



**eConf C000911**  
**SLAC-R-579**

A [word](#) about these proceedings

[eConf C000911](#) [eProceedings](#) [Committees](#) [Participants](#) [Program](#) [RADCOR 2000](#) [eConf](#)

## **Proceedings of the 5th International Symposium on Radiative Corrections (RADCOR 2000)**

**Carmel Mission Inn**  
**Carmel, California**  
**September 11-15, 2000**

**Editor**  
**Howard E. Haber, University of California, Santa Cruz**

**Co-organized by**  
**Santa Cruz Institute for Particle Physics**  
**Howard E. Haber, Chairman**

**Stanford Linear Accelerator Center**  
**Stanley J. Brodsky, Vice-Chairman**

**Stanford Linear Accelerator Center**  
**Stanford, California**  
**December 2001**

**This work was supported in part by the Department of Energy under contract number DE-AC03-76SF00515**

---

■ [eConf C000911](#) ■ [Proceedings](#) ■ [Committees](#) ■ [Participants](#) ■ [Program](#) ■ [RADCOR 2000](#) ■ [eConf](#)

[Jones](#)

Last Update: Monday, 14 January 2002

---

This document, and the material and data contained therein, was developed under sponsorship of the United States Government. Neither the United States nor the Department of Energy, nor the Leland Stanford Junior University, nor their employees, nor their respective contractors, subcontractors, or their employees, makes any warranty, express or implied, or assumes any liability of responsibility for accuracy, completeness or usefulness of any information, apparatus, product or process disclosed, or represents that its use will not infringe privately owned rights. Mention of any product, its manufacturer, or suppliers shall not, nor is it intended to, imply approval, disapproval, or fitness of any particular use. A royalty-free, nonexclusive right to use and disseminate same for any purpose whatsoever, is expressly reserved to the United States and the University.



# Proceedings of the 5th International Symposium on Radiative Corrections (RADCOR 2000)

[eConf C000911](#) [eProceedings](#) [Committees](#) [Participants](#) [Program](#) [RADCOR 2000](#) [eConf](#)

## A Word About These Proceedings and eConf

These proceedings from the 5th International Symposium on Radiative Corrections (RADCOR 2000) are the first set of true eprint proceedings to appear in the Electronic Conference Proceedings Archive (eConf) at the Stanford Linear Accelerator Center.

Authors were requested to submit their papers to the eprint arXiv server (arXiv.org). Links to the arXiv submissions were organized on a Web page to create the proceedings. In addition, a full-set of proceedings was compiled by pulling copies of the portable document format (PDF) version of the papers from the arXiv server.

Authors may revise and resubmit their paper to the eprint arXiv server at anytime. However, at no time will the full PDF version of the proceedings be updated. The advantages to using the arXiv server include:

- The arXiv number (e.g. hep-ph/0101001) gives SPIRES ability to track citation of the papers.
- Papers are always accessible.

In addition, the goal behind producing electronic conference proceedings is to eliminate the costs involved in printing hardcopy versions of conference proceedings. We hope the eConf archive will help us move towards our goal. Whether you are an author, reader, or both, please give us your [feedback](#) on using the eConf archive to view these proceedings.

Electronic Publications  
SLAC Technical Publications

December 14, 2001

---

■ [eConf C000911](#) ■ [Proceedings](#) ■ [Committees](#) ■ [Participants](#) ■ [Program](#) ■ [RADCOR 2000](#) ■ [eConf](#)

**5th International Symposium on Radiative Corrections**  
Carmel Mission Inn, Carmel, CA  
September 11 - 15, 2000



[Jones](#)

Last Update: Friday, 21 December 2001

## Beyond the Standard Model

Edmond Berger	Next-to-leading Order Calculation of Associated Production of Gauginos and Gluinos
Michael Spira	Higgs Radiation Off Quarks in the Standard Model and Supersymmetric Theories at $e^+ e^-$ Colliders
Sven Heinemeyer	Precision Observables in the MSSM: Leading Electroweak Two-loop Corrections
David Garcia	Quantum corrections for the MSSM Higgs couplings to SM fermions
Maria Herrero	Decoupling Properties of MSSM particles in Higgs and Top Decays
Joan Sola	FCNC top quark decays beyond the Standard Model
D.R. Tim Jones	Anomaly Mediated Supersymmetry Breaking, D-terms and R-symmetry
John Gunion	Hunting the Higgs Boson(s)

## Computational Methods

Robert Harlander	Padé approximation to fixed-order QCD computations
Thomas Gehrmann Vladimir A. Smirnov	Progress on two-loop non propagator integrals ‘Strategy of Regions’: Expansions of Feynman Diagrams in both Euclidean and pseudo-Euclidean Regimes
Davison Soper	Letting Real-Virtual Cancellations Happen by Themselves in QCD Calculations
Pietro Anonio Grassi	On the two-loop electroweak amplitude of the muon decay
Adrian Ghinculov	Electroweak radiative corrections: Towards a two-loop analysis
Dirk Kreimer	Combinatorics of (perturbative) Quantum Field Theory
Zvi Bern	Perturbative Quantization of Gravity Theories

## e+e- Physics at Present and Future Facilities

Tom Junk	Searches at LEP
Stephan Wynhoff	Standard Model Physics Results from LEP2
Stefan Dittmaier	Off-shell W-pair production—universal versus non-universal corrections
Giampiero Passarino	Non-Annihilation Processes, Fermion-Loop and QED Radiation
Bennie Ward	Precision Predictions for (Un)Stable $WW/4f$ Production in $e^+ e^-$ Annihilation: YFSWW3/KoralW1.42/YFSZZ
Zbigniew Was	Coherent Exclusive Exponentiation of $2f$ Processes in $e^+ e^-$ Annihilation

## Electroweak Physics

David Strom	Electroweak Measurements on the Z Resonance
Scott Willenbrock	Precision Top-Quark Physics
Andrzej Czarnecki	Radiative corrections to bound-state properties in QED
Wolfgang Hollik	2-loop electroweak contributions to $\Delta r$
Ansgar Denner	Leading electroweak logarithms at one loop
Ralf Prigl	Status of the BNL Muon ( $g-2$ ) Experiment
Bill Marciano	The Muon Anomalous Magnetic Moment: Standard Model Theory and Beyond

## Heavy Quark Physics

Christos Touramanis	Physics at <i>BaBar</i>
Asish Satpathy	First Physics Results from Belle
Xin Zhao	The Measurement of $ V_{cb} $ and Charmless Hadronic B Decays at CLEO
Salvatore Mele	Indirect Determination of the Vertex and Angles of the Unitarity Triangle
Martin Beneke	Conceptual aspects of QCD factorization in hadronic $B$ decays

Ulrich Nierste	The width difference of $B_s$ mesons
Stefano Bertolini	Theory of $\varepsilon'/\varepsilon$
Gino Isidori	Supersymmetric effects in rare semileptonic decays of $B$ and $K$ mesons
Richard Lebed	On Radiative Weak Annihilation Decays
Adam Leibovich	$ V_{ub} $ from Semileptonic Decay and $b$ to $s\gamma$
Michael Luke	Determining $ V_{ub} $ from the $\bar{B}$ to $X_u l \bar{\nu}$ dilepton invariant mass spectrum
Daniel Wyler	$CP$ -Violation, the CKM Matrix and New Physics
Tobias Hurth	Inclusive Rare B Decays

## Precision Physics at Future Colliders

Francois Charles	Higgs and Supersymmetry searches at the Large Hadron Collider
Doreen Wackerroth	Theoretical Challenges for a Precision Measurement of the W Mass at Hadron Colliders
Tim Barklow	WW Physics at Future $e^+e^-$ Linear Colliders
David Rainwater	Precision Higgs Physics at a Future Linear Collider
Jens Erler	Giga Z: High Precision Tests of the SM and the MSSM

## QCD Physics

John Womersley	QCD at the Tevatron: Status and Prospects
Johan Rathsman	Conformal Expansions: A Template for QCD Predictions
Johannes Bluemlein	The Drell-Yan-Levy Relation: $ep$ vs $e^+e^-$ Scattering to $O(\alpha_s^2)$
Rik Yoshida	HERA Small- $x$ and/or Diffraction
Carl Schmidt	Review of BFKL
Antonio Pich	$\varepsilon'/\varepsilon$ and Chiral Dynamics
Andre Hoang	Light Quark Mass Effects in Bottom Quark Mass Determinations
Markus Diehl	Exclusive QCD

ANL-HEP-CP-01-002  
July 27, 2001  
hep-ph/0101164

# Next-to-leading Order Calculation of Associated Production of Gauginos and Gluinos

EDMOND L. BERGER AND T. M. P. TAIT

*High Energy Physics Division\**, Argonne National Laboratory, Argonne, IL 60439,  
USA

*E-mail: berger@anl.gov, tait@hep.anl.gov*

M. KLASSEN

*II. Institut für Theoretische Physik, Universität Hamburg, D-22761 Hamburg,  
Germany*

*E-mail: michael.klasen@desy.de*

Results are presented of a next-to-leading order calculation in perturbative QCD of the production of charginos and neutralinos in association with gluinos at hadron colliders. Predictions for total and differential cross sections are shown at the energies of the Fermilab Tevatron and CERN Large Hadron Collider for a typical supergravity model of the sparticle mass spectrum and for a light gluino model.

Presented by E. L. Berger at the  
5th International Symposium on Radiative Corrections  
(RADCOR-2000)  
Carmel CA, USA, 11–15 September, 2000

---

\*Work supported by the U.S. Department of Energy, High Energy Physics Division, under Contract No. W-31-109-Eng-38.

# 1 Introduction

The mass spectrum in typical supergravity and gauge-mediated models of supersymmetry (SUSY) breaking favors much lighter masses for gauginos than for squarks. Because the masses are smaller, there is greater phase space at the Tevatron and greater partonic luminosities for gaugino pair production, and for associated production of gauginos and gluinos, than for squark pair production. Another point in favor of associated production is the relative simplicity of the final state. For example, the lowest lying neutralino is the (stable) lightest supersymmetric particle (LSP) in supergravity (SUGRA) models, manifest only as missing energy in the events, and it is the second lightest in gauge-mediated models. The charginos and higher mass neutralinos may decay leptonically leaving a lepton signature plus missing transverse energy; relatively clean events ensue. Furthermore, associated production may be the best channel for measurement of the gluino mass.

The search for direct experimental evidence of supersymmetry at colliders requires a good understanding of theoretical predictions of the total and differential cross sections for production of the superparticles. In the case of hadron colliders, where collisions of strongly interacting hadrons are studied, the large strong coupling strength ( $\alpha_s$ ) leads to potentially large contributions beyond the leading order (LO) in a perturbation series expansion of the cross section. To have accurate theoretical estimates of production rates, it is necessary to include corrections at next-to-leading order (NLO) or beyond. In this contribution, we summarize our recent calculations at next-to-leading order in perturbative quantum chromodynamics (QCD) of the total and differential cross sections for associated production of gauginos and gluinos at hadron colliders[1,2]. Associated production offers a chance to study the parameters of the soft SUSY-breaking Lagrangian. Rates are controlled by the magnitudes and phases of the gaugino ( $\tilde{\chi}$ ) and gluino ( $\tilde{g}$ ) masses and by mixing in the squark and gaugino sectors. Our analysis is general in that it is not tied to a particular SUSY breaking model. We can provide cross sections for arbitrary gluino and gaugino masses.

## 2 NLO SUSY-QCD Formalism

Associated production of a gluino and a gaugino proceeds in leading order (LO) through a quark-antiquark initial state and the exchange of an intermediate squark in the  $t$ -channel or  $u$ -channel[3]. At NLO, loop corrections must be included. In addition, there are 2 to 3 parton processes initiated either by quark-antiquark scattering, with a gluon radiated into the final state,  $q + \bar{q} \rightarrow g + \tilde{g} + \tilde{\chi}$ , or by quark-gluon scattering with a light quark radiated into the final state,  $q + g \rightarrow q + \tilde{g} + \tilde{\chi}$ . For the quark-antiquark initial state, the loop diagrams involve the exchange of intermediate

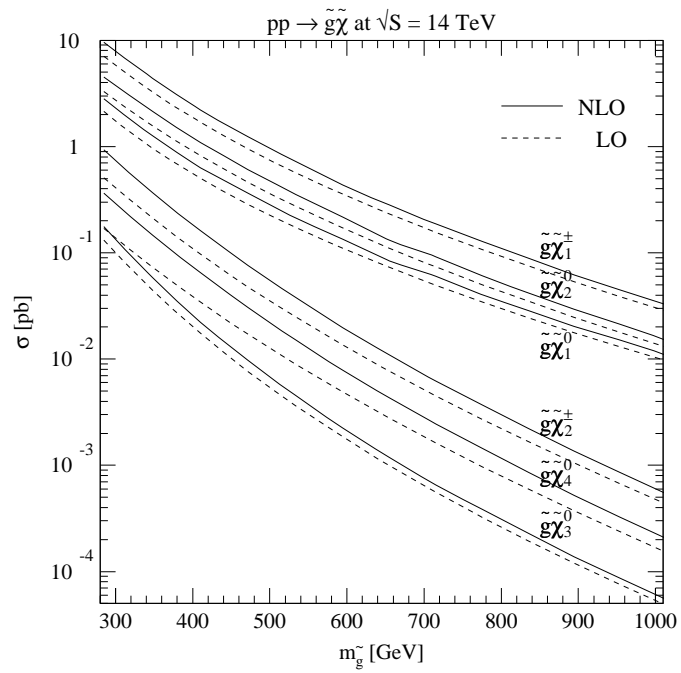
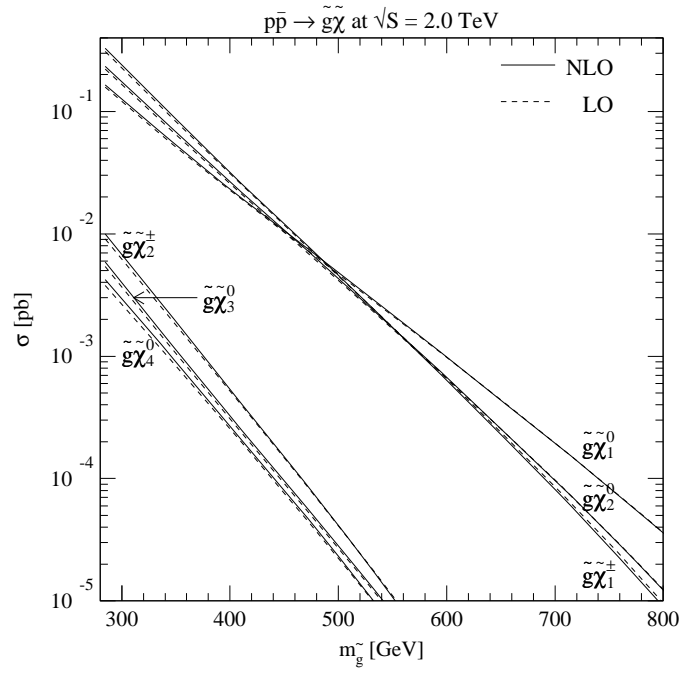


Figure 1: Predicted total hadronic cross sections at Run II of the Tevatron and at the LHC for all six  $\tilde{g}\tilde{\chi}$  channels in a typical SUGRA model as functions of the gluino mass.

Standard Model or SUSY particles in self-energy, vertex, or box diagrams. Ultraviolet and infrared divergences appear at the upper and lower boundaries of integration over unobserved loop momenta. They are regulated dimensionally and removed through renormalization or cancellation with corresponding divergences in the 2 to 3 parton (real emission) diagrams that have an additional gluon radiated into the final state. In addition to soft divergences, real emission contributions have collinear divergences that are factored into the NLO parton densities.

The set of Feynman diagrams with light quark emission includes diagrams in which an intermediate squark splits into a quark and either a gluino or gaugino. After all initial state collinear singularities are removed by mass factorization, the matrix elements may still contain integrable singularities if the mass of the squark is larger than the mass of the gluino or gaugino. In these cases, the intermediate squark state can be on its mass-shell. These singularities represent the LO production of a squark and a gluino or gaugino, followed by the LO decay of the squark. They may be regulated if one includes the full Breit-Wigner form for the squark propagator including a finite squark width. There is a further subtlety associated with the requirement that we not double-count the region of phase space in which the squark is on-shell. The kinematic configuration with an on-shell squark is included in the LO production of a squark and a gluino or a squark and a gaugino, and it should not be considered as a genuine higher order correction to the production of gluinos with gauginos. To avoid double counting, we thus subtract the on-shell squark contribution. It can be subtracted leaving a genuine NLO contribution in the limit of small squark width.

The full treatment of the NLO analysis is presented in our long paper[2].

### 3 Tevatron and LHC Cross Sections

To obtain numerical predictions for hadronic cross sections, we choose an illustrative SUGRA model with parameters  $m_0 = 100$  GeV,  $A_0=300$  GeV,  $\tan \beta = 4$ , and sign  $\mu = +$ . Because the gluino, gaugino, and squark masses all increase with parameter  $m_{1/2}$  (but are insensitive to  $m_0$ ), we vary  $m_{1/2}$  between 100 and 400 GeV. The resulting masses for  $\tilde{\chi}_{1...4}^0$  vary between 31...162, 63...317, 211...665, and 241...679 GeV;  $\tilde{\chi}_{1,2}^\pm$  are almost degenerate in mass with  $\tilde{\chi}_{2,4}^0$ . The mass  $m_{\tilde{\chi}_3^0} < 0$  inside a polarization sum. Our approach is general, and results can be obtained for any set of gaugino and gluino masses. For our second model, we select one[4] with an intermediate-mass gluino as the lightest SUSY particle (LSP), fixing  $m_{\tilde{g}} = 30$  GeV, and  $m_{\tilde{q}} = 450$  GeV. We choose a weak sector identical to the SUGRA case. In our paper[2], we also quote results for anomaly mediated, gauge mediated, and gaugino mediated models.

We convolve LO and NLO partonic cross sections with CTEQ5 parton densities in LO and NLO ( $\overline{\text{MS}}$ ) along with 1- and 2-loop expressions for  $\alpha_s$ , the corresponding values of  $\Lambda$ , and five active quark flavors.

For the SUGRA case, we present total hadronic cross sections in Fig. 1 as functions of the gluino mass. The common renormalization and factorization scale  $\mu$  is set equal to the average particle mass  $m$ . The light gaugino channels should be observable at both colliders. At the Tevatron, for  $2 \text{ fb}^{-1}$  of integrated luminosity, 10 or more events could be produced in each of the lighter gaugino channels if  $m_{\tilde{g}} < 450 \text{ GeV}$ . The heavier Higgsino channels are suppressed by about one order of magnitude and might be observable only at the LHC. As a rough estimate of uncertainty associated with the choice of parton densities, we note that the NLO cross section for  $\tilde{\chi}_2^0$  production is lower by 12% at the Tevatron with the CTEQ5 set than for the CTEQ4 set, and 4% lower at the LHC. The impact of the NLO corrections can be seen more readily in the ratio of NLO to LO cross sections computed at a renormalization scale set equal to the average mass of the final state particles. The NLO effects are moderate (of  $\mathcal{O}(10\%)$ ) at the Tevatron, while at the LHC the NLO contributions can increase the cross sections by as much as a factor of two. The second initial-state channel, initiated by gluon quark scattering, plays a significant role at the energy of the LHC.

For the case of a gluino with mass 30 GeV, the total hadronic cross sections are shown in Fig. 2 as functions of  $m_{1/2}$ . At the Tevatron, for  $2 \text{ fb}^{-1}$  of integrated luminosity, 100 or more events could be produced in each of the lighter gaugino channels if  $m_{1/2} < 400 \text{ GeV}$ . In this case, NLO enhancement factors lie in the ranges 1.3 to 1.4 at the Tevatron and 2 to 4 at the LHC.

An important measure of the theoretical reliability is the variation of the hadronic cross section with the renormalization and factorization scales. At LO, these scales enter only in the strong coupling constant and the parton densities, while at NLO they appear also explicitly in the hard cross section. The scale dependence is reduced considerably after NLO effects are included, as shown in Fig. 3. The Tevatron (LHC) cross sections vary by  $\pm 23(12)\%$  at LO, but only by  $\pm 8(4.5)\%$  in NLO when the scale is varied by a factor of two around the central scale.

For experimental searches, distributions in transverse momentum are important since cuts on  $p_T$  help to enhance the signal. In our long paper[2], we show that NLO contributions can have a large impact on  $p_T$  spectra at the LHC, owing to contributions from the  $gq$  initial state. At the Tevatron the NLO  $p_T$ -distribution is shifted moderately to lower  $p_T$  with respect to the LO expectation. Examples for the  $\tilde{g}\tilde{\chi}_1^\pm$  channel are shown in Fig. 4. The shapes of the rapidity distributions of the gauginos are not altered appreciably by NLO contributions.

## 4 Summary

In our long paper we report a complete next-to-leading order analysis of the associated production of gauginos and gluinos at hadron colliders. If supersymmetry exists at the electroweak scale, the cross section for this process is expected to be observable

at the Fermilab Tevatron and/or the CERN LHC. It is enhanced by the large color charge of the gluino and the relatively small mass of the light gauginos in many SUSY models. Associated production offers a chance to study in detail the parameters of the soft SUSY-breaking Lagrangian. The rates are proportional to the phases of the gaugino and gluino masses, and to the mixings in the squark and chargino/neutralino sectors. In combination with other channels, associated production could allow one to measure some or all of these quantities.

The physical gluino and gaugino masses that we use, as well as the gaugino mixing matrices, are based on four popular SUSY breaking models plus a fifth scenario in which the gluino mass is relatively light. Because the LO cross sections in gauge-mediated, gaugino-mediated, and anomaly-mediated supersymmetry breaking models are not too dissimilar from those of the SUGRA case at Tevatron energies, we focus our NLO work on the SUGRA model and on a model in which a light gluino, with mass  $m_{\tilde{g}} = 30$  GeV, is the lightest supersymmetric particle (LSP).

In the SUGRA model, the largest cross sections at the Fermilab Tevatron energy are those for neutralino  $\tilde{\chi}_2^0$ , enhanced by its  $\tilde{W}_3$ -like coupling with respect to the  $\tilde{B}$ -like  $\tilde{\chi}_1^0$ , and the chargino  $\tilde{\chi}_1^\pm$ , about equal in mass with the  $\tilde{\chi}_2^0$ . The NLO corrections to associated production are generally positive, but they can be modest in size, ranging in the SUGRA model from a few percent at the energy of the Tevatron to 100% at the energy of the LHC, depending on the sparticle masses. In the light-gluino case, NLO contributions increase the cross section by factors of 1.3 to 1.4 at the energy of the Tevatron and by factors of 2 to 3.5 at the energy of the LHC. The large enhancements owe their origins to the important role of the  $gq$  channel that enters first at NLO.

Owing to the NLO enhancements, collider searches for signatures of associated production will generally discover or exclude sparticles with masses larger than one would estimate based on LO production rates alone. More significant from the viewpoint of reliability, the renormalization and factorization scale dependence of the cross sections is reduced by a factor of more than two when NLO contributions are included.

At Run II of the Fermilab Tevatron, for an integrated luminosity of  $2 \text{ fb}^{-1}$ , we expect that 10 or more events could be produced in each of the lighter gaugino channels of the SUGRA model,  $\tilde{g}\tilde{\chi}_1^0$ ,  $\tilde{g}\tilde{\chi}_2^0$ , and  $\tilde{g}\tilde{\chi}_1^\pm$ , provided that the gluino mass  $m_{\tilde{g}}$  is less than 450 GeV. The cross sections for the three heavier gaugino channels,  $\tilde{g}\tilde{\chi}_3^0$ ,  $\tilde{g}\tilde{\chi}_4^0$ , and  $\tilde{g}\tilde{\chi}_2^\pm$ , are smaller by an order of magnitude or more than those of the lighter gaugino channels. In the light gluino LSP model, more than 100 events could be produced in the three lighter gaugino channels provided that the common GUT-scale fermion mass  $m_{1/2}$  is less than 400 GeV, and as many as 10 events in the three heavier gaugino channels as long as  $m_{1/2}$  is less than 200 GeV. At the higher energy and luminosity of the LHC, at least a few events should be produced in every channel in the SUGRA model and many more in the light gluino model.

The relatively large cross sections suggest that associated production is a good

channel for discovery of a light gluino at the Tevatron, for closing the window on this possibility, and/or for setting limits on light gaugino masses. The usual searches for a light gluino LSP are based on the assumption that gluinos are produced in pairs. In this situation, the dominant background is QCD production of hadronic jets. Hard cuts on transverse momentum must be made to reduce this background to tolerable levels. The cuts, in turn, mitigate against gluinos of modest mass. By contrast, if light gluinos are produced in association with gauginos, one can search for light gluino monojets accompanied by leptons and/or missing transverse energy from gaugino decays.

## Acknowledgments

Work is the High Energy Physics Division at Argonne National Laboratory is supported by the U.S. Department of Energy, High Energy Physics Division, under Contract No. W-31-109-Eng-38. The work of M. Klasen is supported by Deutsche Forschungsgemeinschaft (DFG) under contract KL 1266/1-1.

## References

- [1] E. L. Berger, M. Klasen, and T. Tait, *Phys. Lett.* **B459** (1999) 165 and Proceedings of the 35th Rencontres de Moriond on *QCD and High Energy Hadronic Interactions*, Les Arcs, France, 2000, hep-ph/0005199.
- [2] E. L. Berger, M. Klasen, and T. Tait, *Phys. Rev.* **D62** (2000) 095014.
- [3] S. Dawson, E. Eichten, and C. Quigg, *Phys. Rev.* **D31** (1985) 1581; H. Baer, D.D. Karatas, and X. Tata, *Phys. Rev.* **D42** (1990) 2259.
- [4] S. Raby, *Phys. Lett.* **B422** (1998) 158; H. Baer, K. Cheung, and J. F. Gunion, *Phys. Rev.* **D59** (1999) 075002; A. Mafi and S. Raby, *Phys. Rev.* **D62** (2000) 035003.

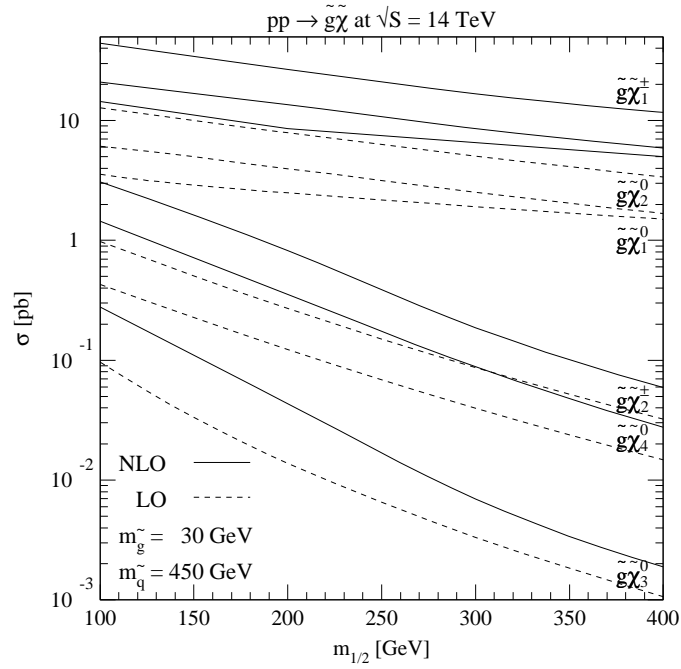
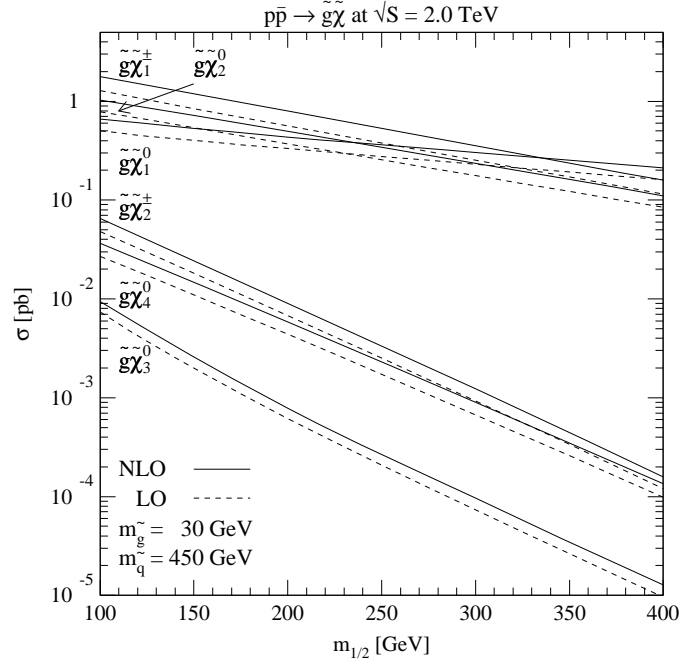


Figure 2: Predicted total hadronic cross sections at Run II of the Tevatron and at the LHC for all six  $g\tilde{\chi}$  channels in our model with a gluino of mass 30 GeV, as functions of the parameter  $m_{1/2}$ .

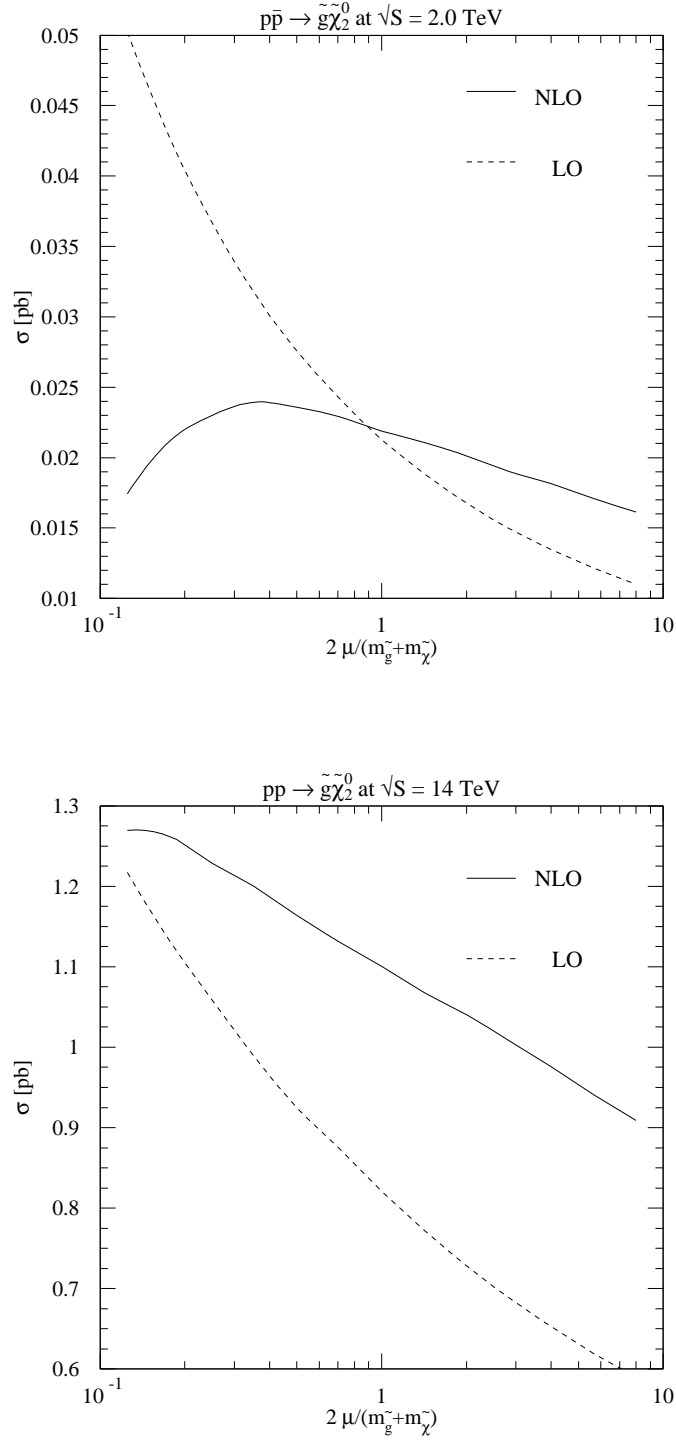


Figure 3: Dependence of the predicted NLO and LO total cross sections at the Tevatron and at the LHC on the renormalization and factorization scale. We show the case of  $\tilde{g}\tilde{\chi}_2^0$  production in the SUGRA model, with  $m_{\tilde{g}} = 410$  GeV and  $m_{\tilde{\chi}_2^0} = 104$  GeV.

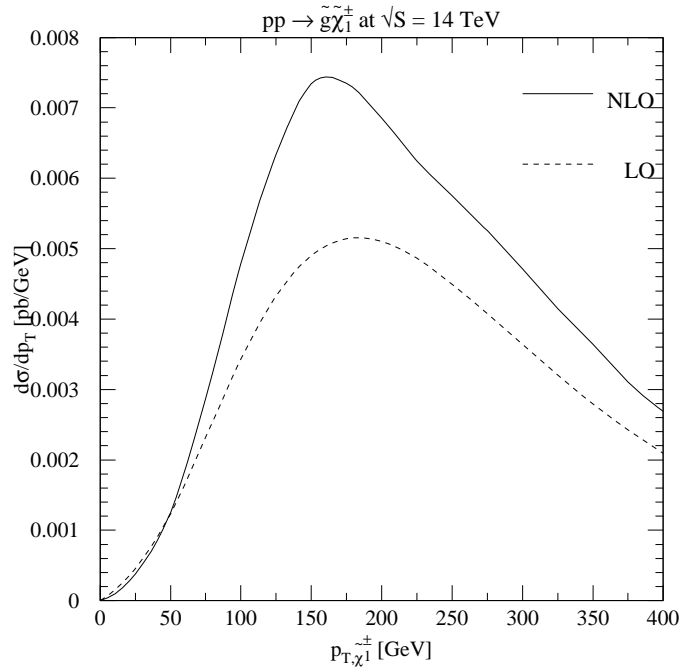
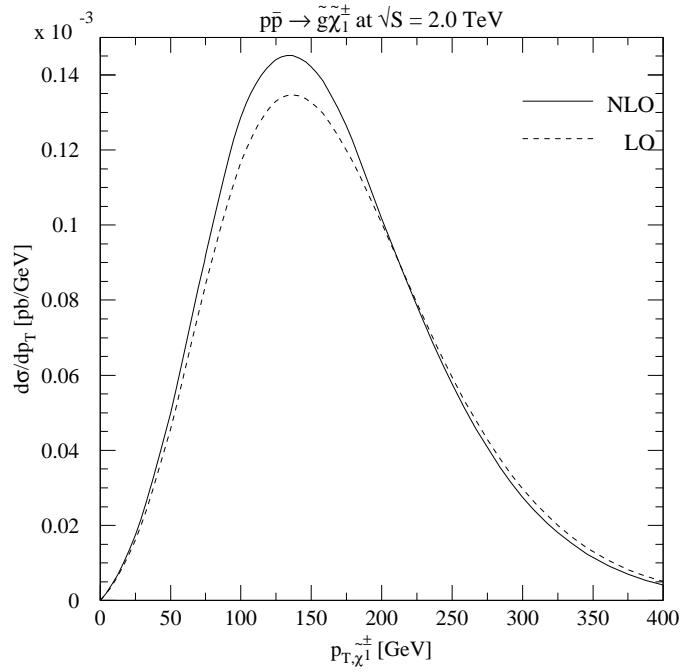


Figure 4: Differential cross section in transverse momentum  $d\sigma/dp_T$  for the production of  $\tilde{\chi}_1^\pm$  with mass 101 GeV in association with a  $\tilde{g}$  of mass 410 GeV at the Tevatron and at the LHC.

HIGGS RADIATION OFF QUARKS  
IN THE STANDARD MODEL AND SUPERSYMMETRIC THEORIES  
AT  $e^+e^-$  COLLIDERS

MICHAEL SPIRA

*Paul-Scherrer-Institut, CH-5232 Villigen PSI, Switzerland*

**Abstract**

Yukawa couplings between Higgs bosons and quarks in the Standard Model (SM) and supersymmetric theories can be measured in the processes  $e^+e^- \rightarrow Q\bar{Q} + \text{Higgs}$ . The cross sections and Higgs energy distributions of these processes in the SM and minimal supersymmetric model have been determined including the complete set of next-to-leading order QCD corrections for all channels.

Presented at the

5th International Symposium on Radiative Corrections  
(RADCOR-2000)  
Carmel CA, USA, 11–15 September, 2000

# 1 Introduction

In the Standard Model (SM) and its supersymmetric extensions, the masses of electroweak gauge bosons, leptons, and quarks are generated by interactions with Higgs fields [1]. The Yukawa couplings between Higgs particles and fermions therefore grow with the masses  $M_f$  of the fermions. The couplings obey a universal scaling law  $g_{ffH} = M_f/v$  in the SM, with  $v \approx 246$  GeV being the ground-state value of the Higgs field. In supersymmetric models, which involve at least two Higgs doublets, the size of the Yukawa couplings is also set by the fermion masses, yet the relationship is more complex owing to the mixing among the Higgs fields. The Yukawa couplings [2] of the two CP-even light/heavy Higgs bosons  $h/H$  and of the CP-odd Higgs boson  $A$  in the minimal supersymmetric extension of the Standard Model (MSSM) [3, 4], expressed in units of the SM couplings, are determined by the parameters  $\text{tg}\beta = v_2/v_1$ , the ratio of the vacuum expectation values of the two Higgs fields generating the masses of up- and down-type particles, and  $\alpha$ , the mixing angle in the CP-even sector. In the decoupling limit, in which the light Higgs mass reaches the maximum value for a given parameter  $\text{tg}\beta$ , the  $h$  Yukawa couplings approach the SM values. In general, they are suppressed for up-type fermions and enhanced for down-type fermions; the enhancement increases with  $\text{tg}\beta$  and can therefore be very strong.

Higgs radiation off top or off bottom quarks in  $e^+e^-$  collisions,

$$e^+e^- \rightarrow Q\bar{Q}\phi \quad [Q = t, b; \phi = H_{SM}, h, H, A], \quad (1)$$

lends itself as a suitable process for measuring the Yukawa couplings of all Higgs bosons [5], particularly for the SM Higgs bosons, the light Higgs boson  $h$  and for moderately heavy Higgs bosons  $H$  and  $A$ . Within the SM it has been demonstrated that the top Yukawa coupling can be measured with an accuracy of 2–3% at linear colliders with  $\sqrt{s} = 800$  GeV [6]. We present the cross sections for these processes including the next-to-leading order (NLO) QCD corrections [7, 8]. In this analysis we have calculated the complete set of  $\mathcal{O}(\alpha_s)$  QCD corrections to all subchannels in (1) systematically. The large number of interfering subchannels in supersymmetric theories renders this program more complex than the corresponding calculation in the SM, in particular since the relative weight of the subchannels varies over the supersymmetric parameter space and over the phase space for different mass ratios. Moreover, the Higgs-energy distributions haven been obtained at NLO [9]. They turn out to be relevant in the separation of the resonant parts and those, which depend on the Yukawa couplings. Introducing appropriate cuts in the Higgs energy the sensitivity to the Yukawa couplings can be increased experimentally.

## 2 QCD Corrections

The QCD corrections can be categorized into five classes. Virtual corrections of the internal quark lines, of the  $\gamma/Z$ -quark vertices, of the Higgs-quark vertices, and box diagrams interfere with the Born amplitude. Gluon radiation off internal and external quark lines adds incoherently to the cross sections. The value of the electromagnetic

coupling is taken to be  $\alpha = 1/128$  and the Weinberg angle as  $\sin^2\theta_W = 0.23$ . The mass of the  $Z$  boson is set to  $M_Z = 91.187\text{ GeV}$ , and the pole masses of the top and bottom quarks are set to  $M_t = 174\text{ GeV}$  [10] and<sup>1</sup>  $M_b = 4.62\text{ GeV}$  [11], respectively. The masses of the MSSM Higgs bosons and their couplings are related to  $\text{tg}\beta$  and the pseudoscalar Higgs boson mass  $M_A$ . In the relation we use, higher-order corrections up to two loops in the effective-potential approach are included [12]. The SUSY parameters are chosen as  $\mu = A_t = A_b = 0$  and  $M_{\tilde{Q}} = 1\text{ TeV}$ ; this simple choice is sufficient to illustrate the main results.

The production of  $b\bar{b}\phi$  final states can be mediated by resonance channels  $e^+e^- \rightarrow ZH_{SM}, Zh, ZH$  and  $e^+e^- \rightarrow Ah, AH$ . We describe the resonance structures as Breit-Wigner forms by substituting  $M^2 \rightarrow M^2 - iM\Gamma$  in all boson propagators. The decay widths of the Higgs bosons are calculated including higher-order corrections, as described in Refs. [13, 14], while the  $Z$  width is set to  $\Gamma_Z = 2.49\text{ GeV}$ . For  $t\bar{t}\phi$  production the widths can be neglected, since the Higgs masses are taken below the  $t\bar{t}$  threshold. The renormalization scale of the QCD coupling  $\alpha_s$ , which is evaluated in NLO with five active flavors normalized to  $\alpha_s(M_Z^2) = 0.119$  [10], is chosen at  $\mu_R^2 = s$ , where  $s = E_{\text{CM}}^2$  is the center-of-mass (CM) energy squared.

The QCD radiative corrections have been calculated in the standard way. The Feynman diagrams have been evaluated within dimensional regularization. Ultraviolet divergences are consistently regularized in  $D = 4 - 2\epsilon$  dimensions, with  $\gamma_5$  treated naively since no anomalies are involved. The renormalization of the  $Q\bar{Q}\phi$  vertices is connected to the renormalization of the quark masses, which, in the case of the top quark, is defined on shell (see e.g. Refs. [15, 16] for details). In the case of bottom quarks large logarithms are mapped into the running mass  $\overline{m}_b(Q_{\text{Higgs}}^2)$  for the Yukawa couplings of the  $b$  quark, with  $Q_{\text{Higgs}}^2$  denoting the squared momentum flow through the corresponding Higgs-boson line. The infrared divergences encountered in the virtual corrections and in the cross section for real gluon emission, are treated in two different ways. Both calculations follow subtraction procedures, one using dimensional regularization and one introducing an infinitesimal gluon mass [17]. The results obtained by the two different procedures are in mutual numerical agreement after adding the contributions from virtual gluon exchange and real gluon emission. A second, completely independent calculation of the QCD corrections to the total cross section was based on the evaluation of all relevant cut diagrams of the photon and  $Z$ -boson self-energies in two-loop order, generalizing the method applied to  $t\bar{t}(g)$  intermediate states in Ref. [18]. The results of the two approaches are in numerical agreement. Moreover, the parts that have been calculated in Refs. [19, 20], i.e. photon exchange and resonant contributions, are in full agreement with our corresponding partial results.

---

<sup>1</sup>This value for the perturbative pole mass of the bottom quark corresponds in NLO to an  $\overline{\text{MS}}$  mass  $\overline{m}_b(\overline{m}_b) = 4.28\text{ GeV}$ .

### 3 Results

**a.) Asymptotic behaviour.** The QCD corrections to the top final states  $t\bar{t}\phi$  can be interpreted easily in two kinematical areas. Whenever the invariant mass of the  $t\bar{t}$  pair is close to threshold, the gluonic Sommerfeld rescattering-correction is positive and becomes large. In the threshold region the  $K$  factor approaches the asymptotic form [7]

$$K_{\text{thr}}^{t\bar{t}\phi} \rightarrow 1 + \frac{32\alpha_s}{9\beta_t} \quad (2)$$

with the maximal quark velocity  $\beta_t = \sqrt{(\sqrt{s} - M_\phi)^2 - 4M_t^2}/2M_t$  in the  $(t\bar{t})$  rest frame.

For high energies, on the other hand, the QCD corrections are of order  $\alpha_s/\pi$ . In the energy region  $s \gg 4M_t^2 \gg M_H^2$  but  $\log s/M_t^2 \not\gg \mathcal{O}(1)$ , which is relevant for the present analysis, the QCD corrections can qualitatively be traced back to vertex corrections and infrared gluon radiation. Since scalar Higgs bosons are radiated off top quarks preferentially with small energy [ $x = E_\phi/E_t \rightarrow 0$ ], as is evident from the leading (universal) part of the fragmentation function

$$f(t \rightarrow tH; x) = \frac{g_{ttH}^2}{16\pi^2} \left[ 4 \frac{1-x}{x} + x \log \frac{s}{M_t^2} \right], \quad (3)$$

the QCD correction of the scalar Yukawa vertex, regularized by soft gluon radiation, approaches the value [19]

$$\Delta_H^{V+IR} = \frac{4\alpha_s}{3\pi} \left[ -1 + \frac{2-x}{x} \log(1-x) \right] \rightarrow -4 \frac{\alpha_s}{\pi}. \quad (4)$$

The scalar Yukawa vertex is therefore reduced by four units in  $\alpha_s/\pi$  which are compensated only partly by one unit due to the increase of the  $t\bar{t}$  production probability, leading in total [7, 19] to

$$K_{\text{cont}}^{t\bar{t}\phi} \rightarrow 1 - 3 \frac{\alpha_s}{\pi} + \dots \quad \text{for } \phi = H_{SM}, h, H. \quad (5)$$

The ellipsis accounts for hard Higgs and gluon radiation (of order  $+\alpha_s/\pi$ ). Thus, the QCD corrections are expected negative for scalar Higgs particles in the high energy continuum.

By contrast, the corresponding fragmentation function for the pseudoscalar Higgs boson [21]

$$f(t \rightarrow tA; x) = \frac{g_{ttA}^2}{16\pi^2} x \log \frac{s}{M_t^2} \quad (6)$$

is hard so that the average of the vertex and IR gluon corrections over the Higgs spectrum amounts to

$$\Delta_A^{V+IR} \rightarrow \frac{4\alpha_s}{3\pi} \left\langle \left[ 1 + \frac{2-x}{x} \log(1-x) \right] \right\rangle \sim -\frac{3}{2} \frac{\alpha_s}{\pi}. \quad (7)$$

Adding to this correction the increase of the  $t\bar{t}$  production probability of one unit, the  $K$  factor is very close to unity

$$K_{\text{cont}}^{t\bar{t}A} \rightarrow 1 - \frac{1}{2} \frac{\alpha_s}{\pi} + \dots \quad (8)$$

After hard gluon bremsstrahlung is taken into account (symbolized by the ellipsis), the overall QCD corrections for the pseudoscalar Higgs boson are therefore expected slightly positive. [For ultra-high energies, i.e.  $\log s/M_t^2 \gg 1$ , hard gluon bremsstrahlung becomes important. Similarly to the leading terms in the fragmentation functions eqs. (3) and (6), the QCD corrections for scalar and pseudoscalar Higgs bosons approach each other as a result of chiral symmetry restoration in *asymptotia*; this has been verified in a numerical calculation.]

Similar estimates can be applied to bottom final states which in general are dominated by resonance decays. After absorbing the large logarithms  $\log(Q_\phi^2/M_b^2)$  into the Yukawa couplings, the non-leading effects are positive:

$$K_{\text{res}}^{b\bar{b}\phi} \approx 1 + \left\{ \frac{17}{3}, 1 \right\} \frac{\alpha_s}{\pi} \quad \text{for } \{\text{Higgs}, Z\} \rightarrow b\bar{b} \quad . \quad (9)$$

Also close to the thresholds and in the high-energy limit the QCD corrections remain positive after mapping the large (negative) corrections into the running Yukawa couplings. Since different channels are activated at the same time, only a qualitative estimate can be given in the continuum regime,

$$K_{\text{cont}}^{b\bar{b}\phi} = 1 + c \frac{\alpha_s}{\pi} \quad \text{with } c = \mathcal{O}(1), \quad (10)$$

while details must be left to the numerical analysis.

**b.) Numerical results.** The total cross sections for  $Ht\bar{t}$  production in the SM are

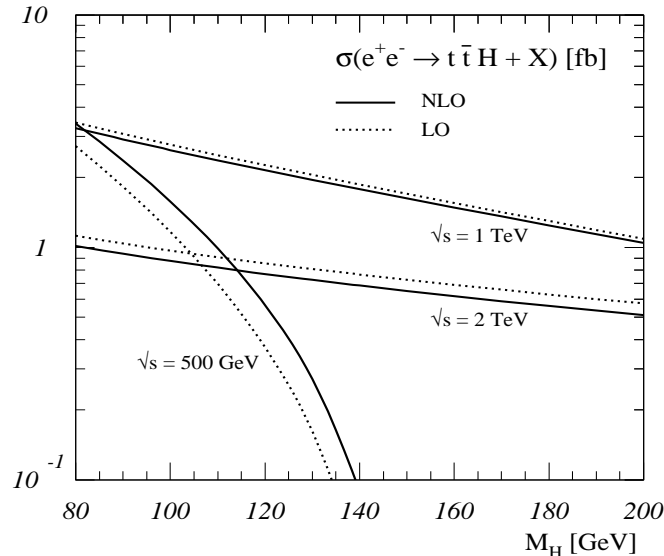


Figure 1: *The total cross section for the process  $e^+e^- \rightarrow t\bar{t}H+X$ , including QCD radiative corrections (full curve) and at LO (dashed curve) as a function of the scaled Higgs energy  $x_H$  [7].*

presented in Fig. 1 as a function of the Higgs mass for different collider energies [7]. The

NLO (LO) cross sections are given by the full (dotted) curves. The QCD corrections are large for  $\sqrt{s} = 500$  GeV due to the Coulomb singularity at threshold and moderate for high energies. At high energies the results agree with the approximation of eq. (5). The cross sections amount to more than about 0.1 fb, which leads to a significant number of events at the TESLA collider, being designed to reach integrated luminosities of about  $\int \mathcal{L} \sim 1 \text{ ab}^{-1}$  in three years of operation. The corresponding Higgs-energy distribution is presented in Fig. 2 for  $M_H = 120$  GeV as a function of the scaled variable  $x_H = 2E_H/\sqrt{s}$  [9]. The shape of the distribution is shifted towards larger values of  $x_H$  due to the Coulomb singularity at threshold. The results for small values of  $x_H$  reproduce the approximation of eq. (5).

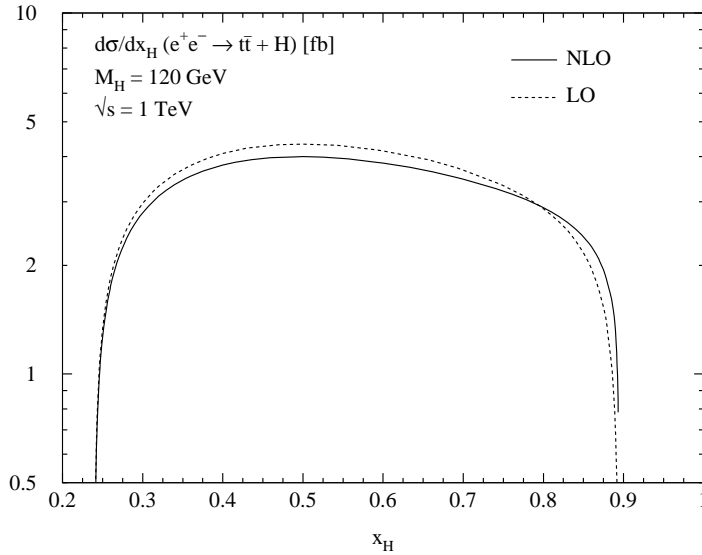


Figure 2: *The Higgs-energy distribution for the process  $e^+e^- \rightarrow t\bar{t}H + X$ , including QCD radiative corrections (full curve) and at LO (dashed curve) as a function of the scaled Higgs energy  $x_H$  [9].*

The results for the MSSM are exemplified in Fig. 3 for  $\text{tg}\beta = 3^2$  and 30 and for the collider energy  $E_{\text{CM}} = 500$  GeV [8]. If required by the size of the cross section, which should not fall below  $\sim 10^{-2}$  fb in order to be accessible experimentally, we switched to  $E_{\text{CM}} = 1$  TeV. The Born terms are shown by the dotted curves, while the final results for the cross sections, including QCD corrections, are given by the full curves.

For  $E_{\text{CM}} = 500$  GeV the QCD corrections to Higgs-boson production in association with  $t\bar{t}$  pairs increase the scalar Higgs-production cross sections significantly, as can be inferred from Fig. 3. Close to threshold the numerical results clearly exhibit the strong increase of the cross sections due to the Coulomb singularity (2). Moreover, for  $\text{tg}\beta = 30$  the cross sections are strongly suppressed except for the regions where the light (heavy)

<sup>2</sup>Although the value  $\text{tg}\beta = 3$  is already excluded for vanishing mixing in the stop sector, this choice exemplifies the complete result for smaller values of  $\text{tg}\beta$  and can easily be extended to the non-vanishing stop mixing case.

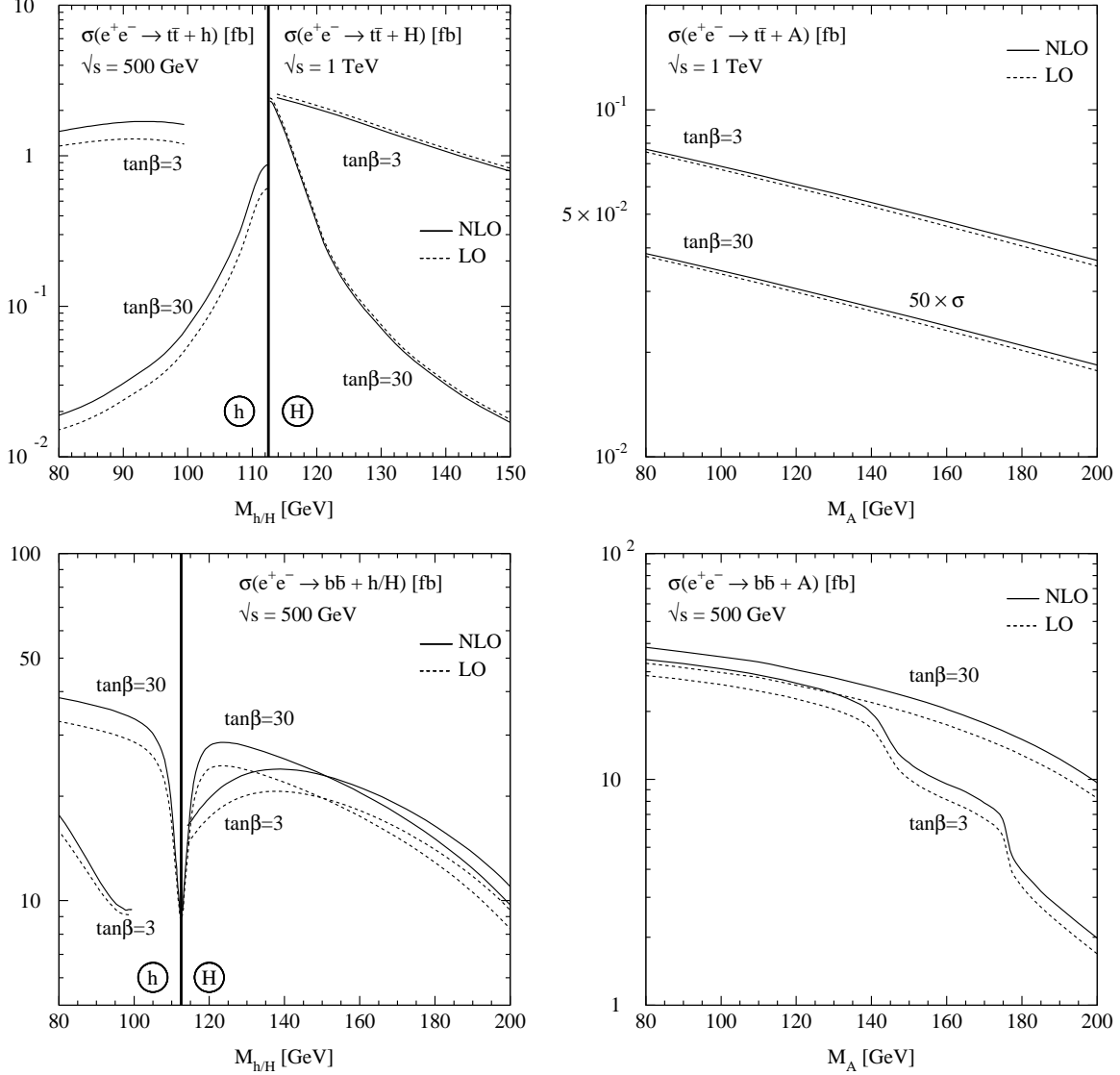


Figure 3: Production cross sections for the MSSM Higgs bosons  $h, H$  and  $A$  in association with heavy  $t, b$  quark pairs [8]; Born approximation: dashed, QCD corrections included: full curves. The rapid drops in the  $b\bar{b}A$  cross section at  $t\beta = 3$  are due to the kinematical opening of the resonant  $H \rightarrow WW, hh$  decays, which reduce the branching ratio of the resonant  $H \rightarrow b\bar{b}$  decay.

scalar Higgs mass is close to its upper (lower) bound. For  $\text{tg}\beta = 3$  the cross section amounts to about 1 fb, which leads to a significant number of events at the TESLA collider.

For CM energies of 1 TeV the QCD corrections to scalar Higgs production in association with  $t\bar{t}$  pairs are of moderate size. They decrease the cross sections by about 3–5%. This is in accordance with the asymptotic form of the  $K$  factor [7]. For pseudoscalar Higgs production, the size of the QCD corrections is slightly positive at 1 TeV, in agreement with the qualitative discussion above.

The cross sections for Higgs-boson production associated with  $b\bar{b}$  pairs are significantly larger due to the resonance contributions from on-shell  $Z$  and Higgs-boson decays into  $b\bar{b}$  pairs. The QCD corrections increase these cross sections by about 5–25%. The drop in the  $b\bar{b}A$  production cross section for  $\text{tg}\beta = 3$  at  $M_A \sim 140$  GeV and 175 GeV can be attributed to the crossing of the thresholds for resonant  $H \rightarrow WW$  and  $H \rightarrow hh$  decays, respectively, in  $HA$  final states.

Without cuts, the intermediate resonance decays  $Z, h, H, A \rightarrow b\bar{b}$  dominate all  $b\bar{b}\phi$  production processes, whenever they are kinematically allowed, and it will be difficult to extract the bottom Yukawa couplings experimentally in regions where resonant Higgs decays to  $b\bar{b}$  pairs are dominant. This is the case at large values of  $\text{tg}\beta$  for all neutral Higgs particles and at small values of  $\text{tg}\beta$  for Higgs masses below the  $WW$  threshold. In these cases the branching ratios, which determine the size of the  $b\bar{b}\phi$  cross sections, will be nearly independent of the bottom Yukawa couplings. Resonance decays  $R \rightarrow b\bar{b}$  in the  $b\bar{b}h/H/A$  final states can however be eliminated by cutting out the resonance energy of the final-state Higgs boson,  $E_{\phi,\text{res}} = (s + M_\phi^2 - M_R^2)/2\sqrt{s}$ . After subtracting these resonance parts, the non-resonant contributions are suppressed by about one to three orders of magnitude. The resonances have been removed from the cross sections in the examples of Fig. 4 by subtracting the two-particle cross sections in the Breit–Wigner bands  $M_R \pm \Delta$  of the energy  $E_{\phi,\text{res}}$  with the resolution  $\Delta = 5$  GeV. This theoretical definition is used for the sake of simplicity; wider cuts may be required in experimental analyses. Peaks and dips in the cross sections are the result of overlapping Breit-Wigner bands. For the scalar Higgs particles they arise from overlapping  $Z$  and  $A$  boson bands; in pseudoscalar Higgs production the light and heavy scalar resonance bands overlap for  $100 \text{ GeV} \lesssim M_A \lesssim 120 \text{ GeV}$  for  $\text{tg}\beta = 30$ . The dips occur whenever the two resonance bands touch each other, while the peaks between the dips occur when the resonance masses coincide exactly. As shown in Fig. 4, the QCD-corrected cross sections are still close to 1 fb or slightly below, except for heavy masses at small values of  $\text{tg}\beta$ . Thus, ensembles of order  $10^3$  events can be collected at a high-luminosity collider [8].

Fig. 5 presents the pseudoscalar Higgs-energy distribution in  $t\bar{t}A$  production at  $\sqrt{s} = 1$  TeV for  $M_A = 120$  GeV and  $\text{tg}\beta = 3$  as a function of the scaled Higgs energy  $x_A = 2E_A/\sqrt{s}$  [9]. As in the case of the SM Higgs boson the distribution is shifted towards larger Higgs energies due to the Coulomb singularity at threshold. Moreover, it is clearly visible from the comparison of Figs. 2 and 5 that the pseudoscalar energy spectrum is harder than the scalar one, which is related to the absence of the  $1/x$  enhancement in eq. (6).

The corresponding Higgs-energy distributions of  $b\bar{b}h$  production for  $M_h = 110$  GeV is

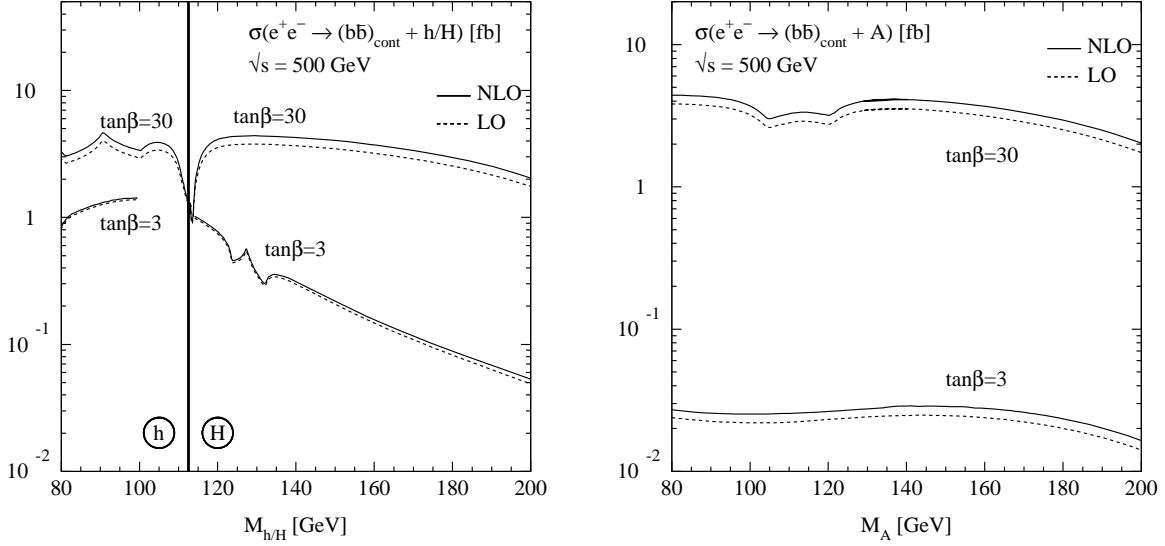


Figure 4: Continuum production of MSSM Higgs bosons  $h, H, A$  in association with a  $b\bar{b}$  pair after subtraction of resonance decays to  $b\bar{b}$  pairs in the Breit-Wigner bands  $M_R \pm 5$  GeV [8].

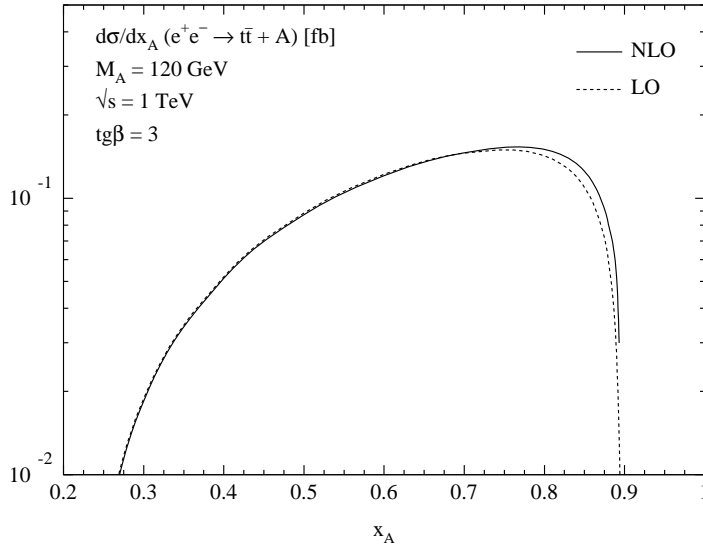


Figure 5: The Higgs-energy distribution for the process  $e^+e^- \rightarrow t\bar{t}A + X$ , including QCD radiative corrections (full curve) and at LO (dashed curve) as a function of the scaled Higgs energy  $x_A$  for  $M_A = 120$  GeV at  $\sqrt{s} = 1$  TeV [9].

exemplified in Fig. 6 and for  $b\bar{b}A$  production for  $M_A = 120$  GeV in Fig. 7 as functions of the corresponding scaled Higgs energies for  $\tan\beta = 30$  at  $\sqrt{s} = 500$  GeV [9]. The resonance peaks of  $A, Z \rightarrow b\bar{b}$  are dominating the distribution of  $b\bar{b}h$  production and of  $h, H \rightarrow b\bar{b}$  the distribution of  $b\bar{b}A$  production. The continuum contributions are suppressed by several orders of magnitude. The QCD corrections are moderate for all Higgs energies.

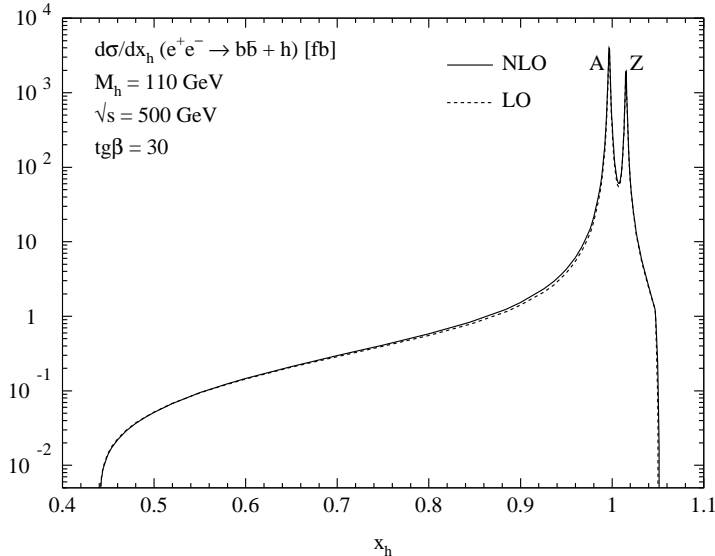


Figure 6: *The Higgs-energy distribution for the process  $e^+e^- \rightarrow b\bar{b}h + X$ , including QCD radiative corrections (full curve) and at LO (dashed curve) as a function of the scaled Higgs energy  $x_h$  for  $M_h = 110$  GeV at  $\sqrt{s} = 500$  GeV [9].*

## 4 Conclusions

Top- and bottom-Yukawa couplings in the SM and supersymmetric theories can be measured at future linear  $e^+e^-$  colliders in Higgs radiation off top and bottom quarks. We have presented the total cross sections and Higgs-energy distributions including the full NLO QCD corrections. The corrections turn out to be large for Higgs radiation off top quarks at c.m. energies  $\sqrt{s} = 500$  GeV, while they are moderate at larger energies. The QCD corrections to Higgs radiation off bottom quarks are moderate after absorbing large logarithms in the running bottom Yukawa couplings.

Measurements of the top Yukawa coupling in SM Higgs radiation off top quarks can be performed quite accurately at the future TESLA collider thanks to the high luminosities. Measurements of Yukawa couplings in supersymmetric Higgs radiation off heavy quarks at  $e^+e^-$  linear colliders are difficult. This is a result of the large number of subchannels contributing to the  $Q\bar{Q}h/H/A$  final states in supersymmetric theories in general, and the contamination by two-Higgs final states in particular. Nevertheless, the continuum cross sections appear large enough to allow for a solution of this experimental problem as shown in the present analysis. Even though experimental simulations are beyond the scope of this note, it may be concluded from earlier SM analyses that the method will work at

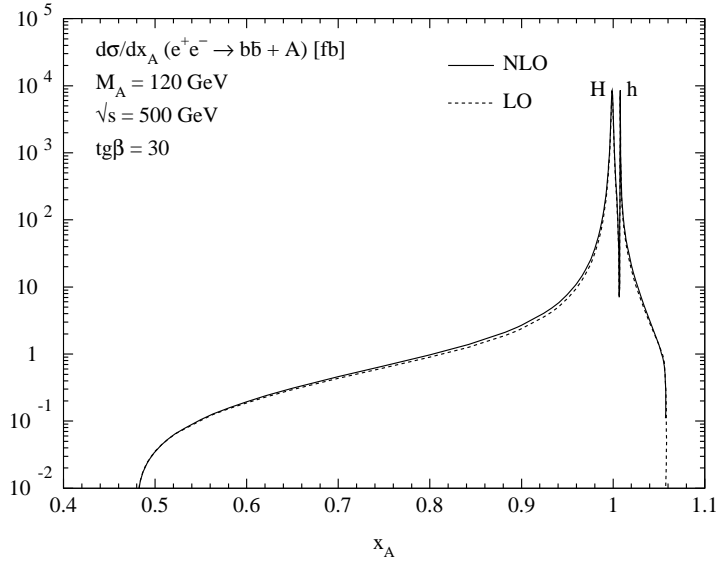


Figure 7: *The Higgs-energy distribution for the process  $e^+e^- \rightarrow b\bar{b}A + X$ , including QCD radiative corrections (full curve) and at LO (dashed curve) as a function of the scaled Higgs energy  $x_A$  for  $M_A = 120$  GeV at  $\sqrt{s} = 500$  GeV [9].*

least in part of the MSSM parameter space, thus providing us with the absolute size of the quark–Higgs Yukawa couplings in the minimal supersymmetric theory.

**Acknowledgements.** I would like to thank S. Dittmaier, M. Krämer, Y. Liao and P.M. Zerwas for the pleasant collaboration on the topic presented here. Moreover, I am grateful to the organizers of RADCOR–2000 for the stimulating atmosphere during the symposium and financial support.

## References

- [1] P.W. Higgs, Phys. Lett. **12** (1964) 132; F. Englert and R. Brout, Phys. Rev. Lett. **13** (1964) 321; G.S. Guralnik, C.R. Hagen and T.W. Kibble, Phys. Rev. Lett. **13** (1964) 585.
- [2] J.F. Gunion and H.E. Haber, Nucl. Phys. **B272** (1986) 1 and **B278** (1986) 449; J.F. Gunion, H.E. Haber, G.L. Kane and S. Dawson, *The Higgs Hunters Guide*, Addison-Wesley 1990.
- [3] P. Fayet and S. Ferrara, Phys. Rep. **32** (1977) 249; H.P. Nilles, Phys. Rep. **110** (1984) 1; H.E. Haber and G.L. Kane, Phys. Rep. **117** (1985) 75; R. Barbieri, Riv. Nuovo Cim. **11** (1988) 1.
- [4] M. Spira and P.M. Zerwas, Lectures, 36th Int. Universitätswochen, Schladming 1997, [hep-ph/9803257].

- [5] A. Djouadi, J. Kalinowski and P.M. Zerwas, *Mod. Phys. Lett.* **A7** (1992) 1765 and *Z. Phys.* **C54** (1992) 255.
- [6] A. Juste and G. Merino, Proceedings, Sitges Conference, Barcelona AU Report [hep-ph/9910301]; H. Baer, S. Dawson and L. Reina, *Phys. Rev.* **D61** (2000) 013002; S. Moretti, *Phys. Lett.* **B452** (1999) 338; TESLA Collaboration, Technical Design Report, to appear.
- [7] S. Dittmaier, M. Krämer, Y. Liao, M. Spira and P.M. Zerwas, *Phys. Lett.* **B441** (1998) 383.
- [8] S. Dittmaier, M. Krämer, Y. Liao, M. Spira and P.M. Zerwas, *Phys. Lett.* **B478** (2000) 247.
- [9] S. Dittmaier, M. Krämer, M. Spira and P.M. Zerwas, in preparation.
- [10] C. Caso et al., Particle Data Group, *Eur. Phys. J.* **C3** (1998) 1.
- [11] S. Narison, *Phys. Lett.* **B341** (1994) 73; M. Jamin and A. Pich, *Nucl. Phys.* **B507** (1997) 334; M. Beneke and A. Signer, *Phys. Lett.* **B471** (1999) 233.
- [12] M. Carena, H.E. Haber, S. Heinemeyer, W. Hollik, C.E.M. Wagner and G. Weiglein, *Nucl. Phys.* **B580** (2000) 29, and references therein.
- [13] A. Djouadi, J. Kalinowski and P.M. Zerwas, *Z. Phys.* **C70** (1996) 435.
- [14] A. Djouadi, *Int. J. Mod. Phys.* **A10** (1995) 1; M. Spira, *Fortschr. Phys.* **46** (1998) 203; A. Djouadi, J. Kalinowski and M. Spira, *Comput. Phys. Commun.* **108** (1998) 56.
- [15] A. Denner, *Fortschr. Phys.* **41** (1993) 307.
- [16] E. Braaten and J.P. Leveille, *Phys. Rev.* **D22** (1980) 715; M. Drees and K. Hikasa, *Phys. Lett.* **B240** (1990) 455; (E) **B262** (1991) 497.
- [17] S. Dittmaier, *Nucl. Phys.* **B565** (2000) 69.
- [18] A. Djouadi and P. Gambino, *Phys. Rev.* **D49** (1994) 3499; (E) **D53** (1996) 4111.
- [19] S. Dawson and L. Reina, *Phys. Rev.* **D57** (1998) 5851 and **D59** (1999) 054012.
- [20] S. Dawson and L. Reina, *Phys. Rev.* **D60** (1999) 015003.
- [21] W. Beenakker, R. Höpker, M. Spira and P.M. Zerwas, *Nucl. Phys.* **B492** (1997) 51.

BNL-HET-01/7  
CERN-TH/2001-056  
August 25, 2001  
hep-ph/0102317

# Precision Observables in the MSSM: Leading Electroweak Two-loop Corrections

S. HEINEMEYER\* AND G. WEIGLEIN†

\**HET, Brookhaven Natl. Lab., Upton NY 11973, USA*

†*CERN, TH Division, CH-1211 Geneva 23, Switzerland*

The leading electroweak MSSM two-loop corrections to the  $\rho$ -parameter are calculated. They are obtained by evaluating the two-loop self-energies of the  $Z$  and the  $W$  boson at  $\mathcal{O}(G_F^2 m_t^4)$  in the limit of heavy scalar quarks. A very compact expression is derived, depending on the ratio of the  $\mathcal{CP}$ -odd Higgs boson mass,  $M_A$ , and the top quark mass,  $m_t$ . Expressions for the limiting cases  $M_A \gg m_t$  and  $M_A \ll m_t$  are also given. The decoupling of the non-SM contribution in the limit  $M_A \rightarrow \infty$  is verified at the two-loop level. The numerical effect of the leading electroweak MSSM two-loop corrections is analyzed in comparison with the leading corrections of  $\mathcal{O}(G_F^2 m_t^4)$  in the SM and with the  $\mathcal{O}(\alpha\alpha_s)$  corrections in the MSSM.

Presented by S. Heinemeyer at the

5th International Symposium on Radiative Corrections  
(RADCOR-2000)

Carmel CA, USA, 11–15 September, 2000

# 1 Introduction

Theories based on Supersymmetry (SUSY) [1] are widely considered as the theoretically most appealing extension of the Standard Model (SM). They predict the existence of scalar partners  $\tilde{f}_L, \tilde{f}_R$  to each SM chiral fermion, and spin-1/2 partners to the gauge bosons and to the scalar Higgs bosons. So far, the direct search for SUSY particles has not been successful. One can only set lower bounds of  $\mathcal{O}(100)$  GeV on their masses [2]. Contrary to the SM, two Higgs doublets are required in the Minimal Supersymmetric Standard Model (MSSM) resulting in five physical Higgs bosons [3]. The direct search resulted in lower limits of about 90 GeV for the neutral Higgs bosons [4].

An alternative way to probe SUSY is to search for the virtual effects of the additional particles via precision observables. The most prominent role in this respect plays the  $\rho$ -parameter [5]. The leading radiative corrections to the  $\rho$ -parameter,  $\Delta\rho$ , constitute the leading process-independent corrections to many electroweak precision observables, such as the  $W$  boson mass,  $M_W$ , and the effective leptonic weak mixing angle,  $\sin^2\theta_{\text{eff}}$ . Within the MSSM the full one-loop corrections to  $M_W$  and  $\sin^2\theta_{\text{eff}}$  have been calculated already several years ago [6,7]. More recently also the leading two-loop corrections of  $\mathcal{O}(\alpha\alpha_s)$  to the quark and scalar quark loops for  $\Delta\rho$  and  $M_W$  have been obtained [8,9]. Contrary to the SM case, these two-loop corrections turned out to increase the one-loop contributions, leading to an enhancement of the latter of up to 35% [8].

We summarize here the result for the leading two-loop corrections to  $\Delta\rho$  at  $\mathcal{O}(G_F^2 m_t^4)$  [10]. For a large SUSY scale,  $M_{SUSY} \gg M_Z$ , the SUSY contributions decouple from physical observables. This has been verified with existing results at the one-loop [11] and at the two-loop level [8,10]. Therefore, in the case of large  $M_{SUSY}$  the leading electroweak two-loop corrections in the MSSM are obtained in the limit where besides the SM particles only the two Higgs doublets needed in the MSSM are active. We derive the result for the  $\mathcal{O}(G_F^2 m_t^4)$  [10] corrections in this case and provide a compact analytical formula for it, depending on the  $\mathcal{CP}$ -odd Higgs boson mass,  $M_A$ , and the top quark mass,  $m_t$ . Furthermore, we present formulas for the limiting cases  $M_A \gg m_t$  (i.e. the SM limit) and  $M_A \ll m_t$ . The numerical effect of the  $\mathcal{O}(G_F^2 m_t^4)$  corrections is compared with the corresponding SM result [12] and the gluon-exchange correction of  $\mathcal{O}(\alpha\alpha_s)$  in the MSSM.

## 2 Calculation of the $\mathcal{O}(G_F^2 m_t^4)$ corrections

### 2.1 $\Delta\rho$ and the Higgs sector

The quantity  $\Delta\rho$ ,

$$\Delta\rho = \frac{\Sigma_Z(0)}{M_Z^2} - \frac{\Sigma_W(0)}{M_W^2}, \quad (1)$$

parameterizes the leading universal corrections to the electroweak precision observables induced by the mass splitting between fields in an isospin doublet [5].  $\Sigma_{Z,W}(0)$  denote the transverse parts of the unrenormalized  $Z$  and  $W$  boson self-energies at zero momentum transfer, respectively. The shifts induced by  $\Delta\rho$  in the prediction for the  $W$  boson mass,  $M_W$ , and the effective leptonic weak mixing angle,  $\sin^2\theta_{\text{eff}}$ , are approximately given by

$$\delta M_W \approx \frac{M_W}{2} \frac{c_W^2}{c_W^2 - s_W^2} \Delta\rho, \quad \delta \sin^2\theta_{\text{eff}} \approx -\frac{c_W^2 s_W^2}{c_W^2 - s_W^2} \Delta\rho. \quad (2)$$

Contrary to the SM, in the MSSM two Higgs doublets are required [3]. At the tree-level, the Higgs sector can be described in terms of two independent parameters (besides  $g$  and  $g'$ ): the ratio of the two vacuum expectation values,  $\tan\beta = v_2/v_1$ , and  $M_A$ , the mass of the  $\mathcal{CP}$ -odd  $A$  boson. The diagonalization of the bilinear part of the Higgs potential, i.e. the Higgs mass matrices, is performed via orthogonal transformations with the angle  $\alpha$  for the  $\mathcal{CP}$ -even part and with the angle  $\beta$  for the  $\mathcal{CP}$ -odd and the charged part. The mixing angle  $\alpha$  is determined at lowest order through

$$\tan 2\alpha = \tan 2\beta \frac{M_A^2 + M_Z^2}{M_A^2 - M_Z^2}; \quad -\frac{\pi}{2} < \alpha < 0. \quad (3)$$

One gets the following Higgs spectrum:

$$\begin{aligned} 2 \text{ neutral bosons, } \mathcal{CP} = +1 & : h^0, H^0 \\ 1 \text{ neutral boson, } \mathcal{CP} = -1 & : A^0 \\ 2 \text{ charged bosons} & : H^+, H^- \\ 3 \text{ unphysical scalars} & : G^0, G^+, G^-. \end{aligned} \quad (4)$$

The tree-level masses, expressed through  $M_Z$ ,  $M_W$  and  $M_A$ , are given by

$$\begin{aligned} m_h^2 &= \frac{1}{2} \left[ M_A^2 + M_Z^2 - \sqrt{(M_A^2 + M_Z^2)^2 - 4M_A^2 M_Z^2 \cos^2 2\beta} \right] \\ m_H^2 &= \frac{1}{2} \left[ M_A^2 + M_Z^2 + \sqrt{(M_A^2 + M_Z^2)^2 - 4M_A^2 M_Z^2 \cos^2 2\beta} \right] \\ m_{H^\pm}^2 &= M_A^2 + M_W^2 \\ m_G^2 &= M_Z^2 \\ m_{G^\pm}^2 &= M_W^2, \end{aligned} \quad (5)$$

where the last two relations, which assign mass parameters to the unphysical scalars  $G^0$  and  $G^\pm$ , are to be understood in the Feynman gauge.

## 2.2 Evaluation of the $\mathcal{O}(G_F^2 m_t^4)$ contributions

In order to calculate the  $\mathcal{O}(G_F^2 m_t^4)$  corrections to  $\Delta\rho$  in the approximation that all superpartners are heavy so that their contribution decouples, the Feynman diagrams generically depicted in Fig. 1 have to be evaluated for the  $Z$  boson ( $V = Z$ ) and the  $W$  boson ( $V = W$ ) self-energy. We have taken into account all possible combinations of the  $t/b$  doublet and the full Higgs sector of the MSSM, see Sect. 2.1.

The two-loop diagrams shown in Fig. 1 have to be supplemented with the corresponding one-loop diagrams with subloop renormalization, depicted generically in Fig. 2. The corresponding insertions for the fermion and Higgs mass counter terms are shown in Fig. 3.

The amplitudes of all Feynman diagrams, shown in Figs. 1–3, have been created with the program *FeynArts2.2* [13], making use of a recently completed model file for the MSSM<sup>1</sup>. The algebraic evaluation and reduction to scalar integrals has been performed with the program *TwoCalc* [14]. (Further details about the evaluations with *FeynArts2.2* and *TwoCalc* can be found in Ref. [15].) As a result we obtained the analytical expression for  $\Delta\rho$  depending on the one-loop functions  $A_0$  and  $B_0$  [16] and on the two-loop function  $T_{134}$  [14,17]. For the further evaluation the analytical expressions for  $A_0$ ,  $B_0$  and  $T_{134}$  have been inserted. In order to derive the leading contributions of  $\mathcal{O}(G_F^2 m_t^4)$  we extracted a prefactor  $h_t^4 \sim G_F^2 m_t^4$ . Its coefficient can be evaluated in the limit where  $M_W$  and  $M_Z$  (and also  $m_b$ ) are set to zero. Furthermore we made use of the mass relations in the MSSM Higgs sector, see eq. (5). In the limit  $M_W, M_Z \rightarrow 0$  they reduce to

$$\begin{aligned}
m_h^2 &= 0 \\
m_H^2 &= M_A^2 \\
m_{H^\pm}^2 &= M_A^2 \\
m_G^2 &= 0 \\
m_{G^\pm}^2 &= 0.
\end{aligned} \tag{6}$$

In the limit  $M_Z \rightarrow 0$  the relation between the angles  $\alpha$  and  $\beta$ , see eq. (3), becomes very simple,  $\alpha = \beta - \pi/2$ , i.e.  $\sin \alpha = -\cos \beta$ ,  $\cos \alpha = \sin \beta$ . The coefficient of the leading  $\mathcal{O}(G_F^2 m_t^4)$  term thus depends only on the top quark mass,  $m_t$ , the  $\mathcal{CP}$ -odd Higgs boson mass,  $M_A$ , and  $\tan \beta$  (or  $s_\beta = \tan \beta / \sqrt{1 + \tan^2 \beta}$ ).

We explicitly verified the UV-finiteness of our result. As a further consistency check of our method we also recalculated the SM result for the  $\mathcal{O}(G_F^2 m_t^4)$  corrections

---

<sup>1</sup> Only the non-SM like counter terms had to be added.

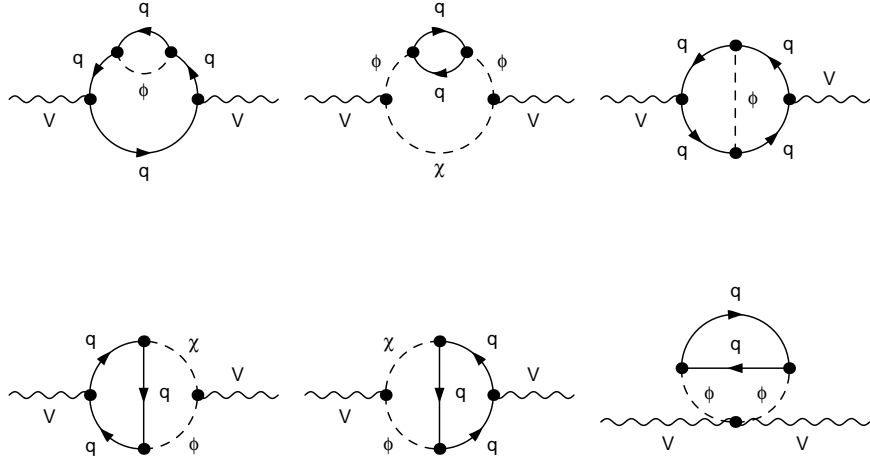


Figure 1: Generic Feynman diagrams for the vector boson self-energies ( $V = \{Z, W\}$ ,  $q = \{t, b\}$ ,  $\phi, \chi = \{h, H, A, H^\pm, G, G^\pm\}$ ).

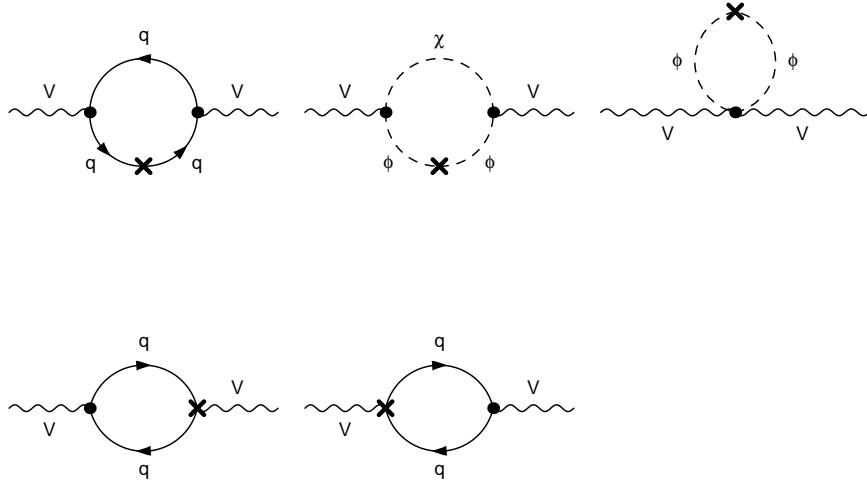


Figure 2: Generic Feynman diagrams for the vector boson self-energies with counter term insertion ( $V = \{Z, W\}$ ,  $q = \{t, b\}$ ,  $\phi, \chi = \{h, H, A, H^\pm, G, G^\pm\}$ ).

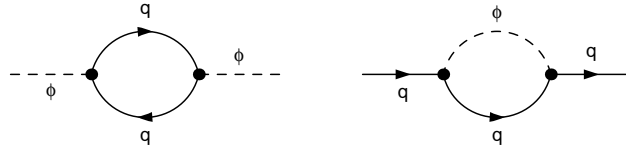


Figure 3: Generic Feynman diagrams for the counter term insertions ( $q = \{t, b\}$ ,  $\phi = \{h, H, A, H^\pm, G, G^\pm\}$ ).

with arbitrary values of the Higgs boson mass, as given in Ref. [18], and found perfect agreement.

### 3 Analytical results

#### 3.1 The full result

The analytical result obtained as described in Sect. 2.2 can conveniently be expressed in terms of

$$a \equiv \frac{m_t^2}{M_A^2}. \quad (7)$$

The corresponding two-loop contribution to  $\Delta\rho$  then reads:

$$\begin{aligned} \Delta\rho_{1,\text{Higgs}}^{\text{SUSY}} = & 3 \frac{G_F^2}{128 \pi^4} m_t^4 \frac{1 - s_\beta^2}{s_\beta^2 a^2} \times \\ & \left\{ \text{Li}_2 \left( \left( (1 - \sqrt{1 - 4a}) / 2 \right) \frac{8}{\sqrt{1 - 4a}} \Lambda \right) \right. \\ & - 2 \text{Li}_2 \left( 1 - \frac{1}{a} \right) [5 - 14a + 6a^2] \\ & + \log^2(a) \left[ 1 + \frac{2}{\sqrt{1 - 4a}} \Lambda \right] - \log(a) [2 - 20a] \\ & - \log^2 \left( \frac{1 - \sqrt{1 - 4a}}{2} \right) \frac{4}{\sqrt{1 - 4a}} \Lambda \\ & + \log \left( \frac{1 - \sqrt{1 - 4a}}{1 + \sqrt{1 - 4a}} \right) \sqrt{1 - 4a} (1 - 2a) \\ & - \log(|1/a - 1|) (a - 1)^2 \\ & \left. + \pi^2 \left[ \frac{2\sqrt{1 - 4a}}{-3 + 12a} \Lambda + \frac{1}{3} - 2a^2 \frac{s_\beta^2}{1 - s_\beta^2} \right] - 17a + 19 \frac{a^2}{1 - s_\beta^2} \right\}, \quad (8) \end{aligned}$$

with

$$\Lambda = 3 - 13a + 11a^2. \quad (9)$$

In the limit of large  $\tan\beta$  (i.e.  $(1 - s_\beta^2) \ll 1$ ) one obtains

$$\Delta\rho_{1,\text{Higgs}}^{\text{SUSY}} = 3 \frac{G_F^2}{128 \pi^4} m_t^4 \left[ \frac{19}{s_\beta^2} - 2\pi^2 + \mathcal{O}(1 - s_\beta^2) \right]. \quad (10)$$

Thus for large  $\tan\beta$  the SM limit with  $M_H^{\text{SM}} \rightarrow 0$  [12] is reached.

### 3.2 The expansion for large $M_A$

The result for  $\Delta\rho_{1,\text{Higgs}}^{\text{SUSY}}$  in eq. (8) can be expanded for small values of  $a$ , i.e. for large values of  $M_A$ :

$$\begin{aligned} \Delta\rho_{1,\text{Higgs}}^{\text{SUSY}} = & 3 \frac{G_F^2}{128 \pi^4} m_t^4 \times \\ & \left\{ 19 - 2\pi^2 \right. \\ & - \frac{1 - s_\beta^2}{s_\beta^2} \left[ \left( \log^2 a + \frac{\pi^2}{3} \right) (8a + 32a^2 + 132a^3 + 532a^4) \right. \\ & + \log(a) \frac{1}{30} (560a + 2825a^2 + 11394a^3 + 45072a^4) \\ & - \frac{1}{1800} (2800a + 66025a^2 + 300438a^3 + 1265984a^4) \\ & \left. \left. + \mathcal{O}(a^5) \right] \right\}. \end{aligned} \quad (11)$$

In the limit  $a \rightarrow 0$  one obtains

$$\Delta\rho_{1,\text{Higgs}}^{\text{SUSY}} = 3 \frac{G_F^2}{128 \pi^4} m_t^4 [19 - 2\pi^2] + \mathcal{O}(a), \quad (12)$$

i.e. exactly the SM limit for  $M_H^{\text{SM}} \rightarrow 0$  is reached. This constitutes an important consistency check: in the limit  $a \rightarrow 0$  the heavy Higgs bosons decouple from the theory. Thus only the lightest  $\mathcal{CP}$ -even Higgs boson remains, which has in the  $\mathcal{O}(G_F^2 m_t^4)$  approximation the mass  $m_h = 0$ , see eq. (6). This decoupling of the non-SM contributions in the limit where the new scale (i.e. in the present case  $M_A$ ) is made large is explicitly seen here at the two-loop level.

### 3.3 The expansion for small $M_A$

The result for  $\Delta\rho_{1,\text{Higgs}}^{\text{SUSY}}$  in eq. (8) can also be expanded for large values of  $a$ , i.e. for small values of  $M_A$  (with  $\hat{a} = 1/a$ ):

$$\begin{aligned} \Delta\rho_{1,\text{Higgs}}^{\text{SUSY}} = & 3 \frac{G_F^2}{128 \pi^4} m_t^4 \times \\ & \left\{ \log^2(\hat{a}) \hat{a}^2 \left[ -1 + \frac{1}{s_\beta^2} \right] \right. \\ & + \log(\hat{a}) \frac{1 - s_\beta^2}{210 s_\beta^2} [-2100\hat{a} + 350\hat{a}^2 + 504\hat{a}^3 + 341\hat{a}^4] \\ & \left. + \pi^2 \frac{2}{3 s_\beta^2} [-3 + 7\hat{a}(1 - s_\beta^2) - 2\hat{a}^2(1 - s_\beta^2)] \right\} \end{aligned}$$

$$\begin{aligned}
& -\pi\sqrt{\hat{a}}\frac{1-s_\beta^2}{256s_\beta^2}\left[1024-640\hat{a}+56\hat{a}^2+3\hat{a}^3\right] \\
& +\frac{19}{s_\beta^2}-\frac{1-s_\beta^2}{22050s_\beta^2}\left[970200\hat{a}-376075\hat{a}^2+24843\hat{a}^3+6912\hat{a}^4\right]+\mathcal{O}(\hat{a}^5)\Big\}.
\end{aligned} \tag{13}$$

In the limit  $\hat{a} \rightarrow 0$  or  $a \rightarrow \infty$  one obtains

$$\Delta\rho_{1,\text{Higgs}}^{\text{SUSY}} = 3\frac{G_F^2}{128\pi^4}m_t^4\frac{1}{s_\beta^2}\left[19-2\pi^2\right]+\mathcal{O}(\hat{a}). \tag{14}$$

## 4 Numerical analysis

### 4.1 The expansion formula

We first analyze the validity of the two expansion formulas, eqs. (11) and (14). In Fig. 4 we show the result for  $\delta_{1,\text{Higgs}}^{\text{SUSY}}$ , defined by

$$\Delta\rho_{1,\text{Higgs}}^{\text{SUSY}} = 3\frac{G_F^2}{128\pi^4}m_t^4\times\delta_{1,\text{Higgs}}^{\text{SUSY}}, \tag{15}$$

as a function of  $b = M_A/m_t (\equiv 1/\sqrt{a})$  for  $\tan\beta = 3$ . The expansion for  $b \ll 1$  is sufficiently accurate nearly up to  $b = 1$ . The other expansion gives accurate results for  $b \gtrsim 2$ . For larger  $\tan\beta$  the expansion becomes better, enlarging the validity region for the large  $M_A$  expansion up to  $b \gtrsim 1$ .

### 4.2 Effects on precision observables

In this section we analyze the numerical effect on the precision observables  $M_W$  and  $\sin^2\theta_{\text{eff}}$ , see eq. (2), induced by the additional contribution to  $\Delta\rho$ . In Fig. 5 the size of the leading  $\mathcal{O}(\alpha^2)$  MSSM corrections, eq. (8), is compared for  $\tan\beta = 3, 40$  with the leading  $\mathcal{O}(\alpha^2)$  contribution in the SM for  $M_H^{\text{SM}} = 0$  [12], with the leading MSSM corrections arising from the  $\tilde{t}/\tilde{b}$  sector at  $\mathcal{O}(\alpha)$  [7], and with the corresponding gluon-exchange contributions of  $\mathcal{O}(\alpha\alpha_s)$  [8] (the  $\mathcal{O}(\alpha\alpha_s)$  gluino-exchange contributions [8], which go to zero for large  $m_{\tilde{g}}$ , have been omitted here). For illustration, the left plot ( $\tan\beta = 3$ ) is shown as a function of  $M_A$ , which affects only the  $\mathcal{O}(\alpha^2)$  MSSM contributions, while the right plot ( $\tan\beta = 40$ ) is given as a function of the common SUSY mass scale in the scalar quark sector,  $M_{\text{SUSY}}$ , which affects only the  $\mathcal{O}(\alpha)$  and  $\mathcal{O}(\alpha\alpha_s)$  MSSM contributions. We have furthermore chosen the case of ‘‘maximal mixing’’ in the scalar top sector, which is realized by setting the off-diagonal term in the  $\tilde{t}$  mass matrix,  $X_t$ , to  $X_t = 2M_{\text{SUSY}}$  and yields the maximal value for  $m_h$  for a given  $\tan\beta$  (see Ref. [19] for details). In the right plot the case of no mixing,  $X_t = 0$ , is also shown. The mixing in the scalar bottom sector has been determined by using

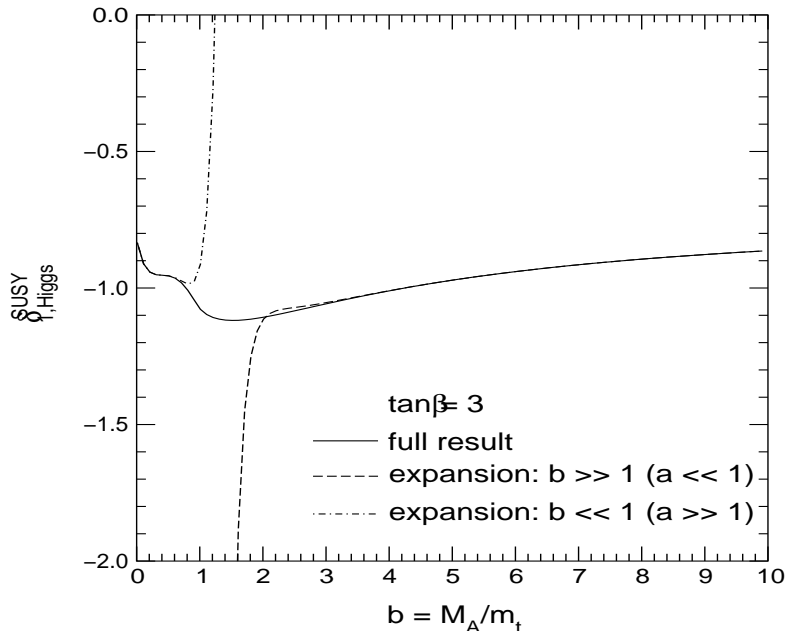


Figure 4: The quality of the expansion formulas, eqs. (11) and (14), is shown as a function of  $b = M_A/m_t (\equiv 1/\sqrt{a})$ .

a bottom quark mass of  $m_b = 4.5$  GeV, and by setting the trilinear couplings to  $A_b = A_t$  and the Higgs mixing parameter to  $\mu = 200$  GeV. The  $\mathcal{O}(\alpha^2)$  contributions in the SM and the MSSM are negative and are for comparison shown with reversed sign.

While for small values of  $M_{SUSY}$  the  $\mathcal{O}(\alpha\alpha_s)$  gluon-exchange contribution in the MSSM is much larger than the  $\mathcal{O}(\alpha^2)$  contribution from eq. (8) (note that in this region of parameter space the approximation of neglecting the scalar-quark contributions in the  $\mathcal{O}(\alpha^2)$  result is no longer valid), they are of approximately equal magnitude for  $M_{SUSY} \approx 500$  GeV (this refers to both the no-mixing and the maximal-mixing case) and compensate each other as they enter with different sign. In this region the two-loop contributions are about one order of magnitude smaller than the  $\mathcal{O}(\alpha)$  MSSM contribution. For  $M_{SUSY} = 1000$  GeV the leading MSSM  $\mathcal{O}(\alpha^2)$  contribution is about three times bigger than the  $\mathcal{O}(\alpha\alpha_s)$  gluon-exchange contribution in the MSSM.

For small  $\tan\beta$  (left plot of Fig. 5) and moderate  $M_A$  ( $M_A \approx 300$  GeV) the new  $\mathcal{O}(\alpha^2)$  MSSM corrections are about two times larger than the leading  $\mathcal{O}(\alpha^2)$  contributions in the SM for  $M_H^{\text{SM}} = 0$ . For large  $M_A$  the decoupling of the extra contributions in the MSSM takes place and the  $\mathcal{O}(\alpha^2)$  MSSM correction approaches the value of the leading  $\mathcal{O}(\alpha^2)$  contributions in the SM for  $M_H^{\text{SM}} = 0$ , as indicated in eqs. (11), (12). For large  $\tan\beta$  (right plot of Fig. 5) the  $\mathcal{O}(\alpha^2)$  MSSM correction and

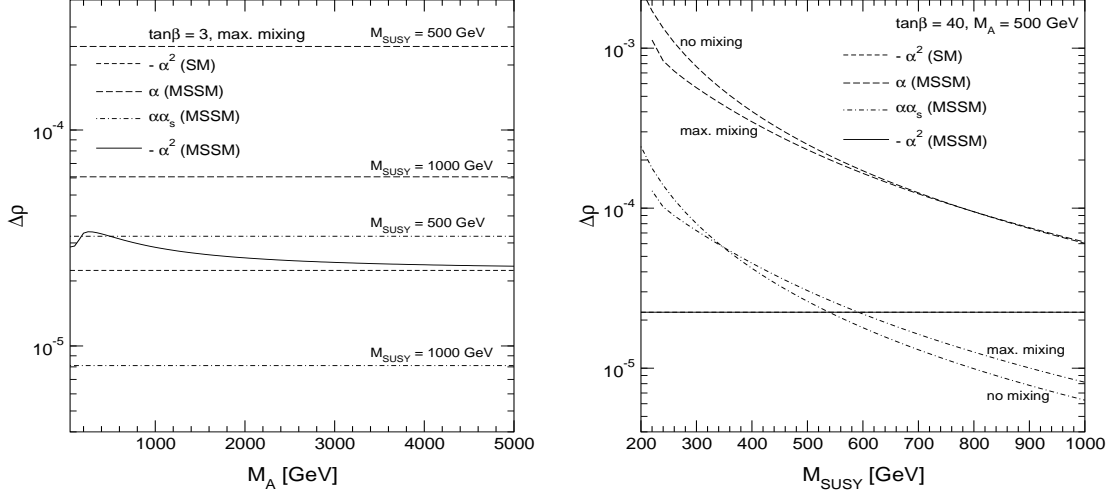


Figure 5: The contribution of the leading  $\mathcal{O}(\alpha^2)$  MSSM corrections,  $\Delta\rho_{1,\text{Higgs}}^{\text{SUSY},\alpha^2}$ , is shown as a function of  $M_A$  for  $\tan\beta = 3$  (left plot) and as a function of  $M_{SUSY}$  for  $\tan\beta = 40$  (right plot). In the left plot the case of maximal  $\tilde{t}$  mixing is shown, while the right plot displays both the no-mixing and the maximal-mixing case.  $\Delta\rho_{1,\text{Higgs}}^{\text{SUSY},\alpha^2}$  is compared with the leading  $\mathcal{O}(\alpha^2)$  SM contribution with  $M_H^{\text{SM}} = 0$  and with the leading MSSM corrections originating from the  $\tilde{t}/\tilde{b}$  sector of  $\mathcal{O}(\alpha)$  and  $\mathcal{O}(\alpha\alpha_s)$ . Both  $\mathcal{O}(\alpha^2)$  contributions are negative and are for comparison shown with reversed sign.

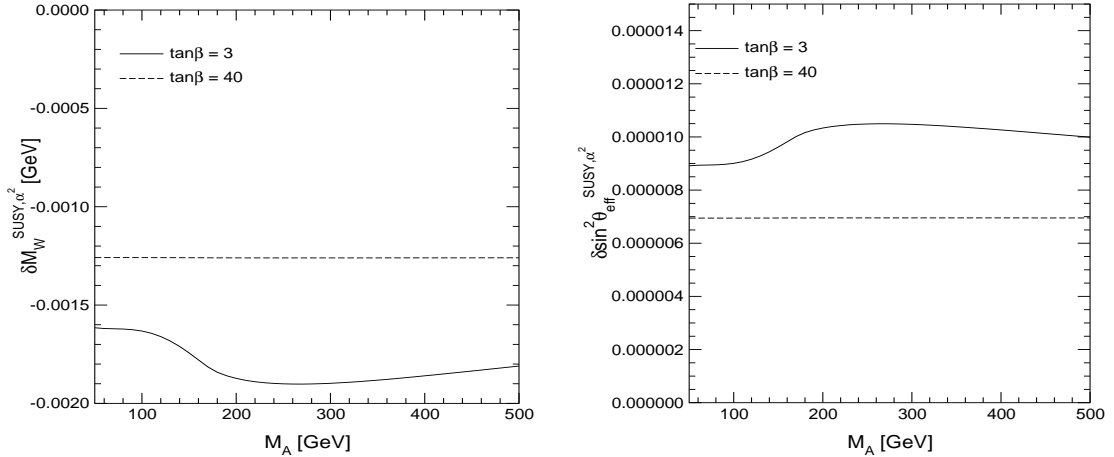


Figure 6: The leading  $\mathcal{O}(\alpha^2)$  MSSM contribution to  $\delta M_W$  (left plot) and  $\delta \sin^2 \theta_{\text{eff}}$  (right plot) is shown as a function of  $M_A$  for  $\tan\beta = 3, 40$ .

the  $\mathcal{O}(\alpha^2)$  contribution in the SM for  $M_H^{\text{SM}} = 0$  are indistinguishable in the plot, in accordance with eq. (10).

It is well known that the  $\mathcal{O}(\alpha^2)$  SM result with  $M_H^{\text{SM}} = 0$  underestimates the result with realistic values of  $M_H^{\text{SM}}$  by about one order of magnitude [18]. One can expect a similar effect in the MSSM once higher order corrections to the Higgs boson sector are properly taken into account, which can enhance  $m_h$  up to  $m_h \lesssim 130$  GeV [19], see Ref. [10].

In Fig. 6 the approximation formulas given in eq. (2) have been employed for determining the shift induced in  $M_W$  and  $\sin^2 \theta_{\text{eff}}$  by the new  $\mathcal{O}(\alpha^2)$  correction to  $\Delta\rho$ . In Fig. 6 the effect for both precision observables is shown as a function of  $M_A$  for  $\tan\beta = 3, 40$ . The effect on  $\delta M_W$  varies between  $-1.5$  MeV and  $-2$  MeV for small  $\tan\beta$  and is almost constant,  $\delta M_W \approx -1.25$  MeV, for  $\tan\beta = 40$ . As above, the constant behavior can be explained by the analytical decoupling of  $\tan\beta$  when  $\tan\beta \gg 1$ , see eq. (10). The induced shift in  $\sin^2 \theta_{\text{eff}}$  lies at or below  $1 \times 10^{-5}$  and shows the same qualitative  $\tan\beta$  dependence as  $\delta M_W$ .

## 5 Conclusions

We have calculated the leading  $\mathcal{O}(G_F^2 m_t^4)$  corrections to  $\Delta\rho$  in the MSSM in the limit of heavy squarks. Short analytical formulas have been obtained for the full result as well as for the cases  $M_A \gg m_t$  and  $M_A \ll m_t$ . As a consistency check we verified that from the MSSM result the corresponding SM result can be obtained in the decoupling limit (i.e.  $M_A \rightarrow \infty$ ).

Numerically we compared the effect of the new contribution with the leading  $\mathcal{O}(\alpha^2)$  SM contribution with  $M_H^{\text{SM}} = 0$  and with the leading MSSM corrections originating from the  $\tilde{t}/\tilde{b}$  sector of  $\mathcal{O}(\alpha)$  and  $\mathcal{O}(\alpha\alpha_s)$ . The numerical effect of the new contribution exceeds the one of the leading QCD correction of  $\mathcal{O}(\alpha\alpha_s)$  in the scalar quark sector for  $M_{\text{SUSY}} \gtrsim 500$  GeV. It is always larger than the leading  $\mathcal{O}(\alpha^2)$  SM contribution with  $M_H^{\text{SM}} = 0$ , reaching approximately twice its value for small  $\tan\beta$  and moderate  $M_A$ .

The numerical effect of the new contribution on the precision observables  $M_W$  and  $\sin^2 \theta_{\text{eff}}$  is relatively small, up to  $-2$  MeV for  $M_W$  and  $+1 \times 10^{-5}$  for  $\sin^2 \theta_{\text{eff}}$ . It should be noted, however, that the  $\mathcal{O}(\alpha^2)$  SM result with  $M_H^{\text{SM}} = 0$ , to which the new result corresponds, underestimates the result with realistic values of  $M_H^{\text{SM}}$  by about one order of magnitude. A similar behavior can also be expected for the MSSM corrections. An extension of our present result to the case of non-zero values of the lightest  $\mathcal{CP}$ -even Higgs boson mass will be undertaken in a forthcoming publication.

## Acknowledgments

S.H. thanks the organizers of “RADCOR2000” for the invitation and the inspiring and constructive atmosphere at the workshop.

## References

- [1] H.P. Nilles, *Phys. Rep.* **110** (1984) 1;  
H.E. Haber and G.L. Kane, *Phys. Rep.* **117**, (1985) 75;  
R. Barbieri, *Riv. Nuovo Cim.* **11**, (1988) 1.
- [2] Part. Data Group, *Eur. Phys. Jour.* **C 15** (2000) 1.
- [3] J. Gunion, H. Haber, G. Kane and S. Dawson, *The Higgs Hunter’s Guide*, Addison-Wesley, 1990.
- [4] S. Andringa et al., *Searches for Higgs Bosons: Preliminary Combined Results using LEP Data Collected at Energies up to 209 GeV*, CERN-EP-2000-055. ALEPH 2000-074 CONF 2000-051, DELPHI 2000-148 CONF 447, L3 Note 2600, OPAL Technical Note TN661.
- [5] M. Veltman, *Nucl. Phys.* **B 123** (1977) 89.
- [6] R. Barbieri and L. Maiani, *Nucl. Phys.* **B 224** (1983) 32;  
C. S. Lim, T. Inami and N. Sakai, *Phys. Rev.* **D 29** (1984) 1488;  
E. Eliasson, *Phys. Lett.* **B 147** (1984) 65;  
Z. Hioki, *Prog. Theo. Phys.* **73** (1985) 1283;  
J. A. Grifols and J. Sola, *Nucl. Phys.* **B 253** (1985) 47;  
B. Lynn, M. Peskin and R. Stuart, CERN Report 86-02, p. 90;  
R. Barbieri, M. Frigeni, F. Giuliani and H.E. Haber, *Nucl. Phys.* **B 341** (1990) 309;  
M. Drees and K. Hagiwara, *Phys. Rev.* **D 42** (1990) 1709.
- [7] M. Drees, K. Hagiwara and A. Yamada, *Phys. Rev.* **D 45** (1992) 1725;  
P. Chankowski, A. Dabelstein, W. Hollik, W. Mösle, S. Pokorski and J. Rosiek, *Nucl. Phys.* **B 417** (1994) 101;  
D. Garcia and J. Solà, *Mod. Phys. Lett.* **A 9** (1994) 211.
- [8] A. Djouadi, P. Gambino, S. Heinemeyer, W. Hollik, C. Jünger and G. Weiglein, *Phys. Rev. Lett.* **78** (1997) 3626, hep-ph/9612363; *Phys. Rev.* **D 57** (1998) 4179, hep-ph/9710438.

- [9] S. Heinemeyer, PhD thesis,  
see <http://www-itp.physik.uni-karlsruhe.de/prep/phd/>;  
G. Weiglein, hep-ph/9901317;  
S. Heinemeyer, W. Hollik and G. Weiglein, *in preparation*.
- [10] S. Heinemeyer and G. Weiglein, *in preparation*.
- [11] T. Appelquist and J. Carazzone, *Phys. Rev. D* **11** (1975) 2856;  
A. Dobado, M. Herrero and S. Peñaranda, *Eur. Phys. Jour. C* **7** (1999) 313,  
hep-ph/9710313, *Eur. Phys. Jour. C* **12** (2000) 673, hep-ph/9903211; *Eur. Phys. Jour. C* **17** (2000) 487, hep-ph/0002134.
- [12] J. van der Bij and F. Hoogeveen, *Nucl. Phys. B* **283** (1987) 477.
- [13] J. Küblbeck, M. Böhm and A. Denner, *Comp. Phys. Comm.* **60** (1990) 165;  
T. Hahn, hep-ph/0012260.  
The program is available via <http://www.feynarts.de>.
- [14] G. Weiglein, R. Scharf and M. Böhm, *Nucl. Phys. B* **416** (1994) 606, hep-ph/9310358;  
G. Weiglein, R. Mertig, R. Scharf and M. Böhm, in *New Computing Techniques in Physics Research 2*, ed. D. Perret-Gallix (World Scientific, Singapore, 1992), p. 617.
- [15] S. Heinemeyer, BNL–HET–00/48, hep-ph/0102318, to appear in the proceedings of the ACAT2000, Fermilab, Oct. 2000.
- [16] G. 't Hooft and M. Veltman, *Nucl. Phys. B* **153** (1979) 365.
- [17] A. Davydychev und J. B. Tausk, *Nucl. Phys. B* **397** (1993) 123;  
F. Berends und J. B. Tausk, *Nucl. Phys. B* **421** (1994) 456.
- [18] R. Barbieri, M. Beccaria, P. Ciafaloni, G. Curci and A. Vicere, *Nucl. Phys. B* **409** (1993) 105;  
J. Fleischer, F. Jegerlehner and O.V. Tarasov, *Phys. Lett. B* **319** (1993) 249.
- [19] S. Heinemeyer, W. Hollik and G. Weiglein, *Phys. Rev. D* **58** (1998) 091701, hep-ph/9803277; *Phys. Lett. B* **440** (1998) 296, hep-ph/9807423; *Eur. Phys. Jour. C* **9** (1999) 343, hep-ph/9812472.

# Quantum corrections for the MSSM Higgs couplings to SM fermions

DAVID GARCIA\*

*CERN, Theory Division  
CH-1211 Geneva 23, Switzerland*

Higgs Yukawa couplings to down-type fermions receive, in the MSSM, supersymmetric quantum corrections that can be of order 1 for large values of  $\tan\beta$ , provided  $|\mu| \sim M_{\text{SUSY}}$ . Therefore, a sensitive prediction for observables driven by any of these couplings can only be obtained after an all-order resummation of the large corrections. We perform this necessary step and show, as an example, the effect of the resummation on the computation of the  $p\bar{p}, pp \rightarrow t\bar{b}H^- + X$  cross-section and on the branching ratio  $\mathcal{BR}(b \rightarrow s\gamma)$  at the next-to-leading order.

Presented at the

5th International Symposium on Radiative Corrections  
(RADCOR-2000)  
Carmel CA, USA, 11–15 September, 2000

---

\*Work supported by the European Commission TMR programme under the grant ERBFMBICT 983539.

# 1 Introduction

The full experimental confirmation of the Standard Model (SM) still requires the finding of the Higgs boson. The last LEP results, suggesting a light Higgs of about 115 GeV [1], are encouraging, but we will have to wait for the upgraded Tevatron or the LHC to see this result either confirmed or dismissed. In any case, there is room for an extended Higgs sector of various kinds (extra doublets, singlets, even triplets).

The Higgs sector of the Minimal Supersymmetric Standard Model (MSSM), well-known nowadays (see [2], for instance), still deserves further studies. In particular, an interesting topic is the effect of supersymmetric corrections on the Yukawa interaction, because many production and decay channels are mediated by these couplings, some of them at the one-loop level (such as  $H \rightarrow \gamma\gamma$  or  $gg \rightarrow H$ ).

For large  $\tan\beta$  values, one expects deviations of order 1 of the Yukawa couplings to down-type fermions from their tree-level values, due to gluino (SUSY-QCD) and, to a lesser extent, higgsino (SUSY-EW) radiative effects. This can be seen, for instance, in the computation of the one-loop correction to the  $t \rightarrow bH^+$  partial decay rate [3], which grows with  $\tan\beta$  as  $(\alpha_{s,w}/4\pi) \tan\beta$ . With contributions of order  $(\alpha_s/4\pi)^n \tan^n\beta$  arising at higher orders in perturbation theory, the one-loop result can only be meaningful for small  $\tan\beta$  values. Let us recall that large  $\tan\beta$  scenarios, such as those derived from supersymmetric SO(10) models with unification of the top and bottom Yukawa couplings at high energies [4,5], have become more appealing since LEP searches for a light neutral Higgs boson,  $h$ , started to exclude the low- $\tan\beta$  region of the MSSM parameter space. The latest analyses rule out the MSSM for  $\tan\beta$  in the range  $0.52 < \tan\beta < 2.25$ , even with maximal stop mixing [6].

In this talk we present the resummation of such corrections into the definition of the bottom Yukawa as a function of the bottom mass, restoring the reliability of the perturbative series for large  $\tan\beta$ . This “improved” formula for the Yukawa is then used in the evaluation of the  $p\bar{p}, pp \rightarrow t\bar{b}H^- + X$  cross-section and of the branching ratio for  $b \rightarrow s\gamma$  at the next-to-leading order (NLO), comparing the result with the case in which no resummation is made.

## 2 Resummation of SUSY corrections

Let us briefly explain how such large corrections could arise. The starting point is the MSSM superpotential. Supersymmetry constrains it to be holomorphic in the chiral superfields, implying that the left-handed components of down-type quarks and leptons only couple to the  $H_1$  Higgs doublet, while the left-handed up-type quarks and leptons only couple to  $H_2$ . For the third-generation quarks, one has

$$\mathcal{L} = -h_b \bar{b}b H_1^0 - h_t \bar{t}t H_2^0 + \dots \quad (1)$$

Soft-SUSY-breaking operators induce the forbidden couplings,  $\bar{b}bH_2^0$  and  $\bar{t}tH_1^0$ , radiatively. After integrating out all R-odd particles in the MSSM, one obtains an effective two-Higgs-doublet model (2HDM) lagrangian

$$\mathcal{L}_{\text{eff}} = -(h_b + \Delta h_b^1) \bar{b}bH_1^0 - (0 + \Delta h_b^2) \bar{b}bH_2^0 + \dots \quad (2)$$

As we have argued above, there is a clear motivation for studying the large  $\tan\beta$  regime of the MSSM. If  $\tan\beta$  is large, and after electroweak symmetry breaking, the  $\Delta h_b^2$  term can induce corrections of order 1 to down-type fermion masses:

$$m_b = h_b v_1 \left( 1 + \Delta h_b^1/h_b + \Delta h_b^2/h_b \tan\beta \right), \quad (3)$$

or conversely, one can express the renormalized bottom Yukawa coupling as a function of the bottom mass through

$$h_b v_1 = \frac{m_b}{1 + \Delta h_b^1/h_b + \Delta h_b^2/h_b \tan\beta} \sim \frac{m_b}{1 + \Delta m_b}. \quad (4)$$

The set of quantum corrections included in (4) are universal, in the sense that they equally affect all amplitudes proportional to the bottom Yukawa. To derive (4), one matches the MSSM to a generic 2HDM at a scale  $M_{\text{SUSY}}$  of the order of the relevant soft-SUSY-breaking parameters. Alternatively, within the MSSM, and using an on-shell renormalization scheme, these corrections are absorbed into the bottom mass counterterm,  $\delta m_b^{\text{SUSY}} \sim -\Delta m_b^{\text{SUSY}}$ .

The quantity  $\Delta m_b$  is dominated by SUSY-QCD virtual effects,<sup>1</sup> and at the one-loop level can be cast into the simple expression [5]

$$\Delta m_b \sim \Delta m_b^{\text{SQCD}} = \frac{2\alpha_s}{3\pi} \mu m_{\tilde{g}} \tan\beta I(m_{\tilde{b}_1}, m_{\tilde{b}_2}, m_{\tilde{g}}), \quad (5)$$

where the function  $I$  is the limit of Passarino–Veltman’s  $C_0$  for vanishing external momenta.

An interesting property of  $\Delta m_b$  is that it does not vanish for  $M_{\text{SUSY}}/m_W \rightarrow \infty$ . The SUSY-QCD contribution, for instance, evaluates to  $\alpha_s/(3\pi) \tan\beta$  in this limit. This should never be understood as a non-decoupling behaviour of the MSSM, because the tree-level  $h_b$  is not an observable. If the masses of both the SUSY partners and the non-standard higgses ( $H$ ,  $A$ ,  $H^\pm$ ) become large, the SUSY radiative corrections to  $h_b$  are cancelled out exactly by one-loop process-dependent corrections. If  $m_A$  is not too large with respect to  $m_W$ , one can expect large deviations from the rule

$$g_{hbb}/g_{h\tau\tau} = m_b/m_\tau, \quad (6)$$

---

<sup>1</sup>An analogous quantity,  $\Delta m_\tau$ , can be defined for the  $\tau$ -Yukawa.  $\Delta m_\tau$ , though, receives (generally) smaller SUSY-EW contributions.

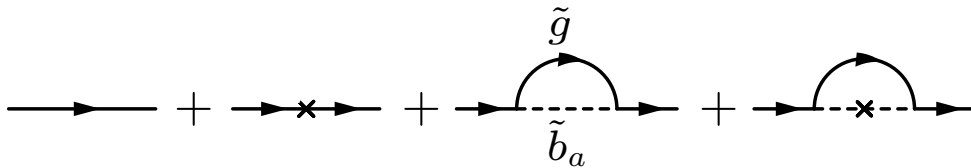


Figure 1: Complete set of Feynman diagrams contributing at order  $\alpha_s^n \tan^n \beta$  to the inverse bottom propagator, in SUSY-QCD with no virtual gluons. Dashed and solid internal lines represent sbottom quarks and gluinos, respectively. A cross denotes, in the second diagram, the insertion of a bottom mass-counterterm, and in the last diagram, the counterterm for the  $\tilde{b}_L \tilde{b}_R H_2^0$  coupling.

which holds not only in the SM, but also in 2HDM of types I and II [2]. For the  $H$ ,  $A$ , neutral higgses, eq. (6) can be violated even in the decoupling limit, their masses being of the order of  $m_A$ . This feature could help in distinguishing the MSSM Higgs sector from a generic type II 2HDM, specially if correlations among various Higgs couplings were checked.

Remarkably enough, it can be shown that, in mass-independent renormalization schemes such as the  $\overline{\text{MS}}$ , the whole set of SUSY-QCD corrections of the form<sup>2</sup>  $\alpha_s^n \tan^n \beta$  are resummed into the above definition for  $h_b$  [7] in eq. (4). The proof involves the consideration of the perturbative series for the inverse bottom propagator, which can be used to determine the functional relation between  $h_b$  and the bottom pole mass. In a first step one restricts the analysis to the set of diagrams with no gluons: only those in fig. 1 contribute at order  $\alpha_s^n \tan^n \beta$ , higher-loop diagrams being suppressed either by inverse powers of  $\tan \beta$  or by  $m_b/M_{\text{SUSY}}$  factors. Requiring the inverse propagator to vanish on-shell, one arrives at (4), apart from  $1/\tan \beta$  and  $m_b/M_{\text{SUSY}}$  suppressed quantities. The full proof, that is, after allowing for diagrams containing virtual gluons, is more delicate. It requires, for instance, a careful analysis of the infrared behaviour of the extra diagrams, as  $1/m_b$  mass singularities would invalidate the counting of  $m_b/M_{\text{SUSY}}$  powers used in the proof.

### 3 Prospects for $H^\pm$ searches at hadron colliders

As a first example of the use of eq. (4), we are going to consider the MSSM associated production of a charged Higgs boson,  $H^\pm$ , with top and bottom at hadron colliders, presenting results for both the Tevatron and the LHC [8]. From our point of view, the relevance of this channel is due to its ability to test the charged Higgs coupling to the third-generation quarks and leptons. Any information obtained about

<sup>2</sup>The only exception being, for  $n = 1$ , the process-dependent one-loop effects that restore the SM low-energy limit of the theory for  $m_A/m_W \rightarrow \infty$ .

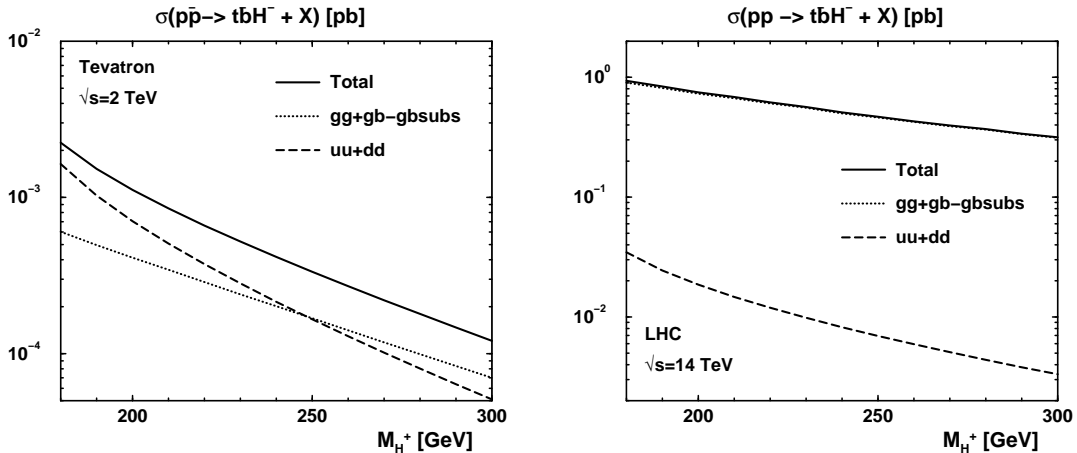


Figure 2: The  $p\bar{p}, pp \rightarrow t\bar{b}H^- + X$  cross-section at the Tevatron Run II (left) and at the LHC (right), for  $\mu = -200$  GeV,  $\tan\beta = 30$  and  $m_{\tilde{g}} = m_{\tilde{t}_1} = m_{\tilde{b}_1} = A_b = A_t = 500$  GeV. The dashed curve corresponds to the  $q\bar{q}$  annihilation channel, the dotted curve to the sum of the  $gg$ -initiated and  $gb$ -initiated channels, after subtracting double counting in the  $gb$  channel. The solid curve is the sum of all channels,  $q\bar{q}$ ,  $gg$  and  $gb$ .

these couplings could provide valuable hints on the exact nature of the Higgs sector.

After the LEP shutdown, charged Higgs searches concentrate on the Tevatron results. Both direct and indirect Tevatron analyses have been limited to the region  $m_{H^+} < m_t - m_b$ , placing constraints on the  $m_{H^+} - \mathcal{BR}_{t \rightarrow bH^+}$  plane [9], which are usually translated to the  $m_{H^+} - \tan\beta$  plane once the relevant MSSM parameters are fixed [10].

Beyond the kinematical limit for  $t \rightarrow bH^+$ , apart from the one considered in this talk, there are two other promising production channels: pair production [11] and associated production with a  $W$  boson [12]. The work presented here on  $p\bar{p}, pp \rightarrow t\bar{b}H^- + X$  adds, with respect to previous analyses [13,14,15,16,17], a resummation of the leading—in powers of  $\alpha_s \tan\beta$ , for  $\tan\beta \gtrsim 10$ —SUSY radiative corrections (both strong and electroweak) and an estimation of the off-shell effects. It will be presented in full detail in [8], including a complete signal and background analysis.

### 3.1 Cross-section computation and results

At the parton level, the reactions  $p\bar{p}, pp \rightarrow t\bar{b}H^- + X$  proceed through three main channels<sup>3</sup>: i)  $q\bar{q} \rightarrow t\bar{b}H^-$ , with  $q = u, d$  (the  $s$  contribution can be safely neglected), a channel only relevant to the Tevatron [14,15]; ii)  $gg \rightarrow t\bar{b}H^-$ , dominant at the LHC,

<sup>3</sup>We shall omit the charge-conjugate process,  $p\bar{p}, pp \rightarrow \bar{t}bH^+ + X$ , for the sake of brevity. Including this process just amounts to multiplying our cross-section by a factor of 2.

and also at the Tevatron for increasing  $H^\pm$  masses [14,15]. Since the bottom mass,  $m_b$ , is small with respect to the energy of the process, parton distribution functions (PDFs) for  $b$ -quarks have to be introduced, allowing for the resummation of collinear logs [18]. This provides an extra  $bg \rightarrow tH^-$  channel contributing to the cross-section. Contrary to i) and ii), in this case the final state contains at most three high- $p_T$   $b$ -quarks and, therefore,  $bg$ -initiated processes cannot be detected by using four high- $p_T$   $b$ -tagging. Once a PDF for the  $b$ -quarks is used, there is some amount of overlap between  $bg$ - and  $gg$ -initiated amplitudes, which has to be removed [18,19]. To this end, we follow here the method described in ref. [19], straightforwardly translated to the  $t\bar{b}H^-$  final state case (see also [14]). Figure 2 shows the relative relevance of the various channels to both the Tevatron Run II and the LHC, as explained above. The solid curve can be used to get a rough estimate of the reach of the process  $p\bar{p}, pp \rightarrow t\bar{b}H^- + X$  in the search for a MSSM charged Higgs boson in these machines for the given parameters (see the caption).

The amplitude for  $p\bar{p}, pp \rightarrow t\bar{b}H^- + X$  is, for large  $\tan\beta$ , approximately proportional to the Yukawa coupling of the bottom quark and, as explained above, receives supersymmetric quantum corrections that can be of order 1. An analysis of the reach of  $p\bar{p}, pp \rightarrow t\bar{b}H^- + X$  in  $H^\pm$  searches demands the appropriate inclusion and resummation (using (4)) of such corrections in the computation of the cross-section. For the present work we have also included the full off-shell SUSY-QCD and SUSY-EW corrections to the  $H^+\bar{t}b$  vertex and to the fermion propagators, although  $\Delta m_b$  in (4) is the only correction contributing at order  $(\alpha_s/4\pi)^n \tan^n\beta$  and thus dominates for large  $\tan\beta$ . In fact, the approximation of neglecting vertex and propagator corrections in the cross-section, which we call “improved Born” approximation, is really justified in that region (see fig. 3).

We disregard virtual supersymmetric effects on the  $gqq$  and  $ggg$  vertices and on the gluon propagators. We expect those to be of order  $(\alpha_s/4\pi) \cdot (\sqrt{s}/M_{\text{SUSY}})$ , with no  $\tan\beta$  enhancement, and thus suppressed both by a loop factor (any reasonable choice for  $\alpha_s(Q)$  will be small) and by a MSSM form factor coming from the loop integrals. Therefore, we can neglect these contributions as we are only considering large  $\tan\beta$  values. Besides, the cross-section for the signal is much smaller for  $\tan\beta$  close to 1, so our approximation is well justified.

The only other source of potentially large radiative corrections is, of course, standard QCD. At least one group is currently addressing the NLO QCD correction to  $p\bar{p}, pp \rightarrow bbH + X$ , which can provide a good guess for the sign and size of the corrections in  $p\bar{p}, pp \rightarrow t\bar{b}H^- + X$ . In the meantime, we can parametrize our ignorance by using a K-factor ranging between 1.2 and 1.5 [22,16,20]. Once the exact value of K will be known, it will be easy to conveniently rescale our plots to take into account the effect of the gluon loops. The only QCD corrections we do incorporate to the cross-

section are those related to the running of  $\alpha_s(Q)$  and  $\overline{m}_b(Q)$ .<sup>4</sup> We choose to work with equal renormalization,  $\mu_R$ , and factorization,  $Q$ , scales fixed at  $\mu_R = Q = m_t + m_{H^+}$ .

Concerning the method employed to compute the squared matrix elements, we have made intensive use of the package CompHEP [24], for both the signal and background processes. Although CompHEP is only able to deal with tree-level calculations, we have managed to add the supersymmetric corrections to the  $t\bar{b}H^-$  vertex and to the fermion propagators in the following way: first, we have modified CompHEP's Feynman rules to allow for the most general off-shell  $t\bar{b}H^-$  vertex, then we have let CompHEP reckon the squared matrix elements and dump the result into REDUCE code. At this point, we have inserted expressions for the coefficients of the off-shell  $t\bar{b}H^-$  vertex that include the one-loop off-shell supersymmetric corrections to the vertex itself and to the off-shell fermion propagators and fermionic external lines.<sup>5</sup> Only half the renormalization of an internal fermion line has to be included, the other half being associated to the  $gq\bar{q}$  vertex. This procedure has allowed us to estimate the relative size of the off-shell effects in the signal cross-section, which never exceeds the few per cent level.

In fig. 3, we compare the above various approximations to the  $p\bar{p} \rightarrow t\bar{b}H^- + X$  cross-section at the Tevatron Run II. The curves correspond to the total cross-section, as a function of  $\tan\beta$ , for a centre-of-mass energy of 2 TeV and a charged Higgs mass of 250 GeV. The tree-level result is given by the dotted line; it grows almost quadratically with  $\tan\beta$ . After including the  $\overline{\text{MS}}$  off-shell one-loop supersymmetric corrections in the  $t\bar{b}H^-$  vertex, in the internal fermion propagators and in the external fermion lines, one obtains the dashed line. For the chosen parameters, that is  $\mu = -200$  GeV,  $m_{\tilde{g}} = m_{\tilde{t}_1} = m_{\tilde{b}_1} = A_b = A_t = 500$  GeV, the overall correction turns out to be positive, as it is driven by the SUSY-QCD correction in (4), which is positive for negative  $\mu$ . The resummation of the order  $\alpha_s^n \tan^n \beta$  supersymmetric corrections further increases the result up to the top solid curve, labelled “improved”  $\overline{\text{MS}}$ . The effect is not dramatic because  $\mu$  is sizeably smaller than the rest of the relevant soft-SUSY-breaking parameters, namely the gluino and sbottom masses. To illustrate the possibility of a suppression of the cross-section due to virtual supersymmetric effects, we also plot the resummed result for the same parameters but taking  $\mu = 200$  GeV and  $A_t = -500$  GeV, which corresponds to the bottom (red) solid line. It does not differ much from the tree-level because of a partial cancellation of the correction due to the effect of the resummed high-order terms in (4). Finally, the dot-dashed curve is obtained by just replacing the  $\overline{m}_b(Q)$  in the tree-level approximation to the cross-section with  $\overline{m}_b(Q)/(1 + \Delta m_b)$ , as suggested by (4). This “improved” tree-level

<sup>4</sup>In the  $t \rightarrow bH^+$  decay rate, this actually accounts for most of the QCD virtual effects (for  $Q = m_t$ ) [23].

<sup>5</sup>We shall not write down here the analytic expressions for the renormalized vertex and propagators. They can easily be derived by just generalizing previous on-shell calculations, such as those for  $t \rightarrow bH^+$  [3].

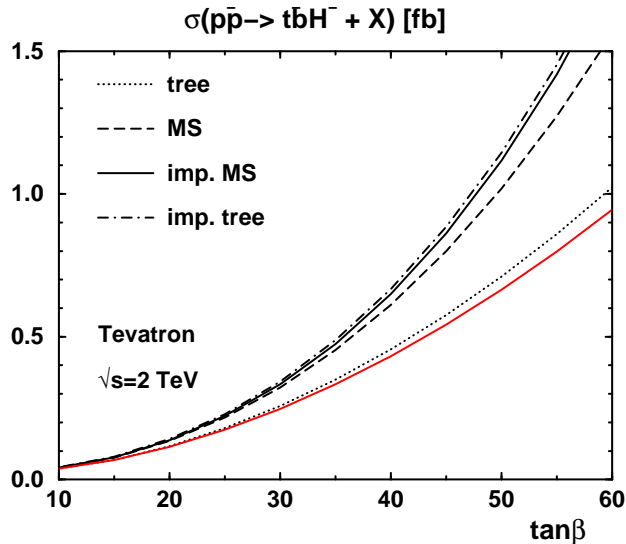


Figure 3: Various approximations to  $\sigma(p\bar{p} \rightarrow t\bar{b}H^- + X)$  at the Tevatron Run II, as a function of  $\tan\beta$ , for a charged Higgs mass of 250 GeV. The remaining MSSM parameters are set as in fig. 2. Shown are the tree-level (dotted line), the one-loop  $\overline{\text{MS}}$  (dashed line), the improved or resummed  $\overline{\text{MS}}$  (top solid line and bottom red solid line, the latter for  $\mu = 200$  GeV and  $A_t = -500$  GeV) and the improved tree-level (dot-dashed line) results.

constitutes a fairly good approximation to the complete resummed  $\overline{\text{MS}}$  result (top solid curve). Similar conclusions apply for  $pp \rightarrow t\bar{b}H^- + X$  at the LHC.

#### 4 $b \rightarrow s\gamma$ and supersymmetry with large $\tan\beta$

The computation of the  $b \rightarrow s\gamma$  branching ratio at the NLO in the MSSM is clearly a complicated matter [25,26], and completely general expressions have not yet been derived. Nevertheless, it turns out that the leading  $\alpha_s^n \tan^{n+1}\beta$  corrections can be calculated and resummed to all orders in perturbation theory by replacing the tree-level Yukawa of the bottom quark by eq. (4) in the Wilson coefficients of the leading-order (LO) computation [27].

To show how this procedure works, let us start by identifying the dominant one-loop Feynman diagrams. In a type II 2HDM, the diagram contributing to the highest  $\tan\beta$  power is that in fig. 4, with the exchange of a virtual charged Higgs in the loop, which is proportional to  $h_b \cdot h_t \cos\beta$  and, therefore, of order  $\tan^0\beta$ . Substituting a chargino by the charged Higgs, one obtains the leading diagram in the MSSM, which is proportional to  $h_b \cdot h_t$  and of order  $\tan\beta$ . We have checked, using the formulae in [25], that the leading—in  $\tan\beta$ — NLO corrections follow from the replacement

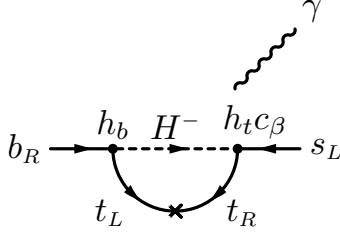


Figure 4: Dominant, in powers of  $\tan\beta$ , LO contribution to the  $b \rightarrow s\gamma$  branching ratio in the 2HDM.

$h_b \rightarrow -h_b\Delta m_b$  (expanding and truncating at first order in  $\alpha_s$ ) in the LO contributions associated to the above-mentioned diagrams. These NLO corrections are to be associated with the insertion of the counterterm for the bottom Yukawa in the LO, and thus have their origin in a one-loop diagram. The resulting effect is of order  $\alpha_s \tan^2\beta$  for the chargino loop, and  $\alpha_s \tan\beta$  for the  $H^-$  loop.

There is one additional source of  $\tan\beta$ -enhanced corrections in the charged Higgs diagrams, which is not related to the bottom mass counterterm [25]: while the tree-level  $H^+\bar{t}_R s_L$  vertex is suppressed by  $1/\tan\beta$ , this suppression is absent at the one-loop level, so that the NLO charged-Higgs contribution to  $\mathcal{BR}(b \rightarrow s\gamma)$  is  $\tan\beta$ -enhanced with respect to the LO one. No enhancement occurs in higher-loop diagrams, which are suppressed either by  $1/\tan\beta$  powers or by  $m_b/M_{\text{SUSY}}$  factors [7].

Now that all sources of  $\tan\beta$ -enhanced terms have been identified, it is an easy matter to proceed with the improvement of the NLO expressions, that is, to resum all terms of order  $\alpha_s^n \tan^{n+1}\beta$ . Just replace, in the LO expressions,  $h_b$  by  $h_b/(1 + \Delta m_b)$ , and remove double counting, i.e.  $-h_b\Delta m_b$  terms, in the NLO formulae (see ref. [27] for a detailed description of the procedure). This is enough to extend the validity of the calculation presented in ref. [25] to large values of  $\tan\beta$ .

The quantitative effect of the improvement can be assessed from fig. 5, where we compare the NLO theoretical prediction for  $\mathcal{BR}(b \rightarrow s\gamma)$  of ref. [25] with (solid line) and without (dashed line) including the all-order resummation of the dominant  $\tan\beta$ -enhanced radiative corrections, for typical values of the supersymmetric parameters. We use a negative value of  $A_t = -500$  GeV at low energies, with  $m_{\tilde{g}}A_t < 0$ . This choice is inspired in supergravity models, where this sign relation holds unless the boundary value of  $A_t$  at the high-energy input scale is one order of magnitude larger than the gaugino soft-supersymmetry-breaking mass parameters [4,28]. For the experimental measurement of the  $b \rightarrow s\gamma$  branching ratio, we use the combined result of CLEO [29] and ALEPH [30],  $\mathcal{BR}(b \rightarrow s\gamma) = (3.14 \pm 0.48) \times 10^{-4}$ . Owing to cancellations among the various contributions, the relative size of the effect turns out to be sizeable only for  $\mu A_t < 0$ : for the set of parameters used in fig. 5, it decreases the NLO result by 20% at  $\tan\beta \simeq 30$ .

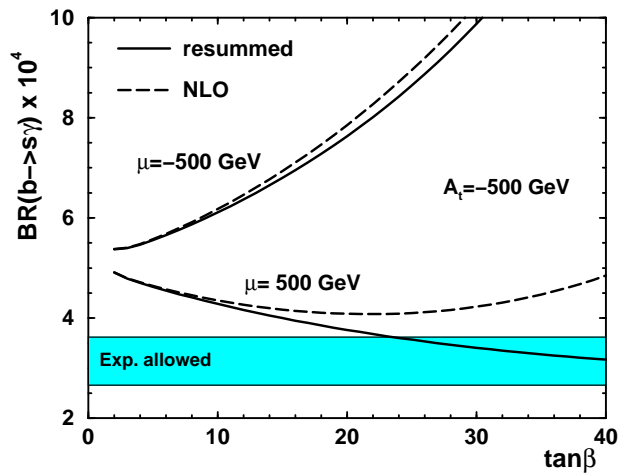


Figure 5: Comparison of the NLO theoretical prediction for  $\mathcal{BR}(b \rightarrow s\gamma)$  of ref. [25] before (solid line) and after (dashed line) performing a resummation of the dominant supersymmetric corrections of order  $\alpha_s^n \tan^{n+1}\beta$ , as explained in the text. The charged-Higgs boson mass is 200 GeV and the light stop mass is 250 GeV. The values of  $\mu$  and  $A_t$  are indicated in the plot, while  $M_2$ , the gluino, heavy-stop and down-squark masses are set at 800 GeV.

Notice that, with our sign conventions, positive values of  $\mu$  are necessary in order to obtain correct values for  $\mathcal{BR}(b \rightarrow s\gamma)$ , even after considering higher-order effects, within minimal supergravity models, for which, as explained in the above paragraph, the sign of  $A_t$  at low energies tends to be negative. This is in contradiction with the results of ref. [31]. We believe sign errors in the charged Goldstone and Higgs couplings to stop and down-like squarks in the published version of [25] are at the origin of this discrepancy (see [27]).<sup>6</sup>

## 5 Conclusions

Motivated by the latest LEP analyses ruling out  $\tan\beta$  values around 1 [6] and by large  $\tan\beta$  supersymmetric SO(10) models, we have analysed the Yukawa couplings of down-type fermions in the MSSM, which receive potentially large supersymmetric corrections when  $\tan\beta$  is large. We claim that, in observables where these couplings are relevant, a resummation of the leading—in powers of  $\tan\beta$ —subset of corrections is needed if the observables are to be computed for large  $\tan\beta$ . We perform such resummation, which is essentially independent of the particular process under consideration, and explore its numerical impact on two exemplary processes: the  $p\bar{p}, pp \rightarrow t\bar{b}H^- + X$  cross-section and the branching ratio of  $b \rightarrow s\gamma$ .

<sup>6</sup>The authors of [25] have independently detected these sign errors, and posted a corrected version of the paper to the hep-ph archive.

## Acknowledgments

The author thanks C.E.M Wagner, M. Carena, J. Solà, M.J. Herrero and A. Pineda for useful discussions, U. Nierste and J. Guasch for revising the text, J. Guasch and A. Belyaev for their collaboration in the computation of the  $p\bar{p}$ ,  $pp \rightarrow t\bar{b}H^- + X$  cross-section.

## Note added

After presentation of this talk, and concerning the  $b \rightarrow s\gamma$  branching ratio, similar formulae for the improvement of the NLO computation in the MSSM with large  $\tan\beta$  have been given in [32].

## References

- [1] R. Barate *et al.* [ALEPH Collaboration], hep-ex/0011045; M. Acciarri *et al.* [L3 Collaboration], hep-ex/0011043; P. Igo-Kemenes for the LEP Working Group on Higgs boson searches, talk given at the LEPC on 3 Nov. 2000.
- [2] J.F. Gunion, H.E. Haber, G.L. Kane and S. Dawson, “The Higgs Hunter’s Guide,” Addison-Wesley, Menlo-Park, 1990.
- [3] J. Guasch, R.A. Jiménez and J. Solà, *Phys. Lett.* **B360** (1995) 47; J.A. Coarasa, D. Garcia, J. Guasch, R.A. Jiménez and J. Solà, *Eur. Phys. J.* **C2** (1998) 373.
- [4] B. Ananthanarayan, G. Lazarides and Q. Shafi, *Phys. Rev.* **D44** (1991) 1613; T. Banks, *Nucl. Phys.* **B303** (1988) 172; M. Olechowski and S. Pokorski, *Phys. Lett.* **B214** (1988) 393; S. Dimopoulos, L.J. Hall and S. Raby, *Phys. Rev. Lett.* **68** (1992) 1984 and *Phys. Rev.* **D45** (1992) 4192; G.W. Anderson, S. Raby, S. Dimopoulos and L.J. Hall, *Phys. Rev.* **D47** (1993) 3702; R. Hempfling, *Phys. Rev.* **D49** (1994) 6168;
- [5] L.J. Hall, R. Rattazzi and U. Sarid, *Phys. Rev.* **D50** (1994) 7048; M. Carena, M. Olechowski, S. Pokorski and C.E.M. Wagner, *Nucl. Phys.* **B426** (1994) 269.
- [6] C. Tully for the LEP Working Group on Higgs boson searches, talk given at the LEPC on 5 Sept. 2000.
- [7] M. Carena, D. Garcia, U. Nierste and C.E.M. Wagner, *Nucl. Phys.* **B577** (2000) 88.

- [8] S. Belyaev, D. Garcia, J. Guasch and J. Solà, in preparation.
- [9] Talk given by D. Chakraborty at the SUSY 99 conference, Fermilab, June 1999; B. Abbott *et al.* [D0 Collaboration], *Phys. Rev. Lett.* **82** (1999) 4975; F. Abe *et al.* [CDF Collaboration], *Phys. Rev. Lett.* **79** (1997) 357.
- [10] J. Guasch and J. Solà, *Phys. Lett.* **B416** (1998) 353.
- [11] S.S. Willenbrock, *Phys. Rev.* **D35** (1987) 173; A. Krause, T. Plehn, M. Spira and P.M. Zerwas, *Nucl. Phys.* **B519** (1998) 85; A.A. Barrientos Bendezú and B.A. Kniehl, *Nucl. Phys.* **B568** (2000) 305; O. Brein and W. Hollik, *Eur. Phys. J.* **C13** (2000) 175.
- [12] Z. Kunszt and F. Zwirner, *Nucl. Phys.* **B385** (1992) 3; A.A. Barrientos Bendezú and B.A. Kniehl, *Phys. Rev.* **D59** (1999) 015009. S. Moretti and K. Odagiri, *Phys. Rev.* **D59** (1999) 055008.
- [13] J. F. Gunion, *Phys. Lett.* **B322** (1994) 125; V. Barger, R.J. Phillips and D.P. Roy, *Phys. Lett.* **B324** (1994) 236.
- [14] F. Borzumati, J. Kneur and N. Polonsky, *Phys. Rev.* **D60** (1999) 115011.
- [15] J.A. Coarasa, J. Guasch and J. Solà, hep-ph/9909397. Contributed to Physics at Run II: Workshop on Supersymmetry / Higgs: Summary Meeting, Batavia, Ill, 19–21 Nov. 1998.
- [16] D.J. Miller, S. Moretti, D.P. Roy and W.J. Stirling, *Phys. Rev.* **D61** (2000) 055011.
- [17] S. Moretti and K. Odagiri, *Phys. Rev.* **D55** (1997) 5627; S. Moretti and D. P. Roy, *Phys. Lett.* **B470** (1999) 209; C.S. Huang and S. Zhu, *Phys. Rev.* **D60** (1999) 075012; L.G. Jin, C.S. Li, R.J. Oakes and S.H. Zhu, *Eur. Phys. J.* **C14** (2000) 91.
- [18] F.I. Olness and W. Tung, *Nucl. Phys.* **B308** (1988) 813; R.M. Barnett, H.E. Haber and D.E. Soper, *Nucl. Phys.* **B306** (1988) 697.
- [19] D. Dicus, T. Stelzer, Z. Sullivan and S. Willenbrock, *Phys. Rev.* **D59** (1999) 094016.
- [20] M. Spira, hep-ph/9810289. Contributed to same meeting as in Ref. [15].
- [21] A. S. Belyaev, E. E. Boos and L. V. Dudko, *Phys. Rev.* **D59** (1999) 075001.
- [22] S. Dawson and L. Reina, *Phys. Rev.* **D57** (1998) 5851.

- [23] C.S. Li and T.C. Yuan, *Phys. Rev.* **D42** (1990) 3088; M. Drees and D.P. Roy, *Phys. Lett.* **B269** (1991) 155; C. Li, Y. Wei and J. Yang, *Phys. Lett.* **B285** (1992) 137; A. Czarnecki and S. Davidson, *Phys. Rev.* **D48** (1993) 4183.
- [24] A. Pukhov *et al.*, “CompHEP - a package for evaluation of Feynman diagrams and integration over multi-particle phase space. User’s manual for version 33,” preprint INP MSU 98-41/542, hep-ph/9908288.
- [25] M. Ciuchini, G. Degrassi, P. Gambino and G.F. Giudice, *Nucl. Phys.* **B534** (1998) 3.
- [26] M. Ciuchini, G. Degrassi, P. Gambino and G.F. Giudice, *Nucl. Phys.* **B527** (1998) 21; P. Ciafaloni, A. Romanino and A. Strumia, *Nucl. Phys.* **B524** (1998) 361; F. M. Borzumati and C. Greub, *Phys. Rev.* **D58** (1998) 074004; C. Bobeth, M. Misiak and J. Urban, *Nucl. Phys.* **B567** (2000) 153.
- [27] M. Carena, D. Garcia, U. Nierste and C.E.M. Wagner, hep-ph/0010003, to be published in *Physics Letters B*.
- [28] L.E. Ibáñez, C. López and C. Muñoz, *Nucl. Phys.* **256** (1985) 218; R. Barbieri and G.F. Giudice, *Nucl. Phys.* **B306** (1988) 63; M. Carena, M. Olechowski, S. Pokorski and C.E.M. Wagner, *Nucl. Phys.* **B419** (1994) 213.
- [29] CLEO Collaboration, CLEO CONF 98-17, ICHEP98 1011.
- [30] R. Barate *et al.* (ALEPH Collaboration), *Phys. Lett.* **B429** (1998) 169.
- [31] W. de Boer, M. Huber, A. Gladyshev and D.I. Kazakov, hep-ph/0007078.
- [32] G. Degrassi, P. Gambino and G.F. Giudice, *JHEP* **0012** (2000) 009.

IFT-UAM/CSIC 01-03, FTUAM 01/02, KA-TP-3-2001  
April 19, 2001  
hep-ph/0102169

## Decoupling Properties of MSSM particles in Higgs and Top Decays

H. E. HABER<sup>a</sup>, M. J. HERRERO<sup>b</sup>, H. E. LOGAN<sup>c</sup>,  
S. PEÑARANDA<sup>d</sup>, S. RIGOLIN<sup>e</sup> AND D. TEMES<sup>b\*</sup>

<sup>a</sup> *Santa Cruz Institute for Particle Physics, University of California.*

<sup>b</sup> *Departamento de Física Teórica, Universidad Autónoma de Madrid.*

<sup>c</sup> *Theoretical Physics Department, Fermi National Accelerator Laboratory.*

<sup>d</sup> *Institut für Theoretische Physik, Universität Karlsruhe.*

<sup>e</sup> *Department of Physics, University of Michigan.*

We study the supersymmetric (SUSY) QCD radiative corrections, at the one-loop level, to  $h^0$ ,  $H^\pm$  and  $t$  quark decays, in the context of the Minimal Supersymmetric Standard Model (MSSM) and in the decoupling limit. The decoupling behaviour of the various MSSM sectors is analyzed in some special cases, where some or all of the SUSY mass parameters become large as compared to the electroweak scale. We show that in the decoupling limit of both large SUSY mass parameters and large CP-odd Higgs mass, the  $\Gamma(h^0 \rightarrow b\bar{b})$  decay width approaches its Standard Model value at one loop, with the onset of decoupling being delayed for large  $\tan\beta$  values. However, this decoupling does not occur if just the SUSY mass parameters are taken large. A similar interesting non-decoupling behaviour, also enhanced by  $\tan\beta$ , is found in the SUSY-QCD corrections to the  $\Gamma(H^+ \rightarrow t\bar{b})$  decay width at one loop. In contrast, the SUSY-QCD corrections in the  $\Gamma(t \rightarrow W^+b)$  decay width do decouple and this decoupling is fast.

Presented at the

5th International Symposium on Radiative Corrections  
(RADCOR-2000)

Carmel CA, USA, 11–15 September, 2000

---

\*e-mails: haber@scipp.ucsc.edu, herrero@delta.ft.uam.es, logan@fnal.gov,  
siannah@particle.uni-karlsruhe.de, srigolin@umich.edu, temes@delta.ft.uam.es

# 1 Introduction

The study of radiative corrections to Standard Model (SM) couplings may provide crucial clues in exploring new physics beyond the reach of present accelerators. In particular, suppose that a light Higgs boson,  $h^0$ , were discovered in the mass range predicted by the minimal supersymmetric extension of the Standard Model (MSSM), but supersymmetric (SUSY) particles were not found. Then, a precise measurement of Higgs couplings to SM particles, which are sensitive to radiative corrections, could provide indirect information about the existence of SUSY in Nature and some indication of the preferred region of the SUSY parameter space. For example, one could predict (in the context of the MSSM) whether the data favored a SUSY spectrum below the 1 TeV energy scale. Similar studies can be performed by considering alternative observables as, for instance, the partial widths of top and Higgs decays into SM particles, and by comparing their predictions in the MSSM and the SM.

In this comparison of the MSSM and SM predictions for observables involving SM particles in the external legs, it is interesting to consider some particular limiting situations. The first one is when the genuine SUSY spectrum is very heavy as compared to the electroweak scale,  $M_{SUSY} \gg M_Z$ , where  $M_{SUSY}$  represents generically the masses of the SUSY particles. This situation corresponds to the decoupling of SUSY particles from the rest of the MSSM spectrum, namely, the SM particles and the MSSM Higgs sector containing  $h^0$ ,  $H^0$ ,  $A^0$  and  $H^\pm$ . The second one is when the extra Higgs bosons,  $H^0$ ,  $A^0$  and  $H^\pm$  are very heavy, but  $h^0$  and the genuine SUSY particles are closer to the electroweak scale. This decoupling limit can be reached by considering  $M_A \gg M_Z$ , where  $M_A$  is the mass of the CP-odd neutral Higgs boson of the MSSM. In addition, there is the limiting situation where both  $M_{SUSY}$  and  $M_A$  are large, and the decoupling of all non-standard particles from the SM physics is expected. This decoupling is known to occur in tree-level physics and in some one-loop physics. In particular, the tree-level couplings of  $h^0$  to fermion pairs and gauge bosons tend to their SM values if  $M_A \gg M_Z$  [1]. As a consequence of this decoupling, distinguishing the lightest MSSM Higgs boson in the large  $M_A$  limit from the Higgs boson of the SM will be very difficult.

Formally, the decoupling of all non-standard MSSM particles implies that in the effective low-energy theory, all observables involving SM particles in the external legs tend to their SM values in the limit of large SUSY masses and large  $M_A$ . It has been shown that all the genuine SUSY particles in the MSSM and the heavy Higgs bosons  $H^0$ ,  $A^0$  and  $H^\pm$ , decouple at one-loop order from the low-energy electroweak gauge boson physics [2]. In particular, the contributions of the SUSY particles to low-energy processes either fall as inverse powers of the SUSY mass parameters or can be absorbed into counterterms for the tree-level couplings of the low-energy theory and, therefore, they decouple in the same spirit as established in the *Appelquist-Carazzone Theorem* [3]. As a result, the radiative corrections involving SUSY particles go to

zero in the asymptotic large SUSY mass limit.

Our purpose here is to determine the decoupling behaviour in the previous limiting situations of several observables, including radiative corrections at one-loop, with the hope that for some of them either the decoupling does not occur totally or, in case it occurs, it proceeds slowly such that there may remain significant signals of new physics beyond SM, even for a heavy SUSY spectra.

In this paper we focus on the partial widths of  $h^0 \rightarrow b\bar{b}$ ,  $H^+ \rightarrow t\bar{b}$  and  $t \rightarrow W^+b$  decays, with special emphasis on the first one, whose corresponding branching ratio will be crucial for the experimental Higgs boson searches at the upcoming Tevatron Run 2 [4,5]. We study the MSSM radiative corrections to these observables at the one-loop level and to leading order in  $\alpha_s$ , and we analyze in detail their behavior in the previously mentioned decoupling limits. These corrections are due to the SUSY-QCD (SQCD) sector and arise from gluinos and third generation-squark exchange. Because of the dependence on the strong coupling constant, these are expected to be the most significant one-loop MSSM contributions over much of the MSSM parameter space. We will show that in the limit of large  $M_A$  (in this limit one also has  $M_{H^0}, M_{H^\pm} \gg M_Z$ ) and large sbottom and gluino masses ( $M_{\tilde{b}_i}, M_{\tilde{g}} \gg M_Z$ ), the SM expression for the  $h^0 \rightarrow b\bar{b}$  one-loop partial width is recovered [6]. That is, the SQCD corrections to the  $\Gamma(h^0 \rightarrow b\bar{b})$  partial width decouple in the limit of large SUSY masses and large  $M_A$ . In particular, we examine the case of large  $\tan\beta$ , for which the SQCD corrections are enhanced. This enhancement can delay the onset of decoupling and give rise to a significant one-loop correction, even for moderate to large values of the SUSY masses. This decoupling, however, does not occur, if either  $M_{SUSY}$  (characterizing a common mass scale for gluino and sbottom masses) or  $M_A$  are kept fixed while the other is taken large. A similar non-decoupling phenomenon of the SQCD corrections to one-loop when  $M_A$  is fixed and the sbottom, stop and gluinos masses are considered large is found in the  $H^+ \rightarrow t\bar{b}$  decay [7]. The SQCD corrections to one-loop in the  $t \rightarrow W^+b$  decay, however, do decouple and this decoupling proceeds fast. We present here just a summary of the main results and refer the reader to refs. [6,7] for more details.

## 2 Decoupling limit in the Higgs sector

The decoupling limit in the Higgs sector of the MSSM was first studied in ref. [1]. In short, it is defined by considering the CP-odd Higgs mass much larger than the electroweak scale,  $M_A \gg M_Z$ , and leads to a particular spectrum in the Higgs sector with very heavy  $H^0$ ,  $H^\pm$  and  $A^0$  bosons, and a light  $h^0$  boson. For a review of the MSSM Higgs sector, see ref. [8].

At tree level, if  $M_A \gg M_Z$ , the Higgs masses are,

$$M_{H^0} \simeq M_{H^\pm} \simeq M_A \gg M_Z, \quad M_{h^0} \simeq M_Z |\cos 2\beta|.$$

That is, at tree-level there exists a CP-even Higgs,  $h^0$ , lighter than the  $Z$  boson.

Concerning the neutral Higgs couplings, their tree-level values in the MSSM normalized to SM couplings and for arbitrary  $M_A$ , are given in table 1.

$\phi$		$g_{\phi\bar{t}t}$	$g_{\phi\bar{b}b}$	$g_{\phi VV}$
SM	$H$	1	1	1
MSSM	$h^\circ$	$\cos\alpha/\sin\beta$	$-\sin\alpha/\cos\beta$	$\sin(\beta-\alpha)$
	$H^\circ$	$\sin\alpha/\sin\beta$	$\cos\alpha/\cos\beta$	$\cos(\beta-\alpha)$
	$A^\circ$	$1/\tan\beta$	$\tan\beta$	0

Table 1: Higgs couplings in the MSSM normalized to SM couplings

Notice that by expanding in inverse powers of  $M_A$ , we get:

$$\frac{\cos\alpha}{\sin\beta} \simeq 1 + \mathcal{O}(M_Z^2/M_A^2), \quad -\frac{\sin\alpha}{\cos\beta} \simeq 1 + \mathcal{O}(M_Z^2/M_A^2)$$

$$\sin(\beta-\alpha) \simeq 1 + \mathcal{O}(M_Z^4/M_A^4).$$

Therefore, the  $h^0$  tree-level couplings in the decoupling limit,  $M_A \gg M_Z$ , tend to their SM values, as expected.

Beyond tree level, it has been shown [9] that, in this same decoupling limit, the Higgs masses keep a similar pattern as at tree level, that is, very heavy  $H^0$ ,  $H^\pm$  and  $A^0$  bosons, and a light  $h^0$  boson. The particular values of their masses depend of course on the MSSM parameters, but for  $M_A \gg M_Z$ ,

$$M_{H^\circ} \simeq M_{H^\pm} \simeq M_A \gg M_Z,$$

$$M_{h^\circ} \leq 130 - 135 \text{ GeV}.$$

In this work we will go beyond tree level and study the decoupling behaviour of heavy SUSY particles and heavy Higgses, at one-loop level, in Higgs bosons and top quark decays.

### 3 Decoupling limit in the SUSY-QCD sector

The sbottom and stop mass matrices, in the MSSM, are given respectively by:

$$\hat{M}_b^2 = \begin{pmatrix} M_{\tilde{Q}}^2 + m_b^2 - M_Z^2(\frac{1}{2} + Q_b s_w^2) \cos 2\beta & m_b(A_b - \mu \tan \beta) \\ m_b(A_b - \mu \tan \beta) & M_{\tilde{D}}^2 + m_b^2 + M_Z^2 Q_b s_w^2 \cos 2\beta \end{pmatrix}$$

and

$$\hat{M}_t^2 = \begin{pmatrix} M_{\tilde{Q}}^2 + m_t^2 + M_Z^2(\frac{1}{2} - Q_t s_w^2) \cos 2\beta & m_t(A_t - \mu \cot \beta) \\ m_t(A_t - \mu \cot \beta) & M_{\tilde{U}}^2 + m_t^2 + M_Z^2 Q_t s_w^2 \cos 2\beta \end{pmatrix}$$

In order to get heavy squarks and heavy gluinos, we need to choose properly the soft SUSY breaking parameters and the  $\mu$ -parameter. Since here we are interested in the limiting situation where the whole SUSY spectrum is heavier than the electroweak scale, we have made the following assumptions for the soft breaking squark mass parameters, trilinear terms,  $\mu$ -parameter and gluino mass (see ref. [6] for more details),

$$M_{SUSY} \sim M_{\tilde{Q}} \sim M_{\tilde{D}} \sim M_{\tilde{U}} \sim M_{\tilde{g}} \sim \mu \sim A_b \sim A_t \gg M_Z,$$

where  $M_{SUSY}$  represents generically a common SUSY large mass scale.

Besides, we have considered two extreme cases, maximal and minimal mixing, which, for the large mass limit we are studying, imply certain constraints on the squark mass differences. Thus, given the generic mass matrix,

$$\hat{M}_{\tilde{q}}^2 \equiv \begin{pmatrix} M_L^2 & m_q X_q \\ m_q X_q & M_R^2 \end{pmatrix},$$

the two limiting cases are reached by choosing the relative size of  $M_{L,R}$  and  $X_q$  as follows,

A.-Close to maximal mixing:  $\theta_{\tilde{q}} \sim \pm 45^\circ$

$$|M_L^2 - M_R^2| \ll m_q X_q \Rightarrow |M_{\tilde{q}_1}^2 - M_{\tilde{q}_2}^2| \ll |M_{\tilde{q}_1}^2 + M_{\tilde{q}_2}^2|$$

B.-Close to minimal mixing:  $\theta_{\tilde{q}} \sim 0^\circ$

$$|M_L^2 - M_R^2| \gg m_q X_q \Rightarrow |M_{\tilde{q}_1}^2 - M_{\tilde{q}_2}^2| \sim \mathcal{O}|M_{\tilde{q}_1}^2 + M_{\tilde{q}_2}^2|$$

Here we have included the corresponding implications for the squark mass differences.

## 4 SUSY-QCD corrections to $h^0 \rightarrow \bar{b}b$ in the decoupling limit

In this section we study the SUSY-QCD corrections to the partial decay width  $\Gamma(h^0 \rightarrow \bar{b}b)$  at the one-loop level and to leading order in perturbative QCD, that is  $\mathcal{O}(\alpha_S)$ . We will then explore the decoupling behaviour of these corrections for large SUSY masses,  $M_{SUSY}$ , and/or large  $M_A$ . Both numerical and analytical results will be presented [6].

For the  $h^0$  mass range predicted by the MSSM, the decay channel  $h^0 \rightarrow \bar{b}b$  is by far the dominant one (except in some special regions of parameter space at large  $\tan\beta$ ), and the precise value of its branching ratio will be crucial for the  $h^0$  final experimental reach at the Tevatron.

Among the various contributions to this decay width, the QCD corrections are known to be the dominant ones. At the one-loop level and to order  $\alpha_S$  these can be written as,

$$\Gamma_1(h^0 \rightarrow \bar{b}b) \equiv \Gamma_0(h^0 \rightarrow \bar{b}b)(1 + 2\Delta_{QCD} + 2\Delta_{SQCD}),$$

where,  $\Gamma_0(h^o \rightarrow b\bar{b})$  is the tree level width,  $\Delta_{QCD}$  is the one-loop contribution from standard QCD and,  $\Delta_{SQCD}$  is the one-loop contribution from the SUSY-QCD sector of the MSSM. The QCD correction,  $\Delta_{QCD}$ , gives a  $\sim 50\%$  reduction in the  $\Gamma(h^o \rightarrow b\bar{b})$  decay rate for  $M_{h^o}$  in its MSSM range [10]. This correction has the same form in the MSSM as in the SM, so that it gives no information in distinguishing the MSSM from the SM. The SQCD correction,  $\Delta_{SQCD}$ , was first computed in the on-shell scheme by using a diagrammatic approach in ref. [11] and later studied in detail in [12]. The SQCD corrections to the  $h^o b\bar{b}$  coupling were also computed in an effective Lagrangian approach in ref. [4], using the SUSY contributions to the  $b$ -quark self energy [13,14] and neglecting terms suppressed by inverse powers of SUSY masses. The size of the SQCD correction,  $\Delta_{SQCD}$ , and the QCD correction,  $\Delta_{QCD}$ , are comparable for a wide window of the MSSM parameter space. In some regions of the MSSM parameter space, the SQCD corrections become so large that it is important to take into account higher-order corrections. The two-loop SQCD corrections have been studied in a diagrammatic approach in ref. [15]. A higher-order analysis has also been carried out in refs. [16,17] by resumming the leading  $\tan\beta$  contributions to all orders of perturbation theory and by using an effective Lagrangian approach. However, this resummation is not important in our present work because we are interested in the decoupling limit, in which the one-loop corrections to the  $h^o b\bar{b}$  coupling are small. Thus, for the present analysis we will just keep the one-loop corrections.

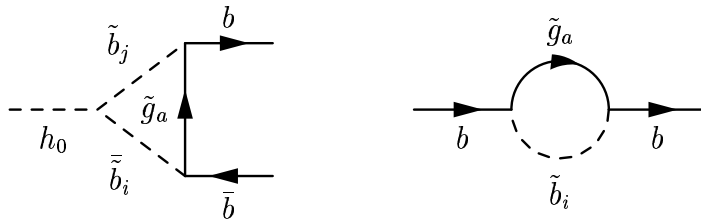


Figure 1: One-loop SUSY diagrams contributing to  $\mathcal{O}(\alpha_S)$  to  $h^o \rightarrow b\bar{b}$  decay

To one-loop and  $\mathcal{O}(\alpha_S)$  there are two type of diagrams, shown in Fig. 1, that contribute to

$$\Delta_{SQCD} = \Delta_{SQCD}^{\text{loops}} + \Delta_{SQCD}^{\text{CT}}.$$

The triangle diagram, with exchange of sbottoms and gluinos, contributes to  $\Delta_{SQCD}^{\text{loops}}$ , whereas the bottom self-energy diagram contributes to the counter-terms part  $\Delta_{SQCD}^{\text{CT}}$ . The exact results in the on-shell scheme are summarized by,

$$\begin{aligned}
\Delta_{SQCD}^{\text{loops}} &= \frac{\alpha_s}{3\pi} \left\{ \left[ \frac{2M_Z^2 \cos\beta \sin(\alpha+\beta)}{m_b \sin\alpha} (I_3^b \cos^2 \theta_{\tilde{b}} - Q_b s_W^2 \cos 2\theta_{\tilde{b}}) + 2m_b + Y_b \sin 2\theta_{\tilde{b}} \right] \right. \\
&\quad \times \left[ m_b C_{11} + M_{\tilde{g}} \sin 2\theta_{\tilde{b}} C_0 \right] (m_b^2, M_{h^o}^2, m_b^2; M_{\tilde{g}}^2, M_{\tilde{b}_1}^2, M_{\tilde{b}_1}^2) \\
&\quad + \left[ \frac{2M_Z^2 \cos\beta \sin(\alpha+\beta)}{m_b \sin\alpha} (I_3^b \sin^2 \theta_{\tilde{b}} + Q_b s_W^2 \cos 2\theta_{\tilde{b}}) + 2m_b - Y_b \sin 2\theta_{\tilde{b}} \right] \\
&\quad \times \left[ m_b C_{11} - M_{\tilde{g}} \sin 2\theta_{\tilde{b}} C_0 \right] (m_b^2, M_{h^o}^2, m_b^2; M_{\tilde{g}}^2, M_{\tilde{b}_2}^2, M_{\tilde{b}_2}^2) \\
&\quad + \left[ -\frac{M_Z^2 \cos\beta \sin(\alpha+\beta)}{m_b \sin\alpha} (I_3^b - 2Q_b s_W^2) \sin 2\theta_{\tilde{b}} + Y_b \cos 2\theta_{\tilde{b}} \right] \\
&\quad \times \left[ 2M_{\tilde{g}} \cos 2\theta_{\tilde{b}} C_0 (m_b^2, M_{h^o}^2, m_b^2; M_{\tilde{g}}^2, M_{\tilde{b}_1}^2, M_{\tilde{b}_2}^2) \right] \left. \right\}, \\
\Delta_{SQCD}^{\text{CT}} &= -\frac{\alpha_s}{3\pi} \left\{ \frac{M_{\tilde{g}}}{m_b} \sin 2\theta_{\tilde{b}} \left[ B_0(m_b^2; M_{\tilde{g}}^2, M_{\tilde{b}_1}^2) - B_0(m_b^2; M_{\tilde{g}}^2, M_{\tilde{b}_2}^2) \right] \right. \\
&\quad - 2m_b^2 \left[ B'_1(m_b^2; M_{\tilde{g}}^2, M_{\tilde{b}_1}^2) + B'_1(m_b^2; M_{\tilde{g}}^2, M_{\tilde{b}_2}^2) \right] \\
&\quad \left. - 2m_b M_{\tilde{g}} \sin 2\theta_{\tilde{b}} \left[ B'_0(m_b^2; M_{\tilde{g}}^2, M_{\tilde{b}_1}^2) - B'_0(m_b^2; M_{\tilde{g}}^2, M_{\tilde{b}_2}^2) \right] \right\},
\end{aligned}$$

where we have used the standard notation for masses, couplings and mixing angles, and we have followed the definitions and conventions for the one-loop integrals  $B_0$ ,  $B'_0$ ,  $B'_1$ ,  $C_0$  and  $C_{11}$  of ref. [18]. Notice that

$$Y_b \equiv A_b + \mu \cot \alpha$$

appears in  $h^o \tilde{b}_R \tilde{b}_L$  coupling and, therefore, will be responsible for sizeable contributions in the large  $A_b$  and/or  $\mu$  limit. Our results agree with those of refs. [11,12].

In order to compute  $\Delta_{SQCD}$  in the decoupling limit of very heavy sbottoms and gluinos, we have considered the following simple assumption for the MSSM parameters,

$$M_{SUSY} \sim M_{\tilde{Q}} \sim M_{\tilde{D}} \sim M_{\tilde{g}} \sim \mu \sim A_b \gg M_Z$$

where the symbol ' $\sim$ ' means 'of the order of' but not necessarily equal. We have performed a systematic expansion of the one-loop integrals and the mixing angle  $\theta_{\tilde{b}}$  in inverse powers of the large SUSY mass parameters. The resulting formulas of these expansions can be found in ref. [6]. Thus, by defining

$$\tilde{M}_S^2 \equiv \frac{1}{2}(M_{\tilde{b}_1}^2 + M_{\tilde{b}_2}^2), \quad R \equiv \frac{M_{\tilde{g}}}{\tilde{M}_S}, \quad X_b \equiv A_b - \mu \tan \beta$$

and including terms up to  $\mathcal{O}(M_{Z,h^o}^2/\tilde{M}_S^2)$  in the expansion, we get the following result for the maximal mixing case,  $\theta_{\tilde{b}} \sim \pm 45^\circ$ :

$$\begin{aligned}
\Delta_{SQCD} &= \frac{\alpha_s}{3\pi} \left\{ \frac{-\mu M_{\tilde{g}}}{\tilde{M}_S^2} (\tan \beta + \cot \alpha) f_1(R) - \frac{Y_b M_{\tilde{g}} m_b^2}{12 \tilde{M}_S^4} f_4(R) \right. \\
&\quad \left. + \frac{2}{3} \frac{M_Z^2 \cos\beta \sin(\alpha+\beta)}{M_S^2 \sin\alpha} I_3^b \left( f_5(R) + \frac{M_{\tilde{g}} X_b}{M_S^2} f_2(R) \right) + \mathcal{O} \left( \frac{m_b^2}{M_S^2} \right) \right\}
\end{aligned}$$

where the functions  $f_i(R)$  are defined in ref. [6] and have been normalized as  $f_i(1) = 1$ .

Notice that the first term is the dominant one in the limit of large  $M_{SUSY}$  mass parameters and does not vanish in the asymptotic limit of infinitely large  $M_S$ ,  $M_{\tilde{g}}$  and  $\mu$ . The second and third terms are respectively of  $\mathcal{O}(M_{h^0}^2/M_{SUSY}^2)$  and  $\mathcal{O}(M_Z^2/M_{SUSY}^2)$  and vanish in the previous asymptotic limit. Therefore the first term gives a non-decoupling SUSY contribution to the  $\Gamma(h^0 \rightarrow b\bar{b})$  partial width which can be of phenomenological interest. Moreover, since this term is enhanced at large  $\tan\beta$  it can provide important corrections to the branching ratio  $BR(h^0 \rightarrow b\bar{b})$ , even for a very heavy SUSY spectrum. The sign of these corrections are fixed by the sign of  $\mu M_{\tilde{g}}$ . The previous result when expressed in terms of the  $h^0$  effective coupling to  $b\bar{b}$  agrees with the result in ref. [4] based on the zero external momentum approximation or, equivalently, the effective Lagrangian approach.

From our previous result, we conclude that there is no decoupling of sbottoms and gluinos in the limit of large SUSY mass parameters for fixed  $M_A$ . Notice that this result is at first sight surprising, since most numerical studies done so far on this subject indicate decoupling of heavy SUSY particles from SM physics<sup>1</sup>. How do we then recover decoupling of the heavy MSSM spectra from the SM low energy physics? The answer to this question relies in the fact that in order to converge to SM predictions we need to consider not just a heavy SUSY spectra but also a heavy Higgs sector. That is, besides large  $M_{SUSY}$ , the condition of large  $M_A$  is also needed. Thus, if  $M_A \gg M_Z$  the light Higgs  $h^0$  behaves as the SM Higgs boson, and the extra heavy Higgses  $A$ ,  $H^\pm$  and  $H^0$  decouple. The decoupling of SUSY particles and the extra Higgs bosons in  $\Delta_{SQCD}$  is seen explicitly once the large  $M_A$  limit of the mixing angle  $\alpha$  is considered,

$$\cot \alpha = -\tan \beta - 2\frac{M_Z^2}{M_A^2} \tan \beta \cos 2\beta + \mathcal{O}\left(\frac{M_Z^4}{M_A^4}\right).$$

By substituting this into our previous result we see that the non-decoupling terms cancel out and we get finally,

$$\begin{aligned} \Delta_{SQCD} &= \frac{\alpha_s}{3\pi} \left\{ \frac{2\mu M_{\tilde{g}}}{M_S^2} f_1(R) \tan \beta \cos 2\beta \frac{M_Z^2}{M_A^2} - X_b \frac{M_{\tilde{g}} m_{h^0}^2}{12M_S^4} f_4(R) \right. \\ &\quad \left. + \frac{2}{3} \frac{M_Z^2}{M_S^2} \cos 2\beta I_3^b \left( f_5(R) + \frac{M_{\tilde{g}} X_b}{M_S^2} f_2(R) \right) + \mathcal{O}\left(\frac{m_b^2}{M_S^2}\right) \right\} \end{aligned}$$

which clearly vanishes in the asymptotic limit of  $M_{SUSY}$  and  $M_A \rightarrow \infty$ .

In conclusion, we get decoupling of the SQCD sector in  $h^0 \rightarrow b\bar{b}$  decays, if and only if, both  $M_{SUSY}$  and  $M_A$  are large. In this limit, the dominant terms go as,

$$\Delta_{SQCD} \sim C_1 \frac{M_Z^2}{M_A^2} + C_2 \frac{M_{Z,h^0}^2}{M_{SUSY}^2},$$

---

<sup>1</sup>It should also be noticed that, strictly speaking, the *decoupling theorem* [3] is not applicable to the MSSM case, since it is a theory that incorporates the SM chiral fermions and the SM electroweak spontaneous symmetry breaking. For a more detailed discussion on this, see ref. [2]

and, since both  $C_1$  and  $C_2$  are enhanced by  $\tan\beta$ , we expect this decoupling to be delayed for large  $\tan\beta$  values. Last but not least, we see that the sign of  $\Delta_{SQCD}$  is given by the sign of  $\mu$  and  $M_{\tilde{g}}$ . All these results are similar for the near zero mixing case,  $\theta_{\tilde{b}} \sim 0^\circ$ ; for brevity we do not show these here (see ref. [6]).

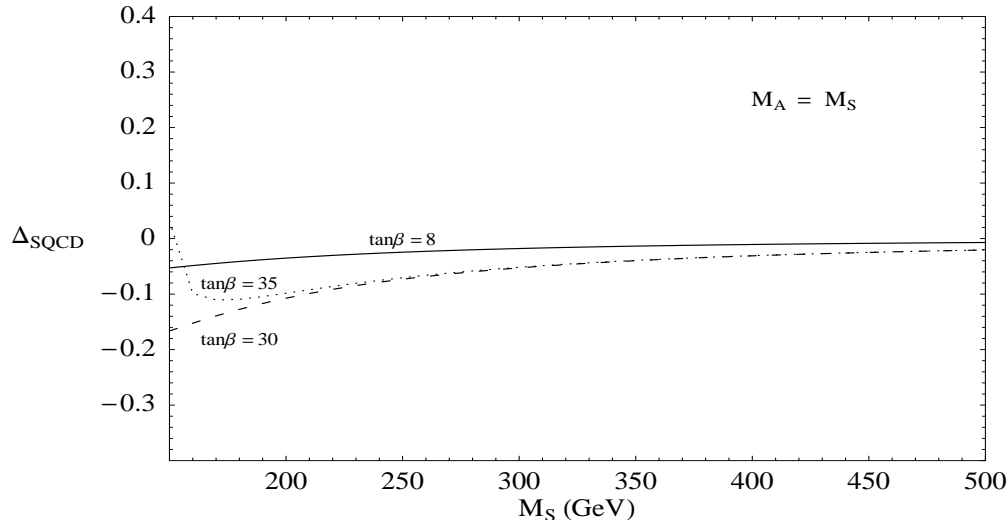


Figure 2: Exact numerical results for  $\Delta_{SQCD}$  in  $h^0 \rightarrow b\bar{b}$  decay as a function of a common MSSM scale  $M_S$  and for several values of  $\tan\beta$

Finally, in order to show this decoupling numerically, we have studied a simple example where there is just one relevant MSSM scale,  $M_S$ . More specifically, we have chosen,

$$M_S = M_{\tilde{Q}} = M_{\tilde{D}} = \mu = A_b = M_{\tilde{g}} = M_A,$$

which, in the limit  $M_S \gg M_Z$ , gives maximal mixing,  $\theta_{\tilde{b}} \sim 45^\circ$ . In Fig. 2 we show the numerical results for the exact one-loop SQCD corrections, as a function of this common MSSM mass scale  $M_S$ , and for several values of  $\tan\beta$ . We can see in this figure clearly the decoupling of  $\Delta_{SQCD}$  with  $M_S$ . This decoupling goes as  $1/M_S^2$ , in agreement with our analytical result, and is delayed for large  $\tan\beta$  values. The typical size of this correction is  $\Delta_{SQCD} \leq -10\%$  for  $M_S \geq 250 \text{ GeV}$ . Notice that the sign of  $\Delta_{SQCD}$  here is negative because of our choice of positive  $\mu$  and  $M_{\tilde{g}}$ .

## 5 Comparing the decoupling behaviour of the various MSSM sectors in $h^o \rightarrow b\bar{b}$ decay

In this section we study and compare the decoupling behaviour of the different MSSM sectors that are relevant in the one-loop SQCD corrections to  $h^o \rightarrow b\bar{b}$  decay.

As we have discussed in the previous section, these are: the extra Higgs bosons,  $H^0$ ,  $A^0$ ,  $H^\pm$ , gluinos  $\tilde{g}$  and sbottoms  $\tilde{b}_{1,2}$ . As regard to the Higgs sector, we have seen that there is no independent decoupling of these heavy  $H^0$ ,  $A^0$ ,  $H^\pm$  Higgs bosons in  $\Delta_{SQCD}$ , unless the SQCD sector is also considered heavy. To illustrate this, we have plotted in Fig. 3 the numerical results of  $\Delta_{SQCD}$  as a function of  $M_A$  for several fixed values of the common SUSY scale  $M_S = M_{\tilde{Q}} = M_{\tilde{D}} = \mu = A_b = M_{\tilde{g}}$  and for  $\tan\beta = 8$ . The fact that  $\Delta_{SQCD}$  does not tend to zero for large  $M_A$  but to a

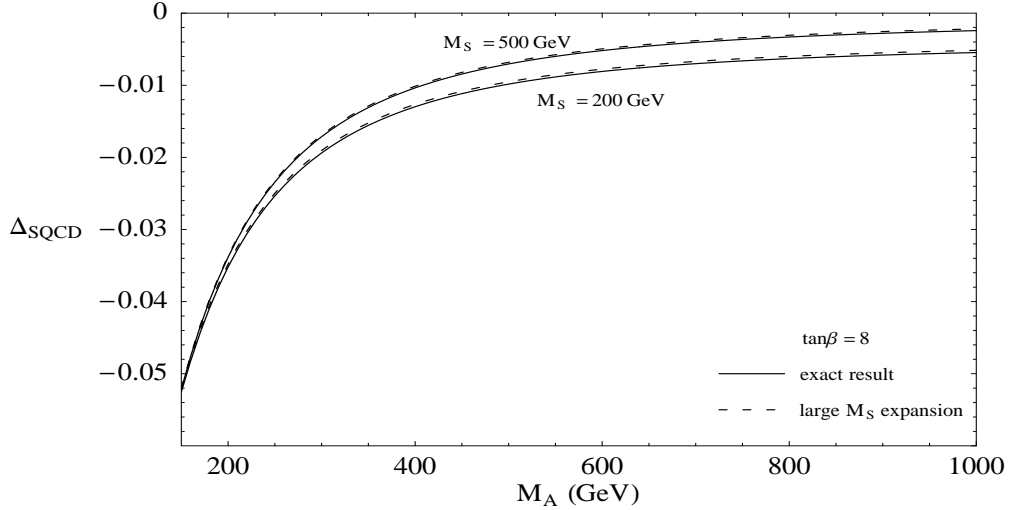


Figure 3:  $\Delta_{SQCD}$  in  $h^0 \rightarrow b\bar{b}$  decay as a function of  $M_A$  for fixed  $M_S$

non-vanishing constant is a clear indication of a non-decoupling behaviour with  $M_A$  for fixed  $M_S$ . Similarly, we have shown that there is no independent decoupling of the SQCD particles. That is, if we consider large values of the common SQCD scale  $M_S$ , while keeping  $M_A$  fixed,  $\Delta_{SQCD}$  approaches to a non-vanishing constant. This is illustrated clearly in Fig. 4. In these Figs. 3 and 4 we also show a comparison of the exact formula with our asymptotic expansion, valid for large  $M_S$ . We have seen that the large  $M_S$  expansion provides a very good approximation to the exact result for most of the  $(M_S, \tan\beta)$  parameter space, except for sufficiently low  $M_S$  and large  $\tan\beta$  values.

Next, we consider the independent decoupling of gluinos. By performing a second expansion in inverse powers of the gluino mass  $M_{\tilde{g}}$ , which is relevant in the heavy gluino limit  $M_{\tilde{g}} \gg M_S \sim \mu \sim A_b \gg M_Z$ , we get:

$$\Delta_{SQCD} = \frac{\alpha_s}{3\pi} \left\{ \frac{2\mu}{M_{\tilde{g}}} (\tan\beta + \cot\alpha) \left( 1 - \log\left(\frac{M_{\tilde{g}}^2}{M_S^2}\right) \right) + \frac{2X_b}{M_{\tilde{g}}} \frac{M_Z^2}{M_S^2} \frac{\cos\beta \sin(\alpha+\beta)}{\sin\alpha} I_3^b - \frac{Y_b}{3M_{\tilde{g}}} \frac{m_h^2}{M_S^2} + \mathcal{O}\left(\frac{M^2}{M_{\tilde{g}}^2}\right) \right\}.$$

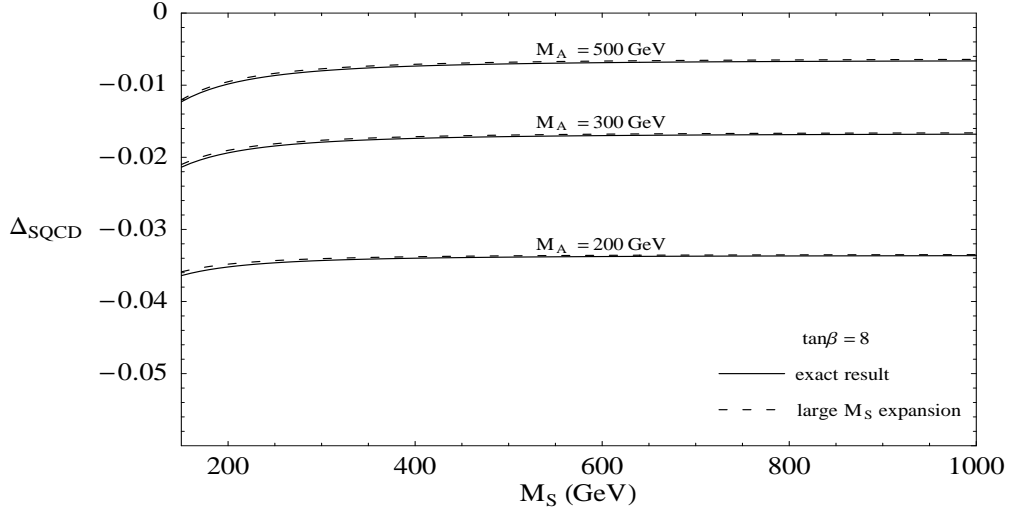


Figure 4:  $\Delta_{SQCD}$  in  $h^0 \rightarrow b\bar{b}$  decay as a function of  $M_S$  for fixed  $M_A$

This yields a very slow decoupling with  $M_{\tilde{g}}$ , due to the logarithmic dependence, and agrees with the previous exact numerical results of ref. [12]. For illustration we show in Fig. 5 our exact numerical results for  $\Delta_{SQCD}$  as a function of  $M_{\tilde{g}}$ , for fixed  $M_A = M_S$  value and for several  $\tan\beta$  values. This very slow decoupling with  $M_{\tilde{g}}$  may have important phenomenological consequences, in the large  $\tan\beta$  regime, because the SQCD correction can reach sizeable values, even for large gluino masses. For instance, for  $\tan\beta = 30$  and  $M_{\tilde{g}} = 1TeV$  we get  $\Delta_{SQCD} = -12\%$ , which is not a small effect.

Finally, we have studied the independent decoupling of sbottoms. By performing an expansion in inverse powers of the average sbottom mass  $\tilde{M}_S$ , which is relevant in the heavy sbottoms limit,  $\tilde{M}_S \gg M_{\tilde{g}} \sim \mu \sim A_b \gg M_Z$  we find the following result:

$$\Delta_{SQCD} = \frac{\alpha_s}{3\pi} \left\{ \frac{-2\mu M_{\tilde{g}}}{\tilde{M}_S^2} (\tan\beta + \cot\alpha) + \frac{M_Z^2 \cos\beta \sin(\alpha + \beta)}{\tilde{M}_S^2 \sin\alpha} I_3^b + \mathcal{O}\left(\frac{m_b^2}{\tilde{M}_S^2}\right) \right\}$$

It shows a fast decoupling behaviour as  $\tilde{M}_S$  is taken large. This same behaviour is also manifest in our exact numerical results shown in Fig. 6

## 6 SUSY-QCD corrections to $H^+ \rightarrow t\bar{b}$ in the decoupling limit

In this section we study the SUSY-QCD corrections to the partial decay width  $\Gamma(H^+ \rightarrow t\bar{b})$  at the one-loop level and to  $\mathcal{O}(\alpha_s)$ . We will then analyze these corrections in the decoupling limit of large SUSY masses. We will present here just a short

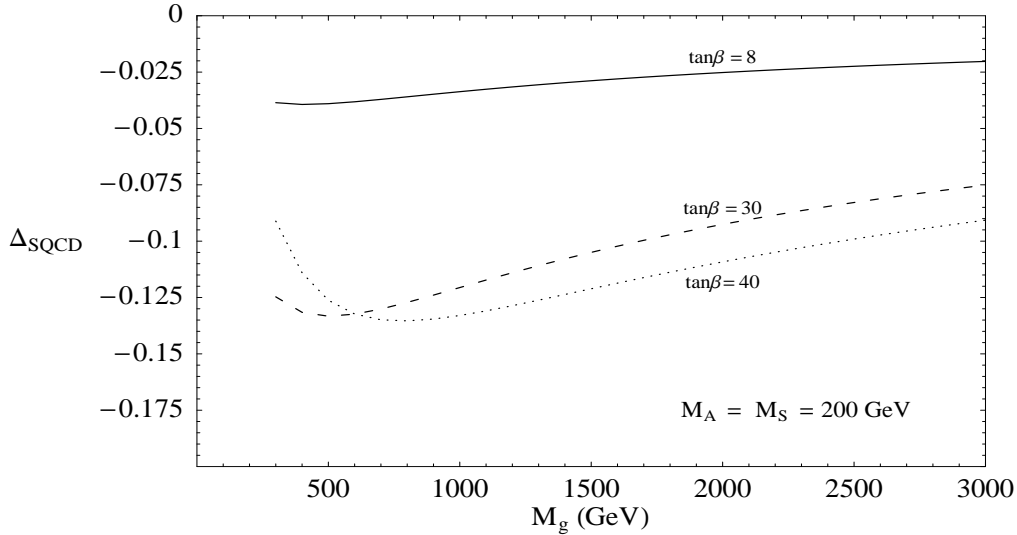


Figure 5:  $\Delta_{SQCD}$  in  $h^0 \rightarrow b\bar{b}$  decay as a function of  $M_{\tilde{g}}$

summary of the main numerical and analytical results, and refer the reader to ref. [7] for a more detailed study.

If all SUSY particles are heavy enough,  $H^+$  decays dominantly into  $t\bar{b}$  above the  $t\bar{b}$  threshold. As in the case of  $h^0 \rightarrow b\bar{b}$ , the dominant radiative corrections to  $H^+ \rightarrow t\bar{b}$  decay are the QCD corrections. At the one-loop level and to  $\mathcal{O}(\alpha_S)$  the corresponding partial width can be written as,

$$\Gamma_1(H^+ \rightarrow t\bar{b}) \equiv \Gamma_0(H^+ \rightarrow t\bar{b})(1 + 2\Delta_{QCD} + 2\Delta_{SQCD}),$$

where  $\Gamma_0(H^+ \rightarrow t\bar{b})$  is the tree-level width,  $\Delta_{QCD}$  is the correction from standard QCD, and  $\Delta_{SQCD}$  is the correction from SUSY-QCD. The standard QCD corrections were computed in ref. [19] and can be large (+10% to -50%). The SUSY-QCD corrections were computed by using a diagrammatic approach in refs. [20,21] and can be comparable or even larger than the standard QCD corrections in a large region of the SUSY parameter space.

At the one-loop level and to  $\mathcal{O}(\alpha_S)$  there are two type of diagrams that contribute to

$$\Delta_{SQCD} = \Delta_{SQCD}^{\text{loops}} + \Delta_{SQCD}^{\text{CT}},$$

as shown in Fig. 6. The triangle diagram, with exchange of sbottoms, stops and gluinos, contributes to  $\Delta_{SQCD}^{\text{loops}}$ , whereas the bottom and top self-energy diagrams contribute to the counter-terms part  $\Delta_{SQCD}^{\text{CT}}$ . The exact results in the on-shell scheme are summarized by,

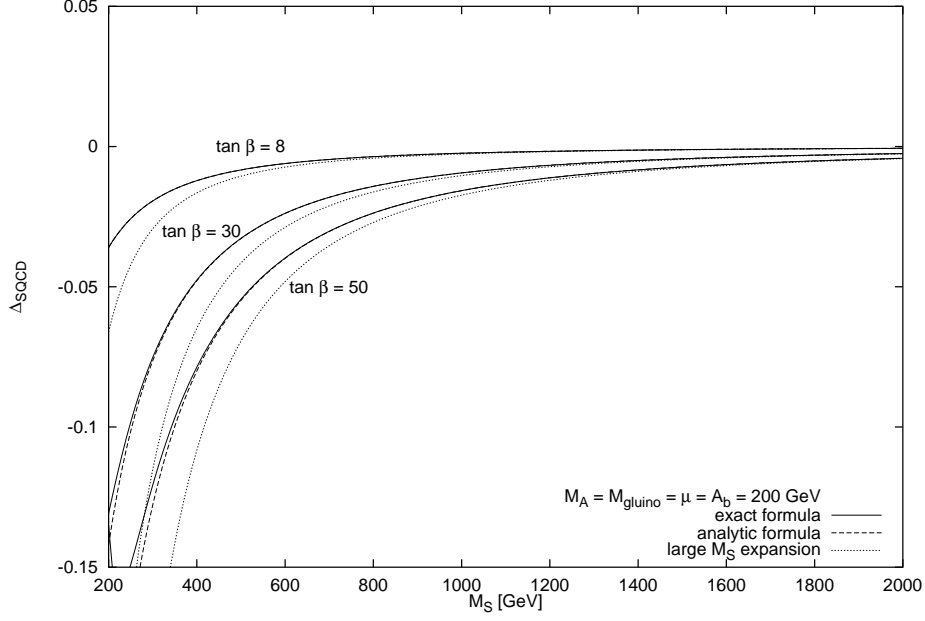


Figure 6:  $\Delta_{SQCD}$  in  $h^0 \rightarrow b\bar{b}$  decay as a function of  $\tilde{M}_S$

$$\Delta_{SQCD}^{loops} = \frac{U_t}{D} H_t + \frac{U_b}{D} H_b,$$

$$\Delta_{SQCD}^{CT} = \frac{U_t}{D} \left( \frac{\delta m_t}{m_t} + \frac{1}{2} \delta Z_L^b + \frac{1}{2} \delta Z_R^t \right) + \frac{U_b}{D} \left( \frac{\delta m_b}{m_b} + \frac{1}{2} \delta Z_L^t + \frac{1}{2} \delta Z_R^b \right),$$

where,

$$D = (M_{H^+}^2 - m_t^2 - m_b^2) (m_t^2 \cot^2 \beta + m_b^2 \tan^2 \beta) - 4m_t^2 m_b^2,$$

$$U_t = (M_{H^+}^2 - m_t^2 - m_b^2) m_t^2 \cot^2 \beta - 2m_t^2 m_b^2,$$

$$U_b = (M_{H^+}^2 - m_t^2 - m_b^2) m_b^2 \tan^2 \beta - 2m_t^2 m_b^2,$$

$$H_t = -\frac{2\alpha_s}{3\pi} \frac{G_{ab}^*}{m_t \cot \beta} [m_t R_{1b}^{(t)} R_{1a}^{(b)*} (C_{11} - C_{12}) + m_b R_{2b}^{(t)} R_{2a}^{(b)*} C_{12} \\ + M_{\tilde{g}} R_{2b}^{(t)} R_{1a}^{(b)*} C_0] (m_t^2, m_{H^+}^2, M_{\tilde{g}}^2, M_{\tilde{t}_b}^2, M_{\tilde{b}_a}^2),$$

$$H_b = -\frac{2\alpha_s}{3\pi} \frac{G_{ab}^*}{m_b \tan \beta} [m_t R_{2b}^{(t)} R_{2a}^{(b)*} (C_{11} - C_{12}) + m_b R_{1b}^{(t)} R_{1a}^{(b)*} C_{12} \\ + M_{\tilde{g}} R_{1b}^{(t)} R_{2a}^{(b)*} C_0] (m_t^2, m_{H^+}^2, M_{\tilde{g}}^2, M_{\tilde{t}_b}^2, M_{\tilde{b}_a}^2),$$

and the counter-terms are given in the on-shell scheme by,

$$\frac{\delta m_{(t,b)}}{m_{(t,b)}} + \frac{1}{2} \delta Z_L^{(b,t)} + \frac{1}{2} \delta Z_R^{(t,b)} = \Sigma_S^{(t,b)}(m_{(t,b)}^2) + \frac{1}{2} \Sigma_L^{(t,b)}(m_{(t,b)}^2) - \frac{1}{2} \Sigma_L^{(b,t)}(m_{(b,t)}^2)$$

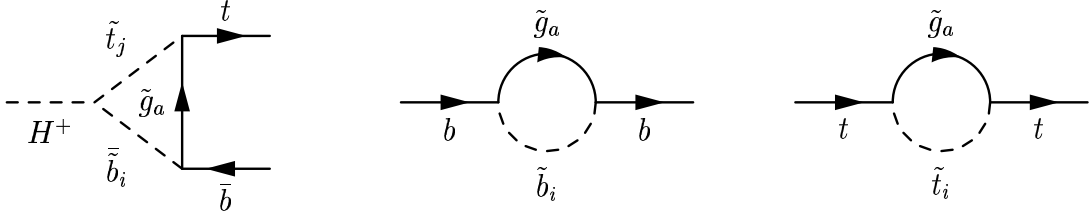


Figure 7: One-loop SUSY diagrams contributing to  $\mathcal{O}(\alpha_S)$  to  $H^+ \rightarrow t\bar{b}$  decay

$$-\frac{m_t^2}{2} \left[ \Sigma_L^{t'}(m_t^2) + \Sigma_R^{t'}(m_t^2) + 2\Sigma_S^{t'}(m_t^2) \right] - \frac{m_b^2}{2} \left[ \Sigma_L^{b'}(m_b^2) + \Sigma_R^{b'}(m_b^2) + 2\Sigma_S^{b'}(m_b^2) \right]$$

where,

$$\begin{aligned} \Sigma_L^q(p^2) &= -\frac{2\alpha_s}{3\pi} |R_{1a}^{(q)}|^2 B_1(p^2, m_{\tilde{g}}^2, m_{\tilde{q}_a}^2), \\ \Sigma_R^q(p^2) &= -\frac{2\alpha_s}{3\pi} |R_{2a}^{(q)}|^2 B_1(p^2, m_{\tilde{g}}^2, m_{\tilde{q}_a}^2), \\ \Sigma_S^q(p^2) &= -\frac{2\alpha_s}{3\pi} \frac{m_{\tilde{g}}}{m_q} \text{Re}(R_{1a}^{(q)} R_{2a}^{(q)*}) B_0(p^2, m_{\tilde{g}}^2, m_{\tilde{q}_a}^2). \end{aligned}$$

The  $G_{ab}$  parametrize the  $H^+ \tilde{b}_a \tilde{t}_b$  couplings, and the  $R^{(q)}$  are the rotation matrices that relate the interaction-eigenstate squarks to the mass-eigenstates. Their values in the MSSM can be found, for instance, in ref. [7]. The above result agrees with the original computation of refs. [20,21].

In order to compute  $\Delta_{SQCD}$  in the decoupling limit of large SUSY masses, we have considered all the soft-SUSY-breaking mass parameters and the  $\mu$  parameter to be of the same order (collectively denoted by  $M_{SUSY}$ ) and much heavier than the electroweak scale,

$$M_{SUSY} \sim M_{\tilde{Q}} \sim M_{\tilde{U}} \sim M_{\tilde{D}} \sim M_{\tilde{g}} \sim \mu \sim A_t \sim A_b \gg M_{EW},$$

and we have performed a systematic expansion in inverse powers of the large SUSY mass parameters. Notice that in this case it does not make sense to consider the alternative limit of large  $M_A$ , since this parameter provides the charged Higgs mass value and, therefore, it must be fixed. We have obtained analytical expansions for  $\Delta_{SQCD}$  that include up to  $\mathcal{O}(M_{EW}^2/M_{SUSY}^2)$  corrections, for all the interesting limiting cases of maximal and minimal mixing, in both the stop and the sbottom sectors. For brevity, we do not present here the complete results, which can be found in ref. [7], and we just show the most relevant result, that is, the dominant term in this expansion for the particular choice of maximal mixing. Thus, for  $\theta_{\tilde{b},\tilde{t}} \sim 45^\circ$  and

$\tilde{M}_S^2 \equiv \frac{1}{2}(M_{\tilde{b}_1}^2 + M_{\tilde{b}_2}^2) \equiv \frac{1}{2}(M_{\tilde{t}_1}^2 + M_{\tilde{t}_2}^2)$  we get:

$$\Delta_{SQCD} = \frac{\alpha_s}{3\pi} \left\{ \frac{-\mu M_{\tilde{g}}}{M_S^2} (\tan \beta + \cot \beta) f_1(R) + \mathcal{O}\left(\frac{M_{EW}^2}{M_S^2}\right) \right\}$$

This leading term does not vanish in the heavy SUSY particle limit and, therefore, there is no decoupling of stops, sbottoms and gluinos in the  $\Gamma(H^+ \rightarrow t\bar{b})$  decay width to one-loop level. This can be seen clearly, for instance, for the simplest case of equal mass scales,  $\mu = M_{\tilde{g}} = \tilde{M}_S$ , where  $f_1(R) = 1$ . This leading term, when expressed in terms of an effective coupling of  $H^+$  to  $b\bar{t}$  is in agreement with the previous results of refs. [16,17] that were obtained in the zero external momentum approximation by using an effective Lagrangian approach. We see in this result the enhancement of  $\Delta_{SQCD}$  by  $\tan \beta$ , so that this non-decoupling effect can be numerically important for large  $\tan \beta$  values. As in the case of  $h^0$ , the sign of the SQCD correction is determined by the sign of  $M_{\tilde{g}}$  and  $\mu$ . We have obtained similar results for the case of minimal mixing, as can be seen in [7].

Finally, in order to illustrate this non-decoupling behaviour numerically, we present in Fig. 8 the  $\Delta_{SQCD}$  correction as a function of a common SUSY mass scale  $M_S = M_{\tilde{Q}} = M_{\tilde{U}} = M_{\tilde{D}} = M_{\tilde{g}} = A_b = A_t = \mu$ . The Higgs mass has been fixed to  $m_{H^+} = 250 \text{ GeV}$ , and several values of  $\tan \beta$  have been considered. The fact that  $\Delta_{SQCD}$  tends to a non-vanishing value for very large  $M_S$  shows precisely this non-decoupling effect. The correction is quite sizeable, even for a very heavy SUSY spectrum. This is particularly noticeable for large  $\tan \beta$ .

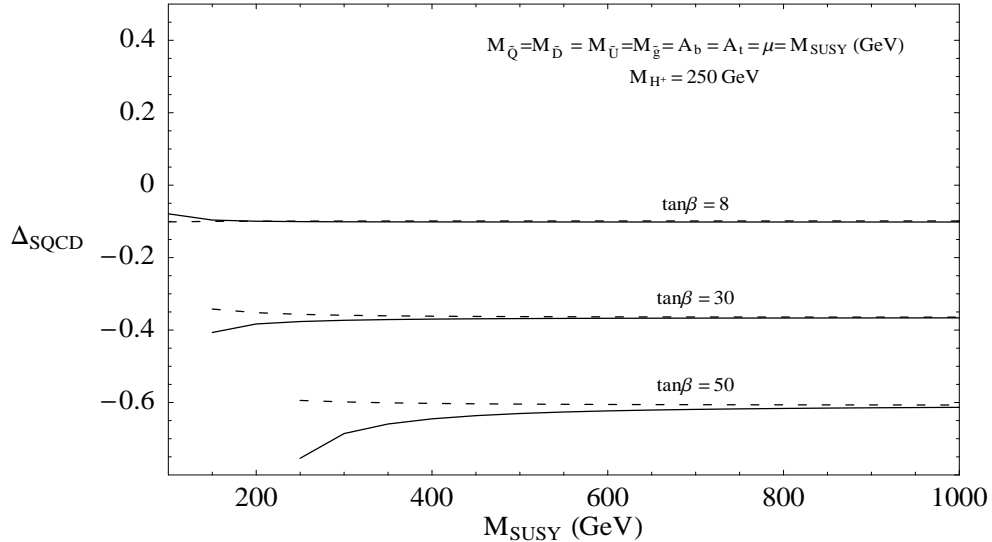


Figure 8:  $\Delta_{SQCD}$  in  $H^+ \rightarrow t\bar{b}$  decay as a function of the common SUSY scale  $M_S$

In addition, we have proved the independent decoupling of the gluinos and squarks

whenever they are considered separately very heavy as compared to the electroweak scale. Furthermore, the decoupling of gluinos is much slower than the decoupling of squarks due again to the logarithmic dependence on the gluino mass. In Fig. 9 we show the exact numerical results for  $\Delta_{SQCD}$  as a function of the gluino mass and for  $M_{\tilde{Q}} = M_{\tilde{U}} = M_{\tilde{D}} = A_b = A_t = \mu = 1 \text{ TeV}$  and  $m_{H^+} = 250 \text{ GeV}$ . We see clearly the very slow decoupling of the correction with the gluino mass and notice the large size of  $\Delta_{SQCD}$ , specially for large  $\tan\beta$ . For instance, if  $\tan\beta = 30$  and  $M_{\tilde{g}} = 2 \text{ TeV}$  we get  $\Delta_{SQCD} = -40\%$ . Notice that the size can be so large that the validity of the perturbative expansion can be questionable. We refer the reader to refs. [16,17] where this subject is studied and some techniques of resummation for a better convergence of the series are proposed.

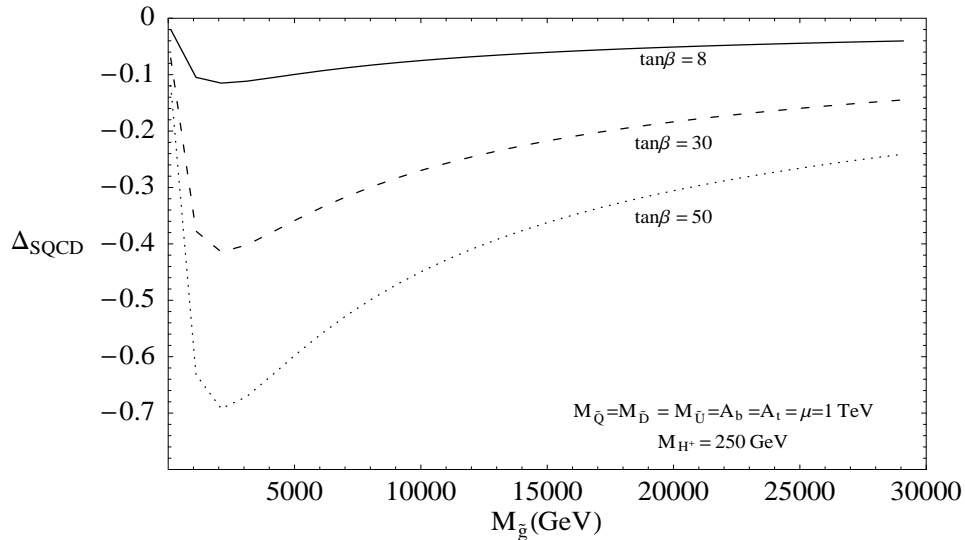


Figure 9:  $\Delta_{SQCD}$  in  $H^+ \rightarrow t\bar{b}$  decay as a function of  $M_{\tilde{g}}$

## 7 SUSY-QCD corrections to $t \rightarrow W^+b$ in the decoupling limit

In this section we briefly comment on the SUSY-QCD corrections to  $t \rightarrow W^+b$  at the one-loop level and to  $\mathcal{O}(\alpha_S)$ , and we study them in the decoupling limit. These radiative corrections were studied in the context of the MSSM in ref. [22] and are known to be important for some regions of the MSSM parameter space. The standard QCD corrections are also known to be important and give a  $\sim -10\%$  reduction in  $\Gamma(t \rightarrow W^+b)$  [23]. The Feynman diagrams that contribute to the SQCD corrections are shown in Fig. 10. The size of the SQCD corrections has been estimated to range between  $-5\%$  and  $-10\%$  and are quite insensitive to  $\tan\beta$  [22]. In contrast, the

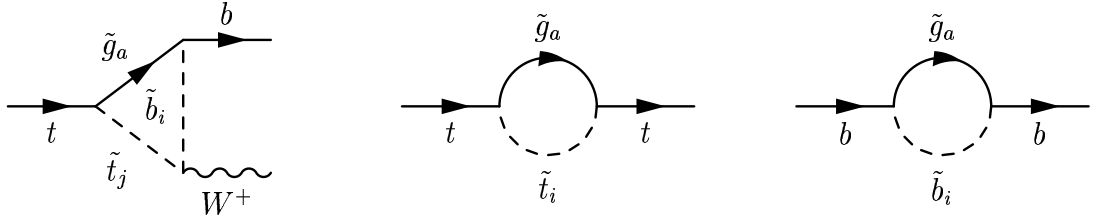


Figure 10: One-loop SUSY diagrams contributing to  $\mathcal{O}(\alpha_S)$  in  $t \rightarrow W^+b$  decay

SUSY-Electroweak corrections that range between  $-1\%$  and  $-10\%$  are known to grow with  $\tan\beta$  [24].

In order to analyze the decoupling limit in this observable we have chosen the simplest case with just one SUSY scale,  $M_S$ , which is considered very large as compared to the electroweak scale,  $M_{EW}$ ,

$$M_{\tilde{Q}} = M_{\tilde{U}} = M_{\tilde{D}} = A_t = A_b = \mu = M_{\tilde{g}} = M_S \gg M_{EW}.$$

After performing an expansion of  $\Delta_{SQCD}$  (we use here an analogous notation as in previous sections) in inverse powers of  $M_S$  we have obtained the following result for the dominant contribution,

$$\Delta_{SQCD} = -\frac{\alpha_s}{3\pi} \frac{m_t^2}{M_S^2} \left( \frac{1}{6} + \frac{1}{24}(1 - \cot\beta)^2 + \frac{1}{6}(1 - \cot\beta) \right) + \mathcal{O}\left(\frac{m_t m_W, m_W^2, \dots}{M_S^2}\right)$$

From this result, we conclude that there is decoupling as  $M_S$  becomes large in the SQCD corrections to the dominant top decay,  $t \rightarrow W^+b$ , and this decoupling which behaves as  $(m_t^2/M_S^2)$  is not delayed. Indeed, we see in the previous equation that these corrections are not enhanced by  $\tan\beta$ . Thus, we do not expect relevant indirect signals from a heavy SUSY-QCD sector in this decay channel.

## 8 Conclusions

In this work we have studied the one-loop SQCD corrections to the partial widths of  $h^0 \rightarrow b\bar{b}$ ,  $H^+ \rightarrow t\bar{b}$  and  $t \rightarrow W^+b$  decays, in the limit of large SUSY masses. In order to understand analytically the behavior of the SQCD corrections in this limit, we have performed expansions of the one-loop partial widths that are valid for large values of the SUSY mass parameters compared to the electroweak scale. We have shown that for the SUSY mass parameters and  $M_A$  large and all of the same order, the SQCD corrections in  $h^0 \rightarrow b\bar{b}$  decay decouple like the inverse square of these

mass parameters, and the one-loop partial width  $\Gamma(h^0 \rightarrow b\bar{b})$  tends to its SM value. In this case the effective low energy theory that one obtains after integrating out all the heavy non-standard modes of the MSSM is precisely the SM. However, if the mass parameters are not all of the same size, then this behavior can be modified. If  $M_A$  is light, then the SQCD corrections to the  $\Gamma(h^0 \rightarrow b\bar{b})$  decay width do not decouple in the limit of large SUSY mass parameters. We have also presented and discussed here a similar non-decoupling SQCD correction to the  $\Gamma(H^+ \rightarrow t\bar{b})$  decay width. Given the closely related structure of the various Higgs bosons couplings to the SM fermions, one expects that similar SUSY non-decoupling effects will appear as well in other decay channels such as  $H^0 \rightarrow b\bar{b}$ ,  $A^0 \rightarrow b\bar{b}$  and  $t \rightarrow H^+b$ . In the limit of large SUSY mass parameters and light  $M_A$  the effective low-energy theory, valid at the electroweak scale, should contain two full Higgs doublets with Higgs-fermion couplings of the general type-III model [25] that have no restrictions (other than those imposed by the SM symmetries), since supersymmetry is not anymore a symmetry of this low-energy theory. The particular values of the couplings in this low-energy effective Lagrangian are generated by integrating out all the heavy SUSY particles from the original MSSM Lagrangian, and they can be computed [26]. These non-decoupling SQCD corrections can be of phenomenological interest at present and future colliders. In particular they can provide some clues in the indirect search of a heavy SUSY spectrum at the LHC [27].

We have also examined, in Higgs decays, some special cases in which there is a hierarchy among the SUSY mass parameters. In the case of maximal squark mixing with  $M_S$  large and the other SUSY mass parameters and  $M_A$  of order a common mass scale  $M$  (chosen such that  $M_{EW} \ll M \ll M_S$ ), the SQCD corrections decouple like  $M^2/M_S^2$ . Second, we examined the case of a large gluino mass with the other SUSY mass parameters of order a common mass scale  $M$  (chosen such that  $M_{EW} \ll M \ll M_{\tilde{g}}$ ). In this case we found that the SQCD corrections decouple more slowly, like  $(M/M_{\tilde{g}}) \log(M_{\tilde{g}}^2/M_S^2)$ .

Finally we have studied the dominant decay of the top quark, in the decoupling limit of large SUSY mass parameters, and we have found that the SQCD corrections decouple as  $\mathcal{O}(\frac{m_t^2}{M_S^2})$ . It will be, therefore, very difficult to look for indirect heavy SUSY signals in this channel.

## Acknowledgments

M.J.H. wish to thank Howard E. Haber and the Organizing Committee for the kind invitation to give a talk at this Symposium and for the enjoyable atmosphere at this interesting conference. S.P. acknowledges H.E. Haber for the invitation to attend this Symposium. This work has been supported in part by the Spanish Ministerio

de Educacion y Cultura under project CICYT AEN97-1678. S.P. has been partially supported by the U.S. Department of Energy under contract DE-FG03-92ER40689 and by Ramon Areces Foundation. S.R. has been partially supported by the European Union through contract ERBFMBICT972474. H.E.H. is supported in part by the U.S. Department of Energy under contract DE-FG03-92ER40689. Fermilab is operated by Universities Research Association Inc. under contract no. DE-AC02-76CH03000 with the U.S. Department of Energy.

## References

- [1] H. E. Haber and Y. Nir, Nucl. Phys. **B335**, 363 (1990); H. E. Haber, in Proceedings of the US–Polish Workshop, Warsaw, Poland, September 21–24, 1994, edited by P. Nath, T. Taylor, and S. Pokorski (World Scientific, Singapore, 1995) pp. 49–63.
- [2] A. Dobado, M. J. Herrero and S. Peñaranda, Eur. Phys. J. **C7**, 313 (1999); Eur. Phys. J. **C12**, 673 (2000); Eur. Phys. J. **C17**, 487 (2000).
- [3] T. Appelquist and J. Carazzone, Phys. Rev. **D11**, 2856 (1975).
- [4] M. Carena, S. Mrenna and C. E. M. Wagner, Phys. Rev. **D60**, 075010 (1999); Phys. Rev. **D62**, 055008 (2000).
- [5] M. Carena, J. S. Conway, H. E. Haber and J. D. Hobbs, *Report of the Tevatron Higgs Working Group*, hep-ph/0010338
- [6] H. E. Haber, M. J. Herrero, H. E. Logan, S. Penaranda, S. Rigolin and D. Temes, Phys. Rev. **D 63**, 055004 (2001),
- [7] M. J. Herrero, S. Peñaranda and D. Temes, *SUSY-QCD decoupling properties in  $H^+ \rightarrow t\bar{b}$  decay*, FTUAM 00/20; IFT-UAM/CSIC 00/42
- [8] J. F. Gunion, H. E. Haber, G. Kane and S. Dawson, *The Higgs Hunter’s Guide* (Addison–Wesley, Reading, MA, 1990) [errata: hep-ph/9302272].
- [9] H. E. Haber, *Nonminimal Higgs sector: The decoupling limit and its phenomenological implications* (1994), hep-ph/9501320.
- [10] E. Braaten and J. P. Leveille, Phys. Rev. **D22**, 715 (1980); N. Sakai, Phys. Rev. **D22**, 2220 (1980); T. Inami and T. Kubota, Nucl. Phys. **B179**, 171 (1981).
- [11] A. Dabelstein, Nucl. Phys. **B456**, 25 (1995).
- [12] J. A. Coarasa, R. A. Jiménez and J. Solà, Phys. Lett. **B389**, 312 (1996).

- [13] L. J. Hall, R. Rattazzi and U. Sarid, Phys. Rev. **D50**, 7048 (1994); R. Hempfling, Phys. Rev. **D49**, 6168 (1994); M. Carena, M. Olechowski, S. Pokorski and C. E. M. Wagner, Nucl. Phys. **B426**, 269 (1994).
- [14] D. M. Pierce, J. A. Bagger, K. Matchev and R.-J. Zhang, Nucl. Phys. **B491**, 3 (1997).
- [15] S. Heinemeyer, W. Hollik and G. Weiglein, Eur. Phys. J. **C16**, 139 (2000).
- [16] M. Carena, D. Garcia, U. Nierste and C. E. M. Wagner, Nucl. Phys. **B577**, 88 (2000).
- [17] H. Eberl, K. Hidaka, S. Kraml, W. Majerotto and Y. Yamada, Phys. Rev. **D62** 055006 (2000).
- [18] W. Hollik, in *Precision Tests of the Standard Electroweak Model*, edited by P. Langacker (World Scientific, Singapore, 1995), p. 37–116.
- [19] A. Mendez and A. Pomarol, Phys. Lett. **B252**, 461 (1990); C. S. Li and R. Oakes, Phys. Rev. **D43**, 855 (1991); A. Djouadi and P. Gambino, Phys. Rev. **D51**, 218 (1995).
- [20] R. A. Jimenez and J. Sola, Phys. Lett. **B389**, 53 (1996).
- [21] A. Bartl, H. Eberl, K. Hidaka, T. Kon, W. Majerotto and Y. Yamada, Phys. Lett. **B378**, 167 (1996).
- [22] A. Dabelstein, W. Hollik, R. A. Jimenez, C. Junger and J. Sola, Nucl. Phys. **B454**, 75 (1995).
- [23] M. Jezabek and J. H. Kühn, Nucl. Phys. **B314**, 1 (1989); *ibid* **B320**, 20 (1989); C. S. Li, R. J. Oakes and T. C. Yuan, Phys. Rev. **D43** 3759 (1991); A. Denner and T. Sack, Z. Phys. **C46** 653 (1990); Nucl. Phys. **B358**, 46 (1991).
- [24] D. Garcia, W. Hollik, R. A. Jimenez and J. Sola, Nucl. Phys. **B427**, 53 (1994); J. M. Yang and C. S. Li, Phys. Lett. **320** 117 (1994).
- [25] W. S. Hou, Phys. Lett. **B296**, 179 (1992) ; D. Chang, W. S. Hou and W. Y. Keung, Phys. Rev. **D48**, 217 (1993); D. Atwood, L. Reina and A. Soni, Phys. Rev. **D55**, 3156 (1997).
- [26] A. Dobado, M. J. Herrero and D. Temes, in progress.
- [27] A. M. Curiel, M. J. Herrero, D. Temes and J. F. de Troconiz, in progress.

# FCNC top quark decays beyond the Standard Model

KA-TP-1-2001  
UAB-FT-506  
January 2001  
hep-ph/0101294

SANTI BÉJAR<sup>a\*</sup>, JAUME GUASCH<sup>b†</sup>, JOAN SOLÀ<sup>a‡</sup>

<sup>a</sup> *Grup de Física Teòrica and Institut de Física d'Altes Energies, Universitat Autònoma de Barcelona, E-08193, Bellaterra, Barcelona, Catalonia, Spain*

<sup>b</sup> *Institut für Theoretische Physik, Universität Karlsruhe, Kaiserstraße 12, D-76128 Karlsruhe, Germany.*

Flavor Changing Neutral Current decays of the top quark within the strict context of the Standard Model are known to be extremely rare. In fact, they are hopelessly undetectable at the Tevatron, LHC and LC in any of their scheduled upgradings. Therefore, if a few of these events eventually show up in the future we will have certainly discovered new physics. We argue that this could well be the case for the LHC and the LC both within the Minimal Supersymmetric Standard Model (MSSM) and in a general two-Higgs-doublet model (2HDM), especially if we look for FCNC top quark decays into Higgs bosons.

Invited talk presented at the

5th International Symposium on Radiative Corrections  
(RADCOR–2000)

Carmel CA, USA, 11–15 September, 2000

---

\*Supported in part by CICYT under project No. AEN99-0766.

†Supported by the European Union under contract No. HPMF-CT-1999-00150.

‡Supported in part by the Direcció General de Recerca de la Generalitat de Catalunya and by CICYT under project No. AEN99-0766.

# 1 Introduction

At the tree-level there are no Flavor Changing Neutral Current (FCNC) processes in the Standard Model (SM), and at one-loop they are induced by charged-current interactions, which are GIM-suppressed. In particular, FCNC decays of the top quark into gauge bosons ( $t \rightarrow cV$ ;  $V \equiv \gamma, Z, g$ ) are very unlikely ( $BR(t \rightarrow c\gamma, Z) \sim 10^{-13}$  and  $BR(t \rightarrow cg) \sim 10^{-11}$ ) [1]. These are much smaller than the FCNC rates of a typical low-energy meson decay, e.g.  $B(b \rightarrow s\gamma) \sim 10^{-4}$ . The reason is simple: for FCNC top quark decays in the SM, the loop amplitudes are controlled by down-type quarks, mainly by the bottom quark. Therefore, the scale of the loop amplitudes is set by  $m_b^2$  and the partial widths are of order

$$\Gamma(t \rightarrow Vc) \sim |V_{tb}^* V_{bc}|^2 \alpha G_F^2 m_t m_b^4 F \sim |V_{bc}|^2 \alpha_{em}^2 \alpha m_t \left(\frac{m_b}{M_W}\right)^4 F, \quad (1)$$

where  $\alpha$  is  $\alpha_{em}$  for  $V = \gamma, Z$  and  $\alpha_s$  for  $V = g$ . The factor  $F \sim (1 - m_V^2/m_t^2)^2$  results, upon neglecting  $m_c$ , from phase space and polarization sums. The fourth power mass ratio, in parenthesis in eq. (1), stems from the GIM mechanism and is responsible for the ultralarge suppression beyond naive expectations based on pure dimensional analysis, power counting and CKM matrix elements. From that simple formula, the approximate orders of magnitude mentioned above ensue immediately.

Even more dramatic is the situation with the top quark decay into the SM Higgs boson,  $t \rightarrow cH_{SM}$ :  $BR(t \rightarrow cH_{SM}) \sim 10^{-13} - 10^{-15}$  ( $m_t = 175 \text{ GeV}$ ;  $M_Z \leq M_H \leq 2 M_W$ ) [2]. This extremely tiny rate is far out of the range to be covered by any presently conceivable high luminosity machine. On the other hand, the highest FCNC top quark rate in the SM, namely that of the gluon channel  $t \rightarrow cg$ , is still 6 orders of magnitude below the feasible experimental possibilities at the LHC. All in all the detection of FCNC decays of the top quark at visible levels (viz.  $BR(t \rightarrow cX) > 10^{-5}$ ) by the high luminosity colliders round the corner seems doomed to failure in the absence of new physics. Unfortunately, although the FCNC decay modes into electroweak gauge bosons  $V_{ew} = \gamma, Z$  may be enhanced a few orders of magnitude, it proves to be insufficient to raise the meager SM rates mentioned before up to detectable limits, and this is true both in the 2HDM – where  $BR(t \rightarrow V_{ew}c) < 10^{-6}$  [1] – and in the MSSM – where  $BR(t \rightarrow V_{ew}c) < 10^{-7}$  [3]. In this respect it is a lucky fact that these bad news need not to apply to the gluon channel, which could be barely visible ( $BR(t \rightarrow gc) \lesssim 10^{-5}$ ) both in the MSSM [4,5] and in the general 2HDM [1]. But, most significant of all, they may not apply to the non-SM Higgs boson channels  $t \rightarrow (h^0, H^0, A^0) + c$  either. As we shall show, these Higgs decay channels of the top quark could lie above the visible threshold for a parameter choice made in perfectly sound regions of parameter space.

A systematic discussion of these “gifted” Higgs channels has been made in Ref. [5] for the MSSM and more recently in Ref. [6] for the general 2HDM. Here we will present

the results in the 2HDM and the MSSM, and make a close comparison between them. We believe that this study is necessary, not only to assess what are the chances to see traces of new physics in the new colliders but also to clear up the nature of the virtual effects; in particular to disentangle whether the origin of the hypothetically detected FCNC decays of the top quark is ultimately triggered by SUSY or by some alternative renormalizable extension of the SM such as the 2HDM or generalizations thereof. Of course the alleged signs of new physics could be searched for directly through particle tagging, if the new particles were not too heavy. However, even if accessible, the corresponding signatures could be far from transparent. In contrast, the indirect approach based on the FCNC processes has the advantage that one deals all the time with the dynamics of the top quark. Thus by studying potentially new features beyond the well-known SM properties of this quark one can hopefully uncover the existence of the underlying new interactions [7].

## 2 Relevant fields and interactions

We will mainly focus our interest on the loop induced FCNC decays

$$t \rightarrow c h \quad (h = h^0, H^0, A^0), \quad (2)$$

in which any of the three possible neutral Higgs bosons from a general 2HDM can be in the final state. However, as a reference we shall compare throughout our analysis the Higgs channels with the more conventional gluon channel  $t \rightarrow c g$ .

Although other quarks could participate in the final state of these processes, their contribution is negligible. The lowest order diagrams entering these decays are one-loop diagrams in which Higgs, quarks, gauge and Goldstone bosons – in the Feynman gauge – circulate around. In the MSSM also the SUSY-partners of the above fields, namely squarks and charginos, circulate in the loops. In addition there exists the possibility that the squark-squared-mass-matrix is not simultaneously diagonal to the quark-mass-matrix. In this latter case there exist tree-level FCNC couplings in the interactions quark-squark-gluino and quark-squark-neutralino. This possibility is not unnatural. If one computes the evolution of the squark-squared-mass-matrix using the Renormalization Group Equations, assuming alignment at a certain scale (e.g. a supposed Unification Scale), one finds that non-diagonal terms for the squark-left–squark-left entries are generated [8]. We have computed the MSSM decay widths under two different approximations: in the first one we assume alignment, and the only induced FCNC are generated through the charged sector of the model with the same mixing matrix as in the SM – the CKM-matrix; in the second approach we give up the alignment hypothesis, and assume a free – though restricted by experiment [9]– squark-mass-matrix and compute the SUSY-QCD induced FCNC partial decay widths, which are the leading ones under this approximation.

Here we follow the standard notation [10], namely  $h^0, H^0$  are CP-even Higgs bosons and  $A^0$  is a CP-odd one. When the quark mass matrices are diagonalized in non-minimal extensions of the Higgs sector of the SM, the Yukawa couplings do not in general become simultaneously diagonalized, so that one would expect Higgs mediated FCNC's at the tree-level. These are of course unwanted, since they would lead to large FCNC processes in light quark phenomenology, which are stringently restricted by experiment. One has two canonical choices to get rid of them, called Type I 2HDM and Type II 2HDM [10]. The Higgs sector of the MSSM is that of a Type II 2HDM, with restrictions between the parameters due to the SUSY constraints.

When analyzing the 2HDM I, II cases we will use the following set of free parameters:

$$(m_{h^0}, m_{H^0}, m_{A^0}, m_{H^\pm}, \tan \alpha, \tan \beta), \quad (3)$$

where  $m_{H^\pm}$  is the mass of the charged Higgs companions  $H^\pm$ ,  $\tan \alpha$  defines the mixing angle  $\alpha$  in the diagonalization of the CP-even sector, and  $\tan \beta$  gives the mixing angle  $\beta$  in the CP-odd sector. The latter is a key parameter in our analysis. It is given by the quotient of the vacuum expectation values (VEV's) of the two Higgs doublets  $\Phi_{2,1}$ , viz.  $\tan \beta = v_2/v_1$  [10]. The most general (Type I or Type II) 2HDM Higgs potential subject to hermiticity,  $SU(2) \times U(1)$  and gauge invariance involves six scalar operators with six free (real) coefficients  $\lambda_i$  ( $i = 1, \dots, 6$ ) and the two VEV's [10]. We will furthermore assume that  $\lambda_5 = \lambda_6$  in the general 2HDM Higgs potential [6]. The alternative set (3) is just a (more physical) reformulation of this fact after diagonalization of the mass matrices and imposing the aforementioned set of constraints. The constraints imposed by SUSY reduce the number of free parameters in eq. (3) to two, which we take to be  $(m_{A^0}, \tan \beta)$ , since the radiative corrections to the rest of parameters (3) are large we make use of the one-loop expressions to compute them [11]<sup>1</sup>.

The two canonical types of 2HDM's only differ in the couplings to fermions but they share the rest of Feynman rules. Of particular relevance are the rules for the trilinear Higgs vertices in the 2HDM case, which depend on the Higgs boson mass differences and can be enhanced for large and small  $\tan \beta$  – see Ref. [6]. In the MSSM, however, the mass differences are correlated and one can further simplify their form to a combination of trigonometric functions of  $\alpha$  and  $\beta$ , using the relations between the parameters (3) – see Ref. [10]. We refrain from giving here the interaction Lagrangian [5,6,10,13].

Both in the generic 2HDM II and in the MSSM, the Feynman rules for the lightest CP-even Higgs,  $h^0$ , go over to the SM Higgs boson ones in the limit  $\sin(\beta - \alpha) \rightarrow 1$ . In the particular case of the MSSM, this limit is equivalent to  $m_{A^0} \rightarrow \infty$ . Moreover, in the MSSM one has  $m_{h^0} \lesssim 135 \text{ GeV}$  [12] whereas in the general Type II model there

---

<sup>1</sup>The two-loop corrections to the Higgs sector of the MSSM have also recently become available [12]. Their effect, however, cannot significantly modify our one-loop results.

is no upper bound on  $m_{h^0}$ , and by the same token the corresponding lower bound is considerably less stringent – see Ref. [6].

Since we shall perform our calculation in the on-shell scheme, we understand that the physical inputs are given by the electromagnetic coupling and the physical masses of all the particles. It should be clear that, as there are no tree-level FCNC decays of the top quark, there is no need to introduce counterterms for the physical inputs. In fact, the calculation is carried out in lowest order with respect to the effective  $tch$  and  $tcg$  couplings and so the sum of all the one-loop diagrams (as well as of certain subsets of them) should be finite in a renormalizable theory, and indeed it is.

From the interaction Lagrangians and Feynman rules it is straightforward to compute the loop induced FCNC rates for the decays (2) and  $t \rightarrow c g$  [5,6]. We shall refrain from listing the lengthy analytical formulae. The computation in the MSSM was reported in great detail in Ref. [5], and the one in the 2HDM [6] is very similar. Therefore, we will limit ourselves to exhibit the final numerical results. The fiducial ratio on which we will apply our numerical computation is the following:

$$B^j(t \rightarrow h + c) = \frac{\Gamma^j(t \rightarrow h + c)}{\Gamma(t \rightarrow W^+ + b) + \Gamma^j(t \rightarrow H^+ + b)} , \quad (4)$$

for each Type  $j = I, II$  of 2HDM and the MSSM and for each neutral Higgs boson  $h = h^0, H^0, A^0$ . While this ratio is not the total branching fraction, it is enough for most practical purposes and it is useful in order to compare with previous results in the literature. We define the fiducial branching ratio for  $t \rightarrow g + c$  in a similar way.

We have performed a fully-fledged independent analytical and numerical calculation of  $\Gamma^j(t \rightarrow g + c)$  at one-loop in the context of 2HDM I, II and the MSSM. Where there is overlapping, we have checked the numerical results of Ref. [1]<sup>2</sup>.

Charged Higgs bosons from Type II models are subject to an indirect bound from the experimental measurement by CLEO of the branching fraction  $BR(B \rightarrow X_s \gamma)$  [14]. From the various analysis in the literature one finds  $m_{H^\pm} > (165 - 200) GeV$  for virtually any  $\tan\beta \gtrsim 1$  [15,16]. This bound does not apply to Type I models. Therefore, in principle the top quark decay  $t \rightarrow H^+ + b$  is still possible in 2HDM I; but also in 2HDM II, if  $m_{H^\pm}$  lies near the lowest end of the previous bound, and in this case that decay can contribute to the denominator of eq. (4). In SUSY models this limit does not apply provided  $\mu A_t < 0$  – see e.g. [17].

### 3 $t \rightarrow ch$ and $t \rightarrow cg$ in the MSSM

Under the alignment hypothesis FCNC's are generated at the one-loop level through the charged interactions of quarks with Higgs bosons and squarks with charginos, that

---

<sup>2</sup>In Ref. [1]  $B(t \rightarrow g + c)$  is defined without including the charged Higgs channel contribution in the fiducial branching ratio. The agreement is achieved, however, only if it is included.

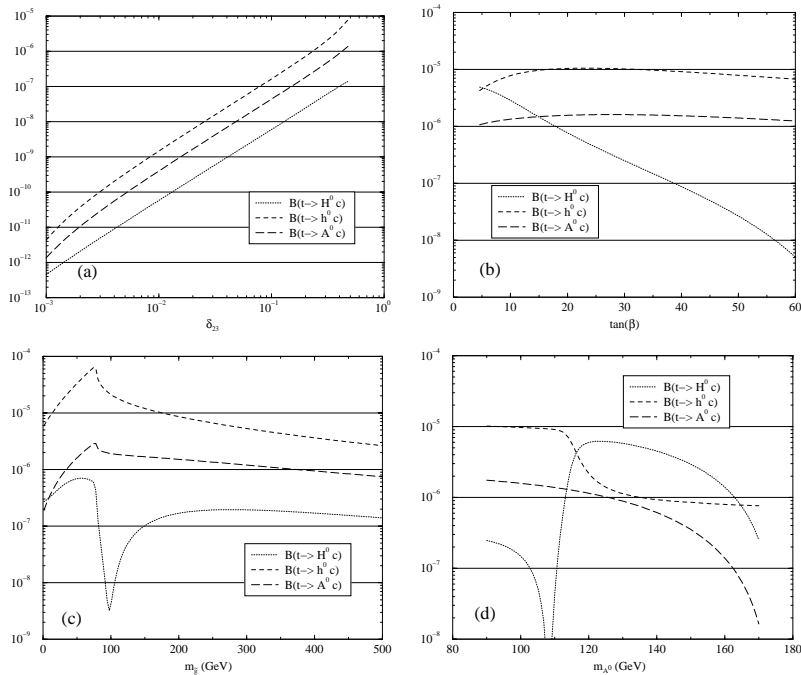


Figure 1: Evolution of the SUSY-QCD contributions to the ratio (4) with **(a)** the mixing parameter  $\delta_{23}$  between the 2nd and 3rd squark generations; **(b)**  $\tan\beta$ ; **(c)** the gluino mass  $m_{\tilde{g}}$ ; and **(d)** the pseudoscalar Higgs mass  $M_{A^0}$ . The rest of inputs are given in eq. (6)

is, they are of electroweak (EW) nature. In this case the largest rates are driven by the trilinear scalar coupling  $\tilde{d}_a \tilde{d}_b h$ , although the down-type-quark loops contributions are non-negligible. As a consequence the largest FCNC decay rates are obtained at large  $\tan\beta$ .

Giving up alignment the leading FCNC rates are driven by means of the SUSY-QCD tree-level vertex  $u_a \tilde{u}_b \tilde{g}$  for  $a \neq b$ . The mixing terms between generations are encoded in the parameter

$$\delta_{ij} \equiv \frac{(M_{LL}^2)_{ij}}{m_i m_j} \quad (i \neq j), \quad (5)$$

where  $(M_{LL}^2)_{ij}$  is the non-diagonal squared-mass-matrix element between the  $i$ th and  $j$ th generations, and  $m_i$  is the mass parameter of the  $i$ th generation. Low energy experiments are used to give upper bounds to the  $\delta_{ij}$ , but, whereas the mixing between the 1st and 2nd generation are strongly restricted, the one between the 2nd and the 3rd turns out to be basically free [9], and this is the one which has a greatest impact in the process under study. We assume that inter-generational mixing only exists between the left-handed squarks, since this is the most natural scenario [8]. A detailed

analysis showed that the presence of mixing in the right-handed squark sector does not lead to a significant increase of the computed branching ratios [4,5].

Since the EW contributions lie about two orders of magnitude below the SUSY-QCD ones [5], we will concentrate in the latter ones. In Fig. 1 we present the fiducial ratio (4) as a function of the most important parameters: the mixing parameter between the 2nd and the 3rd generation  $\delta_{23}$ , eq. (5); the gluino mass  $m_{\tilde{g}}$ ;  $\tan\beta$ ; and the mass of the pseudoscalar Higgs  $m_{A^0}$ . The set of reference parameters used is:

$$\begin{aligned} \tan\beta &= 35, m_{A^0} = 100\text{GeV}, \mu = -200\text{GeV}, A_t = A_q = -A_b = 300\text{GeV}, \\ m_{\tilde{t}_1} &= 150\text{GeV}, m_{\tilde{q}} \simeq 200\text{GeV}, m_{\tilde{g}} = 180\text{GeV}, \delta_{12} = \delta_{13} = 0.03, \delta_{23} = 0.5. \quad (6) \\ m_t &= 175\text{GeV}, m_b = 5\text{GeV}, \alpha_s(m_t) = 0.11, V_{cb} = 0.040, \end{aligned}$$

and the remaining ones are as in [18].

As anticipated, the most important parameter is  $\delta_{23}$ . In Fig. 1a we see that an increase in three orders of magnitude on  $\delta_{23}$  corresponds to a change in six orders of magnitude on  $B(t \rightarrow ch)$ , a fact that can be traced down to the quadratic dependence of the latter on  $\delta_{23}$ . The dependence on  $\tan\beta$  is rather mild since it enters the amplitude through the  $\tilde{u}_\alpha \tilde{u}_\beta h$  coupling as  $1/\tan\beta$ , and also indirectly through the determination of the squark masses. For the chosen set of parameters (6) it has a non-negligible impact on the  $H^0$  channel (Fig. 1b). Although all Feynman diagrams proceed through gluino exchange, the gluino mass turns out not to be a critical quantity. In Fig. 1c we see that the decoupling of the gluino is slow, a fact observed also in other Higgs bosons observables related to the top quark [13]. This fact can be traced back to the presence of chirality-changing couplings, which imply a corresponding gluino mass-insertion in the amplitude. Finally in Fig. 1d we see that the smallest value for the  $H^0$  branching ratio is not due to the smaller phase space available, but to the value of the couplings. In fact  $B(t \rightarrow cH^0)$  grows with  $m_{A^0}$  (and thus with  $m_{H^0}$ ), until it dies out near the phase space kinematical limit.

In Fig. 2 we display the theoretical prediction for  $B(t \rightarrow cg)$  as a function of the gluino mass and  $\delta_{23}$ , assuming  $m_{H^\pm} > m_t$ . The values for the ratio are below that of the neutral Higgs bosons channels, but still some orders of magnitude above the SM expected value for experimentally allowed values of  $m_{\tilde{g}} > 180\text{GeV}$ . Again the branching ratio grows quadratically with the mixing parameter  $\delta_{23}$  (Fig. 2a). In contrast with the Higgs bosons channels (Fig. 1c), the gluon channel  $B(t \rightarrow cg)$  shows a fast decoupling with the gluino mass (Fig. 2b).

In Fig. 3 we present the maximum rates for  $B(t \rightarrow ch)$  and  $B(t \rightarrow cg)$  – eq. (4) – in the MSSM. We have made a comprehensive scan of the MSSM parameter space, taking into account present constraints from experiment. Perhaps the most noticeable result is that the decay into the lightest MSSM Higgs boson ( $t \rightarrow ch^0$ ) is the one that can be maximally enhanced, and reaching values of order  $B^{\text{MSSM}}(t \rightarrow ch^0) \sim 10^{-4}$  that stay fairly stable all over the parameter space. The FCNC top quark decay into the lightest Higgs scalar can have an observable ratio in a large portion of the

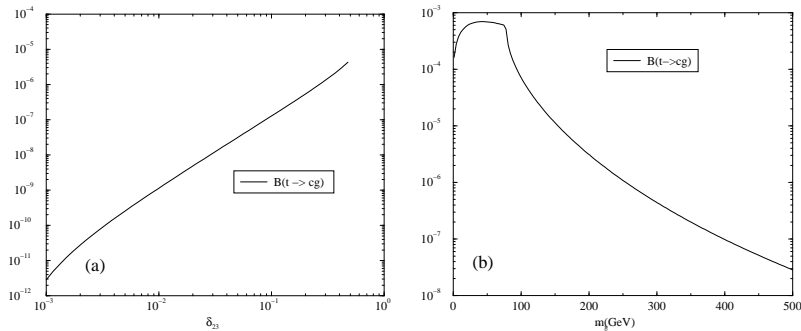


Figure 2: Evolution of the SUSY-QCD effects on  $B(t \rightarrow cg)$  as a function of **(a)** the mixing parameter  $\delta_{23}$ , and **(b)** the gluino mass  $m_{\tilde{g}}$ .

parameter space, and in particular for almost all the range of Higgs boson masses. Needless to say, not all of the maxima can be simultaneously attained as they are obtained for different values of the parameters. The maximum FCNC rate of the gluon channel in the MSSM reads (Fig. 3b)  $B^{\text{MSSM}}(t \rightarrow cg) \lesssim 10^{-5}$ , but it never really reaches the critical value  $10^{-5}$ , which can be considered as the visible threshold for the next generation of colliders (see Sec. 5).

#### 4 $t \rightarrow ch$ and $t \rightarrow cg$ in the general 2HDM

In the 2HDM case a highly relevant parameter is  $\tan \beta$ , which must be restricted to the approximate range

$$0.1 < \tan \beta \lesssim 60 \quad (7)$$

in perturbation theory. It is to be expected from the various couplings involved in the processes under consideration that the low  $\tan \beta$  region could be relevant for both the Type I and Type II 2HDM's. In contrast, the high  $\tan \beta$  region is only potentially important for the Type II. However, the eventually relevant regions of parameter space are also determined by the value of the mixing angle  $\alpha$ , as we shall see below.

Of course there are several restrictions that must be respected by our numerical analysis. First, the one-loop corrections to the  $\rho$ -parameter from the 2HDM sector cannot deviate from the reference SM contribution in more than one per mil [18]:  $|\delta\rho^{2\text{HDM}}| \leq 0.001$ . From the analytical expression for  $\delta\rho$  in the general 2HDM we have introduced this numerical condition in our codes.

For both models we have imposed the condition that the (absolute value) of the trilinear Higgs self-couplings do not exceed the maximum unitarity limit tolerated for the SM trilinear coupling:  $|\lambda_{HHH}| \leq \left| \lambda_{HHH}^{(SM)}(m_H = 1 \text{ TeV}) \right| = 3g(1 \text{ TeV})^2/(2M_W)$ .

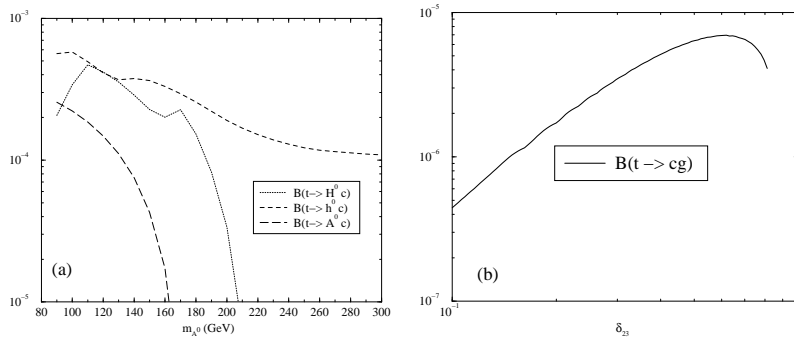


Figure 3: Maximum value of  $B(t \rightarrow ch)$  in the MSSM, obtained by taking into account only the SUSY-QCD contributions, as a function of  $m_{A0}$ ; **(b)** maximum value of  $B(t \rightarrow cg)$  as a function of the intergenerational mixing parameter  $\delta_{23}$  in the LH sector. In all cases the scanning for the rest of parameters of the MSSM has been performed within the phenomenologically allowed region.

In the MSSM case it was not necessary to impose this restriction because the Higgs self-couplings are purely gauge. As for the  $\delta\rho$  constraint in the MSSM, we have checked that it is satisfied. It is in the 2HDM case that one has to keep an eye very seriously on  $\delta\rho$  because it grows with the Higgs boson mass squared differences, whereas in the MSSM the mass differences are much more tamed in all sectors of the theory.

The combined set of independent conditions turns out to be quite effective in narrowing down the permitted region in the parameter space, as can be seen in Figs. 4-7 where we plot the fiducial FCNC rate (4) and the corresponding one for the gluon channel versus the parameters (3). The cuts in some of these curves just reflect the fact that at least one of these conditions is not fulfilled.

After scanning the parameter space, we see in Figs. 4-5 that the 2HDM I (resp. 2HDM II) prefers low values (resp. high values) of  $\tan\alpha$  and  $\tan\beta$  for a given channel, e.g.  $t \rightarrow h^0 c$ . Therefore, the following choice of mixing angles will be made to optimize the presentation of our numerical results:

$$2\text{HDM I} : \tan\alpha = \tan\beta = 1/4 ; \quad 2\text{HDM II} : \tan\alpha = \tan\beta = 50 . \quad (8)$$

We point out that, for the same values of the masses, one obtains the same maximal FCNC rates for the alternative channel  $t \rightarrow H^0 c$  provided one just substitutes  $\alpha \rightarrow \pi/2 - \alpha$ . Equation (8) defines the eventually relevant regions of parameter space and, as mentioned above, depend on the values of the mixing angles  $\alpha$  and  $\beta$ , namely  $\beta \simeq \alpha \simeq 0$  for Type I and  $\beta \simeq \alpha \simeq \pi/2$  for Type II. Despite naive expectations, and due to the structure of the Yukawa couplings of Type II models, there is a cancellation of the contributions in the low  $\tan\beta$  end. This is in contrast to Type I models where

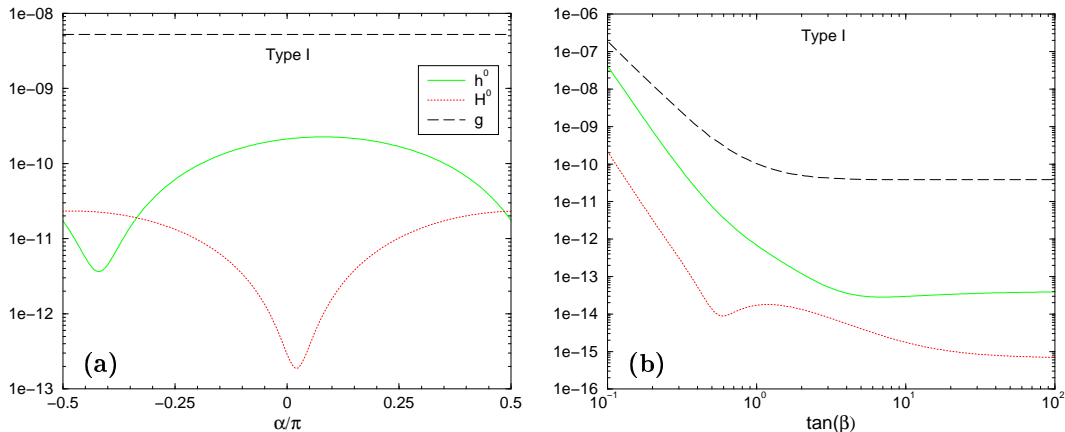


Figure 4: Evolution of the FCNC top quark fiducial ratio (4) – and the corresponding one for  $B(t \rightarrow g + c)$  – in Type I 2HDM versus: **(a)** the mixing angle  $\alpha$  in the CP-even Higgs sector, in units of  $\pi$ ; **(b)**  $\tan\beta$ . The values of the fixed parameters are as in eqs. (8) and (9).

the maximal ratios occur. So the most favoured region of Type II models definitely is the high  $\tan\beta$  one.

Due to the  $\alpha \rightarrow \pi/2 - \alpha$  symmetry of the maximal rates for the CP-even Higgs channels, it is enough to concentrate the numerical analysis on one of them, but one has to keep in mind that the other channel yields the same rate in another region of parameter space. Whenever a mass has to be fixed, we choose conservatively the following values for both models:

$$m_{h^0} = 100 \text{ GeV}, \quad m_{H^0} = 150 \text{ GeV}, \quad m_{A^0} = m_{H^\pm} = 180 \text{ GeV}. \quad (9)$$

The variation of the results with respect to the masses is studied in Figs. 6-7. In particular, in Fig. 6 we can see the (scanty) rate of the channel  $t \rightarrow A^0 c$  when it is kinematically allowed. This is easily understood as it is the only one that does not have trilinear couplings with the other Higgs particles. While it does have trilinear couplings involving Goldstone bosons, these are not enhanced. The crucial role played by the trilinear Higgs self-couplings in our analysis cannot be underestimated as they can be enhanced by playing around with both (large or small)  $\tan\beta$  and also with the mass splittings among Higgses. This feature is particularly clear in Fig. 6a where the rate of the channel  $t \rightarrow h^0 c$  is dramatically increased at large  $m_{A^0}$ , for fixed values of the other parameters and preserving our list of constraints.

From Figs. 4a and 4b it is pretty clear that the possibility to see FCNC decays of the top quark into Type I Higgs bosons is plainly hopeless even in the most favorable regions of parameter space – the lowest (allowed)  $\tan\beta$  end. In fact, the highest rates remain neatly down  $10^{-6}$ , and therefore they are (at least) one order of magnitude

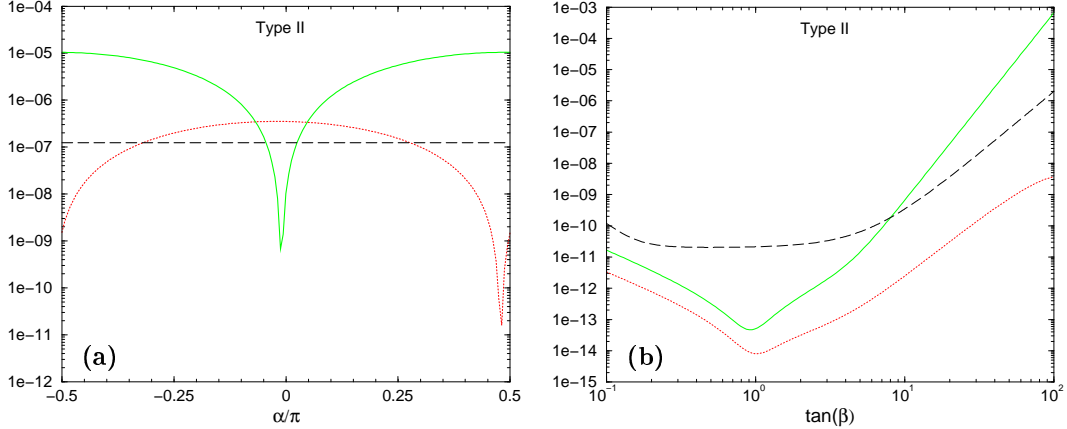


Figure 5: As in Fig. 4, but for the 2HDM II. The plot in (b) continues above the bound in eq. (7) just to better show the general trend.

below the threshold sensibility of the best high luminosity top quark factory in the foreseeable future (see Section 5).

Fortunately, the meager situation just described does not replicate for Type II Higgs bosons. For, as shown in Figs. 5a and 5b, the highest potential rates are of order  $10^{-4}$ , and so there is hope for being visible. In this case the most favorable region of parameter space is the high  $\tan\beta$  end in eq. (7). Remarkably, there is no need of risking values over and around 100 to obtain the desired rates. But it certainly requires to resort to models whose hallmark is a large value of  $\tan\beta$  of order or above  $m_t/m_b \gtrsim 35$ . As for the dependence of the FCNC rates on the various Higgs boson masses (Cf. Figs. 6-7) we see that for large  $m_{A^0}$  the decay  $t \rightarrow h^0 c$  can be greatly enhanced as compared to  $t \rightarrow g c$ . We also note (from the combined use of Figs. 5b, 6a and 6b) that in the narrow range where  $t \rightarrow H^+ b$  could still be open in the 2HDM II, the rate of  $t \rightarrow h^0 c$  becomes the more visible the larger and larger is  $\tan\beta$  and  $m_{A^0}$ . Indeed, in this region one may even overshoot the  $10^{-4}$  level without exceeding the upper bound (7) while also keeping under control the remaining constraints. Finally, the evolution of the rate (4) and  $B(t \rightarrow g + c)$  with respect to the two CP-even Higgs boson masses is shown in Figs. 7a and 7b.

## 5 Discussion and conclusions

In the near and middle future, with the upgrades of the Tevatron (Run II, TeV33), the advent of the LHC, and the construction of an  $e^+e^-$  linear collider (LC), new results on top quark physics, and possibly also on Higgs physics, will be obtained. With datasets from LHC and LC increasing to several  $100fb^{-1}/\text{year}$  in the high-

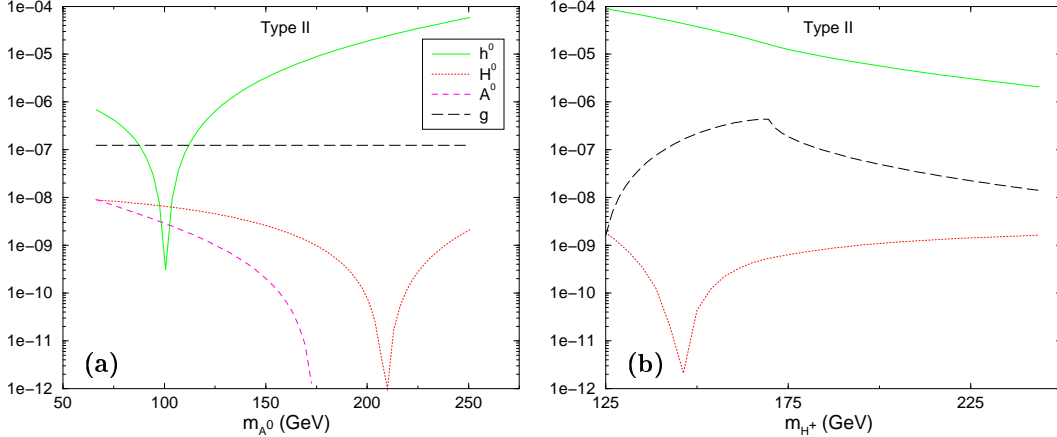


Figure 6: Evolution of the FCNC top quark fiducial ratios (4) – and the corresponding one for  $B(t \rightarrow g + c)$  – in Type II 2HDM versus: **(a)** the CP-odd Higgs boson mass  $m_{A^0}$ ; **(b)** the charged Higgs boson mass  $m_{H^\pm}$ . The values of the fixed parameters are as in eqs. (8) and (9). The plot in (b) starts below the bound  $m_{H^\pm} > 165 \text{ GeV}$  mentioned in the text to better show the general trend.

luminosity phase, one should be able to pile up an enormous wealth of statistics on top quark decays. Therefore, these machines should be very useful to analyze rare decays of the top quark, viz. decays whose branching fractions are extremely small ( $\lesssim 10^{-5}$ ).

The sensitivities to FCNC top quark decays for  $100 \text{ fb}^{-1}$  of integrated luminosity in the relevant colliders are estimated to be [19]:

$$\begin{aligned} \text{LHC} : B(t \rightarrow cX) &\gtrsim 5 \times 10^{-5}, & \text{LC} : B(t \rightarrow cX) &\gtrsim 5 \times 10^{-4}, \\ \text{TEV33} : B(t \rightarrow cX) &\gtrsim 5 \times 10^{-3}. \end{aligned} \quad (10)$$

This estimation has been confirmed by a full signal-background analysis for the hadron colliders and also for the LC in the case of gauge boson decays [20]. From these experimental expectations and our numerical results it becomes patent that whilst the Tevatron will remain essentially blind to this kind of physics, the LHC and the LC will have a significant potential to observe FCNC decays of the top quark beyond the SM. Above all there is a possibility to pin down top quark decays into neutral Higgs particles, eq. (2), within the framework of the general 2HDM II provided  $\tan \beta \gtrsim m_t/m_b \sim 35$ , and within the MSSM provided  $\delta_{23}$ –eq. (5)– is large. The maximum rates are of order  $10^{-4}$  in both models and correspond to the two CP-even scalars. In the MSSM the lightest Higgs boson is highlighted all over the  $m_{A^0}$  range. This conclusion is remarkable from the practical (quantitative) point of view, and also qualitatively because the top quark decay into the SM Higgs particle is the less favorable top quark FCNC rate in the SM. On the other hand, we deem practically hopeless to see FCNC

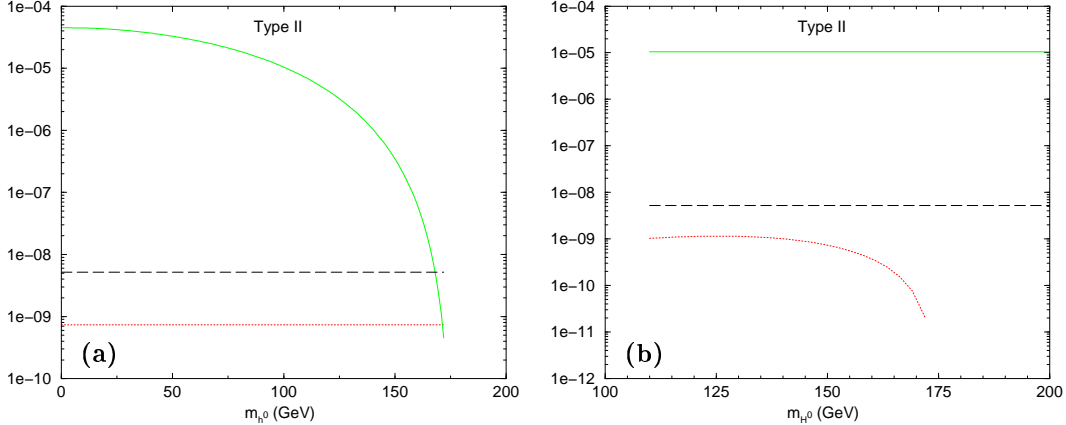


Figure 7: As in Fig. 6, but plotting versus: **(a)** the lightest CP-even Higgs boson mass  $m_{h^0}$ ; **(b)** the heaviest CP-even Higgs boson mass  $m_{H^0}$ .

decays of the top quark in a general 2HDM I for which the maximum rates are of order  $10^{-7}$ . This order of magnitude cannot be enhanced unless one allows  $\tan\beta \ll 0.1$ , but the latter possibility is unrealistic because perturbation theory breaks down and therefore one cannot make any prediction within our approach.

We have made a parallel numerical analysis of the gluon channel  $t \rightarrow c g$ . We confirm that this is another potentially important FCNC mode of the top quark in extensions of the SM [1,4,5,6] but, unfortunately, it still falls a bit too short to be detectable. The maximum rates for this channel lie below  $10^{-6}$  in the 2HDM I (for  $\tan\beta > 0.1$ ) and in the 2HDM II (for  $\tan\beta < 60$ ), and below  $10^{-5}$  for the MSSM, and so it will be hard to deal with it even at the LHC.

We are thus led to the conclusion that the Higgs channels (2), more specifically the CP-even ones, give the highest potential rates for top quark FCNC decays in a general 2HDM II and the MSSM. Most significant of all: they are *the only* FCNC decay modes of the top quark, within the simplest renormalizable extensions of the SM, that have a real chance to be seen in the next generation of high energy, high luminosity, colliders.

Although the 2HDM II and the MSSM show similar behaviour, there exist some conspicuous differences on which we wish to elaborate a bit in what follows. First, in the general 2HDM II the two channels  $t \rightarrow (h^0, H^0) c$  give the same maximum rates, provided we look at different (disjoint) regions of the parameter space. The  $t \rightarrow A^0 c$  channel is, as mentioned, negligible with respect to the CP-even modes. Hereafter we will discard this FCNC top quark decay mode from our discussions within the 2HDM context. On the other hand, in the MSSM there is a most distinguished channel, viz.  $t \rightarrow h^0 c$ , which can be high-powered by the SUSY stuff all over the parameter space. In this framework the mixing angle  $\alpha$  becomes stuck once  $\tan\beta$  and the rest of

the independent parameters are given, and so there is no possibility to reconvert the couplings between  $h^0$  and  $H^0$  as in the 2HDM. Still, we must emphasize that in the MSSM the other two decays  $t \rightarrow H^0 c$  and  $t \rightarrow A^0 c$  can be competitive with  $t \rightarrow h^0 c$  in certain portions of parameter space. For example,  $t \rightarrow H^0 c$  becomes competitive when the pseudoscalar mass is in the range  $110 \text{ GeV} < m_{A^0} \lesssim 170 \text{ GeV}$  – Cf. Fig. 1d. The possibility of having more than one FCNC decay (2) near the visible level is a feature which is virtually impossible in the 2HDM II. Second, the reason why  $t \rightarrow h^0 c$  in the MSSM is so especial is that it is the only FCNC top quark decay (2) which is always kinematically open throughout the whole MSSM parameter space, while in the 2HDM all of the decays (2) could be, in the worst possible situation, dead closed. Nevertheless, this is not the most likely situation in view of the fact that all hints from high precision electroweak data seem to recommend the existence of (at least) one relatively light Higgs boson [21,22]. This is certainly an additional motivation for our work, as it leads us to believe that in all possible (renormalizable) frameworks beyond the SM, and not only in SUSY, we should expect that at least one FCNC decay channel (2) could be accessible. Third, the main origin of the maximum FCNC rates in the MSSM traces back to the tree-level FCNC couplings of the gluino [5]. These are strong couplings, and moreover they are very weakly restrained by experiment. In the absence of such gluino couplings, or perhaps by further experimental constraining of them in the future, the FCNC rates in the MSSM would boil down to just the EW contributions, to wit, those induced by charginos, squarks and also from SUSY Higgses. The associated SUSY-EW rate is of order  $10^{-6}$  at most [5], and therefore it is barely visible, most likely hopeless even for the LHC. In contrast, in the general 2HDM the origin of the contributions is purely EW and the maximum rates are two orders of magnitude higher than the full SUSY-EW effects in the MSSM. It means that we could find ourselves in the following situation. Suppose that the FCNC couplings of the gluino get severely restrained in the future and that we come to observe a few FCNC decays of the top quark into Higgs bosons, perhaps at the LHC and/or the LC. Then we would immediately conclude that these Higgs bosons could not be SUSY-MSSM, whilst they could perhaps be CP-even members of a 2HDM II. Fourth, the gluino effects are basically insensitive to  $\tan \beta$ , implying that the maximum MSSM rates are achieved equally well for low, intermediate or high values of  $\tan \beta$ , whereas the maximum 2HDM II rates (comparable to the MSSM ones) are attained only for high  $\tan \beta$ .

The last point brings about the question of whether it would be possible to discern between different models if these decays are detected. The answer is, most likely yes. There are many possibilities and corresponding strategies, but we will limit ourselves to point out some of them. For example, let us consider the type of signatures involved in the tagging of the Higgs channels. In the favorite FCNC region (8) of the 2HDM II, the combined decay  $t \rightarrow h c \rightarrow c b \bar{b}$  is possible only for  $h^0$  or for  $H^0$ , but not for both – Cf. Fig. 5a – whereas in the MSSM,  $h^0$  together with  $H^0$ , are

highlighted for  $110 \text{ GeV} < m_{A^0} < m_t$ , with no preferred  $\tan \beta$  value. And similarly,  $t \rightarrow A^0 c$  is also non-negligible for  $m_{A^0} \lesssim 120 \text{ GeV}$  – Cf. Fig. 1d. Then the process  $t \rightarrow h c \rightarrow cb\bar{b}$  gives rise to high  $p_T$  charm-quark jets and a recoiling  $b\bar{b}$  pair with large invariant mass. It follows that if more than one distinctive signature of this kind would be observed, the origin of the hypothetical Higgs particles could not probably be traced back to a 2HDM II.

One might worry that in the case of  $h^0$  and  $H^0$  they could also (in principle) decay into electroweak gauge boson pairs  $h^0, H^0 \rightarrow V_{ew} \bar{V}_{ew}$ , which in some cases could be kinematically possible. But this is not so in practice for the 2HDM II [6]. Again, at variance with this situation, in the MSSM case  $H^0 \rightarrow V_{ew} \bar{V}_{ew}$  is perfectly possible – not so  $h^0 \rightarrow V_{ew} \bar{V}_{ew}$  due to the aforementioned upper bound on  $m_{h^0}$  – because  $\tan \beta$  has no preferred value in the most favorable MSSM decay region of  $t \rightarrow H^0 c$ . Therefore, detection of a high  $p_T$  charm-quark jet against a  $V_{ew} \bar{V}_{ew}$  pair of large invariant mass could only be advantageous in the MSSM, not in the 2HDM. Similarly, for  $\tan \beta \gtrsim 1$  the decay  $H^0 \rightarrow h^0 h^0$  (with real or virtual  $h^0$ ) is competitive in the MSSM in a region where the parent FCNC top quark decay is also sizeable. Again this is impossible in the 2HDM II and therefore it can be used to distinguish the two (SUSY and non-SUSY) Higgs frames.

Finally, even if we place ourselves in the high  $\tan \beta$  region both for the MSSM and the 2HDM II, then the two frameworks could still possibly be separated provided that two Higgs masses were known, perhaps one or both of them being determined from the tagged Higgs decays themselves, eq. (2). Suppose that  $\tan \beta$  is numerically known (from other processes or from some favorable fit to precision data), then the full spectrum of MSSM Higgs bosons would be approximately determined (at the tree level) by only knowing one Higgs mass, a fact that could be used to check whether the other measured Higgs mass becomes correctly predicted. Of course, the radiative corrections to the MSSM Higgs mass relations can be important at high  $\tan \beta$  [12], but these could be taken into account from the approximate knowledge of the relevant sparticle masses obtained from the best fits available to the precision measurements within the MSSM. If there were significant departures between the predicted mass for the other Higgs and the measured one, we would probably suspect that the tagged FCNC decays into Higgs bosons should correspond to a non-supersymmetric 2HDM II.

At the end of the day we see that even though the maximum FCNC rates for the MSSM and the 2HDM II are both of order  $10^{-4}$  – and therefore potentially visible – at some point on the road it should be possible to disentangle the nature of the Higgs model behind the FCNC decays of the top quark. Needless to say, if all the recent fuss at CERN [21] about the possible detection of a Higgs boson would eventually be confirmed in the future (e.g. by the LHC), this could still be interpreted as the discovery of one neutral member of an extended Higgs model.

We emphasize our most essential conclusions in a nutshell: i) Detection of FCNC top quark decay channels into a neutral Higgs boson would be a blazing signal of

physics beyond the SM; ii) There is a real chance for seeing rare events of that sort both in generic Type II 2HDM's and in the MSSM. The maximum rates for the leading FCNC processes (2) and  $t \rightarrow c g$  in the 2HDM II (resp. in the MSSM) satisfy the relations

$$BR(t \rightarrow g c) < 10^{-6}(10^{-5}) < BR(t \rightarrow h c) \sim 10^{-4}, \quad (11)$$

where it is understood that  $h$  is  $h^0$  or  $H^0$ , but not both, in the 2HDM II; whereas  $h$  is most likely  $h^0$ , but it could also be  $H^0$  and  $A^0$ , in the MSSM ; iii) Detection of more than one Higgs channel would greatly help to unravel the type of underlying Higgs model.

The pathway to seeing new physics through FCNC decays of the top quark is thus potentially open. It is now an experimental challenge to accomplish this program using the high luminosity super-colliders round the corner.

## Acknowledgments

One of the authors (J.S) would like to thank H. Haber and T. Junk for helpful discussions. J.G. thanks S. Peñaranda for suggestions.

## References

- [1] G. Eilam, J. L. Hewett, A. Soni, *Phys. Rev.* **D44** (1991) 1473–1484.
- [2] B. Mele, S. Petrarca, A. Soddu, *Phys. Lett.* **B435** (1998) 401, [hep-ph/9805498](#); G. Eilam, J. L. Hewett, A. Soni, *Phys. Rev.* **D59** (1999) 039901, Erratum.
- [3] J. L. Lopez, D. V. Nanopoulos, R. Rangarajan, *Phys. Rev.* **D56** (1997) 3100–3106, [hep-ph/9702350](#).
- [4] G. M. de Divitiis, R. Petronzio, L. Silvestrini, *Nucl. Phys.* **B504** (1997) 45–60, [hep-ph/9704244](#).
- [5] J. Guasch, J. Solà, *Nucl. Phys.* **B562** (1999) 3–28, [hep-ph/9906268](#).
- [6] S. Béjar, J. Guasch, J. Solà, [hep-ph/0011091](#).
- [7] M. Beneke, I. Efthymiopoulos, M.L. Mangano, J. Womersley (conveners), *Top Quark Physics*, proc. of the workshop *Standard Model physics (and more) at the LHC*, p. 419, eds. G. Altarelli and M.L. Mangano, [hep-ph/0003033](#).
- [8] M. J. Duncan, *Nucl. Phys.* **B221** (1983) 285; *Phys. Rev.* **D31** (1985) 1139.

- [9] F. Gabbiani *et al.*, *Nucl. Phys.* **B477** (1996) 321–352, [hep-ph/9604387](#);  
M. Misiak, S. Pokorski, J. Rosiek, *Supersymmetry and FCNC Effects*, in:  
“Heavy Flavours II”, p. 795, eds. A.J. Buras, M. Lindner, Advanced Series on  
directions in High Energy Physics, World Scientific 1998, [hep-ph/9703442](#).
- [10] J. Gunion, H. Haber, G. Kane, S. Dawson, *The Higgs Hunter’s Guide*  
(Addison-Wesley, Menlo-Park, 1990).
- [11] A. Dabelstein, *Z. Phys.* **C67** (1995) 495–512, [hep-ph/9409375](#); *Nucl. Phys.*  
**B456** (1995) 25–56, [hep-ph/9503443](#).
- [12] M. Carena *et al.*, *Nucl. Phys.* **B580** (2000) 29–57, [hep-ph/0001002](#);  
J. R. Espinosa, R.-J. Zhang, *Nucl. Phys.* **B586** (2000) 3–38, [hep-ph/0003246](#),  
and references therein.
- [13] J. Guasch, R. A. Jiménez, J. Solà, *Phys. Lett.* **B360** (1995) 47–56,  
[hep-ph/9507461](#); J. A. Coarasa *et al.*, *Eur. Phys. J.* **C2** (1998) 373,  
[hep-ph/9607485](#).
- [14] M. S. Alam *et al.*, CLEO Collaboration, *Phys. Rev. Lett.* **74** (1995) 2885–2889;  
CLEO Collaboration, proc. of the *29th International Conference on*  
*High-Energy Physics (ICHEP 98)*, Vancouver, B.C., Canada, 1998; S. Ahmed  
*et al.*, CLEO Collaboration, [hep-ex/9908022](#).
- [15] F. M. Borzumati, C. Greub, *Phys. Rev.* **D58** (1998) 074004, [hep-ph/9802391](#);  
*ibid.* **D59** (1999) 057501, [hep-ph/9809438](#); Proc. of ICHEP 98, Vancouver,  
Canada, 23-29 Jul 1998, vol. 2, 1735-1739; [hep-ph/9810240](#).
- [16] P. H. Chankowski, M. Krawczyk, J. Zochowski, *Eur. Phys. J.* **C11** (1999) 661,  
[hep-ph/9905436](#), and references therein.
- [17] M. Ciuchini *et al.*, *Nucl. Phys.* **B534** (1998) 3, [hep-ph/9806308](#); M. Carena *et*  
*al.*, [hep-ph/0010003](#); D. Garcia, these proceedings, [hep-ph/0101206](#).
- [18] D. E. Groom *et al.*, *Eur. Phys. J.* **C15** (2000) 1.
- [19] R. Frey *et al.*, FERMILAB-CONF-97-085, April 1997, [hep-ph/9704243](#).
- [20] J. A. Aguilar-Saavedra, G. C. Branco, *Phys. Lett.* **B495** (2000) 347–356,  
[hep-ph/0004190](#); J. A. Aguilar-Saavedra, [hep-ph/0012305](#).
- [21] T. Junk, these proceedings, [hep-ex/0101015](#),
- [22] K. Hagiwara, these proceedings.

LTH 492  
July 30, 2001  
hep-ph/0101159

# Anomaly Mediated Supersymmetry Breaking, D-terms and R-symmetry

D.R.T. JONES\*

*Department of Mathematical Sciences  
University of Liverpool, Liverpool L69 3BX, U.K.*

We explore two distinct resolutions to the tachyonic slepton puzzle in the Anomaly Mediated Supersymmetry Breaking scenario. Both are based on extending the MSSM by an anomaly free  $U_1$  symmetry, and in both cases exact RG invariance is preserved.

Presented at the

5th International Symposium on Radiative Corrections  
(RADCOR-2000)

Carmel CA, USA, 11–15 September, 2000

---

\*Work supported by the Leverhulme Trust and by PPARC

# 1 Introduction

Recently there has been interest in a specific and predictive framework for the origin of soft supersymmetry breaking within the MSSM, known as Anomaly Mediated Supersymmetry Breaking (AMSB). The basic AMSB solution is given by[1]:

$$\begin{aligned} M &= M_0 \frac{\beta_g}{g} \\ h^{ijk} &= -M_0 \beta_Y^{ijk} \\ (m^2)^i_j &= \frac{1}{2} |M_0|^2 \mu \frac{d\gamma^i_j}{d\mu}. \end{aligned} \tag{1}$$

where  $M$  is the gaugino mass,  $h^{ijk}$  the  $\phi^3$  coupling  $Y^{ijk}$  the superpotential Yukawa coupling and  $(m^2)^i_j$  the  $\phi\phi^*$ -mass. They are all given in terms of the gravitino mass,  $M_0$ , and the RG functions  $\beta_g$  and  $\gamma^i_j$  of the unbroken theory. It is interesting that two of these relations were first developed in an attempt to construct RG trajectories[2]; the results for  $M, h, m^2$  satisfy exactly the formulae for the corresponding  $\beta$ -functions given, for example in [2]).

Direct application of the AMSB solution to the MSSM leads, unfortunately, to negative (mass)<sup>2</sup> sleptons: in other words, to a theory without a vacuum preserving the  $U_1$  of electromagnetism. We explore two distinct resolutions[3][4] of this dilemma, both based on generalising the AMSB solution, while retaining the crucial property of RG invariance, which makes the low energy theory insensitive to the nature of new physics at high scales. (For some other approaches see Refs. [5]-[14]). Both our ideas are based on extending the MSSM with an extra  $U_1$ ; in the second case this  $U_1$  being associated with an  $R$ -symmetry. In both cases it transpires that requiring RG invariance of the generalised AMSB solution means that the  $U_1$  must have no mixed anomalies with the MSSM gauge group. Also in both cases, a distinguishing feature of the results is the existence of sum rules for the sparticle masses.

# 2 Fayet-Iliopoulos D-terms

A modification of the AMSB solution which has been studied in some detail is the simple replacement  $m^2 \rightarrow \hat{m}^2$  where

$$(\hat{m}^2)^i_j = (m^2)^i_j + m_0^2 \delta^i_j. \tag{2}$$

Here  $m^2$  is the basic AMSB solution from Eq. (1) and  $m_0^2$  is constant. This is not RG invariant (for constant  $m_0^2$ ), but if instead we have

$$(\hat{m}^2)^i_j = (m^2)^i_j + m_0^2 \sum_{a=1}^{\mathcal{N}} k_a (Y_a)^i_j \tag{3}$$

then  $\hat{m}^2$  is RG invariant, as long as each  $Y_a$  corresponds to a  $U_1$  invariance of the superpotential  $W$  and also has vanishing mixed anomaly with each MSSM gauge group factor. This apparent miracle occurs because in fact the modification to  $m^2$  proposed in Eq. (3) is precisely that introduced by a set of Fayet-Iliopoulos (FI)  $D$ -terms.

In the MSSM, there is a non-zero FI-term, but this cannot alone solve the slepton problem because its (mass)<sup>2</sup> contributions to the LH and RH sleptons have opposite signs, being dictated by the hypercharge of the relevant field. The minimal solution we proposed was the introduction of a single extra  $U_1$ , which we denote  $U'_1$ . The MSSM does not admit such a generation independent) anomaly-free  $U_1$  so we need to introduce some new fields to cancel the associated anomalies. However cancellation of the *mixed* anomalies can be achieved within the MSSM itself; the hypercharges of the quark and Higgs multiplets are determined in terms of the lepton hypercharges, so that the MSSM admits two independent mixed-anomaly-free  $U_1$  groups, the existing  $U_1^Y$  and another (which could be chosen to be  $U_1^{B-L}$ [14]). If we also require absence of  $(U'_1)^3$  and  $U'_1$ -gravitational anomalies this can be achieved by introducing a set of MSSM singlets with  $U'_1$  charges  $s_i$  and imposing the constraints[15]

$$\begin{aligned} \sum_{i=1}^N s_i &= -3(2Y'_L + Y'_{\tau^c}), \quad \text{and} \\ \sum_{i=1}^N s_i^3 &= -3(2Y'_L + Y'_{\tau^c})^3, \end{aligned} \quad (4)$$

where the existing MSSM  $U_1$  corresponds of course to  $s_i = 2Y'_L + Y'_{\tau^c} = 0$ .

The classification of rational solutions to Eq. (4) is an interesting Diophantine problem; but as explained in [3], all we require for the RG invariance of Eq. (3) is the existence of the sets of charges  $Y_a$ ; there need be no relic of the associated gauge symmetry (or the singlets  $S_i$ ) in the low energy theory. This is the point of view we will take from now on.

In Table (1) we give a possible set of  $U'_1$  charges with the  $U_1^Y$  ones for comparison. This set of  $Y'$  charges correspond to requiring  $\text{Tr}(YY') = 0$ ; of course the result is a linear combination of  $U_1^Y$  and  $U_1^{B-L}$ . The outcome is that the squark and slepton masses are given by

$$\begin{aligned} \overline{m}_Q^2 &= m_Q^2 + \frac{1}{6}\zeta_1 + \zeta_2 Y'_Q, & \overline{m}_{t^c}^2 &= m_{t^c}^2 - \frac{2}{3}\zeta_1 + \zeta_2 Y'_{t^c}, \\ \overline{m}_{b^c}^2 &= m_{b^c}^2 + \frac{1}{3}\zeta_1 + \zeta_2 Y'_{b^c}, & \overline{m}_L^2 &= m_L^2 - \frac{1}{2}\zeta_1 + \zeta_2 Y'_L, \\ \overline{m}_{\tau^c}^2 &= m_{\tau^c}^2 + \zeta_1 + \zeta_2 Y'_{\tau^c} \end{aligned} \quad (5)$$

where dependence on the FI coefficients, the Higgs vevs and the singlet sector is subsumed into the parameters  $\zeta_{1,2}$ . There is a substantial region of the  $\zeta_{1,2}$ -plane

Table 1: Table of  $U_1$  and  $U_1'$  hypercharges.

	$Q$	$L$	$t^c$	$b^c$	$\tau^c$	$H_1$	$H_2$	$S_i$
$Y$	$\frac{1}{6}$	$-\frac{1}{2}$	$-\frac{2}{3}$	$\frac{1}{3}$	1	$-\frac{1}{2}$	$\frac{1}{2}$	0
$Y'$	$\frac{7}{3}$	-7	$\frac{5}{3}$	$-\frac{19}{3}$	3	4	-4	$s_i$

such that all the above  $\overline{m}^2$  parameters are positive (the precise region depending on the input  $\tan\beta$ ). The result is interesting phenomenology. The gaugino spectrum is the same as in previous AMSB scenarios, with a near degenerate wino and neutralino, the latter being (in some regions of parameter space) the LSP.

For a choice of  $m_0 = 40\text{TeV}$ ,  $\tan\beta = 5$ ,  $\zeta_1 = 0.2$ ,  $\zeta_2 = -.02$ , we find  $|\mu_s| = 645\text{GeV}$  and (choosing  $\mu_s > 0$ ) a mass spectrum given by:

$$\begin{aligned}
m_{\tilde{t}_1} &= 575, & m_{\tilde{t}_2} &= 861, & m_{\tilde{b}_1} &= 825, & m_{\tilde{b}_2} &= 1040, & m_{\tilde{\tau}_1} &= 137, & m_{\tilde{\tau}_2} &= 339, \\
m_{\tilde{u}_L} &= 931, & m_{\tilde{u}_R} &= 851, & m_{\tilde{d}_L} &= 935, & m_{\tilde{d}_R} &= 1045, & m_{\tilde{e}_L} &= 139, & m_{\tilde{e}_R} &= 339, \\
m_{\tilde{\nu}} &= 112, & m_{h,H} &= 110, 455, & m_A &= 453, & m_{H^\pm} &= 461, & m_{\tilde{\chi}_{1,2}^\pm} &= 104, 649 \\
m_{\tilde{\chi}_{1\dots 4}} &= 103, 366, 648, 658, & m_{\tilde{g}} &= 1007,
\end{aligned} \tag{6}$$

where all masses are given in GeV.

A characteristic feature of the present setup is the existence of sparticle mass sum rules such as

$$m_{\tilde{t}_1}^2 + m_{\tilde{t}_2}^2 + m_{\tilde{b}_1}^2 + m_{\tilde{b}_2}^2 - 2(m_t^2 + m_b^2) = 2.75m_{\tilde{g}}^2. \tag{7}$$

The numerical coefficient here depends only on the input  $\tan\beta$  (here taken to be  $\tan\beta = 5$ ), and also (weakly) on  $m_0$ , here taken to be 40TeV.

### 3 R-symmetry and Yukawa textures

There is an alternative generalisation of the AMSB solution for  $m^2$  from Eq. (1) as follows:

$$(m^2)^i_j = \frac{1}{2}|m_0|^2\mu\frac{d\gamma^i_j}{d\mu} + \overline{m}_0^2(\gamma^i_j + \overline{q}^i\delta^i_j). \tag{8}$$

This is also RG invariant to all orders as long as  $\overline{q}^i$  satisfy the following constraints:

$$\begin{aligned}
(\bar{q}^i + \bar{q}^j + \bar{q}^k)Y_{ijk} &= 0 \\
2 \text{Tr} [\bar{q}C(R)] + Q &= 0,
\end{aligned} \tag{9}$$

where  $Q$  is the one loop  $\beta_g$  coefficient and  $C(R)$  is the quadratic matter Casimir. It is easy to show[5][6] that Eq. (9) corresponds precisely to requiring that the theory have a non-anomalous  $\mathcal{R}$ -symmetry (which we denote  $\mathcal{R}$ , to avoid confusion with our notation  $R$  for group representations). If we set

$$\bar{q}^i = 1 - \frac{3}{2}r^i, \tag{10}$$

then we see that Eq. (9) corresponds to  $(r^i + r^j + r^k)Y_{ijk} = 2Y_{ijk}$ , which is the conventional  $\mathcal{R}$ -charge normalisation.

Turning to the MSSM we find that, as in the previous section, our solution will retain the crucial RG invariance as long as all the *mixed* anomalies of the  $\mathcal{R}$ -symmetry with the MSSM gauge group vanish. The MSSM does not admit such a generation independent  $\mathcal{R}$ -symmetry; however it *does* admit one that permits only 3rd generation Yukawa couplings and has identical  $\mathcal{R}$ -charges for the first two generations. We find that this can be achieved for arbitrary values of the leptonic charges with the quark and Higgs charges determined as follows (we work with the fermionic charges, related to the  $\mathcal{R}$ -charges by  $q_f = r - 1$ ):

$$\begin{aligned}
q_3 &= \frac{4}{9} - \frac{1}{3}l_3 - \frac{1}{9}\bar{\kappa} \\
u_3 &= -\frac{22}{9} - \frac{2}{3}l_3 - e_3 + \frac{1}{9}\bar{\kappa} \\
d_3 &= -\frac{4}{9} + \frac{4}{3}l_3 + e_3 + \frac{1}{9}\bar{\kappa} \\
q_1 &= -\frac{101}{90} - \frac{1}{3}\kappa + \frac{1}{15}l_3 + \frac{1}{5}e_3 + \frac{1}{30}\bar{\kappa} + \frac{1}{18}\frac{\bar{\kappa}}{\kappa} \\
u_1 &= -\frac{79}{90} - \frac{2}{3}\kappa - \frac{16}{15}l_3 - \frac{6}{5}e_3 - \frac{1}{30}\bar{\kappa} - \frac{1}{18}\frac{\bar{\kappa}}{\kappa} \\
d_1 &= \frac{101}{90} + \frac{4}{3}\kappa + \frac{14}{15}l_3 + \frac{4}{5}e_3 - \frac{1}{30}\bar{\kappa} - \frac{1}{18}\frac{\bar{\kappa}}{\kappa} \\
h_2 &= -h_1 = l_3 + e_3 + 1,
\end{aligned} \tag{11}$$

where  $\kappa = l_1 - l_3 + e_1 - e_3 - 3$ , and  $\bar{\kappa} = -12l_3 - 16e_3 + 10e_1 - 23$ . As explained above, we have imposed  $q_1 = q_2$  etc.

Thus for any set of rational values for the leptonic charges there exist rational values for all the charges. it is clear therefore that we can potentially resolve the

Table 2: The fermionic  $\mathcal{R}$ -charges for the case  $\Delta_d = \Delta_L$

$q_3$	$l_3$	$u_3$	$d_3$	$e_3$	$q_1$
$\frac{e}{6} - \frac{2}{9}$	$-\frac{e}{2} - \frac{1}{6}$	$-\frac{2e}{3} - \frac{29}{18}$	$\frac{e}{3} + \frac{1}{18}$	$e$	$\frac{e}{6} - \frac{43}{72}$
$l_1$	$u_1$	$d_1$	$e_1$	$H_1$	$H_2$
$-\frac{e}{2} + \frac{5}{24}$	$-\frac{2e}{3} + \frac{19}{72}$	$\frac{e}{3} - \frac{77}{72}$	$e + \frac{9}{8}$	$-\frac{e}{2} - \frac{5}{6}$	$\frac{e}{2} + \frac{5}{6}$

tachyonic slepton problem, since we can choose the lepton  $\mathcal{R}$ -charges so that all the  $\bar{q}$  contributions to Eq. (8) are positive for the sleptons. Of course we will need to check that the corresponding contributions for the squarks and Higgses do not cause problems.

We can get a different handle on the  $\mathcal{R}$ -charge assignments by relating them to a possible origin of the light quark and lepton masses. Suppose[17] there are higher-dimension terms in the effective field theory of the form (for the up-type quarks)  $H_2 Q_i u_j^c (\frac{\theta}{M_U})^{a_{ij}}$  or  $H_2 Q_i u_j^c (\frac{\bar{\theta}}{M_U})^{\bar{a}_{ij}}$ , where  $\theta, \bar{\theta}$  is a pair of MSSM singlet fields with  $\mathcal{R}$ -charges  $\pm r_\theta$  that get equal vacuum expectation values, and  $M_U$  represents some high energy new physics scale (with similar terms for the light down quarks and leptons). Evidently the  $\mathcal{R}$ -charge assignments will then dictate the texture of the Yukawa couplings, via the relation  $h_2 + q_1 + u_1 + a_{11} r_\theta = -1$  and similar identities. if we suppose identical textures for the down quarks and leptons then we find

$$\kappa = -\frac{3}{2}, \quad \bar{\kappa} = -\frac{21}{2} - \frac{9}{4}\lambda, \quad (12)$$

where  $\lambda = 2l_3 + e_3$ . The only value of  $\lambda$  we have found which leads to nice textures with only one pair of  $\theta, \bar{\theta}$  fields is  $\lambda = -\frac{1}{3}$ , which leads to the set of fermionic  $\mathcal{R}$ -charges shown in Table (2).

With this charge assignment we find, (for arbitrary  $e$ ) but setting  $r_\theta = \frac{3}{8}$ , Yukawa textures of the form

$$\Delta_u = \begin{pmatrix} \epsilon^4 & \epsilon^4 & \epsilon \\ \epsilon^4 & \epsilon^4 & \epsilon \\ \epsilon^5 & \epsilon^5 & 1 \end{pmatrix}, \quad \Delta_d = \Delta_L = \begin{pmatrix} \epsilon^4 & \epsilon^4 & \epsilon \\ \epsilon^4 & \epsilon^4 & \epsilon \\ \epsilon^3 & \epsilon^3 & 1 \end{pmatrix} \quad (13)$$

The quark and lepton mass hierarchies and the CKM matrix can be produced with matrices of these generic structures, see [4]. The phenomenology of Flavour Changing Neutral Currents (in both hadronic and leptonic sectors) and CP-violation effects clearly deserve a detailed investigation.

It is easy to show that as long as  $-\frac{1}{3} < e < \frac{1}{3}$  and  $\overline{m}_0^2 < 0$ , the contribution to each slepton mass term due to the  $\overline{q}$  term in Eq. (8) will be positive, and we may expect to achieve a viable spectrum; however, it turns out that it is still non-trivial to obtain an acceptable minimum because, for example, if  $e = 0$  and  $\overline{m}_0^2 < 0$ , the  $\overline{m}_0^2 \overline{q}$  contributions to Eq. (8) from  $u_3$ ,  $q_1$  and  $d_1$  are negative. We find in fact that we need to have  $e < 0$ .

A variety of mass spectra for  $m_0 = 40\text{TeV}$  (corresponding to a gluino mass of around  $1\text{TeV}$ ), but with different values of  $\tan\beta$ ,  $e$  and  $\overline{m}_0^2$ , is presented in table 3; we were unable to find any values of  $e$  and  $\overline{m}_0^2$  corresponding to an acceptable spectrum for  $\tan\beta$  significantly larger than 10. The heaviest sparticle masses scale with  $m_0$  and are given roughly by  $M_{\text{SUSY}} = \frac{1}{40}m_0$ . A characteristic feature of AMSB models is the near-degenerate light charged and neutral winos; this prediction, as in the FI case, is preserved in the scenario presented here. The main distinction from the FI case is the large splitting between the third generation and the other two, caused by the generation-dependent  $\mathcal{R}$ -charge assignments. Moreover, unusual is the possibility (exemplified in the first three columns of table 3) that the  $\tilde{\nu}_\tau$  is the LSP. As is well known, radiative corrections give a sizeable upward contribution to the mass of the light CP-even Higgs, and so we have included the one-loop calculation.

As in the FI case, however, a salient feature of the model is the existence of sum rules for the sparticle masses. These sum rules follow from Eq. (11); and thus for the particular solution exhibited in table 3, they are independent of  $e$ . We find for example the following relation:

$$m_{\tilde{t}_1}^2 + m_{\tilde{t}_2}^2 + m_{\tilde{b}_1}^2 + m_{\tilde{b}_2}^2 - 2(m_t^2 + m_b^2) - 2.75m_g^2 = 0.92\overline{m}_0^2\text{TeV}^2, \quad (14)$$

where we have again taken  $\tan\beta = 5$  and  $m_0 = 40\text{TeV}$ .

Note the similarity with the corresponding one in the FI scenario described in the previous section, Eq. (7); the distinction lies in the non-zero RHS in Eq. (14), which can be traced back to the dependence on  $\gamma$  in Eq. (8).

## 4 Conclusions

We have shown that by extending the MSSM with a  $U_1$  or a  $U_1^R$  (which may or may not be associated with a physical vector boson), it is possible to construct solutions to the running equations for  $m^2$ ,  $M$  and  $h$  that are completely RG invariant, and leads to a phenomenologically acceptable theories, resulting in a distinctive spectrum with sum

Table 3: The sparticle masses (given in GeV) for the  $U_1^R$  case

$\tan \beta(\text{sign } \mu_s)$	2(+)	2(-)	5(+)	5(+)	10(+)
$e$	-1/9	-1/9	-1/9	-2/9	-2/9
$\overline{m}_0^2(\text{TeV}^2)$	-0.1	-0.1	-0.1	-0.25	-0.2
$\tilde{t}_{1,2}$	652,882	615,908	567,876	302,879	404,875
$\tilde{b}_{1,2}$	865,977	865,977	843,974	853,1009	843,987
$\tilde{\tau}_{1,2}$	94,110	87,116	75,127	136,289	86,251
$\tilde{u}_{L,R}$	918,997	918,997	917,997	880,1084,	892,1057
$\tilde{d}_{L,R}$	920,887	920,887	921,887	884,776	896,814
$\tilde{e}_{L,R}$	260,423	260,423	261,423	473,664	418,590
$\tilde{\nu}_\tau$	83	83	73	277	234
$\tilde{\nu}_e$	251	251	249	467	410
$h$	96	105	119	114	124
$H$	598	598	585	121	308
$A$	593	593	584	110	307
$H^\pm$	599	599	590	137	318
$\tilde{\chi}_1^\pm$	98	116	104	101	106
$\tilde{\chi}_2^\pm$	628	625	663	449	530
$\tilde{\chi}_1$	98	115	103	99	103
$\tilde{\chi}_2$	364	372	367	357	365
$\tilde{\chi}_3$	619	620	662	446	532
$\tilde{\chi}_4$	637	628	672	470	544
$\tilde{g}$	1008	1008	1008	1008	1008

rules for the sparticle masses. In both cases the additional source of supersymmetry-breaking may be provided by the vacuum expectation value of a  $D$ -term.

In a recent paper[14], it was shown how our first scenario can be compatible with currently fashionable braneworld scenarios, with breaking of both supersymmetry and the extra  $U_1$  occurring on a hidden brane; the incorporation of massive neutrinos

was also considered. It would be interesting to perform a similar construction for the  $\mathcal{R}$ -symmetry case.

## Acknowledgements

Warm thanks to Ian Jack, with whom all the work described here, and more, was done. I am also grateful to the Leverhulme Trust and PPARC for financial support, and to Howie Haber and the other organisers of RADCOR 2000 for the opportunity to visit Carmel and participate in this meeting.

## References

- [1] L. Randall and R. Sundrum, *Nucl. Phys.* **B557** (1999) 79;  
G.F. Giudice, M.A. Luty, H. Murayama and R. Rattazzi, *JHEP* 9812 (1998) 27;  
I. Jack and D.R.T. Jones, *Phys. Lett.* **B465** (1999) 148.
- [2] I. Jack, D.R.T. Jones and A. Pickering, *Phys. Lett.* **B426** (1998) 73.
- [3] I. Jack and D.R.T. Jones, *Phys. Lett.* **B482** (2000) 167.
- [4] I. Jack and D.R.T. Jones, *Phys. Lett.* **B491** (2000) 151.
- [5] A. Pomarol and R. Rattazzi, *JHEP* **9905** (1999) 013.
- [6] M.A. Luty and R. Rattazzi, *JHEP* **9911** (1999) 001.
- [7] E. Katz, Y. Shadmi and Y. Shirman, *JHEP* **9908** (1999) 015.
- [8] Z. Chacko, M.A. Luty, I. Maksymyk and E. Ponton, *JHEP* **0004** (2000) 001.
- [9] T. Gherghetta, G.F. Giudice and J.D. Wells, *Nucl. Phys.* **B559** (1999) 27.
- [10] K.I. Izawa, Y. Nomura and T. Yanagida, *Prog. Th. Phys.* **102** (1999) 1181.
- [11] D.E. Kaplan and G.D. Kribs, *JHEP* **0009** (2000) 048.
- [12] M. Carena, K. Huitu and T. Kobayashi, *Nucl. Phys.* **B592** (2000) 164.
- [13] B.C. Allanach and A. Dedes, *JHEP* **0006** (2000) 017.
- [14] N. Arkani-Hamed, D.E. Kaplan, H. Murayama and Y. Nomura, LBNL-47184, [hep-ph/0012103].

- [15] A.H. Chamseddine and H. Dreiner, *Nucl. Phys.* **B447** (1995) 195.
- [16] A.H. Chamseddine and H. Dreiner, *Nucl. Phys.* **B458** (1996) 65;  
D.J. Castano, D.Z. Freedman and C. Manuel, *Nucl. Phys.* **B461** (1996) 50.
- [17] C.D. Froggatt and H.B. Nielsen, *Nucl. Phys.* **B147** (1979) 277.

UCD-01-05  
June 19, 2001  
hep-ph/0106154

## Hunting the Higgs Boson(s)

JOHN F. GUNION \*

*Davis Institute for High Energy Physics, Department of Physics  
University of California at Davis, Davis CA, USA*

I give a brief review of some of the opportunities and challenges that could arise in our quest to unravel the Higgs sector that very probably underlies electroweak symmetry breaking. In particular, I review scenarios with an extended Higgs sector that allow for a heavy SM-like Higgs boson and/or make discovery more difficult while at the same time maintaining consistency with current limits and precision electroweak constraints.

Presented at the

5th International Symposium on Radiative Corrections  
(RADCOR-2000)

Carmel CA, USA, 11-15 September, 2000

and at

8th International Symposium on Particles, Strings and  
Cosmology  
(PASCOS-2001)

University of North Carolina, Chapel Hill, 10-15 April, 2001

---

\*Work supported in part by the U.S. Department of Energy and by the Davis Institute for High Energy Physics.

# 1 The Standard Model

The most important and immediate goal in our quest to understand nature at the microscopic level is the determination of the mechanism by which elementary particles acquire mass. One very attractive approach is to hypothesize the existence of a Higgs sector (for a review, see [1]) of scalar fields (some of which must have non-zero quantum numbers under the weak  $SU(2) \times U(1)$  electroweak gauge group). The Higgs potential must be such that one or more of the neutral components of the Higgs fields spontaneously acquires a non-zero vacuum expectation value, thereby giving masses to the  $W^\pm$  and  $Z$  gauge bosons. In the minimal Standard Model (SM), mass generation is accomplished through the existence of a Higgs sector containing a single complex scalar field doublet (under weak isospin),  $\phi = \begin{pmatrix} \phi^+ \\ \phi^0 \end{pmatrix}$ . When  $\text{Re}\phi^0$  acquires a vacuum expectation value ( $\frac{v}{\sqrt{2}}$ ), the  $\phi^\pm$  and  $\text{Im}\phi^0$  fields are absorbed by the hitherto massless  $W^\pm$  and  $Z$  fields which thereby acquire mass. At the same time, Yukawa couplings  $\lambda_f \bar{f} f \phi$  lead to the generation of mass for the fermions,  $m_f \propto \lambda_f v$ . The quantum fluctuations of the remaining field  $\text{Re}\phi^0$ , correspond to a physical particle, the neutral Higgs boson, denoted  $h_{\text{SM}}$ . The couplings of the  $h_{\text{SM}}$  to other SM particles are completely constrained. However, the mass of the  $h_{\text{SM}}$  is completely unconstrained in the SM context without referencing physics at higher energy scales.

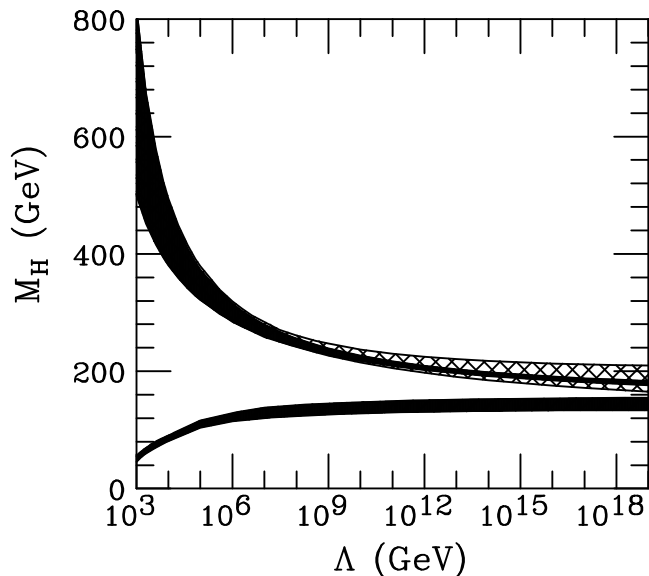


Figure 1: Triviality and (meta)stability bounds for the SM Higgs boson as a function of the new physics scale  $\Lambda$ . From [2].

If the SM is the correct description of electroweak symmetry breaking at current energies, it could still be that the SM is only an effective theory valid below some

higher energy scale  $\Lambda$ . Above  $\Lambda$ , new physics enters and a more complete/fundamental theory would emerge. One possibility is that there is no new physics between electroweak scales and the Planck scale,  $M_P$ . Or it could be that a theory such as supersymmetry emerges at a lower scale. Fig. 1 (from [2]) shows that the SM could remain valid as an effective theory all the way up to  $M_P$  only for a very limited range of  $m_{h_{\text{SM}}}$ , roughly  $140 < m_{h_{\text{SM}}} < 180$  GeV. For  $m_{h_{\text{SM}}}$  outside this range, new physics would have to enter at a much lower scale. For example, if a  $m_{h_{\text{SM}}} \sim 115$  GeV SM Higgs boson is discovered, then  $\Lambda \lesssim 1000$  TeV. The upper bound shown in Fig. 1 derives from requiring that the coupling  $\lambda$  appearing in the Higgs field quartic self-coupling term in the Higgs potential,  $\propto \lambda\phi^4$ , remain perturbative when ‘probed’ at energy scale  $\Lambda$ . Since  $\lambda$  grows with energy scale, this bounds  $\lambda(m_{h_{\text{SM}}})$ , thereby bounding  $m_{h_{\text{SM}}} \sim 2v^2\lambda(m_{h_{\text{SM}}})$ . The lower bound shown derives from requiring stability of the potential. In particular,  $\lambda$  is not allowed to be driven negative at energy scales below  $\Lambda$  (by the large top quark contribution to the running of  $\lambda$ ); *i.e.* we require  $\lambda(\Lambda) > 0$ . Without this constraint the universe would ultimately prefer to tunnel to a state in which the Higgs field  $\phi$  has values with  $|\phi| \gtrsim \Lambda$ , yielding large negative  $V(\Lambda) \propto \lambda(\Lambda)|\phi \sim \Lambda|^4$  if  $\lambda(\Lambda) < 0$ . The meta-stability condition, that the time scale for such tunneling be longer than the age of the universe, is only slightly less constraining.

Precision electroweak data suggests [3] the presence of a light SM-like  $h$ , the best single SM-like Higgs boson fit being obtained for  $m_h \lesssim 100$  GeV. Recent LEP data [4] contain hints (at the roughly  $2.9\sigma$  level) that a SM-like Higgs boson might be present with mass  $m_h \sim 115$  GeV. This same data could also be interpreted as providing weak evidence for a somewhat spread-out Higgs signal in the region  $m_h \lesssim 115$  GeV,

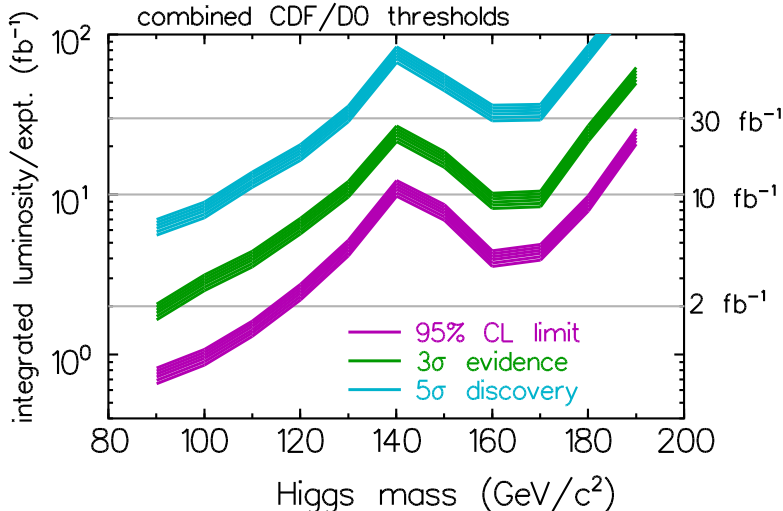


Figure 2: Prospects for SM Higgs discovery at the Tevatron.

such as might arise if there were a number of Higgs bosons with overlapping resonance shapes, each one having  $ZZ$  coupling-squared that is a small fraction of the strength expected for the  $h_{\text{SM}}$ .

If the precision electroweak and LEP hints for a single light SM-like Higgs boson are correct, the Tevatron will have an excellent chance of detecting such an  $h$  with  $L = 15 \text{ fb}^{-1}$  of accumulated luminosity (per experiment). This is illustrated in Fig. 2, from [5]. If  $90 \text{ GeV} \lesssim m_{h_{\text{SM}}} \lesssim 130 \text{ GeV}$  one employs  $q'\bar{q} \rightarrow W^* \rightarrow Wh_{\text{SM}} \rightarrow \ell\nu b\bar{b}$  and  $q\bar{q} \rightarrow Z^* \rightarrow Zh_{\text{SM}} \rightarrow \nu\bar{\nu} b\bar{b}$  and  $\ell^+\ell^- b\bar{b}$ . If  $130 \text{ GeV} \lesssim m_{h_{\text{SM}}} \lesssim 190 \text{ GeV}$  one uses  $gg, W^*W^* \rightarrow h_{\text{SM}}$  as well as  $q'\bar{q} \rightarrow W^* \rightarrow Wh_{\text{SM}}$  and  $q\bar{q} \rightarrow Z^* \rightarrow Zh_{\text{SM}}$ , all with  $h_{\text{SM}} \rightarrow WW^*, ZZ^*$ . Relevant final states for  $h_{\text{SM}}$  decay would be  $\ell^\pm\ell^\pm jjX$  and  $\ell^+\ell^-\nu\bar{\nu}$ . Currently, it is believed that  $L = 15 \text{ fb}^{-1}$  can be accumulated by 2006-2007, i.e. just as LHC will start producing physics results.

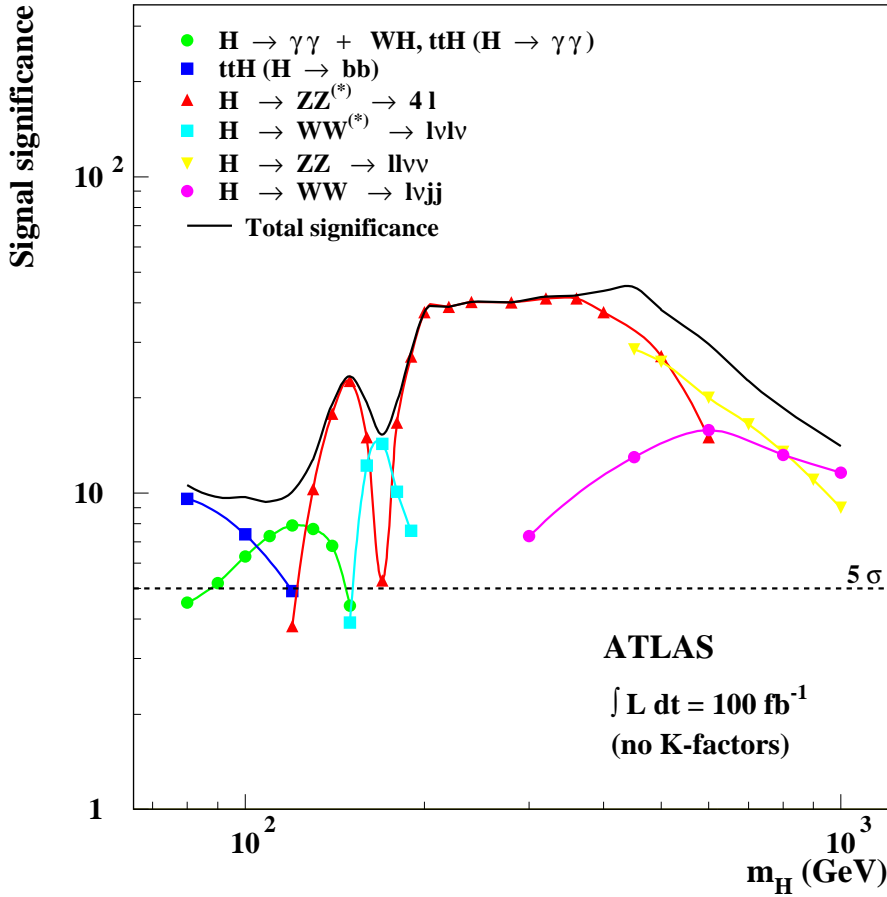


Figure 3: The statistical significance in various channels for a Standard Model Higgs signal with  $L = 100 \text{ fb}^{-1}$  of accumulated luminosity for the ATLAS detector at the LHC. Also shown is the net statistical significance after combining channels. From [6]. The CMS detector finds similar results [7].

The LHC and its detectors have been specifically designed to discover the  $h_{\text{SM}}$  for any  $m_{h_{\text{SM}}} \lesssim 1$  TeV or to see signs of a strongly interacting  $W$  sector if the effective Higgs mass is even larger. The discovery modes are the following. For  $m_{h_{\text{SM}}} \lesssim 130$  GeV, one employs  $gg, W^*W^* \rightarrow h_{\text{SM}} \rightarrow \gamma\gamma, q_i\bar{q}_j \rightarrow W^\pm h_{\text{SM}}$  and  $gg \rightarrow t\bar{t}h_{\text{SM}}$  with  $h_{\text{SM}} \rightarrow \gamma\gamma$  and  $h_{\text{SM}} \rightarrow b\bar{b}$ . For  $m_{h_{\text{SM}}} > 130$  GeV, the best signal is  $gg, W^*W^* \rightarrow h_{\text{SM}} \rightarrow ZZ^{(*)} \rightarrow 4\ell$  ( $gg, W^*W^* \rightarrow h_{\text{SM}} \rightarrow WW^* \rightarrow \ell\nu\ell\nu$  for  $m_{h_{\text{SM}}} \sim 2m_W$ ). If  $m_{h_{\text{SM}}} > 300$  GeV (400 GeV) the  $gg, W^*W^* \rightarrow h_{\text{SM}} \rightarrow WW \rightarrow \ell\nu jj$  ( $\rightarrow ZZ \rightarrow \ell\nu\nu$ ) modes are very robust. The statistical significances for various channels are shown in Fig. 3. For  $L = 100 \text{ fb}^{-1}$ , a signal of at least  $10\sigma$  is achieved for all  $m_{h_{\text{SM}}} < 1$  TeV.

A future linear  $e^+e^-$  collider would also be certain to detect the SM  $h_{\text{SM}}$  unless  $m_{h_{\text{SM}}} > \sqrt{s}$ . Comprehensive reviews are found in [8] and [9]. If  $m_{h_{\text{SM}}} < \sqrt{s} - m_Z$ ,  $e^+e^- \rightarrow Z^* \rightarrow Zh_{\text{SM}}$  production would allow both an inclusive recoil mass determination of  $\sigma(Zh_{\text{SM}})$  and exclusive final state determinations of  $\sigma(Zh_{\text{SM}})B(h_{\text{SM}} \rightarrow X)$  for various final states  $X$ . The ratio of the latter to the former gives a result for  $B(h_{\text{SM}} \rightarrow X)$ . The power of this approach and of the LC detectors to separate the various channels  $X$  is illustrated by the fact that for  $L = 500 \text{ fb}^{-1}$  of accumulated luminosity (1 or 2 years of operation) one can even obtain an accurate determination of  $B(h_{\text{SM}} \rightarrow WW^*)$  if  $m_{h_{\text{SM}}} \gtrsim 120$  GeV and of  $B(h_{\text{SM}} \rightarrow \gamma\gamma)$  if  $m_{h_{\text{SM}}} \lesssim 130$  GeV. Even the very narrow width of the light Higgs can be determined quite accurately by indirect means. For instance, by isolating  $e^+e^- \rightarrow e^+e^-W^*W^* \rightarrow e^+e^-h_{\text{SM}}$  events one can extract  $\Gamma_{h_{\text{SM}}}^{\text{tot}} = \frac{\sigma(W^*W^* \rightarrow h_{\text{SM}} \rightarrow WW^*)}{[B(h_{\text{SM}} \rightarrow WW^*)]^2}$ . The  $\gamma\gamma$  collider option at the LC can also play an important role. In particular, the  $\gamma\gamma \rightarrow h_{\text{SM}}$  coupling can be determined from the ratio  $\sigma(\gamma\gamma \rightarrow h_{\text{SM}} \rightarrow b\bar{b})/B(h_{\text{SM}} \rightarrow b\bar{b})$  (the latter determined using the  $Zh_{\text{SM}}$  techniques). This coupling is very sensitive to the presence of loops containing heavy particles whose mass is acquired via the Higgs mechanism. In addition, at low masses such that the  $W^*W^*$  technique for total width determination is not very accurate,  $\gamma\gamma \rightarrow h_{\text{SM}}$  allows [10] extraction of  $\Gamma_{h_{\text{SM}}}^{\text{tot}} = \frac{\sigma(\gamma\gamma \rightarrow h_{\text{SM}} \rightarrow b\bar{b})}{B(h_{\text{SM}} \rightarrow \gamma\gamma)B(h_{\text{SM}} \rightarrow b\bar{b})}$ . The process  $\gamma\gamma \rightarrow h_{\text{SM}}$  also allows determination of the CP nature of the  $h_{\text{SM}}$  by studying the cross section dependence upon relative orientation of the (transverse) polarizations of the colliding  $\gamma$ 's [11,12,13]. CP=+ (−) implies  $\gamma\gamma \rightarrow h_{\text{SM}}$  cross section proportional to  $\vec{\epsilon}_1 \cdot \vec{\epsilon}_2$  ( $\vec{\epsilon}_1 \times \vec{\epsilon}_2$ ). Finally, by studying angular distributions of the  $t, \bar{t}$  and  $h$  in  $e^+e^- \rightarrow t\bar{t}h$  it is possible to determine the CP of the resonance eigenstate [14,15].

## 2 Non-Exotic Extensions of the SM Higgs Sector

Even within the SM effective field theory context, the Higgs sector need not consist of just a single doublet; one should consider extended Higgs sector possibilities. Indeed, typical models in which the Higgs sector is the result of a new strong interaction at a higher scale  $\Lambda$  produce an effective field theory below  $\Lambda$  that contains at least two doublets and/or extra singlets [16]. Higher representations are also a

possibility. String models also often yield quite a number of Higgs representations at low energy [17]; singlets, doublets and higher representations are all possible.

Addition of singlets poses no particular theoretical problems (or benefits). Addition of one or more extra doublet representation(s) has both attractive and unattractive aspects. On the unattractive side is the fact that the squared-mass(es) of the additional charged Higgs boson(s) become new parameter(s) that must be chosen to be positive definite in order to avoid breaking of electromagnetic symmetry. This unfavorable aspect is, in the view of many, more than compensated by the fact that a multi-Higgs-doublet model allows for the possibility of explaining all CP-violation phenomena as a result of explicit or spontaneous CP violation in the Higgs sector. Triplet representations and higher are deemed ‘exotic’ in that  $\rho$  is no longer computable when they participate in EWSB (*i.e.* when the vev of the neutral member of the representation is non-zero); instead,  $\rho$  becomes infinitely renormalized and must be treated as an input parameter to the model [18]. In this section, we focus our attention on singlet and doublet extensions. In both cases, detection and simulation considerations change dramatically. Triplets will be discussed very briefly in the next section.

The new considerations that arise for an extended SM Higgs sector are brought most immediately into focus by discussing the discovery prospects for Higgs bosons at an  $e^+e^-$  collider; other colliders will encounter even greater difficulty in ensuring discovery of at least one Higgs boson of an extended sector.

## 2.1 A Continuum Signal

As stated above, it is not entirely unreasonable to consider a case in which there are many singlets and/or extra doublets, possibly even triplets, in addition to the original doublet Higgs field  $\phi$ . Each complex neutral field results in an extra scalar and extra pseudoscalar degree of freedom. The former will generally mix with  $\text{Re}\phi^0$  and the interesting question is the extent to which this could make Higgs discovery difficult. The worst case scenario is that in which the physical eigenstates share the  $WW/ZZ$  coupling-squared and are spread out in mass in such a way that their separation is smaller than the  $\sim 10$  GeV or so mass resolution of the detector. The result could be a very spread out and diffuse signal that could only be searched for as a broad excess in the  $M_X$  recoil mass spectrum in  $e^+e^- \rightarrow ZX$  production, where  $M_X$  is computed from  $p_X = p_{e^+} + p_{e^-} - p_Z$  for events in which the  $Z$  decays to  $e^+e^-$ ,  $\mu^+\mu^-$  (and possibly jets). As noted earlier, LEP2 data is consistent with a small spread-out excess of events at high  $M_X$  (in the  $M_X \sim 100 - 110$  GeV region) beyond the number predicted by background computations; this excess could be interpreted in terms of such a diffuse spread-out signal.

Fortunately, there are constraints on this scenario. First, defining  $C_i$  to be the strength of the  $h_iVV$  coupling relative to that of the  $h_{\text{SM}}$ , unitarity for  $WW$  scattering, as well as the general structure of the theory, imply the sumrule  $\sum_i C_i^2 \geq 1$ ;

if only singlet and doublet representations are present  $\sum_i C_i^2 = 1$ . Second, precision electroweak constraints imply that the value of  $\langle M^2 \rangle$  appearing in

$$\sum_i C_i^2 m_{h_i}^2 = \langle M^2 \rangle. \quad (1)$$

should not exceed about  $(200 \text{ GeV})^2$ . For the most general supersymmetric model Higgs sector, imposing the requirement of perturbativity of couplings after evolving up to the GUT scale yields this same result for the maximum possible  $\langle M^2 \rangle$  [19].

To illustrate the consequences [20], assume  $C_i^2$  is constant from  $m_h^{\min}$  to  $m_h^{\max}$ ; using continuum notation,  $C^2(m_h) \geq 1/(m_h^{\max} - m_h^{\min})$  for  $\int dm_h C^2(m_h) \geq 1$ , while Eq. (1) implies  $\frac{1}{3}([m_h^{\max}]^2 + m_h^{\max} m_h^{\min} + [m_h^{\min}]^2) \leq \langle M^2 \rangle$ . Let us also suppose that LEP data can be used to show that  $C^2(m_h)$  is very small for  $m_h < 70 \text{ GeV}$  (this is being examined currently). Then if  $C^2(m_h)$  is constant from  $m_h^{\min} = 70 \text{ GeV}$  out to  $m_h^{\max} = 300 \text{ GeV}$  the sumrule will be saturated.

Clearly, LEP2 would have had great difficulty confirming the presence of such a broad excess. One needs to have  $e^+e^-$  collisions at high enough energy to avoid kinematic suppression over the bulk of the  $M_X$  region in question. A  $\sqrt{s} = 500 \text{ GeV}$  collider would be more or less ideal. In Ref. [21], the backgrounds in the recoil  $M_X$  spectrum for  $ZX$  production were examined for  $\sqrt{s} = 500 \text{ GeV}$  over the interval  $70 \text{ GeV}$  to  $200 \text{ GeV}$ . For the  $m_h^{\min} = 70, m_h^{\max} = 300 \text{ GeV}$  case described, a fraction  $f \sim 0.57$  of the continuum signal resides in this region. In order to avoid the large  $ZZ$  background, it is actually best to restrict consideration to the  $100 - 200 \text{ GeV}$  range in which a fraction  $f \sim 0.43$  of the signal resides. For  $L = 500 \text{ fb}^{-1}$ , the excess signal event rate after cuts would be  $S \sim 1350f \sim 580$  with a background of  $B = 2700$ . The resulting  $\sim 50\%f \sim 22\%$  excess over background would be readily detected, and would yield  $S/\sqrt{B} \sim 26f \sim 11$ . Allowing for some extra weighting of the signal into the  $M_X = m_Z$  region, it still seems safe to say that  $S/\sqrt{B} > 5$  would be achieved for  $L \gtrsim 200 \text{ fb}^{-1}$ .

Obviously, detection of this type of signal would be very difficult, if not impossible, at a hadron collider due to the inability to reconstruct the recoil mass in a  $ZX$  or  $WX$  event (the energies of the colliding quarks being unknown). In this scenario, the LHC would have good evidence that  $WW$  scattering at high- $m_{WW}$  was perturbative, but the continuum of Higgs bosons responsible for this perturbativity would probably not be directly detected. Detection of the Higgs bosons would require that only a few of the Higgs bosons decayed to some particular identifiable final state (e.g.  $b\bar{b}$ ) and that these same Higgs bosons were sufficiently well separated in mass that the individual mass peaks could be reconstructed. This latter is a possibility if some of the Higgs bosons give mass to some fermions and not others, rather than all Higgs bosons contributing roughly equally to the various fermionic masses. Of course, this type of channel separation would make resonance peak reconstruction possible at the LC as well.

## 2.2 The General Two-Higgs-Doublet Model

This is a particularly useful model to consider since it already displays many features that would be present in still more complex Higgs sectors (see [1] for a review and references). We will confine our attention to a type-II two-doublet model (in which one Higgs doublet,  $\phi_u$ , gives mass to up quarks while the second,  $\phi_d$ , gives mass to down quarks and leptons). Of course, the MSSM Higgs sector is a constrained type-II two-doublet model. If CP is conserved in the Higgs sector, then there are two CP-even eigenstates,  $h^0$  and  $H^0$ , one CP-odd eigenstate,  $A^0$  and a charged Higgs pair,  $H^\pm$ . If CP is violated, the  $h^0, H^0, A^0$  would mix to form a trio of mixed-CP eigenstates,  $h_{i=1,2,3}$ . One of the most important parameters of a 2HDM model is  $\tan\beta = v_u/v_d$ , the ratio of vacuum expectation values for the neutral field components of  $\phi_u$  and  $\phi_d$ ;  $v_u^2 + v_d^2 = v_{\text{SM}}^2$  is required to obtain the correct  $W$  and  $Z$  masses.

The most pressing question is again whether or not we are guaranteed that there should be at least one light Higgs boson with properties such that we can detect it at the various colliders. The answer is model dependent.

As we shall review later, in the general 2HDM context (i.e. without the constraints of supersymmetry), it is possible to satisfy precision electroweak constraints even if the only Higgs boson that has substantial  $WW/ZZ$  coupling is quite heavy (but, at most  $\sim 1$  TeV). Precision constraints are most easily satisfied if there is one light Higgs boson (with no  $WW/ZZ$  coupling), all others being quite heavy. Would we discover this light  $\hat{h}$ ?

Again we use the  $e^+e^-$  collider to illustrate. There the relevant production processes would be  $e^+e^- \rightarrow t\bar{t}\hat{h}$ ,  $e^+e^- \rightarrow b\bar{b}\hat{h}$ ,  $e^+e^- \rightarrow Z^* \rightarrow Z\hat{h}\hat{h}$  and  $e^+e^- \rightarrow \nu\bar{\nu}\hat{h}\hat{h}$ . As regards the fermion processes, there are sumrules that guarantee that the  $b\bar{b}\hat{h}$  and  $t\bar{t}\hat{h}$  couplings cannot both be suppressed [22]. In particular, for a  $\hat{h}$  of a general type-II 2HDM with no  $VV$  coupling one finds  $g_{t\bar{t}\hat{h}}/g_{t\bar{t}h_{\text{SM}}} = \cot\beta$  and  $g_{b\bar{b}\hat{h}}/g_{b\bar{b}h_{\text{SM}}} = \tan\beta$ . The  $Z^* \rightarrow Z\hat{h}\hat{h}$  and  $WW \rightarrow \hat{h}\hat{h}$  processes are dominated by the quartic coupling which is determined purely by the covariant gauge derivative structure,  $(D_\mu\Phi)^\dagger(D^\mu\Phi)$ , responsible for the relevant interactions. We will now outline why these processes are not necessarily sufficient to guarantee  $\hat{h}$  discovery.

### Yukawa processes

Because of the  $\tan\beta$  dependence of the couplings,  $e^+e^- \rightarrow t\bar{t}\hat{h}$  will always yield an observable event rate if  $\tan\beta$  is small enough (and the process is kinematically allowed) while  $b\bar{b}\hat{h}$  will be observable for large enough  $\tan\beta$ . However, even for  $L = 2500 \text{ fb}^{-1}$  there is a wedge of  $\tan\beta$ , beginning at  $m_{\hat{h}} \sim 50 \text{ GeV}$  (80 GeV) for  $\sqrt{s} = 500 \text{ GeV}$  (800 GeV), for which neither process will have as many as 50 events [22,23], deemed the absolute minimum number of events for which detection would be possible at the LC. Of course, the upper limit limit for the wedge illustrated up to 400 GeV rises further for still larger  $m_{\hat{h}}$  values, while the lower line delimiting the

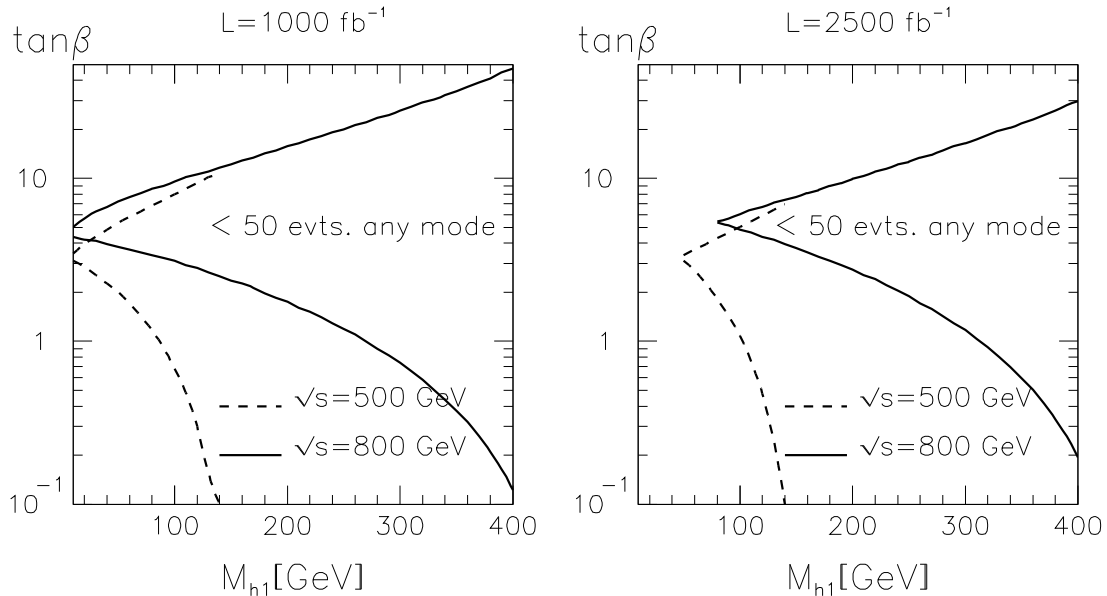


Figure 4: For  $\sqrt{s} = 500$  GeV (dashes) and  $\sqrt{s} = 800$  GeV (solid), we plot the maximum and minimum  $\tan\beta$  values between which  $t\bar{t}\hat{h}$  and  $b\bar{b}\hat{h}$  both have fewer than 50 events assuming (a)  $L = 1000 \text{ fb}^{-1}$  or (b)  $L = 2500 \text{ fb}^{-1}$ .

wedge disappears once  $t\bar{t}\hat{h}$  is kinematically forbidden. In short, the fermionic coupling sum rules do not yield any guarantees. They only restrict the problematical region.

### Double Higgs production processes

In Fig. 5 we [24] plot the cross section for  $e^+e^- \rightarrow Z^* \rightarrow Z\hat{h}\hat{h}$ . We see that this process can probe up to  $m_{\hat{h}} = 150$  GeV (250 GeV) for a 20 event signal with  $L = 1000 \text{ fb}^{-1}$  (50 events for  $L = 2500 \text{ fb}^{-1}$ ). Similar results are obtained for  $WW \rightarrow \hat{h}\hat{h}$  fusion production. Thus, even after combining these process with the Yukawa processes, there is a large range of  $m_{\hat{h}}$  and  $\tan\beta$  values for which the only Higgs boson light enough to be produced in  $e^+e^-$  collisions cannot be detected.

### Precision electroweak constraints in the 2HDM

In this subsection, we demonstrate how a 2HDM can give good agreement with precision electroweak constraints, even if there is only one Higgs boson with  $VV$  decoupling and it has mass  $\sim 1$  TeV [23]. As noted earlier, a heavy SM-like  $h$  gives a large  $\Delta S > 0$  and large  $\Delta T < 0$ , as illustrated by the locations of the stars in Fig. 6. The key is to compensate the negative  $\Delta T$  from the 1 TeV SM-like Higgs with a large  $\Delta T > 0$  from a small mass non-degeneracy (weak isospin breaking) of heavier Higgs. For example, for a light  $\hat{h} = A^0$ , the  $h^0$  would be taken heavy and SM-like and the

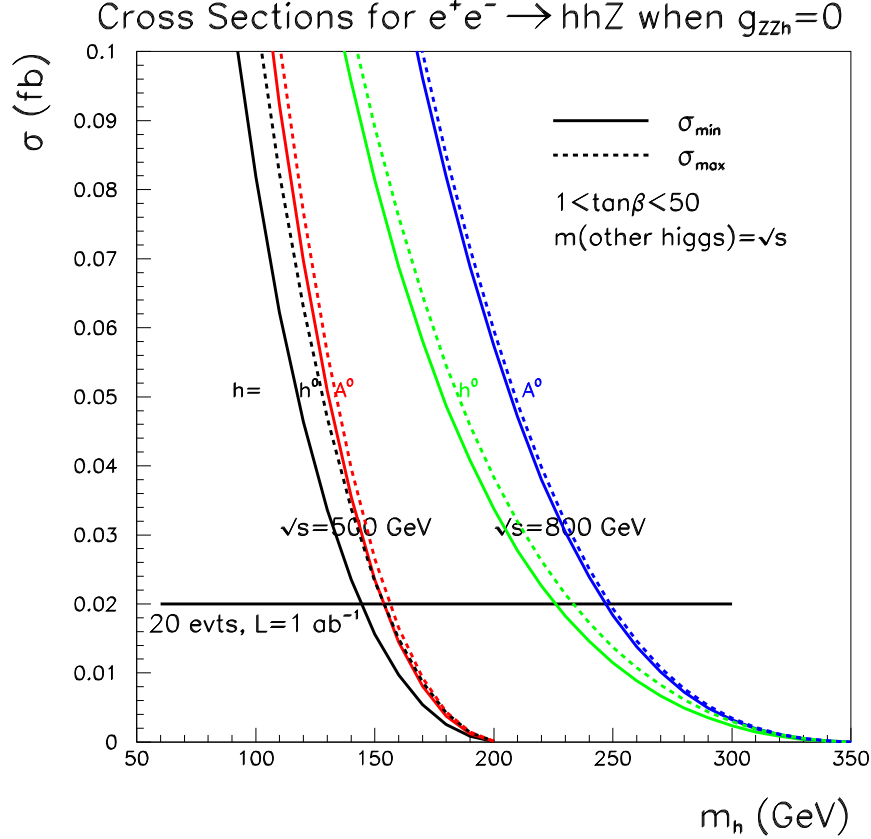


Figure 5: For  $\sqrt{s} = 500$  GeV and  $800$  GeV and for  $\hat{h} = h^0$  and  $\hat{h} = A^0$ , we plot as a function of  $m_{\hat{h}}$  the maximum and minimum values of  $\sigma(e^+e^- \rightarrow \hat{h}\hat{h}Z)$  found after scanning  $1 < \tan\beta < 50$  taking all other Higgs masses equal to  $\sqrt{s}$ . For  $\hat{h} = h^0$ , we require  $\sin(\beta - \alpha) = 0$  during the scan. The 20 event level for  $L = 1 \text{ ab}^{-1}$  is indicated.

value of  $\Delta\rho$  would be approximately given by:

$$\Delta\rho = \frac{\alpha}{16\pi m_W^2 c_W^2} \left\{ \frac{c_W^2}{s_W^2} \frac{m_{H^\pm}^2 - m_{H^0}^2}{2} - 3m_W^2 \left[ \log \frac{m_{h^0}^2}{m_W^2} + \frac{1}{6} + \frac{1}{s_W^2} \log \frac{m_W^2}{m_Z^2} \right] \right\} \quad (2)$$

From this formula, it is clear that one can adjust  $m_{H^\pm} - m_{H^0} \sim \text{few GeV}$  (both  $m_{H^\pm}$  and  $m_{H^0}$  being large) so that the  $S, T$  prediction moves to the location of the blobs shown.

### Possible evidence from $a_\mu$ for a light $\hat{h} = A^0$

The latest BNL result [25] for  $a_\mu$  differs by  $2.6\sigma$  from the SM prediction (for a standard set of inputs for low energy  $\sigma(e^+e^- \rightarrow \text{hadrons})$ ):

$$\Delta a_\mu \equiv a_\mu^{\text{exp}} - a_\mu^{\text{SM}} = 426(165) \times 10^{-11}. \quad (3)$$

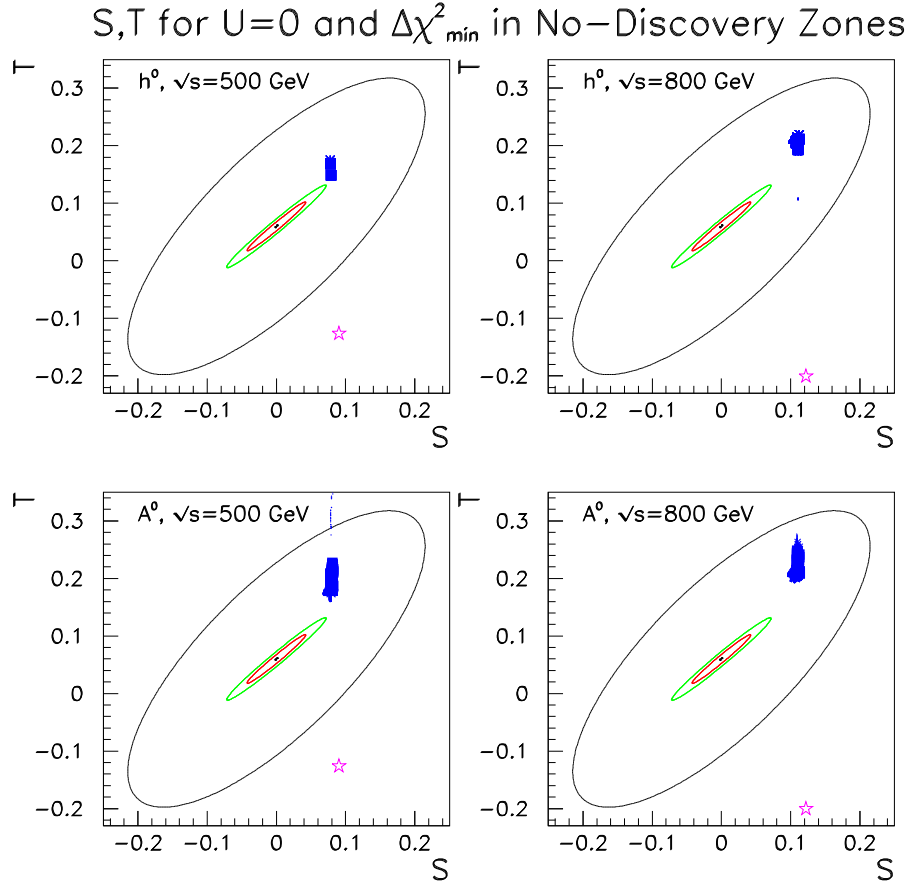


Figure 6: The outer ellipses indicate the current precision electroweak 90% CL region in the  $S, T$  plane for  $U = 0$  and  $m_{h_{\text{SM}}} = 115$  GeV. The innermost (middle) ellipse show the size of the 90% (99.9%) CL region for  $m_{h_{\text{SM}}} = 115$  GeV after new precision electroweak measurements (especially of  $\sin^2 \theta_{\text{leptonic}}$  at a Giga- $Z$  factory and a  $\Delta m_W \lesssim 6$  MeV threshold scan measurement). The blobs indicate the  $S, T$  predictions for points with  $\tan \beta > 2$  that lie within the no-discovery wedges illustrated in Fig. 5, adjusting other model parameters so that the  $\Delta\chi^2$  of the precision electroweak fit is minimized while keeping all but one Higgs boson heavier than  $\sqrt{s}$ . Stars show  $S, T$  predictions for the SM taking  $m_{h_{\text{SM}}} = 500$  or 800 GeV.

Taking the above numbers at face value, the range of  $\Delta a_\mu$  at 95% C.L. ( $\pm 1.96\sigma$ ) is given by  $10.3 \times 10^{-10} < \Delta a_\mu < 74.9 \times 10^{-10}$ . A light  $A^0$  ( $h^0$ ) gives a positive (negative) contribution to  $a_\mu$  dominated (for all but a very light Higgs boson) by the two-loop Bar-Zee graph. If we use a light  $A^0$  as the entire explanation for  $\Delta a_\mu$ , Fig. 7 shows that this leads to constraints such that  $\tan \beta > 15$  is required with  $m_{A^0} < 100$  GeV (smaller values for smaller  $\tan \beta$ ) [26]. For  $\tan \beta > 17$  and  $m_{A^0} < 100$  GeV, the  $A^0$

will be found at a LC for sure, but discovery of such a light state primarily decaying into two (soft) jets will be hard at the LHC. If the size of  $\Delta a_\mu$  should decline with analysis of the final data set, or with alternative input for  $\sigma(e^+e^- \rightarrow \text{hadrons})$  at low energy, higher  $m_{A^0}$  and/or smaller  $\tan\beta$  would be needed to explain  $\Delta a_\mu$ . Thus, for smaller  $\Delta a_\mu$  the  $A^0$  might not be observable at either the LC or the LHC. Of course, there are many other new-physics explanations for  $\Delta a_\mu$ . Possibly a piece could come from the Higgs sector and a piece from these other sources.

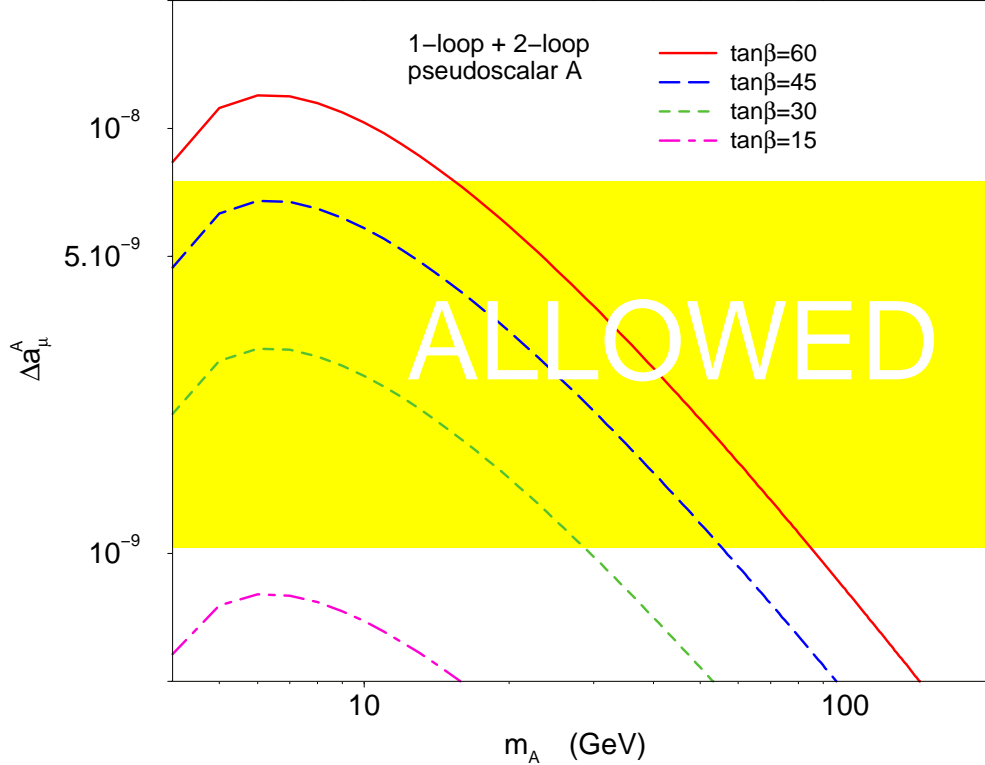


Figure 7: Explanation of new BNL  $a_\mu$  value via light 2HDM  $A^0$ . (Cheung, Chou, Kong)

### 3 Triplet Representations

It is certainly easy to construct models in which the Higgs sector contains one or more triplet representations (see [1] for a review of models). Most interesting would be the presence of a complex  $|Y| = 2$  triplet representation. One can use a  $2 \times 2$  matrix notation for such a representation:

$$\Delta = \begin{pmatrix} \Delta^+/\sqrt{2} & \Delta^{++} \\ \Delta^0 & -\Delta^+/\sqrt{2} \end{pmatrix}. \quad (4)$$

The most dramatic new features of Higgs representations containing a complex triplet are the presence of the doubly-charged Higgs bosons,  $\Delta^{--}$  and  $\Delta^{++}$  and the possibility of lepton-number-violating Majorana-like couplings which take the form

$$\mathcal{L}_M = ih_{ij}\psi_i^T C\tau_2\Delta\psi_j + \text{h.c.}, \quad (5)$$

where  $i, j = e, \mu, \tau$  are generation indices. This coupling will give rise to a see-saw mass term if  $\langle\Delta^0\rangle \equiv v_\Delta \neq 0$ . However, if  $v_\Delta \neq 0$ , then we lose predictivity for  $\rho$ ;  $\rho$  is renormalized and becomes an input parameter for the model [18]. Whether or not  $v_\Delta \neq 0$ ,  $\mathcal{L}_M$  gives rise to  $e^-e^- \rightarrow \Delta^{--}$  and  $\mu^-\mu^- \rightarrow \Delta^{--}$  couplings. Left-right (L-R) symmetric models combine the best of both worlds. They introduce right-handed electroweak isospin in addition to the left-handed isospin of the SM and contain a left-triplet  $\Delta_L$  with  $\langle\Delta_L^0\rangle = 0$  (so that  $\rho = 1$  is natural) and a right-triplet  $\Delta_R$  with  $\langle\Delta_R^0\rangle \neq 0$  so as to generate a Majorana neutrino mass. L-R symmetry requires that if the Majorana  $\mathcal{L}_M$  is present for  $\Delta_R$ , then it must also be present for  $\Delta_L$ . In what follows, we discuss the phenomenology of the  $\Delta_L$ ; that for the Higgs in  $\Delta_R$  is very different [27]. We will drop the  $L$  subscript in the following. Limits on the  $h_{ij}$  by virtue of the  $\Delta^{--} \rightarrow \ell^-\ell^-$  couplings include: Bhabha scattering,  $(g-2)_\mu$ , muonium-antimuonium conversion, and  $\mu^- \rightarrow e^-e^-e^+$ . Writing

$$|h_{\ell\ell}^{\Delta^{--}}|^2 \equiv c_{\ell\ell}m_{\Delta^{--}}^2 (\text{GeV}), \quad (6)$$

$c_{ee} < 10^{-5}$  (Bhabha) and  $\sqrt{c_{ee}c_{\mu\mu}} < 10^{-7}$  (muonium-antimuonium) are the strongest of the limits. There are no limits on  $c_{\tau\tau}$ .

If  $v_\Delta$  is small or 0, the  $\Delta^{--}$  width would be quite small, which can lead to very large  $s$ -channel production rates for  $\Delta^{--}$  in  $e^-e^-$  and  $\mu^-\mu^-$  collisions [28]. The strategy for  $\Delta^{--}$  detection is the following. For small or zero  $v_\Delta$ , we would discover the  $\Delta^{--}$  in  $p\bar{p}, pp \rightarrow \Delta^{--}\Delta^{++}$  with  $\Delta^{--} \rightarrow \ell^-\ell^-, \Delta^{++} \rightarrow \ell^+\ell^+$  ( $\ell = e, \mu, \tau$ ) at the Tevatron or LHC for  $m_{\Delta^{--}} \lesssim 1$  TeV [29]. This is precisely the mass range for which  $s$ -channel production of the  $\Delta^{--}$  would be possible at a  $\sqrt{s} \leq 1$  TeV  $e^-e^-$  LC or  $\mu^-\mu^-$  collider. Event rates can be enormous for  $c_{\ell\ell}$  near the current upper limits [28]. Equivalently,  $e^-e^-$  and  $\mu^-\mu^-$  collisions probe very small  $c_{\ell\ell}$ . For small beam energy spread ( $\delta E/E \equiv R$ ), the number of  $\Delta^{--}$  produced in  $\ell^-\ell^-$  collisions is

$$N(\Delta^{--})_{L=50 \text{ fb}^{-1}} \sim 3 \times 10^{10} \left(\frac{c_{\ell\ell}}{10^{-5}}\right) \left(\frac{0.2\%}{R}\right), \quad (7)$$

where  $R \sim 0.2\%$  is reasonable in  $e^-e^-$  collisions and  $R \lesssim 0.01\%$  is possible in  $\mu^-\mu^-$  collisions. If 100 events (of like sign dilepton pairs of definite known invariant mass) constitute a viable signal, Eq. (7) implies we can probe

$$c_{\ell\ell}|_{100 \text{ events}} \sim 3.3 \times 10^{-14} \left(\frac{R}{0.2\%}\right) \left(\frac{50 \text{ fb}^{-1}}{L}\right), \quad (8)$$

independent of  $m_{\Delta^{--}}$ . This is dramatic sensitivity — at least a factor of  $10^8 - 10^9$  improvement over current limits at an  $e^-e^-$  collider. If  $\Delta^{--} \rightarrow \mu^-\mu^-$  primarily, then 10 events might constitute a viable signal and sensitivity would be further improved.

As a final remark, we note that if triplets are present in a SUSY model, the triplet Higgs field(s) will destroy coupling constant unification if intermediate scale matter is not included; but, this is not a severe problem since such matter is natural in L-R symmetric supersymmetric models.

## 4 Extra Dimensions and Higgs Physics

This is a very large area of recent research and I will say only a few words about a variety of interesting possibilities.

The first important point is that large extra dimensions are associated with much lower Planck scales, possibly as low as  $M_S \sim 1$  TeV [30]. This reduces and can even eliminate the naturalness and hierarchy problems. In particular, the quadratic divergence in the Higgs mass loop calculation would be cutoff at  $M_S$ . As a result, this particular motivation for low-energy supersymmetry is greatly reduced. (Of course, in most such models one must view the MSSM unification of gauge couplings at the GUT scale in the usual four-dimensional theories as being totally accidental.) Other useful possibilities with large extra dimensions include various explanations of the small size of most Yukawa couplings. In one approach [31], the brane on which the SM particles live has significant width, and the Higgs is centered at one location while the weakly coupled fermions are located with significant separations from the Higgs centrum.

Extra dimensions can also provide new contributions to the precision electroweak observables [32]. These can shift expectations for the mass of the SM-like Higgs, in particular allowing it to be much heavier than the light  $m_{h_{\text{SM}}} \sim 100$  GeV values required in the pure SM context. Just as in the general 2HDM case, the extra dimension theory only needs to give a small  $\Delta S$  contribution and a large  $\Delta T > 0$  contribution.

Extra dimensions can also be the source of electroweak symmetry breaking. In one approach [33], the Kaluza Klein (KK) modes mix with Higgs in such a way that the full effective potential takes the form  $\bar{V}_{\text{tot}} = V(\phi) - \bar{D}V^2(\phi)$ , with  $\bar{D} < 0$  from the KK summation. If  $\bar{D} < 0$ , as for instance if the number of extra dimension is  $\delta = 1$ , then the minimum of this potential is at  $V(\phi) = \frac{1}{2\bar{D}}$ , independent of the form of  $V(\phi)$ . In fact, even if  $V(\phi)$  has no quartic term, the  $-\bar{D}V^2(\phi)$  term generates the quartic interactions and EWSB takes place. The physical Higgs boson is a complicated mixture of the usual Higgs field and a sum of KK modes. The main phenomenological implication is that such a Higgs might not have significant Yukawa couplings and invisible decays into KK modes could be dominant.

It is also the case that the Lagrangian could contain a term of form  $-\frac{\zeta}{2}R(g)\phi^\dagger\phi$ , where  $R(g)$  is the usual Ricci scalar. This term introduces mixing between the Higgs bosons and the KK excitations associated with the extra dimensions. The result is a large invisible decay width of the Higgs boson [34].

In the Randall-Sundrum model, there is only one graviscalar. It mixes with the Higgs boson, yielding two mixed physical states with properties that are intermediate between those of the radion and of the Higgs boson [34].

## 5 Detecting an Invisible Higgs Boson

Aside from invisible KK mode decays, there are also the possibilities of Higgs decays to Majorans, to  $\tilde{\chi}_1^0\tilde{\chi}_1^0$  (in supersymmetric models), and to 4th generation neutrinos (with  $m_{\nu_4} > m_Z/2$  to avoid  $Z$  invisible width limits). If the Higgs decays are dominated by the invisible channel(s), alternative Higgs detection strategies are necessary. At a LC, there is no difficulty in seeing an invisibly decay Higgs in Higgsstrahlung production,  $e^+e^- \rightarrow Z^* \rightarrow Zh$ , by looking for a peak in the recoil mass  $M_X$  in the  $ZX$  final state, with  $Z \rightarrow e^+e^-$  and  $Z \rightarrow \mu^+\mu^-$ .

At hadron colliders, detection will be more difficult. The key is to be able to tag the Higgs event using particle(s) produced in association with the Higgs boson. The modes  $t\bar{t}h$  production [35] and  $Wh, Zh$  production [36,37] were identified early on as being very promising, but detailed experimental evaluation/simulation has only recently been begun. The latter modes might even be useful at the Tevatron [38]. More recently,  $WW \rightarrow h$  fusion using double tagging of highly energetic forward jets at the LHC has been proposed [39]. It should be noted that the  $Wh, Zh$  and  $WW$  fusion modes all rely on the  $VV$  coupling of the Higgs boson, whereas the  $t\bar{t}h$  mode relies on the fermionic couplings and would be relevant even for the Higgs bosons of an extended Higgs sector that have small or zero tree-level  $VV$  couplings.

For a SM-like Higgs, it was estimated that the  $Wh + Zh$  and  $t\bar{t}h$  modes have discovery reach at the LHC up to about 200 GeV and 250 GeV, respectively, with  $L = 100 \text{ fb}^{-1}$  of accumulated luminosity. At the Tevatron, the  $Wh + Zh$  modes will only exceed the limits for an invisibly decaying SM-like Higgs boson already established at LEP2 ( $m_h > 100 \text{ GeV}$ ) when  $L > 5 \text{ fb}^{-1}$ . These discovery reaches are substantially less than those for the  $h_{\text{SM}}$  with normal decays. A roughly equal mixture of invisible and normal decays would reduce the reach of both the invisible decay and normal decay detection techniques and possibly make Higgs detection all but impossible at the hadron colliders. A careful study is needed.

## 6 Supersymmetric Model Higgs Bosons

A good summary of the MSSM Higgs sector is found in [1]. At least two doublets are required in supersymmetry in order to give mass to both up quarks and down quarks and leptons. An even number of doublets, plus their higgsino partners, are also required for cancellation of anomalies. The MSSM contains exactly two doublets ( $Y = +1$  and  $Y = -1$ ) with type-II Yukawa couplings. TeV scale supersymmetry as embodied in the MSSM is the most popular cure for the naturalness and hierarchy problems for good reason. First, for two (and only two) doublets one finds perfect coupling constant unification at the GUT scale if the SUSY scale is  $m_{\text{SUSY}} \sim 1$  TeV (actually, a significant number of sparticles with masses nearer 10 TeV gives better  $\alpha_s$  unification with  $\alpha_2$  and  $\alpha_1$ ). If there are more doublets, triplets, etc. then coupling unification generally requires intermediate scale matter between the TeV and  $M_U$  scales. If there are extra dimensions, unification would not necessarily be relevant (although it can be maintained by putting the SM particles in the bulk [40]). In short, the MSSM without extra large dimensions has very strong motivation.

The only extension to the MSSM Higgs sector that does not destroy gauge unification is to add one or more singlet Higgs fields. The model in which one singlet Higgs field is included is called the NMSSM (next-to-minimal supersymmetric model) [41] (see [1] for a review). This is an extremely attractive model in that it provides the most natural explanation for having a  $\mu$  parameter that has TeV scale magnitude. The parameter  $\mu$  is that appearing in the MSSM superpotential  $\mu \hat{\phi}_u \hat{\phi}_d$ , where the  $\hat{\phi}_{u,d}$  are the superfields containing the scalar  $\phi_{u,d}$  Higgs fields of the type-II Higgs sector. In the NMSSM, this interaction is replaced by the superpotential form  $\lambda_S \hat{S} \hat{\phi}_u \hat{\phi}_d$ , which generates an electroweak scale effective  $\mu = \lambda_S s$  when the scalar component of  $\hat{S}$  acquires an electroweak scale vacuum expectation value,  $s \equiv \langle S^0 \rangle$ , as is easily and naturally arranged. In addition, the NMSSM can contain a superpotential piece of the form  $\frac{1}{3} \kappa \hat{S}^3$ .

As is well known, there is a strong bound on the mass of the lightest Higgs boson  $h^0$  of supersymmetric models. In the MSSM, if  $m_{\tilde{t}} \leq 1$  TeV then  $m_{h^0} \lesssim 130 - 135$  GeV after including stop loop corrections with  $A_t \neq 0$ . ( $A_t$  is the magnitude of the trilinear soft supersymmetry breaking term.) This bound is so strong because *at tree-level* one finds  $m_{h^0} \leq m_Z$  due to the fact that all Higgs self couplings are given in terms of gauge couplings,  $g$  and  $g'$ . However, the choice above of  $m_{\tilde{t}} \leq 1$  TeV is a bit arbitrary. As noted earlier, having some SUSY matter nearer 10 TeV actually improves coupling constant unification. For stop masses in this latter range, the upper bound on  $m_{h^0}$  would be larger. Also, increasing the top mass within the current experimental error increases the upper limit on  $m_{h^0}$ . In the NMSSM, the upper bound is less constrained because of the new  $\lambda_S$  parameter introduced. One finds  $m_{h^0} \leq 150$  GeV *assuming perturbativity for  $\lambda_S$  up to  $M_U$* . If one adds more doublet Higgs superfields, this actually lowers the mass bound. Adding triplet Higgs superfields increases the mass

bound (assuming perturbativity up to  $M_U$  again) to  $m_{h^0} \leq 200$  GeV [42]. This is the maximal value employed earlier in the sum rule of Eq. (1).

## 6.1 Experimental limits from LEP2 on MSSM Higgs bosons

Limits from LEP2 in the MSSM context are quite significant. Roughly,  $m_{h^0}, m_{A^0} \lesssim 91$  GeV are excluded [43] for maximal mixing in the stop squark sector (a certain choice of  $X_t \equiv A_t - \mu \cot \beta$ ) and  $m_{\text{SUSY}} = 1$  TeV. Using the theoretical upper bound on  $m_{h^0}$  as a function of  $\tan \beta$ , this translates to exclusion of the region  $0.5 < \tan \beta < 2.4$  at 95% CL. Higher  $m_{\text{SUSY}}$  means that Higgs masses at a given  $\tan \beta$  increase with the result that less of the  $[m_{A^0}, \tan \beta]$  parameter space is excluded.

The above limits on  $m_{h^0}, m_{A^0}$  assume absence of CP violation in the Higgs sector and invisible decays of the  $h^0, A^0$  are not allowed for. CP violation arises in the MSSM through phases of the  $\mu$  and  $A_t$  parameters. This CP violation leads to CP violation in the MSSM two-doublet Higgs sector brought in via the one-loop corrections sensitive to these phases. The two new parameters are:  $\phi_\mu + \phi_A$  and  $\theta$ , the latter being the phase of one of the Higgs doublet fields relative to the other. Studies [44,45] suggest that MSSM Higgs mass limits will be weakened significantly, implying that the disallowed  $\tan \beta$  region is still allowed when CP violation is present.

Allowing for  $h^0$  and  $A^0$  to have some, perhaps substantial, invisible decays would considerably weaken the constraints on the  $h^0 A^0$  cross section. As a result, the  $ZX$  recoil mass analysis would have to be relied upon more heavily. I would guess that the limits on  $m_{h^0}$  and  $m_{A^0}$  deteriorate substantially. This deserves study by the LEP experimental groups.

## 6.2 Discovery prospects for MSSM Bosons at the Tevatron

We recall that the  $H^0$  ( $h^0$ ) has most of the  $WW, ZZ$  coupling when  $m_{A^0} \lesssim m_Z$  ( $m_{A^0} \gtrsim 150$  GeV). For,  $m_Z \lesssim m_{A^0} \lesssim 150$  GeV, the  $h^0$  and  $H^0$  will share the  $WW, ZZ$  coupling strength to a greater or lesser extent depending upon other details of the input parameters. The useful production processes are  $q\bar{q} \rightarrow Vh^0, VH^0$  with  $h^0, H^0 \rightarrow b\bar{b}$  being dominant for  $m_{A^0}$  values such that  $h^0, H^0$  has substantial  $VV$  coupling, respectively. The decoupled Higgs boson,  $h^0$  at low  $m_{A^0}$  or  $H^0$  at high  $m_{A^0}$ , will have  $b\bar{b}$  coupling that is enhanced by a factor of  $\tan \beta$  (relative to the SM-like value) and the processes  $gg, q\bar{q} \rightarrow b\bar{b}h^0$  or  $b\bar{b}H^0$ , respectively, will be enhanced;  $gg, q\bar{q} \rightarrow b\bar{b}A^0$  is always enhanced at high  $\tan \beta$ . Obviously, a Higgs which decouples from  $VV$  and has enhanced  $b\bar{b}$  coupling will decay primarily to  $b\bar{b}$ . A careful study, including a parameterized simulation of detector effects, was performed to study prospects at the Tevatron using these channels [5]. Except for some very special parameter configurations, the results are summarized by Fig. 8. One sees that  $L > 15 \text{ fb}^{-1}$  is needed to guarantee  $5\sigma$  discovery at lower  $m_{A^0}$ . For larger  $m_{A^0}$ , as typically needed for successful generation of EWSB via the RGE running, much higher  $L$  will

be needed. Except in the upper left corner of low  $m_{A^0}$  and high  $\tan\beta$ , only the  $h^0$  is observed. The small white region is where the  $h^0$  and  $H^0$  are sharing the  $VV$  coupling and neither is produced strongly enough for detection. If the root-mean squark mass,  $m_{\text{SUSY}}$ , is increased above 1 TeV, the  $h^0$  mass increases and discovery prospects deteriorate.

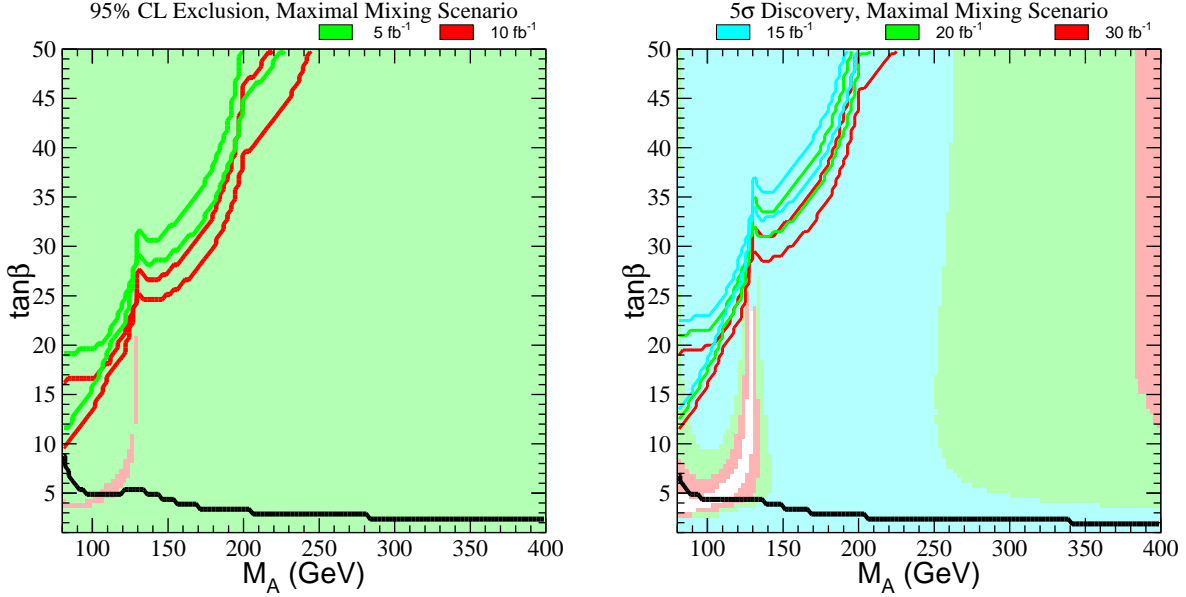


Figure 8: (a) 95% CL exclusion regions and (b)  $5\sigma$  discovery regions in the  $[m_{A^0}, \tan\beta]$  plane, for the maximal mixing scenario (using  $m_{\text{SUSY}} = 1$  TeV) and two different search channels:  $q\bar{q} \rightarrow V\phi$  [ $\phi = h^0, H^0$ ],  $\phi \rightarrow b\bar{b}$  (shaded regions) and  $gg, q\bar{q} \rightarrow b\bar{b}\phi$  [ $\phi = h^0, H^0, A^0$ ],  $\phi \rightarrow b\bar{b}$  (region in the upper left-hand corner bounded by the solid lines). The region below the solid black line is excluded by no  $e^+e^- \rightarrow Z\phi$  events at LEP2.

### 6.3 Discovery Prospects for MSSM Higgs Bosons at the LHC

Focusing on large  $m_{A^0}$ , discovery of the SM-like  $h^0$  will typically be possible using the same production/decay modes as for a light  $h_{\text{SM}}$  at the LHC. At high  $\tan\beta$  and large  $m_{A^0}$ , the decoupled  $H^0$  and  $A^0$  can be found using  $gg, q\bar{q} \rightarrow b\bar{b}H^0, b\bar{b}A^0$ , with  $H^0, A^0 \rightarrow \tau^+\tau^-$  or  $\mu^+\mu^-$  and  $gb \rightarrow H^\pm t$  with  $H^\pm \rightarrow \tau^\pm\nu$ . These are the main modes of importance since LEP2 limits pretty much exclude  $\tan\beta < 2.5$ , for which other modes could be dominant. The contours for  $5\sigma$  discovery are shown in Fig. 9. Discovery of at least one of the MSSM Higgs bosons is guaranteed for  $L = 300 \text{ fb}^{-1}$ . If  $m_{A^0} \gtrsim 200$  GeV and  $\tan\beta$  is not large enough, it could happen that only the SM-like  $h^0$  will be observable.

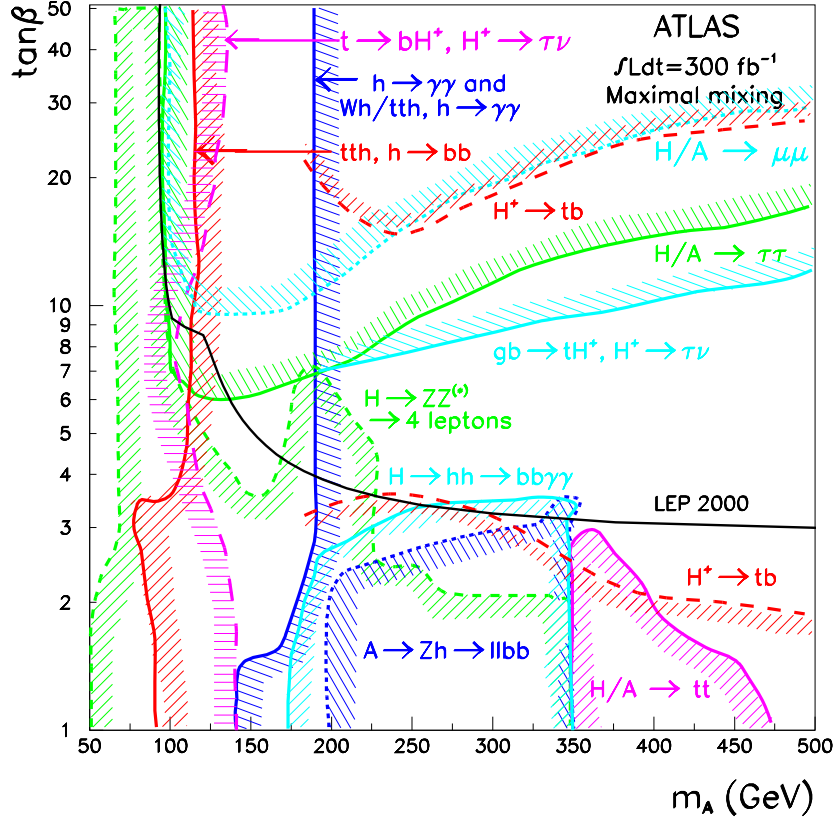


Figure 9:  $5\sigma$  discovery contours for MSSM Higgs boson detection in various channels are shown in the  $[m_{A^0}, \tan\beta]$  parameter plane, assuming maximal mixing,  $m_{\text{SUSY}} = 1$  TeV and an integrated luminosity of  $L = 300 \text{ fb}^{-1}$  for the ATLAS detector. This figure is preliminary [46].

#### 6.4 Discovery Prospects for MSSM Higgs Bosons at the LC

Recent reviews of this topic include [8] and [9]. Any Higgs boson with even very modest  $VV$  coupling can be detected using the Higgsstrahlung  $e^+e^- \rightarrow Z^* \rightarrow Zh$  process. For  $m_{A^0} \gtrsim 150$  GeV (as probable for RGE driven EWSB), decoupling has set in and it is the  $h^0$  that will be detected in this way. In particular, the upper limit of  $m_{h^0} \lesssim 135$  GeV guarantees that a  $\sqrt{s} = 350$  GeV LC would suffice. For the  $H^0, A^0, H^\pm$ , the production mechanisms  $e^+e^- \rightarrow H^0 + A^0$  and  $e^+e^- \rightarrow H^+ + H^-$  would be full strength. However, at large  $m_{A^0}$ , one finds  $m_{H^0} \sim m_{A^0} \sim m_{H^\pm}$  so that pair production requires  $m_{A^0} < \sqrt{s}/2$ . If  $m_{A^0}$  exceeds  $\sqrt{s}/2$ , then one must turn to  $e^+e^- \rightarrow b\bar{b}A^0, b\bar{b}H^0, btH^\pm$ . As we have already discussed, the event rates for these processes are not large enough for observation unless  $\tan\beta$  is quite large. In the problematical moderate  $\tan\beta$  wedge, where the LHC will also not find the  $H^0, A^0, H^\pm$ , observation might be possible using  $\gamma\gamma \rightarrow H^0, A^0$ . In particular, this

will be possible if the value of  $m_{A^0}$  is constrained to within  $\pm 50$  GeV, since then the expected yearly luminosity would be such that an appropriately designed scan, using a peaked  $\gamma\gamma$  luminosity spectrum, would reveal a  $H^0, A^0$  signal when  $E_{\gamma\gamma}^{\text{peak}} \sim m_{A^0}$  [49].

A model-dependent constraint on  $m_{A^0}$  of this type might be possible. If one assumes a non-conspiratorial MSSM parameter scenario,  $h^0$  vs.  $h_{\text{SM}}$  branching ratio differences reflect the value of  $m_{A^0}$  rather accurately. Further, expected LC precisions for the branching ratios are such that these differences could be measured with sufficient accuracy to determine  $m_{A^0}$  within  $\pm 50$  GeV if  $m_{A^0} \lesssim 400$  GeV [47,48]. This is precisely the range of relevance for a  $\gamma\gamma$  collisions at a  $\sqrt{s} = 500$  GeV LC. Alternatively, if the properties of the observed light Higgs are found not to deviate from those predicted for the  $h_{\text{SM}}$ , then the most natural conclusion would be that  $m_{A^0}$  is substantially heavier than 500 GeV. In this case, a  $\gamma\gamma$  scan over the  $E_{\gamma\gamma} \lesssim 400$  GeV range would not be useful. However, if one does not accept this model-dependent indirect determination of the magnitude of  $m_{A^0}$ , a full scan, say from  $m_{A^0} \sim 250$  GeV up to  $m_{A^0} \sim 400$  GeV would be called for. However, luminosity expectations for the NLC design might not suffice [49] to find the  $H^0, A^0$  if one has to scan such a large range of mass. Much higher  $L_{\gamma\gamma}$  luminosity is claimed by TESLA. This might be a rather crucial difference [49,50]. Once the mass of any of the  $h^0, H^0, A^0$  is known, we can run with  $E_{\gamma\gamma}^{\text{peak}}$  equal to the Higgs mass and determine the CP nature of the Higgs boson by adjusting the linear polarization orientations of the initial laser beams [11,12,13]. In particular, we can separate  $A^0$  from  $H^0$  when these are closely degenerate (as typical for  $\tan\beta \gtrsim 4$  and  $m_{A^0} > 2m_Z$ ).

## 6.5 Special Cases in the MSSM

As already noted, the above summaries assume relatively canonical MSSM parameter choices and absence of CP violation in the Higgs sector. These expectations need not apply. If there are substantial  $h^0 \rightarrow \tilde{\chi}_1^0 \tilde{\chi}_1^0$  decays, as still possible even given LEP2 lower bounds on  $m_{\tilde{\chi}_1^0}$ , observation of the  $h^0$  at hadron colliders (but not the LC) would be more difficult. For low stop masses, corrections to the one-loop induced  $ggh^0$  and  $\gamma\gamma h^0$  couplings would be substantial. The stop and top loops negatively interfere leading to reduction of  $gg$  fusion production and some increase in  $B(h^0 \rightarrow \gamma\gamma)$  [1,51].

There can be substantial radiative corrections to the tree-level couplings. This would be especially important for  $b\bar{b}$  decays of the  $h^0$  when the  $h^0$  is SM-like. In particular, after including radiative corrections, for the  $b\bar{b}$  Yukawa Lagrangian one obtains  $\mathcal{L} \simeq \lambda_b \phi_d^0 b\bar{b} + \Delta\lambda_b \phi_u^0 b\bar{b}$ . The coupling  $\Delta\lambda_b$  is one-loop and arises from  $\tilde{b} - \tilde{g}$  and  $\tilde{t} - \tilde{\phi}_{u,d}$  loops. Typically,  $\frac{\Delta\lambda_b}{\lambda_b} \sim 0.01$  (either sign). Further,  $\frac{\Delta\lambda_b}{\lambda_b}$  does not vanish in the limit of large SUSY masses (there is no decoupling). The result for the full

$h^0 \rightarrow b\bar{b}$  coupling takes the form:

$$\lambda_b^{h^0} \simeq -\frac{m_b \sin \alpha}{v \cos \beta} \frac{1}{1 + \frac{\Delta\lambda_b}{\lambda_b} \tan \beta} \left[ 1 - \frac{\frac{\Delta\lambda_b}{\lambda_b}}{\tan \alpha} \right], \quad (9)$$

implying that if  $\tan \alpha \simeq \frac{\Delta\lambda_b}{\lambda_b}$  then  $\lambda_b^{h^0} \simeq 0$ . In particular, this can happen when  $m_{A^0} \rightarrow \infty$  if  $\Delta\lambda_b/\lambda_b < 0$ , since, at large  $m_{A^0}$ ,  $\alpha \rightarrow \pi/2 - \beta$  and  $\tan \alpha \rightarrow -1/\tan \beta$  is small. Conversely, for  $\Delta\lambda_b/\lambda_b > 0$ , substantial enhancement of  $\lambda_b^{h^0}$  is possible.

If parameters are such that the  $h^0$  decouples from  $b$ 's (i.e.  $h^0 \simeq \text{Re}\phi_u^0$ ), discovery strategies could not rely on the  $b\bar{b}$  decay mode. However, since  $\Gamma(h^0 \rightarrow \gamma\gamma)$  is dominated by  $W$  and  $t$  loops, small or vanishing  $\lambda_b^{h^0}$  will affect the  $h^0 \rightarrow \gamma\gamma$  partial width very little. There is also little impact on the  $gg$  partial width. Thus, suppressed  $\Gamma(h^0 \rightarrow b\bar{b})$  implies enhanced  $B(h^0 \rightarrow \gamma\gamma), B(h^0 \rightarrow WW^*)$ . In fact, the  $\gamma\gamma$  mode can be viable for some range of  $m_{h^0}$  at the Tevatron if  $h^0 \sim \phi_u$  [52]. More generally, allowing for either suppressed or enhanced  $\lambda_b^{h^0}$ , LHC  $gg \rightarrow h^0 \rightarrow \gamma\gamma$  and Tevatron  $Wh^0[\rightarrow WW^*]$  modes improve when LHC, Tevatron  $W, Zh^0[\rightarrow b\bar{b}]$  modes deteriorate. One also finds that the Tevatron and the LHC are complementary as  $\lambda_b^{h^0}$  and  $m_{h^0}$  vary in that  $h^0$  discovery will occur at one or the other machine, even if not both [53].

Turning next to the  $H^0, A^0, H^\pm$ , discovery will typically become more difficult if these Higgs bosons have substantial branching ratios for decay to pairs of neutralinos, or charginos or sleptons, . . . Such decays will, however, only be significant if  $\tan \beta$  is in the low to moderate range, a significant part of which has already been excluded by LEP2 data. For larger  $\tan \beta$ , the  $H^0, A^0 \rightarrow b\bar{b}$  and  $H^\pm \rightarrow t\bar{b}$  decay modes and their  $\tau$  analogues are sufficiently enhanced that sparticle pair channels will have small branching ratios.

## 6.6 Discovery of NMSSM Higgs Bosons

The addition of the singlet superfield results in a third CP-even Higgs boson and a second CP-odd Higgs boson. The CP-even bosons mix, as do the CP-odd bosons. There is still a strong constraint of  $m_{h_1^0} \leq 150$  GeV on the mass of the lightest CP-even physical state. If it does not have substantial coupling to  $VV$ , then it can be shown that one of the other two states ( $h_2^0$  or  $h_3^0$ ) must have at least moderate  $VV$  coupling *and* must be relatively light. As a result, discovery of one (or more) of the CP-even Higgs bosons of the NMSSM is guaranteed at a LC with  $\sqrt{s} > 350$  GeV [54]. An important question is whether the sharing of the  $VV$  coupling that is possible in the NMSSM means that discovery of one of the NMSSM Higgs bosons at the LHC cannot be guaranteed. A study for Snowmass 96 [55] showed that parameters could be chosen so that no Higgs boson would be observed employing the experimentally verified modes available at that time, even for  $L = 600 \text{ fb}^{-1}$ . For example, for  $m_{h_1^0} = 105$  GeV and  $\tan \beta = 5$ , event rates in the  $h_{1,2,3} \rightarrow \gamma\gamma, ZZ^*$ ,

$WW^*$ , *etc.* final states could all be suppressed by virtue of a shared  $VV$  coupling configuration, while  $\tan\beta$  was too small to sufficiently enhance the  $b\bar{b}h_{1,2,3}$  and  $b\bar{b}a_{1,2}$  (with  $h_{1,2,3}, a_{1,2} \rightarrow \tau^+\tau^-$ ) modes to the  $5\sigma$  level. What was missing in 1996 was a discovery mode based on the  $b\bar{b}$  decays, especially those of the lightest Higgs bosons,  $h_{1,2}$ . Recently, the  $t\bar{t}h \rightarrow t\bar{t}b\bar{b}$  mode (originally discussed in [56]) has been shown to be viable for a SM-like Higgs by the ATLAS and CMS groups [57]. Rescaling these results to the NMSSM, a preliminary study [58] finds that all points for which discovery was found to be impossible without this mode would allow  $> 5\sigma$  discovery of  $h_1$  or  $h_2$  in the  $t\bar{t}b\bar{b}$  final state. Further study is needed, but it now appears that there is a ‘no-lose’ theorem for NMSSM Higgs discovery at the LHC once both ATLAS and CMS have each accumulated  $L \geq 300 \text{ fb}^{-1}$  of luminosity.

## 7 Conclusions

This brief overview of discovery prospects for Higgs bosons necessarily omitted many interesting topics, and almost completely ignored the very interesting programs for precision measurements of the properties of the Higgs bosons at the LHC and LC and how such measurements impact our ability to determine, for instance, the MSSM or NMSSM soft-supersymmetry-breaking parameters. It is these latter which are needed to connect TeV scale physics to the GUT scale physics that we ultimately hope to probe.

## Acknowledgments

This work was supported in part by the U.S. Department of Energy and by the Davis Institute for High Energy Physics.

## References

- [1] J.F. Gunion, H.E. Haber, G. Kane and S. Dawson, *The Higgs Hunters Guide*, Addison-Wesley.
- [2] T. Hambye and K. Riesselmann, *Phys. Rev.* **D55** (1997) 7255.
- [3] A. Freitas, W. Hollik, W. Walter and G. Weiglein, *Phys. Lett.* **B495** (2000) 338 [hep-ph/0007091]; A. Freitas, S. Heinemeyer, W. Hollik, W. Walter and G. Weiglein, *Nucl. Phys. Proc. Suppl.* **89** (2000) 82 [hep-ph/0007129]; hep-ph/0101260.
- [4] R. Barate *et al.* [ALEPH Collaboration], *Phys. Lett.* **B495** (2000) 1 [hep-ex/0011045]; P. Abreu *et al.* [DELPHI Collaboration], *Phys. Lett.* **B499** (2001)

- 23 [hep-ex/0102036]; M. Acciarri *et al.* [L3 Collaboration], hep-ex/0012019; G. Abbiendi *et al.* [OPAL Collaboration], *Phys. Lett.* **B499** (2001) 38 [hep-ex/0101014].
- [5] M. Carena, J.S. Conway, H.E. Haber and J.D. Hobbs *et al.*, hep-ph/0010338 [FERMILAB-CONF-00/270-T].
- [6] For a recent review, see V.A. Mitsou, ATLAS-CONF-2000-002.
- [7] K. Lassila-Perini, ETH Dissertation thesis No. 12961 (1998).
- [8] TESLA Technical Design Report, R. Heuer, D. Miller, F. Richard, A. Wagner and P.M. Zerwas (editors), obtainable from [www.desy.de/~lcnotes/tdr/](http://www.desy.de/~lcnotes/tdr/) .
- [9] The NLC Orange Book, . . . .
- [10] J.F. Gunion and P.C. Martin, hep-ph/9610417; J. F. Gunion and P. C. Martin, *Phys. Rev. Lett.* **78** (1997) 4541 [hep-ph/9607360].
- [11] B. Grzadkowski and J.F. Gunion, *Phys. Lett.* **B294** (1992) 361 [hep-ph/9206262].
- [12] J.F. Gunion and J.G. Kelly, *Phys. Lett.* **B333** (1994) 110 [hep-ph/9404343].
- [13] M. Krämer, J. Kühn, M.L. Stong and P.M. Zerwas, *Z. Phys.* **C64** (1994) 21 [hep-ph/9404280].
- [14] J.F. Gunion and X.G. He, Proceedings of Snowmass96, hep-ph/9609453.
- [15] J.F. Gunion, B. Grzadkowski and X. He, *Phys. Rev. Lett.* **77** (1996) 5172 [hep-ph/9605326].
- [16] B.A. Dobrescu, hep-ph/9903407 and hep-ph/0103038.
- [17] M. Cvetič, H. Lu, C. N. Pope, A. Sadzadeh and T.A. Tran, *Nucl. Phys.* **B586** (2000) 275 [hep-th/0003103].
- [18] J.F. Gunion, R. Vega and J. Wudka, *Phys. Rev.* **D43** (1991) 2322.
- [19] J.R. Espinosa and M. Quirós, *Phys. Rev. Lett.* **81** (1998) 516 [hep-ph/9804235].
- [20] J.R. Espinosa and J.F. Gunion, *Phys. Rev. Lett.* **82** (1999) 1084 [hep-ph/9807275].
- [21] J. F. Gunion, T. Han and R. Sobey, *Phys. Lett.* **B429** (1998) 79 [hep-ph/9801317].

- [22] B. Grzadkowski, J.F. Gunion and J. Kalinowski, *Phys. Lett.* **B480** (2000) 287 [hep-ph/0001093].
- [23] T. Farris, B. Grzadkowski, J.F. Gunion, J. Kalinowski and M. Krawczyk, *Phys. Lett.* **B496** (2000) 195 [hep-ph/0009271].
- [24] T. Farris and J.F. Gunion, LC note in preparation.
- [25] H. N. Brown *et al.* [Muon g-2 Collaboration], *Phys. Rev. Lett.* **86** (2001) 2227 [hep-ex/0102017].
- [26] K. Cheung, C. Chou and O. C. Kong, hep-ph/0103183.
- [27] R.N. Mohapatra, *Fortsch. Phys.* **31** (1983) 185; J.F. Gunion, J. Grifols, A. Mendez, B. Kayser and F. Olness, *Phys. Rev.* **D40** (1989) 1546; N.G. Deshpande, J.F. Gunion, B. Kayser and F. Olness, *Phys. Rev.* **D44** (1991) 837.
- [28] J.F. Gunion, *Int. J. Mod. Phys.* **A11** (1996) 1551 [hep-ph/9510350]; **A13** (1998) 2277 [hep-ph/9803222]. See also: P.H. Frampton, *Int. J. Mod. Phys.* **A15** (2000) 2455 [hep-ph/0002017]; F. Cuyper and M. Raidal, *Nucl. Phys.* **B501** (1997) 3 [hep-ph/9704224].
- [29] J. F. Gunion, C. Loomis and K. T. Pitts, Snowmass96 Proceedings, hep-ph/9610237.
- [30] N. Arkani-Hamed, S. Dimopoulos and G. Dvali, *Phys. Lett.* **B429** (1998) 263 [hep-ph/9803315].
- [31] E. A. Mirabelli and M. Schmaltz, *Phys. Rev.* **D61** (2000) 113011 [hep-ph/9912265].
- [32] T. G. Rizzo and J. D. Wells, *Phys. Rev.* **D61** (2000) 016007 [hep-ph/9906234].
- [33] B. Grzadkowski and J. F. Gunion, *Phys. Lett.* **B473** (2000) 50 [hep-ph/9910456].
- [34] G. F. Giudice, R. Rattazzi and J. D. Wells, *Nucl. Phys.* **B595** (2001) 250 [hep-ph/0002178].
- [35] J. F. Gunion, *Phys. Rev. Lett.* **72** (1994) 199 [hep-ph/9309216].
- [36] S. G. Frederiksen, N. Johnson, G. Kane and J. Reid, *Phys. Rev.* **D50** (1994) 4244.
- [37] D. Choudhury and D. P. Roy, *Phys. Lett.* **B322** (1994) 368 [hep-ph/9312347].
- [38] S. P. Martin and J. D. Wells, *Phys. Rev.* **D60** (1999) 035006 [hep-ph/9903259].

- [39] O. J. Eboli and D. Zeppenfeld, *Phys. Lett.* **B495** (2000) 147 [hep-ph/0009158].
- [40] K. R. Dienes, E. Dudas and T. Gherghetta, *Nucl. Phys.* **B537** (1999) 47 [hep-ph/9806292].
- [41] J. Ellis, J. F. Gunion, H. E. Haber, L. Roszkowski and F. Zwirner, *Phys. Rev.* **D39** (1989) 844.
- [42] J. R. Espinosa and M. Quiros, *Phys. Lett.* **B302** (1993) 51 [hep-ph/9212305].
- [43] The ALEPH, DELPHI, L3 and OPAL Collaborations and the LEP Higgs Working Group, LHWG note 2001-2 (26 March 2001).
- [44] G. L. Kane and L. Wang, *Phys. Lett.* **B488** (2000) 383 [hep-ph/0003198].
- [45] M. Carena, J. Ellis, A. Pilaftsis and C. E. Wagner, *Phys. Lett.* **B495** (2000) 155 [hep-ph/0009212].
- [46] The results of Fig. 9 were provided by F. Gianotti on behalf of the ATLAS collaboration. They are the preliminary results available as of March 3, 2001.
- [47] J.F. Gunion, L. Poggioli, R. Van Kooten, C. Kao, P. Rowson *et al.*, “Higgs boson discovery and properties,” in *New Directions for High Energy Physics*, Proceedings, Snowmass ’96 pp. 541–587 [hep-ph/9703330].
- [48] See, for example, J.F. Gunion, hep-ph/9705282.
- [49] D. Asner, J. Gronberg, J. Gunion and T. Hill, in preparation.
- [50] M.M. Mühlleitner, M. Krämer, M. Spira and P.M. Zerwas, hep-ph/0101083.
- [51] A. Djouadi, *Phys. Lett.* **B435** (1998) 101 [hep-ph/9806315].
- [52] S. Mrenna and J. Wells, *Phys. Rev.* **D63** (2001) 015006 [hep-ph/0001226].
- [53] M. Carena, S. Mrenna and C. E. Wagner, *Phys. Rev.* **D62** (2000) 055008 [hep-ph/9907422].
- [54] U. Ellwanger and C. Hugonie, hep-ph/9909260.
- [55] J. F. Gunion, H. E. Haber and T. Moroi, Proceedings, Snowmass ’96 [hep-ph/9610337].
- [56] J. Dai, J. F. Gunion and R. Vega, *Phys. Rev. Lett.* **71** (1993) 2699 [hep-ph/9306271].

- [57] ATLAS Collaboration, “Detector and Physics Performance Technical Design Report”, CERN/LHCC/99-15 (1999); CMS Collaboration, Technical Design Reports, CMS TDR 1-5 (1997/98).
- [58] U. Ellwanger, J.F. Gunion and C. Hugonie, in preparation.

# Padé approximation to fixed order QCD calculations

ROBERT V. HARLANDER\*

*HET, Physics Department*  
*Brookhaven National Laboratory, Upton, NY 11973, U.S.A.*  
rharlan@bnl.gov

Padé approximations appear to be a powerful tool to extend the validity range of expansions around certain kinematical limits and to combine expansions of different limits to a single interpolating function. After a brief outline of the general method, we will review a number of recent applications and describe the modifications that have to be applied in each case. Among these applications are the  $\overline{\text{MS}}$ /on-shell conversion factor for quark masses and the top decay rate at NNLO in QCD.

Presented at the

5th International Symposium on Radiative Corrections  
(RADCOR-2000)  
Carmel CA, USA, 11–15 September, 2000

---

\*Supported by *Deutsche Forschungsgemeinschaft*.

# 1 Introduction

The field of radiative corrections in quantum field theory has always been exciting and rapidly developing. At this conference various new methods were presented that allow us to keep up with the ever increasing complexity of the problems posed by modern particle physics. Some of these methods are concerned with the analytic evaluation of certain classes of Feynman diagrams (see, e.g., [1]). Equally important, however, is the development of systematic approximations for complex problems. As demonstrated in various physical applications, asymptotic expansions of Feynman diagrams prove to be a very efficient tool for this purpose: they provide recipes to reduce the number of dimensional scales (masses, momenta) that a diagram depends on (see, e.g., [2]). The result is a series (possibly asymptotic) in terms of ratios of these dimensional parameters.

However, the validity of an expansion is restricted to a certain – in general finite – region of convergence. As we will see, Padé approximations have been used to enlarge the validity range of these expansions. In some of the cases described below, expansions from different limits could be combined to construct an interpolating function which connects the individual, often non-overlapping regions of convergence.<sup>1</sup>

The outline of this review is as follows: we will begin by describing the general method on the basis of the hadronic  $R$  ratio. This quantity is extremely important in particle physics: not only is it directly measurable at  $e^+e^-$  colliders, but it also influences other quantities, for example the running of the electro-magnetic coupling constant  $\alpha_{\text{QED}}(s)$  or the anomalous magnetic moment of the muon. The continuous efforts for an accurate evaluation of this quantity have presently reached an accuracy of order  $\alpha_s^3$ , even though only in the high energy limit. At order  $\alpha_s^2$ , due to the successful application of the Padé procedure described below, the full energy dependence is known. At first, the method was applied to non-singlet diagrams which clearly give the major contribution to  $R$  (cf. Sect. 2). Sect. 3 will describe the generalizations that were necessary to evaluate the singlet contributions. Let us note that recently also non-diagonal currents have been taken into account. This opens a new field of applications related to charged current reactions, like single top production at hadron colliders.

The sections that follow are concerned with a different class of applications of the Padé procedure, namely the evaluation of on-shell quantities. First we describe a recent calculation of the conversion factor from the quark mass in the  $\overline{\text{MS}}$  scheme to the on-shell scheme at order  $\alpha_s^3$ . Due to the progress in the field of heavy quark and top threshold physics, the evaluation of this factor was of utmost importance.

---

<sup>1</sup>It might be appropriate to remark that Padé approximations have also been used in the literature to estimate higher order corrections in perturbation theory (e.g. [3]). These considerations are of completely different nature than the fixed-order predictions which will be discussed in this talk.

The second application is the determination of NNLO QCD corrections to the top quark decay rate which is a necessary input for a precise experimental determination of the top quark properties at future colliders. Closely related is the evaluation of the muon decay rate at second order in QED, as well as  $\Gamma(b \rightarrow ue\bar{\nu}_e)$  to  $\mathcal{O}(\alpha_s^2)$ . Each of the on-shell quantities above has been calculated by two independent groups with complementary methods. The agreement of the results once again confirms the validity and accuracy of the Padé method.

## 2 General procedure

We are not going to describe all the details of the procedure for constructing Padé approximants, because this has been done in the literature to a sufficient extent (see in particular [4,5,6,7,8,9]). Nevertheless, for the sake of a closed presentation, let us give the main ideas by considering the by now “classic” example of the hadronic  $R$  ratio:

$$R(s) = \frac{\sigma(e^+e^- \rightarrow \text{hadrons})}{\sigma(e^+e^- \rightarrow \mu^+\mu^-)}. \quad (1)$$

The leading two orders in  $\alpha_s$  for  $R(s)$  are known in analytic form. An analytic evaluation of the complete corrections at  $\mathcal{O}(\alpha_s^2)$  currently seems to be excluded. The exact answer is known only for certain contributions, in particular the terms involving a light fermion pair [10].

For the other contributions one has to rely on approximations. There are two obvious limiting cases for which this can be achieved: On the one hand, if the center-of-mass energy is very large, one may set the quark masses  $m$  to zero. One may then use the equation

$$R(s) = 12\pi \text{Im}\Pi(s/(4m^2) + i0_+) \quad (2)$$

which relates  $R(s)$  to the imaginary part of the polarization function  $\Pi(z)$  along the upper branch of the cut  $z \in [1, \infty]$  in the complex plane. Sample diagrams for  $\Pi(z)$  are shown in Fig. 1. For the moment we will restrict the discussion to diagrams where the external currents are connected by a single massive quark line (Fig. 1 (a) and (b)). Contributions where the external currents are connected by a *massless* quark line and where the massive quarks couple only to gluons (“gluon-splitting diagrams”) are numerically unimportant and shall not be addressed here. The modifications for diagrams where each of the external currents is connected to a separate Fermion line (“singlet diagrams”, Fig. 1 (c)) will be discussed in the next section.

Taking  $m = 0$  leads to massless propagator diagrams which can be calculated using the integration-by-parts algorithm [11] as implemented in the FORM program [12]

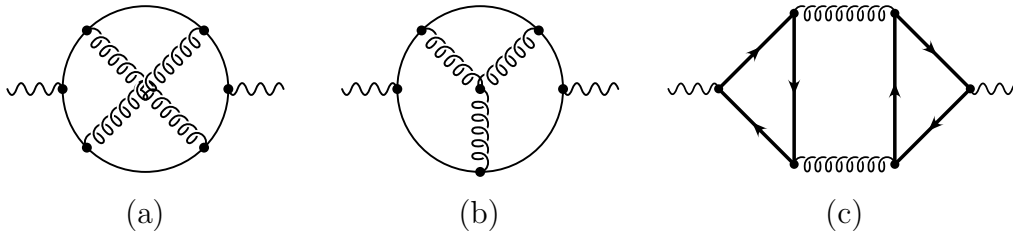


Figure 1: Diagrams contributing to the polarization function  $\Pi(z)$ . The solid lines are quarks, the springy ones are gluons. The wavy lines represent the external currents. (a) and (b) are non-singlet, (c) is a singlet diagram.

MINCER [13]. One obtains

$$R(s) = 3 \left\{ 1 + \frac{\alpha_s}{\pi} + \left( \frac{\alpha_s}{\pi} \right)^2 \left[ \frac{365}{24} - 11\zeta_3 + n_f \left( -\frac{11}{12} + \frac{2}{3}\zeta_3 \right) \right] \right\} + \dots, \quad (3)$$

where the ellipse indicates higher order terms in  $\alpha_s$  and in  $m^2/s$ .

On the other hand, the leading behavior in the opposite limit, where the center-of-mass energy is close to threshold, i.e.  $v \equiv \sqrt{1 - 4m^2/s} \ll 1$ , can be deduced from the Sommerfeld-Sakharov formula and the two-loop result of the QCD potential (for details see [6,7]). In general, these considerations allow one to deduce the terms that are singular for  $v \rightarrow 0$  (cf. Coulomb singularity) as well as the constant term.

In both limits, however, one can do better. There are well-defined methods to obtain *expansions* around the exact limits  $m = 0$  and  $s = 4m^2$  (for reviews see [2,14]). These methods reduce the original diagrams that depend on the two scales  $m^2$  and  $q^2$  to single-scale integrals which can be solved analytically. In this way one obtains approximations that are valid in certain ranges away from the actual limits. Fig. 2 shows the behavior of these expansions as dashed and dotted lines. It immediately becomes clear that their validity is restricted to a finite kinematical region. It is the purpose of this section to outline the procedure that leads to the *solid* lines in this figure, i.e. the construction of an approximation which is valid over the full  $v$  range.

The limits discussed above are the only two kinematically distinguished points for  $R(s)$  at  $\mathcal{O}(\alpha_s^2)$  (we disregard the four-particle threshold at  $s = 16m^2$  here). Considering its connection to the polarization function  $\Pi(z)$ , however, (cf. Eq. (1)) there clearly is another interesting point, namely  $z = 0$ . The coefficients of an expansion of  $\Pi(z)$  around  $z = 0$  are called “moments”. Because of the cut at  $z = 1$ , this expansion is expected to converge only for  $|z| < 1$ , and at first it seems to be impossible to extract any information on  $R(s)$  from it. However, one has to recall that  $\Pi(z)$  is analytic everywhere in the complex plane, except along the cut. A mapping of the

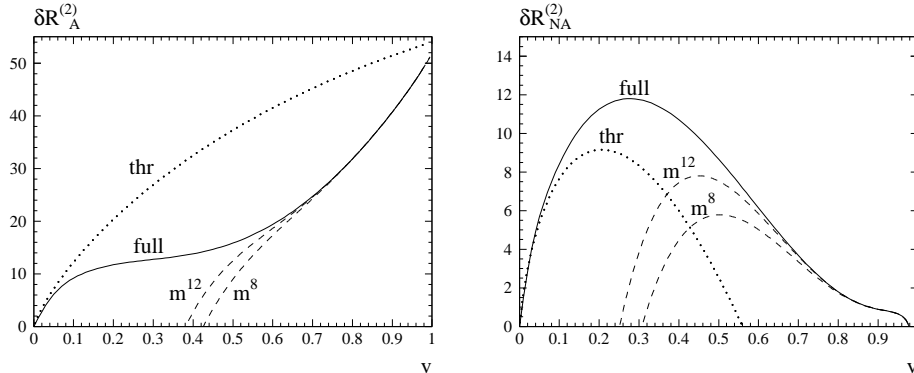


Figure 2: Threshold expansion up to terms of order  $v \ln v$  [15] (dotted), high-energy expansion up to  $m^{12}/s^6$  [16] (dashed), and Padé result [6] (solid). The singular and constant terms in  $v$  have been subtracted and the renormalization scale is set to  $\mu^2 = m^2$ . Left:  $C_F^2$ -term; Right:  $C_F C_A$ -term ( $C_F = 4/3$  and  $C_A = 3$  are the Casimir operators of the fundamental and the adjoint representation of  $SU(3)$ ).

form

$$\omega = \frac{1 - \sqrt{1 - z}}{1 + \sqrt{1 - z}} \quad (4)$$

transforms the whole  $z$ -plane into the unit circle of the  $\omega$ -plane, such that the upper (lower) branch of the cut gets mapped to the upper (lower) semi-circle. The points at  $|z| = \infty$  go to  $\omega = -1$ , while  $z = 0$  and  $z = 1$  correspond to  $\omega = 0$  and  $\omega = 1$ , respectively.

In order to arrive at a smooth function that is easy to approximate, one subtracts the threshold singularities from  $\Pi(z)$  (see above) as well as the logarithms of the asymptotic high-energy expansion (this has to be done in a suitable way in order not to generate logarithms for  $z \rightarrow 0$ ). After some more manipulations one arrives at a function  $P(\omega)$  whose value at  $\omega = -1$  and whose first few Taylor coefficients around  $\omega = 0$  are in one-to-one correspondence to the expansion coefficients of  $\Pi(z)$  around  $z = 0$  and  $z = \infty$ .

$P(\omega)$  is analytic within  $|\omega| < 1$  and thus its Taylor series around  $\omega = 0$  converges inside this region. However, we need the values of  $\Pi(z)$  on the cut, or equivalently,  $P(|\omega| = 1)$ . Thus one has to make sure that convergence of  $P(\omega)$  is given not only for  $|\omega| < 1$ , but also for  $|\omega| = 1$ .

This is the point where Padé approximants come into play. The definition of an  $[n/m]$ -Padé approximant on a function  $P(\omega)$  is

$$P_{[n/m]}(\omega) = \frac{a_0 + a_1\omega + \dots + a_n\omega^n}{1 + b_1\omega + \dots + b_m\omega^m}. \quad (5)$$

It has been demonstrated in [4,5] that such an approximant extends the convergence region of the Taylor expansion to its border  $|\omega| = 1$ . Performing the mapping back to the  $z$ -plane, and applying the inverse operations that led from  $\Pi(z)$  to  $P(\omega)$ , we thus have constructed a function that approximates  $\Pi(z)$  all over the complex plane, including the branches of the cut from  $z = 1$  to  $z = \infty$ . The imaginary part of this function gives rise to the solid lines in Fig. 2.

A nice feature of Padé approximation is that one has the freedom in varying the parameters  $n$  and  $m$  in Eq. (5). If convergence of the Padé approximants was *not* given, this would manifest itself in strong variations of the result for different values in  $n$  and  $m$ . For  $\Pi(z)$ , for example, this dependence is so weak that different Padé approximants produce curves that would be hardly distinguishable from one another in Fig. 2 (see, e.g., [9]).

As it was mentioned above, this procedure was applied for the first time in [5] to the three-loop QED vacuum polarization. It was later on generalized to the QCD case [6] for various external currents [7] (vector, axial-vector, scalar, pseudo-scalar). In all of these papers, only the leading two terms in the asymptotic expansion around  $z \rightarrow \infty$  were taken into account. After higher order terms in this limit became available [16], the method was extended to include them [8] and a further stabilization of the Padé predictions was observed [17,9]. Recently [18] the method has been applied to non-diagonal currents in order to derive the dominant contributions to single top production at hadron colliders.

### 3 Padé approximation for singlet diagrams

Above we described in some sense the “optimal case”: information on both the limits  $z \rightarrow 0$  and  $z \rightarrow \infty$  was available, and the leading threshold behavior was known. Furthermore, the analytic structure of  $\Pi(z)$  was such that the expansion around  $z = 0$  had the form of a plain Taylor expansion as opposed to an asymptotic series, i.e., it did not contain any logarithms of  $z$ . This is due to the fact that the discussion was restricted to the non-singlet contributions. The corresponding diagrams (cf. Fig. 1 (a) and (b)) do not have massless cuts: the external currents are connected by a single massive quark line, and cutting the diagram in halves always involves a cut through this line.

In the remaining part of this review we will be concerned with exceptions to this “optimal procedure.” The first case we will consider are the singlet contributions to  $\Pi(z)$ . They are distinguished from the non-singlet diagrams in the sense that the external currents are each connected to separate Fermion lines which in turn are connected to each other by gluons (cf. Fig. 1 (c)). If the external currents are vector-like, these diagrams vanish at  $\mathcal{O}(\alpha_s^2)$  due to Furry’s theorem. If, however, one is

concerned with axial-vector, scalar, or pseudo-scalar currents, massless cuts occur.<sup>2</sup> These massless cuts spoil the analyticity of  $P(\omega)$  (see Sect.2) within  $|\omega| < 1$ , and thus also the convergence of its expansion around  $\omega = 0$ . Luckily, for the singlet diagrams the analytic expressions of the massless cuts are known. Thus, denoting these massless cuts as  $R_{\text{ml}}(s)$ , we may employ the dispersion relation to write

$$\begin{aligned} \Pi_{\text{S}}(z) &= \Pi_{\text{ml}}(z) + \hat{\Pi}(z), \quad \text{with} \quad \hat{\Pi}(z) = C^{-1} \int_1^{\infty} ds \frac{R_{\text{S}}(s)}{s - 4m^2z} \\ \text{and} \quad \Pi_{\text{ml}}(z) &= C^{-1} \int_0^1 ds \frac{R_{\text{S}}(s)}{s - 4m^2z} = C^{-1} \int_0^1 ds \frac{R_{\text{ml}}(s)}{s - 4m^2z} \end{aligned} \quad (6)$$

( $C = 12\pi$  for external vector and axial-vector currents,  $C = 8\pi$  for scalar and pseudo-scalar currents). Here,  $\Pi_{\text{S}}(z)$  is the singlet contribution to the polarization function and

$$R_{\text{S}}(s) = C \text{Im}\Pi_{\text{S}}(s/(4m^2) + i0_+). \quad (7)$$

$\hat{\Pi}(z)$  is analytic in the complex plane cut along  $z \in [1, \infty]$ . It can be obtained by evaluating  $\Pi_{\text{ml}}(z)$  through Eq. (6) and subtracting it from  $\Pi_{\text{S}}(z)$ , i.e., the result for the singlet diagrams (see Fig. 1 (c)). One can then apply the Padé procedure outlined in Sect. 2 to  $\hat{\Pi}(z)$ .

For details on the evaluation of the integral for  $\Pi_{\text{ml}}(z)$  in Eq. (6) and the results we refer to [8]. At this point it shall be sufficient to mention that the combination of [7,19] (non-singlet) and [8] (singlet) provides the current knowledge of  $R(s)$  at  $\mathcal{O}(\alpha_s^2)$ . Some contributions are known analytically, and the accuracy of the approximations in all the other cases is extremely good. Let us also remark that at  $\mathcal{O}(\alpha_s^3)$ ,  $\Pi(z)$  is known in its high-energy expansion up to the terms  $\propto m^4/s^2$  [20,21,22]. No moments for  $z \rightarrow 0$  are available yet, and therefore a Padé approximation along the lines of the previous section is still out of reach.

As another application of the methods described above let us note that the results at  $\mathcal{O}(\alpha_s^2)$  were combined with the one-loop electro-weak corrections in order to predict the total cross section for  $e^+e^- \rightarrow t\bar{t}$  at a linear collider [23].

## 4 Relation between $\overline{\text{MS}}$ and on-shell quark mass

The  $\overline{\text{MS}}$  scheme is a very convenient renormalization scheme, in particular from the technical point of view. Renormalization constants in the  $\overline{\text{MS}}$  scheme do not depend

---

<sup>2</sup> In the axial-vector case, the purely gluonic cuts are zero according to the Landau-Yang theorem; but in order to avoid the axial anomaly, it is convenient to consider a full SU(2) doublet like  $(t, b)$ . Taking  $m_b = 0$ , the massless cuts arise from cuts involving  $b$  quarks.

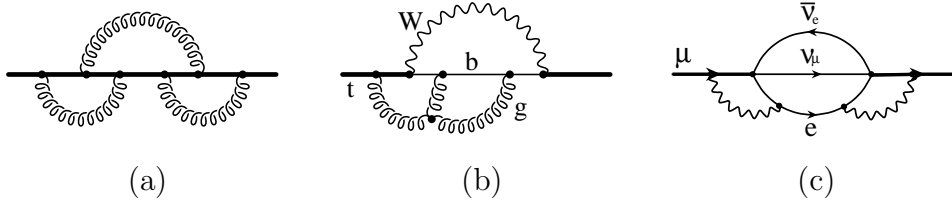


Figure 3: Diagrams contributing to (a)  $z_m$ , (b)  $\Gamma(t \rightarrow bW)$ , and (c)  $\Gamma(\mu \rightarrow e\bar{\nu}_e\nu_\mu)$ .

on any masses or momenta, which means that their evaluation provides a certain freedom in choosing the particular set of diagrams to calculate. For example, the four-loop quark anomalous dimension was computed using two completely different approaches [24].

However, comparison of the theoretical results to experimental data often requires to express the involved quantities in terms of their on-shell values. This is why the conversion factor

$$z_m = \frac{M}{\bar{m}} \quad (8)$$

that relates the on-shell to the  $\overline{\text{MS}}$  quark mass is of great importance. In order to obtain this quantity, one has to evaluate the quark propagator

$$\Sigma(q) = \not{q} \Sigma_V(q^2) + m \Sigma_S(q^2) \quad (9)$$

at the on-shell point  $q^2 = m^2$ , where  $q$  is the external momentum and  $m$  is the quark mass. A sample diagram that contributes to  $\Sigma(q)$  at order  $\alpha_s^3$  is shown in Fig. 3 (a).

Technically, these diagrams carry only a single scale and should be accessible through the integration-by-parts algorithm [11]. However, it turns out that the level of complexity for  $n$ -loop on-shell diagrams is comparable to  $(n + 1)$ -loop massive tadpole diagrams, for example. At the two-loop level, the problem of finding the recurrence relations was solved in [25].

The three-loop case seemed to be out of reach for quite some time. This is why the first calculation of the conversion factor was performed using a different, semi-analytic approach with the help of Padé approximants [26]. Looking at the Fermion propagator as a function of  $z = q^2/m^2$  in the complex  $z$  plane, we find a similar structure as for the polarization function  $\Pi(z)$  in Sect. 2.  $\Sigma_{S,V}(q^2)$  is analytic in the complex plane cut along  $z \in [1, \infty]$ . Thus, in principle one can follow the same strategy as for  $\Pi(z)$ : based on the expansions around  $q^2 = 0$  and  $q^2 = \infty$  one constructs an approximation for  $\Sigma_{S,V}(q^2)$  in the whole  $q^2$  plane, including  $q^2 = m^2$  ( $z = 1$ ), the point of interest.

A complication one has to face here is that the functions  $\Sigma_{S,V}(q^2)$  depend on the

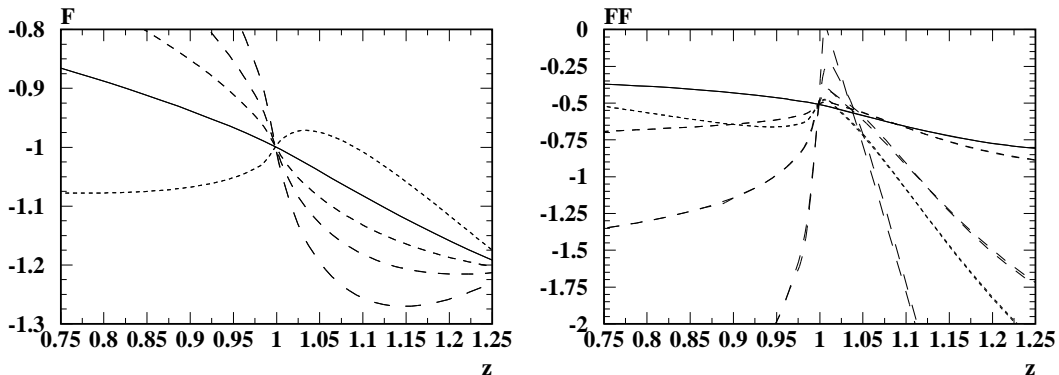


Figure 4: Gauge parameter dependence of  $-g(z)$ . ( $g(z)$  is constructed from  $\Sigma_{S,V}(q^2)$  in such a way that  $g(1) = -z_m$  — for details see [26]). “F” denotes the  $\mathcal{O}(\alpha_s)$  contribution, “FF” the  $C_F^2$  term at  $\mathcal{O}(\alpha_s^2)$ . The solid line corresponds to  $\xi = -2$ , the others to  $\xi = -5, 0, +2, +5$  (from short to long dashes) [Figures taken from [26]].

strong gauge parameter  $\xi$  in general.<sup>3</sup> Only at the on-shell point  $q^2 = m^2$  are they gauge independent. Thus, the expansions around  $z = 0$  and  $z = \infty$  explicitly contain  $\xi$ . If they could be re-summed exactly,  $\xi$  would drop out in the limit  $z \rightarrow 1$ . But here the exact re-summation will be replaced by a Padé approximation and thus the result depends on  $\xi$  even for  $z = 1$ . However, the argumentation is that the dependence on  $\xi$  is weak at  $z = 1$ , in the sense that any “reasonable” choice of  $\xi$  leads to valid predictions, with the spread among different choices being within the error of the Padé approximation. The question of what a “reasonable” choice is can be answered by making the natural assumption that a smooth curve gets better reproduced by Padé approximants than a strongly varying one. Looking at Fig. 4, it is not hard to decide that the favored values for  $\xi$  are within a few units around  $\xi = 0$ .

Following the outlined procedure, the authors of [26] were able to deduce the value of  $z_m$  with an uncertainty of around  $\pm 3\%$ . Shortly after this result was presented, a second group published the analytical result for the conversion factor  $z_m$  [27]. They managed to establish the recurrence relations for three-loop on-shell diagrams derived by integration-by-parts, which provides an extremely useful tool for various other applications (see also [28]).

---

<sup>3</sup>We define the gluon propagator in  $R_\xi$  gauge as  $i(-g_{\mu\nu} + \xi q_\mu q_\nu / q^2) / (q^2 + i0_+)$ .

## 5 Top decay to $\alpha_s^2$ and second order QED corrections to muon decay

The decay rate of the top quark is expected to be measured at future colliders with about 10% accuracy. This is roughly the size of the  $\mathcal{O}(\alpha_s)$  corrections to this quantity, which is why the evaluation of the  $\alpha_s^2$  contribution was necessary. One option to evaluate this decay rate is to calculate the on-shell top quark propagator to the appropriate order and to take the imaginary part. A typical diagram whose imaginary part contributes to the rate  $\Gamma(t \rightarrow bW)$  at order  $\alpha_s^2$  is shown in Fig. 3 (b). In a first approximation, one may take the bottom quark and the  $W$  boson to be massless. Then the lowest order diagram is a massless propagator. Starting from  $\mathcal{O}(\alpha_s)$ , however, one is again faced with proper on-shell diagrams. In contrast to the problem of the  $\overline{\text{MS}}$ /on-shell conversion factor (see Sect. 4) the diagrams for  $t \rightarrow bW$  contain massless cuts due to the presence of the  $b$  and the  $W$ . The solution of [29] (see also [30]) to this problem was to evaluate the expansion around  $q^2/m_t^2 = 0$  and to take the imaginary part *before* evaluating a Padé approximation. It is therefore not possible to take information from the limit  $q^2 \rightarrow \infty$  into account, because otherwise one receives contributions to the imaginary part coming from the cut starting at  $q^2 = m_t^2$ .

Nevertheless, the Padé approximants constructed from the expansion around  $q^2 = 0$  alone give a fairly accurate result (judging from the spread of the different approximants). In addition, it agrees well with an earlier result [31] which relied on an expansion around  $1 - m_b^2/m_t^2 = 0$ . Considering the fact that these approaches are based on expansions around two completely different limits – which, in addition, are both far from the physical point – their agreement within very small error bars is a clear demonstration of the power of the applied methods.

Another example of this kind is the decay rate of the muon. Following a strategy closely related to the one described above for top decay, it was possible to evaluate the second order QED corrections to this quantity in a semi-analytical way [32]. Note, however, that the corresponding diagrams contain four closed loops here (cf. Fig. 3 (c)), even though one of them (made up by the neutrino lines) is always a massless self-energy insertion. Also in this case the Padé approximants agree nicely with the previously known analytical result [33] which provides an important check on the latter.

Along the same lines one can also obtain the corrections of order  $\alpha_s^2$  to the decay rate  $\Gamma(b \rightarrow ue\bar{\nu}_e)$ , the only technical difference being the presence of non-Abelian diagrams. Also here the semi-analytical result [32] approximates the analytical formula [34] to high accuracy.

## 6 Conclusions

We reviewed the method and recent applications of Padé approximation to fixed order calculations in QCD. Originally developed for the hadronic  $e^+e^-$  cross section, the approach proved to be useful also for a completely different class of problems related to on-shell phenomena, for example in heavy quark physics. Let us conclude by pointing out that the continuously refining field of expansion techniques for Feynman diagrams (see [2]) should pave the way to numerous new applications for the Padé method.

**Acknowledgments.** I would like to thank the organizers of the RADCOR-2000 symposium for the invitation, and all the participants for the pleasant and fruitful atmosphere during the conference. Travel support from the High Energy Group at BNL, DOE contract number DE-AC02-98CH10886, is acknowledged.

## References

- [1] T. Gehrmann and E. Remiddi, these proceedings [hep-ph/0101147].
- [2] V.A. Smirnov, these proceedings [hep-ph/0101152].
- [3] M.A. Samuel, J. Ellis, and M. Karliner, *Phys. Rev. Lett.* **74** (1995) 4380; J. Ellis, M. Karliner, and M.A. Samuel, *Phys. Lett.* **B 400** (1997) 176.
- [4] D.J. Broadhurst, J. Fleischer, and O.V. Tarasov, *Z. Phys.* **C 60** (1993) 287; J. Fleischer and O.V. Tarasov, *Z. Phys.* **C 64** (1994) 413.
- [5] P.A. Baikov and D.J. Broadhurst, Proc. of the *4th International Workshop on Software Engineering and Artificial Intelligence for High Energy and Nuclear Physics* (AIHENP95), Pisa, Italy, 3-8 April 1995; [hep-ph/9504398].
- [6] K.G. Chetyrkin, J.H. Kühn, and M. Steinhauser, *Phys. Lett.* **B 371** (1996) 93; *Nucl. Phys.* **B 482** (1996) 213.
- [7] K.G. Chetyrkin, J.H. Kühn, and M. Steinhauser, *Nucl. Phys.* **B 505** (1997) 40.
- [8] K.G. Chetyrkin, R. Harlander, and M. Steinhauser, *Phys. Rev.* **D 58** (1998) 014012.
- [9] J.H. Kühn, Proc. of the *4th International Symposium on Radiative Corrections* (RADCOR 98), Barcelona, Spain, 8-12 Sep 1998; [hep-ph/9901330].

- [10] A.H. Hoang, J.H. Kühn, and T. Teubner, *Nucl. Phys.* **B 452** (1995) 173;  
A.H. Hoang, M. Jezabek, J.H. Kühn, and T. Teubner, *Phys. Lett.* **B 338** (1994) 330.
- [11] F.V. Tkachov, *Phys. Lett.* **B 100** (1981) 65;  
K.G. Chetyrkin and F.V. Tkachov, *Nucl. Phys.* **B 192** (1981) 159.
- [12] J.A.M. Vermaseren, [math-ph/0010025].
- [13] S.A. Larin, F.V. Tkachov, and J.A.M. Vermaseren, Rep. No. NIKHEF-H/91-18 (Amsterdam, 1991).
- [14] R. Harlander, *Act. Phys. Pol.* **B 30** (1999) 3443.
- [15] A. Czarnecki and K. Melnikov, *Phys. Rev. Lett.* **80** (1998) 2531.
- [16] K.G. Chetyrkin, R. Harlander, J.H. Kühn, and M. Steinhauser, *Nucl. Phys.* **B 503** (1997) 339;  
R. Harlander and M. Steinhauser, *Phys. Rev.* **D 56** (1997) 3980; *Eur. Phys. J.* **C 2** (1998) 151.
- [17] R. Harlander, PhD thesis, Karlsruhe University (Shaker Verlag, Aachen, 1998).
- [18] K.G. Chetyrkin and M. Steinhauser, [hep-ph/0012002].
- [19] A.H. Hoang, M. Jezabek, J.H. Kühn, and T. Teubner, *Phys. Lett.* **B 338** (1994) 330; A.H. Hoang, J.H. Kühn, and T. Teubner, *Nucl. Phys.* **B 452** (1995) 173;  
A.H. Hoang and T. Teubner, *Nucl. Phys.* **B 519** (1998) 285.
- [20] S.G. Gorishny, A.L. Kataev, and S.A. Larin, *Phys. Lett.* **B 259** (1991) 144;  
L.R. Surguladze and M.A. Samuel, *Phys. Rev. Lett.* **66** (1991) 560; (E) *ibid.*, 2416;  
K.G. Chetyrkin, *Phys. Lett.* **B 391** (1997) 402.
- [21] K.G. Chetyrkin and J.H. Kühn, *Phys. Lett.* **B 248** (1990) 359.
- [22] K.G. Chetyrkin, R.V. Harlander, and J.H. Kühn, *Nucl. Phys.* **B 586** (2000) 56.
- [23] J. Kühn, T. Hahn, and R. Harlander, Proc. of the *4th International Workshop on Linear Colliders* (LCWS 99), Sitges, Barcelona, Spain, 28 Apr-5 May 1999; [hep-ph/9912262].
- [24] K.G. Chetyrkin, *Phys. Lett.* **B 404** (1997) 161;  
J.A.M. Vermaseren, S.A. Larin, and T. van Ritbergen, *Phys. Lett.* **B 405** (1997) 327.

- [25] N. Gray, D.J. Broadhurst, W. Grafe, and K. Schilcher, *Z. Phys. C* **48** (1990) 673.
- [26] K.G. Chetyrkin and M. Steinhauser, *Phys. Rev. Lett.* **83** (1999) 4001; *Nucl. Phys. B* **573** (2000) 617.
- [27] K. Melnikov and T. van Ritbergen, *Phys. Lett. B* **482** (2000) 99.
- [28] A. Czarnecki, these proceedings.
- [29] K.G. Chetyrkin, R. Harlander, T. Seidensticker, M. Steinhauser, *Phys. Rev. D* **60** (1999) 114015.
- [30] A. Czarnecki and K. Melnikov, Proc. of the *Lake Louise Winter Institute: Quantum Chromodynamics*, Lake Louise, Alberta, Canada, 15-21 Feb 1998; [hep-ph/9806258].
- [31] A. Czarnecki and K. Melnikov, *Nucl. Phys. B* **544** (1999) 520.
- [32] T. Seidensticker and M. Steinhauser, *Phys. Lett. B* **467** (1999) 271.
- [33] T. van Ritbergen and R.G. Stuart, *Phys. Rev. Lett.* **82** (1999) 488.
- [34] T. van Ritbergen, *Phys. Lett. B* **454** (1999) 353.

## Progress on two-loop non-propagator integrals

T. GEHRMANN<sup>a,b</sup> AND E. REMIDDI<sup>c</sup>

<sup>a</sup> *Theory Division, CERN, CH-1211 Geneva 23, Switzerland*

<sup>b</sup> *Institut für Theoretische Teilchenphysik, Universität Karlsruhe,  
D-76128 Karlsruhe, Germany*

<sup>c</sup> *Dipartimento di Fisica, Università di Bologna and INFN, Sezione di Bologna,  
I-40126 Bologna, Italy*

At variance with fully inclusive quantities, which have been computed already at the two- or three-loop level, most exclusive observables are still known only at one loop, as further progress was hampered up to very recently by the greater computational problems encountered in the study of multi-leg amplitudes beyond one loop. We discuss the progress made lately in the evaluation of two-loop multi-leg integrals, with particular emphasis on two-loop four-point functions.

Presented at the

5th International Symposium on Radiative Corrections  
(RADCOR-2000)

Carmel CA, USA, 11–15 September, 2000

# 1 Introduction

Precision applications of particle physics phenomenology often demand theoretical predictions at the next-to-next-to-leading order in perturbation theory. Corrections at this order are known for many inclusive observables, such as total cross sections or sum rules, which correspond from a technical point of view to propagator-type Feynman amplitudes. For  $2 \rightarrow 2$  scattering and  $1 \rightarrow 3$  decay processes, the calculation of next-to-next-to-leading order corrections is a yet outstanding task. One of the major ingredients for these calculations are the two-loop virtual corrections to the corresponding four-point Feynman amplitudes. Depending on the process under consideration, these calculations require two-loop four-point functions with massless internal propagators and all legs on-shell (high energy limit of Bhabha scattering, hadronic two-jet production) or one leg off-shell (three-jet production and event shapes in electron-positron annihilation, two-plus-one-jet production in deep inelastic scattering, hadronic vector-boson-plus-jet production).

During the past two years, many new results on two-loop four-point functions became available, thus enabling the first calculations of two-loop virtual corrections to  $2 \rightarrow 2$  scattering processes. A variety of newly developed techniques made this progress possible. In this talk, we describe these new techniques and their applications, and we summarise recent results. In an outlook, we discuss the remaining steps to be taken towards the completion of next-to-next-to-leading order calculations of  $2 \rightarrow 2$  scattering and  $1 \rightarrow 3$  decay processes.

## 2 New technical developments

Using dimensional regularization [1,2] with  $d = 4 - 2\epsilon$  dimensions as regulator for ultraviolet and infrared divergences, the integrals appearing in the calculation of two-loop corrections take the generic form

$$I(p_1, \dots, p_n) = \int \frac{d^d k}{(2\pi)^d} \frac{d^d l}{(2\pi)^d} \frac{1}{D_1^{m_1} \dots D_t^{m_t}} S_1^{n_1} \dots S_q^{n_q}, \quad (1)$$

where the  $D_i$  are massless scalar propagators, depending on  $k, l$  and the external momenta  $p_1, \dots, p_n$  while  $S_i$  are scalar products of a loop momentum with an external momentum or of the two loop momenta. The topology (interconnection of propagators and external momenta) of the integral is uniquely determined by specifying the set  $(D_1, \dots, D_t)$  of  $t$  different propagators in the graph. The integral itself is then specified by the powers  $m_i$  of all propagators and by the selection  $(S_1, \dots, S_q)$  of scalar products and their powers  $(n_1, \dots, n_q)$  (all the  $m_i$  are positive integers greater or equal to 1, while the  $n_i$  are greater or equal to 0). Integrals of the same topology with the same dimension  $r = \sum_i m_i$  of the denominator and same total number

$s = \sum_i n_i$  of scalar products are denoted as a class of integrals  $I_{t,r,s}$ . The integration measure and scalar products appearing in the above expression are in Minkowskian space, with the usual causal prescription for all propagators. The loop integrations are carried out for arbitrary space-time dimension  $d$ , which acts as a regulator for divergences appearing due to the ultraviolet or infrared behaviour of the integrand. For each topology appearing in the calculation, a sizable number of different scalar integrals has to be computed.

Recent progress in the computation of two-loop corrections to four-point amplitudes was based on three technical developments: an efficient procedure to reduce the large number of different scalar integrals to a very limited number of so-called master integrals, new techniques for the computation of these master integrals, and a new class of functions (harmonic polylogarithms), which can be extended to suit the needs of a particular calculation. We discuss these developments in the following.

## 2.1 Reduction to master integrals

The number  $N(I_{t,r,s})$  of the integrals grows quickly as  $r, s$  increase, but the integrals are related among each other by various identities. One class of identities follows from the fact that the integral over the total derivative with respect to any loop momentum vanishes in dimensional regularization

$$\int \frac{d^d k}{(2\pi)^d} \frac{\partial}{\partial k^\mu} J(k, \dots) = 0, \quad (2)$$

where  $J$  is any combination of propagators, scalar products and loop momentum vectors.  $J$  can be a vector or tensor of any rank. The resulting identities [2,3] are called integration-by-parts (IBP) identities.

In addition to the IBP identities, one can also exploit the fact that all integrals under consideration are Lorentz scalars (or, perhaps more precisely, “ $d$ -rotational” scalars), which are invariant under a Lorentz (or  $d$ -rotational) transformation of the external momenta [4]. These Lorentz invariance (LI) identities are obtained from:

$$\left( p_1^\nu \frac{\partial}{\partial p_{1\mu}} - p_1^\mu \frac{\partial}{\partial p_{1\nu}} + \dots + p_n^\nu \frac{\partial}{\partial p_{n\mu}} - p_n^\mu \frac{\partial}{\partial p_{n\nu}} \right) I(p_1, \dots, p_n) = 0. \quad (3)$$

In the case of two-loop four-point functions, one has a total of 13 equations (10 IBP + 3 LI) for each integrand corresponding to an integral of class  $I_{t,r,s}$ , relating integrals of the same topology with up to  $s + 1$  scalar products and  $r + 1$  denominators, plus integrals of simpler topologies (*i.e.* with a smaller number of different denominators). The 13 identities obtained starting from an integral  $I_{t,r,s}$  do contain integrals of the following types:

- $I_{t,r,s}$ : the integral itself.

- $I_{t-1,r,s}$ : simpler topology.
- $I_{t,r+1,s}, I_{t,r+1,s+1}$  : same topology, more complicated than  $I_{t,r,s}$ .
- $I_{t,r-1,s}, I_{t,r-1,s-1}$ : same topology, simpler than  $I_{t,r,s}$ .

Quite in general, single identities of the above kind can be used to obtain the reduction of  $I_{t,r+1,s+1}$  or  $I_{t,r+1,s}$  integrals in terms of  $I_{t,r,s}$  and simpler integrals - rather than to get information on the  $I_{t,r,s}$  themselves.

If one considers the set of all the identities obtained starting from the integrand of all the  $N(I_{t,r,s})$  integrals of class  $I_{t,r,s}$ , one obtains  $(N_{\text{IBP}} + N_{\text{LI}})N(I_{t,r,s})$  identities which contain  $N(I_{t,r+1,s+1}) + N(I_{t,r+1,s})$  integrals of more complicated structure. It was first noticed by S. Laporta [5] that with increasing  $r$  and  $s$  the number of identities grows faster than the number of new unknown integrals. As a consequence, if for a given  $t$ -topology one considers the set of all the possible equations obtained by considering all the integrands up to certain values  $r^*, s^*$  of  $r, s$ , for large enough  $r^*, s^*$  the resulting system of equations, apparently overconstrained, can be used for expressing the more complicated integrals, with greater values of  $r, s$  in terms of simpler ones, with smaller values of  $r, s$ . An automatic procedure to perform this reduction by means of computer algebra using FORM [6] and MAPLE [7] is discussed in more detail in [4].

For any given four-point two-loop topology, this procedure can result either in a reduction towards a small number (typically one or two) of integrals of the topology under consideration and integrals of simpler topology (less different denominators), or even in a complete reduction of all integrals of the topology under consideration towards integrals with simpler topology. Left-over integrals of the topology under consideration are called irreducible master integrals or just master integrals.

## 2.2 Computation of master integrals

The IBP and LI identities allow to express integrals of the form (1) as a linear combination of a few master integrals, i.e. integrals which are not further reducible, but have to be computed by some different method.

For the case of massless two-loop four-point functions, several techniques have been proposed in the literature, such as for example the application of a Mellin–Barnes transformation to all propagators [8] or the negative dimension approach [9]. Both techniques rely on an explicit integration over the loop momenta, with differences mainly in the representation used for the propagators.

A method for the analytic computation of master integrals avoiding the explicit integration over the loop momenta is to derive differential equations in internal propagator masses or in external momenta for the master integral, and to solve these with appropriate boundary conditions. This method has first been suggested by Kotikov [10] to relate loop integrals with internal masses to massless loop integrals.

It has been elaborated in detail and generalized to differential equations in external momenta in [11]; first applications were presented in [12]. In the case of four-point functions with one external off-shell leg and no internal masses, one has three independent invariants, resulting in three differential equations.

The derivatives in the invariants  $s_{ij} = (p_i + p_j)^2$  can be expressed by derivatives in the external momenta:

$$\begin{aligned} s_{12} \frac{\partial}{\partial s_{12}} &= \frac{1}{2} \left( +p_1^\mu \frac{\partial}{\partial p_1^\mu} + p_2^\mu \frac{\partial}{\partial p_2^\mu} - p_3^\mu \frac{\partial}{\partial p_3^\mu} \right), \\ s_{13} \frac{\partial}{\partial s_{13}} &= \frac{1}{2} \left( +p_1^\mu \frac{\partial}{\partial p_1^\mu} - p_2^\mu \frac{\partial}{\partial p_2^\mu} + p_3^\mu \frac{\partial}{\partial p_3^\mu} \right), \\ s_{23} \frac{\partial}{\partial s_{23}} &= \frac{1}{2} \left( -p_1^\mu \frac{\partial}{\partial p_1^\mu} + p_2^\mu \frac{\partial}{\partial p_2^\mu} + p_3^\mu \frac{\partial}{\partial p_3^\mu} \right). \end{aligned} \quad (4)$$

It is evident that acting with the right hand sides of (4) on a master integral  $I_{t,t,0}$  will, after interchange of derivative and integration, yield a combination of integrals of the same type as appearing in the IBP and LI identities for  $I_{t,t,0}$ , including integrals of type  $I_{t,t+1,1}$  and  $I_{t,t+1,0}$ . Consequently, the scalar derivatives (on left hand side of (4)) of  $I_{t,t,0}$  can be expressed by a linear combination of integrals up to  $I_{t,t+1,1}$  and  $I_{t,t+1,0}$ . These can all be reduced (for topologies containing only one master integral) to  $I_{t,t,0}$  and to integrals of simpler topology by applying the IBP and LI identities. As a result, we obtain for the master integral  $I_{t,t,0}$  an inhomogeneous linear first order differential equation in each invariant. For topologies with more than one master integral, one finds a coupled system of first order differential equations. The inhomogeneous term in these differential equations contains only topologies simpler than  $I_{t,t,0}$ , which are considered to be known if working in a bottom-up approach.

The master integral  $I_{t,t,0}$  is obtained by matching the general solution of its differential equation to an appropriate boundary condition. Quite in general, finding a boundary condition is a simpler problem than evaluating the whole integral, since it depends on a smaller number of kinematical variables. In some cases, the boundary condition can even be determined from the differential equation itself.

To solve the differential equations for two-loop four-point functions with one off-shell leg [4,13], we express the system of differential equations for any master integral in the variables  $s_{123} = s_{12} + s_{13} + s_{23}$ ,  $y = s_{13}/s_{123}$  and  $z = s_{23}/s_{123}$ . We obtain a homogeneous equation in  $s_{123}$ , and inhomogeneous equations in  $y$  and  $z$ . Since  $s_{123}$  is the only quantity carrying a mass dimension, the corresponding differential equation is nothing but the rescaling relation obtained by investigating the behaviour of the master integral under a rescaling of all external momenta by a constant factor. The master integral can be determined by solving one of the inhomogeneous equations, the second equation can then serve as a check on the result.

In the  $y$  differential equation for the master integral under consideration, the coefficient of the homogeneous term as well as the full inhomogeneous term (coefficients

and subtopologies) are then expanded as a series in  $\epsilon$ . From the leading coefficient of the homogeneous term, one can determine a rational prefactor  $\mathcal{R}$  for the master integral. Rescaling the master integral by this prefactor, one obtains a differential equation in which the coefficient of the homogeneous term is of  $\mathcal{O}(\epsilon)$ . This equation can then be solved order by order in  $\epsilon$  by direct integration. The remaining constants of integration, which correspond to the boundary condition of the equation, are subsequently determined by using the fact that the master integral is regular in the whole kinematic plane with the exception of a few (at most three) branch cuts.

For each master integral, we obtain a result of the form

$$\sum_i \mathcal{R}_i(y, z; s_{123}, \epsilon) \mathcal{H}_i(y, z; \epsilon), \quad (5)$$

where the prefactor  $\mathcal{R}_i(y, z; s_{123}, \epsilon)$  is a rational function of  $y$  and  $z$ , which is multiplied with an overall normalization factor to account for the correct dimension in  $s_{123}$ , while  $\mathcal{H}_i(y, z; \epsilon)$  is a Laurent series in  $\epsilon$ . The coefficients of its  $\epsilon$ -expansion are then written as the sum of two-dimensional harmonic polylogarithms up to a weight determined by the order of the series:

$$\mathcal{H}_i(y, z; \epsilon) = \frac{\epsilon^p}{\epsilon^4} \sum_{n=0}^4 \epsilon^n \left[ T_n(z) + \sum_{j=1}^n \sum_{\vec{m}_j \in V_j(z)} T_{n, \vec{m}_j}(z) H(\vec{m}_j; y) \right], \quad (6)$$

where the  $H(\vec{m}_j; y)$  are two-dimensional harmonic polylogarithms (2dHPL), which were introduced in [13] and  $T_n(z)$ ,  $T_{n, \vec{m}_j}(z)$  are  $z$ -dependent coefficients.

### 2.3 Harmonic polylogarithms

Harmonic polylogarithms (HPL) were introduced in [14] as an extension of the generalized polylogarithms of Nielsen [15,16]. They are constructed in such a way that they form a closed, linearly independent set under a certain class of integrations. We observe that the class of allowed integrations on this set can be extended *à la carte* by enlarging the definition of harmonic polylogarithms in order to suit the needs of a particular calculation. We made use of this feature by generalizing the one-dimensional HPL of [14] to two-dimensional harmonic polylogarithms (2dHPL), which appear in the solution of the differential equations for the three-scale master integrals discussed in [13]. We briefly recall the HPL formalism [14]:

1. The one-dimensional HPL  $H(\vec{m}_w; x)$  is described by a  $w$ -dimensional vector  $\vec{m}_w$  of parameters and by its argument  $x$ .  $w$  is called the weight of  $H$ .
2. The HPL of parameters  $(+1, 0, -1)$  form a closed set under the class of integrations

$$\int_0^x dx' \left( \frac{1}{x'}, \frac{1}{1-x'}, \frac{1}{1+x'} \right) H(\vec{b}; x'). \quad (7)$$

3. The HPL fulfil an algebra, such that a product of two HPL (with weights  $w_1$  and  $w_2$ ) of the same argument  $x$  is a combination of HPL of argument  $x$  with weight  $w = w_1 + w_2$ .
4. The HPL fulfil integration-by-parts identities.
5. The HPL are linearly independent.

The generalization from one-dimensional to two-dimensional HPL starts from (7), which defines the class of integrations under which the HPL form a closed set. By inspection of the various inhomogeneous terms of the  $y$  differential equations for the three-scale master integrals discussed in this paper, we find that, besides the denominators  $1/y$  and  $1/(1-y)$ , also  $1/(1-y-z)$  and  $1/(y+z)$  appear. It is therefore appropriate to introduce an extension of the HPL, which forms a closed set under the class of integrations

$$\int_0^y dy' \left( \frac{1}{y'}, \frac{1}{1-y'}, \frac{1}{1-y'-z}, \frac{1}{y'+z} \right) H(\vec{b}; y'). \quad (8)$$

Allowing  $(z, 1-z)$  as components of the vector  $\vec{m}_w$  of parameters does then define the extended set of HPL, which we call two-dimensional harmonic polylogarithms (2dHPL). They retain all properties of the HPL, in particular the algebra and the linear independence.

Two-dimensional harmonic polylogarithms can be expressed in terms of Nielsen's generalized polylogarithms up to weight 3, which is the maximum weight appearing in the divergent terms of two-loop four-point functions with one leg off-shell. These relations are tabulated in [13]. At weight 4, only some special cases relate to generalized polylogarithms.

### 3 Summary of recent results

For two-loop four-point functions with massless internal propagators and all legs on-shell, which are relevant for example in the next-to-next-to-leading order calculation of two-jet production at hadron colliders, all master integrals have been calculated over the past two years. The calculations were performed using the Mellin–Barnes method [8] and the differential equation technique [17]. The resulting master integrals can be expressed in terms of Nielsen's generalized polylogarithms. Very recently, these master integrals were already applied in the calculation of two-loop virtual corrections to Bhabha scattering [18] in the limit of vanishing electron mass and to quark–quark scattering [19].

In [13], we have used the differential equation approach to compute all master integrals for two-loop four-point functions with one off-shell leg. Earlier partial results

on these functions were obtained in [9,20], and a purely numerical approach to these functions was presented in [21]. Our results [13] for these master integrals are in terms of two-dimensional harmonic polylogarithms. All 2dHPL appearing in the divergent parts of the master integrals can be expressed in terms of Nielsen’s generalized polylogarithms of suitable non-simple arguments, while the 2dHPL appearing in the finite parts are one-dimensional integrals over generalized polylogarithms. An efficient numerical implementation of these functions is currently being worked out. Our results correspond to the kinematical situation of a  $1 \rightarrow 3$  decay, their analytic continuation into the region of  $2 \rightarrow 2$  scattering processes requires the analytic continuation of the 2dHPL, which is outlined in [13].

These four-point two-loop master integrals with one leg off-shell are a crucial ingredient to the virtual next-to-next-to-leading order corrections to processes such as three-jet production in electron–positron annihilation, two-plus-one-jet production in deep inelastic scattering and vector-boson-plus-jet production at hadron colliders.

## 4 Outlook

Owing to numerous technical developments in the past two years, virtual two-loop corrections to four-point amplitudes are now becoming available for a variety of phenomenologically relevant processes. One must however keep in mind that these corrections form only one part of a full next-to-next-to-leading order calculation, which also has to include the one-loop corrections to processes with one soft or collinear real parton [22] as well as tree-level processes with two soft or collinear partons [23]. Only after summing all these contributions (and including terms from the renormalization of parton distributions for processes with partons in the initial state), the divergent terms cancel among one another. The remaining finite terms have to be combined into a numerical programme implementing the experimental definition of jet observables and event-shape variables. A first calculation involving the above features was presented for case of photon-plus-one-jet final states in electron–positron annihilation in [23], thus demonstrating the feasibility of this type of calculations.

## Acknowledgments

TG would like to acknowledge a travel grant from the Deutsche Forschungsgemeinschaft (DFG) under contract number Ge1138/2-1.

## References

- [1] C.G. Bollini and J.J. Giambiagi, *Nuovo Cim.* **12B** (1972) 20; G.M. Cicuta and E. Montaldi, *Nuovo Cim. Lett.* **4** (1972) 329.
- [2] G. 't Hooft and M. Veltman, *Nucl. Phys.* **B44** (1972) 189.
- [3] F.V. Tkachov, *Phys. Lett.* **100B** (1981) 65; K.G. Chetyrkin and F.V. Tkachov, *Nucl. Phys.* **B192** (1981) 159.
- [4] T. Gehrmann and E. Remiddi, *Nucl. Phys.* **B580** (2000) 485.
- [5] S. Laporta and E. Remiddi, *Phys. Lett.* **B379** (1996) 283.
- [6] J.A.M. Vermaseren, *Symbolic Manipulation with FORM*, Version 2, CAN, Amsterdam, 1991.
- [7] *MAPLE V Release 3*, Copyright 1981-1994 by Waterloo Maple Software and the University of Waterloo.
- [8] V.A. Smirnov, *Phys. Lett.* **B460** (1999) 397; J.B. Tausk, *Phys. Lett.* **B469** (1999) 225; C. Anastasiou, J.B. Tausk and M.E. Tejeda-Yeomans, *Nucl. Phys. B* (Proc. Suppl.) **89** (2000) 262.
- [9] C. Anastasiou, E.W.N. Glover and C. Oleari, *Nucl. Phys.* **B565** (2000) 445.
- [10] A.V. Kotikov, *Phys. Lett.* **B254** (1991) 158.
- [11] E. Remiddi, *Nuovo Cim.* **110A** (1997) 1435 (hep-th/9711188).
- [12] M. Caffo, H. Czyż and E. Remiddi, *Nuovo Cim.* **111A** (1998) 365 (hep-th/9805118), *Nucl. Phys.* **B581** (2000) 274.
- [13] T. Gehrmann and E. Remiddi, Karlsruhe preprint TTP00-20 (hep-ph/0008287); CERN preprint CERN-TH/2001-005 (hep-ph/0101124).
- [14] E. Remiddi and J.A.M. Vermaseren, *Int. J. Mod. Phys.* **A15** (2000) 725.
- [15] N. Nielsen, *Nova Acta Leopoldiana (Halle)* **90** (1909) 123.
- [16] K.S. Kölbig, J.A. Mignaco and E. Remiddi, *BIT* **10** (1970) 38.
- [17] V.A. Smirnov and O.L. Veretin, *Nucl. Phys.* **B566** (2000) 469; C. Anastasiou, T. Gehrmann, C. Oleari, E. Remiddi and J.B. Tausk, *Nucl. Phys.* **B580** (2000) 577; T. Gehrmann and E. Remiddi, *Nucl. Phys. B* (Proc. Suppl.) **89** (2000) 251.

- [18] Z. Bern, L. Dixon and A. Ghinculov, Stanford preprint SLAC-PUB-8655 (hep-ph/0010075).
- [19] C. Anastasiou, E.W.N. Glover, C. Oleari and M.E. Tejeda-Yeomans, Durham preprints IPPP-00-05 (hep-ph/0010212), IPPP-00-08 (hep-ph/0011094), IPPP-00-11 (hep-ph/0012007).
- [20] V.A. Smirnov, Phys. Lett. **B491** (2000) 130; Karlsruhe preprint TTP00-24 (hep-ph/0011056).
- [21] T. Binoth and G. Heinrich, Nucl. Phys. **B585** (2000) 741.
- [22] D.A. Kosower and P. Uwer, Nucl. Phys. **B563** (1999) 477; Z. Bern, V. Del Duca, W.B. Kilgore and C.R. Schmidt, Phys. Rev. **D60** (1999) 116001; S. Catani and M. Grazzini, Nucl. Phys. **B591** (2000) 435.
- [23] A. Gehrmann-De Ridder and E.W.N. Glover, Nucl. Phys. **B517** (1998) 269.

April 19, 2001  
hep-ph/0101152

**‘Strategy of Regions’:  
Expansions of Feynman Diagrams  
both in Euclidean and  
Pseudo-Euclidean Regimes**

V.A. SMIRNOV\*

*Nuclear Physics Institute of Moscow State University  
Moscow 119899, Russia*

The strategy of regions [1] turns out to be a universal method for expanding Feynman integrals in various limits of momenta and masses. This strategy is reviewed and illustrated through numerous examples. In the case of typically Euclidean limits it is equivalent to well-known prescriptions within the strategy of subgraphs. For regimes typical for Minkowski space, where the strategy of subgraphs has not yet been developed, the strategy of regions is characterized in the case of threshold limit, Sudakov limit and Regge limit.

Presented at the

5th International Symposium on Radiative Corrections  
(RADCOR–2000)

Carmel CA, USA, 11–15 September, 2000

---

\* The participation in the Symposium supported by the Organizing Committee and by the Russian State Research Program ‘High Energy Physics’. Work supported by the Volkswagen Foundation, contract No. I/73611, and by the Russian Foundation for Basic Research, project 98–02–16981.

## 1 Introduction

The problem of asymptotic<sup>1</sup> expansions of Feynman integrals in momenta masses is very important and has been analyzed in a large number of papers. For limits typical for Euclidean space, an adequate solution has been found [2] (see a brief review in [3]) and mathematically proven. It is expressed by a simple formula with summation in a certain family of subgraphs of a given graph so that let us refer to it as ‘the strategy of subgraphs’. For limits typical for Minkowski space, the strategy of subgraphs has not yet been rigorously developed.

Quite recently a new method for expanding Feynman integrals in limits of momenta and masses has been suggested [1]. It is based on the analysis of various regions in the space of loop momenta of a given diagram and denoted as ‘the strategy of regions’. The purpose of this talk is to review and illustrate this strategy through numerous examples. First, the problem of asymptotic expansion in limits of momenta and masses is characterized. Then the two basic strategies are formulated and compared for limits typical for Euclidean space. For regimes typical for Minkowski space, the strategy of regions is checked through typical examples, up to two-loop level, in the case of threshold limit, Sudakov limit and Regge limit. Finally, the present status of the strategy of regions is characterized.

## 2 Limits of momenta and masses

Let  $\Gamma$  be a graph and  $F_\Gamma(m_1, m_2, \dots, q_1, q_2, \dots)$  the corresponding Feynman integral constructed according to Feynman rules and depending on masses  $m_i$  and external momenta  $q_j$ . It can be represented as a linear combination of tensors composed of the external momenta with coefficients which are scalar Feynman integrals that depend on the masses and kinematical invariants  $s_{ij} = q_i \cdot q_j$ .

The problem of asymptotic expansion of Feynman integrals in some limit of momenta and masses is of the physical origin and arises quite naturally. If one deals with phenomena that take place at a given energy scale it is natural to consider large (small) all the masses and kinematical invariants that are above (below) this scale. Therefore a limit (regime) is nothing but a decomposition of the given family of these parameters into small and large ones.

---

<sup>1</sup>The word ‘asymptotic’ is also usually applied to perturbative series with zero radius of convergence. For expansions of Feynman integrals in momenta and masses, this word just means that the remainder of an asymptotic expansion satisfies a desired estimate provided we pick up a sufficiently large number of first terms of the expansion. It should be stressed that the radius of convergence of any series in the right-hand side of any expansion in momenta and masses is non-zero. This is not a rigorously proven mathematical theorem but at least examples where such a radius of convergence is zero are unknown for the moment.

For limits typical for Euclidean space, an external momentum is called large if at least one of its components is large and small if all its four components are large. Thus such a limit is characterized by a decomposition  $\{m_i\}, \{q_i\} \rightarrow \{m_i\}, \{q_i\}; \{M_i\}, \{Q_i\}$ , with  $m_i, |q_j| \ll M_{i'}, |Q_{j'}|$ , where  $|q_j|$  is understood in the Euclidean sense.

For limits typical for pseudo-Euclidean space, it is impossible to characterize the external momenta in this way and one turns to a decomposition written through kinematical invariants:  $\{m_i\}, \{s_{jj'}\} \rightarrow \{m_i\}, \{s_{jj'}\}; \{M_i\}, \{S_{jj'}\}$ , with  $m_i, |s_{jj'}| \ll M_{i'}, |S_{jj'}|$ . However, instead of the kinematical invariants themselves, some linear combinations can be used (for example, in the case of the threshold limit).

Feynman integrals are generally quite complicated functions depending on a large number of arguments. When a given Feynman integral is considered in a given limit it looks natural to expand it in ratios of small and large parameters and then replace the initial complicated object by a sufficiently large number of first terms of the corresponding asymptotic expansion. Experience shows that Feynman integrals are always expanded in powers and logarithms of the expansion parameter which is a ratio of the large and the small scales of the problem. In particular, when a given Feynman integral depends only on a small mass squared and a large external momentum squared,  $m^2 \ll -q^2$ , we have

$$F_\Gamma(q^2, m^2) \sim (-q^2)^\omega \sum_{n=n_0}^{\infty} \sum_{j=0}^{2h} C_{nj} \left(\frac{m^2}{-q^2}\right)^n \ln^j \left(\frac{m^2}{-q^2}\right), \quad (1)$$

where  $h$  is the number of loops of  $\Gamma$  and  $\omega$  ultraviolet (UV) degree of divergence. The maximal power of the logarithm equals the number of loops for typically Euclidean limits and is twice the number of loops for limits typical for Minkowski space.

To expand Feynman diagrams one can either

1. Take a given diagram in a given limit and expand it by some special technique, or,
2. Formulate prescriptions for a given limit and then apply them to any diagram (e.g. with 100 loops).

Of course, the second (global) solution is preferable because

- *no analytical work* is needed when applying it to a given diagram: just follow formulated prescriptions and write down a result in terms of Feynman integrals (with integrands expanded in Taylor series in some parameters);
- a natural requirement can be satisfied: individual terms of the expansion are homogeneous (modulo logs) in the expansion parameter.

Two kinds of such global prescriptions are known:

\* *Strategy of Subgraphs* and

\* *Strategy of Regions*

We shall now formulate both strategies in the case of limits typical for Euclidean space.

### 3 Strategy of subgraphs and strategy of regions for limits typical for Euclidean space

For limits typical for Euclidean space, the solution of the problem of asymptotic expansion is described [2] by the following simple formula, with summation in subgraphs, supplied with some explanations:

$$F_\Gamma \sim \sum_\gamma F_{\Gamma/\gamma} \circ \mathcal{T}_\gamma F_\gamma, \quad (2)$$

where the sum runs in a certain class of subgraphs  $\gamma$  of  $\Gamma$ . For example, in the off-shell (Euclidean) limit  $m^2 \ll -q^2$  (when  $q$  is considered large in Euclidean sense), one can distribute the flow of  $q$  through *all* the lines of  $\gamma$ . (This is a ‘physical’ definition.) Moreover  $F_\gamma$  and  $F_{\Gamma/\gamma}$  are the Feynman integrals respectively for  $\gamma$  and  $\Gamma/\gamma$  (the reduced graph  $\Gamma/\gamma$  is obtained from  $\Gamma$  by collapsing  $\gamma$  to a point). The operator  $\mathcal{T}_\gamma$  expands the integrand of  $F_\gamma$  in Taylor series in its small masses and small external momenta which are either the small external momenta of  $\Gamma$ , or loop momenta of the whole graph that are external for  $\gamma$  (they are *by definition* small). The symbol  $\circ$  denotes insertion of the second factor (polynomial) into  $F_{\Gamma/\gamma}$  (like an insertion of a counterterm within dimensional renormalization).

All quantities are supposed to be dimensionally regularized [4] by  $d = 4 - 2\varepsilon$ . Even if the initial Feynman integral is UV and IR finite, the regularization is necessary because individual terms in the right-hand side become divergent starting from some minimal order of expansion. The necessity to run into divergences is a negligible price to have the simplest prescription for expanding Feynman integrals. Moreover the cancellation of divergences in the right-hand side of expansions of finite Feynman integrals is a very crucial practical check of the expansion procedure.

Operator analogs of limits typical for Euclidean space (the off-shell large momentum limit and the large mass limit) are operator product expansion and large mass expansion described by an effective Lagrangian — see a review with applications in [5].

Consider, for example, the scalar diagram shown in Fig. 1 in the off-shell limit  $m^2 \ll -q^2$  which can be treated as a Euclidean limit with the external momentum  $q$  large in the Euclidean sense. The propagator of the dashed line is massless and

the dot on the solid line denotes the second power of the massive propagator. The corresponding Feynman integral is

$$F_{\Gamma}(q^2, m^2; \varepsilon) = \int \frac{d^d k}{(k^2 - m^2)^2 (q - k)^2} . \quad (3)$$

The causal  $i0$  in the propagators  $k^2 - m^2 + i0$ , etc. are omitted for brevity.

According to (2) two subgraphs give non-zero contributions. The graph  $\Gamma$  itself generates Taylor expansion of the integrand in  $m$ , with resulting massless integrals evaluated (e.g. by Feynman parameters) in gamma functions for general  $\varepsilon$ :

$$\begin{aligned} \int \frac{d^d k}{(q - k)^2} \mathcal{T}_m \frac{1}{(k^2 - m^2)^2} &= \int \frac{d^d k}{(k^2)^2 (q - k)^2} - 2m^2 \int \frac{d^d k}{(k^2)^3 (q - k)^2} + \dots \\ &= \frac{i\pi^{d/2}}{(-q^2)^{1+\varepsilon}} \frac{\Gamma(1 - \varepsilon)^2 \Gamma(\varepsilon)}{\Gamma(1 - 2\varepsilon)} \left[ 1 + 2\varepsilon \frac{m^2}{q^2} + \dots \right] . \end{aligned} \quad (4)$$

The second contribution originates from the subgraph  $\gamma_1$  which is the upper line. It is given by Taylor expansion of its propagator in the loop momentum  $k$  which is external for this subgraph, with resulting massive vacuum integrals also evaluated in gamma functions for general  $\varepsilon$ :

$$\begin{aligned} \int \frac{d^d k}{(k^2 - m^2)^2} \mathcal{T}_k \frac{1}{(q - k)^2} &= \frac{1}{q^2} \int \frac{d^d k}{(k^2 - m^2)^2} + \frac{1}{(q^2)^2} \int \frac{(2q \cdot k - k^2) d^d k}{(k^2 - m^2)^2} + \dots \\ &= \frac{i\pi^{d/2}}{q^2 (m^2)^\varepsilon} \Gamma(\varepsilon) \left[ 1 + \frac{\varepsilon}{1 + \varepsilon} \frac{m^2}{q^2} + \dots \right] . \end{aligned} \quad (5)$$

The contribution of another subgraph consisting of two lower lines generates a zero contribution because this is a massless vacuum diagram:

$$\int \frac{d^d k}{k^2} \mathcal{T}_{k,m} \frac{1}{((q - k)^2 - m^2)^2} = \frac{1}{(q^2)^2} \int \frac{d^d k}{k^2} + \dots = 0 .$$

This contribution would be however non-zero in the case of a non-zero mass in the lower lines.

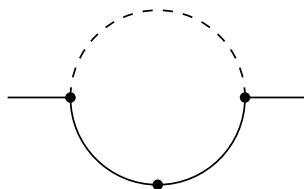


Figure 1: One-loop propagator diagram

When  $\varepsilon \rightarrow 0$ , infrared (IR) poles in the first non-zero contribution are canceled against ultraviolet (UV) poles in the second one, with the finite result

$$F_{\Gamma}(q^2, m^2; 0) \sim \frac{i\pi^2}{q^2} \left[ \ln \left( \frac{-q^2}{m^2} \right) - \frac{m^2}{q^2} + \dots \right]. \quad (6)$$

It turns out that at present there are no simple generalizations of the strategy of subgraphs to typical Minkowskian regimes.<sup>2</sup> Before formulating what the strategy of regions is let us remind that a (*standard*) strategy of regions was used for many years for analyzing leading power and (sub)leading logarithms. It reduces to the following prescriptions:

- Consider various regions of the loop momenta and expand, in every region, the integrand in a Taylor series with respect to the parameters that are considered small in the given region;
- pick up the leading asymptotic behaviour generated by every region.

Let us stress that cut-offs that specify the regions are not removed within this strategy. In fact, it was sufficient to analyze rather limited family of regions because the leading asymptotics are generated only by specific regions.

The (*generalized*) strategy of regions has been suggested in [1] (and immediately applied to the threshold expansion):

- Consider various regions ...
- Integrate the integrand expanded, in every region in its own way, over the whole integration domain in the loop momenta;
- Put to zero any integral without scale.

Let us stress that, for typically Euclidean limits, integrals without scale (tadpoles) are *automatically* put to zero. For general limits, this is an *ad hoc* prescription.

An experimental observation tell us that this strategy of regions gives asymptotic expansions for any diagram in any limit. In particular, it has been checked in numerous examples when comparing results of expansion with existing explicit analytical results. We have also an indirect confirmation because, for limit typical for Euclidean space, the strategy of regions leads to the same prescriptions as the strategy of subgraphs. To see this it is in fact sufficient to take any loop momentum to be either

$$\begin{aligned} \textit{large} : & \quad k \sim q, \quad \text{or} \\ \textit{small} : & \quad k \sim m \end{aligned}$$

---

<sup>2</sup> With the exception of the large momentum off-shell limit and one of the versions of the Sudakov limit — see [6].

and then observe that one obtains eq. (2).

Still to see how the strategy of regions works let us consider the previous example of Fig. 1. We consider the loop momentum  $k$  to be either large or small and obtain

$$\begin{aligned} k \text{ large:} & \rightarrow \mathcal{T}_m \frac{1}{(k^2 - m^2)^2} \leftrightarrow \Gamma \\ k \text{ small:} & \rightarrow \mathcal{T}_k \frac{1}{(q - k)^2} \leftrightarrow \gamma_1 \end{aligned}$$

Thus the region of the large momenta reproduces the contribution of the subgraph  $\Gamma$  and the region of the small momenta reproduces the contribution of the subgraph  $\gamma_1$  present according to the strategy of subgraphs (2).

From now on we turn to various examples of limits typical for Minkowski space.

## 4 Strategy of regions for limits typical for Minkowski space

### 4.1 Threshold expansion [1]

Consider first the threshold limit when an external momentum squared tends to a threshold value. Our primary task is to see what kinds of regions are relevant here. Let us consider the same example of Fig. 1 but in the new limit,  $q^2 \rightarrow m^2$ . In this case, it is reasonable to choose the loop momentum in another way to make explicit the dependence on the expansion parameter:

$$F_{\Gamma}(q^2, y; \varepsilon) = \int \frac{d^d k}{k^2((q - k)^2 - m^2)^2} = \int \frac{d^d k}{k^2(k^2 - 2q \cdot k - y)^2}. \quad (7)$$

So we have turned to the new variables  $(q^2, m^2) \rightarrow (q^2, y)$  with  $y = m^2 - q^2 \rightarrow 0$  the expansion parameter of the problem.

Let us look for relevant regions. The region of large (let us from now on use the term *hard* instead) momenta,  $k \sim q$ , always contributes. It gives

$$\int \frac{d^d k}{k^2} \mathcal{T}_y \frac{1}{(k^2 - 2q \cdot k - y)^2} = \int \frac{d^d k}{k^2(k^2 - 2q \cdot k)^2} + \dots = \frac{i\pi^{d/2}}{(q^2)^{1+\varepsilon}} \frac{\Gamma(1 + \varepsilon)}{2\varepsilon} + \dots, \quad (8)$$

where each integral is evaluated in gamma functions for general  $\varepsilon$ .

If we consider the region of small loop momenta,  $k \sim \sqrt{y}$  (which from now on we will call *soft*) we shall obtain an integral without scale which we put to zero according to one of the prescriptions of the strategy of regions:

$$\int \frac{d^d k}{k^2(-2q \cdot k)^2} + \dots = 0.$$

It is the *ultrasoft* (us) region,  $k \sim y/\sqrt{q^2}$ , which gives here the second non-zero contribution:

$$\int \frac{d^d k}{k^2} \mathcal{T}_{k^2} \frac{1}{(k^2 - 2q \cdot k - y)^2} = \int \frac{d^d k}{k^2 (-2q \cdot k - y)^2} + \dots = -i\pi^{d/2} \frac{\Gamma(1-\varepsilon)\Gamma(2\varepsilon)}{(q^2)^{1-\varepsilon} y^{2\varepsilon}}. \quad (9)$$

Only the leading term survives because, in the next terms the factor  $k^2$  resulting from expansion cancels the massless propagator so that a scaleless integral appears.

If we combine the hard and ultrasoft contributions we shall obtain, in the limit  $\varepsilon \rightarrow 0$ , the known explicit result for the given diagram expanded at threshold:

$$\frac{i\pi^{d/2}}{q^2} \left[ \ln \frac{y}{q^2} - \frac{y}{q^2} + \dots \right].$$

It turns out that for diagrams consisting of massless and massive (with the same mass  $m$ ) lines and having thresholds only with one massive line, i.e. at  $q^2 = m^2$ , only hard and ultrasoft regions are relevant. To find other characteristic regions we turn to an example with two massive lines — see Fig. 2. We have

$$F_\Gamma(q^2, y; \varepsilon) = \int \frac{d^d k}{(k^2 - m^2)((q - k)^2 - m^2)} = \int \frac{d^d k}{(k^2 + q \cdot k - y)(k^2 - q \cdot k - y)}, \quad (10)$$

where the loop momentum is again chosen in another way, and we have turned to the new variables:  $(q^2, m^2) \rightarrow (q^2, y)$  where  $y = m^2 - q^2/4 \rightarrow 0$  is the small parameter of the problem. Keeping in mind the non-relativistic flavour of the problem we choose the frame  $q = \{q_0, \vec{0}\}$ .

Let us look for relevant regions. The hard region,  $k \sim q$ , gives

$$\begin{aligned} \int d^d k \mathcal{T}_y \frac{1}{(k^2 + q_0 k_0 - y)(k^2 - q_0 k_0 - y)} + \dots &= \int d^d k \frac{1}{(k^2 + q_0 k_0)(k^2 - q_0 k_0)} + \dots \\ &= i\pi^{d/2} \left( \frac{4}{q^2} \right)^\varepsilon \frac{\Gamma(\varepsilon)}{1 - 2\varepsilon} + \dots \end{aligned} \quad (11)$$

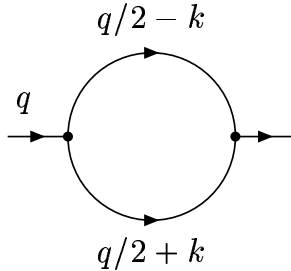


Figure 2: One-loop propagator diagram with two non-zero masses in the threshold

The soft and ultrasoft regions generate zero contributions because of the appearance of scaleless integrals:

$$-\frac{1}{q^2} \int \frac{d^d k}{k_0^2} + \dots = 0, \quad -\frac{1}{q^2} \int \frac{dk_0 d^d \vec{k}}{(q_0 k_0 - y + i0)(q_0 k_0 + y - i0)} + \dots = 0. \quad (12)$$

It turns out that the missing non-zero contribution here comes from the *potential* (p) [1] region,  $k_0 \sim y/q_0$ ,  $\vec{k} \sim \sqrt{y}$ . It generates Taylor expansion in  $k_0^2$  and is evaluated by closing the integration contour in  $k_0$  and taking a residue, e.g. in the upper half-plane, and then evaluating  $(d-1)$ -dimensional integral in  $\vec{k}$  using Feynman parameters. Here again only the leading term survives because the next terms involve scaleless integrals:

$$\begin{aligned} & \int dk_0 d^{d-1} \vec{k} \mathcal{T}_{k_0^2} \frac{1}{(k^2 + q_0 k_0 - y + i0)(k^2 - q_0 k_0 - y + i0)} \\ &= \int \frac{dk_0 d^{d-1} \vec{k}}{(\vec{k}^2 - q_0 k_0 + y - i0)(\vec{k}^2 + q_0 k_0 + y - i0)} + \dots = i\pi^{d/2} \Gamma(\varepsilon - 1/2) \sqrt{\frac{\pi y}{q^2}} y^{-\varepsilon}. \end{aligned} \quad (13)$$

The sum of the hard and potential contributions successfully reproduces the known analytical result for the given diagram.

The next example is given by the triangle diagram with two non-zero masses in the threshold — see Fig. 3. It is considered at  $q = p_1 + p_2$ ,  $p = (p_1 - p_2)/2$ ,  $p_1^2 = p_2^2 = m^2$  and is given by the following Feynman integral:

$$\int \frac{d^d k}{(k^2 + q \cdot k - y)(k^2 - q \cdot k - y)(k - p)^2}, \quad (14)$$

where again  $y = m^2 - q^2/4 \rightarrow 0$  and  $q = \{q_0, \vec{0}\}$ .

The situation is quite similar to the previous diagram. There are two non-zero contributions generated by the hard and potential regions [1]: the (h) contribution

$$\int d^d k \frac{1}{(k^2 + q_0 k_0)(k^2 - q_0 k_0)(k - p)^2} = -i\pi^{d/2} \left(\frac{4}{q^2}\right)^{1+\varepsilon} \frac{\Gamma(\varepsilon)}{2(1+2\varepsilon)} + \dots \quad (15)$$

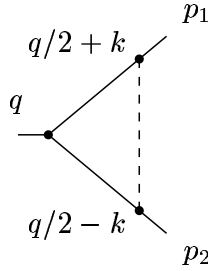


Figure 3: Triangle diagram with two non-zero masses in the threshold

and the (p) contribution

$$\int \frac{dk_0 d^{d-1}\vec{k}}{(\vec{k}^2 - q_0 k_0 + y - i0)(\vec{k}^2 + q_0 k_0 + y - i0)(-\vec{k} - \vec{p})^2} = i\pi^{d/2} \frac{y^{-\varepsilon}}{\sqrt{q^2 y}} \frac{\sqrt{\pi}\Gamma(\varepsilon + 1/2)}{2\varepsilon}. \quad (16)$$

One can check that their sum equals the whole analytical result for the given diagram.

It turns out that we have already seen the whole list of regions relevant to the threshold expansion, with the qualification that soft regions did not yet contribute in the examples. We refer for two-loop examples to [1]. For example, the threshold expansion of Fig. 4 at  $y = m^2 - q^2/4 \rightarrow 0$  consists of contributions generated by the following regions: (h-h), (h-p)=(p-h), (p-p), (p-us) (where two loop momenta are characterized, and the ultrasoft momentum in the last contribution refers to the momentum of the middle line).

Similarly, the threshold expansion of Fig. 5 at  $y = m^2 - q^2/4 \rightarrow 0$  consists of (h-h), (h-p), (p-h), (p-p), (p-s) (where the loop momentum of the box subgraph is soft) and (p-us) (where the momentum of the middle line is ultrasoft) contributions — see details in [1].

It should be stressed that the knowledge about expansions of individual Feynman diagram gives the possibility to derive expansions at the operator level. The threshold expansion with one zero (small) and one non-zero mass in the threshold leads to HQET (see [7] for review), while the situation with two non-zero masses in

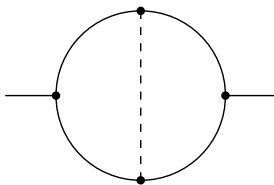


Figure 4: Two-loop master self-energy diagram with two non-zero masses in the threshold

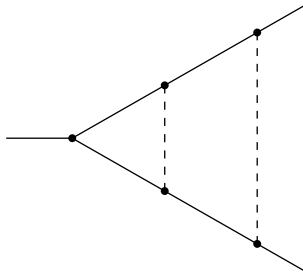


Figure 5: Two-loop vertex diagram with two non-zero masses in the threshold

the threshold provides the transition from QCD to NRQCD [8] and then further to pNRQCD [8]. Historically, the development of HQET was performed without the knowledge of the corresponding diagrammatical expansion. This can be explained by the combinatorial simplicity of HEQT with the structure similar to that of the large mass expansion, where there are only two scales in the problem.

The case of the threshold expansion with two non-zero masses in the threshold is much more complicated. At the diagrammatical level, this is described by the multiplicity of relevant regions in the problem which correspond to three different scales:  $m$  (mass of the quark), the momentum  $mv$ , where  $v$  is relative velocity of the quarks (straightforwardly expressed through the variable  $y$  in the above examples), and the energy  $mv^2$ . An adequate description of the transition from NRQCD (which is obtained from QCD by ‘integrating out’ the hard scale,  $m$ ) to pNRQCD has been obtained not so easily (see a discussion from the point of view of 1997 in [1]), and the development of the diagrammatical threshold expansion helped to unambiguously identify all relevant scales in the problem and the form of the corresponding terms in the effective Lagrangian.

The threshold expansion resulted in a number of applications. The first of them was analytical evaluation of the two-loop matching coefficients of the vector current in NRQCD and QCD [10]. Another class of important results was the two-loop description of the  $t\bar{t}$  production in  $e^+e^-$  annihilation near threshold — see [11].

## 4.2 Sudakov limit

There are three different versions of the Sudakov limit  $m^2 \ll Q^2 \equiv -s = -(p_1 - p_2)^2$  or  $M^2 \ll -s$  which are exemplified by scalar triangle diagram in Fig. 6, where dashed lines denote massless propagators. Within the ‘standard’ strategy of regions, summing up (sub)leading logarithms (at the leading power) using evolution equations

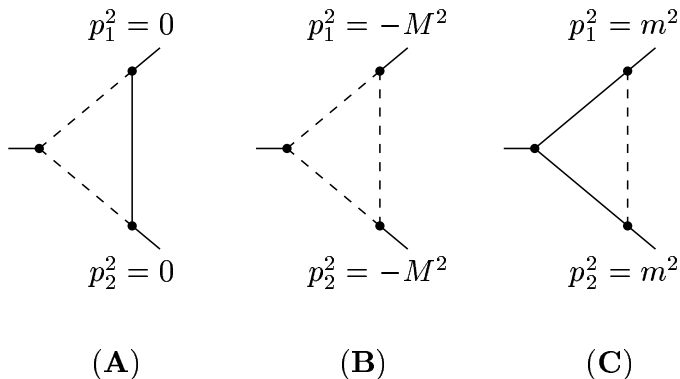


Figure 6: Triangle diagram in the Sudakov limit

has been analyzed in a large number of papers [12].

Let us expand the triangle diagram in Limit A by the strategy of regions. With the standard choice  $p_{1,2} = (Q/2, 0, 0, \mp Q/2)$ , we have

$$\begin{aligned} & \int \frac{d^d k}{(k^2 - 2p_1 \cdot k)(k^2 - 2p_2 \cdot k)(k^2 - m^2)} \\ &= \int \frac{dk_+ dk_- d^{d-2} \underline{k}}{(k_+ k_- - \underline{k}^2 - Qk_+)(k_+ k_- - \underline{k}^2 - Qk_-)(k_+ k_- - \underline{k}^2 - m^2)}, \end{aligned}$$

where  $k_{\pm} = k_0 \pm k_3$ ,  $\underline{k} = (k_1, k_2)$ , with  $2p_{1,2} \cdot k = Qk_{\pm}$ .

Let us look for relevant regions. The hard region,  $k \sim q$ , generates Taylor expansion of the integrand in  $m^2$

$$\int \frac{d^d k}{(k^2 - 2p_1 \cdot k)(k^2 - 2p_2 \cdot k)k^2} + \dots = -i\pi^{d/2} \frac{1}{(Q^2)^{1+\varepsilon}} \frac{\Gamma(1+\varepsilon)\Gamma(-\varepsilon)^2}{\Gamma(1-2\varepsilon)} + \dots \quad (17)$$

The soft ( $k \sim m$ ) and ultrasoft ( $k \sim m^2/Q$ ) regions generate scaleless integrals which are zero:

$$\int \frac{d^d k}{(-2p_1 \cdot k)(-2p_2 \cdot k)k^2} + \dots = 0, \quad \int \frac{d^d k}{(-2p_1 \cdot k)(-2p_2 \cdot k)(-m^2)} + \dots = 0. \quad (18)$$

What is yet missing is the contribution of collinear regions<sup>3</sup>:

$$\begin{aligned} 1\text{-collinear (1c):} & \quad k_+ \sim m^2/Q, \quad k_- \sim Q, \quad \underline{k} \sim m, \\ 2\text{-collinear (2c):} & \quad k_+ \sim Q, \quad k_- \sim m^2/Q, \quad \underline{k} \sim m. \end{aligned}$$

The (1c) region generates Taylor expansion of propagator 2 in  $k^2$ :

$$\int \frac{d^d k}{(k^2 - 2p_1 \cdot k)(-2p_2 \cdot k)(k^2 - m^2)} + \dots, \quad (19)$$

and the (2c) contribution is symmetrical. These contributions are not however individually regularized by dimensional regularization. A natural way to overcome this obstacle is to introduce an auxiliary analytic regularization [14], calculate (1c) and (2c) contributions and switch it off in the sum. Then the (1c) and (2c) regions give, in the leading power,

$$-i\pi^{d/2} \frac{\Gamma(\varepsilon)}{Q^2(m^2)^\varepsilon} \left[ \ln(Q^2/m^2) + \psi(\varepsilon) - \gamma_E - 2\psi(1-\varepsilon) \right] + \dots \quad (20)$$

---

<sup>3</sup>introduced within the ‘standard strategy of regions’ [13]

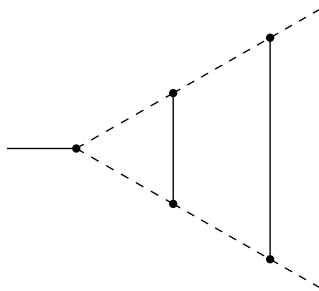


Figure 7: Two-loop vertex diagram in Limit A

After we combine the (h) and (c) contributions we shall see that IR/collinear poles in the (h) contribution and UV/collinear poles in (c) contribution are canceled, and at  $\varepsilon \rightarrow 0$  we obtain

$$\frac{i\pi^2}{Q^2} \left[ \text{Li}_2(x) - \frac{1}{2} \ln^2 x + \ln x \ln(1-x) - \frac{\pi^2}{3} \right], \quad (21)$$

where  $\text{Li}_2(x)$  is dilogarithm and  $x = m^2/Q^2$ .

The triangle diagrams of Fig. 5 in Limits B and C are similarly expanded. In Limit B one meets (h), (1c), (2c) and (us) regions, and, in Limit C, one has (h), (1c) and (2c) regions.

Two-loop examples for the Sudakov limit, within the strategy of regions, can be found in [15]. For example, the following regions contribute to the expansion of Fig. 7 in Limit A: (h-h), (1c-h)+(2c-h), (1c-1c)+(2c-2c), and (h-s) where the soft momentum refers to the middle line. For Limit B, one has (h-h), (1c-h)=(2c-h), (1c-1c)=(2c-2c), (us-h), (us-1c), (us-2c), (us-us).

For the diagram of Fig. 5 (considered above in the threshold limit), with  $p_{1,2} = \tilde{p}_{1,2} + (m^2/Q^2)\tilde{p}_{2,1}$ , with  $\tilde{p}_{1,2} = (Q/2, 0, 0, \mp Q/2)$ , obvious regions (h-h), (1c-h)=(2c-h), (1c-1c)=(2c-2c) are not sufficient because the poles of the fourth order do not cancel. It turns out that it is necessary to consider also ultracollinear regions:

$$\begin{aligned} (1\text{uc}): \quad & k_+ \sim m^4/Q^3, \quad k_- \sim m^2/Q, \quad \underline{k} \sim m^3/Q^2, \\ (2\text{uc}): \quad & k_+ \sim m^2/Q, \quad k_- \sim m^4/Q^3, \quad \underline{k} \sim m^3/Q^2. \end{aligned}$$

After one adds contributions of the (1uc-2c) and (1c-2uc) regions the leading power of expansion satisfies the check of poles [15].

The (generalized) strategy of regions combined with evolution equations derived within the ‘standard’ strategy of regions has been applied to summing up next-to-leading logarithms for Abelian form factor and four-fermion amplitude in the  $SU(N)$  gauge theory [16].

### 4.3 Regge limit

The Regge limit for scattering diagrams is characterized as  $|t| \ll |s|$ , where  $s = (p_1 + p_2)^2$  and  $t = (p_1 + p_3)^2$  are Mandelstam variables.

Let us expand, using the strategy of regions, the box diagram shown in Fig. 8. The Feynman integral is

$$\int \frac{d^d k}{(k^2 + 2p_1 \cdot k)(k^2 - 2p_2 \cdot k)k^2(k + p_1 + p_3)^2}. \quad (22)$$

Let  $s = -Q^2$ ,  $t = -T$ , and let us choose  $p_{1,2} = (\mp Q/2, 0, 0, Q/2)$ , and  $p_1 + p_3 = (T/Q, 0, \sqrt{T + T^2/Q^2}, 0)$ . It turns out that in the Regge limit one meets contributions of (h) and (c) regions. The collinear regions are now characterized as

$$(1(2)c): \quad k_{\pm} \sim T/Q, \quad k_{\mp} \sim Q, \quad \underline{k} \sim \sqrt{T}.$$

The sum of (1c) and (2c) gives, in the leading power,  $1/t$ ,

$$i\pi^{d/2} \frac{\Gamma(-\varepsilon)^2 \Gamma(1 + \varepsilon)}{\Gamma(-2\varepsilon) s (-t)^{1+\varepsilon}} [\ln(t/s) + \psi(-\varepsilon) - 2\psi(1 + \varepsilon) + \gamma_E]. \quad (23)$$

The hard contribution starts from the NLO. If we sum up the (h) and (c) contributions we shall see that, at  $\varepsilon \rightarrow 0$ , only the LO (c) contribution survives and gives

$$\frac{i\pi^{d/2} e^{-\gamma_E \varepsilon}}{st} \left[ \frac{4}{\varepsilon^2} - (\ln(-s) + \ln(-t)) \frac{2}{\varepsilon} + 2 \ln(-s) \ln(-t) - \frac{4\pi^2}{3} \right]. \quad (24)$$

In the case of on-shell massless double box,  $p_i^2 = 0$ , given by the integral

$$\int \int \frac{d^d k d^d l}{(l^2 + 2p_1 \cdot l)(l^2 - 2p_2 \cdot l)(k^2 + 2p_1 \cdot k)(k^2 - 2p_2 \cdot k)} \times \frac{1}{k^2(k-l)^2(l+r)^2} \equiv \frac{(i\pi^{d/2} e^{-\gamma_E \varepsilon})^2}{(-s)^{2+2\varepsilon} (-t)} K(t/s; \varepsilon), \quad (25)$$

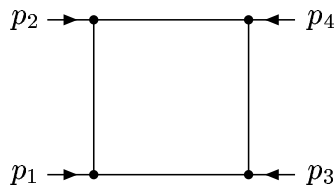


Figure 8: Box diagram

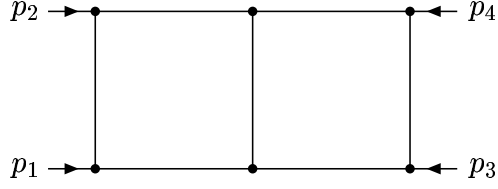


Figure 9: Double box

there are (h-h), (1c-1c) and (2c-2c) contributions in the Regge limit. The (h-h) contribution starts from the NLO,  $t^0$ , and the (c-c) contribution from LO,  $t^{-1}$ . This is a result for the sum of the LO and NLO contributions [17]

$$\begin{aligned}
K(x, \varepsilon) &= -\frac{4}{\varepsilon^4} + \frac{5 \ln x}{\varepsilon^3} - \left(2 \ln^2 x - \frac{5}{2} \pi^2\right) \frac{1}{\varepsilon^2} \\
&- \left(\frac{2}{3} \ln^3 x + \frac{11}{2} \pi^2 \ln x - \frac{65}{3} \zeta(3)\right) \frac{1}{\varepsilon} + \frac{4}{3} \ln^4 x + 6\pi^2 \ln^2 x - \frac{88}{3} \zeta(3) \ln x + \frac{29}{30} \pi^4 \\
&+ 2x \left[ \frac{1}{\varepsilon} \left( \ln^2 x - 2 \ln x + \pi^2 + 2 \right) - \frac{1}{3} \left( 4 \ln^3 x + 3 \ln^2 x \right. \right. \\
&\left. \left. + (5\pi^2 - 36) \ln x + 2(33 + 5\pi^2 - 3\zeta(3)) \right) \right] + O(x^2 \ln^3 x) .
\end{aligned} \tag{26}$$

The on-shell double box has provided a curious example of a situation when the evaluation of large number terms of the expansion is rather complicated while an explicit analytical result<sup>4</sup> [18] is known:

$$\begin{aligned}
K(x, \varepsilon) &= -\frac{4}{\varepsilon^4} + \frac{5 \ln x}{\varepsilon^3} - \left(2 \ln^2 x - \frac{5}{2} \pi^2\right) \frac{1}{\varepsilon^2} \\
&- \left(\frac{2}{3} \ln^3 x + \frac{11}{2} \pi^2 \ln x - \frac{65}{3} \zeta(3)\right) \frac{1}{\varepsilon} + \frac{4}{3} \ln^4 x + 6\pi^2 \ln^2 x - \frac{88}{3} \zeta(3) \ln x + \frac{29}{30} \pi^4 \\
&- \left[ 2\text{Li}_3(-x) - 2 \ln x \text{Li}_2(-x) - \left(\ln^2 x + \pi^2\right) \ln(1+x) \right] \frac{2}{\varepsilon} \\
&- 4 \left( S_{2,2}(-x) - \ln x S_{1,2}(-x) \right) + 44\text{Li}_4(-x) - 4 \left( \ln(1+x) + 6 \ln x \right) \text{Li}_3(-x) \\
&+ 2 \left( \ln^2 x + 2 \ln x \ln(1+x) + \frac{10}{3} \pi^2 \right) \text{Li}_2(-x) \\
&+ \left( \ln^2 x + \pi^2 \right) \ln^2(1+x) - \frac{2}{3} \left( 4 \ln^3 x + 5\pi^2 \ln x - 6\zeta(3) \right) \ln(1+x) .
\end{aligned} \tag{27}$$

Still the evaluation of those first two terms of the expansion was used as a very crucial check of (27). Observe that the asymptotic expansion within the strategy of regions was successfully applied in [20] also to double boxes with one leg off shell.

<sup>4</sup>See [19] for a review of recent results on the evaluation of double box diagrams.

## 5 Present status of the strategy of regions

To characterize the present status of the strategy of regions let us first point out that at present there are no mathematical proofs, similar to the case of the strategy of subgraphs (applied only to the limits typical for Euclidean space), although this looks to be a very good mathematical problem. (Moreover, the very word ‘region’ is understood in the physical sense so that one does not bother about ‘the decomposition of unity’.) Its solution is expected to be specific for each concrete regime typical for Minkowski space. Another reasonable problem is to develop the strategy of regions for phase space integrals arising in evaluation of real radiation processes.

Let us conclude with advice that could be useful when studying a new limit:

- Look for regions, typical for the limit (probably, they are similar to regions connected with known limits<sup>5</sup>);
- Test one- and two-loop examples by comparison with explicit results;
- Check poles in  $\varepsilon$ ; if this check is not satisfied look for missing regions;
- Check expansion numerically;
- Use the strategy of regions formulated in  $\alpha$ -parameters [15], e.g., to avoid double counting;
- Stay optimistic because, up to now, the strategy of regions successfully worked in all known examples!

## Acknowledgments

I am thankful to S. Brodsky, L. Dixon, H. Haber and K. Melnikov for support and kind hospitality at the symposium.

---

<sup>5</sup>As a recent example of using the strategy of regions in a new situation let us refer to ref. [21] where non-relativistic integrals describing bound states within NRQCD were further expanded in the ratio of the small and the large mass  $m/M$ . The relevant regions turned out to be (non-relativistic) hard and soft regions of three-dimensional momenta.

## References

- [1] M. Beneke and V.A. Smirnov, *Nucl. Phys.* **B522** (1998) 321.
- [2] S.G. Gorishny, *Nucl. Phys.* **B319** (1989) 633; K.G. Chetyrkin, *Teor. Mat. Fiz.* **75** (1988) 26; *ibid.* **76** (1988) 207; V.A. Smirnov, *Commun. Math. Phys.* **134** (1990) 109.
- [3] V.A. Smirnov, *Mod. Phys. Lett.* **A10** (1995) 1485.
- [4] G. 't Hooft and M. Veltman, *Nucl. Phys.* **B44** (1972) 189; C.G. Bollini and J.J. Giambiagi, *Nuovo Cim.* **12B** (1972) 20.
- [5] K.G. Chetyrkin, J.H. Kühn and A. Kwiatkowski, *Phys. Reports* **277** (1997) 189.
- [6] V.A. Smirnov, *Phys. Lett.* **B394** (1997) 205; **B404** (1997) 101; A. Czarnecki and V.A. Smirnov, *Phys. Lett.* **B394** (1997) 211.
- [7] M. Neubert, *Phys. Rep.* **245** (1994) 259.
- [8] W.E. Caswell and G.P. Lepage, *Phys. Lett.* **B167** (1986) 437.
- [9] A. Pineda and J. Soto, *Nucl. Phys. Proc. Suppl.* **64** (1998) 428; *Phys. Rev.* **D59** (1999) 016005.
- [10] A. Czarnecki and K. Melnikov, *Phys. Rev. Lett.* **80** (1998) 2531; M. Beneke, A. Signer and V.A. Smirnov, *Phys. Rev. Lett.* **80** (1998) 2535.
- [11] A. Hoang et al., *Eur. Phys. J. direct* **C3** (2000) 1; A. Hoang, these proceedings.
- [12] V.V. Sudakov, *Zh. Eksp. Teor. Fiz.* **30** (1956) 87; R. Jackiw, *Ann. Phys.* **48** (1968) 292; **51** (1969) 575; J.M. Cornwall and G. Tiktopoulos, *Phys. Rev. Lett.* **35** (1975) 338; **D13** (1976) 3370; J. Frenkel and J.C. Taylor, *Nucl. Phys.* **B116** (1976) 185; J.C. Collins, *Phys. Rev.* **D22** (1980) 1478; in *Perturbative QCD*, ed. A.H. Mueller, 1989, p. 573. A. Sen, *Phys. Rev.* **D24** (1981) 3281; **D28** (1983) 860; G. Korchemsky, *Phys. Lett.* **B217** (1989) 330; **B220** (1989) 629.
- [13] G. Sterman, *Phys. Rev.* **D17** (1978) 2773; S. Libby and G. Sterman, *Phys. Rev.* **D18** (1978) 3252; A.H. Mueller, *Phys. Rep.* **73** (1981) 35.
- [14] E.R. Speer, *J. Math. Phys.* **9** (1968) 1404.
- [15] V.A. Smirnov and E.R. Rakhmetov, *Teor. Mat. Fiz.* **120** (1999) 64; V.A. Smirnov, *Phys. Lett.* **B465** (1999) 226.
- [16] J.H. Kühn, A.A. Penin and V.A. Smirnov, *Eur. Phys. J.* **C17** (2000) 97.

- [17] V.A. Smirnov and O.L. Veretin, *Nucl. Phys.* **B566** (2000) 469.
- [18] V.A. Smirnov, *Phys. Lett.* **B460** (1999) 397.
- [19] T. Gehrmann, these proceedings.
- [20] V.A. Smirnov, *Phys. Lett.* **B491** (2000) 130; V.A. Smirnov, hep-ph/0011056.
- [21] A. Czarnecki and K. Melnikov, hep-ph/0012053.

April 19, 2001  
hep-ph/0102031

# Letting Real-Virtual Cancellations Happen by Themselves in QCD Calculations

DAVISON E. SOPER\*

*Institute of Theoretical Science  
University of Oregon, Eugene, OR 97403 USA*

Calculations of observables in quantum chromodynamics are typically performed using a method that combines numerical integrations over the momenta of final state particles with analytical integrations over the momenta of virtual particles. I review a method for performing all of the integrations numerically. In this method, the real-virtual cancellations happen inside the integrals – simply because they are built into the Feynman rules. I indicate promising topics for further research on this subject.

Presented at the

5th International Symposium on Radiative Corrections  
(RADCOR–2000)

Carmel CA, USA, 11–15 September, 2000

---

\*Work supported by the U. S. Department of Energy

# 1 Introduction

There is an important class of computer programs that do calculations in quantum chromodynamics (QCD) in which the calculation is performed at next-to-leading order in perturbation theory and allows for the determination of a variety of characteristics of the final state. This talk reviews a program of this class in which a “completely numerical” integration algorithm is used.

I consider the calculation of “three-jet-like” observables in  $e^+e^-$  annihilation. A program that does this can be used to calculate a jet cross section (with any infrared safe choice of jet definition) or observables like the thrust distribution. Such a program generates random partonic events consisting of three or four final state quarks, antiquarks, and gluons. Each event comes with a calculated weight. A separate routine then calculates the contribution to the desired observable for each event, averaging over the events with their weights.

The weights are treated as probabilities. However, these weights can be both positive or negative. This is an almost inevitable consequence of quantum mechanics. The calculated observable is proportional to the square of a quantum amplitude and is thus positive. However, as soon as one divides the amplitude into pieces for purposes of calculation, one finds that, while the square of each piece is positive, the interference terms between different pieces can have either sign. Thus the kind of program discussed here stands in contrast to the tree-level event generators in which, by simplifying the physics, one can generally arrange to have all the weights be positive, or, even, all be equal to 1.

To understand the algorithms used in the class of programs described above, it is best to think of the calculations as performing integrations over momenta in which the quantum matrix elements and the measurement functions form the integrand. There are two basic algorithms for performing the integrations. The older is due to Ellis, Ross, and Terrano (ERT) [1]. In this method, some of the integrations are performed analytically ahead of time. The other integrations are performed numerically by the Monte Carlo method. The integrations are divergent and are regulated by analytical continuation to  $3 - 2\epsilon$  space dimensions and a scheme of subtractions or cutoffs. The second method is much newer [2,3,4]. In this method, all of the momentum integrations are done by Monte Carlo numerical integration. With this method, the integrals are all convergent (after removal of the ultraviolet divergences by a straightforward renormalization procedure).

In its current incarnation, the numerical method is not as good as older programs in analyzing three jet configurations that are close to being two jet configurations. On the other hand, the numerical method offers evident advantages in flexibility to modify the integrand. Since this method is quite new, one cannot yet say for what problems it might do better than the now standard ERT method.

The numerical integration method exists as computer code with accompanying

technical notes [4] and many of the basic ideas behind it have been described in two papers [2,3]. In this talk, I briefly review the basics of the numerical integration method. Then, I display some graphs that illustrate the cancellation of singularities that occurs inside the integrand in the numerical method. Finally, I discuss some avenues for future research.

## 2 Review of the numerical method

Let us begin with a precise statement of the problem. We consider an infrared safe three-jet-like observable in  $e^+e^- \rightarrow \text{hadrons}$ , such as a particular moment of the thrust distribution. The observable can be expanded in powers of  $\alpha_s/\pi$ ,

$$\sigma = \sum_n \sigma^{[n]}, \quad \sigma^{[n]} \propto (\alpha_s/\pi)^n. \quad (1)$$

The order  $\alpha_s^2$  contribution has the form

$$\begin{aligned} \sigma^{[2]} &= \frac{1}{2!} \int d\vec{p}_1 d\vec{p}_2 \frac{d\sigma_2^{[2]}}{d\vec{p}_1 d\vec{p}_2} \mathcal{S}_2(\vec{p}_1, \vec{p}_2) \\ &+ \frac{1}{3!} \int d\vec{p}_1 d\vec{p}_2 d\vec{p}_3 \frac{d\sigma_3^{[2]}}{d\vec{p}_1 d\vec{p}_2 d\vec{p}_3} \mathcal{S}_3(\vec{p}_1, \vec{p}_2, \vec{p}_3) \\ &+ \frac{1}{4!} \int d\vec{p}_1 d\vec{p}_2 d\vec{p}_3 d\vec{p}_4 \frac{d\sigma_4^{[2]}}{d\vec{p}_1 d\vec{p}_2 d\vec{p}_3 d\vec{p}_4} \mathcal{S}_4(\vec{p}_1, \vec{p}_2, \vec{p}_3, \vec{p}_4). \end{aligned} \quad (2)$$

Here the  $d\sigma_n^{[2]}$  are the order  $\alpha_s^2$  contributions to the parton level cross section, calculated with zero quark masses. Each contains momentum and energy conserving delta functions. The  $d\sigma_n^{[2]}$  include ultraviolet renormalization in the  $\overline{\text{MS}}$  scheme. The functions  $\mathcal{S}$  describe the measurable quantity to be calculated. We wish to calculate a “three-jet-like” quantity. That is,  $\mathcal{S}_2 = 0$ . The normalization is such that  $\mathcal{S}_n = 1$  for  $n = 2, 3, 4$  would give the order  $\alpha_s^2$  perturbative contribution to the total cross section. There are, of course, infrared divergences associated with Eq. (2). For now, we may simply suppose that an infrared cutoff has been supplied.

The measurement, as specified by the functions  $\mathcal{S}_n$ , is to be infrared safe, as described in Ref. [5]: the  $\mathcal{S}_n$  are smooth, symmetric functions of the parton momenta and

$$\mathcal{S}_{n+1}(\vec{p}_1, \dots, \lambda\vec{p}_n, (1-\lambda)\vec{p}_n) = \mathcal{S}_n(\vec{p}_1, \dots, \vec{p}_n) \quad (3)$$

for  $0 \leq \lambda < 1$ . That is, collinear splittings and soft particles do not affect the measurement.

It is convenient to calculate a quantity that is dimensionless. Let the functions  $\mathcal{S}_n$  be dimensionless and eliminate the remaining dimensionality in the problem by

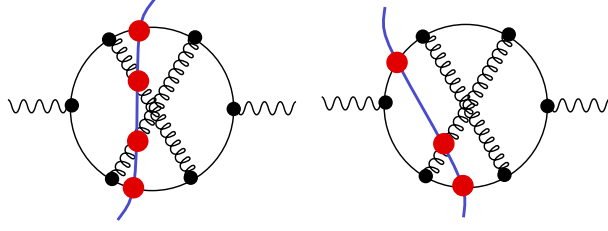


Figure 1: Two cuts of one of the Feynman diagrams that contribute to  $e^+e^- \rightarrow \text{hadrons}$ .

dividing by  $\sigma_0$ , the total  $e^+e^-$  cross section at the Born level. Let us also remove the factor of  $(\alpha_s/\pi)^2$ . Thus, we calculate

$$\mathcal{I} = \frac{\sigma^{[2]}}{\sigma_0 (\alpha_s/\pi)^2}. \quad (4)$$

Let us now see how to set up the calculation of  $\mathcal{I}$  in a convenient form. We note that  $\mathcal{I}$  is a function of the c.m. energy  $\sqrt{s}$  and the  $\overline{\text{MS}}$  renormalization scale  $\mu$ . We will choose  $\mu$  to be proportional to  $\sqrt{s}$ :  $\mu = A_{UV}\sqrt{s}$ . Then  $\mathcal{I}$  depends on  $A_{UV}$ . But, because it is dimensionless, it is independent of  $\sqrt{s}$ . This allows us to write

$$\mathcal{I} = \int_0^\infty d\sqrt{s} h(\sqrt{s}) \mathcal{I}(A_{UV}, \sqrt{s}), \quad (5)$$

where  $h$  is any function with

$$\int_0^\infty d\sqrt{s} h(\sqrt{s}) = 1. \quad (6)$$

The quantity  $\mathcal{I}$  can be expressed in terms of cut Feynman diagrams, as in Fig. 1. The dots where the parton lines cross the cut represent the function  $\mathcal{S}_n(\vec{p}_1, \dots, \vec{p}_n)$ . Each diagram is a three loop diagram, so we have integrations over loop momenta  $l_1^\mu$ ,  $l_2^\mu$  and  $l_3^\mu$ . We first perform the energy integrations. For the graphs in which four parton lines cross the cut, there are four mass-shell delta functions  $\delta(p_j^2)$ . These delta functions eliminate the three energy integrals over  $l_1^0$ ,  $l_2^0$ , and  $l_3^0$  as well as the integral (5) over  $\sqrt{s}$ . For the graphs in which three parton lines cross the cut, we can eliminate the integration over  $\sqrt{s}$  and two of the  $l_j^0$  integrals. One integral over the energy  $E$  in the virtual loop remains. We perform this integration by closing the integration contour in the lower half  $E$  plane. This gives a sum of terms obtained from the original integrand by some simple algebraic substitutions. Having performed the energy integrations, we are left with an integral of the form

$$\mathcal{I} = \sum_G \int d\vec{l}_1 d\vec{l}_2 d\vec{l}_3 \sum_C g(G, C; \vec{l}_1, \vec{l}_2, \vec{l}_3). \quad (7)$$

Here there is a sum over graphs  $G$  (of which one is shown in Fig. 1) and there is a sum over the possible cuts  $C$  of a given graph. The problem of calculating  $\mathcal{I}$  is now set up in a convenient form for calculation.

If we were using the Ellis-Ross-Terrano method, we would put the sum over cuts outside of the integrals in Eq. (7). For those cuts  $C$  that have three partons in the final state, there is a virtual loop. We can arrange that one of the loop momenta, say  $\vec{l}_1$ , goes around this virtual loop. The essence of the ERT method is to perform the integration over the virtual loop momentum analytically ahead of time. The integration is often ultraviolet divergent, but the ultraviolet divergence is easily removed by a renormalization subtraction. The integration is also typically infrared divergent. This divergence is regulated by working in  $3 - 2\epsilon$  space dimensions and then taking  $\epsilon \rightarrow 0$  while dropping the  $1/\epsilon^n$  contributions (after proving that they cancel against other contributions). After the  $\vec{l}_1$  integration has been performed analytically, the integrations over  $\vec{l}_2$  and  $\vec{l}_3$  can be performed numerically. For the cuts  $C$  that have four partons in the final state, there are also infrared divergences. One uses either a ‘phase space slicing’ or a ‘subtraction’ procedure to get rid of these divergences, cancelling the  $1/\epsilon^n$  pieces against the  $1/\epsilon^n$  pieces from the virtual graphs. In the end, we are left with an integral  $\int d\vec{l}_1 d\vec{l}_2 d\vec{l}_3$  in exactly three space dimensions that can be performed numerically.

In the numerical method, we keep the sum over cuts  $C$  inside the integrations. We take care of the ultraviolet divergences by simple renormalization subtractions on the integrand. We make certain deformations on the integration contours so as to keep away from poles of the form  $1/[E_F - E_I + i\epsilon]$ . Then the integrals are all convergent and we calculate them by Monte Carlo numerical integration.

Let us now look at the contour deformation in a little more detail. We denote the momenta  $\{\vec{l}_1, \vec{l}_2, \vec{l}_3\}$  collectively by  $l$  whenever we do not need a more detailed description. Thus

$$\mathcal{I} = \sum_G \int dl \sum_C g(G, C; l). \quad (8)$$

For cuts  $C$  that leave a virtual loop integration, there are singularities in the integrand of the form  $E_F - E_I + i\epsilon$  (or  $E_F - E_I - i\epsilon$  if the loop is in the complex conjugate amplitude to the right of the cut). Here  $E_F$  is the energy of the final state defined by the cut  $C$  and  $E_I$  is the energy of a possible intermediate state. These singularities do not create divergences. The Feynman rules provide us with the  $i\epsilon$  prescriptions that tell us what to do about the singularities: we should deform the integration contour into the complex  $l$  space so as to keep away from them. Thus we write our integral in the form

$$\mathcal{I} = \sum_G \int dl \sum_C \mathcal{J}(G, C; l) g(G, C; l + i\kappa(G, C; l)). \quad (9)$$

Here  $i\kappa$  is a purely imaginary nine-dimensional vector that we add to the real nine-dimensional vector  $l$  to make a complex nine-dimensional vector. The imaginary part

$\kappa$  depends on the real part  $l$ , so that when we integrate over  $l$ , the complex vector  $l+i\kappa$  lies on a surface, the integration contour, that is moved away from the real subspace. When we thus deform the contour, we supply a jacobian  $\mathcal{J} = \det(\partial(l+i\kappa)/\partial l)$ . (See Ref. [3] for details.)

The amount of deformation  $\kappa$  depends on the graph  $G$  and, more significantly, the cut  $C$ . For cuts  $C$  that leave no virtual loop, each of the momenta  $\vec{l}_1$ ,  $\vec{l}_2$ , and  $\vec{l}_3$  flows through the final state. For practical reasons, we want the final state momenta to be real. Thus we set  $\kappa = 0$  for cuts  $C$  that leave no virtual loop. On the other hand, when the cut  $C$  does leave a virtual loop, we choose a non-zero  $\kappa$ . We must, however, be careful. When  $\kappa = 0$  there are singularities in  $g$  on certain surfaces that correspond to collinear parton momenta. These singularities cancel between  $g$  for one cut  $C$  and  $g$  for another. This cancellation would be destroyed if, for  $l$  approaching the collinear singularity,  $\kappa = 0$  for one of these cuts but not for the other. For this reason, we insist that for all cuts  $C$ ,  $\kappa \rightarrow 0$  as  $l$  approaches one of the collinear singularities. The details can be found in Ref. [3].

Much has been left out in this brief overview, but we should now have enough background to see how the method works.

### 3 Example

I present here a simple example, taken from Ref. [3]. Instead of working with QCD at three loops with many graphs, let's work with one graph for  $\phi^3$  theory at two loops, as shown in Fig. 2.

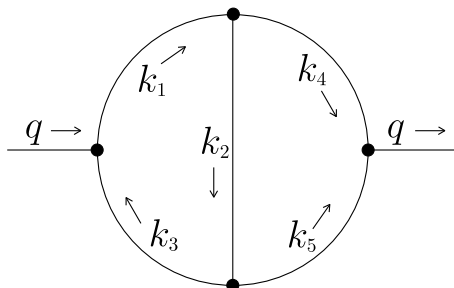


Figure 2: Sample graph in  $\phi^3$  theory.

This graph has four final state cuts, as shown in Fig. 3. We will fix the incoming momentum  $\vec{q}$  and integrate over the incoming energy  $q^0$ . For a measurement function, we take  $\mathcal{S}(p) = \sum |\vec{p}_{T,i}|$ , where  $\vec{p}_T$  is the part of  $\vec{p}$  orthogonal to  $\vec{q}$ . We make a choice of contour deformations and of the density  $\rho$  of Monte Carlo integration points as described in [3]. Then we can plot the integrand  $f$  divided by the density of points  $\rho$  versus the loop momentum. In a Monte Carlo integration, large  $f/\rho$  corresponds to

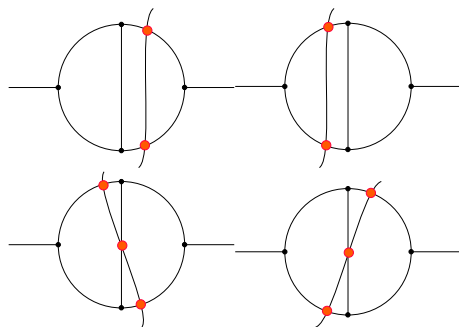


Figure 3: Cuts of the sample graph.

large fluctuations, so  $f/\rho$  should never be too large. In the two figures that follow, I plot  $f/\rho$  versus the momentum in the left hand loop. Specifically, using the  $\vec{k}_n$  defined in Fig. 2, I plot  $f/\rho$  versus  $\vec{l} \equiv \vec{k}_2$  at fixed  $\vec{k}_4$  for  $\vec{l}$  in the  $\{\vec{k}_4, \vec{q}\}$  plane.

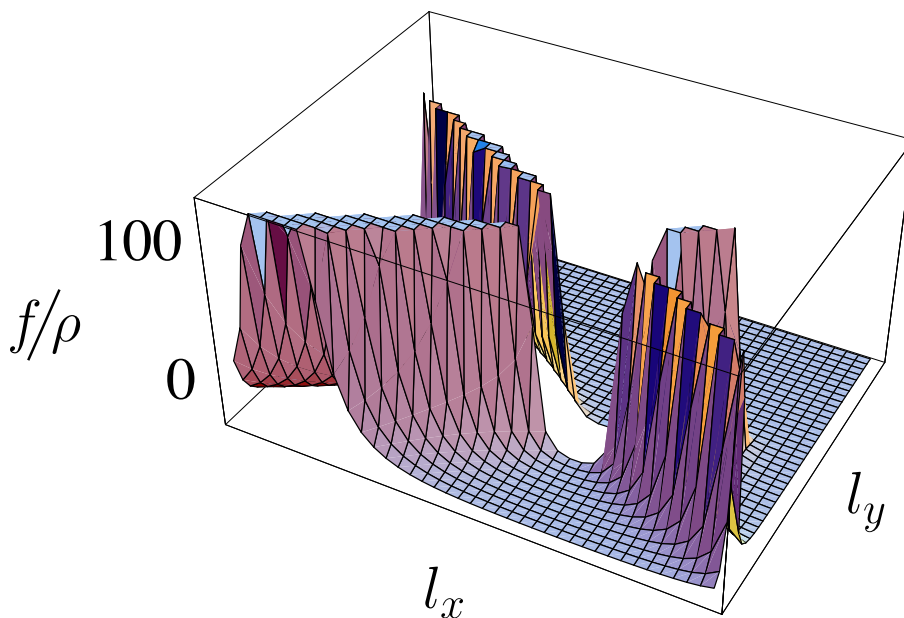


Figure 4: Integrand divided by the density of points for the three parton cuts. The collinear singularities are visible.

In Fig. 4, I show  $f/\rho$  summed over the two cut Feynman graphs that have three partons in the final state, leaving no virtual loop. Evidently, there are singularities. There is a soft parton singularity (at  $\vec{l} = 0$ ) that I have cut out of the diagram and there are collinear parton singularities that are visible in the picture. In the Ellis-Ross-Terrano method, these cut graphs would be calculated using a numerical integration. But first a cutoff or other method for eliminating the singularities would

be needed to eliminate the singular region. The two cuts that leave virtual subgraphs also lead to singularities along the collinear lines in the space of the loop momentum. I omit displaying a graph of  $f/\rho$  for these two cut Feynman graphs because the result simply looks like an upside down version of Fig. 4. In the Ellis-Ross-Terrano method, one takes care of the singularities in the virtual loop by integrating in  $3 - 2\epsilon$  space dimensions. In the numerical method, one combines the integrands for all of the cuts. Then the collinear singularities disappear, while the soft singularity is weakened enough that it can be eliminated in  $f/\rho$  by building a suitable singularity into  $\rho$ . As suggested by the title for this talk, the cancellation of singularities between real and virtual graphs happens by itself because it is built into the Feynman rules. The result for  $f/\rho$  summed over all four cuts is shown in Fig. 5. The collinear singularities are gone, while the soft parton singularity in  $f$  has been weakened enough that it is cancelled by a corresponding singularity in  $\rho$ . Thus a Monte Carlo integration of  $f$  using a density of integration points  $\rho$  can converge nicely because  $f/\rho$  is not singular.

What remains visible in Fig. 5 is a ridge in  $f/\rho$  for  $\vec{l}$  lying on the ellipsoidal surface defined by  $|\vec{k}_1| + |\vec{k}_3| = |\vec{k}_4| + |\vec{k}_5|$ , where the intermediate state energy in the virtual graphs matches the final state energy. This ridge is related to an energy denominator factor  $1/[E_F - E_I + i\epsilon]$  in old fashioned perturbation theory. The numerical integration method has taken advantage of the  $i\epsilon$  prescription in the Feynman rules to deform the integration contour and avoid the singularity.

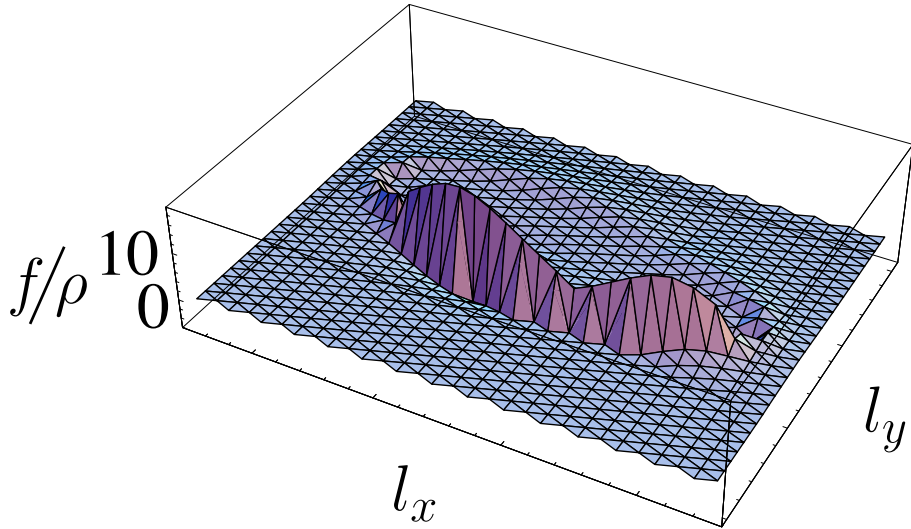


Figure 5: Integrand divided by the density of points for all cuts together. The collinear singularities disappear while the soft parton singularity in  $f$  is weakened so that it can be cancelled by a singularity in  $\rho$ .

## 4 Prospects

There are a number of promising areas for further research along these lines.

The current program, *beowulf* [4], does  $e^+ + e^- \rightarrow 3$  jets at next-to-leading order. The partons are all massless. With some modifications, the partons could have masses. Then one could include massive quarks and one could extend the theory to the complete Standard Model with its massive vector bosons. Furthermore, one could add supersymmetry interactions.

The current program is confined to processes with no hadrons in the initial state. Presumably the same idea can be applied to processes with initial state hadrons, that is electron-proton collisions and proton-proton or proton-antiproton collisions. Again, one should be able to make the particles massive so that one can extend the calculations to the complete Standard Model and supersymmetry.

It should also be possible to have more final state partons. That is, one could attempt to calculate  $e^+ + e^- \rightarrow 4$  jets or  $p + \bar{p} \rightarrow 3$  jets at next-to-leading order.

The challenge of the legendary hero Beowulf was to kill the monster Grendel. The monsters listed above are already dead or at least gravely injured. In particular, all that *beowulf* can do could already have been accomplished by the program of Kunszt and Nason eleven years ago [6]. However, the challenge of calculating  $e^+ + e^- \rightarrow 3$  jets at next-to-next-to-leading order remains unmet, and it may be that a completely numerical attack would be successful.

A less difficult goal is to use the flexibility inherent in the numerical method to go beyond fixed order perturbation theory. For instance, one could use running couplings inside the next-to-leading order graphs as a method for investigating power suppressed (“renormalon”) contributions to the theory. More importantly, one could put a next-to-leading order calculation inside a parton shower event generator (or attach parton showers to the outside of the next-to-leading order calculation) in order to have a full parton shower event generator that is correct at next-to-leading order for three jet quantities in  $e^+e^-$  annihilation. This is, of course, not quite trivial [7]. As far as I can see, the first step is to convert the current algorithms so that they operate in Coulomb gauge instead of Feynman gauge. In this way, the partons propagating into the final state have physical polarizations only. Then these physically polarized partons can split many times to make parton showers. One simply has to avoid counting the same splittings twice.

## References

- [1] R. K. Ellis, D. A. Ross and A. E. Terrano, Nucl. Phys. **B178**, 421 (1981).
- [2] D. E. Soper, Phys. Rev. Lett. **81**, 2638 (1998) [hep-ph/9804454].

- [3] D. E. Soper, Phys. Rev. **D 62**, 014009 (2000) [hep-ph/9910292].
- [4] D. E. Soper, *beowulf* Version 1.0, <http://zebu.uoregon.edu/~soper/beowulf/> .
- [5] Z. Kunszt and D. E. Soper, Phys. Rev. **D 46**, 192 (1992).
- [6] Z. Kunszt, P. Nason, G. Marchesini and B. R. Webber in *Z Physics at LEP1*, Vol. 1, edited by B. Altarelli, R. Kleiss and C. Verzegnassi (CERN, Geneva, 1989), p. 373
- [7] D. E. Soper and M. Kramer, work in progress.

## On the two-loop electroweak amplitude of the muon decay<sup>1</sup>

P.A. GRASSI<sup>a</sup> AND T. HURTH<sup>b</sup>

(a) *Physics Department, New York University ,  
4 Washington Place, New York, NY, 10003, USA.*

(b) *Theory Division, CERN,  
CH-1211, Geneva 23, Switzerland.*

We present an analysis of the two-loop amplitude of the muon decay in the Standard Model (SM) using algebraic renormalization techniques. In addition, we discuss a manifestly BRST invariant IR regulator for the photon within the SM.

---

<sup>1</sup>To appear in the Proceedings of the 5th International Symposium on Radiative Corrections (RADCOR-2000) Carmel CA, USA, 11–15 September, 2000. Talk by P. A. G..

# 1 Introduction

In perturbative multi-loop calculations, the subtraction of UV-divergences in quantum field theory generally leads to Green functions which fail to respect the symmetries of the theory. With the exception of the well-known  $\gamma_5$  problem, the method of dimensional regularization is compatible with the gauge symmetry but it breaks the supersymmetry. In these cases a practical method is needed to restore the symmetry identities of the gauge symmetry or of the supersymmetry. Here the method of algebraic renormalization [1] supplies a complete solution. However, this method has rarely been used in practical calculations although it has been applied intensively in order to demonstrate the renormalizability of various models.

In a recent papers [2, 3], we reviewed the method of algebraic renormalization from a practical point of view and proposed an algebraic method combining the advantages of the background field method (BFM) and the simplification of (intermediate) Taylor subtractions. The method is independent of the regularization scheme; since the local breaking terms are under control, one can use the most convenient regularization scheme in a specific application. After a straightforward analysis of the corresponding (Ward-Takahashi Identities) WTIs and (Slavnov-Taylor Identities) STIs, the spurious anomalies introduced by a non-invariant regularization scheme were shown to reduce to a few universal breaking terms which depend only on finite Green's functions. The method was already applied to several phenomenologically relevant examples in the SM, such as the two-loop contributions to the processes  $H \rightarrow \gamma\gamma$ , to  $B \rightarrow X_s\gamma$  and to the three-gauge boson vertices [2, 4, 3].

Because of the experimental precision of standard model observables at LEP (CERN, Geneva), at SLC (SLAC, Stanford) and at TEVATRON (FERMILAB), calculations of quantum corrections on the two-loop level are necessary; and the  $\gamma_5$  play a critical role here. The purpose of this note is to offer a theoretical analysis of the electroweak two-loop contribution to the muon decay using our algebraic method, and to show its efficiency.

Since a detailed self-contained discussion of the fundamental symmetry constraints for the SM, of the algebraic renormalization procedure in the BFM, and of our specific subtraction method can be found in [2, 3], we restrict ourselves here to reviewing briefly the basic steps of our method (Sec. 2). Then we discuss the muon-decay amplitude, in particular the gauge-invariant subset of two-loop diagrams which is sensitive to the  $\gamma_5$  problem (Sec. 3). It is well-known that there is a physical infrared divergence present in the muon-decay amplitude. For this purpose, we propose an IR regulator that is manifestly compatible with all the symmetries of the SM (Sec. 4).

## 2 General Strategy

In the following, we briefly review the main steps elaborated in [2, 3] to renormalize a gauge model with a non-invariant regularization technique. The BFM turns out to be very important for our purposes and, therefore, we quantize the SM in the ‘t Hooft background gauge [5, 6, 7].

The use of a non-invariant regularization scheme induces breaking terms into the STIs

$$\mathcal{S}(\Gamma^{(n)}) = \hbar^n \Delta^{(n),S} + \mathcal{O}(\hbar^{n+1}), \quad (1)$$

which implement the Becchi-Rouet-Stora-Tyutin (BRST) symmetry, and into the WTIs

$$\mathcal{W}_{(\lambda)}(\Gamma^{(n)}) = \hbar^n \Delta^{(n),W} + \mathcal{O}(\hbar^{n+1}), \quad (2)$$

which implement the background gauge invariance of the SM. The definition of  $\mathcal{S}$  and  $\mathcal{W}_{(\lambda)}$  is given in [2].

The local breaking terms are denoted by  $\Delta^{(n),S}$  and  $\Delta^{(n),W}$ . Note that the locality is a consequence of the Quantum Action Principle. Here and in the following,  $\Gamma^{(n)}$  denotes the  $n$ -loop order regularized and (minimally) subtracted one-particle-irreducible (1PI) function.  $\Gamma^{(n)}$  includes the renormalization of all subdivergences. The STIs and the WTIs are not able to fix the Green functions completely. Indeed it is possible to add invariant local terms to the action changing the normalization conditions of the Green functions. A complete analysis on the normalization conditions for the SM can, for instance, be found in [7].

Acting on the broken WTIs (2) with the Taylor operator  $(1 - T^\delta)$  one gets

$$(1 - T^\delta)\mathcal{W}_{(\lambda)}(\Gamma^{(n)}) = 0, \quad (3)$$

where  $\delta$  has to be chosen in such a way that  $(1 - T^\delta)\Delta^{(n),S/W} = 0$ . After commuting the Taylor operator  $(1 - T^\delta)$  with  $\mathcal{W}_{(\lambda)}$ , we obtain

$$\mathcal{W}_{(\lambda)}[(1 - T^{\delta'})\Gamma^{(n)}] = [T^\delta\mathcal{W}_{(\lambda)} - \mathcal{W}_{(\lambda)}T^{\delta'}]\Gamma^{(n)} \equiv \hbar^n \Psi^{(n),W}(\lambda), \quad (4)$$

where  $\delta'$  is the naive power-counting degree of  $\Gamma^{(n)}$ . In general, one has  $\delta \geq \delta'$ , hence the commutation of the Taylor operator with  $\mathcal{W}_{(\lambda)}$  leads to over-subtractions of  $\Gamma^{(n)}$  and, thus, to the new breaking terms  $\Psi^{(n),W}(\lambda)$  occurring on the r.h.s. of Eq. (4) (for more details see [2, 3]). The breaking terms  $\Psi^{(n),S}(\lambda)$  for the STIs are defined in the same way. Therefore, the application of the Taylor subtraction on Eqs. (1) and (2) transforms them into

$$\mathcal{S}(\hat{\Gamma}^{(n)}) = \hbar^n \Psi^{(n),S} + \mathcal{O}(\hbar^{n+1}) \quad \text{and} \quad \mathcal{W}_{(\lambda)}(\hat{\Gamma}^{(n)}) = \hbar^n \Psi^{(n),S} + \mathcal{O}(\hbar^{n+1}), \quad (5)$$

where  $\hat{\Gamma}^{(n)} = (1 - T^\delta)\Gamma^{(n)}$ .

The breaking terms  $\Psi^{(n),S}$  and  $\Psi^{(n),W}$  can be expressed in terms of a linear combination of ultra-violet (UV) finite Green functions. Here we assumed that up to the  $(n - 1)$ -loop order the Green functions are already correctly renormalized. The main difference between  $\Psi^{(n),S}$  and  $\Psi^{(n),W}$  is due to the linearity of the corresponding operators  $\mathcal{S}$  and  $\mathcal{W}_{(\lambda)}$ . In the former case one has to consider non-linear terms arising from lower loop orders. On the contrary, the linearity of the WTIs enormously simplifies the evaluation of the breaking terms and of counterterms.

Finally, we introduce

$$\mathbb{I}^{(n)} = \hat{\Gamma}^{(n)} - \Xi^{(n)} = (1 - T^\delta)\Gamma^{(n)} - \Xi^{(n)}, \quad (6)$$

where  $\Xi^{(n)}$  is chosen in such a way that the following identities are fulfilled:

$$\mathcal{S}(\mathbb{I}^{(n)}) = 0, \quad \mathcal{W}_{(\lambda)}(\mathbb{I}^{(n)}) = 0. \quad (7)$$

In general, it is quite simple to compute the counterterm,  $\Gamma^{C.T.} = T^\delta\Gamma^{(n)} + \Xi^{(n)}$ , as it can be expressed in terms of Green functions expanded around zero external momenta.

As already mentioned above, there is still the freedom to add invariant counterterms. In other words, we have the freedom to impose normalization conditions that lead in addition to Eqs. (7) to the following equation being fulfilled:

$$\mathcal{N}_i(\mathbb{I}^{(n)}) = 0, \quad (8)$$

where the index  $i$  runs over all independent parameters of the SM. As the Green function  $\Gamma^{(n)}$  also has to fulfill this condition we have for the counterterm

$$\mathcal{N}_i(T^\delta\Gamma^{(n)} + \Xi^{(n)}) = 0, \quad (9)$$

which is a local equation. This means that, whenever the effort to impose the normalization conditions is done the changes due to the subtraction are only a local changes which can be easily compensated. For clarity let us consider an example: for the condition on the  $W$  boson mass we could choose  $\mathcal{N}_1(\Gamma_{\hat{W}^+\hat{W}^-}^{(n)}) = \Gamma_{\hat{W}^+\hat{W}^-}^{(n),T}(p^*) = 0$  where the superscript  $T$  stands for the transverse part and  $\text{Re}(p^*) = M_W$ . Notice that the imposition of normalization conditions is a very important ingredient for the computation in order to compare with other schemes and in order to simplify the breaking terms themselves.

The procedure described so far is heavily based on the Taylor operator  $T^\delta$ . In the presence of massless particles this may introduce infra-red (IR) divergences. In [4] we presented a modified procedure which resolves this spurious IR problem generally.

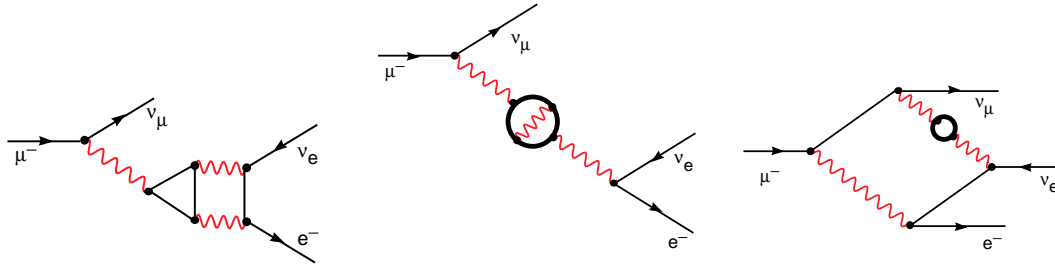


Figure 1: Example of  $O(N_f\alpha^2)$  contributions to the muon decay amplitude with a two-loop three-point, two-loop two-point function and with box contribution

### 3 Muon Decay Amplitude

#### 3.1 General settings

- *Muon decay amplitude*

We want to focus on the  $O(N_f\alpha^2)$  contributions including the two-loop three-point functions  $\Gamma_{\hat{W}_\mu^+ \bar{\nu}_e}(p_\nu, p_e)$  \* with a  $\hat{W}$  and an electron (muon) and electron- (muon-) neutrino. This subgroup of  $O(N_f\alpha^2)$  contributions to the muon decay amplitude is the most delicate one regarding the  $\gamma_5$ -problem. An example is given in Fig. 1.

There are further contributions at the two-loop level such as the diagrams including the two-loop-two-point function  $\Gamma_{\hat{W}_\mu^+ \hat{W}_\nu^-}(p)$  (Fig. 1). These have already been discussed within our approach in [4], but there are no problems with  $\gamma_5$  there. Moreover, there are two-loop box diagrams with a gauge-boson self-energy inside (as shown in the last diagram of Fig. 1).

Thus, let us focus on contributions like the one shown in the first picture of Fig. 1. We have to consider the complete gauge-invariant subset of two-loop contributions to the three-point function  $\Gamma_{\hat{W}_\mu^+ \bar{\nu}_e}(p_\nu, p_e)$ . Actually, there are various types of diagrams shown in Fig. 2. Here we note that only the first two diagrams in Fig. 2 change when switching from a conventional gauge to the 't Hooft-background gauge.

---

\*All momenta are considered as incoming. In the Green functions  $\Gamma_{\phi_1 \dots \phi_n}$  they are assigned to the corresponding fields starting from the right. The momentum of the most left field is determined via momentum conservation.  $\hat{W}$  denotes the background field corresponding to the quantum field  $W$ .

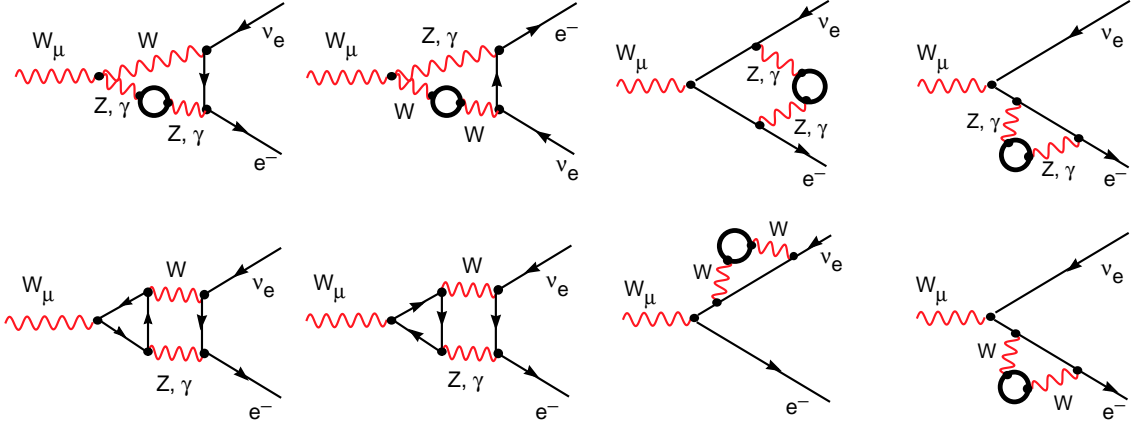


Figure 2: Gauge-invariant subset of  $O(N_f\alpha^2)$  contributions to the muon decay including vertex and external leg corrections.

- *IR problems*

Among the  $O(N_f\alpha^2)$  gauge-invariant subset of diagrams (see Fig. (2)), one has to consider those with a virtual photon. Those diagrams are potentially IR divergent and only the  $O(N_f\alpha^2)$  contributions to the physical amplitude, after the inclusion of the Bremsstrahlung radiation of the external electron and muon, turn out to be finite.

Historically [8], the virtual photon contributions, namely the pure QED corrections, are analysed separately from the electroweak corrections by using a suitable decomposition of massless propagators. In that spirit, the pure QED corrections have been computed in [9, 10, 11] and the remaining complete electroweak corrections are IR finite. In paper [12] the  $O(N_f\alpha^2)$  corrections are computed in the  $\overline{\text{MS}}$  scheme and the massless quark approximation has been used. In [13, 14] the exact fermionic contributions, in on-shell scheme, are taken into account. However, since we are not interested in the explicit evaluation of the muon amplitude, but only to present a procedure to handle the  $\gamma_5$  problem in the present process, we will not disentangle the QED corrections in our considerations.

As a consequence, we have to keep the possible IR divergences under control, namely we have to be sure that all the steps of the computation are IR regulated. The situation is worsened by the fact that, according to our procedure, the Taylor expansion in Eqs. (4) is performed at zero momentum. For those purposes, we propose a BRST invariant IR regularization for the photon within the SM (see Sec. 4). This method regulates both physical and spurious IR divergences simultaneously.

An alternative approach to IR problems is the following: regarding  $\gamma_5$ , the delicate diagram is shown in the first picture of Fig. (1) which belong to the pure vertex corrections  $\Gamma_{\hat{W}_\mu^+\bar{\nu}e}(p_\nu, p_e)$ . Luckily, this vertex Green function is the simplest one – compared to box and external-leg corrections – from the IR perspective. This is because its physical IR singularities are induced only by the on-shell wave-function renormalization.

Therefore, we can also avoid the physical IR problems by choosing an off-shell renormalization procedure. There are two ways of doing this: *i*) either one imposes an on-shell renormalization for the neutrino and, as a consequence of WTIs, an off-shell renormalization prescription of the electron is automatically provided (see next section), *ii*) or one can also choose a MS wave-function renormalization for external fermions which is infrared finite and compatible with the background gauge invariance.

Finally, to handle the spurious IR problems generated by means of the Taylor subtraction, a modification of the procedure is discussed in [4]. Here, the modified breaking terms  $\Psi^{(2),W}$ , occurring in the WTI for the Green function  $\Gamma_{\hat{W}_\mu^+\bar{\nu}e}(p_\nu, p_e)$ , is written explicitly.

- *Kinematic approximations*

The specific kinematic situation allows for some simplifications: in  $\Gamma_{\hat{W}_\mu^+\bar{\nu}e}(p_\nu, p_e)$  the  $W$  is off-shell, while both the electron and the electron-neutrino are on-shell. We can make the approximation  $p_W^2 = 0$  and neglect  $m_{muon}/m_W$ -terms, because the muon is almost at rest. All momenta squared are zero, and hence

$$p_W = p_\nu = p_e = 0. \quad (10)$$

In the following we will derive all symmetry constraints for the general kinematic case and then specify to the zero-momentum setting (10).

- *Subdivergences*

Considering only the  $O(N_f\alpha^2)$  contributions to the two-loop three-point vertex function  $\Gamma_{\hat{W}_\mu^+\bar{\nu}e}^{(2)}(p_\nu, p_e)$ , we have to take into account three kinds of one-loop subdivergences: the three-gauge boson vertices with one background and two quantum fields (they have been largely discussed in [4] within the BFM framework), the quantum gauge boson self-energies (they have been analysed in [2, 3] without and with the BFM; in particular, in [3] the conversion from background field amplitudes to quantum ones is completely exploited) and the one-loop  $\Gamma_{\hat{W}_\mu^+\bar{\nu}e}^{(1)}(p_\nu, p_e)$  amplitude together with their corresponding scalar vertices where the gauge boson is replaced by the Goldstone boson (notice that this amplitude appears also as subdivergence for two-loop three-gauge boson vertices and it is extensively discussed in [4]).

Moreover, the renormalization of one-loop amplitudes can be quite easily handled within different regularization techniques, therefore we can assume, for the time being, that the one-loop Green functions already satisfy the WTIs (or the STIs) and fulfill certain normalization conditions. Nevertheless, to apply our procedure, we have to compute the one-loop counterterms which must be inserted in one-loop graphs. By using the notation of the introduction, these counterterms are given by

$$\begin{aligned}\mathbb{\Pi}^{(n)} &= \hat{\Gamma}^{(n)} - \Xi^{(n)} = \Gamma^{(n)} - [T^\delta \Gamma^{(n)} + \Xi^{(n)}] \\ &= \Gamma_{\text{bare}}^{(n)} - \Gamma_{\text{UV}}^{(n)} - [T^\delta \Gamma_{\text{bare}}^{(n)} + T^\delta \Gamma_{\text{UV}}^{(n)} + \Xi^{(n)}].\end{aligned}\quad (11)$$

In the second line we have introduced the bare Green function  $\Gamma_{\text{bare}}^{(n)}$  in addition. This quantity is defined by  $\Gamma^{(n)} = \Gamma_{\text{bare}}^{(n)} - \Gamma_{\text{UV}}^{(n)}$  where  $\Gamma_{\text{UV}}^{(n)}$  denotes the necessary UV counterterms computed in the specific regularization used in the calculation. Of course, the complete one-loop counterterms, namely  $\mathbb{\Pi}^{(n)} - \Gamma_{\text{bare}}^{(n)}$ , have to be taken into account at the two-loop level.

For instance, in the case of charged gauge-boson self-energies, given  $\mathbb{\Pi}_{W_\mu^+ W_\nu^-}^{(1)}(p)$  (which satisfy the normalization conditions and the corresponding STIs) and given  $\Gamma_{W_\mu^+ W_\nu^-}^{(1)}(p)$ , computed in the same regularization as will be used in the two-loop computation of  $\Gamma_{W_\mu^+ \bar{\nu}_e}^{(2)}(p_\nu, p_e)$ , the counterterms are

$$\begin{aligned}\Gamma_{W_\mu^+ W_\nu^-}^{(1), C.T.}(p) &= T_p^2 \left( \Gamma_{W_\mu^+ W_\nu^-}^{(1)}(p) \right) + \Xi_{W_\mu^+ W_\nu^-}^{(1)}(p), \\ \Xi_{W_\mu^+ W_\nu^-}^{(1)}(p) &= \xi_{W,1}^{(1)} p^2 g_{\mu\nu} + \xi_{W,2}^{(1)} p_\mu p_\nu + \xi_{M_W}^{(1)} g_{\mu\nu},\end{aligned}\quad (12)$$

where

$$\begin{aligned}\xi_{W,1}^{(1)} &= \frac{1}{144} \left( 5 \partial_p^2 \mathbb{\Pi}_{W_\mu^+ W_\nu^-}^{(1)}(p) \Big|_{p=0} - 2 \partial_{p^\mu} \partial_{p^\nu} \mathbb{\Pi}_{W_\mu^+ W_\nu^-}^{(1)}(p) \Big|_{p=0} \right), \\ \xi_{W,2}^{(1)} &= \frac{1}{72} \left( -\partial_p^2 \mathbb{\Pi}_{W_\mu^+ W_\nu^-}^{(1)}(p) \Big|_{p=0} + 4 \partial_{p^\mu} \partial_{p^\nu} \mathbb{\Pi}_{W_\mu^+ W_\nu^-}^{(1)}(p) \Big|_{p=0} \right), \\ \xi_{M_W}^{(1)} &= \frac{1}{4} \mathbb{\Pi}_{W_\mu^+ W_\nu^-}^{(1)}(p) \Big|_{p=0}.\end{aligned}\quad (13)$$

In the same way, all the other possible one-loop divergences can be computed once the renormalized Green functions  $\mathbb{\Pi}^{(1)}$  are known.

In some cases, the BFM does not achieve great advantages (for instance, in the cases of amplitudes with external fermions only) at the practical level and, on the other hand, it could be convenient to use the conventional gauge fixing. However, the Green functions computed with external background fields can be easily related to those with external quantum fields by using the extended versions of the BRST symmetry.

## 3.2 Two-loop vertex function

Working in the framework of the BFM, there is only one WTI for the vertex function  $\Gamma_{\hat{W}_\mu^+ \bar{\nu}_e}^{(2)}(p_\nu, p_e)$  that has to be evaluated at two loops (cf. [2]):

$$i(p_\nu + p_e)_\rho \Gamma_{\hat{W}_\rho^+ \bar{\nu}_e}^{(2)}(p_\nu, p_e) + i M_W \Gamma_{\hat{G}^+ \bar{\nu}_e}^{(2)}(p_\nu, p_e) + \frac{ie}{s_W \sqrt{2}} \left[ \Gamma_{\bar{\nu}_\nu}^{(2)}(-p_\nu) P_L - P_R \Gamma_{\bar{e}e}^{(2)}(p_e) \right] = \Delta_{\lambda^+ \bar{\nu}_e}^{(2),W}(p_\nu, p_e). \quad (14)$$

Here  $\Delta_{\lambda^+ \bar{\nu}_e}^{(2),W}(p_\nu, p_e)$  is a polynomial of the external momenta  $p_\nu$  and  $p_e$  of maximum degree 1. We define the weak mixing angle through the on-shell relation  $c_W = M_W/M_Z$  as we want to maintain the form of the WTIs to be the same to all orders.  $P_{L/R} = (1 \mp \gamma_5)/2$  are the chiral projectors.

The breaking terms in (14) are generated by a non-invariant regularization procedure, for instance by using the 't Hooft-Veltman definition of  $\gamma_5$  [15]. To remove them, according to the procedure described in [2, 4], we apply the Taylor operator  $(1 - T_{p_\nu, p_e}^1)$ , obtaining

$$i(p_\nu + p_e)_\rho \left[ (1 - T_{p_\nu, p_e}^0) \Gamma_{\hat{W}_\rho^+ \bar{\nu}_e}^{(2)}(p_\nu, p_e) \right] + i M_W \left[ (1 - T_{p_\nu, p_e}^0) \Gamma_{\hat{G}^+ \bar{\nu}_e}^{(2)}(p_\nu, p_e) \right] + \frac{ie}{s_W \sqrt{2}} \left\{ \left[ (1 - T_{p_\nu}^1) \Gamma_{\bar{\nu}_\nu}^{(2)}(-p_\nu) \right] P_L - P_R \left[ (1 - T_{p_e}^1) \Gamma_{\bar{e}e}^{(2)}(p_e) \right] \right\} = \Psi_{\lambda^+ \bar{\nu}_e}^{(2),W}(p_\nu, p_e). \quad (15)$$

where

$$\Psi_{\lambda^+ \bar{\nu}_e}^{(2),W}(p_\nu, p_e) = i M_W \left( p_\nu^\rho \partial_{p_\nu^\rho} + p_e^\rho \partial_{p_e^\rho} \right) \Gamma_{\hat{G}^+ \bar{\nu}_e}^{(2)}(p_\nu, p_e) \Big|_{p_\nu = p_e = 0}, \quad (16)$$

are finite and are generated by means of the over-subtraction.

Notice that the computation of  $\Psi_{\lambda^+ \bar{\nu}_e}^{(2),W}$  can be also performed without encountering any UV divergences. For that purpose, it is sufficient to implement the subtraction of UV subdivergences directly in such a way that all the diagrams are always finite. Technically, we suggest the use of Zimmermann's subtraction formula [16]. Since all the integrals involved can be performed analytically,  $\Psi_{\lambda^+ \bar{\nu}_e}^{(2),W}$  can be evaluated exactly. In this way, we use the Dirac algebra in 4 dimensions without any ambiguities.

Notice that the zero momentum subtraction in Eq. (15) removes exactly the contribution that we would like to evaluate to compute the muon decay amplitude in the approximation (10). However, this contribution can be computed as a counterterm. Notice in fact that, the local part of the muon decay amplitude is totally fixed when the normalization conditions for fermion two-point functions and the WTIs are used.

By using the parametrization

$$\begin{aligned}\Xi_{\psi}^{(2)}(p) &= \xi_{2,\psi}^{(2)}(\not{p} - m_\psi) + \xi_\psi^{(2)}m_\psi, \quad \psi = \nu, e \\ \Xi_{\hat{W}_\mu^+\bar{\nu}e}^{(2)}(p_\nu, p_e) &= \xi_{L,\hat{W}^+\bar{\nu}e}^{(2)}\gamma^\mu P_L + \xi_{R,\hat{W}^+\bar{\nu}e}^{(2)}\gamma^\mu P_R,\end{aligned}\quad (17)$$

for two- and three-point functions, and decomposing the breaking terms into scalar functions

$$\Psi_{\lambda^+\bar{\nu}e}^{(2),W}(p_\nu, p_e) = i\left(\psi_1^{(2)}\not{p}_\nu P_L + \psi_2^{(2)}\not{p}_\nu P_R + \psi_3^{(2)}\not{p}_e P_L + \psi_4^{(2)}\not{p}_e P_R\right), \quad (18)$$

we have the solution

$$\begin{aligned}\xi_{R,\hat{W}^+\bar{\nu}e}^{(2)} &= \psi_2^{(2)} = \psi_4^{(2)}, \\ \xi_{L,\hat{W}^+\bar{\nu}e}^{(2)} &= \frac{e}{s_W\sqrt{2}}\xi_{2,\nu}^{(2)} + \psi_1^{(2)}, \\ \xi_{2,e}^{(2)} &= \xi_{2,\nu}^{(2)} + \frac{s_W\sqrt{2}}{e}\left(\psi_1^{(2)} - \psi_3^{(2)}\right),\end{aligned}\quad (19)$$

for the coefficients. Notice that the equality  $\psi_2^{(2)} = \psi_4^{(2)}$  follows from the consistency conditions (see, for example, the discussion in [2]) and it provides a check of the computation of the breaking terms. In addition, from Eqs. (19), it emerges that  $\xi_{2,e}^{(2)} = \xi_{2,\nu}^{(2)}$  in the case of invariant regularization techniques, namely when  $\psi_i^{(2)} = 0$ ,  $\forall i$ . This means that we are not allowed to impose any arbitrary normalization conditions for fermion residues. If the neutrino is renormalized in such a way that its residues is equal to 1, the electron residue will be clearly different from 1. In this way, we have a partial on-shell scheme, we maintain the background gauge symmetry and we can avoid the physical IR divergences for the vertex amplitude.

The final result, namely diagram computation plus counterterms, can be written in the following way

$$\begin{aligned}\Pi_{\hat{W}_\mu^+\bar{\nu}e}^{(2)}(p_\nu, p_e) &= \Gamma_{\hat{W}_\mu^+\bar{\nu}e}^{(2)}(p_\nu, p_e) \\ &\quad - \left[T_{p_\nu, p_e}^0 \Gamma_{\hat{W}_\mu^+\bar{\nu}e}^{(2)}(p_\nu, p_e) + \xi_{L,\hat{W}^+\bar{\nu}e}^{(2)}\gamma^\mu P_L + \xi_{R,\hat{W}^+\bar{\nu}e}^{(2)}\gamma^\mu P_R\right].\end{aligned}\quad (20)$$

The parameters  $\xi_\nu^{(2)}$  and  $\xi_e^{(2)}$  are used to impose mass renormalization conditions on the fermion self-energies.

From this we learn that the symmetric amplitude  $\Pi_{\hat{W}_\mu^+\bar{\nu}e}^{(2)}$  at zero momentum is just given by the universal counterterm:

$$\Pi_{\hat{W}_\mu^+\bar{\nu}e}^{(2)}(p_\nu = 0, p_e = 0) = -\xi_{L,\hat{W}^+\bar{\nu}e}^{(2)}\gamma^\mu P_L - \xi_{R,\hat{W}^+\bar{\nu}e}^{(2)}\gamma^\mu P_R. \quad (21)$$

The proposed procedure allows for an efficient computation of the amplitude  $\Pi_{\hat{W}_\mu^+\bar{\nu}e}^{(2)}$  at two-loop order avoiding the  $\gamma_5$  problem. In the literature, different techniques with different prescription of  $\gamma_5$  have been used to evaluate the Feynman diagrams of  $\Pi_{\hat{W}_\mu^+\bar{\nu}e}^{(2)}$ , however we believe that a rigorous check of these result is desirable.

## 4 Massive U(1) BRST symmetry within the SM

It is a well-known problem that in the computation of Green's function there are IR divergences due to the vanishing photon mass. In this brief section, we will describe how to perform a regularization of the photonic IR divergences in a way that is consistent with the BRST symmetry of the SM and, thus, preserves the unitarity of the model (see also [18]). The choice of such a regulator is motivated essentially by the fact that it regulates both the physical and spurious IR divergences.

We will refer to the Stueckelberg method (see [19, 20] and references therein). This method gives rise to unsolvable renormalization problems in the case of Yang-Mills fields, which only can only be resolved through the Higgs mechanism. However, in the abelian case it provides a manifestly BRST (and the background gauge) invariant model of massive QED.

For pedagogical purposes, we present a short digression regarding the Stueckelberg formalism in QED. The Lagrangian is given by

$$\begin{aligned}\mathcal{L} &= -\frac{1}{4g^2}F_{\mu\nu}^2 + \frac{m^2}{2g^2}(A_\mu - \frac{1}{m}\partial_\mu\varphi)^2 + s(\bar{c}\mathcal{F}) + \mathcal{L}_{\text{matter}}, \\ \mathcal{L}_{\text{matter}} &= \bar{\Psi}(i\not{\partial} - M)\Psi + \bar{\Psi}\gamma^\mu(A_\mu - \frac{1}{m}\partial_\mu\varphi)\Psi,\end{aligned}\tag{22}$$

where  $F_{\mu\nu} = \partial_\mu A_\nu - \partial_\nu A_\mu$ .

The apparent non-renormalizable derivative coupling  $\bar{\Psi}\gamma^\mu\partial_\mu\varphi\Psi$  can be absorbed by a field redefinition

$$\psi = e^{\frac{i}{m}\varphi}\Psi, \quad \mathcal{L}_{\text{matter}} = \bar{\psi}(\gamma^\mu(i\partial_\mu + A_\mu) - M)\psi.\tag{23}$$

Notice that in the non-abelian case a redefinition of fields of type (23) will generate new non-eliminable non-renormalizable terms [20].

The BRST transformations of the fundamental fields are given by

$$\begin{aligned}s\hat{A}_\mu &= 0, & \hat{A}_\mu &= A_\mu - \frac{1}{m}\partial_\mu\varphi, \\ s\varphi &= mc, & sc &= 0, \\ s\bar{c} &= b, & sb &= 0.\end{aligned}\tag{24}$$

Thus, the BRST multiplets consist of two trivial pairs  $(\varphi, c)$ ,  $(\bar{c}, b)$  and one singlet  $\hat{A}_\mu = A_\mu - \frac{1}{m}\partial_\mu\varphi$ . This means that the physical spectrum will be independent of  $(\varphi, c)$  and  $(\bar{c}, b)$ .

In the gauge-fixing-ghost term  $s(\bar{c}\mathcal{F})$ ,  $\mathcal{F}$  is a real bosonic function of all the fields and their derivatives. For example, the 't Hooft-Feynman gauge fixing

$$\mathcal{F} = \frac{1}{g^2}\left(\frac{1}{2}b - \partial^\mu A_\mu - m\varphi\right),\tag{25}$$

leads directly to noninteracting ghosts  $\bar{c}$  and  $c$ . Moreover, the  $\hat{A} - \varphi$  sector does not contain higher derivatives or dipoles. The field strengths  $F_{\mu\nu}$  calculated from  $A$  and from  $\hat{A}$  coincide. The field  $b$  is auxiliary with the algebraic equation of motion  $b = \partial^\mu A_\mu + m\varphi$ . Thus, the  $\mathcal{L}$  defines a massive abelian gauge field coupled to matter fields.

To extend the Stueckelberg formalism to the SM quantized in the background gauge, the scalar field  $\varphi$  transforms under the BRST symmetry<sup>†</sup> and under the background gauge transformations in the following way

$$s\varphi = \mu c, \quad \delta_{(\lambda)}\varphi = \mu\lambda, \quad (26)$$

where  $\lambda$  is the infinitesimal parameter of the background gauge transformations.  $\mu$  is the IR regulator and  $c$  is the  $U(1)$  ghost. The latter can be written in terms of the combination  $c = c_W c_A + s_W c_Z$ , where  $c_A$  and  $c_Z$  are the photon ghost and the ghost associated with the  $Z$  boson, respectively. It follows that a term like

$$\Gamma^{\text{Stu}} = \int d^4x \left( \frac{1}{2} \partial_\mu \varphi \partial^\mu \varphi - \mu \partial_\mu \varphi B^\mu + \frac{\mu^2}{2} B^\mu B_\mu \right), \quad (27)$$

is BRST and background gauge invariant for all the values of the parameter  $\mu$  and the last term provides a mass term for the  $B_\mu$  fields. Other  $\varphi$ -dependent invariant terms can be constructed, however it is easy to show that all of them, but (27), can be reabsorbed by a simple redefinition of the field  $B_\mu$  (cf. [20]). In addition, in order to deal with diagonal two-point functions the ‘t Hooft gauge fixing

$$\begin{aligned} \Gamma^{\text{Stu,g.f.}} &= s \int d^4x \bar{c} (\partial^\mu B_\mu - \rho\mu\varphi + \xi_0 b) \\ &= \int d^4x \left[ b (\partial^\mu B_\mu - \rho\mu\varphi + \xi_0 b) - \bar{c} \partial^2 c + \rho\mu^2 \bar{c} c \right], \end{aligned} \quad (28)$$

is used. Here  $\xi_0$  is the conventional gauge fixing parameter of the  $U(1)$  sector and  $\rho$  is the ‘t Hooft parameter. With this gauge fixing, it is easy to see that the gauge field  $B_\mu$ , the scalar field  $\varphi$  and the ghosts  $\bar{c}, c$  (with masses  $\mu^2, \rho^2\mu^2/\xi_0$  and  $\rho\mu^2$ ) form a quartet which ensures the unitarity of the model. Notice that the BRST variation of  $\varphi$  says that this field corresponds to a would-be-Goldstone boson, and the spontaneous symmetry breaking mechanism – in the abelian case – can be implemented without the Higgs counterpart.

In the SM framework, the field  $B_\mu$  does not coincide with the physical photon field, but the mixing with the third component of  $SU(2)$  gauge boson triplet  $W_\mu^3$  has to be considered. We have to cancel this term by modifying the gauge fixing function  $\mathcal{F}_B$  (cf. [2], Eq. (A.3)) for the abelian field in the following way

$$\mathcal{F}_B = \partial^\mu B_\mu + \rho_0 (\hat{\Phi} + v)^{i t_{ij}^0} (\Phi + v)^j + \frac{\xi_0}{2} b \longrightarrow \mathcal{F}_B - \rho\mu\varphi, \quad (29)$$

---

<sup>†</sup>Notation, definitions, and quantum numbers can be found in [2].

where  $\rho$  is the t'Hooft parameter for the  $\varphi$  field. By eliminating the Lagrange multiplier  $b$ , we have the gauge fixing terms

$$\begin{aligned}
\mathcal{L}^{\text{g.f.}} &= -\frac{1}{2\xi_0} \left[ \partial^\mu B_\mu - \rho\mu\varphi + \rho_0(\hat{\Phi} + v)^i t_{ij}^0 (\Phi + v)^j \right]^2 \\
&= -\frac{1}{2\xi_0} (\partial^\mu B_\mu)^2 - \frac{\rho^2 \mu^2}{2\xi_0} \varphi^2 - \frac{\rho_0 g'^2 v^2}{2\xi_0} G^2 + \frac{\rho\rho_0 \mu v g'}{2\xi_0} \varphi G \\
&\quad + \frac{\rho\mu}{\xi_0} \partial^\mu B_\mu \varphi - \frac{\rho_0 v g'}{\xi_0} \partial^\mu B_\mu G \\
&\quad - \frac{\rho v g'}{2\xi_0} (\partial^\mu B_\mu - \mu\rho\varphi) (H \hat{G} - \hat{H} G) - \frac{\rho^2 g'^2 v^2}{2\xi_0} (H \hat{G} - \hat{H} G)^2, \quad (30)
\end{aligned}$$

where  $g'$  is the  $U(1)$  gauge coupling,  $v$  is the vacuum expectation value,  $G$  and  $H$  are the Goldstone boson and the Higgs field, respectively, while  $\hat{G}$  and  $\hat{H}$  are their background partners. The first line contains the contribution to the quadratic part of the action, this shows that also the masses of the Goldstone boson  $G$  are modified by the introduction of the Stueckelberg field  $\varphi$ . The mixed terms  $\varphi \partial^\mu B_\mu$  and  $G \partial^\mu B_\mu$  are cancelled (in the restricted 't Hooft gauge) by the mixing terms coming from the covariant derivatives of the kinetic terms (i.e. from Eq. (27)). Finally the last terms describe the interactions between  $\varphi$  and the other fields. As can be noticed all the interaction terms depend on the background fields. Therefore, the Stueckelberg  $\varphi$  field can be generated only if the fields  $\hat{G}$  or  $\hat{H}$  appear as external vertices of the amplitude or due to the mixing with the neutral Goldstone boson. This is the only difference between the Stueckelberg formalism and its application to the SM quantized in the background gauge.

## ACKNOWLEDGEMENTS

We thank P. Gambino, W. Hollik, G. Weiglein, A. Ferrogliia and M. Pernici for useful comments and discussions. We also warmly thank our collaborator Matthias Steinhauser. The work of P.A.G. is supported by NSF grants no. PHY-9722083 and PHY-0070787.

## References

- [1] O. Piguet and S.P. Sorella, *Algebraic Renormalization* Lecture Notes in Physics Monographs, Springer-Verlag Berlin Heidelberg, 1995 and references therein.
- [2] P.A. Grassi, T. Hurth, and M. Steinhauser, [hep-ph/9907426] to appear in *Annals of Physics* (NY).

- [3] P.A. Grassi, T. Hurth, and M. Steinhauser, Rep. No. CERN-TH/2001-002, NYU-TH/00/09/9.
- [4] P.A. Grassi, T. Hurth, and M. Steinhauser, [hep-ph/0011067] to appear in JHEP.
- [5] G. 't Hooft, Nucl. Phys. **B33**, 436 (1971); H. Kluberg-Stern and J. Zuber, Phys. Rev. D **12**, 467 (1975); Phys. Rev. D **12**, 482 (1975); L.F. Abbott, Nucl. Phys. **B185**, 189 (1981); S. Ichinose and M. Omote, Nucl. Phys. **B203**, 221 (1982); D.M. Capper and A. MacLean, Nucl. Phys. **B203**, 413 (1982); D.G. Boulware, Phys. Rev. D **12**, 389 (1981).
- [6] A. Denner, G. Weiglein, and S. Dittmaier, Phys. Lett. **B333**, 420 (1994); Nucl. Phys. **B440**, 95 (1995).
- [7] P.A. Grassi, Nucl. Phys. **B462**, 524 (1996); Nucl. Phys. **B537**, 527(1999); Nucl. Phys. **B560**, 499 (1999).
- [8] A. Sirlin, Phys. Rev. D **22**, 971 (1980). A. Sirlin, Phys. Rev. D **29**, 89 (1984).
- [9] T. van Ritbergen and R. G. Stuart, Phys. Rev. Lett. **82**, 488 (1999) [hep-ph/9808283]. T. van Ritbergen and R. G. Stuart, Nucl. Phys. **B564**, 343 (2000) [hep-ph/9904240].
- [10] M. Steinhauser and T. Seidensticker, Phys. Lett. **B467**, 271 (1999) [hep-ph/9909436].
- [11] A. Ferroglia, G. Ossola, and A. Sirlin, Nucl. Phys. **B560**, 23 (1999) [hep-ph/9905442].
- [12] P. Malde and R. G. Stuart, Nucl. Phys. **B552**, 41 (1999) [hep-ph/9903403].
- [13] A. Freitas, W. Hollik, W. Walter, and G. Weiglein, Phys. Lett. **B495**, 338 (2000) [hep-ph/0007091].
- [14] A. Freitas, S. Heinemeyer, W. Hollik, W. Walter, and G. Weiglein, Nucl. Phys. Proc. Suppl. **89**, 82 (2000) [hep-ph/0007129].
- [15] G. 't Hooft and M. Veltman, Nucl. Phys. **B44**, 189 (1972); P. Breitenlohner and D. Maison, Comm. Math. Phys. **52**, 11, 39, 55 (1977).
- [16] W. Zimmermann, *Local Operator Products and Renormalization in Quantum Field Theory* in 1970 Brandeis University Summer Institute Lectures, Cambridge, Mass. M.I.T. Press.

- [17] C. Becchi, A. Rouet, and R. Stora, *Comm. Math. Phys.* **42**, 127(1975); *Ann. of Phys. (NY)* **98**, 287(1976); I.V. Tyutin, Lebedev Institute preprint N39 (1975); see also C. Becchi, *Lectures on Renormalization of Gauge Theories* in Relativity, group and topology II, Les Houches 1983.
- [18] P.A. Grassi, Ph. D. Thesis, University of Milano, Italy, 1997.
- [19] E.C.G. Stueckelberg, *Helv. Phys. Acta* **30**, 209 (1957).
- [20] N. Dragon, T. Hurth, and P. van Nieuwenhuizen, *Nucl. Phys. Proc. Suppl.* **B56**, 318 (1997) [hep-th/9703017]; T. Hurth, *Helv. Phys. Acta* **70**, 406 (1997).

May 2001  
hep-ph/0106020

## Electroweak radiative corrections: Towards a full two-loop analysis

ADRIAN GHINCULOV<sup>a\*</sup> AND YORK-PENG YAO<sup>b†</sup>

<sup>a</sup>*Department of Physics and Astronomy, UCLA,  
Los Angeles, California 90095-1547, USA*

<sup>b</sup>*Randall Laboratory of Physics, University of Michigan,  
Ann Arbor, Michigan 48109-1120, USA*

In calculating electroweak radiative corrections at two-loop level, one encounters Feynman graphs with several different masses on the internal propagators and on the external legs, which lead to complicated scalar functions. We describe a general analytic-numerical reduction scheme for evaluating any two-loop diagrams with general kinematics and general renormalizable interactions, whereby ten basic functions form a complete set after tensor reduction. We illustrate this scheme by applying it to two- and three-point functions. We discuss the treatment of infrared singularities within this numerical approach.

Presented at the

5th International Symposium on Radiative Corrections  
(RADCOR-2000)

Carmel CA, USA, 11–15 September, 2000

---

\*Work supported by the US Department of Energy.

†Work supported by the US Department of Energy.

Because of the level of experimental precision attained in measuring the electroweak parameters at LEP, SLC, and Tevatron, a full two-loop analysis is desirable. This will be even more necessary in view of the precision envisioned at future colliders such as the LHC, NLC, and the GigaZ.

While several two-loop quantities are already included in standard electroweak fitting programs such as ZFITTER [1], they are often obtained within certain approximations where one can neglect certain masses or can perform a mass expansion of Feynman graphs. These approximation techniques, while ingenious, were used because the exact Feynman integrals typically lead to complicated scalar functions which often cannot be evaluated analytically, in a closed form, in terms of usual special functions. During the past decade, the existing work on massless [2] and massive [3]–[11] two-loop graphs made it clear that for the general mass case, a certain amount of numerical work is unavoidable.

Here we discuss the status of a hybrid, analytical-numerical approach to two-loop radiative corrections with arbitrary masses. The aim is to treat any two-loop graph, of any topology, by using the same algorithm, so that the general recipe can be encoded in a computer program. Such an approach was developed in ref. [5], and was successfully applied to several physical processes [6]–[8].

At the center of this approach is the introduction of a set of ten basic functions,  $h_1$ – $h_{10}$ , defined by the following one-dimensional integral representations:

$$\begin{aligned}
h_1(m_1, m_2, m_3; k^2) &= \int_0^1 dx \tilde{g}(x) \\
h_2(m_1, m_2, m_3; k^2) &= \int_0^1 dx [\tilde{g}(x) + \tilde{f}_1(x)] \\
h_3(m_1, m_2, m_3; k^2) &= \int_0^1 dx [\tilde{g}(x) + \tilde{f}_1(x)] (1-x) \\
h_4(m_1, m_2, m_3; k^2) &= \int_0^1 dx [\tilde{g}(x) + \tilde{f}_1(x) + \tilde{f}_2(x)] \\
h_5(m_1, m_2, m_3; k^2) &= \int_0^1 dx [\tilde{g}(x) + \tilde{f}_1(x) + \tilde{f}_2(x)] (1-x) \\
h_6(m_1, m_2, m_3; k^2) &= \int_0^1 dx [\tilde{g}(x) + \tilde{f}_1(x) + \tilde{f}_2(x)] (1-x)^2 \\
h_7(m_1, m_2, m_3; k^2) &= \int_0^1 dx [\tilde{g}(x) + \tilde{f}_1(x) + \tilde{f}_2(x) + \tilde{f}_3(x)] \\
h_8(m_1, m_2, m_3; k^2) &= \int_0^1 dx [\tilde{g}(x) + \tilde{f}_1(x) + \tilde{f}_2(x) + \tilde{f}_3(x)] (1-x) \\
h_9(m_1, m_2, m_3; k^2) &= \int_0^1 dx [\tilde{g}(x) + \tilde{f}_1(x) + \tilde{f}_2(x) + \tilde{f}_3(x)] (1-x)^2 \\
h_{10}(m_1, m_2, m_3; k^2) &= \int_0^1 dx [\tilde{g}(x) + \tilde{f}_1(x) + \tilde{f}_2(x) + \tilde{f}_3(x)] (1-x)^3, \quad (1)
\end{aligned}$$

where:

$$\begin{aligned}
\tilde{g}(m_1, m_2, m_3; k^2; x) &= Sp\left(\frac{1}{1-y_1}\right) + Sp\left(\frac{1}{1-y_2}\right) + y_1 \log \frac{y_1}{y_1-1} + y_2 \log \frac{y_2}{y_2-1} \\
\tilde{f}_1(m_1, m_2, m_3; k^2; x) &= \frac{1}{2} \left[ -\frac{1-\mu^2}{\kappa^2} + y_1^2 \log \frac{y_1}{y_1-1} + y_2^2 \log \frac{y_2}{y_2-1} \right] \\
\tilde{f}_2(m_1, m_2, m_3; k^2; x) &= \frac{1}{3} \left[ -\frac{2}{\kappa^2} - \frac{1-\mu^2}{2\kappa^2} - \left(\frac{1-\mu^2}{\kappa^2}\right)^2 \right. \\
&\quad \left. + y_1^3 \log \frac{y_1}{y_1-1} + y_2^3 \log \frac{y_2}{y_2-1} \right] \\
\tilde{f}_3(m_1, m_2, m_3; k^2; x) &= \frac{1}{4} \left[ -\frac{4}{\kappa^2} - \left(\frac{1}{3} + \frac{3}{\kappa^2}\right) \left(\frac{1-\mu^2}{\kappa^2}\right) - \frac{1}{2} \left(\frac{1-\mu^2}{\kappa^2}\right)^2 - \left(\frac{1-\mu^2}{\kappa^2}\right)^3 \right. \\
&\quad \left. + y_1^4 \log \frac{y_1}{y_1-1} + y_2^4 \log \frac{y_2}{y_2-1} \right] . \quad (2)
\end{aligned}$$

Here we use the following notations:

$$\begin{aligned}
y_{1,2} &= \frac{1 + \kappa^2 - \mu^2 \pm \sqrt{\Delta}}{2\kappa^2} \\
\Delta &= (1 + \kappa^2 - \mu^2)^2 + 4\kappa^2\mu^2 - 4i\kappa^2\eta , \quad (3)
\end{aligned}$$

and

$$\begin{aligned}
\mu^2 &= \frac{ax + b(1-x)}{x(1-x)} \\
a &= \frac{m_2^2}{m_1^2}, \quad b = \frac{m_3^2}{m_1^2}, \quad \kappa^2 = \frac{k^2}{m_1^2} . \quad (4)
\end{aligned}$$

The evaluation of these ten functions is best done by numerical integration. By using an adaptative deterministic numerical integration algorithm, these one-dimensional integrals can be calculated fast and very precisely. By numerical integration, we plot these ten basic functions in figure 1 for a range of their kinematic variables.

Within the method we discuss here, any two-loop diagram with arbitrary masses is first reduced to multi-dimensional scalar integrals involving these ten basic functions  $h_i$ . In ref. [5] we have shown that this can always be done for any two-loop diagrams occuring in renormalizable theories. We note in passing that for the case of non-renormalizable theories this set of ten functions  $h_i$  in general needs to be extended to include additional functions.

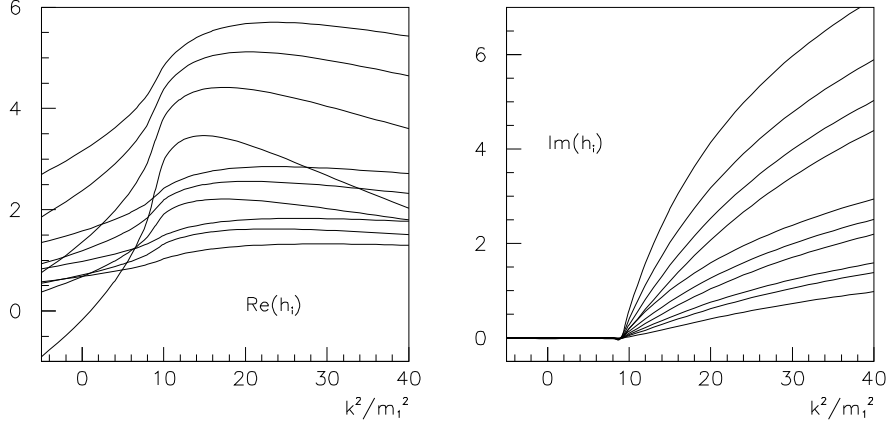


Figure 1: Plots of the ten basic functions  $h_i(m_1^2, m_2^2, m_3^2; -k^2)$  as a function of the external momentum variable  $k^2$ . The plots given here are for  $m_1^2 = m_2^2 = m_3^2 = 1$ .

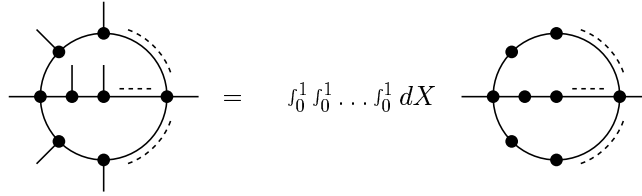


Figure 2: Expressing generic massive two-loop Feynman diagrams as integrals over sunset-type functions.

This reduction procedure starts by introducing Feynman parameters in the original Feynman graph in order to relate the integral to sunset-type integrals. This is illustrated in figure 2.

At this point, the Feynman graph is written as a multi-dimensional integral over tensor integrals of the following type:

$$\int d^n p d^n q \frac{p^{\mu_1} \dots p^{\mu_i} q^{\mu_{i+1}} \dots q^{\mu_j}}{[(p+k)^2 + m_1^2]^{\alpha_1} (q^2 + m_2^2)^{\alpha_2} (r^2 + m_3^2)^{\alpha_3}} \quad (5)$$

In the following step, these tensor integrals are decomposed into scalar integrals, whereby the Lorentz structure is constructed from the vector  $k^\mu$  and the metric tensor  $g^{\mu\nu}$ . This can be carried out systematically by decomposing the loop momenta  $p$  and  $q$  into components parallel and orthogonal to  $k^\mu$ . For instance, the decomposition of all tensor integrals up to rank three is the following:

$$\begin{aligned}
\frac{1}{[211]} &= {}_1A_1, & \frac{p^\mu}{[211]} &= k^\mu {}_2A_1, & \frac{q^\mu}{[211]} &= k^\mu {}_3A_1 \\
\frac{p^\mu p^\nu}{[211]} &= \tau^{\mu\nu} {}_4A_1 + g^{\mu\nu} {}_4A_2, & \frac{p^\mu q^\nu}{[211]} &= \tau^{\mu\nu} {}_5A_1 + g^{\mu\nu} {}_5A_2, & \frac{q^\mu q^\nu}{[211]} &= \tau^{\mu\nu} {}_6A_1 + g^{\mu\nu} {}_6A_2 \\
\frac{p^\mu p^\nu p^\lambda}{[211]} &= (\tau^{\mu\nu} k^\lambda + \tau^{\mu\lambda} k^\nu + \tau^{\nu\lambda} k^\mu) {}_7A_1 + (g^{\mu\nu} k^\lambda + g^{\mu\lambda} k^\nu + g^{\nu\lambda} k^\mu) {}_7A_2 \\
\frac{q^\mu p^\nu p^\lambda}{[211]} &= (\tau^{\mu\nu} k^\lambda + \tau^{\mu\lambda} k^\nu + \tau^{\nu\lambda} k^\mu) {}_8A_1 + (g^{\mu\nu} k^\lambda + g^{\mu\lambda} k^\nu + g^{\nu\lambda} k^\mu) {}_8A_2 \\
\frac{p^\mu q^\nu q^\lambda}{[211]} &= (\tau^{\mu\nu} k^\lambda + \tau^{\mu\lambda} k^\nu + \tau^{\nu\lambda} k^\mu) {}_9A_1 + (g^{\mu\nu} k^\lambda + g^{\mu\lambda} k^\nu + g^{\nu\lambda} k^\mu) {}_9A_2 \\
&\quad + (g^{\mu\nu} k^\lambda + g^{\mu\lambda} k^\nu - 2g^{\nu\lambda} k^\mu) {}_9A_3 \\
\frac{q^\mu q^\nu q^\lambda}{[211]} &= (\tau^{\mu\nu} k^\lambda + \tau^{\mu\lambda} k^\nu + \tau^{\nu\lambda} k^\mu) {}_{10}A_1 + (g^{\mu\nu} k^\lambda + g^{\mu\lambda} k^\nu + g^{\nu\lambda} k^\mu) {}_{10}A_2
\end{aligned} \tag{6}$$

In the formulae above, a loop integration  $\int d^n p d^n q$  is understood, and we used the following notations:

$$[211] = [(p+k)^2 + m_1^2]^2 (q^2 + m_2^2) (r^2 + m_3^2), \quad \tau^{\mu\nu} = g^{\mu\nu} - \frac{k^\mu k^\nu}{k^2} \tag{7}$$

In ref. [5] we have shown that all the scalar coefficients  ${}_iA_j$  involved in this tensor decomposition are directly expressible in terms of the ten basic functions  $h_i$ , up to trivial one-loop tadpole integrals. In all the formulae above, we have considered only integrals with a special combination of propagator powers, namely [211] of eq. 6. Where integrals with higher powers are needed, they can be obtained directly by mass differentiation. The only two-loop combination with lower power, [111], can be obtained from [211] by a recursion formula obtained by partial integration [5].

After performing these steps, the Feynman graph is decomposed into scalar integrals expressed essentially as multiple integrals over  $h_i$  functions, plus trivial one-loop tadpole-type contributions. All necessary formulae to perform this reduction are given in ref. [5]. They were encoded into computer algebra programs for automatizing the reduction.

Once this standard integral representation is obtained for all Feynman graphs involved in a physical process, the final step consists in a numerical multi-dimensional integration of these expressions. The numerical integration uses an adaptative deterministic algorithm, similar to the numerical integration for the  $h_i$  functions. This ensures an efficient and precise evaluation of the integrals.

Several physical calculations have been performed so far by using this method. As a two-point example to test the reduction algorithm and the reliability of the numerical integration, in figure 3 we show the mixed electroweak-QCD Feynman

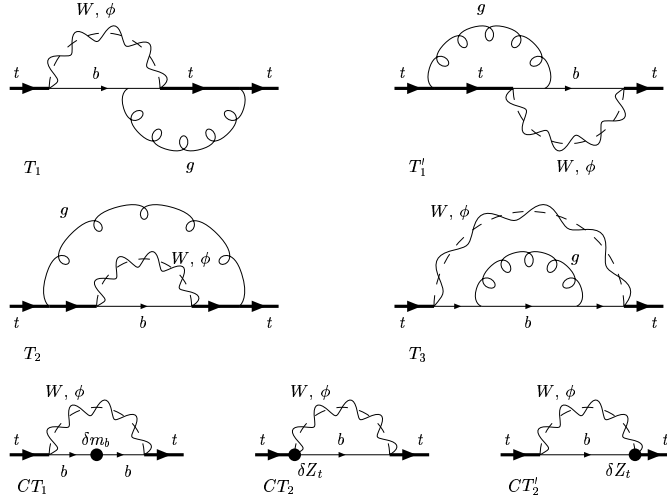


Figure 3: The two-loop Feynman graphs which contribute to the  $b$ -mass dependent correction of  $\mathcal{O}(\alpha_s g^2)$  to the top self-energy. Only the counterterm diagrams are shown which are needed for subtracting the infinities of the imaginary part of the self-energy, which gives the  $\mathcal{O}(\alpha_s)$  correction to the  $t \rightarrow W + b$  decay.

$m_t$ [GeV]	160	165	170	175	180
$\Gamma_t^{tree}$ [GeV]	1.127	1.260	1.402	1.553	1.712
$\delta\Gamma_t^{1-loop}$ [GeV]	-.092	-.104	-.117	-.132	-.149

Table 1: The  $\mathcal{O}(\alpha_s)$  correction to the top decay  $t \rightarrow W + b$  as obtained from the imaginary part of the two-loop top self-energy of figure 1, integrated numerically. We took  $G_F = 1.16637 \cdot 10^{-5} \text{ GeV}^{-2}$ ,  $m_W = 80.41 \text{ GeV}$ ,  $m_b = 4.7 \text{ GeV}$ , and  $\alpha_s(m_t) = .108$ .

graphs which contribute to the top quark self-energy at two-loop. By calculating the self-energy function  $\Sigma(p \cdot \gamma) = \Sigma_1(p \cdot \gamma) + \gamma_5 \cdot \Sigma_{\gamma_5}(p \cdot \gamma)$  at two-loop, from its imaginary part one can extract the top decay width up to  $\mathcal{O}(\alpha_s)$ , as  $\Gamma_t = 2 \cdot \text{Im}\Sigma_1(p \cdot \gamma = m_t)$ . Since this correction is known in an analytic form, this provides a good check on our two-loop algorithm. The results for the correction to the width, obtained from the imaginary part of the two-loop self-energy, are given in table 1. They agree with the existing analytic results.

As a three-point example, in figure 4 we show the diagrams which contribute to the top-dependent decay process  $Z \rightarrow b\bar{b}$ .

A point which deserves special attention in this case is the presence of IR divergences. Because the general formulae of the  $h_i$  functions are derived for general, finite masses, IR divergences in our method are not automatically extracted as poles in the space-time regulator, as is customary in QCD calculations. IR divergences

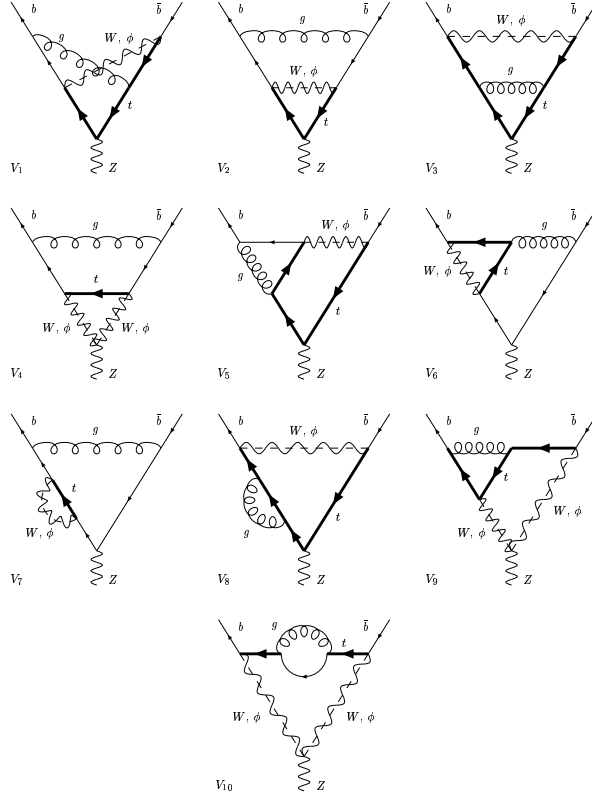


Figure 4: Two-loop three-point diagrams contributing to  $Z \rightarrow b\bar{b}$  at  $\mathcal{O}(\alpha_s g^2)$ .

in our approach usually appear as end-point singularities in the Feynman parameter integration over  $h_i$  functions, and therefore require a special treatment.

For both cases at hand – the top quark self-energy and the  $Z \rightarrow b\bar{b}$  decay – one possible approach is to use a mass regulator for the gluon. While in general this is not possible for non-abelian theories because it does not preserve the Slavnov-Taylor identities, in the particular case of these mixed electroweak-QCD corrections this is a correct procedure because at this order the IR structure is the same as in the abelian case.

Another approach is to extract the IR structure of the graphs analytically before numerical integration. This can be done in the form of one-loop integrals which can be handled separately in an analytical way, by usual dimensional regularization. This is illustrated in fig. 5. Once the IR divergences are extracted in the form of one-loop integrals, the two-loop integration can be carried out numerically.

We give in table 2 numerical results for all two-loop Feynman graphs involved in this process. The numerical results are after the extraction of the UV poles. The IR singularities are subtracted as shown in figure 5. The numerical integration accuracy

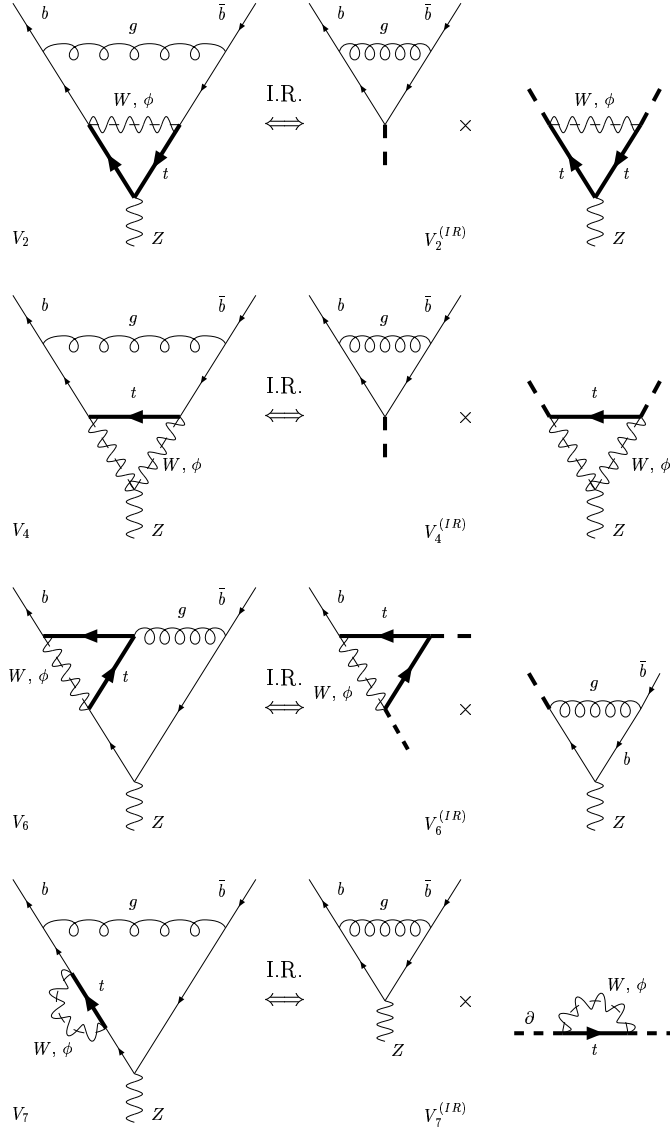


Figure 5: *Extracting the infrared divergent pieces of the two-loop diagrams analytically. The infrared divergency of the two-loop diagram is the same as the infrared divergency of the product of the two one-loop diagrams obtained by “freezing” the common line in the loop momenta integration.*

diagram	$m_t = 165 \text{ GeV}$	$m_t = 175 \text{ GeV}$	$m_t = 185 \text{ GeV}$
$V_1$	$-1.009 \cdot 10^{-3}$	$-7.187 \cdot 10^{-4}$	$-4.057 \cdot 10^{-4}$
$V_2 - V_2^{(IR)}$	$(-2.873 + i2.122) \cdot 10^{-3}$	$(-2.490 + i1.147) \cdot 10^{-3}$	$(-2.087 + i.09274) \cdot 10^{-3}$
$V_3$	$1.545 \cdot 10^{-3}$	$2.255 \cdot 10^{-3}$	$3.034 \cdot 10^{-3}$
$V_4 - V_4^{(IR)}$	$(1.215 - i2.481) \cdot 10^{-2}$	$(1.242 - i2.570) \cdot 10^{-2}$	$(1.266 - i2.660) \cdot 10^{-2}$
$V_5$	$2.107 \cdot 10^{-2}$	$2.469 \cdot 10^{-2}$	$2.861 \cdot 10^{-2}$
$V_6 - V_6^{(IR)}$	$(3.089 - i4.257) \cdot 10^{-2}$	$(3.500 - i4.824) \cdot 10^{-2}$	$(3.950 - i5.445) \cdot 10^{-2}$
$V_7 - V_7^{(IR)}$	$(-.7778 + i1.281) \cdot 10^{-2}$	$(-.8001 + i1.349) \cdot 10^{-2}$	$(-.8232 + i1.420) \cdot 10^{-2}$
$V_8$	$-1.059 \cdot 10^{-3}$	$-1.474 \cdot 10^{-3}$	$-1.942 \cdot 10^{-3}$
$V_9$	$6.289 \cdot 10^{-2}$	$6.703 \cdot 10^{-2}$	$7.143 \cdot 10^{-2}$
$V_{10}$	$-1.402 \cdot 10^{-2}$	$-1.389 \cdot 10^{-2}$	$-1.380 \cdot 10^{-2}$

Table 2: Numerical values for the two-loop diagrams shown in figure 4.  $V_1$ - $V_{10}$  are the sums of the corresponding  $W$  and  $\phi$  exchange graphs. An overall color and coupling constant factor of  $i\gamma_\mu(1-\gamma_5)\alpha_s(g^3/12 \cos\theta_W)$  is understood. The UV and IR divergences are removed as discussed in the text.

is  $10^{-3}$ . The evaluation of a total of 78 Feynman graph evaluations with this precision required 100 hours computing time on a 600 MHz Pentium machine.

To conclude, we developed an algorithm for the tensor reduction of massive two-loop diagrams. It applies in principle to any massive two-loop graph, and it can be automatized in the form of a computer algebra program. The tensor decomposition algorithm results in a multi-dimensional integral over a set of ten basic functions  $h_i$ , which are defined in terms of one-dimensional integral representations. We described the numerical methods which we used for carrying out the remaining integrations.

We have shown how these techniques work in the case of two realistic calculations of mixed electroweak-QCD radiative corrections. The first example is the two-loop top quark self-energy from which the  $O(\alpha_s)$  correction to the top quark decay width can be extracted and compared with the analytical result. The second example is a three-point calculation involving all two-loop diagrams which contribute to the top-dependent decay process  $Z \rightarrow b\bar{b}$ . Thus we have shown that the techniques we described can be used in realistic calculations, where several internal mass and external momenta scales are involved.

This approach works for any such combination of kinematic variables, apart from possible infrared complications. In the context of the  $Z \rightarrow b\bar{b}$  example, we discussed the analytical separation of the infrared divergencies. Within our two-loop methods, if a process involves infrared singularities, these have to be dealt with in a special way because the numerical nature of our methods.

## References

- [1] D. Bardin, P. Christova, M. Jack, L. Kalinovskaya, A. Olchevski, S. Riemann, T. Riemann, *Comput. Phys. Commun.* **133** (2001) 229.
- [2] Z. Bern, L. Dixon, A. Ghinculov, *Phys. Rev.* **D63** (2001) 053007; C. Anastasiou, E.W.N. Glover, M.E. Tejeda-Yeomans, C. Oleari, *Nucl. Phys.* **0B601** (2001) 318; *Nucl. Phys.* **0B601** (2001) 341; *hep-ph/0011094*; *hep-ph/0010212*; E.W.N. Glover, C. Oleari, M.E. Tejeda-Yeomans, *hep-ph/0102201*; Z. Bern, L. Dixon, D.A. Kosower, *JHEP* **0001** (2000) 027; J.B. Tausk, *Phys. Lett.* **B469** (1999) 225; C. Anastasiou, T. Gehrmann, C. Oleari, E. Remiddi, J.B. Tausk, *hep-ph/0003261*; *Nucl. Phys.* **B580** (2000) 577; V.A. Smirnov, *Phys. Lett.* **B460** (1999) 397; V.A. Smirnov, O.L. Veretin, *Nucl. Phys.* **B566** (2000) 469; J.A.M. Vermaseren, S.A. Larin, T. van Ritbergen, *Phys. Lett.* **B405** (1997) 327; *Phys. Lett.* **B404** (1997) 153; *Phys. Lett.* **B400** (1997) 379.
- [3] G. Weiglein, R. Scharf, M. Bohm, *Nucl. Phys.* **B416** (1994) 606.
- [4] S. Bauberger and G. Weiglein, *Phys. Lett.* **B419** (1998) 333; *Nucl. Instrum. Meth.* **A389** (1997) 318.
- [5] A. Ghinculov and Y.-P. Yao, *Nucl. Phys.* **B516** (1998) 385; *Phys. Rev.* **D63** (2001) 054510.
- [6] A. Ghinculov and Y.-P. Yao, *Mod. Phys. Lett.* **A15** (2000) 509.
- [7] A. Ghinculov and Y.-P. Yao, *Mod. Phys. Lett.* **A15** (2000) 1967; *Mod. Phys. Lett.* **A15** (2000) 925.
- [8] A. Ghinculov and J.J. van der Bij, *Nucl. Phys.* **B436** (1995) 30; A. Ghinculov, *Phys. Lett.* **B337** (1994) 137; *(E)* **B346** (1995) 426; *Nucl. Phys.* **B455** (1995) 21.
- [9] L. Durand, B.A. Kniehl and K. Riesselmann, *Phys. Rev.* **D51** (1995) 5007; *Phys. Rev. Lett.* **72** (1994) 2534; *(E)* *Phys. Rev. Lett.* **74** (1995) 1699; A. Frink, B.A. Kniehl, D. Kreimer, K. Riesselmann, *Phys. Rev.* **D54** (1996) 4548.
- [10] F.A. Berends, M. Buza, M. Böhm and R. Scharf, *Z. Phys.* **C63** (1994) 227.
- [11] R. Harlander, T. Seidensticker, M. Steinhauser, *Phys. Lett.* **B426** (1998) 125; J. Fleischer, O.V. Tarasov, F. Jegerlehner, P. Raczka, *Phys. Lett.* **B293** (1992) 437; J. Fleischer, F. Jegerlehner, M. Tentyukov, O. Veretin, *Phys. Lett.* **B459** (1999) 625.

# Combinatorics of (perturbative) Quantum Field Theory\*

D. KREIMER<sup>†</sup>  
Lyman Lab., Harvard University

September 2000

## Abstract

We review the structures imposed on perturbative QFT by the fact that its Feynman diagrams provide Hopf and Lie algebras. We emphasize the role which the Hopf algebra plays in renormalization by providing the forest formulas. We exhibit how the associated Lie algebra originates from an operadic operation of graph insertions. Particular emphasis is given to the connection with the Riemann–Hilbert problem. Finally, we outline how these structures relate to the numbers which we see in Feynman diagrams.

---

\*hep-th/0010059, MZ-TH/00-42

<sup>†</sup>Heisenberg Fellow at Mainz Univ., D-55099 Mainz, Germany, kreimer@thep.physik.uni-mainz.de

# 1 Introduction

Renormalization (see [1] for a classical textbook treatment) has been settled as a self-consistent approach to the treatment of short-distance singularities in the perturbative expansion of quantum field theories thanks to the work of Bogoliubov, Parasiuk, Hepp, Zimmermann, and followers. Nevertheless, its intricate combinatorics went unrecognized for a long time. In this review we want to describe the results in a recent series of papers devoted to the Hopf algebra structure of quantum field theory (QFT) [2, 3, 4, 5, 6, 7, 8, 9, 10, 11, 12, 13, 14, 15, 16]. These results were obtained during the last three years, starting from first papers on the subject [2, 3, 4] and flourishing in intense collaborations with Alain Connes [5, 6, 7, 8, 9] and David Broadhurst [10, 11, 12].

We will review the results obtained so far in a fairly informative style, emphasizing the underlying ideas and concepts. Technical details and mathematical rigor can be found in the above-cited papers, while it is our present purpose to familiarize the reader with the key ideas. Furthermore, we intend to spell out lines for further investigation, as it more and more becomes clear that this Hopf algebra structure provides a very fine tool for a better understanding of a correct mathematical formulation of QFT as well as for applications in particle and statistical physics.

Nevertheless, we will use one concept for the first time in this paper: we will introduce an operad of Feynman graphs, as it is underlying many of the operations involved in the Hopf and Lie algebras built on Feynman graphs.

## 2 The Hopf algebra structure: trees and graphs

Let us start right away with the consideration of how rooted trees and Feynman graphs are connected in perturbative QFT.

### 2.1 Basic considerations

There are two basic operations on Feynman graphs which govern their combinatorial structure as well as the process of renormalization. The question to what extent they also determine analytic properties of Feynman graphs is one of these future lines of investigations, with first results in [13, 14]. We will comment in some detail on this aspect later on.

These two basic operations are the disentanglement of a graph into subgraphs, and the opposite operation, plugging a subgraph into another one. Let us consider the disentanglement of a graph first.

We consider the following three-loop vertex-correction  $\Gamma$

$$\Gamma = \text{triangle with a loop inside}$$

We regard it as a contribution to the perturbative expansion of  $\phi^3$  theory in six spacetime dimensions, where this theory is renormalizable.<sup>1</sup>  $\Gamma$  contains one interesting subgraph, the one-loop self-energy graph

$$\gamma = \text{---} \bigcirc \text{---} .$$

We are interested in it because it is the only subgraph which provides a divergence, and the whole UV-singular structure comes from this subdivergence and from the overall divergence of  $\Gamma$  itself. Let

$$\Gamma_0 := \Gamma/\gamma = \text{---} \triangleleft \text{---}$$

be the graph where we shrink  $\gamma$  to a point. From the analytic expressions corresponding to  $\Gamma$ , to  $\Gamma_0$  and to  $\gamma$  we can form the analytic expression corresponding to the renormalization of the graph  $\Gamma$ . It is given by

$$\Gamma - R(\Gamma) - R(\gamma)\Gamma_0 + R(R(\gamma)\Gamma_0), \quad (1)$$

where we still abuse, in these introductory remarks, notation by using the same symbol  $\Gamma$  for the graph and the analytic expression corresponding to it. We do so as we want to emphasize for the moment that the crucial step in obtaining this expression is the use of the graph  $\Gamma$  and its disentangled pieces,  $\gamma$  and  $\Gamma_0 = \Gamma/\gamma$ . The analytic expressions will come as characters on these Hopf algebra elements, and we will discuss these characters in detail below. Diagrammatically, the above expression reads

$$\text{---} \triangleleft \text{---} - R(\text{---} \triangleleft \text{---}) - R(\text{---} \bigcirc \text{---}) \text{---} \triangleleft \text{---} + R(R(\text{---} \bigcirc \text{---}) \text{---} \triangleleft \text{---}).$$

The unavoidable arbitrariness in the so-obtained expression lies in the choice of the map  $R$  which we suppose to be such that it does not modify the short-distance singularities (UV divergences) in the analytic expressions corresponding to the graphs. This then renders the above combination of four terms finite. If there were no subgraphs, a simple subtraction  $\Gamma - R(\Gamma)$  would suffice to eliminate the short-distance singularities, but the necessity to obtain local counterterms forces us to first subtract subdivergences, which is achieved by Bogoliubov's famous  $\bar{R}$  operation [1], which delivers here:

$$\Gamma \rightarrow \bar{R}(\Gamma) = \Gamma - R(\gamma)\Gamma_0. \quad (2)$$

---

<sup>1</sup>External lines are amputated, but still drawn, in a convenient abuse of notation. In the massless case considered here no further notation is needed for insertions into propagators. In the general case (massive theories, spin) the external structures defined in [5] are a sufficient tool.

This provides two of the four terms above. Amongst them, these two are free of subdivergences and hence provide only a local overall divergence. The projection of these two terms into the range of  $R$  provides the other two terms, which combine to the counterterm

$$Z_\Gamma = -R(\Gamma) + R(R(\gamma)\Gamma_0) \quad (3)$$

of  $\Gamma$ , and subtracting them delivers the finite result above by the fact that the UV divergences are not changed by the renormalization map  $R$ .<sup>2</sup>

The basic operation here is the disentanglement of the graph  $\Gamma$  into pieces  $\gamma$  and  $\Gamma/\gamma$ , and this very disentanglement gives rise to a Hopf algebra structure, as was first observed in [2]. This Hopf algebra has a role model: the Hopf algebra of rooted trees. We first want to get an idea about this universal Hopf algebra after which all the Hopf algebras of Feynman graphs are modeled.

Consider the two graphs

$$\Gamma_1 = \text{---} \triangleleft \text{---}, \quad \Gamma_2 = \text{---} \triangleleft \text{---}.$$

They have one common property: both of them can be regarded as the graph

$$\Gamma_0 = \Gamma_1/\gamma = \Gamma_2/\gamma = \text{---} \triangleleft \text{---}$$

into which the subgraph

$$\gamma = \text{---} \bigcirc \text{---}$$

is inserted, at two different places though. But as far as their UV-divergent sectors go they both realize a rooted tree of the form given in Fig.(1), in the language of [2] both graphs  $\Gamma_1, \Gamma_2$  correspond to a parenthesized word of the form

$$((\text{---} \bigcirc \text{---}) \triangleleft \text{---}).$$

In [2] such graphs were considered to be equivalent, as the combinatorial process of renormalization produces exactly the same terms for both of them. We will formulate this equivalence in a later section using the language of operads.

The combinatorics of renormalization is essentially governed by this bookkeeping process of the hierarchies of subdivergences, and this bookkeeping is what is delivered by rooted trees. They are just the appropriate tool to store the hierarchy of disjoint and nested subdivergences. Another example given in Fig.(2) might be better suited than any formalism to make this clear.

<sup>2</sup>Locality is connected to the absence of subdivergences: if a graph has a sole overall divergence, UV singularities only appear when all loop momenta tend to infinity jointly. Regarding the analytic expressions corresponding to a graph as a Taylor series in external parameters like masses or momenta, powercounting establishes that only the coefficients of the first few polynomials in these parameters are UV singular. Hence they can be subtracted by a counterterm polynomial in fields and their derivatives. The argument fails as long as one has not eliminated all subdivergences: their presence can force each term in the Taylor series to be divergent.

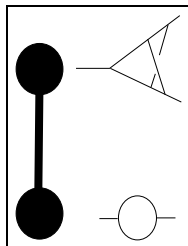


Figure 1: A decorated rooted tree with two vertices, each decorated by a graph without subdivergences (assuming this is an example in  $\phi^3$  theory in six dimensions). The root (by our convention the uppermost vertex) is decorated by the graph  $\Gamma_0 = \Gamma_1/\gamma = \Gamma_2/\gamma$  which we obtain when we shrink the subdivergence  $\gamma$  to a point in either  $\Gamma_1$  or  $\Gamma_2$ . The vertex decorated by the one-loop self-energy  $\gamma$  corresponds to this subdivergence, and the rooted tree stores the information that this divergence is nested in the other graph. The information at which place the subdivergence is to be inserted is not stored in this notation. The hierarchy which determines the recursive mechanism of renormalization is independent of this information. It can easily be restored allowing marked graphs as decorations, or one could directly formulate the Hopf algebra on graphs as we do below.

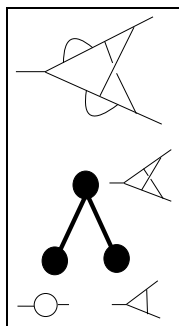


Figure 2: This graph has a hierarchy of divergences given by two disjoint subdivergences, the self-energy  $\gamma$  and a one-loop vertex-correction  $\tilde{\gamma}$ , so that its divergent structure represents the decorated rooted tree indicated. As a parenthesized word, the graph corresponds to  $((\gamma)(\tilde{\gamma})\Gamma_0)$ . There are, by the way,  $5 \times 6 = 30$  graphs which are all equivalent in the sense that they represent this rooted tree or parenthesized word, generated by the 5 internal vertices and 6 internal edges which provide places for insertion in  $\Gamma_0$ .

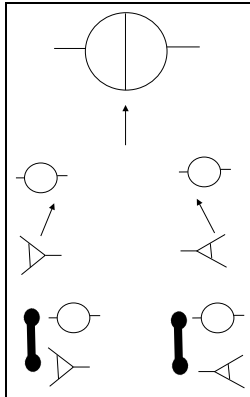


Figure 3: Finding the two ways of getting the overlapping graph  $\Omega$ . There are two vertices in the one-loop self-energy into which the one-loop vertex correction can be inserted. Both result in the same graph. The short-distance singularities in  $\Omega$  arise from two sectors, described by two decorated rooted trees.

At this stage, the reader should wonder what to make out of graphs which have overlapping divergences. This can be best understood when we turn to the other basic operation on graphs: plugging them into each other. On the one hand, for the non-overlapping graphs  $\Gamma_1, \Gamma_2$  above there is a unique way to obtain them from

$$\Gamma_0 = \Gamma_1/\gamma = \Gamma_2/\gamma = \text{---}\triangleleft$$

and the self-energy  $\gamma$ . We plug  $\gamma$  into the vertex-correction at an appropriate internal line to obtain these graphs. This operation will be considered in some more detail in a later section. On the other hand, for a graph which contains overlapping divergences we have typically no unique manner, but several ways instead, how to obtain it. For example,

$$\Omega = \text{---}\bigcirc\text{---}$$

can be obtained in the two ways indicated in Fig.(3).

Each of these ways corresponds to a rooted tree [4], and the sum over all these rooted trees bookkeeps the subdivergent structures of a graph with overlapping divergences correctly. The resolution of overlapping divergences into rooted trees corresponds to the determination of Hepp sectors, and amounts to a resolution of overlapping subsets into nested and disjoint subsets generally [4].<sup>3</sup>

---

<sup>3</sup>The remarks above are specific to theories which have trivalent couplings. In general, the determination of divergent sectors still leads to rooted trees [4]. A concrete example how the Hopf algebra structure appears in  $\phi^4$ -theory can be found in [20]. Also, resolving the

One remark is in order: the very fact that overlapping divergences can be reduced to divergences which have a tree-hierarchy has a deeper reason: the short-distance singularities of QFT result from confronting products of distributions which are well-defined on the configuration space of vertices located at distinct space-time points, but which become ill-defined along diagonals [17, 18]. But then, the various possible ways how an ensemble of distinct points can collapse to (sub-)diagonals is known to be stratified by rooted trees [19], and this is what essentially ensures that the Hopf algebra structure of these trees can reproduce the forest formulas of perturbative QFT. Let us then have a closer look at the connection between graphs and rooted trees.

## 2.2 Sector decomposition and rooted trees

Consider the Feynman graph  $\Omega$  once more, as given in Fig.(4). It corresponds to a contribution to the perturbative expansion in the coupling constant  $g$  of the theory to order  $g^4$ . It has short-distance (UV) singularities which are apparent in the following sectors

$$I_1 := \{1, 2, 3\}, I_2 := \{2, 3, 4\}, I = \{1, 2, 3, 4\},$$

which give the label of the vertices participating in the divergent (sub-)graphs. Note that the sectors overlap:  $I_1 \cap I_2 \neq \emptyset$ . The singularities are stratified so that they can be represented as rooted trees, as described in Fig.(4). In this stratification of sectors each node at the rooted tree corresponds to a Feynman graph which connects the vertices attached to the node by propagators in a manner such that it has no subdivergences. We call such graphs primitive graphs. Each primitive graph is only overall divergent.

Now, where do singularities reside? Typically, if we write down analytic expressions in terms of momentum integrals, UV-divergences appear when the loop momenta involved in a primitive graph tend to infinity jointly, and this can be detected by powercounting over edges and vertices in the graph. On the other hand, we can consider Feynman rules in coordinate space. Then, the UV-singular integrations over momenta become short distance singularities. Again, they creep in from the very fact that closed loops, cycles in the graph, force the integration over the positions of vertices to produce ill-defined products of distributions with coinciding support. Powercounting amounts to a check of the scaling degree of the relevant distributions and ultimately determines the appearance of a short distance singularity at the diagonal under consideration.

The short distance singularities of Feynman graphs then come solely from regions where all vertices are located at coinciding points. One has no problem to define the Feynman integrand in the configuration space of vertices at distinct locations, while a proper extension to diagonals is what is required.

---

overlapping divergences in terms of decorated rooted trees determines the appropriate set of primitive elements of the Hopf algebra, which can for example be systematically achieved by making use of Dyson–Schwinger equations [2, 15], see also [21].



In the above, the two divergent subgraphs are ill-defined along the diagonals  $x_1 = x_2 = x_3$  and  $x_2 = x_3 = x_4$  while the overall divergence corresponds to the main diagonal  $x_1 = x_2 = x_3 = x_4$ .

Due to the Hopf algebra structure of Feynman graphs we can define the renormalization of all such sectors without making recourse to any specific analytic properties of the expressions (Feynman integrals) representing those sectors. The only assumption we make is that in a sufficiently small neighborhood of such an ultralocal region (the neighborhood of a diagonal) we can define the scaling degree, –the powercounting–, in a sensible manner.

Apart from this assumption our approach is purely combinatorial and in particular independent of the geometry of the underlying spacetime manifold.

Fig.(4) also gives a first idea why the Hopf algebra of undecorated rooted trees is the universal object underlying the Hopf algebras of Feynman graphs. The essential combinatorics needed to obtain local counterterms will solely use cuts on these rooted trees which are drawn in bold black lines in the figure, with no further operation on decorations. Different theories just differ by having different types of chords and vertices, while to each chord and vertex in the figure we assign the appropriate scaling degree, the weight with which they contribute to the powercounting.

One further remark is in order: the existence of a purely combinatorial solution coincides with the result of Brunetti and Fredenhagen [22], who showed that the renormalization mechanism is indeed unchanged in the context of curved manifolds in a detailed local analysis using the Epstein–Glaser mechanism. To my mind, quite generally, the Hopf algebra can be used to make sense out of extensions of products of distributions to diagonals of configuration spaces even before we decide by which class of (generalized) functions we want to realize these extensions. While consistency of the Hopf algebra approach to renormalization with the Epstein–Glaser formalism was settled once the Hopf algebra was directly formulated on graphs [4, 8], it was also addressed at a notational level making use of configuration space Feynman graphs in [20]. Still, one should regard the splitting of distributions itself as the first instance where a representation of the Hopf algebra is realized, so that properties like Lorentz covariance appear as properties of the representation alone, maintaining a proper separation of the combinatorics of the Bogoliubov recursion from the analytic properties of the functions defined over the configuration space, enabling also a direct formulation on the level of time-ordered products instead of Feynman graphs.

Once more, that the Hopf algebra structure coming in is the one of rooted trees should be no surprise: limits to diagonals in configuration spaces are stratified by rooted trees [19], and it is the Hopf algebra structure of these rooted trees which describes the combinatorics of renormalization, as we will see. The Hopf algebra of rooted trees will be the role model for all the Hopf algebras of Feynman graphs for a specifically chosen QFT, a classifying space in technical terms (see Theorem 2, section 3 in [5]), while each such chosen QFT probes

$$\boxed{B_-( \text{tree} ) = \text{rootless tree}}$$

Figure 5: The action of  $B_-$  on an undecorated rooted tree.

the short distance singularities according to its Feynman graphs. The resulting iterative procedure gives rise to the Hopf algebra of rooted trees which was first described, in the equivalent language of parenthesized words, in [2] and then in its final notation in [5]. It is now time to describe this Hopf algebra of rooted trees in some detail.

### 2.3 The Hopf algebra of undecorated rooted trees

We follow section II of [5] closely. A *rooted tree*  $t$  is a connected and simply-connected set of oriented edges and vertices such that there is precisely one distinguished vertex which has no incoming edge. This vertex is called the root of  $t$ . Further, every edge connects two vertices and the *fertility*  $f(v)$  of a vertex  $v$  is the number of edges outgoing from  $v$ . The trees being simply-connected, each vertex apart from the root has a single incoming edge (we could attach, if we like, an extra edge to the root as well, for a more common treatment). Each vertex in such a rooted tree corresponds to a divergent sector in a Feynman diagram. The rooted trees store the hierarchy of such sectors. We will always draw the root as the uppermost vertex in figures, and agree that all edges are oriented away from the root.

As in [5], we consider the (commutative) algebra of polynomials over  $\mathbb{Q}$  in rooted trees, where the multiplication  $m(t, t')$  of two rooted trees is their disjoint union, so we can draw them next to each other in arbitrary order, and the unit with respect to this multiplication is the empty set.<sup>4</sup> Note that for any rooted tree  $t$  with root  $r$  which has fertility  $f(r) = n \geq 0$ , we have trees  $t_1, \dots, t_n$  which are the trees attached to  $r$ .

Let  $B_-$  be the operator which removes the root  $r$  from a tree  $t$ , as in Fig.(5):

$$B_- : t \rightarrow B_-(t) = t_1 t_2 \dots t_n. \tag{4}$$

We extend the action of  $B_-$  to a product of rooted trees by a Leibniz rule,  $B_-(XY) = B_-(X)Y + XB_-(Y)$ . We also set  $B_-(t_1) = 1$ ,  $B_+(1) = t_1$ , where  $t_1$  is the rooted tree corresponding to the root alone.

Let  $B_+$  be the operation which maps a monomial of  $n$  rooted trees to a new rooted tree  $t$  which has a root  $r$  with fertility  $n$  which connects to the  $n$  roots

---

<sup>4</sup>We restrict ourselves to one-particle irreducible diagrams for the moment. Then, the disjoint union of trees corresponds to the disjoint union of graphs. One could also set up the Hopf algebra structure such that one-particle reducible graphs correspond to products of rooted trees [2].

$$\boxed{\mathbf{B}_+(\cdot \text{ : } \text{ :}) = \text{ : } \text{ :}}$$

Figure 6: The action of  $B_+$  on a monomial of trees.

of  $t_1, \dots, t_n$ :

$$B_+ : t_1 \dots t_n \rightarrow B_+(t_1 \dots t_n) = t. \quad (5)$$

This is clearly the inverse to the action of  $B_-$  on single rooted trees. One has

$$B_+(B_-(t)) = B_-(B_+(t)) = t \quad (6)$$

for any rooted tree  $t$ . Fig.(6) gives an example.

All the operations described here have a straightforward generalization to decorated rooted trees, in which case the operator  $B_+$  carries a further label to indicate the decoration of the root [5]. We will not use decorated rooted trees later, as we will directly formulate the Hopf algebras of specific QFTs on Feynman graphs. The Hopf algebra of undecorated rooted trees is the universal object [5] for all those Hopf algebras, and hence we describe it here in some detail.

Note that while  $[B_+, B_-](t) = 0$  for any single rooted tree  $t$ , this commutator is non-vanishing on products of trees. Obviously, one always has  $\text{id} = B_- B_+$ , while  $B_+ B_-$  acts trivially only on single rooted trees, not on their product.<sup>5</sup>

We will introduce a Hopf algebra on our rooted trees by using the possibility to cut such trees in pieces. For the reader not familiar with Hopf algebras, let us mention a few very elementary facts first. An algebra  $A$  is essentially specified by a binary operation  $m : A \times A \rightarrow A$  (the product) fulfilling the associativity  $m(m(a, b), c) = m(a, m(b, c))$  so that to each two elements of the algebra we can associate a new element in the algebra, and by providing some number field  $\mathbb{K}$  imbedded in the algebra via  $E : \mathbb{K} \rightarrow A, k \rightarrow k1$ . In a coalgebra we do the opposite, we disentangle each algebra element: each element  $a$  is decomposed by the coproduct  $\Delta : A \rightarrow A \times A$  in a coassociative manner,  $(\Delta \times \text{id})\Delta(a) = (\text{id} \times \Delta)\Delta(a)$ . Further, the unit 1 of the algebra,  $m(1, a) = m(a, 1) = a$ , is dualized to the counit  $\bar{e}$  in the coalgebra,  $(\bar{e} \times \text{id})\Delta(a) = (\text{id} \times \bar{e})\Delta(a) = a$ . If the two operations  $m, \Delta$  are compatible (the coproduct of a product is the product of the coproducts), we have a bialgebra, and if there is a coinverse, the celebrated antipode  $S : H \rightarrow H$ , as well, we have a Hopf algebra. While in the algebra the

<sup>5</sup>This has far reaching consequences and is closely connected to the fact that logarithmic derivatives (with respect to the log of some scale say) of  $Z$ -factors are finite quantities. Indeed,  $Z$ -factors can be regarded as formal series over Feynman diagrams graded by the loop number starting with 1, and their logarithm defines a series in graphs which typically demands that commutators like  $[B_+, B_-](t_1 t_1)$  are a primitive element in the Hopf algebra, and hence provide only a first order pole [16, 12]. This is a first instance of a t'Hooft relation to which we turn later when we review the results of [9].

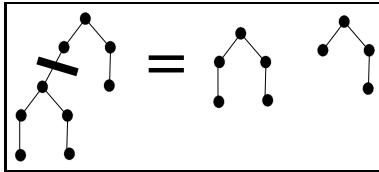


Figure 7: An elementary cut  $c$  splits a rooted tree  $t$  into two components. We remove the chosen edge and get two components. Both are rooted trees in an obvious manner: one contains the vertex which was the old root and the root of the other is provided by the vertex which was at the endpoint (edges are oriented away from the root) of the removed edge.

unit, the inverse and the product are related by  $m(a, a^{-1}) = m(a^{-1}, a) = 1$ , the counit, the coproduct and the coinverse are related by  $m(S \times \text{id})\Delta = E \circ \bar{e}$ . A thorough introduction can be found for example in [23].

To define a coproduct for rooted trees we are hence looking for a map which disentangles rooted trees. We start with the most elementary possibility. An *elementary cut* is a cut of a rooted tree at a single chosen edge, as indicated in Fig.(7). By such a cutting procedure, we will obtain the possibility to define a coproduct, as we can use the resulting pieces on either side of the coproduct. It is this cutting operation which corresponds to the disentanglements of graphs discussed before.

Still before introducing the coproduct we introduce the notion of an *admissible cut*, also called a *simple cut* [5]. It is any assignment of elementary cuts to a rooted tree  $t$  such that any path from any vertex of the tree to the root has at most one elementary cut, as in Fig.(8). An admissible cut  $C$  maps a tree to a monomial in trees. If the cut  $C$  contains  $n$  elementary cuts, it induces a map

$$C : t \rightarrow C(t) = \prod_{i=1}^{n+1} t_{j_i}. \quad (7)$$

Note that precisely one of these trees  $t_{j_i}$  will contain the root of  $t$ . Let us denote this distinguished tree by  $R^C(t)$ . The monomial which is delivered by the  $n - 1$  other factors is denoted by  $P^C(t)$ . In graphs,  $P^C(t)$  corresponds to a set of disjoint subgraphs  $\cup_i \gamma_i$  which we shrink to a point and take out of the initial graph  $\Gamma$  corresponding to  $t$ , while  $R^C(t)$  corresponds to the remaining graph  $\Gamma / (\cup_i \gamma_i)$ . Admissibility means that there are no further disentanglements in the set  $\cup_i \gamma_i$ . Hence, a sum over all such sets provides a sum over all unions of subgraphs, as we will discuss below. Arbitrary non-admissible cuts correspond to the notion of forests in the sense of Zimmermann [2, 5].

Let us now establish the Hopf algebra structure. Following [2, 5] we define the counit and the coproduct. The *counit*  $\bar{e}: H \rightarrow \mathbb{Q}$  is simple:

$$\bar{e}(X) = 0$$

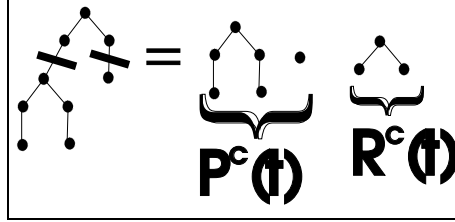


Figure 8: An admissible cut  $C$  acting on a tree  $t$ . It produces a monomial of trees. One of the factors,  $R^C(t)$ , contains the root of  $t$ .

$$\begin{aligned}
 \Delta(\cdot) &= \cdot \otimes 1 + 1 \otimes \cdot \\
 \Delta(\downarrow) &= \downarrow \otimes 1 + 1 \otimes \downarrow + \cdot \otimes \cdot \\
 \Delta(\downarrow \downarrow) &= \downarrow \otimes 1 + 1 \otimes \downarrow \downarrow + \cdot \otimes \downarrow + \downarrow \otimes \cdot \\
 \Delta(\downarrow \downarrow \downarrow) &= \downarrow \otimes 1 + 1 \otimes \downarrow \downarrow \downarrow + 2 \cdot \otimes \downarrow + \cdot \otimes \cdot
 \end{aligned}$$

Figure 9: The coproduct. We work it out for the trees  $t_1, t_2, t_{3_1}, t_{3_2}$ , from top to bottom.

for any  $X \neq 1$ ,

$$\bar{e}(1) = 1.$$

The *coproduct*  $\Delta$  is defined by the equations

$$\begin{aligned}
 \Delta(1) &= 1 \otimes 1, \\
 \Delta(t_1 \dots t_n) &= \Delta(t_1) \dots \Delta(t_n), \\
 \Delta(t) &= t \otimes 1 + (id \otimes B_+)[\Delta(B_-(t))],
 \end{aligned} \tag{8}$$

which defines the coproduct on trees with  $n$  vertices iteratively through the coproduct on trees with a lesser number of vertices.

The coproduct can be written in a non-recursive manner as [2, 5]

$$\Delta(t) = 1 \otimes t + t \otimes 1 + \sum_{\text{adm. cuts } C \text{ of } t} P^C(t) \otimes R^C(t). \tag{9}$$

Up to now we have established a bialgebra structure. It is actually a Hopf algebra. Following [2, 5] we find the antipode  $S$  as

$$S(1) = 1,$$

$$\begin{array}{l}
\mathbf{S}(\bullet) = -\bullet \\
\mathbf{S}(\downarrow) = -\downarrow + \dots \\
\mathbf{S}(\downarrow \downarrow) = -\downarrow \downarrow + 2 \cdot \downarrow - \dots \\
\mathbf{S}(\downarrow \downarrow \downarrow) = -\downarrow \downarrow \downarrow + 2 \cdot \downarrow \downarrow - \dots
\end{array}$$

Figure 10: The antipode. Again we work it out for the trees  $t_1, t_2, t_{3_1}, t_{3_2}$ .

$$\begin{aligned}
S(t_1 \dots t_k) &= S(t_1) \dots S(t_k), \\
S(t) &= -t - \sum_{\text{adm. cuts } C \text{ of } t} S[P^C(t)]R^C(t). \tag{10}
\end{aligned}$$

Fig.(10) gives examples for the antipode.

Let us give yet another formula to write the antipode, which one easily derives using induction on the number of vertices [2, 5]:

$$S(t) = - \sum_{\text{all cuts } C \text{ of } t} (-1)^{n_C} P^C(t)R^C(t), \tag{11}$$

where  $n_C$  is the number of elementary cuts in  $C$ . This time, we have a non-recursive expression, summing over all cuts  $C$ , relaxing the restriction to admissible cuts.

By now we have established a Hopf algebra  $H$  on rooted trees, using the set of rooted trees, the commutative multiplication  $m$  for elements of this set, the unit 1 and counit  $\bar{e}$ , the coproduct  $\Delta$  and antipode  $S$ . Still following [2, 5] we allow to label the vertices of rooted trees by Feynman graphs without subdivergences, in the sense described before. Quite general, if  $Y$  is a set of primitive elements providing labels, we get a similar Hopf algebra  $H(Y)$ . The determination of all primitive graphs which can appear as labels corresponds to a skeleton expansion and is discussed in detail in [4]. Instead of using the language of a decorated Hopf algebra we use directly the corresponding Hopf algebra of graphs below.

Let us also mention again that

$$m[(S \otimes \text{id})\Delta(t)] = E \circ \bar{e}(t) \quad (= 0 \text{ for any non-trivial } t \neq 1). \tag{12}$$

As the divergent sectors in Feynman graphs are stratified by rooted trees, we can use the Hopf algebra structure to describe the disentanglement of graphs into

pieces, and it turns out that this delivers the forest formulas of renormalization theory.

Let us now come back to the graph  $\Omega$  and its representation in Fig.(4). We want to look at the relevant Hopf algebra operations in some detail, which we describe in Fig.(11). The operations described in this figure go through for any QFT whose ultraviolet divergences are local, stratified by rooted trees that is. A renormalizable field theory will only demand a finite number of counterterms in the action, while an effective theory is finite in the number of needed counterterms only for a finite loop order, but the number will actually increase with the loop order. A superrenormalizable theory gives only a truncated representation of rooted trees: higher orders in the perturbative expansion do not deliver new short-distance singularities, and hence the existent divergences are stratified by rooted trees with a restricted number of vertices.

Each short-distance singularity corresponds to a sector which can be described by a rooted tree, which itself notates the hierarchy of singularities. We have a coproduct which describes the job-list [10] of renormalization: we use it to disentangle the singularities located at (sub-)diagonals. The Feynman rules are then providing a character  $\phi : H \rightarrow V$  on this Hopf algebra. They map a Hopf algebra element to an analytic expression, typically evaluating in a suitable ring  $V$  of Feynman integrands or Laurent polynomials in a regularization parameter. These maps being characters, we have

$$\phi(\gamma_1 \gamma_2) = \phi(\gamma_1)\phi(\gamma_2). \quad (13)$$

Then, renormalization comes from the very simple Hopf algebra property Eq.(12), as we now explain. Let us describe carefully how to use the Hopf algebra structure in the example of Fig.(11). The first thing which we have to introduce, together with our Feynman rules, is a map  $R : V \rightarrow V$  which is essentially determined by the choice of a renormalization scheme. The freedom in this choice is essentially what makes up the renormalization group.

The presence of the antipode  $S$  allows to consider, for each  $\phi$ , its inverse character  $\phi^{-1} = \phi \circ S$ . Actually, we have a group structure on characters: to each two characters  $\phi, \psi$  we can assign a new character

$$\phi \star \psi = m_V \circ (\phi \otimes \psi) \circ \Delta,$$

and a unit of the  $\star$ -product is provided as

$$\phi \star \eta = \eta \star \phi = \phi$$

and the inverse is indeed provided by the antipode:

$$\phi^{-1} \star \phi = \phi \star \phi^{-1} = \eta,$$

where  $\eta$  comes from the counit and is uniquely defined as  $\eta = \psi \circ E \circ \bar{e}$  so that  $\eta(1) = 1_V$ ,  $\eta(X) = 0$ ,  $\forall X \neq 1$ , and for any arbitrarily chosen character  $\psi$  (any character fulfills  $\psi(1) = 1_V$ ).

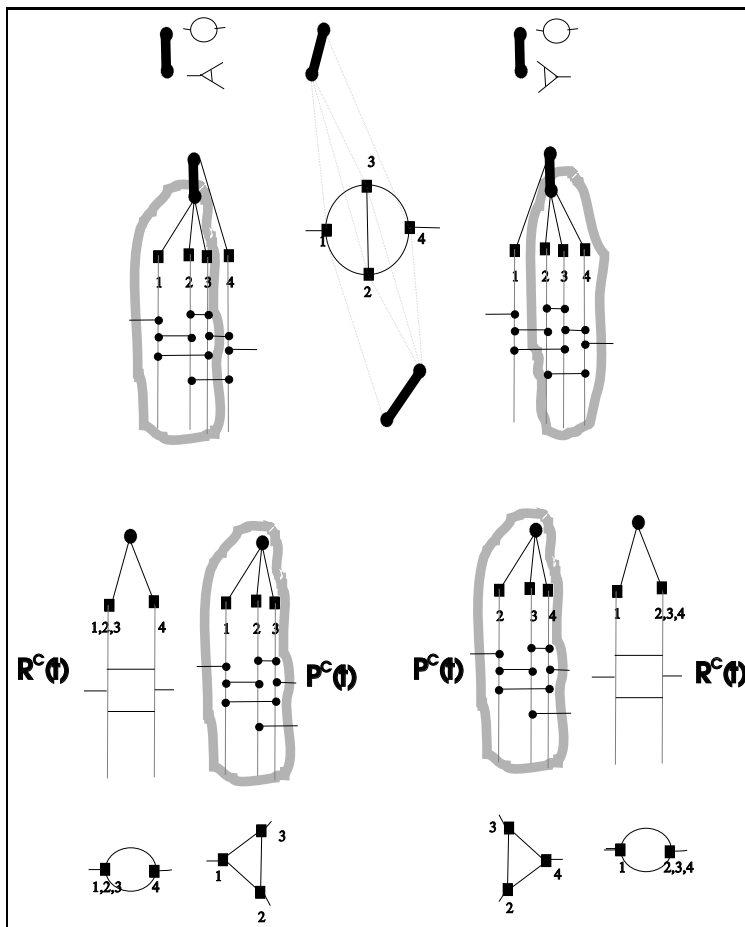


Figure 11: The graph  $\Omega$  gives rise to two rooted trees corresponding to its two (overlapping) divergent sectors. Each of the two rooted trees allows for a single admissible cut. We implement it in each case by the gray curve which encircles the one vertex which constitutes  $P^C(t)$  and the whole chord diagram attached to this subtree. It hence corresponds to a subgraph which is a three-point graph, as three chords are crossed by this gray curve. The cut at the rooted tree then corresponds to shrinking the subgraph to a point, which is a vertex in the remaining graph (a one-loop self-energy). This vertex we have decorated by  $\{2, 3, 4\}$  or  $\{1, 2, 3\}$ . It amounts to a local polynomial insertion in the self-energy. If the vertices so-generated always give rise to polynomial insertions which are part of the action already, we have a renormalizable theory. For a general theory, one will have a variety of different chords represented by different propagators, and a variety of vertices as well. For a renormalizable theory there will be only a finite number of each. It may happen that there are various different vertices into which a graph can shrink, in which case a sum over the corresponding external structures is involved [8].

The next thing to do is to use  $\phi$  and  $R$  to define a further character  $S_R : H \rightarrow V$  by

$$S_R = -R[\phi(t) + \sum S_R(t')\phi(t'')],$$

where we used the notation  $\Delta(t) = t \otimes 1 + 1 \otimes t + \sum t' \otimes t''$ . By construction, if we choose  $R = \text{id}_V$ , the identity map from  $V \rightarrow V$ , we have  $S_{\text{id}_V} = \phi \circ S$ .

Now, consider  $S_R \star \phi$ . We have

$$S_{\text{id}_V} \star \phi = \phi \circ m \circ (S \otimes \text{id}) \circ \Delta = \eta$$

by the Hopf algebra property Eq.(12) above. This guarantees that from regions where  $R$  becomes the identity map  $\text{id}_V : V \rightarrow V$ , we get a vanishing contribution from any non-trivial sector  $t$  realized in a Feynman graph  $\Gamma$ , as  $\eta(t) = 0$ . So if we demand that  $R$  leaves short distance singularities unaltered, so that  $R = \text{id}_V$  for large loop momenta, we automatically have a vanishing contribution of those singularities to  $S_R \star \phi$ .<sup>6</sup>

What we see at work here is a general principle of multiplicative subtraction [5]: while for a primitive Hopf algebra element  $t$ ,  $\Delta(t) = t \otimes 1 + 1 \otimes t$ ,  $S_R \star \phi$  amounts simply to the additive operation

$$\phi(t) - R[\phi(t)],$$

for a general Hopf algebra element the coproduct provides a much more refined multiplicative subtraction mechanism, which can obviously be considered for a wide class of Hopf algebras. This principle can certainly be applied in the future not only in the problem of short distance singularities, but in a much wider class of problems, with asymptotic expansions coming to mind immediately.

Fig.(12) describes how the Hopf algebra is realized on the sectors of the graph  $\Omega$  and how this relates to the Hopf algebra of Feynman graphs to which we now turn.

## 2.4 The Hopf algebra of graphs

As we already have emphasized the Hopf algebra of rooted trees is the role model for the Hopf algebras of Feynman graphs which underly the process of renormalization when formulated perturbatively at the level of Feynman graphs. The following formulas should be of no surprise after our previous discussions.

First of all, we start considering one-particle irreducible graphs as the linear generators of the Hopf algebra, with their disjoint union as product. We then define a Hopf algebra by a coproduct

$$\Delta(\Gamma) = \Gamma \otimes 1 + 1 \otimes \Gamma + \sum_{\gamma \subset \Gamma} \gamma \otimes \Gamma/\gamma, \quad (14)$$

---

<sup>6</sup>That  $R$  leaves short-distance singularities unaltered typically requires that the first few Taylor coefficients in the Feynman integrands, as determined by powercounting, are left unaltered.

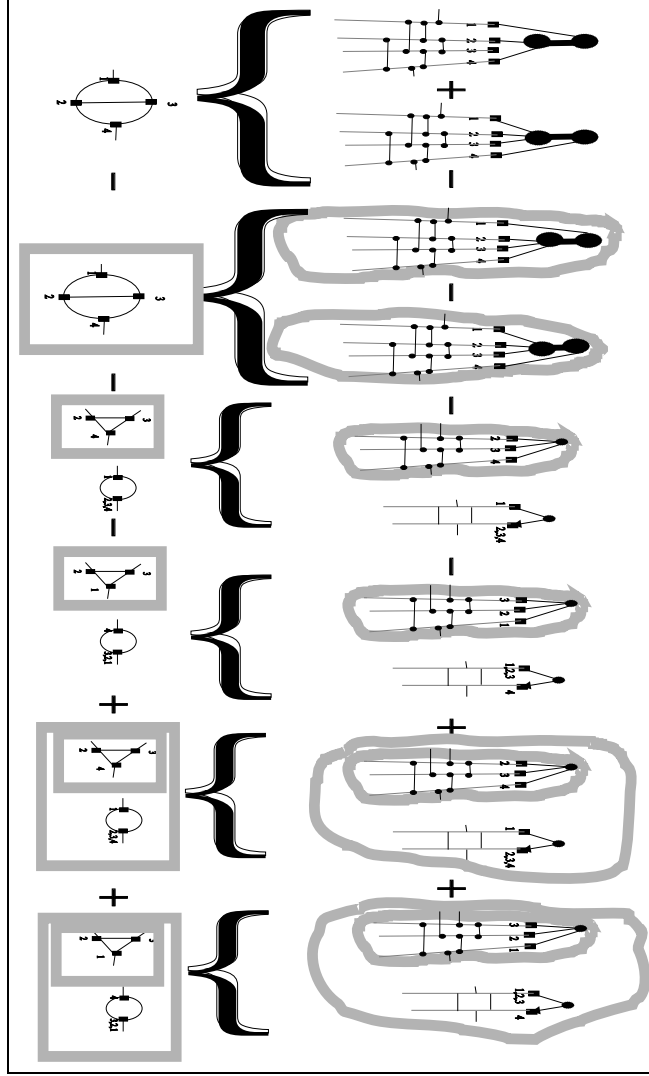


Figure 12: The result of the operation  $S_R \star \phi(\Omega)$  graphically, where an application of the operation  $R$  is indicated by encircling the graph whose corresponding analytic expression is to be mapped to the range of  $R$  by a thick grey line. In the upper row, we see the result in terms of the decorated rooted trees of Fig.(11) while in the second row we see the result directly expressed in terms of Feynman integrals. Again, the map  $\phi$  is not explicitly written out. The grey boxes indicate the full and normal forests of classical renormalization theory [1] and are in one-to-one correspondence with the cuts at the corresponding rooted trees if we incorporate the empty and the full cut in the sum over cuts, so that the two terms  $T \otimes 1 + 1 \otimes T$  which appear in any coproduct  $\Delta(T) = T \otimes 1 + 1 \otimes T + \sum_{adm.C} P^C(T) \otimes R^C(T)$  can be regarded as generated by the full  $(T \otimes 1)$  and the empty cut  $(1 \otimes T)$  [5].

where the sum is over all unions of one-particle irreducible (1PI) superficially divergent proper subgraphs and we extend this definition to products of graphs so that we get a bialgebra [8]. The above sum should, when needed, also run over appropriate external structures to specify the appropriate type of local insertion [8] which appear in local counterterms, which we omitted in the above sum for simplicity.<sup>7</sup>

The counit  $\bar{\epsilon}$  vanishes, as before, on any non-trivial Hopf algebra element. At this stage we have a commutative, but typically not cocommutative bialgebra. It actually is a Hopf algebra as the antipode in such circumstances comes almost for free as

$$S(\Gamma) = -\Gamma - \sum_{\gamma \subset \Gamma} S(\gamma)\Gamma/\gamma. \quad (15)$$

The next thing we need are Feynman rules, which we regard as maps  $\phi : H \rightarrow V$  from the Hopf algebra of graphs  $H$  into an appropriate space  $V$ .

Over the years, physicists have invented many calculational schemes in perturbative quantum field theory, and hence it is of no surprise that there are many choices for this space. For example, if we want to work on the level of Feynman integrands in a BPHZ scheme, we could take as this space a suitable space of Feynman integrands (realized either in momentum space or configuration space, whatever suits). An alternative scheme would be the study of regularized Feynman integrals, for example the use of dimensional regularization would assign to each graph a Laurent-series with poles of finite order in a variable  $\varepsilon$  near  $\varepsilon = 0$ , and we would obtain characters evaluating in this ring. In any case, we will have  $\phi(\Gamma_1\Gamma_2) = \phi(\Gamma_1)\phi(\Gamma_2)$ .

Then, with the calculational scheme chosen and the Feynman rules providing a canonical character  $\phi$ , we will have to make one further choice: a renormalization scheme. This is a map  $R : V \rightarrow V$ , and we demand that it does not modify the UV-singular structure: in BPHZ language, it should not modify the Taylor expansion of the integrand for the first couple of terms divergent by powercounting. In dimensional regularization, we demand that it does not modify the pole terms in  $\varepsilon$ .

Finally, the principle of multiplicative subtraction works as before: we define a further character  $S_R$  which deforms  $\phi \circ S$  slightly and delivers the counterterm for  $\Gamma$ :

$$S_R(\Gamma) = -R[\phi(\Gamma)] - R \left[ \sum_{\gamma \subset \Gamma} S_R(\gamma)\phi(\Gamma/\gamma) \right] \quad (16)$$

which should be compared with the undeformed

$$\phi \circ S = -\phi(\Gamma) - \sum_{\gamma \subset \Gamma} \phi \circ S(\gamma)\phi(\Gamma/\gamma). \quad (17)$$

---

<sup>7</sup>A simple example exhibited in [8] is the self-energy in massive  $\phi^3$  theory in six dimensions. It provides two external structures, corresponding to local insertions of counterterms for the  $m^2\phi^2$  and for the  $(\partial_\mu\phi)^2$  term.

Then, the classical results of renormalization theory follow suit [2, 4, 5]. We obtain the renormalization of  $\Gamma$  by the application of a renormalized character

$$\Gamma \rightarrow S_R \star \phi(\Gamma)$$

and the  $\bar{R}$  operation as

$$\bar{R}(\Gamma) = \phi(\Gamma) + \sum_{\gamma \subset \Gamma} S_R(\gamma) \phi(\Gamma/\gamma), \quad (18)$$

so that we have

$$S_R \star \phi(\Gamma) = \bar{R}(\Gamma) + S_R(\Gamma). \quad (19)$$

In the above, we have given all formulas in their recursive form. Zimmermann's original forest formula solving this recursion is obtained when we trace our considerations back to the fact that the coproduct of rooted trees can be written in non-recursive form, and similarly the antipode. It is not difficult to see that the sum over all cuts corresponds to a sum over all forests, and the notion of full and normal forests of Zimmermann [1] gives rise to appropriate sums over cuts [2, 5], making use of the graphical implementation of cuts as for example in Fig.(12).

### 3 Rescalings and renormalization schemes

Let us come back to unrenormalized Feynman graphs, and their evaluation by some chosen character  $\phi$ , and let us also choose a renormalization scheme  $R$ . The group structure of such characters on the Hopf algebra can be used in an obvious manner to describe the change of renormalization schemes. This has very much the structure of a generalization of Chen's Lemma [3].

#### 3.1 Chen's Lemma

Consider  $S_R \star \phi$ . Let us change the renormalization scheme from  $R$  to  $R'$ . How is the renormalized character  $S_{R'} \star \phi$  related to the renormalized character  $S_R \star \phi$ ? The answer lies in the group structure of characters:

$$S_{R'} \star \phi = [S_{R'} \star S_R \circ S] \star [S_R \star \phi]. \quad (20)$$

We inserted a unit  $\eta$  with respect to the  $\star$ -product in form of  $\eta = S_R \circ S \star S_R \equiv S_R^{-1} \star S_R$ , and can now read the renormalization, switching between the two renormalization schemes, as composition with the renormalized character  $S_{R'} \star S_R^{-1}$ .<sup>8</sup>

---

<sup>8</sup> $S_{R'} \star S_R \circ S$  is a renormalized character indeed: if  $R, R'$  are both self-maps of  $V$  which do not alter the short-distance singularities as discussed before, then in the ratio  $S_{R'} \star S_R \circ S$  those singularities drop out.

Similar considerations apply to a change of scales which determine a character [3]. If  $\rho$  is a dimensional parameter which appears in a character  $\phi = \phi(\rho)$ ,<sup>9</sup> then the transition  $\rho \rightarrow \rho'$  is implemented in the group by acting on the right with the renormalized character  $\psi_{\rho, \rho'}^\phi := \phi(\rho) \circ S \star \phi(\rho')$  on  $\phi(\rho)$ ,

$$\phi(\rho') = \phi(\rho) \star \psi_{\rho, \rho'}^\phi. \quad (21)$$

Let us note that this Hopf algebra structure can be efficiently automated as an algorithm for practical calculations exhibiting the full power of this combinatorics [10].

Now, assume we compute Feynman graphs by some Feynman rules in a given theory and decide to subtract UV singularities at a chosen renormalization point  $\mu$ . This amounts, in our language, to saying that the map  $S_R$  is parametrized by this renormalization point:  $S_R = S_R(\mu)$ . Then, let  $\Phi(\mu, \rho)$  be the ratio  $\Phi(\mu, \rho) = S_R(\mu) \star \phi(\rho)$ . We then have the groupoid law generalizing the before-mentioned Chen's lemma [3]

$$\Phi(\mu, \eta) \star \Phi(\eta, \rho) = \Phi(\mu, \rho). \quad (22)$$

While this looks like a groupoid law, the product of two unrelated ratios  $\Phi(\mu_1, \mu_2) \star \Phi(\mu_3, \mu_4)$ , as any other product of characters, is always well-defined in the group of characters of the Hopf algebra.

### 3.2 Automorphisms of the Hopf algebra

In the set-up discussed so far, the combinatorics of renormalization was attributed to a Hopf algebra, while characters of this Hopf algebra took care of the specific Feynman rules and chosen renormalization schemes. Renormalized quantities appear as the ratio of two characters, while divergences drop out in this ratio  $S_R \star \phi$ .

Typically, such characters introduce a renormalization scale (cut-off, the 't Hooft mass  $\mu$  in dimensional regularization), and we can use these parameters to describe the change of schemes in a fairly unified manner, as discussed in [3].

These considerations of changes of renormalization schemes are related to another interesting aspect discussed in [3]. So far, we regarded the map  $R$  as a self-map in a certain space  $V$ . We will not have  $R(XY) = R(X)R(Y)$  (for example, minimal subtraction cannot possibly fulfill that the poleterms of a product is the product of the poleterms), but  $R$  obeys the multiplicativity constraints

$$R(XY) + R(X)R(Y) = R(XR(Y)) + R(R(X)Y), \quad (23)$$

which ensure that  $S_R(\Gamma_1\Gamma_2) = S_R(\Gamma_1)S_R(\Gamma_2)$  [3, 8]. This leads to the Riemann-Hilbert problem to be discussed below.

---

<sup>9</sup>Typically, it could be a scale which dominates the process under consideration.

We now want to investigate to what extent the map  $R : V \rightarrow V$  can be lifted to an automorphism  $\Theta_R : H \rightarrow H$  of the Hopf algebra. We regard  $V$  as the space in which Feynman graphs evaluate by the Feynman rules, as discussed above. Let again the Feynman rules be implemented by  $\phi$ . The map  $S_R$  is then a character constructed with the help of  $\phi$ , so we should write  $S_R \equiv S_R^\phi$  to be exact.

The question is if one can construct, for any  $R$ , an automorphism  $\Theta_R : H \rightarrow H$  of the Hopf algebra such that one has

$$\bar{\phi} \equiv S_R^\phi \circ S = \phi \circ \Theta_R, \quad (24)$$

so that (using  $S^2 = \text{id}$  which is true in any commutative Hopf algebra)

$$S_R \star \phi = \bar{\phi} \circ S \star \phi = \phi \circ \Theta_R \circ S \star \phi = \phi \circ [\Theta_R^{-1} \star \text{id}]. \quad (25)$$

The answer is affirmative [3]. Following [3] and the use of one-parameter group of automorphisms in the renormalization group [9] to be discussed below, we make the following *Ansatz* for  $\Theta_R$ :

$$\Theta_R(\Gamma) = \Gamma e^{-\varepsilon \text{deg}(\Gamma) \rho_R(\Gamma)}, \quad (26)$$

where, in the context of dimensional regularization or any other analytic regularization,  $\rho_R(\Gamma)$  will be a character evaluating in the ring of Taylor series in  $\varepsilon$  regular at  $\varepsilon = 0$  and  $\text{deg}(\Gamma) = n$  if  $\Gamma$  has  $n$  loops.<sup>10</sup> Then, one determines

$$\rho_R(\Gamma) = \frac{-1}{\varepsilon \text{deg}(\Gamma)} \log \left( \frac{S_R^\phi \circ S(\Gamma)}{\phi(\Gamma)} \right), \quad (27)$$

so that indeed  $\rho_R(\Gamma)$  is free of poleterms, as one easily shows

$$\frac{S_R^\phi \circ S(\Gamma)}{\phi(\Gamma)} = 1 + \mathcal{O}(\varepsilon),$$

for arbitrary graphs  $\Gamma$ . This gives a unifying approach to the treatment of renormalization schemes and changes between them.<sup>11</sup>

## 4 The insertion operad of Feynman graphs

In this section, we want to describe an operad structure on Feynman graphs. This operad was implicitly present in many results in [5, 8, 9], and so it is worth

<sup>10</sup>It is convenient but not necessary to work with dimensional regularization here. In BPHZ, one could work for example with the ratio of Taylor series in external parameters.

<sup>11</sup>From here, one can start considering categorical aspects of renormalization theory and in particular address the question posed in [2] if a modified coproduct  $\Delta_R = (\Theta_R \otimes \text{id}) \circ \Delta$  is (weak-)coassociative in dependence of  $R$ , with first results upcoming in a recent thesis [24].

to describe it shortly at this stage, also with regard to the fact that it will prove to be a useful construct to investigate the number-theoretic aspects of Feynman graphs [13, 14] to be discussed below.

While the previous two sections discussed the process of disentangling a Feynman graph into subgraphs according to the presence of UV singularities, we now turn to the process of plugging graphs into each other. This will lead us in the next section to Lie algebras of Feynman graphs. Here, we want to study the most basic operation: plugging one graph  $\Gamma_1$  into another graph  $\Gamma_2$ . Typically, there are various places in  $\Gamma_2$ , provided by edges and vertices of  $\Gamma_2$ , which can be replaced by  $\Gamma_1$ . To obtain a sensible notion of this operation we should fulfill operad laws in this process. These operad laws can be described as follows. Operad laws are concerned with rules which should be fulfilled when we insert several times. First, assume we have graphs  $\gamma_1, \gamma_2$  and want to plug both of them into different places of a graph  $\Gamma$ . Then, the result should be independent of the order in which we do it. Next, when we plug  $\gamma_1$  into  $\gamma_2$  at some place, and insert the result into  $\Gamma$ , the result should be the same as inserting  $\gamma_2$  at the same place in  $\Gamma$ , and then  $\gamma_1$  into the corresponding relabelled place of  $\gamma_2$ . Finally, the permutation of places should be compatible with the composition (see for example [25] for a formal definition of these requirements).

We only describe the operad in the context of massless  $\phi^3$  theory in six dimensions, the generalizations to more general cases are obvious and will be discussed elsewhere.

A Feynman graph provides vertices and edges connecting these vertices. The operad essentially consists of regarding these vertices and edges as places into which other graphs can be inserted. Naturally, a vertex correction can replace a vertex of a similar type, and a propagator-function can replace a line which represents a free propagator of a similar type. In massless  $\phi^3$  theory, we only have one type of lines and one type of vertices.

First, we note that the overall divergent Feynman graphs in this theory are given by 1PI graphs with two or three amputated external lines. Thus, vertices in the graphs are either internal three-point vertices, or two-point vertices resulting from the amputation of an external leg from a three-point vertex. Hence, self-energies can be described as graphs which precisely have two two-point vertices, while three-point graphs, –vertex corrections–, have precisely three two-point vertices. Propagator-functions then have two external edges.

When we want to replace an internal vertex, we just replace it by a vertex correction. When we want to replace an internal edge, a free propagator, we replace it by a propagator-function, as described by Figs.(13,14).

How many places are there? Let  $\Gamma(p_1, p_2)$  be a 1PI vertex function given by a three point graph  $\Gamma$  with  $l$  loops, which then provides  $2l + 1$  vertices and  $3l$  internal lines, hence  $5l + 1$  places for insertion altogether. Let  $\Pi(p)$  be a propagator function given by a (not necessarily one-particle irreducible) two-point graph  $\Pi$  with  $l$  loops, it then provides  $2l$  vertices and  $3l + 1$  lines, hence again  $5l + 1$  places (we not necessarily have to label all edges and vertices, for

example dropping the label at an external edge of the propagator function takes into account quite naturally the fact that self-energies are proportional to an inverse propagator, and, in a massless theory, cancel one of the external lines).

We label all edges and vertices in arbitrary order, and the composition laws described in the figure captions of Figs.(13,14) fulfill the operad laws (the before-mentioned requirements are fulfilled), so that Figs.(13,14) define this operad by way of example.

So, with these rules for insertion (we also understand that insertion of a propagator-function at a vertex place or a vertex-function at an edge vanishes trivially by definition), one gets indeed an (partial) operad. Note further that insertion of a free propagator or vertex leaves the result unchanged.

One easily extends this construction to the case that one has vertices of other valencies and with different sorts of lines coming in.

This operad can be conveniently used to study the Lie algebraic structure of diagrams as well as for the investigation of number-theoretic aspects as we will see below. Also, the operad viewpoint is helpful in understanding the equivalence classes discussed in [2]. For example, the two graphs  $\Gamma_1$  and  $\Gamma_2$  of section 2.1 belong to the same equivalence class,  $\Gamma_1 \sim \Gamma_2$ , given by the parenthesized word  $((\gamma)\Gamma_0)$ , and are distinguished only by the place into which we insert  $\gamma$ . In general, two graphs are equivalent if one is obtained via a permutation of concatenation labels of the other, while maintaining the tree structure of its subdivergences: all Feynman graphs which represent the same rooted tree or parenthesized word can be obtained from each other by the change of labels of places where we insert the primitive graphs into each other.

Also, typical equations in field theory like Schwinger-Dyson equations are naturally formulated by this operad, using the fact that the sum over all diagrams can be written as a sum over all primitive ones into which all diagrams are plugged in all possible places. Details will be given in future work.

## 5 The Lie algebra structure

In [5, 8, 9] the reader finds various Lie algebra structures which appear in the dual of the Hopf algebra which is the universal enveloping algebra of a Lie algebra. Here, we describe the Lie algebra of Feynman graphs. There is also one for rooted trees, which can be found in [5].

Study of these Lie algebras is a very convenient way of understanding the structure of Feynman graphs. These Lie algebras play a crucial role when one wants to understand the connection between the group of diffeomorphisms of physical parameters like coupling constants with the group of characters of the Hopf algebra, to which we will turn in the next section.

It is also quite useful in determining the Hopf algebra structure of a chosen QFT correctly, because, once it is found, the corresponding enveloping algebra will be the dual of a commutative non-cocommutative Hopf algebra (by the

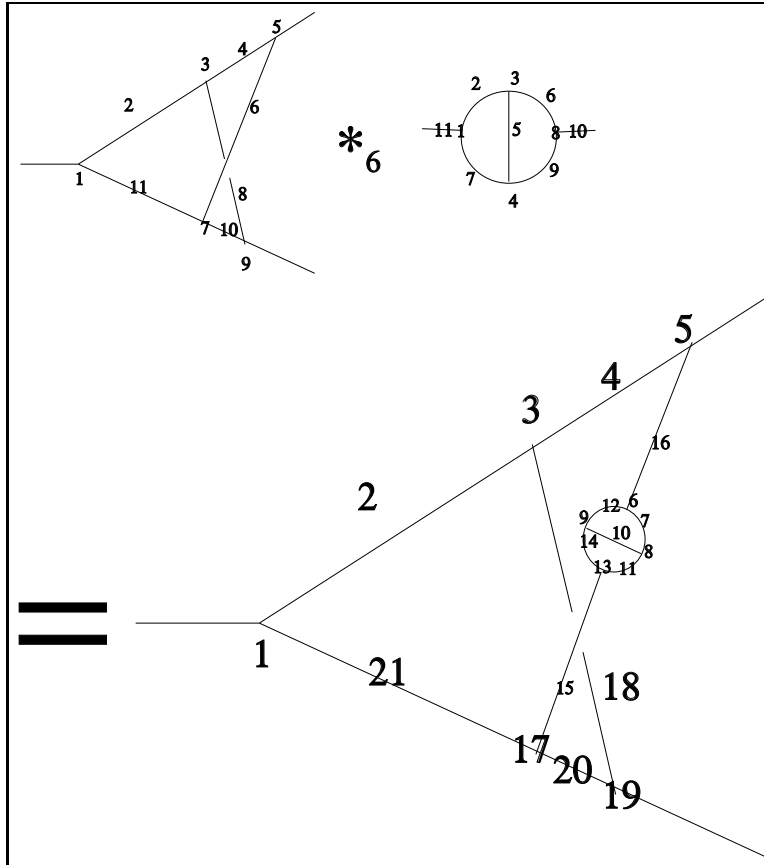


Figure 13: We consider a propagator-graph  $\gamma$  and a vertex-function  $\Gamma$  and as an example their concatenation  $\Gamma \star_6 \gamma$ . The propagator function replaces the line with label 6 in the vertex-function. The propagator-function provides four vertices (labelled 1,3,4,8) and seven edges (labelled 2,5,6,7,9,10,11). Two of the edges, 10 and 11, are external. The vertex-function provides five vertices (labelled 1,3,5,7,9) and six edges (labelled 2,4,6,8,10,11). The vertices 1,5,9 are external, they connect to edges which are not part of the vertex function. We still indicated them by open-ended lines at those vertices, but one should regard vertices 1,5,9 as two-point vertices. Note that each internal edge ends in two labelled vertices. We replace the edge labelled 6 by the propagator-function, connecting the external edges 10 and 11 of the latter to the vertices 5 and 7 of the vertex-function. We glue the edge with the lower label (10) to the vertex with the lower label (5). Relabelling is done in the obvious way: labels 1 to 5 in the vertex-function remain unchanged, the labels at the inserted propagator function become labels 6 to 16, and labels 7 to 11 become labels 17 to 21, increasing their labels by  $4 + 7 - 1 = 10$ .

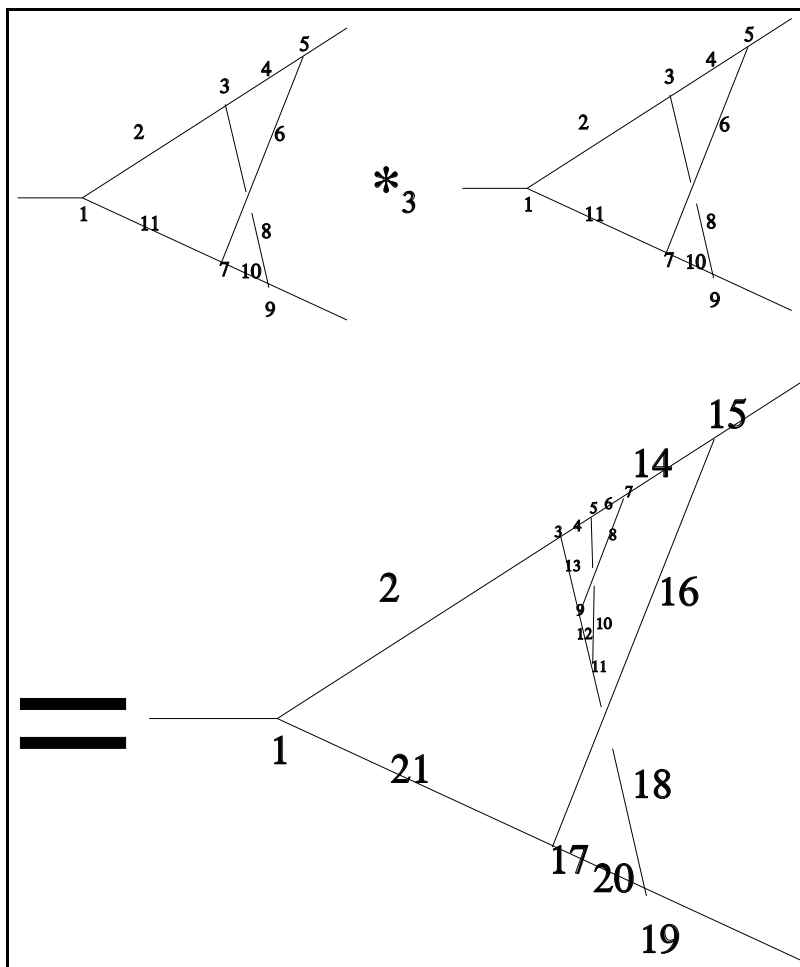


Figure 14: To explain the insertion of a vertex-function, we replace in this example vertex 3 of a vertex-function by the very same vertex-function, so we describe  $\Gamma \star_3 \Gamma$ . We do it by connecting edges 2,4,8 which are attached to vertex 3 to the three two-point vertices 1,5,9, respecting the order: edge 2 connects to vertex 1, edge 4 to vertex 5, edge 8 to vertex 9. Relabelling is done in the obvious way: labels 1 and 2 in the vertex-function remain unchanged, the labels at the inserted vertex-function become labels 3 to 13, and labels 4 to 11 become labels 14 to 21.

celebrated Milnor–Moore theorem [5, 8]) whose coproduct gives us the forests formulas of renormalization.<sup>12</sup> To find these Lie algebras, one defines a Lie-bracket of two 1PI graphs  $\Gamma_1, \Gamma_2$  by plugging  $\Gamma_1$  into  $\Gamma_2$  in all possible ways and subtracts all ways of plugging  $\Gamma_2$  into  $\Gamma_1$ .

These Lie algebras all arise from a pre-Lie structure which we can describe in Fig.[15]. The operation of inserting one graph  $\Gamma_1$  in another graph  $\Gamma_2$  in all possible ways is a pre-Lie operation  $\Gamma_2 \star \Gamma_1$ , which means that it fulfills

$$\Gamma_3 \star (\Gamma_2 \star \Gamma_1) - (\Gamma_3 \star \Gamma_2) \star \Gamma_1 = \Gamma_3 \star (\Gamma_1 \star \Gamma_2) - (\Gamma_3 \star \Gamma_1) \star \Gamma_2.$$

Antisymmetrization then gives automatically a bracket  $[\Gamma_1, \Gamma_2] = \Gamma_1 \star \Gamma_2 - \Gamma_2 \star \Gamma_1$ , which fulfills the Jacobi identity. This operation of inserting one graph in another in all possible ways can obviously written with the help of the operad structure of the previous section as a sum over all places where to insert (plus a sum over all permutations of the labels of identical external vertices of the graph which is to be inserted) and the operad laws then guarantee that the pre-Lie property is fulfilled, making use of the intimate connection between rooted trees, operads and pre-Lie algebras [28].

Once this Lie algebra is found, one knows that dually one obtains a commutative, non-cocommutative Hopf algebra which is the basis of the forest formulas of renormalization as discussed in the previous section.

It is not difficult to work out the corresponding pre-Lie structure for QED for example, and indeed, reading the graphs of Fig.(15) as QED graphs in the obvious possible manners only demands to cancel a few of the terms in that figure, because a photon propagator can only replace a photon line, and not a fermion line. Similarly, for any local QFT, one can determine the corresponding Hopf and Lie algebras, incorporating external structures whenever necessary as in [8].

The resulting Lie algebras of Feynman graphs play a fundamental role in understanding how the combinatorial properties of renormalization connect to the renormalization group, to the running of physical parameters. We now turn to study these results of [7, 8, 9].

## 6 The Birkhoff decomposition and the renormalization group

In [7, 8, 9] the reader finds an amazing connection between the Riemann–Hilbert problem and renormalization. This result was first announced in [7]. It is

<sup>12</sup>For example one easily determines the Lie algebra of QED, having one type of vertex connecting to two different type of lines for fermion and photon propagators. This then confirms the corresponding Hopf algebra structure of 1PI graphs to be commutative non-cocommutative. One-particle reducible graphs can be treated as in [16]. In the literature, there are other attempts to describe the renormalization of QED by binary rooted trees [26]. But the singularities of QED are stratified along diagonals as in any local QFT, and the rather artificial restriction to binary rooted trees ultimately runs into trouble [27].

$$\begin{aligned}
& \text{---} \circ \text{---} * (\text{---} \triangle \text{---} * \text{---} \circ \text{---}) \\
& - (\text{---} \circ \text{---} * \text{---} \triangle \text{---}) * \text{---} \circ \text{---} \\
= & \text{---} \circ \text{---} * (\text{---} \triangle \text{---} + \text{---} \triangle \text{---} + \text{---} \triangle \text{---}) \\
& - (2 \text{---} \bigcirc \text{---}) * \text{---} \circ \text{---} \\
= & \text{---} \bigcirc \text{---} + \text{---} \bigcirc \text{---} + 2 \text{---} \bigcirc \text{---} + \text{---} \bigcirc \text{---} + \text{---} \bigcirc \text{---} \\
& - 2 (\text{---} \bigcirc \text{---} + \text{---} \bigcirc \text{---} + \text{---} \bigcirc \text{---} + \text{---} \bigcirc \text{---} + \text{---} \bigcirc \text{---}) \\
= & \text{---} \bigcirc \text{---} - \text{---} \bigcirc \text{---} - \text{---} \bigcirc \text{---} - \text{---} \bigcirc \text{---} \\
= & 2 (\text{---} \bigcirc \text{---} + \text{---} \bigcirc \text{---}) \\
& - (2 \text{---} \bigcirc \text{---} + \text{---} \bigcirc \text{---} + \text{---} \bigcirc \text{---} + 2 \text{---} \bigcirc \text{---} + \text{---} \bigcirc \text{---} + \text{---} \bigcirc \text{---}) \\
= & \text{---} \circ \text{---} * (2 \text{---} \bigcirc \text{---}) \\
& - (\text{---} \bigcirc \text{---} + \text{---} \bigcirc \text{---}) * \text{---} \triangle \text{---} \\
= & \text{---} \circ \text{---} * (\text{---} \circ \text{---} * \text{---} \triangle \text{---}) \\
& - (\text{---} \circ \text{---} * \text{---} \circ \text{---}) * \text{---} \triangle \text{---}
\end{aligned}$$

Figure 15: The (pre-)Lie algebra structure of Feynman graphs. The fact that the operation of plugging a graph into another one in all possible ways is pre-Lie is essentially due to the fact that the ways of plugging (in all possible ways)  $\Gamma_1$  into  $\Gamma_2$ , and the result into  $\Gamma_3$ , subtracted from the ways of plugging (in all possible ways)  $\Gamma_1$  into the result of plugging (in all possible ways)  $\gamma_2$  into  $\Gamma_3$  is the sum over all possible ways to plug  $\Gamma_1, \Gamma_2$  disjointly into  $\Gamma_3$ .

based on the use of a complex regularization parameter. Typically, dimensional regularization provides such a parameter as the deviation  $\varepsilon$  from the relevant integer dimension of spacetime, but for example analytic regularization would do as well.

With such a regularization parameter, the Feynman rules map a Feynman graph to a Laurent series with poles of finite order in this regularization parameter, hence the Feynman rules provide a character from the Hopf algebra of Feynman graphs to the ring of Laurent polynomials with poles of finite order in  $\varepsilon$ .

As mentioned before, the multiplicativity constraints [3, 7, 8]

$$R[xy] + R[x]R[y] = R[R[x]y] + R[xR[y]]$$

ensure that the corresponding counterterm map  $S_R$  is a character as well,

$$S_R[xy] = S_R[x]S_R[y], \quad \forall x, y \in H.$$

We now study how this set-up leads to the Riemann–Hilbert problem and the Birkhoff decomposition.

## 6.1 Minimal subtraction: the Birkhoff decomposition

To make contact with the Riemann–Hilbert problem, the crucial step is to recognize that, for  $R = MS$  being chosen to be projection onto these poles of finite order (the minimal subtraction scheme MS),  $\phi = S_{MS} \circ S_\star[S_{MS} \star \phi]$  is a decomposition of the character  $\phi$  into a part which is holomorphic at  $\varepsilon = 0$ :  $S_{MS} \star \phi \equiv \phi_+$  is a character evaluating in the ring of functions holomorphic at  $\varepsilon = 0$ , while  $S_{MS} \equiv \phi_-$  maps to polynomials in  $1/\varepsilon$  without constant term, it delivers, when evaluated on Feynman graphs, the MS counterterms for those graphs. This corresponds to a Birkhoff decomposition  $\phi = \phi_-^{-1} \phi_+$ . For an introduction to the Riemann–Hilbert problem and the associated Birkhoff decomposition we refer the reader to [29]. Suffices it here to say that the Riemann–Hilbert problem is a type of inverse problem. For a given complex differential equation

$$y'(z) = A(z)y(z), \quad A(z) = \sum_i \frac{A_i}{z - z_i}$$

with given regular singularities  $z_i$  and matrices  $A_i$ , one can determine monodromy matrices  $M_i$  integrating around curves encircling the singularities. The inverse problem, finding the differential equation from knowledge of the singular places and monodromy matrices, is the Riemann–Hilbert problem. A crucial role in its solution plays the Birkhoff decomposition: for a closed curve  $C$  in the Riemann sphere, and a matrix-valued loop  $\gamma : z \rightarrow \gamma(z)$  well-defined on  $C$ , decompose it into parts  $\gamma_\pm$  well-defined in the interior/exterior of  $C$ .

Thus, renormalization in the MS scheme can be summarized in one sentence: with the character  $\phi$  given by the Feynman rules in a suitable regularization

scheme and well-defined on any small curve around  $\varepsilon = 0$ , find the Birkhoff decomposition  $\phi_+(\varepsilon) = \phi_- \phi$ , where now and in the following the product in expressions like  $\phi_- \phi$  is meant to be just the convolution product  $\phi_- \star \phi$  of characters used before.

The unrenormalized analytic expression for a graph  $\Gamma$  is then  $\phi[\Gamma](\varepsilon)$ , the MS-counterterm is  $S_{MS}(\Gamma) \equiv \phi_-[\Gamma](\varepsilon)$  and the renormalized expression is the evaluation  $\phi_+[\Gamma](0)$ . Once more, note that the whole Hopf algebra structure of Feynman graphs is present in this group: the group law demands the application of the coproduct,  $\phi_+ = \phi_- \phi \equiv S_{MS} \star \phi$ .

The transition from here to other renormalization schemes can be achieved in the group of characters in accordance with our previous considerations in section 3.

But still, one might wonder what a huge group this group of characters really is. What one confronts in QFT is the group of diffeomorphisms of physical parameter: low and behold, changes of scales and renormalization schemes are just such (formal) diffeomorphisms. So, for the case of a massless theory with one coupling constant  $g$ , for example, this just boils down to formal diffeomorphisms of the form

$$g \rightarrow \psi(g) = g + c_2 g^2 + \dots$$

The group of one-dimensional diffeomorphisms of this form looks much more manageable than the group of characters of the Hopf algebras of Feynman graphs of this theory.

Thus, it would be very nice if the whole Birkhoff decomposition could be obtained at the level of diffeomorphisms of the coupling constants, and this is what was achieved in [9].

## 6.2 The $\beta$ -function

Following [8] in the above we have seen that perturbative renormalization is a special case of a general mathematical procedure of extraction of finite values based on the Riemann-Hilbert problem. The characters of the Hopf algebra of Feynman graphs form a group whose concatenation, unit and inverse are given by the coproduct, the counit and the antipode. So we can associate to any given renormalizable quantum field theory an (infinite dimensional) complex Lie group  $G$  of characters of its Hopf algebra  $H$  of Feynman graphs. Passing from the unrenormalized theory to the renormalized one corresponds to the replacement of the loop  $\varepsilon \rightarrow \gamma(\varepsilon) \in G$  (obtained by restricting the character  $\phi$  to an arbitrarily chosen curve  $C$  around  $\varepsilon = 0$ ) of elements of  $G$  obtained from dimensional regularization (still,  $\varepsilon \neq 0$  is the deviation from the integer dimension of space-time) by the value  $\gamma_+(\varepsilon)$  of its Birkhoff decomposition,  $\gamma(\varepsilon) = \gamma_-(\varepsilon)^{-1} \gamma_+(\varepsilon)$ .

In [9] it was shown how to use the very concepts of a Hopf and Lie algebra of graphs to lift the usual concepts of the  $\beta$ -function and renormalization group

from the space of coupling constants of the theory to the complex Lie group  $G$ . We now exhibit these results.

The original loop  $\varepsilon \rightarrow \gamma(\varepsilon)$  not only depends upon the parameters of the theory but also on the additional *unit of mass*  $\mu$ , –the 't Hooft mass in dimensional regularization–, required by dimensional analysis.

But although the loop  $\gamma(\varepsilon)$  does depend on the additional parameter  $\mu$ ,

$$\mu \rightarrow \gamma(\varepsilon; \mu),$$

the negative part  $\gamma_{\mu^-}$  in the Birkhoff decomposition, the character delivering the MS counterterms,

$$\gamma(\varepsilon; \mu) = \gamma_-(\varepsilon; \mu)^{-1} \gamma_+(\varepsilon; \mu)$$

is actually independent of  $\mu$ ,

$$\frac{\partial}{\partial \mu} \gamma_-(\varepsilon; \mu) = 0. \quad (28)$$

This is a remnant of the fact that our Hopf algebra is constructed so as to achieve local counterterms:  $\phi$  is a character which can be easily shown to be a series in  $\log(q^2/\mu^2)$  so that a remaining  $\mu^2$  dependence in MS counterterms would be accompanied by a remaining  $q^2$  dependence, and would hence violate locality.<sup>13</sup>

The Lie group  $G$  turns out to be graded, with grading,

$$\theta_\rho \in \text{Aut } G, \quad \rho \in \mathbb{R},$$

inherited from the grading of the Hopf algebra  $H$  of Feynman graphs given by the loop number,

$$\text{deg}(\Gamma) = \text{loop number of } \Gamma \quad (29)$$

for any 1PI graph  $\Gamma$ , so that  $\theta_\rho(\Gamma) = e^{\rho \text{deg}(\Gamma)} \Gamma$ .<sup>14</sup>

This leads to

$$\gamma(\varepsilon; e^\rho \mu) = \theta_{\rho\varepsilon}(\gamma(\varepsilon; \mu)) \quad \forall \rho \in \mathbb{R},$$

---

<sup>13</sup>A similar argument applies when the Feynman rules provide a character parametrized by several scales. Again, by a group action which is a finite renormalization, we can reduce the unrenormalized theory to a dependence on a single scale. This reduction can constrain the renormalization group flow to a submanifold though, in which case an explicit group action is needed to switch from mass-independent to mass-dependent renormalization group functions, as it is well-known [30].

<sup>14</sup>Here  $\rho$  is to be regarded as a constant. If we promote it to a character evaluating in the ring of functions holomorphic at  $\varepsilon = 0$  we obtain the automorphisms used in section 3 to lift the renormalization map  $R$  to automorphisms of the Hopf algebra. Note that a constant  $\rho$  is sufficient to describe momentum schemes for example, using that one only has to use  $\rho = \varepsilon \log(\mu^2/q^2)$  to compensate for the canonical  $q^2$ -dependence [2, 3, 16, 10].

so that the loops  $\gamma(\mu)$  associated to the unrenormalized theory have the property that the negative part of their Birkhoff decomposition is unaltered by the operation,

$$\gamma(\varepsilon) \rightarrow \theta_{\rho\varepsilon}(\gamma(\varepsilon)) :$$

if we replace  $\gamma(\varepsilon)$  by  $\theta_{\rho\varepsilon}(\gamma(\varepsilon))$  we do not change the negative part of its Birkhoff decomposition. A complete characterization of the loops  $\gamma(\varepsilon) \in G$  fulfilling this invariance can be found in [9]. This characterization only involves the negative part  $\gamma_-(\varepsilon)$  of their Birkhoff decomposition which by hypothesis fulfills,

$$\gamma_-(\varepsilon) \theta_{\rho\varepsilon}(\gamma_-(\varepsilon))^{-1} \text{ is convergent for } \varepsilon \rightarrow 0. \quad (30)$$

It is then easy to see that this defines in the limit  $\varepsilon \rightarrow 0$  a one parameter subgroup,

$$F_\rho \in G, \quad \rho \in \mathbb{R}. \quad (31)$$

Now, the role of the  $\beta$ -function is revealed: the generator  $\beta := \left( \frac{\partial}{\partial \rho} F_\rho \right)_{\rho=0}$  of this one parameter group is related to the *residue* of the loop  $\gamma$

$$\text{Res}_{\varepsilon=0} \gamma = - \left( \frac{\partial}{\partial u} \gamma_- \left( \frac{1}{u} \right) \right)_{u=0} \quad (32)$$

by the simple equation,

$$\beta = Y \text{ Res } \gamma, \quad (33)$$

where  $Y = \left( \frac{\partial}{\partial \rho} \theta_\rho \right)_{\rho=0}$  is the grading. In a moment, we will see how this generator  $\beta$  relates to the common  $\beta$ -function of physics.

All this is a simple consequence of the set-up described so far and is worked out in detail in [9] (essentially, at the moment we quote a summary of the results of that paper), while the central result of [9] gives  $\gamma_-(\varepsilon)$  in closed form as a function of  $\beta$ . Let us use an additional generator in the Lie algebra of  $G$  (i.e. primitive elements of  $H^*$ ) implementing the grading such that  $[Z_0, X] = Y(X) \forall X \in \text{Lie } G$ . Then, the loop  $\gamma_-(\varepsilon)$  corresponding to the MS counterterm evaluated on any close curve around  $\varepsilon = 0$  can be written by a scattering type formula for  $\gamma_-(\varepsilon)$  as

$$\gamma_-(\varepsilon) = \lim_{t \rightarrow \infty} e^{-t(\frac{\beta}{\varepsilon} + Z_0)} e^{tZ_0}. \quad (34)$$

Both factors in the right hand side belong to the semi-direct product,

$$\tilde{G} = G \rtimes_{\theta} \mathbb{R}$$

of the group  $G$  by the grading, but their product belongs to the group  $G$ .

As a consequence the higher pole structure of the divergences is uniquely determined by the residue and this gives a strong form of the t'Hooft relations, which come indeed as an immediate corollary.<sup>15</sup>

The most fundamental result of [9] is obtained though when considering two competing Hopf algebra structures: diffeomorphisms of physical parameters carry, being formal diffeomorphisms, with them the Hopf algebra structure of such diffeomorphisms. This structure was recognized for the first time by Alain Connes and Henri Moscovici in [31]. On the other hand, a variation of physical parameters induced by a variation of scales is a renormalization, which directly leads to the Hopf algebra of Feynman graphs. Let us first describe the Hopf algebra structure of the composition of diffeomorphisms in a fairly elementary way, while mathematical detail can be found in [31].

Assume you have formal diffeomorphisms  $\phi, \psi$  in a single variable

$$x \rightarrow \phi(x) = x + \sum_{k>1} c_k^\phi x^k, \quad (35)$$

and similarly for  $\psi$ . How do you compute the Taylor coefficients  $c_k^{\phi \circ \psi}$  for the composition  $\phi \circ \psi$  from the knowledge of the Taylor coefficients  $c_k^\phi, c_k^\psi$ ? It turns out that it is best to consider the Taylor coefficients

$$\delta_k^\phi = \log(\phi'(x))^{(k)}(0) \quad (36)$$

instead, which are as good to recover  $\phi$  as the usual Taylor coefficients. The answer lies then in a Hopf algebra structure:

$$\delta_k^{\phi \circ \psi} = m \circ (\tilde{\psi} \otimes \tilde{\phi}) \circ \Delta_{CM}(\delta_k),$$

where  $\tilde{\phi}, \tilde{\psi}$  are characters on a certain Hopf algebra  $H_{CM}$  (with coproduct  $\Delta_{CM}$ ) so that  $\tilde{\phi}(\prod_i \delta_i) = \prod_i \delta_i^\phi$ . Thus one finds a Hopf algebra with abstract generators  $\delta_n$  such that it introduces a convolution product on characters evaluating to the Taylor coefficients  $\delta_n^\phi, \delta_n^\psi$ , such that the natural group structure of these characters agrees with the diffeomorphism group.

It turns out that this Hopf algebra of Connes and Moscovici is intimately related to rooted trees in its own right [5], signalled by the fact that it is linear in generators on the rhs, as are the coproducts of rooted trees and graphs.<sup>16</sup>

<sup>15</sup>The explicit formulas in [9] allow to find the combinations of primitive graphs into which higher order poles resolve. The weights are essentially given by iterated integrals which produce coefficients which generalize the tree-factorials obtained for the undecorated Hopf algebra in [3, 16, 10]. Iterated application of this formula allows to express inversely the first-order poles contributing to the  $\beta$ -function as polynomials in Feynman graphs free of higher-order poles.

<sup>16</sup>Taking the  $\delta_n$  as naturally grown linear combination of rooted trees imbeds the commutative part of the Connes-Moscovici Hopf algebra in the Hopf algebra of rooted trees, which on the other hand allows for extensions similar to the ones needed by Connes and Moscovici. Details are in [5].

This initiated the collaboration of Alain Connes and the author, when, in a lucky accident, we both stumbled over similar Hopf algebras at about the same time.

Now, following [9], let us specialize to the massless case. Then the formula for the bare coupling constant,

$$g_0 = g Z_1 Z_3^{-3/2} \quad (37)$$

(where both  $g Z_1 = g + \delta g$  and the field strength renormalization constant  $Z_3$  are thought of as power series (in  $g$ ) of elements of the Hopf algebra  $H$ ) does define a Hopf algebra homomorphism,

$$H_{CM} \xrightarrow{g_0} H,$$

from the Hopf algebra  $H_{CM}$  of coordinates on the group of formal diffeomorphisms of  $\mathbb{C}$  (ie such that  $\varphi(0) = 0$ ,  $\varphi'(0) = \text{id}$  as in Eq.(35)) to the Hopf algebra  $H$  of the massless theory.<sup>17</sup> Having this Hopf algebra homomorphism from  $H_{CM}$  to  $H$ , dually one gets a transposed group homomorphism  $\rho$ , a homomorphism from the huge group of characters of the Hopf algebra to the group of diffeomorphism of physical parameters [9]. We finally recover the usual  $\beta$ -function: the image by  $\rho$  of the previously introduced generator  $\beta = Y \text{Res } \gamma$  is then the usual  $\beta$ -function of the coupling constant  $g$ . While this might sound rather abstract, it can be easily translated into the standard notions of renormalization theory (see, for example, [32]).

While in [9] the physical parameter under consideration was a single coupling, similar considerations apply to other physical parameters which run under the renormalization group, making use of the Hopf algebraic description of composition of diffeomorphisms in general.

As a corollary of the construction of  $\rho$  one gets an *action* by (formal) diffeomorphisms of the group  $G$  on the space  $X$  of (dimensionless) coupling constants of the theory. One can then in particular formulate the Birkhoff decomposition *directly* in the group  $\text{Diff}(X)$  of formal diffeomorphisms of the space of coupling constants.

The unrenormalized theory delivers a loop

$$\delta(\varepsilon) \in \text{Diff}(X), \quad \varepsilon \neq 0,$$

whose value at  $\varepsilon \neq 0$  is simply the unrenormalized effective coupling constant. The Birkhoff decomposition  $\delta(\varepsilon) = \delta_+(\varepsilon) \delta_-(\varepsilon)^{-1}$  of this loop gives directly

$$\delta_-(\varepsilon) = \text{bare coupling constant}$$

---

<sup>17</sup>We restrict ourselves to the massless theory so that we can deal with one-dimensional diffeomorphisms. We can regard a mass as a further coupling constant of a two-point vertex which leads to formal diffeomorphisms of higher dimensional spaces.

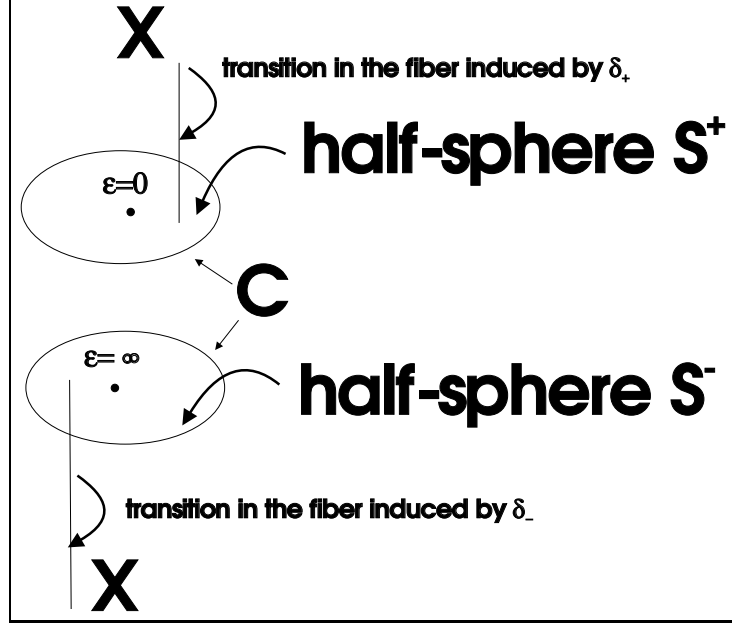


Figure 16: The geometric picture of [9] allows for the construction of a complex bundle,  $P = (S^+ \times X) \cup_{\delta} (S^- \times X)$  over the sphere  $S = P_1(\mathbb{C}) = S^+ \cup S^-$ , and with fiber  $X$ ,  $X \longrightarrow P \xrightarrow{\pi} S$ , where  $X$  is a complex manifold of physical parameters. The transition in this fiber are diffeomorphisms.  $\delta(\varepsilon)$  delivers a diffeomorphism of  $X$  for any  $\varepsilon \in C$ , where  $C$  is the boundary of the two half-spheres  $S^+, S^-$ . It extends to the interiors of the half-spheres via its Birkhoff decomposition. The meaning of this Birkhoff decomposition,  $\delta(\varepsilon) = \delta_+(\varepsilon)\delta_-(\varepsilon)^{-1}$  is then exactly captured by an isomorphism of the bundle  $P$  with the trivial bundle,  $S \times X$ . Note that  $\delta_-(\infty)$  is well-defined due to the fact that  $S_{MS}$  has no constant term in  $\varepsilon$ , which characterizes a minimal subtraction scheme.

and

$$\delta_+(\varepsilon) = \text{renormalized effective coupling constant.}$$

This result is now stated in a manner independent of our group  $G$  or the Hopf algebra  $H$ , its proof makes heavy use of these ingredients though.

Finally, the Birkhoff decomposition of a loop,  $\delta(\varepsilon) \in \text{Diff}(X)$  admits a beautiful geometric interpretation [9], described in Fig.(16).

### 6.3 An example

In [9] the reader can find explicit computational examples up to the three-loop level, and a complete proof to all loop orders, for the group and Hopf algebra homomorphisms described above. We only want to check the Hopf algebra

homomorphism  $H_{CM} \rightarrow H$  up to two loops here. We regard  $g_0$  as a series in a variable  $x$  (which can be thought of as a physical coupling) up to order  $x^4$ , making use of  $g_0 = xZ_1Z_3^{-3/2}$  and the expression of the  $Z$ -factors in terms of 1PI Feynman graphs. The challenge is then to confirm that the coordinates  $\delta_n^{g_0}$ , implicitly defined by [31]

$$\log [g_0(x)]^{(n)},$$

as expected from Eq.(36), commute with the Hopf algebra homomorphism: calculating the coproduct  $\Delta_{CM}$  of  $\delta_n$  and expressing the result in terms of Feynman graphs with the help of the character corresponding to  $g_0$ ,  $\tilde{g}_0(\delta_n) = \delta_n^{g_0}$ , must equal the application of the coproduct  $\Delta$  applied to  $\delta_n^{g_0}$ .

We write  $g_0 = xZ_1Z_3^{-3/2}$ ,

$$Z_1 = 1 + \sum_{k=1}^{\infty} z_{1,2k} x^{2k},$$

$$Z_3 = 1 - \sum_{k=1}^{\infty} z_{3,2k} x^{2k},$$

and

$$Z_g = Z_1Z_3^{-3/2}, \quad z_{i,2k} \in \mathcal{H}_c, \quad i = 1, 3,$$

as formal series in  $x^2$ . Using

$$\log \left( \frac{\partial}{\partial x} x Z_g \right) = \sum_{k=1}^{\infty} \frac{\delta_{2k}^{g_0}}{(2k)!} x^{2k},$$

which defines  $\delta_{2k}^{g_0}$ , we find

$$\begin{aligned} \frac{1}{2!} \delta_2^{g_0} &\equiv \tilde{\delta}_2^{g_0} &= 3z_{1,2} + \frac{9}{2} z_{3,2}, \\ \frac{1}{4!} \delta_4^{g_0} &\equiv \tilde{\delta}_4^{g_0} &= 5[z_{1,4} + \frac{3}{2} z_{3,4}] - \frac{9}{2} z_{1,2}^2 - 6z_{1,2} z_{3,2} - \frac{3}{4} z_{3,2}^2. \end{aligned} \quad (38)$$

The algebra homomorphism  $H_{CM} \rightarrow H$  is effected by expressing the  $z_{i,2k}$  in Feynman graphs, with 1PI graphs with three external legs contributing to  $Z_1$ , and 1PI graphs with two external legs, self-energies, contributing to  $Z_3$ .

Explicitly, we have

$$\begin{aligned} z_{1,2} &= \triangleleft, \\ z_{3,2} &= \frac{1}{2} \circlearrowleft, \\ z_{1,4} &= \triangleleft + \triangleleft + \triangleleft + \frac{1}{2} [\triangleleft + \triangleleft + \triangleleft] + \frac{1}{2} \triangleleft, \\ z_{3,4} &= \frac{1}{2} [\circlearrowleft + \circlearrowright]. \end{aligned}$$

On the level of diffeomorphisms, we have the coproduct

$$\Delta_{CM}[\delta_4] = \delta_4 \otimes 1 + 1 \otimes \delta_4 + 4\delta_2 \otimes \delta_2, \quad (39)$$

where we skip odd gradings (in  $\phi^3$  theory, adding a loop order increases the order in the coupling by  $g^2$ ).

We have to check that the coproduct  $\Delta$  of Feynman graphs reproduces these results.

Applying  $\Delta$  to the rhs of (39) gives, using the expressions for  $z_{i,k}$  in terms of Feynman graphs,

$$\begin{aligned} \Delta(\tilde{\delta}_4) &= 6 \langle \triangleleft \otimes \triangleleft + \frac{9}{2} \left[ \triangleleft \otimes \text{circle} + \text{circle} \otimes \triangleleft \right] \\ &\quad + \frac{27}{8} \text{circle} \otimes \text{circle} + \tilde{\delta}_4 \otimes 1 + 1 \otimes \tilde{\delta}_4. \end{aligned}$$

This has to be compared with  $\tilde{\delta}_4 \otimes 1 + 1 \otimes \tilde{\delta}_4 + \frac{2!2!}{4!} 4\tilde{\delta}_2 \otimes \tilde{\delta}_2$ , which matches nicely, as

$$\begin{aligned} \tilde{\delta}_2 \otimes \tilde{\delta}_2 &= 9 \langle \triangleleft \otimes \triangleleft + \frac{27}{4} \left[ \triangleleft \otimes \text{circle} + \text{circle} \otimes \triangleleft \right] \\ &\quad + \frac{81}{16} \text{circle} \otimes \text{circle}. \end{aligned}$$

## 7 Conclusions and Outlook

In this final section we mainly want to comment on some more future lines of investigation, which in part are already work in progress. We start with the connection between Feynman diagrams and the numbers which we see in their coefficients of ultraviolet divergence, which is a rich source of structure [15].

### 7.1 Numbers and Feynman diagrams

There is an enormous amount of interesting number theory in Feynman diagrams [33, 34, 15]. In particular, the primitive elements in the Hopf algebra, those graphs which have no subdivergences and provide a renormalization scheme independent coefficient of ultraviolet divergence, show remarkable and hard to explain patterns. These coefficients evaluate in Euler–Zagier sums (generalized polylogs evaluated at (suitable roots of) unity so that they generalize multiple zeta values (MZVs) [15, 33, 34]), numbers which have remarkably fascinating algebraic structure [35, 36, 37, 38].

These algebraic structures are believed to be governed by shuffle algebras, and by the much more elusive Grothendieck–Teichmüller group (see, for example, [39] for an introduction to the Grothendieck Teichmüller group which is close in spirit to the consideration of short-distance singularities).

The coefficients of UV-divergence in Feynman diagrams typically evaluate, up to the six loop level, in terms of these Euler–Zagier sums, but the question if this will always be so remains open in light of the failure to identify all these coefficients in this number class at the seven loop level [33, 34, 15]. While the embarrassingly successful heuristic approach summarized in [15], providing a knot-to-number dictionary for those numbers, only emphasizes the need for a more thorough understanding, the algebraic structures in Feynman graphs hopefully lead to such an understanding in the future. It is already remarkable that shuffle products can be detected in Feynman graphs [13], but their are hints for much more structure [14].

But while the existence of shuffle algebras in Feynman graphs can essentially be straightforwardly addressed due to the fact that a shuffle algebra makes use of the  $B_+, B_-$  operators in a natural way [13], these remaining algebraic relations between Feynman graphs will be harder to address.<sup>18</sup> But the very fact that Feynman graphs realize their short-distance singularities in tree-like hierarchies suggests that they can be understood along lines similar to what is known for Euler–Zagier sums.

In particular, Feynman graphs whose subdivergences realize the same rooted tree but with subgraphs inserted at different internal lines provide remarkable number-theoretic features [40]. As mentioned before, in the operad picture, such differences are given by permutations  $\sigma(i) = j$  of places  $i$  at which we compose:

$$\Gamma \circ_i \gamma \rightarrow \Gamma \circ_{\sigma(i)} \gamma.$$

Note that, if we let  $U$  be the difference of the two expressions, we get a primitive element in the Hopf algebra (if the two graphs  $\Gamma$  and  $\gamma$  are both primitive),  $\Delta(U) = U \otimes 1 + 1 \otimes U$ .

Quite often, one finds that these differences are even finite, which means that the coefficients of ultraviolet divergence are the same and drop out in the difference: short distance singularities are invariant under the above permutations. Fig.(17) gives an example of such an invariance observed in [40]. We insert a one-loop bubble at different places  $i, j$  in the graph. We do not have to worry that in one case it is a one-loop fermion self-energy, in the other case a one-loop boson self-energy. In massless Yukawa theory, they both evaluate to the same analytic expression. This makes it very easy to study the effect of a subdivergence being inserted at different places in a larger graph. In this four-loop example, the difference becomes a primitive element and hence delivers only a first order pole  $\sim \zeta(3)/\varepsilon$ , signalling the difference in topology between

<sup>18</sup>But note that these shuffle algebras and shuffle identities only hold for the coefficients of ultraviolet singularity: they hold up to finite parts, up to finite renormalizations that is.

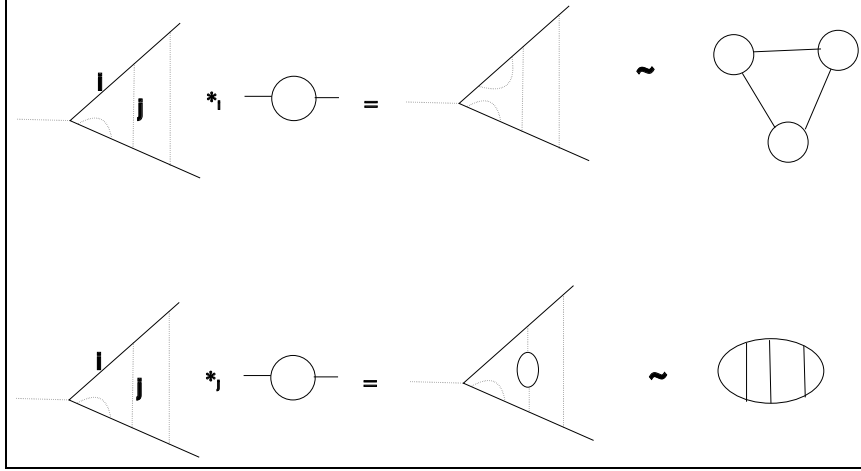


Figure 17: These two Feynman graphs (with their distinct topologies indicated on the rhs of each: the topology of the upper graph is that of disjoint one-loop insertions, the lower is a ladder topology) in massless Yukawa theory have a remarkable relation: their difference is a primitive Hopf algebra element. When evaluating the character  $S_{MS}$  on both, one finds a Laurent series with poles of fourth order from both of them. In the difference, the highest three-pole terms drop out, and the remaining term is  $\sim \zeta(3)/\varepsilon$ . Similar phenomena happen at higher loop orders [40]: higher poleterms are invariants under the permutation of places where we insert subgraphs.

the two diagrams [15]. The ladder diagram evaluates to rational coefficients in the poleterms of its MS counterterm, while the other diagram has the same rational part, but also has  $\zeta(3)$  in the  $1/\varepsilon$  pole. In the difference, only this first order pole  $\sim \zeta(3)/\varepsilon$  remains.

Comparing the two three-loop subgraphs of each diagram, one finds their difference to be finite and  $\sim \zeta(3)$ , so that the three coefficients  $\sum_{i=1}^3 c_i/\varepsilon^i$  are invariant under an exchange of the place where we insert the subgraph: the morphism sending one graph to the other, and thus sending one configuration of internal vertices with its characteristic short-distance singularities to another, is a finite one. Similar observation hold for higher loop orders [40].

A systematic understanding of such phenomena, and a possible relation to finite-type invariants, seems crucial to understand the algebraic relations in Feynman graphs completely. Ultimately, one hopes for a geometric understanding of the analytic challenge posed by Feynman diagrams. Meanwhile, similar relations have been observed in QED [41].

A requirement on the way to such an understanding is the question how in the geometric picture of Fig.(16) one can relate an infinitesimal variation in the base space to a variation in the fiber, ie the quest for a connection?

For the  $\delta_-$  part of the Birkhoff decomposition, this leads to an investigation

as to how a derivative with respect to the regularization parameter  $\varepsilon$  is related to the insertion of a further graph. First results at low loop orders to be discussed elsewhere indicate that this is a source for relations between the coefficients of ultraviolet divergence similar but not quite like the four-term relations discussed in the study of finite-type invariants [15]. This is not impossible: while all higher poleterms are fixed in terms of the residue by the scattering type formula Eq.(34) of the previous section, this formula can by its very nature not deliver relations between residues of graphs.

## 7.2 Gauge symmetries

Clearly, one of the most urgent and fascinating questions is the role of symmetries in quantum field theories. Having, with the Hopf algebra structures reported here, discovered such a wonderful machinery which encapsulates the quest for locality, one should expect interesting structure when considering local gauge symmetries, in particular also with respect to the role which foliations play naturally in noncommutative geometry [31, 42].

There are many aspects which can hopefully be addressed in the near future.

- To what extent can Ward- and Slavnov-Taylor identities be incorporated in this picture? Do these identities form something like an ideal in the algebra of graphs? Note that the language of external structures allows nicely to formulate concepts like the longitudinal and transversal part of a vertex-correction for example, and is hence well-adopted to address such questions.
- Has BRST cohomology a natural formulation in this context?
- Gauge theories provide number-theoretical miracles in abundance, with the most significant observation being Jon Rosner's observation [43] of the vanishing of  $\zeta(3)$  from the  $\beta$ -function of quenched QED. While this can be understood heuristically [44, 15], eventually the role between internal symmetries and number-theoretic properties must be properly understood.

For the practitioner of quantum field theory, the real challenge lies in the treatment of the perturbative expansion in circumstances when there is no regularization available which preserves the symmetries of the initial theory. A notorious and famous problem at hand is the  $\gamma_5$  problem in dimensional regularization [45]. In realistic circumstances like the Standard Model this already demands a formidable effort at the one-loop level if one uses a calculational scheme which violates the BRS symmetry even in the absence of anomalies (see [46] for such an example), which then is an unavoidable effort dictated by the demand to restore the BRS symmetry using the quantum action principle. There is one obvious useful role for the Hopf algebra: the analysis at the one-loop level would in many ways not change when extended to any other primitive element of the

Hopf algebra, which, being primitive, all share with the one-loop graphs that they have no subdivergences. From there, the Hopf algebra structure governs the iteration of graphs into each other.

But then, the prominent role and natural role which field-theoretic ingredients like the Dirac propagator and  $\gamma_5$  itself, a volume form on four-dimensional space essentially, play in non-commutative geometry [6, 42], gives hope for a more profound understanding of this problem in the future.

### 7.3 The exact renormalization group and the non-perturbative regime

Ultimately, the renormalization group is a non-perturbative object, and can indeed be addressed without necessarily making use of the usual concepts of graph-theoretic expansions [47, 48]. This is nicely reflected by the fact that the transition from the perturbative to the non-perturbative just amounts, in the picture outlined here, to a Birkhoff decomposition of an actual instead of a formal diffeomorphism. Integrating out high frequency modes in the functional integral step-by-step produces a sequence of diffeomorphisms of the correlation function under consideration.<sup>19</sup>

The Hopf algebra of rooted trees, thanks to its universality, provides the relevant backbone in any case, and indeed rooted trees underly any iterative equation, like, for example, the Wilson equation

$$\frac{\partial S_\lambda}{\partial \lambda} = \mathcal{F}(S_\lambda),$$

for some action parametrized by some cut-off  $\lambda$  and some suitable functional  $\mathcal{F}$ . Integrating this functional  $\mathcal{F}$  now plays the role of the operator  $B_+$  in the universal setting of the Hopf algebra of rooted trees [5]. Rooted trees are deeply built into solutions of (integro-) differential equations [49, 50]. It is no miracle then that on the other hand one finds that the understanding of the Hopf- and Lie algebras of Feynman graphs not only enables high-loop order calculations [10, 11, 51] which allow to analyze Padé-Borel resummations [11, 51, 52] but also allows to find exact non-perturbative solutions in new problems. A first result can be found in [51].

### 7.4 Further aspects

Combinatorially, rooted trees are very fundamental objects, and their Hopf and Lie algebra structure underlies not only the combinatorial process of renormalization, but can hopefully be used in the future in other expansions in perturbation theory, starting from a disentanglement of infrared divergent sectors

<sup>19</sup>The fact, emphasized by Polchinski [47], that in such an approach one does not see the graph-theoretical notions emphasized in textbook approaches to renormalization theory is a mere reflection of the fact that one can formulate the Birkhoff decomposition directly on the level of diffeomorphisms of physical observables [9], as exhibited in the previous section.

[53] to more general applications in asymptotic expansions [54]. Its universal nature already allowed to use it in a straightforward formulation of block spin transformations, coarse graining and the renormalization of spin networks [55]. Eventually, one hopes, this basic universal combinatorial structure finds its way into other approaches to QFT, from the constructive approach [56] which in its nature is very tree-like from a start [57], to the algebraic school [58, 59], which all have to handle the basic combinatorial step that we can address a problem only after we addressed its subproblems.<sup>20</sup> Note also that applications of forest formulas in the context of noncommutative field theory and string field theory (see [62] for a detailed graphical analysis) naturally change the criteria for the subgraphs  $\gamma$  over which a sum

$$\Delta(\Gamma) = \Gamma \otimes 1 + 1 \otimes \Gamma + \sum_{\gamma} \gamma \otimes \Gamma/\gamma$$

runs, while the results in [4] underline that a Hopf algebra structure can still be established when we vary these criteria.

There is no space here to comment in detail on some other mathematical developments which are related to the discovery of the Hopf algebra structure of renormalization. We can only address the interested reader to [63, 64, 65, 28]. But note that such mathematical investigations are often very useful for a practitioner of QFT: clearly, the classification of all primitive Hopf algebra elements is of importance even for the case of the undecorated Hopf algebra of rooted trees, and leads for example to the notion of a bigrading which characterizes potential higher divergences algebraically [12, 65].

## 7.5 Conclusions

Rooted trees and Feynman graphs are familiar objects for anybody working on the perturbative expansion of a functional integral, and as familiar are forest formulas and the Bogoliubov recursion.

What is new is that there is a universal Hopf algebra on rooted trees, devoted to the problem of singularities along diagonals in configuration spaces and providing a principle of multiplicative subtraction, which reproduces just these recursions and forest formulas. That Feynman graphs, with all their external structure, form a Lie algebra is a very nice consequence which hopefully gives a new and strong handle for the understanding of QFT in the future. The consequences of the connection to the Riemann–Hilbert problem and the Birkhoff decomposition of diffeomorphisms, the connection between short-distance singularities in perturbation theory and polylogarithms, all this indicates what a rich source of mathematical structure and beauty is imposed on a quantum field theory by its infinities.

---

<sup>20</sup>The universality of the Hopf algebra can be used to describe effective actions in a unifying manner, which was indeed one of the main points of [8, 9], while the connection to integrable models promoted in [60, 61] can hopefully be substantiated further in the future.

## Acknowledgments

A large body of the work presented here was done in past and ongoing collaborations with David Broadhurst and Alain Connes. Helpful discussions with Jim Stasheff on operads are gratefully acknowledged. This work was done in part for the Clay Mathematics Institute. Also, the author thanks the DFG for a Heisenberg fellowship.

## References

- [1] Collins, *Renormalization*, Cambridge Univ. Press 1984.
- [2] D. Kreimer, *On the Hopf algebra structure of perturbative quantum field theories*, Adv. Theor. Math. Phys. **2** (1998) 303[q-alg/9707029].
- [3] D. Kreimer, *Chen's iterated integral represents the operator product expansion*, Adv. Theor. Math. Phys. **3** (2000) 627[hep-th/9901099].
- [4] D. Kreimer, *On overlapping divergences*, Commun. Math. Phys. **204** (1999) 669[hep-th/9810022].
- [5] A. Connes and D. Kreimer, *Hopf algebras, renormalization and noncommutative geometry*, Commun. Math. Phys. **199** (1998) 203[hep-th/9808042].
- [6] A. Connes and D. Kreimer, *Lessons from quantum field theory: Hopf algebras and spacetime geometries*, Lett. Math. Phys. **48** (1999) 85[hep-th/9904044].
- [7] A. Connes and D. Kreimer, *Renormalization in quantum field theory and the Riemann-Hilbert problem*, JHEP **9909** (1999) 024[hep-th/9909126].
- [8] A. Connes and D. Kreimer, *Renormalization in quantum field theory and the Riemann-Hilbert problem. I: The Hopf algebra structure of graphs and the main theorem*, Commun. Math. Phys. **210** (2000) 249[hep-th/9912092].
- [9] A. Connes and D. Kreimer, *Renormalization in quantum field theory and the Riemann-Hilbert problem. II: The beta-function, diffeomorphisms and the renormalization group*, Commun. Math. Phys. in press, hep-th/0003188.
- [10] D. J. Broadhurst and D. Kreimer, *Renormalization automated by Hopf algebra*, J. Symb. Comput. **27** (1999) 581[hep-th/9810087].
- [11] D. J. Broadhurst and D. Kreimer, *Combinatoric explosion of renormalization tamed by Hopf algebra: 30-loop Pade-Borel resummation*, Phys. Lett. **B475** (2000) 63[hep-th/9912093].

- [12] D. J. Broadhurst and D. Kreimer, *Towards cohomology of renormalization: Bigrading the combinatorial Hopf algebra of rooted trees*, Commun. Math. Phys. in press, hep-th/0001202.
- [13] D. Kreimer, *Shuffling quantum field theory*, Lett. Math. Phys. **51** (2000) 179[hep-th/9912290].
- [14] D. Kreimer, *Feynman diagrams and polylogarithms: Shuffles and pentagons*, Nucl. Phys. Proc. Suppl. **89** (2000) 289[hep-th/0005279].
- [15] D. Kreimer, *Knots and Feynman Diagrams*, Cambridge Univ. Press 2000.
- [16] D. Kreimer and R. Delbourgo, *Using the Hopf algebra structure of QFT in calculations*, Phys. Rev. **D60** (1999) 105025[hep-th/9903249].
- [17] H. Epstein and V. Glaser, *The role of locality in perturbation theory*, Ann. Inst. H. Poincaré **19** (1973) 211.
- [18] R. Stora, *Renormalized perturbation theory: a theoretical laboratory*, talk given at *Mathematical Physics in Mathematics and Physics*, Siena, June 2000.
- [19] W. Fulton and R. MacPherson, *A compactification of configuration spaces*, Ann. Math. **139** (1994) 183.
- [20] J.M. Gracia-Bondia and S. Lazzarini, *Connes–Kreimer–Epstein–Glaser renormalization*, hep-th/0006106.
- [21] T. Krajewski and R. Wulkenhaar, *On Kreimer’s Hopf algebra structure of Feynman graphs*, Eur. Phys. J. **C7** (1999) 697[hep-th/9805098].
- [22] R. Brunetti and K. Fredenhagen, *Microlocal analysis and interacting quantum field theories: Renormalization on physical backgrounds*, Commun. Math. Phys. **208** (2000) 623[math-ph/9903028].
- [23] C. Kassel, *Quantum Groups* Springer 1995.
- [24] M. Mertens, PhD Thesis (in german), *Über die Rolle von Hopfkategorien in störungstheoretischer Quantenfeldtheorie*, Mainz University, Fall 2000.
- [25] J.L. Loday, *La renaissance des opérades*, (French) [The rebirth of operads] Séminaire Bourbaki, Vol. 1994/95. Astérisque No. 237, (1996), (Exp. No. 792, 3) 47.
- [26] C. Brouder, *On the trees of quantum fields*, hep-th/9906111;  
C. Brouder and A. Frabetti, *Renormalization of QED with planary binary trees*, hep-th/0003202.
- [27] C. Brouder, private communication.

- [28] F. Chapoton and M. Livernet, *Pre-Lie algebras and the rooted trees operad*, math.QA/0002069.
- [29] D.V. Anosov and A.A. Bolibruch, *The Riemann–Hilbert problem*, Vieweg 1994.
- [30] E. Kraus, *The structure of the invariant charge in massive theories with one coupling*, Ann. Phys. **240** (1995) 367[hep-th/9311158];  
E. Kraus, *Asymptotic normalization properties and mass independent renormalization group functions*, Helv. Phys. Acta **67** (1994) 424[hep-th/9406134].
- [31] A. Connes and H. Moscovici, *Hopf algebras, cyclic cohomology and the transverse index theorem*, Commun. Math. Phys. **198** (1998) 199[math.dg/9806109].
- [32] T. Krajewski, talk given at *Non-Commutativity, Geometry and Probability*, Nottingham July 2000 and *General reparametrization invariance in the Connes–Kreimer formalism*, in preparation.
- [33] D. J. Broadhurst and D. Kreimer, *Knots and numbers in  $\Phi_4$  theory to 7 loops and beyond*, Int. J. Mod. Phys. **C6** (1995) 519[hep-ph/9504352].
- [34] D. J. Broadhurst and D. Kreimer, *Association of multiple zeta values with positive knots via Feynman diagrams up to 9 loops*, Phys. Lett. **B393** (1997) 403[hep-th/9609128].
- [35] A.B. Goncharov, *The dihedral Lie algebras and Galois symmetries of  $\pi_1^l(P^1 - 0, \infty$  and  $N$ -th root of unity)*, math.ag/0009121;  
A.B. Goncharov, *Multiple Zeta Values, Galois groups, and geometry of modular varieties*, math.ag/0005069;  
A.B. Goncharov, *The double logarithm and Manin’s complex for modular curves*, Math. Res. Lett. **4**, (1997) 617;  
A.B. Goncharov, *Multiple polylogarithms, cyclotomy and modular complexes*, Math. Res. Lett. **5**, (1998) 497.
- [36] J.M. Borwein and D.M. Bradley and D.J. Broadhurst, *Evaluation of  $k$ -fold Euler–Zagier sums: a compendium of results for arbitrary  $k$* , Elec. J.Comb. **4**(2), R5, (1997);  
D.J. Broadhurst, *Conjectured Enumeration of irreducible Multiple Zeta Values, from Knots and Feynman Diagrams*, Phys.Lett. **B**, in press, hep-th/9612012;  
D.J. Broadhurst, *On the enumeration of irreducible  $k$ -fold Euler sums and their roles in knot theory and field theory*, J.Math.Phys., in press, hep-th/9604128.

- [37] D. Zagier, *Values of Zeta-functions and their applications*, in First European Congress of Mathematics, Vol. II, Birkhauser, Boston, 1994, 497-512.
- [38] M.E. Hoffman, *Quasi Shuffle Products*, J. Algebraic Combin. **11** (2000) 49[math.QA/9907173].
- [39] D. Bar-Natan, *On Associators and the Grothendieck Teichmüller Group I*, Selecta Math. (N.S.) **4** (1998) 183[q-alg/9606021].
- [40] D. Kreimer, *On knots in subdivergent diagrams*, Eur. Phys. J. **C2** (1998) 757[hep-th/9610128].
- [41] I. Bierenbaum, Diploma Thesis *Die Riemann'sche  $\zeta$ -Funktion in iterierten Einschleifenintegralen*, Mainz Univ., wwwthep.physik.uni-mainz.de/Publications/Dip-th.html, (00-D4), to be published.
- [42] A. Connes, *A short survey of Noncommutative Geometry*, hep-th/0003006.
- [43] J.L. Rosner, Phys. Rev. Lett. **17** (1966) 1190; Ann. Phys. **44** (1967) 11.
- [44] D.J. Broadhurst, R. Delbourgo and D. Kreimer, *Unknotting the polarized vacuum of quenched QED*, Phys. Lett. **B366** (1996) 421[hep-ph/9509296].
- [45] F. Jegerlehner, *Facts of life with  $\gamma_5$* , hep-th/0005255.
- [46] C.P. Martin and D. Sanchez-Ruiz, *Action principles, restoration of BRS symmetry and the renormalization group equation for chiral non-Abelian gauge theories in dimensional renormalization with a non-anticommuting  $\gamma_5$* , Nucl. Phys. **B572** (2000) 387[hep-th/9905076].
- [47] J. Polchinski, *Renormalization And Effective Lagrangians*, Nucl. Phys. **B231** (1984) 269.
- [48] C. Bagnuls and C. Bervillier, *Exact renormalization group equations: an introductory review*, hep-th/0002034.
- [49] J.C. Butcher, Math. Comp. **26** (1972) 79.
- [50] C. Brouder, *Runge-Kutta methods and renormalization*, Eur. Phys. J. **C12** (2000) 521[hep-th/9904014].
- [51] D. J. Broadhurst and D. Kreimer, *Dyson-Schwinger tests of Padé-Borel resummation of anomalous dimensions*, MZ-TH/00-28, in preparation.
- [52] U.D. Jentschura, E.J. Weniger, G. Soff, *Asymptotic improvement of resummations and perturbative predictions in quantum field theory*, hep-ph/0005198.
- [53] T. Binoth and G. Heinrich, *An automatized algorithm to compute infrared divergent multi-loop integrals*, hep-ph/0004013.

- [54] V. A. Smirnov, *Problems of the strategy of regions*, Phys. Lett. **B465** (1999) 226[hep-ph/9907471].
- [55] F. Markopoulou, *An algebraic approach to coarse graining*, hep-th/0006199.
- [56] J. Glimm and A. Jaffe, *Positivity of the  $\phi^4$  in three dimensions Hamiltonian*, Fortschr. Phys. **21** (1973) 327.
- [57] G. Benfatto and G. Gallavotti, *Renormalization Group*, Princeton Univ. Press 1995.  
M. Salmhofer, *Renormalization: An Introduction*, Springer 1998.
- [58] D. Buchholz and R. Verch, *Scaling algebras and renormalization group in algebraic quantum field theory*, Rev. Math. Phys. **7** (1995) 1195[hep-th/9501063].
- [59] M. Dütsch and K. Fredenhagen, *Algebraic QFT, perturbation theory and the loop expansion*, hep-th/0001129.
- [60] A. Gerasimov, A. Morozov, K. Selivanov, *Bogoliubov's recursion and integrability of effective actions*, hep-th/0005053.
- [61] A. Mironov and A. Morozov, *On renormalization group in abstract QFT*, hep-th/0005280.
- [62] I. Chepelev, R. Roiban, *Convergence theorem for noncommutative Feynman graphs and renormalization*, hep-th/0008090.
- [63] I. Moerdijk, *On the Connes–Kreimer construction of Hopf algebras*, math-ph/9907010.
- [64] F. Panaite, *Relating the Connes–Kreimer and Grossman-Larson Hopf algebras built on rooted trees*, math.QA/0003074.
- [65] L. Foissy, *Finite dimensional comodules over the Hopf algebras of rooted trees*, Univ. Reims preprint July 2000.

# Perturbative Quantization of Gravity Theories

ZVI BERN\*

*Department of Physics*  
*UCLA, Los Angeles, CA 90095 USA*

We discuss relations between gravity and gauge theory tree amplitudes that follow from string theory. Together with  $D$ -dimensional unitarity, these relations can be used to perturbatively quantize gravity theories, i.e. they contain the necessary information for calculating complete gravity  $S$ -matrices to any loop orders. This leads to a practical method for computing non-trivial gravity  $S$ -matrix elements by relating them to much simpler gauge theory ones. We also describe arguments that  $N = 8$   $D = 4$  supergravity is less divergent in the ultraviolet than previously thought.

Presented at the

5th International Symposium on Radiative Corrections  
(RADCOR-2000)

Carmel CA, USA, 11–15 September, 2000

---

\*Work supported by the US Department of Energy under grant DE-FG03-91ER40662.

# 1 Introduction

In this talk we review work [1,2,3,4,5] that exploits perturbative relations between gravity and gauge theories. Although both theories have a local symmetry, their dynamical behaviors are quite different. Nevertheless, in the context of perturbation theory, it turns out that tree-level gravity amplitudes can, roughly speaking, be expressed as a sum of products of gauge theory amplitudes. These tree-level relations between gravity and gauge theory S-matrices are rather remarkable from a conventional Lagrangian or Hamiltonian point of view but can be most easily understood from the Kawai, Lewellen and Tye (KLT) [6] relations between open and closed string tree amplitudes. When combined with the  $D$ -dimensional unitarity methods described in refs. [7,8], it provides a new tool for investigating the ultra-violet behavior of quantum gravity. (The unitarity methods have also been applied to QCD loop computations of phenomenological interest and to supersymmetric gauge theory computations [7,9,10].)

Ultraviolet properties are a central issue for perturbative gravity. Although gravity is non-renormalizable by power counting, no divergence has, in fact, been established by a direct calculation for any four-dimensional supersymmetric theory of gravity. Explicit calculations have established that non-supersymmetric theories of gravity with matter generically diverge at one loop [11,12,13], and pure gravity diverges at two loops [14]. However, in any supergravity theory in  $D = 4$ , supersymmetry Ward identities [15] forbid all possible one-loop [16] and two-loop [17] counterterms. Thus, at least a three-loop calculation is required to directly address the question of divergences in four-dimensional supergravity. There is a candidate counterterm at three loops for all supergravities including the maximally extended version ( $N = 8$ ) [18,19]. However, no explicit three loop (super) gravity calculations have appeared. It is in principle possible that the coefficient of a potential counterterm can vanish, especially if the full symmetry of the theory is taken into account. Based on explicit calculation, we shall argue that this is indeed the case for the potential three-loop counterterm of  $N = 8$  supergravity.

With traditional perturbative approaches [20] to performing explicit calculations, as the number of loops increases the number of algebraic terms proliferates rapidly beyond the point where computations are practical. We will take a different approach, relying instead on a new formalism for perturbatively quantizing gravity.

## 2 Method for Investigating Perturbative Gravity

Our reformulation of quantum gravity is based on two ingredients:

1. The Kawai, Lewellen and Tye relations between closed and open string tree-level S-matrices [6].

2. The observation that the  $D$ -dimensional tree amplitudes contain all information necessary for building the complete perturbative  $S$ -matrix to any loop order [7,8].

## 2.1 The KLT tree-level relations.

In the field theory limit ( $\alpha' \rightarrow 0$ ) the KLT relations for the four- and five-point amplitudes are [6,21]

$$\begin{aligned} M_4^{\text{tree}}(1, 2, 3, 4) &= -i s_{12} A_4^{\text{tree}}(1, 2, 3, 4) A_4^{\text{tree}}(1, 2, 4, 3), \\ M_5^{\text{tree}}(1, 2, 3, 4, 5) &= i s_{12} s_{34} A_5^{\text{tree}}(1, 2, 3, 4, 5) A_5^{\text{tree}}(2, 1, 4, 3, 5) \\ &\quad + i s_{13} s_{24} A_5^{\text{tree}}(1, 3, 2, 4, 5) A_5^{\text{tree}}(3, 1, 4, 2, 5), \end{aligned} \quad (1)$$

where the  $M_n$ 's are the amplitudes in a gravity theory stripped of couplings, the  $A_n$ 's are the color-ordered gauge theory sub-amplitudes also stripped of couplings and  $s_{ij} \equiv (k_i + k_j)^2$ . We suppress all  $\varepsilon_j$  polarizations and  $k_j$  momenta, but keep the 'j' labels to distinguish the external legs. Full gauge theory amplitudes are given in terms of the partial amplitudes  $A_n$ , via

$$\mathcal{A}_n^{\text{tree}}(1, 2, \dots, n) = g^{(n-2)} \sum_{\sigma \in S_n/Z_n} \text{Tr}(T^{a_{\sigma(1)}} \dots T^{a_{\sigma(n)}}) A_n^{\text{tree}}(\sigma(1), \dots, \sigma(n)),$$

where  $S_n/Z_n$  is the set of all permutations, but with cyclic rotations removed, and  $g$  is the gauge theory coupling constant. The  $T^{a_i}$  are fundamental representation matrices for the Yang-Mills gauge group  $SU(N_c)$ , normalized so that  $\text{Tr}(T^a T^b) = \delta^{ab}$ . For states coupling with the strength of gravity, the full amplitudes including the gravitational coupling constant are,

$$\mathcal{M}_n^{\text{tree}}(1, \dots, n) = \left(\frac{\kappa}{2}\right)^{(n-2)} M_n^{\text{tree}}(1, \dots, n),$$

where  $\kappa^2 = 32\pi G_N$ . The KLT equations generically hold for any closed string states, using their Fock space factorization into pairs of open string states.

Berends, Giele and Kuijf [21] exploited the KLT relations (1) and their  $n$ -point generalizations to obtain an infinite set of maximally helicity violating (MHV) graviton tree amplitudes, using the known MHV Yang-Mills amplitudes [22]. Cases of gauge theory coupled to gravity have recently been discussed in ref. [5]. Interestingly, the color charges associated with any gauge fields appearing in gravity theories are represented through the KLT equations as flavor charges carried either by scalars or fermions. For example, by applying the KLT equations the three-gluon one-graviton amplitude may be expressed as

$$\begin{aligned} \mathcal{M}_4^{\text{tree}}(1_g^-, 2_g^-, 3_g^+, 4_h^+) &= -i g \frac{\kappa}{2} s_{12} A_4^{\text{tree}}(1_g^-, 2_g^-, 3_g^+, 4_h^+) \times A_4^{\text{tree}}(1_s, 2_s, 4_g^+, 3_s) \\ &= g \frac{\kappa}{2} \frac{\langle 12 \rangle^4}{\langle 12 \rangle \langle 23 \rangle \langle 34 \rangle \langle 41 \rangle} \times \sqrt{2} f^{a_1 a_2 a_3} \frac{[43] \langle 32 \rangle}{\langle 24 \rangle}, \end{aligned}$$

where the  $\pm$  superscripts denote the helicities and the subscripts  $h, g$  and  $s$  denote whether a given leg is a graviton, gluon or scalar. On the right-hand side of the equation, the group theory indices are flavor indices for the scalars. On the left-hand side they are reinterpreted as color indices for gluons. For simplicity, the amplitudes have been expressed in terms of  $D = 4$  spinor inner products (see e.g. ref. [23]), although the factorization of the amplitude into purely gauge theory amplitudes holds in any dimension. The spinor inner products are denoted by  $\langle i j \rangle = \langle i^- | j^+ \rangle$  and  $[i j] = \langle i^+ | j^- \rangle$ , where  $|i^\pm\rangle$  are massless Weyl spinors of momentum  $k_i$ , labeled with the sign of the helicity. They are antisymmetric, with norm  $|\langle i j \rangle| = |[i j]| = \sqrt{s_{ij}}$ .

## 2.2 Cut Construction of Loop Amplitudes

We now outline the use of the KLT relations for computing multi-loop gravity amplitudes, starting from gauge theory amplitudes. Although the KLT equations hold only at the classical tree-level,  $D$ -dimensional unitarity considerations can be used to extend them to the quantum level. The application of  $D$ -dimensional unitarity has been extensively discussed for the case of gauge theory amplitudes [7,8], so here we describe it only briefly.

The unitarity cuts of a loop amplitude can be expressed in terms of amplitudes containing fewer loops. For example, the two-particle cut of a one-loop four-point amplitude in the channel carrying momentum  $k_1 + k_2$ , as shown in fig. 1, can be expressed as the cut of,

$$\sum_{\text{states}} \int \frac{d^D L_1}{(4\pi)^D} \frac{i}{L_1^2} \mathcal{M}_4^{\text{tree}}(-L_1, 1, 2, L_3) \frac{i}{L_3^2} \mathcal{M}_4^{\text{tree}}(-L_3, 3, 4, L_1) \Big|_{\text{cut}}, \quad (2)$$

where  $L_3 = L_1 - k_1 - k_2$ , and the sum runs over all states crossing the cut. We label  $D$ -dimensional momenta with capital letters and four-dimensional ones with lower case. We apply the on-shell conditions  $L_1^2 = L_3^2 = 0$  to the amplitudes appearing in the cut even though the loop momentum is unrestricted; only functions with a cut in the given channel under consideration are reliably computed in this way.

Complete amplitudes are found by combining all cuts into a single function with the correct cuts in all channels. If one works with an arbitrary dimension  $D$  in

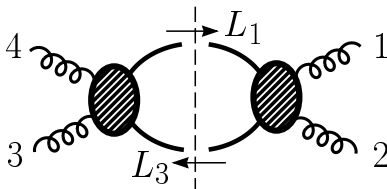


Figure 1: The two-particle cut at one loop in the channel carrying momentum  $k_1 + k_2$ .

eq. (2), and takes care to keep the full analytic behavior as a function of  $D$ , then the results will be free of subtraction ambiguities that are commonly present in cutting methods [24,7,8]. (The regularization scheme dependence remains, of course.) An advantage of the cutting approach is that the gauge-invariant amplitudes on either side of the cut may be simplified before attempting to evaluate the cut integral [8].

### 3 Recycling Gauge Theory Into Gravity Loop amplitudes

As a relatively simple example, consider the one-loop amplitude with four identical helicity external gravitons and a scalar in the loop [2,3]. The cut in the  $s_{12}$  channel is

$$\int \frac{d^D L_1}{(2\pi)^D} \frac{i}{L_1^2} M_4^{\text{tree}}(-L_1^s, 1_h^+, 2_h^+, L_3^s) \frac{i}{L_3^2} M_4^{\text{tree}}(-L_3^s, 3_h^+, 4_h^+, L_1^s) \Big|_{\text{cut}}, \quad (3)$$

where the superscript  $s$  indicates that the cut lines are scalars and the subscript  $h$  indicates that the external particles are gravitons. Using the KLT expressions (1) we may replace the gravity tree amplitudes appearing in the cuts with products of gauge theory amplitudes. The required gauge theory tree amplitudes, with two external scalar legs and two gluons, are relatively simple to obtain using Feynman diagrams and are,

$$A_4^{\text{tree}}(-L_1^s, 1_g^+, 2_g^+, L_3^s) = i \frac{\mu^2 [12]}{\langle 12 \rangle [(\ell_1 - k_1)^2 - \mu^2]},$$

$$A_4^{\text{tree}}(-L_1^s, 1_g^+, L_3^s, 2_g^+) = -i \frac{\mu^2 [12]}{\langle 12 \rangle} \left[ \frac{1}{(\ell_1 - k_1)^2 - \mu^2} + \frac{1}{(\ell_1 - k_2)^2 - \mu^2} \right],$$

where  $L_1 = \ell_1 + \mu$ , where the subscript  $g$  means the lines are gluons. The gluon momenta are four-dimensional, but the scalar momenta are allowed to have a  $(-2\epsilon)$ -dimensional component  $\vec{\mu}$ , with  $\vec{\mu} \cdot \vec{\mu} = \mu^2 > 0$ . The overall factor of  $\mu^2$  appearing in these tree amplitudes means that they vanish in the four-dimensional limit, in accord with a supersymmetry Ward identity [15]. In the KLT relation (1), one of the propagators cancels, leaving

$$M_4^{\text{tree}}(-L_1^s, 1_h^+, 2_h^+, L_3^s) = -i \left( \frac{\mu^2 [12]}{\langle 12 \rangle} \right)^2 \left[ \frac{1}{(\ell_1 - k_1)^2 - \mu^2} + \frac{1}{(\ell_1 - k_2)^2 - \mu^2} \right].$$

By symmetry, the tree amplitudes appearing in any of the other cuts are the same up to relabelings. We then inserting these trees, with appropriate leg labels, into the cut (3).

After combining all three cuts into a single function that has the correct cuts in

all channels one obtains the one-loop graviton amplitude with a scalar in the loop,

$$M_4^{1\text{-loop}}(1_h^+, 2_h^+, 3_h^+, 4_h^+) = 2 \frac{[12]^2 [34]^2}{\langle 12 \rangle^2 \langle 34 \rangle^2} \left( \mathcal{I}_4^{1\text{-loop}}[\mu^8](s, t) + \mathcal{I}_4^{1\text{-loop}}[\mu^8](s, u) + \mathcal{I}_4^{1\text{-loop}}[\mu^8](t, u) \right), \quad (4)$$

where  $s = s_{12}$ ,  $t = s_{14}$ ,  $u = s_{13}$  are the usual Mandelstam variables and

$$\mathcal{I}_4^{1\text{-loop}}[\mathcal{P}](s, t) = \int \frac{d^D L}{(2\pi)^D} \frac{\mathcal{P}}{L^2(L-k_1)^2(L-k_1-k_2)^2(L+k_4)^2} \quad (5)$$

is the scalar box integral depicted in fig. 2 with the external legs arranged in the order 1234. In eq. (4) the numerator  $\mathcal{P}$  is  $\mu^8$ . The two other scalar integrals that appear correspond to the two other distinct orderings of the four external legs. The spinor factor  $[12]^2 [34]^2 / (\langle 12 \rangle^2 \langle 34 \rangle^2)$  in eq. (4) is actually completely symmetric, although not manifestly so. By rewriting this factor and extracting the leading  $\mathcal{O}(\epsilon^0)$  contribution from the integral, the final one-loop  $D = 4$  result after reinserting the gravitational coupling is

$$\mathcal{M}_4^{1\text{-loop}}(1_h^+, 2_h^+, 3_h^+, 4_h^+) = -\frac{i}{(4\pi)^2} \left(\frac{\kappa}{2}\right)^4 \left(\frac{st}{\langle 12 \rangle \langle 23 \rangle \langle 34 \rangle \langle 41 \rangle}\right)^2 \frac{s^2 + t^2 + u^2}{120}, \quad (6)$$

in agreement with a previous calculation [25].

## 4 Maximal Supergravity

Maximal  $N = 8$  supergravity can be expected to be the least divergent of the four-dimensional supergravity theories due to its high degree of symmetry. Moreover, from a technical viewpoint maximally supersymmetric  $N = 8$  amplitudes are by far the easiest to deal with in our formalism because of spectacular supersymmetric cancellations. For these reasons it is logical to re-investigate the divergence properties of this theory first [1]. It should be possible to apply similar methods to theories with less supersymmetry.

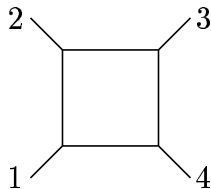


Figure 2: The one loop box integral.

## 4.1 Cut Construction

Again we obtain supergravity amplitudes by recycling gauge theory calculations. For the  $N = 8$  case, we factorize each of the 256 states of the multiplet into a tensor product of  $N = 4$  super-Yang-Mills states. The key equation for obtaining the two-particle cuts is,

$$\begin{aligned}
\sum_{\substack{N=8 \\ \text{states}}} M_4^{\text{tree}}(-L_1, 1, 2, L_3) \times M_4^{\text{tree}}(-L_3, 3, 4, L_1) \\
= s^2 \sum_{\substack{N=4 \\ \text{states}}} A_4^{\text{tree}}(-L_1, 1, 2, L_3) \times A_4^{\text{tree}}(-L_3, 3, 4, L_1) \\
\times \sum_{\substack{N=4 \\ \text{states}}} A_4^{\text{tree}}(L_3, 1, 2, -L_1) \times A_4^{\text{tree}}(L_1, 3, 4, -L_3),
\end{aligned} \tag{7}$$

where we have suppressed the particle labels. The external labels are those for any particles in the supermultiplet, while the sum on the left-hand side runs over all states in the  $N = 8$  super-multiplet. On the right-hand side the two sums run over the states of the  $N = 4$  super-Yang-Mills multiplet: a gluon, four Weyl fermions and six real scalars. Given the corresponding  $N = 4$  Yang-Mills two-particle sewing equation [9],

$$\begin{aligned}
\sum_{\substack{N=4 \\ \text{states}}} A_4^{\text{tree}}(-L_1, 1, 2, L_3) \times A_4^{\text{tree}}(-L_3, 3, 4, L_1) \\
= -ist A_4^{\text{tree}}(1, 2, 3, 4) \frac{1}{(L_1 - k_1)^2} \frac{1}{(L_3 - k_3)^2},
\end{aligned}$$

it is a simple matter to evaluate eq. (7), yielding

$$\begin{aligned}
\sum_{\substack{N=8 \\ \text{states}}} M_4^{\text{tree}}(-L_1, 1, 2, L_3) \times M_4^{\text{tree}}(-L_3, 3, 4, L_1) \\
= istu M_4^{\text{tree}}(1, 2, 3, 4) \left[ \frac{1}{(L_1 - k_1)^2} + \frac{1}{(L_1 - k_2)^2} \right] \\
\times \left[ \frac{1}{(L_3 - k_3)^2} + \frac{1}{(L_3 - k_4)^2} \right].
\end{aligned} \tag{8}$$

The sewing equations for the  $t$  and  $u$  channels are similar.

A remarkable feature of the cutting equation (8) is that the external-state dependence of the right-hand side is entirely contained in the tree amplitude  $M_4^{\text{tree}}$ . This fact allows us to iterate the two-particle cut algebra to *all* loop orders! Although this is not sufficient to determine the complete multi-loop four-point amplitudes, it does provide a wealth of information.

Applying eq. (8) at one loop to each of the three channels yields the one-loop four

graviton amplitude of  $N = 8$  supergravity,

$$\begin{aligned} \mathcal{M}_4^{1\text{-loop}}(1, 2, 3, 4) &= -i\left(\frac{\kappa}{2}\right)^4 stuM_4^{\text{tree}}(1, 2, 3, 4) \\ &\times \left(\mathcal{I}_4^{1\text{-loop}}(s, t) + \mathcal{I}_4^{1\text{-loop}}(s, u) + \mathcal{I}_4^{1\text{-loop}}(t, u)\right), \end{aligned}$$

in agreement with previous results [26]. We have reinserted the gravitational coupling  $\kappa$  in this expression. The scalar integrals are defined in eq. (5) with  $\mathcal{P} = 1$ .

At two loops, the two-particle cuts are given by a simple iteration of the one-loop calculation. The three-particle cuts can be obtained by recycling the corresponding cuts for the case of  $N = 4$  super-Yang-Mills. It turns out that the three-particle cuts introduce no other functions than those already detected in the two-particle cuts. Combining all the cuts into a single function yields the  $N = 8$  supergravity two-loop amplitude [1],

$$\begin{aligned} \mathcal{M}_4^{2\text{-loop}}(1, 2, 3, 4) &= \left(\frac{\kappa}{2}\right)^6 stuM_4^{\text{tree}}(1, 2, 3, 4) \\ &\times \left(s^2 \mathcal{I}_4^{2\text{-loop,P}}(s, t) + s^2 \mathcal{I}_4^{2\text{-loop,P}}(s, u) \right. \\ &\left. + s^2 \mathcal{I}_4^{2\text{-loop,NP}}(s, t) + s^2 \mathcal{I}_4^{2\text{-loop,NP}}(s, u) + \text{cyclic}\right), \end{aligned} \quad (9)$$

where ‘+ cyclic’ instructs one to add the two cyclic permutations of legs (2,3,4), and  $\mathcal{I}_4^{2\text{-loop,P/NP}}$  are depicted in fig. 3.

We comment that using the two-loop amplitude (9), Green, Kwon and Vanhove [27] provided an explicit demonstration of the non-trivial M theory duality between  $D = 11$  supergravity and type II string theory.

## 4.2 Divergence Properties of $N = 8$ Supergravity

Though a momentum cutoff scheme leads to a one-loop divergence for  $N = 1$ ,  $D = 11$  supergravity, in dimensional regularization there are no one-loop divergences

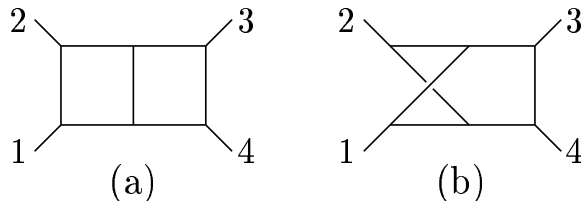


Figure 3: The planar (a) and non-planar (b) scalar integrals,  $\mathcal{I}_4^{2\text{-loop,P}}(s, t)$  and  $\mathcal{I}_4^{2\text{-loop,NP}}(s, t)$ , appearing in the two-loop  $N = 8$  amplitudes. Each internal line represents a scalar propagator.

in  $D = 11$ , so the first potential divergence in this theory is at two loops. Dimensional regularization is a rather convenient way to extract divergence properties as an analytic function of dimension, allowing us to directly relate properties of the  $N = 1$ ,  $D = 11$  supergravity to  $N = 8$   $D = 4$  supergravity. (Some care is needed, however, to preserve supersymmetry [28].)

Since the two-loop  $N = 8$  supergravity amplitude (9) has been expressed in terms of scalar  $\phi^3$  loop momentum integrals, it is straightforward to extract the divergence properties. The scalar integrals diverge only for  $D \geq 7$ ; hence the two-loop  $N = 8$  amplitude is manifestly finite in  $D = 5$  and 6, contrary to earlier expectations based on superspace power-counting arguments [19]. The discrepancy between the above explicit results and the earlier superspace power counting arguments is due to a previously unaccounted higher dimensional gauge symmetry. Once this symmetry is accounted for, superspace power counting gives the same degree of divergence as the explicit calculation [29].

The manifest  $D$ -independence of the cutting algebra allowed us to extend the calculation to  $D = 11$ , though there is no corresponding  $D = 11$  super-Yang-Mills theory. The result (9) then explicitly demonstrates that  $N = 1$   $D = 11$  supergravity diverges even when using dimensional regularization. The  $D = 11$  two-loop divergence may be extracted from the amplitude in eq. (9) yielding [1] a non-vanishing counterterm. Further work on the structure of the  $D = 11$  counterterm has been carried out in refs. [30].

Since the two-particle cut sewing equation iterates to all loop orders, one can compute all contributions which can be assembled solely from two-particle cuts [1]. Counting powers of loop momenta in these contributions suggests the simple finiteness formula,

$$L < \frac{10}{(D-2)}, \quad (\text{with } L > 1), \quad (10)$$

where  $L$  is the number of loops. This formula indicates that  $N = 8$  supergravity is finite in some other cases where the previous superspace bounds suggest divergences [19], e.g.  $D = 4$ ,  $L = 3$ . The first  $D = 4$  counterterm detected via the two-particle cuts of four-point amplitudes occurs at five, not three loops. Further evidence that the finiteness formula is correct stems from the maximally helicity violating contributions to  $m$ -particle cuts, in which the same supersymmetry cancellations occur as for the two-particle cuts [1]. Moreover, a recent superspace power counting analysis taking the appropriate symmetries into account confirms the finiteness bound [29]. Further work would, however, be required to prove that there are no additional hidden cancellations which could improve the finiteness condition beyond eq. (10). Interestingly, there has been a suggestion by Chalmers that dualities might accomplish this [31].

## 5 Concluding Comments

There are also a number of other interesting open questions. For example, the methods described here have been used to investigate only maximal supergravity. It would be interesting to systematically re-examine the divergence structure of non-maximal theories. (Some interesting recent work on this may be found in ref. [32].) Using the methods described in this talk it might, for example, be possible to systematically determine finiteness conditions order-by-order in the loop expansion. A direct derivation of the Kawai-Lewellen-Tye decomposition of gravity amplitudes in terms of gauge theory ones starting from the Einstein-Hilbert Lagrangian perhaps might lead to a useful reformulation of gravity. Some initial steps to gain an understanding of the Kawai-Lewellen-Tye relations, starting from the Lagrangian was presented in ref. [4]. (See also ref. [33].) Connected with this is the question of whether the heuristic notion that gravity is the square of gauge theory can be given meaning outside of perturbation theory. In particular, an intriguing question is whether it is possible to relate more general solutions of the classical equations of motion for gravity to those for gauge theory.

## Acknowledgments

The research reported on here was supported by the US Department of Energy under grants DE-FG03-91ER40662, DE-AC03-76SF00515 and DE-FG02-97ER41029. The work was performed in collaborations with L. Dixon, D. Dunbar, A.K. Grant, M. Perelstein, and J. Rozowsky. An expanded version of this talk appears in the proceedings of the Third Meeting on Constrained Dynamics and Quantum Gravity, Villasimius (Sardinia, Italy) September 13-17, 1999.

## References

- [1] Z. Bern, L. Dixon, D. C. Dunbar, M. Perelstein and J. S. Rozowsky, Nucl. Phys. B **530**, 401 (1998) [hep-th/9802162].
- [2] Z. Bern, L. Dixon, M. Perelstein and J. S. Rozowsky, Phys. Lett. B **444**, 273 (1998) [hep-th/9809160].
- [3] Z. Bern, L. Dixon, M. Perelstein and J. S. Rozowsky, Nucl. Phys. B **546**, 423 (1999) [hep-th/9811140].
- [4] Z. Bern and A. K. Grant, Phys. Lett. B **457**, 23 (1999) [hep-th/9904026].

- [5] Z. Bern, A. De Freitas and H. L. Wong, Phys. Rev. Lett. **84**, 3531 (2000) [hep-th/9912033].
- [6] H. Kawai, D. C. Lewellen and S. H. Tye, Nucl. Phys. B **269**, 1 (1986).
- [7] Z. Bern, L. Dixon, D. C. Dunbar and D. A. Kosower, Nucl. Phys. B **425**, 217 (1994) [hep-ph/9403226]; Z. Bern, L. Dixon, D. C. Dunbar and D. A. Kosower, Nucl. Phys. B **435**, 59 (1995) [hep-ph/9409265]; Z. Bern and A. G. Morgan, Nucl. Phys. B **467**, 479 (1996) [hep-ph/9511336]; Z. Bern, L. Dixon, D. A. Kosower and S. Weinzierl, Nucl. Phys. B **489**, 3 (1997) [hep-ph/9610370]; Z. Bern, L. Dixon and D. A. Kosower, Nucl. Phys. B **513**, 3 (1998) [hep-ph/9708239]; J. S. Rozowsky, hep-ph/9709423.
- [8] Z. Bern, L. Dixon and D. A. Kosower, Ann. Rev. Nucl. Part. Sci. **46**, 109 (1996) [hep-ph/9602280].
- [9] Z. Bern, J. S. Rozowsky and B. Yan, Phys. Lett. B **401**, 273 (1997) [hep-ph/9702424]; in Proceedings of the 5th International Workshop on Deep Inelastic Scattering and QCD (DIS 97), Chicago, IL, 14-18 Apr 1997, [hep-ph/9706392]
- [10] Z. Bern, L. Dixon and D. A. Kosower, JHEP**0001**, 027 (2000) [hep-ph/0001001].
- [11] G. 't Hooft and M. Veltman, Annales Poincare Phys. Theor. A **20**, 69 (1974).
- [12] G. 't Hooft, Nucl. Phys. B **62**, 444 (1973).
- [13] S. Deser and P. van Nieuwenhuizen, Phys. Rev. D **10**, 401 (1974). Phys. Rev. D **10**, 411 (1974). S. Deser, H. Tsao and P. van Nieuwenhuizen, Phys. Rev. D **10**, 3337 (1974).
- [14] M. H. Goroff and A. Sagnotti, Phys. Lett. B **160**, 81 (1985); Nucl. Phys. B **266**, 709 (1986); A. E. van de Ven, Nucl. Phys. B **378**, 309 (1992).
- [15] M. T. Grisaru, H. N. Pendleton and P. van Nieuwenhuizen, Phys. Rev. D **15**, 996 (1977); M. T. Grisaru and H. N. Pendleton, Nucl. Phys. B **124**, 81 (1977); S. J. Parke and T. R. Taylor, Phys. Lett. B **157**, 81 (1985).
- [16] M. T. Grisaru, P. van Nieuwenhuizen and J. A. Vermaseren, Phys. Rev. Lett. **37**, 1662 (1976).
- [17] M. T. Grisaru, Phys. Lett. B **66**, 75 (1977). E. Tomboulis, Phys. Lett. B **67**, 417 (1977).
- [18] R. E. Kallosh, Phys. Lett. B **99**, 122 (1981).

- [19] S. Deser, J. H. Kay and K. S. Stelle, Phys. Rev. Lett. **38**, 527 (1977). P. S. Howe, K. S. Stelle and P. K. Townsend, Nucl. Phys. B **191**, 445 (1981). P. S. Howe and K. S. Stelle, Phys. Lett. B **137**, 175 (1984); Int. J. Mod. Phys. A **4**, 1871 (1989).
- [20] B.S. DeWitt, Phys. Rev. **162** 1239 (1967); M. Veltman, in Les Houches 1975, Proceedings, Methods In Field Theory (Amsterdam 1976).
- [21] F. A. Berends, W. T. Giele and H. Kuijf, Phys. Lett. B **211**, 91 (1988).
- [22] S. J. Parke and T. R. Taylor, Phys. Rev. Lett. **56**, 2459 (1986).
- [23] M. L. Mangano and S. J. Parke, Phys. Rept. **200**, 301 (1991). L. Dixon, in Proceedings of Theoretical Advanced Study Institute in Elementary Particle Physics (TASI 95), ed. D.E. Soper, hep-ph/9601359.
- [24] W. L. van Neerven, Nucl. Phys. B **268**, 453 (1986).
- [25] D. C. Dunbar and P. S. Norridge, Nucl. Phys. B **433**, 181 (1995) [hep-th/9408014]; D. C. Dunbar and P. S. Norridge, Class. Quant. Grav. **14**, 351 (1997) [hep-th/9512084].
- [26] M. B. Green, J. H. Schwarz and L. Brink, Nucl. Phys. B **198**, 474 (1982).
- [27] M. B. Green, H. Kwon and P. Vanhove, Phys. Rev. D **61**, 104010 (2000) [hep-th/9910055].
- [28] W. Siegel, Phys. Lett. B **84**, 193 (1979); D. M. Capper, D. R. Jones and P. van Nieuwenhuizen, Nucl. Phys. B **167**, 479 (1980).
- [29] K.S. Stelle, private communication.
- [30] S. Deser and D. Seminara, Phys. Rev. Lett. **82**, 2435 (1999) [hep-th/9812136]. Phys. Rev. D **62**, 084010 (2000) [hep-th/0002241]; Z. Bern *et al.*, hep-th/0012230.
- [31] G. Chalmers, hep-th/0008162.
- [32] D. C. Dunbar, B. Julia, D. Seminara and M. Trigiante, JHEP**0001**, 046 (2000) [hep-th/9911158].
- [33] W. Siegel, Phys. Rev. D **47**, 5453 (1993) [hep-th/9302036]; W. Siegel, Phys. Rev. D **48**, 2826 (1993) [hep-th/9305073]. W. Siegel, in Proceedings of Strings 1993, eds. M.B. Halpern, A. Sevrin and G. Rivlis (World Scientific, Singapore, 1994), [hep-th/9308133].

OPAL Conference Report CR460  
September 7, 2001  
hep-ex/0101015

# Searches at LEP

Tom Junk

*Carleton University*  
*1125 Colonel By Drive, Ottawa, Canada K1S 5B6*

## Abstract

Searches have been conducted for a broad range of new phenomena by the four experiments ALEPH, DELPHI, L3, and OPAL, at LEP2. Each experiment contributes approximately  $150 \text{ pb}^{-1}$  of  $e^+e^-$  annihilation data with a mean  $\sqrt{s}$  of 205.9 GeV in 2000 to these searches (data prepared for the September 5 LEPC meeting). The statistical procedure for setting limits and evaluating the significance of excesses observed in the data is reviewed. Search results are presented for the Standard Model Higgs boson, the neutral Higgs bosons in the MSSM, charged Higgs bosons, invisibly decaying Higgs bosons produced by Higgs-strahlung, and fermiophobic Higgs bosons. Search results are briefly summarized for gauginos, stops, and staus. The photon recoil spectrum is checked for hints of new physics.

Results presented here have been prepared by the four LEP Collaborations, ALEPH, DELPHI, L3, and OPAL, and by the LEP Higgs and SUSY working groups, for presentation at the September 5 open meeting of the LEP experiments committee (LEPC).

Presented at the 5<sup>th</sup> International Symposium on  
Radiative Corrections  
Carmel, California, September 11–15, 2000

# 1 Introduction

In 1995, LEP finished taking large samples of data on the  $Z^0$  resonance and began a program of increasing the beam energy in order to study in detail known phenomena at higher energies and to search for new particles and interactions. The very highest beam energies were reached in 2000, and in that year each experiment collected  $\approx 150 \text{ pb}^{-1}$  of  $e^+e^-$  annihilation data at an average  $\sqrt{s}$  of approximately 205.9 GeV for inclusion in the results presented at the September 5, 2000 meeting of the LEP Experiments Committee (LEPC). In addition, the searches for the SM and MSSM Higgs bosons were combined by the LEP Higgs Working Group and shown at the LEPC meeting and are summarized here. The search for a neutral Higgs boson produced in association with a  $Z^0$  boson is emphasized here because of recent interest generated by excess events observed by the ALEPH collaboration in the summer of 2000. In addition, a brief selection of searches for supersymmetric particles is given, and a summary of the running strategy for the rest of 2000 is presented.

The main Standard Model backgrounds for the searches described here are

- Two-photon processes,  $e^+e^- \rightarrow e^+e^-\bar{f}f$ , where the  $\bar{f}f$  pair has a very low invariant mass and is produced in  $t$ -channel exchange of two photons.
- Radiative returns to the  $Z^0$ . Initial state radiation (ISR) reduces the effective  $\sqrt{s}$  to the  $Z^0$  pole energy and produces boosted  $Z^0$  events. The photon usually escapes down the beampipe, but may be observed, and the probability of two hard photons increases with increasing  $\sqrt{s}$ . These events are backgrounds to analyses requiring missing energy, and electromagnetic coverage is needed very close to the beam axis in order to suppress this background to searches requiring missing transverse momentum.
- W-pair production  $e^+e^- \rightarrow W^+W^-$ . These produce four-jet final states, or jets+a lepton+missing energy, or two leptons and missing energy. The last is classified as an “acoplanar dilepton” because the plane containing the two leptons does not in general contain the beam axis. Very few b quarks are produced in W decay and so this background can be suppressed in Higgs searches with b-tags with good background rejection. Searches for acoplanar dileptons have  $W^+W^-$  production as an

irreducible background in some kinematic regions, while the two-photon background dominates in other regions.

- Z-pair production,  $e^+e^- \rightarrow Z^0Z^0$ . These events may have four jets, two jets and missing energy, two jets and two like-flavor but opposite-sign leptons, four leptons, or two leptons and missing energy. They have a high b quark content and constitute a primary irreducible background to Higgs boson searches.
- Single W production,  $e^+e^- \rightarrow W^+e^-\bar{\nu}_e$ . This can produce jets+missing energy (“acoplanar dijets”), jets+a forward electron, or a lepton+missing energy or a lepton+a forward electron+missing energy.
- Single Z production  $e^+e^- \rightarrow Z^0e^+e^-$ . This process can produce acoplanar dijets or acoplanar dileptons if the electrons are not detected. One or both of the electrons may be detected however.

## 2 Statistical Procedure

A single procedure is used by the four experiments and by the LEP Higgs and SUSY working groups to determine whether a model of new physics is excluded by LEP search data or if the background hypothesis is disfavored relative to a particular signal hypothesis. The procedure begins with a full specification of the model to test, with the masses, production cross-sections, and decay branching ratios specified. If the model under test allows many possibilities for the parameters, then in general the parameters are scanned and excluded regions are given in the parameter space that is allowed. For a specific model with a specific choice of its free parameters, histograms of the expected signal, background, and data events are formed in variables that separate the expected signal from the expected background. Then all possible experimental outcomes are considered, and they are ordered according to those that are more signal-like (more candidate events in bins where a signal is expected), and those that are more background-like (fewer such candidates). The variable used for ordering the outcomes is the “likelihood ratio,” the ratio of the probability of observing the particular outcome in the signal+background hypothesis to the probability of observing the same

outcome in the background-only hypothesis:

$$Q = \frac{P_{poiss}(data|signal + background)}{P_{poiss}(data|background)}. \quad (1)$$

Each bin of each histogram may be considered as an independent counting experiment, and the Poisson probabilities multiply. The expression for  $\log Q$  is convenient for combinations of many bins in many experiments:

$$\log Q = \sum_i \left( n_i^{data} \log \left( 1 + \frac{s_i}{b_i} \right) - s_i \right), \quad (2)$$

where  $s_i$  is the signal estimation for a bin of a search channel,  $b_i$  is the background estimation,  $n_i^{data}$  is the number of observed data events, and the sum runs over all bins in all search channels. Some searches may have just one bin in them, while others may have some regions of histograms of measured variables with good separation of the signal from the background and other regions with poorer separation. Because  $\log Q$  reduces to a sum of event weights, events may be classified by the  $s/b$  in the bins in which they appear.

A particular value of  $\log Q$  will be obtained for each model hypothesis and the available data and background estimates. In order to determine whether an outcome is sufficient to exclude that model, the probability of obtaining that outcome in the signal+background hypothesis is computed:

$$CL_{s+b} = P(Q \leq Q_{obs}|signal + background). \quad (3)$$

If  $CL_{s+b} < 0.05$  then the signal+background hypothesis is ruled out at the 95% confidence level. Another important confidence level to compute is the consistency of the observation with the background hypothesis:

$$CL_b = P(Q \leq Q_{obs}|background), \quad (4)$$

which is the probability of having observed no more than was observed, if only background processes contribute. This variable is used as the “discovery” variable, requiring  $1 - CL_b < 5.7 \times 10^{-7}$  in order to claim a  $5\sigma$  discovery. These confidence levels may be computed using Monte Carlo techniques [1], or by various convolution methods [2], [3].

One defect of the  $CL_{s+b}$  variable is that it is a test of the signal+background hypothesis and not of just the signal hypothesis. A consequence of this is that

a deficit of selected events relative to the background estimation can rule out the background hypothesis alone, and therefore also any signal+background hypothesis, even if the signal is vanishingly small. In fact, this is expected to happen 5% of the time at the 95% confidence level. In order not to produce misleading limits or exclusions of parts of parameter space to which the experiments are not sensitive, the following quantity is used [1]:

$$CL_s = CL_{s+b}/CL_b, \quad (5)$$

which is expected to approach unity in the absence of sensitivity to a particular signal.

### 3 Standard Model Higgs Boson Searches

The Standard Model Higgs boson is expected to be produced in  $e^+e^-$  collisions mainly by the Higgs-strahlung process when it is kinematically allowed, and to a lesser extent by the  $W^+W^-$ -fusion process. The main attraction of the latter process is that its cross-section does not drop rapidly near  $\sqrt{s} - m_Z$ , although its total rate is very small. The total production cross-section near the kinematic edge is of the order of 50 to 500 fb, depending on how close  $m_H$  is to  $\sqrt{s} - m_Z$ . The Standard Model Higgs boson is expected to decay predominantly into  $b\bar{b}$  pairs in the mass range of interest, with a branching ratio of 78% at  $m_H=110$  GeV and a branching ratio of 74% at  $m_H=115$  GeV. The second most important decay mode is to tau pairs, with a branching ratio of approximately 7%, and the  $W^+W^-$  decays take 8%, which rises quickly with  $m_H$ . Decays to charm and gluons account for the remainder. Efficient and pure b-tagging is therefore important for search for Higgs bosons at LEP2. The Standard Model Higgs search channels are differentiated by the  $Z^0$  decay mode that they select. There is the four-jet channel ( $H^0 \rightarrow b\bar{b}, Z^0 \rightarrow q\bar{q}$ ), the missing-energy channel ( $H^0 \rightarrow b\bar{b}, Z^0 \rightarrow \nu\bar{\nu}$ ), the tau channels ( $H^0 \rightarrow b\bar{b}, Z^0 \rightarrow \tau^+\tau^-$  and  $H^0 \rightarrow \tau^+\tau^-, Z^0 \rightarrow q\bar{q}$ ), and the lepton channels ( $H^0 \rightarrow b\bar{b}, Z^0 \rightarrow e^+e^-$  or  $Z^0 \rightarrow \mu^+\mu^-$ ).

Precision electroweak measurements may be used to estimate the value of the Higgs boson mass, assuming the Standard Model framework for radiative corrections. The combined prediction of  $m_H$  is  $62^{+53}_{-39}$  GeV, where the errors are symmetric and Gaussian in the variable  $\log m_H$ , as reported at ICHEP 2000 [4]. This prediction changes, however, when  $\alpha_{EM}(m_Z)$  is computed

differently or computed using additional low-energy  $e^+e^- \rightarrow q\bar{q}$  cross-section data from BES.

In the absence of new particles and interactions, the mass of the Standard Model Higgs boson can be from approximately 140 GeV to 180 GeV, where the lower bound arises from a vacuum stability argument, and the upper bound from the requirement that the Higgs self-coupling remains finite at all energies. For new physics interactions with a scale of the order of a TeV, the Higgs boson mass is much less constrained by these arguments, lying between 50 to 800 GeV [5]. Fine tuning arguments [6], requiring that the magnitude of the radiative corrections to  $m_H$  are not too many orders of magnitude larger than  $m_H$  itself, further restrict the possible ranges of  $m_H$  although these restrictions are relaxed if new physics appears on the 1–10 TeV scale.

The combined distribution of the reconstructed masses in the four experiments' Standard Model Higgs boson searches is shown in Figure 1 for a fairly tight set of selection requirements [7]. Along with the background expectation and the observed data counts is shown the expected signal from a Higgs boson of mass 114 GeV. The contributions to the histogram are given by experiment in Table 1.

The distribution of the reconstructed mass and the the total number of selected events may be uninformative or misleading in several ways. The distribution of the reconstructed mass is summed over different experiments, and over different search channels at different center-of-mass energies. The reconstructed mass resolutions are different and depend on how close  $m_H$  is to the kinematic limit which changes with  $\sqrt{s}$ , and the relative amounts of the signal and background are different from channel to channel, depending on the background rates and signal branching ratios. In a summed histogram of the reconstructed mass, candidates in relatively clean channels are included in the same bins as signal and background estimates from other channels with poorer performance. Additional cuts have been applied after the standard analysis cuts in order that the contributions from the different experiments are roughly equal in their total size. If an experiment has a large amount of the expected signal just failing the cut needed to make the reconstructed mass distribution plot, it may be more sensitive than another experiment with more expected signal on its side of its cut. Because all bins of all histograms in all variables (each search channel from each experiment at each center of mass energy has its own histogram, and the variables can be the reconstructed mass, the b-tags, or combinations of these and other

information) can be combined using the uniform procedure outlined above, there is no loss of sensitivity in the confidence level calculations, but an amount of information is necessarily lost when producing a histogram of the reconstructed mass and tables listing its contents.

The full amount of information in the searches is retained and displayed in a compact form if the histograms are rebinned in the variable  $s/b$ . For each bin of each histogram to be combined, the  $s/b$  is uniquely determined. Because the test-statistic  $\log Q$  is additive and depends only on the  $s/b$  in the bins where the candidates are found and also on the total signal sum, the contents of bins with the same  $s/b$  may be simply added. The result is shown in Figure 2 along with its integral from the high  $s/b$  side [7]. The integral of this distribution at a particular cut in  $s/b$  is the optimal answer to “How many events are observed” and “How many are expected in the signal+background and the background-only hypotheses,” for each possible setting of the cuts.

One observes in this distribution three events with rather high values of the local  $s/b$ . These three are all four-jet candidates from ALEPH, with strong b-tags and high reconstructed masses [8]. The selection of these events and the stability of their assigned significance has been checked in several ways. A cut-based analysis is used to cross-check the primary neural-net-based analysis and similar results are obtained. All lower-energy data have been analyzed to look for biases in the reconstructed mass distribution towards a peak at the maximum kinematically allowed value, and no such bias is seen. The b-tag and neural net distributions also are modeled well [8]. One feature however, is that if all possible jet pairings are considered and events are removed if even one of these pairings yields jet-pair masses within 10 GeV of either  $m_W$  or  $m_Z$ , then the excess vanishes. It was found in a Monte Carlo study, however, that the signal efficiency drops by 50% by removing such events, and that this procedure does not enhance the separation of signal from background.

There is a small excess observed in the DELPHI four-jet channel, but not in the L3 or OPAL four-jet channels. Also, no excesses are observed in the combined missing-energy ( $Z^0 \rightarrow \nu\bar{\nu}$ ) channels, the lepton channels, or the tau channels. Combining all missing-energy, lepton, and tau channels together has about the same statistical power of all four-jet channels combined together.

The combined test-statistic is shown in Figure 3. It has a minimum at  $m_H=114-115$  GeV, and is the most compatible with the median expected

signal at  $m_H=114$  GeV. The confidence levels are used to quantify how significant this observation is.

The exclusion limit is computed by finding the lowest  $m_H$  for which  $CL_s = 0.05$ . It is computed for each experiment separately, and for each search channel separately, combining the results of the experiments. The expected limit is the median in a large ensemble of possible experiments in which only Standard Model background processes contribute. The value of  $CL_s$  and its expectation for the all channels combined from all experiments is shown in Figure 4. The exclusion limits are listed in Table 2. The branching ratios of the  $Z^0$  are well known and hence the separation by channel is not that interesting, except for the tau channel, which covers also Higgs boson decays to tau leptons.

In order to test for the compatibility of the observation with the expected background,  $1 - CL_b$  is shown as a function of the tested  $m_H$  in Figure 5.  $1 - CL_b$  reaches its minimum at  $m_H=115$  GeV, with a probability of consistency of the data with the background of  $7 \times 10^{-3}$ , for a significance of approximately  $2.6\sigma$ , due mainly to the excess four-jet events in ALEPH, but also to events with lower values of  $s/b$  which also contribute.

In the case that there is no signal truly present, the excess would take approximately  $60 \text{ pb}^{-1}$  per experiment at  $\sqrt{s} = 206.6$  GeV to fade away to a  $2\sigma$  excess for test mass hypotheses near 115 GeV. On the other hand, if the Higgs boson does have Standard Model couplings and branching fractions, then one would expect the significance of the excess to increase as more data are collected. As can be seen in Figure 6, it would take approximately  $100 \text{ pb}^{-1}$  of data at  $\sqrt{s} = 206.6$  GeV to obtain a  $4\sigma$  effect for  $m_H=113$  GeV, and around  $140 \text{ pb}^{-1}$  for  $m_H=114$  GeV. On the other hand, significances of  $3\sigma$  can be obtained within  $60 \text{ pb}^{-1}$  for  $m_H$  all the way up to 115 GeV, and that amount can be collected in approximately 60 days of running.

## 4 Searches for Non-Standard Higgs Bosons

### 4.1 Neutral Higgs Bosons in the MSSM

One of the simplest extensions to the Higgs sector of the Standard Model is to add a second Higgs field doublet. The Minimal Supersymmetric Extension of the SM (MSSM) requires this structure. One field couples to up-type quarks and the other to down-type quarks, and there is a mixing angle  $\alpha$

between these two fields in order to produce the physical Higgs states, which number five: the  $h^0$ , the  $A^0$ , the  $H^0$ , and two charged Higgs bosons  $H^+$  and  $H^-$ . The ratio of the vacuum expectation values of the two fields is denoted  $\tan\beta$ . In the CP-conserving, low-energy effective MSSM studied here [9], the remaining parameters are the mass of the  $A^0$ , the CP-odd Higgs boson (the other two neutral bosons are CP even), the mass scale of the sfermions  $M_{\text{SUSY}}$  (here set to 1 TeV), the Higgs mass matrix parameter  $\mu$  (here set to -200 GeV), the gaugino mass parameter  $M_2$  (here set to 200 GeV), and the amount of stop mixing, chosen here to be zero or maximal. Recent calculations of  $m_h$  including the dominant 2-loop terms are used [10]. The gluino mass is also a free parameter; it affects the Higgs masses and branching ratios through radiative corrections.

For the case of maximal stop mixing, and the choices of the other parameters given above, the value of  $m_h$  assumes its maximal value<sup>1</sup> as a function of  $\tan\beta$  and is used to set conservative limits on  $\tan\beta$ . This scenario is called the  $m_h$ -max scenario.

The searches used to set limits in this space are the same searches for the  $h^0Z^0$  final state used in the Standard Model section, but in addition, searches for  $h^0A^0$  are performed in the  $b\bar{b}b\bar{b}$  and  $b\bar{b}\tau^+\tau^-$  final states. The production cross-section for  $e^+e^- \rightarrow h^0A^0$  is proportional to  $\cos^2(\beta - \alpha)$ , which is largest for  $m_h \approx m_A$  while the cross-section for  $e^+e^- \rightarrow h^0Z^0$  is proportional to  $\sin^2(\beta - \alpha)$ . The cross-section for  $h^0A^0$  production grows more slowly along the diagonal  $m_h = m_A$  than the  $h^0Z^0$  cross-section does for large  $m_A$ . Therefore, the absolute lower limits on  $m_h$  will come from the case in which  $h^0Z^0$  production is suppressed, and the limits for  $m_A \rightarrow \infty$  are those obtained in the Standard Model, as can be seen from Figure 7.

For the case of no stop mixing, the maximal value of  $m_h$  as a function of  $\tan\beta$  is much less, although a second problem opens up at low  $\tan\beta$ : the branching ratio for  $h^0 \rightarrow b\bar{b}$  can be suppressed by a larger decay width for  $h^0 \rightarrow A^0A^0$ , and for low  $\tan\beta$  or low  $m_A$ , the decay rate of the  $A^0$  to  $b\bar{b}$  pairs is suppressed either by the coupling strength or the kinematics if  $m_A < 10$  GeV. In this case, an "L"-shaped unexcluded region opens up for low  $\tan\beta$  and low  $m_A$ , shown in Figure 8. Additional flavor-independent searches, and searches specifically targeted at this region are being developed and will

---

<sup>1</sup>Another calculation [11] using a renormalization-group improved one-loop calculation, does in fact give slightly higher values of  $m_h$  for  $\tan\beta < 1$ , but also smaller values of  $m_h$  for  $\tan\beta > 1$  – we choose the calculation which gives the lowest upper end of the excluded  $\tan\beta$  region.

soon be included in the combination. The limits on  $m_h$  and  $m_A$  presented in Table 3 ignore this unexcluded region, although the limits on  $\tan\beta$  in the no-stop-mixing scenario include its effects. In both the  $m_h$ -max scenario and the no stop mixing scenario,  $\tan\beta$  is considered only up to 30, because for larger values of  $\tan\beta$  the  $h^0$  decay width can exceed the experimental mass resolution, and additional Monte Carlo signal samples are needed to assess the effect of lower  $s/b$  in these channels.

A third scenario has been proposed, called the “large- $\mu$ ” scenario [9], in which  $M_{\text{SUSY}}$  is taken to be 400 GeV,  $M_2 = 400$  GeV,  $\mu = 1$  TeV, and the gluino mass is 200 GeV. This setting of parameters is designed to highlight loop effects which can suppress the decay  $h^0 \rightarrow b\bar{b}$ , without a corresponding enhancement of  $h^0 \rightarrow \tau^+\tau^-$ . In this case, the  $h^0$  decays rather into gluons, charmed quarks, or W pairs, but only for high  $\tan\beta$ . The decay widths of the  $h^0$  and the  $A^0$  remain much smaller than the experimental mass resolution up to  $\tan\beta = 50$ . The maximum value of  $m_h$  in this scenario is approximately 108 GeV, and for the region where  $\sin^2(\beta - \alpha)$  is low and  $m_h + m_A$  is kinematically out of reach at LEP2, the process  $e^+e^- \rightarrow H^0 Z^0$  is accessible with a cross-section proportional to  $\cos^2(\beta - \alpha)$ . Nearly all model points except those with difficult decay branching fractions can therefore be excluded. These difficult regions are at  $\tan\beta > 10$  and  $80 < m_A < 180$ , as seen in Figure 9.

## 4.2 Charged Higgs Bosons

At LEP, charged Higgs bosons are expected to be pair-produced via the  $s$ -channel exchange of a  $\gamma$  or a  $Z^0$ , and the production cross-section depends only on the mass of the  $H^\pm$  and on well-measured electroweak parameters. The decay modes of the  $H^\pm$  are considered for the purpose of these searches to be limited to  $q\bar{q}'$  and  $\tau\nu_\tau$ . The mass limits are produced therefore as a function of  $\text{Br}(H^+ \rightarrow \tau^+\nu_\tau)$ . The search channels include a four-jet search without b-tagging, a semileptonic search, and a fully leptonic search, in which the final state consists of an acoplanar pair of taus. The predominant background is  $e^+e^- \rightarrow W^+W^-$ , which can produce all of the available final states, although the acoplanar tau pair rate is significantly lower than the four-jet rate due to the branching ratios of the W. The large  $W^+W^-$  background sets the scale for the limits in the hadronic and semileptonic searches. The limits are shown in Figure 10. For  $\text{Br}(H^+ \rightarrow \tau^+\nu_\tau)=0$ , the observed mass limit is 80.5 GeV and the median expected limit is 79.8 GeV. For  $\text{Br}(H^+ \rightarrow \tau^+\nu_\tau)=1$ , the ob-

served mass limit is 89.2 GeV and the median expected limit is 90.9 GeV. The lowest limit obtained at any branching ratio is 78.7 GeV, with a median expectation of 78.5 GeV. A small excluded “island” appears in Figure 10 for  $\text{Br}(H^+ \rightarrow \tau^+ \nu_\tau) = 0$ , where the search sensitivity above the  $W^+W^-$  background peak is beginning to become sufficient to exclude a small region. More data would allow this island to grow and eventually connect with the main excluded region, leaving a hole near  $m_W$  which can be excluded only with a larger amount of integrated luminosity.

### 4.3 Searches for $H^0 \rightarrow \gamma\gamma$

The final states  $q\bar{q}\gamma\gamma$ ,  $\ell^+\ell^-\gamma\gamma$ , and  $\gamma\gamma$ +missing energy are sought by the four LEP experiments and combined. Because the branching ratio  $\text{Br}(H^0 \rightarrow \gamma\gamma)$  is small in the Standard Model (of the order  $10^{-3}$ ), mass limits cannot be set on the SM Higgs from this search only. This search is more interesting when considering models in which the  $H^0$  decays are non-standard. In particular, if the  $H^0$  fails to couple to fermions entirely, then the available decay modes are into  $\gamma\gamma$  and  $W^+W^-$ , the first of which proceeds only at the one-loop level mediated by a  $W$  boson. As the mass of the  $H^0$  increases, the  $W^+W^-$  branching fraction gradually becomes more important and the mass limits obtained at LEP2 are mainly determined by this behavior than by the power of the searches. The limits are expressed in Figure 11 by assuming the SM production cross-section for  $e^+e^- \rightarrow H^0Z^0$ , and by ignoring the results of searches for other decays of the  $H^0$  to set limits on the branching ratio  $\text{Br}(H^0 \rightarrow \gamma\gamma)$ . Alternatively, this can be interpreted as a limit on the production cross-section as a fraction of the SM cross-section, with  $\text{Br}(H^0 \rightarrow \gamma\gamma) = 1$ . In the fermiophobic model, the observed mass limit is 107.7 GeV, with a median expected limit of 105.8 GeV.

### 4.4 $h^0 \rightarrow$ Invisible Particles

The Higgs boson may decay invisibly in the MSSM if the lightest neutralino has a mass of less than half the mass of the Higgs. Two important advantages of an  $e^+e^-$  collider are that the center-of-mass energy of each interaction is known with a high degree of precision, and that the total momentum is zero. These features can be used to search for the process  $e^+e^- \rightarrow h^0Z^0$ , where the  $h^0$  decays invisibly, because the  $Z^0$  decay products can be measured and the missing mass can be inferred. In this case,  $Z^0$  decays to quarks are exploited

for the search. Neutrino decays are not useful, and the leptonic decays have a low relative branching ratio. Tau decays in particular pollute the leptonic sample because the neutrinos in such events carry a large amount of missing energy.

The limits are shown in Figure 12 assuming the Standard Model production cross-section and are limits on the invisible branching ratio of the Higgs, ignoring the results of searches for visible Higgs decays. Alternatively, these limits can be interpreted as limits on the production cross-section divided by the Standard Model production cross-section, assuming 100% invisible decays of the  $h^0$ . For the SM cross-section and 100% invisible decays, the mass limits obtained are 113.7 GeV (observed) and 112.8 GeV (median expectation).

## 5 Gaugino, Squark, Slepton Searches

Charginos may be produced either in the  $s$ -channel via photon or  $Z^0$  exchange, or in the  $t$ -channel via exchange of an electron sneutrino. These diagrams interfere destructively, although the  $t$ -channel diagram is important only for light electron sneutrinos. The chargino may decay into a  $W$  and a neutralino, or into a slepton and a neutrino, where the slepton decays into a neutralino and a lepton, or directly into a lepton and a sneutrino. All of these decay modes produce similar final states – two leptons (or jets) and missing energy. The branching ratios for these processes depend on the slepton and sneutrino masses, and the mass difference  $\Delta M$  between the chargino and the LSP (either the neutralino or sneutrino) strongly affects the final state kinematic distributions. For a small mass difference, the visible decay products of the chargino have low visible energies. These final states are similar to the two-photon background processes which have large cross-sections in  $e^+e^-$  collisions at high energies. For very large  $\Delta M$ , the final states resemble  $W^+W^-$  production. The search analyses are therefore optimized in separate regions of  $\Delta M$  due to the different makeup of the signal and background estimations.

An important feature of the chargino searches is that the limits obtained approach the maximum possible kinematic limits rapidly due to the high expected production cross-sections, and so the extra data taken at  $\sqrt{s} \geq 208$  GeV is very useful in these searches. OPAL presents limits on the chargino production cross section in Figure 13. No evidence for a signal

is observed, although for the search with  $\Delta M \approx 10$  GeV, there is an excess observed [12] in the OPAL experiment: five events are counted in the data, while 0.74 events are expected from the sum of all Standard Model backgrounds. None of the other experiments sees a similar excess, and the significance is diluted by the fact that many different search regions in four experiments were independently investigated and that a fluctuation can happen in any of them.

Neutralinos may also be produced via  $s$ -channel  $Z^0$  exchange, or via  $t$ -channel selectron exchange, and the lightest neutralino  $\tilde{\chi}_1^0$  is assumed to be the lightest supersymmetric particle (LSP). Pair production of  $\tilde{\chi}_1^0\tilde{\chi}_1^0$  is impossible to detect aside from the signature of the residual initial state radiation. Instead, associated production of  $\tilde{\chi}_2^0\tilde{\chi}_1^0$  is sought, where  $\tilde{\chi}_2^0 \rightarrow \tilde{\chi}_1^0 Z^0$ , and the  $Z^0$  decay products are observed. The observable final states are then two jets and missing energy, or two leptons and missing energy, with similar backgrounds to the chargino searches. OPAL's limits on the neutralino production cross-section are shown in Figure 13.

Searches for sleptons similarly focus on the final state of two like-flavored, opposite-signed leptons with missing energy, produced by the process  $e^+e^- \rightarrow \tilde{\ell}^+\tilde{\ell}^-$  followed by  $\tilde{\ell}^+ \rightarrow \tilde{\chi}_1^0\ell^+$ . In the 1999 data, there was an excess of events passing the requirements of the stau searches in all four detectors – no single experiment had a significant effect, but in combination the significance was greater:  $1 - \text{CL}_b = 0.001$  when 1998 and 1999 data were combined [13], with a stau mass hypothesis of 85 GeV and a neutralino mass hypothesis of 22 GeV. However, the excess did not persist in the 2000 data collected by the four experiments, and the particular hypothesis mentioned above is now excluded at the 95% CL [14].

After the July 20 LEPC presentation by ALEPH reporting an excess in a preliminary search [15] for a very light sbottom (of mass between 3 and 4 GeV), the DELPHI and OPAL collaborations performed similar searches. OPAL sees a deficit of events, with 15 events observed and 20.5 events expected from Standard Model background processes [16]. DELPHI similarly does not see an excess [17]. The ALEPH experiment updated the search with an improved Monte Carlo and a lepton identification algorithm which is more appropriate for identifying leptons inside dense jets and does not report a significant excess, with 24 events observed and 20 events expected from Standard Model backgrounds [8].

## 6 The Photon Recoil Spectrum

Events containing a single high-energy photon are valuable for searching for non-interacting new particles, such as LSP neutralinos (already mentioned), or  $\tilde{\chi}_2^0 \rightarrow \tilde{\chi}_1^0 \gamma$ . In Gauge-mediated SUSY-breaking models, the gravitino can be the LSP, and  $\tilde{\chi}_1^0 \rightarrow \tilde{G} \gamma$  is possible. An excited neutrino may decay radiatively. In general, any invisible process may also be accompanied by initial state radiation which may be detected, giving a sign for new physics. Unfortunately, no excess is observed in the recoil mass spectrum to single and multiple photons, as shown in Figure 14, which combines [14] the four LEP experiments' results for all data taken with  $\sqrt{s} \geq 130$  GeV.

## 7 Prospects for Further LEP Running

The hint of an excess in the Standard Model Higgs searches near with  $m_H=115$  GeV has generated a good deal of interest in extending the LEP run through 2001 with an energy upgrade.

Since the RADCOR2K conference, there have been two additional updates of the significance of the SM Higgs search results, at the LEPC presentations of October 10, 2000 [18] and on November 3, 2000 [19], with significances reported of  $2.5\sigma$  and  $2.9\sigma$ , respectively. Some variation is expected in both the signal and background cases due to statistical fluctuations – large jumps in the significance occur with the discrete arrival of candidates with large local values of  $s/b$ .

At the November 3 LEPC open session, the ALEPH, DELPHI, L3 and OPAL collaborations and the LEP Higgs Working Group jointly recommended running LEP in 2001. On the same day, the LEP Experiments Committee met in a closed session and was undecided on the recommendation, balancing the construction schedule, the cost, and the staffing of the LHC against the LEP run request. The research board also failed to make a recommendation, and on November 8, 2000, a press release was issued that LEP was closed, and on November 15, 2000 a committee of the CERN council was convened, which also failed to endorse the run extension request. Dismantling LEP began in early December, 2000.

## Acknowledgements

The LEP accelerator has performed outstandingly well due to the hard work of the members of the accelerator divisions at CERN. In particular, the RF performance has improved throughout the year, miniramps and the bending-field spreading technique were commissioned, and the accelerator had a high reliability and short turnaround times, all due to hard work and good organization. The author would like to thank the members of the four LEP collaborations, and the members of the LEP Higgs working group for the exemplary cooperation and openness in supplying search results for combination.

## References

- [1] A. L. Read, *Optimal Statistical Analysis of Search Results Based on the Likelihood Ratio and its Application to the Search for the MSM Higgs boson at 161 and 172 GeV*, DELPHI note 97-158 PHYS 737 (1997).
- [2] H. Hu and J. Nielsen, *Analytic Confidence Level Calculations using the Likelihood Ratio and Fourier Transform*, physics/9906010 (1999).
- [3] T. Junk, Nucl. Instrum. Meth. **A434**, 435 (1999).
- [4] B. Pietrzyk, presentation given at the 30<sup>th</sup> International Conference on High Energy Physics, July 27 - August 2, 2000, Osaka, Japan.
- [5] P. Igo-Kemenes, Eur. Phys. J. **C15**, 274 (2000).
- [6] C. Kolda and H. Murayama, hep-ph/0003170 (2000).
- [7] C. Tully, presentation given to the open session of the LEP Experiments Committee, September 5, 2000. Available at [http://lephiggs.web.cern.ch/LEPHIGGS/talks/tully\\_talk.pdf](http://lephiggs.web.cern.ch/LEPHIGGS/talks/tully_talk.pdf).
- [8] D. Schlatter, presentation given to the open session of the LEP Experiments Committee, 5 September 2000. Available at [http://alephwww.cern.ch/ALPUB/seminar/lepc\\_sep00/lepc\\_0509.pdf](http://alephwww.cern.ch/ALPUB/seminar/lepc_sep00/lepc_0509.pdf).
- [9] M. Carena, S. Heinemeyer, C.E.M. Wagner, and G. Weiglein, “Suggestions for Improved Benchmark Scenarios for Higgs Boson Searches at LEP2”, hep-ph/9912223 (1999).
- [10] S. Heinemeyer, W. Hollik and G. Weiglein, Phys. Rev. **D58** 091701 (1998);  
S. Heinemeyer, W. Hollik and G. Weiglein, Eur. Phys. J. **C9** 343 (1999).
- [11] M. Carena, M. Quirós and C.E.M. Wagner, Nucl. Phys. **B461** (1996) 407, hep-ph/9508343.
- [12] C. Rembser, OPAL Collaboration presentation given to the LEPC open session, 5 September, 2000. Available at [http://opal.web.cern.ch/Opal/talks/rembser\\_lepc00/main.ps.gz](http://opal.web.cern.ch/Opal/talks/rembser_lepc00/main.ps.gz)

- [13] A. Favara, presentation given at SUSY2K, CERN, June 26 – July 1, 2000.
- [14] S. Lees-Rosier, LEP SUSY Working Group presentation given to the LEPC open session, 5 September, 2000. Available at [http://13www.cern.ch/conferences/ps/RosierLEPC\\_susyww.ps.gz](http://13www.cern.ch/conferences/ps/RosierLEPC_susyww.ps.gz)
- [15] G. Taylor, ALEPH Collaboration presentation given at the LEPC open session, July 20, 2000. Available at <http://alephwww.cern.ch/ALPUB/seminar/lepcjul00/lepc.ps>.
- [16] K. Hoffman, presentation given at the 30<sup>th</sup> International Conference on High Energy Physics, July 27 - August 2, 2000, Osaka, Japan.
- [17] T. Camporesi, DELPHI Collaboration presentation given to the LEPC open session, September 5, 2000. Available at [http://delphiwww.cern.ch/~pubxx/delsec/talks/LEPCsep2000/tc\\_lepc.pdf](http://delphiwww.cern.ch/~pubxx/delsec/talks/LEPCsep2000/tc_lepc.pdf)
- [18] T. Junk, LEP Higgs Working Group presentation given at the LEP Fest, October 10, 2000. Available at [http://lephiggs.web.cern.ch/LEPHIGGS/talks/tom\\_lepfest.ps](http://lephiggs.web.cern.ch/LEPHIGGS/talks/tom_lepfest.ps).
- [19] P. Igo-Kemenes, LEP Higgs Working Group presentation given at the LEPC open session, November 3, 2000. Available at <http://lephiggs.web.cern.ch/LEPHIGGS/talks/index.html>.

Experiment	Data	Background	Signal
ALEPH	7	3.3	1.0
DELPHI	5	5.4	1.3
L3	4	4.0	0.3
OPAL	11	9.6	0.9
<b>LEP</b>	<b>27</b>	<b>22.2</b>	<b>3.6</b>

Table 1: Numbers of observed events and the expected event counts from a 114 GeV Higgs boson signal and the Standard Model background processes.

Experiment	Observed (GeV)	Expected (GeV)
ALEPH	109.1	112.5
DELPHI	110.5	110.9
L3	108.8	110.2
OPAL	109.5	111.7
Channel	Observed (GeV)	Expected (GeV)
Leptons	109.9	108.8
Neutrinos	112.1	110.7
Taus	105.4	104.2
Four Jets	109.0	113.5
<b>LEP</b>	<b>112.3</b>	<b>114.5</b>

Table 2: Limits on the mass of the Higgs boson, assuming the Standard Model production cross-section and branching fractions, by experiment, by channel, and combined. These have been computed with a uniform procedure and may vary by small amounts from the ones quoted by the individual experiments. In the lepton channel, there is a small unexcluded region below 100.7 GeV.

Scenario	$m_h$ limit obs (GeV)	$m_h$ limit exp (GeV)	$m_A$ limit obs (GeV)	$m_A$ limit exp (GeV)	$\tan\beta$ limit obs	$\tan\beta$ limit exp
$m_h$ -max	89.5	93.8	90.2	94.1	0.53–2.25	0.48–2.48
No stop mix	89.4	94.3	89.6	94.6	0.9–7.2	0.8–15

Table 3: Limits on  $m_h$ ,  $m_A$ , and  $\tan\beta$  in the  $m_h$ -max and no-mixing scenarios. The limits obtained by the combination of the four LEP experiments’ data are indicated with “obs,” while the median limits expected to be obtained in a large ensemble of background-only experiments are labeled “exp.”

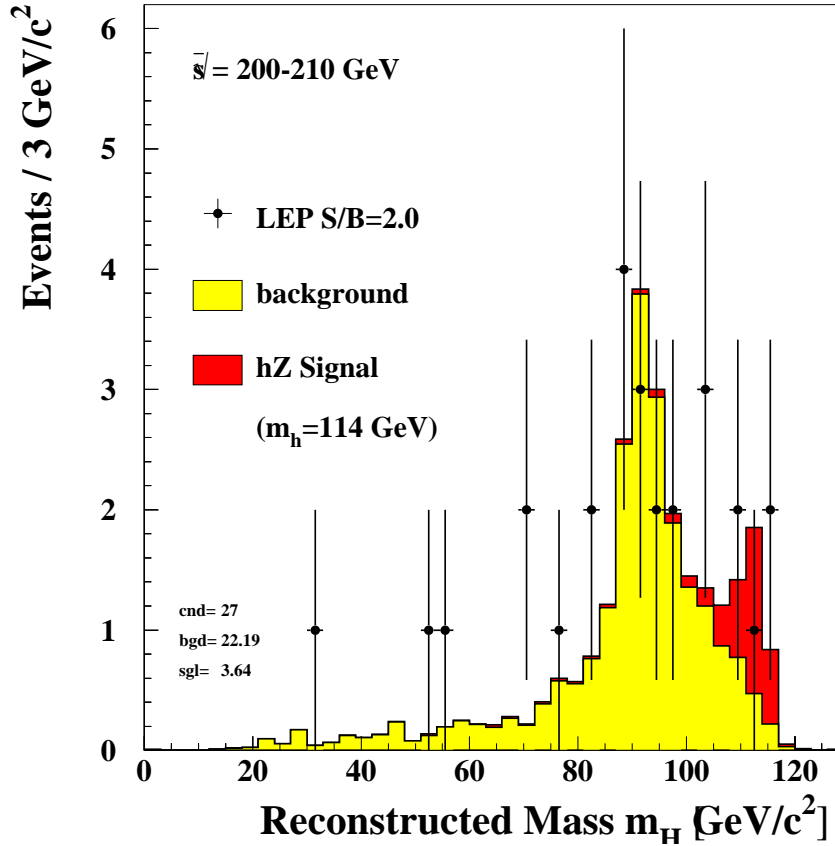


Figure 1: Distribution of the reconstructed masses of candidates selected by the Higgs search analyses summed over the four LEP experiments, summed over all search channels for the data taken in 2000. The selection cuts have been chosen such that the integrated signal divided by the integrated background for reconstructed masses above 109 GeV, for a SM signal hypothesis of 114 GeV, is roughly 2.0, in order to keep the contributions from the four experiments roughly similar. Each bin contains contributions from several sources with different s/b. The light histogram shows the sum of all SM background expectations, the dark histogram shows the expected signal from a 114 GeV Higgs boson, and the points show the data.

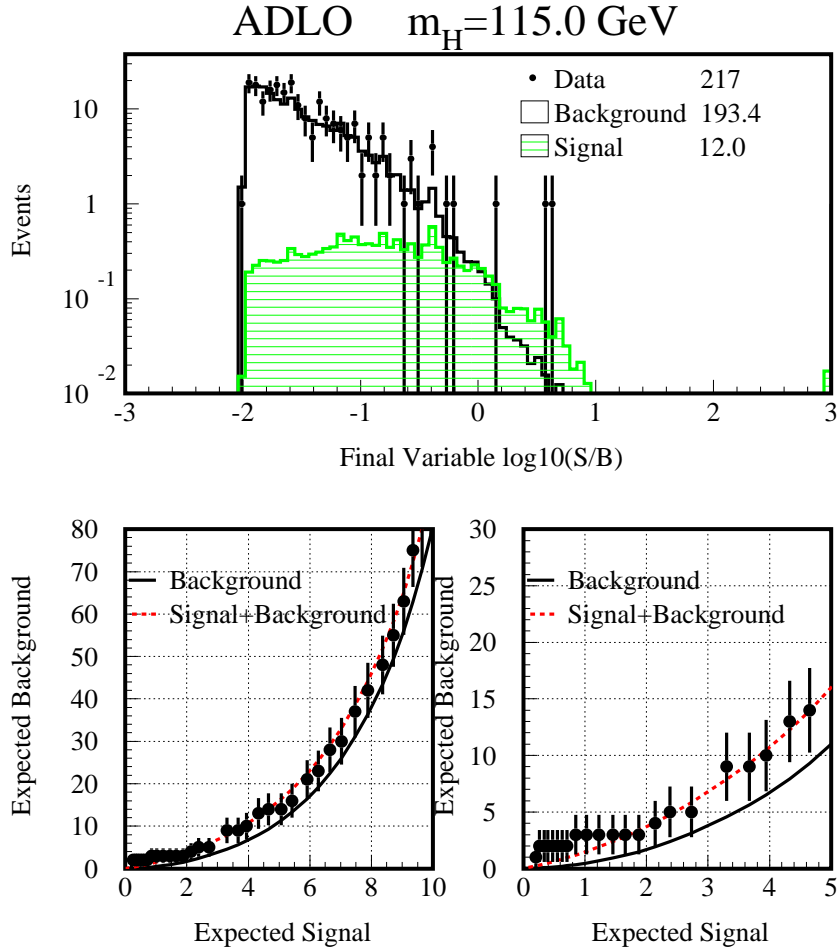


Figure 2: Distribution of the  $s/b$  for all bins of all search channels in all experiments at all energies. The signal is shown with a hatched histogram and the background with the open histogram. The data are shown with the points with error bars. The most significant candidates from the ALEPH experiment's four-jet channels are the three rightmost data points. The lower graphs show the integral of the  $s/b$  distribution shown in the upper panel, from the high  $s/b$  side. The background integral is the solid curve, the signal+background is the dashed curve, and the observed data are the points with error bars. Neighboring points are highly correlated because of the cumulative sum. The two lower panes show the same integrals, but on different horizontal scales.

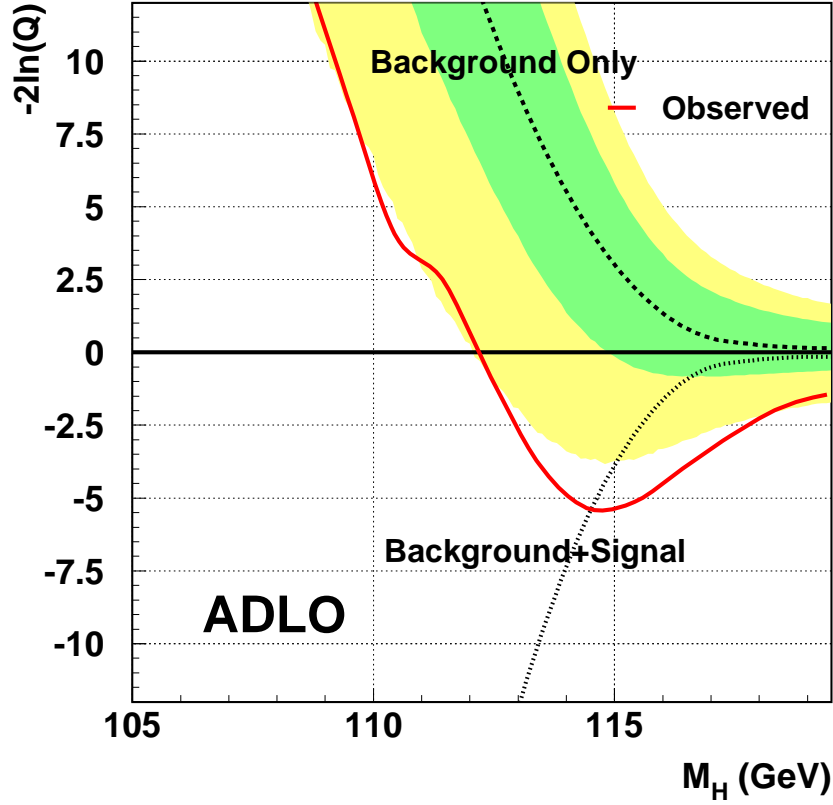


Figure 3: The value of the likelihood ratio test statistic  $-2\ln Q$  as a function of the test mass  $m_H$ . Values below zero indicate a preference of the data for the signal hypothesis. The solid curve shows the observation in the combined LEP data, the dashed curve shows the median expectation in an ensemble of background experiments, and the dotted curve shows the median expectation in an ensemble of experiments in which the background and a signal originating from a SM Higgs boson of mass equal to the test mass. The dark band around the median background expectation is the 68% probability interval for the background ensemble, centered on the median expectation, and the light bands indicate the 95% interval. The minimum of the observed  $-2\ln Q$  curve is at  $m_H=115$  GeV and has a value below zero, indicating that the signal hypothesis is preferred. The median expectation from a 115 GeV Higgs boson is very close to the observed value.

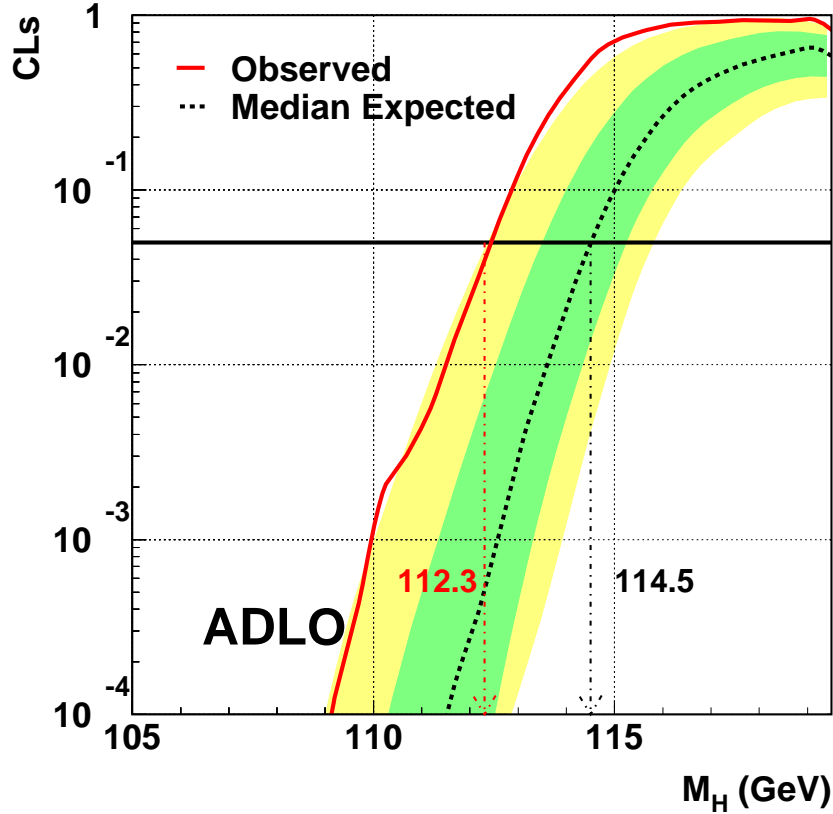


Figure 4: The exclusion confidence level  $CL_s$ , as a function of the test mass  $m_H$ . The solid curve shows the value of  $CL_s$  computed from the selected events observed in the data, for the four LEP experiments combined. The dashed curve is the median expectation in an ensemble of background-only experiments, and the dark and light shaded bands indicate the 68% and 95% probability intervals around the expected median. The 95% CL exclusion limit is the lowest point at which the observed  $CL_s$  crosses 0.05, and the median expected limit is where the median expectation cross the line at 0.05. A lower bound on  $m_H$  is obtained at 112.3 GeV, while the expected limit is 114.5 GeV.

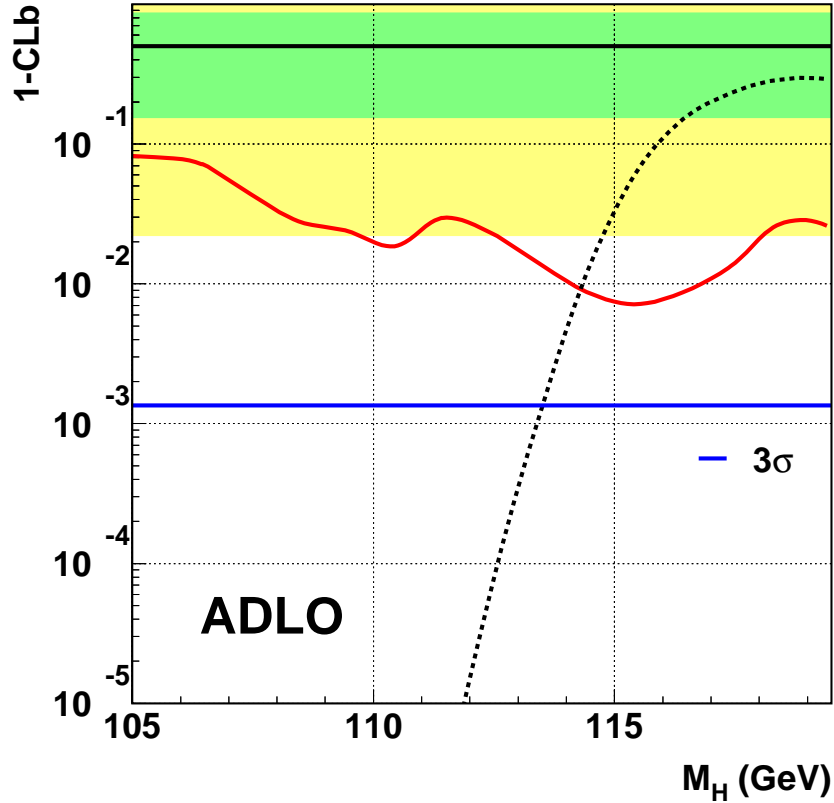


Figure 5: The background confidence level  $1 - CL_b$  as a function of the test mass  $m_H$ . This is the probability of a fluctuation of the background to be at least as signal-like as observed at that particular test mass; a small value indicates an excess of selected events. If  $1 - CL_b < 5.7 \times 10^{-7}$  then a discovery may be claimed at the  $5\sigma$  level. The lowest  $1 - CL_b$  observed in the data is  $7 \times 10^{-3}$  at  $m_H \approx 115$  GeV, which corresponds to a significance of approximately  $2.6\sigma$ .

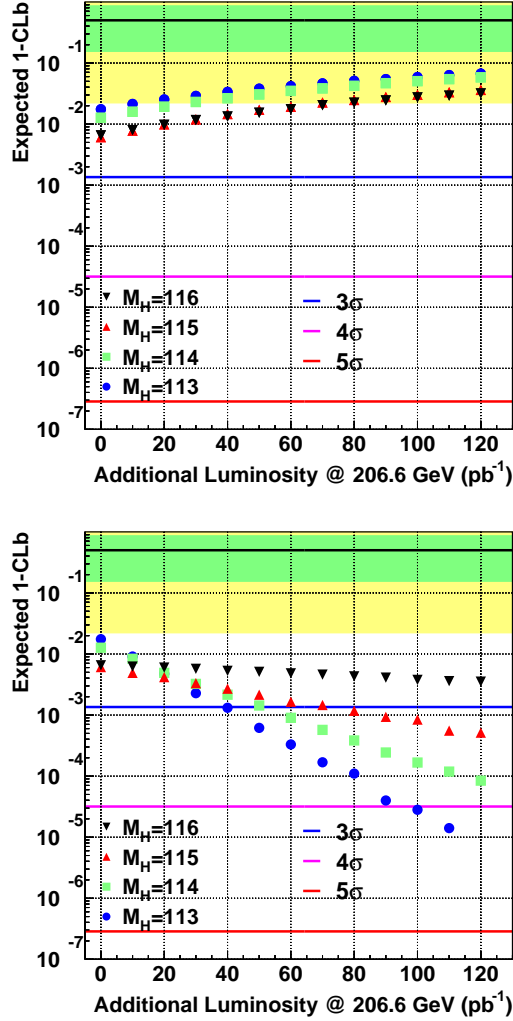


Figure 6: Scenarios for additional LEP running in 2000 beyond the September 5 LEPC. The top pane indicates the expected behavior of  $1 - CL_b$  as a function of the amount of luminosity collected, assuming a beam energy of 206.6 GeV and the absence of a signal, for four different values of the test mass. This quantifies the rapidity with which a background fluctuation should disappear with additional data accumulated. The lower pane indicates the speed with which the significance of an excess will grow with time if the signal were actually present, for different choices of the Higgs boson mass hypothesis  $m_H$ . A 113 GeV Higgs boson would be discoverable with a few months of extra running, but to extend the sensitivity out to 115 GeV requires a run in 2001. LEP typically collects in excess of 1 pb<sup>-1</sup> per day.

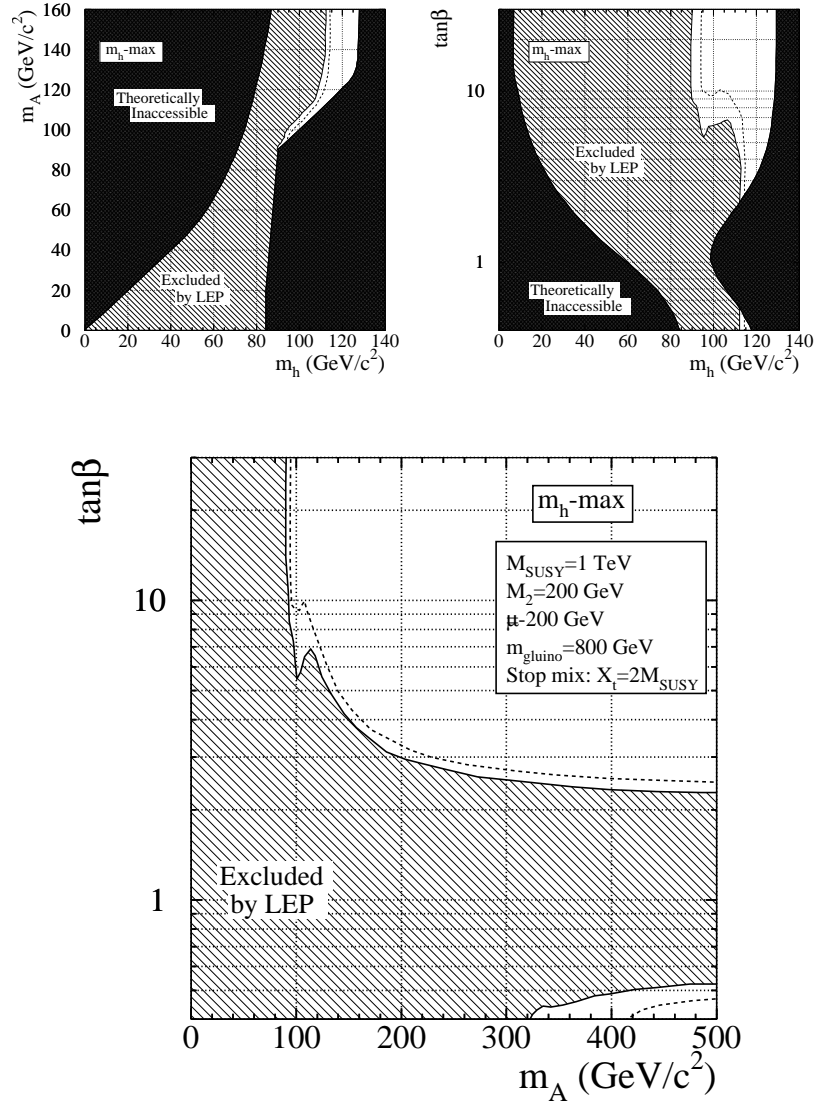


Figure 7: Limits on  $m_h$ ,  $m_A$ , and  $\tan\beta$  in the  $m_h$ -max MSSM benchmark scenario, described in the text. The limits are shown in the  $(m_h, m_A)$  plane (upper left), the  $(m_h, \tan\beta)$  plane (upper right), and in the  $(m_A, \tan\beta)$  plane (lower plot). The excluded regions are shown with diagonal hatching, and the regions which are not allowed by the theory are shown with dark hatching. The median expected boundaries of the excluded regions are shown with dashed lines. The  $m_h$ -max scenario is designed to give the most conservative limits on  $\tan\beta$  from the intersection of the limit curve with the theoretically unallowed region on the right of the  $(m_h, \tan\beta)$  plot.

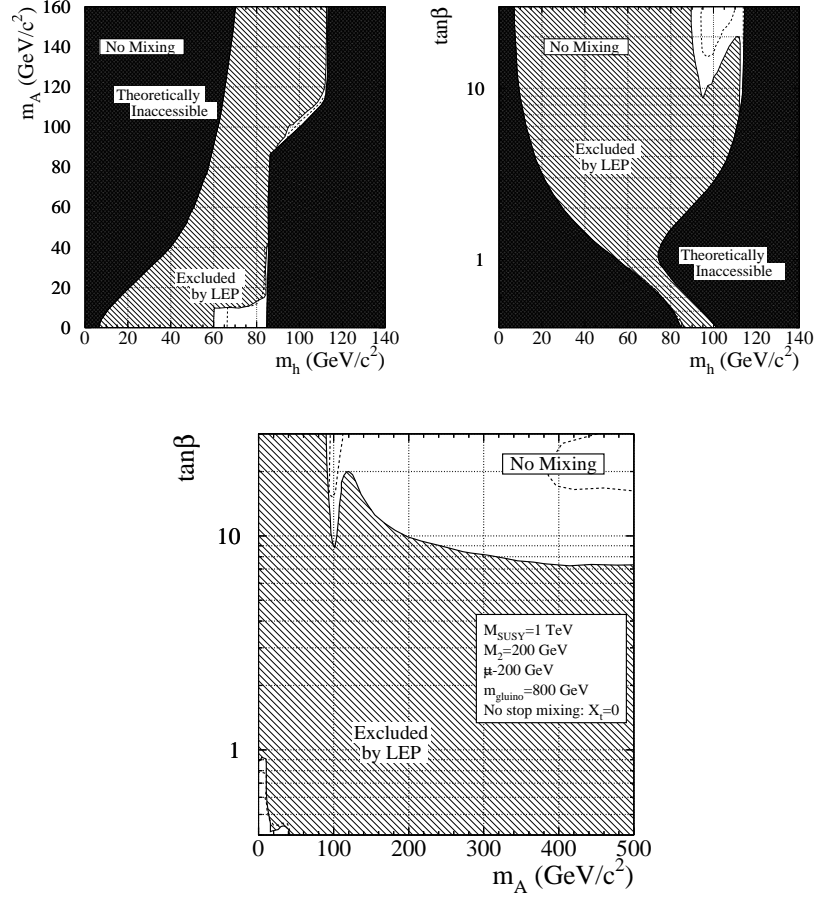


Figure 8: Exclusions in the no-stop-mixing MSSM benchmark scenario, described in the text. The limits are shown in the  $(m_h, m_A)$  plane (upper left), the  $(m_h, \tan\beta)$  plane (upper right), and in the  $(m_A, \tan\beta)$  plane (lower plot). The excluded regions are shown with diagonal hatching, and the regions which are not allowed by the theory are shown with dark hatchings. The median expected boundaries of the excluded regions are shown with dashed lines. In this scenario, the limits are similar for  $m_H \approx m_A$  and also the same for  $m_H$  at low  $\tan\beta$  as they are in the  $m_h$ -max scenario, but the limits on  $\tan\beta$  from the intersection on the right-hand side of the  $(m_h, \tan\beta)$  plot are much more stringent. On the other hand, more parameter space is opened up at low  $\tan\beta$  for values of  $m_h$  between 60 and 85 GeV. In this region, the  $h^0$  decays into  $A^0 A^0$  and/or charm and gluons, because the  $b\bar{b}$  decay is suppressed by the low value of  $\tan\beta$ , and the  $b\bar{b}$  decays of the  $A^0$  are also suppressed. In this region, flavor-independent searches, under development, will be used to search for possible signals, and if none are found, to exclude the remaining part.

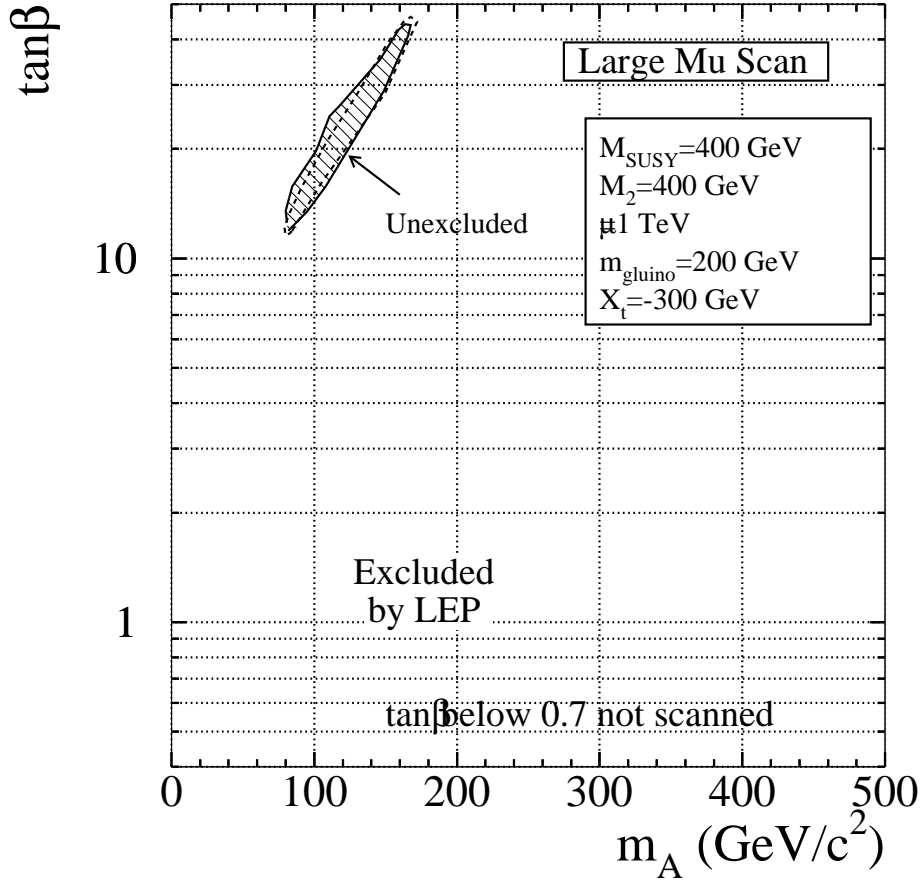


Figure 9: The exclusion in the large- $\mu$  MSSM benchmark scenario, described in the text. Only the  $(m_A, \tan\beta)$  projection is shown because the unexcluded region is not easily visible in the other projections. This scenario is designed to highlight portions of SUSY parameter space where the  $h^0 \rightarrow b\bar{b}$  decay is suppressed, and the tau decays are not enhanced, the remainder being taken up by  $W^{(*)+}W^{(*)-}$  and  $c\bar{c}$  decays. The unexcluded region is shown with diagonal hatching in this case, and the median expected boundary of this region is shown with a dashed line. For some points in this parameter space, the heavy Higgs boson  $H^0$  is kinematically accessible, and the searches for  $h^0 Z^0$  are re-interpreted as searches for  $H^0 Z^0$  where the latter searches have a better expected sensitivity.

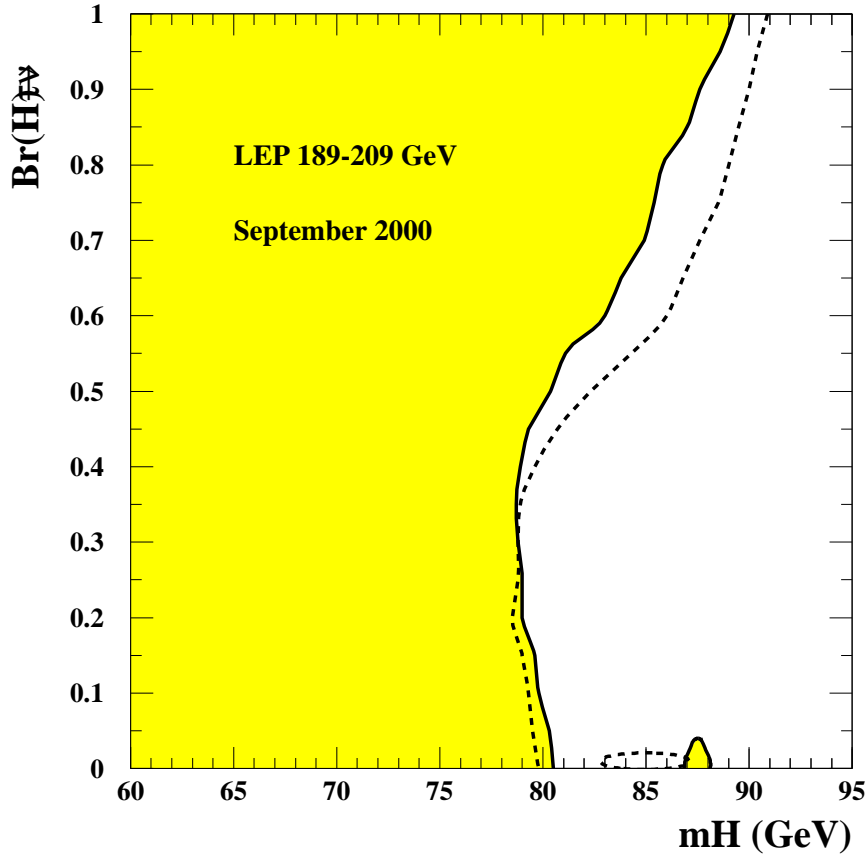


Figure 10: Limits on the production of charged Higgs bosons, as a function of the branching ratio  $\text{Br}(H^+ \rightarrow \tau^+ \nu_\tau)$ , assuming that  $\text{Br}(H^+ \rightarrow \tau^+ \nu_\tau) + \text{Br}(H^+ \rightarrow q\bar{q}') = 1$ . The excluded region is shown with light shading and the boundary is indicated with the heavy solid lines. The boundary of the region expected to be excluded in 50% of background-only experiments is indicated by the dashed lines. The background from  $W^+W^-$  decays is more severe for the four-jet search because of the  $W^\pm$  branching ratios, and impedes efforts to search for charged Higgs bosons with masses close to the mass of the  $W^\pm$ . As data accumulate, though, the sensitivity increase for  $m_{H^\pm}$  significantly in excess of  $m_W$ , and a small island of exclusion is appearing in both the observed and expected limits above  $m_W$  for  $\text{Br}(H^+ \rightarrow \tau^+ \nu_\tau) = 0$ . The result is from the combination of the charged Higgs boson searches from the four LEP experiments.

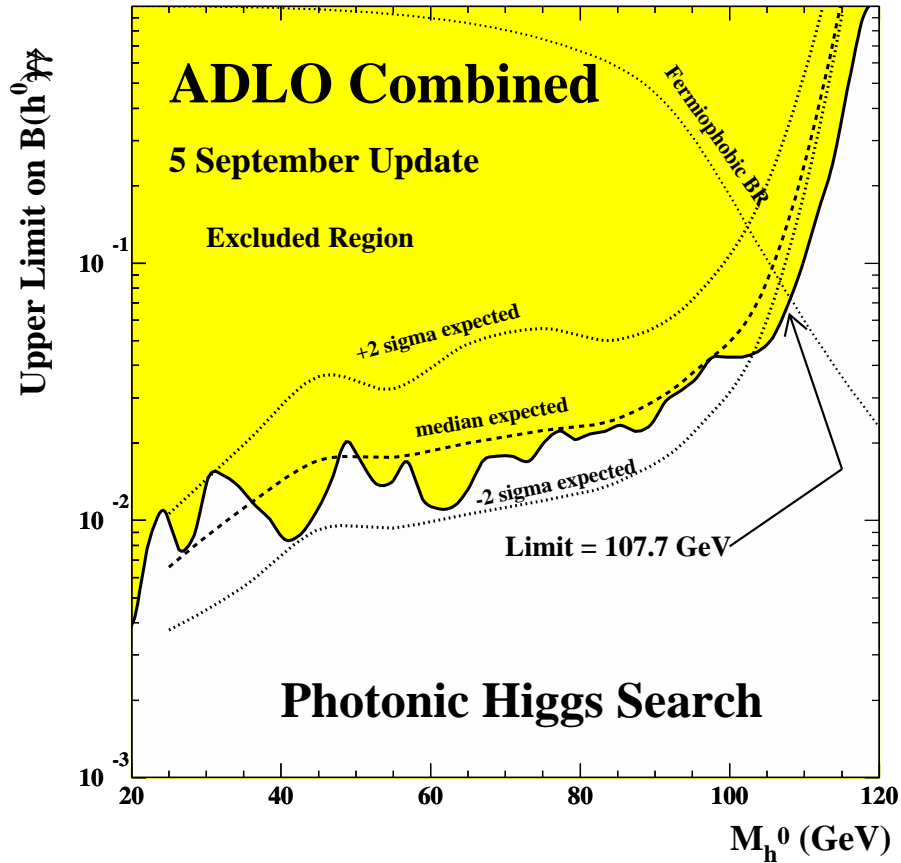


Figure 11: Limits obtained on the production of  $e^+e^- \rightarrow H^0 Z^0 \rightarrow \gamma\gamma Z^0$ , combining all search channels from the four LEP experiments for all decay modes of the  $Z^0$ . These searches are not combined with the searches for the non-photonic decays of the Higgs boson, and are therefore limits on the production cross-section of a Higgs boson which decays only into photons, relative to the Standard Model production cross-section. Alternatively, they are interpreted as limits on the photonic branching ratio of the Higgs boson, ignoring the other search results. A prediction of the photonic branching ratio of the Higgs boson in a model in which the couplings of the Higgs boson to fermions are all zero is shown with the dashed line. In such a fermiophobic model, a lower mass limit of 107.7 GeV is obtained.

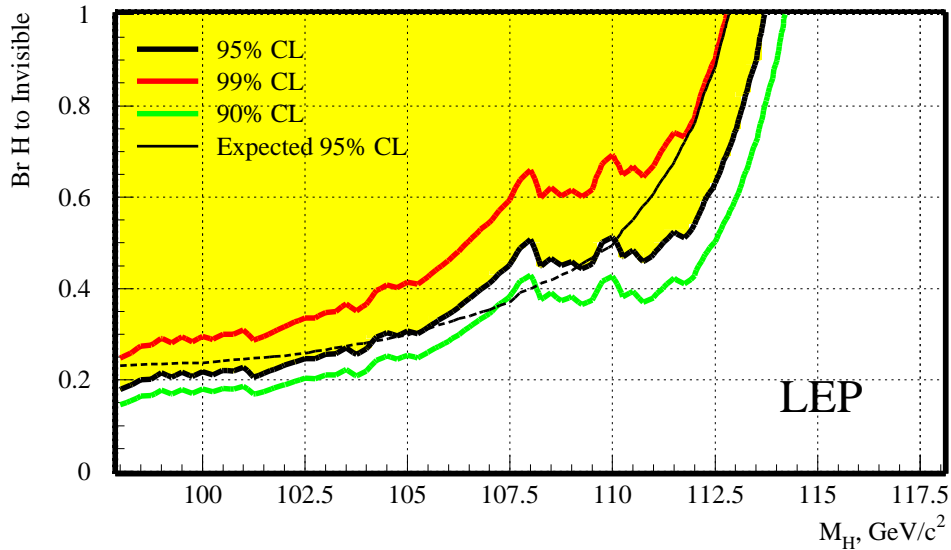


Figure 12: Limits obtained on the production of  $e^+e^- \rightarrow H^0 Z^0$ , where the  $H^0$  decays invisibly, combining all search channels from the four LEP experiments for the included decay modes of the  $Z^0$ . These searches are not combined with the searches for the visible decays of the Higgs boson, and are therefore limits on the production cross-section of a Higgs boson which decays only invisibly, relative to the Standard Model production cross-section. Alternatively, they are interpreted as limits on the invisible branching ratio of the Higgs boson, ignoring the other search results. A lower bound on a Higgs boson produced with the SM production cross-section and decaying invisibly is set at 113.7 GeV, and the median expectation is 112.8 GeV.

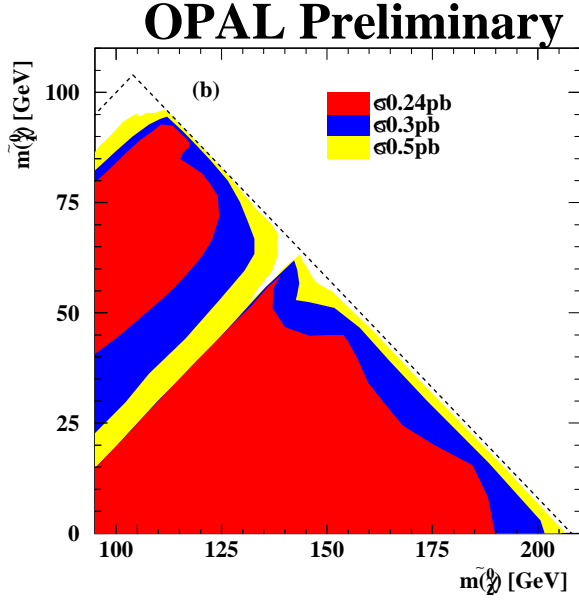
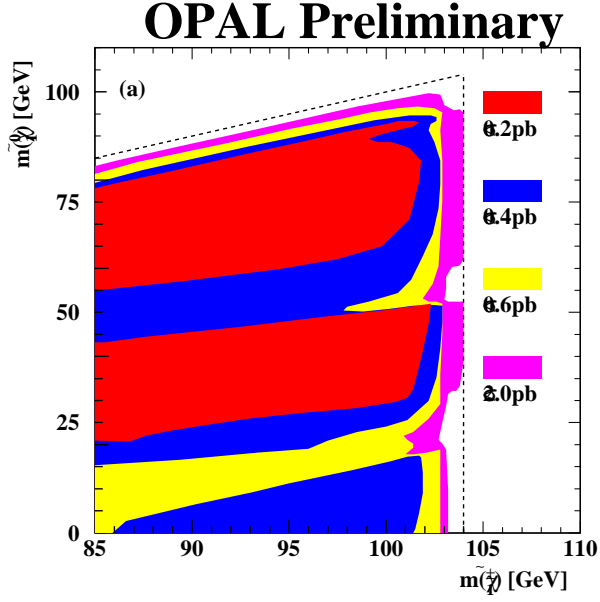


Figure 13: Contours of the 95% C.L. upper limits for (a) the  $e^+e^- \rightarrow \tilde{\chi}_1^+ \tilde{\chi}_1^-$  production cross-sections at  $\sqrt{s} = 208$  GeV are shown assuming  $\text{Br}(\tilde{\chi}_1^+ \rightarrow \tilde{\chi}_1^0 W^{(*)+}) = 100\%$ . (b) the  $e^+e^- \rightarrow \tilde{\chi}_2^0 \tilde{\chi}_1^0$  production cross-sections at  $\sqrt{s} = 208$  GeV are shown assuming  $\text{Br}(\tilde{\chi}_2^0 \rightarrow \tilde{\chi}_1^0 Z^{(*)0}) = 100\%$ . The region for which  $m_{\tilde{\chi}_2^0} + m_{\tilde{\chi}_1^0} < m_Z$  is not considered in this analysis. The limits use only the data taken in 2000.

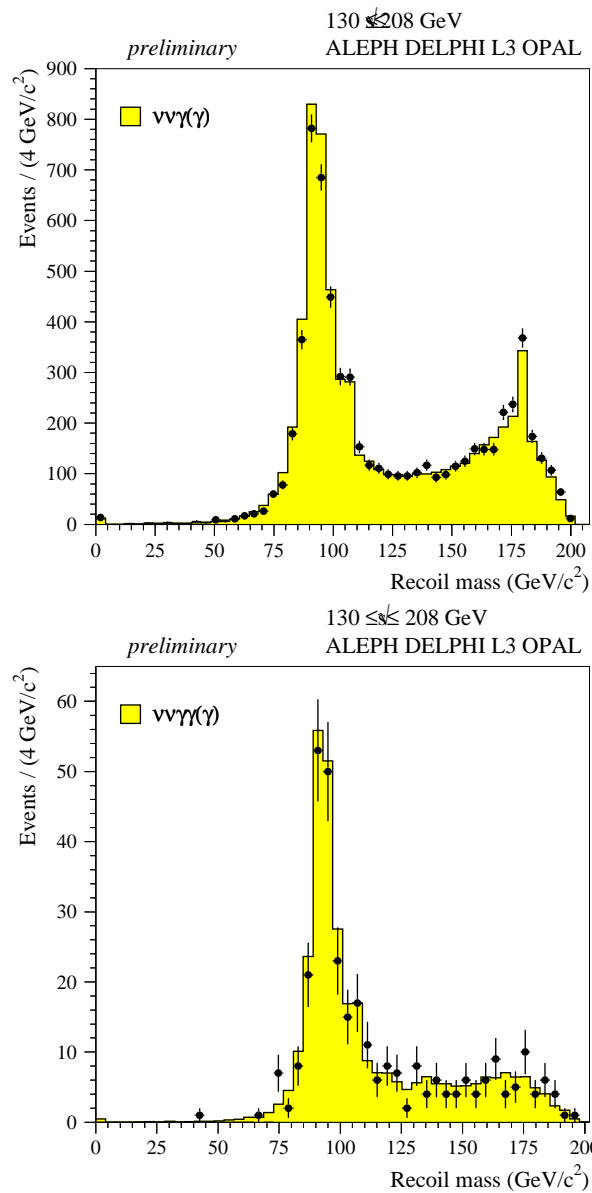


Figure 14: Spectrum of the recoil mass in events with one single high-energy photon (top) and with two or more photons (bottom). Data with  $130 \leq \sqrt{s} \leq 208$  GeV from the four LEP experiments are combined.

October 19, 2001  
hep-ex/0101016

## Standard Model Physics Results from LEP2

STEPHAN WYNHOFF

*CERN*

*1211 Geneva 23, Switzerland  
Email: Stephan.Wynhoffcern.ch*

At LEP2 many Standard Model predictions are tested up to centre-of-mass energies of 209 GeV. Fermion pair production cross sections and asymmetries agree well with the theoretical expectation over the entire energy range. The measurements are used to determine the  $\gamma/Z$  interference and to search for contact interactions up to 20 TeV. The cross sections for single-W, ZZ and  $W^+W^-$  production agree well with the expectations. The branching fractions of the W boson into hadrons and leptons are determined as well as the CKM matrix element  $|V_{cs}|$ . Precise measurements of the W mass and width are presented yielding  $M_W = 80.427 \pm 0.046$  GeV and  $\Gamma_W = 2.12 \pm 0.11$  GeV. All electroweak data are very consistent with the Standard Model predictions. In a combined fit using the recent value of  $\Delta\alpha_{\text{had}}^{(5)}(s)$  the mass of the Higgs boson is constrained to  $M_H = 88_{-37}^{+60}$  GeV.

Presented at the

5th International Symposium on Radiative Corrections  
(RADCOR-2000)  
Carmel CA, USA, 11–15 September, 2000

## 1 Introduction

The LEP accelerator has provided since its start in 1989 many possibilities to check Standard Model [1,2] (SM) predictions. During the first years the accelerator was operated at the Z-pole (LEP1) and the four LEP experiments, ALEPH, DELPHI, L3 and OPAL collected some 15 million hadronic and 2 million leptonic Z decays. These data allowed a precise determination of the properties of the Z boson [3]. In the second phase of LEP, LEP2, the centre-of-mass energy,  $\sqrt{s}$ , was successively increased up to  $\sqrt{s} = 209$  GeV allowing the production of  $W^+W^-$  and ZZ pairs. More than 8000 W-pair events have been collected per experiment and are used to determine in particular the mass and width of the W boson [4]. Combining the LEP results with other electroweak precision measurements allows thorough consistency tests of the SM and to constrain the mass of the Higgs boson [5,6].

To match the statistical accuracy of the large data samples collected at LEP – especially at energies above the Z-pole – the corresponding theory programs have been improved. For 2-fermion processes the programs ZFITTER [7], TOPAZ0 [8] and KKMC [9] have now a precision better than 0.2% for the total hadronic and leptonic<sup>1</sup> cross sections at high energies. The KKMC program covers the entire energy range from  $\tau$ - and  $b$ -factories over LEP to linear colliders. Also for 4-fermion processes adequate precision has been reached. Using the double-pole approximation [10] RacoonWW [11] and YFSWW3 [12] calculate the  $W^+W^-$  cross section within 0.4% above the production threshold. The cross section for the process  $e^+e^- \rightarrow We\nu$  is calculated within 4-5% accuracy by WPHACT [13], grc4f [14] and WTO [15] using the fermion loop scheme [16]. The programs YFSZZ [17] and ZZTO [18] predict the Z-pair production cross section within 2%. Details can be found in the proceedings of the LEP2MC workshop [19,20]. Generally there is now an excellent match in precision between theoretical predictions and experimental measurements.

## 2 Fermion Pair Production

At centre-of-mass energies well above the Z-pole photon radiation becomes important. The effects to consider are initial and final state photon radiation, interference between these and the production of additional fermion pairs by a photon or Z boson. The main interest is in events where the annihilation took place at a high effective centre-of-mass energy,  $\sqrt{s'}$ , which is defined as the mass of the outgoing lepton pair or of the  $\gamma^*/Z$  propagator. Results are given by all four experiments for events with  $\sqrt{s'} > 0.85 \cdot \sqrt{s}$ . The results for the reactions  $e^+e^- \rightarrow \text{hadrons}(\gamma)$ ,  $e^+e^- \rightarrow \mu^+\mu^-(\gamma)$  and  $e^+e^- \rightarrow \tau^+\tau^-(\gamma)$  are combined taking properly into account the statistical and systematical uncertainties and their correlations [21].

---

<sup>1</sup>For Bhabha scattering the precision is estimated to 2% for an angular range of  $30^\circ < \vartheta < 150^\circ$ .

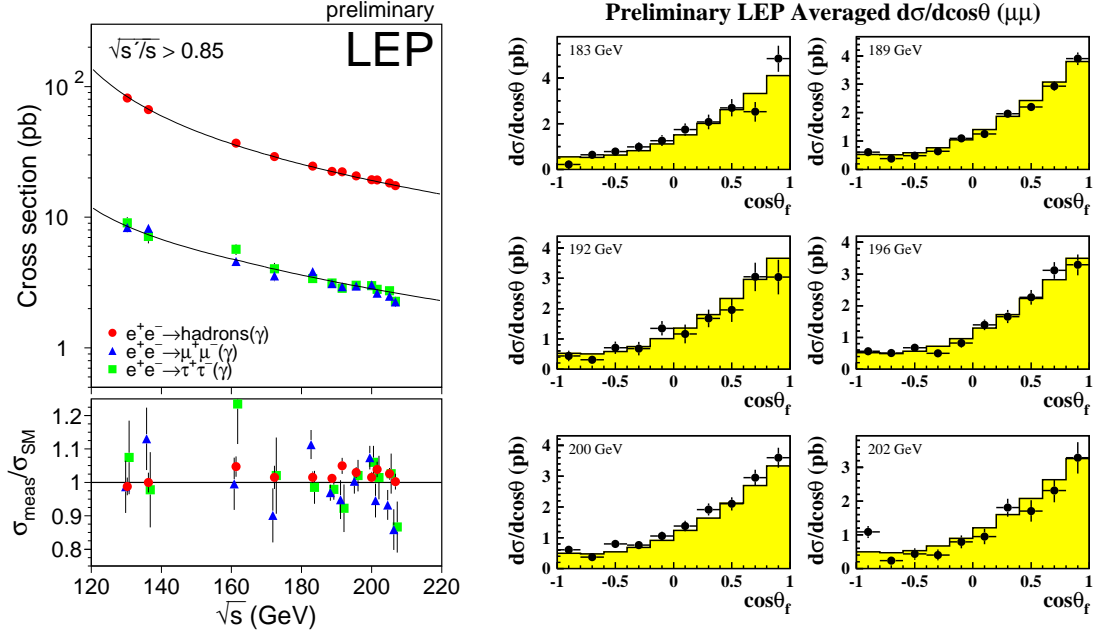


Figure 1: The measured cross sections of fermion pair production and the differential cross section for muon pair production at LEP2.

The combined results for the total cross sections are in Figure 1 compared to the SM predictions for all three processes. The measurements agree well with the theoretical expectations. For muon and tau pair production also the differential cross sections,  $d\sigma/d\cos(\vartheta)$ , have been determined. The result for muon pair production is also shown in Figure 1 for centre-of-mass energies from 183 GeV to 202 GeV. Also the forward-backward asymmetries for these processes are in good agreement with the SM. For hadronic final states the ratios of cross sections for b quarks and c quarks to the total hadronic cross section,  $R_b$  and  $R_c$ , as well as the forward-backward asymmetries for these flavours are determined. Within the limited statistics of the measurements good agreement with the SM is observed.

The reaction  $e^+e^- \rightarrow f\bar{f}$  has contributions from photon exchange, from Z boson exchange and from  $\gamma/Z$  interference. Within the S-Matrix approach [22] the lowest-order total cross sections and forward-backward asymmetries are parametrised in the following way:

$$\sigma_a^0(s) = \frac{4}{3}\pi\alpha^2 \left[ \frac{g_f^a}{s} + \frac{j_f^a(s - \bar{m}_Z^2) + r_f^a s}{(s - \bar{m}_Z^2)^2 + \bar{m}_Z^2 \Gamma_Z^2} \right], \text{ for } a = \text{tot, fb},$$

$$A_{\text{fb}}^0(s) = \frac{3}{4} \frac{\sigma_{\text{fb}}^0(s)}{\sigma_{\text{tot}}^0(s)}, \quad \text{with} \quad \sigma_{fb}^0 = \frac{4}{3} (\sigma_f - \sigma_b).$$

The S–Matrix ansatz defines the Z resonance using a Breit–Wigner denominator with an  $s$ –independent width. In other approaches, a Breit–Wigner denominator with an  $s$ –dependent width is used, which implies the following transformation of the values of the Z boson mass and width:  $M_Z = \bar{m}_Z + 34.1 \text{ MeV}$  and  $\Gamma_Z = \bar{\Gamma}_Z + 0.9 \text{ MeV}$ . In the following, the fit results are quoted after applying these transformations. The S–Matrix parameters  $r_f$ ,  $j_f$  and  $g_f$  give the Z exchange,  $\gamma/Z$  interference and photon exchange contributions for fermions of type  $f$ , respectively. For hadronic final states the parameters  $r_{\text{had}}^{\text{tot}}$ ,  $j_{\text{had}}^{\text{tot}}$  and  $g_{\text{had}}^{\text{tot}}$  are sums over all produced quark flavours.

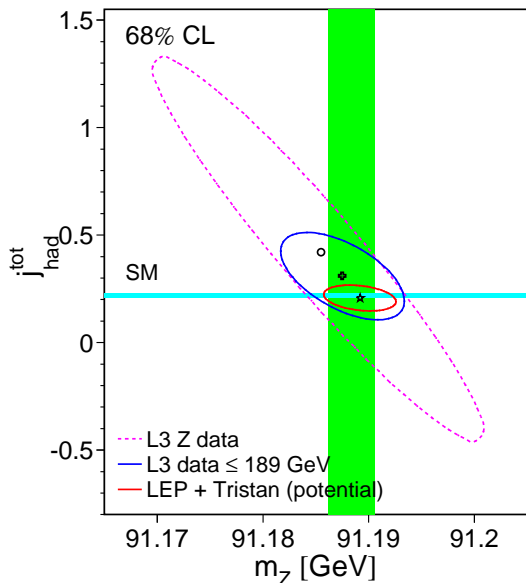


Figure 2: Contours in the  $(M_Z, j_{\text{had}}^{\text{tot}})$  plane at 68% confidence level under the assumption of lepton universality. The dashed line is obtained from Z data only; the inclusion of 130 GeV to 189 GeV data gives the solid line. The circle (Z data) and the cross (all data) indicate the central values of the fits. The SM prediction for  $j_{\text{had}}^{\text{tot}}$  is shown as the horizontal band. The vertical band corresponds to the 68% confidence level interval on  $M_Z$  in a fit assuming the Standard Model value for  $\gamma/Z$  interference. The smallest contour shows the result of a fit to all LEP and TRISTAN data.

While in the standard fits to determine the Z boson mass the  $\gamma/Z$  interference is fixed to its SM expectation in S-matrix fits it is left free leading to an additional uncertainty on  $M_Z$ . Figure 2 shows the 68% confidence level contours in the  $(M_Z, j_{\text{had}}^{\text{tot}})$  plane for the L3 data taken at the Z–pole and after including the 130–189 GeV measurements [23]. The improvement resulting from the inclusion of the high energy measurements is clearly visible. The S-matrix fit agrees well with the results from the standard fit indicated by the vertical band. Figure 2 also shows the potential <sup>2</sup> result when combining all LEP data [21] and the Tristan [24] results. The total error on  $M_Z$  is expected to be 2.3 MeV showing that it is possible to remove the additional uncertainty from the  $\gamma/Z$  interference on  $M_Z$  almost completely.

The measured fermion pair cross sections and asymmetries can also be used to set limits on contact interactions, fermion sizes, extra space dimensions, TeV strings, gravitons and other new physics effects. For example, contact interactions setting

<sup>2</sup>Only some preliminary LEP1 results within the S-Matrix framework are available and systematic errors are not fully taken into account.

Table 1: Preliminary limits on contact interactions from LEP combined data collected at centre-of-mass energies from 130 GeV to 202 GeV.

	Helicity configuration				Energy scale [TeV]	
	$\eta_{RR}$	$\eta_{LL}$	$\eta_{LR}$	$\eta_{RL}$	$\Lambda_-$	$\Lambda_+$
AA	$\pm 1$	$\pm 1$	$\mp 1$	$\mp 1$	13.9	17.6
VV	$\pm 1$	$\pm 1$	$\pm 1$	$\pm 1$	17.2	20.4
RR	$\pm 1$	0	0	0	9.7	12.3
LL	0	$\pm 1$	0	0	10.2	12.8

in at an energy scale  $\Lambda$  can be described by the following Lagrangian [25] where by convention the couplings  $g$  are normalised by  $g^2/4\pi = 1$  and the helicity amplitudes obey  $|\eta_{ij}| = 0, 1$ :

$$\mathcal{L} = \frac{1}{1 + \delta_{ef}} \sum_{i,j=L,R} \eta_{ij} \frac{g^2}{\Lambda_{ij}^2} (\bar{e}_i \gamma^\mu e_i) (\bar{f}_j \gamma_\mu f_j),$$

$\delta_{ef}$  is the Kronecker symbol being one for Bhabha scattering and zero otherwise. A contact interaction, even at very high energy scales, can be detected at LEP2 by its interference effects with the SM by modifications to the differential cross sections.

$$\frac{d\sigma}{d\cos\theta} = \frac{d\sigma^{\text{SM}}}{d\cos\theta} + c_{\text{int}}(s, \cos\theta) \frac{1}{\Lambda^2} + c_{\text{ci}}(s, \cos\theta) \frac{1}{\Lambda^4}.$$

Such fits are done to the LEP combined measurements [21] and the resulting limits on the energy scale are in the range from 10 TeV to 20 TeV depending on the helicity configuration. The results are summarised in Table 1.

### 3 Boson Production Cross Sections

The high centre-of-mass energies obtained at LEP2 allow the production not only of fermion pairs but also of boson pairs,  $W^+W^-$  and  $ZZ$ , and the production of single  $W$  bosons.

The production of  $Z$  boson pairs tests the SM in the neutral-current sector and is sensitive to scenarios for new physics like extra space dimensions or couplings between neutral gauge bosons. All experiments have measured the  $ZZ$  cross section at  $\sqrt{s}$  up to 208 GeV. The results are combined using the expected statistical error and systematic uncertainties [26]. They are compared to predictions from YFSZZ and ZZTO in Figure 3 and show no significant deviation from these theoretical models.

No new measurement for single  $W$  production ( $e^+e^- \rightarrow We\nu$ ) has been provided above  $\sqrt{s} = 202$  GeV but the fermion loop scheme [16] has been introduced as an

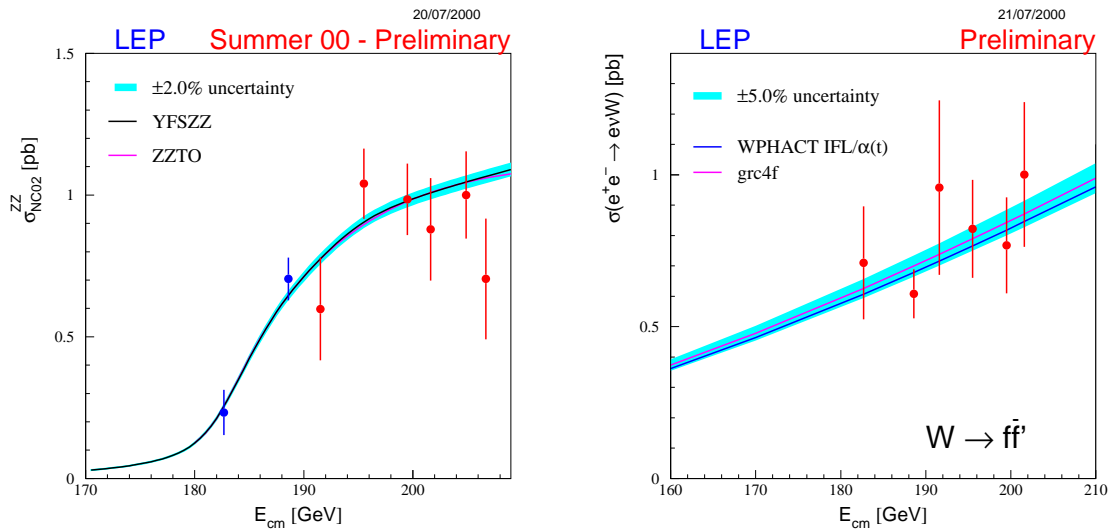


Figure 3: The measured cross sections for Z pair production and for single W production.

additional theoretical model. The data are compared with the updated, slightly lower theoretical predictions in Figure 3 showing good agreement.

## 4 $W^+W^-$ Production

At centre-of-mass energies above 160 GeV the production of  $W^+W^-$  pairs is possible. Both W bosons decay into two fermions each producing three different types of final states. About 45.6% of the events decay fully hadronically. These are balanced events of high multiplicity. In  $3 \times 14.6\%$  one W decays hadronically while the other one decays leptonically resulting in 2 jets and a high energetic lepton. A  $\tau$  lepton can decay into a third, narrow jet instead of an electron or muon. Fully leptonic decays are characterised by low multiplicity and a lot of missing energy. The leptons are typically acoplanar.

Events of all three topologies are selected by the four LEP experiments to measure the total production cross section of  $W^+W^-$  pairs. The combined LEP cross section [26] is shown in Figure 4 and compared to the predictions of the programs Gentle 2.1 [27] (at centre-of-mass energies below 170 GeV) and RacoonWW and YFSWW 1.14 above threshold. Over the full energy range an excellent agreement between the measurements and the SM is found.

From the selected events also the decay fractions of the W boson into hadrons and the three lepton flavours are determined. DELPHI and L3 used data from centre-of-mass energies of 161 GeV to 202 GeV while ALEPH and OPAL analysed

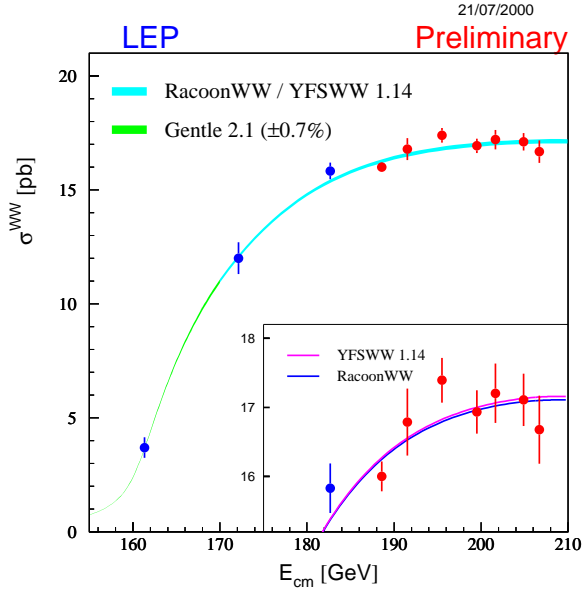


Figure 4:  $W^+W^-$  production cross section at LEP. The points correspond to the combined measurements of all four LEP experiments for all decay channels. The lines represent the Standard Model predictions. The Gentle program is used for  $\sqrt{s} < 170$  GeV .

data up to 207 GeV . The results are listed in Table 2. The branching fractions for the three lepton flavours agree with each other and support the hypothesis of lepton universality. The LEP combined leptonic branching fraction of the W boson is  $Br(W \rightarrow l\nu) = 10.74 \pm 0.10$  %. This direct measurement can be compared to the indirect extraction at the TEVATRON where the combined results from CDF and D0 [28] yield  $Br(W \rightarrow l\nu) = 10.43 \pm 0.25$  %.

From the hadronic branching fraction it is possible to determine the element  $|V_{cs}|$

Table 2: Preliminary hadronic and leptonic branching fractions of the W boson measured by the four LEP experiments and the combined results. All numbers are given in percent.

	W→hadrons	W→eν	W→μν	W→τν
ALEPH	$67.22 \pm 0.53$	$11.19 \pm 0.34$	$11.05 \pm 0.32$	$10.53 \pm 0.42$
DELPHI	$67.81 \pm 0.61$	$10.33 \pm 0.45$	$10.68 \pm 0.34$	$11.28 \pm 0.56$
L3	$68.47 \pm 0.59$	$10.22 \pm 0.36$	$9.87 \pm 0.38$	$11.64 \pm 0.51$
OPAL	$67.86 \pm 0.62$	$10.52 \pm 0.37$	$10.56 \pm 0.35$	$10.69 \pm 0.49$
LEP	$67.78 \pm 0.32$	$10.62 \pm 0.20$	$10.60 \pm 0.18$	$11.07 \pm 0.25$

of the Cabbibo-Kobayashi-Maskawa mixing matrix exploiting the formula:

$$\frac{Br(W \rightarrow \text{hadrons})}{1 - Br(W \rightarrow \text{hadrons})} = \sum |V_{ij}^2| \left(1 + \frac{\alpha_s}{\pi}\right).$$

With LEP data a value of  $|V_{cs}| = 0.989 \pm 0.016$  is obtained. This value is in good agreement with the more direct determination using events with tagged charm of  $|V_{cs}| = 0.95 \pm 0.08$  [26].

## 5 W Mass Measurement

The mass of the W boson is determined at LEP in two different ways. Close to the production threshold the total cross section depends strongly on  $M_W$ . For  $\sqrt{s} = 161 - 172$  GeV the mass is determined from  $\sigma_{WW}$  to be  $M_W = 80.40 \pm 0.22$  GeV [4]. At higher centre-of-mass energies where the dependence of  $M_W$  on  $\sigma_{WW}$  is reduced the mass is reconstructed directly from the W decay products.

Table 3: The values obtained for the mass and the width of the W boson obtained by the four LEP experiments and their combination from data taken at  $\sqrt{s} = 172 - 202$  GeV. All numbers are preliminary.

	$M_W$ [GeV]	$\Gamma_W$ [GeV]
ALEPH	$80.440 \pm 0.064$	$2.17 \pm 0.20$
DELPHI	$80.380 \pm 0.071$	$2.09 \pm 0.15$
L3	$80.375 \pm 0.077$	$2.19 \pm 0.21$
OPAL	$80.485 \pm 0.065$	$2.04 \pm 0.18$
LEP	$80.427 \pm 0.046$	$2.12 \pm 0.11$

From the three possible final states,  $qqqq$ ,  $qq\nu$  and  $l\nu l\nu$ , the fully leptonic is not used because the two undetectable neutrinos inhibit the complete determination of the event kinematics. For the other events leptons and jets are reconstructed and  $M_W$  is determined in a kinematic fit to the measured fermion energies and angles. Constraints from energy and momentum conservation – one for semileptonic and four for hadronic decays – are imposed to improve the resolution. In some analyses the two reconstructed W masses are required to be equal as an additional constraint. For hadronic decays choosing the correct jet pairing poses an additional problem. The pairing giving the best  $\chi^2$  in the fit is chosen. Possible gluon radiation is taken into account by splitting the hadronic events into a 4- and 5-jet sample improving the mass resolution (DELPHI, OPAL).

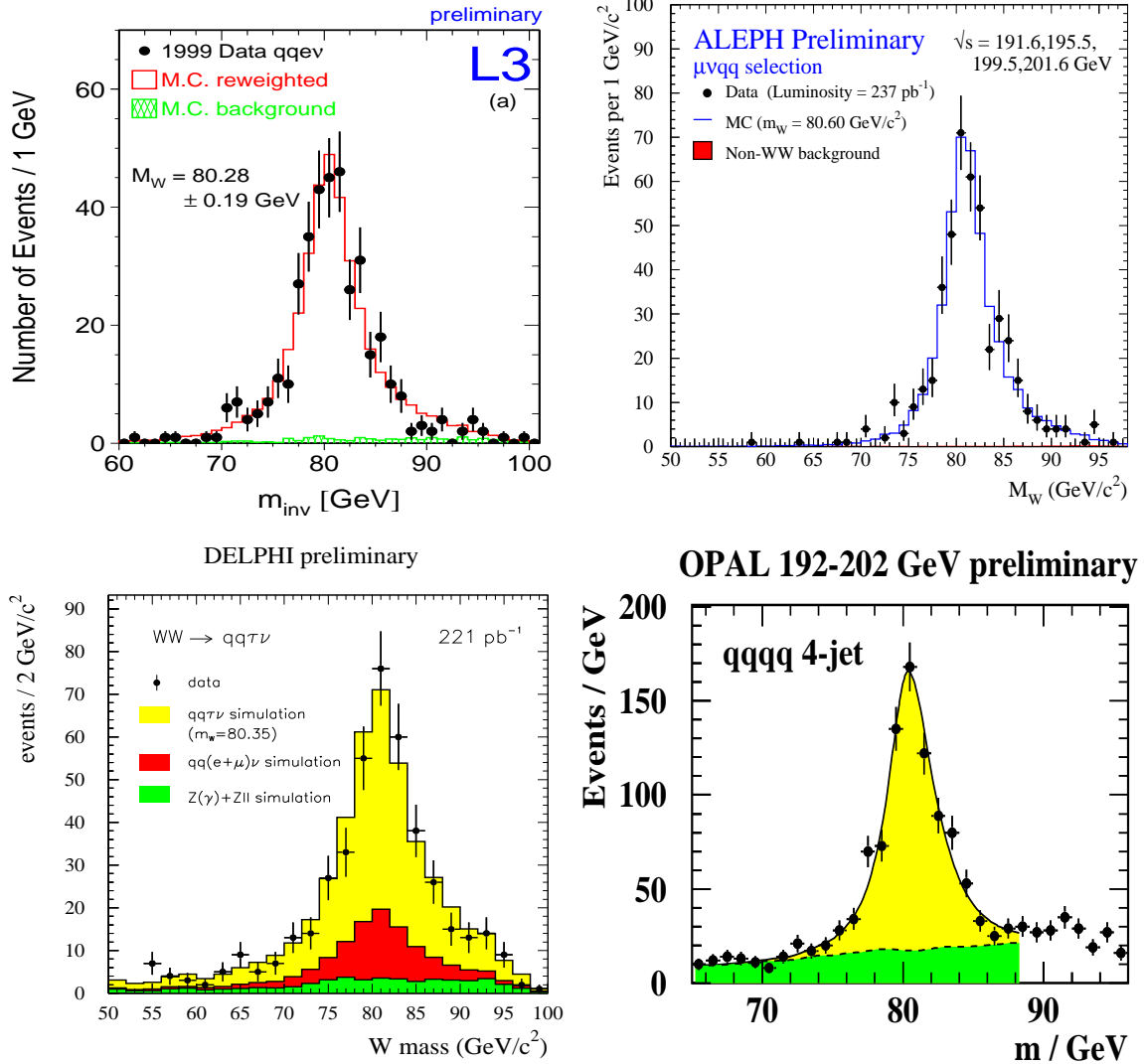


Figure 5: Invariant mass spectra for the four  $W^+W^-$  production topologies used for direct reconstruction at  $\sqrt{s} = 192 - 202$  GeV compared to the W mass fit results. L3, ALEPH and DELPHI use reweighted Monte-Carlo samples while OPAL took a relativistic Breit-Wigner function instead.

Table 4: Breakdown of the systematic and statistical errors on  $M_W$  for the different decay topologies in the LEP combined measurement.

Source	Systematic Errors on $M_W$ in MeV		
	$qq\ell\nu$	qqqq	Combined
Colour Reconnection	–	50	13
Bose-Einstein Correlations	–	25	7
LEP Beam Energy	17	17	17
ISR / FSR	8	10	8
Hadronisation	26	23	24
Detector Systematics	11	8	10
Other	5	5	4
Total Systematic	35	64	36
Statistical	38	34	30
Total	51	73	47

The invariant mass distributions obtained from data taken at  $\sqrt{s} = 192 - 202$  GeV are shown in Figure 5. The W boson mass is extracted from these spectra by comparing reweighted Monte-Carlo event samples corresponding to different mass hypotheses to data (ALEPH, L3, OPAL). Alternatively, the differential cross sections are convoluted with resolution functions (DELPHI, OPAL) or the mass is determined from a Breit-Wigner fit to the measured mass spectrum (OPAL).

The results for  $M_W$  are listed in Table 3. The LEP value is a combination of individual measurements performed at 172 - 202 GeV from the experiments for different channels and years taking errors and correlations into account. The resulting  $\chi^2/\text{dof}$  is 27.1/29. The statistical contribution to the error is 30 MeV, that from systematic uncertainties amounts to 36 MeV.

Currently, the systematic uncertainties dominate the total error on  $M_W$ . A part common to all measurements comes from the LEP beam energy determination and amounts to 17 MeV at highest energies [29]. A new beam energy spectrometer that has been installed in 1999 is expected to reduce this error to 7 - 12 MeV [30]. Other systematic uncertainties relevant for all decay channels are hadronisation effects, detector related systematics and effects of initial state and final state radiation.

The fully hadronic decays suffer from specific uncertainties due to hadronic final state interactions (FSI). They occur because the distance between the two decaying W bosons of about 0.1 fm is much smaller than the typical hadronic interactions length of 1 fm. This can give rise to colour reconnection effects [31] or Bose-Einstein correlations [32]. Both can affect the reconstruction of the invariant masses by mo-

momentum transfers between particles that stem from different W bosons. Combining the results from the four experiments common uncertainties of 50 MeV for colour reconnection and 25 MeV for Bose-Einstein effects are estimated by comparing different Monte-Carlo models. FSI effects may also show up in the difference between  $M_W$  values measured from semi-leptonic or from fully hadronic events. The difference, determined removing systematic errors due to possible FSI effects, amounts to

$$\Delta M_W = M_W(\text{qqqq}) - M_W(\text{qql}\nu) = +5 \pm 50 \text{ MeV}$$

and is compatible with zero. Recently, possible effects of FSI are also studied in other observable than the W mass which are sensitive to FSI [33], e.g. the particle flow in the overlap region between two jets and particle correlation functions. In future it may be possible to exclude some of the FSI models in a combined LEP analysis, which should reduce the systematic uncertainty on  $M_W$ .

Table 4 shows a breakdown of all systematic errors for semileptonic and hadronic final states. Due to the uncertainties related to FSI effects the contribution of hadronic final states to the combined  $M_W$  measurement is only 27% while the weight of the semileptonic events is 73%.

The W boson mass  $M_W = 80.427 \pm 0.046 \text{ GeV}$  measured at LEP is in striking agreement with its determination at  $p\bar{p}$  colliders [34] of  $M_W = 80.452 \pm 0.062 \text{ GeV}$ . The resulting average from direct measurements is

$$M_W = 80.436 \pm 0.037 \text{ GeV} .$$

The method of direct reconstruction is also adequate to measure the width of the W boson,  $\Gamma_W$ . The results of the four LEP experiments are shown in Table 3. The combination of the individual measurements is done in the same way as for the determination of  $M_W$ . The resulting LEP value is  $\Gamma_W = 2.12 \pm 0.11 \text{ GeV}$  and is in agreement with the direct determination by CDF [35] of  $\Gamma_W = 2.06 \pm 0.13 \text{ GeV}$ .

## 6 Standard Model Fits

Many SM parameters are measured at LEP1 and SLD like the mass and width of the Z boson,  $M_Z$  and  $\Gamma_Z$ , the hadronic pole cross section,  $\sigma_{\text{had}}^0$ , the ratios of leptonic to hadronic widths,  $R_l$ , the asymmetry parameters for leptons and  $b$  and  $c$ - quarks,  $A_{\text{FB}}^0$ , the  $\tau$  polarisation and quark charge asymmetry,  $Q_{\text{FB}}$ . At SLD the measurement of left-right forward-backward asymmetry and recently the asymmetry for  $s$  quarks [36] are done. Finally, the result for the on-shell value of  $\sin^2 \vartheta_W = 0.2255 \pm 0.0021$  measured by NuTeV/CCFR in  $\nu$ -nucleon scattering [37] and the value of  $\alpha(M_Z^2)$  are added. The latter can be expressed as

$$\alpha(s) = \frac{\alpha(0)}{1 - \Delta\alpha_{\text{lep}}(s) - \Delta\alpha_{\text{had}}^{(5)}(s) - \Delta\alpha_{\text{had}}^{\text{top}}(s)}$$

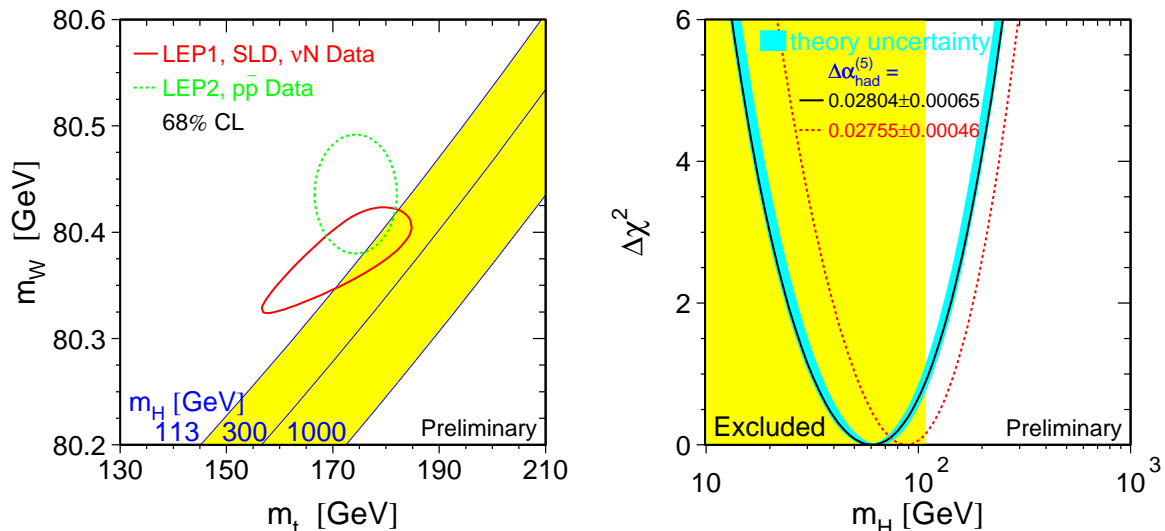


Figure 6: Left: Contours obtained from direct measurements and from a fit to electroweak precision data in the  $M_W$ - $m_t$  plane testing the consistency of the SM. The results are compared to different values of  $M_H$

Right:  $\Delta\chi^2$  of SM fits as a function of  $M_H$  for different values of  $\Delta\alpha_{\text{had}}^{(5)}(s)$ . The blue band indicates theoretical uncertainties due to higher order corrections. Higgs masses in the shaded area are excluded by direct searches.

where all terms except the contribution from the five light quark flavours,  $\Delta\alpha_{\text{had}}^{(5)}(s)$ , are known with high accuracy. Here a value  $\Delta\alpha_{\text{had}}^{(5)}(s) = 0.02804 \pm 0.00065$  [38] is used. A fit within the Standard Model is performed to these inputs to determine the parameters  $M_Z$ ,  $m_t$ ,  $M_H$ ,  $\alpha_s$  and  $\Delta\alpha_{\text{had}}^{(5)}(s)$ .

In Figure 6 the result of the fit is shown in the  $M_W$ - $m_t$  plane and compared to the direct measurements of  $M_W$  at LEP and  $p\bar{p}$  colliders and of  $m_t$  at the TEVATRON [39]. The measurements are nicely consistent with the indirect determination from the SM fit. A similar fit using all data except the direct measurement of the top quark mass result in  $m_t = 179_{-10}^{+13}$  GeV and when using all data except direct  $M_W$  determinations  $M_W = 30.386 \pm 0.025$  GeV is obtained. Again, these results are in good agreement with the respective direct measurements. This demonstrates the compatibility and the internal consistency of the SM within the existing precision and confirms the SM parameter relations at 1-loop level.

The SM fits can also be used to estimate the mass of the Higgs boson. To do this a series of fits with fixed values of  $M_H$  is performed and the difference in the  $\chi^2$  values as shown in Figure 6 is considered. Since the leading radiative correction terms

depend on  $\log(M_H)$  the constraints that can be obtained are not very stringent. The result using  $\Delta\alpha_{\text{had}}^{(5)}(s) = 0.02804 \pm 0.00065$  is

$$M_H = 60_{-29}^{+52} \text{ GeV}; \quad \log(M_H / \text{GeV}) = 1.78_{-0.28}^{+0.27}.$$

The slight decrease with respect to the previous result [40] is mainly caused by the change in  $M_W$ . The central value depends strongly on the top quark mass and the value of  $\Delta\alpha_{\text{had}}^{(5)}(s)$  used.

The value of  $\Delta\alpha_{\text{had}}^{(5)}(s)$  is obtained by integrating the  $R_{\text{had}}$  distribution measured in  $e^+e^-$  annihilation or calculated in perturbative QCD:

$$\Delta\alpha_{\text{had}}^{(5)}(s) \propto \int_{4M_\pi^2}^{\infty} \frac{R(s') ds'}{s'(s' - s)}$$

Recent results obtained at BES [41] have been used to extract the more precise value  $\Delta\alpha_{\text{had}}^{(5)}(s) = 0.02755 \pm 0.00046$  [6] yielding a higher value for  $M_H$ :

$$M_H = 88_{-37}^{+60} \text{ GeV}; \quad \log(M_H / \text{GeV}) = 1.94_{-0.24}^{+0.22}$$

Relying on perturbative QCD the error on  $\Delta\alpha_{\text{had}}^{(5)}(s)$  is further reduced. With the value  $\Delta\alpha_{\text{had}}^{(5)}(s) = 0.02738 \pm 0.00020$  [42] one obtains  $M_H = 104_{-39}^{+59} \text{ GeV}$ .

Depending on the value of  $\Delta\alpha_{\text{had}}^{(5)}(s)$  used in the fit upper limits on the Higgs boson mass of 162 – 215 GeV are obtained at 95% confidence level. The fits suggest that the Standard Model Higgs is light. They are compatible with the results from direct searches for the Higgs that exclude values of  $M_H$  below 113.5 GeV at 95% C.L. and strongly indicate the observation of a Higgs with a mass [43] of

$$M_H = 115_{-0.9}^{+1.3} \text{ GeV}.$$

## 7 Conclusions

Since its start in 1989 the energy range studied at LEP has more than doubled. Up to  $\sqrt{s} = 209 \text{ GeV}$  the measurements of fermion pair production are in good agreement with the Standard Model predictions. The data taken above the Z pole allow to improve the determination of  $M_Z$  and the  $\gamma/Z$  interference within the S-Matrix ansatz significantly. It also allows to exclude new (contact) interactions below energy scales of 10 TeV to 20 TeV.

The cross sections for single W production,  $W^+W^-$  and ZZ production agree with the SM predictions as well.

From the large number of selected  $W^+W^-$  pairs the mass and width of the W boson can be directly reconstructed. The values

$$\begin{aligned}
M_W &= 80.427 \pm 0.046 \text{ GeV} \\
\Gamma_W &= 2.12 \pm 0.11 \text{ GeV}
\end{aligned}$$

are in perfect agreement with the indirect determination of these quantities in fits to electroweak data. The impressive consistency between all direct measurements and indirectly determined parameters confirms the Standard Model at 1-loop level. Fits to all electroweak data profit from the recent progress in the determination of  $\alpha(M_Z^2)$  and predict the mass of the Higgs boson to be

$$M_H = 88_{-37}^{+60} \text{ GeV}$$

which is consistent with the possible direct observation at LEP at  $M_H \approx 115 \text{ GeV}$ .

## Acknowledgments

I thank the experiments ALEPH, DELPHI, L3, OPAL and SLD for making their most recent and preliminary results available. I also thank the LEP and SLD working groups on electroweak physics for their effort combining the measurements and performing the fits. I am grateful to Arno Straessner for discussion of the  $W$  mass measurement.

## References

- [1] S.L. Glashow, *Nucl. Phys.* **22** 579 (1961); S. Weinberg, *Phys. Rev. Lett.* **19** 1264 (1967); A. Salam, "Elementary Particle Theory", Ed. N. Svartholm, (Almqvist and Wiksell, Stockholm, 1968), 367
- [2] M. Veltman, *Nucl. Phys.* **B 7** 637 (1968); G.M. 't Hooft, *Nucl. Phys.* **B 35** 167 (1971); G.M. 't Hooft and M. Veltman, *Nucl. Phys.* **B 44** 189 (1972); *Nucl. Phys.* **B 50** 318 (1972)
- [3] The LEP electroweak working group *LEP-EWWG LS 2000-01*. Contributed paper to ICHEP 2000.
- [4] The LEP WW working group *LEP-EWWG MASS 2000-01*.
- [5] A. Gurtu, *Precision tests of the electroweak gauge theory*, to be published in *Proc. of ICHEP 2000*, World Scientific.
- [6] B. Pietrzyk, *The global fit to electroweak data*, to be published in *Proc. of ICHEP 2000*, World Scientific.

- [7] D. Bardin *et al.*, *hep-ph/9908433*; *Z. Phys.* **C 44** (1989) 493; *Nucl. Phys* **B 351** (1991) 1; *Phys. Lett.* **B 255** (1991) 290.
- [8] G. Montagna *et al.*, *Nucl. Phys* **B401** (1993) 3; *Comp. Phys. Comm.* **76** (1993) 328
- [9] S. Jadach, B. Ward & Z. Was, *Nucl. Phys. Proc. Suppl.* **89** 106 (2000); *Comp. Phys. Comm.* **130** 260 (2000)
- [10] W. Beenakker, F. Berends & A. Chaposvsky *Nucl. Phys* **B 548** 3 (1999)
- [11] A. Denner *et al.*, *hep-ph/0007245*; *Nucl. Phys. Proc. Suppl.* **89** 100 (2000); *hep-ph/0006307*; *hep-ph/9912447*; *hep-ph/007245*; *J. Phys.* **G26** 593 (2000)
- [12] G. Gounaris, J. Layssac & F. Reynard, *Phys. Rev.* **D61** 073013 (2000)
- [13] E. Accomando & A. Ballestrero, *Comp. Phys. Comm.* **99** 270 (1997)
- [14] T. Ishikawa *et al.*, *GRACE* manual, KEK report 92-19 (1993)
- [15] G. Passarino, *Comp. Phys. Comm.* **97** 261 (1996); *hep9810416*; *Nucl. Phys.* **B574** 451 (2000)
- [16] G. Passarino, *Nucl. Phys.* **B578** 3 (2000)
- [17] S. Jadach, W. Placzek & B. Ward, *Phys. Rev.* **D56** 6369 (1997)
- [18] G. Passarino in *hep-ph/0005309*
- [19] M. Kobel *et al.*, *hep-ph/0007180*
- [20] M. Grünewald, G. Passarino *et al.*, *hep-ph/0005309*
- [21] LEP electroweak working group,  $f\bar{f}$  subgroup, *LEP2FF 00-03* (2000)
- [22] A. Leike, T. Riemann and J. Rose, *Phys. Lett.* **B 273** 513 (1991); T. Riemann, *Phys. Lett.* **B 293** 451 (1992)
- [23] L3 collab., M. Acciari *et al.*, *Phys. Lett.* **B 489** 93 (2000)
- [24] TOPAZ Collab., K. Miyabayashi *et al.*, *Phys. Lett.* **B 347** 171 (1995); VENUS Collab., K. Yusa *et al.*, *Phys. Lett.* **B 447** 167 (1999)
- [25] E. Eichten, K. Lane & M. Peskin, *Phys. Rev. Lett.* **50** 811 (1983)
- [26] LEP electroweak working group *LEPEWWG/XSEC 2000-01* (2000)
- [27] D. Bardin *et al.*, *Comp. Phys. Comm.* **104** 161 (1997)

- [28] U. Bassler, *Electroweak Measurements at the Tevatron*, talk presented at XXXVth Rencontres de Moriond, Electroweak Interactions and Unified Theories, Les Arcs, March 11-18, 2000; F. Abe *et al.*, CDF collab., *Phys Rev D* **52** 2624 (1995); B. Abbott *et al.*, D0 collab., *Phys Rev D* **61** 072001 (2000).
- [29] The LEP energy calibration working group, A. Blondel *et al.*, *Eur. Phys. J.* **C11** (1999) 573; The LEP energy calibration working group, *LEP ECAL* **99-01**.
- [30] G. Wilkinson, Energy Calibration: Status and Prospects, *Proc. of the 10th Chamonix Workshop on LEP-SPS*, Ed. P. Le Roux *CERN-SL* **2000-007**
- [31] G. Gustafson, U. Petterson & P.M. Zerwas, *Phys. Lett.* **B 209** 90 (1988); T. Sjöstrand & V.A. Khoze, *Z. Phys.* **C 62** 281 (1994), *Phys. Rev. Lett.* **72** 28 (1994); E. Accomando, A. Ballestrero & E. Maina, *Phys. Lett.* **B 362** 141 (1995); G. Gustafsson & J. Häkkinen, *Z. Phys.* **C 64** 659 (1994); L. Lönnblad, *Z. Phys.* **C 70** 107 (1996); J. Ellis & K. Geiger, *Phys. Rev.* **D 54** 1967 (1996), *Phys. Lett.* **B 404** 230 (1997).
- [32] K. Fialkowski & R. Wit, *Z. Phys.* **C 74** 145 (1997); K. Fialkowski, R. Wit & J. Wosiek, *Phys. Rev.* **D 58** 094013 (1998); S. Jadach & K. Zalewski, *Acta. Phys. Pol.* **B 28** 1363 (1997); V. Kartvelishvili, R. Kvatadze & R. Møller, *Phys. Lett.* **B 408** 331 (1997); L. Lönnblad & T. Sjöstrand, *Phys. Lett.* **B 351** 293 (1995); L. Lönnblad & T. Sjöstrand, *Eur. Phys. J.* **C 2** 165 (1998).
- [33] A. Valassi, *Bose-Einstein correlations in W decays at LEP*, and P. de Jong, *Colo(u)r reconnection in W decays*, to be published in *Proc. of ICHEP 2000*, World Scientific.
- [34] The UA2 Collaboration, J. Alitti *et al.*, *Phys. Lett.* **B 241** 150 (1990); *Phys. Lett.* **B 276** 354 (1992); The DO Collaboration, B. Abbott *et al.*, *Phys. Rev. Lett.* **84** 222 (2000); B. Carithers, *New W Mass Measurements from CDF/DO*, talk presented at the EPS conference, Tampere, Finland, July 1999.
- [35] T. Affolder *et al.*, CDF collab., *Phys. Rev. Lett.* **85** 3347 (2000)
- [36] D. Su, *First Direct Measurement of the Parity-Violating Coupling of the Z0 to the s-Quark*, to be published in *Proc. of ICHEP 2000*, World Scientific.
- [37] CCFR/NuTeV Collaboration, K. McFarland *et al.*, *Eur. Phys. Jour.* **C1** 509 (1998); NuTeV Collaboration, K. McFarland, *hep-ex/9806013*.
- [38] S. Eidelmann and F. Jegerlehner, *Z. Phys.* **C 67** 585 (1995).
- [39] R. Partridge, *Heavy Quark Production and Decay (t, b, and onia)*, talk presented at ICHEP'98, Vancouver, B.C., Canada, July 1998.

- [40] The LEP collaborations ALEPH, DELPHI, L3, OPAL, the LEP electroweak working group and the SLD heavy flavour and electroweak groups, *CERN-EP 2000-16* (2000)
- [41] Z. Zhao, *Measurements of  $R$  at 2-5 GeV*, to be published in *Proc. of ICHEP 2000*, World Scientific.
- [42] A.D. Martin, *et al.*, *hep-ph/0008078*.
- [43] P. Igo-Kemenes, LEP-Seminar, Nov. 3rd 2000

DESY 01/003  
LU-ITP 01/01  
PSI-PR-01-01  
UR-1630, ER/40685/965  
August 15, 2001  
hep-ph/0101257

## Off-shell W-pair production — universal versus non-universal corrections

A. DENNER

*Paul Scherrer Institut, CH-5232 Villigen PSI, Switzerland*

S. DITTMAYER\*

*Deutsches Elektronen-Synchrotron DESY, D-22603 Hamburg, Germany*

M. ROTH

*Institut für Theoretische Physik, Universität Leipzig, D-04109 Leipzig, Germany*

D. WACKEROTH

*Department of Physics and Astronomy, University of Rochester,  
Rochester, NY 14627-0171, USA*

Electroweak radiative corrections to  $e^+e^-$  scattering processes typically amount to  $\mathcal{O}(10\%)$  at LEP energies. Their logarithmic increase with energy renders them even more important at future colliders. Although the bulk of these corrections is due to universal process-independent effects, the remaining non-universal corrections are nevertheless phenomenologically important. We describe the structure of the universal corrections to  $e^+e^- \rightarrow WW \rightarrow 4f$  in detail and discuss the numerical size of universal and non-universal effects using the Monte Carlo generator RACONWW<sup>†</sup>.

Presented at the

5th International Symposium on Radiative Corrections  
(RADCOR–2000)

Carmel CA, USA, 11–15 September, 2000

---

\*Heisenberg fellow of the Deutsche Forschungsgemeinschaft

<sup>†</sup>Program available from <http://www.hep.psi.ch/racoonww/racoonww.html>

# 1 Introduction

At present, the investigation of W-pair production at LEP2 plays an important role in the verification of the Electroweak Standard Model (SM). Apart from the direct observation of the triple-gauge-boson couplings in  $e^+e^- \rightarrow W^+W^-$ , the increasing accuracy in the W-pair-production cross-section and W-mass measurements has put this process into the row of SM precision tests [ 1]. The W-pair cross section is measured at the per-cent level, and the W-boson-mass determination aims at a final accuracy of 30 MeV. Experiments at a future  $e^+e^-$  linear collider (LC) with higher luminosity and higher energy will even exceed this precision.

To account for the high experimental accuracy on the theoretical side is a great challenge: the W bosons have to be treated as resonances in the full four-fermion processes  $e^+e^- \rightarrow 4f$ , and radiative corrections need to be included. While several lowest-order predictions are based on the full set of Feynman diagrams, only very few calculations include radiative corrections beyond the level of universal radiative corrections (see Refs. [ 2, 3] and references therein). These universal corrections comprise the leading process-independent effects; for  $e^+e^- \rightarrow WW \rightarrow 4f$  these include universal renormalization effects (running or effective couplings), the Coulomb singularity at the W-pair-production threshold, and initial-state radiation (ISR) in leading-logarithmic approximation. The remaining corrections are usually viewed as non-universal and can only be included by an explicit diagrammatic calculation. In this article we describe the structure of the universal corrections in detail and discuss the size of the non-universal corrections for LEP2 und LC energies. This issue is not only theoretically interesting, it is also important in practice, since many Monte Carlo generators for W-pair production that are in use neglect non-universal electroweak corrections.

The size of non-universal corrections was already estimated by inspecting the pair production of stable W bosons quite some time ago [ 2, 4, 5]. For LEP2 energies these effects reduce the total W-pair cross section at the level of 1–2%, but for energies in the TeV range the impact grows to  $\mathcal{O}(10\%)$ . For differential distributions the size of the non-universal corrections is usually much larger. In the following we investigate the corresponding corrections to off-shell W-pair production,  $e^+e^- \rightarrow WW \rightarrow 4f$ , by inspecting total cross sections as well as angular and invariant-mass distributions with the Monte Carlo generator RACOONWW [ 6].

## 2 Radiative corrections to off-shell W-pair production — state of the art

Fortunately, to match the experimental precision for W-pair production a full one-loop calculation for the four-fermion processes is not needed for most purposes,

in particular for LEP2 physics. Instead it is sufficient to take into account only those radiative corrections that are enhanced by two resonant W bosons. For centre-of-mass (CM) energies  $E_{\text{CM}}$  not too close to the W-pair-production threshold, say for  $E_{\text{CM}} \gtrsim 170 \text{ GeV}$ , the neglected  $\mathcal{O}(\alpha)$  corrections are of the order  $(\alpha/\pi)(\Gamma_{\text{W}}/M_{\text{W}})$ , i.e. below 0.5% even if possible enhancement factors are taken into account. The theoretically clean way to carry out this approximation is the expansion about the two resonance poles, which is called *double-pole approximation* (DPA). A full description of this strategy and of different variants used in the literature (some of them involving further approximations) can be found in Refs. [ 6, 7, 8, 9].

At present, two Monte Carlo programs include  $\mathcal{O}(\alpha)$  corrections to  $e^+e^- \rightarrow \text{WW} \rightarrow 4f$  in DPA and further numerically important higher-order effects: YFSWW3 [ 7] and RACOONWW [ 6]. The salient features of the two approaches, which are conceptually very different, as well as detailed comparisons of numerical results are summarized in Ref. [ 3]. Further numerical results of the two programs can be found in Refs. [ 10, 11]. Both programs have reached an accuracy of roughly  $\sim 0.5\%$  for CM energies between 170 GeV and 500 GeV. For higher energies also leading electroweak two-loop effects become important (see also below).

Figure 1 shows a comparison of the results of RACOONWW and YFSWW3 with recent LEP2 data, as given by the LEP Electroweak Working Group [ 12] for the Summer 2000 conferences. The data are in good agreement with the predictions of the two programs, which differ by about 0.3% at LEP2 energies. Below a CM energy of 170 GeV, the prediction in Figure 1 is continued by GENTLE [ 13], which does not include the non-universal electroweak corrections. In its new version GENTLE is tuned to reproduce the DPA prediction of RACOONWW and YFSWW3 on the total cross section at LEP2 within a few per mill (see Ref. [ 3]).

### 3 Universal electroweak corrections — improved Born approximation

#### 3.1 Preliminaries

Universal radiative corrections are those parts of the full correction that are connected to specific subprocesses, such as collinear photon emission or running couplings, and lead to characteristic enhancement factors. Owing to their universality such corrections are often related to the lowest-order matrix element of the underlying process. In the following we construct an *improved Born approximation* (IBA) for the processes  $e^+e^- \rightarrow \text{WW} \rightarrow 4f$  that is based on universal corrections only. For the production subprocess the IBA closely follows the approximation formulated in Ref. [ 4] for on-shell W-pair production. For the W decay the IBA is identical with the lowest-order prediction in the  $G_\mu$  scheme, as suggested in Ref. [ 14].

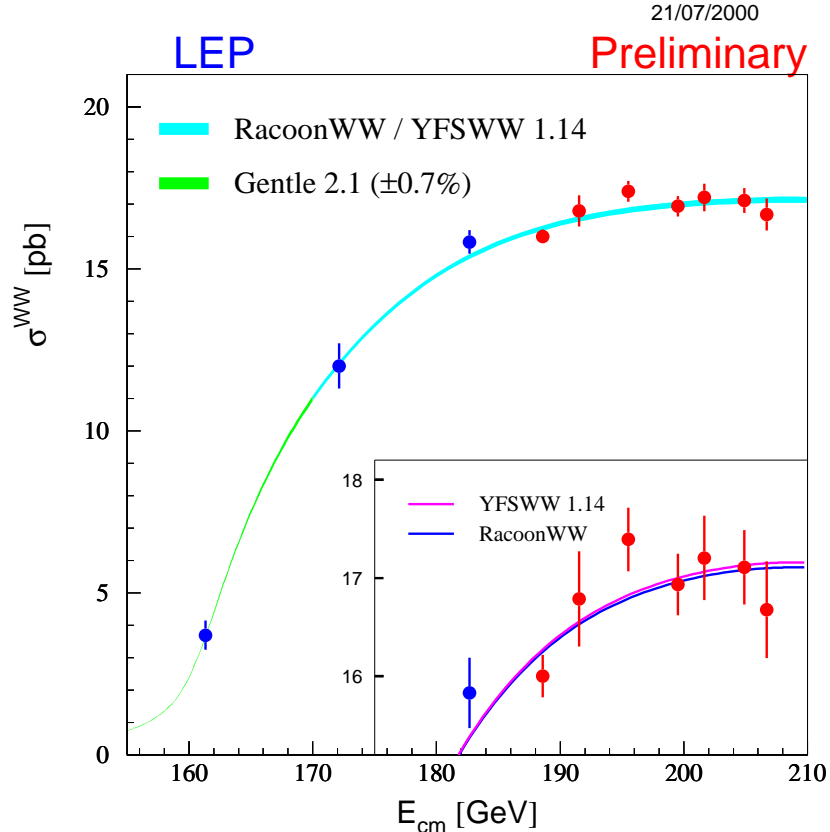


Figure 1: Total WW production cross section at LEP2 as given by the LEPEWWG [ 12]

In order to define the IBA, we first need the lowest-order matrix element of the process

$$\begin{aligned}
 e^+(p_+, \sigma_+) + e^-(p_-, \sigma_-) &\rightarrow W^+(k_+, \lambda_+) + W^-(k_-, \lambda_-) \\
 &\rightarrow f_1(k_1, \sigma_1) + \bar{f}_2(k_2, \sigma_2) + f_3(k_3, \sigma_3) + \bar{f}_4(k_4, \sigma_4). \quad (3.1)
 \end{aligned}$$

The arguments label the momenta  $p_{\pm}$ ,  $k_i$  and helicities  $\sigma_i = \pm 1/2$ ,  $\lambda_j = 0, \pm 1$  of the corresponding particles. The cross section that is defined by including only the so-called *signal diagrams* for W-pair-mediated four-fermion production, which are shown in Figure 2, is called CC03 cross section<sup>1</sup>. Note that the masses of the external fermions (not the ones in closed fermion loops) are neglected whenever possible. In the absence of photon radiation this, in particular, implies that we have helicity conservation for the initial  $e^+e^-$  system, i.e. only the combination  $\sigma_- = -\sigma_+$  con-

<sup>1</sup>Of course, the CC03 cross section is a non gauge-invariant quantity. However, evaluated in the 't Hooft-Feynman gauge it approximates the full cross sections for W-pair-mediated  $4f$  production very well, as long as no electrons or positrons are in the final state. Therefore, the CC03 cross section is widely used in the literature (see also Refs. [ 2, 3]).

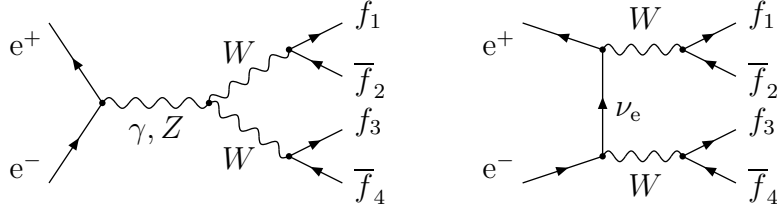


Figure 2: Lowest-order signal diagrams for  $e^+e^- \rightarrow WW \rightarrow 4f$

tributes, and we can define  $\sigma = \sigma_- = -\sigma_+$ . For definite electron helicity  $\sigma$ , the lowest-order CC03 matrix element is given by

$$\mathcal{M}_{\text{Born,CC03}}^{e^+e^- \rightarrow WW \rightarrow 4f, \sigma}(p_+, p_-, k_+, k_-, k_+^2, k_-^2) = \sum_{n=1}^3 F_{n, \text{Born}}^\sigma(s, t) \mathcal{M}_n^\sigma(p_+, p_-, k_+, k_-, k_+^2, k_-^2), \quad (3.2)$$

where  $\mathcal{M}_n^\sigma$  are so-called standard matrix elements (SME) containing the spinor chains of the external fermions, and  $F_{n, \text{Born}}^\sigma(s, t)$  are invariant functions containing couplings and propagator factors. In lowest order only three SME and invariant functions contribute. Following the notation and conventions of Ref. [6], these read ( $\omega_\pm = (1 \pm \gamma_5)/2$ )

$$\begin{aligned} \mathcal{M}_1^\sigma &= \bar{v}(p_+) \not{\epsilon}_+^* (\not{k}_+ - \not{p}_+) \not{\epsilon}_-^* \omega_\sigma u(p_-), \\ \mathcal{M}_2^\sigma &= \bar{v}(p_+) \frac{1}{2} (\not{k}_+ - \not{k}_-) \omega_\sigma u(p_-) (\varepsilon_+^* \varepsilon_-^*), \\ \mathcal{M}_3^\sigma &= \bar{v}(p_+) \not{\epsilon}_+^* \omega_\sigma u(p_-) (\varepsilon_-^* k_+) - \bar{v}(p_+) \not{\epsilon}_-^* \omega_\sigma u(p_-) (\varepsilon_+^* k_-) \end{aligned} \quad (3.3)$$

with “effective W-polarization vectors”

$$\begin{aligned} \varepsilon_+^{*, \mu} &= \frac{e}{\sqrt{2} s_w} \frac{1}{k_+^2 - M_W^2 + i M_W \Gamma_W} \bar{u}(k_1) \gamma^\mu \omega_- v(k_2), \\ \varepsilon_-^{*, \mu} &= \frac{e}{\sqrt{2} s_w} \frac{1}{k_-^2 - M_W^2 + i M_W \Gamma_W} \bar{u}(k_3) \gamma^\mu \omega_- v(k_4), \end{aligned} \quad (3.4)$$

and

$$\begin{aligned} F_{1, \text{Born}}^\sigma(s, t) &= \frac{e^2}{2 s_w^2 t} \delta_{\sigma-}, \\ F_{3, \text{Born}}^\sigma(s, t) &= -F_{2, \text{Born}}^\sigma(s, t) = \frac{2e^2}{s} - \frac{2e^2}{s - M_Z^2} \left( 1 - \frac{\delta_{\sigma-}}{2 s_w^2} \right). \end{aligned} \quad (3.5)$$

The actual values of the input parameters  $e$ ,  $M_W$ ,  $M_Z$ , and  $s_w$  depend on the input-parameter scheme. In the  $G_\mu$ -scheme the electromagnetic coupling  $e$  is deduced from the Fermi constant  $G_\mu$  using the tree-level relation  $e^2 = 4\sqrt{2} G_\mu M_W^2 s_w^2$ , and the weak

mixing angle is fixed by the gauge-boson masses, which are independent input parameters,  $s_w^2 = 1 - M_W^2/M_Z^2$ .

Before we define the IBA we comment on the calculation of the full factorizable one-loop correction in DPA<sup>2</sup>, which is described in Ref. [ 6], and its relation to the decomposition (3.2). In this case six independent SME contribute for each value of  $\sigma$ , and the functions  $F_n^\sigma$  contain standard loop integrals. Moreover, in order to guarantee the gauge invariance of the corrections, which is mandatory for consistency, it is necessary to perform an on-shell projection of the external fermion momenta  $k_i$ . This means that the  $k_i$  are changed to related momenta  $\hat{k}_i$  in such a way that  $\hat{k}_\pm^2 = M_W^2$ . The off-shell values  $k_\pm^2$  are kept only in the propagator factors of (3.4).<sup>3</sup>

### 3.2 Improved Born approximation

The first step in the construction of the IBA consists in a modification of the Born matrix element in such a way that the universal renormalization effects induced by the running of  $\alpha$  and by  $\Delta\rho$  are absorbed. This is achieved [ 4] by the replacements

$$\frac{e^2}{s_w^2} \rightarrow 4\sqrt{2}G_\mu M_W^2, \quad e^2 \rightarrow 4\pi\alpha(s) \quad (3.6)$$

in the lowest-order functions  $F_{i,\text{Born}}^\sigma$  of (3.5), which implies that weak-isospin exchange involves the coupling  $G_\mu M_W^2$  and pure photon exchange the coupling  $\alpha(s)$ . The running of the electromagnetic coupling is induced by light (massless) charged fermions only, i.e. we evaluate  $\alpha(s)$  by

$$\alpha(s) = \frac{\alpha(M_Z^2)}{1 - \frac{\alpha(M_Z^2)}{3\pi} \ln(s/M_Z^2) \sum_{f \neq t} N_f^c Q_f^2} \quad (3.7)$$

with the value  $\alpha(M_Z^2) = 1/128.887$  taken from the fit [ 15] of the hadronic vacuum polarization to the empirical ratio  $R = \sigma(e^+e^- \rightarrow \text{hadrons})/\sigma(e^+e^- \rightarrow \mu^+\mu^-)$ . Thus, the basic matrix element for the IBA reads

$$\mathcal{M}_{\text{IBA}}^{e^+e^- \rightarrow \text{WW} \rightarrow 4f, \sigma}(p_+, p_-, k_+, k_-, k_+^2, k_-^2) = \sum_{n=1}^3 F_{n,\text{IBA}}^\sigma(s, t) \mathcal{M}_n^\sigma(p_+, p_-, k_+, k_-, k_+^2, k_-^2) \quad (3.8)$$

---

<sup>2</sup> In DPA the virtual one-loop correction consists of *factorizable* and *non-factorizable* contributions. The factorizable corrections are the ones that are related to the W-pair-production and W-decay subprocesses. The non-factorizable corrections comprise the remaining doubly-resonant virtual corrections and include all diagrams with photon exchange between the production and decay subprocesses.

<sup>3</sup>This on-shell projection also renders the CC03 cross section gauge-invariant, leading to the so-called DPA Born cross section. However, the DPA Born cross section is a much worse approximation for the  $4f$  cross section than the CC03 variant (see also Refs. [ 3, 8]).

with

$$\begin{aligned}
F_{1,\text{IBA}}^\sigma(s, t) &= \frac{2\sqrt{2}G_\mu M_W^2}{t} \delta_{\sigma-}, \\
F_{3,\text{IBA}}^\sigma(s, t) &= -F_{2,\text{IBA}}^\sigma(s, t) = \frac{4\sqrt{2}G_\mu M_W^2}{s - \hat{M}_Z^2} \delta_{\sigma-} - \frac{8\pi\alpha(s)\hat{M}_Z^2}{s(s - \hat{M}_Z^2)}. \tag{3.9}
\end{aligned}$$

Note that we have used the complex Z-boson mass  $\hat{M}_Z^2 = M_Z^2 - iM_W\Gamma_Z$  in order to regularize the Z resonance below the W-pair-production threshold; otherwise the ISR convolution over the reduced CM energy would lead to complications (see below).

Another important virtual correction is induced by the Coulomb singularity near the W-pair-production threshold. We include this effect in the calculation of the ‘‘hard’’ IBA cross section  $\hat{\sigma}_{\text{IBA}}^{e^+e^- \rightarrow \text{WW} \rightarrow 4f}$ ,

$$\int d\hat{\sigma}_{\text{IBA}}^{e^+e^- \rightarrow \text{WW} \rightarrow 4f}(p_+, p_-) = \frac{1}{2s} \int d\Phi_{4f} |\mathcal{M}_{\text{IBA}}^{e^+e^- \rightarrow \text{WW} \rightarrow 4f}|^2 \left[ 1 + \delta_{\text{Coul}}(s, k_+^2, k_-^2) g(\bar{\beta}) \right], \tag{3.10}$$

where the correction factor  $\delta_{\text{Coul}}$  is given by [ 16, 17]

$$\begin{aligned}
\delta_{\text{Coul}}(s, k_+^2, k_-^2) &= \frac{\alpha(0)}{\bar{\beta}} \text{Im} \left\{ \ln \left( \frac{\beta - \bar{\beta} + \Delta_M}{\beta + \bar{\beta} + \Delta_M} \right) \right\}, \\
\bar{\beta} &= \frac{\sqrt{s^2 + k_+^4 + k_-^4 - 2sk_+^2 - 2sk_-^2 - 2k_+^2 k_-^2}}{s}, \\
\beta &= \sqrt{1 - \frac{4(M_W^2 - iM_W\Gamma_W)}{s}}, \quad \Delta_M = \frac{|k_+^2 - k_-^2|}{s} \tag{3.11}
\end{aligned}$$

with the fine-structure constant  $\alpha(0)$ . The auxiliary function

$$g(\bar{\beta}) = (1 - \bar{\beta}^2)^2 \tag{3.12}$$

restricts the impact of  $\delta_{\text{Coul}}$  to the threshold region where it is valid. Its actual form (and its occurrence) is somewhat ad hoc but justified by a numerical comparison to the full  $\mathcal{O}(\alpha)$  correction. Omitting this factor would lead to a constant positive correction of a few per mill above threshold, although the correct non-universal correction is even negative.

The last ingredient in the IBA is the leading-logarithmic contribution induced by initial-state radiation (ISR). We follow the structure-function approach [ 18], where the full IBA cross section  $\sigma_{\text{IBA}}$  reads

$$\int d\sigma_{\text{IBA}} = \int_0^1 dx_1 \int_0^1 dx_2 \Gamma_{\text{ee}}^{\text{LL}}(x_1, Q^2) \Gamma_{\text{ee}}^{\text{LL}}(x_2, Q^2) \int d\hat{\sigma}_{\text{IBA}}^{e^+e^- \rightarrow \text{WW} \rightarrow 4f}(x_1 p_+, x_2 p_-). \tag{3.13}$$

The structure functions  $\Gamma_{ee}^{\text{LL}}(x, Q^2)$  include the leading logarithms  $[\alpha \ln(Q^2/m_e^2)]^n$  up to order  $n = 3$ , and the soft-photon effects are exponentiated; the explicit expressions can also be found in Refs. [ 2, 6]. The QED splitting scale  $Q^2$  is not fixed in leading-logarithmic approximation and has to be set to a typical momentum scale of the process. It can be used to adjust the IBA to the full correction, but also to estimate the intrinsic uncertainty of the IBA by choosing different values for  $Q^2$ .

Finally, we have to fix the W-boson width  $\Gamma_W$  in the evaluation of the IBA. In order to avoid any kind of mismatch with the decay,  $\Gamma_W$  should be calculated in lowest order using the  $G_\mu$  scheme. This choice guarantees that the “effective branching ratios”, which result after integrating out the decay parts, add up to one when summing over all channels. Of course, if naive QCD corrections are taken into account by multiplying with  $(1 + \alpha_s/\pi)$  for each hadronically decaying W boson, these QCD factors also have to be included in the calculation of the total W width.

Note that unlike the full one-loop calculation in DPA, the IBA is also applicable near the W-pair production threshold, since no pole expansion is involved.

## 4 Comparison of the improved Born approximation with state-of-the-art results

### 4.1 Total cross section

In order to investigate the reliability of the IBA defined in (3.13), we have implemented this IBA in the Monte Carlo program RACOONWW, which provides state-of-the-art predictions for the full  $\mathcal{O}(\alpha)$  corrections in DPA, as discussed above. For the following numerical evaluations we have adopted the input-parameter set of Refs. [ 3, 6].

Figure 3 compares different predictions for the total cross section (without any phase-space cuts) for the semileptonic process  $e^+e^- \rightarrow u\bar{d}\mu^-\bar{\nu}_\mu(\gamma)$  for CM energies  $E_{\text{CM}}$  up to 1 TeV. The IBA is evaluated for the two different scales  $Q^2 = s = E_{\text{CM}}^2$  and  $Q^2 = |t_{\text{min}}| = E_{\text{CM}}^2 \left(1 - \sqrt{1 - 4M_W^2/E_{\text{CM}}^2}\right) / 2 - M_W^2$ , and “best” labels the RACOONWW prediction including all universal and non-universal corrections as described in detail in Ref. [ 6]. The motivation for  $Q^2 = s$  is obvious;  $Q^2 = |t_{\text{min}}|$  is motivated by the fact that  $t_{\text{min}}$  corresponds to the minimal momentum transfer in the  $t$ -channel diagrams for forward scattering of on-shell W bosons, which dominates the cross section. The comparison of the corresponding relative corrections (normalized to the CC03 Born cross section in  $G_\mu$  scheme) is shown in Figure 4.

For LEP2 energies, i.e. energies below 210 GeV, the difference between the two IBA versions reflects the typical uncertainty of 1–2% inherent in all predictions that neglect non-universal electroweak corrections. It turns out that the IBA with  $Q^2 = s$  is closer to the “best” prediction, with a maximal deviation at the upper LEP2

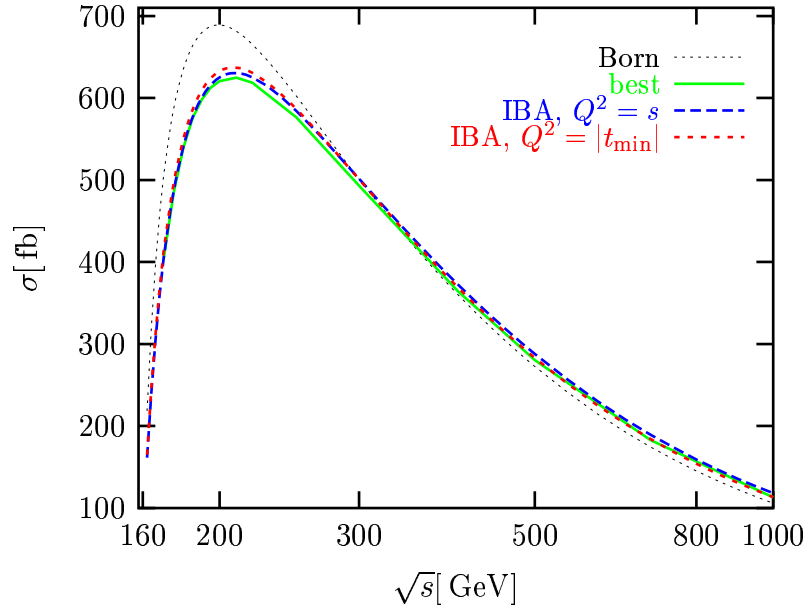


Figure 3: Predictions for the total cross section for the process  $e^+e^- \rightarrow u\bar{d}\mu^-\bar{\nu}_\mu$  based on various approximations for radiative corrections

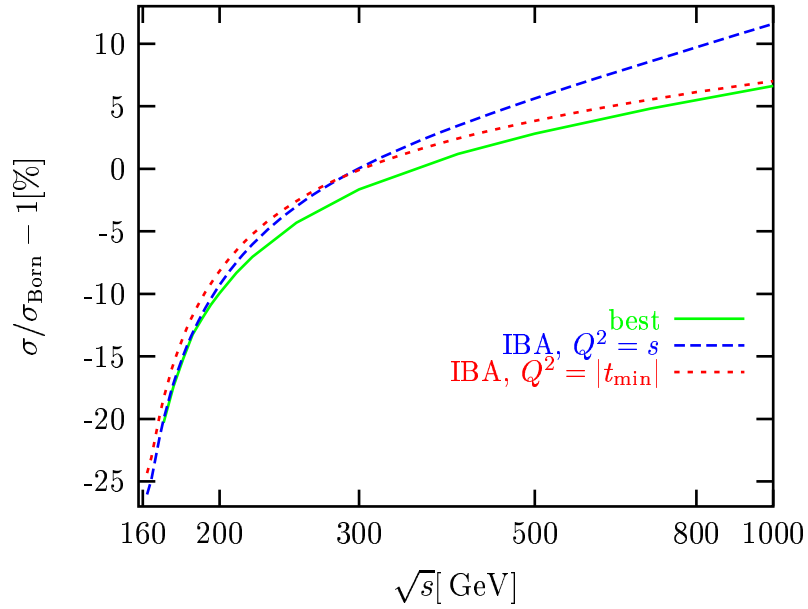


Figure 4: Relative corrections to the total cross section for the process  $e^+e^- \rightarrow u\bar{d}\mu^-\bar{\nu}_\mu$  in various approximations

energies:  $\sim 0.6\%$  at 200 GeV and  $\sim 0.8\%$  at 210 GeV. Note that the “best” prediction is not included below 170 GeV, since the uncertainty of all predictions based on a DPA formally runs out of control near the  $W$ -pair-production threshold. On the other hand, the IBA does not suffer from this constraint. Since the IBA with  $Q^2 = s$  agrees with the “best” prediction near 170 GeV at the per-mill level this IBA version is an appropriate extrapolation of the “best” RACOONWW prediction down to the  $W$ -pair-production threshold. Of course, the theoretical uncertainty below 170 GeV is then of the order of one to a few per cent.

For LC energies the IBA becomes more and more uncertain; for 1 TeV the two IBA versions differ already by  $\sim 5\%$ . This signals that non-leading electroweak corrections become more and more important. The dominant effects are due to Sudakov logarithms [ 19] of the type  $\alpha \ln^2(s/M_W^2)$  which originate from the exchange of soft and collinear massive gauge bosons, i.e.  $W$  and  $Z$  bosons. The IBA does not account for these effects. Nevertheless the IBA with  $Q^2 = |t_{\min}|$  follows the “best” prediction within  $\sim 1\text{--}2\%$  even for high energies. This is plausible, because the total cross section is strongly dominated by the  $t$ -channel pole for forward scattering for high energies, and this contribution is well approximated by the IBA. Note, however, that the good agreement could not be predicted without a comparison with the full DPA correction including non-universal electroweak corrections. On the other hand, it can be expected that the quality of the IBA with  $Q^2 = |t_{\min}|$  also becomes worse if forward scattering is excluded or suppressed by phase-space cuts; this issue is further discussed below in the context of differential distributions.

## 4.2 Differential distributions

In order to define differential distributions, the kinematic information on the fermion momenta in  $e^+e^- \rightarrow WW \rightarrow 4f(\gamma)$  is required. In the presence of photon radiation, a consistent treatment of photons that are soft or collinear to charged fermions is crucial. If such photons are not recombined with the nearest charged fermion, i.e. if these photon–fermion systems are not treated as single “quasi-particles”, the bare fermion momenta in general lead to distributions that are not IR-safe, i.e. they involve mass-singular logarithms of the form  $\alpha \ln m_f$ . For fermions other than muons such effects are definitely unphysical. In order to avoid such artifacts, we recombine soft and collinear photons according to the procedure<sup>4</sup> described in Refs. [ 3, 6].

---

<sup>4</sup>In this approach, first photons close to the beams are dropped in events, i.e. their momenta are set to zero. If the photon survives the cut to the beam, it is recombined with the charged fermion  $f$  if  $M_{f\gamma} < M_{\text{rec}}$ , where  $f$  is the fermion with the smallest invariant mass  $M_{f\gamma}^2 = (p_f + k_\gamma)^2$  with the photon. Finally, events are discarded in which charged fermions are close to the beam. The size of the recombination cut  $M_{\text{rec}}$ , thus, determines how many photons are recombined with the charged fermions. In Refs. [ 3, 6] the two values  $M_{\text{rec}} = 5$  GeV and 25 GeV are chosen, defining a “bare” and a “calo(rimetric)” setup, respectively.

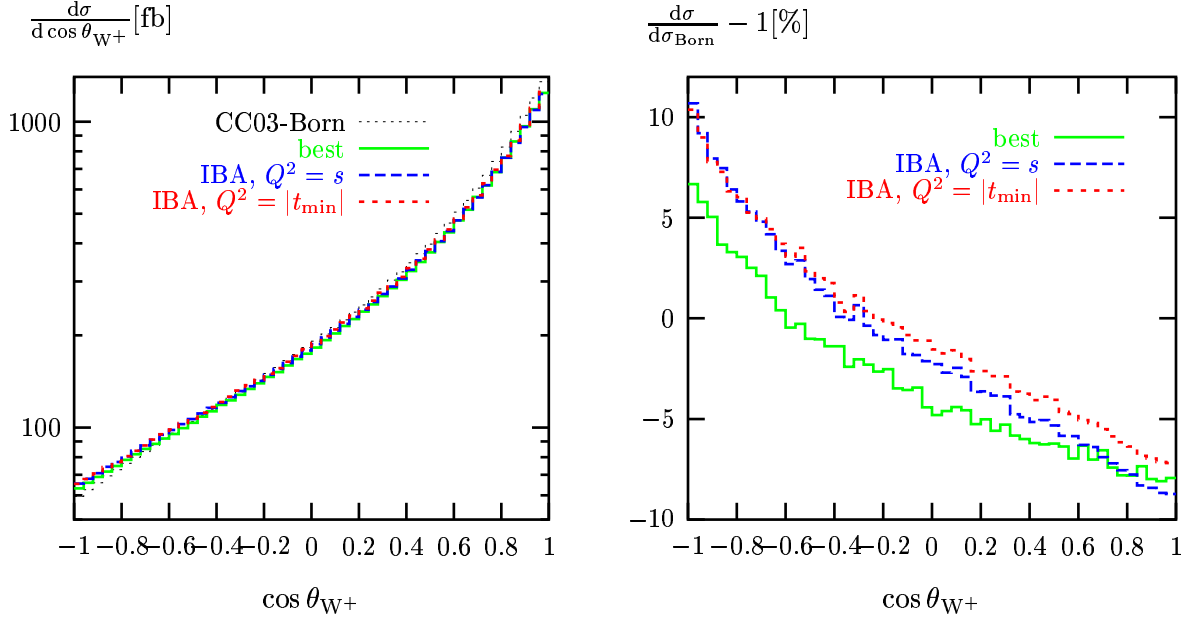


Figure 5: Predictions for the  $W^+$ -production-angle distribution (left) and corresponding relative corrections (right) for the process  $e^+e^- \rightarrow u\bar{d}\mu^-\bar{\nu}_\mu$  at  $E_{\text{CM}} = 200$  GeV based on various approximations for radiative corrections

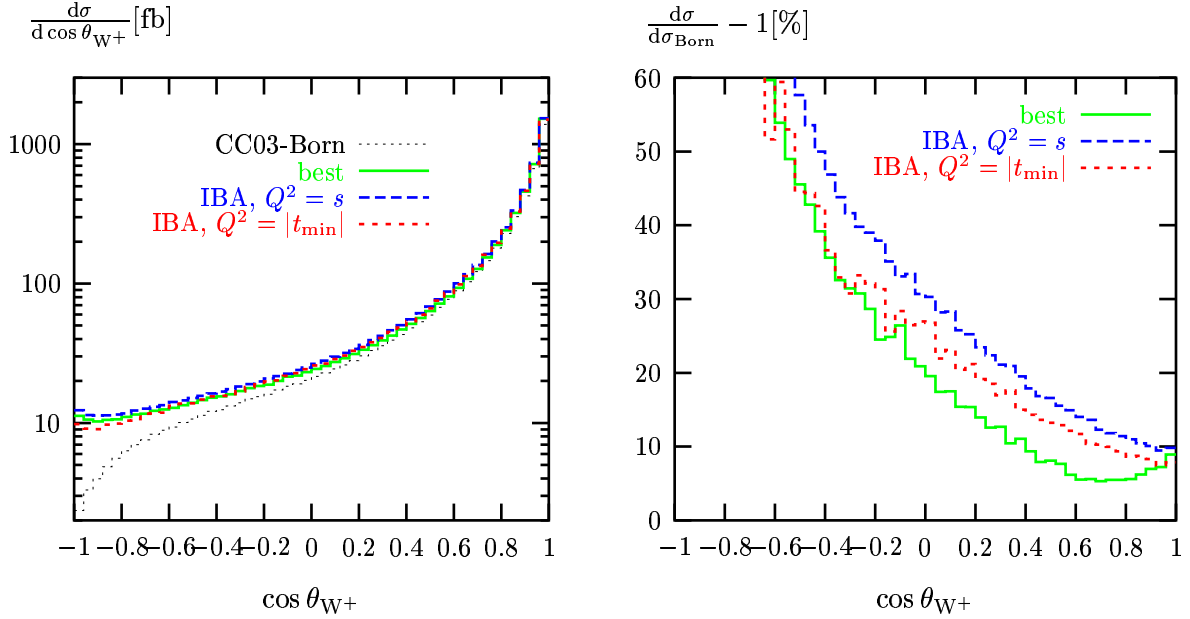


Figure 6: Predictions for the  $W^+$ -production-angle distribution (left) and corresponding relative corrections (right) for the process  $e^+e^- \rightarrow u\bar{d}\mu^-\bar{\nu}_\mu$  at  $E_{\text{CM}} = 500$  GeV based on various approximations for radiative corrections

In Figures 5 and 6 the full RACOONWW and IBA predictions for the  $W^+$ -production-angle distribution are compared for the process  $e^+e^- \rightarrow u\bar{d}\mu^-\bar{\nu}_\mu$  at the typical LEP2 energy of  $E_{\text{CM}} = 200 \text{ GeV}$  and the LC energy  $E_{\text{CM}} = 500 \text{ GeV}$ . The uncertainty of the IBA predictions induced by the QED splitting scale  $Q$  is about 1–2% and  $\sim 5\%$  for LEP and LC energies, respectively. The deviation of the IBA prediction from the full result is up to  $\sim 5\%$  and  $\sim 5\text{--}10\%$ , where the agreement is best for forward scattering ( $\cos\theta_{W^+} \rightarrow 1$ ), as anticipated above. The IBA uncertainty and the deviation from the full result further grow with increasing energy. This comparison is performed using the “calo” setup for the photon recombination of photons, but the sensitivity of the  $W$ -production-angle distribution to the recombination procedure is very weak (see Refs. [ 3, 6]).

The sensitivity to photon recombination is maximal in the invariant-mass distributions of the reconstructed  $W$  bosons, which can be seen by comparing Figures 7 and 8. The full correction shows a very strong dependence on the recombination procedure, which was discussed in Ref. [ 10] in detail. The more inclusive recombination (“calo”) leads to large positive corrections above resonance and thus to a shift of the resonance to the right, which can be of the order of some 10 MeV [ 10]. Since this distortion of the  $W$  line shape is mainly induced by final-state radiation and radiation off the  $W$  bosons, the IBA, as defined above, does not account for this effect. It is obvious that the  $W$ -invariant-mass distributions can only be properly described if photon radiation from the  $W$ -decay processes is taken into account properly. Figures 7 and 8 refer to the LEP energy  $E_{\text{CM}} = 200 \text{ GeV}$ , but this conclusion is, of course, valid for all energies.

## 5 Conclusions

Electroweak radiative corrections to  $e^+e^- \rightarrow WW \rightarrow 4f$  typically amount to  $\mathcal{O}(10\%)$  at LEP2 energies and further increase for higher energies. We have explicitly given analytical results for the universal process-independent corrections, which include effective coupling constants, the Coulomb singularity near the  $W$ -pair-production threshold, and leading ISR effects. They have been implemented in the Monte Carlo generator RACOONWW, which calculates the full  $\mathcal{O}(\alpha)$  corrections in double-pole approximation. Using this program a comparison between universal effects and the full correction has been presented.

For LEP2 energies the universal corrections are dominant, and the remaining non-universal contributions reduce the total  $W$ -pair cross section by 1–2%. In angular distributions non-universal effects can reach several per cent, mainly in regions where the cross section is small. The radiative corrections to  $W$ -invariant-mass distributions lead to a distortion of the  $W$  resonance, which is mainly due to photon radiation off

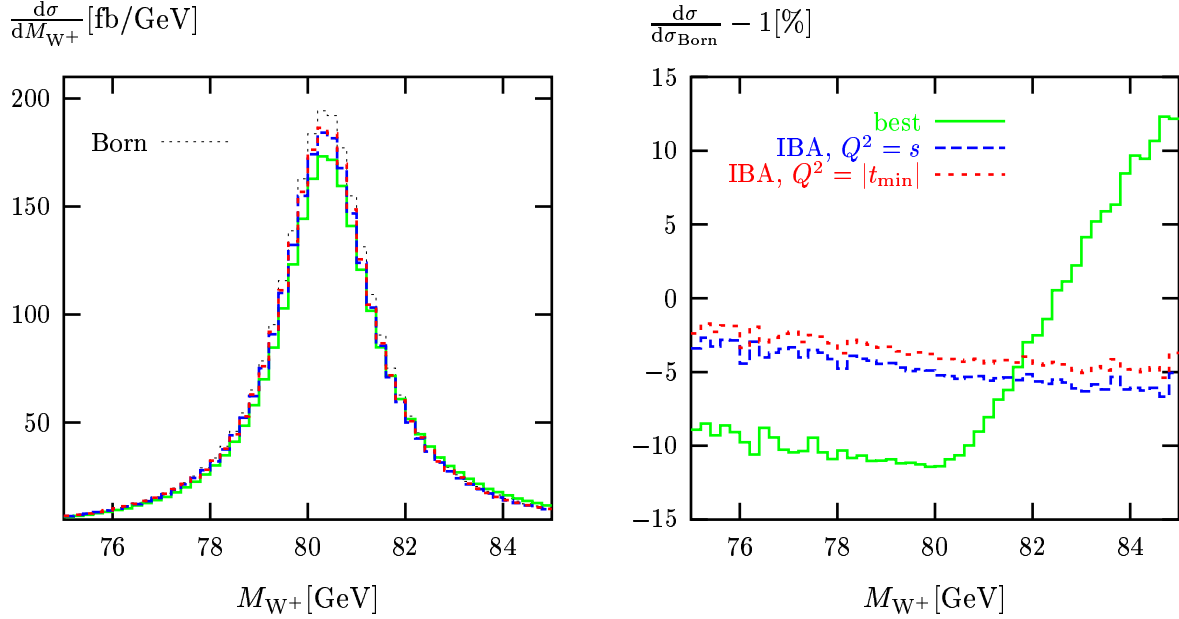


Figure 7: Predictions for the  $W^+$ -invariant-mass distribution (left) and corresponding relative corrections (right) for the process  $e^+e^- \rightarrow u\bar{d}\mu^-\bar{\nu}_\mu$  at  $E_{\text{CM}} = 200$  GeV based on various approximations for radiative corrections, using the “calo” setup for photon recombination

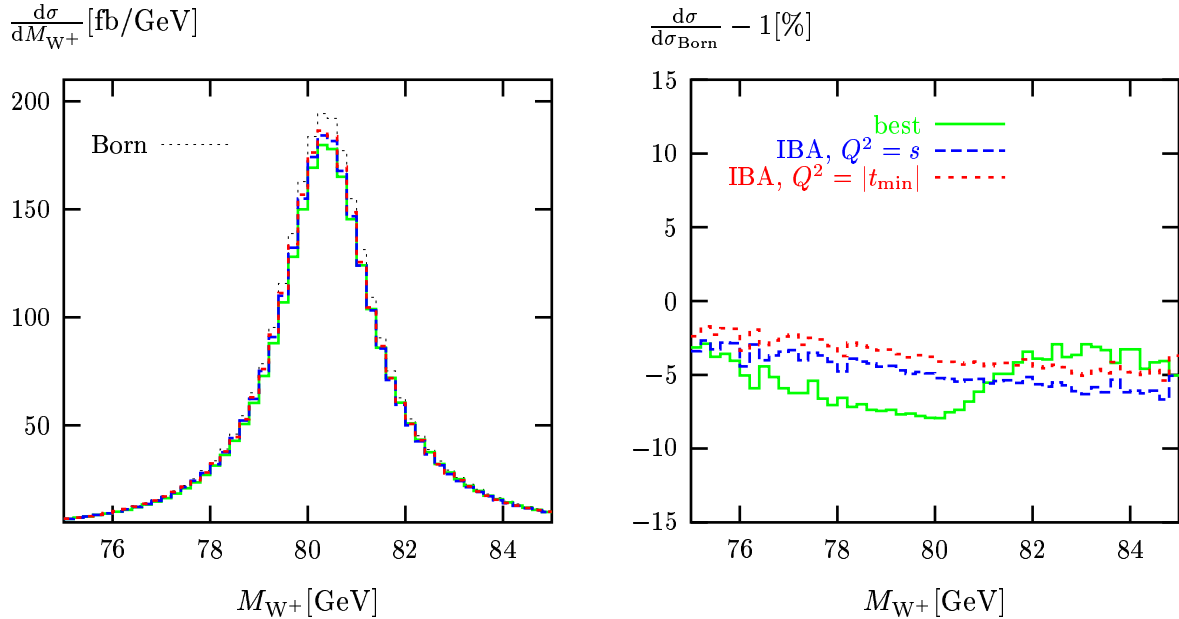


Figure 8: Predictions for the  $W^+$ -invariant-mass distribution (left) and corresponding relative corrections (right) for the process  $e^+e^- \rightarrow u\bar{d}\mu^-\bar{\nu}_\mu$  at  $E_{\text{CM}} = 200$  GeV based on various approximations for radiative corrections, using the “bare” setup for photon recombination

the charged final-state fermions and off the W bosons. This line-shape distortion is not accounted for by the above-mentioned universal effects.

For LC energies, i.e. energies up to the TeV range, non-universal effects become more and more important. While the universal effects still describe W-pair production in the forward region within some per cent, non-universal corrections reach the order of several 10% for intermediate and large W-production angles.

## Acknowledgments

We would like to thank the organizers of the conference, in particular Howard Haber, for providing a very pleasant atmosphere during the whole conference. Two of us (A.D. and S.D.) would like to thank the organizers for financial support. This work was supported in part by the Swiss Bundesamt für Bildung und Wissenschaft, by the European Union under contract HPRN-CT-2000-00149, by the U.S. Department of Energy under grant DE-FG02-91ER40685 and by the U.S. National Science Foundation under grant PHY-9600155.

## References

- [1] T. Barklow, these proceedings;  
S. Wynnhoff, these proceedings.
- [2] W. Beenakker et al., in *Physics at LEP2* (Report CERN 96-01, Geneva, 1996), Vol. 1, p. 79, hep-ph/9602351.
- [3] M. Grünewald et al., in *Reports of the Working Groups on Precision Calculations for LEP2 Physics* (Report CERN 2000-009, Geneva, 2000), p. 1, hep-ph/0005309.
- [4] M. Böhm, A. Denner and S. Dittmaier, *Nucl. Phys.* **B376** (1992) 29; E: **B391** (1993) 483.
- [5] S. Dittmaier, *Acta Phys. Pol.* **B28** (1997) 619;  
A. Denner and S. Dittmaier, *Proceedings of the Joint ECFA/DESY Study: Physics and Detectors for a Linear Collider*, Frascati, London, Munich, Hamburg, 1996, ed. R. Settles, DESY 97-123E (Hamburg, 1997), p. 131 (hep-ph/9706388);  
M. Kuroda, I. Kuss and D. Schildknecht, *Phys. Lett.* **B409** (1997) 405.
- [6] A. Denner, S. Dittmaier, M. Roth and D. Wackerroth, *Nucl. Phys.* **B587** (2000) 67.

- [7] S. Jadach *et al.*, *Phys. Lett.* **B417** (1998) 326; *Phys. Rev.* **D61** (2000) 113010; hep-ph/0007012.
- [8] W. Beenakker, A.P. Chapovsky and F.A. Berends, *Nucl. Phys.* **B548** (1999) 3.
- [9] Y. Kurihara, M. Kuroda and D. Schildknecht, *Nucl. Phys.* **B565** (2000) 49.
- [10] A. Denner, S. Dittmaier, M. Roth and D. Wackeroth, *Phys. Lett.* **B475** (2000) 127; *EPJdirect* **Vol. 2 C4** (2000) 1 (hep-ph/9912447).
- [11] S. Jadach *et al.*, hep-ph/0009352.
- [12] Homepage of the LEP Electroweak Working Group, <http://lepewwg.web.cern.ch/LEPEWWG/>.
- [13] D. Bardin, M. Bilenky, A. Olchevski and T. Riemann, *Phys. Lett.* **B308** (1993) 403;  
D. Bardin *et al.*, *Comput. Phys. Commun.* **104** (1997) 161.
- [14] A. Denner and T. Sack, *Z. Phys.* **C46** (1990) 653.
- [15] S. Eidelmann and F. Jegerlehner, *Z. Phys.* **C67** (1995) 585.
- [16] V.S. Fadin, V.A. Khoze and A.D. Martin, *Phys. Lett.* **B311** (1993) 311;  
D. Bardin, W. Beenakker and A. Denner, *Phys. Lett.* **B317** (1993) 213;  
V.S. Fadin *et al.*, *Phys. Rev.* **D52** (1995) 1377.
- [17] A. Denner, S. Dittmaier and M. Roth, *Nucl. Phys.* **B519** (1998) 39.
- [18] E.A. Kuraev and V.S. Fadin, *Yad. Fiz.* **41** (1985) 753 [*Sov. J. Nucl. Phys.* **41** (1985) 466];  
G. Altarelli and G. Martinelli, in “*Physics at LEP*”, eds. J. Ellis and R. Peccei, CERN 86-02 (CERN, Geneva, 1986), Vol. 1, p. 47;  
O. Nicrosini and L. Trentadue, *Phys. Lett.* **B196** (1987) 551; *Z. Phys.* **C39** (1988) 479;  
F.A. Berends, G. Burgers and W.L. van Neerven, *Nucl. Phys.* **B297** (1988) 429, **E:B304** (1988) 921.
- [19] W. Beenakker *et al.*, *Phys. Lett.* **B317** (1993) 622; *Nucl. Phys.* **B410** (1993) 245.

October 19, 2001  
hep-ph/0101139

# Non-Annihilation Processes, Fermion-Loop and QED Radiation

GIAMPIERO PASSARINO\*

*Dipartimento di Fisica Teorica, Università di Torino, Italy  
INFN, Sezione di Torino, Italy*

The bulk of large radiative corrections to any process can be obtained by promoting coupling constants to be running ones and by including QED radiation at the leading logarithmic level via structure functions evolved at some scale. The problem of *fixing* the proper scale in running coupling constants and in structure functions for non-annihilation processes is briefly addressed and the general solution is analyzed.

Presented at the

5th International Symposium on Radiative Corrections  
(RADCOR-2000)

Carmel CA, USA, 11–15 September, 2000

---

\*Work supported by the European Union under contract HPRN-CT-2000-00149.

# 1 Introduction

At the eve of LEP shutdown it is of some importance to summarize the present status of high precision physics [1]. For  $e^+e^- \rightarrow \bar{f}f$  all one-loop terms are known, including re-summation of leading terms. At the two-loop level leading and next-to-leading terms have been computed and included in codes like TOPAZ0 [2,3] and ZFITTER [4]. For realistic observables initial state QED radiation is included via the structure function method, or equivalent ones. Final state QED is also available as well as the interference between initial and final states [5]. Fine points in QED for  $2 \rightarrow 2$  are as follows. For  $s$ -channel all the  $\mathcal{O}(\alpha^2 L^n)$ ,  $n = 0, 1, 2$  terms are known from explicit calculations, the leading  $\mathcal{O}(\alpha^3 L^3)$  is also available and they are important for the studies of the  $Z$  lineshape.

Differences and uncertainties amount to at most  $\pm 0.1$  MeV on  $M_Z$  and  $\Gamma_Z$  and  $\pm 0.01\%$  on  $\sigma_h^0$  (MIZA, TOPAZ0 and ZFITTER) [6]. For non-annihilation processes (Bhabha) both structure-function and parton-shower methods have been analyzed and the uncertainty is estimated to be 0.061% from BHLUMI [7]. Certainly, full two-loop electroweak corrections are needed for GigaZ ( $10^9 Z$  events) with a quest for a fast numerical evaluation of the relevant diagrams.

For  $e^+e^- \rightarrow 4$  fermions all tree-level processes are available and  $\mathcal{O}(\alpha)$  electroweak corrections are known only for the  $WW$ -signal and in double-pole approximation (DPA) [8] and [9].  $e^+e^- \rightarrow 4f + \gamma$  in Born approximation is also available for all processes [10].

Fine points in QED for  $2 \rightarrow 4$  are as follows. For  $e^+e^- \rightarrow WW \rightarrow 4f$  DPA gives the answer but, for a generic process  $e^+e^- \rightarrow 4f$  QED radiation is included by using  $s$ -channel structure-functions, i.e. in leading-log approximation. The latter are strictly applicable only if ISR can be separated unambiguously. Otherwise their implementation may lead to an excess of radiation. Preliminary investigations towards non- $s$  SF by GRACE and by SWAP [10] gives an indication on how to implement the bulk of the non-annihilation effect but still represent *ad hoc* solutions. These methods, which are essentially based on a matching with the soft photon emission, still contain an ambiguity on the energy scale selection with consequences on the predicted observables.

## 2 Non-Annihilation processes

There are several processes, namely those with  $t$ -channel photons that are not dominated by annihilation. Typical examples are single- $W$  production and two-photon processes. The main question can be summarized as follows: how to include the bulk of radiative corrections?

At the Born level we still require the notion of input parameter set (IPS, i.e. the

choice of some set of input parameters (improperly called renormalization scheme (RS) in the literature) and of certain relations among them, e.g.

$$s_\theta^2 = 1 - \frac{M_W^2}{M_Z^2}, \quad \alpha \equiv \alpha_{G_F} = 4\sqrt{2} \frac{G_F M_W^2 s_\theta^2}{4\pi}, \quad (1)$$

Roughly speaking the theoretical uncertainty associated with the choice of the RS is most severe whenever low- $q^2$  photons dominate.

The first step in getting the right scales is represented by the Complex-Mass Renormalization in the Fermion-Loop approximation which gives [11]

$$\text{Couplings} \quad \Longrightarrow \quad \text{Running Couplings}$$

$$\text{Transitions} \quad \Longrightarrow \quad \text{Diagonal Propagator-Functions}$$

showing a pole in the 2nd sheet, and

$$\text{Born Vertices} \quad \Longrightarrow \quad \text{one fermion-loop corrected Vertices}$$

A typical example is shown by the following identities among diagrams:

Here open circles denote re-summed propagators and the dot a vertex.

Running of coupling constants is shown in Fig. 2. In Fig. 2 the running of  $e^2(q^2)$  is shown for  $q^2 \rightarrow 0_+$ , compared with the fixed value in the  $G_F$ -scheme. Furthermore, the evolution of  $g^2(q^2)$  is shown for  $q^2$  time-like or space-like.

The sizeable difference that one gets between  $e^2$  running in  $t$ channel and  $e^2$  fixed in the  $G_F$ -scheme is one of the major improvements induced by the FL-scheme in non-annihilation, Born processes.

However, the original formulation of the FL-scheme works only for conserved external currents. The extension to external massive fermions exists [13] and requires one additional replacement: one perform the calculation in the  $\xi = 1$  gauge, neglects contributions from unphysical scalars and uses

$$\delta_{\mu\nu} \text{ (in propagators)} \quad \Longrightarrow \quad \delta_{\mu\nu} + \frac{p_\mu p_\nu}{M^2(p^2)}, \quad (2)$$

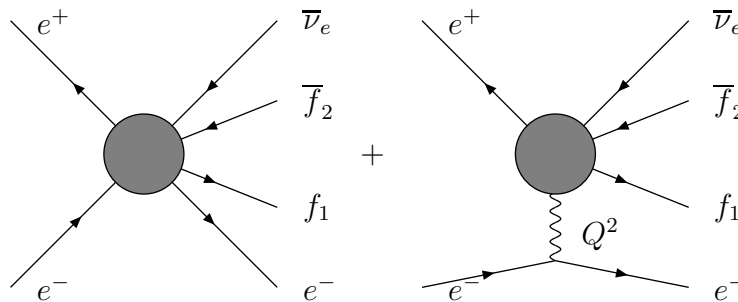
where  $M(p^2)$  is the (complex) running mass. The connection with complex-poles,  $p_w, p_z$  (here only for a massless internal world) is simple

$$\begin{aligned}
 W &\implies M^2(p^2) = \frac{g^2(p^2)}{g^2(p_w)} p_w, \\
 Z &\implies \frac{1}{M_0^2(p^2)} = \frac{g^2(p_z)}{g^2(p^2)} \frac{c^2(p^2)}{c^2(p_z)} \frac{1}{p_z} \\
 &\implies \frac{1}{M_0^2(p^2)} = \frac{c^2(p^2)}{M^2(p^2)}
 \end{aligned} \tag{3}$$

and gives the M(assive)FL-scheme, where gauge invariance is respected and collinear regions, e.g. outgoing electrons at zero scattering angle, are accessible for safe theoretical predictions.

### 3 Applications to single- $W$

The single- $W$  production mechanism is represented in the following figure.



The CC20 family of diagrams with the explicit component containing a  $t$ -channel photon.

The main consequences of applying the MFL-scheme are as follows:

- there is a maximal decrease of about 7% in the result if we compare with the  $G_F$ -scheme predictions but,
- the effect is rather sensitive to the relative weight of multi-peripheral contributions and is process and cut dependent [12].

## 4 QED radiation for arbitrary processes

Here the relevant question can be formulated as follows: is multi-photon radiation a one-scale or a multi-scale convolution phenomenon?

$$\begin{aligned} \sigma(p_+ p_- \rightarrow q_1 \dots q_n + \text{QED}) &\stackrel{?}{=} \int dx_+ dx_- D(x_+, ?) D(x_-, ?) \\ &\times \sigma(x_+ p_+ x_- p_- \rightarrow q_1 \dots q_n) \end{aligned} \quad (4)$$

In the above equation the question mark means that the corresponding scale has to be guessed. We need to understand how the standard SF-method is related to the exact YFS exponentiation. In the standard YFS treatment of multiple photon emission we have

$$\sigma\left(p_+ + p_- \rightarrow \sum_{i=1,2l} q_i + \sum_{j=1,n} k_j\right) \sim \int dPS_q |M_0|^2 E\left(p_+ + p_- - \sum_i q_i\right), \quad (5)$$

where  $E$  is the spectral function defined by

$$\begin{aligned} E(K) &= \frac{1}{(2\pi)^4} \int d^4x \exp(iK \cdot x) E(x), \\ E(x) &= \exp\left\{\frac{\alpha}{2\pi^2} \int d^4k e^{ik \cdot x} \delta^+(k^2) |j^\mu(k)|^2\right\} \end{aligned} \quad (6)$$

At this point we choose an alternative procedure where we do not separate the soft component from the hard one and compute some exact result valid for an arbitrary number of dimensions  $n$  and for on-shell photons, i.e.  $k^2 = 0$ ,

$$I = \int d^n k e^{ik \cdot x} \frac{\delta^+(k^2)}{p_i \cdot k p_j \cdot k} \quad (7)$$

In dimensional-regularization one has the following result, valid  $\forall x^2$ :

$$I(x) = -\pi \rho \int_0^1 \frac{du}{P^2} \left( \frac{1}{\hat{\varepsilon}} + 2 \ln 2 - \ln x^2 - \xi \ln \frac{\xi + 1}{\xi - 1} \right), \quad (8)$$

where we have defined a variable  $\xi$  as the ratio

$$\xi = \frac{|x_0|}{r}, \quad (9)$$

with an infinitesimal imaginary part attributed to  $x_0$ ,

$$x_0 \rightarrow x_0 + i\delta. \quad \delta \rightarrow 0_+. \quad (10)$$

Furthermore,  $P$  is the linear combination

$$P = p_j + (\rho p_i - p_j) u, \quad (11)$$

where we have defined  $\rho$  to satisfy

$$(\rho p_i - p_j)^2 = 0, \quad (12)$$

and  $x_0, r$  are rewritten in covariant form as follows:

$$x_0 = -\frac{P \cdot x}{\sqrt{-P^2}}, \quad r^2 = x_0^2 + x^2. \quad (13)$$

The last integral shows the infrared pole  $\frac{1}{\hat{\epsilon}}$  and a collection of  $\text{Li}_2$ -functions. Therefore,  $E(K)$  is not available in close form. The scheme that we want to propose defines a coplanar approximation [14] to the exact spectral function,

$$\begin{aligned} I_{ij}^c &\stackrel{\text{def}}{=} -\frac{2}{3} \pi \rho_{ij} \mathcal{F}_{\text{cp}} \frac{1}{p_j^2 - \rho_{ij}^2 p_i^2} \ln \frac{\rho_{ij}^2 p_i^2}{p_j^2}, \\ I_{ii}^c &\stackrel{\text{def}}{=} -\frac{2}{3} \pi \rho_{ij} \mathcal{F}_{\text{cp}} \frac{1}{m_i^2}, \\ \mathcal{F}_{\text{cp}} &= \ln \left\{ e^{-\Delta_{\text{IR}}} \frac{p_i \cdot x p_j \cdot x}{m_i m_j} \right\}, \\ \Delta_{\text{IR}} &= \frac{1}{\hat{\epsilon}} + \text{constants}. \end{aligned} \quad (14)$$

Within the coplanar approximation we have

$$\begin{aligned} E^{\text{pair} \langle ij \rangle}(K) &\xrightarrow{\text{cp}} \frac{1}{(2\pi)^2} \left\{ \frac{e^{-\Delta_{\text{IR}}}}{m_i m_j} \right\}^{-\alpha A_{ij}} \frac{1}{\Gamma^2(\alpha A_{ij})} \\ &\times \int_0^\infty d\sigma d\sigma' (\sigma\sigma')^{\alpha A_{ij}-1} \delta^4(\sigma p_i + \sigma' p_j - K). \end{aligned} \quad (15)$$

This results explains why we have introduced the term *coplanar*. Note that  $\alpha A \sim \beta$  only when the corresponding invariant is much larger than mass<sup>2</sup> but the above expression is valid for all regimes and it is easily generalized to  $n$  emitters with the result that <sup>1</sup> in a process  $2 \rightarrow n$  any external charged leg  $i$  talks to all other charged legs, each time with a known scale  $s_{ij}$  and with a known total weight proportional to

$$x_i^{\alpha(A_1^i + \dots + A_I^i) - 1} / \Gamma(\alpha(A_1^i + \dots + A_I^i)), \quad 0 \leq x_i \leq 1 \quad (16)$$

<sup>1</sup>A.Ballestrero, G.P. work in progress

Note that each  $A$  has the appropriate sign, in/out, part/antp. Furthermore,  $I(i)$  is the number of pairs  $\langle ij \rangle$  with  $i$  fixed. The IR exponent is given by

$$\alpha A = \frac{2\alpha}{\pi} \left\{ \frac{1+r^2}{1-r^2} \ln \frac{1}{r} - 1 \right\}, \quad \frac{m_e^2}{|t|} = \frac{r}{(1-r)^2} \quad (17)$$

For Bhabha scattering we will have the following combination:

$$-A(s, m_e) - A(t, m_e) + A(u, m_e) = \frac{2}{\pi} \left[ \ln \frac{st}{m_e^2 u} - 1 \right], \quad (18)$$

obtained as an exact result, not a guess.

## 5 Conclusions for QED

The structure-function language is still applicable but initial state structure functions evaluated for one scale is, quite obviously, not enough. In any process each external leg brings one structure function; since all charged legs talk to each other, each SF is not function of one *ad hoc* scale but all  $\langle ij \rangle$  scales enter into  $SF_i$ . The exact spectral-function is a convolution of SF

$$\begin{aligned} E^{\text{pair}\langle ij \rangle}(K) &= \int d^4 K' \Phi(K') E_{\text{cp}}^{\text{pair}\langle ij \rangle}(K - K'), \\ \Phi(K) &= \frac{1}{(2\pi)^4} \int d^4 x \exp \{i K \cdot x + \alpha (I - I_{\text{cp}})\} \\ &= \delta(K) + \mathcal{O}(\alpha) \end{aligned} \quad (19)$$

Furthermore, IR-finite reminders and virtual parts can be added according to the standard approach of reorganizing the perturbative expansion.

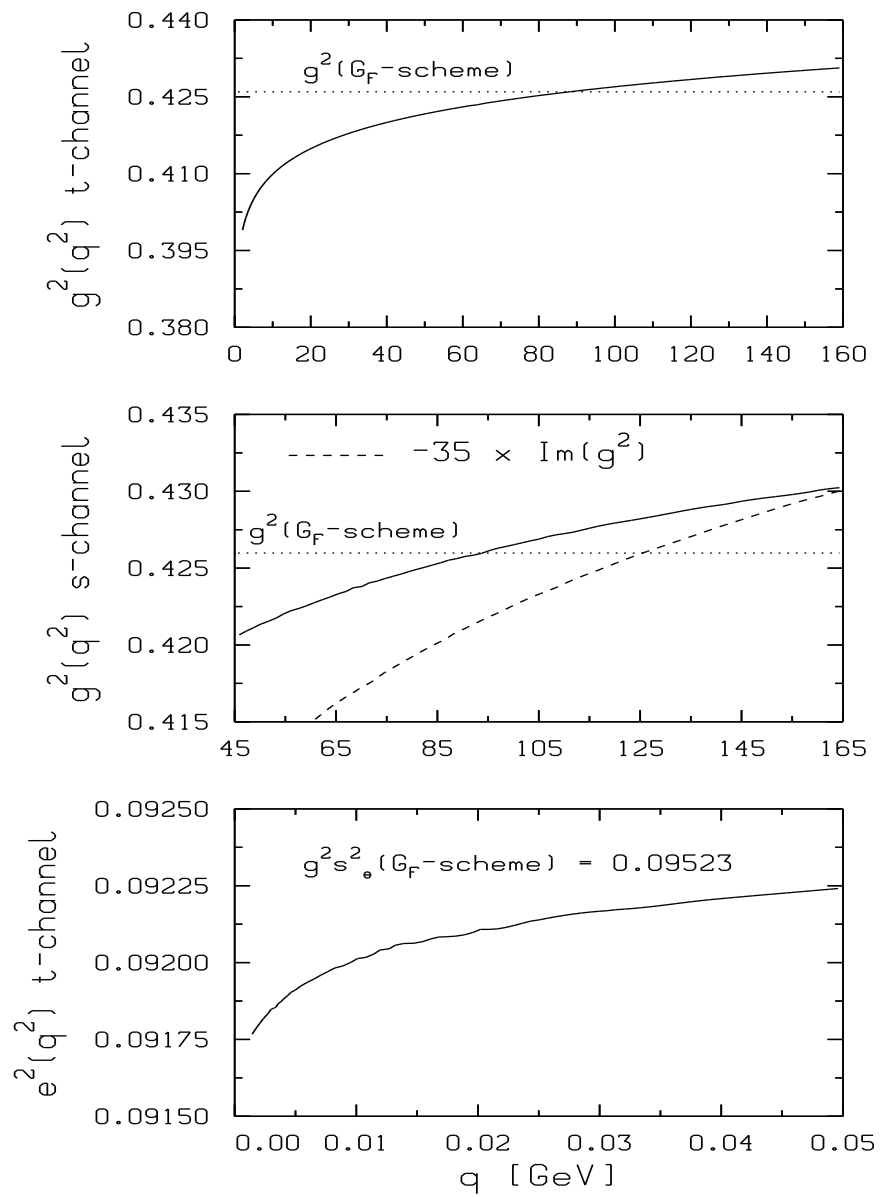
## Acknowledgments

I am grateful to A. Ballestrero for the collaboration in this research and to H. Haber for the invitation and for the very pleasant stay at Carmel.

## References

- [1] D. Bardin, M. Grunewald and G. Passarino, hep-ph/9902452.
- [2] G. Montagna, F. Piccinini, O. Nicosini, G. Passarino and R. Pittau, Comput. Phys. Commun. **76** (1993) 328.

- [3] G. Montagna, F. Piccinini, O. Nicrosini, G. Passarino and R. Pittau, Nucl. Phys. **B401** (1993) 3.
- [4] D. Bardin, P. Christova, M. Jack, L. Kalinovskaya, A. Olchevski, S. Riemann and T. Riemann, hep-ph/9908433.
- [5] S. Jadach, B. F. Ward and Z. Was, Comput. Phys. Commun. **130** (2000) 260 [hep-ph/9912214].
- [6] LEP EWWG/LS 2000-01.
- [7] S. Jadach, W. Placzek, E. Richter-Was, B. F. Ward and Z. Was, Comput. Phys. Commun. **102** (1997) 229.
- [8] A. Denner, S. Dittmaier, M. Roth and D. Wackerroth, Nucl. Phys. **B587** (2000) 67 [hep-ph/0006307].
- [9] S. Jadach, W. Placzek, M. Skrzypek, B. F. Ward and Z. Was, hep-ph/0007012.
- [10] M. W. Grunewald *et al.*, hep-ph/0005309.
- [11] W. Beenakker *et al.*, Nucl. Phys. **B500** (1997) 255 [hep-ph/9612260].
- [12] G. Passarino, Nucl. Phys. **B578** (2000) 3 [hep-ph/0001212].
- [13] G. Passarino, Nucl. Phys. **B574** (2000) 451 [hep-ph/9911482].
- [14] C. Chahine, Phys. Rev. **D18** (1978) 4617.



**Precision Predictions for (Un)Stable  
 $WW/4f$  Production in  $e^+e^-$  Annihilation:  
YFSWW3/KoralW-1.42/YFSZZ\***

B.F.L. WARD<sup>a,b,c</sup>, S. JADACH<sup>c,d,e</sup>, W. PŁACZEK<sup>c,f</sup>, M. SKRZYPEK<sup>c,e</sup>  
AND Z. WĄS<sup>c,e</sup>

*<sup>a</sup>Department of Physics and Astronomy*

*University of Tennessee, Knoxville, TN 37996-1200, USA*

*<sup>b</sup>SLAC, Stanford University, Stanford, California 94309, USA,*

*<sup>c</sup>CERN, Theory Division, CH-1211 Geneva 23, Switzerland,*

*<sup>d</sup>DESY-Zeuthen, Theory Division, D-15738 Zeuthen, Germany,*

*<sup>e</sup>Institute of Nuclear Physics, ul. Kawoory 26a, 30-055 Cracow, Poland,*

*<sup>f</sup>Institute of Computer Science, Jagellonian University,*

*ul. Nawojki 11, 30-072 Cracow, Poland*

---

\*Work partly supported by the Maria Skłodowska-Curie Joint Fund II PAA/DOE-97-316, the European Commission 5-th Framework contract HPRN-CT-2000-00149, and the US Department of Energy Contracts DE-FG05-91ER40627 and DE-AC03-76ER00515.

We present precision calculations of the processes  $e^+e^- \rightarrow 4\text{-fermions}$  in which the double resonant  $W^+W^-$  and  $ZZ$  intermediate states occur. Referring to these latter intermediate states as the 'signal processes', we show that, by using the YFS Monte Carlo event generators [YFSWW3-1.14](#) and [KoralW-1.42](#) in an appropriate combination, we achieve a physical precision on the  $WW$  signal process, as isolated with LEP2 MC Workshop cuts, [below 0.5%](#). We stress the full gauge invariance of our calculations and we compare our results with those of other authors where appropriate. In particular, sample Monte Carlo data are explicitly illustrated and compared with the results of the program [RacoonWW](#) of Denner *et al.*. In this way, we cross check that the total (physical $\oplus$ technical) precision tag for the  $WW$  signal process cross section is [0.4% for 200 GeV](#), for example. Results are also given for 500 GeV with an eye toward the LC. For the analogous  $ZZ$  case, we cross check that our [YFSZZ](#) calculation yields a total precision tag of [2%](#), when it is compared to the results of [ZZTO](#) and [GENTLE](#) of Passarino and Bardin *et al.*, respectively.

Presented at the

5th International Symposium on Radiative Corrections  
(RADCOR-2000)

Carmel CA, USA, 11-15 September, 2000

# 1 Introduction

The theoretical paradigm affirmed by the award of the 1999 Nobel Prize to G. 't Hooft and M. Veltman for the success of the predictions of their formulation [1] of the renormalised non-Abelian quantum loop corrections for the **Standard Model** [2] of the electroweak interaction focuses our efforts on the need to continue to test this theory at the quantum loop level in the gauge boson sector itself. This then emphasises the importance of the on-going (the data are under analysis and will be for some time even though the LEP2 accelerator was recently shutdown) precision studies of the processes  $e^+e^- \rightarrow W^+W^-(ZZ) + n(\gamma) \rightarrow 4f + n(\gamma)$  at LEP2 energies [3,4,5], as well as the importance of the planned future higher energy studies of such processes in LC physics programs [6,7,8,9]. We need to stress also that hadron colliders also have considerable reach into this physics and we hope to come back to their roles elsewhere [10].

In what follows, we present precision predictions for the event selections (ES) of the LEP2 MC Workshop [11] for the processes  $e^+e^- \rightarrow W^+W^- + n(\gamma) \rightarrow 4f + n(\gamma)$  based on our new exact  $\mathcal{O}(\alpha)_{prod}$  YFS exponentiated LL  $\mathcal{O}(\alpha^2)$  **FSR leading pole approximation (LPA)** formulation as it is realized in the MC program **YFSWW3-1.14** [12,13] in combination with the all four-fermion processes MC event generator **KoralW-1.42** [14] so that the respective four-fermion background processes are taken into account in a gauge invariant way. In addition, we also present the current status of the predictions of our YFS MC approach to the processes  $e^+e^- \rightarrow ZZ + n(\gamma) \rightarrow 4f + n(\gamma)$  as it was also illustrated in the **2000 LEP2 MC Workshop** [11] using the MC event generator YFSZZ [15], which realizes **YFS exponentiated LL  $\mathcal{O}(\alpha^2)$  ISR in the LPA** in a gauge invariant way. Indeed, gauge invariance is a crucial aspect of our work and we stress that we maintain it through-out our calculations. Here, **ISR** denotes initial state radiation, **FSR** denotes final-state radiation and LL denotes leading-log as usual.

This realization which we present of the YFS MC approach is the **exclusive exponentiation (EEX)** [16] and it is already well established in its applications to the **MC event generators for LEP1 physics calculations in the MC's KORALZ/YFS3** [17,18], **BHLUMI** [19,20] and **KoralW** [14]. In our applications in YFSWW3-1.14 and in KoralW-1.42, the **FSR is implemented using the program PHOTOS** [21], so that not only is the FSR calculated to the LL  $\mathcal{O}(\alpha^2)$  but the **FSR photons have the correct finite  $p_T$  in the soft limit to  $\mathcal{O}(\alpha)$** . We always use the ratio of branching ratios (BR's) to correct the respective decay rates through  $\mathcal{O}(\alpha)$  accordingly. Recently, we have introduced the **coherent exclusive exponentiation (CEEX)** [22] approach to the YFS MC event generator calculation of radiative corrections and we will present the application of this new approach to the  $4f$  production processes elsewhere [10]. **For a description of its application to the  $2f$  production processes see Ref. [23].**

Recently, the authors in Refs. [24,25] have also presented MC program results for

the processes  $e^+e^- \rightarrow W^+W^- + n(\gamma) \rightarrow 4f + n(\gamma)$ ,  $n = 0, 1$  in combination with the complete background processes which feature the exact LPA  $\mathcal{O}(\alpha)$  correction, the complete  $\mathcal{O}(\alpha)$  result for  $e^+e^- \rightarrow 4f + \gamma$ , and soft photon KF [26] exponentiation for the LL  $\mathcal{O}(\alpha^3)$  ISR via structure functions. Thus, we will compare our results where possible with those in Refs. [24] in an effort to check the over-all precision of our work. As we argue below, the two sets of results should agree at a level below 0.5% on observables such as the total cross section. The authors in Refs. [5] have used semi-analytical methods to compute the exact LPA  $\mathcal{O}(\alpha)$  correction  $e^+e^- \rightarrow W^+W^- \rightarrow 4f$  with no higher order resummation. Thus, while we have compared our results with theirs in Ref. [13] for example, here we do not present such comparisons because the expected precision tag of their results is larger than the desired 0.5% needed by the LEP2 experiments [11].

For the processes  $e^+e^- \rightarrow ZZ + (n\gamma) \rightarrow 4f + (n'\gamma)$ , the authors in Refs. [27,28] have presented calculations in the LEP2 MC Workshop [11] at the NC02 and all-4f level [28] as well. The calculations in Ref. [27] are done with the program ZZTO and feature universal ISR corrections,  $\mathcal{O}(\alpha)$  FSR<sub>QED</sub> corrections,  $\mathcal{O}(\alpha_s)$  FSR<sub>QCD</sub> corrections, and running masses in the fermion loop scheme of Ref. [29]. The results in Ref. [28] feature the structure function approach to the ISR QED corrections and the  $\mathcal{O}(\alpha)$  FSR<sub>QED</sub> corrections. We will compare our YFSZZ results with these two sets of results as well, as the three approaches should agree at the level of the 2% precision needed by the LEP2 experiments [11] on observables such as the total cross section.

Our presentation is organised as follows. In the next Section, we discuss the current status YFSWW3-1.14. In Section 3, we present the current status of KoralW-1.42 from the standpoint of its use to calculate the 4f background processes in combination with YFSWW3-1.14. In Section 4, we present the current status of YFSZZ. In Sections 5, 6 and 7, we illustrate the results we have obtained with our calculations for YFSWW3, KoralW-1.42 and YFSZZ, respectively, for the ES of the LEP2 MC Workshop [11], wherein we include comparisons with the respective results in Refs. [24,27,28]. Section 8 contains our summary remarks.

## 2 YFSWW3-1.14

In this section we present the current status of **YFSWW3-1.14**. We start with the **process of interest and its cross section**,

$$\begin{aligned}
 e^-(p_1) + e^+(p_2) &\rightarrow f_1(r_1) + \bar{f}_2(r_2) + f'_1(r'_1) + \bar{f}'_2(r'_2) + \gamma(k_1), \dots, \gamma(k_n), \\
 \sigma_n &= \frac{1}{flux} \int d\tau_{n+4}(p_1 + p_2; r_1, r_2, r'_1, r'_2, k_1, \dots, k_n) \\
 &\quad \sum_{\text{ferm. spin}} \sum_{\text{phot. spin}} |\mathcal{M}_{4f}^{(n)}(p_1, p_2, r_1, r_2, r'_1, r'_2, k_1, \dots, k_n)|^2,
 \end{aligned} \tag{1}$$

and the corresponding expressions for the  **$W^+W^-$  production and decay in the leading pole approximation (LPA)**,

$$\begin{aligned}
 e^-(p_1) + e^+(p_2) &\rightarrow W^-(q_1) + W^+(q_2), \\
 W^-(q_1) &\rightarrow f_1(r_1) + \bar{f}_2(r_2), \quad W^+(q_2) \rightarrow f'_1(r'_1) + \bar{f}'_2(r'_2), \\
 \sigma_n &= \frac{1}{flux} \int d\tau_{n+4}(p_1 + p_2; r_1, r_2, r'_1, r'_2, k_1, \dots, k_n) \\
 &\quad \sum_{\text{ferm. spin}} \sum_{\text{phot. spin}} |\mathcal{M}_{LPA}^{(n)}(p_1, p_2, r_1, r_2, r'_1, r'_2, k_1, \dots, k_n)|^2.
 \end{aligned} \tag{2}$$

Here, we realize the **LPA<sub>a,b</sub>** as follows:

$$\begin{aligned}
 \mathcal{M}_{4f}^{(n)}(p_1, p_2, r_1, r_2, r'_1, r'_2, k_1, \dots, k_n) &\stackrel{LPA}{\Rightarrow} \mathcal{M}_{LPA}^{(n)}(p_1, p_2, r_1, r_2, r'_1, r'_2, k_1, \dots, k_n) \\
 &= \sum_{\text{Phot. Partitions}} \mathcal{M}_{Prod}^{(n), \lambda_1 \lambda_2}(p_1, p_2, q_1, q_2, k_1, \dots, k_n) \\
 &\times \frac{1}{D(q_1)} \mathcal{M}_{Dec1, \lambda_1}^{(n)}(q_1, r_1, r_2, k_{a+1}, \dots, k_b) \\
 &\times \frac{1}{D(q_2)} \mathcal{M}_{Dec2, \lambda_2}^{(n)}(q_2, r'_1, r'_2, k_{b+1}, \dots, k_n), \\
 D(q_i) &= q_i^2 - M^2, \quad M^2 = (M_W^2 - i\Gamma_W M_W)(1 - \Gamma_W^2/M_W^2 + \mathcal{O}(\alpha^3)), \\
 q_1 &= r_1 + r_2 + k_{a+1} + \dots + k_b; \quad q_2 = r'_1 + r'_2 + k_{b+1} + \dots + k_n,
 \end{aligned} \tag{3}$$

where the two formulations of the **LPA, LPA<sub>a,b</sub>**, are based on the results in **Eden Refs. [30,31]** as one can see from the representation of our amplitudes  $\mathcal{M}$  as

$$\mathcal{M} = \sum_j \ell_j A_j(\{q_k q_l\}). \tag{4}$$

Here, the  $\{\ell_j\}$  are a complete set of spinor covariants and the  $\{A_j\}$  are the respective scalar functions. For **LPA<sub>(a)b</sub>**, we do (not) evaluate the

spinor covariants on-pole in realizing the respective  $\mathcal{M}_{LPA}^{(n)}$ . We do both in YFSWW3-1.14.

We use standard YFS methods(EEX-Type)to write

$$d\sigma = e^{2\Re\alpha B' + 2\alpha\tilde{B}} \frac{1}{(2\pi)^4} \int d^4y e^{iy(p_1+p_2-q_1-q_2)+D} [\bar{\beta}_0 + \sum_{n=1}^{\infty} \frac{d^3k_j}{k_j^0} e^{-iyk_j} \bar{\beta}_n(k_1, \dots, k_n)] \times \frac{d^3r_1}{E_1} \frac{d^3r_2}{E_2} \frac{d^3r'_1}{E'_1} \frac{d^3r'_2}{E'_2}, \quad (5)$$

where

$$D = \int \frac{d^3k}{k_0} \tilde{S} [e^{-iy \cdot k} - \theta(K_{max} - |\vec{k}|)] \quad (6)$$

$$2\alpha\tilde{B} = \int \frac{d^3k}{k_0} \theta(K_{max} - |\vec{k}|) \tilde{S}(k).$$

Here,  $K_{max}$  is a dummy parameter of which eq.(5) is independent. In realizing eq.(5) in YFSWW3, we employ the following schemes, which are related by the renormalization group:

- Version 1.13:  $G_\mu$ -Scheme of Fleischer *et al.* [32]
- Version 1.14: Scheme A – only the hard EW correction has  $\alpha_{G_\mu}$ ; Scheme B – the entire  $\mathcal{O}(\alpha)$  correction has  $\alpha(0)$

As it was shown in the LEP2 MC Workshop [11], there is a  $\Rightarrow -0.3 \div -0.4\%$  shift of the normalisation of version 1.14 relative to that of version 1.13. This can be seen as follows. The universal LL ISR  $\mathcal{O}(\alpha)$  soft plus virtual correction is

$$\delta_{ISR,LL}^{v+s} = \beta \ln k_0 + \frac{\alpha}{\pi} \left( \frac{3}{2} L + \frac{\pi^2}{3} - 2 \right), \quad (7)$$

with  $\beta = \frac{2\alpha}{\pi}(L-1)$  and with  $k_0$  equal to the usual soft cut-off and  $L = \ln s/m_e^2$ . From eq.(7), we get the estimate of the shift in normalisation between version 1.13 and version 1.14 at 200 GeV as

$$(\alpha(0) - \alpha_{G_\mu}) \left( \frac{3}{2} L - 2 \right) \sim -0.33\%. \quad (8)$$

This is consistent with what is observed as reported in Ref. [11]. See Dittmaier's talk [25] for more details and references.

### 3 KoralW-1.42

For the **process of interest**,  $e^-(p_1) + e^+(p_2) \rightarrow f_1(r_1) + \bar{f}_2(r_2) + f'_1(r'_1) + \bar{f}'_2(r'_2) + \gamma(k_1), \dots, \gamma(k_n)$ , we use **KoralW-1.42** which realizes the  $\mathcal{O}(\alpha^3)$  **LL YFS exponentiated ISR**. The respective input Born matrix elements are the **GRACE v. 2** [33] all 4f library of Born matrix elements and **our independent CC03 Born matrix elements**. This allows us to **combine YFSWW3-1.14 and KoralW-1.42 to correct for background diagram effects**: using  $\text{LPA}_a$  in YFSWW3-1.14, whose cross section we denote by  $\sigma(Y_a)$ , we get

$$\sigma_{Y/K} = \sigma(Y_a) + \Delta\sigma(K), \quad (9)$$

where  $\Delta\sigma(K)$  is defined by

$$\Delta\sigma(K) = \sigma(K_1) - \sigma(K_3). \quad (10)$$

Here,  $\sigma(K_1)$  is the 4-f KoralW-1.42 result and  $\sigma(K_3)$  is the CC03 KoralW-1.42 result. This means that  $\sigma_{Y/K}$  is accurate to  $\mathcal{O}(\frac{\alpha}{\pi} \frac{\Gamma_W}{M_W})$ .

Alternatively, using  $\text{LPA}_i$ ,  $i = a, b$  in YFSWW3-1.14, whose cross section we denote by  $\sigma(Y_i)$ , we get

$$\sigma_{K/Y} = \sigma(K_1) + \Delta\sigma(Y) \quad (11)$$

where

$$\Delta\sigma(Y) = \sigma(Y_i) - \sigma(Y_4), \quad (12)$$

and  $\sigma(Y_4)$  is the respective YFSWW3-1.14 result with **NL  $\mathcal{O}(\alpha)$  corrections to  $\bar{\beta}_n$ ,  $n = 0, 1$ , switched off**. This means that  $\sigma_{K/Y}$  is also accurate to  $\mathcal{O}(\frac{\alpha}{\pi} \frac{\Gamma_W}{M_W})$ .

**Above WW threshold,  $\sigma_{K/Y}$  and  $\sigma_{Y/K}$  agree to the 0.1% level. We advocate the latter as our best result in the following.**

Note that we sometimes identify  $\sigma(Y_1) = \sigma(Y_a)$ ,  $\sigma(Y_2) = \sigma(Y_b)$ ,  $\sigma(Y_3) = \sigma(K_3)$  with  $\sigma(K_2)$  equal to the cross section from KoralW-1.42 with the **on-pole CC03 Born level matrix element with YFS exponentiated  $\mathcal{O}(\alpha^3)$  LL ISR** – this  $\sigma(K_2)$  should be available soon. It is useful for further cross checks on our work.

### 4 YFSZZ

In our calculation in YFSZZ-1.02 [15] **the process of interest is  $e^-(p_1) + e^+(p_2) \rightarrow Z(q_1)Z(q_2) + (\gamma(k_1), \dots, \gamma(k_m)) \rightarrow f_1(r_1) + \bar{f}_1(r_2) + f'_1(r'_1) + \bar{f}'_1(r'_2) + \gamma(k_1), \dots, \gamma(k_n)$** . We proceed as follows in realizing the **MC YFSZZ-1.02**:

- We use  $LPA_a$  as described above for the NC02 process to calculate  $\mathcal{O}(\alpha^2)$  LL YFS exponentiated ISR for the input NCO2 Born matrix elements of Ref. [34].
- Anomalous couplings are supported following the conventions of Ref. [34] – this is also true for YFSWW3/KORALW.

We stress that YFSZZ is in wide use at LEP and that it was tested in the LEP2 MC Workshop, just as YFSWW3-1.14 was tested. We now turn to such results.

## 5 Results-YFSWW3-1.14

In this section we illustrate the effects of the NL  $\mathcal{O}(\alpha)$  correction as it is calculated in YFSWW3-1.14. We do this with the hardest photon angular distribution. Similar calculations of other observables can be found in Ref. [13,11].

Specifically, in Fig. 1, we show the distribution of the cosine of the production angle of the hardest photon in the cms system with respect to the  $e^+$  beam. We see that away from the beams the NL  $\mathcal{O}(\alpha)$  correction is important for precision studies of this photonic observable. Similar conclusions follow from the more complete set of observables studied in Refs. [13,11].

Indeed, in the LEP2 MC Workshop, we compared our results with those of RacoonWW by the authors in Ref. [24]. For a complete description of these comparisons we refer the reader to Ref. [11]. Here, we show in Table 1 the comparison of the total cross sections at 200 GeV with no cuts as defined Ref. [11].

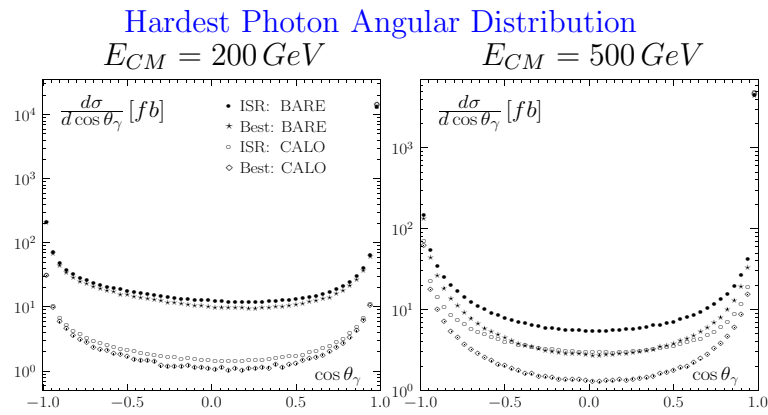


Figure 1:  $\cos\theta_\gamma$  w.r.t. the  $e^+$  beam in the cms system for  $e^+e^- \rightarrow W^+W^- \rightarrow u\bar{d}\mu^-\bar{\nu}_\mu$ . We see that NL corrections are important away from the beams, for example.

### Comparison with RacoonWW

<b>no cuts</b>		$\sigma_{\text{tot}}[\text{fb}]$	
final state	program	Born	best
$\nu_{\mu}\mu^{+}\tau^{-}\bar{\nu}_{\tau}$	YFSWW3	219.770(23)	199.995(62)
	RacoonWW	219.836(40)	199.551(46)
	(Y-R)/Y	-0.03(2)%	0.22(4)%
$u\bar{d}\mu^{-}\bar{\nu}_{\mu}$	YFSWW3	659.64(07)	622.71(19)
	RacoonWW	659.51(12)	621.06(14)
	(Y-R)/Y	0.02(2)%	0.27(4)%
$u\bar{d}s\bar{c}$	YFSWW3	1978.18(21)	1937.40(61)
	RacoonWW	1978.53(36)	1932.20(44)
	(Y-R)/Y	-0.02(2)%	0.27(4)%

Table 1: Total cross sections, CC03 from RacoonWW, YFSWW3,  $\sqrt{s} = 200$  GeV without cuts. Statistical errors correspond to the last digits in ( ).

From the results in Table 1 and the related results given in Ref. [11] we conclude that the TU of the calculations is 0.4% at 200 GeV for the total signal cross section. This is a considerable improvement over previously quoted precision of 2% in Ref. [35].

## 6 Results-YFSWW3/KoralW

One of the important aspects of the isolation and study of the  $WW$  signal processes is the control of the corresponding background  $4f$  processes. This we do with our all- $4f$  MC KoralW-1.42 as we described above. Here, we illustrate the size of the corresponding  $4f$  background corrections to the YFSWW3-1.14 cross sections.

Specifically, in Tabs. 2 and 3, we show the size of this  $4f$  background correction in comparison to the NL correction of YFSWW3-1.14 for the total cross section, for example, both for the case of no cuts and the case of cuts, respectively, as defined in Ref. [11]. These results show that the  $4f$  background correction at 200 GeV to the total YFSWW3-1.14 cross section is below 0.1%.

## 7 Results-YFSZZ

In this section we show the results of our comparison with ZZTO for the total  $ZZ$  pair signal processes as carried out in Ref. [11]. In that same set of comparisons, ZZTO was also compared with the results of GENTLE by the authors in Refs. [28]. In this way, a cross check was made on all three calculations.

### WW/4f Cross Section

NO CUTS		$\sigma_{WW} [fb]$		$\delta_{4f} [\%]$		$\delta_{WW}^{NL} [\%]$
Final state	Program	Born	ISR	Born	ISR	
$\nu_\mu \mu^+ \tau^- \bar{\nu}_\tau$	YFSWW3	219.793 (16)	204.198 (09)	—	—	-1.92 (4)
	KoralW	219.766 (26)	204.178 (21)	0.041	0.044	—
	(Y-K)/Y	0.01 (1)%	0.01 (1)%	—	—	—
$u\bar{d}\mu^-\bar{\nu}_\mu$	YFSWW3	659.69 (5)	635.81 (3)	—	—	-1.99 (4)
	KoralW	659.59 (8)	635.69 (7)	0.073	0.073	—
	(Y-K)/Y	0.02 (1)%	0.02 (1)%	—	—	—
$u\bar{d}s\bar{c}$	YFSWW3	1978.37 (14)	1978.00 (09)	—	—	-2.06 (4)
	KoralW	1977.89 (25)	1977.64 (21)	0.060	0.061	—
	(Y-K)/Y	0.02 (1)%	0.02 (1)%	—	—	—

Table 2: Total WW YFSWW3 and KoralW cross sections: Born and ISR level, KoralW 4f correction, YFSWW3  $\mathcal{O}(\alpha)$  NL correction, at 200 GeV, no cuts. The last digits in (...) correspond to the statistical errors.

Specifically, we show in Table 4 the ZZ signal cross section at 188.6 GeV as predicted by YFSZZ and ZZTO for the case of no cuts as defined in Ref. [11]. For ZZTO, results are shown for two schemes, the  $G_\mu$  and  $\alpha$  schemes [27]. The agreement between the programs in this comparison and between the programs in the other related comparisons carried out in Ref. [11] show that the TU for the respective NC02 signal process is 2% at the respective LEP2 energies.

## 8 Conclusions

We are currently at an exciting point in the tests of the EW Theory in gauge boson physics. The WW pair production is an important aspect of these tests. The radiative corrections which we realize in YFSWW3-1.14 play a significant role in these tests as follows:

- Mass distributions: these are affected by FSR, yielding peak position and height shifts
- W Angular distributions: these are affected by LL and NL corrections
- $\ell$  Angular distributions: these are affected by LL and NL corrections
- Photon Angular distributions: these are affected by LL and NL corrections

*WW/4f* Cross Section

<b>WITH CUTS</b>		$\sigma_{WW}$ [fb]		$\delta_{4f}$ [%]		$\delta_{WW}^{NL}$ [%]
Final state	Program	Born	ISR	Born	ISR	
$\nu_\mu \mu^+ \tau^- \bar{\nu}_\tau$	YFSWW3	210.938 (16)	196.205 (09)	—	—	-1.93 (4)
	KoralW	210.911 (26)	196.174 (21)	0.041	0.044	—
	(Y-K)/Y	0.01 (1)%	0.02 (1)%	—	—	—
$u\bar{d}\mu^-\bar{\nu}_\mu$	YFSWW3	627.22 (5)	605.18 (3)	—	—	-2.00 (4)
	KoralW	627.13 (8)	605.03 (7)	0.074	0.074	—
	(Y-K)/Y	0.01 (1)%	0.02 (1)%	—	—	—
$u\bar{d}s\bar{c}$	YFSWW3	1863.60 (15)	1865.00 (09)	—	—	-2.06 (4)
	KoralW	1863.07 (25)	1864.62 (21)	0.065	0.064	—
	(Y-K)/Y	0.03 (2)%	0.02 (1)%	—	—	—

Table 3: Total *WW* YFSWW3 and KoralW cross sections: Born and ISR level, KoralW 4*f* correction, YFSWW3  $\mathcal{O}(\alpha)$  NL correction, at 200 GeV, with cuts. The last digits in (...) correspond to the statistical errors.

Comparison with ZZTO

channel	YFSZZ	ZZTO $G_F$ -scheme	ZZTO $\alpha$ -scheme
$qqqq$	294.6794(490)	298.4411(60)	294.5715(59)
$qq\nu\nu$	175.4404(302)	175.5622(35)	174.9855(35)
$qqll$	88.1805(134)	88.7146(18)	87.9881(18)
$ll\nu\nu$	26.2530(463)	26.0940(5)	26.1342(5)
$llll$	6.5983(15)	6.5929(1)	6.5706(1)
$\nu\nu\nu\nu$	26.1080(71)	25.8192(5)	25.9868(5)
total	617.2596(755)	621.2241(124)	616.2366(123)

Table 4: NC02 cross sections, YFSZZ vs ZZTO, 188.6 GeV, in fb. The statistical errors correspond to the last digits in ( ).

- Photon Energy distributions: these are affected by LL corrections
- Normalisation: this is affected by LL AND NL corrections; the current 200 GeV TU is 0.4% from the {YFSWW3/RacoonWW} results.

Concerning our results on calculating the 4*f* background to YFSWW3-1.14 using KoralW-1.42, we have shown the following:

- Two different combinations of YFSWW3 and KoralW-1.42 cross sections reach the total precision  $\mathcal{O}(\frac{\alpha}{\pi} \frac{\Gamma_W}{M_W})$ .

- The size of the  $4f$  correction to **YFSWW3-1.14** is  $\lesssim 0.1\%$ , as expected.
- The future extension to a single platform is possible.

It follows that **YFSWW3/KoralW** is a complete MC event generator solution for precision **WW/4f** production at **LEP2** ( and **LC's**).

From our studies of the **NC02** signal process we conclude that **YFSZZ**, a multiple photon MC event generator for **NC02** with  $\bar{\beta}_0$  level LPA YFS exponentiation (**EEX**), is tested in the **LEP2 MC Workshop vs ZZTO** and **GENTLE** to 2% TU. An upgrade to higher precision is possible but is not needed, apparently?

## Acknowledgments

Two of us (S.J. and B.F.L.W.) acknowledge the kind hospitality of Prof. G. Altarelli and the CERN Theory Division while this work was being completed. Three of us (B.F.L.W., W.P. and S.J.) acknowledge the support of Prof. D. Schlatter and Prof. D. Plane and of the ALEPH, DELPHI, L3 and OPAL Collaborations in the final stages of this work. One of us (S.J.) is thankful for the kind support of the DESY Directorate and one of us (Z.W.) acknowledges the support of the L3 Group of ETH Zurich during the time this work was performed. All us thank the members of the LEP2 MC Workshop for valuable interactions and stimulation during the course of this work. The authors especially thank Profs. A. Denner, S. Dittmaier and F. Jegerlehner and Drs. M. Roth and D. Wackerath for useful discussions and interactions.

## References

- [1] G. 't Hooft and M. Veltman, Nucl. Phys. **B44**,189 (1972); *ibid.* **B50**, 318 (1972); G. 't Hooft, *ibid.* **B35**, 167 (1971); M. Veltman, *ibid.* **B7**, 637 (1968).
- [2] S.L. Glashow, Nucl. Phys. **22** (1961) 579;  
S. Weinberg, Phys. Rev. Lett. **19** (1967) 1264;  
A. Salam, in *Elementary Particle Theory*, ed. N. Svartholm (Almqvist and Wiksells, Stockholm, 1968), p 367.
- [3] W. Beenakker et al., *WW Cross-Sections and Distributions*, in *Physics at LEP2*, edited by G. Altarelli, T. Sjöstrand and F. Zwirner (CERN 96-01, Geneva, 1996), Vol. 1, p. 79.
- [4] W. Beenakker, F. A. Berends and A. P. Chapovsky, Phys. Lett. **B435** (1998) 233.

- [5] W. Beenakker, F. A. Berends and A. P. Chapovsky, Nucl. Phys. **B548** (1999) 3; in *Barcelona 1998, Radiative corrections: Application of quantum field theory to phenomenology*, ed. J. Sola ( World Sci. Publ. Co., Singapore, 1999) pp. 528-536.
- [6] D. L. Burke, in Beyond the Standard Model 4, eds. J. F. Gunion *et al.* (World Sci. Publ. Co., Singapore, 1995) p.125.
- [7] Y. Kurihara, ed., Japan Linear Collider (JLC) Proceedings, 5th Workshop, (KEK, Tsukuba, 1995).
- [8] M. Piccolo, in Frascati 1998, Bruno Touschek and the Birth of  $e^+e^-$  Physics, ed. G. Isidori (INFN, Frascati, 1999) p. 131.
- [9] P. M. Zerwas, in \*Moscow 1999, High energy physics and quantum field theory\* 152-170.
- [10] S. Jadach *et al.*, to appear.
- [11] Proc. of LEP2 MC Workshop, edited by S. Jadach, G. Passarino and F. Pittau, CERN Yellow Report 2000-009.
- [12] S. Jadach, W. Płaczek, M. Skrzypek, B.F.L. Ward and Z. Wąs, Phys. Lett. **B417** (1998) 326.
- [13] S. Jadach, W. Płaczek, M. Skrzypek, B.F.L. Ward and Z. Wąs, Phys. Rev. **D61** (2000) 113010.
- [14] S. Jadach, W. Płaczek, M. Skrzypek, B. F. L. Ward and Z. Wąs, Comp. Phys. Commun. **119** (1999) 272; M. Skrzypek, S. Jadach, W. Płaczek and Z. Wąs, *ibid.* **94** (1996) 216.
- [15] S. Jadach, W. Płaczek and B.F.L. Ward, Phys. Rev. **D56** (1997) 6939.
- [16] D. R. Yennie, S. Frautschi and H. Suura, Ann. Phys. **13** (1961) 379.
- [17] S. Jadach, B.F.L. Ward and Z. Wąs, Comp. Phys. Commun. **79** (1994) 503.
- [18] S. Jadach and B.F.L. Ward, Phys. Lett. **B274** (1992) 470.
- [19] S. Jadach, W. Płaczek, E. Richter-Wąs, B.F.L. Ward and Z. Wąs, Comput. Phys. Commun. **102** (1997) 229.
- [20] S. Jadach, E. Richter-Wąs, B.F.L. Ward and Z. Wąs, Comput. Phys. Commun. **70** (1992) 305.
- [21] E. Barberio and Z. Wąs, Comput. Phys. Commun. **79** (1994) 291 and references therein.

- [22] S. Jadach, B.F.L. Ward and Z. Wąs, Phys. Lett. **B449** (1999) 97; Comp. Phys. Commun. **130** (1999) 260; CERN-TH-2000-087.
- [23] Z. Wąs, in these *Proceedings*, ed H. Haber (SLAC, Stanford, 2001).
- [24] A. Denner, S. Dittmaier, M. Roth and D. Wackerth, Phys.Lett. B475 (2000) 127; J.Phys. G26 (2000) 593; BI-TP-99-47, DOE-ER-40685-941, LU-ITP-1999-023, PSI-PR-99-34, UR-1594, hep-ph/9912447; Nucl.Phys. B587 (2000) 67; private communication.
- [25] S. Dittmaier, in these *Proceedings*, ed H. Haber (SLAC, Stanford, 2001).
- [26] E. A. Kuraev and V. F. Fadin, Sov. J. Nucl. Phys. **41** (1985) 466.
- [27] G. Passarino, in *CERN Yellow Report 2000-009*, eds. S. Jadach, R. Pittau and G. Passarino (CERN, Geneva, 2000) p. 134.
- [28] D. Bardin *et al.*, in *CERN Yellow Report 2000-009*, eds. S. Jadach, R. Pittau and G. Passarino (CERN, Geneva, 2000) p. 135; Comput. Phys. Commun. **104** (1997) 161.
- [29] W. Beenakker *et al.*, Nucl. Phys. **B500** (1997) 255; G. Passarino, Nucl. Phys. **B574** (2000) 451.
- [30] R. J. Eden, P. V. Landshoff, D. I. Olive, and J. C. Polkinghorne, “*The Analytic S-Matrix*”, (Cambridge University Press, Cambridge, 1966).
- [31] R. G. Stuart, Nucl. Phys. **B498** (1997) 28; Eur. Phys. J. **C4** (1998) 259; in \*Tegernsee 1996, The Higgs puzzle\*, pp. 47-54; in \*Merida 1996, High energy physics - Particles and fields\*, pp. 199-206.
- [32] J. Fleischer, F. Jegerlehner and M. Zralek, Z. Phys. **C42** (1989) 409; M. Zralek and K. Kołodziej, Phys. Rev. **D43** (1991) 43; J. Fleischer, K. Kołodziej and F. Jegerlehner, Phys. Rev. **D47** (1993) 830; J. Fleischer *et al.*, Comput. Phys. Commun. **85** (1995) 29 and references therein.
- [33] J. Fujimoto *et al.*, MINAMI-TATEYA Coll., GRACE User’s Manual, v. 2.0; Comput. Phys. Commun. **100** (1997) 128;
- [34] K. Hagiwara *et al.*, Nucl. Phys. **B282** (1987) 253.
- [35] D. G. Charlton, eConf C990809 (2000) 352-367, and references therein.

# Coherent Exclusive Exponentiation of 2f Processes in $e^+e^-$ Annihilation\*

Z. WĄS,<sup>†</sup> S. JADACH<sup>‡</sup> and B.F.L. WARD<sup>§</sup>,

In the talk we present the Coherent Exclusive Exponentiation (CEEX) which is implemented in the  $\mathcal{KCMC}$  event generator for the process  $e^+e^- \rightarrow f\bar{f} + n\gamma$ ,  $f = \mu, \tau, d, u, s, c, b$  for center of mass energies from  $\tau$  lepton threshold to 1TeV, that is for LEP1, LEP2, SLC, future Linear Colliders,  $b, c, \tau$ -factories etc. We will attempt a short discussion of the theoretical concepts necessary in our approach, in particular the relations between the rigorous calculation of spin amplitudes (perturbation expansion), phase space parametrisation and exponentiation. In CEEX effects due to photon emission from the initial beams and outgoing fermions are calculated in QED up to second-order, including all interference effects. Electroweak corrections are included in first-order, at the amplitude level. The beams can be polarised longitudinally and transversely, and all spin correlations are incorporated in an exact manner. Precision predictions, in particular the photon emission at LEP2 energies, are also shown.

Presented at the

5th International Symposium on Radiative Corrections  
(RADCOR-2000)

Carmel CA, USA, 11–15 September, 2000

---

\*Work supported in part by the US DoE contracts DE-FG05-91ER40627 and DE-AC03-76SF00515, the European Commission 5-th framework contract HPRN-CT-2000-00149 and the Polish-French Collaboration within IN2P3 through LAPP Annecy.

<sup>†</sup>Institute of Nuclear Physics, Cracow, ul. Kawory 26A, Poland

<sup>‡</sup>Theory Group DESY, Platanenallee 6, D-15738 Zeuthen, Germany  
and Institute of Nuclear Physics, Cracow, ul. Kawory 26A, Poland

<sup>§</sup>Department of Physics and Astronomy, The University of Tennessee, Knoxville, Tennessee 37996-1200, USA

# 1 Introduction

At the end of LEP2 operation the total cross section for the process  $e^-e^+ \rightarrow f\bar{f} + n\gamma$  has to be calculated with the precision 0.2% – 1%, depending on the event selection. The arbitrary differential distributions have to be calculated with the corresponding precision. Even now, this is not always the case [1] and the calculations are still continuing. In the future, for linear colliders (LC's), the precision requirement can be even more demanding. These requirements necessitate development of the appropriate calculational schemes for the QED corrections and the construction of new dedicated MC programs. We present here an effort in this direction. Our report is based on refs. [2,3,4] and the Monte Carlo program is described in ref. [5]. The pedagogical introduction to some concepts necessary in understanding exponentiation can be found e.g. in [6].

Feature	KORALB	KORALZ	$\mathcal{K}\mathcal{K}$ 4.13	$\mathcal{K}\mathcal{K}$ 2000+?
QED type	$\mathcal{O}(\alpha)$	EEX	CEEX, EEX	CEEX, EEX
CEEX(ISR+FSR)	none	none	$\{\alpha, \alpha L; \alpha^2 L^2, \alpha^2 L^1\}$	$\{\dots\alpha^2 L^1; \alpha^3 L^3\}$
EEX(ISR+FSR)	none	$\{\alpha, \alpha L, \alpha^2 L^2\}$	$\{\alpha, \alpha L, \alpha^2 L^2, \alpha^3 L^3\}$	$\{\dots\alpha^2 L^2, \alpha^3 L^3\}$
ISRFSR int.	$\mathcal{O}(\alpha)$	$\mathcal{O}(\alpha)$	$\{\alpha, \alpha L\}_{\text{CEEX}}$	$\{\alpha, \alpha L\}_{\text{CEEX}}$
Exact brems.	1 $\gamma$	1, 2 coll. $\gamma$	1, 2, 3 coll. $\gamma$	up to 3 $\gamma$
Electroweak	No Zres.	DIZET 6.x	DIZET 6.x	New version?
Beam polar.	long+trans.	longit.	long+trans.	long+trans.
$\tau$ polar.	long+trans.	longit.	long+trans.	long+trans.
Hadronization	—	JETSET	JETSET	PYTHIA
$\tau$ decay	TAUOLA	TAUOLA	TAUOLA	TAUOLA
Inclusive mode	—	No	Yes	Yes
Beamstrahlung	—	No	Yes	Yes
Beam spread	—	No	Yes	Yes
$\nu\nu$ channel	—	Yes	No	Yes
$ee$ channel	—	No	No	Yes
$tt$ channel	—	No	No	yes?
$WW$ channel	—	No	No	yes?

Table 1: Overview of the  $\mathcal{K}\mathcal{K}\text{MC}$  event generator as compared with KORALZ and KORALB.

## 2 What is precision calculation

New results from high energy particle experiments are obtained as a result of the huge effort of hundreds of experimental physicists over many years. In the cases when

theoretical calculations are needed to interpret the results, it is fair to require, whenever possible, the uncertainty of the calculations to be smaller at least by a factor of 3 than the experimental error. Once the condition is fulfilled, in the final interpretation of experimental data for quantities such as coupling constants, total cross sections or particle masses, the final combined theoretical and experimental uncertainty would not increase more than 10 % with respect to experimental uncertainty alone. This rule of thumb is motivated in cases when the theoretical calculations are possible and require an effort much smaller than that of the experiments.

The crucial requirement of the high precision calculation is however not only that its results agree with the measured data, but also, that the relation of the results with the foundation of the Standard Model field theory is fully controlled. At present, requirements for precision, as defined by experiments, do not exceed the 0.1 % tag. That is why, in general, predictions including complete Standard Model corrections of  $\mathcal{O}(\alpha_{QED})$ , are sufficient. Only those terms of the higher orders which include enhancement factors such as  $\ln \frac{s}{m_f^2}$ ,  $\ln \frac{M_Z}{\Gamma_Z}$ ,  $\frac{m_t}{m_W}$  etc., have to be taken into account.

Thanks to this, one can define schemes of calculation where QED calculations can be separated from the rest, and dealt with to large degree individually<sup>1</sup>. As it was presented in [1,7] this was indeed the solution successful for LEP2  $e^+e^- \rightarrow 2f$  and  $e^+e^- \rightarrow 4f$  processes. Exponentiation is a convenient way of dealing with the QED corrections, which are large, and depend on the detection conditions (cuts).

### 3 What is coherent exclusive exponentiation CEEEX?

The *exponentiation* is generally a method of summing up real and virtual photon contributions to infinite order such that infrared (IR) divergences cancel. The *exclusivity* means that the procedure of exponentiation, that is summing up the infrared (IR) real and virtual contribution, within the standard perturbative scheme of quantum field theory, is done at the level of the fully differential (multiphoton) cross section, or even better, at the level of the scattering matrix element (spin amplitude), *before any phase-space integration over photon momenta is done*. The other popular type of the exponentiation is *inclusive* exponentiation (IEX), which is done at the level of inclusive distributions, structure functions, etc. see discussion in ref. [8]. The classical work of Yennie-Frautschi-Suura [9] (YFS) represents the best example of the exclusive exponentiation and we nickname it as EEX. Finally, why do we use word *coherent*? In CEEEX the essential part of the summation of the IR real and virtual photon contributions is done at the amplitude level. Of course, IR cancellations occur as usual at the probability level, however, the transition from spin amplitudes to dif-

---

<sup>1</sup>Even further separation is possible: emission of additional real fermion pairs can be calculated separately. At the same step, the appropriate virtual corrections have to be included into predictions for  $2f$ -processes.

ferential cross sections, and the phase space integration are done entirely numerically! As a consequence of the above *coherent* approach it follows that CEEX is friendly to coherence among Feynman diagrams, narrow resonances, interferences, etc. This is a great practical advantage. In our many previous works which led to the development of the Monte Carlo event generators like YFS2, YFS3, KORALZ, KORALW, YFS3WW, BHLUMI, BHWIDE, see refs. [10,11,12,13,14,15], we have generally employed EEX, which is closely related to the YFS work [8]. The CEEX is a recent development and is so far used only in the new  $\mathcal{K}\mathcal{K}\mathcal{M}\mathcal{C}$  program [5].

Let us now show in a very simplified schematic way what is the the main difference between the old EEX/YFS and the CEEX for the fermion pair production the process:

$$e^-(p_1, \lambda_1) + e^+(p_2, \lambda_2) \rightarrow f(q_1, \lambda'_1) + \bar{f}(q_2, \lambda'_2) + \gamma(k_1, \sigma_1) + \dots + \gamma(k_n, \sigma_n). \quad (1)$$

The EEX total cross section is

$$\sigma = \sum_{n=0}^{\infty} \int_{m_\gamma} d\Phi_{n+2} e^{Y(m_\gamma)} D_n(q_1, q_2, k_1, \dots, k_n), \quad (2)$$

where in the  $\mathcal{O}(\alpha^1)$  the distributions for  $n_\gamma = 0, 1, 2$  are

$$\begin{aligned} D_0 &= \bar{\beta}_0 \\ D_1(k_1) &= \bar{\beta}_0 \tilde{S}(k_1) + \bar{\beta}_1(k_1) \\ D_2(k_1, k_2) &= \bar{\beta}_0 \tilde{S}(k_1) \tilde{S}(k_2) + \bar{\beta}_1(k_1) \tilde{S}(k_2) + \bar{\beta}_1(k_2) \tilde{S}(k_1) \end{aligned} \quad (3)$$

and the real soft factors are defined as usual

$$4\pi \tilde{S}(k) = \sum_{\sigma} |\mathfrak{s}_\sigma(k)|^2 = |\mathfrak{s}_+(k)|^2 + |\mathfrak{s}_-(k)|^2 = -\frac{\alpha}{\pi} \left( \frac{q_1}{kq_1} - \frac{q_2}{kq_2} \right)^2. \quad (4)$$

What is important for our discussion is that the IR-finite building blocks

$$\begin{aligned} \bar{\beta}_0 &= \sum_{\lambda} |\mathcal{M}_\lambda|^2, \\ \bar{\beta}_1(k) &= \sum_{\lambda\sigma} |\mathcal{M}_{\lambda\sigma}^{1\text{-phot}}|^2 - \sum_{\sigma} |\mathfrak{s}_\sigma(k)|^2 \sum_{\lambda} |\mathcal{M}_\lambda^{\text{Born}}|^2 \end{aligned} \quad (5)$$

in the multiphoton distributions are all in terms of  $\sum_{spin} |\dots|^2$ !! We denoted:  $\lambda =$  fermion helicities and  $\sigma =$  photon helicity.

The above is to be contrasted with the analogous  $\mathcal{O}(\alpha^1)$  case of CEEX

$$\sigma = \sum_{n=0}^{\infty} \int_{m_\gamma} d\Phi_{n+2} \sum_{\lambda, \sigma_1, \dots, \sigma_n} |e^{B(m_\gamma)} \mathcal{M}_{n, \sigma_1, \dots, \sigma_n}^\lambda(k_1, \dots, k_n)|^2, \quad (6)$$

where the differential distributions for  $n_\gamma = 0, 1, 2$  photons are the following:

$$\begin{aligned}\mathcal{M}_0^\lambda &= \hat{\beta}_0^\lambda, \quad \lambda = \text{fermion helicities}, \\ \mathcal{M}_{1,\sigma_1}^\lambda(k_1) &= \hat{\beta}_0^\lambda \mathfrak{s}_{\sigma_1}(k_1) + \hat{\beta}_{1,\sigma_1}^\lambda(k_1), \\ \mathcal{M}_{2,\sigma_1,\sigma_2}^\lambda(k_1, k_2) &= \hat{\beta}_0^\lambda \mathfrak{s}_{\sigma_1}(k_1) \mathfrak{s}_{\sigma_2}(k_2) + \hat{\beta}_{1,\sigma_1}^\lambda(k_1) \mathfrak{s}_{\sigma_2}(k_2) + \hat{\beta}_{1,\sigma_2}^\lambda(k_2) \mathfrak{s}_{\sigma_1}(k_1)\end{aligned}\quad (7)$$

and the IR-finite building blocks are

$$\begin{aligned}\hat{\beta}_0^\lambda &= (e^{-B} \mathcal{M}_\lambda^{\text{Born+Virt.}})|_{\mathcal{O}(\alpha^1)}, \\ \hat{\beta}_{1,\sigma}^\lambda(k) &= \mathcal{M}_{1,\sigma}^\lambda(k) - \hat{\beta}_0^\lambda \mathfrak{s}_\sigma(k).\end{aligned}\quad (8)$$

As shown explicitly, this time everything is in terms of  $\mathcal{M}$ -spin-amplitudes! This is the basic difference between EEX/YFS and CEEEX. The complete expressions for spin amplitudes with CEEEX exponentiation, for any number of photons, are shown in ref. [2] for the  $\mathcal{O}(\alpha^1)$  case and in ref. [4] for the  $\mathcal{O}(\alpha^2)$  case.

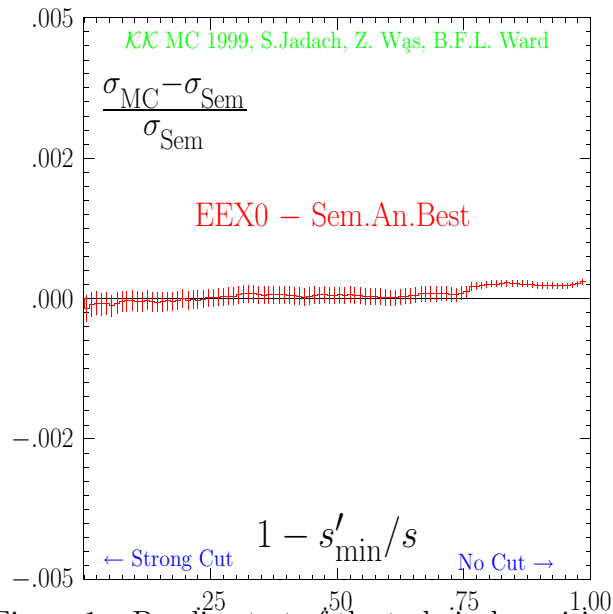


Figure 1: Baseline test of the technical precision.

## 4 Monte Carlo numerical results

The  $\mathcal{O}(\alpha^2)$  CEEEX-style matrix element is implemented in  $\mathcal{K}\mathcal{K}\mathcal{M}\mathcal{C}$  which simulates the production of muon, tau and quark pairs. Electrons (Bhabha scattering) and neutrino channels are not available. The program includes for the optional use the older, EEX-style matrix element. It is then functionally similar to KORALZ [11] and the older KORALB [16] programs. In Table 1 we provide the complete comparison of the features of  $\mathcal{K}\mathcal{K}\mathcal{M}\mathcal{C}$  and the older programs.

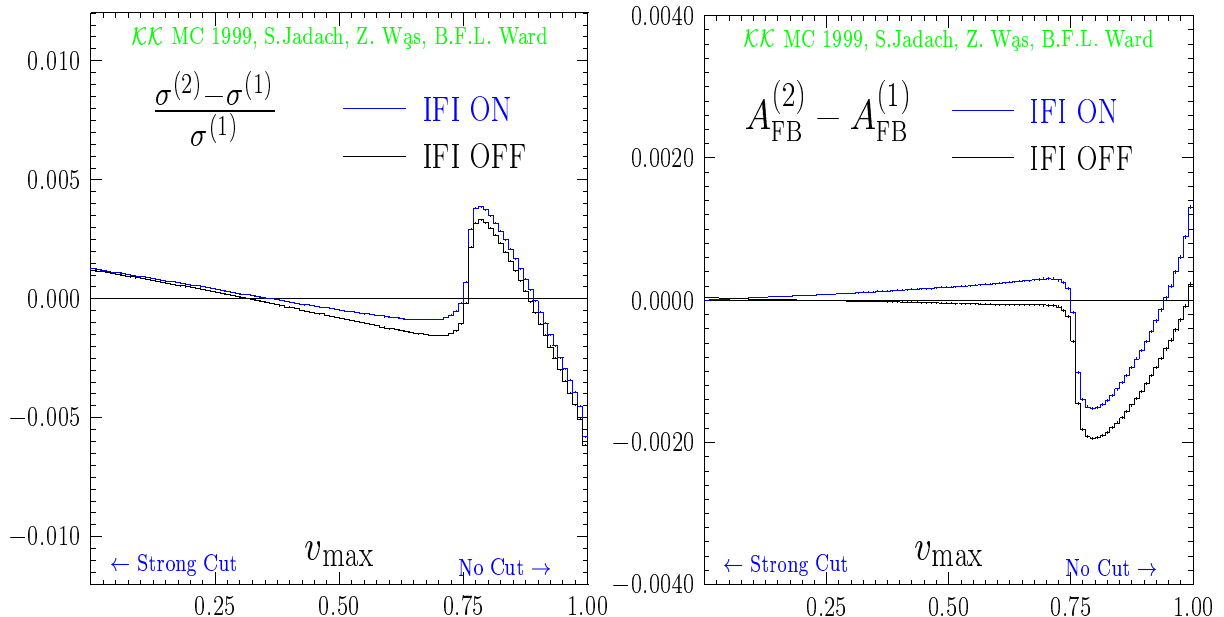


Figure 2: Test of the technical precision of  $\mathcal{K}\mathcal{K}\text{MC}$ .

#### 4.1 Technical precision

For the new MC program of the high complexity like  $\mathcal{K}\mathcal{K}\text{MC}$  it is important to check very precisely the overall normalisation. This is the cornerstone of the evaluation of the *technical precision* of the program, especially for  $\mathcal{K}\mathcal{K}\text{MC}$  which is aimed at the end of testing at the total precision of 0.1%. In Fig. 1 we present the comparison of the  $\mathcal{K}\mathcal{K}\text{MC}$  with simple semi-analytical integration for the total cross section, as a function of the minimum mass  $\sqrt{s'_{\min}}$  of the final muon pair. It is done for muon-pair final state at  $\sqrt{s} = 200\text{GeV}$ . For  $\sqrt{s'_{\min}} \rightarrow \sqrt{s}$ , when emission of hard photons is suppressed, there is an agreement  $< 0.02\%$  between  $\mathcal{K}\mathcal{K}\text{MC}$  and the analytical calculation. For  $\sqrt{s'_{\min}} < M_Z$  the on-shell Z-boson production due to emission of the hard initial state radiation (ISR), the so called Z radiative return (ZRR), is allowed kinematically. Even in this case (more sensitive to higher orders) the agreement  $< 0.02\%$  is reached. For the above exercise we used the simplified  $\mathcal{O}(\alpha^0)$  CEEEX matrix element, because in this case the precise phase-space analytical integration is relatively easy.

#### 4.2 Physical precision

The equally important component of the overall error is the physical error which we estimate conservatively as the half of the difference  $\mathcal{O}(\alpha^2) - \mathcal{O}(\alpha^1)$ . In Fig. 2 we show the corresponding result for the total cross section and charge asymmetry for  $\sqrt{s} = 189\text{GeV}$  as a function of the cut on energies of all photons ( $s'_{\min} < s$  limits the total photon energy.) We obtain in this way the estimate 0.2% for the physical

precision of the total cross section and 0.1% for the charge asymmetry. Both plots in Fig. 2 show as expected a strong variation at the position of the ZRR. The quoted precision is good enough for the LEP2 combined data.

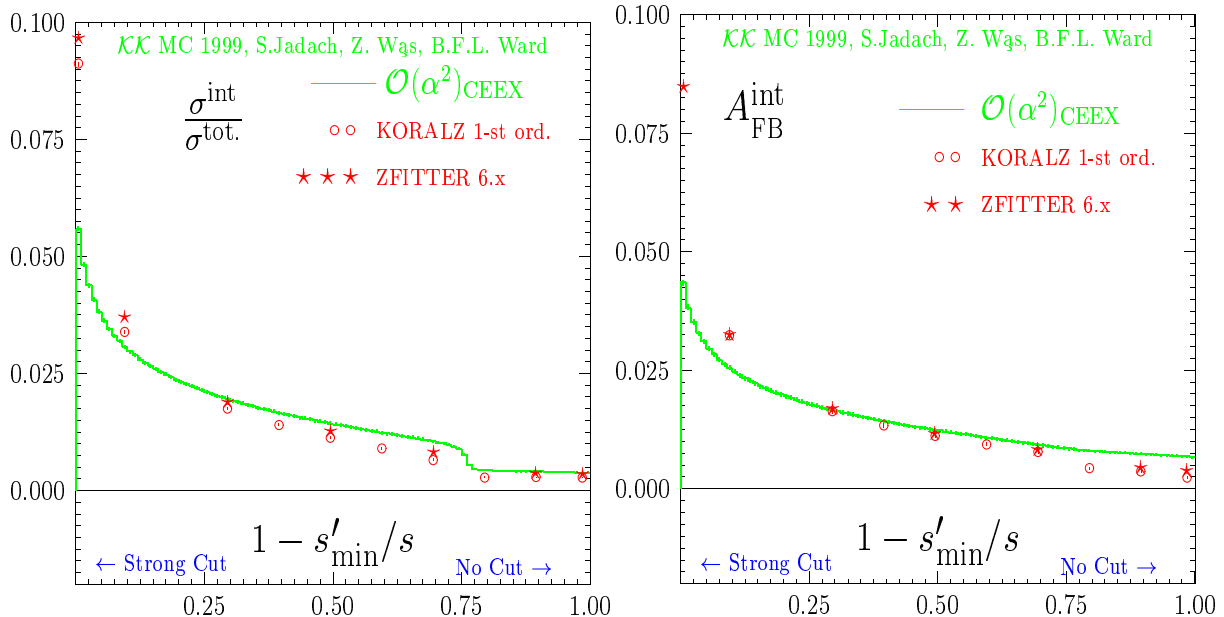


Figure 3: The effect of the initial-final state QED interference in total cross-section and charge asymmetry.

### 4.3 Initial-final state QED interference

One important benefit from CEEX with respect to the older EEX is the inclusion of the Initial-Final state QED Interference (IFI). The effect of the IFI is comparable with the precision of the LEP2 combined data and should be under good control. Results of our analysis of the size of the IFI at LEP2 energies ( $\sqrt{s} = 189\text{GeV}$ ) are shown in Fig. 3. In this figure we compare the CEEX result of  $\mathcal{K}\mathcal{K}\text{MC}$  first of all with the result of KORALZ which is run in the  $\mathcal{O}(\alpha^1)$  mode without exponentiation (The IFI is neglected for KORALZ with the EEX matrix element.) The  $\mathcal{O}(\alpha^1)$  IFI contribution from KORALZ was extensively cross-checked in the past with the dedicated semi-analytical calculations [17]; it is therefore a good reference and starting point. As we see the IFI contribution of CEEX differs slightly from the pure  $\mathcal{O}(\alpha^1)$  result. It is related to exponentiation which makes the angular dependence (in the muon scattering angle) of the IFI contribution less sharp and it is also due to the convolution of the IFI with the  $\mathcal{O}(\alpha^2)$  ISR. The expected modification of the interference correction due to higher orders is about 20% for the cross section and asymmetry, if the ZRR is excluded, (the size of the ISR correction in the cross section) and it is indeed of this size. Apparently, this principle works also in the case of ZRR included, remembering

that in this case the ISR correction is 100% or more. However, we feel that this case requires further study. We have also included results of the semianalytical program ZFITTER [18] in our plots<sup>2</sup>. They agree well with the  $\mathcal{O}(\alpha^1)$  IFI of KORALZ. This is expected because they are without exponentiation.

## 5 Outlook and summary

The most important new features in the present CEEX are the ISR-FSR interference, the second-order subleading corrections, the exact matrix element for two hard photons, and the full density matrix treatment for the spin states of initial and final state fermions<sup>3</sup>. This makes CEEX already a unique source of SM predictions for the LEP2 physics program and for the LC physics program. Note that for these the electroweak correction library has to be reexamined at LC energies. The most important omission in the present version is the lack of neutrino and electron channels. Let us stress that the present program is an excellent starting platform for the construction of the second-order Bhabha MC generator based on CEEX exponentiation. We hope to be able to include the Bhabha and neutrino channels soon, possibly in the next version<sup>4</sup>. The other important directions for the development are the inclusion of the exact matrix element for three hard photons, together with virtual corrections up to  $\mathcal{O}(\alpha^3 L^3)$  and the emission of the light fermion pairs. The inclusion of the  $W^+W^-$  and  $t\bar{t}$  final states is still in a farther perspective.

## References

- [1] M. Kobel *et al.* [Two Fermion Working Group Collaboration], “Two-fermion production in electron positron collisions,” hep-ph/0007180.
- [2] S. Jadach, B. F. L. Ward, and Z. Wąs, Phys. Lett. **B449**, 97 (1999).
- [3] S. Jadach, B. F. L. Ward, and Z. Was, Global positioning of spin GPS scheme for half spin massive spinors, 1998, preprint hep-ph/9905452, CERN-TH-98-235, submitted to Eur. J. Phys. C.
- [4] S. Jadach, B. F. L. Ward, and Z. Wąs, Coherent Exclusive Exponentiation For Precision Monte Carlo Calculations, 2000, preprint CERN-TH/2000-087,UTHEP-99-09-01.

---

<sup>2</sup> We would like to thank D. Bardin for providing us results from ZFITTER.

<sup>3</sup>The recent presentation of the  $\tau$  lepton decay library TAUOLA can be found in ref [19].

<sup>4</sup>At the time of the completion of the conference contribution, the program version including the neutrino channel can be obtained upon individual request only. It is still at the stage of the pre-release tests.

- [5] S. Jadach, Z. Wąs, and B. F. L. Ward, The Precision Monte Carlo Event Generator  $\mathcal{KK}$  For Two-Fermion Final States In  $e^+e^-$  Collisions, Computer Physics Communications in print, 2000, preprint DESY-99-106, CERN-TH/99-235, UTHEP-99-08-01, source version 4.13 available from <http://home.cern.ch/jadach/>.
- [6] Z. Was, “Radiative corrections,” CERN-TH-7154-94, *Written on the basis of lectures given at the 1993 European School of High Energy Physics, Zakopane, Poland, 12-25 Sep 1993*.
- [7] M. W. Grunewald *et al.*, “Four fermion production in electron positron collisions,” hep-ph/0005309.
- [8] S. Jadach and B. Ward, in *Electroweak Physics*, edited by N. Dombey and F. Boudjema (Plenum Publ. Co., London, 1989), Proc. of Sussex University Conference.
- [9] D. R. Yennie, S. Frautschi, and H. Suura, *Ann. Phys. (NY)* **13**, 379 (1961).
- [10] S. Jadach and B. F. L. Ward, *Comput. Phys. Commun.* **56**, 351 (1990).
- [11] S. Jadach, B. F. L. Ward, and Z. Wąs, *Comput. Phys. Commun.* **79**, 503 (1994).
- [12] S. Jadach *et al.*, *Comput. Phys. Commun.* **119**, 272 (1999).
- [13] S. Jadach, W. Płaczek, M. Skrzypek, and B. F. L. Ward, *Phys. Rev.* **D54**, 5434 (1996).
- [14] S. Jadach *et al.*, *Comput. Phys. Commun.* **102**, 229 (1997).
- [15] S. Jadach, W. Płaczek, and B. F. L. Ward, *Phys. Lett.* **B390**, 298 (1997), also hep-ph/9608412; The Monte Carlo program BHWIDE is available from <http://hephp01.phys.utk.edu/pub/BHWIDE>.
- [16] S. Jadach and Z. Was, *Comput. Phys. Commun.* **85**, 453 (1995).
- [17] S. Jadach and Z. Wąs, *Phys. Rev.* **D41**, 1425 (1990).
- [18] D. Bardin *et al.*, ZFITTER v.6.21: A Semianalytical program for fermion pair production in  $e^+ e^-$  annihilation, 1999, e-print: hep-ph/9908433.
- [19] Z. Was, “TAUOLA the library for tau lepton decay, and KKMC/KORALB/KORALZ/... status report,” hep-ph/0011305.

# Electroweak Measurements on the Z Resonance

DAVID STROM \*

*Department of Physics  
University of Oregon, Eugene, OR 97403 USA*

Almost all precision electroweak measurements from the Z resonance made at the LEP storage ring by the ALEPH, DELPHI, L3 and OPAL experiments and those made using a polarized electron beam at the SLC by the SLD experiment are now final and have been published. Changes in the measurements since the last RADCOR meeting are discussed. The internal consistency of the measurements is considered. The impact of remaining theoretical uncertainties in the QCD sector are examined as well as the impact of experimental and theoretical uncertainties on the value of  $\alpha_{\text{QED}}(m_Z)$ .

Presented at the

5th International Symposium on Radiative Corrections  
(RADCOR-2000)

Carmel CA, USA, 11–15 September, 2000

---

\*Work supported by the US Department of Energy grant DE-FG03-96ER40969.

## 1 Introduction

Between 1989 and 1995 the LEP collaborations collected more than 200 pb<sup>-1</sup> per experiment, which resulted in more than 17 million recorded Z decays. The LEP data included almost 50 pb<sup>-1</sup> of off-peak data, which is needed to determine the mass and width of the Z. The SLD at the SLC recorded collisions with a polarized electron beam and an unpolarized positron beam from 1992 until 1998, achieving electron polarizations as high as 80% and a total data sample of more than 500,000 recorded Z decays. These large data samples provide the basis for well-known tests of the Standard Model.

Almost all of the precision measurements made at the Z resonance have now been published and the LEP and SLD electroweak working groups have almost completed a comprehensive review of these measurements which will shortly appear in *Physics Reports*[1]. Furthermore, several very complete reviews of the theory necessary for the interpretation of these measurements already exist, see, for example, References [2,3,4]. Rather than attempting to summarize this entire work in a few pages, I will briefly review changes in theory and measurement since the last RADCOR meeting and then consider three areas where some controversy exists: the determination of strong coupling constant,  $\alpha_s$ , the possible discrepancy between the Standard Model and measurements of forward-backward asymmetries in  $b\bar{b}$  final states, and finally the impact on Higgs mass limits of the contribution of hadronic vacuum polarization to the running value of the electromagnetic coupling constant at the Z resonance,  $\alpha(m_Z^2)$ .

## 2 Changes since RADCOR 1998

The LEP and SLD collaborations present their measurements in terms of pseudo-observables which are closely related to the actual measurements, but include corrections for effects such as electromagnetic radiation and interference between photon mediated and Z mediated processes. These variables, together with other variables commonly used in electroweak fits are summarized in Table 1. The values of the Z mass,  $m_Z$ , the Z width,  $\Gamma_Z$  and the peak hadronic cross section  $\sigma_{\text{had}}^{\text{pole}}$  require quite large corrections as illustrated in Figure 1 taken from Reference [9]. Large corrections are also needed to the forward-backward asymmetries of leptons and quarks. The largest corrections of all are for electron final states, where t-channel effects dominate in many regions of phase space. Radiative corrections for the left-right asymmetries measured by SLD and for polarized forward-backward asymmetries are much smaller, but nevertheless important. For example, the largest change between the preliminary SLD measurement of the left-right asymmetry ( $A_{\text{LR}}$ ) and the final published value of  $A_{\text{LR}}$  came from a correction to the beam energy which was based

Table 1: The summary of measurements included in the combined analysis of Standard Model parameters used by the LEP and SLD electroweak groups reproduced from References [5] and [6]. The electroweak measurements from  $p\bar{p}$  colliders,  $\nu N$  scattering, and LEP2  $m_W$  are described elsewhere in the RADCOR 2000 proceedings [7,8].

	2000 Result	1998 Result	Standard Model fit	2000 Pull
$\Delta\alpha_{\text{had}}^{(5)}(m_Z^2)$	$0.02804 \pm 0.00065$	$0.02804 \pm 0.00065$	0.02804	0.0
<u>LEP</u>				
$m_Z$ [GeV]	$91.1875 \pm 0.0021$	$91.1867 \pm 0.0021$	91.1874	0.0
$\Gamma_Z$ [GeV]	$2.4952 \pm 0.0023$	$2.4939 \pm 0.0024$	2.4962	-0.4
$\sigma_{\text{had}}^{\text{pole}}$ [nb]	$41.540 \pm 0.037$	$41.491 \pm 0.058$	41.480	1.6
$R_\ell$	$20.767 \pm 0.025$	$20.765 \pm 0.026$	20.740	1.1
$A_{\text{FB}}^0$	$0.0171 \pm 0.0010$	$0.0169 \pm 0.0010$	0.0164	0.8
$\tau$ polarization:				
$A_\tau$	$0.1439 \pm 0.0042$	$0.1431 \pm 0.0045$	0.1480	-1.0
$A_e$	$0.1498 \pm 0.0048$	$0.1479 \pm 0.0051$	0.1480	0.4
q $\bar{q}$ charge asym.:				
$\sin^2\theta_{\text{eff}}^{\text{lept}}$	$0.2321 \pm 0.0010$	$0.2321 \pm 0.0010$	0.23140	0.7
$m_W$ [GeV]	$80.427 \pm 0.046$	$80.37 \pm 0.09$	80.402	0.5
<u>SLD</u>				
$\sin^2\theta_{\text{eff}}^{\text{lept}} (A_\ell)$	$0.23098 \pm 0.00026$	$0.23109 \pm 0.00029$	0.23140	-1.6
<u>Heavy Flavor</u>				
$R_b$	$0.21653 \pm 0.00069$	$0.21656 \pm 0.00074$	0.21578	1.1
$R_c$	$0.1709 \pm 0.0034$	$0.1735 \pm 0.0044$	0.1723	-0.4
$A_{\text{FB}}^{0,b}$	$0.0990 \pm 0.0020$	$0.0990 \pm 0.0021$	0.1038	-2.4
$A_{\text{FB}}^{0,c}$	$0.0689 \pm 0.0035$	$0.0709 \pm 0.0044$	0.0742	-1.5
$A_b$	$0.922 \pm 0.023$	$0.867 \pm 0.035$	0.935	-0.6
$A_c$	$0.631 \pm 0.026$	$0.647 \pm 0.040$	0.668	-1.4
<u><math>p\bar{p}</math> and <math>\nu N</math></u>				
$m_W$ [GeV]	$80.452 \pm 0.062$	$80.41 \pm 0.09$	80.402	0.8
$\sin^2\theta_W$	$0.2255 \pm 0.0021$	$0.2254 \pm 0.0021$	0.2226	1.2
$m_t$ [GeV]	$174.3 \pm 5.1$	$173.8 \pm 5.0$	174.3	0.0

on a scan of the Z resonance [10].

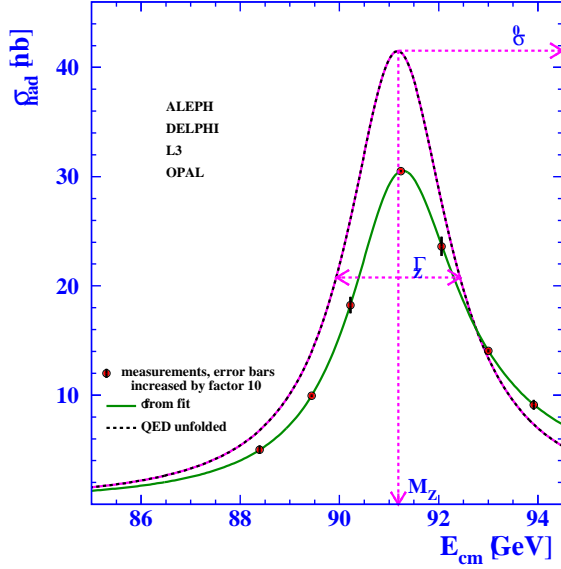


Figure 1: Illustration of LEP line-shape parameter definitions[9].

For the five Z line-shape parameters (assuming lepton universality) as measured at LEP[11,12,13,14], the total error and the theoretical error on the determination of the pseudo-observables is shown in Table 2. In terms of the effective vector and axial and vector couplings of a given fermion to the Z,  $g_{Af}$  and  $g_{Vf}$ :

$$\Gamma_{f\bar{f}} = \frac{G_F N_c m_Z^3}{6\pi\sqrt{2}} \left( R_V^f g_{Vf}^2 + R_A^f g_{Af}^2 \right) + \Delta_{\text{QCD}} \quad (1)$$

$$A_f = 2 \frac{g_{Vf} g_{Af}}{g_{Vf}^2 + g_{Af}^2}. \quad (2)$$

Here,  $R_V^f$  and  $R_A^f$  give corrections for final-state QED and QCD effects as well as quark masses,  $\Delta_{\text{QCD}}$  for non-factorizable QCD effects. Note that  $A_f$  depends only on the ratio of couplings.

In almost all cases the theory error on the extraction of the pseudo-observables is at least five times smaller than the experimental error. The exceptions occur for theory corrections involving electron final states where t-channel photon mediated processes are important. For example, the theoretical error on luminosity determined with small angle Bhabha scattering drives the error on  $\sigma_{\text{had}}^{\text{pole}}$  [15,16] and the effects of interference corrections on  $R_e \equiv \frac{\Gamma_{\text{had}}}{\Gamma_e}$ , and on  $A_{\text{FB}}^{0,e} \equiv \frac{3}{4} A_e^2$  give a theoretical error which is of the same order as the total error on these quantities when lepton universality is assumed.

Table 2: The total and theoretical errors for the five parameters in a fit assuming lepton universality. If lepton universality is not assumed, the theory errors for electrons are larger, i.e. 0.024 for  $R_e$  and  $0.0014A_{\text{FB}}^0$ .

Quantity	Total Error	Theory Error
$m_Z$	2.1 MeV ( $0.2 \times 10^{-4}$ )	0.3 MeV ( $0.03 \times 10^{-4}$ )
$\Gamma_Z$	2.3 MeV ( $9.2 \times 10^{-4}$ )	0.2 MeV ( $0.8 \times 10^{-4}$ )
$\sigma_{\text{had}}^0 \quad \equiv \quad \frac{12\pi}{m_Z^2} \frac{\Gamma_{e^+e^-} \Gamma_{\text{had}}}{\Gamma_Z^2}$	0.037nb ( $8.9 \times 10^{-4}$ )	0.022nb ( $5.3 \times 10^{-4}$ )
$R_\ell \quad \equiv \quad \frac{\Gamma_{\text{had}}}{\Gamma_\ell}$	0.025 ( $12 \times 10^{-4}$ )	0.004 ( $1.9 \times 10^{-4}$ )
$A_{\text{FB}}^0 \quad \equiv \quad \frac{3}{4} A_e A_f$	0.0010 (5.6%)	0.0001 (0.6%)

It should be stressed that because of the complexity of the fitting procedure used to extract the pseudo-observables from the several hundred cross section and asymmetries of each of the LEP experiments, it will be extremely difficult to incorporate any future improvements in the theory needed to determine the pseudo-observables. It is encouraging that, in general, these theory errors are quite small. The theory used to extract the pseudo-observables from the raw measurements has been very stable since RADCOR 1998 (also shown in Table 1) with two exceptions. The inclusion of third order initial state radiation correction shifted  $\sigma_{\text{had}}^0$  by 0.023 nb or 70% of its present total error[17], and also led to a  $\sim 0.5$  MeV. shift on  $m_Z$ . Inclusion of initial-state radiation of  $e^+e^-$  pairs gave rise to a  $\sim 0.5$  MeV shift on  $m_Z$  and  $\sim 0.8$  MeV shift on  $\Gamma_Z$  [18].

The largest change in the experimental handling of the data was due to improved treatment of the errors on the determination of the beam energy. A lower energy systematic error was obtained for the 1995 LEP run than for the 1993 LEP run[19]. To properly take this into account, the four experiments combined should give more weight to the 1995 data than each do individually. To test the effects of this reweighting, separate values of  $m_Z$  were determined for each year as shown in Figure 2. Because of the consistency of  $m_Z$  for the different periods, the numerical effect of this new procedure was small[9].

In terms of the parameters derived from the LEP line shape, the largest change between RADCOR 1998 and these results is that the ratio of the invisible width to the width for a single generation of charged leptons,  $\frac{\Gamma_{\text{inv}}}{\Gamma_\ell}$ , is now slightly less than the Standard Model prediction giving a value for the number of neutrinos,

$$N_\nu = 2.984 \pm 0.008,$$

approximately  $2\sigma$  smaller than expected. In 1998, the  $N_\nu$  value was almost exactly 3. The change in the central value is largely due to an improved treatment of initial-state radiation that changed the value of  $\sigma_{\text{had}}^{\text{pole}}$ . The error has also been significantly reduced because of a reduction in the luminosity theoretical error [15] since RADCOR 1998.

As is apparent from Table 1 there have been big improvements in the heavy quark measurements made by SLD. These are discussed in detail in Section 4.

### 3 Theoretical errors in the determination of $\alpha_s$

The LEP line-shape data allows a precise determination of  $\alpha_s$  from the effect of QCD final state corrections to the hadronic width. To lowest order, the hadronic width scales as  $\Gamma_{\text{had}} \propto 1 + \frac{\alpha_s}{\pi}$  which leads to the following dependences of LEP

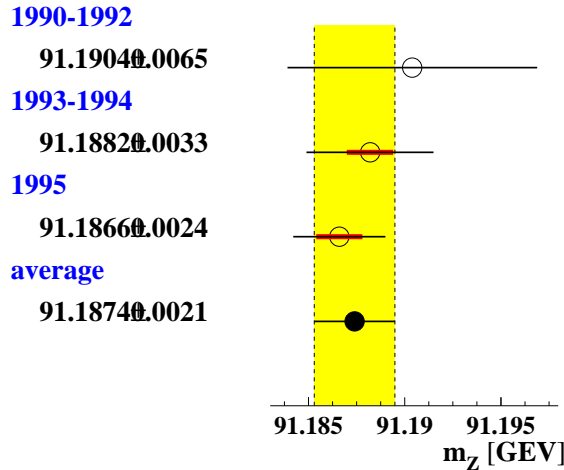


Figure 2: The value of  $m_Z$  determined in separate running periods of the LEP accelerator.

pseudo-observables on  $\alpha_s$ :

$$\begin{aligned}
\Gamma_Z &= \Gamma_{\text{had}} + 3\Gamma_\ell + 3\Gamma_\nu &\propto 1 + 0.7 \frac{\alpha_s}{\pi} \\
R_\ell &= \frac{\Gamma_{\text{had}}}{\Gamma_\ell} &\propto 1 + \frac{\alpha_s}{\pi} \\
\sigma_{\text{had}}^0 &= \frac{12\pi}{m_Z^2} \frac{\Gamma_\ell \Gamma_{\text{had}}}{\Gamma_Z^2} &\propto 1 - 0.4 \frac{\alpha_s}{\pi} \\
\sigma_\ell^0 &= \frac{12\pi}{m_Z^2} \frac{\Gamma_\ell^2}{\Gamma_Z^2} &\propto 1 - 1.4 \frac{\alpha_s}{\pi}
\end{aligned}$$

Here charged lepton universality has been assumed and the invisible width of the Z has been assumed to consist of the contribution from the three generations of neutrinos ( $3\Gamma_\nu$ ). Theoretically, the dependence of these quantities on  $\alpha_s$  comes from the same contribution to  $\Gamma_{\text{had}}$ . (There are additional small top mass ( $m_t$ ) contributions to the partial widths from  $\alpha_s m_t^2$  and  $\alpha_s^2 m_t^2$  corrections to the couplings  $g_{Af}$  and  $g_{Vf}$ . The uncertainty on these corrections correspond to less than a 1.0 GeV uncertainty in the top mass and can therefore be ignored. This is discussed in more detail below.) The cleanest measurements of  $\alpha_s$  come from quantities which depend on the ratio of partial widths such as  $R_\ell$ ,  $\sigma_{\text{had}}^0$  and  $\sigma_\ell^0$  where additional uncertainties from  $m_t$  and from the Higgs mass ( $m_h$ ) cancel.

The parameters  $R_\ell$ ,  $\sigma_{\text{had}}^0$ , and  $\sigma_\ell^0$  are not independent since  $R_\ell = \frac{\sigma_{\text{had}}^0}{\sigma_\ell^0}$ . The LEP parameter set includes  $R_\ell$  and  $\sigma_{\text{had}}^0$ , hiding the constraint imposed by  $\sigma_\ell^0$  in the correlation matrix. The value of  $\alpha_s$  determined using  $R_\ell$  alone is (for  $m_h = 100$  GeV)

$$\alpha_s(m_Z) = 0.1228 \pm 0.0038 \begin{array}{l} +0.0033(m_h=900 \text{ GeV}) \\ -0.0000(m_h=100 \text{ GeV}) \end{array}$$

which can be compared to that obtained from  $\sigma_\ell^0$  alone

$$\alpha_s(m_Z) = 0.1183 \pm 0.0030 \begin{array}{l} +0.0026(m_h=900 \text{ GeV}) \\ -0.0000(m_h=100 \text{ GeV}) \end{array}$$

The discrepancy between these two values is another manifestation of the small value of  $N_\nu$  determined from these data. The result of the grand electroweak fit that uses other electroweak data to constrain the unknown Higgs mass and includes information from  $\Gamma_Z$  is

$$\alpha_s(m_Z) = 0.1183 \pm 0.0027.$$

The error does not include any theoretical error from the QCD calculation of  $\Gamma_{\text{had}}$ .

The line-shape value of  $\alpha_s(m_Z)$  is comparable to the recent world averages, such as the PDG average[20],  $\alpha_s(m_Z) = 0.1181 \pm 0.002$  and an average of measurements based on NNLO calculations[21]  $\alpha_s(m_Z) = 0.1178 \pm 0.0034$ . There is some controversy concerning the theoretical error for the line-shape  $\alpha_s(m_Z)$ . Values in the literature differ by nearly an order of magnitude ranging from 0.0005 [22] to 0.003 [21]. Given the statistical precision of the line-shape  $\alpha_s(m_Z)$  measurement it is worth examining the errors in some detail.

The most complete analysis of the error on  $\alpha_s(m_Z)$  is given in Reference [23] which gives a detailed examination of the QCD calculations presently implemented in the commonly used programs TOPAZ0[24] and ZFITTER[25]. The treatment here closely follows that of Reference [23], however, calculations which were not available at the time that this work was completed are also considered here. The effects of QCD on  $\Gamma_{\text{had}}$  can be divided into 4 different categories: the dominant non-singlet terms which have the same effect on axial and vector neutral currents; corrections due to quark masses, dominated by uncertainties in the b-quark mass; singlet contributions and finally propagator corrections associated with the top mass  $m_t$ .

### 3.1 Uncertainties in massless non-singlet terms

The non-singlet axial and vector QCD corrections for massless quarks in  $R_V^f$  and  $R_A^f$  are equal (see Equation 1). This correction is known to third order and is given[22] by:

$$1 + \frac{\alpha_s}{\pi} + 1.40932\left(\frac{\alpha_s}{\pi}\right)^2 - 12.76706\left(\frac{\alpha_s}{\pi}\right)^3. \quad (3)$$

One way to assess the errors due to missing higher order terms is by changing the QCD renormalization scale, which is explained in some detail in Reference [21]. In Reference [22] the renormalization scale  $\mu$  is varied in the interval  $e^{-2}(0.14) < \mu/m_Z < e^2(7.4)$ . The total fractional variation of  $\Gamma_{\text{had}}$  for this range of renormalization scales corresponds to a variation in  $\alpha_s$  of 2.6%, giving errors of approximately  $\pm 1.3\%$ . A similar study has been done in Reference [23] and a total variation in  $\alpha_s$  of 1.0% is obtained when  $\mu$  is varied in the smaller interval  $0.5 < \mu/m_Z < 2.0$ .

An alternative method, employed in Reference [23], is simply to estimate the possible error due to missing higher orders as equal to the last evaluated term. When this is applied to Equation 3, the cubic term corresponds to an estimated error on  $\alpha_s$  of  $\pm 1.8\%$ .

These uncertainties can be reduced by summing a large class of “ $\pi^2$ -terms”, as is done in Reference [22]. For the measurement of  $\alpha_s$  from the Z line shape, considering scale variations ( $e^{-2}(0.14) < \mu/m_Z < e^2(7.4)$ ) and scheme dependence, Reference [22] suggests an error  $\pm 0.4\%$  from QCD theory and that the value of  $\alpha_s$  be scaled by

$$\alpha_s^{\text{improved}} = 1.006\alpha_s^{\text{ZFITTER}}. \quad (4)$$

In Reference [26] a similar technique is applied to  $e^+e^- \rightarrow \text{hadrons}$  at  $\sqrt{s} = 31.6\text{GeV}$ . In this case the improved value of  $\alpha_s$  was 0.8% greater than the standard one, in agreement with Equation 4. Reference [26] does criticize Reference [22] for not having varied the scheme dependence sufficiently, but this would appear to be a technical objection as opposed to a practical one, as the variation in the scheme dependence made only a small contribution to the error.

The main controversy surrounding the  $\alpha_s$  error centers on the validity of the summation of the higher order terms such as done in Reference [22]. This summation

has also been applied to the determination of  $\alpha_s$  using information from hadronic decays of the tau lepton,  $R_\tau$ . Given the much larger value of  $\alpha_s$  at this scale, it might be expected that any problems in the summation procedure would be amplified. Using a method called Contour Improved Fixed Order Perturbation Theory (CIPT) [27], which is similar to the  $\pi^2$  summation of Reference [22], OPAL[33] obtains  $\alpha_s(m_\tau^2) = 0.348 \pm 0.010(\text{exp}) \pm 0.019(\text{theory})$ . However, it has also been found that when “renormalon” effects referred to as “renormalon chain resummation” (RCPT) [29] are included,  $\alpha_s(m_\tau^2) 0.306 \pm 0.005(\text{exp}) \pm 0.011(\text{theory})$  is obtained.

Since these two methods of determining  $\alpha_s$  with  $R_\tau$  marginally disagree by more than the theoretical error estimates, it is important that an error due to renormalon effects be included in any analysis of  $\alpha_s$  from the Z line shape. Fortunately, the effects of renormalons were also included in the calculations of Reference [22] for  $\Gamma_{\text{had}}$  and were found to have almost no effect.

Since these renormalon effects are small at the Z resonance, I conclude that the studies of  $R_\tau$  give no evidence for additional QCD uncertainties in the non-singlet term and the 0.4% error estimate is appropriate. Of course, it cannot be excluded that there are other unknown effects, but this is true for all of the theoretical errors in the Z resonance studies as well.

### 3.2 Mass correction

The only significant contribution from the uncertainty in the mass corrections is from the b-quark mass. The uncertainties associated with these corrections can be significantly reduced if the running b-quark mass,  $\overline{m}_b(m_Z) \simeq 2.77$  GeV is used.

These corrections are known to  $\mathcal{O}(\alpha_s^3)$  for  $R_V$  (vector current), but only to  $\mathcal{O}(\alpha_s^2)$  for  $R_A$  (axial-vector current). In Reference [23] uncertainties from missing orders are evaluated using scale variations ( $0.5 < \mu/m_Z < 2.0$ ) and from the size of the  $\mathcal{O}(\alpha_s^2)$  terms. The scale variation gave a total variation in  $\alpha_s$  of 0.04%. The size of the axial-vector  $\mathcal{O}(\alpha_s^2)$  term dominates the uncertainty, and corresponds to 0.05%. I adopt  $\pm 0.05\%$  as the error estimate from unknown higher orders in the mass corrections.

Propagating the error of the pole mass of the b-quark,  $M_b = 4.7 \pm 0.2$  GeV, an error on  $\alpha_s(m_Z)$  of  $\pm 0.31\%$  is obtained.

### 3.3 Singlet contributions

The error on the singlet contribution is due to uncertainties from the top quark mass and from possible missing higher orders. The error due to the top-quark mass is evaluated using ZFITTER or TOPAZ0 and is not included in the QCD error estimate. The QCD singlet contribution (including top mass dependent contributions with  $m_t = 174$  GeV) scales  $\Gamma_{\text{had}}$  by

$$1 - 0.63(\alpha_s/\pi)^2 - 2.69(\alpha_s/\pi)^3. \quad (5)$$

Varying the renormalization scale in the range ( $0.5 < \mu/m_Z < 2.0$ ) in this expression gives a total variation of  $\alpha_s$  of 0.26%, whereas dropping the third term changes  $\alpha_s$  by 0.38%. The larger value is taken as the error.

### 3.4 Propagator corrections

The behavior of the widths themselves, such as  $\Gamma_Z$  or  $\Gamma_{\text{had}}$ , will differ from observables that depend on the ratio of widths,  $R_\ell$ ,  $\sigma_{\text{had}}^0$  and  $\sigma_\ell^0$ . Since the  $\alpha_s$  correction to the propagator affects all partial widths equally, its effects will cancel in these observables. This correction is parameterized[30] by

$$\delta\rho_{m_t} = \frac{3\sqrt{2}G_F m_t^2}{16\pi^2} \left(1 - 2.8599\frac{\alpha_s}{\pi} - 14.594\left(\frac{\alpha_s}{\pi}\right)^2\right) \quad (6)$$

where  $m_t$  is the top pole mass and  $\alpha_s = \alpha_s(m_t) \simeq 0.11$ . For  $m_t = 175$  GeV the partial widths of leptonic and neutrino final states scale with  $\alpha_s$  as

$$1 + \delta\rho_{m_t}^{\text{QCD}} = 1 - 0.027\frac{\alpha_s}{\pi} - 0.140\left(\frac{\alpha_s}{\pi}\right)^2. \quad (7)$$

Although this propagator correction is only a few percent of the QCD hadronic final-state correction, its theoretical uncertainty can be disproportionately large. Measurements of  $\alpha_s$  through quantities in which the propagator effects cancel, such as  $R_\ell$ ,  $\sigma_{\text{had}}^0$  and  $\sigma_\ell^0$  are therefore favored. Such observables also benefit from the cancelation of other effects in the propagator, such as  $m_b$  and  $m_t$  dependence, which are in fact much larger than the QCD effects.

The scheme and renormalization dependence of the QCD propagator correction has been evaluated in Reference [30] and is less than  $5 \times 10^{-5}$ . Taking into account the Z branching ratio to hadrons ( $\sim 70\%$ ), the corresponding additional error on  $\alpha_s$  determined from  $\Gamma_Z$  is 0.21%.

This renormalization scale uncertainty could also be viewed as an error on  $m_t$ . For  $m_t = 175$  GeV, this corresponds to an uncertainty of 0.4 GeV, which is much smaller than the corresponding experimental uncertainty of 5 GeV.

In the extreme alternative approach of taking the last calculated term as the error estimate, a fractional error on  $\Gamma_Z$  of  $17 \times 10^{-5}$  is obtained, corresponding to an additional error on  $\alpha_s$  determined from  $\Gamma_Z$  of 0.7%.

Effects from the uncertainties of the QCD corrections (also known to second order) on the ratio of couplings for different fermions,  $g_{Vf}/g_{Af}$ , or equivalently  $\sin^2\theta_W^{\text{eff}}$ , have been justifiably neglected[31] in these error estimates. These corrections give rise to slight differences in the  $\alpha_s$  dependence of the Standard Model predictions for  $\Gamma_\nu$  and  $\Gamma_\ell$ .

Table 3: Summary of the QCD error on  $\alpha_s$  derived from various line shape observables based on the ratio of partial widths,  $R_\ell$ ,  $\sigma_{\text{had}}^0$  and  $\sigma_\ell^0$  and from the total width of the Z,  $\Gamma_Z$ .

effect	$\alpha_s$ from ratio of widths	$\alpha_s$ from $\Gamma_Z$
missing orders, massless, non-singlet	0.40%	0.40%
missing orders, singlet	0.38%	0.38%
missing orders, mass	0.05%	0.05%
b-quark mass	0.31%	0.31%
propagator effects	-	0.21%
Total	0.84%	0.87%

### 3.5 $\alpha_s$ summary

The effects discussed above are summarized in Table 3. I conservatively assume that the singlet and non-singlet contributions could be 100% correlated and sum their errors linearly. Another approach to possible correlation between theoretical uncertainties in different parts of the QCD calculation is taken by Reference [21]. This approach is based on an attempt to extract the overall dependence of  $R_\ell$  on  $\alpha_s$ , including all contributions to the running quark masses and any residual propagator effects from a third order fit in  $\alpha_s$  to the ZFITTER output as a function of  $\alpha_s$  [32]. Note that because of the running quark masses and the propagator corrections the expansion contains terms beyond the third-order. The effects of these terms are included by the fit in the effective coefficients of the lower-order terms. The renormalization group equations are then applied to the resulting expansion. An error from renormalization scale uncertainties of +2.4%, -0.3% is obtained which is compatible to the result one obtains from adding the errors of the singlet and non-singlet contributions *without* the correction of Equation 4. Note that neither ZFITTER nor TOPAZ0 presently include this correction.

The other effects in Table 3 are added in quadrature. The contribution of the QCD uncertainty in the measurement of  $\alpha_s$  from  $R_\ell$ ,  $\sigma_{\text{had}}^0$  and  $\sigma_\ell^0$  is slightly smaller than that from  $\Gamma_Z$  (or the derived quantity  $\Gamma_{\text{had}}$ ) because the propagator corrections are smaller. Since the constraints on  $m_t$  and  $m_h$  are presently much looser than the uncertainty on the QCD effect in the propagator, this additional source of error could be ignored in the grand electroweak fit. However, at present this is numerically unimportant. Rounding the QCD theoretical uncertainty to 0.9% and applying the correction of Equation 4 gives an improved value of the strong coupling constant

$$\alpha_s(m_Z) = 0.1190 \pm 0.0027(\text{Exp.} + \text{EW}) \pm 0.0011(\text{QCD})$$

where the first error includes statistical, systematic and electroweak errors and the second error is due to QCD effects. This result is nearly as precise as the 2000 PDG[20] world average of  $\alpha_s(m_Z) = 0.1181 \pm 0.002$ .

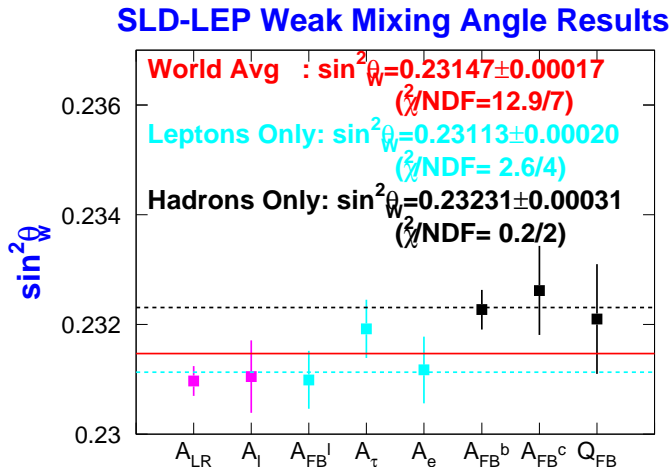


Figure 3: Comparison of  $\sin^2\theta_{\text{eff}}^{\text{lept}}$  measured at SLD and LEP[36].

#### 4 Measurements of $\sin^2\theta_{\text{eff}}^{\text{lept}}$ and $A_b$

The effective value of the weak mixing angle is given by ratio of effective vector and axial couplings

$$\sin^2\theta_{\text{eff}}^{\text{lept}} \equiv \frac{1}{4} \left(1 - \frac{g_{V\ell}}{g_{A\ell}}\right) \quad (8)$$

and is closely related to  $A_\ell$  as given by Equation 2. The most accurate value of  $\sin^2\theta_{\text{eff}}^{\text{lept}}$  comes from the left-right asymmetry  $A_{\text{LR}} = A_\ell$  as measured by SLD[10]. Additional constraints come from polarized forward-backward asymmetries of leptons measured at SLD and from forward-backward asymmetries measured at LEP (see Table 2). LEP can also probe  $A_e$  and  $A_\tau$  directly using the tau polarization. The values presented here include an improved preliminary measurement from OPAL [34] and a recent final result from DELPHI [35]. The resulting values of  $\sin^2\theta_{\text{eff}}^{\text{lept}}$  are given in Figure 3.

The forward-backward asymmetries of  $b\bar{b}$  and  $c\bar{c}$  events can also be used to determine  $\sin^2\theta_{\text{eff}}^{\text{lept}}$  through the relations  $A_{\text{FB}}^{0,c} \equiv \frac{3}{4}A_eA_c$  and  $A_{\text{FB}}^{0,b} \equiv \frac{3}{4}A_eA_b$  as long as the Standard Model is used to calculate  $A_c$  and  $A_b$ . The figure shows that there is a significant discrepancy between the quark based forward-backward measurements

Table 4: Comparison of measured and Standard Model values of  $A_c$  and  $A_b$ . The LEP values are extracted using the LEP/SLD average of  $A_\ell = 0.1500 \pm 0.0016$

	$A_b$	$A_c$
SLD	$0.922 \pm 0.023$ (-0.6 $\sigma$ )	$0.631 \pm 0.026$ (-1.4 $\sigma$ )
LEP/SLD Average	$0.898 \pm 0.015$ (-2.5 $\sigma$ )	$0.623 \pm 0.020$ (-2.2 $\sigma$ )
Standard Model	0.935	0.668

and those made in the leptonic sector alone.

Since the leptonic measurements agree well, a possible explanation for this effect would be that the values of either or both  $A_c$  and  $A_b$  deviate from the Standard Model prediction. Using the polarized forward-backward asymmetry for  $b\bar{b}$  and  $c\bar{c}$  events  $A_c$  and  $A_b$  can be obtained directly [37]. The comparison of the SLD result and Standard Model is given in Table 4. The precision of the preliminary SLD result has been considerably improved since the 1998 RADCOR [37], (see Table 1 and Reference [5]) but the SLD data are not statistically precise enough to indict the Standard Model by themselves. It is unfortunate that SLD was prevented from running long enough to settle this issue.

Given that the SLD data cannot confirm a deviation in the values of  $A_c$  and  $A_b$ , the remaining possibilities are a large statistical fluctuation or an unstated systematic error in some of the measurements. The most economical solution would be a systematic error affecting the LEP heavy quark measurements. However, there is no obvious source of such an error. On the experimental side, the total systematic error for  $A_{\text{FB}}^{0,b}$  would have to be inflated by more than a factor of 5 to account for the discrepancy. The theoretical systematics are dominated by the correction to the observed asymmetry for gluon radiation. For a completely inclusive selection, the total QCD correction applied to the data is approximately 4%, of order the discrepancy between the LEP  $A_{\text{FB}}^{0,b}$  average and the expected value from the Standard Model. However, most experimental analyses tend to reject events strongly affected by gluon radiation so the actual corrections are much smaller [38]. Furthermore, the experimental techniques used in jet-charged measurements uses data driven correction which attenuate the QCD effects still further. The residual QCD error on the LEP  $A_{\text{FB}}^{0,b}$  measurements, largely from missing higher orders in the QCD calculation and from hadronization, is estimated to be 0.2%.

The LEP heavy quark results are not all published or final and it is expected that some of the techniques developed for b-mixing studies will result in an increase in the precision of some of the LEP results [39,40].

Table 5: Limits and values for Higgs mass determined from fits with the “usual” experiment driven value[41] of  $\Delta\alpha_{\text{had}}^5(m_Z^2)$  traditionally used by the LEP electroweak group and the value of  $\Delta\alpha_{\text{had}}^5(m_Z^2)$  presented at ICHEP2000 including BES data [50].

$\Delta\alpha_{\text{had}}^5$	$0.02804 \pm 0.00065$	$0.02755 \pm 0.00046$
$m_h$	$60_{-29}^{+52}$ GeV	$90_{-39}^{+63}$ GeV
$m_h$ 95% C.L. upper limit	$m_{\text{Higgs}} < 170\text{GeV}$	$m_{\text{Higgs}} < 210\text{GeV}$

## 5 Impact of uncertainties in hadronic vacuum polarization

The constraint given by the LEP and SLD asymmetry data on the Higgs mass is strongly dependent on the running value of  $\alpha$  parameterized by

$$\alpha(m_Z^2) = \frac{\alpha(0)}{1 - \Delta\alpha_\ell(m_Z^2) - \Delta\alpha_{\text{had}}^5(m_Z^2) - \Delta\alpha_{\text{top}}(m_Z^2)}$$

where  $\Delta\alpha_\ell(m_Z^2)$  is the contribution to vacuum polarization from leptons,  $\Delta\alpha_{\text{top}}(m_Z^2)$  the contribution from top quarks and  $\Delta\alpha_{\text{had}}^5(m_Z^2)$  the contribution from the five lightest quarks. The value of  $\Delta\alpha_{\text{had}}^5(m_Z^2)$  is derived from the measured cross section for the process  $e^+e^- \rightarrow \text{hadrons}$  at low energies and currently limits the precision with which  $\alpha(m_Z^2)$  can be determined.

The correlation between  $\Delta\alpha_{\text{had}}^5(m_Z^2)$  and the determination of the Higgs mass from the electroweak data is shown in Figure 4. The value of the Higgs mass determined from the fit is strongly correlated with the  $\Delta\alpha_{\text{had}}^5(m_Z^2)$  input. In Figure 5 various determinations [41,42,43,44,45,46,47,48,49,50] of the  $\Delta\alpha_{\text{had}}^5(m_Z^2)$  are shown. The LEP Electroweak group has generally used the value from Eidelmann and Jegerlehner [41] which is primarily data driven. It is interesting that the new determination from Pietrzyk [50], based on new data from BES [51] presented at ICHEP 2000 agrees well with the result of theory driven results [43,44,45,46,47,48,49] which makes use of perturbative QCD. In any case the result of using the Pietrzyk result is to move the Higgs mass prediction of the grand electroweak fit towards higher values (see Table 5). We can expect that the error on  $\Delta\alpha_{\text{had}}^5(m_Z^2)$  will continue to decline in the future as more data is collected by BES and other low energy electron-positron storage rings.

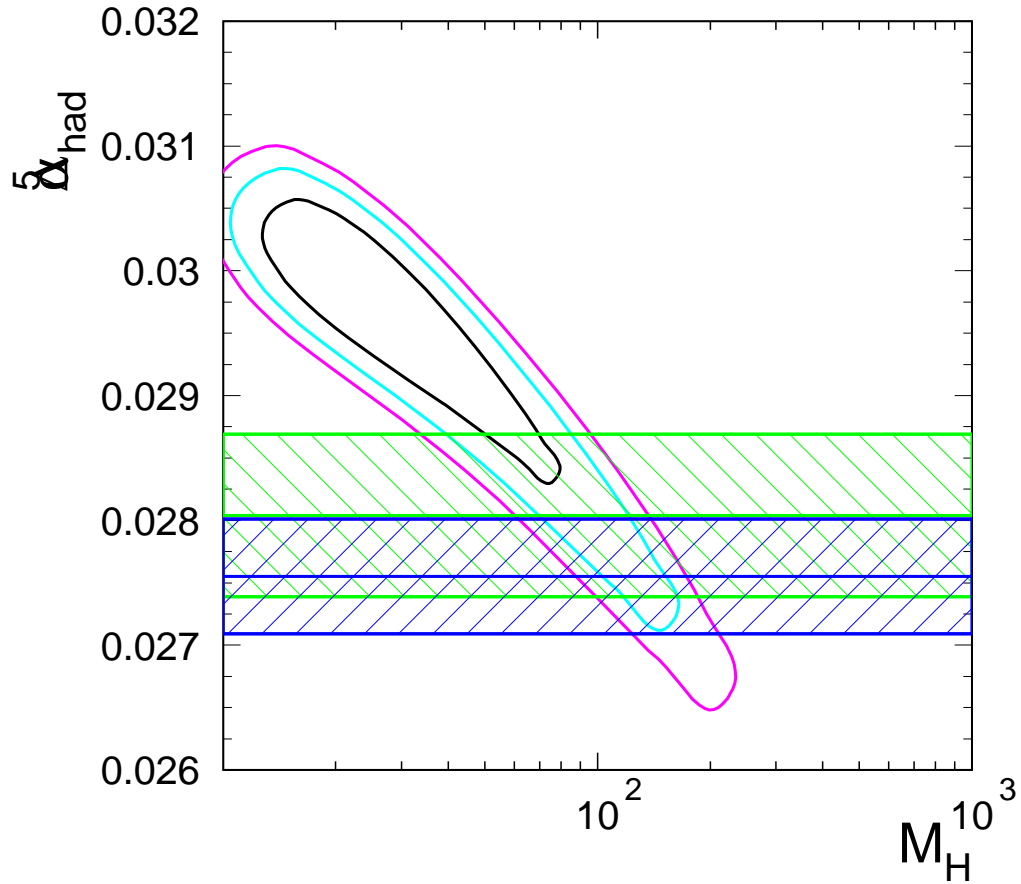


Figure 4: The contours show the  $1\sigma$  (47% C.L.),  $2\sigma$  (91% C.L.) and  $3\sigma$  (99.5% C.L.) limits in the  $\Delta\alpha_{\text{had}}^5(m_Z^2)-m_h$  plane, for a data similar, but not identical to that of Table 1[36]. The upper bands show the value from  $\Delta\alpha_{\text{had}}^5(m_Z^2)-m_h$  from Reference [41] and the lower band shows preliminary results using the new preliminary BES data from Reference [50]

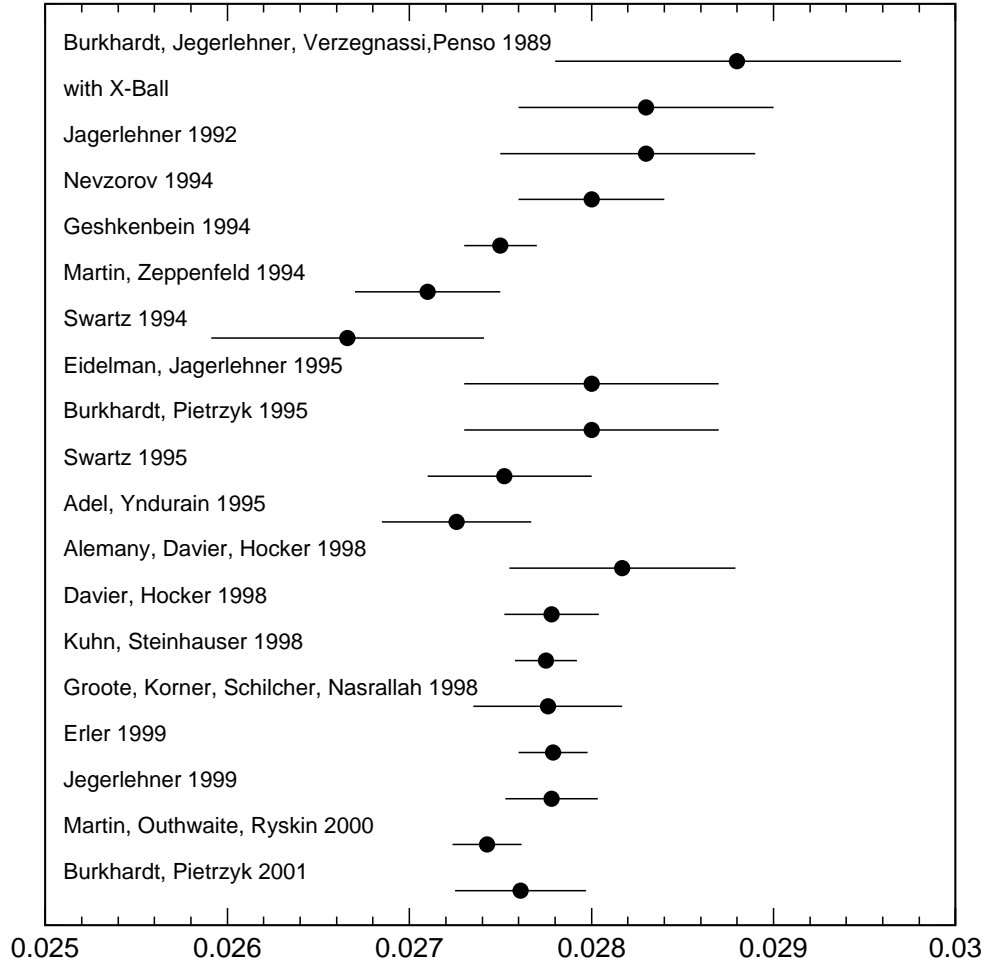


Figure 5: Compilation of values of  $\Delta\alpha_{\text{had}}^5(m_Z^2)$  as a function of time. (See References [41,42,43,44,45,46,47,48,49], for older values see citation in Reference [42]). The last two results incorporate the new BES data[51].

## 6 Conclusions

The LEP results for the Z line shape and lepton asymmetries have been stable for some time and are now final and published[9]. The theoretical error assigned to  $\alpha_s$  determined from these data remains controversial. If the correction of Reference [22] is applied,

$$\alpha_s(m_Z) = 0.1190 \pm 0.0027(\text{Exp.} + \text{EW}) \pm 0.0011(\text{QCD})$$

is obtained. This is competitive with the 2000 PDG[20] world average of  $\alpha_s(m_Z) = 0.1181 \pm 0.002$ .

The SLD measurement of  $\sin^2\theta_{\text{eff}}^{\text{lept}}$ , based primarily on the left-right polarized asymmetry, is also now final and published[10]. Its value agrees with that obtained from lepton asymmetries and  $\tau$  polarization at LEP. However, the average from these lepton based results is in disagreement with the LEP heavy-quark measurements of  $\sin^2\theta_{\text{eff}}^{\text{lept}}$ . It is possible that the discrepancy could be explained by anomalous values of  $A_b$  or  $A_c$ , but the direct measurements of these quantities by SLD are in agreement with both the Standard Model and the LEP values, assuming a Standard Model value for  $A_e$ .

The interpretation of these electroweak results in terms of limits on the Higgs boson mass depends on the value of  $\Delta\alpha_{\text{Had}}^5(m_Z^2)$ . New  $e^+e^-$  cross section measurements from BES gives a data driven value  $\Delta\alpha_{\text{had}}^5(m_Z^2)$  which agrees with previous theory driven determinations, resulting in a higher prediction for the Higgs boson mass.

## Acknowledgments

I would like to thank the ALEPH, DELPHI, L3, OPAL and SLD collaborations and the LEP and SLD Electroweak Working Groups for their assistance in preparing this report. I am especially grateful to Martin Grünewald and Günter Quast for providing the electroweak fits used in this report. I would also like to thank Dave Soper and Sigi Bethke for useful discussions about the application of QCD to the LEP line-shape results. Finally I wish to thank Dick Kellogg for his suggestions and encouragement.

## References

- [1] ALEPH, DELPHI, L3, OPAL and SLD Collaborations, the LEP Electroweak Working Group and the SLD Electroweak and Heavy Flavor Groups, “Precision Electroweak Measurements on the Z Resonance”, in preparation.
- [2] G. Montagna, O. Nicosini and F. Piccinini, Riv. Nuovo Cim. **21N9** (1998) 1.

- [3] D. Bardin, M. Grunewald and G. Passarino, “Precision calculation project report,” hep-ph/9902452.
- [4] D. Bardin and G. Passarino, “The Standard Model in the making: Precision study of the electroweak interactions,” *Oxford, UK: Clarendon (1999) 685 p.*
- [5] ALEPH, DELPHI, L3, OPAL and SLD Collaborations, the LEP Electroweak Working Group and the SLD Electroweak and Heavy Flavor Groups, “A combination of preliminary electroweak measurements and constraints on the standard model,” hep-ex/0103048.
- [6] ALEPH, DELPHI, L3, OPAL and SLD Collaborations, the LEP Electroweak Working Group and the SLD Electroweak and Heavy Flavor Groups, “A combination of preliminary electroweak measurements and constraints on the standard model,” CERN-EP-99-015.
- [7] K. McFarland, “Electroweak Physics at the Tevatron”, RADCOR 2000.
- [8] S. Wynnhoff, “Standard model physics results from LEP2,” hep-ex/0101016.
- [9] LEP Collaborations, “Combination procedure for the precise determination of Z boson parameters from results of the LEP experiments,” hep-ex/0101027.
- [10] K. Abe *et al.*, SLD Collaboration, Phys. Rev. Lett. **84** (2000) 5945.
- [11] R. Barate *et al.*, ALEPH Collaboration, Eur. Phys. J. C **14** (2000) 1.
- [12] P. Abreu *et al.*, DELPHI Collaboration, Eur. Phys. J. C **16** (2000) 371.
- [13] M. Acciarri *et al.*, L3 Collaboration, Eur. Phys. J. C **16** (2000) 1.
- [14] G. Abbiendi *et al.*, OPAL Collaboration, Eur. Phys. J. C **19** (2001) 587.
- [15] B. F. Ward, S. Jadach, M. Melles and S. A. Yost, Phys. Lett. B **450** (1999) 262.
- [16] G. Montagna, M. Moretti, O. Nicosini, A. Pallavicini and F. Piccinini, Nucl. Phys. B **547** (1999) 39.  
G. Montagna, M. Moretti, O. Nicosini, A. Pallavicini and F. Piccinini, Phys. Lett. B **459** (1999) 649.
- [17] G. Montagna, O. Nicosini and F. Piccinini, Phys. Lett. B **406** (1997) 243.
- [18] A. B. Arbuzov, “Light pair corrections to electron positron annihilation at LEP/SLC,” hep-ph/9907500.
- [19] L. Arnaudon *et al.*, Z. Phys. C **66** (1995) 45.

- [20] L. Montanet *et al.*, Phys. Rev. D **50** (1994) 1173.
- [21] S. Bethke, J. Phys. G **G26** (2000) R27.
- [22] D. E. Soper and L. R. Surguladze, Phys. Rev. D **54** (1996) 4566.
- [23] K. G. Chetyrkin, J. H. Kuhn and A. Kwiatkowski, Phys. Rept. **277** (1996) 189.
- [24] G. Montagna, O. Nicosini, F. Piccinini and G. Passarino, Comput. Phys. Commun. **117** (1999) 278.
- [25] D. Bardin, P. Christova, M. Jack, L. Kalinovskaya, A. Olchevski, S. Riemann and T. Riemann, Comput. Phys. Commun. **133** (2001) 229.
- [26] P. A. Raczka and A. Szymacha, Phys. Rev. D **54** (1996) 3073.
- [27] F. Le Diberder and A. Pich, Phys. Lett. B **289** (1992) 165.
- [28] K. Ackerstaff *et al.*, OPAL Collaboration, Eur. Phys. J. C **7** (1999) 571.
- [29] P. Ball, M. Beneke and V. M. Braun, Nucl. Phys. B **452** (1995) 563.
- [30] K.G. Chetyrkin, J.H. Kühn, and M. Steinhauser, Phys. Lett. **B351** (1995) 331.
- [31] K. G. Chetyrkin, J. H. Kühn and M. Steinhauser, Phys. Rev. Lett. **75** (1995) 3394.
- [32] E. Tournefier, “Extraction of  $\alpha_s$  and constraint on the Higgs mass from electroweak fits at the Z resonance,” hep-ex/9810042.
- [33] K. Ackerstaff, *et al.*, OPAL Collaboration, Eur. Phys. J. C **7** (1999) 571.
- [34] OPAL Collaboration, “Precision Tau and Electron Neutral Current Asymmetry Measurements from the Tau Polarization at OPAL”, OPAL Physics Note PN438.
- [35] P. Abreu *et al.*, DELPHI Collaboration, Eur. Phys. J. C **14** (2000) 585.
- [36] Private communication, T. Abe.
- [37] K. Abe *et al.*, SLD Collaboration, hep-ex/0009064.  
K. Abe *et al.*, SLD Collaboration, SLAC-PUB-8542 *Talk given at the 30th International Conference on High-Energy Physics (ICHEP 2000), Osaka, Japan, 27 Jul - 2 Aug 2000.*  
K. Abe *et al.*, SLD Collaboration, Phys. Rev. D **63** (2001) 032005.
- [38] D. Abbaneo *et al.*, LEP Heavy Flavor Working Group Collaboration, Eur. Phys. J. C **4** (1998) 185.

- [39] DELPHI Collaboration, “Measurement of the Forward-Backward Asymmetries of  $e^+e^- \rightarrow Zb\bar{b}$  and  $c\bar{c}$  using prompt leptons”, DELPHI 2000-101 CONF 400.
- [40] ALEPH collaboration, “Inclusive semileptonic branching ratios of b hadrons produced in Z decays”, ALEPH 2000-069, CONFG 2000-047, Contributed paper to ICHEP2000 #133.
- [41] S. Eidelman and F. Jegerlehner, Z. Phys. C **67** (1995) 585.
- [42] H. Burkhardt and B. Pietrzyk, Phys. Lett. B **356** (1995) 398.
- [43] R. Alemany, M. Davier and A. Hocker, Eur. Phys. J. C **2**, 123 (1998).
- [44] M. Davier and A. Hocker, Phys. Lett. B **419** (1998) 419.
- [45] J. H. Kuhn and M. Steinhauser, Phys. Lett. B **437** (1998) 425.
- [46] S. Groote, J. G. Korner, K. Schilcher and N. F. Nasrallah, Phys. Lett. B **440** (1998) 375.
- [47] J. Erler, Phys. Rev. D **59** (1999) 054008.
- [48] F. Jegerlehner, “Hadronic effects in  $(g - 2)(\mu)$  and  $\alpha_{\text{QED}}(m_Z)$ : Status and perspectives,” hep-ph/9901386.
- [49] A. D. Martin, J. Outhwaite and M. G. Ryskin, Phys. Lett. B **492** (2000) 69.
- [50] B. Pietrzyk, “The global fit to electroweak data”, talk presented at ICHEP 2000, Osaka, July 27- August 2, 2000. LAP-EXP-2000-06. H. Burkhardt and B. Pietrzyk, LAPP-EXP-2001-03.
- [51] Z.G. Zhao, BES Collaboration, “New R values in 2-5 GeV from BES” talk presented at ICHEP2000, OSKA, July 27- August 2, 2000.

## Precision Top-Quark Physics

SCOTT WILLENBROCK

*Department of Physics  
University of Illinois at Urbana-Champaign  
1110 W. Green St., Urbana, IL 61801*

I consider the measurement of the top-quark mass, the CKM matrix element  $V_{tb}$ , and the top-quark Yukawa coupling to the Higgs boson at the Tevatron, the LHC, and a Linear Collider. The theoretical motivations for these measurements, as well as the experimental possibilities, are discussed.

Presented at the

5th International Symposium on Radiative Corrections  
(RADCOR-2000)

Carmel CA, USA, 11–15 September, 2000

# 1 Introduction

The top quark was discovered in 1995 by the CDF [1] and D0 [2] experiments at Fermilab, during Run I of the Tevatron  $p\bar{p}$  collider ( $\sqrt{S} = 1.8$  TeV,  $\int \mathcal{L} dt \approx 100$  pb $^{-1}$ ). In Table 1 I briefly summarize the top-quark measurements made in Run I and compare them with the expectations from the standard model. The standard model does not predict the top-quark mass, but it can be inferred indirectly from precision electroweak experiments [3], and this indirect mass is in good agreement with the measured mass. The strong interaction of the top quark is probed by measuring the top-quark cross section, which proceeds via the strong processes  $q\bar{q}, gg \rightarrow t\bar{t}$ ; this cross section is in good agreement with next-to-leading-order QCD. The weak interaction of the top quark is probed in a variety of ways. In the three-generation standard model, top decays almost exclusively to bottom, as confirmed by experiment. The branching ratios of top to longitudinal (zero-helicity)  $W$  bosons and to right-handed (positive-helicity)  $W$  bosons are predicted to be approximately 0.7 and zero, respectively, in agreement with experiment. The weak interaction of the top quark is also probed indirectly by precision electroweak experiments and  $b$ -quark physics, as illustrated in Figs. 1 and 2. All of these experiments are consistent with the three-generation standard model. Thus, although the properties of the top quark have thus far been measured only crudely, there is no evidence for physics beyond the standard model in top-quark physics.

Table 1: Comparison of theory and experiment for top-quark physics from Run I of the Fermilab Tevatron. [ $W_{0,+}$  denote a longitudinal (zero-helicity) and right-handed (positive-helicity)  $W$  boson.] For discussion and references, see Refs. [4,5].

	Experiment	Theory
$m_t$	$174.3 \pm 5.1$ GeV	$168.2_{-7.4}^{+9.6}$ GeV
$\sigma(t\bar{t})$	$6.2 \pm 1.7$ pb	$4.75 \pm 0.5$ pb
$BR(t \rightarrow Wb)/BR(t \rightarrow Wq)$	$0.94_{-0.24}^{+0.31}$	$\approx 1$
$BR(t \rightarrow W_0b)$	$0.91 \pm 0.39$	$\approx 0.7$
$BR(t \rightarrow W_+b)$	$0.11 \pm 0.15$	$\approx 0$

Let us assume that the top quark is indeed a standard quark. What parameters of the top quark do we want to measure? There are only a few standard-model parameters associated with the top quark; its mass ( $m_t$ ), its Cabibbo-Kobayashi-Maskawa matrix elements ( $V_{tb}, V_{ts}, V_{td}$ ), and its Yukawa coupling to the Higgs field ( $y_t$ ). This last parameter is not truly independent, as it is related to the top-quark mass (at leading order) via  $y_t = \sqrt{2}m_t/v$ , where  $v \approx 246$  GeV is the vacuum-expectation value of the Higgs field. However, this parameter is especially interesting, as it is related

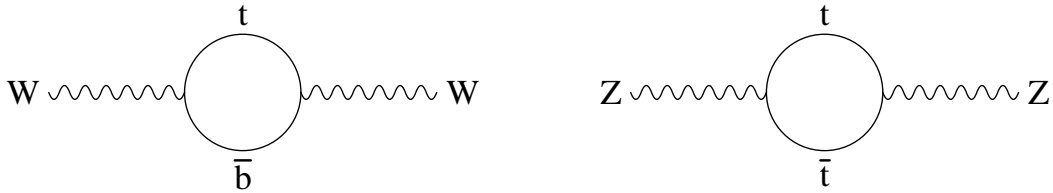


Figure 1: The weak interaction of the top quark is probed indirectly by the vector-boson self energies.

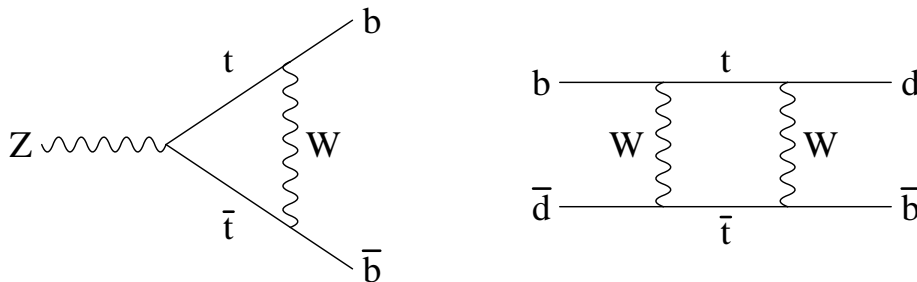


Figure 2: The weak interaction of the top quark is also probed indirectly by  $b$  physics.

to the electroweak-symmetry-breaking sector, which has yet to be directly probed experimentally. A measurement of the top-quark Yukawa coupling therefore probes the mechanism that generates the top-quark mass.

In this talk I discuss the measurement of the parameters  $m_t$ ,  $V_{tb}$ , and  $y_t$ . I first ask how accurately we desire these parameters. I then ask how accurately we can measure them with present and future colliders. I consider the upgraded Fermilab Tevatron ( $\sqrt{S} = 2$  TeV), with an integrated luminosity of  $2 \text{ fb}^{-1}$  (Run IIa) and  $15 \text{ fb}^{-1}$  (Run IIb), the CERN Large Hadron Collider (LHC,  $\sqrt{S} = 14$  TeV  $pp$  collider), and the Linear Collider, an  $e^+e^-$  collider running at the  $t\bar{t}$  threshold [as well as at the  $W^+W^-$  threshold and at the  $Z$  mass (Giga  $Z$ )].

The standard-model parameters of the top quark are interesting in their own right. Furthermore, any discrepancies between theory and experiment would indicate new physics. Thus top-quark physics could serve to further solidify the standard model, or to indicate physics beyond the standard model.

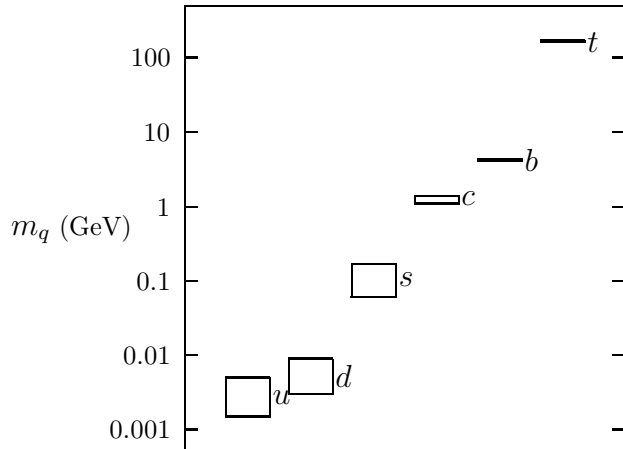


Figure 3: The quark mass spectrum. The bands indicate the running  $\overline{\text{MS}}$  mass, evaluated at the quark mass (for  $c, b, t$ ) or at 2 GeV (for  $u, d, s$ ), and the associated uncertainty.

## 2 Top-quark mass

The top-quark mass has been measured by the CDF and D0 collaborations to be [6]<sup>1</sup>

$$m_t = 174.3 \pm 5.1 \text{ GeV (CDF + D0)} . \quad (1)$$

To put this into context, I plot all the quark masses in Fig. 3, on a logarithmic scale. The width of each band is proportional to the fractional uncertainty in the quark mass. We see that, at present, the top-quark mass is the best-known quark mass, with the  $b$ -quark mass a close second ( $m_b^{\overline{\text{MS}}}(m_b) = 4.25 \pm 0.15 \text{ GeV}$ ) [3].

An important question for the future is what precision we desire for the top-quark mass. There are at least two avenues along which to address this question. One is in the context of precision electroweak data. Fig. 4 summarizes the world's precision electroweak data on a plot of  $M_W$  vs.  $m_t$ . The solid ellipse is the  $1\sigma$  contour. If the standard electroweak model is correct, the predicted top-quark mass from precision electroweak data is  $m_t = 168.2_{-7.4}^{+9.6} \text{ GeV}$  [3]. We conclude that the present uncertainty of 5 GeV in the top-quark mass is sufficient for the purpose of precision electroweak physics at this time.

There is one electroweak measurement,  $M_W$ , whose precision will increase significantly. An uncertainty of 20 MeV is a realistic goal for Run IIb at the Tevatron and the LHC [9,10,11]. Let us take this uncertainty and project it onto a line of

<sup>1</sup>This is the top-quark pole mass, which is defined to order  $\Lambda_{QCD} \approx 200 \text{ MeV}$  [7]. The corresponding  $\overline{\text{MS}}$  mass is  $m_t^{\overline{\text{MS}}}(m_t^{\overline{\text{MS}}}) = 165.2 \pm 5.1 \text{ GeV}$  [8].

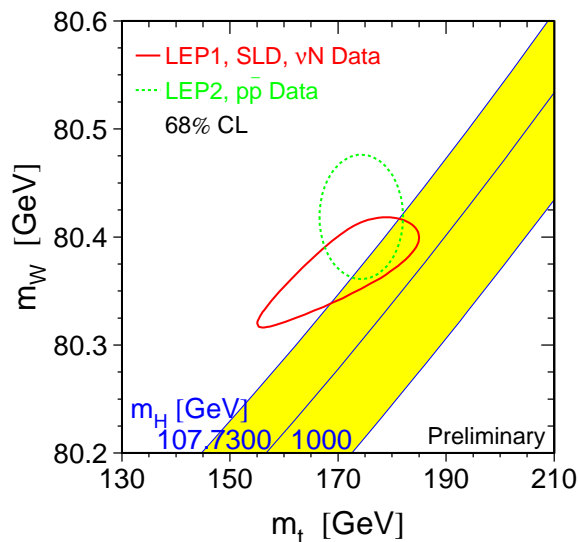


Figure 4:  $W$  mass *vs.* top-quark mass, with lines of constant Higgs mass. The solid ellipse is the  $1\sigma$  (68% CL) contour from precision electroweak experiments. The dashed ellipse is the  $1\sigma$  (68% CL) contour from direct measurements. Only the shaded region is allowed in the standard electroweak model. Figure from LEP Electroweak Working Group, <http://www.cern.ch/LEPEWWG/>.

constant Higgs mass in Fig. 4. This is appropriate, because once a Higgs boson is discovered, even a crude knowledge of its mass will define a narrow line in Fig. 3, since precision electroweak measurements are sensitive only to the logarithm of the Higgs mass. An uncertainty in  $M_W$  of 20 MeV projected onto a line of constant Higgs mass corresponds to an uncertainty of 3 GeV in the top-quark mass. Thus we desire a measurement of  $m_t$  to 3 GeV in order to make maximal use of the precision measurement of  $M_W$  at the Tevatron and the LHC.

Looking further ahead, a high-luminosity Linear Collider running at the  $WW$  threshold could measure the  $W$  mass with an accuracy of 6 MeV [12]. This would require a measurement of  $m_t$  to 1 GeV. The same machine running at the  $Z$  mass (Giga  $Z$ ) could make a measurement of  $\sin^2 \theta_W$  with an accuracy of  $1 \times 10^{-5}$  [12]. This would also require a measurement of  $m_t$  with an uncertainty of order 1 GeV [13].

Another avenue along which to address the desired accuracy of the top-quark mass is to recall that the top-quark mass is a fundamental parameter of the standard model. Actually, the fundamental parameter is the Yukawa coupling of the top quark

to the Higgs field, given at leading order by

$$y_t = \sqrt{2} \frac{m_t}{v} \approx 1 \quad (2)$$

where  $v \approx 246$  GeV is the vacuum-expectation value of the Higgs field. The fact that this coupling is of order unity suggests that it may be a truly fundamental parameter. We hope someday to have a theory that relates the top-quark Yukawa coupling to that of its weak-interaction partner, the  $b$  quark.<sup>2</sup> The  $b$ -quark mass is currently known with an accuracy of 3.5% [3]. Since the uncertainty is entirely theoretical, it is likely that it will be reduced in the future. If we assume that future work reduces the uncertainty to 1%, the corresponding uncertainty in the top-quark mass would be 2 GeV.

We conclude that both precision electroweak experiments and  $m_t$  as a fundamental parameter lead us to the desire to measure the top-quark mass with an accuracy of 1–3 GeV. This is well matched with future expectations. An uncertainty of 3 GeV per experiment is anticipated in Run IIa [18,19], and 2 GeV per experiment in Run IIb [9]. The LHC could potentially reduce the uncertainty to 1 GeV, although that has not been established [10].

Recall that the need to reduce the uncertainty in the top-quark mass to 1 GeV is driven by the precision measurement of  $M_W$  and  $\sin^2 \theta_W$  at the Linear Collider. Such a machine, operating at the  $t\bar{t}$  threshold, could make a much more accurate determination of the top-quark mass. It is interesting to ask if there is any motivation to go beyond 1 GeV in the accuracy of the measurement of  $m_t$ .

No such motivation appears to exist solely within the context of the standard model, but it is plausible that physics beyond the standard model could lead us to desire  $m_t$  with an accuracy much less than 1 GeV. I offer two examples. Imagine that nature is supersymmetric, and the Higgs sector consists of two Higgs doublets, as in the minimal supersymmetric standard model. There is an upper bound on the mass of the lightest Higgs scalar, and this bound is saturated in the limit that the pseudoscalar Higgs mass and the ratio of vacuum-expectation values,  $\tan \beta$ , are large. The mass of the lightest Higgs scalar is predicted to be [20,21,22]

$$m_h^2 = M_Z^2 + \frac{3G_F}{\pi^2 \sqrt{2}} m_t^4 \ln \frac{M_S^2}{m_t^2} \quad (3)$$

where  $M_S^2$  is the average of the two top-squark squared masses and I have assumed no top-squark mixing, for simplicity. The second term is from loops of top quarks and top squarks, as shown in Fig. 5, and since it depends on the top-quark mass

---

<sup>2</sup>A particularly compelling model that relates the  $b$  and  $t$  masses is SO(10) grand unification [14,15]. This model may be able to account for the masses of all the third-generation fermions, including the tau neutrino, whose mass is given by the “see-saw” mechanism [16] as  $m_{\nu_\tau} \approx m_t^2/M_{GUT} \approx 10^{-2}$  eV [17].

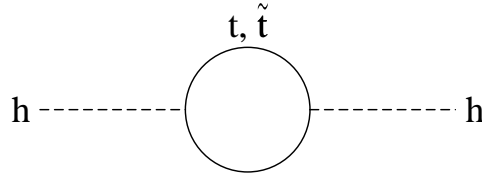


Figure 5: Corrections to the mass of the lightest supersymmetric Higgs boson from loops of top quarks and top squarks.

to the fourth power, an uncertainty in the top-quark mass implies an uncertainty in the predicted Higgs mass. The Higgs mass will be measured with an accuracy of about 0.1% at the LHC [10]; this requires a measurement of  $m_t$  to about 100 MeV (where I have taken  $M_S \approx 1$  TeV). However, there is an uncertainty in the predicted Higgs mass due to the unknown three-loop contributions to Eq. (3), which has been estimated to be about 3 GeV [23,24]. This corresponds to an uncertainty in the top-quark mass of about 2 GeV. Thus the motivation to go beyond 1 GeV accuracy hinges on the knowledge of higher-order terms in Eq. (3).

A second motivation for going beyond 1 GeV in the accuracy of the top-quark mass measurement is a more model-independent one. The generation of mass is related to the breaking of the electroweak symmetry. The electroweak interaction has been measured with an accuracy of about 0.07% (the accuracy in our present knowledge of  $\sin^2 \theta_W$ ). If the mechanism that breaks the weak interaction is related to the weak interaction itself, then a measurement of  $m_t$  to 0.07%, *i.e.*, 100 MeV, may be warranted.

Both of these arguments, although speculative, lead to a goal of about 100 MeV for the accuracy of the top-quark mass measurement. Such an accuracy may be within the reach of a Linear Collider operating at the  $t\bar{t}$  threshold. Recent next-to-next-to-leading-order (NNLO) calculations of the  $t\bar{t}$  threshold in a nonrelativistic expansion yield a line shape with sufficient accuracy to extract the mass within 100 MeV [25]. It is essential to use a short-distance “threshold mass” in such calculations [26,27]. The threshold mass has recently been related to the more commonly-used  $\overline{\text{MS}}$  mass to  $\mathcal{O}(\alpha_s^3)$  [28,29], so the theoretical work required for a NNLO extraction of the top-quark mass from the  $t\bar{t}$  threshold is complete. However, at the time of this symposium, there remained a mystery in the normalization of the line shape. Work performed after this symposium has resolved that mystery via renormalization-group improvement, as shown in Fig. 6, so the normalization is now also known with good accuracy [30].

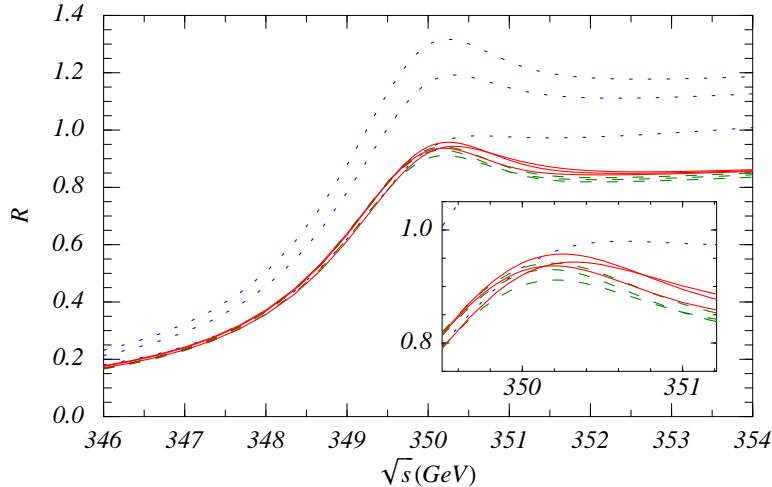


Figure 6: Renormalization-group-improved NNLO calculation of the  $t\bar{t}$  threshold at a Linear Collider. The curves are leading log (dotted), next-to-leading log (dashed), and next-to-next-to-leading log (solid), for three different renormalization scales. From Ref. [30].

### 3 $V_{tb}$

It is remarkable that, although it has not yet been directly measured,  $V_{tb}$  is the best-known Cabibbo-Kobayashi-Maskawa (CKM) matrix element (as a percentage of its value), if we assume three generations:  $V_{tb} = 0.9990 - 0.9993$  [3]. This is due to the small measured values of  $V_{ub}$  and  $V_{cb}$  and the three-generation unitarity constraint  $|V_{ub}|^2 + |V_{cb}|^2 + |V_{tb}|^2 = 1$ . Thus, if there are three generations, we desire a measurement of  $V_{tb}$  with an accuracy of 0.0002. Unfortunately, there is no known way to achieve such an accuracy.

If there are more than three generations,  $V_{tb}$  is almost completely unknown:  $V_{tb} = 0.07 - 0.993$  [3]. In this case, a measurement of  $V_{tb}$  with any accuracy is worthwhile. The existence of a fourth generation is disfavored by precision electroweak data at the 97% C.L., however [3]. If there are only three generations, then a measurement of  $V_{tb}$  may be considered as a probe of physics beyond the standard model [31,32].

CDF has measured [33]

$$\frac{BR(t \rightarrow Wb)}{BR(t \rightarrow Wq)} = \frac{|V_{tb}|^2}{|V_{td}|^2 + |V_{ts}|^2 + |V_{tb}|^2} = 0.94_{-0.24}^{+0.31} \quad (4)$$

and it is interesting to ask what this tells us about  $V_{tb}$ . If we assume that there are just three generations of quarks, then unitarity of the CKM matrix implies that the denominator of Eq. (4) is unity, and we can immediately extract

$$|V_{tb}| = 0.97_{-0.12}^{+0.16} (> 0.75 \text{ 95\% CL}) \text{ (3 generations)}. \quad (5)$$

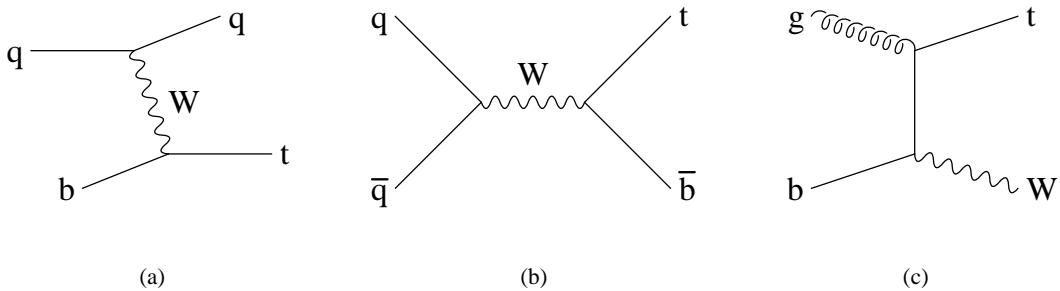


Figure 7: Single-top-quark production via (a)  $t$ -channel  $W$  exchange, (b)  $s$ -channel  $W$  exchange, and (c) associated production with a  $W$ .

However, we already know that  $V_{tb} = 0.9990 - 0.9993$  if we assume three generations, which is far more accurate than the above measurement. If we assume more than three generations, then we lose the constraint that the denominator of Eq. (4) is unity. All we can conclude from Eq. (4) is that  $|V_{tb}| \gg |V_{ts}|, |V_{td}|$ ; we learn nothing about its absolute magnitude.

Fortunately, there is a direct way to measure  $|V_{tb}|$  at the Tevatron and the LHC, which makes no assumptions about the number of generations. One uses the weak interaction to produce the top quark; the three relevant processes are shown in Fig. 7. The cross sections for these “single top” processes are proportional to  $|V_{tb}|^2$ . The first process involves a  $t$ -channel  $W$  boson [34,35,36], the second process involves an  $s$ -channel  $W$  boson [37,38], and the third process is associated production of a single top quark with a real  $W$  boson [39,40]. The cross sections for these processes are given in Table 2, along with the cross section for  $t\bar{t}$  pair production. The largest single-top cross section comes from the  $t$ -channel process, which is about 1/3 of the cross section for  $t\bar{t}$  pair production. The  $s$ -channel process is relatively larger at the Tevatron than the LHC, since it is a quark-antiquark initiated process. It has the advantage of small theoretical uncertainty. The cross section for associated production is only significant at the LHC.

Thus far there are only upper bounds on the cross sections from CDF and D0. The upper bounds on the  $t$ -channel cross sections are [41,42]

$$\sigma(qb \rightarrow qt) < 13.5 \text{ pb (95\% CL) (CDF)} \quad (6)$$

$$\sigma(qb \rightarrow qt) < 58 \text{ pb (95\% CL) (D0)} \quad (7)$$

which is an order of magnitude away from the theoretical expectation. There is a similar bound on the  $s$ -channel process [41,42]

$$\sigma(q\bar{q} \rightarrow t\bar{b}) < 12.9 \text{ pb (95\% CL) (CDF)} \quad (8)$$

$$\sigma(q\bar{q} \rightarrow t\bar{b}) < 39 \text{ pb (95\% CL) (D0)} \quad (9)$$

Table 2: Total cross sections (pb) for single-top-quark production and top-quark pair production at the Tevatron and LHC, for  $m_t = 175$  GeV. The NLO  $t$ -channel cross section is from Ref. [45]. The NNLO  $s$ -channel cross section is from Refs. [46,47]. The cross section for the  $Wt$  process is from Ref. [40]; it is leading order, with a subset of the NLO corrections included. The uncertainties are due to variation of the factorization and renormalization scales; uncertainty in the parton distribution functions; and uncertainty in the top-quark mass (2 GeV).

	Tevatron	LHC
$t$ -channel	$2.12 \pm 0.24$	$238 \pm 27$
$s$ -channel	$0.88 \pm 0.06$	$10.2 \pm 0.7$
$Wt$	$0.088 \pm 0.023$	$51 \pm 9$
$t\bar{t}$	$\approx 6.5$	$\approx 770$

which is even further from the theoretical expectation. The  $t$ - and  $s$ -channel processes will be first observed in Run II [9,43,44], while the associated-production process must await the LHC [10,11,40].

The most accurate measurements of  $V_{tb}$  will come from the  $t$ - and  $s$ -channel processes. Both the  $t$ -channel [45] and the  $s$ -channel [46] total cross sections have been calculated at next-to-leading order (NLO) in QCD, with an uncertainty of about 5% from varying the factorization and renormalization scales. After this symposium, a calculation of the leading (in the large  $N_c$  limit) next-to-next-to-leading-order (NNLO) QCD correction to the  $s$ -channel process appeared [47]; this essentially eliminates the uncertainty from varying the factorization and renormalization scales. It is also desirable to have a calculation of the differential cross section at NLO; this work is in progress [48]. Taking all uncertainties into account, it seems possible that  $V_{tb}$  can be measured at the Tevatron and the LHC with an uncertainty of 5% [11,43].

At a Linear Collider,  $V_{tb}$  can be extracted by measuring the top-quark width from a scan of the  $t\bar{t}$  threshold. The anticipated uncertainty in  $V_{tb}$  from such a measurement is about 10% [49]. The width is known with very good theoretical precision, thanks to recent calculations at NNLO in QCD [50,51]. The recent renormalization-group-improved calculation of the  $t\bar{t}$  threshold (Fig. 6)), mentioned in the previous section, removes any theoretical uncertainty in the normalization of the cross section that would impede the extraction of the width [30].

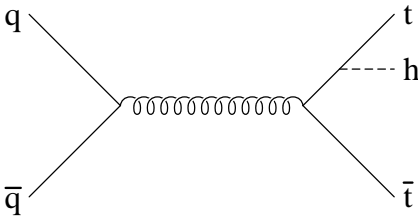


Figure 8: Higgs-boson production in association with a top-quark pair.

## 4 Yukawa coupling

As mentioned in the introduction, the top-quark Yukawa coupling is related to the top-quark mass (at leading order) via  $y_t = \sqrt{2}m_t/v$ , where  $v$  is the vacuum-expectation value of the Higgs field. However, it is the Yukawa coupling, not the mass, which is the truly fundamental parameter. The Yukawa coupling transmits the information that the Higgs field has acquired a vacuum expectation value to the top quark, thereby generating its mass. Since the Yukawa coupling is associated both with electroweak symmetry breaking and with fermion mass generation, it may be the most interesting parameter in top-quark physics.

How accurately do we desire to measure the top-quark Yukawa coupling? Since it is linearly related to the top quark mass, it would be desirable to measure it with the same fractional precision as the top-quark mass. A measurement of the top-quark mass with an accuracy of 1–2 GeV would correspond to a measurement of the Yukawa coupling to about 1%. Unfortunately, there is no known way to make a measurement with this accuracy.

The most direct way to measure the top-quark Yukawa coupling at a hadron collider is via the associated production of the Higgs boson with a top-quark pair, as shown in Fig. 8. If the Higgs boson decays to  $b\bar{b}$ , there are four  $b$  quarks in the final state, and tagging three or more of them reduces the background to an acceptable level. It has recently been argued that this process can be used to discover the Higgs boson in Run II of the Tevatron, given  $15 \text{ fb}^{-1}$  of integrated luminosity [52]. This process would yield only a crude measurement of the Yukawa coupling, however, due to the limited statistics. Even at the LHC, the anticipated accuracy is only about 16% via this process [10,11]. A next-to-leading-order calculation of the production cross section is still needed. This calculation has thus far been performed only in the limit  $m_h \ll m_t$  [53].

A less direct way to measure the top-quark Yukawa coupling at a hadron collider is to produce the Higgs boson via gluon fusion, as shown in Fig. 9 [54]. In the standard model this process is dominated by a top-quark loop, but if there are other heavy colored particles that couple to the Higgs boson (such as squarks), they too

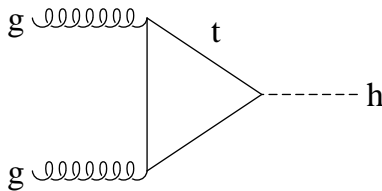


Figure 9: Higgs-boson production from gluon fusion via a top-quark loop.

contribute to the amplitude, complicating the extraction of the top-quark Yukawa coupling. Assuming only the top quark contributes substantially to this process, the Yukawa coupling can be measured with an accuracy of about 10%. The next-to-leading order calculation of this cross section is already in hand, but the remaining scale dependence is significant, about 15% [55]. The gluon luminosity contributes another 10% to the uncertainty in the cross section [56].

The top-quark Yukawa coupling can also be measured at a Linear Collider, using the analogue of Fig. 8 with the initial quark-antiquark replaced by electron-positron and the intermediate gluon replaced by  $\gamma, Z$ . The measurement is limited by statistics, and depends on the machine energy. In Table 3 I list the accuracy of the measurement of the Yukawa coupling at a 500 GeV and a 1 TeV Linear Collider for two Higgs masses [57]. At the 500 GeV machine one is limited by phase space. One does much better at the 1 TeV machine, but cannot achieve the desired 1% accuracy. The next-to-leading-order calculation of this cross section is already available [58,59].

Table 3: Accuracy of the measurement of the top-quark Yukawa coupling from  $e^+e^- \rightarrow t\bar{t}h$  at a Linear Collider of energy 500 GeV and 1 TeV. From Ref. [57].

$m_h$	500 GeV	1 TeV
110 GeV	12%	6%
130 GeV	44%	8%

## 5 Conclusions

Thus far the properties of the top quark have been tested only crudely. This decade will witness measurements of the top quark with increasing precision at the Tevatron and the LHC, and perhaps eventually at a Linear Collider. These measurements will either confirm that the top quark is an ordinary standard-model quark, or will indicate the presence of new physics. In either case, the study of the top quark will be rewarding.

In this talk I concentrated on the measurement of the fundamental parameters associated with the top quark. I argued that the desire to measure the top-quark mass to an accuracy of 1–3 GeV, the goal of the Tevatron and LHC, is well motivated by precision electroweak analyses, and by comparison with the anticipated accuracy in the  $b$ -quark mass. Although the Linear Collider can measure the mass with an accuracy of 100 MeV, there is no compelling motivation within the standard model to pursue such an accuracy. I considered two speculative motivations for pursuing this accuracy from physics beyond the standard model.

The CKM matrix element  $V_{tb}$  will be measured with an accuracy of about 5% at the Tevatron and the LHC via single-top-quark production. If there are only three generations, this measurement is not nearly accurate enough to help determine the CKM matrix. A Linear Collider cannot make a more accurate measurement.

The top-quark Yukawa coupling to the Higgs boson is perhaps the most interesting parameter, since it is associated with electroweak symmetry breaking and fermion mass generation. Since the Yukawa coupling is proportional to the top-quark mass, it would be desirable to measure them both with the same percentage accuracy. Unfortunately, this is well out of reach. Only a crude measurement of the top-quark Yukawa coupling can be made at the LHC. A Linear Collider with energy significantly above 500 GeV can measure the Yukawa coupling with an accuracy below 10%, but cannot achieve the desired 1% accuracy.

## Acknowledgments

I am grateful for conversations with and assistance from S. Heinemeyer, A. Hoang, and K. Paul. This work was supported in part by Department of Energy grant DE-FG02-91ER40677.

## References

- [1] F. Abe *et al.* [CDF Collaboration], Phys. Rev. Lett. **74**, 2626 (1995) [hep-ex/9503002].
- [2] S. Abachi *et al.* [D0 Collaboration], Phys. Rev. Lett. **74**, 2632 (1995) [hep-ex/9503003].
- [3] D. E. Groom *et al.*, “Review of particle physics,” Eur. Phys. J. **C15**, 1 (2000).
- [4] S. Willenbrock, Rev. Mod. Phys. **72**, 1141 (2000) [hep-ph/0008189].
- [5] E. H. Simmons, “Top Physics”, lectures given at TASI 2000, hep-ph/0011244.
- [6] L. Demortier, R. Hall, R. Hughes, B. Klima, R. Roser and M. Strovink [The Top Averaging Group Collaboration], FERMILAB-TM-2084.
- [7] M. C. Smith and S. S. Willenbrock, Phys. Rev. Lett. **79**, 3825 (1997) [hep-ph/9612329].
- [8] N. Gray, D. J. Broadhurst, W. Grafe and K. Schilcher, Z. Phys. **C48**, 673 (1990).
- [9] D. Amidei *et al.* [TeV-2000 Study Group Collaboration], “Future electroweak physics at the Fermilab Tevatron: Report of the TeV-2000 Study Group,” FERMILAB-PUB-96-082.
- [10] ATLAS Technical Design Report, Vol. II, CERN/LHCC/99-15 (1999).
- [11] M. Beneke *et al.*, “Top quark physics,” hep-ph/0003033, in “Proceedings of the Workshop on Standard Model Physics at the LHC,” eds. G. Altarelli and M. Mangano, CERN 2000-004.
- [12] P. M. Zerwas, “Physics with an e+ e- linear collider at high luminosity,” hep-ph/0003221.
- [13] J. Erler, S. Heinemeyer, W. Hollik, G. Weiglein and P. M. Zerwas, Phys. Lett. **B486**, 125 (2000) [hep-ph/0005024].
- [14] H. Georgi, AIP Conf. Proc. **23**, 575 (1975).
- [15] H. Fritzsch and P. Minkowski, Annals Phys. **93**, 193 (1975).
- [16] M. Gell-Mann, P. Ramond, and R. Slansky, in *Supergravity*, eds. P. van Nieuwenhuizen and D. Freedman (North Holland, Amsterdam, 1979), p. 315.
- [17] F. Wilczek, Nucl. Phys. Proc. Suppl. **77**, 511 (1999) [hep-ph/9809509].

- [18] R. Blair *et al.* [CDF-II Collaboration], “The CDF-II detector: Technical design report,” FERMILAB-PUB-96-390-E.
- [19] S. Abachi *et al.* [The D0 Collaboration], “The D0 upgrade: The detector and its physics,” FERMILAB-PUB-96-357-E.
- [20] H. E. Haber and R. Hempfling, *Phys. Rev. Lett.* **66**, 1815 (1991).
- [21] Y. Okada, M. Yamaguchi and T. Yanagida, *Prog. Theor. Phys.* **85**, 1 (1991).
- [22] J. Ellis, G. Ridolfi and F. Zwirner, *Phys. Lett.* **B257**, 83 (1991).
- [23] S. Heinemeyer, W. Hollik and G. Weiglein, *Eur. Phys. J.* **C9**, 343 (1999) [hep-ph/9812472].
- [24] S. Heinemeyer and G. Weiglein, hep-ph/0102117.
- [25] A. H. Hoang *et al.*, *Eur. Phys. J. direct***C3**, 1 (2000) [hep-ph/0001286].
- [26] M. Beneke, *Phys. Lett.* **B434**, 115 (1998) [hep-ph/9804241].
- [27] A. H. Hoang, M. C. Smith, T. Stelzer and S. Willenbrock, *Phys. Rev. D* **59**, 114014 (1999) [hep-ph/9804227].
- [28] K. G. Chetyrkin and M. Steinhauser, *Nucl. Phys.* **B573**, 617 (2000) [hep-ph/9911434].
- [29] K. Melnikov and T. v. Ritbergen, *Phys. Lett.* **B482**, 99 (2000) [hep-ph/9912391].
- [30] A. H. Hoang, A. V. Manohar, I. W. Stewart and T. Teubner, hep-ph/0011254.
- [31] F. del Aguila, M. Perez-Victoria and J. Santiago, *Phys. Lett. B* **492**, 98 (2000) [hep-ph/0007160].
- [32] T. Tait and C. P. Yuan, *Phys. Rev. D* **63**, 014018 (2001) [hep-ph/0007298].
- [33] T. Affolder *et al.* [CDF Collaboration], hep-ex/0012029.
- [34] S. S. Willenbrock and D. A. Dicus, *Phys. Rev. D* **34**, 155 (1986).
- [35] C. P. Yuan, *Phys. Rev. D* **41**, 42 (1990).
- [36] R. K. Ellis and S. Parke, *Phys. Rev. D* **46**, 3785 (1992).
- [37] S. Cortese and R. Petronzio, *Phys. Lett.* **B253**, 494 (1991).
- [38] T. Stelzer and S. Willenbrock, *Phys. Lett.* **B357**, 125 (1995) [hep-ph/9505433].

- [39] A. P. Heinson, A. S. Belyaev and E. E. Boos, Phys. Rev. D **56**, 3114 (1997) [hep-ph/9612424].
- [40] T. M. Tait, Phys. Rev. D **61**, 034001 (2000) [hep-ph/9909352].
- [41] T. Kikuchi, S. K. Wolinski, L. Demortier, S. Kim and P. Savard [CDF Collaboration], FERMILAB-CONF-00-290-E, *Presented at DPF 2000: The Meeting of the Division of Particles and Fields of the American Physical Society, Columbus, Ohio, 9-12 Aug 2000*.
- [42] B. Abbott *et al.* [D0 Collaboration], Phys. Rev. D **63**, 031101 (2001) [hep-ex/0008024].
- [43] T. Stelzer, Z. Sullivan and S. Willenbrock, Phys. Rev. D **58**, 094021 (1998) [hep-ph/9807340].
- [44] A. S. Belyaev, E. E. Boos and L. V. Dudko, Phys. Rev. D **59**, 075001 (1999) [hep-ph/9806332].
- [45] T. Stelzer, Z. Sullivan and S. Willenbrock, Phys. Rev. D **56**, 5919 (1997) [hep-ph/9705398]; update by Z. Sullivan, presented at the Top Thinkshop 2, Fermilab, November 10-12, 2000.
- [46] M. C. Smith and S. Willenbrock, Phys. Rev. D **54**, 6696 (1996) [hep-ph/9604223].
- [47] K. G. Chetyrkin and M. Steinhauser, hep-ph/0012002.
- [48] B. W. Harris, E. Laenen, L. Phaf, Z. Sullivan and S. Weinzierl, hep-ph/0102126.
- [49] P. Comas, R. Miquel, M. Martinez and S. Orteu, CERN-PPE/96-40, in “Proceeding of the Workshop on Physics with  $e^+e^-$  Linear Colliders” (Annecy, Gran Sasso, Hamburg, February 1995 – September 1995).
- [50] A. Czarnecki and K. Melnikov, Nucl. Phys. **B544**, 520 (1999) [hep-ph/9806244].
- [51] K. G. Chetyrkin, R. Harlander, T. Seidensticker and M. Steinhauser, Phys. Rev. D **60**, 114015 (1999) [hep-ph/9906273].
- [52] J. Goldstein, C. S. Hill, J. Incandela, S. Parke, D. Rainwater and D. Stuart, hep-ph/0006311.
- [53] S. Dawson and L. Reina, Phys. Rev. D **57**, 5851 (1998) [hep-ph/9712400].
- [54] H. M. Georgi, S. L. Glashow, M. E. Machacek and D. V. Nanopoulos, Phys. Rev. Lett. **40**, 692 (1978).

- [55] M. Spira, A. Djouadi, D. Graudenz and P. M. Zerwas, Nucl. Phys. **B453**, 17 (1995) [hep-ph/9504378].
- [56] J. Huston, S. Kuhlmann, H. L. Lai, F. Olness, J. F. Owens, D. E. Soper and W. K. Tung, Phys. Rev. D **58**, 114034 (1998) [hep-ph/9801444].
- [57] H. Baer, S. Dawson and L. Reina, Phys. Rev. D **61**, 013002 (2000) [hep-ph/9906419].
- [58] S. Dawson and L. Reina, Phys. Rev. D **59**, 054012 (1999) [hep-ph/9808443].
- [59] S. Dittmaier, M. Kramer, Y. Liao, M. Spira and P. M. Zerwas, Phys. Lett. **B441**, 383 (1998) [hep-ph/9808433].

Alberta Thy 09-01  
May 2001  
hep-ph/0105118

# Radiative corrections to bound-state properties in QED

ANDRZEJ CZARNECKI

*Department of Physics, University of Alberta  
Edmonton, AB, Canada T6G 2J1*

This talk summarizes some results on bound-state properties obtained since the previous (1998) RADCOR meeting. Recent results on radiative corrections to positronium decay width and the  $g$ -factor of a bound electron are described. A new approach to evaluating recoil corrections in systems consisting of particles with different masses is discussed.

Presented at the

5th International Symposium on Radiative Corrections  
(RADCOR-2000)  
Carmel CA, USA, 11–15 September, 2000

# 1 Introduction

Studies of bound-state properties in Quantum Electrodynamics (QED) are important on their own for a variety of practical applications, but also stimulate development of theoretical tools useful in many other areas of physics. High-precision QED calculations, including evaluation of high orders in the perturbation theory, are necessary to match the precision of atomic physics experiments, particularly in the spectroscopy of simple atoms. In those cases where theory and experiment can both attain high accuracy, comparisons of measurements with predictions often enable determination of various fundamental physical constants, such as the fine structure constant, masses or mass ratios of the electron, muon, and proton, ratios of various magnetic moments, proton charge radius, etc.

In other cases, when the relevant constants are known from other sources, one can very precisely test theoretical understanding of bound states. An impressive example, discussed at the previous RADCOR meeting [1], is the hyperfine splitting in the positronium ground state. There, the two-loop effects change the leading order prediction by about 12 MHz, or only 0.006%, but this effect is still larger than the experimental error by more than an order of magnitude! Rarely is computing of high-order loop effects more rewarding than it is in the spectroscopy of simple atoms like the positronium or muonium.

Such high-precision comparisons of theory and experiment are possible in simple atoms because on the one hand, measurements can be made very accurately with the modern spectroscopic methods, and on the other there are hardly any principal limitations of the theory. Since electrons are much lighter than any hadrons, the computations are not hindered by non-perturbative QCD uncertainties. Spectra and lifetimes of simple atoms can, in principle, be evaluated with any accuracy required by current experiments within pure QED.

Theoretical tools developed in this way, such as the computational techniques for the Feynman integrals or the machinery of non-relativistic effective theories [2], can subsequently be applied to solve problems in other areas of physics, such as hadronic properties or thermal field theory.

In this talk I would like to present some results obtained in the last couple of years since the previous RADCOR meeting in Barcelona. Those results include the positronium lifetime, bound electron gyromagnetic factor, and a new approach to computing properties of bound states consisting of particles with widely different masses.

## 2 Positronium decay

Lifetimes of the singlet and triplet positronium ground-states, p-Ps and o-Ps, can be measured with high precision [3]. For several years there was a very significant discrepancy between the theoretical predictions for the o-Ps lifetime and the experimental results. More recently, studies performed at the University of Tokyo gave results consistent with the theory. The most accurate experimental results are summarized in Table 1. Recently, the results obtained in gases were reexamined and new corrections were taken into account. The preliminary updated central value for the o-Ps decay rate measured in this method is approximately  $7.047/\mu\text{s}$  [4], in very good agreement with the vacuum measurement, but still significantly higher than the QED prediction.

Table 1: Recent experimental results for the o-Ps lifetime. “Method” in the second column refers to the medium in which the o-Ps decays. The last column shows the value of the two-loop coefficient  $B_o$ , necessary to bring the theoretical prediction (4) into agreement with the given experimental value. The last line gives the present theoretical prediction.

Reference	Method	$\Gamma(\text{o-Ps}) [\mu\text{s}^{-1}]$	$B_o$
Ann Arbor [5]	Gas	7.0514(14)	338(36)
Ann Arbor [6]	Vacuum	7.0482(16)	256(41)
Tokyo [7]	SiO <sub>2</sub> powder	7.0398(29)	41(74)
Tokyo (preliminary) [8]	SiO <sub>2</sub> powder	7.0398(15)	41(37)
	QED prediction [9]	7.0399	44.87(26)

The gas and vacuum results led to the suspicion that the two-loop QED corrections, which were not fully known, may be very large. The coefficient of  $(\alpha/\pi)^2$  in the correction relative to the lowest-order decay rate is denoted by  $B_o$ . Its value, necessary to reconcile a given experimental result with the QED prediction, is given in the last column of Table 1.

If such unusually enhanced effects existed, one would expect them to modify the p-Ps decay rate as well. Since p-Ps decay is much simpler than that of o-Ps, we

undertook a full two-loop QED study of this process [10,11].

The parapositronium decay rate into two photons agrees with predictions and had previously attracted less theoretical attention. However, it is also measured sufficiently precisely [12],

$$\Gamma_{\text{p-Ps}}^{\text{exp}}(\text{gas}) = 7990.9(1.7) \mu\text{s}^{-1}, \quad (1)$$

to warrant a calculation of  $\mathcal{O}(\alpha_s^2)$  corrections. The prediction for this decay width can be parameterized as

$$\begin{aligned} \Gamma_{\text{p-Ps}} = & \frac{m\alpha^5}{2} \left[ 1 + A_p \frac{\alpha}{\pi} + 2\alpha^2 \ln \frac{1}{\alpha} + B_p \left( \frac{\alpha}{\pi} \right)^2 - \frac{3\alpha^3}{2\pi} \ln^2 \frac{1}{\alpha} \right. \\ & \left. + \frac{\alpha^3}{\pi} \ln \alpha \left( 10 \ln 2 - \frac{367}{90} - 2A_p \right) + \dots \right], \quad A_p = \frac{\pi^2}{4} - 5. \end{aligned} \quad (2)$$

Our aim was the evaluation of the second order non-logarithmic correction  $B_p$ . It receives contributions from both soft and hard scales,  $B_p = B_p^{\text{soft}} + B_p^{\text{hard}}$ . We found

$$\begin{aligned} B_p^{\text{soft}} + 2\pi^2 \ln \frac{1}{\alpha} &= \frac{\pi^2}{2\epsilon} + 2\pi^2 \ln \frac{1}{m\alpha} + \frac{107\pi^2}{24}, \\ B_p^{\text{hard}} &= -\frac{\pi^2}{2\epsilon} + 2\pi^2 \ln(m) - 40.46(30) + \frac{1}{4}A_p^2, \end{aligned} \quad (3)$$

and the final result is  $B_p = 5.1(3)$ . There is a significant cancelation between soft and hard pieces and the final result is almost eight times smaller than the magnitude of the finite constant in the hard scale contribution computed in dimensional regularization.

Using the above result for  $B_p$  we arrive at the following result for the decay rate:

$$\Gamma_{\text{p-Ps}}^{\text{theory}} = 7989.64(2)\mu\text{s}^{-1},$$

which agrees very well with the measured value, Eq. (1).

Most recently, the two-loop corrections were also computed for the o-Ps decay,

$$\begin{aligned} \Gamma_{\text{o-Ps}} &= m\alpha^6 \frac{2(\pi^2 - 9)}{9\pi} \left[ 1 - A_o \frac{\alpha}{\pi} - \frac{\alpha^2}{3} \ln \frac{1}{\alpha} + B_o \left( \frac{\alpha}{\pi} \right)^2 - \frac{3\alpha^3}{2\pi} \ln^2 \frac{1}{\alpha} \right. \\ & \quad \left. - \frac{\alpha^3}{\pi} \ln \frac{1}{\alpha} \left( 8 \ln 2 - \frac{229}{30} + \frac{A_o}{3} \right) + \dots \right] \\ &= 7.03994(1)/\mu\text{s}, \quad A_o = 10.286606(10). \end{aligned} \quad (4)$$

The non-logarithmic two-loop coefficient is (with the small light-by-light contribution shown explicitly)  $B_o = 44.52(26) + 0.350(4) = 44.87(26)$  [9,13]. For both o-Ps and p-Ps, the leading logs in the order  $\alpha^3$  were found in [14] and the next-to-leading logarithms were computed only recently [15,16,17].

Can we claim that the positronium lifetime puzzle has been solved? It would certainly be very valuable to have another measurement of the o-Ps lifetime, especially that the powder measurement is somewhat controversial. An independent calculation of the theoretical prediction would also be useful, although it is unlikely that any unusually large effects are there to be uncovered.

### 3 Expansion of bound-state energies in the constituent mass ratio

A new approach to computing energy levels of a non-relativistic bound-state of two constituents with masses  $M$  and  $m$ , by a systematic expansion in powers of  $m/M$ , was described in [18].

Simple atoms of experimental interest often consist of two particles (constituents), widely separated in mass. An extreme example is the hydrogen, where the ratio of the proton and electron masses is of the order of 2000. Smaller ratios characterize muonium, muonic hydrogen, and exotic hadronic atoms. The goal of [18] was to find a practical algorithm which would allow evaluation of the bound-state energy levels (in a given order of perturbation theory in  $\alpha$  and  $Z\alpha$ ) as an expansion in powers and logarithms of  $m/M$  with an arbitrary precision.

That algorithm is useful in finding the so-called “hard-scale corrections”. In the language of an effective field theory, this corresponds to determining the Wilson coefficients of the short-distance operators, generated by virtual momenta much larger than the characteristic momenta of the atomic constituents. In practical terms, what is needed is the scattering amplitude of the two particles, with masses  $m$  and  $M$ , at the threshold, that is when the particles have vanishing velocities. The relevant Feynman diagrams depend on only the two mass scales  $m$  and  $M$  (since the external spatial momenta vanish). Since, however, at the two-loop level, which is of interest for the current theoretical studies, such integrals cannot in general be evaluated exactly, we need a method of expanding them in powers and logs of  $m/M$ .

As is already well known in the theory of asymptotic expansions (for reviews and further references see e.g. [19,20,21]), such expansion consists first of all in expanding the Feynman integrand in the small parameter  $m$ . In general, this gives rise to non-integrable singularities at small values of some momenta for which, before the expansion, the mass  $m$  provided a regulator. The difficulty in constructing a correct algorithm is to find the necessary counterterms and to evaluate the resulting new integrals.

Such a procedure was carried out in [18] with the example of radiative-recoil corrections, such as the diagram shown in Fig. 1.

In the language of characteristic scales of the momenta in the counterterm integrals, there are 3 “regions”. Fig. 2 depicts the Taylor expansion in  $m$  (2(a)) and the

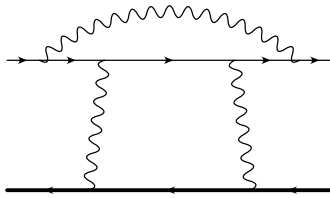


Figure 1: An example of a forward-scattering radiative-recoil diagram. The bold line represents the heavy constituent of the bound-state (e.g. proton if we consider hydrogen) and the thin line — the light one (an electron).

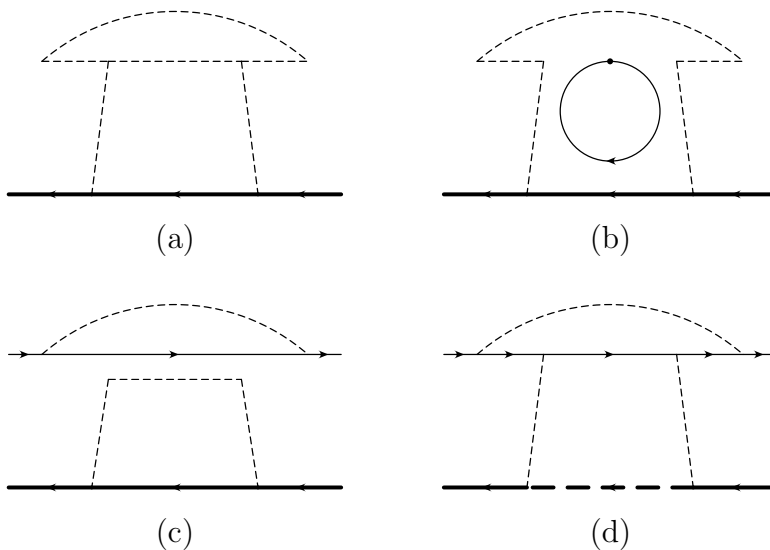


Figure 2: Elements of the expansion of the diagram in Fig. 1 in powers and logs of  $m/M$  (see text). Thick and thin solid lines denote propagators with  $M$  and  $m$ , respectively. Thin dashed lines are massless, and the thick dashed line denotes a static (“eikonal”) propagator.

3 counterterms. In the diagram 2(b), the momentum flowing through one of the light constituent lines is of the order of  $m$ , while the second loop momentum is  $\mathcal{O}(M)$  (so that the propagators along its flow can be Taylor-expanded in  $m$  and in the corresponding small momentum). In 2(c) we have the same sizes of the loop momenta, but now the large momentum takes a different route to flow through the upper part of the diagram. The last contribution, 2(d), arises when both loop momenta are  $\mathcal{O}(m)$ . In this case, the heavy propagator  $1/(k^2 + 2k.P)$  can be expanded in  $k^2$ , and becomes an “eikonal” [22] propagator  $1/2k.P$ .

This last contribution was least easy to evaluate and a procedure for computing the resulting integrals was described in [18]. It is interesting that the same integrals arise in very different problems, for example in certain corrections to the radiative

quark decays [23].

## 4 Anomalous magnetic moment of a bound electron

In [24] the binding corrections to the gyromagnetic factor  $g_e$  of an electron in hydrogen-like ions were studied. The interaction of an electron with an external magnetic field  $\mathbf{B}$  is described by the potential  $V = -\boldsymbol{\mu} \cdot \mathbf{B}$ . The electron magnetic moment  $\boldsymbol{\mu}$  is given by  $\boldsymbol{\mu} = g_e \frac{e}{2m} \mathbf{s}$ , with  $m$ ,  $\mathbf{s} = \boldsymbol{\sigma}/2$ , and  $g_e$  denoting the mass, spin and the so-called gyromagnetic or Landé factor of the electron.

If the electron is bound in a ground state of a hydrogen-like ion,  $g_e$  becomes a function of the nuclear charge  $Z$  and its measurements [25,26,27] provide a sensitive test of the bound-state theory based on the QED. The theoretical prediction can be cast in the following form [28]

$$g_e(Z) = g_D + \Delta g_{\text{rec}} + \Delta g_{\text{rad}}. \quad (5)$$

The first term corresponds to the lowest order expansion in  $\alpha/\pi$  and has been calculated to all orders in  $Z\alpha$  [29],

$$g_D = \frac{2}{3} \left[ 1 + 2\sqrt{1 - (Z\alpha)^2} \right]. \quad (6)$$

$\Delta g_{\text{rec}}$  denotes the recoil corrections [30],  $\Delta g_{\text{rec}} = \mathcal{O}\left((Z\alpha)^2 \frac{m}{m_N}\right)$ , where  $m_N$  is the nucleus mass. Further references to the studies of those effects can be found in [28].

Our main interest were the radiative corrections. They can be presented as an expansion in two parameters,  $Z\alpha$  and  $\alpha/\pi$ ,

$$\frac{\Delta g_{\text{rad}}}{2} = C_e^{(2)}(Z\alpha) \left(\frac{\alpha}{\pi}\right) + C_e^{(4)}(Z\alpha) \left(\frac{\alpha}{\pi}\right)^2 + \dots \quad (7)$$

Powers of  $\alpha/\pi$  correspond to electron–electron interactions, while  $Z\alpha$  governs binding effects due to electron interactions with the nucleus. The first coefficient function in (7),  $C_e^{(2)}(Z\alpha)$ , has been computed numerically to all orders in  $Z\alpha$  [31,32]. Its first two terms in the  $Z\alpha$  expansion are also known analytically [33,34]

$$C_e^{(2)}(Z\alpha) = \frac{1}{2} \left[ 1 + \frac{1}{6}(Z\alpha)^2 + \mathcal{O}\left((Z\alpha)^4\right) \right]. \quad (8)$$

The main theoretical uncertainty for  $g_e$  in light ions is, at present, connected with the unknown coefficient  $C'$  in the next coefficient function,

$$\begin{aligned} C_e^{(4)}(Z\alpha) &= C_e^{(4)}(0) \left[ 1 + C' \cdot (Z\alpha)^2 + \mathcal{O}\left((Z\alpha)^4\right) \right], \\ C_e^{(4)}(0) &= -0.328\,478\,444\,00\dots \quad [35, 36, 28]. \end{aligned} \quad (9)$$

At present, the most accurate experimental value of the bound electron gyromagnetic factor has been obtained [37,38] with a hydrogen-like carbon ion  $^{12}\text{C}^{5+}$  ( $Z = 6$ ),

$$g_e(Z = 6; \text{exp}) = 2.001\,041\,596(5). \quad (10)$$

The theoretical prediction is [39]

$$g_e(Z = 6; \text{theory}) = 2.001\,041\,591(7) \quad (11)$$

where 70% of the error is caused by the unknown coefficient  $C'$  of the  $\left(\frac{\alpha}{\pi}\right)^2 (Z\alpha)^2$  effects in (9) (for carbon, higher powers of  $Z\alpha$  are assumed to be negligible).

The purpose of our paper [24] was to demonstrate that  $C' = 1/6$ , in analogy to the corresponding coefficient in the lower order in  $\alpha/\pi$ . In fact, we found that the coefficient of  $(Z\alpha)^2$  is the same in all coefficient functions  $C_e^{(2n)}(Z\alpha)$ , so that the theoretical prediction for  $\Delta g_{\text{rad}}$  accurate up to  $(Z\alpha)^2$  and exact in  $\alpha/\pi$  reads

$$\Delta g_{\text{rad}} = (g_{\text{free}} - 2) \cdot \left[ 1 + \frac{(Z\alpha)^2}{6} \right], \quad (12)$$

where  $g_{\text{free}}$  is the gyromagnetic factor of a free electron, presently known to  $\mathcal{O}((\alpha/\pi)^4)$  [40] (the same result had been obtained in a different way in [41]). With this result, the theoretical uncertainty in (11) is reduced from  $7 \cdot 10^{-9}$  to about  $2 \cdot 10^{-9}$ .

## 5 Conclusions

Three examples of problems in the bound-state theory, solved since the last RAD-COR meeting, were summarized in this talk. Of course, other groups have made important progress in other aspects of bound-state physics, which was not reported here. I would like to mention two examples. Important new corrections to the hydrogen Lamb shift were found in [42,43]. In [42], an algorithm was constructed to compute a class of 3-loop propagator-type massive integrals (the so-called master integrals had been computed in [44]).

Another class of recently studied problems is connected with the “velocity renormalization group” [45]. This approach allows better understanding and at least partial resummation of large logarithms  $\ln \frac{1}{\alpha}$  arising in the non-relativistic bound-state calculations. A review of the recent progress in this area can be found in [46].

Hopefully, the recent significant progress in the theory will be followed by new measurements. It would be very important to re-measure the positronium hyperfine splitting, to resolve the present (more than 3 standard deviations) discrepancy between the old measurements and the improved theory [1,47,48,49]. Similarly important would be an independent study of the ortho-positronium lifetime. Now that

the theory has in most cases taken control of the two-loop quantum effects, it is particularly exciting to test those predictions experimentally.

## Acknowledgments

I am grateful to Kirill Melnikov and Alexander Yelkhovsky, with whom the results described here were obtained, for the continuing collaboration and for helpful remarks about this paper. This research was supported by the Natural Sciences and Engineering Research Council of Canada. I thank the organizers of the RADCOR-2001, especially Howard Haber, for partially supporting my participation.

## References

- [1] A. Czarnecki, K. Melnikov, and A. Yelkhovsky, in *Radiative Corrections*, edited by J. Sola (World Scientific, Singapore, 1999), p. 125, hep-ph/9904479.
- [2] W. E. Caswell and G. P. Lepage, *Phys. Lett.* **B167**, 437 (1986).
- [3] A. Czarnecki and S. G. Karshenboim, in *Proc. XIV Intl. Workshop on High Energy Physics and Quantum Field Theory (QFTHEP'99, Moscow 1999)*, edited by B. B. Levchenko and V. I. Savrin (MSU-Press, Moscow, 2000), p. 538, hep-ph/9911410.
- [4] R. S. Conti *et al.*, Experimental tests of QED in positronium: recent advances, 2000, talk given at the Conference *Hydrogen Atom II*, Castiglione della Pescaia, Italy, June 2000; <http://positrons.physics.lsa.umich.edu/atomic/psreview.pdf>.
- [5] C. I. Westbrook, D. W. Gidley, R. S. Conti, and A. Rich, *Phys. Rev.* **A40**, 5489 (1989).
- [6] J. S. Nico, D. W. Gidley, A. Rich, and P. W. Zitzewitz, *Phys. Rev. Lett.* **65**, 1344 (1990).
- [7] S. Asai, S. Orito, and N. Shinohara, *Phys. Lett.* **B357**, 475 (1995).
- [8] S. Asai, private communication; O. Jinnouchi, University of Tokyo Ph.D. Thesis, 2001.
- [9] G. S. Adkins, R. N. Fell, and J. Sapirstein, *Phys. Rev. Lett.* **84**, 5086 (2000).
- [10] A. Czarnecki, K. Melnikov, and A. Yelkhovsky, *Phys. Rev. Lett.* **83**, 1135 (1999), erratum: *ibid.* **85**, 2221 (2000).

- [11] A. Czarnecki, K. Melnikov, and A. Yelkhovsky, Phys. Rev. A **61**, 052502 (2000), erratum: *ibid.* **62**, 059902 (2000), hep-ph/9910488.
- [12] A. H. Al-Ramadhan and D. W. Gidley, Phys. Rev. Lett. **72**, 1632 (1994).
- [13] G. S. Adkins, R. N. Fell, and J. Sapirstein, Phys. Rev. **A63**, 032511 (2001).
- [14] S. G. Karshenboim, JETP **76**, 541 (1993), Zh. Eksp. Teor. Fiz. **103**, 1105 (1993).
- [15] K. Melnikov and A. Yelkhovsky, Phys. Rev. **D62**, 116003 (2000).
- [16] R. Hill and G. P. Lepage, Phys. Rev. **D62**, 111301 (2000).
- [17] B. A. Kniehl and A. A. Penin, Phys. Rev. Lett. **85**, 1210 (2000), erratum: *ibid.* **85**, 3065 (2000).
- [18] A. Czarnecki and K. Melnikov, hep-ph/0012053, in press in Phys. Rev. Lett.
- [19] K. G. Chetyrkin, preprint MPI-Ph/PTh 13/91 (unpublished).
- [20] F. V. Tkachev, Sov. J. Part. Nucl. **25**, 649 (1994).
- [21] V. A. Smirnov, Mod. Phys. Lett. **A10**, 1485 (1995).
- [22] A. Czarnecki and V. Smirnov, Phys. Lett. **B394**, 211 (1997).
- [23] A. J. Buras, A. Czarnecki, M. Misiak, and J. Urban, work in progress.
- [24] A. Czarnecki, K. Melnikov, and A. Yelkhovsky, Phys. Rev. **A63**, 012509 (2001).
- [25] N. Hermanspahn *et al.*, Acta Phys. Pol. **B27**, 357 (1996).
- [26] W. Quint, Phys. Scr. **T59**, 203 (1995).
- [27] G. Werth, Phys. Scr. **T59**, 206 (1995).
- [28] P. J. Mohr and B. N. Taylor, Rev. Mod. Phys. **72**, 351 (2000).
- [29] G. Breit, Nature **122**, 649 (1928).
- [30] H. Grotch, Phys. Rev. **A2**, 1605 (1970).
- [31] A. Blundell, K. T. Cheng, and J. Sapirstein, Phys. Rev. **A55**, 1857 (1997).
- [32] H. Persson, S. Salomonson, P. Sunnergren, and I. Lindgren, Phys. Rev. **A56**, R2499 (1997).
- [33] J. Schwinger, Phys. Rev. **73**, 416 (1948).

- [34] H. Grotch, Phys. Rev. Lett. **24**, 39 (1970).
- [35] C. M. Sommerfield, Phys. Rev. **107**, 328 (1957).
- [36] A. Petermann, Nucl. Phys. **3**, 689 (1957).
- [37] N. Hermanspahn *et al.*, Phys. Rev. Lett. **84**, 427 (2000).
- [38] H. Häffner *et al.*, The  $g$ -Factor of Hydrogenic Ions: A Test of QED, 2000, contribution to the Conference *Hydrogen Atom II*, Castiglione della Pescaia, Italy, June 2000.
- [39] T. Beier *et al.*, Phys. Rev. **A62**, 032510 (2000).
- [40] V. W. Hughes and T. Kinoshita, Rev. Mod. Phys. **71**, S133 (1999).
- [41] M. I. Eides and H. Grotch, Ann. Phys. **260**, 191 (1997).
- [42] K. Melnikov and T. van Ritbergen, Phys. Rev. Lett. **84**, 1673 (2000).
- [43] K. Pachucki, Phys. Rev. **A63**, 042503 (2001).
- [44] S. Laporta and E. Remiddi, Phys. Lett. **B379**, 283 (1996).
- [45] M. E. Luke, A. V. Manohar, and I. Z. Rothstein, Phys. Rev. **D61**, 074025 (2000).
- [46] A. V. Manohar and I. W. Stewart, Nucl. Phys. Proc. Suppl. **94**, 130 (2001).
- [47] R. J. Hill, Phys. Rev. Lett. **86**, 3280 (2001).
- [48] K. Melnikov and A. Yelkhovsky, Phys. Rev. Lett. **86**, 1498 (2001).
- [49] B. A. Kniehl and A. A. Penin, Phys. Rev. Lett. **85**, 5094 (2000).

CERN-TH/2001-018  
KA-TP-2-2001  
September 28, 2001  
hep-ph/0101260

## Two-loop electroweak contributions to $\Delta r$ \*

A. FREITAS<sup>a</sup>, S. HEINEMEYER<sup>b</sup>, W. HOLLIK<sup>c</sup>, W. WALTER<sup>c</sup>, G. WEIGLEIN<sup>d</sup>

<sup>a</sup> *DESY Theorie, Notkestr. 85, D-22603 Hamburg, Germany*

<sup>b</sup> *HET, Physics Department, Brookhaven Nat. Lab., Upton, NY 11973, USA*

<sup>c</sup> *Institut für Theoretische Physik, Universität Karlsruhe,  
D-76128 Karlsruhe, Germany*

<sup>d</sup> *CERN, TH Division, CH-1211 Geneva 23, Switzerland*

A review is given on the quantum correction  $\Delta r$  in the  $W$ - $Z$  mass correlation at the electroweak two-loop level, as derived from the calculation of the muon lifetime in the Standard Model. Exact results for  $\Delta r$  and the  $W$ -mass prediction including  $\mathcal{O}(\alpha^2)$  corrections with fermion loops are presented and compared with previous results of a next-to-leading order expansion in the top-quark mass.

Presented by W. HOLLIK at the

5th International Symposium on Radiative Corrections  
(RADCOR-2000)

Carmel CA, USA, 11-15 September, 2000

---

\*Work supported by the Deutsche Forschungsgemeinschaft and by the European Union.

# 1 Introduction

The interdependence between the  $W$ -boson mass,  $M_W$ , and the  $Z$ -boson mass,  $M_Z$ , with the help of the Fermi constant  $G_F$  and the fine structure constant  $\alpha$  is one of the most important relations for testing the electroweak Standard Model (SM) with high precision. At present, the world-average for the  $W$ -boson mass is  $M_W^{\text{exp}} = 80.434 \pm 0.037$  GeV [1]. The experimental precision on  $M_W$  will be further improved with the data taken at LEP2 in their final analysis, at the upgraded Tevatron and at the LHC, where an error of  $\delta M_W = 15$  MeV can be expected [2]. At a high-luminosity linear collider running in a low-energy mode at the  $W^+W^-$  threshold, a reduction of the experimental error down to  $\delta M_W = 6$  MeV may be feasible [3]. This offers the prospect for highly sensitive tests of the electroweak theory [4], provided that the accuracy of the theoretical prediction matches the experimental precision. The basic physical quantity for the  $M_W$ - $M_Z$  correlation is the muon lifetime  $\tau_\mu$ , which defines the Fermi constant  $G_F$  according to

$$\frac{1}{\tau_\mu} = \frac{G_F^2 m_\mu^5}{192\pi^3} F\left(\frac{m_e^2}{m_\mu^2}\right) \left(1 + \frac{3}{5} \frac{m_\mu^2}{M_W^2}\right) (1 + \Delta_{\text{QED}}), \quad (1)$$

with  $F(x) = 1 - 8x - 12x^2 \ln x + 8x^3 - x^4$ . By convention, the QED corrections within the Fermi Model,  $\Delta_{\text{QED}}$ , are included in this defining equation for  $G_F$ . The one-loop result for  $\Delta_{\text{QED}}$  [5], which has already been known for several decades, has recently been supplemented by the two-loop correction [6], yielding

$$\Delta_{\text{QED}} = 1 - 1.81 \frac{\alpha(m_\mu)}{\pi} + 6.7 \left(\frac{\alpha(m_\mu)}{\pi}\right)^2, \quad \text{with} \quad \alpha(m_\mu) \simeq \frac{1}{135.90}. \quad (2)$$

The tree-level  $W$ -propagator effect giving rise to the (numerically insignificant) term  $3m_\mu^2/(5M_W^2)$  in (1), is conventionally also included in the definition of  $G_F$ , although not part of the Fermi Model prediction. From the precisely measured muon-decay width the value [7]  $G_F = (1.16637 \pm 0.00001) 10^{-5}$  GeV $^{-2}$  for the Fermi constant is derived.

Calculating the muon lifetime within the SM and comparing the SM result with (1) yields the relation

$$M_W^2 \left(1 - \frac{M_W^2}{M_Z^2}\right) = \frac{\pi\alpha}{\sqrt{2}G_F} (1 + \Delta r), \quad (3)$$

where the radiative corrections are summarized in the quantity  $\Delta r$ , first calculated in [8] at one-loop. This relation can be used for deriving the prediction of  $M_W$  within the SM (or possible extensions), to be confronted with the experimental result for  $M_W$ .

The one-loop result for  $\Delta r$  within the SM can be decomposed as follows (with the notation  $s_w^2 = 1 - M_W^2/M_Z^2$ ,  $c_w^2 = 1 - s_w^2$ ),

$$\Delta r^{(\alpha)} = \Delta\alpha - \frac{c_w^2}{s_w^2} \Delta\rho + \Delta r_{\text{rem}}(M_H), \quad (4)$$

exhibiting the leading fermion-loop contributions  $\Delta\alpha$  and  $\Delta\rho$ , which originate from the charge and mixing-angle renormalization; the remainder part  $\Delta r_{\text{rem}}$  contains in particular the dependence on the Higgs-boson mass,  $M_H$ . The QED-induced shift  $\Delta\alpha$  in the fine structure constant contains large logarithms of light-fermion masses. The leading contribution to the  $\rho$  parameter from the top/bottom weak-isospin doublet,  $\Delta\rho$ , gives rise to a term with a quadratic dependence on the top-quark mass,  $m_t$  [9].

Beyond the one-loop order, resummations of the leading one-loop contributions  $\Delta\alpha$  and  $\Delta\rho$  are known [10]. They correctly take into account the terms of the form  $(\Delta\alpha)^2$ ,  $(\Delta\rho)^2$ ,  $(\Delta\alpha\Delta\rho)$ , and  $(\Delta\alpha\Delta r_{\text{rem}})$  at the two-loop level and the leading powers in  $\Delta\alpha$  to all orders.

QCD corrections to  $\Delta r$  are known at  $\mathcal{O}(\alpha\alpha_s)$  [11] and  $\mathcal{O}(\alpha\alpha_s^2)$  [12]. Concerning the electroweak two-loop contributions, only partial results are available up to now. Approximative calculations were performed based on expansions for asymptotically large values of  $M_H$  [13] and  $m_t$  [14,15,16]. The terms derived by expanding in the top-quark mass of  $\mathcal{O}(G_F^2 m_t^4)$  [14] and  $\mathcal{O}(G_F^2 m_t^2 M_Z^2)$  [15] were found to be numerically sizeable. The  $\mathcal{O}(G_F^2 m_t^2 M_Z^2)$  term, involving three different mass scales, has been obtained by two separate expansions in the regions  $M_W, M_Z, M_H \ll m_t$  and  $M_W, M_Z \ll m_t, M_H$  and by an interpolation between the two expansions. This formally next-to-leading order term turned out to be of a magnitude similar to that of the formally leading term of  $\mathcal{O}(G_F^2 m_t^4)$ , entering with the same sign. Its inclusion (both for  $M_W$  and the effective weak mixing angle) had important consequences on the indirect constraints on the Higgs-boson mass derived from the SM fit to the precision data.

A more complete calculation of electroweak two-loop effects is hence desirable. As a first step in this direction, exact results were derived for the Higgs-mass dependence of the fermionic two-loop corrections to the precision observables [17]. They have been compared with the results of expanding up to  $\mathcal{O}(G_F^2 m_t^2 M_Z^2)$  [15], specifically analysing the effects of the  $m_t$  expansion, and good agreement has been found [18]. Beyond the two-loop order, complete results for the pure fermion-loop corrections (*i.e.* contributions containing  $n$  fermion loops at  $n$ -loop order) have recently been obtained up to four-loop order [19]. These results contain in particular the contributions of the leading powers in  $\Delta\alpha$  as well as the ones in  $\Delta\rho$  and the mixed terms.

In this talk the complete fermionic electroweak two-loop corrections to  $\Delta r$  are discussed, as calculated exactly without an expansion in the top-quark or the Higgs-boson mass [20]. These are all two-loop diagrams contributing to the muon-decay amplitude and containing at least one closed fermion loop (except the pure QED corrections already contained in the Fermi model result, according to (1)). Fig. 1

displays some typical examples. The considered class of diagrams includes the potentially large corrections both from the top/bottom doublet and from contributions proportional to  $N_{lf}$  and  $N_{lf}^2$ , where  $N_{lf}$  is the number of light fermions (a partial result for the light-fermion contributions is given in [21]). The results presented here improve on the previous results of an expansion in  $m_t$  up to next-to-leading order [15] in containing the full dependence on  $m_t$  as well as the complete light-fermion contributions at the two-loop order, while in [15] higher-order corrections from light fermions have only been taken into account via a resummation of the one-loop light-fermion contribution.

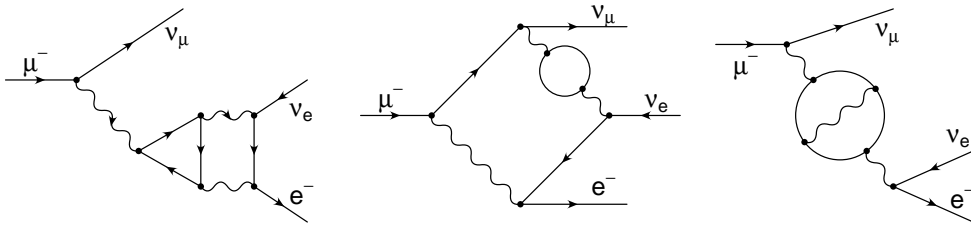


Figure 1: Examples for various types of fermionic two-loop diagrams contributing to muon decay.

## 2 Outline of the calculation

Since all possibly infrared (IR) divergent photonic corrections are already contained in the definition (1) of the Fermi constant  $G_F$  and mass singularities are absorbed in the running of the electromagnetic coupling,  $M_W$  represents the scale for the electroweak corrections in  $\Delta r$ . Therefore it is possible to neglect all fermion masses except the top-quark mass and the momenta of the external leptons so that the Feynman diagrams for muon decay reduce to vacuum diagrams.

All QED contributions to the Fermi Model have to be excluded in the computation of  $\Delta r$  since they have already been separated off in the definition of  $G_F$ , see eq. (1). Apart from the one-loop contributions, this comprises two-loop QED corrections and mixed contributions of QED and weak corrections of each one-loop order, which have to be removed from  $\Delta r^{(\alpha^2)}$ . For fermionic two-loop diagrams it is possible to find a one-to-one correspondence between QED graphs in Fermi-Model and SM contributions.

After extracting the IR-divergent QED corrections, the generic diagrams contributing to the muon-decay amplitude can be reduced to vacuum-type diagrams, since the masses of the external particles and the momentum transfer are negligible. The renormalization of is performed in the on-shell scheme. Thus, the mass-

renormalization of the gauge bosons requires the evaluation of two-loop two-point functions with non-zero external momentum, which is more involved from a technical point of view regarding the tensor structure and the evaluation of the scalar integrals. This complication cannot be avoided by performing the calculation within another renormalization scheme, *e.g.* the  $\overline{MS}$  scheme, since ultimately one is interested in the relation between the physical parameters  $M_W$ ,  $M_Z$ ,  $\alpha$ ,  $G_F$ , where the two-point functions for non-zero momenta enter.

All diagrams and amplitudes for the decay and counterterm contributions have been generated with the program *FeynArts 2.2* [22]. The amplitudes are algebraically reduced by means of a general tensor-integral decomposition for two-loop two-point functions with the program *TwoCalc* [23], leading to a fixed set of standard scalar integrals. Analytic expressions are known for the scalar one-loop [24] and two-loop [25] vacuum integrals, whereas the two-loop self-energy diagrams can be evaluated numerically by means of one-dimensional integral representations [26].

In order to apply an additional check the calculations were performed within a covariant  $R_\xi$  gauge, with individual gauge parameters  $\xi_i$  for each gauge boson. It has been explicitly checked at the algebraic level that the gauge-parameter dependence of the final result drops out.

At the subloop level, also the Faddeev-Popov ghost sector has to be renormalized. The gauge-fixing part of the Lagrangian, in terms of the gauge fields  $A^\mu$ ,  $Z^\mu$ ,  $W^{\pm\mu}$  and the unphysical Higgs scalars  $\chi$ ,  $\phi^\pm$  given by

$$\begin{aligned} \mathcal{L}_{\text{gf}} &= -\frac{1}{2} \left[ (F^\gamma)^2 + (F^Z)^2 + F^+ F^- + F^- F^+ \right], & \text{with} \\ F^\gamma &= (\xi_1^\gamma)^{-\frac{1}{2}} \partial_\mu A^\mu + \frac{\xi^{\gamma Z}}{2} \partial_\mu Z^\mu, \\ F^Z &= (\xi_1^Z)^{-\frac{1}{2}} \partial_\mu Z^\mu + \frac{\xi^{Z\gamma}}{2} \partial_\mu A^\mu - (\xi_2^Z)^{\frac{1}{2}} M_Z \chi, \\ F^\pm &= (\xi_1^W)^{-\frac{1}{2}} \partial_\mu W^{\pm\mu} \mp i (\xi_2^W)^{\frac{1}{2}} M_W \phi^\pm, \end{aligned} \tag{5}$$

does not need renormalization. Accordingly, one can either introduce the gauge-fixing term after renormalization or renormalize the gauge parameters in such a way that they compensate the renormalization of the fields and masses. Both ensure that no counterterms arise from the gauge-fixing sector but they differ in the treatment of the ghost Lagrangian, which is given by the variation of the functionals  $F^a$  under infinitesimal gauge transformations  $\delta\theta_b$ ,

$$\mathcal{L}_{\text{FP}} = \sum_{a,b=\gamma,Z,\pm} \bar{u}^a \frac{\delta F^a}{\delta\theta^b} u^b. \tag{6}$$

In the latter case, which was applied in our work for simplification of the automatized treatment, additional counterterm contributions for the ghost sector arise from the gauge-parameter renormalization. The parameters  $\xi_i^a$  in (5) are renormalized such that their counterterms  $\delta\xi_i^a$  exactly cancel the contributions from the renormalization of the fields and masses and that the renormalized gauge parameters comply with the  $R_\xi$  gauge.

### 3 On the $\gamma_5$ -problem

In four dimensions the algebra of the  $\gamma_5$ -matrix is defined by the two relations

$$\{\gamma_5, \gamma_\alpha\} = 0 \quad \text{for} \quad \alpha = 1, \dots, 4 \quad (7)$$

$$\text{Tr}\{\gamma_5\gamma^\mu\gamma^\nu\gamma^\rho\gamma^\sigma\} = 4i\epsilon^{\mu\nu\rho\sigma}. \quad (8)$$

It is impossible to translate both relations simultaneously into  $D \neq 4$  dimensions without encountering inconsistencies [27].

A certain treatment of  $\gamma_5$  might break symmetries, *i.e.* violate Slavnov-Taylor (ST) identities which would have to be restored with extra counterterms. Even after this procedure a residual scheme dependence can persist which is associated with  $\epsilon$ -tensor expressions originating from the treatment of (8). Such expressions cannot be canceled by counterterms. If they broke ST identities this would give rise to anomalies.

't Hooft and Veltman [27] suggested a consistent scheme, formalized by Breitenlohner and Maison [28], as a separation of the first four and the remaining dimensions of the  $\gamma$ -Matrices (HVBM-scheme). It has been shown [29] that the SM with HVBM regularization is anomaly-free and renormalizable. This shows that  $\epsilon$ -tensor terms do not get merged with divergences.

The naively anti-commuting scheme, which is widely used for one-loop calculations, extends the rule (7) to  $D$  dimensions but abandons (8),

$$\{\gamma_5, \gamma_\alpha\} = 0 \quad \text{for} \quad \alpha = 1, \dots, D \quad (9)$$

$$\text{Tr}\{\gamma_5\gamma^\mu\gamma^\nu\gamma^\rho\gamma^\sigma\} = 0. \quad (10)$$

This scheme is unambiguous but does not reproduce the four-dimensional case.

In the SM, particularly triangle diagrams (like the ones in Figure 2) containing chiral couplings are sensitive to the  $\gamma_5$ -problem. In our context, the one-loop triangle diagrams have been explicitly calculated in both schemes. While the naive scheme immediately respects all ST identities the HVBM scheme requires the introduction of additional finite counterterms. Even after this procedure finite differences remain between the results of the two schemes, showing that the naive scheme is inapplicable in this case.

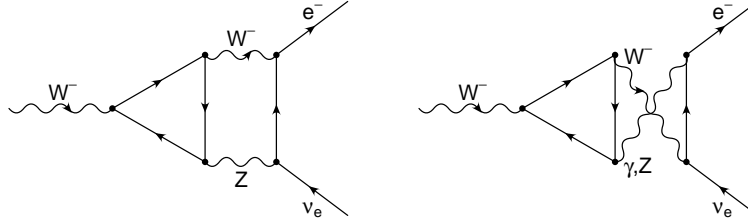


Figure 2: Charged-current vertex diagrams with fermion-triangle subgraphs.

In the calculation of  $\Delta r$  triangle diagrams appear as subloops of two-loop charged current (CC) vertex diagrams (Fig. 2). One finds that for the difference terms between both schemes this loop can be evaluated in four dimensions without further difficulties. This can be explained by the fact that renormalizability forbids divergent contributions to  $\epsilon$ -tensor terms from higher loops in the HVBM scheme. The  $\epsilon$ -tensor contributions from the triangle subgraph in the HVBM scheme meet a second  $\epsilon$ -tensor term from the outer fermion lines in Fig. 2, thereby resulting in a non-zero contribution to  $\Delta r$ .

Computations in the HVBM scheme can in general get very tedious because of the necessity of additional counterterms. For our specific problem, however, it is possible to apply another, simplified, method. One can consider a “mixed” scheme that uses both relations (7) and (8) in  $D$  dimensions, despite their mathematical inconsistency, to evaluate the one-loop triangle subgraphs. These results immediately respect all ST identities. As checked explicitly, they differ from the HVBM results (with the appropriate counterterms to restore the ST identities) only by terms of  $\mathcal{O}(D - 4)$ ,

$$\Gamma_{\Delta(1)}^{\text{HVBM}} = \Gamma_{\Delta(1)}^{\text{mix}} + \mathcal{O}(D - 4). \quad (11)$$

Inserting the one-loop expressions into the the two-loop diagrams one finds that the second loop integration gives a finite result and hence can be performed in four dimensions yielding

$$\Gamma_{\text{CC}(2)}^{\text{HVBM}} = \Gamma_{\text{CC}(2)}^{\text{mix}} + \mathcal{O}(D - 4). \quad (12)$$

Thus the mixed scheme can serve in this case as a technically easy prescription for the correct calculation of the CC two-loop contributions. Practical ways of treating  $\gamma_5$  in higher-order calculations are also discussed in [30].

## 4 Two-loop renormalization

For the determination of the one-loop counterterms and renormalization constants the conventions of [31] are adopted. Two-loop renormalization constants enter via the

counterterms for the transverse  $W$  propagator and the charged current vertex (the counterterms for the transverse  $Z$  propagator are analogous):

$$\left[ \text{wavy line } \otimes \text{ wavy line} \right]_{\text{T}} = \delta Z_{(2)}^W (k^2 - M_W^2) - \delta M_{W(2)}^2 - \delta Z_{(1)}^W \delta M_{W(1)}^2, \quad (13)$$

$$\begin{aligned} \text{wavy line } \otimes \begin{array}{l} \nearrow v_e \\ \searrow e^- \end{array} &= i \frac{e}{\sqrt{2}s_W} \gamma_\mu \omega_- \left[ \delta Z_{e(2)} - \frac{\delta s_{W(2)}}{s_W} + \frac{1}{2} \left( \delta Z_{(2)}^{eL} + \delta Z_{(2)}^W + \delta Z_{(2)}^{\nu L} \right) \right. \\ &\quad \left. + (1\text{-loop renormalization constants}) \right]. \end{aligned} \quad (14)$$

$\delta Z^{W,eL,\nu L}$  denote the field-renormalization constants,  $\delta M_{W,Z}^2$  the  $W$ - and  $Z$ -mass counterterms, and  $\delta Z_e$  denotes the charge-renormalization constant. The lower indices in parentheses indicate the loop order. The mixing-angle counterterm  $\delta s_{W(2)}$  can be derived from the gauge-boson mass counterterms. The two-loop contributions always include the subloop renormalization.

The on-shell masses are defined as the position of the propagator poles. Starting at the two-loop level, it has to be taken into account that there is a difference between the definition of the mass  $\widetilde{M}^2$  as the pole of the real part of the (transverse) propagator,

$$\text{Re} \left\{ (D_{\text{T}})^{-1}(\widetilde{M}^2) \right\} = 0, \quad (15)$$

and the real part  $\overline{M}^2$  of the complex pole,

$$(D_{\text{T}})^{-1}(\mathcal{M}^2) = 0, \quad \mathcal{M}^2 = \overline{M}^2 - i\overline{M}\overline{\Gamma}. \quad (16)$$

The imaginary part of the complex pole is associated with the width  $\overline{\Gamma}$ . The defining condition (16) yields for the  $W$ -mass counterterm

$$\delta \overline{M}_{W(2)}^2 = \text{Re} \{ \Sigma_{\text{T}(2)}^W(\overline{M}_W^2) \} - \delta Z_{(1)}^W \delta \overline{M}_{W(1)}^2 + \text{Im} \{ \Sigma_{\text{T}(1)}^{W'}(\overline{M}_W^2) \} \text{Im} \{ \Sigma_{\text{T}(1)}^W(\overline{M}_W^2) \}, \quad (17)$$

whereas for the real-pole definition the last term of eq. (17) is missing.  $\Sigma_{\text{T}}^W$  denotes the transverse  $W$  self-energy and  $\Sigma_{\text{T}}^{W'}$  its momentum derivative. Similar expressions hold for the  $Z$  boson.

The  $W$  and  $Z$  mass counterterms determine the two-loop counterterm for the mixing angle,  $\delta s_{W(2)}$ , which has to be gauge invariant since  $s_W$  is an observable quantity. With the use of a general  $R_\xi$  gauge it has explicitly been checked that  $\delta s_{W(2)}$  is gauge-parameter independent for the complex-pole mass definition, whereas the real-pole definition leads to a gauge dependent  $\delta s_{W(2)}$ . This is in accordance with the expectation from  $S$ -matrix theory [32], where the complex pole represents a gauge-invariant mass definition.

It should be noted that the mass definition via the complex pole corresponds to a Breit-Wigner parameterization of the resonance shape with a constant width. For

the experimental determination of the gauge-boson masses, however, a Breit-Wigner ansatz with a running width is used. This has to be accounted for by a shift of the values for the complex pole masses [33],

$$\overline{M} = M - \frac{\Gamma^2}{2M}. \quad (18)$$

which yields the relations

$$\begin{aligned} \overline{M}_Z &= M_Z - 34.1 \text{ MeV}, \\ \overline{M}_W &= M_W - 27.4 (27.0) \text{ MeV} \quad \text{for} \quad M_W = 80.4 (80.2) \text{ GeV}. \end{aligned} \quad (19)$$

For  $M_Z$  and  $\Gamma_Z$  the experimental numbers are taken. The  $W$  mass is a calculated quantity, and therefore also a theoretical value for the  $W$ -boson width should be applied here. The results above are obtained from the approximate, but sufficiently accurate expression for the  $W$  width,

$$\Gamma_W = 3 \frac{G_F M_W^3}{2\sqrt{2}\pi} \left( 1 + \frac{2\alpha_s}{3\pi} \right). \quad (20)$$

## 5 Results

In the previous sections the characteristics of the calculation of electroweak two-loop contributions to  $\Delta r$  have been pointed out. Combining the fermionic  $\mathcal{O}(\alpha^2)$  contributions with the one-loop and the QCD corrections yields the total result

$$\Delta r = \Delta r^{(\alpha)} + \Delta r^{(\alpha\alpha_s)} + \Delta r^{(\alpha\alpha_s^2)} + \Delta r^{(N_f\alpha^2)} + \Delta r^{(N_f^2\alpha^2)}. \quad (21)$$

Here  $N_f, N_f^2$  symbolize one and two fermionic loops, respectively. Fig. 3 shows that both the QCD and electroweak two-loop corrections give sizeable contributions of 10–15% with respect to the one-loop result.

In Fig. 4 the prediction for  $M_W$  derived from the result (21) and the relation (3) is compared with the experimental value for  $M_W$ . Dotted lines indicate one standard deviation bounds. The main uncertainties of the prediction originate from the experimental errors of  $m_t = (174.3 \pm 5.1) \text{ GeV}$  [7] and  $\Delta\alpha = 0.05954 \pm 0.00065$  [34]. It is obvious that low Higgs masses are favored; the new results on  $\Delta r$  strengthen the tendency towards a lighter Higgs boson (according to the following comparison).

These results can be compared with the results obtained by expansion of the two-loop contributions up to next-to-leading order in  $m_t$  [15]. The predicted values for  $M_W$  for several values of  $M_H$  are given in Tab. 1. For the input parameters the values of [15] have been chosen, *i.e.*  $m_t = 175 \text{ GeV}$ ,  $M_Z = 91.1863 \text{ GeV}$ ,  $\Delta\alpha = 0.0594$ ,  $\alpha_s(M_Z) = 0.118$ . Agreement is found between the results with maximal deviations of less than 5 MeV in  $M_W$ . The deviations in the last column of Tab. 1 can of course not

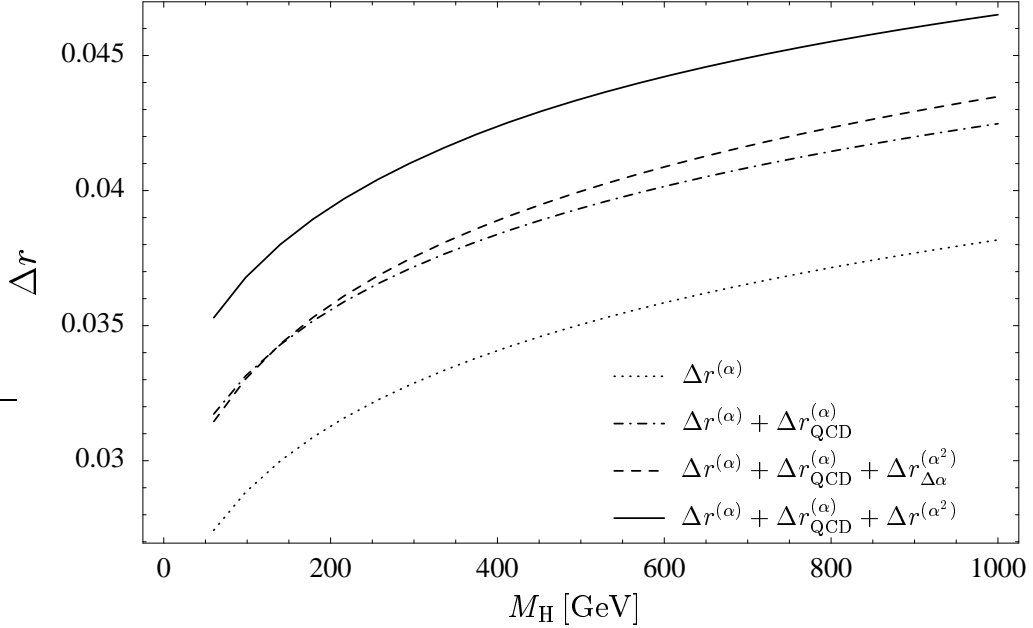


Figure 3: Various stages of  $\Delta r$ , as a function of  $M_H$ . The one-loop contribution,  $\Delta r^{(\alpha)}$ , is supplemented by the two-loop and three-loop QCD corrections,  $\Delta r_{\text{QCD}}^{(\alpha)} \equiv \Delta r^{(\alpha\alpha_s)} + \Delta r^{(\alpha\alpha_s^2)}$ , and the fermionic electroweak two-loop contributions,  $\Delta r^{(\alpha^2)} \equiv \Delta r^{(N_f\alpha^2)} + \Delta r^{(N_f^2\alpha^2)}$ . For comparison, the effect of the two-loop corrections induced by a resummation of  $\Delta\alpha$ ,  $\Delta r_{\Delta\alpha}^{(\alpha^2)}$ , is shown separately.

be attributed exclusively to differences in the two-loop top-quark and light-fermion contributions, because the results also differ by a slightly different treatment of those higher-order terms that are not yet under control, such as purely bosonic two-loop contributions, and effects from scheme dependence.

Similar to [35], a simple numerical parametrization of our result for  $M_W$  can be given by the following expression:

$$M_W = M_W^0 - c_1 dH - c_5 dH^2 + c_6 dH^4 - c_2 d\alpha + c_3 dt - c_7 dH dt - c_4 d\alpha_s, \quad (22)$$

where

$$dH = \ln\left(\frac{M_H}{100 \text{ GeV}}\right), \quad dt = \left(\frac{m_t}{174.3 \text{ GeV}}\right)^2 - 1, \\ d\alpha = \frac{\Delta\alpha}{0.05924} - 1, \quad d\alpha_s = \frac{\alpha_s(M_Z)}{0.119} - 1, \quad (23)$$

with the coefficients  $M_W^0 = 80.3767 \text{ GeV}$ ,  $c_1 = 0.05613$ ,  $c_2 = 1.081$ ,  $c_3 = 0.5235$ ,  $c_4 = 0.0763$ ,  $c_5 = 0.00936$ ,  $c_6 = 0.000546$ ,  $c_7 = 0.00573$ . and with  $M_Z = 91.1785 \text{ GeV}$ . The quality of the approximation (22) to our full result for  $M_W$  is within 0.4 MeV, allowing  $M_H$  between 65 GeV and 1 TeV.

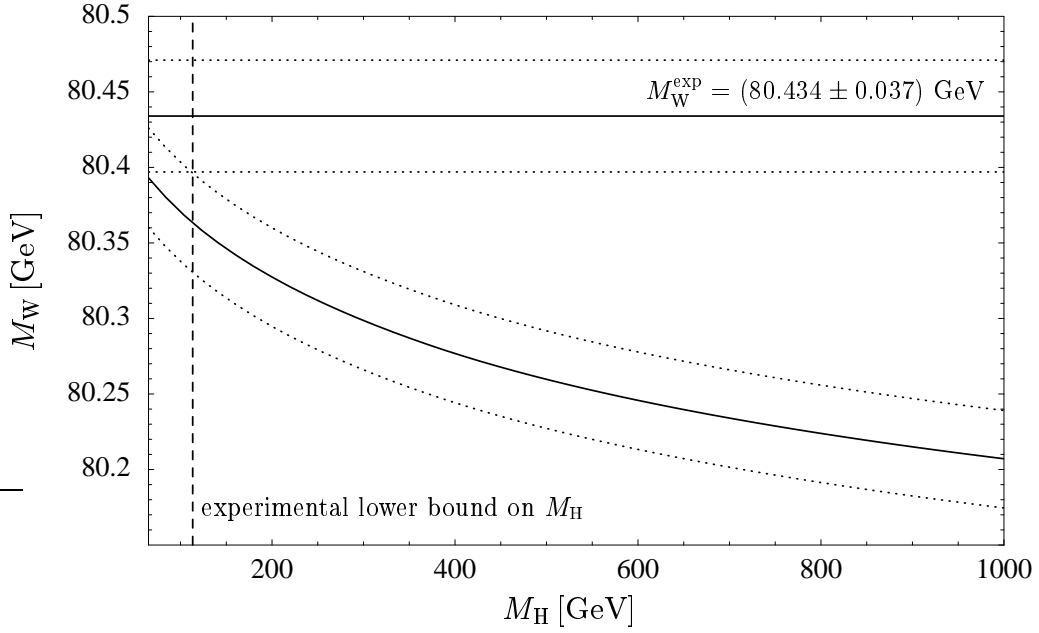


Figure 4: The SM prediction for  $M_W$  as a function of  $M_H$  for  $m_t = 174.3 \pm 5.1$  GeV is compared with the current experimental value,  $M_W^{\text{exp}} = 80.434 \pm 0.037$  GeV [1].

## 6 Conclusion

In this talk the realization of an exact two-loop calculation of fermionic contributions in the full electroweak SM and its application to the precise computation of  $\Delta r$  has been reviewed. Numerical illustrations were given for the results, which might serve as ingredients for future SM fits.

Table 1: Comparison between  $M_W$ -predictions from an NLO expansion in  $m_t$  ( $M_W^{\text{expa}}$ ) and the full calculation ( $M_W^{\text{full}}$ ).  $\delta M_W$  denotes the difference.

$M_H$ [GeV]	$M_W^{\text{expa}}$ [GeV]	$M_W^{\text{full}}$ [GeV]	$\delta M_W$ [MeV]
65	80.4039	80.3997	4.2
100	80.3805	80.3771	3.4
300	80.3061	80.3051	1.0
600	80.2521	80.2521	0.0
1000	80.2129	80.2134	-0.5

## Acknowledgments

This work was supported by the Deutsche Forschungsgemeinschaft (Forschergruppe “Quantenfeldtheorie, Computeralgebra und Monte Carlo Simulation”) and by the European Union (HPRN-CT-2000-00149).

## References

- [1] A. Gurtu, Plenary Talk at *XXXth International Conference on High Energy Physics*, Osaka (Japan) 2000;  
B. Pietrzyk, Talk at *XXXth International Conference on High Energy Physics*, Osaka (Japan) 2000.
- [2] ATLAS Collaboration, “Detector and Physics Performance Technical Design Report”, CERN/LHCC/99-15 (1999);  
CMS Collaboration, Technical Design Reports, CMS TDR 1–5 (1997/98);  
S. Haywood et al., *Electroweak physics*, hep-ph/0003275, in *Proceedings of the Workshop on Standard Model Physics (and more) at the LHC*, eds. G. Altarelli and M.L. Mangano (Report CERN 2000–004).
- [3] G. Wilson, Proceedings of the *Worldwide Study on Physics and Experiments with Future Linear  $e^+e^-$  Colliders*, Sitges 1999 (p. 411), eds. E. Fernández and A. Pacheco, Universitat Autònoma Barcelona 2000.
- [4] S. Heinemeyer, Th. Mannel and G. Weiglein, DESY 99-117, hep-ph/9909538, Proceedings of the *Worldwide Study on Physics and Experiments with Future Linear  $e^+e^-$  Colliders*, Sitges 1999 (p. 417), eds. E. Fernández and A. Pacheco, Universitat Autònoma Barcelona 2000;  
J. Erler, S. Heinemeyer, W. Hollik, G. Weiglein and P.M. Zerwas, *Phys. Lett.* **B486** (2000) 125.
- [5] R.E. Behrends, R.J. Finkelstein and A. Sirlin, *Phys. Rev.* **101** (1956) 866;  
S.M. Berman, *Phys. Rev.* **112** (1958) 267;  
T. Kinoshita and A. Sirlin, *Phys. Rev.* **113** (1959) 1652.
- [6] T. van Ritbergen and R.G. Stuart, *Phys. Rev. Lett.* **82** (1999) 488; *Nucl. Phys.* **B564** (2000) 343;  
M. Steinhauser and T. Seidensticker, *Phys. Lett.* **B467** (1999) 271.
- [7] Particle Data Group, *Eur. Jour. Phys.* **C15** (2000) 1.
- [8] A. Sirlin, *Phys. Rev.* **D22** (1980) 971;  
W.J. Marciano and A. Sirlin, *Phys. Rev.* **D22** (1980) 2695.

- [9] M. Veltman, *Nucl. Phys.* **B123** (1977) 89.
- [10] W.J. Marciano, *Phys. Rev.* **D20** (1979) 274;  
A. Sirlin, *Phys. Rev.* **D29** (1984) 89;  
M. Consoli, W. Hollik and F. Jegerlehner, *Phys. Lett.* **B227** (1989) 167.
- [11] A. Djouadi and C. Verzegnassi, *Phys. Lett.* **B195** (1987) 265;  
A. Djouadi, *Nuovo Cimento* **A100** (1988) 357;  
B.A. Kniehl, *Nucl. Phys.* **B347** (1990) 89;  
F. Halzen and B.A. Kniehl, *Nucl. Phys.* **B353** (1991) 567;  
B.A. Kniehl and A. Sirlin, *Nucl. Phys.* **B371** (1992) 141, *Phys. Rev.* **D47** (1993) 883;  
A. Djouadi and P. Gambino, *Phys. Rev.* **D49** (1994) 3499.
- [12] L. Avdeev, J. Fleischer, S.M. Mikhailov and O. Tarasov, *Phys. Lett.* **B336** (1994) 560; E: *Phys. Lett.* **B349** (1995) 597;  
K. Chetyrkin, J. Kühn and M. Steinhauser, *Phys. Lett.* **B351** (1995) 331; *Phys. Rev. Lett.* **75** (1995) 3394.
- [13] J. van der Bij and F. Hoogeveen, *Nucl. Phys.* **B283** (1987) 477;  
J. van der Bij and M. Veltman, *Nucl. Phys.* **B231** (1984) 205.
- [14] J. van der Bij and F. Hoogeveen, *Nucl. Phys.* **B283** (1987) 477;  
R. Barbieri, M. Beccaria, P. Ciafaloni, G. Curci and A. Vicere, *Phys. Lett.* **B288** (1992) 95, E: *Phys. Lett.* **B312** (1993) 511; *Nucl. Phys.* **B409** (1993) 105;  
J. Fleischer, O.V. Tarasov and F. Jegerlehner, *Phys. Lett.* **B319** (1993) 249; *Phys. Rev.* **D51** (1995) 3820.
- [15] G. Degrassi, P. Gambino and A. Vicini, *Phys. Lett.* **B383** (1996) 219;  
G. Degrassi, P. Gambino and A. Sirlin, *Phys. Lett.* **B394** (1997) 188.
- [16] J. van der Bij, K. Chetyrkin, M. Faisst, G. Jikia, T. Seidensticker, hep-ph/0011373.
- [17] S. Bauberger and G. Weiglein, *Phys. Lett.* **B419** (1998) 333;  
G. Weiglein, hep-ph/9901317, in *Proceedings of the IVth International Symposium on Radiative Corrections*, ed. J. Solà (World Scientific, Singapore, 1999), p. 410.
- [18] P. Gambino, A. Sirlin and G. Weiglein, *JHEP* **04** (1999) 025.
- [19] G. Weiglein, *Acta Phys. Pol.* **B29** (1998) 2735;  
A. Stremplat, Diploma thesis (Univ. of Karlsruhe, 1998).

- [20] A. Freitas, W. Hollik, W. Walter, G. Weiglein, *Phys. Lett.* **B495** (2000) 338;  
A. Freitas, S. Heinemeyer, W. Hollik, W. Walter, G. Weiglein, *Nucl. Phys. Proc. Suppl.* **89** (2000) 82.
- [21] P. Malde and R.G. Stuart, *Nucl. Phys.* **B552** (1999) 41.
- [22] J. Küblbeck, M. Böhm and A. Denner, *Comput. Phys. Commun.* **60** (1990) 165;  
H. Eck and J. Küblbeck, *Guide to FeynArts1.0* (Univ. of Würzburg, 1992);  
T. Hahn, KA-TP-5-1999, hep-ph/9905354; KA-TP-23-2000, hep-ph/0012260;  
*FeynArts2.2 User's Guide* (Univ. of Karlsruhe, 2000).
- [23] G. Weiglein, R. Scharf and M. Böhm, *Nucl. Phys.* **B416** (1994) 606;  
G. Weiglein, R. Mertig, R. Scharf and M. Böhm, in *New Computing Techniques in Physics Research 2*, ed. D. Perret-Gallix (World Scientific, Singapore, 1992), p. 617.
- [24] G. 't Hooft and M. Veltman, *Nucl. Phys.* **B153** (1979) 365.
- [25] A.I. Davydychev and J.B. Tausk, *Nucl. Phys.* **B397** (1993) 123.
- [26] S. Bauberger, F.A. Berends, M. Böhm and M. Buza, *Nucl. Phys.* **B434** (1995) 383;  
S. Bauberger, F.A. Berends, M. Böhm, M. Buza and G. Weiglein, *Nucl. Phys. B (Proc. Suppl.)* **37B** (1994) 95, hep-ph/9406404;  
S. Bauberger and M. Böhm, *Nucl. Phys.* **B445** (1995) 25.
- [27] G. 't Hooft and M. Veltman, *Nucl. Phys.* **B44** (1972) 189.
- [28] P. Breitenlohner and D. Maison, *Commun. Math. Phys.* **52** (1977) 11.
- [29] D. J. Gross und R. Jackiw, *Phys. Rev.* **D6** (1972) 477;  
G. Costa, T. Marinucci, M. Tonin, J. Julve, *Nuovo Cimento* **A38** (1977) 373.
- [30] F. Jegerlehner, DESY 00-075, hep-th/0005255;  
P.A. Grassi, T. Hurth and M. Steinhauser, BUTP-99-13, hep-ph/9907426.
- [31] A. Denner, *Fortschr. Phys.* **41** (1993) 307.
- [32] A. Sirlin, *Phys. Rev. Lett.* **67** (1991) 2127;  
R.G. Stuart, *Phys. Lett.* **B262** (1991) 113;  
S. Willenbrock and G. Valencia, *Phys. Lett.* **B259** (1991) 373;  
H. Veltman, *Z. Phys.* **C62** (1994) 35;  
M. Passera and A. Sirlin, *Phys. Rev.* **D58** (1998) 113010;  
P. Gambino and P.A. Grassi, TUM-HEP-352/99, hep-ph/9907254;  
A.R. Bohm and N.L. Harshman, hep-ph/0001206.

- [33] D. Bardin, A. Leike, T. Riemann and M. Sachwitz, *Phys. Lett.* **B206** (1988) 539.
- [34] S. Eidelman and F. Jegerlehner, *Z. Phys.* **C67** (1995) 585.
- [35] G. Degrassi, P. Gambino, M. Passera and A. Sirlin, *Phys. Lett.* **B418** (1998) 209.

# Leading electroweak logarithms at one loop

ANSGAR DENNER

*Paul Scherrer Institut, CH-5232 Villigen PSI, Switzerland*

STEFANO POZZORINI

*Institute of Theoretical Physics, University of Zürich, Switzerland*

*and*

*Paul Scherrer Institut, CH-5232 Villigen PSI, Switzerland*

We summarize results for the complete one-loop electroweak logarithmic corrections for general processes at high energies and fixed angles. Our results are applicable to arbitrary matrix elements that are not mass-suppressed. We give explicit results for W-boson-pair production in  $e^+e^-$  annihilation.

Presented at the

5th International Symposium on Radiative Corrections  
(RADCOR-2000)  
Carmel CA, USA, 11–15 September, 2000

# 1 Introduction

Future colliders, such as the LHC [1] or an  $e^+e^-$  linear collider (LC) [2], will explore the energy range  $\sqrt{s} \gg M_Z$ . It is known since many years (see, for instance, Refs. [3,4]) that above the electroweak scale the structure of the leading electroweak corrections changes and double logarithms of Sudakov type [5] as well as single logarithms involving the ratio of the energy to the electroweak scale become dominating. These logarithms arise from virtual (or real) gauge bosons emitted by the initial and final-state particles. They correspond to the well-known soft and collinear singularities observed in QCD.

In the electroweak theory, unlike in massless gauge theories, the large logarithms originating from virtual corrections are of physical significance. In fact, real Z-boson and W-boson bremsstrahlung need not be included, since the masses of the weak gauge bosons, Z and W, provide a physical cutoff, and the massive gauge bosons can be detected as distinguished particles.

The typical size of double-logarithmic (DL) and single-logarithmic (SL) corrections is given by

$$\frac{\alpha}{4\pi s_w^2} \log^2 \frac{s}{M_W^2} = 6.6\%, \quad \frac{\alpha}{4\pi s_w^2} \log \frac{s}{M_W^2} = 1.3\% \quad (1.1)$$

at  $\sqrt{s} = 1$  TeV and increases with energy. If the experimental precision is at the few-percent level like at the LHC, both DL and SL electroweak contributions have to be included at the one-loop level. In view of the precision objectives of a LC, between the percent and the permil level, besides the complete one-loop corrections also two-loop DL effects have to be taken into account.

Owing to this phenomenological relevance, the infrared (IR) structure of the electroweak theory is receiving increasing interest recently. The one-loop structure and the origin of the DL corrections have been discussed for  $e^+e^- \rightarrow f\bar{f}$  [6,7] and are by now well established. Recipes for the resummation of the DL corrections have been developed [8,7,9,10] and explicit calculations of the leading DL corrections for the processes  $g \rightarrow f\bar{f}$  and  $e^+e^- \rightarrow f\bar{f}$  have been performed [11,12,13]. On the other hand, for the SL corrections complete one-loop calculations are only available for 4-fermion neutral-current processes [14,9] and W-pair production [4]. The subleading two-loop logarithmic corrections have been evaluated for  $e^+e^- \rightarrow f\bar{f}$  in Ref. [9]. A general recipe for a subclass of SL corrections to all orders has been proposed in Ref. [15], based on the infrared-evolution-equation method.

Here, we summarize the results for all DL and SL contributions to the electroweak one-loop virtual corrections published in Ref. [16]. The results apply to exclusive processes with arbitrary external states, including transverse and longitudinal gauge bosons as well as Higgs fields.

The paper is organized as follows: in Section 2 we introduce our notations and discuss the origin of the leading electroweak logarithms. The leading logarithms orig-

inating from the soft–collinear region, from the soft or collinear regions, and from parameter renormalization are considered in Sections 3, 4, and 5, respectively. In Section 6 we apply our general results to W-boson-pair production in  $e^+e^-$  annihilation.

## 2 Form and origin of enhanced logarithmic corrections

We consider electroweak processes involving  $n$  arbitrary incoming<sup>1</sup> particles (or antiparticles) associated to the fields  $\varphi_{i_k}$ ,

$$\varphi_{i_1}(p_1) \dots \varphi_{i_n}(p_n) \rightarrow 0. \quad (2.1)$$

The indices  $i_k$  correspond to the reducible representation of  $SU(2) \times U(1)$  including all fields in the standard model, and we restrict ourselves to Born matrix elements  $\mathcal{M}_0^{i_1 \dots i_n}(p_1, \dots, p_n)$  that are not suppressed in the limit where all invariants are much larger than the gauge-boson masses,

$$r_{kl} := (p_k + p_l)^2 \sim 2p_k p_l \gg M_W^2. \quad (2.2)$$

In the high-energy limit (2.2), we split all enhanced DL and SL corrections into a “symmetric electroweak” (ew) part given by logarithms of the ratio between the energy and the electroweak scale (1.1) and a remaining part that we denote as “pure electromagnetic contribution” (em), which involves logarithms of the light-fermion masses and the infinitesimal photon mass  $\lambda$  used to regularize IR singularities. For the symmetric electroweak logarithms we introduce the shorthands

$$L(s) := \frac{\alpha}{4\pi} \log^2 \frac{s}{M_W^2}, \quad l(s) := \frac{\alpha}{4\pi} \log \frac{s}{M_W^2}. \quad (2.3)$$

We assume that the masses  $M_H$ ,  $m_t$ ,  $M_Z$ , and  $M_W$  have the same order of magnitude and neglect all logarithms of ratios of these masses.

In logarithmic approximation (LA) the one-loop corrections to (2.1) assume the form

$$\delta \mathcal{M}^{i_1 \dots i_n}(p_1, \dots, p_n) = \mathcal{M}_0^{i'_1 \dots i'_n}(p_1, \dots, p_n) \delta_{i'_1 i_1 \dots i'_n i_n}, \quad (2.4)$$

i.e. they factorize into the lowest-order matrix element times an  $SU(2) \times U(1)$  matrix. For matrix elements that are not mass-suppressed the factorization formula is universal. The matrix  $\delta_{i'_1 i_1 \dots i'_n i_n}$  can be expressed using the couplings  $ieI^{V_a}(\varphi)$  of the external fields  $\varphi_{i_k}$  to the gauge bosons  $V_a$ . These correspond to the generators of infinitesimal global  $SU(2) \times U(1)$  transformations of these fields,<sup>2</sup>

$$\delta_{V_a} \varphi_i = ieI_{\varphi_i \varphi_{i'}}^{V_a}(\varphi) \varphi_{i'}. \quad (2.5)$$

<sup>1</sup>Usual scattering processes are obtained by crossing symmetry

<sup>2</sup>Details about the explicit form of the generators and other group theoretical quantities can be found in the appendix of Ref. [16].

In terms of the electric charge  $Q$  and weak isospin  $T^a$  they are given by

$$I^A = -Q, \quad I^Z = \frac{T^3 - s_w^2 Q}{s_w c_w}, \quad I^\pm = \frac{T^1 \pm iT^2}{\sqrt{2}s_w} \quad (2.6)$$

and depend on the weak mixing angle, which is fixed by  $c_w^2 = 1 - s_w^2 = M_W^2/M_Z^2$ .

In general, large logarithms contributing to (2.4) are shared between the loop diagrams and the coupling- and field-renormalization constants, depending on the gauge-fixing and the renormalization scheme. We work within the 't Hooft–Feynman gauge and adopt the on-shell scheme [17] for field and parameter renormalization. We use dimensional regularization and choose the regularization scale  $\mu^2 = s$  so that the logarithms  $\log(\mu^2/s)$  related to the UV singularities are not enhanced, and only the mass-singular logarithms  $\log(\mu^2/M^2)$  or  $\log(s/M^2)$  are large. In this setup large logarithms are distributed as follows:

- The DL contributions originate from those one-loop diagrams where soft–collinear gauge bosons are exchanged between pairs of external legs. These double logarithms are obtained with the eikonal approximation.
- The SL mass-singular contributions from loop diagrams originate from the emission of virtual collinear gauge bosons from external lines [18]. These SL contributions are extracted from the loop diagrams in the collinear limit by means of Ward identities, and are found to factorize into the Born amplitude times “collinear factors” [19].
- The remaining SL contributions originating from soft and collinear regions are contained in the field renormalization constants (FRCs).
- The parameter renormalization (PR) constants, i.e. the charge- and weak-mixing-angle renormalization constants, as well as the renormalization of dimensionless mass ratios associated with the Yukawa and the scalar self-couplings, involve the SL contributions of UV origin. These are the logarithms that are controlled by the renormalization group.

The DL and SL mass-singular terms are extracted from loop diagrams by setting all masses to zero in the numerators of the loop-integrals. For processes involving external longitudinal gauge bosons, this approach is not directly applicable, owing to the longitudinal polarization vectors

$$\epsilon_L^\mu(p) = \frac{p^\mu}{M} + \mathcal{O}\left(\frac{M}{p^0}\right), \quad (2.7)$$

which are inversely proportional to the gauge boson mass. However, since we are only interested in the high-energy limit, we can use the Goldstone-boson equivalence theorem [20] taking into account the correction factors from higher-order contributions [21].

### 3 Soft-collinear contributions

The DL corrections originate from loop diagrams where virtual gauge bosons  $V_a = A, Z, W^\pm$  are exchanged between pairs of external legs (Figure 1), and arise from the integration region where the gauge-boson momenta are soft and collinear to one of the external legs. They are obtained using the eikonal approximation, and result in a double sum over pairs of external legs

$$\delta^{\text{DL}} \mathcal{M}^{i_1 \dots i_n} = \frac{\alpha}{8\pi} \sum_{k=1}^n \sum_{l \neq k} \sum_{V_a=A, Z, W^\pm} I_{i'_k i_k}^{V_a}(k) I_{i'_l i_l}^{\bar{V}_a}(l) \mathcal{M}_0^{i_1 \dots i'_k \dots i'_l \dots i_n} \times \left[ \log^2 \left( \frac{|r_{kl}|}{M_{V_a}^2} \right) - \delta_{V_a A} \log^2 \left( \frac{m_k^2}{\lambda^2} \right) \right], \quad (3.1)$$

where  $\bar{V}_a$  represents the charge conjugated of  $V_a$ . Formula (3.1) applies to chiral fermions, Higgs bosons, and transverse gauge bosons and depends on their gauge couplings  $I^{V_a}(k)$ . The DL corrections for external longitudinal gauge bosons  $Z_L$  and  $W_L^\pm$  are obtained from the corrections (3.1) for the corresponding external would-be Goldstone bosons  $\chi$  and  $\phi^\pm$ , respectively, using the equivalence theorem

$$\begin{aligned} \delta^{\text{DL}} \mathcal{M} \dots W_L^\pm \dots &= \delta^{\text{DL}} \mathcal{M} \dots \phi^\pm \dots, \\ \delta^{\text{DL}} \mathcal{M} \dots Z_L \dots &= i \delta^{\text{DL}} \mathcal{M} \dots \chi \dots. \end{aligned} \quad (3.2)$$

#### Leading soft-collinear contributions

The DL term in (3.1) containing the invariant  $r_{kl}$  depends on the angle between the momenta  $p_k$  and  $p_l$ . Writing

$$\log^2 \left( \frac{|r_{kl}|}{M^2} \right) = \log^2 \left( \frac{s}{M^2} \right) + 2 \log \left( \frac{s}{M^2} \right) \log \left( \frac{|r_{kl}|}{s} \right) + \log^2 \left( \frac{|r_{kl}|}{s} \right), \quad (3.3)$$

one can isolate an angular-independent part proportional to  $L(s)$ , and this part, together with the additional contributions from photon loops in (3.1), gives the leading

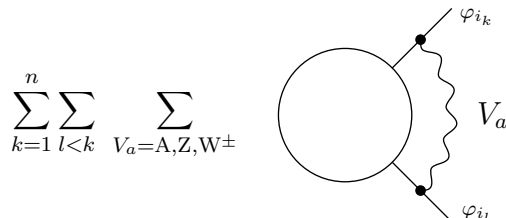


Figure 1: Feynman diagrams leading to DL corrections

soft-collinear (LSC) contribution. Using the invariance of the  $S$  matrix with respect to global  $SU(2) \times U(1)$  transformations, the LSC contribution in (3.1) can be written as a single sum over external legs,

$$\delta^{\text{LSC}} \mathcal{M}^{i_1 \dots i_n} = \sum_{k=1}^n \delta_{i'_k i_k}^{\text{LSC}}(k) \mathcal{M}_0^{i_1 \dots i'_k \dots i_n}, \quad (3.4)$$

where the correction factors reads

$$\delta_{i'_k i_k}^{\text{LSC}}(k) = -\frac{1}{2} \left[ C_{i'_k i_k}^{\text{ew}}(k) L(s) + \delta_{i'_k i_k} Q_k^2 L^{\text{em}}(s, \lambda^2, m_k^2) \right]. \quad (3.5)$$

The first term represents the DL symmetric-electroweak part and is proportional to the effective electroweak Casimir operator<sup>3</sup>

$$C^{\text{ew}} := \sum_{V_a=A,Z,W^\pm} I^{V_a} I^{\bar{V}_a} = \frac{1}{c_w^2} \left( \frac{Y}{2} \right)^2 + \frac{1}{s_w^2} C^{\text{SU}(2)}, \quad (3.6)$$

which depends on the weak hypercharge  $Y = 2(Q - T^3)$  and the  $SU(2)$  Casimir operator  $C^{\text{SU}(2)}$ . The second term in (3.5) originates from photon loops and reads

$$L^{\text{em}}(s, \lambda^2, m_k^2) := 2l(s) \log \left( \frac{M_W^2}{\lambda^2} \right) + \frac{\alpha}{4\pi} \left[ \log^2 \frac{M_W^2}{\lambda^2} - \log^2 \frac{m_k^2}{\lambda^2} \right]. \quad (3.7)$$

### Subleading soft-collinear contributions

The remaining part of (3.1) is a subleading soft-collinear (SSC) contribution,

$$\delta^{\text{SSC}} \mathcal{M}^{i_1 \dots i_n} = \sum_{k=1}^n \sum_{l < k} \sum_{V_a=A,Z,W^\pm} \delta_{i'_k i_k i'_l i_l}^{V_a, \text{SSC}}(k, l) \mathcal{M}_0^{i_1 \dots i'_k \dots i'_l \dots i_n}. \quad (3.8)$$

This remains a sum over pairs of external legs with angular-dependent factors<sup>4</sup>

$$\delta_{i'_k i_k i'_l i_l}^{V_a, \text{SSC}}(k, l) = \left[ 2l(s) + \delta_{V_a A} \frac{\alpha}{2\pi} \log \frac{M_W^2}{\lambda^2} \right] \log \frac{|r_{kl}|}{s} I_{i'_k i_k}^{V_a}(k) I_{i'_l i_l}^{\bar{V}_a}(l). \quad (3.9)$$

Owing to the non-diagonal matrices  $I^\pm(k)$  (cf. appendix of Ref. [16]), the exchange of soft charged gauge bosons involves  $SU(2)$ -transformed Born matrix elements on the right-hand side of (3.8).

<sup>3</sup> As explained in Ref. [16] care must be taken for reducible representations, where owing to mixing, (3.6) can be non-diagonal.

<sup>4</sup> Double logarithms of  $r_{kl}/s$  are neglected in the limit (2.2).

## 4 Collinear and soft single logarithms

The collinear and soft SL corrections originate from field renormalization and from mass-singular loop diagrams. On one hand the FRCs give the well-known factors  $\delta Z_\varphi/2$  for each external leg, containing collinear as well as soft SL contributions. On the other hand, mass-singular logarithms arise from the collinear limit of loop diagrams where an external line splits into two internal lines [18], one of these internal lines being a virtual gauge boson A, Z, or W. Both contributions factorize as a sum over the external legs,

$$\delta^C \mathcal{M}^{i_1 \dots i_n} = \sum_{k=1}^n \delta_{i'_k i_k}^C(k) \mathcal{M}_0^{i_1 \dots i'_k \dots i_n} \quad (4.1)$$

with

$$\delta_{i'_k i_k}^C(k) = \frac{1}{2} \delta Z_{i'_k i_k}^\varphi + \delta_{i'_k i_k}^{\text{coll}}(k) \Big|_{\mu^2=s}. \quad (4.2)$$

The factorization of the mass-singular loop diagrams will be presented in a forthcoming publication [19]. Therein, we derive the factorization identities

$$\sum_{V_a=A,Z,W^\pm} \left\{ \begin{array}{c} \text{Diagram 1: } \varphi_{i_k} \text{ line splits into } \varphi_{i'_k} \text{ and } V_a \text{ into a loop} \\ \text{Diagram 2: } \varphi_{i_k} \text{ line splits into } \varphi_{i'_k} \text{ and } V_a \text{ into a loop} \end{array} \right\} - \sum_{l \neq k} \left[ \begin{array}{c} \text{Diagram 3: } \varphi_{i_k} \text{ and } \varphi_{i_l} \text{ lines split into } \varphi_{i'_k} \text{ and } V_a \text{ into a loop} \\ \text{Diagram 4: } \varphi_{i_k} \text{ and } \varphi_{i_l} \text{ lines split into } \varphi_{i'_k} \text{ and } V_a \text{ into a loop} \end{array} \right] \Big|_{\text{eik. appr.}} \Big|_{\text{coll.}} = \sum_{\varphi_{i'_k}} \varphi_{i'_k} \text{ loop} \delta_{\varphi_{i'_k} \varphi_{i_k}}^{\text{coll}}. \quad (4.3)$$

for fermions, gauge bosons and scalar bosons. These identities are obtained by evaluation of the loop diagrams involving the collinear splitting processes  $\varphi_{i_k}(p) \rightarrow V^a(q) \varphi_{i'_k}(p-q)$ , after subtraction of the contributions already contained in the FRCs and the soft collinear corrections. In the limit of collinear gauge-boson emission, the left-hand side of (4.3) is proportional to

$$\sum_{V_a, \varphi_{i'_k}} \int \frac{dq^D}{(2\pi)^D} \frac{-ie I_{\varphi_{i'_k} \varphi_{i_k}}^{\bar{V}^a} q^\mu}{(q^2 - M_{V_a}^2)[(p-q)^2 - M_{\varphi_{i'_k}}^2]} \times \left\{ \begin{array}{c} \text{Diagram 5: } \varphi_{i'_k}(p-q) \text{ line splits into } \varphi_{i'_k} \text{ and } V_\mu^a(q) \text{ into a loop} \\ \text{Diagram 6: } \varphi_{i'_k}(p-q) \text{ line splits into } \varphi_{i'_k} \text{ and } V_\mu^a(q) \text{ into a loop} \end{array} \right\}, \quad (4.4)$$



$A, Z, W^\pm$  these coefficients generalize to a matrix  $b_{ab}^{\text{ew}}$  in the adjoint representation (cf. appendix of Ref. [16]). The charged component reads

$$b_{W^\sigma W^{\sigma'}}^{\text{ew}} = \delta_{\sigma\sigma'} \frac{19}{6s_w^2}, \quad (4.9)$$

and determines the running of the SU(2) gauge coupling. In the neutral sector we have

$$b_{AA}^{\text{ew}} = -\frac{11}{3}, \quad b_{AZ}^{\text{ew}} = b_{ZA}^{\text{ew}} = -\frac{19 + 22s_w^2}{6s_w c_w}, \quad b_{ZZ}^{\text{ew}} = \frac{19 - 38s_w^2 - 22s_w^4}{6s_w^2 c_w^2}. \quad (4.10)$$

The  $AA$  component determines the running of the electric charge, and the  $AZ$  component is associated with the running of the weak mixing angle [cf. (5.3)]. The SL corrections for transverse gauge bosons are given by

$$\delta_{V_a V_b}^{\text{C}}(V_{\text{T}}) = \frac{1}{2} \left[ b_{V_a V_b}^{\text{ew}} + E_{V_a V_b} b_{AZ}^{\text{ew}} \right] l(s) + \delta_{V_a V_b} Q_{V_a}^2 l^{\text{em}}(M_{\text{W}}^2) - \frac{1}{2} \delta_{V_a A} \delta_{V_b A} \Delta\alpha(M_{\text{W}}^2). \quad (4.11)$$

The first term corresponds to the result for a symmetric massless gauge theory like QCD (see for instance Ref. [22]). The second term is proportional to the antisymmetric matrix  $E_{V_a V_b}$ , with non-vanishing components  $E_{AZ} = -E_{ZA} = 1$ . This term results from the on-shell renormalization condition [17] and ensures that the correction factor for external photons does not involve mixing with Z bosons,

$$\delta_{ZA}^{\text{C}}(V_{\text{T}}) = 0. \quad (4.12)$$

The third term in (4.11) represents an electromagnetic contribution for charged external gauge bosons. Finally, the  $AA$  component receives a pure electromagnetic contribution associated with the light-fermion loops,

$$\Delta\alpha(M_{\text{W}}^2) = \frac{\alpha}{3\pi} \sum_{f,i,\sigma \neq t} N_{\text{C}}^f Q_{f\sigma}^2 \log \frac{M_{\text{W}}^2}{m_{f\sigma,i}^2} \quad (4.13)$$

where the sum runs over the generations  $i = 1, 2, 3$  of leptons and quarks  $f = l, q$  with isospin  $\sigma$  and colour factor  $N_{\text{C}}^f$ , omitting the top-quark contribution.

### Longitudinally polarized gauge bosons Z, $W^\pm$

The mass singular corrections for external longitudinal gauge bosons Z,  $W^\pm$ , are obtained from the corrections for the corresponding would-be Goldstone bosons  $\chi$ ,  $\phi^\pm$  using the equivalence theorem. For renormalized amputated Green functions we have the relations

$$\begin{aligned} p^\mu \langle W_\mu^\pm(p) \dots \rangle &= \pm M_{\text{W}} (1 + \delta C_\phi) \langle \phi_0^\pm(p) \dots \rangle, \\ p^\mu \langle Z_\mu(p) \dots \rangle &= i M_{\text{Z}} (1 + \delta C_\chi) \langle \chi_0(p) \dots \rangle. \end{aligned} \quad (4.14)$$

Besides the lowest-order contribution, (4.14) contains non-trivial higher-order corrections owing to the mixing between gauge bosons and would-be Goldstone bosons [21]. These corrections correspond to the FRC's for would-be Goldstone bosons in (4.2), and combining them with the collinear factors for would-be Goldstone bosons one obtains

$$\begin{aligned}\delta_{\phi^\pm\phi^\pm}^{\text{C}}(\Phi) &= \delta C_\phi + \delta_{\phi^\pm\phi^\pm}^{\text{coll}}(\Phi) = \left[2C_\Phi^{\text{ew}} - \frac{3}{4s_w^2} \frac{m_t^2}{M_W^2}\right] l(s) + Q_W^2 l^{\text{em}}(M_W^2), \\ \delta_{\chi\chi}^{\text{C}}(\Phi) &= \delta C_\chi + \delta_{\chi\chi}^{\text{coll}}(\Phi) = \left[2C_\Phi^{\text{ew}} - \frac{3}{4s_w^2} \frac{m_t^2}{M_W^2}\right] l(s).\end{aligned}\tag{4.15}$$

The result is written in terms of the eigenvalue of  $C^{\text{ew}}$  for the scalar doublet  $\Phi$  and contains large Yukawa contributions.

### Higgs bosons

The SL corrections (4.2) for Higgs bosons read

$$\delta_{HH}^{\text{C}}(\Phi) = \left[2C_\Phi^{\text{ew}} - \frac{3}{4s_w^2} \frac{m_t^2}{M_W^2}\right] l(s).\tag{4.16}$$

Note that up to pure electromagnetic contributions, longitudinal gauge bosons and Higgs bosons receive the same collinear SL corrections.

## 5 Logarithms connected to parameter renormalization

The logarithms related to UV divergences originate from the renormalization of the dimensionless parameters

$$e, \quad c_w = \frac{M_W}{M_Z}, \quad h_t = \frac{m_t}{M_W}, \quad h_H = \frac{M_H^2}{M_W^2},\tag{5.1}$$

i.e. the electric charge, the weak mixing angle, and the dimensionless mass ratios related to the top-quark Yukawa coupling and to the scalar self-coupling, respectively. These SL corrections determine the running of the couplings, and in one-loop approximation they are obtained from the Born matrix element  $\mathcal{M}_0 = \mathcal{M}_0(e, c_w, h_t, h_H)$  in the high-energy limit by

$$\delta^{\text{PR}} \mathcal{M} = \frac{\delta \mathcal{M}_0}{\delta e} \delta e + \frac{\delta \mathcal{M}_0}{\delta c_w} \delta c_w + \frac{\delta \mathcal{M}_0}{\delta h_t} \delta h_t + \frac{\delta \mathcal{M}_0}{\delta h_H} \delta h_H^{\text{eff}} \Big|_{\mu^2=s}.\tag{5.2}$$

The contribution from the tadpole renormalization to the renormalization of the scalar self-coupling (cf. Ref. [23]) is included in the effective counterterm  $\delta h_{\text{H}}^{\text{eff}}$ . In the on-shell scheme (and in LA) the counterterms read

$$\begin{aligned}
\frac{\delta c_{\text{w}}^2}{c_{\text{w}}^2} &= \frac{s_{\text{w}}}{c_{\text{w}}} b_{AZ}^{\text{ew}} l(\mu^2), & \frac{\delta e^2}{e^2} &= -b_{AA}^{\text{ew}} l(\mu^2) + \Delta\alpha(M_{\text{W}}^2), \\
\frac{\delta h_{\text{t}}}{h_{\text{t}}} &= \left\{ \frac{1}{2} b_{WW}^{\text{ew}} - \frac{3}{2} (C_{\text{tR}}^{\text{ew}} + C_{\text{tL}}^{\text{ew}}) + \frac{9}{8s_{\text{w}}^2} \frac{m_{\text{t}}^2}{M_{\text{W}}^2} \right\} l(\mu^2), \\
\frac{\delta h_{\text{H}}^{\text{eff}}}{h_{\text{H}}} &= \left\{ b_{WW}^{\text{ew}} + \frac{3}{2s_{\text{w}}^2} \left[ \frac{M_{\text{W}}^2}{M_{\text{H}}^2} \left( 2 + \frac{1}{c_{\text{w}}^4} \right) - \left( 2 + \frac{1}{c_{\text{w}}^2} \right) + \frac{M_{\text{H}}^2}{M_{\text{W}}^2} \right] \right. \\
&\quad \left. + \frac{3}{s_{\text{w}}^2} \frac{m_{\text{t}}^2}{M_{\text{W}}^2} \left( 1 - 2 \frac{m_{\text{t}}^2}{M_{\text{H}}^2} \right) \right\} l(\mu^2).
\end{aligned} \tag{5.3}$$

In the case of processes with longitudinal gauge bosons, the renormalization (5.2) must be performed in the matrix elements resulting from the equivalence theorem.

## 6 Application to W-boson-pair production

In this section, the above results for Sudakov DL, collinear or soft SL, and PR corrections are applied to W-pair production. Similar results for neutral gauge-boson-pair production and neutral current processes  $e^+e^- \rightarrow f\bar{f}$  can be found in Ref. [16].

We consider the polarized scattering process<sup>5</sup>  $e_{\kappa}^+ e_{\kappa}^- \rightarrow W_{\lambda_+}^+ W_{\lambda_-}^-$ , where  $\kappa = \text{R, L}$  is the electron chirality, and  $\lambda_{\pm} = 0, \pm$  represent the gauge-boson helicities. In the high-energy limit only the following helicity combinations are non-suppressed [4,24]: the purely longitudinal final state  $(\lambda_+, \lambda_-) = (0, 0)$ , which we denote by  $W_{\text{L}}^+ W_{\text{L}}^-$ , and the purely transverse and opposite final states  $(\lambda_+, \lambda_-) = (\pm, \mp)$ , which we denote by  $W_{\text{T}}^+ W_{\text{T}}^-$ . The Mandelstam variables are  $s = (p_{e^+} + p_{e^-})^2$ ,  $t = (p_{e^+} - p_{W^+})^2 \sim -s(1 - \cos\theta)/2$ , and  $u = (p_{e^+} - p_{W^-})^2 \sim -s(1 + \cos\theta)/2$ , where  $\theta$  is the angle between  $e^+$  and  $W^+$ . The Born amplitude gets contributions of the  $s$ - and  $t$ -channel diagrams in Figure 2 and reads

$$\mathcal{M}_0^{e_{\kappa}^+ e_{\kappa}^- \rightarrow W_{\text{L}}^+ W_{\text{L}}^-} = e^2 R_{e_{\kappa}^- \phi^-} \frac{A_s}{s}, \quad \mathcal{M}_0^{e_{\kappa}^+ e_{\kappa}^- \rightarrow W_{\text{T}}^+ W_{\text{T}}^-} = \delta_{\kappa\text{L}} \frac{e^2}{2s_{\text{w}}^2} \frac{A_t}{t} \tag{6.1}$$

up to terms of order  $M_{\text{W}}^2/s$ , where  $R_{\varphi_i \varphi_k} := I_{\varphi_i}^A I_{\varphi_k}^A + I_{\varphi_i}^Z I_{\varphi_k}^Z$  is given by

$$R_{e_{\text{R}}^- \phi^-} = \frac{1}{2c_{\text{w}}^2}, \quad R_{e_{\text{L}}^- \phi^-} = \frac{1}{4s_{\text{w}}^2 c_{\text{w}}^2}, \quad R_{e_{\text{L}}^- W_{\text{T}}^-} = \frac{1}{2s_{\text{w}}^2}. \tag{6.2}$$

The amplitude for transverse gauge-boson production is non-suppressed only for left-handed electrons in the initial state. In the following we give the one-loop correc-

---

<sup>5</sup>The momenta and fields of the initial states are incoming, and those of the final states are outgoing.

tions as relative corrections to the Born matrix elements (6.1). The LSC contributions (3.4) read

$$\delta_{e_\kappa^+ e_\kappa^- \rightarrow W_\lambda^+ W_{-\lambda}^-}^{\text{LSC}} = - \sum_{\varphi=e_\kappa, W_\lambda} \left[ C_\varphi^{\text{ew}} L(s) + L^{\text{em}}(s, \lambda^2, m_\varphi^2) \right]. \quad (6.3)$$

Here and in the following formulas, the quantum numbers of the would-be Goldstone bosons  $\phi^\pm$  have to be used for longitudinally polarized gauge bosons  $W_L^\pm$ . The eigenvalues of the effective electroweak Casimir operator are

$$C_{e_R}^{\text{ew}} = \frac{1}{c_w^2}, \quad C_{e_L}^{\text{ew}} = C_\Phi^{\text{ew}} = \frac{1 + 2c_w^2}{4s_w^2 c_w^2}, \quad C_{W_T}^{\text{ew}} = \frac{2}{s_w^2}. \quad (6.4)$$

The SSC corrections are obtained by applying (3.8) to the crossing symmetric process  $e_\kappa^+ e_\kappa^- W_\lambda^- W_{-\lambda}^+ \rightarrow 0$ . The contribution of the neutral gauge bosons  $V_a = A, Z$  gives

$$\sum_{V_a=A,Z} \delta_{e_\kappa^+ e_\kappa^- \rightarrow W_\lambda^+ W_{-\lambda}^-}^{V_a, \text{SSC}} = - \left[ 4R_{e_\kappa^- W_\lambda^-} l(s) + \frac{\alpha}{\pi} \log \frac{M_W^2}{\lambda^2} \right] \log \frac{t}{u}, \quad (6.5)$$

The contribution of soft  $W^\pm$  bosons to (3.8) yields

$$\begin{aligned} \sum_{V_a=W^\pm} \delta^{V_a, \text{SSC}} \mathcal{M}^{e_\kappa^+ e_\kappa^- \phi^- \phi^+} &= \frac{2l(s)\delta_{\kappa L}}{\sqrt{2}s_w} \left[ \frac{1}{2s_w} \left( \mathcal{M}_0^{\bar{\nu}_\kappa e_\kappa^- H \phi^+} + \mathcal{M}_0^{e_\kappa^+ \nu_\kappa \phi^- H} \right) \right. \\ &\quad \left. + \frac{i}{2s_w} \left( \mathcal{M}_0^{\bar{\nu}_\kappa e_\kappa^- \chi \phi^+} - \mathcal{M}_0^{e_\kappa^+ \nu_\kappa \phi^- \chi} \right) \right] \log \frac{|t|}{s}, \\ \sum_{V_a=W^\pm} \delta^{V_a, \text{SSC}} \mathcal{M}^{e_L^+ e_L^- W_T^+ W_T^-} &= \frac{2l(s)}{\sqrt{2}s_w} \left[ \left( \mathcal{M}_0^{\bar{\nu}_L e_L^- A_T W_T^+} + \mathcal{M}_0^{e_L^+ \nu_L W_T^- A_T} \right) \right. \\ &\quad \left. - \frac{c_w}{s_w} \left( \mathcal{M}_0^{\bar{\nu}_L e_L^- Z_T W_T^+} + \mathcal{M}_0^{e_L^+ \nu_L W_T^- Z_T} \right) \right] \log \frac{|t|}{s}, \quad (6.6) \end{aligned}$$

and after explicit evaluation of the SU(2)-transformed Born matrix elements on the left-hand side of (6.6), we find the relative corrections

$$\sum_{V_a=W^\pm} \delta_{e_\kappa^+ e_\kappa^- \rightarrow W_L^+ W_L^-}^{V_a, \text{SSC}} = -l(s) \frac{\delta_{\kappa L}}{s_w^4 R_{e_L^- \phi^-}} \log \frac{|t|}{s},$$

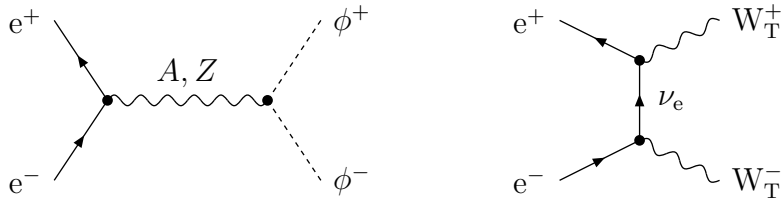


Figure 2: Dominant lowest-order diagrams for  $e^+e^- \rightarrow \phi^+\phi^-$  and  $e^+e^- \rightarrow W_T^+W_T^-$

$$\sum_{V_a=W^\pm} \delta_{e_L^+ e_L^- \rightarrow W_T^+ W_T^-}^{V_a, \text{SSC}} = -\frac{2}{s_w^2} \left(1 - \frac{t}{u}\right) l(s) \log \frac{|t|}{s}. \quad (6.7)$$

The collinear and soft SL corrections can be read off from (4.7), (4.11), and (4.15),

$$\begin{aligned} \delta_{e_\kappa^+ e_\kappa^- \rightarrow W_L^+ W_L^-}^{\text{C}} &= \left[3C_{e_\kappa}^{\text{ew}} + 4C_\Phi^{\text{ew}}\right] l_C - \frac{3}{2s_w^2} \frac{m_t^2}{M_W^2} l_{\text{Yuk}} + \sum_{\varphi=e, W} 2l^{\text{em}}(m_\varphi^2), \\ \delta_{e_L^+ e_L^- \rightarrow W_T^+ W_T^-}^{\text{C}} &= \left[3C_{e_L}^{\text{ew}} + b_{WW}^{\text{ew}}\right] l_C + \sum_{\varphi=e, W} 2l^{\text{em}}(m_\varphi^2). \end{aligned} \quad (6.8)$$

Here the Yukawa and non-Yukawa  $l(s)$  terms have been denoted by  $l_{\text{Yuk}}$  and  $l_C$ , respectively. Note that the (large) Yukawa contributions occur only for longitudinal gauge bosons.

The PR logarithms are obtained from the renormalization of (6.1). The corresponding  $l(s)$  terms are denoted by  $l_{\text{PR}}$ , and according to (5.3) given by

$$\begin{aligned} \delta_{e_R^+ e_R^- \rightarrow W_L^+ W_L^-}^{\text{PR}} &= -\left[\frac{s_w}{c_w} b_{AZ}^{\text{ew}} + b_{AA}^{\text{ew}}\right] l_{\text{PR}} + \Delta\alpha(M_W^2), \\ \delta_{e_L^+ e_L^- \rightarrow W_L^+ W_L^-}^{\text{PR}} &= -\left[\left(1 - \frac{c_w^2}{s_w^2}\right) \frac{s_w}{c_w} b_{AZ}^{\text{ew}} + b_{AA}^{\text{ew}}\right] l_{\text{PR}} + \Delta\alpha(M_W^2), \\ \delta_{e_L^+ e_L^- \rightarrow W_T^+ W_T^-}^{\text{PR}} &= -b_{WW}^{\text{ew}} l_{\text{PR}} + \Delta\alpha(M_W^2). \end{aligned} \quad (6.9)$$

In order to give an impression of the size of the correction, we give a numerical evaluation of the symmetric electroweak part (ew) (2.3) of the above results. Using the physical parameters

$$M_W = 80.35 \text{ GeV}, \quad M_Z = 91.1867 \text{ GeV}, \quad m_t = 175 \text{ GeV}, \quad \alpha = \frac{1}{137.036}, \quad (6.10)$$

we obtain

$$\begin{aligned} \delta_{e_L^+ e_L^- \rightarrow W_T^+ W_T^-}^{\text{ew}} &= -12.6 L(s) - 8.95 \left[ \log \frac{t}{u} + \left(1 - \frac{t}{u}\right) \log \frac{|t|}{s} \right] l(s) + 25.2 l_C - 14.2 l_{\text{PR}}, \\ \delta_{e_L^+ e_L^- \rightarrow W_L^+ W_L^-}^{\text{ew}} &= -7.35 L(s) - \left(5.76 \log \frac{t}{u} + 13.9 \log \frac{|t|}{s}\right) l(s) + 25.7 l_C - 31.8 l_{\text{Yuk}} \\ &\quad - 9.03 l_{\text{PR}}, \\ \delta_{e_R^+ e_R^- \rightarrow W_L^+ W_L^-}^{\text{ew}} &= -4.96 L(s) - 2.58 \left(\log \frac{t}{u}\right) l(s) + 18.6 l_C - 31.8 l_{\text{Yuk}} + 8.80 l_{\text{PR}}. \end{aligned} \quad (6.11)$$

These correction factors are shown in Figures 3 and 4 as a function of the scattering angle and the energy, respectively. If the electrons are left-handed, large negative DL and PR corrections originate from the SU(2) interaction. Instead, for right-handed

electrons the DL corrections are smaller, and the PR contribution is positive. For transverse W bosons, there are no Yukawa contributions and the other contributions are in general larger than for longitudinal W bosons. Nevertheless, for energies around 1 TeV, the corrections are similar. Finally, note that the angular-dependent contributions are very important for the LL and LT corrections: at  $\sqrt{s} \approx 1$  TeV they vary from +15% to -5% for scattering angles  $30^\circ < \theta < 150^\circ$ , whereas the angular-dependent part of the RL corrections remains between  $\pm 2\%$ .

## 7 Conclusion

We have considered general electroweak processes at high energies. We have given recipes and explicit formulas for the extraction of the one-loop leading electroweak logarithms. Like the well-known soft-collinear double logarithms, also the collinear single logarithms can be expressed as simple correction factors that are associated with the external particles of the considered process. Up to electromagnetic terms, the collinear SL corrections for external longitudinal gauge bosons and for Higgs bosons are equal. The subleading single logarithms arising from the soft-collinear limit are angular-dependent and can be associated to pairs of external particles. Their

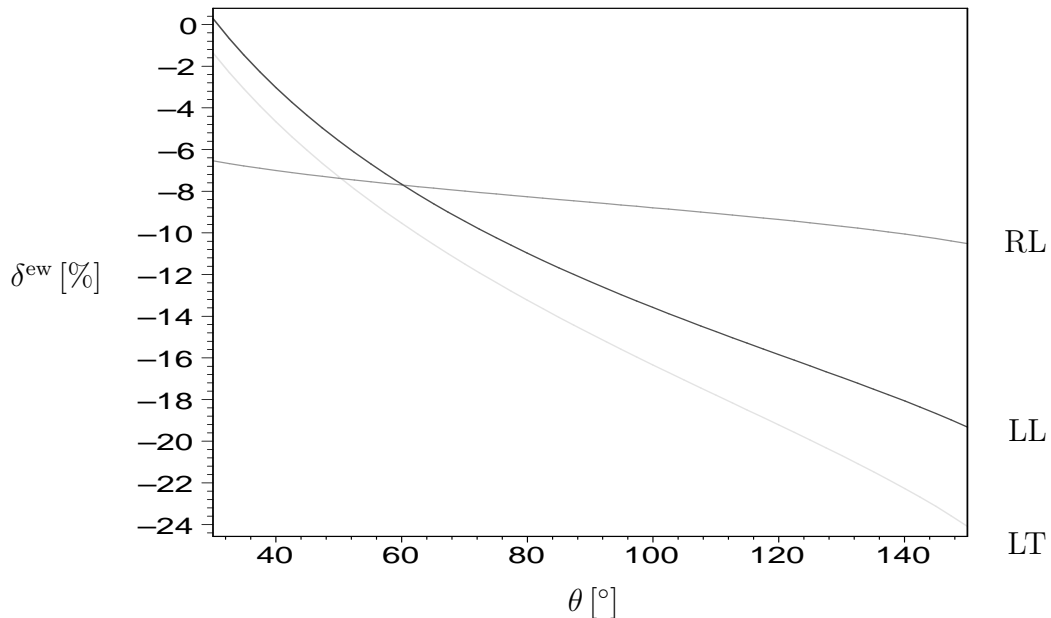


Figure 3: Dependence of the electroweak correction factor  $\delta_{e_{\kappa^+}^+ e_{\kappa^-}^- \rightarrow W_{\lambda}^+ W_{-\lambda}^-}^{\text{ew}}$  on the scattering angle  $\theta$  at  $\sqrt{s} = 1$  TeV for polarizations RL, LL, and LT

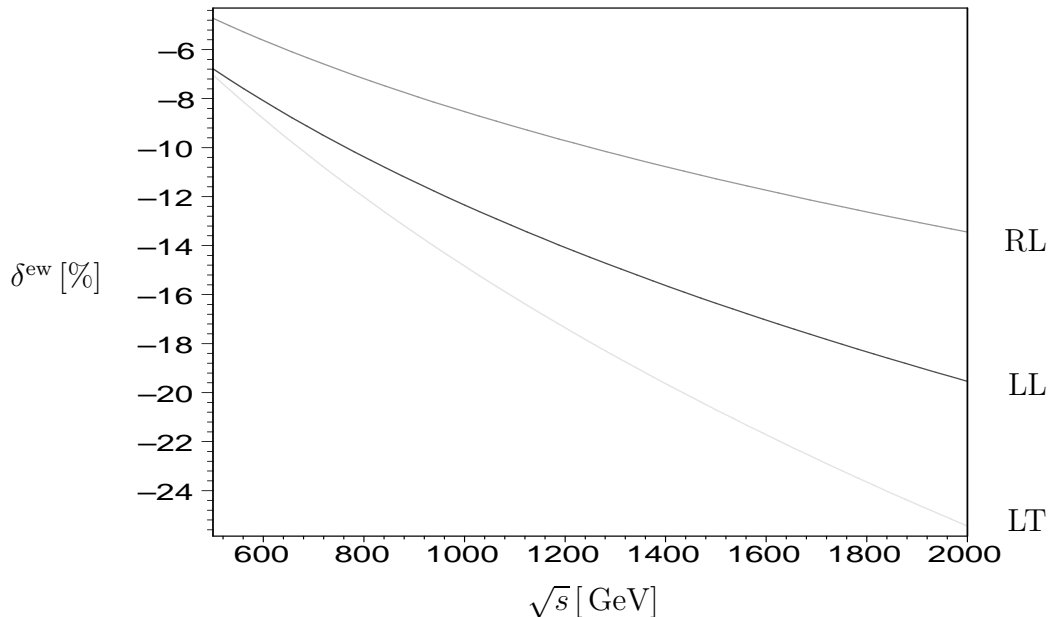


Figure 4: Dependence of the electroweak correction factor  $\delta_{e_{\kappa^+}^+ e_{\kappa^-}^- \rightarrow W_{\lambda}^+ W_{-\lambda}^-}^{\text{ew}}$  on the energy  $\sqrt{s}$  at  $\theta = 90^\circ$  for polarizations RL, LL, and LT

evaluation requires in general all matrix elements that are linked to the lowest-order matrix element via global SU(2) rotations. Finally, the logarithms originating from coupling-constant renormalization are associated with the explicit dependence of the lowest-order matrix element on the coupling parameters. Our results are applicable to general amplitudes that are not mass-suppressed, as long as all invariants are large compared to the masses. As illustration, we have applied our general results to W-boson-pair production.

## Acknowledgments

A.D. would like to thank the organizers of the conference, in particular Howard Haber, for providing a very pleasant atmosphere during the whole conference and for financial support. This work was supported in part by the Swiss Bundesamt für Bildung und Wissenschaft and by the European Union under contract HPRN-CT-2000-00149.

## References

- [1] S. Haywood, P.R. Hobson, W. Hollik, Z. Kunszt et al., hep-ph/0003275, in *Standard Model Physics (and more) at the LHC*, eds. G. Altarelli and M.L. Mangano, (CERN-2000-004, Genève, 2000) p. 117.
- [2] E. Accomando et al., *Phys. Rep.* **299** (1998) 1 [hep-ph/9705442].
- [3] M. Kuroda, G. Moulataka and D. Schildknecht, *Nucl. Phys.* **B350** (1991) 25;  
G. Degrassi and A. Sirlin, *Phys. Rev.* **D46** (1992) 3104;  
A. Denner, S. Dittmaier and R. Schuster, *Nucl. Phys.* **B452** (1995) 80 [hep-ph/9503442];  
A. Denner, S. Dittmaier and T. Hahn, *Phys. Rev.* **D56** (1997) 117 [hep-ph/9612390].
- [4] W. Beenakker et al., *Nucl. Phys.* **B410** (1993) 245 and *Phys. Lett.* **B317** (1993) 622.
- [5] V.V. Sudakov, *JETP* **3** (1956) 65.
- [6] P. Ciafaloni and D. Comelli, *Phys. Lett.* **B446** (1999) 278 [hep-ph/9809321].
- [7] J.H. Kühn and A.A. Penin, TTP-99-28, hep-ph/9906545.
- [8] P. Ciafaloni and D. Comelli, *Phys. Lett.* **B476** (2000) 49 [hep-ph/9910278].
- [9] J.H. Kühn, A.A. Penin and V.A. Smirnov, *Eur. Phys. J.* **C17** (2000) 97 [hep-ph/9912503].
- [10] V.S. Fadin, L.N. Lipatov, A.D. Martin and M. Melles, *Phys. Rev.* **D61** (2000) 094002 [hep-ph/9910338].
- [11] M. Melles, *Phys. Lett.* **B495** (2000) 81 [hep-ph/0006077].
- [12] W. Beenakker and A. Werthenbach, *Phys. Lett.* **B489** (2000) 148 [hep-ph/0005316].
- [13] M. Hori, H. Kawamura and J. Kodaira, *Phys. Lett.* **B491** (2000) 275 [hep-ph/0007329].
- [14] M. Beccaria, P. Ciafaloni, D. Comelli, F. Renard and C. Verzegnassi, *Phys. Rev.* **D61** (2000) 073005 and 011301 [hep-ph/9906319 and hep-ph/9907389];  
M. Beccaria, F.M. Renard and C. Verzegnassi, PM-00-23, hep-ph/0007224.
- [15] M. Melles, *Phys. Rev. D* **63** (2001) 034003 [hep-ph/0004056].
- [16] A. Denner and S. Pozzorini, *Eur. Phys. J. C* **18** (2001) 461 [hep-ph/0010201].

- [17] A. Denner, *Fortschr. Phys.* **41** (1993) 307.
- [18] T. Kinoshita, *J. Math. Phys.* **3** (1962) 650.
- [19] A. Denner and S. Pozzorini, *Eur. Phys. J. C* **21** (2001) 63 [hep-ph/0104127].
- [20] J.M. Cornwall, D.N. Levin and G. Tiktopoulos, *Phys. Rev.* **D10** (1974) 1145;  
G.J. Gounaris, R. Kögerler and H. Neufeld, *Phys. Rev.* **D34** (1986) 3257.
- [21] Y.P. Yao and C.P. Yuan, *Phys. Rev.* **D38** (1988) 2237;  
J. Bagger and C. Schmidt, *Phys. Rev.* **D41** (1990) 264;  
H.J. He, Y.P. Kuang and X. Li, *Phys. Rev. Lett.* **69** (1992) 2619 and  
*Phys. Rev.* **D49** (1994) 4842;  
D. Espriu and J. Matias, *Phys. Rev.* **D52** (1995) 6530 [hep-ph/9501279].
- [22] Z. Kunszt, A. Signer and Z. Trocsanyi, *Nucl. Phys.* **B420** (1994) 550 [hep-ph/9401294].
- [23] A. Denner, S. Dittmaier and G. Weiglein, *Nucl. Phys.* **B440** (1995) 95 [hep-ph/9410338].
- [24] W. Beenakker and A. Denner, *Int. J. Mod. Phys.* **A9** (1994) 4837.

## Status of the BNL Muon ( $g - 2$ ) Experiment\*

R. Prigl (2), H.N. Brown (2), G. Bunce (2), R.M. Carey (1), P. Cushman (8), G.T. Danby (2), P.T. Debevec (7), H. Deng (12), W. Deninger (7), S.K. Dhawan (12), V.P. Druzhinin (9), L. Duong (8), W. Earle (1), E. Efstathiadis (1), F.J.M. Farley (12), G.V. Fedotov (9), S. Giron (8), F. Gray (7), M. Grosse Perdekamp (12), A. Grossmann (5), U. Haeberlen (6), M. Hare (1), E.S. Hazen (1), D.W. Hertzog (7), V.W. Hughes (12), M. Iwasaki (11), K. Jungmann (5), D. Kawall (12), M. Kawamura (11), B.I. Khazin (9), J. Kindem (8), F. Krienen (1), I. Kronkvist (8), R. Larsen (2), Y.Y. Lee (2), W. Liu (12), I. Logashenko (9), R. McNabb (8), W. Meng (2), J.-L. Mi (2), J.P. Miller (1), W.M. Morse (2), P. Neumayer (5), D. Nikas (2), C.J.G. Onderwater (7), Y. Orlov (3), C. Ozben (2), J. Paley (1), C. Pai (2), C. Polly (7), J. Pretz (12), G. zu Putlitz (5), S.I. Redin (12), O. Rind (1), B.L. Roberts (1), N. Ryskulov (9), S. Sedykh (7), Y.K. Semertzidis (2), Yu.M. Shatunov (9), E. Sichtermann (12), E. Solodov (9), M. Sossong (7), A. Steinmetz (12), L.R. Sulak (1), M. Tanaka (2), C. Timmermans (8), A. Trofimov (1), D. Urner (7), D. Warburton (2), D. Winn (4), A. Yamamoto (10), D. Zimmerman (8).

(1) Department of Physics, Boston University, Boston, MA 02215, USA, (2) Brookhaven National Laboratory, Upton, NY 11973, USA, (3) Newman Laboratory, Cornell University, Ithaca NY 14853, USA, (4) Fairfield University, Fairfield, CT 06430, USA, (5) Physikalisches Institut der Universität Heidelberg, 69120 Heidelberg, Germany, (6) MPI für Med. Forschung, 69120 Heidelberg, Germany, (7) Department of Physics, University of Illinois, Urbana, IL 61820, USA, (8) Department of Physics, University of Minnesota, Minneapolis, MN 55455, USA, (9) Budker Institute of Nuclear Physics, Novosibirsk, Russia, (10) KEK, Japan, (11) Tokyo Institute of Technology, Tokyo, Japan, (12) Department of Physics, Yale University, New Haven, CT 06511, USA.

The muon ( $g - 2$ ) experiment at Brookhaven has been taking data since 1997. Analyses of the data taken in 1997 and 1998, which include about 2% of the data taken so far, have improved the experimental accuracy in the muon anomalous magnetic moment to  $a_{\mu(\text{expt})} = 1165921(5) \times 10^{-9} (4 \text{ ppm})$ . The value agrees with standard theory. Analysis of the 1999 data, about 25% of the existing data set, is nearing completion and analysis of the 2000 data has started. The experiment is preparing for another major data taking run, this time storing negative instead of positive muon beams.

Presented at the

5th International Symposium on Radiative Corrections  
(RADCOR-2000)  
Carmel CA, USA, 11–15 September, 2000

---

\*This work was supported in part by the US Dept. of Energy, The U.S. National Science Foundation, the German Bundesminister für Bildung und Forschung, the Russian Ministry of Science, and the US-Japan Agreement in High Energy Physics. A. Steinmetz acknowledges support by the Alexander von Humboldt Foundation.

# 1 Introduction

The Brookhaven g-2 experiment E821 is designed to provide a precision test of the standard model prediction for  $a_\mu$  which is dominated by the QED radiative corrections but has sizeable contributions from hadronic loops,  $a_\mu^{Had} = 6739(67) \times 10^{-11}$  or  $57.8(7) ppm$  in  $a_\mu$ , as well as electroweak loops,  $a_\mu^{EW} = 1.30(4) ppm$ . The theory of  $a_\mu$  is discussed in detail in another contribution to these proceedings [1]. The goal of E821 is to reduce the error in  $a_\mu$  to  $0.35 ppm$ , a fraction of the electroweak contribution.

The experiment measures the muon anomaly  $a_\mu$  directly rather than the g-factor. Therefore we commonly express contributions and errors in units of  $a_\mu$ . Any numbers given in ppm here have to be multiplied by  $1.165... \times 10^{-9}$  for comparison with the absolute numbers found in [1] and most other theoretical papers on the muon g-factor.

# 2 The Brookhaven Experiment

The principle of the measurement is similar to the third CERN experiment [2]. Polarized muons are stored in a uniform dipole magnetic field with electrostatic quadrupoles providing weak vertical focussing. The muon spin precesses relative to the momentum vector with the frequency

$$\vec{\omega}_a = -\frac{e}{m_\mu} \left[ a_\mu \vec{B} - \left( a_\mu - \frac{1}{\gamma_\mu^2 - 1} \right) \vec{\beta} \times \vec{E} \right], \quad (1)$$

where  $\vec{\beta} = \vec{v}/c$ ,  $\gamma = 1/\sqrt{1 - v^2/c^2}$ , and assuming that  $\frac{E}{c} \ll B$  and  $\vec{\beta} \cdot \vec{B} \approx 0$ . The dependence of  $\omega_a$  on the electric field  $\vec{E}$  can be eliminated by storing muons with the “magic”  $\gamma_\mu = 29.3$ , corresponding to a muon momentum  $p_\mu = 3.094 \text{ GeV}/c$ . In this ideal case,  $a_\mu - 1/(\gamma_\mu^2 - 1) = 0$ , and the focussing electric field does not affect the spin precession frequency.  $a_\mu$  is then extracted from  $\omega_a \approx 2\pi \times 230 \text{ kHz}$  through

$$a_\mu = \frac{\omega_a/\omega_p}{\mu_\mu/\mu_p - \omega_a/\omega_p} \quad (2)$$

where  $\omega_p \approx 2\pi \times 62 \text{ MHz}$  is the free proton precession frequency in the same magnetic field seen by the muons. The ratio of muon to proton magnetic moments is  $\mu_\mu/\mu_p = 3.18334539(10)$  [3,4].

The source of the stored muons is the Alternating Gradient Synchrotron (AGS) proton beam, which delivers 6-12 bunches with a total of  $40-60 \times 10^{12}$  protons at  $24 \text{ GeV}/c$  onto a nickel production target every 2.7 s. The individual bunches have a total width of about 100 ns and are spaced apart by 33 ms.

From each bunch about  $4 \times 10^7$  pions at  $\approx 3.1 \text{ GeV}/c$  are transported from the target along a 116 m beam line. About 50% of the pions decay along the transport line and a momentum slit followed by a bending magnet near the downstream end selects either pions or forward decay muons from a slightly higher momentum pion beam for injection

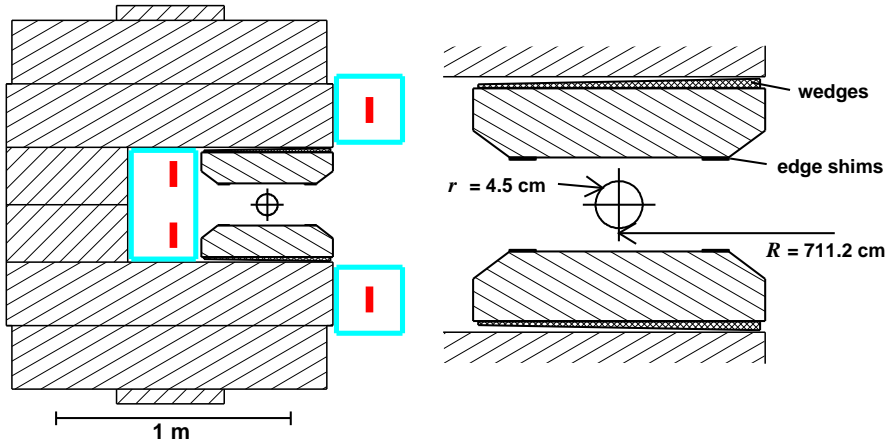


Figure 1: Storage ring magnet cross section and detailed view of the magnet gap region.

into the storage ring. After passing through a hole in the back of the storage ring magnet yoke and a field free region supplied by a superconducting inflector magnet [5], the pion or muon beam enters the toroidal storage region which has a radius of 7.112 m and a 9 cm diameter cross section. The storage ring magnet is described in detail in [6].

One of the major improvements over the last CERN experiment is the use of direct muon injection. In pion injection mode a small fraction of muons from pion decay,  $\pi^+ \rightarrow \mu^+ \nu_\mu$ , are launched onto a stable orbit and are stored. In muon injection mode, a total kick of  $\approx 11$  mrad on the first one or two turns is needed to store the muons born in the pion decay channel. The muon kicker is a pulsed magnet consisting of three sections of pairs of current sheets, each 1.7 m long. The peak current through the plates during a 400 ns wide pulse is about 4100 A, providing a vertical field of 0.016 T superimposed on the 1.45 T field of the storage ring magnet.

The continuous superferric ‘C’-shaped storage ring magnet, Fig. 1, is excited by superconducting coils which carry a current of 5177 A. The yoke consists of twelve 30 degree sections bolted together at the four corners, with azimuthal gaps of less than 1 mm. The pole pieces are 10 degrees long and aligned with the yoke sectors. The azimuthal gap between adjacent pole pieces of about  $75 \mu\text{m}$  is filled with insulating Kapton foils to avoid irregular eddy current effects. The vertical gap between pole and yoke decouples the yoke and pole pieces, which are fabricated from high quality steel, and allows the insertion of iron wedges to compensate for the C-magnet quadrupole. The 10 cm wide wedges are radially adjustable. This allows us to locally change the total air gap and thus the dipole field component for better field homogeneity in azimuth. The four edge shims, 5 cm wide and about 3 mm high, are the main tool for reducing field variations over the beam cross section. Continuous current sheets glued to the pole pieces are used to further reduce the fractional inhomogeneity in the integral field. The gradual improvement of the field integral across the aperture is shown in Fig. 2.

During data taking an array of nuclear magnetic resonance (NMR) probes embedded in the top and bottom plates of the twelve vacuum chambers is used to monitor and

## 1ppm field contours

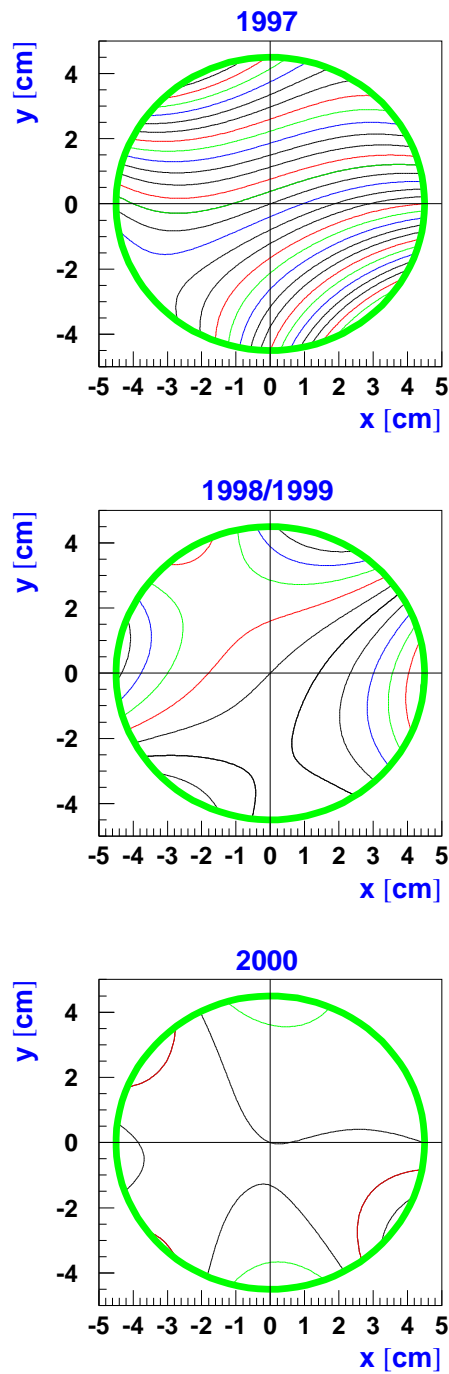


Figure 2: Typical contour plot of the magnetic field integrated over azimuth during the 1997 run (top), 1998 (1999) run (middle), and the 2000 run (bottom).  $x$  denotes the radial and  $y$  the vertical direction. Each contour line represents a fractional change of  $1 \times 10^{-6}$ . No efforts were made to improve the field quality between the 1998 and 1999 run and the field quality was the same for these runs. The most significant improvement for 2000 came from the installation of a new inflector magnet.

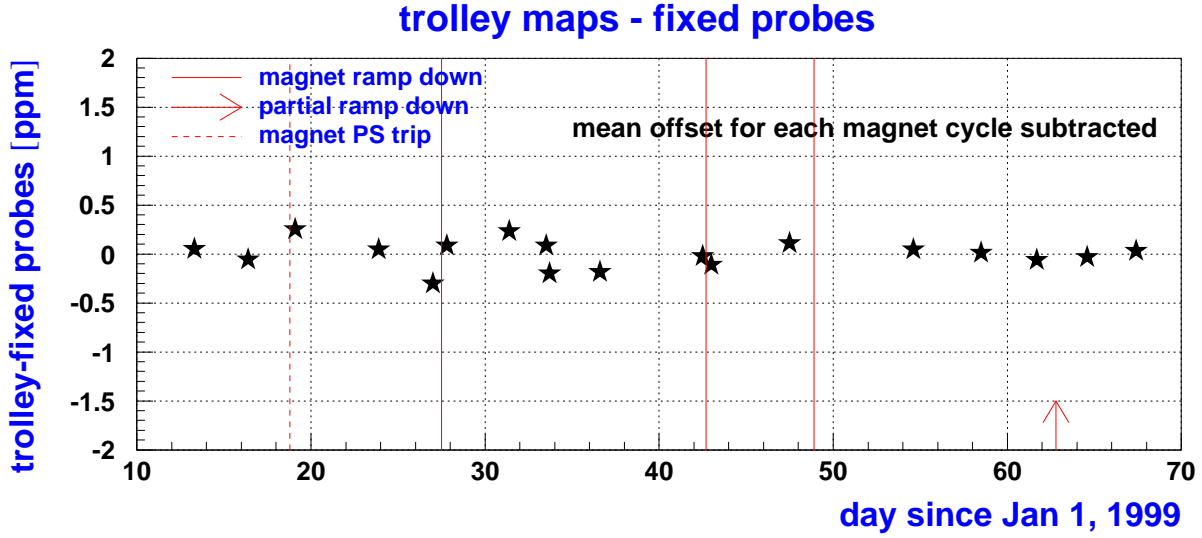


Figure 3: Difference between the field average measured by the trolley and the field average predicted by the monitoring probes. It is assumed that the true difference is constant during each magnet-on period and fluctuations are caused by the limited accuracy of the individual measurements.

stabilize the magnetic field [7]. About one third of the 375 probes installed are typically used in the field analysis. The field inside the storage region is mapped twice a week using a hermetically sealed trolley operating in vacuum and containing a matrix of 17 NMR probes. The probes in the trolley are calibrated in place against a standard probe [8]. The first trolley run in a magnet cycle establishes the offset between the average field measured by the monitoring probes and the average field seen by the muon beam. Subsequent trolley runs can then be used to determine the accuracy of the continuous field “tracking” with the monitoring probes. The quality of the field tracking is shown in Fig. 3 for the 1999 run.

The decay positrons from  $\mu^+ \rightarrow e^+ \nu_e \bar{\nu}_\mu$ , which constitute our signal, range in energy from 0 GeV to 3.1 GeV, and are detected with 24 Pb-scintillating fiber calorimeters placed symmetrically around the inside of the storage ring. Because of the parity violating nature of the weak decay, the high-energy positrons are preferentially emitted along the muon spin direction. The muon spin precession is reflected in the decay positron spectrum,  $N(t)$ , where we expect

$$N(t) = N_0(E) e^{-t/\tau_\mu} [1 - A(E) \cos(\omega_a t + \phi)]. \quad (3)$$

The normalization constant  $N_0$  depends on the energy threshold  $E$  as does the asymmetry parameter  $A$ . For  $E=2.0$  GeV,  $A$  is  $\approx 0.4$ .

The arrival times of the positrons are recorded in multi-hit time-to-digital converters (TDCs), and the calorimeter pulses are also sampled by a 400 MHz waveform digitizer (WFD). A laser and light emitting diode (LED) system are used to monitor potential time

and gain shifts. Several detector stations are outfitted with a finely segmented hodoscope array of  $20 \times 32$  small scintillating elements connected to a multianode phototube, which provide position sensitive information on the muon decay positron. Additional event information is derived from stations equipped with five scintillator paddles oriented horizontally. Finally, a set of wire chambers in one section of the ring provides information on the stored muon phase space by measuring the flight path of the decay electrons and tracing them back to their origin. The distribution of the muon beam across the aperture has to be convoluted with the magnetic field to determine the average field seen by the muons. The mean radial distribution of the stored muons can also be obtained from the fast rotation signal from the initial time structure of the injected beam.

### 3 Present Status of Results

In the first data taking run of the experiment in 1997 pion injection was used because the muon kicker was still under construction. This mode suffers from a low efficiency - only about 20 muons get stored per  $10^6$  pions injected into the storage ring - as well as from a significant flash caused by hadronic interactions of pions that do not decay and hit the inflector channel wall at the end of the first turn. The result from this run,  $a_\mu = 1\,165\,925(15) \times 10^{-9}$ , is discussed in [9]. In 1998 the muon kicker was commissioned and first data were taken in muon injection mode. The run was cut short by a hardware failure in the beamline. The analysis of the 1998 data, most of which taken during the last week of running, resulted in a value of  $a_\mu = 11\,659\,191(59) \times 10^{-10} (\pm 5 \text{ ppm})$  [10]. Combining all experimental data including the old CERN measurement,  $a_\mu^{CERN} = 11\,659\,230(84) \times 10^{-10} (\pm 7.2 \text{ ppm})$  [2], yields  $a_\mu^{expt} = 11\,659\,205(46) \times 10^{-9} (\pm 4 \text{ ppm})$  for the world average. This value agrees with the theoretical value  $a_\mu^{SM} = 11\,659\,160(7) \times 10^{-10} (\pm 0.6 \text{ ppm})$  found in [1].

### 4 Status of the Analysis of the 1999 and 2000 Data

The experiment currently analyses the data collected in 1999 which is about 15 times larger than the 1998 data set. In contrast to the old data, which could quite well be fitted to the basic 5-parameter function in equation (3), the significant increase in statistical power combined with a higher data taking rate revealed a number of subtle effects that slowed down the analysis. Two of the most prominent effects can be illustrated by ignorantly fitting the data to the function in eq. (3), and then looking at the residuals, i.e. the difference between the measured decay spectrum and the 5-parameter fit as shown in Fig. 4. Clearly the fitting function does not describe the data well. The residual in Fig. 4b,c has two prominent features. One is the excess of data at early times, and the other an oscillation of the counts with respect to the fitting function, also decaying with time. The former feature is caused by the high counting rate at early times. Our 400 MHz waveform digitizer does not allow us to distinguish between two decay positrons

that hit the same detector within about 3.5 nsec. Such pairs of pulses pile up to one larger pulse. If each of the single pulses exceed the energy threshold  $E$ , we lose a count. On the other hand, two pulses below threshold can combine to form a larger pulse that exceeds the threshold. Since our energy cuts are relatively high to benefit from the large asymmetry at higher energies, the pulses gained outnumber the pulses lost, leading to excessive counts at early times. An additional complication is that the g-2 phase of the pulses lost is not the same as the phase of the pulses gained because higher energy decay positrons have a larger bend radius in the ring magnet field and on average a longer flight path and flight time before hitting one of the calorimeters. Choosing an energy threshold where the pulses gained and pulses lost cancel does not eliminate the pile-up problem. As the muons decay, the count rate and therefore the fraction of pile-up pulses goes down. The simple 5-parameter fit to the data tries to accomodate the higher counts at early times by increasing the normalization constant, leading to an overestimate of counts at later times as seen in Fig. 4b.

An elegant way to extract the number of pile-up pulses from the data is to artificially increase the deadtime of the pulse finder by a factor of two, see how many more pulses are found above threshold, and then subtract these counts from the original decay positron spectrum. This sample of pulses can also be used to study the phase of the pile-up pulses. An alternative is to parametrize the pile-up fraction and include it in the fitting function. Both methods are used and compared in the analysis.

The oscillations in the residuals are caused by a coherent motion of the stored muon beam with a frequency that depends on the strength of the focusing electrostatic quadrupole field, the betatron tune. Due to a mismatch between the narrow inflector channel aperture, an 18 mm horizontal times 56 mm vertical rectangle, and the 90 mm diameter circular ring magnet aperture, we do not fill the available phase space in the storage ring in muon injection mode. This leads to a modulation of the horizontal beam width at the betatron oscillation frequency from the momentum spread, and a modulation of the horizontal and vertical beam width at twice this frequency from the angular spread of the incoming beam. In addition, our muon kicker runs reliably only a few percent below its design value. The resulting incomplete kick, combined with the fact that we do not fill the storage ring phase space, causes the beam centroid to oscillate about the central orbit at the betatron frequency. This coherent beam motion is known as coherent betatron oscillation or CBO. The dynamic behaviour of the stored muon beam was measured with a set of fiber harps that plunge in and out of the beam. Fig. 5 shows the motion of the beam centroid as an example.

The CBO is visible in the positron spectrum because the acceptance of our detectors is slightly dependent on the radius of the muon at the time of decay. The frequency we see is not the CBO frequency itself but its beating with the frequency of revolution, since we detect the decays at fixed points along the storage ring magnet circumference.

Other effects that need to be studied in detail include the loss of muons before they decay, the gain stability of the calorimeters and timing stability of the readout electronics, background events caused by the loss of protons that we inevitably store together with the muons, and background events called “flashlets”. The flashlets are caused by a small

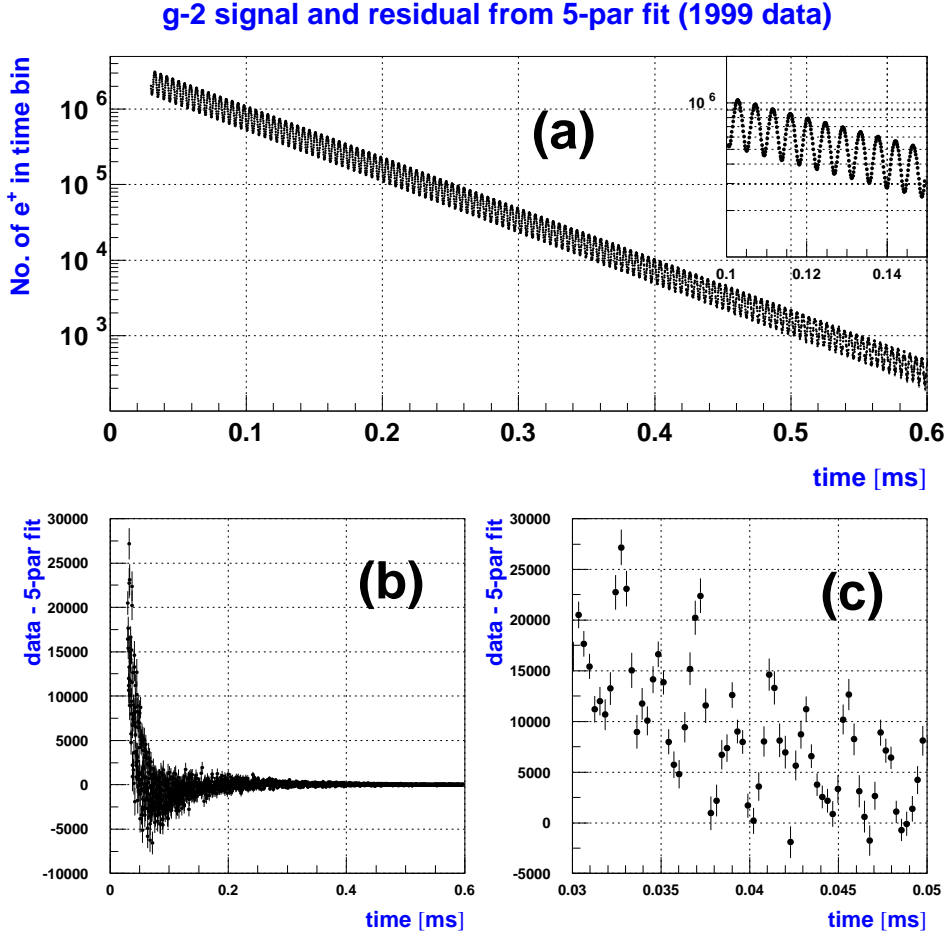


Figure 4: Positron spectrum from a large fraction of the 1999 data set (a), with an enlarged view of the time between 100 and 150  $\mu\text{sec}$  after beam injection in the top right corner. The residuals from fitting the function in eq. (3) to the data show clear structure (b), particularly at early times (c).

fraction of the halo of the primary beam still circulating in the accelerator being scattered into the extraction line and transported to the production target. The resulting low intensity secondary beam does not get kicked and is therefore not stored in our ring magnet, but creates a small flash of background signals. The most troublesome secondary beam component is positrons. Starting with the momentum of the stored muon beam, the positrons spiral inwards due to energy loss in the inflector channel windows and give a signal that cannot be distinguished from true decay positron counts near the upper edge of the decay spectrum. We have developed a sensitive analysis method to detect these flashlets utilizing the discrete time structure associated with the  $2.7 \mu\text{sec}$  revolution time of the beam in the accelerator. The flashlet contamination is very sensitive to the performance of the accelerator and we disregard data taken while there were elevated levels of flashlet contamination. During the 2000 run we installed a sweeper magnet in

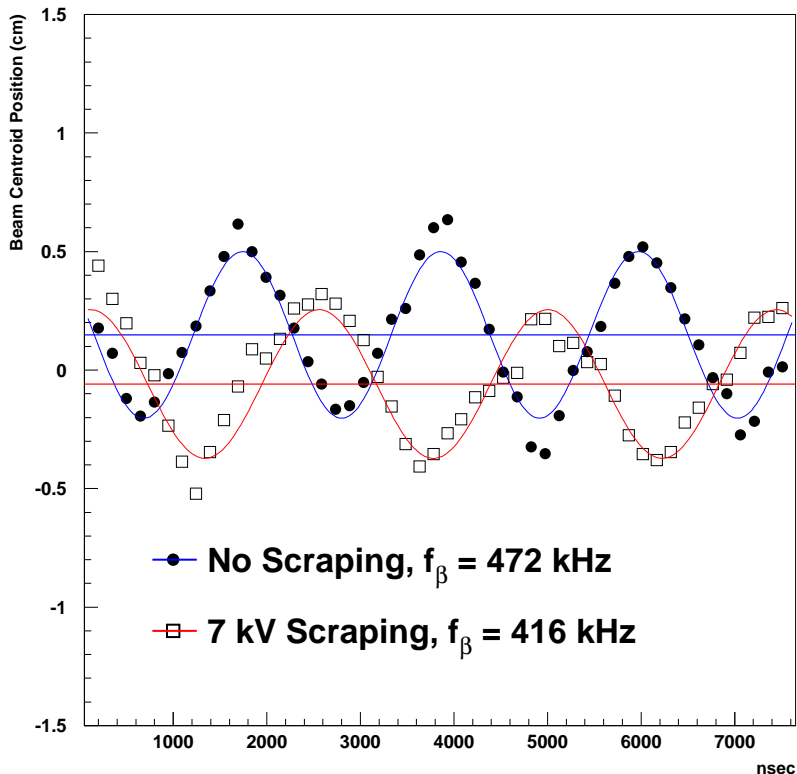


Figure 5: Beam centroid as measured by a set of fibers plunged into the muon beam at two different settings of the electrostatic quadrupoles. In normal running mode, the muon beam gets scraped for the first 15-20  $\mu\text{sec}$  after injection by an imbalance in the quadrupole plate voltages which lowers the center of the electrostatic quadrupole field and therefore the beam centroid. This also changes the betatron tune.

the secondary beam line that turns on microseconds after beam injection into the storage ring and sweeps any late arrivals out of the beamline.

In the course of the data analysis all these effects have to be studied in detail, with different analysis teams developing their own tools to correct for them, parametrize them for inclusion into the fitting function, or estimate their impact on the fit parameters with analytical and Monte Carlo methods in cases where the unwanted or missing counts do not have unique characteristics but mix into other fitting parameters. This process is nearing completion for the 1999 data.

## 5 Future

The experiment is looking forward to another run from February through April 2001. Since the 2000 run we have reversed the polarity of the beam line and ring magnet to store negative muon beam and measure  $a_{\mu^-}$ . We expect a decay positron rate similar to the 2000 run and hope to at least double our data set. Analysis of the 2000 data, 3-4 times larger than the 1999 data set, has started and initial checks e.g. for flashlet contamination suggest that most of the data is of good quality.

## References

- [1] A. Czarnecki and W.J. Marciano, **hep-ph/0010194**, these proceedings.
- [2] J. Bailey et al., *Nucl. Phys.B.* **B150** (1979) 1.
- [3] Particle Data Group, *Eur. Phys. J. C* **3** (1998) 1.
- [4] W. Liu, et al., *Phys. Rev. Lett.* **82** (1999) 711.
- [5] F. Krienen, et al., *Nucl. Instr. Meth. A.* **283** (1989) 5.
- [6] G.D. Danby, et al., *Nucl. Instr. Meth. A* **457** (2001) 151.
- [7] R. Prigl, et al., *Nucl. Instr. Meth. A.* **374** (1996) 118.
- [8] X. Fei, et al., *Nucl. Instr. Meth. A.* **394** (1997) 349.
- [9] R.M. Carey, et al., *Phys. Rev. Lett.* **82** (1999) 1632.
- [10] H.N. Brown, et al., *Phys. Rev. D.* **62** (2000) 091101(R).

Alberta Thy 11-00  
BNL-HET-00/35  
October 2000  
hep-ph/0010194

# The Muon Anomalous Magnetic Moment: Standard Model Theory and Beyond

ANDRZEJ CZARNECKI

*Department of Physics, University of Alberta  
Edmonton, AB, Canada T6G 2J1*

and

*Physics Department, Brookhaven National Laboratory,  
Upton, NY 11973, USA*

and

WILLIAM J. MARCIANO

*Physics Department, Brookhaven National Laboratory,  
Upton, NY 11973, USA*

QED, Hadronic, and Electroweak Standard Model contributions to the muon anomalous magnetic moment,  $a_\mu \equiv (g_\mu - 2)/2$ , are reviewed. Theoretical uncertainties in the prediction  $a_\mu^{\text{SM}} = 116\,591\,597(67) \times 10^{-11}$  are scrutinized. Effects due to “New Physics” are described. Implications of the current experiment vs. theory constraint  $a_\mu^{\text{exp}} - a_\mu^{\text{SM}} = 453(465) \times 10^{-11}$  and anticipated near term error reduction to  $\pm 155 \times 10^{-11}$  are discussed.

Presented at the

5th International Symposium on Radiative Corrections  
(RADCOR–2000)

Carmel CA, USA, 11–15 September, 2000

# 1 Introduction

Leptonic anomalous magnetic moments provide precision tests of the Standard Model and stringent constraints on potential “New Physics” effects. In the case of the electron, comparing the extraordinary measurements of  $a_e \equiv (g_e - 2)/2$  at the University of Washington [1]

$$\begin{aligned} a_{e^-}^{\text{exp}} &= 0.001\,159\,652\,188\,4(43), \\ a_{e^+}^{\text{exp}} &= 0.001\,159\,652\,187\,9(43), \end{aligned} \tag{1}$$

with the prediction [2,3,4,5]

$$\begin{aligned} a_e^{\text{SM}} &= \frac{\alpha}{2\pi} - 0.328\,478\,444\,00 \left(\frac{\alpha}{\pi}\right)^2 + 1.181\,234\,017 \left(\frac{\alpha}{\pi}\right)^3 \\ &\quad - 1.5098(384) \left(\frac{\alpha}{\pi}\right)^4 + 1.66(3) \times 10^{-12} (\text{hadronic \& electroweak loops}) \end{aligned} \tag{2}$$

provides the best determination of the fine structure constant [6],

$$\alpha^{-1}(a_e) = 137.035\,999\,58(52). \tag{3}$$

To test the Standard Model requires an alternative measurement of  $\alpha$  with comparable accuracy. Unfortunately, the next best determination of  $\alpha$ , from the quantum Hall effect [2],

$$\alpha^{-1}(qH) = 137.036\,003\,00(270), \tag{4}$$

has a much larger error. If one assumes that  $|\Delta a_e^{\text{New Physics}}| \simeq m_e^2/\Lambda^2$ , where  $\Lambda$  is the scale of “New Physics”, then the agreement between  $\alpha^{-1}(a_e)$  and  $\alpha^{-1}(qH)$  currently probes  $\Lambda \lesssim \mathcal{O}(100 \text{ GeV})$ . To access the much more interesting  $\Lambda \sim \mathcal{O}(\text{TeV})$  region would require an order of magnitude improvement in  $a_e^{\text{exp}}$  (technically feasible [7]), an improved calculation of the 4-loop QED contribution to  $a_e^{\text{SM}}$  and a much better independent measurement of  $\alpha^{-1}$  by almost two orders of magnitude. The last requirement, although difficult, is perhaps most likely to come [6] from combining the already precisely measured Rydberg constant with a much better determination of  $m_e$ .

We should note that for “New Physics” effects that are linear in the electron mass,  $\Delta a_e^{\text{NP}} \sim m_e/\Lambda$ , naively, one is currently probing a much more impressive  $\Lambda \sim \mathcal{O}(10^7 \text{ GeV})$  and the possible advances described above would explore  $\mathcal{O}(10^9 \text{ GeV})!$  However, we subsequently argue that such linear “New Physics” effects are misleading or unlikely.

The measurement of the muon’s anomalous magnetic moment has also been impressive. A series of experiments at CERN that ended in 1977 found [8]

$$a_\mu^{\text{exp}} = 116\,592\,300(840) \times 10^{-11} \quad (\text{CERN 1977}). \tag{5}$$

More recently, an ongoing experiment (E821) at Brookhaven National Laboratory has been running with much higher statistics and a very stable, well measured magnetic field in its storage ring. Based on data taken through 1998, combined with the earlier CERN result in (5), it found [9]

$$a_{\mu}^{\text{exp}} = 116\,592\,050(460) \times 10^{-11} \quad (\text{CERN'77+BNL'98}). \quad (6)$$

Ongoing analysis of E821's 1999 data is expected to reduce the error in (6) to about  $\pm 140 \times 10^{-11}$  before the end of this year (2000). The ultimate goal of the experiment is  $\pm 40 \times 10^{-11}$ , about a factor of 20 improvement relative to the classic CERN experiments.

Although  $a_{\mu}^{\text{exp}}$  is currently about 1000 times less precise than  $a_e^{\text{exp}}$ , it is much more sensitive to hadronic and electroweak quantum loops as well as “New Physics” effects, since such contributions [10] are generally proportional to  $m_l^2$ . The  $m_{\mu}^2/m_e^2 \simeq 40\,000$  enhancement more than compensates for the reduced experimental precision and makes  $a_{\mu}^{\text{exp}}$  a more sensitive probe of short-distance phenomena. Indeed, as we later illustrate, a deviation in  $a_{\mu}^{\text{exp}}$  from the Standard Model prediction,  $a_{\mu}^{\text{SM}}$ , could quite naturally be interpreted as the appearance of “New Physics” such as supersymmetry, an exciting prospect. Of course, before making such an interpretation, one must have a reliable prediction for  $a_{\mu}^{\text{SM}}$ , an issue that we address in the next section.

Before leaving the comparison between  $a_e^{\text{exp}}$  and  $a_{\mu}^{\text{exp}}$ , we should remark that for cases where “New Physics” contributions to  $a_l$  scale as  $m_l/\Lambda$ , roughly equal sensitivity in  $\Lambda$  ( $\sim 10^7$  GeV) currently exists for both types of measurements. However, as previously mentioned, such examples are in our view artificial.

## 2 Standard Model Prediction For $a_{\mu}$

### 2.1 QED Contribution

The QED contribution to  $a_{\mu}$  has been computed through 5 loops [5,2]

$$\begin{aligned} a_{\mu}^{\text{QED}} = & \frac{\alpha}{2\pi} + 0.765\,857\,376(27) \left(\frac{\alpha}{\pi}\right)^2 + 24.050\,508\,98(44) \left(\frac{\alpha}{\pi}\right)^3 \\ & + 126.07(41) \left(\frac{\alpha}{\pi}\right)^4 + 930(170) \left(\frac{\alpha}{\pi}\right)^5. \end{aligned} \quad (7)$$

Growing coefficients in the  $\alpha/\pi$  expansion reflect the presence of large  $\ln m_{\mu}/m_e \simeq 5.3$  terms coming from electron loops. Employing the value of  $\alpha$  from  $a_e$  in eq. (3) leads to

$$a_{\mu}^{\text{QED}} = 116\,584\,705.7(2.9) \times 10^{-11}. \quad (8)$$

The current uncertainty is well below the  $\pm 40 \times 10^{-11}$  ultimate experimental error anticipated from E821 and should, therefore, play no essential role in the confrontation between theory and experiment.

## 2.2 Hadronic Loop Corrections

Starting at  $\mathcal{O}(\alpha^2)$ , hadronic loop effects contribute to  $a_\mu$  via vacuum polarization. A first principles QCD calculation of that effect does not exist. Fortunately, it is possible to evaluate the leading effect via the dispersion integral [11]

$$a_\mu^{\text{Had}}(\text{vac. pol.}) = \frac{1}{4\pi^3} \int_{4m_\pi^2}^{\infty} ds K(s) \sigma^0(s)_{e^+e^- \rightarrow \text{hadrons}}, \quad (9)$$

where  $\sigma^0(s)_{e^+e^- \rightarrow \text{hadrons}}$  means QED vacuum polarization and other extraneous radiative corrections have been subtracted from measured cross sections, and

$$K(s) = x^2 \left(1 - \frac{x^2}{2}\right) + (1+x)^2 \left(1 + \frac{1}{x^2}\right) \left[ \ln(1+x) - x + \frac{x^2}{2} \right] + \frac{1+x}{1-x} x^2 \ln x$$

$$x = \frac{1 - \sqrt{1 - 4m_\mu^2/s}}{1 + \sqrt{1 - 4m_\mu^2/s}}. \quad (10)$$

Detailed studies of eq. (9) have been carried out by a number of authors [12,13,14,15,16,17,18]. Here, we employ an analysis due to Davier and Höcker [13,14,15] which finds

$$a_\mu^{\text{Had}}(\text{vac. pol.}) = 6924(62) \times 10^{-11}. \quad (11)$$

It used experimental  $e^+e^-$  data, hadronic tau decays, perturbative QCD and sum rules to minimize the uncertainty in that result. The contributions coming from various energy regions are illustrated in Table 1.

Table 1: Contributions to  $a_\mu^{\text{Had}}(\text{vac. pol.})$  from different energy regions as found by Davier and Höcker [13,14,15].

$\sqrt{s}$ (GeV)	$a_\mu^{\text{Had}}(\text{vac. pol.}) \times 10^{11}$
$2m_\pi - 1.8$	$6343 \pm 60$
$1.8 - 3.7$	$338.7 \pm 4.6$
$3.7 - 5 + \psi(1S, 2S)$	$143.1 \pm 5.4$
$5 - 9.3$	$68.7 \pm 1.1$
$9.3 - 12$	$12.1 \pm 0.5$
$12 - \infty$	$18.0 \pm 0.1$
Total	$6924 \pm 62$

It is clear from Table 1 that the final result and its uncertainty are dominated by the low energy region. In fact, the  $\rho(770 \text{ MeV})$  resonance provides about 72% of the total hadronic contribution to  $a_\mu^{\text{Had}}(\text{vac. pol.})$ .

To reduce the uncertainty in the  $\rho$  resonance region, Davier and Höcker employed  $\Gamma(\tau \rightarrow \nu_\tau \pi^- \pi^0)/\Gamma(\tau \rightarrow \nu_\tau \bar{\nu}_e e^-)$  data to supplement  $e^+e^- \rightarrow \pi^+\pi^-$  cross-sections. In the  $I = 1$  channel they are related by isospin. Currently, tau decay data is experimentally more precise.

An issue in the use of tau decay data is the magnitude of isospin violating corrections due to QED and the  $m_d - m_u$  mass difference. A short-distance QED correction [19] of about  $-2\%$  was applied to the hadronic tau decay data and the  $m_{\pi^\pm} - m_{\pi^0}$  phase space difference is easy to account for. Other isospin violating differences are estimated to be about  $\pm 0.5\%$  and included in the hadronic uncertainty.

Although the error assigned to the use of tau decay data appears reasonable, it has been questioned [20,21]. More recent preliminary  $e^+e^- \rightarrow \pi^+\pi^-$  data from Novosibirsk [20] seems to suggest a potential 1.5 sigma difference with corrected hadronic tau decays which would seem to further reduce  $a_\mu^{\text{Had}}$ . It is not clear whether the difference is due to additional isospin violating corrections to hadronic tau decays or radiative corrections to  $e^+e^- \rightarrow \text{hadrons}$  data which must be accounted for in any precise comparison [22]. If that difference is confirmed by further scrutiny, it could lead to a reduction in  $a_\mu^{\text{Had}}(\text{vac. pol.})$ . Resolution of this issue is extremely important. However, we note that a reduction in  $a_\mu^{\text{Had}}$  would further increase the  $a_\mu^{\text{exp}} - a_\mu^{\text{SM}}$  difference given in the abstract which is roughly 1 sigma at present.

Evaluation of the 3-loop hadronic vacuum polarization contribution to  $a_\mu$  has been updated to [23,17]

$$\Delta a_\mu^{\text{Had}}(\text{vac. pol.}) = -100(6) \times 10^{-11}. \quad (12)$$

Light-by-light hadronic diagrams have been evaluated using chiral perturbation theory. An average [13,14,15] of two recent studies [24,25] gives

$$\Delta a_\mu^{\text{Had}}(\text{light-by-light}) = -85(25) \times 10^{-11}. \quad (13)$$

Adding the contributions in Eqs. (11), (12), and (13) leads to the total hadronic contribution

$$a_\mu^{\text{Had}} = 6739(67) \times 10^{-11}. \quad (14)$$

The uncertainty in that result represents the main theoretical error in  $a_\mu^{\text{SM}}$ . It would be very valuable to supplement the above evaluation of  $a_\mu^{\text{Had}}$  with lattice calculations (for the light-by-light contribution) and improved  $e^+e^-$  data. A goal of  $\pm 40 \times 10^{-11}$  or smaller appears to be within reach and is well matched to the prospectus of experiment E821 at Brookhaven which aims for a similar level of accuracy.

### 2.3 Electroweak corrections

The one-loop electroweak radiative corrections to  $a_\mu$  are predicted in the Standard Model to be [26,27,28,29,30,31,32]

$$\begin{aligned}
a_\mu^{\text{EW}}(1 \text{ loop}) &= \frac{5 G_\mu m_\mu^2}{3 \cdot 8 \sqrt{2} \pi^2} \\
&\times \left[ 1 + \frac{1}{5} (1 - 4 \sin^2 \theta_W)^2 + \mathcal{O} \left( \frac{m_\mu^2}{M^2} \right) \right] \\
&\approx 195 \times 10^{-11}
\end{aligned} \tag{15}$$

where  $G_\mu = 1.16637(1) \times 10^{-5} \text{ GeV}^{-2}$ ,  $\sin^2 \theta_W \equiv 1 - M_W^2/M_Z^2 \simeq 0.223$ . and  $M = M_W$  or  $M_{\text{Higgs}}$ . The original goal of E821 at Brookhaven was to measure that predicted effect at about the 5 sigma level (assuming further reduction in the hadronic uncertainty). Subsequently, it was pointed out [33] that two-loop electroweak contributions are relatively large due to the presence of  $\ln m_Z^2/m_\mu^2 \simeq 13.5$  terms. A full two-loop calculation [34,35], including low-energy hadronic electroweak loops [36,35], found for  $m_H \simeq 150 \text{ GeV}$

$$a_\mu^{\text{EW}}(2 \text{ loop}) = -43(4) \times 10^{-11}, \tag{16}$$

where the quoted error is a conservative estimate of hadronic, Higgs, and higher-order corrections. Combining eqs. (15) and (16) gives the electroweak contribution

$$a_\mu^{\text{EW}} = 152(4) \times 10^{-11}. \tag{17}$$

Higher-order leading logs of the form  $(\alpha \ln m_Z^2/m_\mu^2)^n$ ,  $n = 2, 3, \dots$  can be computed via renormalization group techniques [37]. Due to cancellations, they give a relatively small  $+0.5 \times 10^{-11}$  contribution to  $a_\mu^{\text{EW}}$ . It is safely included in the uncertainty of eq. (17).

### 2.4 Comparison with Experiment

The complete Standard Model prediction for  $a_\mu$  is

$$a_\mu^{\text{SM}} = a_\mu^{\text{QED}} + a_\mu^{\text{Had}} + a_\mu^{\text{EW}}. \tag{18}$$

Combining eqs. (8), (14) and (17), one finds

$$a_\mu^{\text{SM}} = 116\,591\,597(67) \times 10^{-11}. \tag{19}$$

Comparing that prediction with the current experimental value in eq. (6) gives

$$a_\mu^{\text{exp}} - a_\mu^{\text{SM}} = 453 \pm 465 \times 10^{-11}. \tag{20}$$

That still leaves considerable room for contributions from “New Physics” beyond the Standard Model. At (one-sided [38]) 95% CL, one finds

$$- 310 \times 10^{-11} \leq a_\mu(\text{New Physics}) \leq 1216 \times 10^{-11}. \quad (21)$$

That constraint is already significant for theories which give additional negative contributions to  $a_\mu$ . Soon, its range will be reduced by a factor of 3 when the new E821 result is unveiled. Will a clear signal for “New Physics” emerge? As we show in the next section, realistic examples of “New Physics” could quite easily lead to  $a_\mu(\text{New Physics}) \sim \mathcal{O}(400 - 500 \times 10^{-11})$  which would appear as about a 3 sigma effect in the near term and increase to a 6 or 7 sigma effect as E821 is completed and the hadronic uncertainties in  $a_\mu^{\text{SM}}$  are further reduced.

### 3 “New Physics” effects

In general, “New Physics” (i.e. beyond the Standard Model expectations) will contribute to  $a_\mu$  via quantum loop effects. Indeed, whenever a new model or Standard Model extension is proposed,  $a_\mu^{\text{exp}} - a_\mu^{\text{SM}}$  is employed to constrain or rule it out. Future improvements in  $a_\mu^{\text{exp}}$  will make such tests even more powerful. Alternatively, they may in fact uncover a significant deviation indicative of “New Physics”.

In this section we describe several generic examples of interesting “New Physics” probed by  $a_\mu^{\text{exp}} - a_\mu^{\text{SM}}$ . Rather than attempting to be inclusive, we concentrate on two general scenarios: 1) Supersymmetric loop effects which can be substantial and would be heralded as the most likely explanation if a deviation in  $a_\mu^{\text{exp}}$  is observed and 2) Models of radiative muon mass generation which predict  $a_\mu(\text{New Physics}) \sim m_\mu^2/M^2$  where  $M$  is the scale of “New Physics”. Other examples of potential “New Physics” contributions to  $a_\mu$  are only briefly mentioned.

#### 3.1 Supersymmetry

The supersymmetric contributions to  $a_\mu$  stem from smuon–neutralino and sneutrino–chargino loops (see Fig. 1). They include 2 chargino and 4 neutralino states and could in principle entail slepton mixing and phases.

Early studies of the supersymmetric contributions  $a_\mu^{\text{SUSY}}$  were carried out in the context of the minimal SUSY standard model (MSSM) [39,40,41,42,43,44,45,46], in an  $E_6$  string-inspired model [47,48], and in an extension of the MSSM with an additional singlet [49,50]. An important observation was made in [51], namely that some of the contributions are enhanced by the ratio of Higgs’ vacuum expectation values,  $\tan \beta$ , which in some models is large (of order  $m_t/m_b \approx 40$ ). The main contribution is generally due to the chargino-sneutrino diagram (Fig. 1a), which is enhanced by a Yukawa coupling in the muon-sneutrino-Higgsino vertex.

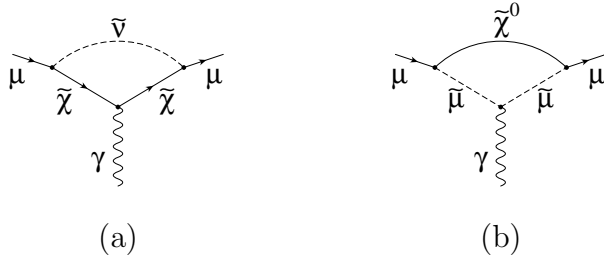


Figure 1: Supersymmetric loops contributing to the muon anomalous magnetic moment.

The leading effect is approximately given in the large  $\tan\beta$  limit by

$$|a_\mu^{\text{SUSY}}| \simeq \frac{\alpha(M_Z)}{8\pi \sin^2\theta_W} \frac{m_\mu^2}{\widetilde{m}^2} \tan\beta \left(1 - \frac{4\alpha}{\pi} \ln \frac{\widetilde{m}}{m_\mu}\right), \quad (22)$$

where  $\widetilde{m}$  represents a typical SUSY loop mass. (Chargino- and sneutrino-masses are assumed degenerate in that expression [52].) Also, we have included a 7–8% suppression factor due to 2-loop EW effects [34,37]. Numerically, one expects

$$|a_\mu^{\text{SUSY}}| \simeq 140 \times 10^{-11} \left(\frac{100 \text{ GeV}}{\widetilde{m}}\right)^2 \tan\beta, \quad (23)$$

where  $a_\mu^{\text{SUSY}}$  generally has the same sign as the  $\mu$ -parameter in SUSY models.

Ref. [51] found that E821 will be a stringent test of a class of supergravity models. In the minimal SU(5) SUGRA model,  $\tan\beta$  is severely constrained by proton decay lifetime and no significant  $a_\mu^{\text{SUSY}}$  is possible. However, extended models, notably SU(5) $\times$ U(1) escape that bound and can induce large effects.

Supersymmetric effects in  $a_\mu$  were subsequently computed in a variety of models. Constraints on MSSM were examined in [52,53]. MSSM with large CP-violating phases was studied in [54]. Ref. [55] examined models with a superlight gravitino. Detailed studies of  $a_\mu^{\text{SUSY}}$  were carried out in models constrained by various assumptions on the SUSY-breaking mechanism: gauge-mediated [56,57], SUGRA [58,59,60], and anomaly-mediated [61].

If we simply employ for illustration the large  $\tan\beta$  approximate formula in eq. (23) and the current constraint in eq. (20), then we find (for positive  $\text{sgn}(\mu)$ )

$$\tan\beta \left(\frac{100 \text{ GeV}}{\widetilde{m}}\right)^2 \simeq 3.2 \pm 3.3. \quad (24)$$

For  $\tan\beta \simeq 40$ , the non-trivial bound  $\widetilde{m} \geq 215 \text{ GeV}$  (95% one-sided CL) follows. It is anticipated that the uncertainty in that constraint will soon be reduced to  $\pm 1$  when the E821 result is announced. One can imagine a variety of outcomes and inferences. If the central value in (24) falls to near zero, then for  $\tan\beta \simeq 40$ ,  $\widetilde{m} \geq 500 \text{ GeV}$

will result, a significant constraint. (Negative  $\text{sgn } \mu$  models are already tightly constrained.) (Of course, in specific models with non-degenerate gauginos and sleptons, a more detailed study is required, but here we only want to illustrate roughly the scale of supersymmetry probed.) More interesting would be the case where the central value in eq. (24) remains fixed and the error is reduced to  $\pm 1$ , thereby signaling at a 3 sigma level the presence of “New Physics”. A natural SUSY interpretation would be that  $\text{sgn } \mu$  is positive,  $\tan \beta$  is large  $\mathcal{O}(20 - 40)$  and  $\widetilde{m} \simeq 250 - 350$  GeV or that  $\tan \beta$  is moderate  $\mathcal{O}(5 - 10)$  and  $\widetilde{m} \simeq 125 - 180$  GeV. Either represents a very exciting prospect with important implications for collider phenomenology as well as other low energy experiments such as  $b \rightarrow s\gamma$ ,  $\mu \rightarrow e\gamma$  etc. Such scenarios are well within the mainstream of SUSY models. Hence, we anticipate a clear deviation in  $a_\mu^{\text{exp}}$  from Standard Model expectations to be heralded as strong evidence for supersymmetry.

### 3.2 Radiative Muon Mass Models

The relatively light masses of the muon and most other known fundamental fermions suggest that they may be radiatively loop induced by “New Physics” beyond the Standard Model. Although no compelling model exists, the concept is very attractive as a natural scenario for explaining the flavor mass hierarchy.

The basic idea is to start off with a naturally zero bare mass due to an underlying chiral symmetry. The symmetry is broken by quantum loop effects. They lead to a finite calculable mass which depends on the mass scales, coupling strengths and dynamics of the underlying symmetry breaking mechanism. One generically expects for the muon

$$m_\mu \propto \frac{g^2}{16\pi^2} M_F, \quad (25)$$

where  $g$  is some new interaction coupling strength and  $M_F \sim 100 - 1000$  GeV is a heavy scale associated with chiral symmetry breaking.

Whatever source of chiral symmetry breaking is responsible for generating the muon’s mass will also give rise to non-Standard Model contributions in  $a_\mu$ . Indeed, fermion masses and anomalous magnetic moments are intimately connected chiral symmetry breaking operators. Remarkably, in such radiative scenarios, the additional contribution to  $a_\mu$  is quite generally given by [62,63]

$$a_\mu(\text{New Physics}) \simeq C \frac{m_\mu^2}{M^2}, \quad C \simeq \mathcal{O}(1), \quad (26)$$

where  $M$  is some physical high mass scale associated with the “New Physics” and  $C$  is a model-dependent number roughly of order 1 (it can be larger).  $M$  need not be the same scale as  $M_F$  in eq. (25). In fact,  $M$  is usually a somewhat larger gauge or scalar boson mass responsible for mediating the chiral symmetry breaking interaction. The

result in eq. (26) is remarkably simple in that it is largely independent of coupling strengths, dynamics, etc. Furthermore, rather than exhibiting the usual  $g^2/16\pi^2$  loop suppression factor,  $a_\mu(\text{New Physics})$  is related to  $m_\mu^2/M^2$  by a (model dependent) constant,  $C$ , roughly of  $\mathcal{O}(1)$ .

To demonstrate how the relationship in eq. (26) arises, we consider a simple toy model example [63] for muon mass generation which is graphically depicted in Fig. 2.

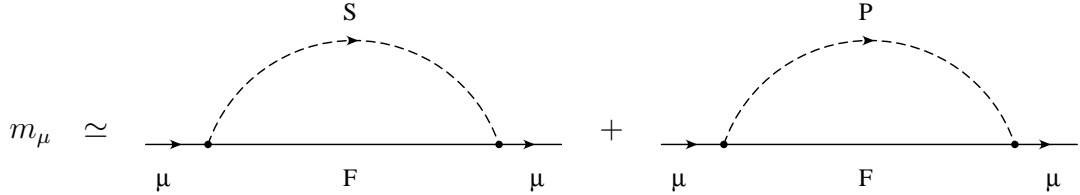


Figure 2: Example of a pair of one-loop diagrams, which can induce a finite radiative muon mass.

If the muon is massless in lowest order (i.e. no bare  $m_\mu^0$  is possible due to a symmetry), but couples to a heavy fermion  $F$  via scalar,  $S$ , and pseudoscalar,  $P$ , bosons with couplings  $g$  and  $g\gamma_5$  respectively, then the diagrams give rise to

$$m_\mu \simeq \frac{g^2}{16\pi^2} M_F \ln \left( \frac{m_S^2}{m_P^2} \right). \quad (27)$$

Note that short-distance ultraviolet divergences have canceled and the induced mass vanishes in the chirally symmetric limit  $m_S = m_P$ .

If we attach a photon to the heavy internal fermion,  $F$  (assumed to have charge  $-1$ ), then a new contribution to  $a_\mu$  is also induced. For  $m_S, m_P \gg M_F$ , one finds [63]

$$a_\mu(\text{New Physics}) \simeq \frac{g^2}{8\pi^2} \frac{m_\mu M_F}{m_P^2} \left( \frac{m_P^2}{m_S^2} \ln \frac{m_S^2}{M_F^2} - \ln \frac{m_P^2}{M_F^2} \right). \quad (28)$$

It also vanishes in the  $m_S = m_P$  chiral symmetry limit. Interestingly,  $a_\mu(\text{New Physics})$  exhibits a linear rather than quadratic dependence on  $m_\mu$  at this point. Recall, that in section 1 we said that such a feature was misleading or artificial. Our subsequent discussion should clarify that point.

Although eqs. (27) and (28) both depend on unknown parameters such as  $g$  and  $M_F$ , those quantities largely cancel when we combine both expressions. One finds

$$a_\mu(\text{New Physics}) \simeq C \frac{m_\mu^2}{m_P^2},$$

$$C = 2 \left[ 1 - \left( 1 - \frac{m_P^2}{m_S^2} \right) \ln \frac{m_S^2}{M_F^2} / \ln \frac{m_S^2}{m_P^2} \right], \quad (29)$$

where  $C$  is very roughly  $\mathcal{O}(1)$ . It can actually span a broad range, depending on the  $m_S/m_P$  ratio. A loop produced  $a_\mu(\text{New Physics})$  effect that started out at  $\mathcal{O}(g^2/16\pi^2)$  has been promoted to  $\mathcal{O}(1)$  by absorbing the couplings and  $M_F$  factor into  $m_\mu$ . Along the way, the linear dependence on  $m_\mu$  has been replaced by a more natural quadratic dependence.

A similar relationship,  $a_\mu(\text{New Physics}) \simeq Cm_\mu^2/M^2$ , has been found in more realistic multi-Higgs models [64], dynamical symmetry breaking scenarios such as extended technicolor [62,63], SUSY with soft masses [65], etc. It is also a natural expectation in composite models [66,67,68] or some models with large extra dimensions [69,70], although studies of such cases have not necessarily made that same connection. Basically, the requirement that  $m_\mu$  remain relatively small in the presence of new chiral symmetry breaking interactions forces  $a_\mu(\text{New Physics})$  to effectively exhibit a quadratic  $m_\mu^2$  dependence.

For models of the above variety, where  $|a_\mu(\text{New Physics})| \simeq m_\mu^2/M^2$ , the current constraint in eq. (21) suggests (very roughly)

$$M \gtrsim \mathcal{O}(1 \text{ TeV}), \quad (30)$$

and that level of sensitivity will expand to about 4 TeV as experiment E821 improves. Of course, a non-null finding of  $a_\mu(\text{New Physics}) \simeq 400 \times 10^{-11}$  could be interpreted as pointing to a source of muon mass generation characterized by a mass scale of  $M \sim 1 - 2 \text{ TeV}$ . Such a scale of “New Physics” could be quite natural in multi-Higgs models and soft SUSY mass scenarios. It would be somewhat low for dynamical symmetry breaking, compositeness and extra dimension models.

### 3.3 Other “New Physics” Examples

Many other examples of “New Physics” contributions to  $a_\mu$  have been considered in the literature. General analysis in terms of effective interactions was presented in [71]. Specific examples include effects due to anomalous  $W$  boson magnetic dipole and electric quadrupole moments [72,73,74,75], muon compositeness [68], extra gauge [76] or Higgs [77] bosons, leptoquarks [78,79], bileptons [80], 2-loop pseudoscalar effects [81], compact extra dimensions [82,83] etc. If a non-Standard Model effect is uncovered, all will certainly be revisited.

## 4 Outlook

After many years of experimental and theoretical toil, studies of the muon anomalous magnetic moment are entering a new exciting phase. Experiment E821 at Brookhaven will soon confront theory at the  $\pm 155 \times 10^{-11}$  level. Such sensitivity could start to unveil “New Physics” at the several sigma level without too much concern about theoretical hadronic uncertainties. Future analysis and runs would then

confirm and refine the discovery. Theorists would have a field day. Alternatively, the experiment could confirm Standard Model expectations and tighten the bounds on “New Physics”, a more traditional role for  $a_\mu$ .

Stay tuned, the show is about to begin.

## Acknowledgments

This work was supported by the DOE under grant number DE-AC02-98CH10886.

## References

- [1] R. S. van Dyck Jr., P. B. Schwinberg, and H. G. Dehmelt, *Phys. Rev. Lett.* **59**, 26 (1987).
- [2] P. J. Mohr and B. N. Taylor, *Rev. Mod. Phys.* **72**, 351 (2000).
- [3] S. Laporta and E. Remiddi, *Acta Phys. Polon.* **B28**, 959 (1997).
- [4] V. W. Hughes and T. Kinoshita, *Rev. Mod. Phys.* **71**, S133 (1999).
- [5] A. Czarnecki and W. J. Marciano, *Nucl. Phys. B (Proc. Suppl.)* **76**, 245 (1999).
- [6] T. Kinoshita, *Rept. Prog. Phys.* **59**, 1459 (1996).
- [7] G. Gabrielse and J. Tan, in *Cavity Quantum Electrodynamics*, edited by P. R. Berman (Academic Press, San Diego, 1994), p. 267.
- [8] C. Caso *et al.* (*Particle Data Group*), *Eur. Phys. J.* **C3**, 1 (1998).
- [9] H. N. Brown *et al.*, hep-ex/0009029 (unpublished).
- [10] T. Kinoshita and W. J. Marciano, in *Quantum Electrodynamics*, edited by T. Kinoshita (World Scientific, Singapore, 1990), pp. 419–478.
- [11] M. Gourdin and E. de Rafael, *Nucl. Phys.* **B10**, 667 (1969).
- [12] R. Alemany, M. Davier, and A. Höcker, *Eur. Phys. J.* **C2**, 123 (1998).
- [13] M. Davier and A. Höcker, *Phys. Lett.* **B435**, 427 (1998).
- [14] M. Davier, hep-ex/9912044 (unpublished).
- [15] M. Davier, *Nucl. Phys. B (Proc. Suppl.)* **76**, 327 (1999).

- [16] S. Eidelman and F. Jegerlehner, *Z. Phys.* **C67**, 585 (1995).
- [17] T. Kinoshita, B. Nizic, and Y. Okamoto, *Phys. Rev.* **D31**, 2108 (1985).
- [18] E. de Rafael, *Phys. Lett.* **B322**, 239 (1994).
- [19] W. J. Marciano and A. Sirlin, *Phys. Rev. Lett.* **61**, 1815 (1988).
- [20] S. Eidelman, private communication.
- [21] F. Jegerlehner, in *Radiative Corrections*, edited by J. Solà (World Scientific, Singapore, 1999), pp. 75–89.
- [22] W. J. Marciano, *Phys. Rev.* **D45**, R721 (1992).
- [23] B. Krause, *Phys. Lett.* **B390**, 392 (1997).
- [24] J. Bijnens, E. Pallante, and J. Prades, *Nucl. Phys.* **B474**, 379 (1996).
- [25] M. Hayakawa and T. Kinoshita, *Phys. Rev.* **D57**, 465 (1998).
- [26] S. J. Brodsky and J. D. Sullivan, *Phys. Rev.* **156**, 1644 (1967).
- [27] T. Burnett and M. J. Levine, *Phys. Lett.* **24B**, 467 (1967).
- [28] R. Jackiw and S. Weinberg, *Phys. Rev.* **D5**, 2473 (1972).
- [29] K. Fujikawa, B. W. Lee, and A. I. Sanda, *Phys. Rev.* **D6**, 2923 (1972).
- [30] I. Bars and M. Yoshimura, *Phys. Rev.* **D6**, 374 (1972).
- [31] G. Altarelli, N. Cabibbo, and L. Maiani, *Phys. Lett.* **B40**, 415 (1972).
- [32] W. A. Bardeen, R. Gastmans, and B. E. Lautrup, *Nucl. Phys.* **B46**, 315 (1972).
- [33] T. V. Kukhto, E. A. Kuraev, A. Schiller, and Z. K. Silagadze, *Nucl. Phys.* **B371**, 567 (1992).
- [34] A. Czarnecki, B. Krause, and W. Marciano, *Phys. Rev. Lett.* **76**, 3267 (1996).
- [35] A. Czarnecki, B. Krause, and W. Marciano, *Phys. Rev.* **D52**, R2619 (1995).
- [36] S. Peris, M. Perrottet, and E. de Rafael, *Phys. Lett.* **B355**, 523 (1995).
- [37] G. Degrassi and G. F. Giudice, *Phys. Rev.* **D58**, 053007 (1998).
- [38] We refer to a 95% one-sided confidence level as roughly equivalent to 90% two-sided.

- [39] P. Fayet, in *Unification of the Fundamental Particle Interactions*, edited by S. Ferrara, J. Ellis, and P. van Nieuwenhuizen (Plenum, New York, 1980), p. 587.
- [40] J. A. Grifols and A. Mendez, Phys. Rev. **D26**, 1809 (1982).
- [41] J. Ellis, J. Hagelin, and D. V. Nanopoulos, Phys. Lett. **B116**, 283 (1982).
- [42] R. Barbieri and L. Maiani, Phys. Lett. **B117**, 203 (1982).
- [43] J. C. Romao, A. Barroso, M. C. Bento, and G. C. Branco, Nucl. Phys. **B250**, 295 (1985).
- [44] D. A. Kosower, L. M. Krauss, and N. Sakai, Phys. Lett. **B133**, 305 (1983).
- [45] T. C. Yuan, R. Arnowitt, A. H. Chamseddine, and P. Nath, Z. Phys. **C26**, 407 (1984).
- [46] I. Vendramin, Nuovo Cim. **A101**, 731 (1989).
- [47] J. A. Grifols, J. Sola, and A. Mendez, Phys. Rev. Lett. **57**, 2348 (1986).
- [48] D. A. Morris, Phys. Rev. **D37**, 2012 (1988).
- [49] M. Frank and C. S. Kalman, Phys. Rev. **D38**, 1469 (1988).
- [50] R. M. Francis, M. Frank, and C. S. Kalman, Phys. Rev. **D43**, 2369 (1991).
- [51] J. L. Lopez, D. V. Nanopoulos, and X. Wang, Phys. Rev. **D49**, 366 (1994).
- [52] T. Moroi, Phys. Rev. **D53**, 6565 (1996).
- [53] G.-C. Cho, K. Hagiwara, and M. Hayakawa, Phys. Lett. **B478**, 231 (2000).
- [54] T. Ibrahim and P. Nath, Phys. Rev. **D62**, 015004 (2000).
- [55] A. Brignole, E. Perazzi, and F. Zwirner, JHEP **9909**, 002 (1999).
- [56] M. Carena, G. F. Giudice, and C. E. M. Wagner, Phys. Lett. **B390**, 234 (1997).
- [57] K. T. Mahanthappa and S. Oh, Phys. Rev. **D62**, 015012 (2000).
- [58] U. Chattopadhyay and P. Nath, Phys. Rev. **D53**, 1648 (1996).
- [59] T. Goto, Y. Okada, and Y. Shimizu, hep-ph/9908499 (unpublished).
- [60] T. Blazek, hep-ph/9912460 (unpublished).
- [61] U. Chattopadhyay, D. K. Ghosh, and S. Roy, hep-ph/0006049 (unpublished).

- [62] W. J. Marciano, in *Radiative Corrections: Status and Outlook*, edited by B. F. L. Ward (World Scientific, Singapore, 1995), pp. 403–414.
- [63] W. Marciano, in *Particle Theory and Phenomenology*, edited by K. Lassila *et al.* (World Scientific, Singapore, 1996), p. 22.
- [64] K. S. Babu and E. Ma, *Mod. Phys. Lett.* **A4**, 1975 (1989).
- [65] F. Borzumati, G. R. Farrar, N. Polonsky, and S. Thomas, *Nucl. Phys.* **B555**, 53 (1999).
- [66] S. J. Brodsky and S. D. Drell, *Phys. Rev.* **D22**, 2236 (1980).
- [67] G. L. Shaw, D. Silverman, and R. Slansky, *Phys. Lett.* **B94**, 57 (1980).
- [68] M. C. Gonzalez-Garcia and S. F. Novaes, *Phys. Lett.* **B389**, 707 (1996).
- [69] H. Davoudiasl, J. L. Hewett, and T. G. Rizzo, hep-ph/0006097 (unpublished).
- [70] R. Casadio, A. Gruppuso, and G. Venturi, hep-th/0010065 (unpublished).
- [71] R. Escribano and E. Masso, *Eur. Phys. J.* **C4** 139 (1998).
- [72] F. Herzog, *Phys. Lett.* **148B**, 355 (1984).
- [73] M. Suzuki, *Phys. Lett.* **153B**, 289 (1985).
- [74] A. Grau and J. A. Grifols, *Phys. Lett.* **154B**, 283 (1985).
- [75] M. Beccaria, F. M. Renard, S. Spagnolo, and C. Verzegnassi, *Phys. Lett.* **B448**, 129 (1999).
- [76] J. P. Leveille, *Nucl. Phys.* **B137**, 63 (1978).
- [77] M. Krawczyk and J. Zochowski, *Phys. Rev.* **D55**, 6968 (1997).
- [78] G. Couture and H. König, *Phys. Rev.* **D53**, 555 (1996).
- [79] S. Davidson, D. Bailey, and B. A. Campbell, *Z. Phys.* **C61**, 613 (1994).
- [80] F. Cuypers and S. Davidson, *Eur. Phys. J.* **C2**, 503 (1998).
- [81] D. Chang, W.-F. Chang, C.-H. Chou, and W.-Y. Keung, hep-ph/0009292 (unpublished).
- [82] M. L. Graesser, *Phys. Rev.* **D61**, 074019 (2000).
- [83] P. Nath and M. Yamaguchi, *Phys. Rev.* **D60**, 116006 (1999).

## Physics at *BABAR*

CHRISTOS TOURAMANIS\*

*Department of Physics  
Oliver Lodge Laboratory, University of Liverpool  
L69 7ZE, Liverpool, U.K.  
(for the BABAR Collaboration)*

The *BABAR* detector at the SLAC PEP-II asymmetric  $e^+e^-$  collider has first started collecting data in May 1999. A study of time-dependent  $CP$ -violating asymmetries in  $B^0 \rightarrow J/\psi K_s^0$  and  $B^0 \rightarrow \psi(2S)K_s^0$  decays has been performed on a data sample of  $9.0\text{fb}^{-1}$  taken at the  $\Upsilon(4S)$  resonance and  $0.8\text{fb}^{-1}$  off-resonance, collected through July 2000. The preliminary result  $\sin 2\beta = 0.12 \pm 0.37$  (stat)  $\pm 0.09$  (syst) is presented here, together with preliminary results on neutral and charged  $B$  meson lifetimes and  $B^0\bar{B}^0$  mixing.

Presented at the

5th International Symposium on Radiative Corrections  
(RADCOR-2000)

Carmel CA, USA, 11–15 September, 2000

---

\* Work supported by the U.K. Particle Physics and Astronomy Research Council, Advanced Research Fellowship GR/L04177

# 1 Introduction

The three-generation Standard Model can accommodate  $CP$  violation through the presence of a non-zero imaginary phase in the Cabibbo-Kobayashi-Maskawa (CKM) quark mixing matrix. However, existing measurements of  $CP$  violation in the neutral kaon system cannot prove that the CKM phase is indeed the origin of  $CP$  violation in nature.

The primary goal of the *BABAR* experiment at PEP-II is to elucidate this question by a series of observations and measurements of  $CP$ -violating effects in the  $B$  meson system. These measurements allow the extraction of the angles  $\alpha$ ,  $\beta$  and  $\gamma$  of the Unitarity Triangle, whose non-zero area [1] is a direct measure of  $CP$  violation.

*BABAR* can also access the sides of the Unitarity Triangle through measurements of  $|V_{ub}|$ ,  $|V_{cb}|$  in semileptonic  $B$  decays and  $|V_{td}|$  in  $B^0\bar{B}^0$  mixing. This allows to overconstrain the Unitarity Triangle and perform stringent tests of the Standard Model.

Thus, high statistics, a clean environment and broad access to the rich phenomenology of the  $B$  sector will allow *BABAR* to improve our knowledge of the overall  $B$  decay picture and probe New Physics at higher energy scales. A broad heavy flavor physics programme is also ongoing in *BABAR*.

## 2 PEP-II

The PEP-II  $B$  Factory [2] is an  $e^+e^-$  colliding beam storage ring complex at SLAC designed to produce a luminosity of  $3 \times 10^{33} \text{ cm}^{-2}\text{s}^{-1}$  at a center-of-mass energy of 10.58 GeV ( $\Upsilon(4S)$  resonance). During the 2000 run PEP-II has exceeded this luminosity, while *BABAR*, with a logging efficiency of  $>95\%$ , has routinely accumulated data above its design daily rate of  $135 \text{ pb}^{-1}$ .

The machine has asymmetric energy beams, with a High Energy Ring (HER, 9.0 GeV electrons) and a Low Energy Ring (LER, 3.1 GeV positrons). These correspond to a center-of-mass boost of  $\beta\gamma=0.56$  and lead to an average separation of  $\beta\gamma c\tau=250 \mu\text{m}$  between the two  $B$  mesons vertices, allowing the measurement of time-dependent  $CP$ -violating decay rate asymmetries.

At the  $\Upsilon(4S)$  resonance  $B$  mesons can only be produced as  $B^+B^-$  or coherent  $B^0\bar{B}^0$  pairs. The time evolution of a coherent  $B^0\bar{B}^0$  pair is coupled in such a way that the  $CP$  or flavor of one  $B$  at decay time  $t_1$  can be described as a function of the other  $B$  ( $B_{tag}$ ) flavor at its decay time  $t_2$  and the signed time difference  $\Delta t = t_1 - t_2$ .

## 3 *BABAR*

### 3.1 Detector description [2]

The volume within the 1.5T *BABAR* superconducting solenoid contains a five layer silicon strip vertex detector (SVT), a central drift chamber (DCH), a quartz-bar Cherenkov radiation detector (DIRC) and a CsI(Tl) crystal electromagnetic calorimeter (EMC). Two layers of cylindrical resistive plate counters (RPCs) are located between the barrel calorimeter and the magnet cryostat. The instrumented flux return (IFR) outside the cryostat is composed of 18 layers of radially increasing thickness steel, instrumented with 19 layers of planar RPCs in the barrel and 18 in the endcaps which provide muon and neutral hadron identification.

## 3.2 Particle reconstruction and identification [2]

Charged particle tracking using the SVT and DCH achieves a resolution of  $(\delta p_T/p_T)^2 = (0.0015 p_T)^2 + (0.005)^2$ , where  $p_T$  is the transverse momentum in GeV/ $c$ . The SVT with a typical resolution of 10  $\mu\text{m}$  per hit provides excellent vertex resolution both in the transverse plane and in  $z$ . The typical fully reconstructed single  $B$  decay vertex resolution in  $z$  is 50  $\mu\text{m}$ . Photons are reconstructed in the EMC, yielding mass resolutions of 6.9 MeV/ $c^2$  for  $\pi^0 \rightarrow \gamma\gamma$  and 10 MeV/ $c^2$  for  $K_S^0 \rightarrow \pi^0 \pi^0$ .

Leptons and hadrons are identified using a combination of measurements from all the *BABAR* components, including the energy loss  $dE/dx$  in the helium-based gas of the DCH (40 samples maximum) and in the silicon of the SVT (5 samples maximum). Electron identification is mainly based on the characteristics of their shower in the EMC, while muons are identified in the IFR and confirmed by their minimum ionising signal in the EMC. Excellent kaon identification in the barrel region is provided by the DIRC, which achieves a separation of  $>3.4\sigma$  in the range 0.25–3.5 GeV/ $c$ .

## 4 $B$ reconstruction

A variety of inclusive, semiexclusive and exclusive reconstruction methods are applied on the *BABAR* data, covering semileptonic and pure hadronic decay modes. The corresponding  $B$  samples have different sizes and purity levels and are used for different types of studies (Branching Fraction measurements, studies of the dynamics of certain decay chains). We will focus here on the cases where some information (final state(s), charge,  $CP$  or flavor content, decay vertex) can be reconstructed for both  $B$  mesons in the event.

### 4.1 Exclusive $B$ sample

$B^0$  and  $B^\pm$  mesons are reconstructed in the following hadronic modes of definite flavor:  $B^0 \rightarrow D^{(*)-}\pi^+, D^{(*)-}\rho^+, D^{(*)-}a_1^+, J/\psi K^{*0}, B^- \rightarrow D^0 \pi^-$  and  $B^- \rightarrow D^{*0} \pi^-$  <sup>†</sup>. All final state particles are reconstructed. The selections have been optimised for signal significance, using on-peak, off-peak and simulated data. Charged particle identification, mass(or mass difference) and vertex constraints are used wherever applicable. The signal for each decay mode is identified in the two-dimensional distribution of the kinematical variables  $\Delta E$  and  $m_{\text{ES}}$ :  $\Delta E = E_{\text{rec}}^* - E_b^*$  is the difference between the  $B$  candidate energy and the beam energy and  $m_{\text{ES}} = \sqrt{E_b^{*2} - \mathbf{p}_{\text{rec}}^{*2}}$  is the mass of a particle with a reconstructed momentum  $\mathbf{p}_{\text{rec}}^* = \sum_i \mathbf{p}_i^*$  assumed to have the beam energy, as is the case for a true  $B$  meson. In events with several  $B$  candidates only the one with the smallest  $\Delta E$  is considered. The  $\Delta E$  and  $m_{\text{ES}}$  variables have minimal correlation. The resolution in  $m_{\text{ES}}$  is  $\approx 3 \text{ MeV}/c^2$  and is dominated by the beam energy spread. The resolution in  $\Delta E$  is mode dependent and varies in the range of 12–40 MeV. For each mode a rectangular signal region is defined by the three standard deviation bands in  $m_{\text{ES}}$  ( $5.27 < m_{\text{ES}} < 5.29 \text{ GeV}/c^2$ ) and  $\Delta E$  (mode dependent interval). For each mode the sample composition is determined by fitting the  $m_{\text{ES}}$  distribution for candidates within the signal region in  $\Delta E$  to the sum of a single Gaussian representing the signal and a background function introduced by the ARGUS collaboration [3]. The purity of each subsample is computed as the ratio of the area of the Gaussian in the  $\pm 3\sigma$  range over the total area in this range. Figure 1 shows the  $m_{\text{ES}}$  distributions for the summed hadronic  $B^0$  and  $B^\pm$  modes with the fits superimposed.

<sup>†</sup>Throughout this paper, conjugate modes are implied.

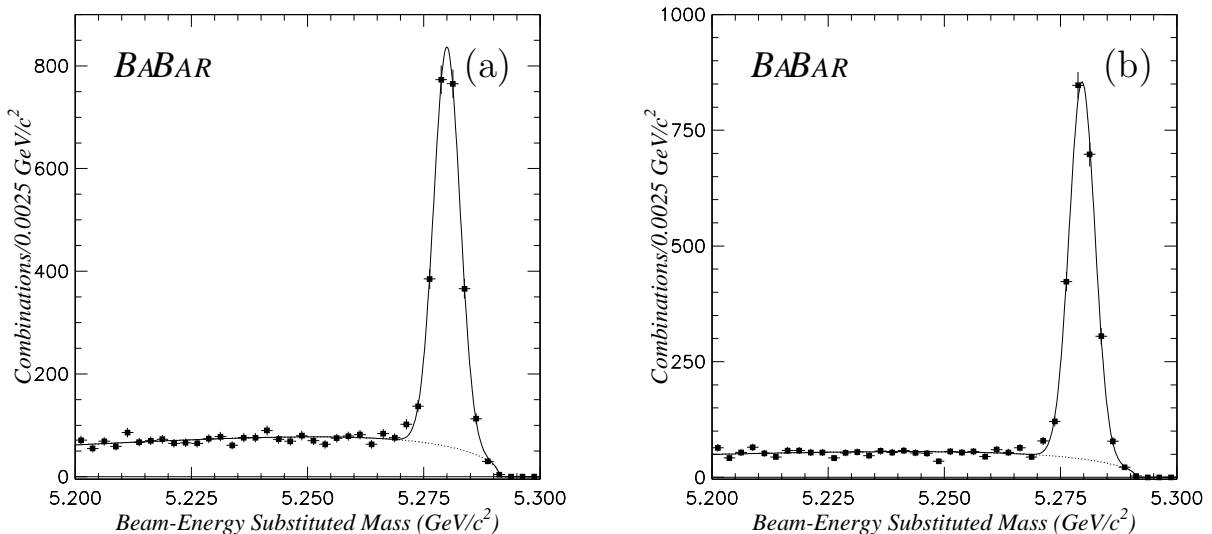


Figure 1:  $m_{ES}$  distribution for all the hadronic modes for (a)  $B^0$  and (b)  $B^\pm$ . The complete fit and its ARGUS [3] background content are also shown. The number of signal events in all  $B^0$  and  $B^\pm$  modes are  $2577 \pm 59$  and  $2636 \pm 56$ , with purity of  $\approx 86\%$  and  $\approx 89\%$  respectively.

## 4.2 Flavor tagging

After removal of the daughter tracks of the reconstructed  $B_{rec}$  in an event, the remaining tracks are used to determine the flavor of the other  $B$  meson ( $B_{tag}$ ), and this ensemble is assigned a tag flavor, either  $B^0$  or  $\bar{B}^0$ .

For each of the tagging methods used we define an effective tagging efficiency  $Q_i = \varepsilon_i \times (1 - 2w_i)^2$ , where  $\varepsilon_i$  is the fraction of events tagged by this method  $i$  and  $w_i$  is the mistag fraction, *i.e.* the probability of incorrectly assigning the opposite tag to an event using this method. A dilution factor is defined as  $\mathcal{D} = 1 - 2w$  and is extracted from the data for each method.

The **Lepton** category uses the presence and charge of a primary lepton from the decaying  $b$  quark. Both electrons and muons are used, with a minimum center-of-mass momentum requirement of  $1.1 \text{ GeV}/c$ . If both an electron and a muon candidate satisfy this requirement, only the electron is taken into account. Mistag arises from (a) pions seen as leptons and (b) softer opposite-sign leptons coming from charm semileptonic decays.

The **Kaon** category is based on the total charge of all identified Kaons. Events with conflicting **Lepton** and **Kaon** tags are excluded from both categories.

For events not tagged with the previous methods, a variety of available particle identification and kinematic variables are fed in a Neural Network whose design and training aims at exploiting the information present in this set of correlated quantities. It is sensitive to the presence of primary and cascade leptons, charged kaons and soft pions from  $D^*$  decays. In addition, the charge of high-momentum particles is exploited in a “jet-charge” type approach. This functionality has been assigned to different sub-nets, to facilitate understanding of the network performance. The output from the full neural network tagger  $x_{NT}$  is mapped onto the interval  $[-1, 1]$ . The assigned flavor

tag is  $B^0$  if  $x_{NT}$  is negative, and  $\bar{B}^0$  otherwise. Events with  $|x_{NT}| > 0.5$  are assigned to the NT1 tagging category and events with  $0.2 < |x_{NT}| < 0.5$  to the NT2 tagging category. Events with  $|x_{NT}| < 0.2$  have very little tagging power and are rejected.

### 4.3 $\Delta t$ calculation and resolution

Since no stable charged particle emerges from the  $\Upsilon(4S)$  decay point, the production point of the  $B$  mesons and thus their individual decay times cannot be determined. However the decay time difference  $\Delta t$  between the two is sufficient for the description of a coherent  $B$  meson pair (decay length difference technique).

The event topology is sketched in Fig. 2. In the *boost approximation* used in *BABAR* the decay time difference is calculated as :  $\Delta t = \Delta z/c < \beta\gamma >$ , where the small flight path of the  $B$  mesons perpendicular to the  $z$  axis is ignored.

Actually, the small effects arising from the tilt of the PEP-II beams with respect to the *BABAR*  $z$  axis (20 mrad), fluctuations in the beam energies, the  $B$  meson transverse momentum in the  $\Upsilon(4S)$  rest frame, have been studied and are taken into account either in the calculations or in the systematic errors as appropriate.

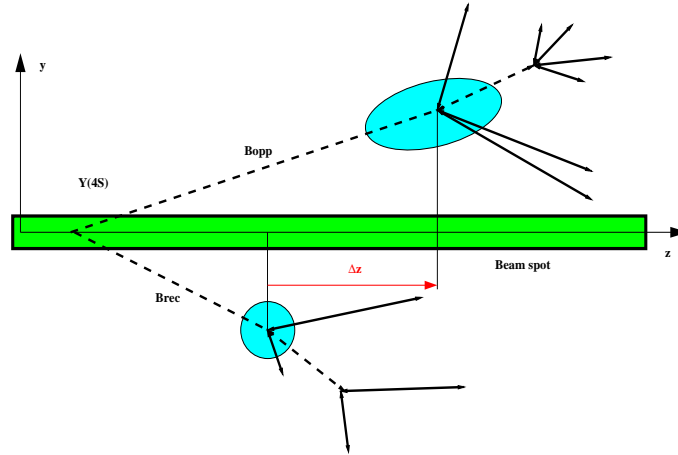


Figure 2: Event topology showing the two  $B$  production and decay points. The figure is not drawn to scale; it has been expanded in the  $y$  direction.

The resolution  $\sigma_z$  for the fully reconstructed  $B$  is found in the simulation to be 45–65  $\mu\text{m}$ , depending on the mode. The resolution  $\sigma_z$  for the tag side is  $\approx 125 \mu\text{m}$ , with a small bias of 25  $\mu\text{m}$  due to forward-going charm decays that cannot be resolved. The resulting resolution in  $\Delta t$  has been parametrised as the sum of three gaussians. The core has a  $\sigma$  of 0.6 ps and contains 75% of the events. The tail has a  $\sigma$  of 1.8 ps. Outliers are described by a gaussian with fixed  $\sigma$  of 8 ps, that contains  $\approx 1\%$  of the total events. This resolution model is used for the lifetime, mixing and  $\sin 2\beta$  fits. Two scale factors (multiplicative to the width of the core and tail gaussians) are included in the fits to the real data for the first two cases, to account for eventual imperfections in the modeling of  $D$  decays and multiple scattering in the simulation. Extensive studies on the different event samples and with variations of the fits (free and fixed parameters) have been performed in order to optimise and validate the method and to obtain reliable estimates of the systematic errors.

## 5 $B$ lifetime measurements

The observed  $\Delta t$  distribution for a set of  $B$  pair events in the presence of the resolution function  $\mathcal{R}$  is :

$$\mathcal{F}(\Delta t) = \Gamma \exp(-\Gamma|\Delta t|) \otimes \mathcal{R}(\Delta t; \hat{a}) \quad (1)$$

where  $\hat{a}$  is the set of parameters describing the resolution function.

The  $B$  meson lifetimes are extracted with unbinned maximum likelihood fits that take individual event  $\Delta t$  errors into account. Our preliminary results are :

$$\begin{aligned} \tau_{B^0} &= 1.506 \pm 0.052 \text{ (stat)} \pm 0.029 \text{ (syst)} \text{ ps} \\ \tau_{B^+} &= 1.602 \pm 0.049 \text{ (stat)} \pm 0.035 \text{ (syst)} \text{ ps} \\ \tau_{B^+}/\tau_{B^0} &= 1.065 \pm 0.044 \text{ (stat)} \pm 0.021 \text{ (syst)} \end{aligned}$$

The only background source is combinatorial and it is estimated from the side-bands of the beam energy substituted mass variable. The main systematic error comes from the resolution modeling and parameters. The two proper time fits are shown in Figure 3.

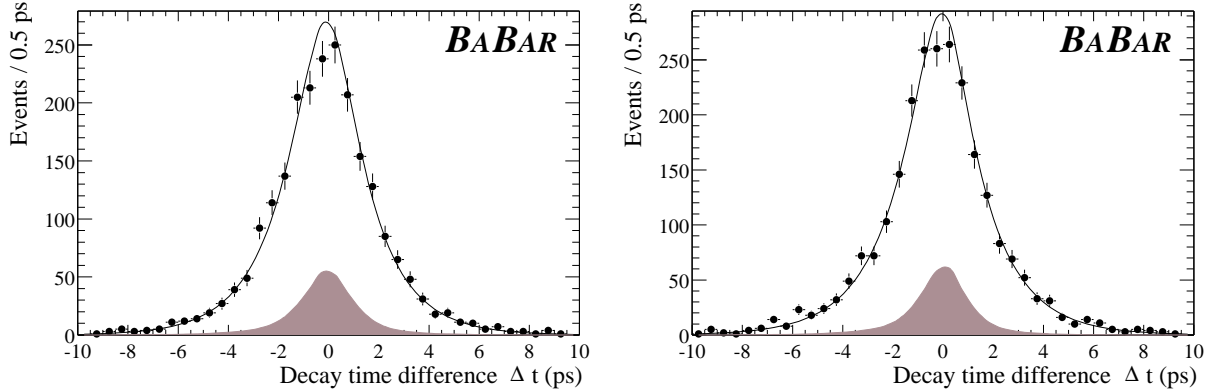


Figure 3:  $\Delta t$  distributions for the  $B^0$  (right) and  $B^\pm$  (left) candidates. The result of the lifetime fit is superimposed. The hatched areas represent the background content of the event samples.

## 6 $B^0$ mixing measurements

Mixing allows the two neutral  $B$  mesons in the  $B^0\bar{B}^0$  coherent state to decay with the same flavor (*mixed events*) or the opposite flavor (*unmixed events*). In a perfect detector one would then observe a time dependent oscillation in the rates of unmixed(+) and mixed(-) events :

$$f_{\pm}(\Delta t; \Gamma, \Delta m_d) = \frac{1}{4} \Gamma e^{-\Gamma|\Delta t|} [1 \pm \cos \Delta m_d \Delta t] \quad (2)$$

where  $\Delta m_d$  is the difference between the mass eigenstates  $B_H^0$  and  $B_L^0$ . Due to imperfect tagging and vertex determination the observed rates become :

$$\mathcal{F}_{\pm}(\Delta t; \Gamma, \Delta m_d, \mathcal{D}, \hat{a}) = \frac{1}{4} \Gamma e^{-\Gamma|\Delta t|} [1 \pm \mathcal{D} \times \cos \Delta m_d \Delta t] \otimes \mathcal{R}(\Delta t; \hat{a}) \quad (3)$$

where  $\mathcal{D}$  is the dilution factor (section 4.2) and  $\mathcal{R}$  is the  $\Delta t$  resolution (section 4.3)

An unbinned maximum likelihood fit that takes into account individual event  $\Delta t$  errors and tagging category is performed on events from the exclusively reconstructed  $B^0$  sample (section 4.1), after tagging (section 4.2) has been performed. The value of  $\Delta m_d$  is fitted simultaneously with the individual dilution factors for each tagging category. This information is later used in the  $\sin 2\beta$  extraction. Our preliminary result for  $\Delta m_d$  is :

$$\Delta m_d = 0.516 \pm 0.031(\text{stat.}) \pm 0.018(\text{syst.}) \hbar \text{ps}^{-1}$$

A sample of events where a semileptonic ( $D^* \ell \nu$ ) instead of a hadronic  $B^0$  decay has been reconstructed (7517 events) are analysed using the same method and fit. The preliminary result for  $\Delta m_d$  from this sample is :

$$\Delta m_d = 0.508 \pm 0.020(\text{stat.}) \pm 0.022(\text{syst.}) \hbar \text{ps}^{-1}$$

Combining the  $\Delta m_d$  results from the hadronic and semileptonic  $B$  samples we obtain the preliminary result :

$$\Delta m_d = 0.512 \pm 0.017(\text{stat.}) \pm 0.022(\text{syst.}) \hbar \text{ps}^{-1}$$

The main sources of systematic errors are the  $\Delta t$  resolution function, Monte Carlo statistics and the  $B^\pm$  background in the semileptonic sample.

In an independent analysis a more abundant but less pure sample of dilepton events has been used. In this inclusive approach the mistag arising from cascade leptons and the  $B^\pm$  fraction are extracted from the same fit as  $\Delta m_d$ . Our preliminary result for  $\Delta m_d$  is :

$$\Delta m_d = 0.507 \pm 0.015(\text{stat.}) \pm 0.022(\text{syst.}) \hbar \text{ps}^{-1}$$

The results from the hadronic and dilepton samples are shown in Figure 4. The tagging performance parameters for each tagging method (category) are extracted from the fully reconstructed sample fits (hadronic and semileptonic) and are shown in Table 1.

Tagging Category	$\varepsilon$ (%)	$w$ (%)	$Q$ (%)
Lepton	$11.2 \pm 0.5$	$9.6 \pm 1.7 \pm 1.3$	$7.3 \pm 0.7$
Kaon	$36.7 \pm 0.9$	$19.7 \pm 1.3 \pm 1.1$	$13.5 \pm 1.2$
NT1	$11.7 \pm 0.5$	$16.7 \pm 2.2 \pm 2.0$	$5.2 \pm 0.7$
NT2	$16.6 \pm 0.6$	$33.1 \pm 2.1 \pm 2.1$	$1.9 \pm 0.5$
all	$76.7 \pm 0.5$		$27.9 \pm 1.6$

Table 1: Tagging performance parameters measured from the mixing maximum-likelihood fit for the fully-reconstructed  $B^0$  sample. The uncertainties on  $\varepsilon$  and  $Q$  are statistical only.

## 7 The $\sin 2\beta$ measurement

If one of the neutral  $B$  mesons ( $B_{tag}$ ) of the coherent  $B^0 \bar{B}^0$  pair decays to a definite flavor eigenstate at time  $t_{tag}$  and the other  $B$  decays to a  $CP$ -even eigenstate like  $J/\psi K_S^0$  or  $\psi(2S)K_S^0$  at time  $t_{CP}$ ,

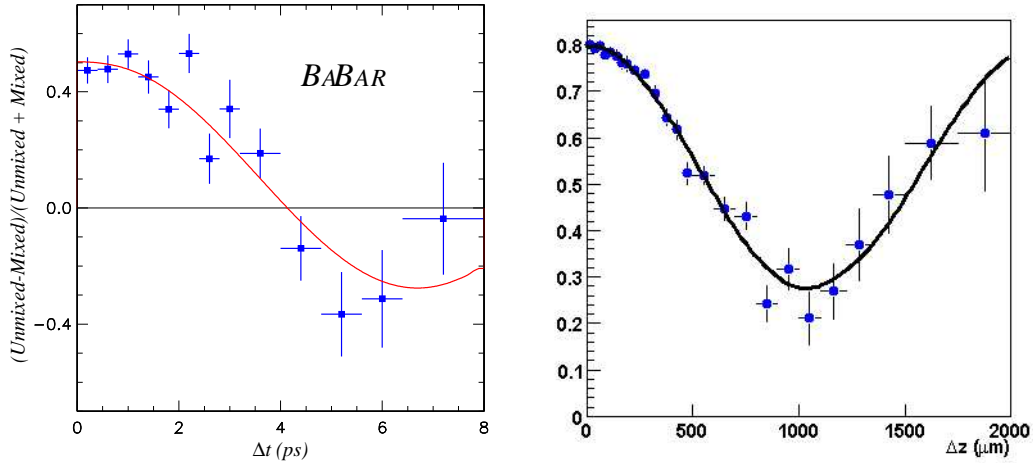


Figure 4: The observed time dependent asymmetries between unmixed and mixed events for the fully reconstructed (left) and dilepton (right)  $B^0$  samples described in the text. The curves show the fit results.

then in a perfect detector the following decay rates would be observed :

$$f_{\pm}(\Delta t; \Gamma, \Delta m_d, \sin 2\beta) = \frac{1}{4} \Gamma e^{-\Gamma|\Delta t|} [1 \pm \sin 2\beta \times \sin \Delta m_d \Delta t] \quad (4)$$

where  $\Delta t = t_{CP} - t_{tag}$  and the (+) or (-) sign indicates whether the  $B_{tag}$  is tagged as a  $B^0$  or a  $\bar{B}^0$  respectively. In the presence of the dilution factor  $\mathcal{D}$  and  $\Delta t$  resolution  $\mathcal{R}$  the observed rates become :

$$\mathcal{F}_{\pm}(\Delta t; \Gamma, \Delta m_d, \mathcal{D} \sin 2\beta, \hat{a}) = \frac{1}{4} \Gamma e^{-\Gamma|\Delta t|} [1 \pm \mathcal{D} \sin 2\beta \times \sin \Delta m_d \Delta t] \otimes \mathcal{R}(\Delta t; \hat{a}) \quad (5)$$

The time dependent decay rate asymmetry  $\mathcal{A}_{CP}(\Delta t)$  is a  $CP$ -violating observable which (neglecting resolution effects) is approximately proportional to  $\sin 2\beta$ :

$$\mathcal{A}_{CP}(\Delta t) = \frac{\mathcal{F}_+(\Delta t) - \mathcal{F}_-(\Delta t)}{\mathcal{F}_+(\Delta t) + \mathcal{F}_-(\Delta t)} \sim \mathcal{D} \sin 2\beta \times \sin \Delta m_d \Delta t \quad (6)$$

## 7.1 Analysis procedure

The extraction of  $\sin 2\beta$  from the data follows the following steps :

- Selection of the signal  $B^0/\bar{B}^0 \rightarrow J/\psi K_S^0$  and  $B^0/\bar{B}^0 \rightarrow \psi(2S)K_S^0$  events, detailed in the following section. Backgrounds and in particular any admixture with the “wrong”  $CP$  content have to be kept at a minimum level.
- Measurement of  $\Delta t$ . The resolution is studied using simulated events and its parameters are actually extracted from real data, as described in section 4.3.
- Determination of the flavor of the  $B_{tag}$ , as described in section 4.2. The dilution factors  $\mathcal{D}_i$  for each tagging category are measured on real data, as described in section 6.

- Extraction of the amplitude of the  $CP$  asymmetry and the value of  $\sin 2\beta$  with an unbinned maximum likelihood fit, described in the following.

A blind analysis has been adopted for the extraction of  $\sin 2\beta$ . A technique that hides the result of the fit by arbitrarily flipping its sign and adding an arbitrary offset, without affecting the error on the fitted parameters or their correlations, was used. Moreover, the visual  $CP$  asymmetry in the  $\Delta t$  distribution is hidden by multiplying  $\Delta t$  by the sign of the tag and adding an arbitrary offset. Such an approach allows to optimise and finalise the event selection and fitting strategy as well as perform a variety of validation and stability checks without the possibility of any experimenter's bias.

## 7.2 Event samples

The  $CP$  sample contains  $B^0$  candidates reconstructed in the  $CP$  eigenstates  $J/\psi K_S^0$  or  $\psi(2S)K_S^0$ . The charmonium mesons are reconstructed through their decays to  $e^+e^-$  and  $\mu^+\mu^-$ , while the  $\psi(2S)$  is also reconstructed through its decay to  $J/\psi\pi^+\pi^-$ . The  $K_S^0$  is reconstructed through its decays to  $\pi^+\pi^-$  and  $\pi^0\pi^0$ .

Utilisation of the exclusively reconstructed  $B$  samples (section 4.1) for the characterisation of the tagging and vertexing performance and quality has already been described. In addition 570  $B^+ \rightarrow J/\psi K^+$  candidates and 237  $B^0 \rightarrow J/\psi(K^{*0} \rightarrow K^+\pi^-)$  candidates have been reconstructed and used extensively in validation analyses.

## 7.3 Selection of events in the $CP$ sample

Events are required to have at least four reconstructed charged tracks, a vertex within 0.5 cm of the average position of the interaction point in the transverse plane, total visible energy greater than 5 GeV, and second-order normalized Fox-Wolfram moment[4] ( $R_2 = H_2/H_0$ ) less than 0.5.

For the  $J/\psi$  or  $\psi(2S) \rightarrow e^+e^-$  ( $\mu^+\mu^-$ ) candidates, at least one of the decay products is required to be positively identified as an electron (muon) in the EMC (IFR). Electrons outside the acceptance of the EMC are accepted if their DCH  $dE/dx$  information is consistent with the electron hypothesis. Looser particle identification criteria are applied on the second electron (muon) candidates. In the muon case, a minimum ionising signature in the EMC is required.

$J/\psi$  candidates are selected with an invariant mass greater than 2.95(3.06)  $\text{GeV}/c^2$  for  $e^+e^-$  ( $\mu^+\mu^-$ ) and smaller than 3.14  $\text{GeV}/c^2$  in both cases. The  $\psi(2S)$  candidates in leptonic modes must have a mass within 50  $\text{MeV}/c^2$  of the  $\psi(2S)$  mass. The lower bound is relaxed to 250  $\text{MeV}/c^2$  for the  $e^+e^-$  mode. For the  $\psi(2S) \rightarrow J/\psi\pi^+\pi^-$  mode, mass-constrained  $J/\psi$  candidates are combined with pairs of oppositely charged tracks considered as pions, and  $\psi(2S)$  candidates with mass between 3.0  $\text{GeV}/c^2$  and 4.1  $\text{GeV}/c^2$  are retained. The mass difference between the  $\psi(2S)$  candidate and the  $J/\psi$  candidate is required to be within 15  $\text{MeV}/c^2$  of the known mass difference.

$K_S^0$  candidates reconstructed in the  $\pi^+\pi^-$  mode are required to have an invariant mass, computed at the vertex of the two tracks, between 486  $\text{MeV}/c^2$  and 510  $\text{MeV}/c^2$  for the  $J/\psi K_S^0$  selection, and between 491  $\text{MeV}/c^2$  and 505  $\text{MeV}/c^2$  for the  $\psi(2S)K_S^0$  selection.

For the  $J/\psi K_S^0$  mode we also consider the decay of the  $K_S^0$  into  $\pi^0\pi^0$ . For pairs of  $\pi^0$  candidates with total energy above 800 MeV we determine the most probable  $K_S^0$  decay point along the path defined by the  $K_S^0$  momentum vector and the primary vertex of the event. The decay-point probability is the product of the  $\chi^2$  probabilities for each photon pair constrained to the  $\pi^0$  mass. We require the distance from the decay point to the primary vertex to be between  $-10$  cm and  $+40$  cm and the  $K_S^0$  mass measured at this point to be between 470 and 536  $\text{MeV}/c^2$ .

$B_{CP}$  candidates are formed by combining mass-constrained  $J/\psi$  or  $\psi(2S)$  candidates with mass-constrained  $K_S^0$  candidates. Cuts on the colinearity of flight vertex and momentum of the  $K_S^0$  (for  $\pi^+\pi^-$  decays), the cosine of the helicity angle of the  $J/\psi$  or  $\psi(2S)$  in the  $B$  candidate rest frame ( $e^+e^-$  and  $\mu^+\mu^-$  modes) or the cosine of the angle between the  $B_{CP}$  candidate three-momentum vector and the thrust vector of the rest of the event ( $\psi(2S) \rightarrow J/\psi\pi^+\pi^-$  mode) are applied to achieve the required signal purity.

$B_{CP}$  candidates are identified in the  $m_{ES}-\Delta E$  plane (see section 4.1). Signal event yields and purities, determined from a fit to the  $m_{ES}$  distributions after selection on  $\Delta E$ , are presented in Table 2. The  $CP$  candidate events are 168 with a purity of 95.6%. In 120 of these events there is information on the flavor of the other  $B$ . These events are used in the final fit for  $\sin 2\beta$ . Distributions of  $\Delta E$  and  $m_{ES}$  are shown in Figures 5 and 6.

Final state	All events	Purity	Tagged events
$J/\psi K_S^0 (K_S^0 \rightarrow \pi^+\pi^-)$	124	96%	85
$J/\psi K_S^0 (K_S^0 \rightarrow \pi^0\pi^0)$	18	91%	12
$\psi(2S)K_S^0$	27	93%	23

Table 2: Event yields for the  $CP$  samples used in this analysis. The total number of events in the  $m_{ES}-\Delta E$  signal box and their purity, as well as the size of the subsamples where the other  $B$  is tagged, are shown.

## 7.4 Extracting $\sin 2\beta$

The  $\Delta t$  of the 120 selected and tagged events is fitted to the expected time evolution (equation 5) with an unbinned maximum likelihood fit. Individual event errors on  $\Delta t$  are taken into account. The resolution determined on the fully reconstructed sample and the mistag factor  $w_i$  corresponding to the tagging category for each event are used in the fit. The  $\Delta m_d$  are fixed to the nominal PDG [5] values of  $\tau_{B^0} = 1.548$  ps and  $\Delta m_d = 0.472 \hbar \text{ps}^{-1}$  respectively. The resulting errors on  $\sin 2\beta$  due to these uncertainties are 0.002 and 0.015.

## 7.5 Fit validation, systematics studies and null $CP$ tests

Knowledge of the mistag fractions, description of the  $\Delta t$  resolution and backgrounds are (in that order) the main sources of systematic errors. All these have been extracted from real data. Real data, fully simulated Monte Carlo, and ‘‘Toy’’ Monte Carlo samples have been used to validate the method and implementation of the fit, to rule out possible biases from the method itself, and to assess the size of systematic errors.

The full  $CP$  analysis and fit were performed on data samples that have no  $CP$  asymmetry. No significant apparent  $CP$  effect was measured, as shown in Table 3. The  $1.9 \sigma$  asymmetry in the  $J/\psi K^{*0}$  channel is interpreted as a statistical fluctuation.

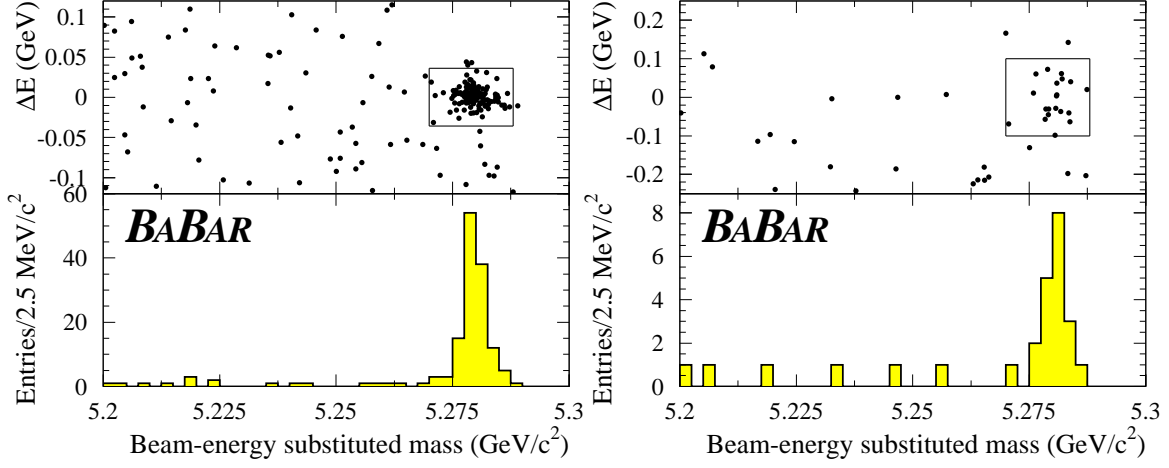


Figure 5:  $J/\psi K_S^0$  signal. Left:  $K_S^0 \rightarrow \pi^+\pi^-$ , Right:  $K_S^0 \rightarrow \pi^0\pi^0$

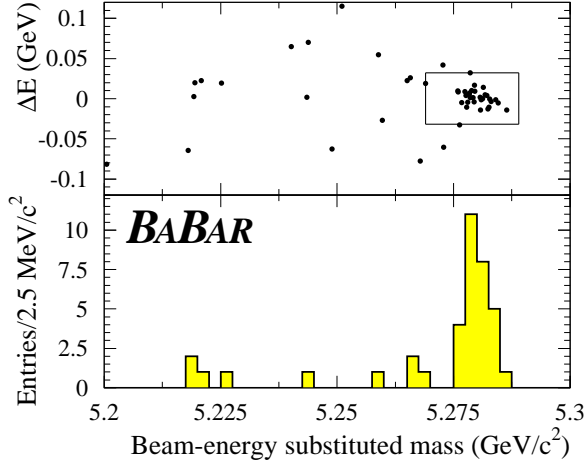


Figure 6:  $\psi(2S)K_S^0$  ( $K_S^0 \rightarrow \pi^+\pi^-$ ) signal.

Sample	Apparent $CP$ -asymmetry
Hadronic charged $B$ decays	$0.03 \pm 0.07$
Hadronic neutral $B$ decays	$-0.01 \pm 0.08$
$J/\psi K^+$	$0.13 \pm 0.14$
$J/\psi K^{*0}$ ( $K^{*0} \rightarrow K^+\pi^-$ )	$0.49 \pm 0.26$

Table 3: Results of fitting for apparent  $CP$  asymmetries in various charged or neutral flavor-eigenstate  $B$  samples.

## 7.6 Results

The maximum-likelihood fit for  $\sin 2\beta$  on the full tagged sample of  $B^0/\bar{B}^0 \rightarrow J/\psi K_S^0$  and  $B^0/\bar{B}^0 \rightarrow \psi(2S)K_S^0$  events yields the preliminary result :

$$\sin 2\beta = 0.12 \pm 0.37 \text{ (stat)} \pm 0.09 \text{ (syst)} \quad (7)$$

The results of the fit for each type of  $CP$  sample and for each tagging category are given in Table 4. The contributions to the systematic uncertainty are summarized in Table 5. The  $\Delta t$  distributions for  $B^0$  and  $\bar{B}^0$  tags are shown in Fig. 7 and the raw asymmetry as a function of  $\Delta t$  is shown in Fig. 8. The probability of obtaining a value of the statistical error larger than the one we observe is estimated at 5%. Based on a large number of full Monte Carlo simulated experiments with the same number of events as our data sample, we estimate that the probability of finding a lower value of the likelihood than our observed value is 20%.

sample	$\sin 2\beta$
<i>CP</i> sample	<b>0.12±0.37</b>
$J/\psi K_S^0$ ( $K_S^0 \rightarrow \pi^+\pi^-$ ) events	$-0.10 \pm 0.42$
other <i>CP</i> events	$0.87 \pm 0.81$
Lepton	$1.6 \pm 1.0$
Kaon	$0.14 \pm 0.47$
NT1	$-0.59 \pm 0.87$
NT2	$-0.96 \pm 1.30$

Table 4:  $\sin 2\beta$  fit results from the entire  $CP$  sample and various subsamples.

Source of uncertainty	Uncertainty on $\sin 2\beta$
uncertainty on $\tau_B^0$	0.002
uncertainty on $\Delta m_d$	0.015
uncertainty on $\Delta z$ resolution for <i>CP</i> sample	0.019
uncertainty on time-resolution bias for <i>CP</i> sample	0.047
uncertainty on measurement of mistag fractions	0.053
different mistag fractions for <i>CP</i> and non- <i>CP</i> samples	0.050
different mistag fractions for $B^0$ and $\bar{B}^0$	0.005
background in <i>CP</i> sample	0.015
<b>total systematic error</b>	<b>0.091</b>

Table 5: Summary of systematic uncertainties on  $\sin 2\beta$

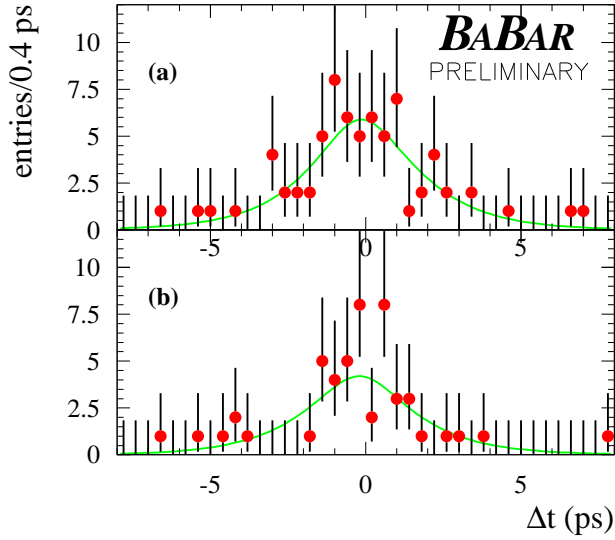


Figure 7: Distribution of  $\Delta t$  for (a) the  $B^0$  tagged events and (b) the  $\bar{B}^0$  tagged events in the  $CP$  sample. The error bars plotted for each data point assume Poisson statistics. The curves correspond to the result of the unbinned maximum-likelihood fit and are each normalized to the observed number of tagged  $B^0$  or  $\bar{B}^0$  events.

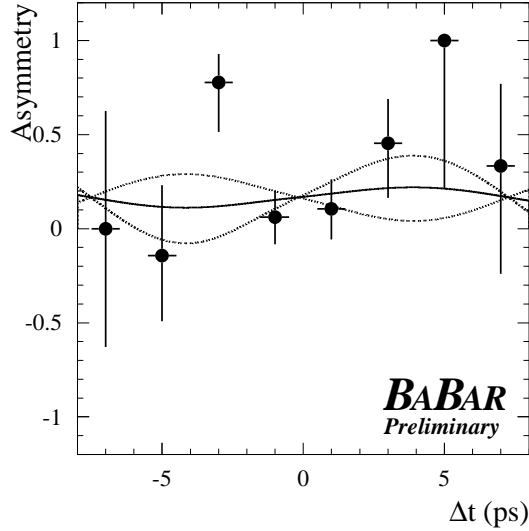


Figure 8: The raw  $B^0$ - $\bar{B}^0$  asymmetry  $(N_{B^0} - N_{\bar{B}^0})/(N_{B^0} + N_{\bar{B}^0})$  with binomial errors as function of  $\Delta t$ . The solid curve represents our central value of  $\sin 2\beta$ . The two dotted curves correspond to one statistical standard deviation from the central value. The curves are not centered at  $(0, 0)$  in part because the probability density functions are normalized separately for  $B^0$  and  $\bar{B}^0$  events, and our  $CP$  sample contains an unequal number of  $B^0$  and  $\bar{B}^0$  tagged events (70  $B^0$  versus 50  $\bar{B}^0$ ). The  $\chi^2$  between the binned asymmetry and the result of the maximum-likelihood fit is 9.2 for 7 degrees of freedom.

## 8 Conclusions and prospects

The first *BABAR* measurement of the *CP*-violating asymmetry parameter  $\sin 2\beta$  has been presented :

$$\sin 2\beta = 0.12 \pm 0.37 \text{ (stat)} \pm 0.09 \text{ (syst)} \quad (\textit{preliminary}) \quad (8)$$

*BABAR* aims at collecting more than  $20 \text{ fb}^{-1}$  of data by the end of Run 1 in fall 2000. A measurement of  $\sin 2\beta$  with a precision better than 0.2 is expected early in 2001.

Very competitive preliminary results have also been presented for the *B* meson lifetimes, as well as the first measurements of  $B^0\bar{B}^0$  mixing at the  $\Upsilon(4S)$ . These measurements will also benefit in the near future from the expected significant increase in statistics.

## References

- [1] C. Jarlskog, in *CP Violation*, C. Jarlskog ed., World Scientific, Singapore (1988).
- [2] *BABAR* Collaboration, B. Aubert *et al.*, "The first year of the *BABAR* experiment at PEP-II", *BABAR-CONF-00/17*, submitted to the XXX<sup>th</sup> International Conference on High Energy Physics, Osaka, Japan.
- [3] ARGUS collaboration, H. Albrecht *et al.*, *Z Phys.* **C48**, 543 (1990).
- [4] G. C. Fox and S. Wolfram, *Phys. Rev. Lett.* **41**, 1581 (1978).
- [5] Particle Data Group, D. E. Groom *et al.*, *Eur. Phys. Jour. C* **15**, 1 (2000).

## First Physics Results From Belle

ASISH SATPATHY<sup>1</sup>

*Department of Physics*  
*University of Cincinnati, Cincinnati, OH 45221-0011, USA*  
*(For The Belle Collaboration)*

The Belle detector at the KEK-B asymmetric  $e^+e^-$  collider has recorded  $6.2 \text{ fb}^{-1}$  data at the  $\Upsilon(4S)$  resonance by July 2000. Using this data sample, several new results on various B meson branching ratio measurements are presented. We also report on the measurement of the Standard Model  $CP$  violation parameter  $\sin(2\phi_1)$ , where  $\phi_1$  is one of angles of the CKM triangle. The preliminary result is  $\sin(2\phi_1) = 0.45^{+0.43\pm 0.07}_{-0.44\pm 0.08}$ .

Presented at the

5th International Symposium on Radiative Corrections  
(RADCOR-2000)  
Carmel CA, USA, 11-15 September, 2000

---

<sup>1</sup>email : satpathy@bsunsv1.kek.jp

# 1 Introduction

The Belle Experiment [1] at the KEK-B asymmetric  $e^+ e^-$  collider has completed its first year of operation in July 2000 accumulating data equivalent to an integrated luminosity of  $6.2 \text{ fb}^{-1}$  on the  $\Upsilon(4S)$ . This corresponds to about  $6.3 \times 10^6 B\bar{B}$ 's. Apart from the early running period, the KEK-B machine operated quite well delivering a record luminosity of  $94 \text{ pb}^{-1}$  per day and  $504 \text{ pb}^{-1}$  per week respectively and has great prospects for further improvement towards its design goal of  $100 \text{ fb}^{-1}$  / Year. We report on some of the new measurements that have been carried out using this dataset with the emphasis on the measurement of the Standard Model CP violation parameter  $\sin(2\phi_1)$ . The results being reported are all preliminary.

## 2 General Features of Data Analysis

$B$  candidates are identified using  $M_b = \sqrt{E_{beam}^2 - |\sum P_i^{cms}|^2}$ , the beam constrained mass and  $\Delta E = E_{beam} - E_B$ , where  $E_{beam} = E_{cms}/2$ . While  $M_b$  expresses the momentum conservation in the decay,  $\Delta E$  expresses the energy conservation of the particles in the decay and is sensitive to the missing particles and  $K/\pi$  misidentification.

In all the decay modes we consider here, the dominant source of background arises from  $e^+e^- \rightarrow q\bar{q}$  ( $q = u, d, c, s$ ) transitions. We exploit the difference between jetty hadronization of continuum events and spherical decay of  $B$ 's at  $\Upsilon(4S)$  center of mass frame. Continuum background is reduced using  $R_2 = H_2/H_0$ , where  $H_l = \sum_{i,j} \frac{|\vec{p}_i||\vec{p}_j|}{E_{cms}^2} P_l(\cos\theta_{i,j})$ , the Fox-Wolfram moment [2], that measures the shape of an event as a whole and  $P_l(\cos\theta_{i,j})$  are Legendre Polynomials. In some decay modes, the continuum background is reduced using modified Fox Wolfram moments [3] where the tracks and showers coming from  $B$  and the rest of the tracks and showers in the event are separated. These modified Fox-Wolfram moments are combined in a Fisher Discriminant to form the Super Fox Wolfram (SFW). The SFW has approximately  $2\sigma$  separation between  $q\bar{q}$  and  $B\bar{B}$  events and provides a 22 % increase in the expected significance for some modes as compared to  $R_2$ . Another popular technique to remove the continuum component in the data is to cut on  $\cos(\theta_{thrust})$  variable, where  $\theta_{thrust}$  is the angle between the thrust axis of the signal  $B$  and the thrust axis of the rest of the event. In some analyses, the continuum variables are combined with kinematic variables in a likelihood fit to determine the signal yield.

## 3 Branching Ratio Measurement

We will highlight selected branching ratio measurements that were either first observation or important new measurements. The preliminary results reported in this

section are based on the first 5.3 million  $B\bar{B}$  events recorded on the  $\Upsilon(4S)$  resonance at KEK-B.

### 3.1 $B \rightarrow \phi K$

This is the first observation of  $B$  decays involving a pure penguin transition,  $b \rightarrow s\bar{s}$ . Two charged tracks identified as kaons are combined to form a  $\phi$  meson candidate with an additional requirement that both tracks are from one vertex. The candidate  $\phi$  is then combined with a charged  $K$  or  $K_s$  to form a  $B$  candidate. Continuum background is suppressed with cuts on  $\cos(\theta_{thrust})$ , the  $\phi$  meson helicity angle which is the angle between the direction of  $K^+$  and the momentum vector of  $\phi(1020)$  and the  $B$  flight direction. The final yield is obtained by fitting the  $M_b$  distribution (Fig. 1). The binned likelihood fit yields  $9.2^{+3.6}_{-2.9}$  ( $B \rightarrow \phi K$ ) events with a statistical significance of  $5.4\sigma$  and  $\mathcal{B}(B^+ \rightarrow \phi(1020)K^\pm) = 1.72^{+0.67}_{-0.54}(\text{stat.}) \pm 0.18(\text{sys.}) \times 10^{-5}$ . We also observed two events of the type  $B \rightarrow \phi K_s$  in the  $3\sigma$  signal box. These are consistent with the fluctuation in the  $q\bar{q}$  background. A more detailed description of the analysis can be found in reference [4]. As statistics improve, this decay mode will be used to determine the CKM angle  $\phi_1$ .

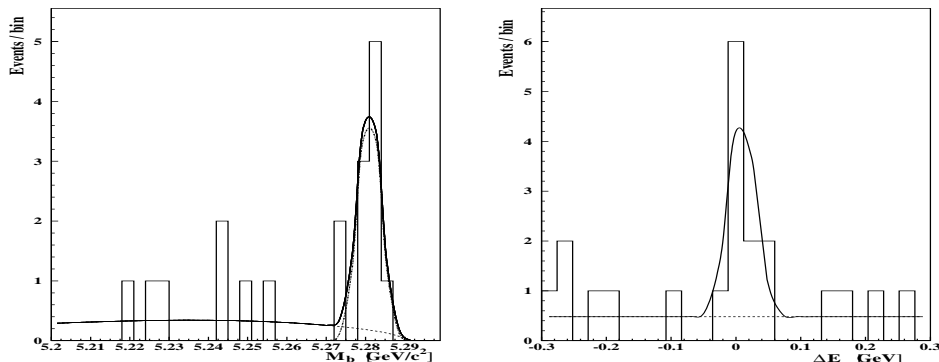


Figure 1:  $B \rightarrow \phi K$  signal yield. [left:] Beam constrained mass distribution [right:]  $\Delta E$  distribution

### 3.2 $B \rightarrow K\pi, KK, \pi\pi$

The study of charmless hadronic  $B$  meson decays offers a variety of test of Standard Model physics and beyond. Our immediate motivation was to measure the branching fraction of those decay modes which are either not measured or are limited by statistics. We have summarized the current Belle branching fraction measurements of charmless  $B \rightarrow hh$  decays in Table 1. Thanks to the excellent performance of the

Decay Modes	Signal Yield	$\mathcal{B}(\times 10^{-5})$	U.L.( $\times 10^{-5}$ )
$B^0 \rightarrow K^+\pi^-$	$25.6_{-6.8}^{+7.5}$	$1.74_{-0.46}^{+0.51} \pm 0.34$	
$B^0 \rightarrow K^+\pi^0$	$32.3_{-8.4}^{+9.4}$	$1.88_{-0.49}^{+0.55} \pm 0.23$	
$B^0 \rightarrow K^0\pi^+$	$5.7_{-2.7}^{+3.4}$	$1.66_{-0.78-0.24}^{+0.98+0.22}$	$< 3.4$
$B^0 \rightarrow K^0\pi^0$	$10.8_{-4.0}^{+4.8}$	$2.10_{-0.78-0.23}^{+0.93+0.25}$	
$B^0 \rightarrow K^+K^-$	$0.8_{-0.8}^{+3.1}$		$< 0.6$
$B^0 \rightarrow K^+K^0$	$0.0_{-0.0}^{+0.5}$		$< 0.51$
$B^0 \rightarrow \pi^+\pi^-$	$9.3_{-5.1}^{+5.3}$	$0.63_{-0.35}^{+0.39} \pm 0.16$	$< 1.65$
$B^0 \rightarrow \pi^+\pi^0$	$5.4_{-4.4}^{+5.7}$	$0.33_{-0.27}^{+0.35} \pm 0.07$	$< 1.01$

Table 1: Belle preliminary results for charmless  $B \rightarrow PP$  decays. The first error is statistical, the second error is systematic. Upper limits are given at the 90 % C.L.

high momentum particle identification system, we have seen very clear signals in some of the decay modes. A detailed account of the analysis can be found in references [5] and [6]. The measurements are all consistent with similar observations in other experiments [7].

### 3.3 Radiative $B$ Meson Decays

Flavor-changing neutral decays involving  $b \rightarrow s$  or  $b \rightarrow d$  transition have received much attention in recent years. The inclusive decay  $B \rightarrow X_s\gamma$  where  $X_s$  is a strange hadronic state, is of particular interest to the experimentalist since the theoretical description of the decay mode is rather clean and can be related to the partonic weak decay  $b \rightarrow s\gamma$ . A short term motivation in this direction was to measure the branching fraction with a better particle identification device and a high resolution electro-magnetic calorimeter. Table 2 summarizes the signal yield and corresponding branching fraction measurement of radiative  $B$  meson decays at Belle. The results are comparable to the recent CLEO results [8]. Our current 90 % C.L. upper limit on the ratio is  $\mathcal{B}(B \rightarrow \rho\gamma)/\mathcal{B}(B \rightarrow K^*\gamma) < 0.28$ . This is an important result because it constrains  $|V_{td}/V_{ts}|$  within the Standard Model. A detailed description of the analysis method can be found in reference [9].

### 3.4 $B \rightarrow D^{(*)}K$

We report the observation of the Cabibbo-suppressed decay modes  $\overline{B}^0 \rightarrow D^{*+}K^-$  and  $B^- \rightarrow D^{*0}K^-$  (Fig. 2). In addition, we also report a new measurement of  $\mathcal{B}(\overline{B}^+ \rightarrow \overline{D}^0K^+)$ . Thanks to the excellent particle identification at Belle, one can clearly separate the signal from the background originating from the Cabibbo-favored decay modes with more than  $3\sigma$  significance. We measured the ratio  $R$  of the branching

Decay Modes	Signal Yield	$\mathcal{B}(\times 10^{-5})$	U.L.( $\times 10^{-5}$ )
$b \rightarrow s\gamma$	$92 \pm 14$	$33.4 \pm 5.0^{+0.34+2.6}_{-0.37-2.8}$	
$B^0 \rightarrow K^{*0}\gamma$	$33.7 \pm 6.9$	$4.94 \pm 0.93^{+0.55}_{-0.52}$	
$B^+ \rightarrow K^{*+}\gamma$	$8.7 \pm 4.2$	$2.87 \pm 1.20^{+0.55}_{-0.40}$	
$B^0 \rightarrow \rho^0\gamma$			$< 0.56$
$B^+ \rightarrow \rho^+\gamma$			$< 2.27$

Table 2: Belle preliminary results for radiative  $B$  meson decays. The first error is statistical, the second error is systematic. Upper limits are given at the 90 % C.L.

Decay Modes	Ratio
$\mathcal{B}(B^- \rightarrow D^0 K^-)/\mathcal{B}(B^- \rightarrow D^0 \pi^-)$	$0.081 \pm 0.014 \pm 0.011$
$\mathcal{B}(B^- \rightarrow D^{*0} K^-)/\mathcal{B}(B^- \rightarrow D^{*0} \pi^-)$	$0.134^{+0.045}_{-0.038} \pm 0.015$
$\mathcal{B}(B^- \rightarrow D^{*+} K^-)/\mathcal{B}(B^- \rightarrow D^{*+} \pi^-)$	$0.062^{+0.030}_{-0.024} \pm 0.013$

Table 3: Belle preliminary results for Cabibbo-suppressed  $B$  meson decays. The first error is statistical, the second error is systematic.

fraction for the Cabibbo suppressed decay  $B \rightarrow D^{(*)}K^-$  normalized relative to the Cabibbo allowed decay  $B \rightarrow D^{(*)}\pi^-$ . The observed ratios are summarized in Table 3. The detailed description of the analysis method can be found in the reference [10]. As statistics improve, the analysis will shift towards the extraction of the CKM angle  $\phi_3$ .

### 3.5 $B \rightarrow J/\psi K_1$

Inclusive  $B \rightarrow J/\psi X$  decays are not saturated by the sum of observed exclusive modes. This motivates the search for new exclusive modes that we are reporting here.  $K_1$  candidates were reconstructed from  $K^+\pi^+\pi^-$ ,  $K^+\pi^-\pi^0$  and  $K^0\pi^+\pi^-$ . We have verified the signal is due to  $B \rightarrow J/\psi K_1(1270)$  (Fig. 3) and determine the branching fractions as summarized in Table 4.

## 4 Measurement of $\sin(2\phi_1)$

Experimentally,  $CP$  asymmetry is observed in the distribution of the proper time difference of two  $B$  decays produced in pairs in the decays of the  $\Upsilon(4S)$ , one to  $CP$  eigenstate and another to any final state where the flavor is identified. For a  $B$  decaying to a  $CP$  eigenstate, the time dependent asymmetry  $a(t)$  can be non-zero,

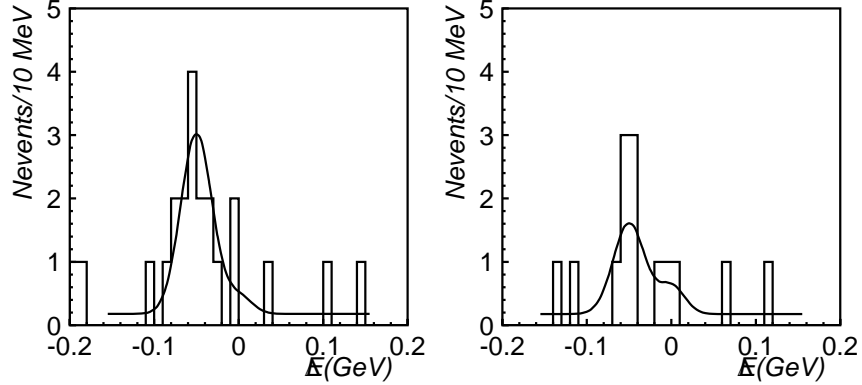


Figure 2:  $\Delta E$  distribution of (left)  $B^0 \rightarrow D^{*-}K^+$  (right)  $B^- \rightarrow D^{*0}K^-$ . The signal yield is obtained from the fit to the distribution with a double Gaussian signal function and a MC determined background shape.

Decay Modes	Branching Ratio ( $\times 10^3$ )
$\mathcal{B}(B^0 \rightarrow J/\psi K_1^0(1270))$	$1.5_{-0.4}^{+0.5} \pm 0.4$
$\mathcal{B}(B^+ \rightarrow J/\psi K_1^+(1270))$	$1.7_{-0.4}^{+0.5} \pm 0.4$

Table 4: Belle preliminary results for  $B \rightarrow J/\psi K_1(1270)$ . The first error is statistical, the second error is systematic.

indicating  $CP$  violation :

$$a(t) = \frac{N(B^0(t) \rightarrow f) - N(\overline{B^0}(t) \rightarrow f)}{N(B^0(t) \rightarrow f) + N(\overline{B^0}(t) \rightarrow f)} = \frac{(1 - |\lambda_f|^2) \cos(\Delta m_d t) - 2Im\lambda_f \sin(\Delta m_d t)}{(1 + |\lambda_f|^2)} \quad (1)$$

where  $\lambda_f = \frac{q A(\overline{B^0} \rightarrow f)}{p A(B^0 \rightarrow f)}$ ,  $\Delta m_d$  is the  $B_d$  mixing frequency,  $\Gamma$  its width and  $Im\lambda_f = \sin(2\phi_1)$  that arises from the interference between the decays with and without mixing.

When  $B^0 \rightarrow f = \overline{B^0} \rightarrow f$  and assuming only one diagram dominates the decay process,  $|\lambda_f|^2=1$ . Then the time dependent asymmetry would be

$$a(t) \sim \eta_{CP} \sin(2\phi_1) \sin(\Delta m_d t) \quad (2)$$

where  $\eta_{CP} = -1$  for  $\psi K_s$  type modes and  $\eta_{CP} = 1$  for  $J/\psi K_L$  and  $\psi\pi^0$  modes. One of the important and immediate goal for the Belle experiment is to measure  $\sin(2\phi_1)$  to see if the CKM model is correct.

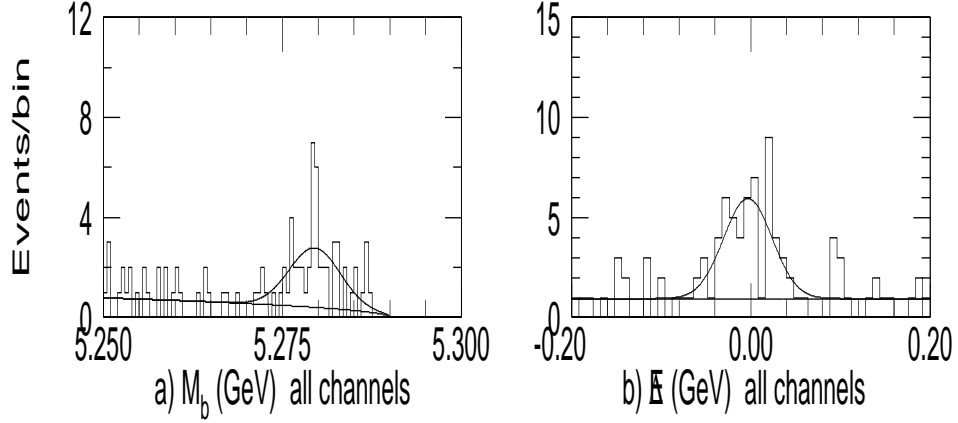


Figure 3: Signal yield for the decay  $B \rightarrow J/\psi K_1(1270)$   
(left)  $M_b$  distribution (right)  $\Delta E$  distribution.

Modes	CP	S / N	Tagged
$J/\psi(l^+l^-)K_s(\pi^+\pi^-)$	-1	70 / 3.4	40
$J/\psi(l^+l^-)K_s(\pi^0\pi^0)$	-1	4 / 0.3	4
$\psi'(l^+l^-)K_s(\pi^+\pi^-)$	-1	5 / 0.2	2
$\psi'(J/\psi\pi^+\pi^-)K_s(\pi^+\pi^-)$	-1	8 / 0.6	3
$\chi_{c1}(J/\psi\gamma)K_s(\pi^+\pi^-)$	-1	5 / 0.75	3
$J/\psi(l^+l^-)\pi^0$	+1	10 / 1	4
Total		102 / 6.25	56
$J/\psi(l^+l^-)K_L$	+1	102 / 48	42

Table 5: Summary of Signal Yield of CP eigenstate  $B$  meson decays.

#### 4.1 Event Reconstruction : $B$ Decaying to CP Eigenstate

Table 5 summarizes the decay modes that are reconstructed for the CP analysis.  $J/\psi$  and  $\psi(2S)$  candidate events were reconstructed from dileptons ( $\mu^+\mu^-$ ,  $e^+e^-$ ), correcting for the final state radiation in the electron channel. For  $\psi(2S)$  candidates we also used the  $J/\psi\pi^+\pi^-$  mode.  $\chi_{c1}$  candidates were reconstructed using only the  $J/\psi\gamma$  decay mode.  $K_s$  candidates were reconstructed in the  $\pi^+\pi^-$  and  $\pi^0\pi^0$  modes. We reconstructed 102 CP eigenstate candidate with 6 estimated background (Fig. 4(left)).

We also reconstructed 102 CP even  $B \rightarrow J/\psi K_L$  candidate events (Fig. 4(right)) with 48 estimated background. Among the backgrounds which contain CP asymmetry, major contributions come from physics events such as  $B$  decays to  $\chi_{c1}K_L$ ,  $J/\psi K_s$ ,  $J/\psi K^*$  and  $J/\psi$  non-resonant  $K_L\pi^0$ .

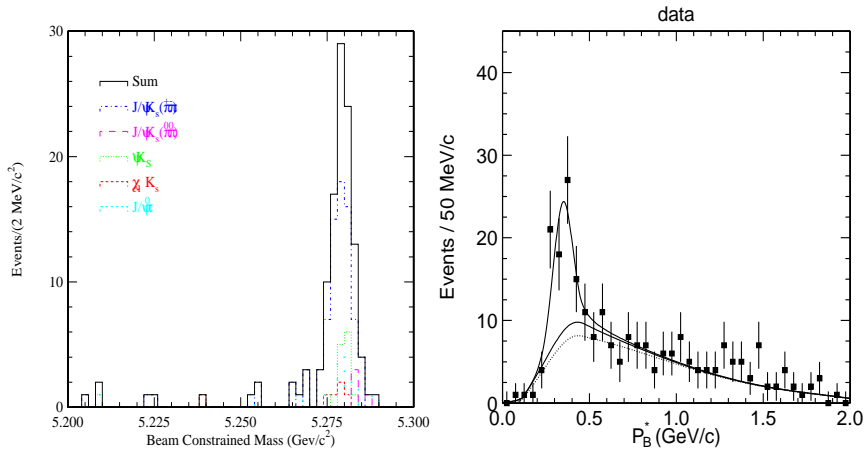


Figure 4:  $B_{CP}$  signal yield. [left:] Beam constrained mass distribution of all the decays modes except the  $K_L$  channel. [right:] Momentum distribution of  $B$  candidate events in CMS where  $B \rightarrow J/\psi K_L$

## 4.2 Measurement of $B$ Life Time : A Benchmark Test

Extraction of  $CP$  asymmetry requires the knowledge of proper time distribution of tagged and fully reconstructed  $B_{CP}$  event. For  $CP$  eigenstate modes, the proper time,  $\Delta t = \Delta z/c\beta\gamma$  at  $\beta\gamma = 0.425$ , was calculated by measuring the difference between the decay vertices of  $B_{CP}$  decay vertex and tagging side  $B_{tag}$  vertex. The vertex point of  $B_{CP}$  was established by the two tracks associated with the  $J/\psi$  decay. The vertex position in the tagging side was determined from the tracks not assigned to  $B_{CP}$  by an algorithm that removes tracks from the secondary vertices or tracks which makes a large increase in the  $\chi^2$  of the vertex fit.

The proper time resolution function  $R_{sig}(\Delta t)$  was parameterized from MC simulation studies and a multi-parameter fit to  $B \rightarrow D^* l \nu$  data (Fig. 5). A double Gaussian parameterization results from various detector characteristics, error in the event by event vertex fit, error in the  $\Delta t$  approximation, the scale factor and charm lifetime.

We measured the  $B$  life time in various decay modes to test the proper time resolution function that we derived from MC studies. The  $B$  lifetime was extracted from an event by event likelihood fit with a P.D.F given by

$$\begin{aligned}
 P(\Delta t) = & f_{sig} \int_{-\infty}^{\infty} d(\Delta t') \frac{e^{-|\Delta t'|/\tau_{sig}}}{2\tau_{sig}} R_{sig}(\Delta t - \Delta t') \\
 & + (1 - f_{sig}) \int_{-\infty}^{\infty} d(\Delta t') [f_{\lambda_{bg}} \frac{\lambda_{bg}}{2} e^{-|\Delta t'|/\lambda_{bg}} + (1 - f_{\lambda_{bg}}) \delta(\Delta t')] R_{bg}(\Delta t - \Delta t')
 \end{aligned}
 \tag{3}$$

Minimization of the likelihood gives  $\tau_B$  which is one of the free parameters determined from the fit. It should be noted that  $R_{bg}(\Delta t)$  was parameterized in the same way

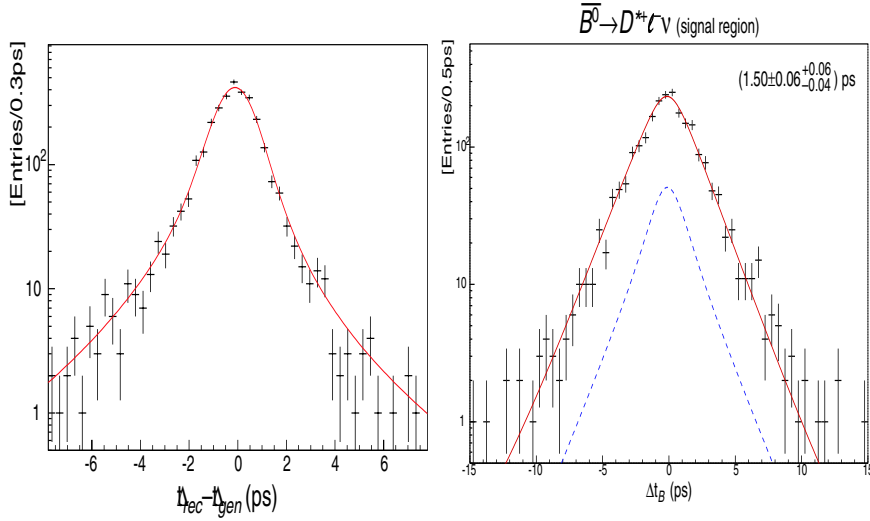


Figure 5: (left): Average shape of the event by event resolution function. (right): Lifetime fit results for  $\overline{B}^0 \rightarrow D^{*+} l^- \nu$ .

	Belle	Particle Data group
$\tau_{\overline{B}^0}$	$1.50 \pm 0.05 \pm 0.07$ ps	$1.548 \pm 0.032$ ps
$\tau_{B^-}$	$1.70 \pm 0.06^{+0.11}_{-0.10}$ ps	$1.653 \pm 0.028$ ps
$\tau_{B^-} / \tau_{\overline{B}^0}$	$1.14 \pm 0.06^{+0.06}_{-0.05}$	$1.062 \pm 0.029$

Table 6: Summary of the measured  $B$  lifetime at Belle.

as of  $R_{sig}(\Delta t)$  using background events from the sideband region of the  $\Delta E$  and  $M_b$  scatter plot.

The superimposed solid line on the data points in the right plot of Fig. 5 is the result of the refit for  $\overline{B}^0 \rightarrow D^{*+} l^- \nu$ . The measured  $\tau_B$  agrees with the world average value proving that the parameterization of the resolution function is correct. Table 6 summarizes the measured combined results for the  $B$  lifetime from various charged and neutral  $B$  decays.

### 4.3 Flavor Tagging and Wrong Tag Fraction

To measure the  $CP$  asymmetry, we need to determine the flavor of the  $B_{CP}$  candidates from the remaining tracks of the event. We use the following algorithm in sequence to tag a certain  $B$  in an event. (0) Require tight PID probability for lepton and kaon selection, (1) Obtain the sign of the high momentum lepton ( $p_l^* > 1.1$  GeV)  $\rightarrow$  positive lepton tags  $B^0$ , (2) Obtain sum of  $K$  charges  $\rightarrow$  positive sum tags  $B^0$ ,

Method	$\epsilon_{tag}$	$w$ (%)	$\epsilon_{eff}$
High $p^*$ Lepton	$14.2 \pm 2.1$	$7.1 \pm 4.5$	$10.5 \pm 2.7$
Kaons	$27.9 \pm 4.2$	$19.9 \pm 7.0$	$10.1 \pm 4.9$
Mid $p^*$ Lepton	$2.9 \pm$	$29.2 \pm 15.0$	0.5
Soft pion	$7.0 \pm 3.5$	$34.1 \pm 15.0$	0.7
Total	52.0		21.2

Table 7: Tagging efficiency and wrong tagging fraction at Belle

(3) Look for medium momentum leptons ( $0.6 < p_l^* < 1.1$  GeV) and large missing momenta  $\rightarrow$  positive charged lepton tags  $B^0$ , (4) Sign of slow pions from  $D^{*+}$  decays  $\rightarrow$  charge of slow pion and hence flavor of  $D^*$  tags the flavor of  $B$ .

The algorithm was tested on a sample of self tagging exclusively reconstructed  $B \rightarrow D^{(*)}l\nu$  decays. We extract the wrong tag fraction ( $w$ ) and  $\Delta m_d$  from a maximum likelihood fit to the  $\Delta t$  distribution (eqn. 4) of  $OF$  (opposite flavor) and  $SF$  (same flavor) events with a function that includes the effect of  $\Delta t$  resolution and background.

$$A_{mix}(\Delta t) = \frac{N(\Delta t)^{OF} - N(\Delta t)^{SF}}{N(\Delta t)^{OF} + N(\Delta t)^{SF}} = (1 - 2w) \cos(\Delta m_d t) \quad (4)$$

The measured value  $\Delta m_d = 0.488 \pm 0.026$  (stat.)  $\text{ps}^{-1}$  verifies the consistency of the tagging algorithm. In an independent approach,  $\Delta m_d$  was determined from the time evolution of dilepton yields in  $\Upsilon(4S)$  decays. The proper-time difference distribution for same-sign and opposite-sign dilepton events were simultaneously fitted to an expression containing  $\Delta m_d$  as a free parameter. Using both electrons and muons, we obtain  $\Delta m_d = 0.463 \pm 0.008$  (stat.)  $\pm 0.016$  (sys)  $\text{ps}^{-1}$  [11]. This is the first determination of  $\Delta m_d$  from time evolution measurements at the  $\Upsilon(4S)$ . Previous measurements at the  $\Upsilon(4S)$  only used time integrated distributions.

Table 7 summarizes the estimated tagging efficiency in each of the above steps. The effective tagging efficiency  $\epsilon_{eff} = \epsilon_{tag}(1 - 2w)^2$  is found to be 21.2 %. We also determined the tagging efficiency from the same test sample. Depending on the tag type, we used the numbers in the table for the fit to extract  $\sin(2\phi_1)$ .

#### 4.4 CP Fit : Extraction of $\sin(2\phi_1)$

Using the tagging method described above, from a sample of 102  $CP$  odd and  $J/\psi\pi^0$  events and 102  $J/\psi K_L$  events, a total of 98 events were tagged. The likelihood for each tagged event is calculated as

$$P(\Delta t) = f_{sig} \int_{-\infty}^{\infty} Sig(\Delta t', \eta_{CP}) R_{sig}(\Delta t - \Delta t') d(\Delta t')$$

$$+(1 - f_{sig}) \int_{-\infty}^{\infty} Bkg(\Delta t') R_{sig}(\Delta t - \Delta t') d(\Delta t') \quad (5)$$

where the P.D.F expected for the signal distribution with  $CP$  eigenvalue  $\eta_{CP}$  is:  $Sig(\Delta t, \eta_{CP}) = \frac{1}{\tau_{B^0}} \exp(-|\Delta t|/\tau_{B^0}) \{1 \mp \eta_{CP}(1 - 2w) \sin(2\phi_1) \sin(\Delta m_d \Delta t)\}$  and that of background distribution is:  $Bkg(\Delta t') = \frac{1}{2\tau_{bkg}} \exp(-|\Delta t'/\tau_{bkg})$  and  $w$  depends on the method of flavor tagging for each event.

The values of  $\Delta m_d$  and  $\tau_{B^0}$  are fixed to the ones in the P.D.G. We use an unbinned maximum likelihood fit to extract the possible  $CP$  asymmetry. Before doing a  $CP$  fit, we wanted to make sure that the whole fitting procedure is bias free. We performed the same analysis procedure including tagging to several non- $CP$  eigenstate decay modes, such as  $B^0 \rightarrow J/\psi K^{*0}$ ,  $B^- \rightarrow J/\psi K^-$ ,  $D^0 \pi^-$  and found  $\sin(2\phi_1)$  is consistent with zero within fitting errors. Our result from the likelihood fit to the fully tagged sample is :  $\sin(2\phi_1) = +0.45_{-0.44}^{+0.43} (stat.)_{-0.09}^{+0.07} (syst.)$  (Fig. 6). Clearly the measurement is statistics limited. It should be noted that the uncertainty in determining the wrong tag fraction is the largest contribution in the systematics.

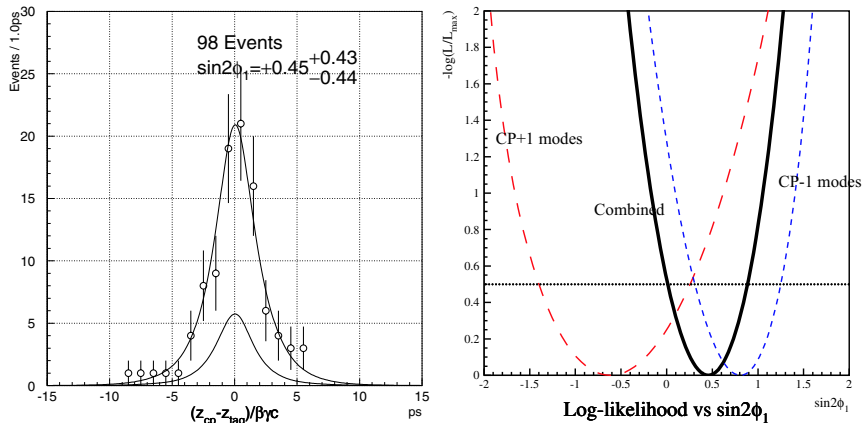


Figure 6: CP fit results for a combined  $CP$  even and  $CP$  odd events.

## 5 Conclusion and Prospect

Belle had a very successful and exciting first year run and is marching along a well defined road to measuring  $\sin(2\phi_1)$  with a very good precision. First preliminary results were reported. We need a lot more data to constrain the CKM triangle with small errors. We observed the first evidence of Cabibbo suppressed  $B \rightarrow D^* K^-$  process, and made first measurements of  $\mathcal{B}(B \rightarrow J/\psi K_1(1270))$  and  $\mathcal{B}(B^+ \rightarrow \phi K^+)$ . New results on many rare decays which will be used to search

for direct  $CP$  violation have also been reported. The physics scope at Belle is not limited to  $B$  physics only. We have reported five different  $\tau$  and two-photon physics related results at the ICHEP2000 conference. Please check out for more: <http://www.bsunsrv1.kek.jp/conferences/ichep2000.html>.

## ACKNOWLEDGMENTS

We gratefully acknowledge the effort of the KEK-B staff in providing us with excellent luminosity and running condition. We thank the rest of the Belle Collaboration for their support and help. Special thanks to the KEK computing research center for their help in many different occasion.

## References

- [1] The Belle Collaboration, KEK Progress Report 2000-4
- [2] G. Fox and S. Wolfram, Phys. Rev. Lett. **41**, 1581 (1978).
- [3] Unpublished lecture note by R. Enomoto, Belle Group (KEK) (1999)
- [4] A. Abashian et. al., Contributed paper for ICHEP2000, BELLE-CONF-0007 (2000)
- [5] A. Abashian et. al., Contributed paper for ICHEP2000, BELLE-CONF-0005 (2000)
- [6] A. Abashian et. al., Contributed paper for ICHEP2000, BELLE-CONF-0006 (2000)
- [7] R. Barate et.al. ALEPH Collaboration, Phys. Lett. **B429**, 169 (1998). OSAKA 2000 Conference papers from BaBar Collaboration and CLEO Collaboration.
- [8] S. Ahmed et. al. CLEO Collaboration, CLEO CONF 99-10, Review of Particle Physics, The European Physical Journal **15**, 1-4 (2000).
- [9] A. Abashian et. al., Contributed paper for ICHEP2000, BELLE-CONF-0003 (2000)
- [10] A. Abashian et. al., Contributed paper for ICHEP2000, BELLE-CONF-0010 (2000)
- [11] K. Abe et. al. (The Belle Collaboration), hep-ex/0011090, KEK Preprint 2000-123, submitted to Phy. Rev. Lett.

# Measurement of $|V_{cb}|$ and Charmless Hadronic B Decays at CLEO

XIN ZHAO\*

*Department of Physics and Astronomy  
University of Kansas, Lawrence, KS 66045 USA*

We review the recent results on the measurement of  $|V_{cb}|$  and charmless hadronic B decays from CLEO based on  $9.7 \times 10^6$   $B\bar{B}$  pairs collected with CLEO II and II.V detectors. The preliminary result on the measurement of  $|V_{cb}|$  is  $|V_{cb}| = (46.4 \pm 2.0 \pm 2.1 \pm 2.1) \times 10^{-3}$ . The comprehensive measurement on exclusive charmless hadronic B decays indicate existence of many contributing and interfering diagrams, especially the gluonic penguin contribution is large.

Presented at the

5th International Symposium on Radiative Corrections  
(RADCOR-2000)

Carmel CA, USA, 11–15 September, 2000

---

\*Work supported by the National Science Foundation and The Department of Energy of the United States.

## 1 CLEO experiment and CLEO III upgrade

CLEO detector has been running at the Cornell Electron Storage Ring(CESR) for 20 years, studies the B physics at the  $\Upsilon(4S)$  energy region. The CLEO II and II.V configurations are described in detail elsewhere [1,2]. It has one of the largest data sample collected at the  $\Upsilon(4S)$  region. The integrated luminosity is  $13.5 \text{ fb}^{-1}$ , among them  $9.1 \text{ fb}^{-1}$  taken at the  $\Upsilon(4S)$  resonance, which corresponds to about  $9.7 \times 10^6 \text{ } B\bar{B}$  pairs, and  $4.4 \text{ fb}^{-1}$  at the energies just below the  $B\bar{B}$  threshold in order to study backgrounds from light quark production(referred to as continuum events). The results reviewed in this paper are based on this full data sample.

Recently the CESR and CLEO detector have been upgraded. The goal is to get to a luminosity of  $1.6 - 2.2 \times 10^{33} \text{ cm}^{-2} \text{ s}^{-1}$ , so as to collect 20-30  $\text{fb}^{-1}$  data per year. The new CLEO III detector consists of a new four layer double sided silicon drift detector, a new 47 layer drift chamber, and a completely new barrel Ring Imaging CHernkov (RICH) detector. The upgraded detector was completed in April of 2000 and started taking physics data in July of 2000.

CLEO analysis covers wide topics in B meson decay. In this talk, we will focus on the CLEO measurements of the CKM matrix elements and CP violation.

## 2 The CKM matrix and Unitary Triangle

In the Standard Model, the Cabibbo-Kobayashi-Maskawa matrix(CKM) [3] describes the mixing between the 3 quark generations. The determination of all of these parameters is required to fully define the Standard Model and may also reveal an underlying structure that will point to new physics. In the framework of the Standard Model the CKM matrix must be unitary, which gives rise to the following relationships between the matrix elements:

$$V_{ud}V_{ub}^* + V_{cd}V_{cb}^* + V_{td}V_{tb}^* = 0, \quad (1)$$

$$V_{ub}V_{us}^* + V_{cb}V_{cs}^* + V_{tb}V_{ts}^* = 0, \quad (2)$$

$$V_{us}V_{ud}^* + V_{cs}V_{cd}^* + V_{ts}V_{td}^* = 0, \quad (3)$$

Chau, Keung [4] and Bjorken have noted that the first equation can be visualized as a triangle in the complex plane with vertices at  $(0,0)$ ,  $(0,1)$  and  $(\rho, \eta)$ . Measurements of the magnitudes of the CKM elements determine the lengths of the sides of the triangle, while measurements of the CP asymmetries determine the interior angles of the triangle. Fig. 1 shows the CKM triangle and the corresponding decay channels by which we can measure the CKM elements. The red decay modes will be discussed in this talk.

### 3 $|V_{cb}|$ from $\overline{B}^0 \rightarrow D^{*+}\ell^{-}\overline{\nu}$

The decay  $\overline{B}^0 \rightarrow D^{*+}\ell^{-}\overline{\nu}$  supplies us with a good channel to measure the CKM element  $|V_{cb}|$ , which is vital to our understanding of the unitary triangle as it sets the scale of the entire triangle. The partial width of  $\overline{B}^0 \rightarrow D^{*+}\ell^{-}\overline{\nu}$  is proportional to  $|V_{cb}|^2$ :

$$\frac{d\Gamma}{dw} = \frac{G_F^2}{48\pi^3} |V_{cb}|^2 [\mathcal{F}(w)]^2 \mathcal{G}(w), \quad (4)$$

where:  $w = v_B \cdot v_{D^*}$  is the relativistic  $\gamma$  of  $D^*$  in the B rest frame;  $\mathcal{G}(w)$  contains kinematic factors and is known by theory;  $\mathcal{F}(w)$  is the form factor describing  $B \rightarrow D^*$  transition.

At zero recoil of  $D^*$  (i.e.  $w = 1$ ),  $\frac{d\Gamma}{dw} \propto (\mathcal{F}(1)|V_{cb}|)^2$ ,  $\mathcal{F}(1)$  can be calculated by theory like HQET(Heavy Quark Effective Theory). This point is where our analysis technique comes from.

#### 3.1 The Analysis Technique

The technique is to measure  $d\Gamma/dw$  and extrapolate to  $w = 1$  to extract  $\mathcal{F}(1)|V_{cb}|$ . For  $D^*\ell\nu$ ,  $w$  runs from 1 to 1.5. We divide it into ten bins. The signal event is full reconstructed as :  $\overline{B}^0 \rightarrow D^{*+}\ell^{-}\overline{\nu}$ ,  $D^{*+} \rightarrow D^0\pi^+$  and  $D^0 \rightarrow K^-\pi^+$ . The  $\overline{B}^0 \rightarrow D^{*+}\ell^{-}\overline{\nu}$  yield in each  $w$  bin is extracted from a likelihood fit to the  $\cos\theta_{B-D^*\ell}$  distribution (the angle between the  $D^*\ell$  combination and  $B$ ). The reason why we fit to this angular distribution is that it can well distinguish between  $\overline{B}^0 \rightarrow D^{*+}\ell^{-}\overline{\nu}$  and  $\overline{B}^0 \rightarrow D^{*+}X\ell^{-}\overline{\nu}$  background events, which include events like  $\overline{B}^0 \rightarrow D^{*+}\ell^{-}\overline{\nu}$  and  $\overline{B}^0 \rightarrow D^{*+}\pi\ell^{-}\overline{\nu}$ . Because these background events don't have zero missing mass as the signal decay, so their  $\cos\theta_{B-D^*\ell}$  distribution will be much broader than the signal  $\overline{B}^0 \rightarrow D^{*+}\ell^{-}\overline{\nu}$  decay. Fig. 2 is a representative fit plot obtained in the first  $w$  bin.

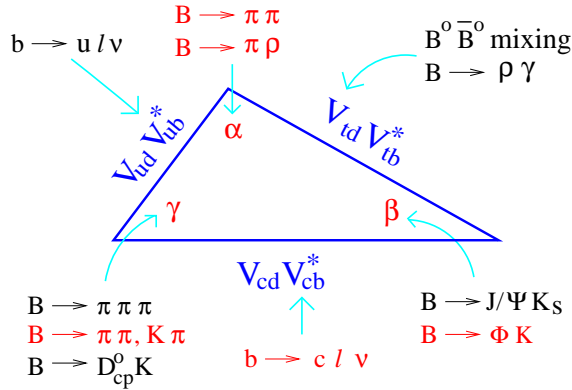


Figure 1: The unitary triangle

We then do a  $\chi^2$  fit on the overall  $w$  distribution taking into account backgrounds, reconstruction efficiency and the  $w$  resolution. We use the dispersion relations [5,6] to constrain the shapes of the form factor  $\mathcal{F}(w)$  and fit for  $\mathcal{F}(1)|V_{cb}|$  and a “slope”,  $\rho^2$  ( $atw = 1$ ), see fig. 3.

This analysis is systematic limited, the major source of uncertainty for the analysis is the efficiency for reconstructing the slow  $\pi$  from  $D^*$  decay( with systematic error of 3.1%), which is due to the uncertainties in the amount of material in the inner detector(2.3%) and the drift chamber hit efficiency(0.8%).

### 3.2 Preliminary results

We find

$$\mathcal{F}(1)|V_{cb}| = (42.4 \pm 1.8 \pm 1.9) \times 10^{-3},$$

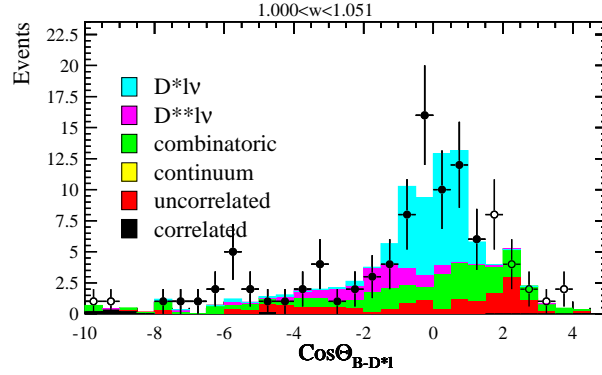


Figure 2: Fit to first  $w$  bin.

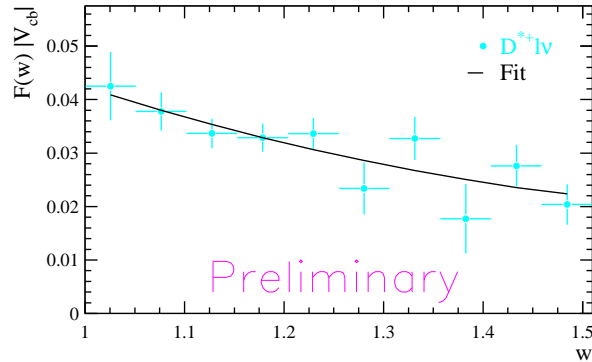


Figure 3: Fit to  $\mathcal{F}(1)|V_{cb}|$ .

$$\mathcal{B}(\overline{B}^0 \rightarrow D^{*+} \ell^- \overline{\nu}) = (5.66 \pm 0.29 \pm 0.33)\%,$$

Using  $\mathcal{F}(1) = 0.913 \pm 0.042$  [7], we calculate

$$|V_{cb}| = (46.4 \pm 2.0 \pm 2.1 \pm 2.1) \times 10^{-3},$$

This result is consistent with our previous measurements, but somewhat higher. The analysis benefits from small backgrounds and good resolution in  $w$ . A measurement using  $D^{*0} \ell \nu$  will come soon. Combining these two channels will give the best single measurement of  $|V_{cb}|$  using the exclusive technique.

## 4 Charmless Hadronic Two-Body B Decays

The rare B decays can occur through two main types of diagrams:  $b \rightarrow u$  spectator diagrams (suppressed by  $V_{ub}$ ) and  $b \rightarrow s$  penguin diagrams (suppressed by loops). Usually for one decay mode, there is more than one contributing diagrams, the interference between them gives rise to the CP violation in the B sector [8,9,10].

### 4.1 Analysis Technique

In CLEO experiment, candidates for B meson decays are distinguished from continuum background using the difference,  $\Delta E$ , between the total energy of the two tracks and the beam energy, and the beam-constrained mass,  $m_B$ . The background for rare B decays arises entirely from the continuum where the two-jet structure of the events can produce high momentum, back-to-back tracks. We suppress the continuum background via event shape because the signal events are spherical while the continuum backgrounds are jetty. Further discrimination between isotropic signal and rather jetty continuum events is provided by a Fisher discriminant technique as described in detail in Ref. [11], which is a linear combination of experimental observables.

We then perform an unbinned maximum-likelihood fit. In this fit the signal and background distributions are defined by probability density functions derived from Monte Carlo studies. The fit determines the relative contributions of the final track combinations to the signal and background. At high momentum, it's hard to separate charged K from charged  $\pi$ , so we simultaneously fit for both components, *e.g.*  $B \rightarrow K^\pm \pi^\mp / \pi^\pm \pi^\mp$ . Fig. 4 shows the fitting plots for the decay modes  $B \rightarrow K^\pm \pi^\mp / \pi^\pm \pi^\mp$ . From the contour plot (fig. 4(a)), we can see the best fit value (cross) is 4 or 5  $\sigma$  away from the point  $N_{\pi\pi} = N_{K\pi} = 0$ . The histograms in fig. 4 are projections of the fitting result onto the variables of energy difference,  $\Delta E$ , and beam constrained mass,  $M$ .

Following I will briefly review the CLEO results for the different decay modes of the charmless hadronic B decays.

## 4.2 Two body B decays to Kaons and Pions: $B \rightarrow K\pi, \pi\pi$

Ratios of various  $B \rightarrow K\pi$  branching fractions were shown [12] to depend explicitly on  $\gamma \equiv \text{Arg}(V_{ub}^*)$  with relatively modest model dependence. Within a factorization model, branching fractions of a large number of rare B decays can be parametrized by a small number of independent physical quantities, including  $\gamma$ , which can then be extracted through a global fit [13] to existing data. Finally, measurement of the time-dependent CP-violation asymmetry in the decay  $B^0 \rightarrow \pi^+\pi^-$  can be used to determine the sum of  $\gamma$  and the phase  $\beta \equiv \text{Arg}(V_{td}^*)$ .

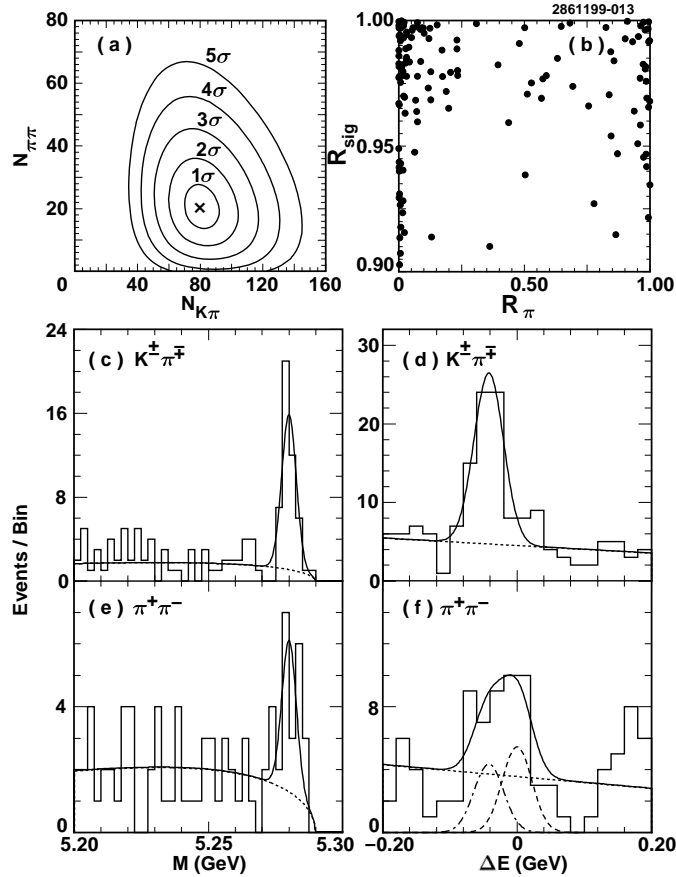


Figure 4: Illustration of Fit Results for  $B \rightarrow K^\pm\pi^\mp, \pi^\pm\pi^\mp$ . Contours of the likelihood function versus  $K\pi$  and  $\pi\pi$  event yield(a); likelihood ratios(b) - signal events cluster near the top of the figure, and separate into  $K\pi$ -like events on the left and  $\pi\pi$ -like events on the right; beam constrained mass for  $K\pi$ -like events(c);  $\Delta E$  for  $K\pi$ -like events(d); beam constrained mass for  $\pi\pi$ -like events(e);  $\Delta E$  for  $\pi\pi$ -like events(f); with both  $\pi\pi$  signal(dashed line) and  $K\pi$  cross-feed (dot-dashed line) shown.

Table 1: Measurements on  $B \rightarrow K\pi, \pi\pi$  modes (All upper limits at 90% C.L.).

Mode	$\epsilon(\%)$	Yield	Signif.	$\mathcal{B}(10^{-6})$
$K^\pm\pi^\mp$	48	$80.2^{+11.8}_{-11.0}$	$11.7\sigma$	$17.2^{+2.5}_{-2.4}\pm 1.2$
$K^0\pi^\pm$	14	$25.2^{+6.4}_{-5.6}$	$7.6\sigma$	$18.2^{+4.6}_{-4.0}\pm 1.6$
$K^\pm\pi^0$	38	$42.1^{+10.9}_{-9.9}$	$6.1\sigma$	$11.6^{+3.0+1.4}_{-2.7-1.3}$
$K^0\pi^0$	11	$16.1^{+5.9}_{-5.0}$	$4.9\sigma$	$14.6^{+5.9+2.4}_{-5.1-3.3}$
$\pi^\pm\pi^\mp$	48	$20.0^{+7.6}_{-6.5}$	$4.2\sigma$	$4.3^{+1.6}_{-1.4}\pm 0.5$
$\pi^\pm\pi^0$	39	$21.3^{+9.7}_{-8.5}$	$3.2\sigma$	$< 12.7$
$\pi^0\pi^0$	29	$6.2^{+4.8}_{-3.7}$	$2.0\sigma$	$< 5.7$
$K^\pm K^\mp$	48	$0.7^{+3.4}_{-0.7}$	$0.0\sigma$	$< 1.9$
$K^\pm K^0$	14	$1.4^{+2.4}_{-1.3}$	$1.1\sigma$	$< 5.1$
$K^0\overline{K^0}$	5	0	$0.0\sigma$	$< 17$

Table 2: Measurements on  $\eta'$  and  $\eta$  modes.

Mode	Signif.	$\mathcal{B} (10^{-6})$
$B^+ \rightarrow \eta' K^+$	$16.8\sigma$	$80^{+10}_{-9}\pm 7$
$B^0 \rightarrow \eta' K^0$	$11.7\sigma$	$89^{+18}_{-16}\pm 9$
$B^+ \rightarrow \eta K^{*+}$	$4.8\sigma$	$26.4^{+9.6}_{-8.2}\pm 3.3$
$B^0 \rightarrow \eta K^{*0}$	$5.1\sigma$	$13.8^{+5.5}_{-4.6}\pm 1.6$

Table 1 summarizes the CLEO results on the  $B \rightarrow K\pi, \pi\pi$  modes. We finally observed all four  $K\pi$  modes. For some decay modes, the significance of the signal is not enough to claim an observation of the decay modes, so we just come up with upper limits.  $B \rightarrow \pi^0\pi^0$  is a new result, while the other results are also improved to the previous ones [14]. These results can be used to set new bound on the angle  $\gamma$  of the unitary triangle [15]. They also indicate that the gluonic penguin diagram contribution to the rare B decays is large.

### 4.3 Modes with $\eta'$ and $\eta$

An earlier search [16] found a large rate for the decay  $B \rightarrow \eta' K$ , and set upper limits on other decays to two-body final states containing  $\eta'$  or  $\eta$  mesons. In table 2, we summarize the latest CLEO measurements on these decay modes, we only observe signals on these four modes shown in table 2, for other modes, there is just upper

Table 3:  $B \rightarrow PV$  Modes

Mode	Yield	Signif.	$\mathcal{B}$ ( $10^{-6}$ )
$B^- \rightarrow \pi^- \rho^0$	$29.8_{-9.6}^{+9.3}$	$5.4\sigma$	$10.4_{-3.4}^{+3.3} \pm 2.1$
$B^- \rightarrow \pi^- \omega$	$28.5_{-7.3}^{+8.2}$	$6.2\sigma$	$11.3_{-2.9}^{+3.3} \pm 1.4$
$B^0 \rightarrow \pi^\pm \rho^\mp$	$31.0_{8.3}^{+0.4}$	$5.6\sigma$	$27.6_{-7.4}^{+8.4} \pm 4.2$

limits [17]. These results confirmed the previous observations that the  $\eta'K$  signal is larger than  $\eta K$ . To explain this phenomenon, a substantial intrinsic charm component of the  $\eta'$  has been proposed [18,19], but the new CLEO results on  $B \rightarrow \eta_c K$  [20]:

$$\text{BR}(B^0 \rightarrow \eta_c K^0) = (1.09_{-0.42}^{+0.55} \pm 0.12 \pm 0.31) \times 10^{-3},$$

$$\text{BR}(B^+ \rightarrow \eta_c K^+) = (0.69_{-0.21}^{+0.26} \pm 0.08 \pm 0.20) \times 10^{-3}$$

shows no enhancement compared to the  $B \rightarrow J/\psi K$  decay.

#### 4.4 B meson decays to Pseudoscalar-Vector final states

CLEO recently made the first observation of the decays  $B^- \rightarrow \pi^- \rho^0$ ,  $B^- \rightarrow \pi^- \omega$  and  $B^0 \rightarrow \pi^\pm \rho^\mp$  (charge-conjugate modes are implied) [21], as summarized in table 3. All of these  $\Delta S=0$  decay modes are expected to be dominated by hadronic  $b \rightarrow u$  transitions. We see no significant yields in any of the  $\Delta S=1$  transitions. This is in contrast to the corresponding charmless hadronic B decays to two pseudoscalar mesons ( $B \rightarrow PP$ )  $B \rightarrow K\pi, \pi\pi$ , where  $\Delta S=1$  transitions clearly dominate. It indicates that gluonic penguin decays play less of a role in  $B \rightarrow PV$  decays than in  $B \rightarrow PP$  decays. This is consistent with theoretical predictions [22] that uses factorization which predicts destructive (constructive) interference between penguin operators of opposite chirality for  $B \rightarrow K\rho$  ( $B \rightarrow K\pi$ ), leading to a rather small (large) penguin contribution in these decays.

#### 4.5 Observation of $B \rightarrow \phi K$ - Preliminary

The decay  $b \rightarrow s\gamma$  produced by the gluonic penguin can be uniquely tagged when the gluon splits into an  $s\bar{s}$  pair as no other b decay can produce this final state. The mode  $B \rightarrow \phi K$  is one such tag of the gluonic penguin and its rate is sensitive to  $\sin 2\beta$  in the CKM matrix. CLEO recently measured  $\text{BR}(B^- \rightarrow \phi K^-) = (6.4_{-2.1-2.0}^{+2.5+0.5}) \times 10^{-6}$  and  $\text{BR}(B^0 \rightarrow \phi K^0) = (5.9_{-2.9-0.9}^{+4.0+1.1}) \times 10^{-6}$ . Assuming that the branching ratio for these two processes should be equal, we obtain

$$\text{BR}(B \rightarrow \phi K) = (6.2_{-1.8-1.7}^{+2.0+0.7}) \times 10^{-6}$$

The first set of errors is statistical, whereas the second set is systematic, dominated by systematics of the unbinned maximum likelihood fit. While statistical significance of the signal in the  $B^- \rightarrow \phi K^-$  mode is  $4.4 \sigma$ , the statistical significance of the  $B^0 \rightarrow \phi K^0$  signal is only  $2.8\sigma$ . Thus, without any theoretical bias, we cannot claim the signal in the  $B^0 \rightarrow \phi K^0$  mode with high confidence and therefore we calculate the upper limit of  $< 1.2 \times 10^{-5}$  at 90% C.L. The signal significance in the combined charged and neutral kaon data is well above 5 standard deviations.

#### 4.6 CP Asymmetry Measurements

Direct CP asymmetry can result from interference of two amplitudes with different strong and weak phases. The asymmetry,  $\mathcal{A}_{CP}$  is defined by the difference between the rates for  $\overline{B} \rightarrow f$  and  $B \rightarrow \overline{f}$  as

$$\mathcal{A}_{CP} \equiv \frac{\mathcal{B}(\overline{B} \rightarrow f) - \mathcal{B}(B \rightarrow \overline{f})}{\mathcal{B}(\overline{B} \rightarrow f) + \mathcal{B}(B \rightarrow \overline{f})}, \quad (5)$$

Precise predictions for  $\mathcal{A}_{CP}$  are not feasible at present as both the absolute value and the strong interaction phases of the contributing amplitudes are not calculable. However, numerical estimates can be made under well-defined model assumptions and the dependence on both model parameters and CKM parameters can be probed. Recent calculations of CP asymmetries under the assumption of factorization have been published by Ali et al. [23].

In table 4, we present results [24] of searches for CP violation in decays of B mesons to the three  $K\pi$  modes,  $K^\pm\pi^\mp$ ,  $K^\pm\pi^0$ ,  $K^0\pi^\pm$ , the mode  $K^\pm\eta'$ , and the vector-pseudoscalar mode  $\omega\pi^\pm$ . These decay modes are selected because they have well measured branching ratios and significant signal yields in our data sample [17,14,21]. In the data analysis, these decays are self-tagging, the flavor of the parent  $b$  or  $\overline{b}$  quark is tagged simply by the sign of the high momentum charged hadron. The asymmetry,  $\mathcal{A}_{CP}$ , is obtained from the maximum likelihood fit as a free parameter.

We see no evidence for CP violation in the five modes and set 90% CL intervals that reduce the possible range of  $\mathcal{A}_{CP}$  by as much as a factor of four. While the sensitivity is not yet sufficient to probe the rather small  $\mathcal{A}_{CP}$  values predicted by factorization models, extremely large  $\mathcal{A}_{CP}$  values that might arise if large strong phase differences were available from final state interactions are firmly ruled out. For the cases of  $K\pi$  and  $\eta'K$ , we can exclude  $|\mathcal{A}_{CP}|$  greater than 0.30 and 0.23 at 90% CL respectively.

## 5 Conclusions

Besides the results discussed above, CLEO has also many other physics results for B decay at  $\Upsilon(4S)$ . However, the unambiguous observation of the gluonic penguin

Table 4: CP asymmetry measurements from CLEO

Mode	Yield	$\mathcal{A}_{CP}$
$K^\pm\pi^\mp$	$80.2^{+11.8}_{-11.0}$	$-0.04 \pm 0.16$
$K^\pm\pi^0$	$42.1^{+10.9}_{-9.9}$	$-0.29 \pm 0.23$
$K^0\pi^\pm$	$25.2^{+6.4}_{-5.6}$	$+0.18 \pm 0.24$
$K^\pm\eta'$	$100^{+13}_{-12}$	$+0.03 \pm 0.12$
$\omega\pi^\pm$	$28.5^{+8.2}_{-7.3}$	$-0.34 \pm 0.25$

and the best single measure of  $|V_{cb}|$  are undoubtedly the highlights in the last year. As the CLEO III starts data taking and the asymmetric B factories gets their first results, we can all look forward to much more exciting physics from the  $\Upsilon(4S)$  in the future.

## Acknowledgments

I am grateful to Alice Bean, Karl Ecklund and the other CLEO and Kansas colleagues for the helpful discussions in preparing for the talk.

## References

- [1] CLEO Collaboration, Y.Kubota *et al.*, *Nucl. Instrum. Methods* **A320**,(1992)66.
- [2] T. Hill, *Nucl. Instrum. Methods* **A418**,(1998)32.
- [3] M. Kobayashi and T. Maskawa, *Progr. Theor. Phys.* **49**,(1973)652.
- [4] L.L.Chau and W.Y.Keung, *Phys. Rev. Lett.* **53**,(1984)1802.
- [5] I. Caprini,L. Lellouch and M. Neubert, *Nucl. Phys.* **B530** (1998)153;
- [6] C.G. Boyd, B. Grinstein and R.F. Lebed, *Phys. Rev.* **D56** (1997)6895;
- [7] BaBar Physics Book, P.F. Harrison and H.R.Quinn ed. *SLAC-R-504* (1998);
- [8] A.J.Buras, Lectures given at the 14th Lake Louise Winter Institute, *hep-ph/9905437*(February, 1999);

- [9] M.Neubert and J.L.Rosner, *Phys. Rev. Lett.* **81** (1998)5076;*Phys. Lett.* **B441**(1998)403
- [10] M.Bander, D.Silverman and A.Soni, *Phys. Rev. Lett.* **43** (1979)242;
- [11] D.M.Asner *et al.*(CLEO Collaboration) *Phys. Rev.* **D53** (1996)1039;
- [12] M.Gronau, J.L.Rosner, and D.London, *Phys. Rev. Lett.* **73** (1994)21; R.Fleischer, *Phys. Lett.* **B365** (1996)399; R.Fleischer, and T.Mannel, *Phys. Rev.* **D57** (1998)2752.
- [13] W.-S. Hou,J.G.Smith and F.Wurthwein, *hep-ex/9910014*.
- [14] D. Cronin-hennessy *et al.* (CLEO Collaboration) *Phys. Rev. Lett.* **85**,(2000)515
- [15] M.Neubert,J.L.Rosner, *Phys. Lett.* **B441** (1998)403.
- [16] B.H.Behrens, *et al.* (CLEO Collaboration) *Phys. Rev. Lett.* **80** (1998)3710.
- [17] S.J.Richichi, *et al.* (CLEO Collaboration) *Phys. Rev. Lett.* **85** (2000)525.
- [18] I.Halperin and A.Zhitnitsky, *Phys. Rev.* **D56** (1997)7247; E.V.Shuryak and A.R.Zhitnitsky *Phys. Rev.* **D57** (1998)2001.
- [19] F.Yuan and K.-T. Chao, *Phys. Rev.* **D56** (1997)2495.
- [20] K.W.Edwards *et al.* (CLEO Collaboration) *Phys. Rev. Lett.* **86** (2001)30.
- [21] C.P. Jessop, *et al.* (CLEO Collaboration) *Phys. Rev. Lett.* **85** (2000)3095.
- [22] K. Lingel, T.Skwarnicki, J.G.Smith, *Ann. Rev. Nucl. Part. Sci.***48** (1998)253; Y-H Chen, H-Y Cheng, B.Tseng and K-C Yang, *Phys. Rev.***D60** (1999)094014.
- [23] A.Ali,G.Kramer and C.D.Lu, *Phys. Rev.***D59** (1999)014005.
- [24] S.Chen *et al.* (CLEO Collaboration) *Phys. Rev. Lett.* **85** (2000)525.

March 3, 2001  
hep-ph/0103040

# Indirect Determination of the Vertex and Angles of the Unitarity Triangle

SALVATORE MELE\*

*CERN, EP Division, CH1211, Genève 23, Switzerland<sup>†</sup>*

The values of the elements of the Cabibbo-Kobayashi-Maskawa matrix are constrained by direct and indirect measurements. A fit to experimental data and theory calculations allows the indirect determination of the vertex and angles of the unitarity triangle as:

$$\rho = 0.18 \pm 0.07 \quad \eta = 0.35 \pm 0.05$$

$$\sin 2\alpha = 0.14_{-0.38}^{+0.25} \quad \sin 2\beta = 0.73 \pm 0.07 \quad \gamma = 63_{-11}^{+8} \text{ degrees.}$$

Information is derived on the presence of CP violation in the matrix, on non-perturbative QCD parameters and on the  $B_s^0$  oscillation frequency.

Presented at the

5th International Symposium on Radiative Corrections  
(RADCOR-2000)

Carmel CA, USA, 11-15 September, 2000

---

\*e-mail: Salvatore.Mele@cern.ch.

<sup>†</sup>On leave of absence from INFN Sezione di Napoli, 80125, Napoli, Italy.

# 1 Introduction

In the Standard Model of the electroweak interactions [1,2,3], a  $3 \times 3$  unitary matrix describes the mixing of the quark mass eigenstates into the weak interaction ones. This matrix is known as the Cabibbo-Kobayashi-Maskawa (CKM) matrix [4,5], and can be written in terms of just four real parameters [6]:

$$V_{\text{CKM}} = \begin{pmatrix} V_{ud} & V_{us} & V_{ub} \\ V_{cd} & V_{cs} & V_{cb} \\ V_{td} & V_{ts} & V_{tb} \end{pmatrix} \simeq \begin{pmatrix} 1 - \frac{\lambda^2}{2} & \lambda & A\lambda^3(\rho - i\eta) \\ -\lambda & 1 - \frac{\lambda^2}{2} & A\lambda^2 \\ A\lambda^3(1 - \rho - i\eta) & -A\lambda^2 & 1 \end{pmatrix}. \quad (1)$$

$A$ ,  $\rho$  and  $\eta$  are of order unity and  $\lambda$  is the sine of the Cabibbo angle. The parameter  $\eta$  is the complex phase of the matrix, directly related to the violation of the CP symmetry in the weak interactions. The measurement of the parameters of the CKM matrix is of fundamental importance for both the description of the weak interaction of quarks and to shed light on the mechanism of CP violation.

The parameters  $A$  and  $\lambda$  are known with an accuracy of a few percent and this work concentrates on the indirect determination of  $\rho$  and  $\eta$ . This is also described as the study of the vertex or the angles of a triangle in the  $\rho - \eta$  plane, whose other two vertices are located in  $(0,0)$  and  $(1,0)$ . This triangle, called the unitarity triangle, is depicted in Figure 1. This study follows the same procedure as a previous publication [7] with an update of the input parameters, as described in the following.

A large number of physical processes are parametrised in terms of the values of the elements of the CKM matrix. Among them, four present the largest sensitivity to  $\rho$  and  $\eta$ , given the knowledge of the involved theoretical and experimental quantities. These processes are discussed in the following and then used in a fit to derive  $\rho$  and  $\eta$ . Conclusions are then drawn from the results of this fit.

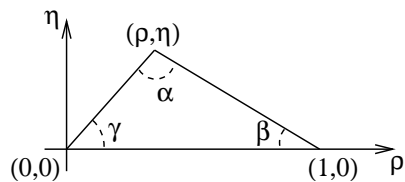


Figure 1: The unitarity triangle.

## 2 Constraints

### 2.1 $\lambda$ and $A$

The value of the sine of the Cabibbo angle is measured as [8]:

$$\lambda = 0.2196 \pm 0.0023.$$

The study of inclusive semileptonic B decays by the CLEO [9] and the LEP [10] experiments yields information on the value of  $|V_{cb}|$ . Further constraints are derived from the study of the  $B^0 \rightarrow D^{*+}\ell\nu$  decay, both at the  $\Upsilon(4S)$  [11] and at the Z pole [10]. From these measurements, a value  $|V_{cb}| = (40.9 \pm 1.9) \times 10^{-3}$  is extracted, which yields:

$$A = \frac{|V_{cb}|}{\lambda^2} = 0.83 \pm 0.04.$$

## 2.2 CP Violation for Neutral Kaons

The mass eigenstates of the neutral kaons can be written as  $|K_S\rangle = p|K^0\rangle + q|\bar{K}^0\rangle$  and  $|K_L\rangle = p|K^0\rangle - q|\bar{K}^0\rangle$ . The relation  $p \neq q$  implies the violation of the CP symmetry that, in the Wu-Yang phase convention [12], is described by the parameter  $\epsilon_K$  defined as:

$$\frac{p}{q} = \frac{1 + \epsilon_K}{1 - \epsilon_K}.$$

The precise measurements of the  $K_S \rightarrow \pi^+\pi^-$  and  $K_L \rightarrow \pi^+\pi^-$  decay rates imply [8]:

$$|\epsilon_K| = (2.280 \pm 0.019) \times 10^{-3}.$$

The relation of  $|\epsilon_K|$  to the CKM matrix parameters is [13,14]:

$$|\epsilon_K| = \frac{G_F^2 f_K^2 m_K m_W^2}{6\sqrt{2}\pi^2 \Delta m_K} B_K (A^2 \lambda^6 \eta) \quad (2)$$

$$\times [y_c (\eta_{ct} f_3(y_c, y_t) - \eta_{cc}) + \eta_{tt} y_t f_2(y_t) A^2 \lambda^4 (1 - \rho)].$$

The functions  $f_3$  and  $f_2$  of the variables  $y_t = m_t^2/m_W^2$  and  $y_c = m_c^2/m_W^2$  are given in Reference [15]. The measured value of the top quark mass,  $174.3 \pm 5.1$  GeV [8], is scaled as proposed in Reference [16], giving:

$$\overline{m}_t(m_t) = 167.3 \pm 5.2 \text{ GeV},$$

while the mass of the charm quark is chosen as [8]:

$$\overline{m}_c(m_c) = 1.25 \pm 0.10 \text{ GeV}.$$

The calculated QCD corrections in Equation (2) are described by the consistent set of parameters [16,17,18,19]:

$$\eta_{cc} = 1.38 \pm 0.53, \quad \eta_{tt} = 0.574 \pm 0.004, \quad \eta_{ct} = 0.47 \pm 0.04.$$

Non-perturbative QCD contributions to this process are affected by a large uncertainty and are summarised by the ‘‘bag’’ parameter  $B_K$ , chosen as [20]:

$$B_K = 0.87 \pm 0.14.$$

The other physical constants appearing in Equation (2) are reported in Table 1. The measurement of  $|\epsilon_K|$  constrains the vertex of the unitarity triangle onto an hyperbola in the  $\rho - \eta$  plane.

Recent measurements of direct CP violation in the neutral kaon sector from the KTeV [21] and NA48 [22] experiments confirm the previous NA31 result [23]. These measurements could result in a lower bound to  $\eta$ . Nonetheless they are not used to constrain the CKM matrix owing to the large uncertainties that affect the corresponding theoretical calculations [24,25].

### 2.3 Oscillations of $B_d^0$ Mesons

The behaviour of neutral mesons containing a  $b$  quark depends on the the mass difference between the heavy and light mass eigenstates,  $B_H$  and  $B_L$ . These are different from the CP eigenstates  $B_d^0$  and  $\bar{B}_d^0$ . The mass difference,  $\Delta m_d = m_{B_H} - m_{B_L}$ , is measured [26] at LEP, the  $\Upsilon(4S)$  and the TEVATRON by means of the study of the oscillations of one CP eigenstate into the other. A recent average is:

$$\Delta m_d = 0.487 \pm 0.014 \text{ ps}^{-1}.$$

Recent results from the Babar [27] and Belle [28] collaborations are not yet included in this average with which they are statistically comparable. The value of  $\Delta m_d$  is related to the CKM parameters as:

$$\Delta m_d = \frac{G_F^2}{6\pi^2} m_W^2 m_B (f_{B_d} \sqrt{B_{B_d}})^2 \eta_B y_t f_2(y_t) A^2 \lambda^6 [(1 - \rho)^2 + \eta^2]. \quad (3)$$

The calculated QCD correction  $\eta_B$  amounts to [16,17,18,19]:

$$\eta_B = 0.55 \pm 0.01,$$

while non-perturbative QCD contributions are summarised by [29]:

$$f_{B_d} \sqrt{B_{B_d}} = 0.206 \pm 0.029 \text{ GeV}.$$

The vertex of the unitarity triangle is constrained by  $\Delta m_d$  onto a circle in the  $\rho - \eta$  plane, with centre in  $(1, 0)$ .

### 2.4 Oscillations of $B_s^0$ Mesons

The  $B_s^0$  mesons are predicted to mix like the  $B_d^0$  mesons, but their larger mass difference,  $\Delta m_s$ , results into faster oscillations. These have eluded direct observation and the current 95% Confidence Level (CL) lower limit on  $\Delta m_s$  from the LEP, SLD and CDF collaborations is [26]:

$$\Delta m_s > 14.9 \text{ ps}^{-1} \text{ (95\% CL)}.$$

The experiments, once combined, are sensitive to values of  $\Delta m_s$  up to  $17.9 \text{ ps}^{-1}$  and a  $2.5\sigma$  indication for the observation of  $B_s^0$  oscillations is observed around  $\Delta m_s = 17.7 \text{ ps}^{-1}$ .

The expression for  $\Delta m_s$  as a function of the CKM parameters is similar to that for  $\Delta m_d$ , and taking their ratio, it follows:

$$\Delta m_s = \Delta m_d \frac{1}{\lambda^2} \frac{m_{B_s}}{m_{B_d}} \xi^2 \frac{1}{(1-\rho)^2 + \eta^2}. \quad (4)$$

All the theoretical parameters and their uncertainties are included in the quantity  $\xi$ , known as [29]:

$$\xi = \frac{f_{B_d} \sqrt{B_{B_d}}}{f_{B_s} \sqrt{B_{B_s}}} = 1.16 \pm 0.07.$$

The lower limit on  $\Delta m_s$  constrains the vertex of the unitarity triangle in a circle in the  $\rho - \eta$  plane with centre in  $(1, 0)$ .

## 2.5 Charmless Semileptonic $b$ Decays

The constraints described so far suffer from the uncertainties in non-perturbative QCD quantities entering their expressions. The determination of either  $|V_{ub}|$  or the ratio  $|V_{ub}|/|V_{cb}|$  constitutes a constraint free from these uncertainties as:

$$|V_{ub}|/|V_{cb}| = \lambda \sqrt{\rho^2 + \eta^2}. \quad (5)$$

The CLEO collaboration has measured this ratio by means of the endpoint of inclusive [30] charmless semileptonic B decays as:  $|V_{ub}|/|V_{cb}| = 0.08 \pm 0.02$ . The ALEPH [31], DELPHI [32] and L3 [33] collaborations have measured at LEP the inclusive charmless semileptonic branching fraction of beauty hadrons; these are averaged [10] as:

$$|V_{ub}| = (4.13_{-0.75}^{+0.63}) \times 10^{-3}.$$

Using the quoted value of  $|V_{cb}|$ , a combination with the CLEO measurement yields:

$$|V_{ub}|/|V_{cb}| = 0.089 \pm 0.010.$$

This constraint is represented by a circle in the  $\rho - \eta$  plane with centre in  $(0,0)$ , shown in Figure 2, that also presents all the other constraints described so far.

## 3 The fit

The  $\rho$  and  $\eta$  parameters are determined from a fit to the constraints described above. The experimental and theoretical quantities appearing in the formulae (2), (3),

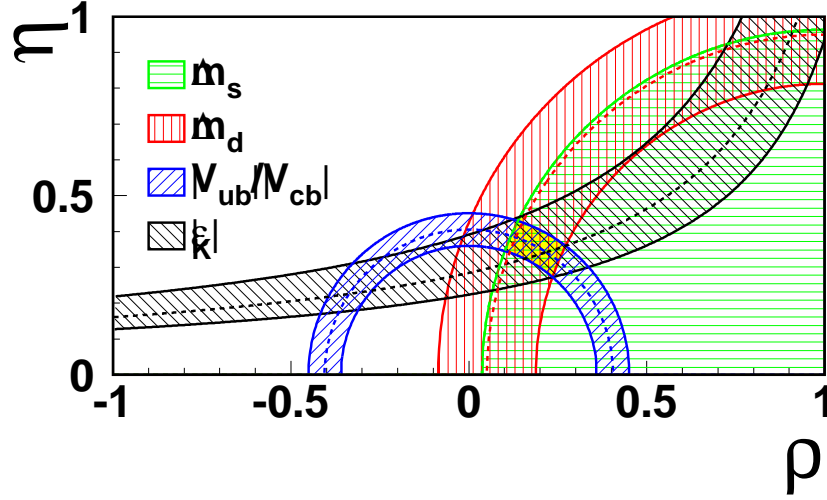


Figure 2: Constraints in the  $\rho - \eta$  plane.  $B_s^0$  oscillations are reported as a 95% CL limit, while the other constraints represent a  $\pm 1\sigma$  variation of the experimental and theoretical parameters entering in the formulae in the text. Central values are indicated by the dashed lines. A darker area shows the overlap among the constraints.

Table 1: Physical constants and parameters of the fit. The values not discussed in the text follow from Reference [8].

$\lambda$	$= 0.2196(23)$	$A$	$= 0.83(4)$
$G_F$	$= 1.16639(1) \times 10^{-5} \text{ GeV}^{-2}$	$\eta_{ct}$	$= 0.47(4)$
$f_K$	$= 0.1598(15) \text{ GeV}$	$\eta_{cc}$	$= 1.38(53)$
$\Delta m_K$	$= 0.5304(14) \times 10^{-2} \text{ ps}^{-1}$	$\overline{m}_c(m_c)$	$= 1.25(10) \text{ GeV}$
$m_K$	$= 0.497672(31) \text{ GeV}$	$\overline{m}_t(m_t)$	$= 167.3(5.2) \text{ GeV}$
$m_W$	$= 80.419(38) \text{ GeV}$	$f_{B_d} \sqrt{B_{B_d}}$	$= 0.206(29) \text{ GeV}$
$m_{B_d}$	$= 5.2792(18) \text{ GeV}$	$B_K$	$= 0.87(14)$
$m_{B_s}$	$= 5.3692(20) \text{ GeV}$	$\xi$	$= 1.16(7)$
$m_B$	$= 5.290(2) \text{ GeV}$	$ \epsilon_K $	$= 2.280(19) \times 10^{-3}$
$\eta_B$	$= 0.55(1)$	$\Delta m_d$	$= 0.487(14) \text{ ps}^{-1}$
$\eta_{tt}$	$= 0.574(4)$	$ V_{ub} / V_{cb} $	$= 0.089(10)$

(4) and (5) are divided in two classes. Those whose uncertainties are below 2% are fixed to their central value as listed in the left half of Table 1. The quantities affected by a larger uncertainty and  $|\epsilon_K|$  are considered as additional parameters of the fit, constraining their values to the estimates summarised in the right half of Table 1.

The following expression is then minimised:

$$\begin{aligned} \chi^2 = & \frac{(\widehat{A} - A)^2}{\sigma_A^2} + \frac{(\widehat{m}_c - m_c)^2}{\sigma_{m_c}^2} + \frac{(\widehat{m}_t - m_t)^2}{\sigma_{m_t}^2} + \frac{(\widehat{B}_K - B_K)^2}{\sigma_{B_K}^2} + \frac{(\widehat{\eta}_{cc} - \eta_{cc})^2}{\sigma_{\eta_{cc}}^2} + \\ & \frac{(\widehat{\eta}_{ct} - \eta_{ct})^2}{\sigma_{\eta_{ct}}^2} + \frac{\left(f_{B_d} \widehat{\sqrt{B_{B_d}}} - f_{B_d} \sqrt{B_{B_d}}\right)^2}{\sigma_{f_{B_d} \sqrt{B_{B_d}}}^2} + \frac{(\widehat{\xi} - \xi)^2}{\sigma_{\xi}^2} + \frac{\left(\frac{|\widehat{V}_{ub}|}{|\widehat{V}_{cb}|} - \frac{|V_{ub}|}{|V_{cb}|}\right)^2}{\sigma_{\frac{|V_{ub}|}{|V_{cb}|}}^2} + \\ & \frac{\left(|\widehat{\epsilon}_K| - |\epsilon_K|\right)^2}{\sigma_{|\epsilon_K|}^2} + \frac{\left(\widehat{\Delta m}_d - \Delta m_d\right)^2}{\sigma_{\Delta m_d}^2} + \chi^2(\mathcal{A}(\Delta m_s), \sigma_{\mathcal{A}}(\Delta m_s)). \end{aligned}$$

The symbols with a hat represent the reference values and the corresponding  $\sigma$  denote their uncertainties. The free parameters of the fit are  $\rho$ ,  $\eta$ ,  $A$ ,  $m_c$ ,  $m_t$ ,  $B_K$ ,  $\eta_{ct}$ ,  $\eta_{cc}$ ,  $f_{B_d} \sqrt{B_{B_d}}$  and  $\xi$ , used to calculate the values of  $|\epsilon_K|$ ,  $\Delta m_d$ ,  $\Delta m_s$  and  $|V_{ub}|/|V_{cb}|$  by means of the formulae (2), (3), (4) and (5).

As  $\Delta m_s$  is not yet measured, its experimental information has to be included in the  $\chi^2$  following a different approach [7]. The results of the search for  $B_s^0$  oscillations are combined [26] in terms of the oscillation amplitude  $\mathcal{A}$  [34], a parameter that is zero in the absence of any signal and compatible with one otherwise, as expressed by the oscillation probability  $P$ :

$$P[B_s^0 \rightarrow (B_s^0, \overline{B}_s^0)] = \frac{1}{2\tau_s} e^{-t/\tau_s} (1 \pm \mathcal{A} \cos \Delta m_s).$$

The results of different experiments are combined in terms of  $\mathcal{A}(\Delta m_s)$  and of its uncertainty  $\sigma_{\mathcal{A}}(\Delta m_s)$ . The 95% CL limit on  $\Delta m_s$  is the value for which the area above one of the Gaussian distribution with mean  $\mathcal{A}(\Delta m_s)$  and variance  $\sigma_{\mathcal{A}}^2(\Delta m_s)$  equals 5% of its total area. In the fit, each value taken by the parameters  $\rho$ ,  $\eta$  and  $\xi$  is converted into a value of  $\Delta m_s$  by means of formula (4). A value of the CL for the oscillation hypothesis is then calculated by integrating the Gaussian distribution with mean  $\mathcal{A}(\Delta m_s)$  and variance  $\sigma_{\mathcal{A}}^2(\Delta m_s)$ . The value  $\chi^2(\mathcal{A}(\Delta m_s), \sigma_{\mathcal{A}}(\Delta m_s))$  of a  $\chi^2$  distribution with one degree of freedom corresponding to this CL is then calculated and finally added to the  $\chi^2$  of the fit.

The fit indicates the following values for the  $\rho$  and  $\eta$  parameters:

$$\rho = 0.18 \pm 0.07 \quad \eta = 0.35 \pm 0.05$$

$$0.05 < \rho < 0.30 \quad 0.26 < \eta < 0.44 \quad (95\%CL).$$

No large change in these results is observed if the theory contribution constraints are removed from the  $\chi^2$  and a flat distribution within the uncertainties is used in their

place. Figure 3 presents the confidence regions for the vertex of the unitarity triangle. The value of the angles of the unitarity triangle are determined as as:

$$\sin 2\alpha = 0.14_{-0.38}^{+0.25} \quad \sin 2\beta = 0.73 \pm 0.07 \quad \gamma = 63_{-11}^{+8} \text{ degrees.}$$

$$-0.77 < \sin 2\alpha < 0.50 \quad 0.59 < \sin 2\beta < 0.87 \quad 44^\circ < \gamma < 82^\circ \quad (95\% \text{CL})$$

The angles  $\alpha$  and  $\beta$  are reported in terms of the functions  $\sin 2\alpha$  and  $\sin 2\beta$ , to which the studies of the CP symmetry usually refer.

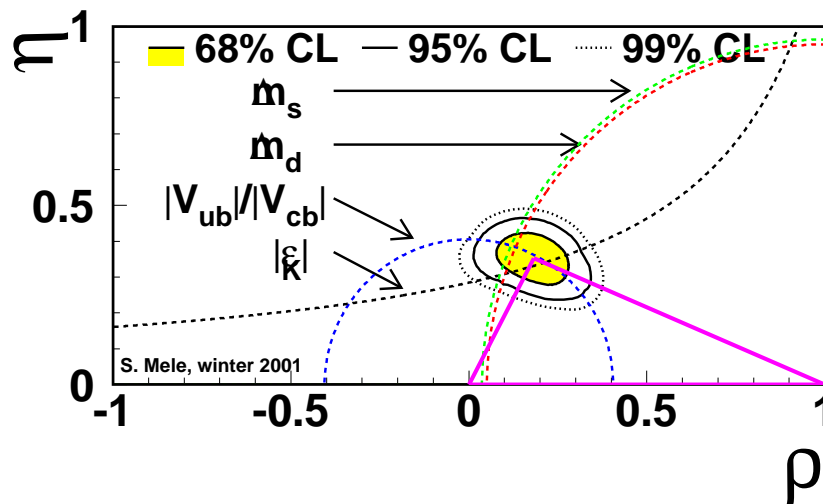


Figure 3: The favoured unitarity triangle and the confidence regions for its vertex; the  $\Delta m_s$  limit and the central values of the other constraints are also shown.

Several direct measurements of  $\sin 2\beta$  were recently reported, as listed in Table 2. Their average,  $\sin 2\beta^{\text{exp.}} = 0.48 \pm 0.16$ , is lower but in agreement with the present estimate, that does not make use of this direct information.

## 4 Consequences of the fit

A strong experimental evidence for CP violation in the CKM matrix, described by values of its complex phase,  $\eta$ , different from zero, comes from the neutral kaon system. It is of interest [39] to investigate whether processes other than kaon physics predict a value of  $\eta$  compatible with zero or not. Figure 4 presents the results of a fit from which the information from the kaon system is removed.. The presence of a CP violating phase in the matrix, *i.e.* its complex nature is strongly favoured.

Table 2: Measurements of  $\sin 2\beta$  and their average, compared with the fit result.

Aleph [35]	$0.93^{+0.64}_{-0.88} \text{ } ^{+0.36}_{-0.24}$
BaBar [36]	$0.34 \pm 0.20 \pm 0.05$
Belle [37]	$0.58^{+0.32}_{-0.34} \text{ } ^{+0.09}_{-0.10}$
CDF [38]	$0.79^{+0.41}_{-0.44}$
Average	$0.48 \pm 0.16$
This fit	$0.73 \pm 0.07$

The values of the parameters  $B_K$  and  $f_{B_d}\sqrt{B_{B_d}}$  that describe non-perturbative QCD effects can be estimated by removing their constraint from the fit. This procedure yields:

$$\rho = 0.17 \pm 0.07 \quad \eta = 0.38^{+0.05}_{-0.06} \quad B_K = 0.76^{+0.21}_{-0.15}$$

in the first case and in the second:

$$\rho = 0.21^{+0.07}_{-0.08} \quad \eta = 0.34 \pm 0.05 \quad f_{B_d}\sqrt{B_{B_d}} = 0.227^{+0.019}_{-0.015} \text{ GeV}.$$

The fit indicates a value of  $B_K$  with an uncertainty larger than the input one, yet

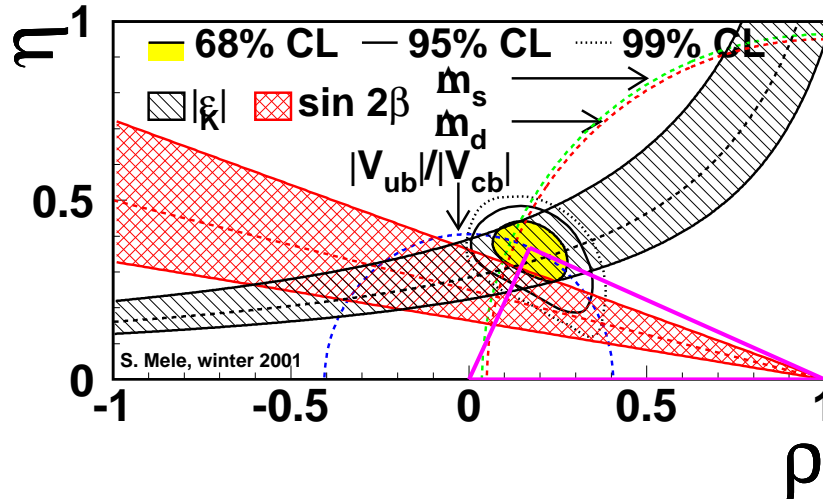


Figure 4: The favoured unitarity triangle and the confidence regions for its vertex, no information from the kaon system is used in the fit. The experimental measurements of CP violation in the neutral kaon and neutral  $b$  meson systems are superimposed.

of similar magnitude. The value of  $f_{B_d}\sqrt{B_{B_d}}$  is found to be well in agreement with the predicted one with a smaller uncertainty, this implies that the high experimental precision of the  $\Delta m_d$  constraint is not fully exploited by the fit, limited by the uncertainty on the  $f_{B_d}\sqrt{B_{B_d}}$  parameter.

The  $\Delta m_s$  constraint heavily affects the  $\rho$  uncertainty. Indeed, a fit that does not make use of the  $\Delta m_s$  information results in:

$$\rho = 0.09_{-0.15}^{+0.10} \quad \eta = 0.40 \pm 0.05.$$

This fit is used to estimate the favoured values of  $\Delta m_s$  as:

$$\begin{aligned} \Delta m_s &= 14.0_{-3.3}^{+3.4} \text{ ps}^{-1} \\ 7.4 \text{ ps}^{-1} &< \Delta m_s < 21.0 \text{ ps}^{-1} \quad (95\% \text{CL}). \end{aligned}$$

## 5 Conclusions

The measurements of  $|\epsilon_K|$ ,  $\Delta m_d$  and  $|V_{ub}|$ , together with the lower limit on  $\Delta m_s$ , effectively constrain the CKM matrix: from a fit to the experimental results and theory parameters, the vertex and the angles of the unitarity triangle are determined as:

$$\begin{aligned} \rho &= 0.18 \pm 0.07 \quad \eta = 0.35 \pm 0.05 \\ \sin 2\alpha &= 0.14_{-0.38}^{+0.25} \quad \sin 2\beta = 0.73 \pm 0.07 \quad \gamma = 63_{-11}^{+8} \text{ degrees}. \end{aligned}$$

These results are in agreement with those of recent similar analyses [40,41,42,43,44].

A coherent picture of the current understanding of the CKM matrix is presented by a fit that does not use any constraint from the kaon system. Its results are displayed in Figure 4. The favoured region for the vertex of the unitarity triangle corresponds to that experimentally indicated by the measurement of the CP violation in the neutral kaon system and overlaps with the one indicated by the recent measurements of  $\sin 2\beta$ .

## Acknowledgments

I am grateful to the organisers of RADCOR-2000 for their invitation to this interesting symposium.

## References

- [1] S. L. Glashow, Nucl. Phys. **22** (1961) 579.
- [2] A. Salam, *Originally printed in \*Svartholm: Elementary Particle Theory, Proceedings Of The Nobel Symposium Held 1968 At Lerum, Sweden\*, Stockholm 1968, 367-377.*
- [3] S. Weinberg, Phys. Rev. Lett. **19** (1967) 1264.
- [4] N. Cabibbo, Phys. Rev. Lett. **10** (1963) 531.
- [5] M. Kobayashi and T. Maskawa, Prog. Theor. Phys. **49** (1973) 652.
- [6] L. Wolfenstein, Phys. Rev. Lett. **51** (1983) 1945.
- [7] S. Mele, Phys. Rev. D **59** (1999) 113011 [hep-ph/9810333].
- [8] D. E. Groom *et al.* [Particle Data Group Collaboration], Eur. Phys. J. C **15** (2000) 1.
- [9] B. Barish *et al.* [CLEO Collaboration], Phys. Rev. Lett. **76** (1996) 1570.
- [10] D. Abbaneo *et al.*, hep-ex/0009052.
- [11] D. Cinabro [CLEO Collaboration], hep-ex/0009045.
- [12] T. T. Wu and C. N. Yang, Phys. Rev. Lett. **13** (1964) 380.
- [13] A. J. Buras, W. Slominski and H. Steger, Nucl. Phys. B **238** (1984) 529.
- [14] A. J. Buras, W. Slominski and H. Steger, Nucl. Phys. B **245** (1984) 369.
- [15] A. Ali and D. London, Z. Phys. C **65** (1995) 431 [hep-ph/9408332].
- [16] A. J. Buras, M. Jamin and P. H. Weisz, Nucl. Phys. B **347** (1990) 491.
- [17] S. Herrlich and U. Nierste, Nucl. Phys. B **419** (1994) 292 [hep-ph/9310311].
- [18] S. Herrlich and U. Nierste, Phys. Rev. D **52** (1995) 6505 [hep-ph/9507262].
- [19] S. Herrlich and U. Nierste, Nucl. Phys. B **476** (1996) 27 [hep-ph/9604330].
- [20] Y. Kuramashi, Nucl. Phys. Proc. Suppl. **83** (2000) 24 [hep-lat/9910032].
- [21] A. Alavi-Harati *et al.* [KTeV Collaboration], Phys. Rev. Lett. **83** (1999) 22 [hep-ex/9905060].

- [22] V. Fanti *et al.* [NA48 Collaboration], Phys. Lett. B **465** (1999) 335 [hep-ex/9909022].
- [23] G. D. Barr *et al.* [NA31 Collaboration], Phys. Lett. B **317** (1993) 233.
- [24] S. Bertolini, hep-ph/0101212.
- [25] A. J. Buras, hep-ph/9806471.
- [26] A. Stocchi, hep-ph/0010222.
- [27] C. Touramanis [BaBar Collaboration], hep-ex/0101035.
- [28] K. Abe *et al.* [Belle Collaboration], hep-ex/0011090.
- [29] D. Becirevic, D. Meloni, A. Retico, V. Gimenez, L. Giusti, V. Lubicz and G. Martinelli, hep-lat/0002025.
- [30] J. Bartelt *et al.* [CLEO Collaboration], Phys. Rev. Lett. **71** (1993) 4111.
- [31] R. Barate *et al.* [ALEPH Collaboration], Eur. Phys. J. C **6** (1999) 555.
- [32] P. Abreu *et al.* [DELPHI Collaboration], Phys. Lett. B **478** (2000) 14.
- [33] M. Acciarri *et al.* [L3 Collaboration], Phys. Lett. B **436** (1998) 174.
- [34] H. G. Moser and A. Roussarie, Nucl. Instrum. Meth. A **384** (1997) 491.
- [35] R. Barate *et al.* [ALEPH Collaboration], Phys. Lett. B **492** (2000) 259 [hep-ex/0009058].
- [36] B. Aubert *et al.* [BABAR Collaboration], hep-ex/0102030.
- [37] A. Abashian *et al.* [BELLE Collaboration], hep-ex/0102018.
- [38] T. Affolder *et al.* [CDF Collaboration], Phys. Rev. D **61** (2000) 072005 [hep-ex/9909003].
- [39] R. Barbieri, L. Hall, A. Stocchi and N. Weiner, Phys. Lett. B **425** (1998) 119 [hep-ph/9712252].
- [40] M. Bargiotti *et al.*, Riv. Nuovo Cim. **23N3** (2000) 1 [hep-ph/0001293].
- [41] P. Faccioli, hep-ph/0011269.
- [42] A. Ali and D. London, hep-ph/0012155.
- [43] M. Ciuchini *et al.*, hep-ph/0012308.
- [44] A. J. Buras, hep-ph/0101336.

# Conceptual aspects of QCD factorization in hadronic $B$ decays\*

M. Beneke

*Institut für Theoretische Physik E, RWTH Aachen, Sommerfeldstr. 28, 52074 Aachen, Germany*

*Email: mbeneke@physik.rwth-aachen.de*

ABSTRACT: I review the meaning of “QCD factorization” in hadronic two-body  $B$  decays and then discuss recent results of theoretical (rather than phenomenological) nature: the proof of factorization at two loops; the identification of “chirally enhanced” power corrections; and the role of annihilation contributions.

## 1. Introduction

Hadronic, two-body  $B$  decays are highly interesting observables for flavour physics, since they depend on CKM matrix elements, including the CP-violating phase of the CKM matrix, and potential other flavour-changing interactions. They also present a formidable challenge for theory, since they involve three fundamental scales, the weak interaction scale  $M_W$ , the  $b$ -quark mass  $m_b$ , and the QCD scale  $\Lambda_{\text{QCD}}$ . From the point of view of fundamental physics, the sensitivity to the weak interaction scale, and potential new phenomena at this scale, is probably most interesting, but since this physics is weakly coupled, it is straightforwardly computable, given a particular model of flavour violation. Most theoretical work therefore concerns strong-interaction corrections. The strong-interaction effects which involve virtualities above the scale  $m_b$  are well understood. They renormalize the coefficients of local operators  $\mathcal{O}_i$  in the weak effective Hamil-

tonian. Assuming the Standard Model of flavour violation, the amplitude for the decay  $B \rightarrow M_1 M_2$  is given by

$$\mathcal{A}(B \rightarrow M_1 M_2) = \frac{G_F}{\sqrt{2}} \sum_i \lambda_i C_i(\mu) \langle M_1 M_2 | \mathcal{O}_i | B \rangle(\mu), \quad (1.1)$$

where  $G_F$  is the Fermi constant. Each term in the sum is the product of a CKM factor  $\lambda_i$ , a coefficient function  $C_i(\mu)$ , which incorporates strong-interaction effects above the scale  $\mu \sim m_b$ , and a matrix element of an operator  $\mathcal{O}_i$ . In extensions of the Standard Model, there may be further operators and different flavour-violating couplings, but the strong-interaction effects below the scale  $\mu$  are still encoded by matrix elements of local operators.

The theoretical problem is therefore to compute these matrix elements. Since they depend on  $m_b$  and  $\Lambda_{\text{QCD}}$ , one should take advantage of the fact that  $m_b \gg \Lambda_{\text{QCD}}$  and compute the short-distance part of the matrix element. The remainder then depends only on  $\Lambda_{\text{QCD}}$ , and – to leading order in  $\Lambda_{\text{QCD}}/m_b$  – turns out to be much simpler than the original matrix element. In this talk I summarize some conceptual aspects of our recent work [1, 2] on this problem. The discussion of the phenomenology of some particular decay modes is omitted here, but can also be found in Refs. [1, 2, 3].

---

\*Talk presented at the UK Phenomenology Workshop on Heavy Flavour and CP Violation, 17 - 22 September 2000, St John’s College, Durham, proceedings to appear in J. Phys. G. Also presented at: 5th International Symposium on Radiative Corrections (RADCOR2000), Carmel, California, September 11 - 15, 2000; 4th Workshop on Continuous Advances in QCD, Minneapolis, U.S.A., 12-14 May 2000; Vth International Workshop on Heavy Quark Physics, Dubna, Russia, 6-8 April 2000. The phenomenological parts of some of the talks have been omitted in this write-up. See Ref. [3] for those parts.

## 2. QCD Factorization

### 2.1 The Physical Picture

Factorization is a property of the heavy-quark limit, in which we assume that the  $b$  quark mass is parametrically large. The  $b$  quark is then decaying into a set of very energetic partons. How these partons and what is left of the  $B$  meson hadronize into two mesons depends on the identity of these mesons.

The simplest case is  $\bar{B}_d \rightarrow D^+\pi^-$ , when the  $D$  meson is also taken to be parametrically heavy. The spectator quark and other light degrees of freedom in the  $B$  meson have to rearrange themselves only slightly to form a  $D$  meson together with the charm quark created in the weak interaction. The other two light quarks are very energetic and for them to form a pion they must be highly collinear and in a colour-singlet configuration. Soft interactions decouple from such a configuration and this allows it to leave the decay region without interfering with the  $D$  meson formation. The probability of such a special configuration to form a pion is described by the leading-twist pion light-cone distribution amplitude (LCDA)  $\Phi_\pi(u)$ . The  $B \rightarrow D$  transition is parameterized by a standard set of form factors. I have repeated essentially the argument of Ref. [4] in favour of the conventional factorization picture, but it is important that this can be converted into a quantitative scheme to compute higher order corrections. For example, if the light quark-anti-quark pair is initially formed in a colour-octet state, we can still show that soft gluons decouple, if this pair is to end up as a pion. This implies that the pair must interact with a hard gluon, and hence this provides a calculable strong-interaction correction to the basic mechanism discussed above. (A correction of this type was computed already in Ref. [5], but it seems to me that the generality and importance of the result went unnoticed.) An important element in demonstrating the suppression of soft interactions (except for those parameterized by the  $B \rightarrow D$  form factor) is the assumption that the pion LCDA vanishes linearly as the longitudinal momentum fraction approaches the endpoints  $u = 0, 1$ . This assumption can be justified by the fact that it is satisfied by the asymptotic

distribution amplitude  $\Phi_\pi(u) = 6u(1-u)$ , which is the appropriate one in the heavy-quark limit. As a consequence

$$\int_0^{\Lambda_{\text{QCD}}/m_b} du u^n \Phi_\pi(u) \sim \left(\frac{\Lambda_{\text{QCD}}}{m_b}\right)^{n+2} \quad (n > -2). \quad (2.1)$$

This guarantees the suppression of soft endpoint contributions.

Note that the above discussion relies crucially on the spectator quark going to the heavy meson in the final state. If, as in the case of a  $D^0\pi^0$  final state, the spectator quark must be picked up by the light meson, the amplitude is suppressed by the  $B \rightarrow \pi$  form factor. But since the  $D$  meson's size is of order  $1/\Lambda_{\text{QCD}}$ , the  $D^0$  formation and  $B \rightarrow \pi$  transition cannot be assumed to not interfere and factorization is violated.

The case of two light final state mesons is the most interesting one. The dominant decay process is indeed the same as for the case of the  $D^+\pi^-$  final state, but this implies that the light meson that picks up the spectator quark is formed in a very asymmetric configuration in which the spectator quark carries a tiny fraction  $\Lambda_{\text{QCD}}/m_b$  of the total energy. Such a configuration is suppressed, see (2.1), and this suppression is equivalent to the well-known  $(\Lambda_{\text{QCD}}/m_b)^{3/2}$ -suppression [6] of heavy-to-light form factors at large recoil. Owing to this suppression there exists a competing process, in which a hard gluon is exchanged with the spectator quark, propelling it to large energy, thus avoiding the penalty factor of (2.1). If the hard gluon connects to the quark-antiquark pair emanating from the weak decay vertex to form the other light meson, this gives rise to another contribution to the factorization formula. (If the gluon connects to the  $b$  quark or the quark that forms the light meson together with the spectator quark, we can consider this as a hard-scattering contribution to the heavy-to-light form factor.) This further contribution, called “hard-spectator interaction”, can be computed with standard methods for light-cone-dominated reactions [7, 8].

There also exist “annihilation” contributions, defined as those diagrams, in which the spectator fermion line connects to the weak decay vertex.

These contributions are suppressed by the factor

$$\frac{\int d\xi \Phi_B(\xi)}{\int d\xi \Phi_B(\xi)/\xi} \equiv \frac{\lambda_B}{M_B} \sim \frac{\Lambda_{\text{QCD}}}{m_b}, \quad (2.2)$$

where  $\Phi_B(\xi)$  is the  $B$  meson LCDA and  $\xi \sim \Lambda_{\text{QCD}}/m_b$  the light-cone momentum fraction of the spectator quark. Hence annihilation contributions can be neglected in the heavy-quark limit (but see the later discussion).

## 2.2 The Factorization Formula

We consider weak decays  $B \rightarrow M_1 M_2$  in the heavy-quark limit. The formal expression of the previous discussion is given by the following result for the matrix element of an operator  $\mathcal{O}_i$  in the weak effective Hamiltonian, valid up to corrections of order  $\Lambda_{\text{QCD}}/m_b$ :

$$\begin{aligned} \langle M_1 M_2 | \mathcal{O}_i | \bar{B} \rangle = & \sum_j F_j^{B \rightarrow M_1}(m_2^2) \int_0^1 du T_{ij}^I(u) \Phi_{M_2}(u) \\ & + (M_1 \leftrightarrow M_2) \\ & + \int_0^1 d\xi du dv T_i^{II}(\xi, u, v) \Phi_B(\xi) \Phi_{M_1}(v) \Phi_{M_2}(u) \\ & \text{if } M_1 \text{ and } M_2 \text{ are both light,} \end{aligned} \quad (2.3)$$

$$\begin{aligned} \langle M_1 M_2 | \mathcal{O}_i | \bar{B} \rangle = & \sum_j F_j^{B \rightarrow M_1}(m_2^2) \int_0^1 du T_{ij}^I(u) \Phi_{M_2}(u) \\ & \text{if } M_1 \text{ is heavy and } M_2 \text{ is light.} \end{aligned} \quad (2.4)$$

Here  $F_j^{B \rightarrow M_{1,2}}(m_{2,1}^2)$  denotes a  $B \rightarrow M_{1,2}$  form factor, and  $\Phi_X(u)$  is the light-cone distribution amplitude for the quark-antiquark Fock state of meson  $X$ .  $T_{ij}^I(u)$  and  $T_i^{II}(\xi, u, v)$  are perturbatively calculable hard-scattering functions;  $m_{1,2}$  denote the light meson masses. Eq. (2.3) is represented graphically in Fig. 1. (The fourth line of (2.3) is somewhat simplified and may require including an integration over transverse momentum in the  $B$  meson starting from order  $\alpha_s^2$ .)

Eq. (2.3) applies to decays into two light mesons, for which the spectator quark in the  $B$  meson can go to either of the final-state mesons. An example is the decay  $B^- \rightarrow \pi^0 K^-$ . If the spectator quark can go only to one of the final-state mesons, as for example in  $\bar{B}_d \rightarrow \pi^+ K^-$ , we call this meson  $M_1$  and the second form-factor term

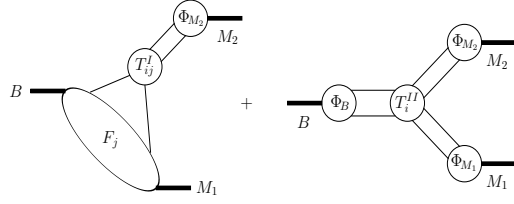


**Figure 1:** Graphical representation of the factorization formula. Only one of the two form-factor terms in (2.3) is shown for simplicity.

on the right-hand side of (2.3) is absent. The factorization formula simplifies when the spectator quark goes to a heavy meson [see (2.4)], such as in  $\bar{B}_d \rightarrow D^+ \pi^-$ . In this case the hard interactions with the spectator quark can be dropped because they are power suppressed in the heavy-quark limit. In the opposite situation that the spectator quark goes to a light meson but the other meson is heavy, factorization does not hold as discussed above.

As an example, consider the matrix element  $\langle \pi^+ \pi^- | (\bar{u}b)_{V-A} (\bar{d}u)_{V-A} | \bar{B} \rangle$ . In leading order the conventional factorization result  $if_\pi F_+^{B \rightarrow \pi}(0) M_B^2$  is obtained. It is convenient to introduce “factorized operators”  $j_1 \otimes j_2$ , whose matrix elements are defined by  $\langle \pi \pi | j_1 \otimes j_2 | B \rangle \equiv \langle \pi | j_1 | B \rangle \langle \pi | j_2 | 0 \rangle$ . The benefit of this notation is that the result of the factorization formula can be expressed in terms of these factorized operators, and this gives a compact representation of the result for *all*  $\pi \pi$  final states. We then find, including the order- $\alpha_s$  corrections,

$$\begin{aligned} (\bar{u}b)_{V-A} (\bar{d}u)_{V-A} = & (\bar{u}b)_{V-A} \otimes (\bar{d}u)_{V-A} \\ & + \frac{1}{3} (\bar{d}b)_{V-A} \otimes (\bar{u}u)_{V-A} \\ & + \frac{\alpha_s}{9\pi} \left[ \{V + H\} (\bar{d}b)_{V-A} \otimes (\bar{u}u)_{V-A} \right. \\ & \left. + P \sum_{q=u,d} (\bar{q}b)_{V-A} \otimes (\bar{d}q)_{V-A} \right], \end{aligned} \quad (2.5)$$

where

$$\begin{aligned} V \equiv & \int_0^1 du \Phi_\pi(u) \left[ 6 \ln \frac{m_b^2}{\mu^2} - 18 \right. \\ & \left. + \frac{3(1-2u)}{1-u} \ln u - 3\pi i \right], \end{aligned} \quad (2.6)$$

$$P \equiv \int_0^1 du \Phi_\pi(u) \left[ \frac{2}{3} \ln \frac{m_b^2}{\mu^2} + \frac{2}{3} + 4 \int_0^1 dz z(1-z) \ln[-z(1-z)u - i\epsilon] \right] \quad (2.7)$$

correspond to the first line of (2.3), which includes vertex ( $V$ ) and penguin ( $P$ ) contractions and

$$H \equiv \frac{4\pi^2}{3} \frac{f_B f_\pi}{M_B \lambda_B F_+^{B \rightarrow \pi}(0)} \int_0^1 \frac{du}{u} \Phi_\pi(u) \times \int_0^1 \frac{dv}{v} \left[ \Phi_\pi(v) + \frac{2\mu_\pi}{m_b} \Phi_p(v) \right], \quad (2.8)$$

accounts for the hard spectator scattering, the second line of (2.3). (I have included a certain power correction, proportional to a twist-3 LCDA  $\Phi_p(v)$ , which will be discussed in some detail later.) After evaluating the matrix elements of all operators in the weak effective hamiltonian, we collect the coefficients of the factorized operators into a set of numbers, conventionally denoted  $a_i$  and express the decay amplitude in terms of these  $a_i$ . In the past, these  $a_i$  have been thought to be uncalculable and have often been assumed to be universal. We now see that they are calculable, but non-universal to the extent that they depend on the identity of the meson.

In the past there have been several attempts at describing exclusive  $B$  decays in terms of hard spectator scattering alone [9, 10, 11, 12, 13, 14, 15, 16] and recently these have been revived in Refs. [17, 18]. The underlying assumption here is that the  $B \rightarrow \pi$  form factors are themselves computable in this approach. The literature quoted reaches different conclusions on the validity of this assumption. The principal difficulty lies in the appearance of an endpoint divergence in the integration over the pion LCDA. This must either be interpreted as an indication of a soft contribution to the form factor, in which case the starting assumption is invalid; or the divergence must be argued away (either by subtracting it into the  $B$  meson wave function [13] or by suppressing it with a Sudakov form factor [16]), in which case the typical (but not unequivocal) result is an unacceptably small form factor at  $q^2 = 0$ . In comparison the advantage of the approach presented here is that it allows us to demonstrate a useful factorization result independent of the validity

of the assumption that the form factor is dominated by hard scattering. (I may mention that form factors themselves obey a formula similar to (2.3) and this may provide a useful framework to investigate the role of hard scattering for form factors [19].)

### 2.3 Implications of Factorization

The significance and usefulness of the factorization formula stems from the fact that the non-perturbative quantities which appear on the right-hand side of (2.3) are much simpler than the original non-leptonic matrix element on the left-hand side. This is because they either reflect universal properties of a single meson state (light-cone distribution amplitudes) or refer only to a  $B \rightarrow$  meson transition matrix element of a local current (form factors). Factorization is a consequence of the fact that only *hard* interactions between the  $(BM_1)$  system and  $M_2$  survive in the heavy quark limit. As a result we can say that

- conventional factorization gives the correct limit, when  $\alpha_s$  and  $\Lambda_{\text{QCD}}/m_b$  corrections are neglected, provided the spectator quark does not go to a heavy meson;
- radiative corrections to conventional factorization can be computed systematically, the result is, in general, non-universal, i.e. there is no reason to suppose that the parameters  $a_i$  should be the same, say for  $D\pi$  and  $\pi\pi$  final states;
- the problem of scheme-dependence in the conventional factorization ansatz is solved in the same way as in any other next-to-leading order computation with the weak effective hamiltonian;
- all strong interaction phases are generated perturbatively in the heavy quark limit, as form factors have no imaginary parts;
- many observables of interest for CP violation become accessible in this way, the current limiting factors being our poor knowledge of  $\lambda_B$  and that of power corrections.

### 3. Discussion

In this section I discuss some aspects that concern factorization beyond the one-loop correction to conventional factorization: the validity of factorization in higher orders of perturbation theory [Sect. 3.1], the issue of final state rescattering [Sect. 3.2] and various sources of power corrections [Sects. 3.3-3.5].

#### 3.1 Factorization in higher orders

A proof of the factorization formula (2.4) for decays into a heavy and a light meson has been given at the two-loop order [2]. Some of the arguments used there have straightforward extensions to all orders, but a technical all-order “proof” has not yet been accomplished. Nonetheless, the arguments used to prove infrared finiteness at two-loop order may be sufficiently convincing to make infrared finiteness at all orders plausible.

It has to be demonstrated that the hard-scattering kernels are infrared finite. To state this more precisely, we write the factorization formula for a heavy-light final state schematically as

$$A \equiv \langle \pi^- D^+ | \mathcal{O} | \bar{B}_d \rangle = F_{B \rightarrow D}(0) \cdot T * \Phi_\pi, \quad (3.1)$$

where the  $*$  represents the convolution and  $\mathcal{O}$  represents a four-quark operator. In order to extract  $T$ , one computes  $A$ ,  $F_{B \rightarrow D}$  and  $\Phi_\pi$  in perturbation theory and uses (3.1) to determine  $T$ . We therefore rewrite (3.1) in perturbation theory,

$$\begin{aligned} A^{(0)} + A^{(1)} + A^{(2)} + \dots = & \\ & \left( F_{B \rightarrow D}^{(0)} + F_{B \rightarrow D}^{(1)} + F_{B \rightarrow D}^{(2)} + \dots \right) \\ & \cdot \left( T^{(0)} + T^{(1)} + T^{(2)} + \dots \right) \\ & * \left( \Phi_\pi^{(0)} + \Phi_\pi^{(1)} + \Phi_\pi^{(2)} + \dots \right), \end{aligned} \quad (3.2)$$

where the superscripts in parentheses indicate the order of perturbation theory, and then compare terms of the same order. Thus up to two-loop order

$$F_{B \rightarrow D}^{(0)} \cdot T^{(0)} * \Phi_\pi^{(0)} = A^{(0)}, \quad (3.3)$$

$$\begin{aligned} F_{B \rightarrow D}^{(0)} \cdot T^{(1)} * \Phi_\pi^{(0)} &= A^{(1)} \quad (3.4) \\ -F_{B \rightarrow D}^{(1)} \cdot T^{(0)} * \Phi_\pi^{(0)} &- F_{B \rightarrow D}^{(0)} \cdot T^{(0)} * \Phi_\pi^{(1)}, \end{aligned}$$

$$\begin{aligned} F_{B \rightarrow D}^{(0)} \cdot T^{(2)} * \Phi_\pi^{(0)} &= A^{(2)} \\ -F_{B \rightarrow D}^{(0)} \cdot T^{(1)} * \Phi_\pi^{(1)} &- F_{B \rightarrow D}^{(1)} \cdot T^{(1)} * \Phi_\pi^{(0)} \\ -F_{B \rightarrow D}^{(2)} \cdot T^{(0)} * \Phi_\pi^{(0)} &- F_{B \rightarrow D}^{(0)} \cdot T^{(0)} * \Phi_\pi^{(2)} \\ -F_{B \rightarrow D}^{(1)} \cdot T^{(0)} * \Phi_\pi^{(1)}. \end{aligned} \quad (3.5)$$

By perturbative expansion of the  $B \rightarrow D$  form factor, we mean the perturbative expansion of the matrix element of  $\bar{c}\Gamma b$ , evaluated between on-shell  $b$ - and  $c$ -quark states. By perturbative expansion of the pion light-cone distribution amplitude, we mean the perturbative expansion of the light-cone matrix element which defines the LCDA, but with the pion state replaced by an on-shell quark with momentum  $uq$  and an on-shell antiquark with momentum  $\bar{u}q$ .

The zeroth order term in (3.3) is trivial. The two terms that need to be subtracted from  $A^{(1)}$  at first order exactly cancel the “factorizable” contributions to  $A^{(1)}$ . The first order term in (3.5) therefore states that  $T^{(1)}$  is given by the “non-factorizable” diagrams. (Here we use “non-factorizable” in the conventional sense, i.e. to denote the diagrams with gluon exchange between the  $(BD)$  system and the pion.) If  $T^{(1)}$  is to be infrared finite, the sum of these diagrams must be infrared finite, which is indeed the case as seen by the explicit one-loop calculation.

The second order term (3.5) has a more complicated structure. The last three terms on the right-hand side exactly cancel the “factorizable” corrections to the two-loop amplitude  $A^{(2)}$ . The remaining two terms that need to be subtracted from  $A^{(2)}$  are non-trivial. The infrared divergences in the sum of “non-factorizable” contributions to  $A^{(2)}$  must then be shown to have precisely the right structure to match the infrared divergences in  $F_{B \rightarrow D}^{(1)}$  and  $\Phi_\pi^{(1)}$ , such that

$$\begin{aligned} A_{\text{non-fact.}}^{(2)} - F_{B \rightarrow D}^{(0)} \cdot T^{(1)} * \Phi_\pi^{(1)} \\ - F_{B \rightarrow D}^{(1)} \cdot T^{(1)} * \Phi_\pi^{(0)} = \text{infrared finite.} \end{aligned} \quad (3.6)$$

Eq. (3.6) is verified by first identifying the regions of phase space which can give rise to infrared singularities. In general these arise when massless lines become soft or collinear with the direction of  $q$ , the momentum of the pion. This requires that one or both of the loop momenta in a two-loop diagram become soft or collinear. Rather than

computing the 62 “non-factorizable” two-loop diagrams (excluding self-energy insertions and field renormalization), the Feynman integrands corresponding to these diagrams in those momentum configurations that can give rise to singularities are then analyzed in all possible combinations: one momentum soft or collinear, the other hard; both momenta soft or collinear; one momentum soft, the other collinear.

The analysis of Ref. [2] shows that infrared divergences cancel in the soft-soft, collinear-collinear and soft-collinear region as required for the validity of (3.6). The non-cancelling divergence in the hard-soft region factorizes into the form

$$A_{\text{hard-soft}}^{(2)} = f_{B \rightarrow D} \cdot T^{(1)} * \Phi_{\pi}^{(0)}, \quad (3.7)$$

where  $f_{B \rightarrow D}$  is precisely the soft contribution to the  $B \rightarrow D$  form factor at the one-loop order; this cancels the second of the two subtraction terms in (3.6). The infrared divergent hard-collinear contributions sum up to the expression

$$A_{\text{hard-collinear}}^{(2)} = F_{B \rightarrow D}^{(0)} \cdot C_F \frac{\alpha_s}{\pi} \ln \frac{\mu_{UV}}{\mu_{IR}} \times \int_0^1 dw du T^{(1)}(w) V(w, u) \Phi_{\pi}^{(0)}(u), \quad (3.8)$$

with  $V(w, u)$  the ERBL evolution kernel [7, 8]. The infrared singular contribution to the (perturbative, one-loop) pion distribution amplitude is determined by

$$\Phi_{\pi}^{(1)}(w) = C_F \frac{\alpha_s}{\pi} \ln \frac{\mu_{UV}}{\mu_{IR}} \int_0^1 du V(w, u) \Phi_{\pi}^{(0)}(u), \quad (3.9)$$

and by combining the previous two equations we find that  $A_{\text{hard-collinear}}^{(2)}$  is precisely equal to the remaining subtraction term in (3.6). It follows from (3.5) that  $T^{(2)}$  is free of infrared singularities.

### 3.2 Rescattering and Parton-Hadron Duality

Final-state interactions are usually discussed in terms of intermediate hadronic states. This is suggested by the unitarity relation (taking  $B \rightarrow \pi\pi$  for definiteness)

$$\text{Im} \mathcal{A}_{B \rightarrow \pi\pi} \sim \sum_n \mathcal{A}_{B \rightarrow n} \mathcal{A}_{n \rightarrow \pi\pi}^*, \quad (3.10)$$

where  $n$  runs over all hadronic intermediate states. In many discussions of final state rescattering the sum on the right hand side of this equation is truncated by keeping only elastic rescattering. It is clear that this approximation is incompatible with the heavy-quark limit, in which the opposite limit of an arbitrarily large number of intermediate states should be considered. Decays of  $B$  mesons lie somewhere in between these limiting cases, but only the heavy-quark limit provides a controlled approximation to the problem. In my opinion, in view of the factorization results, proponents of the elastic scattering limit and methods inspired by Regge physics now need to justify better their motivation for choosing this particular ansatz.

The heavy-quark limit, and the dominance of hard rescattering in this limit, suggest that the sum in (3.10) is interpreted as extending over intermediate states of partons. In this picture the sum over all hadronic intermediate states is approximately equal to the contribution of a quark-anti-quark intermediate state of small transverse extension. The approximation could be further improved by including  $q\bar{q}g$  intermediate states etc. This is similar to the QCD description of  $e^+e^- \rightarrow$  hadrons at large energy; the total cross section of this reaction is well represented by the production cross section of a  $q\bar{q}$  pair, even though the production of every particular final state cannot be computed with perturbative (or any known) methods. There is a limit to the accuracy of such kinds of descriptions, which is discussed under the name of “parton-hadron” duality. Quantifying this accuracy is a formidable, unsolved problem. The same assumption forms the basis for the application of the operator product expansion to *inclusive* non-leptonic heavy-quark decays and there have been some quantitative studies in this context, though in the two-dimensional ’t Hooft model [20, 21, 22]. Parton-hadron duality is also an implicit assumption in applying perturbative QCD techniques to jet observables and hadron-hadron collisions at large momentum transfer. It is probably safe to conclude that the accumulated experience suggests that violations of parton-duality are subdominant effects in the heavy-quark limit, and this is all we need to justify our theoretical framework.

### 3.3 Higher Fock States and Non-factorizable Contributions

The factorization formula needs only the leading-twist LCDAs of the mesons. Higher Fock components of the mesons appear in higher orders of the collinear expansion. The collinear expansion is justified as long as the additional partons carry a finite fraction of the meson's momentum in the heavy-quark limit. Under this assumption, it is easy to see that adding additional partons to the Fock state increases the number of off-shell propagators in a given diagram. This implies power suppression in the heavy-quark expansion.

Soft contributions are also power-suppressed, but it seems difficult to classify them systematically. Again the decay  $\bar{B}_d \rightarrow D^+ \pi^-$  is the simplest case, and I briefly consider the situation, where the “non-factorizable” gluon, i.e. the gluon exchanged between the pion and the  $(\bar{B}D)$  system, is soft. In this case, the “ $q\bar{q}$  Fock state” cannot be described by a light-cone wave function, but such a contribution still receives a power suppression in the heavy-quark limit. The important point is that soft gluons couple very weakly to the  $q\bar{q}$  pair. The coupling can be evaluated (the  $q\bar{q}$  pair being very energetic), and the result is

$$\begin{aligned} \langle D^+ \pi^- | (\bar{c}T^A b)_{V-A} (\bar{d}T^A u)_{V-A} | \bar{B}_d \rangle_{\text{nf}} = & \\ - \int_0^{1/\Lambda_{\text{QCD}}} ds \langle D^+ | \bar{c} \gamma^\mu (1 - \gamma_5) g_s \tilde{G}_{\mu\nu} (-sn) n^\nu b | \bar{B}_d \rangle & \\ \times \int_0^1 du \frac{f_\pi \Phi_\pi(u)}{8N_c u \bar{u}}, & \end{aligned} \quad (3.11)$$

where  $q = En$  is the momentum of the pion. This depends on a *non-local* higher-dimension  $B \rightarrow D$  form factor, but comparing this with the leading order, conventional factorization expression,

$$\begin{aligned} \langle D^+ \pi^- | (\bar{c}b)_{V-A} (\bar{d}u)_{V-A} | \bar{B}_d \rangle_{\text{LO}} = & \quad (3.12) \\ \langle D^+ | \bar{c} \gamma^\mu (1 - \gamma_5) b | \bar{B}_d \rangle i f_\pi E n_\mu \int_0^1 du \Phi_\pi(u), & \end{aligned}$$

we conclude on dimensional arguments that the soft non-factorizable correction is suppressed by one power of  $\Lambda_{\text{QCD}}/m_b$ . (Note that similar considerations for the  $J/\psi K$  final state [23] lead to *local*  $B \rightarrow K$  form factors, because the non-locality is then cut off at a distance  $1/m_c$ .)

Note that power corrections come without a factor of  $\alpha_s$  and we may expect them to be as large as the computable perturbative corrections in general. An important point, however, is that there exists a systematic framework that allows us to classify *both* effects as corrections.

### 3.4 “Chirally enhanced” Corrections

There are two reasons why the hard spectator interaction in (2.3) is particularly sensitive to power-suppressed corrections. The first reason is that the short-distance scale is not  $m_b$  (as is the case for the form factor term in (2.3)), but  $(m_b \Lambda_{\text{QCD}})^{1/2}$ . To see this, note the gluon virtuality is

$$k_g^2 = -\bar{v} \xi M_B^2 + \text{terms of order } \Lambda_{\text{QCD}}^2, \quad (3.13)$$

which on average is around  $1 \text{ GeV}^2$ . To arrive at (2.8) I have neglected the terms of order  $\Lambda_{\text{QCD}}^2$  and this might not be a particularly good approximation. However, there is no (known) systematic way of treating such terms, which amongst other things are sensitive to the off-shellness of the spectator quark in the  $B$  meson (and hence to higher Fock components of the  $B$  meson), and so we must neglect these terms together with many other power corrections.

There is an enhancement of power-suppressed effects for decays into light pseudoscalar mesons connected with the curious numerical fact that

$$2\mu_\pi \equiv \frac{2m_\pi^2}{m_u + m_d} = -\frac{4\langle \bar{q}q \rangle}{f_\pi^2} \approx 3 \text{ GeV} \quad (3.14)$$

is much larger than its naive scaling estimate  $\Lambda_{\text{QCD}}$ . (Here  $\langle \bar{q}q \rangle = \langle 0 | \bar{u}u | 0 \rangle = \langle 0 | \bar{d}d | 0 \rangle$  is the quark condensate.) These “chirally enhanced” corrections have originally been discussed in connection with  $V+A$  penguin operators in the weak effective hamiltonian, but they affect the hard spectator interaction more severely.

Consider first the contribution of the operator  $\mathcal{O}_6 = (\bar{d}_i b_j)_{V-A} (\bar{u}_j u_i)_{V+A}$  to the  $\bar{B}_d \rightarrow \pi^+ \pi^-$  decay amplitude. The parameter  $\mu_\pi$  arises already in the naively factorized matrix element:

$$\begin{aligned} \langle \pi^+ \pi^- | (\bar{d}_i b_j)_{V-A} (\bar{u}_j u_i)_{V+A} | \bar{B}_d \rangle = & \\ iM_B^2 F_+^{B \rightarrow \pi}(0) f_\pi \times \frac{2\mu_\pi}{m_b}. & \end{aligned} \quad (3.15)$$

This is formally a  $\Lambda_{\text{QCD}}/m_b$  power correction but numerically large due to (3.14). We would not have to worry about such terms if they could all be identified and the factorization formula (2.3) applied to them, since in this case higher-order perturbative corrections would not contain non-factorizing infrared logarithms. However, this is not the case.

After including radiative corrections, the matrix element on the left-hand side of (3.15) is expressed as a non-trivial convolution with the pion light-cone distribution amplitude. The terms involving  $\mu_\pi$  can be related to two-particle twist-3 (rather than leading twist-2) distribution amplitudes, conventionally called  $\Phi_p(u)$  and  $\Phi_\sigma(u)$ . The distribution amplitude  $\Phi_p(u)$  does not vanish at the endpoint. As a consequence the hard spectator interaction contains an endpoint divergence. In other words, the ‘‘correction’’ relative to (3.15) is of the form  $\alpha_s \times$  logarithmic divergence, which we interpret as being of the same order as (3.15). It turns out, however, that the  $\alpha_s$  correction to the  $V + A$  operator (giving rise to the parameter  $a_6$  in conventional notation) is free of this potential problem.

As a consequence the most important effect of the chirally enhanced twist-3 LCDAs (with exception of the leading order result for  $a_6$ ) is on the matrix elements that contribute to the coefficients  $a_1$  to  $a_5$ . An example of this is shown in (2.8). Substituting the asymptotic LCDAs,  $H$  is rewritten as

$$H = \frac{12\pi^2 f_B f_\pi}{M_B \lambda_B F_+^{B \rightarrow \pi}(0)} \left[ 1 + \frac{2\mu_\pi}{3m_b} \int_0^1 \frac{dv}{v} \right], \quad (3.16)$$

which exhibits the problem of dealing with the endpoint-divergent integral. I should emphasize that this divergence is not in contradiction with the factorization formula (2.3), in fact it is expected at the level of power-suppressed effects. But from the phenomenological point of view it is somewhat disappointing that these effects are sizeable and can introduce a substantial uncertainty into the hard spectator interaction. The complete set of chirally enhanced terms has been estimated up to now only in Ref. [3], where it was assumed that the divergent integral can be replaced by a universal constant. The variation

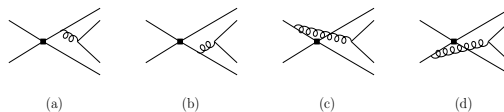


**Figure 2:** Annihilation diagrams.

of this constant constitutes the largest theoretical uncertainty, but it is also shown that the predictivity of the approach is not lost. (Some chirally enhanced terms have been included in Refs. [24, 25], but the correction (2.8), (3.16) to  $a_1$  to  $a_5$ , which contains the endpoint divergence, has been omitted [24] or computed incorrectly [25] in these papers.) As in a related situation for the pion form factor [26] one might argue that the endpoint divergence is suppressed by a Sudakov form factor. However, it is likely that when  $m_b$  is not large enough to suppress these chirally enhanced terms, then it is also not large enough to make Sudakov suppression effective especially since the short-distance scale is not large enough to build up a strong logarithmic evolution.

### 3.5 Annihilation Topologies

My final concern in this section are the annihilation topologies (Fig. 2). The hard part of these diagrams would amount to another contribution to the second hard-scattering kernel,  $T_i^{II}(\xi, u, v)$ , in (2.3). The soft part, if unsuppressed, would violate factorization. However, a straightforward power-counting analysis shows that all annihilation topologies are  $1/m_b$  corrections to the decay amplitudes in the heavy-quark limit [2]. This statement also applies to diagram d, in which case the largest term comes from an endpoint contribution.

As for the hard spectator interaction at leading power in the heavy-quark expansion, there exist ‘‘chirally enhanced’’ contributions from the annihilation topologies related to the corresponding twist-3 light meson LCDAs. It has recently been noted [17, 18] in the context of the hard-scattering approach that these could be non-negligible. To illustrate this effect, I consider the annihilation correction to the coefficient  $a_6$  in the effective transition operator defined in Ref. [1]. Note that  $a_6$  is the coefficient of a power correc-

tion (though chirally enhanced), and I am considering now a power correction to  $a_6$ . For two identical final state mesons, say two pions, only the diagrams a and b contribute to  $a_6$ . To simplify the result, I assume the LCDAs to be the asymptotic ones and obtain for the sum of leading order and annihilation contribution:

$$a_6 \simeq \left( C_6 + \frac{C_5}{N_c} \right) \left[ 1 + \frac{\alpha_s}{9\pi} \frac{96\pi^2 f_B f_\pi}{M_B^2 F_+^{B \rightarrow \pi}(0)} \times \left( X_l^2 - \frac{X_l}{2} \right) \right], \quad (3.17)$$

where  $X_l$  is the divergent integral  $\int_0^1 dv/v$ . Although power-suppressed, the correction is enlarged by a numerical factor and a logarithmic endpoint divergence from each of the two final mesons. We can exhibit this more transparently by comparing the annihilation correction to the generic leading-power hard spectator correction (2.8), (3.16). This gives the ratio

$$\frac{H_{\text{ann}}}{H} \simeq \frac{\lambda_B}{M_B} \times 8 \left( X_l^2 - \frac{X_l}{2} \right), \quad (3.18)$$

suggesting that in this particular case the annihilation topologies are more important than the generic hard spectator interaction. A complete analysis of annihilation contributions to light-light final states (extending the analysis [2] for the  $D\pi$  case) is currently in progress.

## 4. Conclusion

The QCD factorization approach described in this talk constitutes a powerful and systematic approach to non-leptonic decay amplitudes, based on familiar methods of perturbative QCD, and the assumption that the  $b$  quark mass is large. It does not render trivial the problem of accurately computing these amplitudes, but it appears to me that the outstanding issues now are more of numerical than of conceptual character: the best way of dealing with chirally enhanced power corrections; the role of annihilation; the size of power corrections in general and their impact on strong interaction phases; the role of hard scattering in heavy-to-light form factors (and, related to this, the importance of Sudakov form factors) ... It is probable that experimental data will be needed to shed light on some of these issues.

## Acknowledgments

I would like to thank G. Buchalla, M. Neubert and C.T. Sachrajda for their collaboration on the topics of this talk. I would also like to thank the organizers of the conference for their generous support.

## References

- [1] M. Beneke, G. Buchalla, M. Neubert and C.T. Sachrajda, *Phys. Rev. Lett.* **83** (1999) 1914.
- [2] M. Beneke, G. Buchalla, M. Neubert and C.T. Sachrajda, to appear in *Nucl. Phys. B* [hep-ph/0006124].
- [3] M. Beneke, G. Buchalla, M. Neubert and C.T. Sachrajda, to appear in the Proceedings of ICHEP2000, Osaka, Japan [hep-ph/0007256].
- [4] J.D. Bjorken, *Nucl. Phys. Proc. Suppl.* **B 11** (1989) 325.
- [5] H.D. Politzer and M.B. Wise, *Phys. Lett.* **B 257** (1991) 399.
- [6] V.L. Chernyak and I.R. Zhitnitsky, *Nucl. Phys.* **B 345** (1990) 137.
- [7] G.P. Lepage and S.J. Brodsky, *Phys. Rev.* **D 22** (1980) 2157.
- [8] A.V. Efremov and A.V. Radyushkin, *Phys. Lett.* **B 94** (1980) 245.
- [9] A. Szczepaniak, E.M. Henley and S.J. Brodsky, *Phys. Lett.* **B 243** (1990) 287.
- [10] G. Burdman and J.F. Donoghue, *Phys. Lett.* **B 270** (1991) 55.
- [11] H. Simma and D. Wyler, *Phys. Lett.* **B 272** (1991) 395.
- [12] C.E. Carlson and J. Milana, *Phys. Lett.* **B 301** (1993) 237.
- [13] R. Akhouch, G. Sterman and Y.P. Yao, *Phys. Rev.* **D 50** (1994) 358.
- [14] B.F. Ward, *Phys. Rev.* **D 51** (1995) 6253.
- [15] M. Dahm, R. Jakob and P. Kroll, *Z. Physik* **C 68** (1995) 595.
- [16] H. Li and H. Yu, *Phys. Rev.* **D 53** (1996) 2480.
- [17] Y.Y. Keum, H. Li and A.I. Sanda, [hep-ph/0004004] and [hep-ph/0004173].
- [18] C. Lü, K. Ukai and M. Yang, [hep-ph/0004213].

- [19] M. Beneke and T. Feldmann, to appear in *Nucl. Phys. B* [hep-ph/0008255].
- [20] B. Grinstein and R.F. Lebed, *Phys. Rev. D* **57** (1998) 1366.
- [21] I.I. Bigi, M. Shifman, N. Uraltsev and A. Vainshtein, *Phys. Rev. D* **59** (1999) 054011.
- [22] R.F. Lebed and N.G. Uraltsev, [hep-ph/0006346].
- [23] A. Khodjamirian and R. Rückl, in: *Proceedings of the 3rd Workshop on "Continuous Advances in QCD"*, Minneapolis, Minnesota, April 1998, ed. A.V. Smilga (World Scientific, Singapore, 1998) [hep-ph/9807495].
- [24] T. Muta, A. Sugamoto, M.-Z. Yang and Y.-D. Yang, [hep-ph/0006022].
- [25] D. Du, D. Yang and G. Zhu, [hep-ph/0008216].
- [26] B.V. Geshkenbein and M.V. Terentev, *Phys. Lett. B* **117** (1982) 243; *Yad. Fiz.* **39** (1984) 873.

CERN-TH/2001-135  
May 22, 2001  
hep-ph/0105215

## The width difference of $B_s$ mesons

ULRICH NIERSTE

*CERN – Theory Division, 1211 Geneva 23, Switzerland*

Next-to-leading order QCD corrections to the width difference  $\Delta\Gamma$  in the  $B_s$ -meson system are presented. I further discuss how  $\Delta\Gamma$  can be used to detect new physics.

Presented at the

5th International Symposium on Radiative Corrections  
(RADCOR-2000)

Carmel CA, USA, 11–15 September, 2000

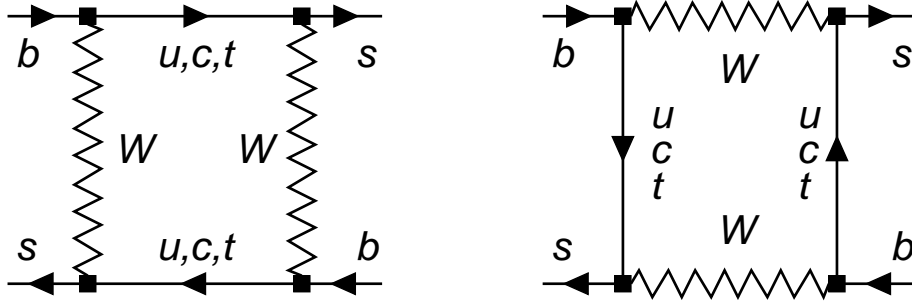


Figure 1: Lowest order contribution to  $B_s - \bar{B}_s$  mixing in the Standard Model.

## 1 Introduction

Currently the prime focus of experimental elementary particle physics is the investigation of the flavor sector of the Standard Model. Transitions between different fermion generations originate from the Higgs-Yukawa sector, which is poorly tested so far. The experimental effort is not only devoted to a precise determination of the Cabibbo-Kobayashi-Maskawa (CKM) matrix [1], which parameterizes the flavor-changing couplings. Flavor-changing neutral currents (FCNC) also provide an ideal testing ground to search for new physics, because they are highly suppressed in the Standard Model: FCNC's are loop-induced, involve the weak coupling constant and the heavy  $W$  boson, are suppressed by small CKM elements or the GIM mechanism [2] and further often suffer from a helicity-suppression, because flavor-changing couplings only involve left-handed fields. Therefore experiments in flavor physics are much more sensitive to new physics than the precision tests of the gauge sector performed in the LEP/SLD/Fermilab-Run-I era. Decays of  $B$  mesons are especially interesting: they allow us to determine three of the four CKM parameters, their rich decay spectrum helps to overconstrain the CKM matrix, they have theoretically clean CP asymmetries (as opposed to  $K \rightarrow \pi\pi$  decays), information from  $B_d$ ,  $B_s$  and  $B^+$  decays can be combined using  $SU(3)_F$  symmetry, the large  $b$  quark mass permits the use of heavy quark symmetries and the heavy quark expansion, and in many extensions of the Standard Model third generation fermions are most sensitive to new physics.

While  $B_s$  mesons cannot be studied at the  $B$  factories running on the  $\Upsilon(4S)$  resonance [3], they are copiously produced at hadron colliders [4].  $B_s$  mesons mix with their antiparticles. Therefore the two mass eigenstates  $B_H$  and  $B_L$  (for “heavy” and “light”), which are linear combinations of  $B_s$  and  $\bar{B}_s$ , differ in their mass and width. In the Standard Model  $B_s - \bar{B}_s$  mixing is described in the lowest order by the box diagrams depicted in Fig. 1. The dispersive part of the  $B_s - \bar{B}_s$  mixing amplitude is called  $M_{12}$ . In the Standard Model it is dominated by box diagrams with internal top quarks. The absorptive part is denoted by  $\Gamma_{12}$  and mainly stems from box diagrams with light charm quarks.  $\Gamma_{12}$  is generated by decays into final states which are common to  $B_s$  and  $\bar{B}_s$ . While  $M_{12}$  can receive siz-

able contributions from new physics,  $\Gamma_{12}$  is induced by the CKM-favored tree-level decay  $b \rightarrow c\bar{c}s$  and is insensitive to new physics. Experimentally  $B_s - \bar{B}_s$  mixing manifests itself in damped oscillations between the  $B_s$  and  $\bar{B}_s$  states. We denote the mass and width differences between  $B_H$  and  $B_L$  by

$$\Delta m = M_H - M_L, \quad \Delta\Gamma = \Gamma_L - \Gamma_H.$$

By solving the eigenvalue problem of  $M_{12} - i\Gamma_{12}/2$  one can relate  $\Delta m$  and  $\Delta\Gamma$  to  $M_{12}$  and  $\Gamma_{12}$ :

$$\Delta m = 2|M_{12}|, \quad \Delta\Gamma = 2|\Gamma_{12}|\cos\phi, \quad (1)$$

where  $\phi$  is defined as

$$\frac{M_{12}}{\Gamma_{12}} = - \left| \frac{M_{12}}{\Gamma_{12}} \right| e^{i\phi}. \quad (2)$$

$\Delta m$  equals the  $B_s - \bar{B}_s$  oscillation frequency and has not been measured yet. In deriving (1) terms of order  $|\Gamma_{12}/M_{12}|^2$  have been neglected.  $\phi$  in (2) is a CP-violating phase, which is tiny in the Standard Model, so that  $\Delta\Gamma_{\text{SM}} = 2|\Gamma_{12}|$ . Unlike in the case of  $B_d$  mesons, the Standard Model predicts a sizable width difference  $\Delta\Gamma$  in the  $B_s$  system, roughly between 5 and 30% of the average total width  $\Gamma = (\Gamma_L + \Gamma_H)/2$ . The decay of an untagged  $B_s$  meson into the final state  $f$  is in general governed by two exponentials:

$$\Gamma[f, t] \propto e^{-\Gamma_L t} |\langle f | B_L \rangle|^2 + e^{-\Gamma_H t} |\langle f | B_H \rangle|^2. \quad (3)$$

If  $f$  is a flavor-specific final state like  $D_s^- \pi^+$  or  $X\ell^+\nu$ , the coefficients of the two exponentials in (3) are equal. A fit of the corresponding decay distribution to a single exponential then determines the average width  $\Gamma$  up to corrections of order  $(\Delta\Gamma)^2/\Gamma$ . In the Standard Model CP violation in  $B_s - \bar{B}_s$  mixing is negligible, so that we can simultaneously choose  $B_L$  and  $B_H$  to be CP eigenstates and the  $b \rightarrow c\bar{c}s$  decay to conserve CP. Then  $B_H$  is CP-odd and cannot decay into a CP-even double-charm final state  $f_{CP+}$  like  $(J/\psi\phi)_{L=0,2}$ , where  $L$  denotes the quantum number of the orbital angular momentum. Thus a measurement of the  $B_s$  width in  $B_s \rightarrow f_{CP+}$  determines  $\Gamma_L$ . By comparing the two measurements one finds  $\Delta\Gamma/2$ . CDF will perform this measurement with  $B_s \rightarrow D_s^- \pi^+$  and  $B_s \rightarrow J/\psi\phi$  in Run-II of the Tevatron [5].

## 2 QCD corrections

Weak decays of  $B$  mesons involve a large range of different mass scales: first there is the  $W$  boson mass  $M_W$ , which appears in the weak  $b \rightarrow c\bar{c}s$  decay amplitude. The second scale in the problem is the mass  $m_b$  of the decaying  $b$  quark. Finally there is the QCD scale

parameter  $\Lambda_{QCD}$ , which sets the scale for the strong binding forces in the  $B_s$  meson. QCD corrections associated with these scales must be treated in different ways. To this end one employs a series of operator product expansions, which factorize the studied amplitude into short-distance Wilson coefficient and matrix elements of local operators, which comprise the long-distance physics. Here in the first step the  $W$ -mediated  $b \rightarrow c\bar{c}s$  decay amplitude is matched to matrix elements of local four-quark operators. We need the two  $|\Delta B| = 1$  current-current operators

$$Q_1 = \bar{c}_i \gamma_\mu (1 - \gamma_5) b_j \bar{s}_j \gamma^\mu (1 - \gamma_5) c_i \quad Q_2 = \bar{c}_i \gamma_\mu (1 - \gamma_5) b_i \bar{s}_j \gamma^\mu (1 - \gamma_5) c_j, \quad (4)$$

where  $i, j$  are color indices.  $Q_2$  is pictorially obtained by contracting the  $W$  line in the  $b \rightarrow c\bar{c}s$  amplitude to a point.  $Q_1$  emerges, once gluon exchange between the two quark lines is included. In the effective hamiltonian

$$\mathcal{H}_{eff} = \frac{G_F}{\sqrt{2}} V_{cb} V_{cs}^* \sum_{r=1}^2 C_r Q_r \quad (5)$$

the Wilson coefficients  $C_r$  are determined in such a way that the Standard Model amplitude is reproduced by  $\langle c\bar{c}s | \mathcal{H}_{eff} | b \rangle$  up to terms of order  $m_b^2/M_W^2$ . The Fermi constant  $G_F$  and the CKM elements have been factored out in (5). The  $C_r$ 's contain the short-distance physics associated with the scale  $M_W$ . QCD corrections to the Wilson coefficients can be computed in perturbation theory. The renormalization group evolution of the  $C_r$ 's down to the scale  $\mu_1 = \mathcal{O}(m_b)$  sums the large logarithms  $\ln(\mu_1/M_W)$  to all orders in perturbation theory. The minimal way to do this is the leading log approximation which reproduces all term of order  $\alpha_s^n \ln^n(\mu_1/M_W)$ ,  $n = 0, 1, \dots$ , of the full Standard Model transition amplitude. The next-to-leading order (NLO) corrections to the coefficients comprise the terms of order  $\alpha_s^{n+1} \ln^n(\mu_1/M_W)$  and have been calculated in [6]. We remark that there are also penguin operators in the effective hamiltonian  $\mathcal{H}_{eff}$ . We have omitted them in (5), because their coefficients are very small. Their impact is discussed in [7,8].

$\Delta\Gamma_{SM} = 2|\Gamma_{12}|$  is related to  $\mathcal{H}_{eff}$  by the optical theorem:

$$\Delta\Gamma_{SM} = 2|\Gamma_{12}| = \left| -\frac{1}{M_{B_s}} \text{Abs} \langle \bar{B}_s | i \int d^4x T \mathcal{H}_{eff}(x) \mathcal{H}_{eff}(0) | B_s \rangle \right|. \quad (6)$$

Here ‘Abs’ denotes the absorptive part of the amplitude, which is obtained by retaining only the imaginary part of the loop integration. The corresponding leading-order diagrams are shown in Fig. 2. In the next step of our calculation we perform an operator product expansion of the RHS in (6) in order to describe  $\Gamma_{12}$  in terms of matrix elements of local  $|\Delta B| = 2$  operators:

$$\begin{aligned} & |\text{Abs} \langle \bar{B}_s | i \int d^4x T \mathcal{H}_{eff}(x) \mathcal{H}_{eff}(0) | B_s \rangle| \\ &= -\frac{G_F^2 m_b^2}{12\pi} |V_{cb}^* V_{cs}|^2 \cdot \\ & \left[ F \left( \frac{m_c^2}{m_b^2} \right) \langle \bar{B}_s | Q | B_s \rangle + F_S \left( \frac{m_c^2}{m_b^2} \right) \langle \bar{B}_s | Q_S | B_s \rangle \right] \left[ 1 + \mathcal{O} \left( \frac{\Lambda_{QCD}}{m_b} \right) \right]. \quad (7) \end{aligned}$$

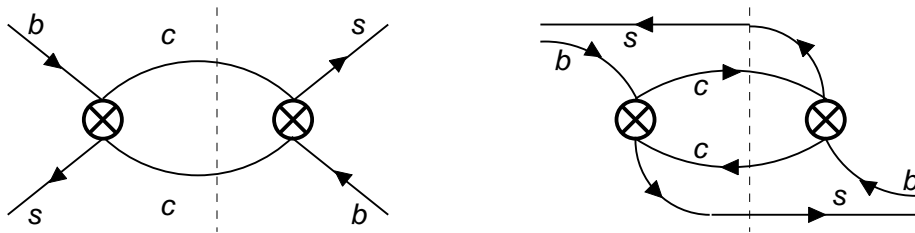


Figure 2: Leading-order diagrams for  $\Gamma_{12}$

The two dimension-6 operators appearing in (7) are

$$Q = \bar{s}_i \gamma_\mu (1 - \gamma_5) b_i \bar{s}_j \gamma^\mu (1 - \gamma_5) b_j, \quad Q_S = \bar{s}_i (1 + \gamma_5) b_i \bar{s}_j (1 + \gamma_5) b_j. \quad (8)$$

In the leading order of QCD the RHS of (7) is pictorially obtained by simply shrinking the  $(c, \bar{c})$  loop in Fig. 2 to a point. Our second operator product expansion is also called *heavy quark expansion* (HQE), which has been developed long ago by Shifman and Voloshin [9]. The new Wilson coefficients  $F$  and  $F_S$  also depend on the charm quark mass  $m_c$ , which is formally treated as a hard scale of order  $m_b$ , since  $m_c \gg \Lambda_{QCD}$ . Strictly speaking, the HQE in (7) is an expansion in  $\Lambda_{QCD}/\sqrt{m_b^2 - 4m_c^2}$ . For the calculation of  $F$  and  $F_S$  it is crucial that these coefficients do not depend on the infrared structure of the process. In particular they are independent of the QCD binding forces in the external  $B_s$  and  $\bar{B}_s$  states in (7), so that they can be calculated in perturbation theory at the parton level. The non-perturbative long-distance QCD effects completely reside in the hadronic matrix elements of  $Q$  and  $Q_S$ . It is customary to parametrize these matrix as

$$\begin{aligned} \langle \bar{B}_s | Q(\mu_2) | B_s \rangle &= \frac{8}{3} f_{B_s}^2 M_{B_s}^2 B(\mu_2) \\ \langle \bar{B}_s | Q_S(\mu_2) | B_s \rangle &= -\frac{5}{3} f_{B_s}^2 M_{B_s}^2 \frac{M_{B_s}^2}{(m_b(\mu_2) + m_s(\mu_2))^2} B_S(\mu_2). \end{aligned} \quad (9)$$

Here  $M_{B_s}$  and  $f_{B_s}$  are mass and decay constant of the  $B_s$  meson. The quark masses  $m_b$  and  $m_s$  in (9) are defined in the  $\overline{\text{MS}}$  scheme. In the so called vacuum insertion approximation  $B(\mu_2)$  and  $B_S(\mu_2)$  are equal to 1.  $\mu_2 = \mathcal{O}(m_b)$  is the scale at which the  $|\Delta B| = 2$  operators are renormalized. It can be chosen different from  $\mu_1$ . The dependence of  $\Delta\Gamma$  on the unphysical scales  $\mu_1$  and  $\mu_2$  diminishes order-by-order in perturbation theory. The residual dependence is usually used as an estimate of the theoretical uncertainty. The  $\mu_1$ -dependence cancels between the  $|\Delta B| = 1$  Wilson coefficients  $C_{1,2}$  in (5) and the radiative corrections to  $F$  and  $F_S$  in (7). The terms in  $F$  and  $F_S$  which depend on  $\mu_2$  cancel with corresponding terms in  $B(\mu_2)$  and  $B_S(\mu_2)$ . The scale  $\mu_2$  enters a lattice calculation of these non-perturbative parameters when the lattice quantities are matched to the continuum.

The leading-order calculation of  $\Delta\Gamma$  requires the calculation of the diagrams in Fig. 2 and has been performed long ago [10]. Subsequently corrections of order  $\Lambda_{QCD}/m_b$  to (7)

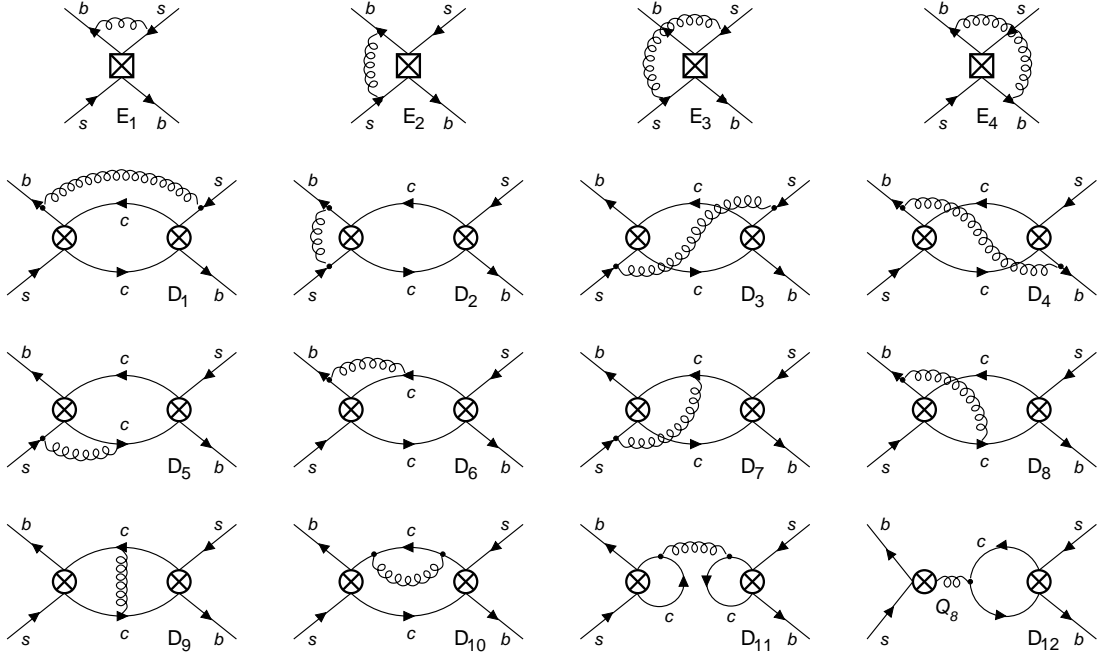


Figure 3: Next-to-leading-order diagrams for  $\Gamma_{12}$ .  $Q_8$  is the chromomagnetic penguin operator.

have been computed in [7]. The next-to-leading order calculation requires the calculation of the diagrams depicted in Fig. 3 [8]. The motivations for this cumbersome calculation are

- 1) to verify the infrared safety of  $F$  and  $F_S$ ,
- 2) to allow for an experimental test of the HQE,
- 3) a meaningful use of lattice results for hadronic matrix elements,
- 4) a consistent use of  $\Lambda_{\overline{MS}}$ ,
- 5) to reduce the sizable  $\mu_1$ -dependence of the LO,
- 6) the large size of QCD corrections, typically of order 30%.

The disappearance of infrared effects from the Wilson coefficients  $F$  and  $F_S$  mentioned in point 1) is necessary for any meaningful operator product expansion. Yet early critics of the HQE had found power-like infrared divergences in individual cuts of diagrams of Fig. 3. In response the cancellation of these divergences has been shown [11], long ago before we have performed the full NLO calculation. However, there are also logarithmic infrared divergences. We found IR-singularities to cancel via two mechanisms:

- Bloch-Nordsieck cancellations among different cuts of the same diagram,

- factorization of IR-singularities, which end up in  $\langle \bar{B}_s | Q | B_s \rangle, \langle \bar{B}_s | Q_S | B_s \rangle$ .

Point 2) above addresses the conceptual basis of the HQE, which is sometimes termed *quark-hadron duality*. It is not clear, whether the HQE reproduces all QCD effects completely. Exponential terms like  $\exp(-\kappa m_b/\Lambda_{QCD})$ , for example, cannot be reproduced by a power series [12]. The relevance of such terms can at present only be addressed experimentally, by confronting HQE-based predictions with data. The only QCD information contained in the LO prediction for  $\Delta\Gamma$  is the coefficients of  $\alpha_s^n \ln^n M_W$ , associated with hard gluon exchange along the  $W$ -mediated  $b \rightarrow c\bar{c}s$  amplitude. The question of quark-hadron duality, however, addresses the non-logarithmic QCD corrections, which belong to the NLO. While it is certainly very interesting to find violations of quark-hadron duality in  $B$  physics, it will be hard to detect them in  $\Delta\Gamma$ : in the LO diagrams in Fig. 2 the heavy  $c, \bar{c}$  quarks recoil back-to-back against each other and are fast in the  $b$  rest frame. The inclusive  $b \rightarrow c\bar{c}s$  decay is more sensitive to uncontrolled long-distance effects, because in some parts of the phase space the  $c, \bar{c}$  quarks move slowly in the  $b$  rest frame or with respect to each other. Still the HQE prediction for  $b \rightarrow c\bar{c}s$  [13] agrees with experiment [14]. If one further takes into account that  $\Delta\Gamma$  has an overall hadronic uncertainty associated with  $f_{B_s}^2 B$  and  $f_{B_s}^2 B_S$ , it appears very unlikely that violations of quark-hadron duality can be detected in  $\Delta\Gamma$ . Points 3) and 4) are related to the fact that leading-order predictions are not sensitive to the renormalization scheme, which impedes the lattice-continuum matching of the non-perturbative parameters. Likewise the  $\mu_2$  dependence of this matching procedure cannot be addressed in the leading-order. The  $\mu_1$ -dependence of  $\Delta\Gamma$  is huge in the leading order. It is reduced in the NLO, but still remains sizable. The results for  $F$  and  $F_S$  can be found in Tab. 2. The reduction of the  $\mu_1$  dependence can be verified from the table. The numerical values of the NLO coefficients depend on the renormalization scheme. The precise definition of this scheme involves the subtraction prescription for the ultraviolet poles (dimensional regularization with  $\overline{\text{MS}}$  subtraction [15]), the treatment of  $\gamma_5$  (for which we have used the NDR scheme) and the chosen definitions of the evanescent operators [16], which can be found in [8]. The lattice-continuum matching must be done in the same renormalization scheme, so that all scheme dependences cancel in the prediction for  $\Delta\Gamma$ .

Including the corrections of order  $\Lambda_{QCD}/m_b$  [7] our NLO prediction reads

$$\frac{\Delta\Gamma_{\text{SM}}}{\Gamma} = \left( \frac{f_{B_s}}{245 \text{ MeV}} \right)^2 [ (0.234 \pm 0.035) B_S(m_b) - 0.080 \pm 0.020 ]. \quad (10)$$

Here  $m_b(m_b) + m_s(m_b) = 4.3 \text{ GeV}$  (in the  $\overline{\text{MS}}$  scheme) and  $m_c^2/m_b^2 = 0.085$  has been used. Since  $F$  is small, the uncertainty in  $B$  is irrelevant, and the term involving  $FB$  has been absorbed into the constant  $-0.080 \pm 0.020$  in (10). Recently the KEK–Hiroshima group succeeded in calculating  $f_{B_s}$  in an unquenched lattice QCD calculation with two dynamical fermions [17]. The result is  $f_{B_s} = (245 \pm 30) \text{ MeV}$ . A recent quenched lattice calculation has found  $B_S(m_b) = 0.87 \pm 0.09$  [18] for the  $\overline{\text{MS}}$  scheme. A similar result has

Table 1:

$\mu_1$	$m_b/2$	$m_b$	$2m_b$
$-F_S$	0.867	1.045	1.111
$-F_S^{(0)}$	1.729	1.513	1.341
$F$	0.042	0.045	0.049
$F^{(0)}$	0.030	0.057	0.103

Table 2: Numerical values of the Wilson coefficients  $F$  and  $F_S$  for  $m_c^2/m_b^2 = 0.085$ . Leading-order results are indicated with the superscript (0). The precise definition of our renormalization scheme can be found in [8].

been obtained in [19]. With these numbers one finds from (10):

$$\frac{\Delta\Gamma_{\text{SM}}}{\Gamma} = 0.12 \pm 0.06. \quad (11)$$

Here we have conservatively added the errors from the two lattice quantities linearly.

### 3 New physics

In the presence of new physics  $\arg M_{12}$  and thereby  $\phi$  in (2) can assume any value. Non-standard contributions to  $\phi$  can be measured from CP-asymmetries, which requires the resolution of the rapid  $B_s - \bar{B}_s$  oscillations and tagging, i.e. the discrimination between  $B_s$  and  $\bar{B}_s$  mesons at the time  $t = 0$  of their production. From (1) one verifies that a non-vanishing  $\phi$  also affects  $\Delta\Gamma$ , which can be measured from untagged data samples and therefore involves better efficiencies than tagged studies. Of course in the search for new physics  $\Delta\Gamma$  is only competitive with CP asymmetries, which determine  $\sin\phi$ , if  $\phi$  is not too close to 0 or  $\pm\pi$ . Nevertheless the information on  $\phi$  from both tagged and untagged data should be combined.

As discussed at the end of Sect. 1,  $\Delta\Gamma$  is most easily found from the lifetimes measured in the decays of an untagged  $B_s$  sample into a flavor-specific final state and into a CP-specific final state  $f_{CP}$ , respectively. In the presence of a non-zero CP-violating phase  $\phi$  the mass eigenstates  $B_L$  and  $B_H$  are no more CP eigenstates, so that now both exponentials in (3) contribute to the decay  $B_s \rightarrow f_{CP}$ . Then this method determines [20,21]:

$$\Delta\Gamma \cos\phi = \Delta\Gamma_{\text{SM}} \cos^2\phi. \quad (12)$$

As first pointed out in [20], one can determine  $|\cos\phi|$  without using the theoretical input in (10): if one is able to resolve both exponentials of (3) in the time evolution of a  $B_s$

decay into a flavor-specific final state, one will measure the true  $|\Delta\Gamma|$ . By comparing with (12) one can then solve for  $|\cos\phi|$ . This method, however, requires to distinguish  $\cosh((\Delta\Gamma)t/2)$  from 1 and is very difficult to carry out. In [21] a different method has been proposed, which only requires to measure lifetimes and branching ratios: first define CP eigenstates  $B_s^{\text{odd}}$  and  $B_s^{\text{even}}$  such that  $B_s^{\text{odd}} \rightarrow D_s^+ D_s^-$ . Then define

$$\Delta\Gamma_{\text{CP}} = \Gamma(B_s^{\text{even}}) - \Gamma(B_s^{\text{odd}}). \quad (13)$$

$\Delta\Gamma_{\text{CP}}$  is related to  $\Gamma_{12}$  as

$$\Delta\Gamma_{\text{CP}} = 2|\Gamma_{12}|.$$

Hence  $\Delta\Gamma_{\text{CP}}$  equals  $\Delta\Gamma_{\text{SM}}$ , but is not affected by the new physics phase  $\phi$  at all! By measuring both  $\Delta\Gamma_{\text{CP}}$  and  $\Delta\Gamma \cos\phi$  one can infer  $|\cos\phi|$  from (12). Loosely speaking,  $\Delta\Gamma_{\text{CP}}$  is measured by counting the CP-even and CP-odd double-charm final states in  $B_s$  decays:

$$\Delta\Gamma_{\text{CP}} = 2\Gamma \sum_{f \in X_{c\bar{c}}} Br(\overset{(-)}{B}_s \rightarrow f) (1 - 2x_f) \left[ 1 + \mathcal{O}\left(\frac{\Delta\Gamma}{\Gamma}\right) \right]. \quad (14)$$

Here  $Br(\overset{(-)}{B}_s \rightarrow f)$  is the branching ratio of an untagged  $B_s$  meson into the final state  $f$ ,  $\Gamma$  is the average  $B_s$  width, the sum runs over all double-charm final states and  $x_f$  is the CP-odd component of the final state  $f$ , e.g.  $x_f$  is 0 for a CP-even state and equals 1 for a CP-odd state. In the Shifman-Voloshin limit [22] one can show that  $\Delta\Gamma_{\text{CP}}$  is exhausted by the  $D_s^{(*)+} D_s^{(*)-}$  final states [23]. Moreover these four final states are purely CP-even in this limit. ALEPH has measured the sum of these branching ratios [24] and found, relying on the SV limit,

$$\Delta\Gamma_{\text{CP}} \approx 2 Br(\overset{(-)}{B}_s \rightarrow D_s^{(*)+} D_s^{(*)-}) = 0.26_{-0.15}^{+0.30}. \quad (15)$$

In the future one can extend this method by including all detected double-charm final states into the sum in (14) and determine the CP-odd fraction  $x_f$  of each final state by measuring the  $B_s$  lifetime in the studied mode [21].

## Acknowledgments

I thank Gudrun Hiller for inviting me to this conference. I gratefully appreciate the financial support from the conference.

## References

- [1] N. Cabibbo, Phys. Rev. Lett. **10** (1963) 531. M. Kobayashi and T. Maskawa, Prog. Theor. Phys. **49** (1973) 652.
- [2] S. L. Glashow, J. Iliopoulos and L. Maiani, Phys. Rev. D **2**, 1285 (1970).
- [3] D. Boutigny et al., *BaBar technical design report*, SLAC-R-0457. M.T. Cheng et al. (Belle collab.), *A study of CP violation in B meson decays: Technical design report*, BELLE-TDR-3-95.
- [4] K. Pitts (for Fermilab D0 and CDF collab.), Proceedings of the 4th Workshop on Heavy Quarks at Fixed Target (HQ 98), Batavia, USA, 1998. R. W. Gardner (BTeV Collaboration), Nucl. Instrum. Meth. **A446** (2000) 208. P. Krizan et al., *HERA-B, an experiment to study CP violation at the HERA proton ring using an internal target*, Nucl. Instrum. Meth. **A351** (1994) 111. David Websdale, *LHC-B: A dedicated B physics detector for the LHC*, Nucl. Phys. Proc. Suppl. **50** (1996) 333.
- [5] F. Azfar, L. Lyons, M. Martin, C. Paus and J. Tseng, CDF note no. 5351. Report of the workshop *B Physics at the Tevatron — Run-II and Beyond*, eds. R. Jesik et al., to appear.
- [6] A. J. Buras and P. H. Weisz, Nucl. Phys. B **333**, 66 (1990).
- [7] M. Beneke, G. Buchalla and I. Dunietz, Phys. Rev. **D54** (1996) 4419.
- [8] M. Beneke, G. Buchalla, C. Greub, A. Lenz and U. Nierste, Phys. Lett. **B459** (1999) 631. U. Nierste, hep-ph/0009203. M. Beneke and A. Lenz, hep-ph/0012222.
- [9] M. Voloshin and M. Shifman, Sov. J. Nucl. Phys. **41** (1985) 120; J. Chay, H. Georgi and B. Grinstein, Phys. Lett. **B247** (1990) 399. I.I. Bigi, N.G. Uraltsev and A.I. Vainshtein, Phys. Lett. **B293** (1992) 430 [(E) Phys. Lett. **B297** (1993) 477]; I.I. Bigi, M. Shifman, N.G. Uraltsev, and A. Vainshtein, Phys. Rev. Lett. **71** (1993) 496. A.V. Manohar and M.B. Wise, Phys. Rev. **D49** (1994) 1310; B. Blok, L. Koyrakh, M. Shifman and A.I. Vainshtein, Phys. Rev. **D49** (1994) 3356; T. Mannel, Nucl. Phys. **B413** (1994) 396. M. Neubert and C. T. Sachrajda, Nucl. Phys. **B483** (1997) 339.
- [10] J.S. Hagelin, Nucl. Phys. **B193**, 123 (1981); E. Franco, M. Lusignoli and A. Pugliese, Nucl. Phys. **B194**, 403 (1982); L.L. Chau, Phys. Rep. **95**, 1 (1983); A.J. Buras, W. Słominski and H. Steger, Nucl. Phys. **B245**, 369 (1984); M.B. Voloshin, N.G. Uraltsev, V.A. Khoze and M.A. Shifman, Sov. J. Nucl. Phys. **46**, 112 (1987); A. Datta, E.A. Paschos and U. Türke, Phys. Lett. **B196**, 382 (1987); A. Datta, E.A. Paschos and Y.L. Wu, Nucl. Phys. **B311**, 35 (1988).
- [11] I. Bigi and N. Uraltsev, Phys. Lett. **B280**, 271 (1992).

- [12] *see e.g.* M. Shifman, hep-ph/9505289.
- [13] E. Bagan, P. Ball, B. Fiol and P. Gosdzinsky, Phys. Lett. B **351**, 546 (1995).
- [14] L. Gibbons *et al.* [CLEO Collaboration], Phys. Rev. D **56**, 3783 (1997). D. Buskulic *et al.* [ALEPH Collaboration], Phys. Lett. B **388**, 648 (1996).
- [15] W. A. Bardeen, A. J. Buras, D. W. Duke and T. Muta, Phys. Rev. **D18** (1978) 3998.
- [16] S. Herrlich and U. Nierste, Nucl. Phys. **B455**, 39 (1995)
- [17] S. Hashimoto, Nucl. Phys. Proc. Suppl. **83-84** (2000) 3.
- [18] N. Yamada et al. (JLQCD coll.), contr. to the *18th Intern. Symposium on Lattice Field Theory (Lattice 2000)*, Bangalore, India, 17-22 Aug 2000, hep-lat/0010089.
- [19] D. Becirevic, D. Meloni, A. Retico, V. Gimenez, V. Lubicz and G. Martinelli, Eur. Phys. J. C **18** (2000) 157.
- [20] Y. Grossman, Phys. Lett. **B380** (1996) 99.
- [21] I. Dunietz, R. Fleischer and U. Nierste, Phys. Rev. D **63**, 114015 (2001).
- [22] M. A. Shifman and M. B. Voloshin, Sov. J. Nucl. Phys. **47** (1988) 511.
- [23] R. Aleksan, A. Le Yaouanc, L. Oliver, O. Pène and J. C. Raynal, Phys. Lett. **B316** (1993) 567.
- [24] R. Barate *et al.* [ALEPH coll.], Phys. Lett. **B486** (2000) 286.

# Theory of $\varepsilon'/\varepsilon$

STEFANO BERTOLINI

*INFN and SISSA  
Via Beirut 4, I-34013 Trieste, Italy*

I shortly review the present status of the theoretical estimates of  $\varepsilon'/\varepsilon$ . I consider a few aspects of the theoretical calculations which may be relevant in understanding the present experimental results. I discuss the role of higher order chiral corrections and in general of non-factorizable contributions for the explanation of the  $\Delta I = 1/2$  selection rule in kaon decays and  $\varepsilon'/\varepsilon$ . Lacking reliable lattice calculations, the  $1/N$  expansion and phenomenological approaches may help in understanding correlations among theoretical effects and the experimental data. The same dynamics which underlies the CP conserving selection rule appears to drive  $\varepsilon'/\varepsilon$  in the range of the recent experimental measurements.

Presented at the

5th International Symposium on Radiative Corrections  
(RADCOR-2000)  
Carmel CA, USA, 11–15 September, 2000

# 1 Introduction

The results announced during the last year by the KTeV [1] and NA48 [2] collaborations have marked a great experimental achievement, establishing 35 years after the discovery of CP violation in the neutral kaon system [3] the existence of a much smaller violation acting directly in the decays.

While the Standard Model (SM) of strong and electroweak interactions provides an economical and elegant understanding of indirect ( $\varepsilon$ ) and direct ( $\varepsilon'$ ) CP violation in term of a single phase, the detailed calculation of the size of these effects implies mastering strong interactions at a scale where perturbative methods break down. In addition, CP violation in  $K \rightarrow \pi\pi$  decays is the result of a destructive interference between two sets of contributions, which may inflate up to an order of magnitude the uncertainties on the hadronic matrix elements of the effective four-quark operators. All that makes predicting  $\varepsilon'/\varepsilon$  a complex and subtle theoretical challenge [4].

The status of the theoretical predictions and experimental data available before the KTeV announcement in February 1999 is summarized in Fig. 1.

The gray horizontal bands show the one-sigma average of the old (early 90's) NA31 (CERN) and E731 (Fermilab) results. The vertical lines show the ranges of the published theoretical *predictions* (before February 1999), identified with the cities where most of the group members reside. The range of the naive Vacuum Saturation

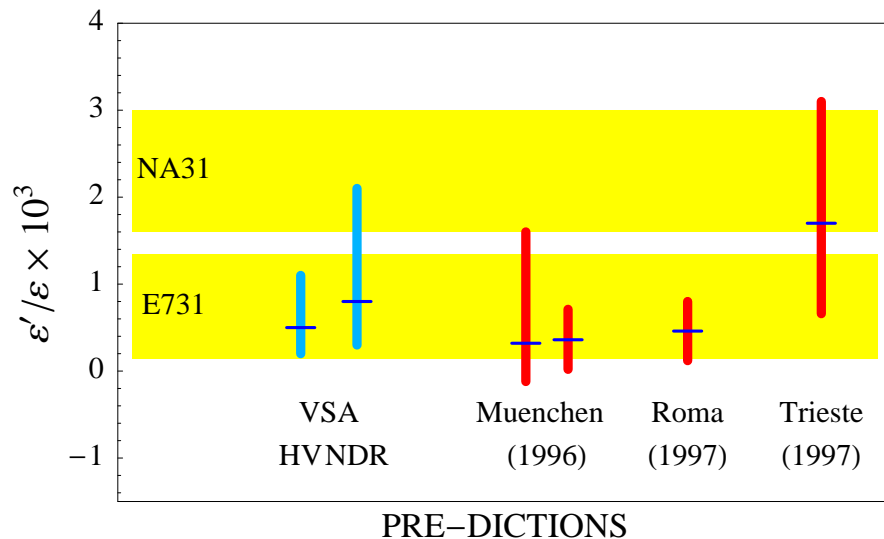


Figure 1: The 1- $\sigma$  results of the NA31 and E731 Collaborations (early 90's) are shown by the gray horizontal bands. The old München, Roma and Trieste theoretical predictions for  $\varepsilon'/\varepsilon$  are depicted by the vertical bars with their central values. For comparison, the VSA estimate is shown using two renormalization schemes.

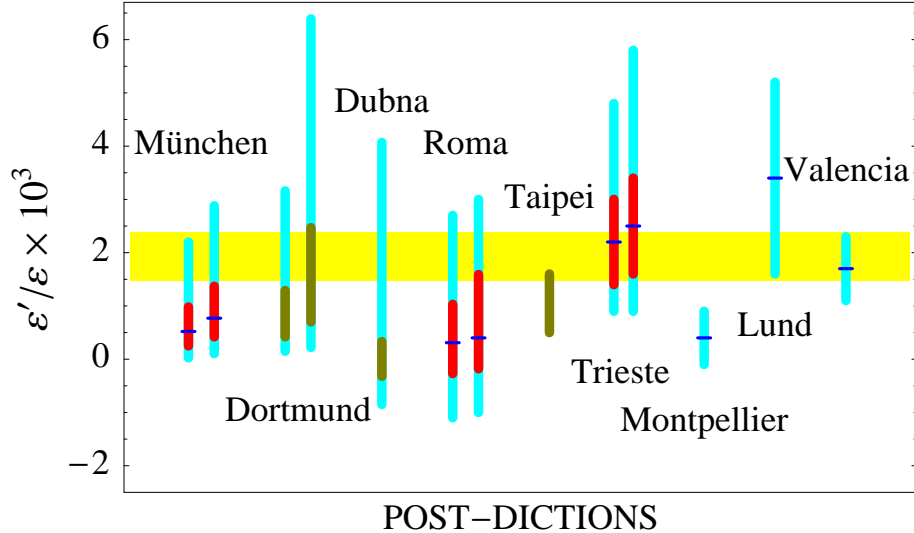


Figure 2: The latest theoretical calculations of  $\varepsilon'/\varepsilon$  are compared with the combined  $1\text{-}\sigma$  average of the NA31, E731, KTeV and NA48 results ( $\varepsilon'/\varepsilon = 19.2 \pm 4.6 \times 10^{-4}$ ), depicted by the gray horizontal band (the error is inflated according to the Particle Data Group procedure when averaging over data with substantially different central values).

Approximation (VSA) is shown for comparison.

The experimental and theoretical scenarios have changed substantially after the first KTeV data and the subsequent NA48 results. Fig. 2 shows the present experimental world average for  $\varepsilon'/\varepsilon$  compared with the revised or new theoretical calculations that appeared during the last year.

Notwithstanding the complexity of the problem, all theoretical calculations show a remarkable overall agreement, most of them pointing to a non-vanishing positive effect in the SM (which is by itself far from trivial).

On the other hand, if we focus our attention on the central values, many of the predictions prefer the  $10^{-4}$  regime, whereas only a few of them stand above  $10^{-3}$ . Is this just a “noise” in the theoretical calculations?

The answer is no. Without entering the details of the various estimates, it is possible to explain most of the abovementioned difference in terms of a single effect: the different size of the hadronic matrix element of the gluonic penguin  $Q_6$  obtained in the various approaches.

While some of the calculations, as the early München and Rome predictions, assume for  $\langle \pi\pi | Q_6 | K \rangle$  values in the neighborhood of the leading  $1/N$  result (naive factorization), other approaches, first of which the Trieste and Dortmund calculations and more recently the Lund and Valencia analyses, find a substantial enhancement of this matrix element with respect to the simple factorization result. The bulk of such

an effect is actually a global enhancement of the  $I = 0$  components of the  $K \rightarrow \pi\pi$  amplitudes, which affects *both* current-current *and* penguin operators, and it can be at least partially understood in terms of chiral dynamics (final-state interactions).

## 2 Final State Interactions

As a matter of fact, one should in general expect an enhancement of  $\varepsilon'/\varepsilon$  with respect to the naive VSA due to final-state interactions (FSI). As Fermi first argued [5], in potential scattering the isospin  $I = 0$  two-body states feel an attractive interaction, of a sign opposite to that of the  $I = 2$  components thus affecting the size of the corresponding amplitudes. This feature is at the root of the enhancement of the  $I = 0$  amplitude over the  $I = 2$  one and of the corresponding enhancement of  $\varepsilon'/\varepsilon$  beyond factorization.

The question is how to make of a qualitative statement a quantitative one. A dispersive analysis of the  $K \rightarrow \pi\pi$  amplitudes has been recently presented in ref. [6]. The Omnès-Mushkelishvili representation [7]

$$M(s + i\epsilon) = P(s) \exp \left( \frac{1}{\pi} \int_{4m_\pi^2}^{\infty} \frac{\delta(s')}{s' - s - i\epsilon} ds' \right) \quad (1)$$

is used in order to resum FSI effects from the knowledge of the  $\pi\pi$  rescattering phase  $\delta(s)$  in the elastic regime ( $s < 1 \text{ GeV}^2$ ).  $P(s)$  is a polynomial function of  $s$  which is related to the factorized amplitude. A solution of the above dispersive relation for the  $A_{0,2}$  amplitudes can be written as

$$A_I(s) = A' (s - m_\pi^2) \mathcal{R}_I(s) e^{i\delta_I(s)} , \quad (2)$$

where  $A'$  is the derivative of the amplitude at the subtraction point  $s = m_\pi^2$ . The coefficient  $\mathcal{R}$  represents the rescaling effect related to the FSI. By replacing  $A'_I$  with the value given by LO chiral perturbation theory, Pich and Pallante found  $\mathcal{R}(m_k^2)_{0,2} \simeq 1.4, 0.9$  thus confirming via the resummation of the leading chiral logs related to FSI the enhancement of the  $I = 0$  amplitudes, together with a mild depletion of the  $I = 2$  components.

The numerical significance of these results has been questioned [8] on the basis that the precise size of the effect depends on boundary conditions of the factorized amplitude which are not unambiguously known, due to higher order chiral corrections. As a matter of fact, while the choice of a low subtraction scale minimizes the effect of momentum dependent chiral corrections the result of ref. [6] cannot account for polynomial corrections due to contact interaction terms whose size is unknown (and renormalization-scheme dependent).

The analysis of ref. [6] shows non-perturbatively the presence of a potentially large departure from factorization which affects the  $I = 0$   $K \rightarrow \pi\pi$  matrix elements. Nevertheless, the question whether the FSI rescaling of the factorized isospin amplitudes leads by itself to a satisfactory calculation of  $\varepsilon'/\varepsilon$  remains open.

### 3 CP conserving versus CP violating amplitudes

Given the possibility that common systematic uncertainties may affect the calculation of  $\varepsilon'/\varepsilon$  and the  $\Delta I = 1/2$  rule (see for instance the present difficulties in calculating on the lattice the “penguin contractions” for CP violating as well as for CP conserving amplitudes [9]) a convincing calculation of  $\varepsilon'/\varepsilon$  must involve at the same time a reliable explanation of the  $\Delta I = 1/2$  selection rule, which is still missing. FSI effects alone are *not* enough to account for the large ratio of the  $I = 0, 2$  CP conserving amplitudes. Other sources of large non-factorizable corrections are needed, which may affect the determination of  $\varepsilon'/\varepsilon$  as well.

The  $\Delta I = 1/2$  selection rule in  $K \rightarrow \pi\pi$  decays is known since 45 years [10] and it states the experimental evidence that kaons are 400 times more likely to decay in the  $I = 0$  two-pion state than in the  $I = 2$  component. This rule is not justified by any general symmetry consideration and, although it is common understanding that its explanation must be rooted in the dynamics of strong interactions, there is no up to date derivation of this effect from first principle QCD.

The ratio of  $I = 2$  over  $I = 0$  amplitudes appears directly in the definition of  $\varepsilon'/\varepsilon$  :

$$\frac{\varepsilon'}{\varepsilon} = \frac{1}{\sqrt{2}} \left\{ \frac{\langle (\pi\pi)_{I=2} | \mathcal{H}_W | K_L \rangle}{\langle (\pi\pi)_{I=0} | \mathcal{H}_W | K_L \rangle} - \frac{\langle (\pi\pi)_{I=2} | \mathcal{H}_W | K_S \rangle}{\langle (\pi\pi)_{I=0} | \mathcal{H}_W | K_S \rangle} \right\}. \quad (3)$$

As a consequence, a self-consistent calculation of  $\varepsilon'/\varepsilon$  must also address the determination of the CP conserving amplitudes.

The way we approach the calculation of the hadronic  $K \rightarrow \pi\pi$  transitions in gauge theories is provided by the Operator Product Expansion which allows us to write the relevant amplitudes in terms of the hadronic matrix elements of effective  $\Delta S = 1$  four quark operators (at a scale  $\mu$ ) and of the corresponding Wilson coefficients, which encode the information about the dynamical degrees of freedom heavier than the chosen renormalization scale:

$$\mathcal{H}_{\Delta S=1} = \frac{G_F}{\sqrt{2}} V_{ud} V_{us}^* \sum_i [z_i(\mu) + \tau y_i(\mu)] Q_i(\mu). \quad (4)$$

The entries  $V_{ij}$  of the  $3 \times 3$  Cabibbo-Kobayashi-Maskawa matrix describe the flavour mixing in the SM and  $\tau = -V_{td}V_{ts}^*/V_{ud}V_{us}^*$ . For  $\mu < m_c$  ( $q = u, d, s$ ), the relevant

quark operators are:

$$\begin{aligned}
\left. \begin{aligned} Q_1 &= (\bar{s}_\alpha u_\beta)_{V-A} (\bar{u}_\beta d_\alpha)_{V-A} \\ Q_2 &= (\bar{s}u)_{V-A} (\bar{u}d)_{V-A} \end{aligned} \right\} && \text{Current-Current} \\
\left. \begin{aligned} Q_{3,5} &= (\bar{s}d)_{V-A} \sum_q (\bar{q}q)_{V\mp A} \\ Q_{4,6} &= (\bar{s}_\alpha d_\beta)_{V-A} \sum_q (\bar{q}_\beta q_\alpha)_{V\mp A} \end{aligned} \right\} && \text{Gluon "penguins"} \\
\left. \begin{aligned} Q_{7,9} &= \frac{3}{2} (\bar{s}d)_{V-A} \sum_q \hat{e}_q (\bar{q}q)_{V\pm A} \\ Q_{8,10} &= \frac{3}{2} (\bar{s}_\alpha d_\beta)_{V-A} \sum_q \hat{e}_q (\bar{q}_\beta q_\alpha)_{V\pm A} \end{aligned} \right\} && \text{Electroweak "penguins"}
\end{aligned} \tag{5}$$

Current-current operators are induced by tree-level W-exchange whereas the so-called penguin (and “box”) diagrams are generated via an electroweak loop. Only the latter “feel” all three quark families via the virtual quark exchange and are therefore sensitive to the weak CP phase. Current-current operators control instead the CP conserving transitions. This fact suggests already that the connection between  $\varepsilon'/\varepsilon$  and the  $\Delta I = 1/2$  rule is by no means a straightforward one.

Using the effective  $\Delta S = 1$  quark Hamiltonian we can write  $\varepsilon'/\varepsilon$  as

$$\frac{\varepsilon'}{\varepsilon} = e^{i\phi} \frac{G_F \omega}{2|\epsilon| \text{Re } A_0} \text{Im } \lambda_t \left[ \Pi_0 - \frac{1}{\omega} \Pi_2 \right] \tag{6}$$

where

$$\begin{aligned}
\Pi_0 &= \frac{1}{\cos \delta_0} \sum_i y_i \text{Re} \langle Q_i \rangle_0 (1 - \Omega_{\eta+\eta'}) \\
\Pi_2 &= \frac{1}{\cos \delta_2} \sum_i y_i \text{Re} \langle Q_i \rangle_2 \quad ,
\end{aligned} \tag{7}$$

and  $\langle Q_i \rangle \equiv \langle \pi\pi | Q_i | K \rangle$ . The rescattering phases  $\delta_{0,2}$  can be extracted from elastic  $\pi - \pi$  scattering data [11] and are such that  $\cos \delta_0 \simeq 0.8$  and  $\cos \delta_2 \simeq 1$ . Given that the phase of  $\varepsilon$ ,  $\theta_\varepsilon$ , is approximately  $\pi/4$ , as well as  $\delta_0 - \delta_2$ ,  $\phi = \frac{\pi}{2} + \delta_2 - \delta_0 - \theta_\varepsilon$  turns out to be consistent with zero.

Two key ingredients appear in eq. 6:

1. The isospin breaking  $\pi^0 - \eta - \eta'$  mixing, parametrized by  $\Omega_{\eta+\eta'}$ , which is estimated to give a *positive* correction to the  $A_2$  amplitude of about 15-35%. The complete inclusion of NLO chiral corrections to the  $\pi^0 - \eta - \eta'$  mixing [12,13] and of additional isospin breaking effects ( $\Delta I = 5/2$  [14,15,16]) in the extraction of the isospin amplitudes may sizeably affect the determination of  $\varepsilon'/\varepsilon$ . Although a partial cancellation of the new terms in  $\varepsilon'/\varepsilon$  reduces their numerical impact, we must await for further analyses in order to confidently assess their relevance.
2. The combination of CKM elements  $\text{Im } \lambda_t \equiv \text{Im}(V_{ts}^* V_{td})$ , which affects directly the size of  $\varepsilon'/\varepsilon$  and the range of the uncertainty. The determination of  $\text{Im } \lambda_t$  depends on B-physics constraints and on  $\varepsilon$  [17]. In turn, the fit of  $\varepsilon$  depends on

the theoretical determination of  $B_K$ , the  $\overline{K}^0 - K^0$  hadronic parameter, which should be consistently determined within every analysis. The theoretical uncertainty on  $B_K$  affects substantially the final uncertainty on  $\text{Im } \lambda_t$ . A better determination of the unitarity triangle is expected from the B-factories and the hadronic colliders. In K-physics, the decay  $K_L \rightarrow \pi^0 \nu \overline{\nu}$  gives the cleanest “theoretical” determination of  $\text{Im } \lambda_t$ , albeit representing a great experimental challenge.

## 4 Summary of theory results

A satisfactory approach to the calculation of  $\varepsilon'/\varepsilon$  should comply with the following requirements:

- A: A consistent definition of renormalized operators leading to the correct scheme and scale matching with the short-distance perturbative analysis.
- B: A self-contained calculation of *all* relevant hadronic matrix elements (including  $B_K$ ).
- C: A simultaneous explanation of the  $\Delta I = 1/2$  selection rule and  $\varepsilon'/\varepsilon$ .

None of the existing calculations satisfies all previous requirements. I summarize very briefly the various attempts to calculate  $\varepsilon'/\varepsilon$  which have appeared so far leading to the estimates shown in Figs. 1 and 2.

- VSA: A simple and naive approach to the problem is the VSA, which is based on two drastic assumptions: the factorization of the four quark operators in products of currents or densities and the saturation of the completeness of the intermediate states by the vacuum. As an example:

$$\begin{aligned} \langle \pi^+ \pi^- | Q_6 | K^0 \rangle &= 2 \langle \pi^- | \overline{u} \gamma_5 d | 0 \rangle \langle \pi^+ | \overline{s} u | K^0 \rangle - 2 \langle \pi^+ \pi^- | \overline{d} d | 0 \rangle \langle 0 | \overline{s} \gamma_5 d | K^0 \rangle \\ &\quad + 2 \left[ \langle 0 | \overline{s} s | 0 \rangle - \langle 0 | \overline{d} d | 0 \rangle \right] \langle \pi^+ \pi^- | \overline{s} \gamma_5 d | K^0 \rangle \end{aligned} \quad (8)$$

The VSA does not allow for a consistent matching of the scale and scheme dependence of the Wilson coefficients (the HV and NDR results are shown in Fig. 1) and it carries potentially large systematic uncertainties [4]. It is best used for LO estimates.

- Taipei’s: Generalized factorization represents an attempt to parametrize the hadronic matrix elements in the framework of factorization without a-priori assumptions [18]. Phenomenological parameters are introduced to account for non-factorizable effects. Experimental data are used in order to extract as much

information as possible on the non-factorizable parameters. This approach has been applied to the  $K \rightarrow \pi\pi$  amplitudes in ref. [19]. The effective Wilson coefficients, which include the perturbative QCD running of the quark operators, are matched to the factorized matrix elements at the scale  $\mu_F$  which is arbitrarily chosen in the perturbative regime. A residual scale dependence remains in the penguin matrix elements via the quark masses. The analysis shows that in order to reproduce the  $\Delta I = 1/2$  rule and  $\varepsilon'/\varepsilon$  sizable non-factorizable contributions are required both in the current-current and the penguin matrix elements. However, some assumptions on the phenomenological parameters and ad hoc subtractions of scheme-dependent terms in the Wilson coefficients make the numerical results questionable. The quoted error does not include any short-distance uncertainty.

- München's: In the München approach (phenomenological  $1/N$ ) some of the matrix elements are obtained by fitting the  $\Delta I = 1/2$  rule at  $\mu = m_c = 1.3$  GeV. On the other hand, the relevant gluonic and electroweak penguin  $\langle Q_6 \rangle$  and  $\langle Q_8 \rangle_2$  remain undetermined and are taken around their leading  $1/N$  values (which implies a scheme dependent result). In Fig. 2 the HV (left) and NDR (right) results are shown [20]. The dark range represents the result of gaussian treatment of the input parameters compared to flat scanning (complete range).
- Dortmund's: In the recent years the Dortmund group has revived and improved the approach of Bardeen, Buras and Gerard [21] based on the  $1/N$  expansion. Chiral loops are regularized via a cutoff and the amplitudes are arranged in a  $p^{2n}/N$  expansion. A particular attention has been given to the matching procedure between the scale dependence of the chiral loops and that arising from the short-distance analysis [22]. The renormalization-scheme dependence remains and it is included in the final uncertainty. The  $\Delta I = 1/2$  rule is reproduced, but the presence of the quadratic cutoff induces a matching scale instability (which is very large for  $B_K$ ). The NLO corrections to  $\langle Q_6 \rangle$  induce a substantial enhancement of the matrix element (right bar in Fig. 2) compared to the leading order result (left bar). The darker ranges correspond to central values of  $m_s$ ,  $\Omega_{\eta+\eta'}$ ,  $\text{Im } \lambda_t$  and  $\Lambda_{QCD}$ .
- Dubna's: In the Nambu, Jona-Lasinio (NJL) modelling of QCD [23] the Dubna group [24] has calculated  $\varepsilon'/\varepsilon$  including chiral loops up to  $O(p^6)$  and the effects of scalar, vector and axial-vector resonances. Chiral loops are regularized via the heat-kernel method, which leaves unsolved the problem of the renormalization-scheme dependence. A phenomenological fit of the  $\Delta I = 1/2$  rule implies deviations up to a factor two on the calculated  $\langle Q_6 \rangle$ . The reduced (dark) range in Fig. 2 corresponds to taking the central values of the NLO chiral couplings and varying the short-distance parameters.

- Trieste's: In the approach of the Trieste group, based on the Chiral Quark Model ( $\chi$ QM) [25], all hadronic matrix elements are computed up to  $O(p^4)$  in the chiral expansion in terms of the three model parameters: the constituent quark mass, the quark condensate and the gluon condensate. These parameters are phenomenologically fixed by fitting the  $\Delta I = 1/2$  rule [26]. This step is crucial in order to make the model predictive, since there is no a-priori argument for the consistency of the matching procedure (dimensional regularization and minimal subtraction are used in the effective chiral theory). As a matter of fact, all computed observables turn out to be very weakly dependent on the scale (and the renormalization scheme) in a few hundred MeV range around the matching scale, which is taken to be 0.8 GeV as a compromise between the ranges of validity of perturbation theory and chiral expansion. The  $I = 0$  matrix elements are strongly enhanced by non-factorizable chiral corrections and drive  $\varepsilon'/\varepsilon$  in the  $10^{-3}$  regime. The dark (light) ranges in Fig. 2 correspond to Gaussian (flat) scan of the input parameters. The bar on the left represents the result of ref. [28] which updates the 1997 calculation [27]. That on the right is a new estimate [29], similarly based on the  $\chi$ QM hadronic matrix elements, in which however  $\varepsilon'/\varepsilon$  is computed by including the explicit computation of  $\varepsilon$  in the ratio as opposed to the usual procedure of taking its value from the experiments. This approach has the advantage of being independent from the determination of the CKM parameters  $\text{Im } \lambda_t$  and of showing more directly the dependence on the long-distance parameter  $\hat{B}_K$  as determined within the model.
- Roma's: Lattice regularization of QCD is *the* consistent approach to the problem. On the other hand, there are presently important numerical and theoretical limitations, like the quenching approximation and the implementation of chiral symmetry, which may substantially affect the calculation of the weak matrix elements. In addition, chiral perturbation theory is needed in order to obtain  $K \rightarrow \pi\pi$  amplitudes from the computed  $K \rightarrow \pi$  transitions. As summarized in ref. [30] lattice cannot provide us at present with reliable calculations of the  $I = 0$  penguin operators relevant to  $\varepsilon'/\varepsilon$ , as well as of the  $I = 0$  components of the hadronic matrix elements of the current-current operators (penguin contractions), which are relevant to the  $\Delta I = 1/2$  rule. This is due to large renormalization uncertainties, partly related to the breaking of chiral symmetry on the lattice. In the recent Roma re-evaluation of  $\varepsilon'/\varepsilon$   $\langle Q_6 \rangle$  is taken at the VSA value with a 100% uncertainty [30]. The result is therefore scheme dependent (the HV and NDR results are shown in Fig. 2). The dark (light) ranges correspond to Gaussian (flat) scan of the input parameters.
- Montpellier's: The analysis in ref. [31] is based on QCD Sum Rules and uses recent data on the  $\tau$  hadronic total decay rates. The value of the  $Q_8$  matrix element thus found is substantially larger than the leading  $1/N$  result. At the

same time, the matrix element of the  $Q_6$  gluonic penguin, computed assuming scalar meson dominance, is found in agreement with leading order  $1/N$ . The combined effect is a strong cancellation between electroweak and gluonic penguins which leads to a vanishingly small  $\varepsilon'/\varepsilon$ . Various sources of uncertainties in the calculation and the comparison with other analyses are discussed in [31].

- Lund's: The  $\Delta I = 1/2$  rule and  $B_K$  have been studied in the NJL framework and  $1/N$  expansion by Bijnsens and Prades [32] showing an impressive scale stability when including vector and axial-vector resonances. The same authors have recently produced a calculation of  $\varepsilon'/\varepsilon$  at the NLO in  $1/N$  [33]. The calculation is done in the chiral limit and it is eventually corrected by estimating the largest  $SU(3)$  breaking effects. Particular attention is devoted to the matching between long- and short-distance components by use of the  $X$ -boson method [34,35]. The couplings of the  $X$ -bosons are computed within the ENJL model which improves the high-energy behavior. The  $\Delta I = 1/2$  rule is reproduced and the computed amplitudes show a satisfactory renormalization-scale and -scheme stability. A sizeable enhancement of the  $Q_6$  matrix element is found which brings the central value of  $\varepsilon'/\varepsilon$  at the level of  $3 \times 10^{-3}$ .
- Valencia's: The standard model estimate given by Pallante and Pich is obtained by applying the FSI correction factors obtained using a dispersive analysis à la Omnès-Mushkelishvili [7] to the leading (factorized)  $1/N$  amplitudes. The detailed numerical outcome has been questioned on the basis of ambiguities related to the choice of the subtraction point at which the factorized amplitude is taken [8]. Large corrections may also be induced by unknown local terms which are unaccounted for by the dispersive resummation of the leading chiral logs. Nevertheless, the analysis of ref. [6] confirms the crucial role of higher order chiral corrections for  $\varepsilon'/\varepsilon$ , even though FSI effects alone leave the problem of reproducing the  $\Delta I = 1/2$  selection rule open.

Other attempts to reproduce the measured  $\varepsilon'/\varepsilon$  using the linear  $\sigma$ -model, which include the effect of a scalar resonance with  $m_\sigma \simeq 900$  MeV, obtain the needed enhancement of  $\langle Q_6 \rangle$  [36]. However, it is not possible to reproduce simultaneously the experimental values of  $\varepsilon'/\varepsilon$  and of the CP conserving  $K \rightarrow \pi\pi$  amplitudes.

Studies on the matching between long- and short- distances in large  $N$  QCD, with the calculation of the  $Q_7$  penguin matrix element and of  $\hat{B}_K$  at the NLO in the  $1/N$  expansion have been presented in ref. [37]. However, a complete calculation of the  $K \rightarrow \pi\pi$  matrix elements relevant to  $\varepsilon'/\varepsilon$  is not available yet.

It has been recently emphasized [38] that cut-off based approaches should pay attention to higher-dimension operators which become relevant for matching scales below 2 GeV and may represent one of the largest sources of uncertainty in present calculations. On the other hand, the calculations based on dimensional regularization

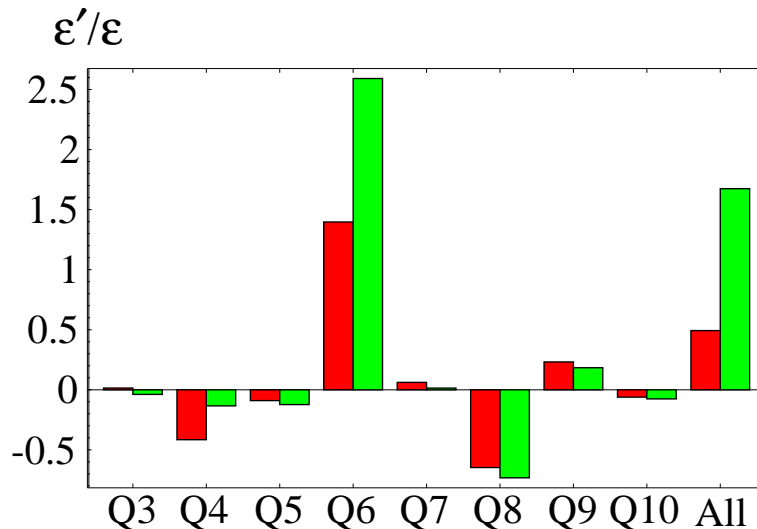


Figure 3: Predicting  $\varepsilon'/\varepsilon$ : a (Penguin) Comparative Anatomy of the München (dark gray) and Trieste (light gray) results in Fig. 1 (in units of  $10^{-3}$ ).

(for instance the Trieste one) may be safe in this respect if phenomenological input is used in order to encode in the hadronic matrix elements the physics at all scales.

Lattice, as a regularization of QCD, is *the* first-principle approach to the problem. Presently, very promising developments are being undertaken to circumvent the technical and conceptual shortcomings related to the calculation of weak matrix elements (for a recent survey see ref. [39]). Among these are the Domain Wall Fermion approach [40,41] which allows us to decouple the chiral symmetry from the continuum limit, and the possibility to circumvent the Maiani-Testa theorem [42] using the fact that lattice calculations are performed in finite volume [43]. All these developments need a tremendous effort in machine power and in devising faster algorithms. Preliminary results for the calculations of both  $\varepsilon'/\varepsilon$  and the  $\Delta I = 1/2$  selection rule are expected during the next year.

## 5 The $\Delta I = 1/2$ selection rule

Without entering into the details of the various calculations I wish to illustrate with a simple exercise the crucial role of higher order chiral corrections (in general of non-factorizable contributions) for  $\varepsilon'/\varepsilon$  and the  $\Delta I = 1/2$  selection rule. In order to do that I focus on two semi-phenomenological approaches.

A commonly used way of comparing the estimates of hadronic matrix elements in different approaches is via the so-called  $B$  factors which represent the ratio of the model matrix elements to the corresponding VSA values. However, care must be

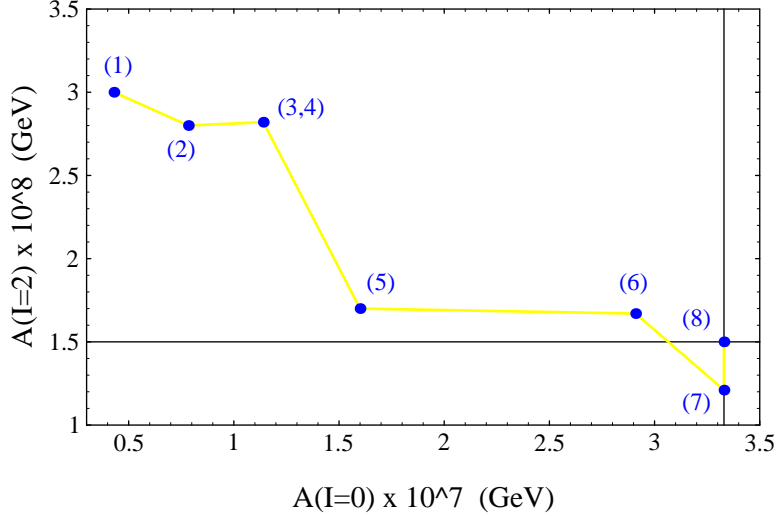


Figure 4: Anatomy of the  $\Delta I = 1/2$  rule in the  $\chi$ QM. See the text for explanations. The cross-hairs indicate the experimental point.

taken in the comparison of different models due to the scale dependence of the  $B$ 's and the values used by different groups for the parameters that enter the VSA expressions. An alternative pictorial and synthetic way of analyzing different outcomes for  $\varepsilon'/\varepsilon$  is shown in Fig. 3, where a “comparative anatomy” of the early Trieste and München predictions is presented.

From the inspection of the various contributions it is apparent that the different outcome on the central value of  $\varepsilon'/\varepsilon$  is almost entirely due to the difference in the size of the  $Q_6$  contribution.

In the München approach [20] the  $\Delta I = 1/2$  rule is used in order to determine phenomenologically the matrix elements of  $Q_{1,2}$  and, via operatorial relations, some of the matrix elements of the left-handed penguins. The approach does not allow for a phenomenological determination of the matrix elements of the penguin operators which are most relevant for  $\varepsilon'/\varepsilon$ , namely the gluonic penguin  $Q_6$  and the electroweak penguin  $Q_8$ . These matrix elements are taken around their leading  $1/N$  values (factorization).

In the semi-phenomenological approach of the Trieste group the size of the effects on the  $I = 0, 2$  amplitudes is controlled by the phenomenological embedding of the  $\Delta I = 1/2$  selection rule which determines the ranges of the model parameters: the constituent quark mass, the quark and the gluon condensates. In terms of these parameters all matrix elements are computed.

Fig. 4 shows an anatomy of the  $\chi$ QM contributions which lead to the experimental value of the  $\Delta I = 1/2$  selection rule for central values of the input parameters.

Point (1) represents the result obtained by neglecting QCD and taking the factorized matrix element for the tree-level operator  $Q_2$ , which is the leading electroweak contribution. The ratio  $A_0/A_2$  is thus found equal to  $\sqrt{2}$ : by far off the experimental point (8). Step (2) includes the effects of perturbative QCD renormalization on the operators  $Q_{1,2}$  [44]. Step (3) shows the effect of including the gluonic penguin operators [45]. Electroweak penguins [46] are numerically negligible in the CP conserving amplitudes and are responsible for the very small shift in the  $A_2$  direction. Therefore, perturbative QCD and factorization lead us from (1) to (4): a factor five away from the experimental ratio.

Non-factorizable gluon-condensate corrections, a crucial model dependent effect entering at the leading order in the chiral expansion, produce a substantial reduction of the  $A_2$  amplitude (5), as it was first observed by Pich and de Rafael [47]. Moving the analysis to  $O(p^4)$ , the chiral loop corrections, computed on the LO chiral lagrangian via dimensional regularization and minimal subtraction, lead us from (5) to (6), while the finite parts of the NLO counterterms calculated in the  $\chi$ QM approach lead to the point (7). Finally, step (8) represents the inclusion of  $\pi$ - $\eta$ - $\eta'$  isospin breaking effects [48].

This model dependent anatomy shows the relevance of non-factorizable contributions and higher-order chiral corrections. The suggestion that chiral dynamics may be relevant to the understanding of the  $\Delta I = 1/2$  selection rule goes back to the work of Bardeen, Buras and Gerard [21] in the  $1/N$  framework with a cutoff regularization. A pattern similar to that shown in Fig. 4 for the chiral loop corrections to  $A_0$  and  $A_2$  was previously obtained, using dimensional regularization in a NLO chiral lagrangian analysis, by Missimer, Kambor and Wyler [49]. The Trieste group has extended their calculation to include the NLO contributions to the electroweak penguin matrix elements [50].

Fig. 5 shows the contributions to  $\varepsilon'/\varepsilon$  of the various penguin operators, providing us with a finer anatomy of the NLO chiral corrections. It is clear that chiral-loop dynamics plays a subleading role in the electroweak penguin sector ( $Q_{8-10}$ ) while enhancing by 60% the gluonic penguin ( $I = 0$ ) matrix elements. The NLO enhancement of the  $Q_6$  matrix element is what drives  $\varepsilon'/\varepsilon$  in the  $\chi$ QM to the  $10^{-3}$  ballpark.

As a consequence, the  $\chi$ QM analysis shows that the same dynamics that is relevant to the reproduction of the CP conserving  $A_0$  amplitude (Fig. 4) is at work in the CP violating sector, albeit with a reduced strength.

In order to ascertain whether these model features represent real QCD effects we must wait for future improvements in lattice calculations [39]. On the other hand, indications for such a dynamics follow also from the analytic properties of the  $K \rightarrow \pi\pi$  amplitudes [6]. It is important to notice however that the size of the effect so derived is generally not enough to fully account for the  $\Delta I = 1/2$  rule. Other non-factorizable contributions are needed to further enhance the CP conserving  $I = 0$  amplitude, and to reduce the large  $I = 2$  amplitude obtained from perturbative QCD

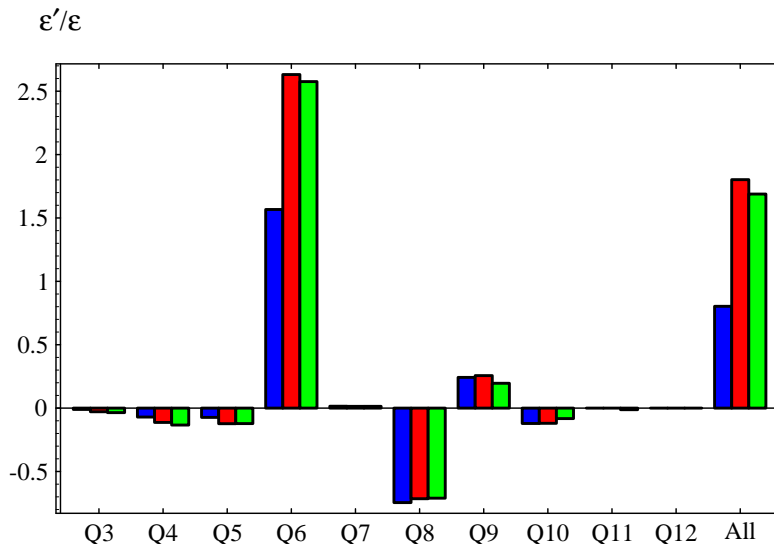


Figure 5: Anatomy of  $\varepsilon'/\varepsilon$  (in units of  $10^{-3}$ ) in the  $\chi$ QM approach. In black the LO results (which includes the non-factorizable gluonic corrections), in half-tone the effect of the inclusion of chiral-loop corrections and in light gray the complete  $O(p^4)$  estimate.

and factorization. In the  $\chi$ QM approach, for instance, the fit of the  $\Delta I = 1/2$  rule is due to the interplay of NLO chiral corrections and non-factorizable soft gluonic contributions (at LO in the chiral expansion).

## 6 Conclusions

In summary, those semi-phenomenological approaches which reproduce the  $\Delta I = 1/2$  selection rule in  $K \rightarrow \pi\pi$  decays, generally agree in the pattern and size of the  $I = 2$  hadronic matrix elements with the existing lattice calculations. On the other hand, the  $\Delta I = 1/2$  rule forces upon us large deviations from the naive factorization for the  $I = 0$  amplitudes:  $B$ -factors of  $O(10)$  are required for  $\langle Q_{1,2} \rangle_0$ . Here is where lattice calculations presently suffer from large systematic uncertainties.

In the Trieste and Dortmund calculations, which reproduce the CP conserving  $K \rightarrow \pi\pi$  amplitudes, non-factorizable effects (mainly due to final-state interactions) enhance the hadronic matrix elements of the gluonic penguins, and give  $B_6/B_8^{(2)} \approx 2$ . Similar indications stem from recent  $1/N$  [33] and dispersive [6] approaches. The direct calculation of  $K \rightarrow \pi\pi$  amplitudes and unquenching are needed in the lattice calculations in order to account for final state interactions. Promising and exciting work in this direction is in progress.

## Acknowledgments

I wish to thank the organizers for their invitation to this interesting meeting hosted in a most enjoyable environment.

## References

- [1] A. Alavi-Harati et al., *Phys. Rev. Lett.* **83** (1999) 22; A. Barker, these Proceedings.
- [2] V. Fanti et al., *Phys. Lett. B* **465** (1999) 335; J. Ocariz, *JHEP Proc.*, Third Latin American Symposium on High Energy Physics, Cartagena de Indias, Colombia, 2-8 April 2000 [PREHEP-silafae-III/027].
- [3] J.H. Christenson et al., *Phys. Rev. Lett.* **13** (1964) 138.
- [4] S. Bertolini, J.O. Eeg and M. Fabbrichesi, *Rev. Mod. Phys.* **72** (2000) 65.
- [5] E. Fermi, *Suppl. Nuovo Cim.* **2** (1955) 17.
- [6] E. Pallante and A. Pich, *Phys. Rev. Lett.* **84** (2000) 2568; *Nucl. Phys. B* **592** (2000) 294; A. Pich, these Proceedings.
- [7] N.I. Mushkelishvili, *Singular Integral Equations* (Noordhoff, Gronigen, 1953), p. 204; R. Omnès, *Nuovo Cim.* **8** (1958) 316.
- [8] A. J. Buras et al., *Phys. Lett. B* **480** (2000) 80.
- [9] M. Ciuchini and G. Martinelli, hep-ph/0006056.
- [10] M. Gell-Mann and A. Pais, *Proc. Glasgow Conf.* (1955) 342.
- [11] J. Gasser and U.G. Meissner, *Phys. Lett. B* **258** (1991) 219; E. Chell and M.G. Olsson, *Phys. Rev. D* **48** (1993) 4076.
- [12] S. Gardner and G. Valencia, *Phys. Lett. B* **466** (1999) 355.
- [13] G. Ecker et al., *Phys. Lett. B* **467** (2000) 88.
- [14] S. Gardner and G. Valencia, *Phys. Rev. D* **62** (2000) 094024.
- [15] K. Maltman and C. Wolfe, *Phys. Lett. B* **482** (2000) 77; *Phys. Rev. D* **63** (2001) 014008.

- [16] V. Cirigliano, J.F. Donoghue and E. Golowich, *Phys. Lett. B* **450** (1999) 241; *Phys. Rev. D* **61** (2000) 093001; *Phys. Rev. D* **61** (2000) 093002; *Eur. Phys. J. C* **18** (2000) 83.
- [17] M. Ciuchini et al., hep-ph/0012308.
- [18] M. Neubert and B. Stech, in "Heavy Flavours", edited by A.J. Buras and M. Lindner (World Scientific, Singapore), hep-ph/9705292.
- [19] H.Y. Cheng, *Chin. J. Phys.* **38** (2000) 1044.
- [20] A.J. Buras, Proceedings of the Kaon 99 Conference, Chicago, USA, hep-ph/9908395.
- [21] W.A. Bardeen, A.J. Buras and J.M. Gerard, *Nucl. Phys. B* **293** (1987) 787.
- [22] T. Hambye et al., *Phys. Rev. D* **58** (1998) 014017; *Nucl. Phys. B* **564** (2000) 391.
- [23] Y. Nambu and G. Jona-Lasinio, *Phys. Rev.* **122** (1961) 345; J. Bijnens, *Phys. Rept.* **265** (1996) 369.
- [24] A.A. Bel'kov et al., hep-ph/9907335;
- [25] S. Weinberg, *Physica A* (327) 961979; A. Manhoar and H. Georgi, *Nucl. Phys. B* **234** (1984) 189.
- [26] S. Bertolini et al., *Nucl. Phys. B* **514** (1998) 63.
- [27] S. Bertolini et al., *Nucl. Phys. B* **514** (1998) 93.
- [28] S. Bertolini, J.O. Eeg and M. Fabbrichesi, hep-ph/0002234 to appear in *Phys. Rev. D* **63** (2001) 0560xx.
- [29] M. Fabbrichesi, *Phys. Rev. D* **62** (2000) 097902.
- [30] G. Martinelli, Proceedings of the Kaon 99 Conference, Chicago, USA, hep-ph/9910237.
- [31] S. Narison, *Nucl. Phys. B* **593** (2001) 3.
- [32] J. Bijnens and J. Prades, *JHEP* **9901** (1999) 023.
- [33] J. Bijnens and J. Prades, *JHEP* **0006** (2000) 035.

- [34] W. A. Bardeen, J. Bijnens and J.-M. Gérard, *Phys. Rev. Lett.* **62** (1989) 1343; J. Bijnens, J.-M. Gérard and G. Klein, *Phys. Lett. B* **257** (1991) 191; J. P. Fatoelo and J.-M. Gérard, *Phys. Lett. B* **347** (1995) 136.
- [35] J. Bijnens and J. Prades, *Phys. Lett. B* **342** (1995) 331; *Nucl. Phys. B* **444** (1995) 523; *JHEP* **9901** (1999) 023; *JHEP* **0001** (2000) 002.
- [36] Y.Y. Keum, U. Nierste and A.I. Sanda, *Phys. Lett. B* **457** (1999) 157; M. Harada et al., *Phys. Rev. D* **62** (2000) 014002; J.C.R. Bloch et al., *Phys. Rev. C* **62** (2000) 025206.
- [37] S. Peris, M. Perrottet and E. de Rafael, *JHEP* **9805** (1998) 011; M. Knecht, S. Peris and E. de Rafael, *Phys. Lett. B* **443** (1998) 255, *Phys. Lett. B* **457** (1999) 227; S. Peris and E. de Rafael, *Phys. Lett. B* **490** (2000) 213.
- [38] V. Cirigliano, J.F. Donoghue and E. Golowich, *JHEP* **0010** (2000) 048.
- [39] L. Lellouch, Proceedings of Lattice 2000, Bangalore, India, hep-lat/0011088.
- [40] D. Kaplan, *Phys. Lett. B* **288** (1992) 342.
- [41] A. Soni, Proceedings of the  $B_{CP}$  99 Conference, Taipei, Taiwan, hep-ph/0003092.
- [42] L. Maiani and M. Testa, *Phys. Lett. B* **245** (1990) 585.
- [43] L. Lellouch and M. Lüscher, hep-lat/0003023.
- [44] M.K. Gaillard and B. Lee, *Phys. Rev. Lett.* **33** (1974) 108; G. Altarelli and L. Maiani, *Phys. Lett. B* **52** (1974) 413.
- [45] M.A. Shifman, A.I. Vainshtein and V.I. Zacharov, *JETP Lett.* **22** (1975) 55; *Nucl. Phys. B* **120** (1977) 316; *JETP* **45** (1977) 670; J. Ellis et al., *Nucl. Phys. B* **131** (1977) 285, (E) 1325411978; F.J. Gilman and M.B. Wise, *Phys. Lett. B* **83** (1979) 83; *Phys. Rev. D* **20** (1979) 2392; R.S. Chivukula, J.M. Flynn and H. Georgi, *Phys. Lett. B* **171** (1986) 453.
- [46] J. Bijnens and M.B. Wise, *Phys. Lett. B* **137** (1984) 245; A.J. Buras and J.M. Gerard, *Phys. Lett. B* **192** (1987) 156; M. Lusignoli, *Nucl. Phys. B* **325** (1989) 33; J.M. Flynn and L. Randall, *Phys. Lett. B* **224** (1989) 221.
- [47] A. Pich and E. de Rafael, *Nucl. Phys. B* **358** (1991) 311.
- [48] B. Holstein, *Phys. Rev. D* **20** (1979) 1187; J.F. Donoghue, E. Golowich, B.R. Holstein and J. Trampetic, *Phys. Lett. B* **179** (1986) 361; A.J. Buras and J.M. Gerard, in ref. [46].

- [49] J. Kambor, J. Missimer and D. Wyler, *Nucl. Phys. B* **346** (1990) 17; *Phys. Lett. B* **261** (1991) 496.
- [50] V. Antonelli et al., *Nucl. Phys. B* **469** (1996) 143; *Nucl. Phys. B* **469** (1996) 181; S. Bertolini, J.O. Eeg and M. Fabbrichesi, *Nucl. Phys. B* **476** (1996) 225;

# Supersymmetric effects in rare semileptonic decays of $B$ and $K$ mesons

GINO ISIDORI

*Theory Division, CERN, CH-1211 Geneva 23, Switzerland \**

Rare flavour-changing neutral-current transitions of the type  $s \rightarrow d \ell^+ \ell^- (\nu \bar{\nu})$  and  $b \rightarrow s \ell^+ \ell^- (\nu \bar{\nu})$  are analysed in supersymmetric extensions of the Standard Model with generic flavour couplings. It is shown that these processes are particularly sensitive to the left-right mixing of the squarks and that, in the presence of non-universal  $A$  terms, they could lead to unambiguous signatures of new physics in exclusive  $K$  and  $B$  meson decays.

Presented at the

5th International Symposium on Radiative Corrections  
(RADCOR-2000)

Carmel CA, USA, 11–15 September 2000

---

\*On leave from INFN, Laboratori Nazionali di Frascati, Via Enrico Fermi 40, I-00044 Frascati (Rome), Italy.

# 1 Introduction

Flavour-changing neutral-current (FCNC) processes are one of the most powerful tools in probing the structure of flavour beyond the Standard Model (SM): the strong suppression of these transitions occurring within the SM, which is due to the Glashow–Iliopoulos–Maiani (GIM) mechanism [1] and to the hierarchy of the Cabibbo–Kobayashi–Maskawa (CKM) matrix [2], ensures a large sensitivity to possible non-standard effects, even if these occur at very high energy scales.

In the present talk we focus on a specific class of  $\Delta F = 1$  FCNC transitions:

$$s \rightarrow d \ell^+ \ell^- (\nu \bar{\nu}) \quad \text{and} \quad b \rightarrow s \ell^+ \ell^- (\nu \bar{\nu}) . \quad (1)$$

As we shall discuss, these are particularly interesting for the following reasons:

- These transitions have a strong sensitivity to supersymmetric extensions of the SM with flavour non-universal soft-breaking terms. Taking into account all the existing phenomenological constraints, within this type of models it is possible to generate sizeable non-standard effects to the partonic processes in (1).
- The existing experimental constraints on these transitions are rather weak, but in the near future it will be possible to perform stringent tests by means of exclusive rare  $K$  and  $B$  meson decays.

In the rest of the talk we shall illustrate these two points in more detail. Section 2 is devoted to the analysis of the supersymmetric contributions to  $d_j \rightarrow d_i \ell^+ \ell^- (\nu \bar{\nu})$  transitions, including a discussion about the indirect bounds obtained by other processes. In Sections 3–5 we analyse how to extract information on these partonic transitions by means of experimental data on  $K \rightarrow \pi \nu \bar{\nu}$ ,  $K_L \rightarrow \pi^0 e^+ e^-$  and exclusive  $b \rightarrow s \ell^+ \ell^- (\nu \bar{\nu})$  decays, respectively.

## 2 SUSY contributions to $d_j \rightarrow d_i \ell^+ \ell^- (\nu \bar{\nu})$ transitions in models with non-universal soft-breaking terms

The class of supersymmetric extensions of the SM that we shall consider is the so-called unconstrained MSSM (see e.g. [3,4]). This model has the minimal number of new fields necessary to build a consistent SUSY version of the SM, namely all the superpartners of the SM fields plus an extra SUSY Higgs doublet. On the contrary, the assumptions made on the soft-breaking terms are very general. The only condition we shall impose on the flavour structure of the soft-breaking terms is a non-universal linear relation between the trilinear terms ( $Y_{ij}^A$ ) and the Yukawa couplings ( $y_k$ ), leading to

$$Y_{ij}^A = \mathcal{O}(y_k M_S) , \quad k = \max(i, j) , \quad (2)$$

where  $M_S$  denotes a common soft-breaking scale [ $M_{ij} = \mathcal{O}(M_S^2)$  for the bilinear terms]. This condition let us to avoid charge- and colour-breaking minima or unbounded directions in the SUSY potential [5]. The proportionality coefficients will be assumed to be  $\mathcal{O}(1)$ , unless more stringent constraints are imposed by experimental data.

Similarly to the SM, also within this context FCNC amplitudes involving external quark fields turn out to be generated only at the quantum level. Given the large number of new off-diagonal flavour couplings, the simplest way to parametrize the new effect is provided by the so-called mass-insertion approximation [3,4]. This consists of choosing a simple basis for the gauge interactions and, in that basis, to perform a perturbative expansion of the squark mass matrices around their diagonal. Being interested in processes with external down-type quarks, we will employ in the following a squark basis where all quark–squark–gaugino vertices involving down-type quarks are flavour-diagonal. In this basis we then define the following adimensional couplings:

$$\left(\delta_{AB}^{[U,D]}\right)_{ij} = \left(M_{[U,D]}^2\right)_{i_A j_B} / \langle M_{[U,D]}^2 \rangle \quad , \quad (3)$$

where  $A, B$  denote the helicity ( $L, R$ ) and  $i, j$  the family. These couplings constitute the basic tool to parametrize and classify the new contributions to FCNC amplitudes arising within the unconstrained MSSM.

SUSY contributions to  $d_j \rightarrow d_i \ell^+ \ell^- (\nu \bar{\nu})$  transitions can also be divided into three groups according to the diagrams (or the effective operators) that generate it: box and helicity-conserving photon-penguins (generic dimension-6 operators), magnetic penguins (dimension-5 operators) and  $Z$  penguins. In each of these classes a different type of delta plays a dominant role.

**Generic dimension-6 operators.** Box diagrams with internal chargino or neutralino fields and, in the case of charged leptons, also photon-penguin diagrams with internal gluino, chargino or neutralino fields, can lead to effective FCNC operators of the type

$$\left(\bar{d}_A^i \gamma^\mu d_A^j\right) \left(\bar{l}_B \gamma_\mu l_B\right) \quad . \quad (4)$$

Since the external quarks have the same helicity, the potentially leading SUSY contributions to the Wilson coefficients of these operators are generated by helicity-conserving couplings:

$$\frac{\left(\delta_{AA}^{[U,D]}\right)_{ij}}{M_S^2} \quad . \quad (5)$$

The dimensional factor in Eq. (5), due to the integration of heavy SUSY degrees of freedom, indicates explicitly that these contributions vanish as  $1/M_S^2$  in the limit of a large SUSY-breaking scale.

The helicity-violating couplings  $\delta_{LR}^Q$  appear in the Wilson coefficients of dimension-6 operators only to second order in the mass expansion, with contributions

of the type [6]

$$\frac{(\delta_{LR}^U)_{i3}(\delta_{RL}^U)_{3j}}{M_S^2} . \quad (6)$$

Since the left–right mixing is generated by the trilinear terms, then  $\delta_{LR}^Q = \mathcal{O}(m_q/M_S)$  and the contribution in (6) vanishes as  $1/M_S^4$  for large  $M_S$ . Thus the effect of helicity-violating couplings is not only disfavoured by the fact that it requires a double insertion, but it is also parametrically suppressed in the limit of a large SUSY-breaking scale. As we shall see below, this is not the case only in a specific type of dimension-6 operators: those generated by  $Z$  penguins.

On the other hand, both helicity-conserving and helicity-violating contributions to generic dimension-6 operators turn out to be negligible with respect to the SM ones, once the bounds from  $\Delta F = 2$  processes are taken into account [7]. This fact can be understood by a naive dimensional argument in the limit of large  $M_S$  [8]. Indeed, considering for simplicity only the case of  $\delta_{AA}^Q$ , it is easy to show that the SUSY contribution to  $\Delta F = 2$  amplitudes –appearing necessarily at the second order in the mass expansion– are of  $\mathcal{O}[(\delta_{AA}^Q/M_S)^2]$ . Thus the limits on  $\delta_{AA}^Q$  arising from  $\Delta F = 2$  amplitudes scale linearly with  $M_S$  and not quadratically, as in the  $\Delta F = 1$  case. As a result, SUSY contributions to  $d_j \rightarrow d_i \ell^+ \ell^- (\nu \bar{\nu})$  transitions generated by box diagrams and helicity-conserving photon-penguins turn out to be extremely suppressed for  $M_S \gtrsim 1$  TeV.<sup>1</sup>

**Magnetic penguins.** The integration of the heavy SUSY degrees of freedom in penguin-like diagrams can also lead to operators with dimension lower than 6, creating an effective FCNC coupling between quarks and SM gauge fields. In the case of the photon field, the unbroken electromagnetic gauge invariance implies that the lowest-dimensional coupling is provided by the so-called magnetic operator

$$\bar{d}_{L(R)}^i \sigma^{\mu\nu} d_{R(L)}^j F_{\mu\nu} . \quad (7)$$

Here the potentially leading SUSY contribution is induced by helicity-violating couplings, and in particular by the left–right mixing of down-type squarks, which can appear in gluino-exchange diagrams:

$$\frac{(\delta_{LR}^D)_{ij}}{M_S} . \quad (8)$$

Since the operator (7) has dimension 5, the explicit dimensional suppression of the left–right mixing contribution is only  $1/M_S$ . Nonetheless, also in this case the overall SUSY effect decouples as  $1/M_S^2$  since  $\delta_{LR}^Q = \mathcal{O}(m_q/M_S)$ .

---

<sup>1</sup>A similar argument holds for SUSY contributions to  $d_j \rightarrow d_i \bar{q} q$  transitions [8], with the notable exception of  $\Delta I = 3/2$  amplitudes [9].

The appearance of a single inverse power of  $M_S$  in Eq. (8) has the important consequence that this contribution can naturally evade the  $\Delta F = 2$  constraints and compete with the SM term [4,12,8]. This is not the case for contributions generated by helicity-conserving couplings or left–right mixing in the up sector, which appear only beyond the first order in the mass insertion.

In the  $b \rightarrow s$  case the most significant constraint on possible non-standard effects in the magnetic operator is provided by the inclusive process  $B \rightarrow X_s \gamma$  (see e.g. [10] for an updated discussion). The recent measurements [11] exclude SUSY contributions substantially larger than the SM one, or imply bounds of  $\mathcal{O}(10^{-2})$  on  $|(\delta_{LR}^D)_{23}|$ . Note, however, that the assumption made on the trilinear terms implies

$$|(\delta_{LR}^D)_{23}| \lesssim \frac{m_b}{M_S} \simeq 10^{-2} \left( \frac{500 \text{ GeV}}{M_S} \right), \quad (9)$$

then the  $B \rightarrow X_s \gamma$  measurement does not pose a serious fine-tuning constraint about the non-universality of  $A$  terms.

Concerning the  $s \rightarrow d$  case, there are no significant constraints on  $|(\delta_{LR}^D)_{12}|$ , whereas a stringent bound on  $|\text{Im}(\delta_{LR}^D)_{12}|$  can be derived from  $\varepsilon'/\varepsilon$  [12]. The latter is obtained by constraining the SUSY contribution to the chromo-magnetic operator (closely related to the magnetic one) and implies [8]:

$$|\text{Im}(\delta_{LR}^D)_{12}| \leq 4 \times 10^{-5} \left( \frac{M_S}{500 \text{ GeV}} \right). \quad (10)$$

This limit is more stringent than the upper bound on  $|(\delta_{LR}^D)_{12}|$  imposed by (2), namely

$$|(\delta_{LR}^D)_{23}| \lesssim \frac{m_s}{M_S} \simeq 2 \times 10^{-4} \left( \frac{500 \text{ GeV}}{M_S} \right), \quad (11)$$

but it is much higher than the value assumed by  $|\text{Im}(\delta_{LR}^D)_{12}|$  within the flavour-constrained MSSM [13]. Interestingly, if  $\text{Im}(\delta_{LR}^D)_{12} = \mathcal{O}(10^{-5})$  it is possible to conceive a scenario where all CP-violating effects observed so far in the kaon sector ( $\varepsilon$  and  $\varepsilon'$ ) are of SUSY origin [14,15]. As we shall discuss in the next sections, this scenario would produce very clear signatures in rare  $K$  decays.

**$Z$  penguins.** Thanks to the spontaneous breaking of  $SU(2)_L$ , in the case of  $Z$  penguins the integration of the SUSY degrees of freedom can lead to an effective FCNC operator of dimension 4:

$$\bar{q}_L^i \gamma^\mu d_L^j Z_\mu. \quad (12)$$

This operator generates a dimension-6 structure like the one in Eq. (4) when the heavy  $Z$  field is integrated out. In this case, however, the dimensional suppression is provided by  $1/M_Z^2$  and there is no explicit trace of  $M_S$ . The

latter is hidden in the dimensionless coupling of the operator (12), denoted by  $Z_{ji}^L$ , that requires a double mixing between  $SU(2)_L$ -singlet and  $SU(2)_L$ -doublet fields,<sup>2</sup> and thus vanishes as  $1/M_S^2$  for large  $M_S$ . The potentially dominant contributions to  $Z_{ji}^L$  arise from chargino loops, either by a double left-right insertion in the up-squark propagators [6] or by a single insertion together with wino-higgsino mixing [7,18]:

$$Z_{ji}^L \sim \begin{cases} (\delta_{LR}^U)_{j3}(\delta_{RL}^U)_{3i} \\ (m_t/M_S)V_{j3}(\delta_{RL}^U)_{3i} \end{cases} \quad (13)$$

As can be noted, in both cases  $Z_{ji}^L = \mathcal{O}(m_t^2/M_S^2)$ , where the  $m_t$  factor arises from the Yukawa coupling of the third generation. Since the left-right mixing in the up sector provides a subleading contribution to generic dimension-6 operators and, in particular, to  $\Delta F = 2$  transitions, the indirect constraints on these effects are rather weak. If  $(\delta_{RL}^U)_{3i}$  lies in the window

$$\frac{m_t}{M_W}|V_{3i}| \lesssim |(\delta_{LR}^U)_{3i}| \lesssim \frac{m_t}{M_S}, \quad (14)$$

then SUSY contributions to  $Z_{ji}^L$  turn out to be comparable or even larger than the SM one. On the contrary, contributions to  $Z_{ji}^L$  from helicity-conserving couplings or left-right mixing in the down sector are always negligible.

In the  $b \rightarrow s$  case some phenomenological constraints on  $|Z_{sb}^L|$  can be obtained directly from exclusive and inclusive  $b \rightarrow s \ell^+ \ell^- (\nu \bar{\nu})$  transitions [18,16]. The latter are certainly cleaner from the theoretical point of view; however, their experimental determination is quite difficult. Indeed the most stringent constraint, at present, is the one extracted from  $B \rightarrow K^* \mu^+ \mu^-$  [16], where the experimental upper bound on the non-resonant branching ratio lies only about a factor of 2 above the SM expectation. This constraint implies a bound of  $\mathcal{O}(1)$  on  $|(\delta_{LR}^U)_{3i}|$ , which is still outside the window (14).

Owing to the smallness of  $V_{td}$ , the window (14) is much larger in the case of  $s \rightarrow d$  transitions. Here the most stringent constraints on  $Z_{ds}^L$  arise from  $K_L \rightarrow \mu^+ \mu^-$  (on the real part) and  $\varepsilon'/\varepsilon$  (on the imaginary part) [19]. Without entering into a detailed discussion about these bounds, which can be found elsewhere [8], we

---

<sup>2</sup>Here and in the following we employ the normalization of  $Z_{ji}^L$  in [8,16]:

$$\mathcal{L}_{\text{FC}}^Z = \frac{G_F}{\sqrt{2}} \frac{e}{\pi^2} M_Z^2 \frac{\cos \Theta_W}{\sin \Theta_W} Z^\mu Z_{ji}^L \bar{q}_L^i \gamma_\mu q_L^j + \text{h.c.} .$$

With this normalization the SM contribution to  $Z_{ji}^L$ , evaluated in the 't Hooft-Feynman gauge, is given by  $Z_{ji}^L|_{\text{SM}} \simeq C_0(x_t)V_{3i}^*V_{3j}$ , where  $V_{ij}$  denote CKM matrix elements,  $x_t = m_t^2/m_W^2$  and the function  $C_0(x)$  can be found in [17]. We further stress that the leading  $\mathcal{O}(x_t)$  contributions to FCNC  $Z$  penguins are gauge-invariant within both SM and MSSM.

simply note that: i) the sizeable uncertainties due to non-perturbative effects in both  $K_L \rightarrow \mu^+\mu^-$  and  $\varepsilon'/\varepsilon$  do not allow us to extract precise constraints; ii) taking into account these uncertainties, the present bounds on  $Z_{ds}^L$  are within the window (14) and allow for  $\mathcal{O}(1)$  deviations from the SM at the amplitude level.

Summarizing, we can say that only the flavour-violating left–right mixing among the squarks can naturally lead to large effects in the transitions (1). In the  $s \rightarrow d$  case this can happen either via magnetic penguins [ruled by  $(\delta_{LR}^D)_{12}$ ] or via  $Z$  penguins [ruled by  $(\delta_{LR}^U)_{13}$  and  $(\delta_{LR}^U)_{23}$ ], whereas  $b \rightarrow s$  magnetic penguins are strongly constrained by  $B \rightarrow X_s\gamma$ . Moreover, we have seen that under the assumption (2) the present constraints about the non-universality of the trilinear terms are all rather weak, both for up- and down-type squarks. We believe that this observation strengthens the interest in searching for sizeable non-standard effects in the transitions (1).

### 3 $K \rightarrow \pi\nu\bar{\nu}$

These decays are considered the golden modes for a precise measurement of the  $s \rightarrow d\nu\bar{\nu}$  transition. Within the SM, separating the contributions to the  $s \rightarrow d\nu\bar{\nu}$  amplitude according to the intermediate up-type quark running inside the loop, one can write

$$\mathcal{A}(s \rightarrow d\nu\bar{\nu})_{\text{SM}} = \sum_{q=u,c,t} V_{qs}^* V_{qd} \mathcal{A}_q \sim \begin{cases} \mathcal{O}(\lambda^5 m_t^2) + i\mathcal{O}(\lambda^5 m_t^2) & (q = t) \\ \mathcal{O}(\lambda m_c^2) + i\mathcal{O}(\lambda^5 m_c^2) & (q = c) \\ \mathcal{O}(\lambda \Lambda_{QCD}^2) & (q = u) \end{cases} \quad (15)$$

The hierarchy of the CKM matrix elements would favour up- and charm-quark contributions; however, the hard GIM mechanism of the parton-level calculation implies  $\mathcal{A}_q \sim m_q^2/M_W^2$ , leading to a completely different scenario. As shown on the r.h.s. of Eq. (15), where we have employed the standard phase convention ( $\text{Im}V_{us} = \text{Im}V_{ud} = 0$ ) and expanded the CKM matrix in powers of the Cabibbo angle ( $\lambda = 0.22$ ) [20], the top-quark contribution dominates both real and imaginary parts. This structure implies that  $\mathcal{A}(s \rightarrow d\nu\bar{\nu})_{\text{SM}}$  is dominated by short-distance dynamics and therefore calculable with high precision in perturbation theory.

The leading short-distance contributions to  $\mathcal{A}(s \rightarrow d\nu\bar{\nu})$ , both within the SM and within its SUSY extension discussed before, can be described by means of a single effective dimension-6 operator:

$$Q_L^\nu = (\bar{s}_L \gamma^\mu d_L)(\bar{\nu}_L \gamma_\mu \nu_L), \quad (16)$$

whose Wilson coefficient has been calculated at the next-to-leading order within the SM [21] (see also [22,23]). The simple structure of  $Q_L^\nu$  has two major advantages:

- the relation between partonic and hadronic amplitudes is very accurate, since the hadronic matrix elements of the  $\bar{s}\gamma^\mu d$  current between a kaon and a pion are related by isospin symmetry to those entering  $K_{l3}$  decays, which are experimentally well known;
- the lepton pair is produced in a state of definite CP and angular momentum, implying that the leading contribution to  $K_L \rightarrow \pi^0 \nu \bar{\nu}$  is CP-violating.

The dominant theoretical error in estimating  $\mathcal{B}(K^+ \rightarrow \pi^+ \nu \bar{\nu})_{\text{SM}}$  is due to the uncertainty of the QCD corrections to the charm contribution (see [23] for an updated discussion), which can be translated into a 5% error in the determination of  $|V_{td}|$  from  $\mathcal{B}(K^+ \rightarrow \pi^+ \nu \bar{\nu})$ <sup>3</sup>. Genuine long-distance effects associated to the up quark have been shown to be substantially smaller [25].

The case of  $K_L \rightarrow \pi^0 \nu \bar{\nu}$  is even cleaner from the theoretical point of view [26]. Indeed, because of the CP structure, only the imaginary parts in (15) –where the charm contribution is absolutely negligible– contribute to  $\mathcal{A}(K_2 \rightarrow \pi^0 \nu \bar{\nu})_{\text{SM}}$ . Thus the dominant direct-CP-violating component of  $\mathcal{A}(K_L \rightarrow \pi^0 \nu \bar{\nu})_{\text{SM}}$  is completely saturated by the top contribution, where the QCD uncertainties are very small (around 1%). Intermediate and long-distance effects in this process are confined to the indirect-CP-violating contribution [27] and to the CP-conserving one [28] which are both extremely small. Taking into account also the isospin-breaking corrections to the hadronic matrix element [29], one can write an expression for  $\mathcal{B}(K_L \rightarrow \pi^0 \nu \bar{\nu})_{\text{SM}}$  in terms of short-distance parameters with a theoretical error below 3% [23,27]:

$$\mathcal{B}(K_L \rightarrow \pi^0 \nu \bar{\nu})_{\text{SM}} = 4.16 \times 10^{-10} \left[ \frac{\overline{m}_t(m_t)}{167 \text{ GeV}} \right]^{2.3} \left[ \frac{\text{Im}\lambda_t}{\lambda^5} \right]^2, \quad (17)$$

where  $\lambda_t = V_{ts}^* V_{td}$ .

Taking into account all the indirect constraints on  $\text{Im}(V_{ts}^* V_{td})$  [30], the present range of SM predictions for the two  $K \rightarrow \pi \nu \bar{\nu}$  branching ratios is reported in the second column of Table 1. In the following three columns, we show the upper bounds obtained within three SUSY scenarios with non-trivial  $(\delta_{LR}^U)_{i3}$  and  $(\delta_{LR}^U)_{12}$ . In all cases the SUSY flavour-mixing terms, as well as CKM matrix elements, have been constrained taking into account the measurement of  $\varepsilon$ ,  $\varepsilon'$ ,  $K_L \rightarrow \mu^+ \mu^-$  and the respective theoretical uncertainties [8]. As can be noticed, the two neutrino modes could provide sizeable unambiguous signatures of SUSY, but only in the presence of a large left–right mixing in the up sector. Interestingly, the present measurement of  $\mathcal{B}(K^+ \rightarrow \pi^+ \nu \bar{\nu})$  [31] is very close to putting serious constraints (or to providing some evidence...) on this scenario.

---

<sup>3</sup>Very recently also the subleading effect of  $\mathcal{O}(m_K^2/m_c^2)$  induced by dimension-8 operators has been estimated [24]. This effect is not calculable precisely, but it is likely to be smaller than (or at most as large as) the uncertainty in the QCD corrections to the leading term [24].

Observable	SM	SUSY scenarios			exp. data
		A	B	C	
$10^{10} \times \mathcal{B}(K^+ \rightarrow \pi^+ \nu \bar{\nu})$	$0.71 \pm 0.12$	$\leq \mathcal{B}_{\text{SM}}$	$\leq 2.1$	$\leq 2.7$	$1.5_{-1.3}^{+3.5}$ [31]
$10^{10} \times \mathcal{B}(K_L \rightarrow \pi^0 \nu \bar{\nu})$	$0.22 \pm 0.05$	$\leq \mathcal{B}_{\text{SM}}$	$\leq 1.7$	$\leq 4.0$	$< 5.9 \times 10^3$ [32]
$10^{11} \times \mathcal{B}(K_L \rightarrow \pi^0 e^+ e^-)_{\text{dir}}$	$0.35 \pm 0.07$	$\leq 2.0$	$\leq 3.0$	$\leq 10$	$< 58$ [33]

Table 1: SM expectations, experimental data and upper bounds within different SUSY scenarios for the branching ratios of the rare decays  $K_L \rightarrow \pi^0 \nu \bar{\nu}$ ,  $K_L \rightarrow \pi^0 e^+ e^-$  and  $K^+ \rightarrow \pi^+ \nu \bar{\nu}$ . The three SUSY scenarios correspond to [8]: A)  $(\delta_{LR}^U)_{i3} = 0$ ,  $(\delta_{LR}^U)_{12} \neq 0$ ,  $0 \leq \text{Im}(\lambda_t) \leq \text{Im}(\lambda_t)_{\text{SM}}$ ; B)  $(\delta_{LR}^U)_{12} = 0$ ,  $(\delta_{LR}^U)_{i3} \neq 0$ ,  $0 \leq \text{Im}(\lambda_t) \leq \text{Im}(\lambda_t)_{\text{SM}}$ ; C)  $(\delta_{LR}^U)_{12} \neq 0$ ,  $(\delta_{LR}^U)_{i3} \neq 0$ ,  $|\text{Im}(\lambda_t)| \leq 1.73 \times 10^{-4}$ .

#### 4 $K_L \rightarrow \pi^0 e^+ e^-$

Similarly to  $K \rightarrow \pi \nu \bar{\nu}$  decays, also the short-distance contributions to  $K \rightarrow \pi \ell^+ \ell^-$  transitions are calculable with high accuracy. Long-distance contributions to the latter, however, are much larger owing to the presence of electromagnetic interactions. Only in few cases (mainly in CP-violating observables) are long-distance contributions suppressed and is it possible to extract the interesting short-distance information.

The single-photon exchange amplitude, dominated by long-distance dynamics, provides the largest contribution to the CP-allowed transitions  $K^+ \rightarrow \pi^+ \ell^+ \ell^-$  and  $K_S \rightarrow \pi^0 \ell^+ \ell^-$ . The former has been observed, both in the electron and in the muon mode, whereas only an upper bound of  $1.6 \times 10^{-7}$  exists on  $\mathcal{B}(K_S \rightarrow \pi^0 e^+ e^-)$  [34]. On the contrary, the long-distance part of the single-photon exchange amplitude is forbidden by CP invariance in the  $K_L \rightarrow \pi^0 \ell^+ \ell^-$  channels, which are much more interesting from the short-distance point of view (especially the electron mode).

In  $K_L \rightarrow \pi^0 e^+ e^-$  we can distinguish three independent (and comparable) contributions: direct-CP-violating, indirect-CP-violating and CP-conserving.

The direct-CP-violating part of the  $K_L \rightarrow \pi^0 e^+ e^-$  amplitude is very similar to the  $K_L \rightarrow \pi^0 \nu \bar{\nu}$  one, but for the fact that it receives an additional short-distance contribution from the photon penguin. Within the SM, this theoretically clean part of the amplitude leads to [35]

$$\mathcal{B}(K_L \rightarrow \pi^0 e^+ e^-)_{\text{dir}}^{\text{SM}} = 6.5 \times 10^{-11} \left[ \frac{\overline{m}_t(m_t)}{167 \text{ GeV}} \right]^2 \left[ \frac{\text{Im}\lambda_t}{\lambda^5} \right]^2. \quad (18)$$

The present range of variation, together with SUSY upper bounds, is reported in the last line of Table 1. Being sensitive also to the photon penguin, the  $K_L \rightarrow \pi^0 e^+ e^-$  amplitude could be substantially modified also in the presence of non-trivial SUSY phases in the down sector. In particular, within the interesting scenario where all CP-violating effects observed in the kaon sector were due to  $\text{Im}(\delta_{LR}^D)_{12} = \mathcal{O}(10^{-5})$ ,

$\mathcal{B}(K_L \rightarrow \pi^0 e^+ e^-)_{\text{dir}}^{\text{SM}}$  would be close to its SM value, whereas  $\mathcal{B}(K_L \rightarrow \pi^0 \nu \bar{\nu})$  would be vanishingly small.

In principle the direct-CP-violating part of the  $K_L \rightarrow \pi^0 e^+ e^-$  amplitude could be experimentally isolated from the other two contributions, especially if it were large. In order to achieve this goal it would be necessary to measure  $\mathcal{B}(K_S \rightarrow \pi^0 e^+ e^-)$  or to put a stringent bound on it. The two CP-violating components of the  $K_L \rightarrow \pi^0 e^+ e^-$  amplitude will in general interfere, and the indirect-CP-violating one alone would lead to

$$\mathcal{B}(K_L \rightarrow \pi^0 e^+ e^-)_{\text{CPV-ind}} = 3 \times 10^{-3} \mathcal{B}(K_S \rightarrow \pi^0 e^+ e^-). \quad (19)$$

Since the relative phase of the two CP-violating amplitudes is known, once  $\mathcal{B}(K_S \rightarrow \pi^0 e^+ e^-)$  will be measured, it will be possible to determine the interference between direct and indirect CP-violating components of  $\mathcal{B}(K_L \rightarrow \pi^0 e^+ e^-)_{\text{CP}}$  up to a sign ambiguity.

The CP-conserving contribution to  $K_L \rightarrow \pi^0 e^+ e^-$ , generated by a two-photon intermediate state, does not interfere with the CP-violating ones and is expected to be in the  $10^{-12}$  range. The relative weight of this contribution can be further constrained by appropriate kinematical cuts; it should therefore not represent a problem if  $\mathcal{B}(K_L \rightarrow \pi^0 e^+ e^-)$  will be found in the  $10^{-11}$  range.

## 5 Exclusive $b \rightarrow s \ell^+ \ell^- (\nu \bar{\nu})$ decays

The starting point for the analysis of  $b \rightarrow s \ell^+ \ell^- (\nu \bar{\nu})$  transitions, both within the SM and the SUSY scenario discussed in Section 2, is the following effective Hamiltonian:

$$\mathcal{H}_{\text{eff}} = -\frac{G_F}{\sqrt{2}} V_{ts}^* V_{tb} \left( \sum_{i=1}^{10} [C_i Q_i + C'_i Q'_i] + C_L^\nu Q_L^\nu + C_R^\nu Q_R^\nu \right) + \text{h.c.} . \quad (20)$$

Here  $Q_i$  denotes the Standard Model basis of operators relevant to  $b \rightarrow s \ell^+ \ell^-$  [17] and  $Q'_i$  their helicity flipped counterparts. In particular, we recall that  $Q_i \sim (\bar{s} \gamma_\mu b)(\bar{\ell} \gamma^\mu \ell)$ , for  $i = 1 \dots 6$ ,  $Q_7 \sim m_b \bar{s}_L (\sigma \cdot F) b_R$ ,  $Q_8 \sim m_b \bar{s}_L (\sigma \cdot G) b_R$ ,  $Q_9 \sim (\bar{s}_L \gamma_\mu b_L)(\bar{\ell} \gamma^\mu \ell)$ ,  $Q_{10} \sim (\bar{s}_L \gamma_\mu b_L)(\bar{\ell} \gamma^\mu \gamma_5 \ell)$  and  $Q_{L(R)}^\nu \sim (\bar{s}_{L(R)} \gamma_\mu b_{L(R)})(\bar{\nu}_L \gamma^\mu \nu_L)$ . The operators that have a non-vanishing matrix element already at the tree level and thus play the dominant role in  $b \rightarrow s \ell^+ \ell^-$  are  $Q_7$ ,  $Q_9$ ,  $Q_{10}$  and their helicity flipped counterparts. On the other hand, only  $Q_{L(R)}^\nu$  have a non-vanishing matrix element in  $b \rightarrow s \nu \bar{\nu}$ .

Rate and CP asymmetry in  $B \rightarrow X_s \gamma$  already provide serious constraints on possible deviations from the SM in  $C_7$  and  $C'_7$  [10], and these bounds will soon improve with new data on  $B \rightarrow X_s \gamma$ . However, as we have discussed in Section 2, even if no new-physics effects are found in the magnetic operator, one could still expect sizeable SUSY contributions mediated by the  $Z$  penguin. In the following we shall concentrate only on the latter type of effects. Under this assumption, a rather simplified scenario

emerges, where  $C_R^{\nu} = C_i^{\nu} = 0$  and only  $C_{10}$  and  $C_L^{\nu}$  are substantially modified from their SM value [16].

Moreover, even though inclusive measurements are certainly more suitable for precise determinations of short-distance parameters, here we shall discuss only exclusive decays, which have a clear advantage from the experimental point of view. Within the SM the following exclusive branching ratios are expected, compared here with the current experimental limits:

$$\begin{aligned}
\mathcal{B}(B \rightarrow K\nu\bar{\nu}) &\approx 4 \times 10^{-6} &< 7.7 \times 10^{-4} & [37] \\
\mathcal{B}(B \rightarrow K^*\nu\bar{\nu}) &\approx 1.3 \times 10^{-5} &< 7.7 \times 10^{-4} & [37] \\
\mathcal{B}(B \rightarrow K\mu^+\mu^-)^{\text{n.r.}} &\approx 6 \times 10^{-7} &< 5.2 \times 10^{-6} & [38] \\
\mathcal{B}(B \rightarrow K^*\mu^+\mu^-)^{\text{n.r.}} &\approx 2 \times 10^{-6} &< 4 \times 10^{-6} & [38] \\
\mathcal{B}(B_s \rightarrow \mu^+\mu^-) &\approx 3 \times 10^{-9} &< 2.6 \times 10^{-6} & [39]
\end{aligned} \tag{21}$$

The corresponding hadronic uncertainties are typically around  $\pm 30\%$  (see e.g. [36] for an updated discussion). As already mentioned, the channel that sets the strongest constraint on the FCNC  $Z$  penguin is  $B \rightarrow K^*\mu^+\mu^-$ . In the optimistic case where  $Z_{bs}^L$  is close to saturating this bound, we would be able to detect the presence of non-standard dynamics already by observing sizeable rate enhancements in the above listed branching ratios. In processes such as  $B \rightarrow K^*\ell^+\ell^-$  and  $B \rightarrow K\ell^+\ell^-$ , where the standard photon-penguin diagrams provide a large contribution, the enhancement could be at most a factor of 2. On the other hand, in processes such as  $B \rightarrow K^*\nu\bar{\nu}$ ,  $B \rightarrow K\nu\bar{\nu}$  and  $B_s \rightarrow \mu^+\mu^-$ , where the photon-exchange amplitude is forbidden, the maximal enhancement could reach a factor of 10 [16].

### 5.1 Forward-backward asymmetry in $B \rightarrow K^*\mu^+\mu^-$

If SUSY effects were not large enough to produce sizeable deviations in the magnitude of the  $b \rightarrow Z^*s$  transition, as expected unless  $|(\delta_{LR}^U)_{32}|$  were very close to the upper bound in Eq. (14), it would be hard to detect them from exclusive rate measurements. A more interesting observable in this respect is provided by the forward-backward (FB) asymmetry of the emitted leptons. In the  $\bar{B} \rightarrow \bar{K}^*\mu^+\mu^-$  case this is defined as

$$\begin{aligned}
\mathcal{A}_{\text{FB}}^{(\bar{B})}(s) &= \frac{1}{d\Gamma(\bar{B} \rightarrow \bar{K}^*\mu^+\mu^-)/ds} \int_{-1}^1 d\cos\theta \\
&\frac{d^2\Gamma(\bar{B} \rightarrow \bar{K}^*\mu^+\mu^-)}{ds d\cos\theta} \text{sgn}(\cos\theta) ,
\end{aligned} \tag{22}$$

where  $s = m_{\mu^+\mu^-}^2/m_B^2$  and  $\theta$  is the angle between the momenta of  $\mu^+$  and  $\bar{B}$  in the dilepton centre-of-mass frame. Assuming that the leptonic current has only a vector (V) or axial-vector (A) structure, then the FB asymmetry provides a direct measure

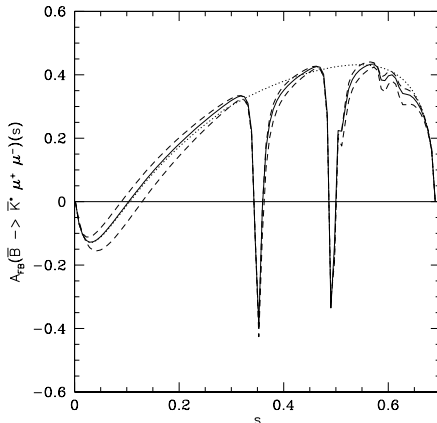


Figure 1: *FB asymmetry of  $\bar{B} \rightarrow \bar{K}^* \mu^+ \mu^-$  within the SM. The solid (dotted) curves have been obtained employing the Krueger–Sehgal [42] approach (using the perturbative end-point effective Hamiltonian [16]). The dashed lines show the effect of varying the renormalization scale of the Wilson coefficients between  $m_b/2$  and  $2m_b$ , within the Krueger–Sehgal approach.*

of the  $A$ - $V$  interference. Since the vector current is largely dominated by the photon-exchange amplitude and the axial one is very sensitive to the  $Z$  exchange,  $\mathcal{A}_{\text{FB}}^{(\bar{B})}$  and  $\mathcal{A}_{\text{FB}}^{(B)}$  provide an excellent tool to probe the  $Z\bar{b}s$  vertex. Indeed  $\mathcal{A}_{\text{FB}}^{(\bar{B})}(s)$  turns out to be proportional to<sup>4</sup>

$$\text{Re} \left\{ C_{10}^* \left[ s C_9^{\text{eff}}(s) + \alpha_+(s) \frac{m_b C_7}{m_B} \right] \right\}, \quad (23)$$

where  $\alpha_+(s)$  is an appropriate ratio of hadronic form factors [16,40]. The overall factor ruling the magnitude of  $\mathcal{A}_{\text{FB}}^{(\bar{B})}(s)$  is affected by sizeable theoretical uncertainties. Nonetheless there are at least three features of this observable that provide a clear short-distance information:

i) Within the SM  $\mathcal{A}_{\text{FB}}^{(\bar{B})}(s)$  has a zero in the low- $s$  region ( $s_0|_{\text{SM}} \sim 0.1$ ) [40]. The exact position of  $s_0$  is not free from hadronic uncertainties at the 10% level; nonetheless, the existence of the zero itself is a clear test of the relative sign between  $C_7$  and  $C_9$ . The position of  $s_0$  is essentially unaffected by possible new-physics effects in the  $Z\bar{b}s$  vertex.

ii) The sign of  $\mathcal{A}_{\text{FB}}^{(\bar{B})}(s)$  around the zero is fixed unambiguously in terms of the relative sign of  $C_{10}$  and  $C_9$  [16]: within the SM one expects  $\mathcal{A}_{\text{FB}}^{(\bar{B})}(s) > 0$  for  $s > s_0$ , as in Fig. 1. This prediction is based on a model-independent relation between the form factors [41]. Interestingly, the sign of  $C_{10}$  could change in the presence of a

<sup>4</sup>To simplify the notation we have introduced the parameter  $C_9^{\text{eff}}(s)$ , which is not a Wilson coefficient but can be identified with  $C_9$  at the leading-log level [16].

non-standard  $Z\bar{b}s$  vertex, leading to a striking signal of new physics in  $\mathcal{A}_{\text{FB}}^{(\bar{B})}(s)$ , even if the rate of  $\bar{B} \rightarrow \bar{K}^*\mu^+\mu^-$  were close to its SM value.

iii) In the limit of CP conservation, one expects  $\mathcal{A}_{\text{FB}}^{(\bar{B})}(s) = -\mathcal{A}_{\text{FB}}^{(B)}(s)$ . This holds at the per-mille level within the SM, where  $C_{10}$  has a negligible CP-violating phase, but again it could be different in the presence of new physics in the  $Z\bar{b}s$  vertex. In this case the ratio  $[\mathcal{A}_{\text{FB}}^{(\bar{B})}(s) + \mathcal{A}_{\text{FB}}^{(B)}(s)]/[\mathcal{A}_{\text{FB}}^{(\bar{B})}(s) - \mathcal{A}_{\text{FB}}^{(B)}(s)]$  could be different from zero, for  $s$  above the charm threshold, even reaching the 10% level in the SUSY scenario of Section 2 [16].

## 6 Conclusions

Rare FCNC transitions of the type  $d_j \rightarrow d_i \ell^+\ell^-(\nu\bar{\nu})$  are very sensitive to simultaneous violations of  $SU(2)_L$  and flavour symmetries. Within generic supersymmetric extensions of the SM, these processes could be substantially modified in the presence of non-diagonal trilinear soft-breaking terms. At present this possibility is still open for both  $b \rightarrow s$  and  $s \rightarrow d$  transitions, but it has more chances to be realized in the  $s \rightarrow d$  case [43]. The future measurements of  $\mathcal{B}(K^+ \rightarrow \pi^+\nu\bar{\nu})$ ,  $\mathcal{B}(K_L \rightarrow \pi^0\nu\bar{\nu})$ ,  $\mathcal{B}(K_L \rightarrow \pi^0e^+e^-)$  and  $\mathcal{A}_{\text{FB}}[B(\bar{B}) \rightarrow \bar{K}^*\mu^+\mu^-]$  will provide very useful insights in this scenario.

## Acknowledgements

It is a pleasure to thank the organisers of RADCOR 2000 for their invitation to this interesting symposium and their financial support.

## References

- [1] S.L. Glashow, J. Iliopoulos and L. Maiani, *Phys. Rev.* **D2** (1970) 1285.
- [2] N. Cabibbo, *Phys. Rev. Lett.* **10** (63) 531; M. Kobayashi and T. Maskawa, *Prog. Theor. Phys.* **49** (73) 652.
- [3] L.J. Hall, V.A. Kostelecky and S. Rabi, *Nucl. Phys.* **B267** (1986) 415.
- [4] J.S. Hagelin, S. Kelley and T. Tanaka, *Nucl. Phys.* **B415** (1994) 293;  
E. Gabrielli, A. Masiero and L. Silvestrini, *Phys. Lett.* **B374** (1996) 80;  
F. Gabbiani, E. Gabrielli, A. Masiero and L. Silvestrini, *Nucl. Phys.* **B477** (1996) 321.
- [5] J.A. Casas and S. Dimopoulos, *Phys. Lett.* **B387** (1996) 107.

- [6] G. Colangelo and G. Isidori, *JHEP* **09** (1998) 009.
- [7] A.J. Buras, A. Romanino and L. Silvestrini, *Nucl. Phys.* **B520** (1998) 3.
- [8] A.J. Buras *et al.*, *Nucl. Phys.* **B566** (2000) 3.
- [9] A.L. Kagan and M. Neubert, hep-ph/9908404.
- [10] E. Gabrielli, S. Khalil and E. Torrente-Lujan, *Nucl. Phys.* **B594** (2001) 3; G. Degrossi, P. Gambino and G. F. Giudice, *JHEP* **12** (2000) 009; M. Carena, D. Garcia, U. Nierste and C. E. Wagner, hep-ph/0010003; D. Bailin and S. Khalil, hep-ph/0010058; M. B. Causse and J. Orloff, hep-ph/0012113; T. Hurth, these proceedings.
- [11] S. Ahmed *et al.* (CLEO Collaboration), hep-ex/9908022.
- [12] A. Masiero and H. Murayama, *Phys. Rev. Lett.* **83** (1999) 907.
- [13] A. J. Buras *et al.*, *Nucl. Phys.* **B592** (2000) 55
- [14] X.-G. He, H. Murayama, S. Pakvasa and G. Valencia, hep-ph/9909562.
- [15] G. D'Ambrosio, G. Isidori and G. Martinelli, *Phys. Lett.* **B480** (2000) 164.
- [16] G. Buchalla, G. Hiller and G. Isidori, *Phys. Rev.* **D63** (2001) 014015.
- [17] G. Buchalla, A.J. Buras and M.E. Lautenbacher, *Rev. Mod. Phys.* **68** (1996) 1125.
- [18] E. Lunghi, A. Masiero, I. Scimemi and L. Silvestrini, *Nucl. Phys.* **B568** (2000) 120; E. Lunghi and I. Scimemi, *Nucl. Phys.* **B574** (2000) 43.
- [19] A.J. Buras and L. Silvestrini, *Nucl. Phys.* **B546** (99) 299.
- [20] L. Wolfenstein, *Phys. Rev. Lett.* **51** (1983) 1945.
- [21] G. Buchalla and A.J. Buras, *Nucl. Phys.* **B398** (1993) 285, **B400** (1993) 225, **412** (1994) 106.
- [22] M. Misiak and J. Urban, *Phys. Lett.* **B451** (1999) 161.
- [23] G. Buchalla and A.J. Buras, *Nucl. Phys.* **BB548** (99) 309.
- [24] A. F. Falk, A. Lewandowski and A. A. Petrov, hep-ph/0012099.
- [25] M. Lu and M. Wise, *Phys. Lett.* **B324** (1994) 461.
- [26] L. Littenberg, *Phys. Rev.* **D39** (1989) 3322.

- [27] G. Buchalla and A.J. Buras, *Phys. Rev.* **D54** (1996) 6782.
- [28] D. Rein and L.M. Sehgal, *Phys. Rev.* **D39** (1989) 3325; G. Buchalla and G. Isidori, *Phys. Lett.* **B440** (1998) 170.
- [29] W.J. Marciano and Z. Parsa, *Phys. Rev.* **D53** (1996) R1.
- [30] M. Ciuchini *et al.*, hep-ph/0012308.
- [31] S. Adler *et al.* (BNL-E787 Collaboration), *Phys. Rev. Lett.* **84** (2000) 3768 and **79** (1997) 2204.
- [32] J. Adams *et al.* (KTeV Collaboration), *Phys. Lett.* **B447** (1999) 240.
- [33] A. Alavi-Harati *et al.* (KTeV Collaboration), hep-ex/0009030.
- [34] V.D. Kekelidze (NA48 Collab.), talk presented at ICHEP2000, Osaka, Japan, 2000.
- [35] A.J. Buras, M.E. Lautenbacher, M. Misiak and M. Münz, *Nucl. Phys.* **B423** (1994) 349.
- [36] A. Ali, P. Ball, L.T. Handoko and G. Hiller, *Phys. Rev.* **D61** (2000) 074024.
- [37] H. Kroha (ALEPH Collaboration), MPI-PHE-96-21, *Prepared for 28th International Conference on High-Energy Physics (ICHEP 96), Warsaw, Poland, July 1996*; W. Adam *et al.* (DELPHI Collaboration), *Z. Phys.* **C72** (1996) 207.
- [38] T. Affolder *et al.* (CDF Collaboration), *Phys. Rev. Lett.* **83** (1999) 3378.
- [39] F. Abe *et al.* (CDF Collaboration), *Phys. Rev.* **D57** (1998) 3811.
- [40] G. Burdman, *Phys. Rev.* **D57** (1998) 4254.
- [41] J. Charles *et al.*, *Phys. Rev.* **D60** (1999) 014001.
- [42] F. Krüger and L.M. Sehgal, *Phys. Lett.* **B380** (1996) 199.
- [43] A. Masiero and O. Vives, hep-ph/0007320.

December, 2000  
hep-ph/0012316

## On Radiative Weak Annihilation Decays

RICHARD F. LEBED\*

*Department of Physics and Astronomy  
Arizona State University, Tempe, AZ 85287 USA*

We discuss a little-studied class of weak decay modes sensitive to only one quark topology at leading order in  $G_F$ :  $M \rightarrow m\gamma$ , where  $M, m$  are mesons with completely distinct flavor quantum numbers. Specifically, they proceed via the annihilation of the valence quarks through a  $W$  and the emission of a single hard photon, and thus provide a clear separation between CKM and strong interaction physics. We survey relevant calculations performed to date, discuss experimental discovery potential, and indicate interesting future directions.

Presented at the

5th International Symposium on Radiative Corrections  
(RADCOR-2000)

Carmel CA, USA, 11–15 September, 2000

---

\*Work supported by the Department of Energy under Grant No. DE-AC05-84ER40150.

The feature that makes heavy quark physics appealing—the decoupling of the heavy quark matrix elements from those of the light degrees of freedom—can prove to be treacherous if one cannot track the processes through which the quarks of various flavors are created or destroyed. Such ambiguities plague the extraction of Cabibbo-Kobayashi-Maskawa (CKM) elements from nonleptonic weak decays.

In this light, processes with unusual flavor quantum numbers are useful since they serve to distinguish the weak interaction and strong interaction physics: As seen below, unusual flavor quantum numbers imply a very limited number of possible Feynman diagram topologies. The price one must pay for this clarity is that such interesting decays tend to be quite rare. In particular, the modes  $M \rightarrow m\gamma$  discussed in this talk are radiative (rates  $\propto \alpha_{\text{EM}}$ ) weak ( $\propto G_F^2 |V^*V|^2$ ) processes with pointlike annihilation ( $\propto f_M/M \cdot f_m/m$ , where  $f$  indicates the meson decay constant). Nevertheless, we argue below that once such modes are produced, they should be relatively easy to detect.

To study the flow of flavor in a flavor-changing weak decay process, it is sufficient to work at the partonic level with simple quark diagrams, since gluons and sea quark pairs carry only flavor-singlet quantum numbers. Only valence quarks and vacuum-produced  $q\bar{q}$  pairs that become valence quarks need be considered. Thus, the complications of QCD are irrelevant if one wishes only to classify weak decay processes. As shown in Ref. [1], only six such classes exist at  $O(G_F^1)$ , since only the  $W$  boson changes flavors in the standard model. These classes are  $T$  (color-unsuppressed tree),  $C$  (color-suppressed tree),  $P$  (penguin),  $A$  (weak annihilation),  $E$  (weak exchange), and  $PA$  (penguin annihilation) diagrams, as depicted in Fig. 1.

One may now enumerate a number of problems inherent to computing weak meson decays of the form  $M \rightarrow m_1 m_2$ . The first such difficulty is the most obvious and endemic to any hadronic process, namely, that hadron wavefunctions are not precisely known and must be modeled in order for a calculation to be performed. Second, for electrically neutral mesons—even with valence quarks with distinct flavors—the asymptotic states are not pure flavor eigenstates, and then one must take into account  $K\bar{K}$ ,  $D\bar{D}$ ,  $B\bar{B}$ , or  $B_s\bar{B}_s$  mixing.

In addition, however, there are complications best seen by using the diagrammatic classification. While it is true that any arbitrarily complicated Feynman diagram for a flavor-changing  $M \rightarrow m_1 m_2$  meson decay falls uniquely into one of these six classes, it is also true that any such decay tends to have contributions from more than one topology. In particular, processes that have a  $T$  diagram often also have a  $C$  diagram, and the two can mix under final-state interactions (FSI's). As an example, consider  $B^+ \rightarrow \pi^+ \bar{D}^0 = \bar{b}u \rightarrow (u\bar{d})(\bar{c}u)$ . The weak decay at the quark level may proceed through  $\bar{b} \rightarrow \bar{c}W^+ \rightarrow \bar{c}u\bar{d}$ , and the  $u$  valence quark in  $\pi^+$  may either come from the weak vertex or the spectator. In other cases, valence quarks may emerge from pair creation due to fragmentation. The basic problem here is one of redundant quark flavor in the final state: Since two  $u$  quarks are indistinguishable, one is faced with

the problem of where each one originates, and this redundancy is forced by the limited number of distinct quark flavors available for hadron formation.

Another affliction of  $M \rightarrow m_1 m_2$  best seen in terms of the diagram topologies is the problem of “generalized penguin pollution,” which we define to be the contribution to a decay from at least two diagrams containing different CKM couplings. A classic example is the decay  $B^0 \rightarrow \pi^+ \pi^- = \bar{b}d \rightarrow (u\bar{d})(d\bar{u})$ . In the  $T$  diagram, the weak decay at the quark level is  $\bar{b} \rightarrow \bar{u}W^+ \rightarrow \bar{u}u\bar{d}$ , where the  $\bar{u}$  quark hadronizes with

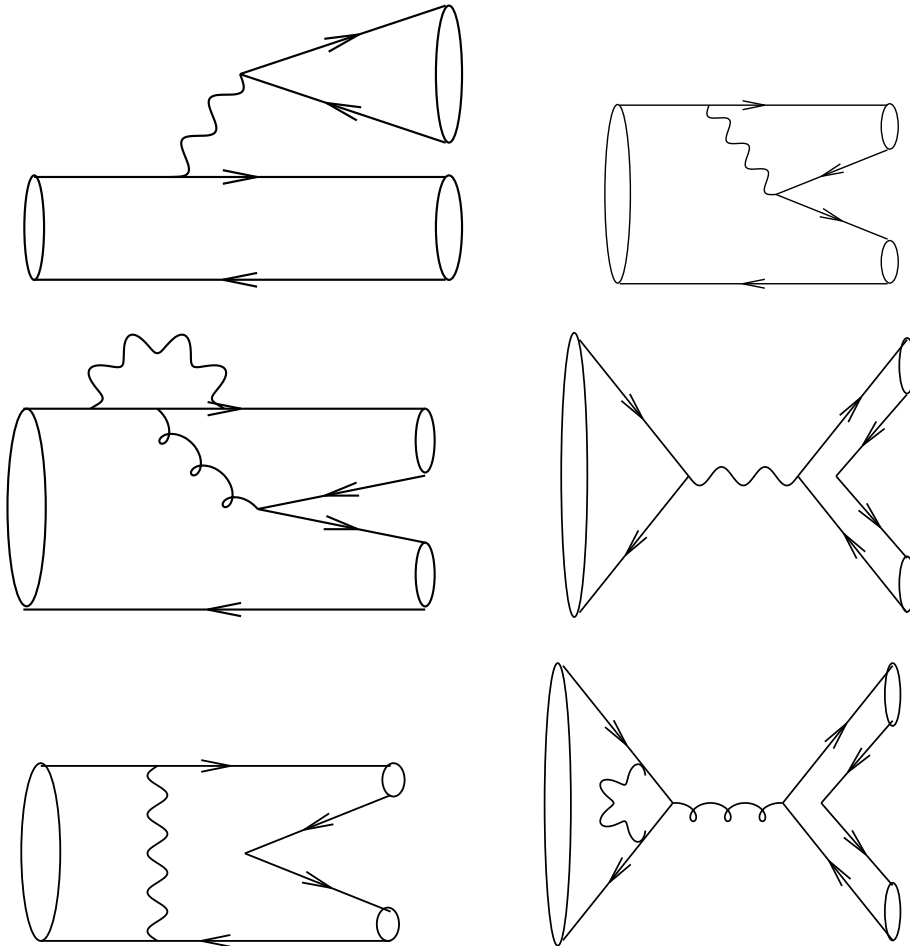


Figure 1: The six flavor-changing weak decay topologies at  $O(G_F^1)$ . Reading across and from top to bottom, these are labeled  $T$ ,  $C$ ,  $P$ ,  $A$ ,  $E$ , and  $PA$ , respectively. Ovals indicate hadronization into color-singlet mesons. For processes with the  $T$  topology, there is often also a  $C$  diagram contribution, so that the two classes can mix through final-state interactions. The  $P$ ,  $A$ ,  $E$ , and  $PA$  diagrams have variants in which the the  $q\bar{q}$  pair from the vacuum hadronize into a single flavor-singlet meson.

the spectator  $d$  quark, and the CKM coefficient is  $V_{ub}^*V_{ud}$ . On the other hand, a  $P$  diagram may also contribute (hence the original name “penguin pollution”), in which  $\bar{b} \rightarrow \bar{d}g \rightarrow \bar{d}u\bar{u}$ . The penguin loop, dominated by the top quark contribution, produces primarily the CKM coupling  $V_{tb}^*V_{td}$ . Again, the ultimate reason that a large proportion of possible modes exhibit generalized penguin pollution is the existence of a limited number of quark flavors available for the decay: In the example, the  $u\bar{u}$  pair can either emerge from a strong or weak process.

Typically,  $M \rightarrow m_1m_2$  meson decays tend to suffer at least one of the latter two problems. It is difficult to find modes proceeding through only one topology, chiefly owing to the limited number of distinct quark flavors; in particular,  $M \rightarrow m_1m_2$  contains six quarks, while only the lightest five quark flavors form mesons.

To evade this problem, let us consider instead the meson decays  $M \rightarrow m\gamma$  [2]. Here one has only four quarks, which can easily be chosen distinct. In this case there is clearly (as a few moments’ study of Fig. 1 should convince the reader) only one weak topology available at  $O(G_F^1)$ : If the meson is charged, then  $M^+ \rightarrow m^+\gamma$  proceeds uniquely through the weak annihilation ( $A$ ) diagram, while if the meson is neutral, then  $M^0 \rightarrow m^0\gamma$  proceeds uniquely through the weak exchange ( $E$ ) diagram. To date, no such decays have been observed, so an order-of-magnitude calculation of their rates serves to guide not only future calculations, but experimental searches as well. The photon may be attached to any charged particle line, and is hard and monochromatic, fixed in energy due to the restrictive kinematics of two-body decays. The  $E$  processes are certainly interesting, but introduce the problem of  $M^0\bar{M}^0$  and  $m^0\bar{m}^0$  mixing mentioned above, so we concentrate below on the  $A$  processes.

Thus far we have considered contributions only at  $O(G_F^1)$ . One may also neglect the diagram in which the photon couples to the  $W^\pm$ , since it produces an extra  $1/M_W^2$  propagator suppression; thus, one need consider only diagrams in which the photon couples to one of the quarks. At a similar numerical size for  $A$  processes are the  $O(G_F^2)$  diagrams depicted in Fig. 2. These consist of “di-penguin” and crossed-box diagrams; however, neither class is expected to be particularly large, since the enhanced significance of ordinary penguin and box diagrams occurs due to virtual  $t$  quark lines in the loops. In the case of charged mesons, one of the valence quarks is necessarily  $u$ -type, and the virtual quark connecting to it through a  $W$  vertex is necessarily  $d$ -type, and thus does not give rise to a large contribution. One concludes that, in the standard model at least, the  $O(G_F^1)$  contribution should dominate the rate for  $A$  processes.

This begs the question of whether any common non-standard physics might contribute to, or even dominate,  $A$  processes. Two very simple possibilities jump immediately to mind. First, the  $s$ -channel exchange of a  $W$  may be replaced with the  $t$ -channel exchange of a flavor-changing neutral current (FCNC) boson  $X$ . Such a

process is important if

$$\frac{V_1 V_2}{M_W^2} \lesssim \frac{g_1 g_2}{M_X^2}, \quad (1)$$

where  $V_i$  and  $g_i$  represent the CKM and new physics couplings, respectively, at the two vertices. The best potential for new physics discovery is when  $g_i$  are  $O(1)$  and  $V_i$  are as small as possible. For example, in the case  $B^+ \rightarrow D^{*+} \gamma$ ,  $V_1 = V_{ub}^* \sim \lambda^3$  and  $V_2 = V_{cd} \approx \lambda$ , with Wolfenstein  $\lambda \approx 0.2$ . Then one immediately finds

$$M_X \lesssim 2 \text{ TeV}, \quad (2)$$

a fairly stringent bound, considering that one must still make sure that  $K\bar{K}$  mixing and other FCNC constraints are properly taken into account.

Another possibility is the  $s$ -channel exchange of a charged Higgs boson. Since the current lower limit [3] is  $M_{H^+} > 130 \text{ GeV}$ , these decays are a possible place to find new physics (using the same tree-level estimation as above) if the corresponding  $H^+ q\bar{q}$  Yukawa couplings are not smaller than the CKM elements  $V_1 V_2$ .

Having discussed the restrictive nature of flavor distinctiveness on generating processes with unique flavor topologies, it is natural to present the complete list [2] of such decays for pure  $A$  processes. One must choose two from the list  $\{b, s, d\}$  and two from the list  $\{c, u\}$ , for a total of six possibilities. Only the lightest pseudoscalar  $M$  of each flavor content decays dominantly weakly. Then angular momentum conservation requires that the spin of the photon must be balanced by a daughter meson  $m$  of spin  $\geq 1$ ; for sake of illustration, we take  $m$  to be the lowest-lying vector meson, which should presumably boast the largest transition rate for any state with the given final flavor quantum numbers. Table 1 presents the modes just described, along with the corresponding CKM coefficients.

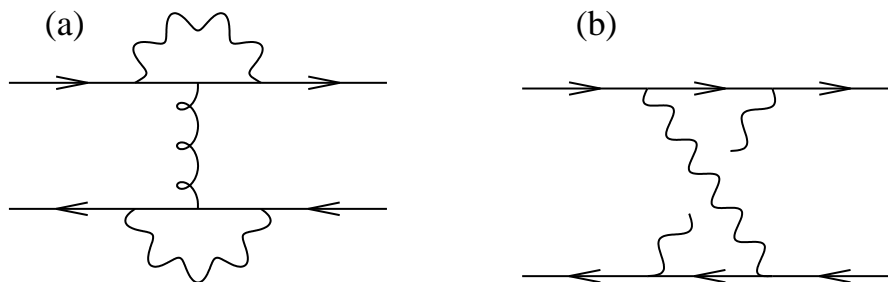


Figure 2: Diagrams contributing at  $O(G_F^2)$  to processes described at  $O(G_F^1)$  by the  $A$  diagram of Fig. 1. These are the (a) “di-penguin” and (b) crossed-box diagrams. The gluons emerging from the  $W$  loops in the di-penguin need not be the same; indeed, the two penguins can be separated by long-distance effects.

Table 1: Flavor structure and mesonic decay modes of weak annihilation radiative decays. The CKM coefficient for each process is accompanied by its magnitude in powers of Wolfenstein  $\lambda \approx 0.2$ .

Valence structure	Decay mode	CKM Elements
$\bar{b}u \rightarrow c\bar{s}\gamma$	$B^+ \rightarrow D_s^{*+}\gamma$	$V_{ub}^*V_{cs} \sim \lambda^3$
$\bar{b}u \rightarrow c\bar{d}\gamma$	$B^+ \rightarrow D^{*+}\gamma$	$V_{ub}^*V_{cd} \sim \lambda^4$
$\bar{b}c \rightarrow u\bar{s}\gamma$	$B_c^+ \rightarrow K^{*+}\gamma$	$V_{cb}^*V_{us} \sim \lambda^3$
$\bar{b}c \rightarrow d\bar{u}\gamma$	$B_c^+ \rightarrow \rho^+\gamma$	$V_{cb}^*V_{ud} \sim \lambda^2$
$c\bar{d} \rightarrow u\bar{s}\gamma$	$D^+ \rightarrow K^{*+}\gamma$	$V_{cd}^*V_{us} \sim \lambda^2$
$c\bar{s} \rightarrow u\bar{d}\gamma$	$D_s^+ \rightarrow \rho^+\gamma$	$V_{cs}^*V_{ud} \sim \lambda^0$

Note that the CKM suppression of the decays varies widely, from none in the case of  $D_s^+ \rightarrow \rho^+\gamma$  to  $\lambda^4$  in the case of  $B^+ \rightarrow D^{*+}\gamma$ . These decays appear to have been discussed only rarely in the literature.  $D_s^+ \rightarrow \rho^+\gamma$  has been considered using the quark model [4], pole and vector meson dominance methods [5], light-cone techniques [6], and effective field theory [7]. The double Cabibbo-suppressed mode  $D^+ \rightarrow K^{*+}\gamma$ , interesting since it is a neutrinoless decay sensitive to  $|V_{cs}|$ , was also considered in Refs. [5,7]. The modes  $B^+ \rightarrow D_s^{*+}\gamma$  and  $D^{*+}\gamma$  (collectively,  $D_{(s)}^{*+}\gamma$ ) were first considered in Ref. [8], where they were suggested as possible probes of  $|V_{ub}|$ . The modes  $B_c \rightarrow \rho^+\gamma$  and  $K^{*+}\gamma$  were first considered [9] in the context of light-cone sum rules.

Let us consider in further detail the calculation of Ref. [8] since its methods and approximations figure large in the rest of this talk. In [8], heavy quark effective theory (HQET) and light-quark SU(3) are used to relate the four-fermion vertex  $(\bar{b}u)(c\bar{d})$  or  $(\bar{b}u)(c\bar{s})$  appearing in the decays  $B^+ \rightarrow D_{(s)}^{*+}\gamma$  to the vertex  $(\bar{b}d)(b\bar{d})$  that appears in  $B\bar{B}$  mixing. Such an approach of course neglects the ‘‘bag parameter’’  $B$  (*i.e.*, the multiplicative long-distance correction to factorization) relevant to each vertex, as well as the mixing and short-distance renormalization of the two different color Fierz orderings of the four-fermion operator.

The next problem is how to incorporate long-distance effects between the weak and electromagnetic vertices. Here, the simplest ansatz is adopted: One assumes that only the lightest meson propagates between the two vertices with the same flavor quantum numbers as the meson on the other side of the photon vertex, and the same spin-parity as the meson on the other side of the weak vertex, . This is depicted in Fig. 3. In each diagram the external states are  $B^+$  and  $D_{(s)}^{*+}$ , while in the first the intermediate meson is  $B^{*+}$ , and in the second it is  $D_{(s)}^+$ . This approximation not only neglects all higher resonances that may contribute in the intermediate state (for example,

$D_{(s)}(2S)$ ), but also vector-dominance diagrams in which the photon is generated by a resonance of a valence quark from one of the mesons and an antiquark from the weak vertex (such as  $B^+ \rightarrow D_s^{*+} \rho^0 \rightarrow D_s^{*+} \gamma$ ), and multiparticle intermediates (such as  $B^+ \rightarrow D^0 K^+ \rightarrow D_s^{*+} \gamma$ ) in which FSI's play an important role.

Finally, HQET is used to relate the  $BB^* \gamma$  and  $D_{(s)} D_{(s)}^* \gamma$  couplings to  $\Gamma(D^{*+} \rightarrow D^+ \gamma)$ , for which an experimental upper bound exists [3]. One finds the branching ratios (BR's)

$$\begin{aligned}
& \text{BR}(B^+ \rightarrow D_s^{*+} \gamma) \\
&= 2 \times 10^{-7} \left( \frac{B_B}{0.98} \right)^2 \left| \frac{V_{ub}^* V_{cs}}{3 \times 10^{-3}} \right| \left( \frac{\Gamma(D^{*+})}{0.131 \text{ MeV}} \right) \left( \frac{\text{BR}(D^{*+} \rightarrow D^+ \gamma)}{3.2\%} \right), \\
& \text{BR}(B^+ \rightarrow D^{*+} \gamma) \\
&= 7 \times 10^{-9} \left( \frac{B_B}{0.98} \right)^2 \left| \frac{V_{ub}^* V_{cd}}{6.6 \times 10^{-4}} \right| \left( \frac{\Gamma(D^{*+})}{0.131 \text{ MeV}} \right) \left( \frac{\text{BR}(D^{*+} \rightarrow D^+ \gamma)}{3.2\%} \right).
\end{aligned} \tag{3}$$

The final approximation, using an on-shell electromagnetic coupling (the  $D^{*+} \rightarrow D^+ \gamma$  transition magnetic moment) to extract the coupling of an intermediate meson, off-shell by the large amount  $m^2(B^+) - m^2(D_{(s)}^+)$  in the second diagram (as fixed by the fact that the real photon has  $q^2 = 0$ ), deserves special comment. In the original calculation [8], a new formal heavy quark limit  $m_b - m_c \lesssim \Lambda_{\text{QCD}} \ll m_{c,b}$  was invented, for which the virtuality of the electromagnetic coupling is parametrically small. It is of course possible to remove this assumption when the photon is virtual, as in  $B^+ \rightarrow D_{(s)}^{*+} e^+ e^-$ ; then one may find a kinematic region where the intermediate meson is approximately at rest [10], or do even better and develop an operator product expansion (OPE) in the variable  $q^2 \gg \Lambda_{\text{QCD}}^2$ . Then one calculates [11], for example,

$$\text{BR}(B^+ \rightarrow D_s^{*+} e^+ e^-) \Big|_{q^2 > 1 \text{ GeV}^2} \approx 1.8 \times 10^{-9}. \tag{4}$$

The authors of Refs. [10,11] also tackle the problem of radiative weak exchange (the  $E$  rather than  $A$  diagram) exclusive processes using the OPE approach in Ref. [12],

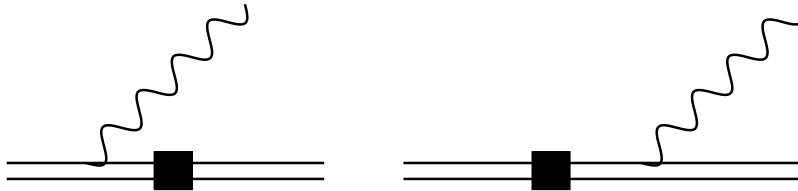


Figure 3: Diagrams for  $B^+ \rightarrow D_{(s)}^{*+}$ , assuming dominance of long-distance physics by single-meson states. The square indicates the weak interaction vertex.

Table 2: Estimates of branching ratios for weak annihilation decays using Eq. (5). Also included are energies of the monochromatic photon.

Decay mode	BR (est.)	Photon Energy (GeV)
$B^+ \rightarrow D_s^{*+}\gamma$	$1 \times 10^{-7}$	2.22
$B^+ \rightarrow D^{*+}\gamma$	$7 \times 10^{-9}$	2.26
$B_c^+ \rightarrow K^{*+}\gamma$	$3 \times 10^{-6}$	3.14
$B_c^+ \rightarrow \rho^+\gamma$	$3 \times 10^{-5}$	3.15
$D^+ \rightarrow K^{*+}\gamma$	$6 \times 10^{-7}$	0.72
$D_s^+ \rightarrow \rho^+\gamma$	$8 \times 10^{-5}$	0.83

finding similar branching ratios. The much smaller rates for  $e^+e^-$  processes compared to those for on-shell photon processes of course arise from the additional factor of  $\alpha_{\text{EM}}$  from conversion of the virtual photon.

One may also consider a simultaneous calculation [2] of all of the decays in Table 1 by using an approach similar to that of Ref. [8] but dropping the heavy quark approximations. In this case, let us consider only the second diagram of Fig. 3, where the photon couples only to the lighter vector meson  $V$ , and denote the initial and intermediate pseudoscalar mesons as  $M$  and  $P$ , respectively. We restrict to this single diagram because no positive measurements of  $MM^*\gamma$  couplings have yet appeared (recall that we used an upper bound for  $DD^*\gamma$ ), while  $\Gamma(K^{*+} \rightarrow K^+\gamma)$  and  $\Gamma(\rho^+ \rightarrow \pi^+\gamma)$  are known. This simple calculation yields

$$\Gamma(M \rightarrow V\gamma) = \frac{3}{2}G_F^2 |V_M V_P|^2 f_M^2 f_P^2 B^2 \Gamma_{V \rightarrow P\gamma} \left[ \frac{\mathcal{C}(M^2 - m_P^2)}{\mathcal{C}(0)} \right]^2 \times \left( \frac{M^2}{M^2 - m_P^2} \right)^2 \left( \frac{M^2 - m_V^2}{m_V^2 - m_P^2} \right)^3 \left( \frac{m_V}{M} \right)^3, \quad (5)$$

where  $B$  is the relevant bag parameter, the width  $\Gamma_{V \rightarrow P\gamma} \propto \alpha_{\text{EM}}$ , and the off-shell extrapolation of the electromagnetic form factor, labeled  $\mathcal{C}$ , is explicitly indicated. Values for branching ratios for the six modes, along with the photon energies, are listed in Table 2.

We see that the Cabibbo-unsuppressed decay  $D_s^+ \rightarrow \rho^+\gamma$  has a rate already large enough that it might already have been produced at Fermilab or CLEO. Certainly it will be produced copiously at BABAR and BELLE, where also the rarer  $B^+$  modes may be observed in smaller but still significant numbers. The  $B_c$  channels must necessarily wait for hadron machines such as LHC or BTeV.

One may also consider information contained in the helicity of the photon. For

an arbitrary  $P(0^-) \rightarrow V(1^-)\gamma$  decay, the generic amplitude is

$$\mathcal{M} = \epsilon_\mu^{*(V)} \epsilon_\nu^{*(\gamma)} \left[ i\mathcal{A}_{PC} \epsilon^{\mu\nu\rho\sigma} p_\rho^{(V)} p_\sigma^{(P)} + \mathcal{A}_{PV} \left( p^{(P)\mu} p^{(P)\nu} - g^{\mu\nu} p^{(\gamma)} \cdot p^{(P)} \right) \right], \quad (6)$$

where  $PC$ ,  $PV$  distinguish parity conserving and violating amplitudes, respectively. Then the total rate is

$$\begin{aligned} \Gamma &= \frac{1}{8\pi} |\mathbf{p}|^3 \left( |\mathcal{A}_{PC} + \mathcal{A}_{PV}|^2 + |\mathcal{A}_{PC} - \mathcal{A}_{PV}|^2 \right) \\ &= \frac{1}{4\pi} |\mathbf{p}|^3 \left( |\mathcal{A}_{PC}|^2 + |\mathcal{A}_{PV}|^2 \right), \end{aligned} \quad (7)$$

where  $|\mathbf{p}| = (m_P^2 - m_V^2)/2m_P$ . The first line of Eq. (7) is separated into contributions in which the two vector particles are both right-handed (RR) and left-handed (LL), respectively. Indeed, the asymmetry is

$$\frac{\Gamma_{RR} - \Gamma_{LL}}{\Gamma} = \frac{2\text{Re} \mathcal{A}_{PC} \mathcal{A}_{PV}^*}{|\mathcal{A}_{PC}|^2 + |\mathcal{A}_{PV}|^2}. \quad (8)$$

The relative weights of the two helicities may prove to be especially interesting since the  $V - A$  nature of weak interactions weights the two photon helicities differently. For example, in the case of penguin  $B^- \rightarrow K^{*-}\gamma$  and  $\rho^-\gamma$  decays, the  $L$  helicity has been found [13] to be enhanced compared to  $R$ . This enhancement persists [14] even when long-distance corrections (including contributions from  $A$  diagrams) are included. Certainly, a measured enhancement of the disfavored helicity would be a signal of new physics. Studies of the role of photon helicities are also underway [15] in the pure  $A$  decays described here.

The radiative weak annihilation decays occupy a unique position in heavy flavor physics, in that they are completely flavor self-tagged and kinematically trivial. Their experimental observation is imminent and promises another handle on the CKM matrix. Once the most common mode  $D_s^{*+} \rightarrow \rho^+\gamma$  is observed, its measured branching ratio may be used to study the other decays. Alternately, lattice simulations may be used to probe the generalized bag parameters, one may relate nonleptonic  $A$  processes to semileptonic radiative modes such as  $B \rightarrow \gamma \ell \nu$  [14,16], or one may consider alternate new physics contributions. On both the theoretical and experimental fronts, many opportunities for advances exist.

## Acknowledgments

I thank the University of Maryland Theoretical Quarks, Hadrons, and Nuclei group for their hospitality.

## References

- [1] M. Gronau, O.F. Hernandez, D. London, and J.L. Rosner, *Phys. Rev.* **D50** (1994) 4529.
- [2] R.F. Lebed, *Phys. Rev.* **D61** (2000) 033004.
- [3] D.E. Groom *et al.* (Particle Data Group), *Eur. Phys. J.* **C15** (2000) 1.
- [4] P. Asthana and A.N. Kamal, *Phys. Rev.* **D43** (1991) 278.
- [5] G. Burdman, E. Golowich, J.L. Hewett, and S. Pakvasa, *Phys. Rev.* **D52** (1995) 6383.
- [6] A. Khodjamirian, G. Stoll, and D. Wyler, *Phys. Lett.* **B358** (1995) 129.
- [7] S. Fajfer, S. Prelovšek, and P. Singer, *Eur. Phys. J.* **C6** (1999) 471; S. Fajfer and P. Singer, *Phys. Rev.* **D56** (1997) 4302; B. Bajc, S. Fajfer, and R.J. Oakes, *ibid.* **51** (1995) 2230.
- [8] B. Grinstein and R.F. Lebed, *Phys. Rev.* **D60** (1999) 031302(R).
- [9] T.M. Aliev and M. Savci, *J. Phys.* **G24** (1998) 2223.
- [10] D.H. Evans, B. Grinstein, and D.R. Nolte, *Phys. Rev.* **D60** (1999) 057301.
- [11] D.H. Evans, B. Grinstein, and D.R. Nolte, *Phys. Rev. Lett.* **83** (1999) 4947.
- [12] D.H. Evans, B. Grinstein, and D.R. Nolte, *Nucl. Phys.* **B577** (2000) 240.
- [13] Y. Grossman and D. Pirjol, *JHEP* **0006** (2000) 029.
- [14] B. Grinstein and D. Pirjol, *Phys. Rev.* **D62** (2000) 093002.
- [15] C.E. Carlson, R.F. Lebed, and A. Petrov, in preparation.
- [16] G.P. Korchemsky, D. Pirjol, and T.-M. Yan, *Phys. Rev.* **D61** (2000) 114510.

FERMILAB-Conf-00/298-T  
August 30, 2001  
hep-ph/0011181

## $|V_{ub}|$ From Semileptonic Decay and $b \rightarrow s\gamma$

ADAM K. LEIBOVICH\*

*Department of Physics, Carnegie Mellon University, Pittsburgh, PA 15213  
Theory Group, Fermilab, P.O. Box 500, Batavia, IL 60510*

Current errors on  $|V_{ub}|$  are dominated by model dependence. For inclusive decays, the model dependence comes from the Fermi motion of the  $b$  quark. By combining the endpoint photon and lepton spectra from the inclusive decays  $B \rightarrow X_s \gamma$  and  $B \rightarrow X_u \ell \bar{\nu}$ , it is possible to remove this model dependence. We show how to combine these rates including the resummation of the endpoint logs at next to leading order. The theoretical errors on  $|V_{ub}|$  on the order of 10% are possible. We also give a brief discussion on comparing different extractions.

Presented at the

5th International Symposium on Radiative Corrections  
(RADCOR-2000)

Carmel CA, USA, 11–15 September, 2000

---

\*This work was supported in part by the U.S. Department of Energy under grant numbers DOE-ER-40682-143 and DE-AC02-76CH03000.

# 1 Introduction

The Cabibbo-Kobayashi-Maskawa matrix element  $V_{ub}$  is very important for understanding CP violation in the Standard Model. An accurate measurement of  $|V_{ub}|$  puts strong constraints on the Unitarity Triangle. Unfortunately,  $V_{ub}$  is very hard to measure. Current measurements have errors that are dominated by model dependence. Some of the best extractions so far have come from exclusive decays, such as  $B \rightarrow \pi \ell \bar{\nu}$  or  $B \rightarrow \rho \ell \bar{\nu}$ . The problem with exclusive decays is the strong hadronic dynamics can not be calculated, and we have to resort to models, light-cone sum rules, or lattice QCD calculations to obtain the form factors [1]. At the present time, all these methods give around 20% errors. A recent measurement from CLEO [2] using  $B \rightarrow \rho \ell \bar{\nu}$  gives  $|V_{ub}| = [3.25 \pm 0.14(\text{stat.})_{-0.29}^{+0.21}(\text{syst.}) \pm 0.55(\text{model})] \times 10^{-3}$ . In the future, the lattice will give accurate predictions for the form factors, but until then, a measurement of 20% is probably the best we can hope for from exclusive decays.

In some ways, inclusive decays should provide a straightforward means to measure  $|V_{ub}|$ . All we need to do is measure the total rate  $b \rightarrow u \ell \bar{\nu}$ , which is proportional to  $|V_{ub}|^2$  and is known to order  $\alpha_s^2$  [3]. If we could measure the total rate, we would not have to worry about quark-hadron duality violations, thus a very accurate measurement would be possible.

Unfortunately, there is a very large background from  $b \rightarrow c$  decays, which is about 100 times more abundant than  $b \rightarrow u$  decays. To remove this large background, kinematic cuts must be made. Three basic cuts are discussed in the literature, each having its own advantages: a cut on the electron energy spectrum, a cut on the hadronic invariant mass spectrum, and a cut on the leptonic invariant mass spectrum. For now we will concentrate on the electron energy spectrum, and return to the other cuts later.

Since the  $u$  quark is much lighter than the  $c$  quark, the electron energy spectrum for  $b \rightarrow u$  decays extends past the endpoint for  $b \rightarrow c$  decays, see Fig. 1. Thus it is possible to remove the charm quark background by cutting above the  $b \rightarrow c$  endpoint. All that is necessary is a theoretical prediction for the integrated rate above the cut. Unfortunately, putting a cut near the endpoint introduces a new small mass scale,  $\Delta E \sim 300$  MeV, which introduces large perturbative  $[\log(m_b/\Delta E)]$  and non-perturbative  $(\Lambda/\Delta E)$  corrections. Therefore both the perturbative and non-perturbative series must be resummed for the rate to be trustworthy.

The calculation of the rate begins with the effective Hamiltonian [4]

$$\begin{aligned} H_{eff} &= \frac{-4G_F}{\sqrt{2}} V_{ub} (\bar{u} \gamma_\mu P_L b) (\bar{\ell} \gamma^\mu P_L \nu_\ell) \\ &= \frac{-4G_F}{\sqrt{2}} V_{ub} J_\mu J_\ell^\mu, \end{aligned} \tag{1}$$

obtained by integrating out the  $t$  quark and  $W$  bosons. The differential decay distri-

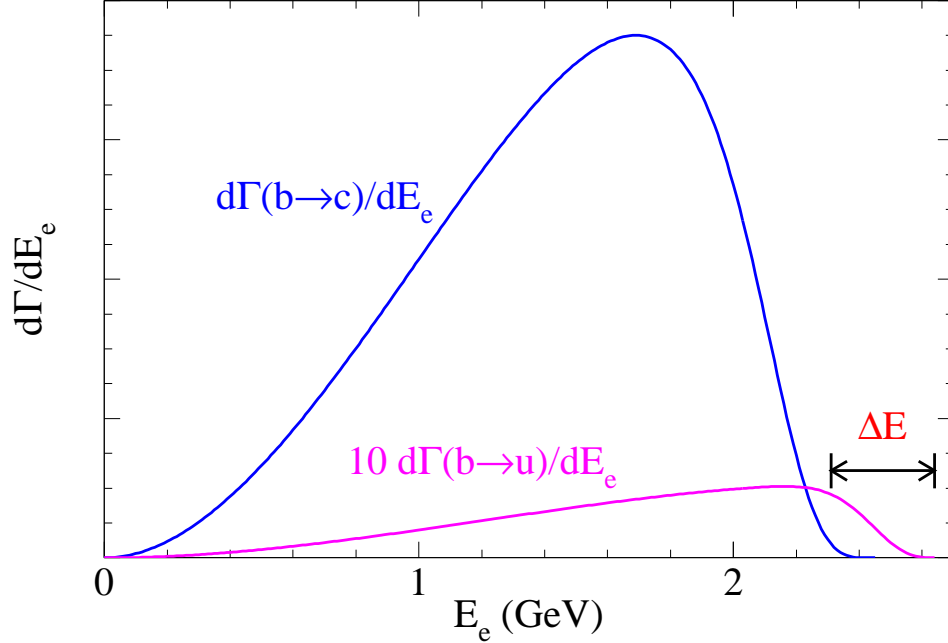


Figure 1: Electron spectrum for semi-leptonic  $b$  decay rates to  $c$  and  $u$  quarks. The rate for  $b \rightarrow ue\bar{\nu}$  has been multiplied by a factor of 10. The region in  $\Delta E$  can only have  $b \rightarrow u$  decays, and thus is useful for extracting  $|V_{ub}|$ .

bution can then be written as the product of leptonic and hadronic tensors

$$d\Gamma \propto |V_{ub}|^2 L^{\alpha\beta} W_{\alpha\beta}. \quad (2)$$

Using the Optical Theorem, the hadronic tensor  $W_{\alpha\beta}$  can be related to the imaginary part of the time ordered product of currents

$$W_{\alpha\beta} = -\frac{1}{\pi} \text{Im} T_{\alpha\beta}, \quad (3)$$

$$T_{\alpha\beta} = -\frac{i}{2M_B} \int d^4x e^{-iq \cdot x} \langle B | T(J_\alpha^\dagger(x) J_\beta(0)) | B \rangle. \quad (4)$$

The time ordered product can be calculated by expanding in an Operator Product Expansion (OPE). The Wilson coefficients can be calculated (over most of phase

space) in perturbation theory [5,6], while higher dimensional operators in the OPE are suppressed (over most of phase space) by powers of  $1/m_b$ . Thus, the leading term in the OPE gives free  $b$  quark decay. The first corrections enter at order  $1/m_b^2$ , and are proportional to the Heavy Quark Effective Theory parameters

$$\lambda_1 = \frac{\langle B | \bar{h}_v (iD)^2 h_v | B \rangle}{2M_B}, \quad (5)$$

$$\lambda_2 = \frac{\langle B | \bar{h}_v g \sigma_{\mu\nu} G^{\mu\nu} | B \rangle}{12M_B}. \quad (6)$$

The problems begin as the energy of the lepton approaches the endpoint. Defining  $x = 2E_\ell/m_b$  to be the rescaled lepton energy, the higher dimensional operators in the OPE are actually suppressed by

$$\frac{\Lambda}{m_b(1-x)} \rightarrow 1 \quad \text{as } x \rightarrow 1. \quad (7)$$

Higher dimensional operators in the expansion are no longer suppressed. In other words, the expansion is becoming singular as we approach the endpoint.

The breakdown in the OPE can be seen in the expression for the rate at order  $1/m_b^2$  [7],

$$\left. \frac{d\Gamma}{dx} \right|_{O(1/m_b^2)} \propto \frac{5\lambda_1 + 33\lambda_2}{3m_b^2} \theta(1-x) - \frac{\lambda_1 + 33\lambda_2}{6m_b^2} \delta(1-x) - \frac{\lambda_1}{6m_b^2} \delta'(1-x), \quad (8)$$

by the appearance of singular functions at the endpoint.

To handle the breakdown of the non-perturbative series, the leading singular terms must be resummed. These corrections resum into a non-perturbative structure function,  $f(k_+)$  [8]. The differential rate is now a convolution of  $f(k_+)$  with the partonic rate [8,9]

$$\frac{d\Gamma}{dE_\ell} = \int dk_+ f(k_+) \frac{d\Gamma_p}{dE_\ell}(m_b^*), \quad (9)$$

where  $m_b^* = m_b + k_+$ . The structure function is universal, meaning that the same function occurs for  $b \rightarrow u\ell\bar{\nu}$  and  $b \rightarrow s\gamma$  decays. Being a non-perturbative function,  $f(k_+)$  is not known; we do know the first few moments of  $f(k_+)$ , however. Thus, to handle the endpoint region, some model for  $f(k_+)$  must be introduced. We could in principle extract the structure function from  $b \rightarrow s\gamma$  decays and then apply it to  $b \rightarrow u\ell\bar{\nu}$ , but this is difficult because of the way  $f(k_+)$  enters the rate (9). Instead, we will skip the step of extracting the structure function and directly use the  $b \rightarrow s\gamma$  rate in the  $b \rightarrow u\ell\bar{\nu}$  rate. But first we need to discuss the perturbative corrections.

Near the endpoint, the perturbative correction to the rate looks like [10]

$$\frac{d\Gamma}{dx} \propto 1 - \frac{2\alpha_s}{3\pi} \left[ \log^2(1-x) + \frac{31}{6} \log(1-x) + \pi^2 + \frac{5}{4} \right]. \quad (10)$$

As  $x \rightarrow 1$ , the logs become large and the perturbative series breaks down. To trust the prediction, the logs need to be resummed. There are similarly large logs in the rate for  $b \rightarrow s\gamma$ , so the logs must be resummed there, too [11].

It is possible to resum the series using Infrared Factorization, which is also used for DIS, Drell-Yan, etc. The idea is that in the endpoint region, the light quark is shot out with large energy, but with small invariant mass. This quark produces a jet of particles through collinear radiation. While the constituents of the jet can talk to each other (and the original  $b$  quark) through soft gluons, hard gluon exchange is disallowed. The soft radiation cannot tell if the jet was initiated by a  $u$  quark or an  $s$  quark, thus it will be the same for  $b \rightarrow u$  and  $b \rightarrow s$  decays.

Mathematically, there is a separation of momentum regions into [12]

$$\text{Hard } (H) : \quad k_+ \sim k_- \sim k_t = O(m_b), \quad (11)$$

$$\text{Jet } (J) : \quad k_+ = O[m_b(1-x)], \quad k_- = O(m_b), \quad k_t = O(m_b\sqrt{1-x}), \quad (12)$$

$$\text{Soft } (S) : \quad k_+ \sim k_- \sim k_t = O[m_b(1-x)]. \quad (13)$$

By introducing a factorization scale  $\mu$  to keep these regions separated, we can write the rate in factorized form as

$$\frac{d\Gamma}{dx} \sim \int dz S(z, \mu) J(z, \mu) H(\mu). \quad (14)$$

The soft function  $S(z, \mu)$  is the same for  $b \rightarrow u$  and  $b \rightarrow s$ , while  $J(z, \mu)$  and  $H(\mu)$  depend on the process.

The rate completely factorizes after taking moments,

$$M_N^\gamma = \int_0^{M_B/m_b} dx x^{n-1} \frac{1}{\Gamma_0^\gamma} \frac{d\Gamma^\gamma}{dx} = S_N J_N^\gamma H_N^\gamma, \quad (15)$$

$$\begin{aligned} M_N^{sl} &= - \int_0^{M_B/m_b} dx x^{n-1} \frac{1}{\Gamma_0^\gamma} \frac{d}{dx} \frac{d\Gamma^\gamma}{dx} \\ &= \int dx_\nu S_N J_N^{sl}(x_\nu) H_N^{sl}(x_\nu), \end{aligned} \quad (16)$$

where  $M_N^\gamma$  and  $M_N^{sl}$  are the moments of the  $b \rightarrow s\gamma$  and  $b \rightarrow u\ell\bar{\nu}$  rates, respectively.

The soft function contains perturbative and non-perturbative pieces

$$S_N = f_N \sigma_N, \quad (17)$$

where  $f_N$  are the moments of the structure function introduced earlier. Thus we can write the moments (15) and (16) as

$$M_N^\gamma = f_N \sigma_N J_N^\gamma H_N^\gamma, \quad (18)$$

$$M_N^{sl} = \int dx_\nu f_N \sigma_N J_N^{sl}(x_\nu) H_N^{sl}(x_\nu). \quad (19)$$

All the large logarithms are contained in the combination  $\sigma_N J_N$ . The only fact we need about the perturbative resummation is that after resumming, including next-to-leading logarithms, there is the relation [13]

$$\sigma_N J_N^{sl} = \sigma_N J_N^\gamma \exp[g_{sl}(\alpha_s \log N)], \quad (20)$$

where  $\exp[g_{sl}(\alpha_s \log N)]$  is a known function.

We can now combine the above results. Substituting first (20) into (19), and then (18) into the result, we get

$$\begin{aligned} M_N^{sl} &= \int dx_\nu f_N \sigma_N J_N^{sl}(x_\nu) H_N^{sl}(x_\nu) \\ &= \int dx_\nu f_N \sigma_N J_N^\gamma \exp[g_{sl}(\alpha_s \log N)] H_N^{sl}(x_\nu) \\ &= \int dx_\nu \frac{M_N^\gamma}{H^\gamma} \exp[g_{sl}(\alpha_s \log N)] H_N^{sl}(x_\nu). \end{aligned} \quad (21)$$

Note that the dependence on the unknown structure function  $f_N$  has been eliminated.

We can go back to  $x$ -space by taking an inverse Mellin transform. The left-hand side of (21) is just the semi-leptonic rate. The right-hand side is a convolution of the  $b \rightarrow s\gamma$  rate with a known function. Rearranging, we can write this as [14]

$$\frac{|V_{ub}|^2}{|V_{ts}^* V_{tb}|^2} = \frac{\int \Gamma(b \rightarrow u\ell\nu)}{\int \int d\Gamma^\gamma/dx^\gamma * K(x^\gamma, \alpha_s)}. \quad (22)$$

So in words, what we have done is written  $|V_{ub}|^2$  as the ratio of the  $b \rightarrow ue\bar{\nu}$  rate over a convolution of the  $b \rightarrow s\gamma$  rate with a known function.

What are the uncertainties? First, there are higher order corrections that we neglected, which enter at the order of  $\Lambda/m_b$ ,  $\alpha_s(1-x)$  and  $(1-x)^3$ . For the value of the electron energy cut,  $x_{\text{cut}} \approx 0.87$ , these corrections should all be less than 10%. Of course, we are estimating the size of the higher order corrections, since they have not been calculated. They may be larger or smaller by a factor of 2 or 3. Without calculating the corrections directly, it is not possible to know. We will come back to this qualification shortly.

Second, there are the violations of quark-hadron duality. These violations are hard to quantify, but they should be small if we are not dominated by a just a few resonances; the more final states, the smaller the duality violations. In the region that we are interested in, it does not appear that we are dominated by resonances, so neglecting them should be okay. It would be better if we could have a larger number of the decay products.

This is possible if we cut on different kinematic variables. The other variables discussed in the literature are the hadronic invariant mass [15], and the lepton invariant mass [16]. The hadronic invariant mass spectrum also has dependence on the

structure function [15,17], which introduces model dependence. However, by using a method analogous to the one described above for the electron spectrum, the dependence on the structure function can be eliminated [18,19]. The errors from higher order corrections are similar to the electron spectrum and should be around 10%. The main advantage of the hadronic invariant mass is that after a cut to remove the charm background, between 40% and 80% of the possible final states will be included. This is much larger than for the electron spectrum, which includes about 10% of the possible final states. Thus the quark-hadron duality violations should be negligible.

The leptonic invariant mass cut has different advantages [16,20]. Here the structure function is not important, so we do not need to do anything to remove this model dependence. Higher order non-perturbative corrections are on the order of  $(\Lambda/m_c)^3$ , which leads to an error again of around 10%. This disadvantage for this cut is the fraction of final states included after the cut is around 20%, so the quark-hadron duality errors may be an issue. There is also some question about how good a resolution can be obtained on the lepton invariant mass, which is the only immediate problem for this method.

All three of the above methods should have a theoretical uncertainty (modulo quark-hadron duality violations) of around 10%. Again, these are estimates of higher order corrections. The actual errors may be bigger or smaller. Also, the duality violations could enter in different ways for each measurement. To really trust any extraction of  $|V_{ub}|$ , we should measure it as many ways as possible, and only after (or if) there is a convergence of the results should we trust the extracted value.

## Acknowledgments

I would like to my collaborators I. Low and I. Z. Rothstein, and the organizers of Radcor 2000 for a very enjoyable conference.

## References

- [1] For a recent review on methods for extracting  $V_{ub}$  along with reasonable assessments of theory errors, see Z. Ligeti, hep-ph/9908432.
- [2] B. H. Behrens *et al.* [CLEO Collaboration], Phys. Rev. **D61**, 052001 (2000).
- [3] T. van Ritbergen, Phys. Lett. **B454**, 353 (1999).
- [4] For a review on calculating the effective weak Hamiltonian, see A. J. Buras, hep-ph/9901409.

- [5] J. Chay, H. Georgi, and B. Grinstein, Phys. Lett. **B247** 399 (1990); M. Voloshin and M. Shifman, Sov. J. Nucl. Phys. **41** 120 (1985).
- [6] I.I. Bigi, M.A. Shifman, N.G. Uraltsev, and A.I. Vainshtein, Int. J. Mod. Phys. **A9** 2467 (1994).
- [7] A.V. Manohar and M.B. Wise, Phys. Rev. **D49** 1310 (1994); I.I. Bigi, M. Shifman, N.G. Uraltsev and A.I. Vainshtein, Phys. Rev. Lett. **71** 496 (1993); B. Blok, L. Koyrakh, M. Shifman and A.I. Vainshtein, Phys. Rev. **D49** (1994), 3356; ERRATUM-ibid. **D50** 3572 (1994); T. Mannel, Nucl. Phys. **B413** 396 (1994).
- [8] M. Neubert, Phys. Rev. **D49** 3392 (1994); T. Mannel and M. Neubert, Phys. Rev. **D50** 2037 (1994).
- [9] R.D. Dikeman, M. Shifman, and N.G. Uraltsev, Int. J. Mod. Phys. **A11** 571 (1996).
- [10] M. Jezabek and J.H. Kühn, Nucl. Phys. **B320** 961 (1989).
- [11] A. K. Leibovich and I. Z. Rothstein, Phys. Rev. **D61**, 074006 (2000).
- [12] G. Sterman and G.P. Korchemsky, Phys. Lett. **B340** 96 (1994).
- [13] R. Akhoury and I.Z. Rothstein, Phys. Rev. **D54** 2349 (1996).
- [14] A. K. Leibovich, I. Low and I. Z. Rothstein, Phys. Rev. **D61**, 053006 (2000).
- [15] A. Falk, Z. Ligeti and M.B. Wise, Phys. Lett. **406** 225 (1997).
- [16] C. W. Bauer, Z. Ligeti and M. Luke, Phys. Lett. **B479**, 395 (2000).
- [17] T. Mannel and S. Recksiegel, Phys. Rev. **D60** 114040 (1999); F. De Fazio and M. Neubert, JHEP **9906**, 017 (1999).
- [18] A. K. Leibovich, I. Low and I. Z. Rothstein, Phys. Rev. **D62**, 014010 (2000).
- [19] A. K. Leibovich, I. Low and I. Z. Rothstein, Phys. Lett. **B486**, 86 (2000).
- [20] M. Luke, these proceedings.

UTPT-01-03  
 UCSD/PTH 01-02  
 LBNL-47132  
 August 8, 2001  
 hep-ph/0101328

## Determining $|V_{ub}|$ from the $\bar{B} \rightarrow X_u \ell \bar{\nu}$ dilepton invariant mass spectrum<sup>\*\*</sup>

CHRISTIAN W. BAUER,<sup>1</sup> ZOLTAN LIGETI,<sup>2</sup> AND MICHAEL LUKE<sup>3</sup>

<sup>1</sup>*Department of Physics, University of California, San Diego,  
 9500 Gilman Drive, La Jolla CA USA 92093*

<sup>2</sup>*Theoretical Physics Group  
 Ernest Orlando Lawrence Berkeley National Laboratory  
 University of California, Berkeley, CA USA 94720*

<sup>3</sup>*Department of Physics, University of Toronto,  
 60 St. George Street, Toronto, Ontario, Canada M5S 1A7*

The invariant mass spectrum of the lepton pair in inclusive semileptonic  $\bar{B} \rightarrow X_u \ell \bar{\nu}$  decay yields a model independent determination of  $|V_{ub}|$  [1]. Unlike the lepton energy and hadronic invariant mass spectra, nonperturbative effects are only important in the resonance region, and play a parametrically suppressed role when  $d\Gamma/dq^2$  is integrated over  $q^2 > (m_B - m_D)^2$ , which is required to eliminate the  $\bar{B} \rightarrow X_c \ell \bar{\nu}$  background. We discuss these backgrounds for  $q^2$  slightly below  $(m_B - m_D)^2$ , and point out that instead of  $q^2 > (m_B - m_D)^2 = 11.6 \text{ GeV}^2$ , the cut can be lowered to  $q^2 \gtrsim 10.5 \text{ GeV}^2$ . This is important experimentally, particularly when effects of a finite neutrino reconstruction resolution are included.

Presented at the

5th International Symposium on Radiative Corrections  
 (RADCOR-2000)

Carmel CA, USA, 11–15 September, 2000

---

<sup>\*\*</sup>Talk given by M.L.

A precise and model independent determination of the Cabibbo-Kobayashi-Maskawa (CKM) matrix element  $V_{ub}$  is important for testing the Standard Model at  $B$  factories via the comparison of the angles and the sides of the unitarity triangle.

If it were not for the huge background from decays to charm, it would be straightforward to determine  $|V_{ub}|$  from inclusive semileptonic decays. Inclusive  $B$  decay rates can be computed model independently in a series in  $\Lambda_{\text{QCD}}/m_b$  and  $\alpha_s(m_b)$  using an operator product expansion (OPE) [2,3,4,5], and the result may schematically be written as

$$d\Gamma = \left( \begin{array}{c} b \text{ quark} \\ \text{decay} \end{array} \right) \times \left\{ 1 + \frac{0}{m_b} + \frac{f(\lambda_1, \lambda_2)}{m_b^2} + \dots + \frac{\alpha_s}{\pi} (\dots) + \frac{\alpha_s^2}{\pi^2} (\dots) + \dots \right\}. \quad (1)$$

At leading order, the  $B$  meson decay rate is equal to the  $b$  quark decay rate. The leading nonperturbative corrections of order  $\Lambda_{\text{QCD}}^2/m_b^2$  are characterized by two heavy quark effective theory (HQET) matrix elements, usually called  $\lambda_1$  and  $\lambda_2$ . These matrix elements also occur in the expansion of the  $B$  and  $B^*$  masses in powers of  $\Lambda_{\text{QCD}}/m_b$ ,

$$m_B = m_b + \bar{\Lambda} - \frac{\lambda_1 + 3\lambda_2}{2m_b} + \dots, \quad m_{B^*} = m_b + \bar{\Lambda} - \frac{\lambda_1 - \lambda_2}{2m_b} + \dots. \quad (2)$$

Similar formulae hold for the  $D$  and  $D^*$  masses. The parameters  $\bar{\Lambda}$  and  $\lambda_1$  are independent of the heavy  $b$  quark mass, while there is a weak logarithmic scale dependence in  $\lambda_2$ . The measured  $B^* - B$  mass splitting fixes  $\lambda_2(m_b) = 0.12 \text{ GeV}^2$ , while  $\bar{\Lambda}$  and  $\lambda_1$  (or, equivalently, a short distance  $b$  quark mass and  $\lambda_1$ ) may be determined from other physical quantities [6,7,8]. Thus, a measurement of the total  $B \rightarrow X_u \ell \bar{\nu}$  rate would provide a  $\sim 5\%$  determination of  $|V_{ub}|$  [9,10].

Unfortunately, the  $\bar{B} \rightarrow X_u \ell \bar{\nu}$  rate can only be measured imposing cuts on the phase space to eliminate the  $\sim 100$  times larger  $\bar{B} \rightarrow X_c \ell \bar{\nu}$  background. Since the predictions of the OPE are only model independent for *sufficiently inclusive* observables, these cuts can destroy the convergence of the expansion. This is the case for two kinematic regions for which the charm background is absent and which have received much attention: the large lepton energy region,  $E_\ell > (m_B^2 - m_D^2)/2m_B$ , and the small hadronic invariant mass region,  $m_X < m_D$  [11,12,13].

The poor behaviour of the OPE for these quantities is slightly subtle, because in both cases there is sufficient phase space for many different resonances to be produced in the final state, so an inclusive description of the decays is still appropriate. However, in both of these regions of phase space the  $\bar{B} \rightarrow X_u \ell \bar{\nu}$  decay products are dominated by high energy, low invariant mass hadronic states,

$$E_X \sim m_b, \quad m_X^2 \sim \Lambda_{\text{QCD}} m_b \gg \Lambda_{\text{QCD}}^2 \quad (3)$$

(where  $E_X$  and  $m_X$  are the energy and invariant mass of the final hadronic state). In this region the differential rate is very sensitive to the details of the wave function of

the  $b$  quark in the  $B$  meson. Since the OPE is just sensitive to local matrix elements corresponding to expectation values of operators in the meson, the first few orders in the OPE do not contain enough information to describe the decay, and as a result the OPE does not converge.

This is simple to see by considering the kinematics. A  $b$  quark in a  $B$  meson has momentum

$$p_b^\mu = m_b v^\mu + k^\mu \quad (4)$$

where  $v^\mu$  is the four-velocity of the quark, and  $k^\mu$  is a small residual momentum of order  $\Lambda_{\text{QCD}}$ . If the hadron decays to leptons with momentum  $q$  and light hadrons with total momentum  $p_X$ , the invariant mass of the light hadrons may be written

$$m_X^2 = (m_b v + k - q)^2 = (m_b v - q)^2 + 2k \cdot (m_b v - q) + O(\Lambda_{\text{QCD}}^2). \quad (5)$$

The first term in the expansion is  $O(m_b^2)$  over most of phase space, while the second is  $O(\Lambda_{\text{QCD}} m_b)$ , and so is suppressed over most of phase space. The OPE presumes that this power counting holds, so that the second term may be treated as a small perturbation. However, if  $E_X$  is large and  $m_X$  is small,  $m_b v - q$  is almost light-like,

$$m_b v^\mu - q^\mu = (E_X, 0, 0, E_X) + O(\Lambda_{\text{QCD}}) \quad (6)$$

in the  $b$  rest frame where  $v^\mu = (1, 0, 0, 0)$ . Since  $E_X \sim O(m_b)$ ,  $(m_b v - q)^2 = O(\Lambda_{\text{QCD}} m_b)$ . Thus, in this region the first two terms in (5) are of the same order (but still parametrically larger than the remaining terms), and the invariant mass of the final hadronic state reflects the distribution of the light-cone component of the residual momentum of the heavy quark in the hadron,

$$m_X^2 = (m_b v - q)^2 + 2E_X k_+ + \dots, \quad k_+ \equiv k_0 + k_3. \quad (7)$$

Since the differential rate in this region depends on the invariant mass of the final state, it is therefore sensitive at leading order to the light-cone wave function of the heavy quark in the meson,  $f(k_+)$ .

In terms of the OPE, this light-cone wave function arises because of subleading terms in the OPE proportional to  $E_X \Lambda_{\text{QCD}} / m_X^2$ , which are suppressed over most of phase space but are  $O(1)$  in the region (3). It has been shown that the most singular terms in the OPE may be resummed into a nonlocal operator whose matrix element in a  $B$  meson is the light-cone structure function of the meson. Since  $f(k_+)$  is a nonperturbative function, it cannot be calculated analytically, so the rate in the region (3) is model-dependent even at leading order in  $\Lambda_{\text{QCD}} / m_b$ .

The situation is illustrated in Fig. 1, where we have plotted the lepton energy and hadronic invariant mass spectra in the parton model (dashed curves) and incorporating a simple one-parameter model for the distribution function (solid curves) [17]

$$f(k_+) = \frac{32}{\pi^2 \Lambda} (1-x)^2 \exp\left[-\frac{4}{\pi}(1-x)^2\right] \Theta(1-x), \quad x \equiv \frac{k_+}{\Lambda}, \quad \Lambda = 0.48 \text{ GeV}. \quad (8)$$

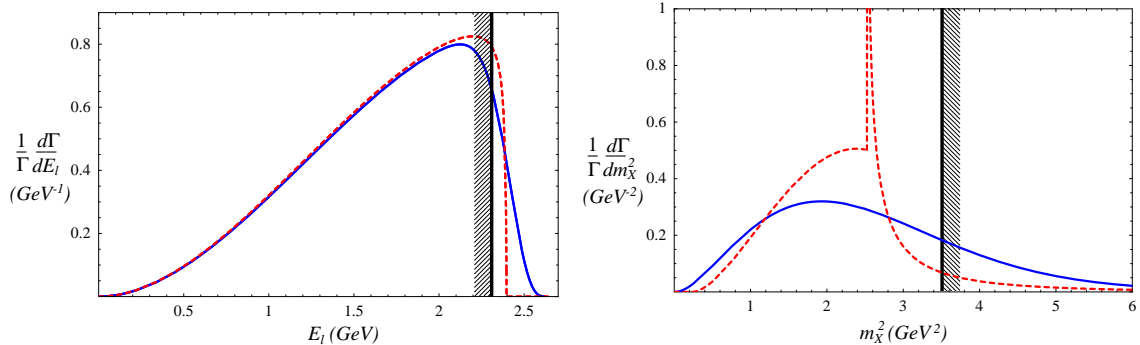


Figure 1: The shapes of the lepton energy and hadronic invariant mass spectra. The dashed curves are the  $b$  quark decay results to  $\mathcal{O}(\alpha_s)$ , while the solid curves are obtained by smearing with the model distribution function  $f(k_+)$  in Eq. (8). The unshaded side of the vertical lines indicate the region free from charm background.

The differences between the curves in the regions of interest indicate the sensitivity of the spectrum to the precise form of  $f(k_+)$ . Currently, there are measurements of  $|V_{ub}|$  from both methods. From the lepton energy cut, the PDG reports  $|V_{ub}/V_{cb}| = 0.08 \pm 0.02$ , while a recent DELPHI measurement using the hadronic invariant mass cut gives  $|V_{ub}/V_{cb}| = 0.103_{-0.012}^{+0.011} (\text{syst.}) \pm 0.016 (\text{stat.}) \pm 0.010 (\text{theory})$  [16]. In both cases, the theoretical error is an estimate based on varying different models of  $f(k_+)$ , and so these measurements are no more model-independent than the exclusive measurement from  $B \rightarrow \rho \ell \bar{\nu}$ . While it may be possible in the future to extract  $f(k_+)$  from the  $B \rightarrow X_s \gamma$  photon spectrum [14,18], unknown order  $\Lambda_{\text{QCD}}/m_b$  corrections arise when relating this to semileptonic  $b \rightarrow u$  decay, limiting the accuracy with which  $|V_{ub}|$  may be obtained.

Clearly, one would like to be able to find a cut which eliminates the charm background but does not destroy the convergence of the OPE, so that the distribution function  $f(k_+)$  is not required. In Ref. [1] we pointed out that this is the situation for a cut on the dilepton invariant mass. Decays with  $q^2 \equiv (p_\ell + p_{\bar{\nu}})^2 > (m_B - m_D)^2$  must arise from  $b \rightarrow u$  transition. Such a cut forbids the hadronic final state from moving fast in the  $B$  rest frame, and simultaneously imposes  $m_X < m_D$  and  $E_X < m_D$ . Thus, the light-cone expansion which gives rise to the shape function is not relevant in this region of phase space [13,19]. The effect of smearing the  $q^2$  spectrum with the model distribution function in Eq. (8) is illustrated in Fig. 2. It is clearly a subleading effect. The Dalitz plots relevant for the charged lepton energy and hadronic invariant mass cuts are shown in Fig. 3. Note that the region selected by a  $q^2$  cut is entirely contained within the  $m_X^2$  cut, but because the dangerous region of high energy, low invariant mass final states is not included with the  $q^2$  cut, the OPE does not break down. It is also important to note, however, that the  $q^2$  cut does make the OPE worse than for the full rate; as we will show, the relative size of the unknown  $\Lambda_{\text{QCD}}^3/m_b^3$  terms grows

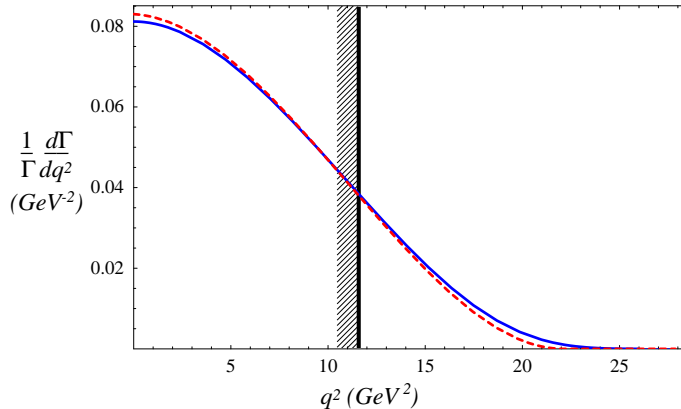


Figure 2: The dilepton invariant mass spectrum. The notation is the same as in Fig. 1.

as the  $q^2$  cut is raised. Equivalently, as was stressed in [20], the effective expansion parameter for this region is  $\Lambda_{\text{QCD}}/m_c$ , not  $\Lambda_{\text{QCD}}/m_b$ .

The  $\overline{B} \rightarrow X_u \ell \overline{\nu}$  decay rate with lepton invariant mass above a given cutoff can therefore be reliably computed working to a fixed order in the OPE (i.e., ignoring the light-cone distribution function),

$$\begin{aligned} \frac{1}{\Gamma_0} \frac{d\Gamma}{d\hat{q}^2} &= \left(1 + \frac{\lambda_1}{2m_b^2}\right) 2(1 - \hat{q}^2)^2 (1 + 2\hat{q}^2) + \frac{\lambda_2}{m_b^2} (3 - 45\hat{q}^4 + 30\hat{q}^6) \\ &+ \frac{\alpha_s(m_b)}{\pi} X(\hat{q}^2) + \left(\frac{\alpha_s(m_b)}{\pi}\right)^2 \beta_0 Y(\hat{q}^2) + \dots, \end{aligned} \quad (9)$$

where  $\hat{q}^2 = q^2/m_b^2$ ,  $\beta_0 = 11 - 2n_f/3$ , and  $\Gamma_0 = G_F^2 |V_{ub}|^2 m_b^5 / (192 \pi^3)$  is the tree level  $b \rightarrow u$  decay rate. The ellipses in Eq. (9) denote terms of order  $(\Lambda_{\text{QCD}}/m_b)^3$  and order  $\alpha_s^2$  terms not enhanced by  $\beta_0$ . The function  $X(\hat{q}^2)$  is known analytically [21], whereas  $Y(\hat{q}^2)$  was computed numerically [22]. The order  $1/m_b^3$  nonperturbative corrections are also known [23], as are the leading logarithmic perturbative corrections proportional to  $\alpha_s^n \log^n(m_c/m_b)$  [20]. The matrix element of the kinetic energy operator,  $\lambda_1$ , only enters the  $\hat{q}^2$  spectrum in a very simple form, because the unit operator and the kinetic energy operator are related by reparameterization invariance [24].

The relation between the total  $\overline{B} \rightarrow X_u \ell \overline{\nu}$  decay rate and  $|V_{ub}|$  is known at the  $\sim 5\%$  level [9,10],

$$|V_{ub}| = (3.04 \pm 0.06 \pm 0.08) \times 10^{-3} \left( \frac{\mathcal{B}(\overline{B} \rightarrow X_u \ell \overline{\nu})|_{q^2 > q_0^2}}{0.001 \times F(q_0^2)} \frac{1.6 \text{ ps}}{\tau_B} \right)^{1/2}, \quad (10)$$

where  $F(q_0^2)$  is the fraction of  $\overline{B} \rightarrow X_u \ell \overline{\nu}$  events with  $q^2 > q_0^2$ , satisfying  $F(0) = 1$ . The errors explicitly shown in Eq. (10) are the estimates of the perturbative and nonperturbative uncertainties in the upsilon expansion [9] respectively. At the

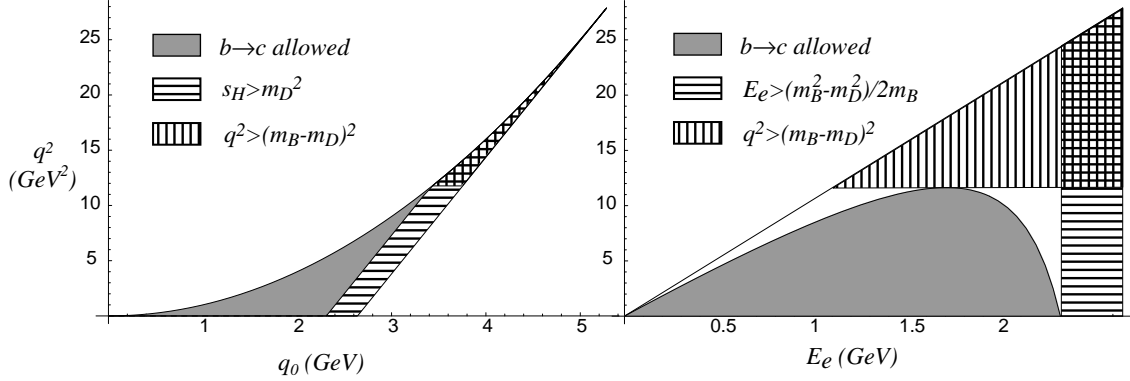


Figure 3: Dalitz plots relevant for  $\bar{B} \rightarrow X_u \ell \bar{\nu}_\ell$ . The shaded regions indicate the part of phase space where  $\bar{B} \rightarrow X_c \ell \bar{\nu}_\ell$  background is present, and the vertical dashed regions corresponds to the cut  $q^2 > (m_B - m_D)^2$ . In the  $q^2 - q_0$  plane, the horizontal dashed region corresponds to an invariant mass cut  $m_X^2 > m_D^2$ , whereas in the  $q^2 - E_\ell$  plane the horizontal dashed region corresponds to the charged lepton energy cut  $E_\ell > (m_B^2 - m_D^2)/2m_B$ . Note that at tree level,  $b \rightarrow u$  semileptonic decay populates the entire triangle on the right-hand plot, but only the right boundary of the left-hand plot.

present time the biggest uncertainty is due to the error of a short distance  $b$  quark mass, whichever way it is defined [20]. (This can be cast into an uncertainty in an appropriately defined  $\bar{\Lambda}$ , or the nonperturbative contribution to the  $\Upsilon(1S)$  mass, etc.) By the time the  $q^2$  spectrum in  $\bar{B} \rightarrow X_u \ell \bar{\nu}$  is measured, this uncertainty should be reduced from extracting  $m_b$  from the hadron mass [6] or lepton energy [7] spectra in  $\bar{B} \rightarrow X_c \ell \bar{\nu}$ , or from the photon energy spectrum [8] in  $B \rightarrow X_s \gamma$ . The uncertainty in the perturbation theory calculation will be largely reduced by computing the full order  $\alpha_s^2$  correction in Eq. (10). The largest “irreducible” uncertainty is from order  $\Lambda_{\text{QCD}}^3/m_b^3$  terms in the OPE, the estimated size of which is shown in Fig. 4, together with our central value for  $F(q_0^2)$ , as functions of  $q_0^2$ .

There is another advantage of the  $q^2$  spectrum over the  $m_X$  spectrum to measure  $|V_{ub}|$ . In the variable  $m_X$ , about 20% of the charm background is located right next to the  $b \rightarrow u$  “signal region”,  $m_X < m_D$ , namely  $\bar{B} \rightarrow D \ell \bar{\nu}$  at  $m_X = m_D$ . In the variable  $q^2$ , the charm background just below  $q^2 = (m_B - m_D)^2$  comes from the lowest mass  $X_c$  states. Their  $q^2$  distributions are well understood based on heavy quark symmetry [25], since this region corresponds to near zero recoil. Fig. 5 shows the  $\bar{B} \rightarrow D \ell \bar{\nu}$  and  $\bar{B} \rightarrow D^* \ell \bar{\nu}$  decay rates using the measured form factors [26] (and  $|V_{ub}| = 0.0035$ ). The  $\bar{B} \rightarrow X_u \ell \bar{\nu}$  rate is the flat curve. Integrated over the region  $q^2 > (m_B - m_{D^*})^2 \simeq 10.7 \text{ GeV}^2$ , the uncertainty of the  $B \rightarrow D$  background is small due to its  $(w^2 - 1)^{3/2}$  suppression compared to the  $\bar{B} \rightarrow X_u \ell \bar{\nu}$  signal. This uncertainty will be further reduced in the near future. This increases the  $b \rightarrow u$  region relevant

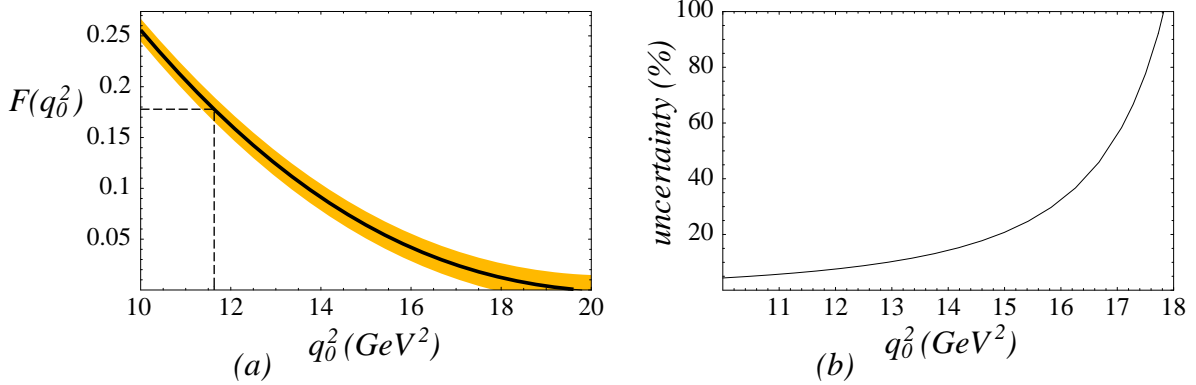


Figure 4: (a) The fraction of  $\overline{B} \rightarrow X_u \ell \overline{\nu}$  events with  $q^2 > q_0^2$ ,  $F(q_0^2)$ , in the upsilon expansion. The dashed line indicates the lower cut  $q_0^2 = (m_B - m_D)^2 \simeq 11.6 \text{ GeV}^2$ , which corresponds to  $F = 0.178 \pm 0.012$ . The shaded region is the estimated uncertainty due to  $\Lambda_{\text{QCD}}^3/m_b^3$  terms; which is shown in (b) as a percentage of  $F(q_0^2)$ .

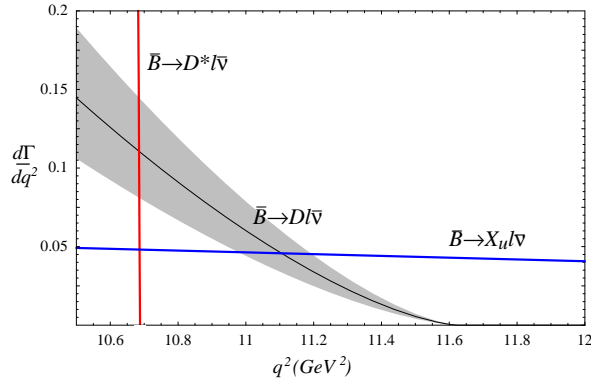


Figure 5: Charm backgrounds near  $q^2 = (m_B - m_D)^2$  (arbitrary units). The shaded region denotes the uncertainty on the  $\overline{B} \rightarrow D \ell \overline{\nu}$  rate.

for measuring  $|V_{ub}|$  by  $\sim 1 \text{ GeV}^2$ . The  $B \rightarrow D^*$  rate is only suppressed by  $(w^2 - 1)^{1/2}$  near zero recoil, and therefore it is more difficult to subtract it reliably from the  $b \rightarrow u$  signal. The nonresonant  $D\pi$  final state contributes in the same region as  $\overline{B} \rightarrow D^*$ , and it is reliably predicted to be small near maximal  $q^2$  (zero recoil) based on chiral perturbation theory [27]. The  $D^{**}$  states only contribute for  $q^2 < 9 \text{ GeV}^2$ , and some aspects of their  $q^2$  spectra are also known model independently [28].

Concerning experimental considerations, measuring the  $q^2$  spectrum requires reconstruction of the neutrino four-momentum, just like measuring the hadronic invariant mass spectrum. A lepton energy cut may be required for this technique, however, the constraint  $q^2 > (m_B - m_D)^2$  automatically implies  $E_\ell > (m_B - m_D)^2/2m_B \simeq 1.1 \text{ GeV}$  in the  $B$  rest frame. Even if the  $E_\ell$  cut has to be slightly larger than this, the utility of our method will not be affected, but a calculation including the effects

of arbitrary  $E_\ell$  and  $q^2$  cuts would be required. If experimental resolution on the reconstruction of the neutrino momentum necessitates a significantly larger cut than  $q_0^2 = (m_B - m_D)^2$ , then the uncertainties in the OPE calculation of  $F(q_0^2)$  increase. In this case, it may be possible to obtain useful model independent information on the  $q^2$  spectrum in the region  $q^2 > m_{\psi(2S)}^2 \simeq 13.6 \text{ GeV}^2$  from the  $q^2$  spectrum in the rare decay  $\bar{B} \rightarrow X_s \ell^+ \ell^-$ , which may be measured in the upcoming Tevatron Run-II.

In conclusion, we have shown that the  $q^2$  spectrum in inclusive semileptonic  $\bar{B} \rightarrow X_u \ell \bar{\nu}$  decay gives a model independent determination of  $|V_{ub}|$  with small theoretical uncertainty. Nonperturbative effects are only important in the resonance region, and play a parametrically suppressed role when  $d\Gamma/dq^2$  is integrated over  $q^2 > (m_B - m_D)^2$ , which is required to eliminate the charm background. This is a qualitatively better situation than other extractions of  $|V_{ub}|$  from inclusive charmless semileptonic  $B$  decay.

## Acknowledgements

This work was supported in part by the Natural Sciences and Engineering Research Council of Canada and by the Director, Office of Science, Office of High Energy and Nuclear Physics, Division of High Energy Physics, of the U.S. Department of Energy under Contract DE-AC03-76SF00098.

## References

- [1] C.W. Bauer, Z. Ligeti, and M. Luke, Phys. Lett. B479 (2000) 395.
- [2] J. Chay, H. Georgi, and B. Grinstein, Phys. Lett. B247 (1990) 399; M. Voloshin and M. Shifman, Sov. J. Nucl. Phys. 41 (1985) 120.
- [3] I.I. Bigi *et al.*, Phys. Lett. B293 (1992) 430; Phys. Lett B297 (1993) 477 (E); I.I. Bigi *et al.*, Phys. Rev. Lett. 71 (1993) 496.
- [4] A.V. Manohar and M.B. Wise, Phys. Rev. D49 (1994) 1310.
- [5] B. Blok *et al.*, Phys. Rev. D49 (1994) 3356.
- [6] A.F. Falk, M. Luke, and M.J. Savage, Phys. Rev. D53 (1996) 2491; Phys. Rev. D53 (1996) 6316; A.F. Falk and M. Luke, Phys. Rev. D57 (1998) 424.
- [7] M. Gremm *et al.*, Phys. Rev. Lett. 77 (1996) 20; M.B. Voloshin, Phys. Rev. D51 (1995) 4934.

- [8] A. Kapustin and Z. Ligeti, Phys. Lett. B355 (1995) 318; C. Bauer, Phys. Rev. D57 (1998) 5611; Erratum *ibid.* D60 (1999) 099907; Z. Ligeti, M. Luke, A.V. Manohar, and M.B. Wise, Phys. Rev. D60 (1999) 034019; A.L. Kagan and M. Neubert, Eur. Phys. J. C7 (1999) 5.
- [9] A.H. Hoang, Z. Ligeti, and A.V. Manohar, Phys. Rev. Lett. 82 (1999) 277; Phys. Rev. D59 (1999) 074017.
- [10] N. Uraltsev, Int. J. Mod. Phys. A14 (1999) 4641.
- [11] V. Barger, C. S. Kim and R. J. Phillips, Phys. Lett. B251, (1990) 629.
- [12] A.F. Falk, Z. Ligeti, and M.B. Wise, Phys. Lett. B406 (1997) 225; I. Bigi, R.D. Dikeman, and N. Uraltsev, Eur. Phys. J. C4 (1998) 453.
- [13] R. D. Dikeman and N. Uraltsev, Nucl. Phys. B509 (1998) 378.
- [14] M. Neubert, Phys. Rev. D49 (1994) 3392; D49 (1994) 4623; I.I. Bigi *et al.*, Int. J. Mod. Phys. A9 (1994) 2467.
- [15] F. De Fazio and M. Neubert, JHEP06 (1999) 017.
- [16] P. Abreu *et al.* [DELPHI Collaboration], Phys. Lett. B478 (2000) 14.
- [17] T. Mannel and M. Neubert, Phys. Rev. D50 (1994) 2037.
- [18] A.K. Leibovich, I. Low, and I.Z. Rothstein, Phys. Rev. D61 (2000) 053006; Phys. Lett. B486 (2000) 86.
- [19] G. Buchalla and G. Isidori, Nucl. Phys. B525 (1998) 333.
- [20] M. Neubert, JHEP 0007 (2000) 022.
- [21] M. Jezabek and J.H. Kuhn, Nucl. Phys. B314 (1989) 1.
- [22] M. Luke, M. Savage, and M.B. Wise, Phys. Lett. B343 (1995) 329.
- [23] C.W. Bauer and C.N. Burrell, Phys. Lett. B469 (1999) 248; hep-ph/9911404.
- [24] M. Luke and A.V. Manohar, Phys. Lett. B286 (1992) 348.
- [25] N. Isgur and M.B. Wise, Phys. Lett. B232 (1989) 113; Phys. Lett. B237 (1990) 527.
- [26] J. Bartelt *et al.*, CLEO Collaboration, hep-ex/9811042; the LEP average for  $B \rightarrow D^*$  is taken from <http://lepvcb.web.cern.ch/LEPVCB/Tampere.html>

- [27] C. Lee, M. Lu, and M.B. Wise, Phys. Rev. D46 (1992) 5040.
- [28] A.K. Leibovich *et al.*, Phys. Rev. Lett. 78 (1997) 3995; Phys. Rev. D57 (1998) 308.

# *CP*-Violation, the CKM Matrix and New Physics

DANIEL WYLER

*Institut für Theoretische Physik  
Universität Zürich  
Winterthurerstrasse 190  
8057 Zürich, Switzerland*

We discuss the influence of new physics on *CP*-violating observables. Assuming the standard model gives a correct description of tree level processes, we show how a consistent procedure can determine the parameters of the standard model and check its validity also in loop induced processes. A method to include new physics in a systematic way is sketched.

Presented at the

5th International Symposium on Radiative Corrections  
(RADCOR-2000)

Carmel CA, USA, 11–15 September, 2000

# 1 Introduction

Observation of novel phenomena often paves the way to new physics. For instance,  $\beta$  decays, parity and flavor violation required the existence of a new force, the weak interactions. At present, it is often thought that  $CP$ -violation could signal new physics beyond the standard model. Although the latter can indeed account for the observed effects <sup>1</sup> (even  $\epsilon'/\epsilon$  may be described by the standard model) its predictions are not well tested (compared to physics at LEP) and therefore a comprehensive study of  $CP$ -violation experiments is important. As sketched in figure 1,  $CP$ -violation manifests itself in many areas; only a comparison between them can determine the correct description. In the standard model, all  $CP$ -violation resides in the CKM matrix <sup>2</sup> which describes the couplings of the W-bosons to the quarks of different charges. Therefore all appreciable  $CP$ -violation occurs within flavor physics. Thus, one obvious strategy to search for new forces and particles would be to look for non-zero  $CP$ -violating effects where no flavour changes are involved, such as in electric dipole moments or asymmetries in nuclear reactions. Unfortunately, the effects of new physics are judged to be quite small (apart from the dipole moments). Therefore more chance is given to the flavor sector instead, that is the physics of Kaons and mostly B-mesons. For a recent extensive review of  $CP$ -violation, see ref. ([1]).

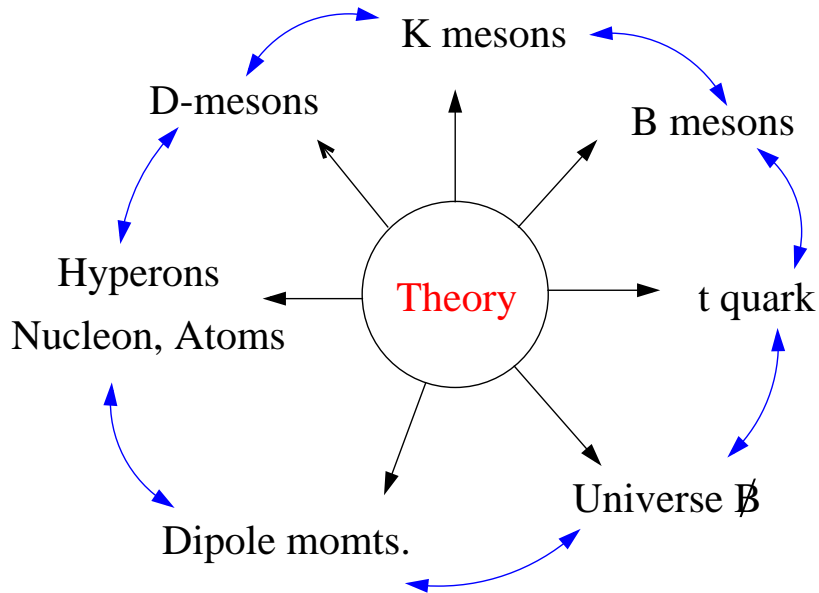


Figure 1: CP-Violation

---

<sup>1</sup>a notable exception is the baryon asymmetry in the universe

<sup>2</sup>I do not discuss the so-called  $\theta$  term

The unitarity of the CKM matrix

$$V = \begin{pmatrix} V_{ud} & V_{us} & V_{ub} \\ V_{cd} & V_{cs} & V_{cb} \\ V_{td} & V_{ts} & V_{tb} \end{pmatrix} \quad (1)$$

implies among others the triangle relation

$$V_{ud}V_{ub}^* + V_{cd}V_{cb}^* + V_{td}V_{tb}^* = 0 \quad (2)$$

which relates observable products of matrix elements and gives stringent tests of the validity of the standard model. Using the Wolfenstein parametrization and scaling as usual the bottom side to one, we can write for the other sides of the scaled triangle

$$R_b = \frac{1}{A\lambda^3}V_{ud}V_{ub}^* = \bar{\varrho} + i\bar{\eta} \quad , \quad R_t = \frac{1}{A\lambda^3}V_{td}V_{tb}^* = 1 - (\bar{\varrho} + i\bar{\eta}). \quad (3)$$

Here, following ref. [2], the quantities

$$\bar{\varrho} = \varrho\left(1 - \frac{\lambda^2}{2}\right) \quad \bar{\eta} = \eta\left(1 - \frac{\lambda^2}{2}\right) \quad (4)$$

are introduced to take into account even higher powers of  $\lambda$ .

An elaborate analysis of superallowed  $\beta$  decay, semileptonic Kaon and  $D$ -meson decays and decays of  $B$  mesons into charmed and charmless final states yields [3]

$$\begin{aligned} V_{ud} &= 0.9736 \pm 0.001 & V_{cs} &= 1.010 \pm 0.16 \\ V_{us} &= 0.2205 \pm 0.0018 & V_{cd} &= 0.224 \pm 0.016 \\ V_{ub} &= 0.04 \pm 0.002 & V_{cb} &= 0.0036 \pm 0.006 \end{aligned} \quad (5)$$

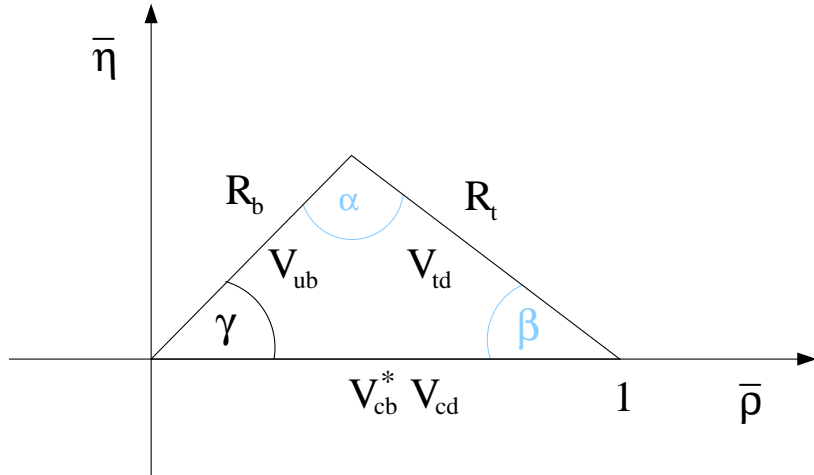


Figure 2: Unitarity triangle in the complex  $(\bar{\varrho}, \bar{\eta})$  plane

These are (apart from corrections) all tree-level processes and therefore thought to be governed by the standard model <sup>3</sup>. They are however not sufficient to check unitarity (unless very precise data from  $t$  decays would be available, or if the sum of the squares would be significantly away from 1).

Further input comes from loop-induced observables. They can be calculated within perturbation theory and input from hadronic physics. While the former are rather reliable and usually give results accurate to 10 percent or so, the latter are generally difficult to estimate. One usually considers the Kaon-mixing quantity  $\epsilon_K$ , the mass difference of the  $B$  and the  $\bar{B}$  mesons (and also of the  $B_s$  and  $\bar{B}_s$  mesons). This analysis has resulted in the range of values for the three angles  $\alpha$ ,  $\beta$  and  $\gamma$  of the unitary triangle and its sides. The hadronic uncertainties are summarized in [4] and are reflected by

$$|R_b| = 0.39 \pm 0.07 \quad |R_t| = 0.98 + 0.04 - 0.22 \quad (6)$$

and by [5,6,7]

$$(\sin 2\beta)_{\text{SM}} = 0.75 \pm 0.20. \quad (7)$$

The new results of last summer and of the beginning of this year concern the angle  $\beta$ . It was found that the coefficient  $a$  of  $\sin(\Delta M_{B_d})$  in the asymmetry for  $B \rightarrow J/\Psi K_S$  is

$$a = 0.79 \pm 0.4(\text{CDF})[8] \quad (8)$$

$$a = 0.58 \pm 0.35(\text{Belle})[9] \quad (9)$$

$$a = 0.34 \pm 0.25(\text{BaBar})[10] \quad (10)$$

In the standard model, one has  $a = \sin(2\beta)$ ; comparing eqs. (7) and (10) we see a surprising inconsistency. Of course, this is a preliminary result, and may disappear as experiments collect more statistics. However, it makes it mandatory to investigate  $CP$ -violation in a (standard) model independent way. Unless  $CP$ -violation within the standard model is grossly wrong, this program essentially amounts to making many measurements and extracting discrepancies between quantities thought to be the same in the standard model. Many authors have discussed this situation; see e.g. [11,12,13,14,15].

## 2 A more general framework

New physics may affect every process. Because the standard model describes the most important weak decays, we will assume that it accounts for semileptonic and tree-level quark decays, at least to the required accuracy. This assumption can be

---

<sup>3</sup>of course, the small  $b \rightarrow u$  transition could be due to new physics

tested, by investigating the consistency of different semileptonic decays, bounds from LEP etc. As an example consider the strengths of the effective Hamiltonians

$$\mathcal{H}_{eff} = G_F(\bar{c}_L\gamma_\mu b_L)(\bar{s}_L\gamma^\mu c_L) \quad (11)$$

$$\mathcal{H}_{eff} = G_F(\bar{u}_L\gamma_\mu b_L)(\bar{s}_L\gamma^\mu u_L). \quad (12)$$

In the standard model, they are proportional to  $\lambda^2$  and  $\lambda^4$ , respectively. On the other hand, a new neutral intermediate boson, say  $Z'$ , may exist, coupled to the currents  $(\bar{s}_L\gamma_\mu b_L)$  and  $(\bar{c}_L\gamma_\mu c_L)$ . If it also couples to quark and lepton pairs, such as  $(\bar{u}_L\gamma_\mu u_L)$  and  $(\bar{c}_L\gamma_\mu c_L)$ , it would contribute to the above Hamiltonians, to  $B_s$  mixing, to  $B_s \rightarrow l^+l^-$  etc. If the couplings are the same for all these pairs, the effective strength would be the same for the two terms in eqs. (11) and (12). Therefore a new  $Z'$ -mediated interaction would induce a deviation from the standard model result that the couplings of the two interactions have a relative strength of  $\lambda^2$ . Thus detailed studies could in principle also test the first assumption. But of course, there are various experimental and theoretical difficulties to overcome before one will obtain accurate enough results.

From fig. 3 we see that the determination of the angle  $\gamma$  from tree level processes involves the interference of amplitudes proportional to  $V_{ub}$  and  $V_{cb}$  respectively. This is achieved in processes where the two diagrams of fig. 3 contribute. A well known example are the decays  $B \rightarrow DK$  [16,17]; more recently the advantage of  $B_c \rightarrow DD_s$  was stressed [18]. The idea is the same as in the previous papers on  $B \rightarrow DK$  : One

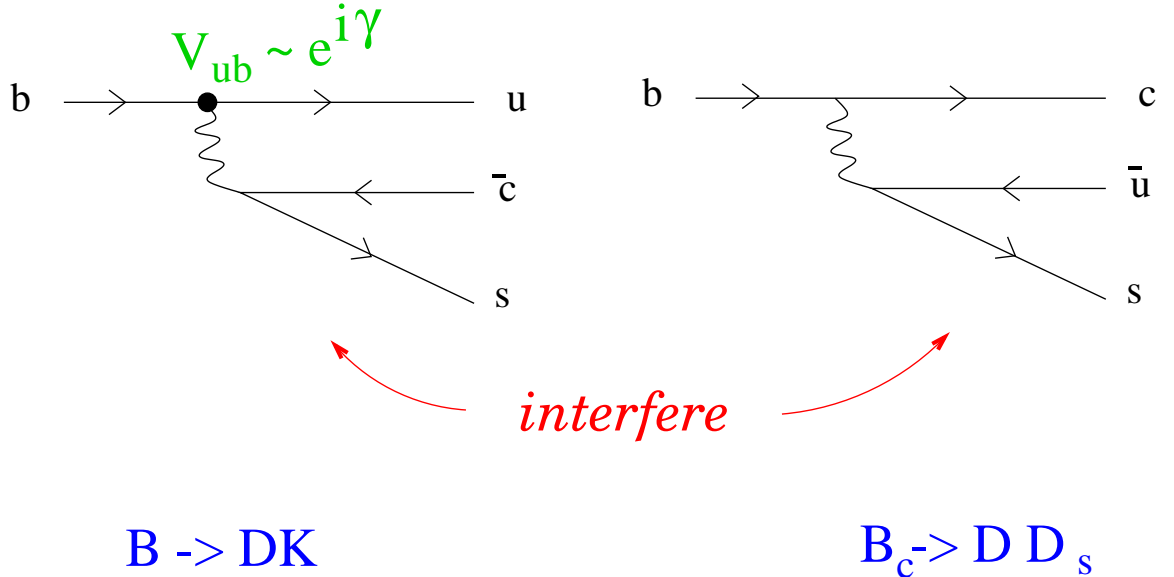


Figure 3: two quark diagrams whose interference gives  $\gamma$

needs to measure the six amplitudes shown in Fig. 4. However due to the different  $CKM$  elements, the sides of the triangles in Fig. 3 are now of similar length and an extraction of  $\gamma$  seems possible with the  $10^{10}$  or so  $B_c$ -mesons expected at LHC. This method does not suffer from hadronic uncertainties.

The experimental difficulties associated with these decays have lead to other possibilities. The decays  $B \rightarrow K\pi$  are sensitive to the interference of the tree level diagram (with  $V_{ub}$ ) and the penguin diagram. This also yields the angle  $\gamma$  if the penguin graph has no extra phase. This decay has been discussed by many people [19].

A third possibility that was investigated are the decays  $B^0 \rightarrow D^\pm \pi^\mp$  [20]. The usual mixing-decay formalism yields for the time dependent asymmetries the coefficients

$$a \sim \text{Im}(e^{-i(2\phi_{mix}+\gamma)})\text{const} \quad (13)$$

$$\bar{a} \sim \text{Im}(e^{-i(2\phi_{mix}+\gamma)})/\text{const}. \quad (14)$$

where const is an unknown hadronic number. It cancels in the product which then yields the combination

$$2\phi_{mix} + \gamma. \quad (15)$$

The  $B\bar{B}$  mixing angle  $\phi_{mix}$  can be determined as usual from the decay  $B \rightarrow J/\Psi K_s$ .

The other angles of the triangle cannot be determined independently by a tree level analysis. But we see, that the tree level analysis allows to determine the unitary triangle of the standard model. It yields, in principle, also the unknown side  $R_t$  and

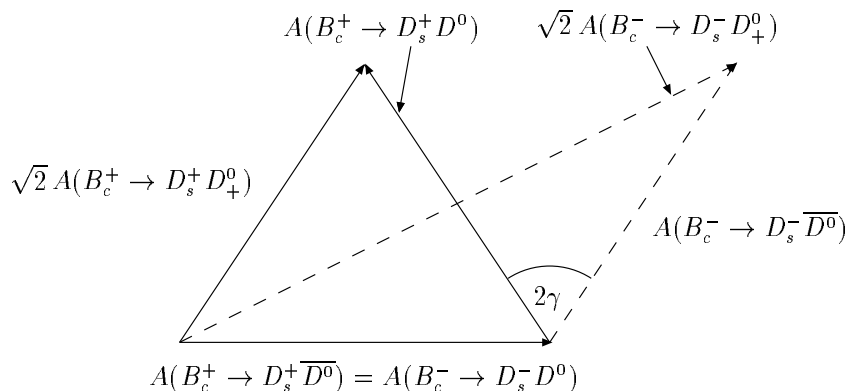


Figure 4: The extraction of  $\gamma$  from  $B_c^\pm \rightarrow D_s^\pm \{D^0, \bar{D}^0, D_+^0\}$  decays

the angle  $\beta$ . Any further independent measurement of these quantities checks the standard model with high accuracy, but it requires loop effects.

### 3 New Physics: Phenomenology

Among the  $CP$ -violating observables, the mixing-decay asymmetry is the cleanest theoretically [21]. It is therefore reasonable to start an investigation of new physics with this quantity. Denoting the coefficient of  $\sin(\Delta mt)$  by  $a$ , one has in general

$$a_{M \rightarrow F} = \text{Im}\left(\left(\frac{p}{q}\right)_M \frac{a}{\bar{a}} \left(\frac{p}{q}\right)_F\right) \quad (16)$$

where  $\left(\frac{p}{q}\right)$  are the mixing parameters and  $a, \bar{a}$  the amplitudes for  $M \rightarrow F$  and  $M \rightarrow \bar{F}$ , respectively.

Setting for the  $B$ -meson mixing element  $M_{12}$

$$M_{12} = r^2 e^{2i\phi^{NP}} e^{2i\beta} |M_{12}^{SM}| \quad (17)$$

to account for a possible new phase and magnitude of the mixing, the asymmetry coefficient is given in the table below:

<i>quarks</i>	$B_d$	$a$	$B_s$	$a$
$b \rightarrow c\bar{c}s$	$\Psi K_s$	$\beta + \phi_d^{NP}$	$DD_s$	$\phi_s^{NP}$
$b \rightarrow s\bar{s}s$	$\Phi K_s$	$\beta + \phi_d^{NP} + \phi^A$	$\Phi\Phi$	$\phi_s^{NP} + \phi^A$
$b \rightarrow u\bar{u}s$	$\pi\pi$			
$b \rightarrow c\bar{c}d$	$D^+ D^-$			
$b \rightarrow u\bar{u}s$	$\pi^0 K_s$			
$b \rightarrow s\bar{s}s$	$\Phi\pi$			

The phase  $\phi^A$  takes into account a possible new phase in the decay. The entries left out receive possibly sizeable contributions from penguin diagrams and cannot be brought to the simple form. This result tells us that comparing the different asymmetries, we can check the consistency of the standard model and determine the phases of new physics.

New physics will also influence other  $CP$ -violating observables, such as the direct asymmetries of, say, charged  $B$ -meson decays. In cases such as  $B \rightarrow K\pi$ , where the asymmetry is small in the standard model new physics may give rise to sizeable asymmetries. Of course, one needs to continue the experimental search for these, but because of the difficulty of calculating direct asymmetries, only quantitative statements are possible.

## 4 New Physics: Analysis

If new physics is associated with a scale  $\Lambda$  much above the weak scale ( $\sim M_W$ ), the total Lagrangian density may be written in the form [22]

$$\mathcal{L} = \mathcal{L}^{SM} + \sum d_i \mathcal{O}_i^{NP} \quad (18)$$

where the  $\mathcal{O}_i$  are operators of dimension six induced by new physics and their coefficients  $d_i$  are of order  $(1/\Lambda^2)$ . This 'effective' Lagrangian is not renormalizable, and therefore one usually uses the new operators only at tree level (see a discussion by). The  $CP$ -violation induced by effective operators  $\mathcal{O}_i^{NP}$  can in most cases only be seen when they are in loops, because the imaginary part (discontinuity) of the corresponding Feynman graph is responsible for  $CP$ -asymmetry. <sup>4</sup> At low energies we then have an effective Hamiltonian

$$\mathcal{H} = \sum c_i \mathcal{O}_i^{SM} + \sum d_i \mathcal{O}_i^{NP}. \quad (19)$$

The amplitudes for a process  $I \rightarrow F$  and the CP conjugated one  $\bar{I} \rightarrow \bar{F}$  then are

$$A(I \rightarrow F) = \sum c_j (R_j + iI_j)^{SM} + \sum d_j (R_j + iI_j)^{NP} \quad (20)$$

where  $R$  and  $I$  are the dispersive and absorptive parts of the matrix elements. For the charge-conjugated process we have similarly

$$A(\bar{I} \rightarrow \bar{F}) = \sum c_j^* (R_j + iI_j)^{SM} + \sum d_j^* (R_j + iI_j)^{NP} \quad (21)$$

When we calculate the  $CP$ -violating asymmetry  $\alpha \sim (|A(I \rightarrow F)|^2 - |A(\bar{I} \rightarrow \bar{F})|^2)$ , we obtain in leading order in QCD and in NP

$$\alpha \sim \text{Im}(cd^*) (R^{SM} I^{NP} - R^{NP} I^{SM}). \quad (22)$$

$R^{NP}$  is a (finite) tree level amplitude, however also the loop  $I^{NP}$  is finite. Therefore the problems associated with a the non-rnormalizable theory  $\sum d_i \mathcal{O}_i^{NP}$  disappear and exact predictions are indeed possible for the the  $CP$ -violating asymmetry. Therefore, an analysis of the effects of new operators is possible also at for CP-violating asymmetries, and not just at tree level!

## 5 New Physics: Models

Virtually any model beyond the standard one carries new sources for flavour and  $CP$ -violations. It is therefore more economical to look at them in increasing complexity.

---

<sup>4</sup>an exception is the electric dipole moment

The simplest one are the minimal flavour violating ones (MFV) where all sources of flavour violation reside in the CKM matrix. This results in many cases in a simple modification of the coefficients in the usual loop expressions. However, there still is a unitary triangle, but its sizes and angles may change. It was analyzed by Ali and London [6]; recently Buras and Buras [15] found a clever lower bound on  $\sin(2\beta)$ . The idea is simple. For both  $\epsilon$  and the  $B$ -meson mass difference, the standard model contribution consists mostly of a  $W - W - t - t$  box diagram; its value might be denoted by  $F_{tt}$ . The MFV modify this to

$$F_{tt} = S_0(m_t) (1 + f) . \quad (23)$$

Then we can write for  $\epsilon_K$

$$\epsilon_K \sim \bar{\eta} \left[ (1 - \bar{\varrho}) A^2 \eta_2 F_{tt} + P_c(\epsilon) \right] A^2 \hat{B}_K \quad (24)$$

while the  $B$ -meson mass difference yields the relation

$$R_t = 1.26 \frac{R_0}{A} \frac{1}{\sqrt{F_{tt}}} , \quad (25)$$

where

$$R_0 = \sqrt{\frac{(\Delta M)_d}{0.47/\text{ps}}} \left[ \frac{200 \text{ mev}}{F_{B_d} \sqrt{\hat{B}_d}} \right] \sqrt{\frac{0.55}{\eta_B}} . \quad (26)$$

With

$$\sin 2\beta = \frac{2\bar{\eta}(1 - \bar{\varrho})}{R_t^2} \quad (27)$$

one gets [2]

$$\sin 2\beta = \frac{1.26}{R_0^2 \eta_2} \left[ \frac{0.226}{A^2 \hat{B}_K} - \bar{\eta} P_c(\epsilon) \right] . \quad (28)$$

Since unitarity implies  $\bar{\eta} \leq R_b$ , there exists a lower bound on  $\sin 2\beta$ . A careful numerical analysis implies [23]

$$\sin 2\beta \geq 0.42. \quad (29)$$

The lower bound in fact corresponds to a  $F_{tt}$  which is three times larger than the standard model value.

Supersymmetry is a attractive candidate for new physics. In general, there are many new  $CP$ -violating phases. Since they can directly affect observables such as the electric dipole moment, it is natural to take them to be small (approximate  $CP$ -violation, [1]). In this situation, also  $CP$ -violating effects in the  $B$ -system are small. This implies a small angle  $\beta$ . This is in contrast to the standard model, where the flavour structure suppresses  $CP$ -violation. The problem with this scheme is that it is hard to get  $\epsilon_K$  right and that  $\epsilon'/\epsilon$  tends to be small.

Similarly, models with left-right symmetry tend to have small  $CP$ -violating phases, thus the effects tend to be small also.

## 6 $CP$ -violation in $D$ -mesons

In the standard model,  $CP$ -violation is small in the  $D$ -System. This is partly due to the rather large tree-level decay rates and small coupling of the third generation. Therefore one would expect new physics  $CP$ -violation mostly in the mixing (see [1] for a more detailed discussion). Recent studies of time-dependent decay rates of  $D^0 \rightarrow K^+\pi^-$  by the CLEO collaboration [24] and measurements of the combination of  $D^0 \rightarrow K^+K^-$  and  $D^0 \rightarrow K^-\pi^+$  rates by the FOCUS collaboration [25] gave first information on the mixing.

As usual, one defines the mixing quantities

$$x \equiv \frac{m_2 - m_1}{\Gamma}, \quad y \equiv \frac{\Gamma_2 - \Gamma_1}{2\Gamma}. \quad (30)$$

$CP$ -violation in the mixing is defined by the angle  $\phi$ . The experiments find that the quantity  $y \cos \phi$  is significantly larger than the expectation in the standard model. The errors being large, this result is not yet significant, but it shows the potential of  $D$ -meson physics.

## 7 $K$ -Physics

Finally let me mention  $K$ -physics. Of course, efforts continue in calculating  $\epsilon'/\epsilon$  and to overcome the hadronic difficulties, and there will be substantial progress. However, the rare decays  $K^+ \rightarrow \pi^+\nu\bar{\nu}$  and  $K^0 \rightarrow \pi^0\nu\bar{\nu}$  provide a theoretically clean way to measure (in the standard model)  $|V_{td}|$  and  $ImV_{td}$  [26]. Clearly, this can be used as a test of the unitary triangle, however the measurement of the neutral decays is not easy and probably many years away.

## 8 Conclusions

The new results on  $\sin 2\beta$  are surprising; they may indicate a failure of the standard model. Several parameters have to be stretched beyond their reasonable values to account for them. One can modify the standard model to accommodate the small value of  $\sin 2\beta$ , but it is not clear that these modifications are consistent.

Nevertheless, the result brings back the (old) view, that a (standard) model independent and broad analysis of  $CP$ -violation is required in order to fully understand this phenomenon and the need for new interaction. This implies in particular measurements of many decay channels.

I have sketched strategies to determine the source of  $CP$ -violation for the case that the standard model accounts for tree level processes and given a phenomenological

framework to calculate the effects of new operators. Needless to say that all of this will take many years of hard work on both the experimental and the theoretical side and that also less perfect measurements have to be pursued.

## Acknowledgments

I thank H. Haber and all speakers for an interesting and exciting meeting. I am grateful to Georgia Hamel and Jacqueline Pizzuti at SCIPP and Ruth McDunn and Terry Anderson at SLAC for their tireless efforts in helping to make RADCOR-2000 a success. I thank my collaborators, especially G. Colangelo and R. Fleischer.

## References

- [1] Y. Nir, hep-ph/0008226.
- [2] A.J. Buras, M.E. Lautenbacher and G. Ostermaier, Phys. Rev. **D50** (1994), 3433 (1994).
- [3] Particle Data Group, Review of Particle Properties, Eur.Phys.J. **C15**, 1 (2000).
- [4] M. Ciuchini, G. D'Agostini, E. Franco, V. Lubicz, G. Martinelli, F. Parodi, P. Roudeau, A. Stocchi, hep-ph/0012308.
- [5] F. Caravaglios, F. Parodi, P. Roudeau, and A. Stocchi, hep-ph/0002171.
- [6] A. Ali and D. London, Eur. Phys. J. **C9** (1999) 687, hep-ph/0002167.
- [7] S. Plaszczynski and M.-H. Schune, hep-ph/9911280.
- [8] T. Affolder et al., CDF collaboration, Phys. Rev. **D61** (2000) 072005.
- [9] E. Abashian et. al., Belle collaboration, Phys.Rev.Lett. 86, 2509 (2001). (Osaka, Japan, July 31, 2000).
- [10] B. Aubert et.al., BaBar collaboration, Phys.Rev.Lett. 86, 2515 (2001).
- [11] G. Eyal, Y. Nir, and G. Perez, JHEP **0008**, 028 (2000), hep-ph/0008009.
- [12] J.P. Silva and L. Wolfenstein, hep-ph/0008004.
- [13] A.L. Kagan and M. Neubert, Phys. Lett. B492, (2000), hep-ph/0007360.

- [14] Z.Z Xing, hep-ph/0008018.
- [15] A. Buras and R. Buras, hep-ph/0008273.
- [16] M. Gronau and D. Wyler, Phys.Lett. **B265**, 172 (1991).
- [17] D. Atwood, I. Dunietz and A. Soni, Phys.Rev. Lett. **78**, 3257 (1997).
- [18] R.Fleischer and D. Wyler, Phys.Rev. **62**, 057503, (2000).
- [19] M. Gronau, J.L. Rosner and D. London, Phys. Rev.Lett. **73**, 21 (1994); R. Fleischer, Phys. Lett. **B365**, 399 (1996); R. Fleischer and T. Mannel, Phys. Rev. **57**, 2752, (1998); M. Neubert and J.L. Rosner, Phys. Rev. Lett. **81**, 5076 (1998).
- [20] R. Fleischer, Nucl. Instrum. Meth. **A446**, (2000), hep-ph/9908340; A. Buras and R. Fleischer, hep-ph/0008298.
- [21] I. Bigi and A. Sanda, Nucl. Phys.**B193**, 85 (1981).
- [22] W. Buchmüller and D. Wyler, Nucl. Phys.**B268**, 621 (1986).
- [23] A. Buras, Flavor dynamics: CP violation and rare decays, hep-ph/0101336.
- [24] R. Godang et al., CLEO collaboration, Phys. Rev. Lett ,**84**,5038, (2000), hep-ex/0001060.
- [25] J.M. Link et al., FOCUS collaboration, Phys. Lett. **B485**, 62 (2000), hep-ex/0004034.
- [26] See A. Buras P. Gambino, M. Gorbahn, S. Jager, L. Silvestrini, Nucl. Phys. **B592**, 55 (2000); hep-ph/0007313.

# Inclusive Rare B Decays

Tobias Hurth

*Theory Division, CERN, CH-1211 Geneva 23, Switzerland*

## Abstract

We review the present status of rare  $B$  decays, focusing on inclusive decay modes and their role in our search for new physics. We also briefly discuss direct CP violation in rare  $B$  decays and the rare kaon decays  $K^+ \rightarrow \pi^+ \nu \bar{\nu}$  and  $K_L \rightarrow \pi^0 \nu \bar{\nu}$ , which offer complementary opportunities for precision flavour physics.

Based on invited talks given at the 8th International Conference on Supersymmetries in Physics (**SUSY2K**), 26 June - 1 July, 2000, CERN, Geneva, Switzerland, and at the 5th International Symposium on Radiative Corrections (**RADCOR 2000**), 11 - 15 September, 2000, Carmel, California.

# 1 Introduction

Flavour physics deals with that part of the standard model (SM) which distinguishes between the three generations of fundamental fermions. It is still a mystery why there are exactly three generations. Also the origin of the fermion masses and their mixing is unknown; in particular, the SM does not explain the hierarchical pattern of these parameters. Flavour physics can be regarded as the least tested part of the SM. This is reflected in the rather large error bars of several flavour parameters such as the mixing parameters at the 20% level [1], which has to be compared with errors smaller than 1% in high energy electroweak precision experiments.

However, the experimental situation concerning flavour physics is drastically changing. There are several  $B$  physics experiments successfully running at the moment and, in the upcoming years, new facilities will start to explore  $B$  physics with increasing sensitivity and within various different experimental settings: Apart from the CLEO experiment (Cornell, USA), located at the Cornell Electron-Positron Storage Ring (CESR) [2], two  $B$  factories, operating at the  $\Upsilon(4S)$  resonance in an asymmetric mode (fig.1), have started successfully: the BaBar experiment at SLAC (Stanford, USA) [3] and the BELLE experiment at KEK (Tsukuba, Japan) [4]. Besides the successfully running hadronic  $B$  physics program at FERMILAB (Batavia, USA) [5] there are independent  $B$  physics experiments planned at the hadronic colliders: the LHC- $B$  experiment at CERN in Geneva [6] and the  $B$ TeV experiment at FERMILAB [7]. The main motivation for a  $B$  physics program at hadron colliders is the huge  $b$  quark production cross section with respect to the one at  $e^+e^-$  machines.

While the time of the electroweak precision physics focusing on the *gauge* sector of the SM draws to a close with the completion of the LEP experiments at CERN and the SLC experiment in Stanford, the era of precision flavour physics focusing on the *scalar* sector of the SM has just begun with the start of the  $B$  factories.

The  $B$  system represents an ideal framework for the study of flavour physics. Since the  $b$  quark mass is much larger than the typical scale of the strong interaction, long-distance strong interactions are generally less important and are under better control than in kaon physics thanks to the heavy mass expansion. Thus, for example the CP violation in the  $B$  system will yield an important independent test of the SM description of CP violation (see [8]).  $B$  meson decays also allow for a rich CKM phenomenology and a stringent test of the unitarity constraints.

The so-called rare decays are of particular interest. These processes represent flavour changing neutral currents (FCNC) and occur in the SM only at the quantum level. The inclusive rare decay modes are theoretically clean observables because no specific model is needed to describe the hadronic final states. Their role is twofold: on the one hand they are relevant to the determination of CKM matrix elements. On the other hand they are particularly sensitive to new physics beyond the SM, since additional contributions to the decay rate, in which SM

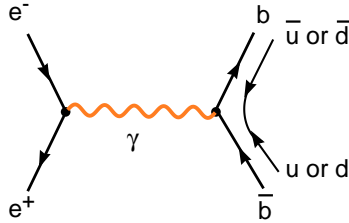


Figure 1:  $e^+e^- \rightarrow Y(4S) \rightarrow B^+B^-, B^0\bar{B}^0$ .

particles are replaced by new particles such as the supersymmetric charginos or gluinos, are not suppressed by additional factors  $\alpha/(4\pi)$  relative to the SM contribution. This makes it possible to observe new physics indirectly - a strategy complementary to the direct production of new (supersymmetric) particles. The latter production is reserved for the planned hadronic machines such as the LHC at CERN, while the indirect search of the  $B$  factories already implies significant restrictions for the parameter space of supersymmetric models and will thus lead to important clues for the direct search of supersymmetric particles. It is even possible that these rare processes lead to the first evidence of new physics by a significant deviation from the SM prediction, for example in the observables concerning direct CP violation, although it will then be difficult to identify in this way the new structures in detail. But also in the long run, after new physics has already been discovered, these decays will play an important role in analyzing in greater detail the underlying new dynamics.

Although the general focus within flavour physics is at present on  $B$  systems, kaon physics offers interesting complementary opportunities in the new physics search such as the rare decays  $K^+ \rightarrow \pi^+\nu\bar{\nu}$  and  $K_L \rightarrow \pi^0\nu\bar{\nu}$ . They are specifically interesting in view of the current experiments at the Brookhaven laboratory (USA) and suggested experiments at FERMILAB (USA) and at KEK (Japan).

The paper is organized as follows: in Section 2 we briefly discuss the role of the strong interaction within flavour physics. In Section 3 the status of rare  $B$  decays within the SM is reviewed. In Section 4 we explore the implications of these decays for our search of physics beyond the SM. In Section 5 we discuss direct CP violation and in Section 6 the complementary role of rare kaon decays within precision flavour physics. In Section 7 we present our summary.

## 2 Strong interaction in $B$ decays

Flavour physics is governed by the interplay of strong and weak interactions. One of the main difficulties in examining the observables in flavour physics is the influence of the strong interaction. As is well known, for matrix elements dominated by long-distance strong interactions there is no adequate quantitative solution available in quantum field theory. The resulting hadronic uncertainties restrict the opportunities in flavour physics significantly. The present discussion

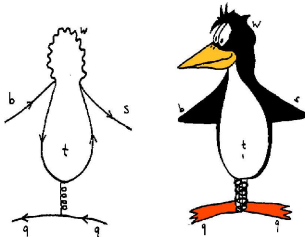


Figure 2: Penguin decays of  $B$  mesons.

on the new  $g - 2$  muon data [9] also reflects this issue. While the hadronic self-energy contribution to the  $g - 2$  observable can be determined by experimental data, the well-known light-by-light contribution can only be modelled at present (see for example [10]).

However, there are several fundamental tools available, which are directly based on QCD. High hopes for precise QCD predictions are placed on lattice gauge theoretical calculations. While there are competitive predictions from lattice gauge theory for form factors of semileptonic decays, pure hadronic decays are less accessible to these methods ([11]). With the help of the so-called QCD sum rules, a consistency test between hadron physics and perturbative QCD, it becomes possible to connect hadronic and fundamental QCD parameters directly. Theoretical predictions via QCD sum rules, however, always have relatively large uncertainties [12]. Another approach is the method of factorization [13]. This method has recently been systematized for nonleptonic decays in the heavy quark limit [14]. However, within this approach a quantitative method to estimate the  $1/m_b$  corrections to this limit is missing. The latter contributions can be specifically large if they are chirally enhanced [15]. Further fundamental methods whose applications and precision are also somewhat restricted are chiral perturbation theory [16] and heavy quark effective theory [17].

In view of this, the goal must be to minimize theoretical uncertainties with the help of an optimized combination of different fundamental methods solely based on QCD. This can only be done for a selected number of observables in flavour physics. However, there are also observables, dominated by purely perturbative contributions, which will make precision flavour physics possible in the near future. Among them inclusive rare  $B$  decays (see fig. 2 [18]) play the most important role.

Inclusive decay modes are theoretically clean and represent a theoretical laboratory of perturbative QCD. In particular, the decay width  $\Gamma(B \rightarrow X_s \gamma)$  is well approximated by the partonic decay rate  $\Gamma(b \rightarrow s \gamma)$ , which can be analysed in renormalization group improved perturbation theory:

$$\Gamma(B \rightarrow X_s \gamma) = \Gamma(b \rightarrow s \gamma) + \Delta^{nonpert.} \quad (2.1)$$

Nonperturbative effects,  $\Delta^{nonpert.}$ , play a subdominant role and are under control

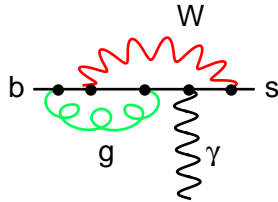


Figure 3: QCD corrections to the decay  $B \rightarrow X_s \gamma$ .

thanks to the heavy mass expansion.

Thus, in general, inclusive decay modes should be preferred to exclusive ones from the theoretical point of view. The inclusive modes  $B \rightarrow X_{s(d)} \gamma$  and  $B \rightarrow X_{s(d)} l^+ l^-$  can be measured by the electron-positron experiments ( $B$  factories, CLEO) with their kinematic constraints and their low background, while they are more difficult to measure at hadronic machines. Exclusive decay modes, however, are more accessible to experiments, in particular at hadronic machines. But in contrast to the inclusive modes, they have in general large nonperturbative QCD contributions. Exclusive decays such as  $B_{d,s} \rightarrow \mu^+ \mu^-$ ,  $B_d \rightarrow K^* \gamma$  and  $B_d \rightarrow K^* \mu^+ \mu^-$  are distinguished observables at the LHC- $B$  experiment.

Within inclusive  $B$  decay modes, short-distance QCD effects lead to a tremendous rate enhancement. These effects are induced by hard gluon exchange between the quark lines of the one-loop electroweak diagrams (fig. 3).

The QCD radiative corrections bring in large logarithms of the form  $\alpha_s^n(m_b) \log^m(m_b/M)$ , where  $M = m_t$  or  $M = m_W$  and  $m \leq n$  (with  $n = 0, 1, 2, \dots$ ). This is a natural feature in any process where two different mass scales are present. In order to get a reasonable result at all, one has to resum at least the leading-log (LL) series

$$\alpha_s^n(m_b) \log^n(m_b/M), \quad (LL) \quad (2.2)$$

with the help of renormalization group techniques. Working to next-to-leading-log (NLL) precision means that one is also resumming all the terms of the form

$$\alpha_s(m_b) (\alpha_s^n(m_b) \log^n(m_b/M)), \quad (NLL). \quad (2.3)$$

A suitable framework to achieve the necessary resummations of the large logs is an effective low-energy theory with five quarks, obtained by integrating out the heavy particles, which, in the SM, are the top quark and the  $W$  boson. The standard method of the operator product expansion allows for a separation of an amplitude of a weak meson decay process into two distinct parts, the long-distance contributions contained in the operator matrix elements and the short-distance physics described by the so-called Wilson coefficients (see fig. 4). In the case of  $B$  decays, the  $W$  boson and the top quark with mass bigger than the factorization scale are integrated out, that is removed from the theory as dynamical variables. The effective hamiltonian can be written

$$H_{eff} = -\frac{4G_F}{\sqrt{2}} \sum C_i(\mu, M_{heavy}) \mathcal{O}_i(\mu) \quad (2.4)$$

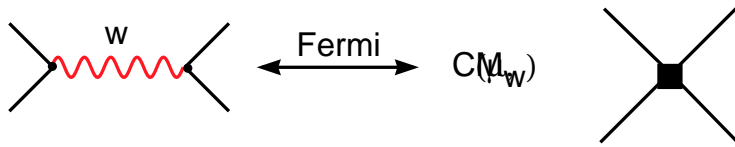


Figure 4: Operator product expansion.

where  $\mathcal{O}_i(\mu)$  are the relevant operators and  $C_i(\mu, M_{heavy})$  are the corresponding Wilson coefficients. As the heavy fields are integrated out, the complete top and  $W$  mass dependence is contained in the Wilson coefficients. Working out a convenient set of quantities, both in the effective (low-energy) theory and in the full (standard model) theory, and requiring equality (matching) up to terms suppressed by higher powers of  $m_W$  or  $m_t$ , these coefficients can be determined.

Within this framework QCD corrections for the decay rates are twofold: the ingredients are the order  $\alpha_s$  corrections to the matrix elements of the various operators and the order  $\alpha_s$  corrections to the Wilson coefficients, of course both at the low-energy scale  $\mu \approx m_b$ . Only the sum of the two contributions is renormalization scheme and scale independent; in fact, from the  $\mu$ -independence of the effective Hamiltonian, one can derive a renormalization group equation (RGE) for the Wilson coefficients  $C_i(\mu)$ :

$$\mu \frac{d}{d\mu} C_i(\mu) = \gamma_{ji} C_j(\mu) \quad , \quad (2.5)$$

where the matrix  $\gamma$  is the anomalous dimension matrix of the operators  $\mathcal{O}_i$ . Then there are the following three principal steps leading to the leading-log (next-to-leading-log) result within the effective field theory approach:

- Step 1: One has to match the full SM theory with the effective theory at the scale  $\mu = \mu_W$ , where  $\mu_W$  denotes a scale of order  $m_W$  or  $m_t$ . At this scale, the matrix elements of the operators in the effective theory lead to the same logarithms as the full theory calculation. Consequently, the Wilson coefficients  $C_i(\mu_W)$  only pick up small QCD corrections, which can be calculated in fixed-order perturbation theory. In the LL (NLL) program, the matching has to be worked out at the  $O(\alpha_s^0)$  ( $O(\alpha_s^1)$ ) level.
- Step 2: Then one performs the evolution of these Wilson coefficients from  $\mu = \mu_W$  down to  $\mu = \mu_b$ , where  $\mu_b$  is of the order of  $m_b$ . As the matrix elements of the operators evaluated at the low scale  $\mu_b$  are free of large logarithms, the latter are contained in resummed form in the Wilson coefficients. For a LL (NLL) calculation, this RGE step has to be done using the anomalous dimension matrix up to order  $\alpha_s^1$  ( $\alpha_s^2$ ).
- Step 3: To LL (NLL) precision, the corrections to the matrix elements of the operators  $\langle s\gamma | \mathcal{O}_i(\mu) | b \rangle$  at the scale  $\mu = \mu_b$  have to be calculated to order  $\alpha_s^0$  ( $\alpha_s^1$ ) precision.

Finally, we stress that the step from the leading (LL) to the next-to-leading (NLL) order within the framework of the renormalization group improved perturbation theory is not only a quantitative one increasing the precision of the theoretical prediction, but also a qualitative one, which tests the validity of the perturbative approach in the given problem.

### 3 Inclusive decay modes

#### 3.1 Experimental data on $B \rightarrow X_s \gamma$

Among inclusive rare  $B$  decays, the  $B \rightarrow X_s \gamma$  mode is the most prominent because it is the only one that is already measured: in 1993, the first evidence for a penguin-induced  $B$  meson decay was found by the CLEO collaboration. At CESR, they measured the exclusive electromagnetic penguin process  $B \rightarrow K^* \gamma$ . The inclusive analogue  $B \rightarrow X_s \gamma$  was also found by the CLEO collaboration through the measurement of its characteristic photon energy spectrum in 1994 (see [23]). As this process is dominated by the two-body decay  $b \rightarrow s \gamma$ , its photon energy spectrum is expected to be a smeared delta function centred at  $E_\gamma \approx m_b/2$ , where the smearing is due to perturbative gluon bremsstrahlung and to the nonperturbative Fermi motion of the  $b$  quark within the  $B$  meson. Only the high part of the photon energy spectrum is sensitive to the rare decay  $B \rightarrow X_s \gamma$ . Some lower cutoff in the photon energy has to be imposed in order to exclude the background, mainly from the nonleptonic charged current processes  $b \rightarrow cq\bar{q}' + \gamma$  or  $b \rightarrow uq\bar{q}' + \gamma$ , which have a typical bremsstrahlung spectrum that is maximal at  $E_\gamma = 0$  and falls off for larger values of  $E_\gamma$ . Therefore only the “kinematic” branching ratio for  $B \rightarrow X_s \gamma$  in the range between  $E_\gamma = 2.2$  GeV and the kinematic endpoint at  $E_\gamma = 2.7$  GeV could be measured directly. To obtain from this measurement the total branching ratio, one has to know the fraction  $R$  of the  $B \rightarrow X_s \gamma$  events with  $E_\gamma \geq 2.2$  GeV. This was done in [19] where the Fermi motion of the  $b$  quark in the  $B$  meson was taken into account by using the phenomenological model of Altarelli et al. (ACCMM model) [20]. Using this *theoretical* input regarding the photon energy spectrum, the value  $R = 0.87 \pm 0.06$  was used by the CLEO collaboration, leading to the CLEO branching ratio [21]

$$\mathcal{B}(B \rightarrow X_s \gamma) = (2.32 \pm 0.57_{stat} \pm 0.35_{sys}) \times 10^{-4}. \quad (3.1)$$

The first error is statistical and the second is systematic (including model dependence). This measurement was based on a sample of  $2.2 \times 10^6 B\bar{B}$  events.

In 1999, CLEO has presented an improved measurement [22], which is based on 53% more data ( $3.3 \times 10^6$  events). They also used the slightly wider  $E_\gamma$  window starting at 2.1 GeV. The relative error drops almost by a factor of  $\sqrt{3}$ :

$$\mathcal{B}(B \rightarrow X_s \gamma) = (3.15 \pm 0.35_{stat} \pm 0.32_{sys} \pm 0.26_{mod}) \times 10^{-4}. \quad (3.2)$$

The errors represent statistics, systematics, and the model dependence, respectively.

There are also data at the  $Z^0$  peak from the LEP experiments. The ALEPH collaboration [24] has measured the inclusive branching ratio

$$\mathcal{B}(H_b \rightarrow X_s \gamma) = (3.11 \pm 0.80_{stat} \pm 0.72_{sys}) \times 10^{-4}. \quad (3.3)$$

It should be noted that the branching ratio in (3.3) involves a weighted average of the  $B$  mesons and  $\Lambda_b$  baryons produced in  $Z^0$  decays (hence the symbol  $H_b$ ) different from the corresponding one given by CLEO, which has been measured at the  $\Upsilon(4S)$  resonance. High luminosity is more difficult to obtain at higher  $e^+e^-$  collision energies. Thus,  $B\bar{B}$  samples obtained by the LEP experiments are smaller than the one at CESR. The rate measured by ALEPH is consistent with the CLEO measurement.

Recently, CLEO presented a refined preliminary analysis (with an lower photon energy cut  $E_\gamma \geq 2.0$  GeV) [25]:

$$\mathcal{B}(B \rightarrow X_s \gamma) = (2.85 \pm 0.35_{stat} \pm 0.22_{sys}) \times 10^{-4} \quad (3.4)$$

and also BELLE has presented preliminary data [25] of competitive experimental accuracy:

$$\mathcal{B}(B \rightarrow X_s \gamma) = (3.37 \pm 0.53_{stat} \pm 0.42_{sys} \pm 0.54_{mod}) \times 10^{-4}. \quad (3.5)$$

More accurate data can be expected in the near future. With the expected high luminosity of the  $B$ -factories, an experimental accuracy below 10% in the inclusive  $B \rightarrow X_s \gamma$  mode appears to be possible.

The uncertainty regarding the fraction  $R$  of the  $B \rightarrow X_s \gamma$  events with  $E_\gamma \geq 2.2$  GeV quoted in the experimental measurement, also cited as model dependence, should be regarded as a purely theoretical uncertainty. As mentioned above, the fraction  $R$  was calculated in [19] using the phenomenological model by Altarelli et al., where the Fermi motion of the  $b$  quark in the  $B$  meson is characterized by two parameters, the average Fermi momentum  $p_F$  of the  $b$  quark and the mass  $m_q$  of the spectator quark. The error on the fraction  $R$  is essentially obtained by varying the model parameters  $p_F$  and  $m_q$  in the range for which the ACCMM model correctly describes the energy spectrum of the charged lepton in the semileptonic decays  $B \rightarrow X_c \ell \nu$  and  $B \rightarrow X_u \ell \nu$ , measured by CLEO and ARGUS. In [19] a first comparison between the calculated photon energy spectrum and the one measured by the CLEO collaboration was presented. The (normalized) measured photon energy spectrum and the theoretical one are in agreement for those values of  $p_F$  and  $m_q$ , that correctly describe the inclusive semileptonic CLEO data  $B \rightarrow X_c \ell \nu$  and  $B \rightarrow X_u \ell \nu$ ; at present, the data from the radiative decays is, however, not precise enough to further constrain the values of  $p_F$  and  $m_q$ . The best fit between the theoretical and measured photon energy spectrum is obtained for  $p_F = 450$  MeV and  $m_q = 0$ . One should mention that the analysis [19] of the photon energy spectrum, in particular the calculation of the fraction  $R$  in the ACCMM model used by CLEO, does not include the full NLL information, which becomes available in the meantime.

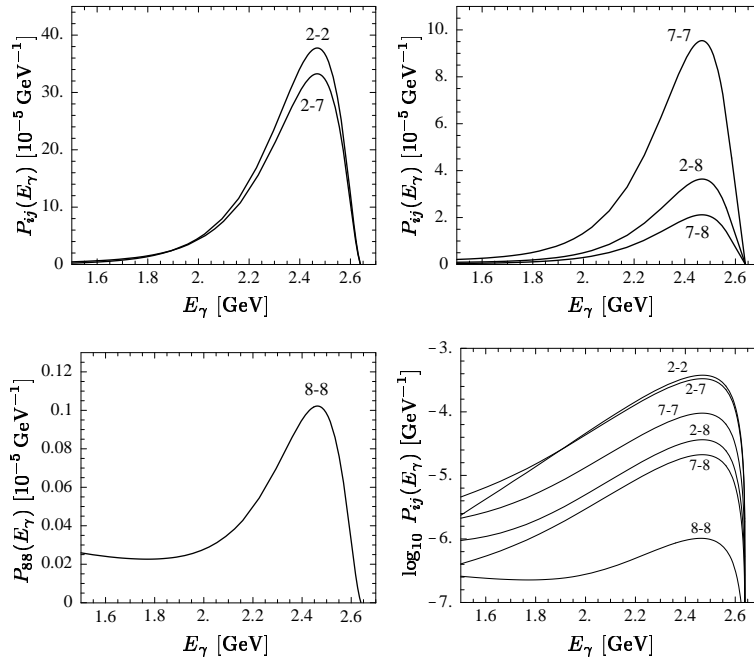


Figure 5: Different components of the photon spectrum in the  $B \rightarrow X_s \gamma$  decay, from [26].

Besides this phenomenological model by Altarelli et al., more fundamental theoretical methods are available today to implement the bound state effects, namely by making use of operator product expansion techniques in the framework of heavy quark effective theory (HQET). A new analysis along these lines was presented in [26]. Unfortunately, the operator product expansion breaks down near the endpoint of the photon energy spectrum; therefore, an infinite number of leading-twist corrections has to be resummed into a nonperturbative universal shape function, which determines the light-cone momentum distribution of the  $b$ -quark in the  $B$  meson [27]. The physical decay distributions are then obtained from a convolution of parton model spectra with this shape function. At present this function cannot be calculated, but there is at least some information on the moments of the shape function, which are related to the forward matrix elements of local operators. Ansätze for the shape function, constrained by the latter information, are used. In contrast to the older analysis based on the ACCMM model, the new analysis of Kagan and Neubert [26] includes the full NLL information. Their fraction  $R = 0.78_{-0.11}^{+0.09}$  (for the energy cut  $E_\gamma > 2.2$  GeV) is smaller than the factor used by CLEO.

An important observation is that the shape of the photon spectrum is not sensitive to physics beyond the SM. As can be seen in fig. 5, all different contributions to the spectrum (corresponding to the interference terms of the various operators involved) have a very similar shape besides the small 8-8 contribution. This implies that we do not have to assume the correctness of the SM in the

experimental analysis and, thus, a precise measurement of the photon spectrum can be used to determine the parameters of the shape function.

Clearly, a lower experimental cut decreases the sensitivity to the parameters of the shape function (or, more generally, the model dependence). With respect to this, the ideal energy cut would be 1.6 GeV. However, in this case a better understanding of the  $\psi$  background would be mandatory. The intermediate  $\psi$  background, namely  $B \rightarrow \psi X_s$  followed by  $\psi \rightarrow X'\gamma$  is more than  $4 \times 10^{-4}$  in the ‘total’ branching ratio. With the present energy cut of 2.1 GeV this contribution is suppressed and estimated to be less than 5% [28].

Another future aim should be to determine the shape function (and analogously the parameter of the ACCMM model) by using the high-precision measurements of the photon energy spectrum.

### 3.2 NLL QCD calculations

As mentioned above, the inclusive decay  $B \rightarrow X_s \gamma$  is a laboratory for perturbative QCD. Nonperturbative effects (see section 3.3) play a subdominant role and are well under control thanks to the heavy quark expansion. The short-distance QCD corrections enhance the partonic decay rate  $\Gamma(b \rightarrow s \gamma)$  by more than a factor of 2. The corresponding large logarithms of the form  $\alpha_s^n(m_b) \log^m(m_b/M)$ , where  $M = m_t$  or  $M = m_W$  and  $m \leq n$  (with  $n = 0, 1, 2, \dots$ ), have to be summed with the help of the renormalization group improved perturbation theory as presented in section 2.

The effective Hamiltonian relevant to  $B \rightarrow X_s \gamma$  in the SM reads

$$H_{eff}(B \rightarrow X_s \gamma) = -\frac{4G_F}{\sqrt{2}} \lambda_t \sum_{i=1}^8 C_i(\mu) \mathcal{O}_i(\mu) \quad , \quad (3.6)$$

where  $\mathcal{O}_i(\mu)$  are the relevant operators,  $C_i(\mu)$  are the corresponding Wilson coefficients, which contain the complete top- and  $W$ - mass dependence (see fig. 6), and  $\lambda_t = V_{tb}V_{ts}^*$  with  $V_{ij}$ , the CKM matrix elements. The CKM dependence globally factorizes, because we work in the approximation  $\lambda_u = 0$  (in the case of  $B \rightarrow X_s \gamma$ ). One neglects the operators with dimension  $> 6$ . which are suppressed by higher powers of  $1/m_W$ .

Using the equations of motion for the operators, one arrives at the following basis of dimension-6 operators:

$$\begin{aligned} \mathcal{O}_1 &= (\bar{c}_{L\beta} \gamma^\mu b_{L\alpha}) (\bar{s}_{L\alpha} \gamma_\mu c_{L\beta}) \quad , \\ \mathcal{O}_2 &= (\bar{c}_{L\alpha} \gamma^\mu b_{L\alpha}) (\bar{s}_{L\beta} \gamma_\mu c_{L\beta}) \quad , \\ \mathcal{O}_3 &= (\bar{s}_{L\alpha} \gamma^\mu b_{L\alpha}) \left[ (\bar{u}_{L\beta} \gamma_\mu u_{L\beta}) + \dots + (\bar{b}_{L\beta} \gamma_\mu b_{L\beta}) \right] \quad , \\ \mathcal{O}_4 &= (\bar{s}_{L\alpha} \gamma^\mu b_{L\beta}) \left[ (\bar{u}_{L\beta} \gamma_\mu u_{L\alpha}) + \dots + (\bar{b}_{L\beta} \gamma_\mu b_{L\alpha}) \right] \quad , \\ \mathcal{O}_5 &= (\bar{s}_{L\alpha} \gamma^\mu b_{L\alpha}) \left[ (\bar{u}_{R\beta} \gamma_\mu u_{R\beta}) + \dots + (\bar{b}_{R\beta} \gamma_\mu b_{R\beta}) \right] \quad , \\ \mathcal{O}_6 &= (\bar{s}_{L\alpha} \gamma^\mu b_{L\beta}) \left[ (\bar{u}_{R\beta} \gamma_\mu u_{R\alpha}) + \dots + (\bar{b}_{R\beta} \gamma_\mu b_{R\alpha}) \right] \quad , \end{aligned}$$

$$\begin{array}{ccc}
C_i(\mu) \langle \text{diagram} \rangle & + & C_7(\mu) \langle \text{diagram} \rangle & + & C_8(\mu) \langle \text{diagram} \rangle \\
\mathcal{O}_i(\mu) & & \mathcal{O}_7(\mu) & & \mathcal{O}_8(\mu)
\end{array}$$

Figure 6: SM Hamiltonian in the case of  $B \rightarrow X_s \gamma$ .

$$\begin{aligned}
\mathcal{O}_7 &= (e/16\pi^2) \bar{s}_\alpha \sigma^{\mu\nu} (\bar{m}_b(\mu)P_R + \bar{m}_s(\mu)P_L) b_\alpha F_{\mu\nu}, \\
\mathcal{O}_8 &= (g_s/16\pi^2) \bar{s}_\alpha \sigma^{\mu\nu} (\bar{m}_b(\mu)P_R + \bar{m}_s(\mu)P_L) T_{\alpha\beta}^A b_\beta G_{\mu\nu}^A.
\end{aligned} \tag{3.7}$$

In the dipole type operators  $\mathcal{O}_7$  and  $\mathcal{O}_8$ ,  $e$  and  $F_{\mu\nu}$  ( $g_s$  and  $G_{\mu\nu}^A$ ) denote the electromagnetic (strong) coupling constant and field strength tensor, respectively;  $T^a$  ( $a = 1, 8$ ) denote  $SU(3)$  colour generators.

The error of the leading logarithmic (LL) result [29] was dominated by a large renormalization scale dependence at the  $\pm 25\%$  level, which already indicated the importance of the NLL series. By convention, the dependence on the renormalization scale  $\mu_b$  is obtained by the variation  $m_b/2 < \mu_b < 2m_b$ . The former measurement of the CLEO collaboration (see (3.1)) overlaps with the estimates based on LL calculations, and the experimental and theoretical errors are comparable. In view of the expected increase in the experimental precision in the near future, it became clear that a systematic inclusion of the NLL corrections was becoming necessary. Moreover, such a NLL program is also important in order to ensure the validity of renormalization group improved perturbation theory in this specific phenomenological application.

This ambitious NLL enterprise was completed some years ago. This was a joint effort of many different groups ([19],[30], [31], [32], [33]),[34]). The theoretical error of the previous LL result was substantially reduced to  $\pm 10\%$ , and the central value of the partonic decay rate increased by about 20%.

All three steps to NLL precision listed below (2.5) involve rather difficult calculations.

- The most difficult part in Step 1 is the two-loop (or order  $\alpha_s$ ) matching of the dipole operators  $\mathcal{O}_7$  and  $\mathcal{O}_8$ . It involves two-loop diagrams both in the full and in the effective theory. It was first worked out by Adel and Yao [32]. As this is a crucial step in the NLL program, Greub and Hurth confirmed their findings in a detailed re-calculation using a different method [34]. Two further recalculations of this result [35, 36] were presented in the meanwhile, confirming the original results in [32]. In order to match the dimension-6 operators  $\mathcal{O}_7$  and  $\mathcal{O}_8$ , it is sufficient to extract the terms of order  $m_b \frac{m_b^2}{M^2}$  ( $M = m_W, m_t$ ) from the SM matrix elements for  $b \rightarrow s\gamma$  and  $b \rightarrow sg$ . Terms suppressed by additional powers of  $m_b/M$  correspond to higher-dimensional operators in the effective theory. In [34] the finite parts

of the two-loop diagrams in the SM were calculated by means of the well-known method of asymptotic mass expansions, which naturally leads to a systematic expansion of Feynman diagrams in inverse powers of  $M$ .

- The order  $\alpha_s^2$  anomalous dimension matrix (Step 2) has been worked out by Chetyrkin, Misiak and Münz [33]. In particular, the calculation of the elements  $\gamma_{i7}$  and  $\gamma_{i8}$  ( $i = 1, \dots, 6$ ) in the  $O(\alpha_s^2)$  anomalous dimension matrix involves a huge number of three-loop diagrams from which the pole parts (in the  $d-4$  expansion) have to be extracted. This extraction was simplified by a clever decomposition of the scalar propagator. Moreover, the number of necessary evanescent operators was reduced by a new choice of a basis of dimension-6 operators. Using the matching result (Step 1), these authors obtained the NLL correction to the Wilson coefficient  $C_7(\mu_b)$ . Numerically, the LL and the NLL value for  $C_7(\mu_b)$  turn out to be rather similar; the NLL corrections to the Wilson coefficient  $C_7(\mu_b)$  lead to a change of the  $B \rightarrow X_s \gamma$  decay rate that does not exceed 6% [33].

It should be stressed that the result of Step 2, in particular the entries  $\gamma_{i7}$  and  $\gamma_{i8}$  ( $i = 1, \dots, 6$ ) of the anomalous dimension matrix to NLL precision, is the only part of the complete NLL enterprise which has not been confirmed by an independent group.

- Step 3 basically consists of bremsstrahlung corrections and virtual corrections. While the bremsstrahlung corrections were worked out some time ago by Ali and Greub [19] and were confirmed and extended by Pott [30], a complete analysis of the virtual two-loop corrections (up to the contributions of the four-quark operators with very small coefficients) was presented by Greub, Hurth and Wyler [31]. The latter calculation involves two-loop diagrams, where the full charm dependence has to be taken into account. By using Mellin-Barnes techniques in the Feynman parameter integrals, the result of these two-loop diagrams was obtained in the form

$$c_0 + \sum_{n=0,1,2,\dots; m=0,1,2,3} c_{nm} \left( \frac{m_c^2}{m_b^2} \right)^n \log^m \frac{m_c^2}{m_b^2}, \quad (3.8)$$

where the quantities  $c_0$  and  $c_{nm}$  are independent of  $m_c$ . The convergence of the Mellin-Barnes series was proved; the practical convergence of the series (3.8) was also checked explicitly. Moreover, a finite result is obtained in the limit  $m_c \rightarrow 0$ , as there is no naked logarithm of  $m_c^2/m_b^2$ . This observation is of some importance in the  $b \rightarrow d\gamma$  process, where the  $u$ -quark propagation in the loop is not CKM-suppressed (see below). The main result of Step 3 consists in a drastic reduction of the renormalization scale uncertainty from about  $\pm 25\%$  to about  $\pm 6\%$ . The central value was shifted by about 20%.

In [31] these results are presented also in the 't Hooft-Veltman scheme, which may be regarded as a first step towards a cross-check of the complete NLL calculation prediction in a different renormalization scheme.

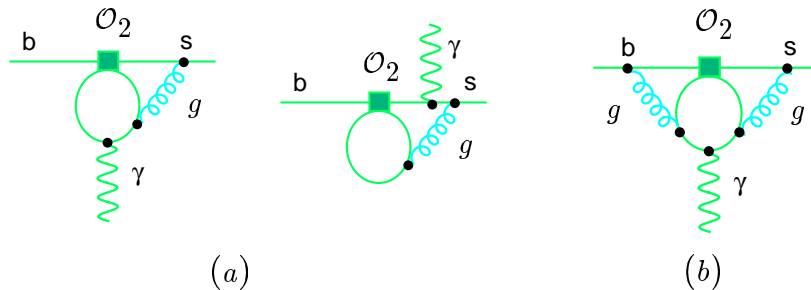


Figure 7: (a) Typical diagrams (finite parts) contributing to the matrix element of the operator  $\mathcal{O}_2$  at the NLL level (Step3); (b) typical diagram (infinite part) contributing to the NLL anomalous dimension matrix (Step2); typical diagram (finite part) contributing in the NLL matching calculation shown in fig.3 (Step1).

Quite recently, the results of the matrix elements based on the operator  $\mathcal{O}_2$  were confirmed by an independent group [37] with the help of the method of asymptotic expansions.

It is clear that many parts of the NLL calculations at the partonic level in the case of  $b \rightarrow s\gamma$  can be straightforwardly taken over to the cases  $b \rightarrow d\gamma$ ,  $b \rightarrow s\text{gluon}$  and  $b \rightarrow sl^+l^-$ . In the latter case, however, many modifications are necessary; in particular the operator basis gets enlarged as will be discussed below.

Combining the NLL calculations of the three steps, the first complete theoretical prediction to NLL precision for the branching ratio of  $B \rightarrow X_s\gamma$  was presented in [33] (see also [38]):

$$\mathcal{B}(B \rightarrow X_s\gamma) = (3.28 \pm 0.33) \times 10^{-4}. \quad (3.9)$$

The theoretical error has two dominant sources. The  $\mu$  dependence, which is now reduced to about 6%. The other main uncertainty of 5% stems from the  $m_c/m_b$  dependence. This first theoretical NLL prediction already included the nonperturbative correction scaling with  $1/m_b^2$ , which are rather small (at the 1% level) (see section 3.3). Surprisingly, these first NLL predictions ([33],[38]) are almost identical to the current prediction quoted in (3.17), in spite of so many important additional refinements such as the electroweak two-loop corrections and the nonperturbative corrections which will be discussed below.

### 3.3 Nonperturbative contributions

Within the framework of the heavy mass expansion, nonperturbative corrections to the branching ratio of decay  $B \rightarrow X_s\gamma$  can be singled out. These contributions also apply to the case of the decay  $B \rightarrow X_d\gamma$  and, with some modifications, to the case of the decay  $B \rightarrow X_sl^+l^-$ .

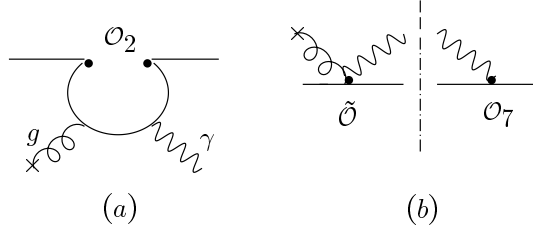


Figure 8: a) Feynman diagram from which the operator  $\tilde{\mathcal{O}}$  arises. b) Relevant cut-diagram for the  $(\mathcal{O}_2, \mathcal{O}_7)$ -interference.

If one neglects perturbative QCD corrections and assumes that the decay  $B \rightarrow X_s \gamma$  is due to the operator  $\mathcal{O}_7$  only, the calculation of the differential decay rate basically amounts to working out the imaginary part of the forward scattering amplitude  $T(q)$ :

$$T(q) = i \int d^4x \langle B | T \mathcal{O}_7^+(x) \mathcal{O}_7(0) | B \rangle \exp(iqx) \quad . \quad (3.10)$$

Using the operator product expansion for  $T \mathcal{O}_7^+(x) \mathcal{O}_7(0)$  and heavy quark effective theory methods, the decay width  $\Gamma(B \rightarrow X_s \gamma)$  reads [39, 40] (modulo higher terms in the  $1/m_b$  expansion):

$$\begin{aligned} \Gamma_{B \rightarrow X_s \gamma}^{(\mathcal{O}_7, \mathcal{O}_7)} &= \frac{\alpha G_F^2 m_b^5}{32\pi^4} |V_{tb} V_{ts}|^2 C_7^2(m_b) \left( 1 + \frac{\delta_{rad}^{NP}}{m_b^2} \right) \quad , \\ \delta_{rad}^{NP} &= \frac{1}{2} \lambda_1 - \frac{9}{2} \lambda_2 \quad , \end{aligned} \quad (3.11)$$

where  $\lambda_1$  and  $\lambda_2$  are the parameters for kinetic energy and the chromomagnetic energy. Using  $\lambda_1 = -0.5 \text{ GeV}^2$  and  $\lambda_2 = 0.12 \text{ GeV}^2$ , one gets  $\delta_{rad}^{NP} \simeq -4\%$ . The  $B \rightarrow X_s \gamma$  decay width is usually normalized by the semileptonic one. The semileptonic decay width gets  $1/m_b^2$  corrections, which are negative; thus, the nonperturbative corrections scaling with  $1/m_b^2$  tend to cancel in the branching ratio  $\mathcal{B}(B \rightarrow X_s \gamma)$ , and only about 1% remains.

Voloshin [41] considered the nonperturbative effects when including also the operator  $\mathcal{O}_2$ . This effect is generated by the diagram in Fig. 8a (and by the one, not shown, where the gluon and the photon are interchanged);  $g$  is a soft gluon interacting with the charm quarks in the loop. Up to a characteristic Lorentz structure, this loop is given by the integral

$$\int_0^1 dx \int_0^{1-x} dy \frac{xy}{m_c^2 - k_g^2 x(1-x) - 2xy k_g k_\gamma} \quad . \quad (3.12)$$

As the gluon is soft, i.e.  $k_g^2, k_g k_\gamma \approx \Lambda^{QCD} m_b/2 \ll m_c^2$ , the integral can be expanded in  $k_g$ . The (formally) leading operator, denoted by  $\tilde{\mathcal{O}}$ , is

$$\tilde{\mathcal{O}} = \frac{G_F}{\sqrt{2}} V_{cb} V_{cs}^* C_2 \frac{e Q_c}{48\pi^2 m_c^2} \bar{s} \gamma_\mu (1 - \gamma_5) g_s G_{\nu\lambda} b \epsilon^{\mu\nu\rho\sigma} \partial^\lambda F_{\rho\sigma} \quad . \quad (3.13)$$

Then working out the cut diagram shown in Fig. 8b, one obtains the nonperturbative contribution  $\Gamma_{B \rightarrow X_s \gamma}^{(\tilde{\mathcal{O}}, \mathcal{O}_7)}$  to the decay width, which is due to the  $(\mathcal{O}_2, \mathcal{O}_7)$  interference. Normalizing this contribution by the LL partonic width, one obtains

$$\frac{\Gamma_{B \rightarrow X_s \gamma}^{(\tilde{\mathcal{O}}, \mathcal{O}_7)}}{\Gamma_{b \rightarrow s \gamma}^{LL}} = -\frac{1}{9} \frac{C_2}{C_7} \frac{\lambda_2}{m_c^2} \simeq +0.03 \quad . \quad (3.14)$$

As the expansion parameter is  $m_b \Lambda_{QCD}/m_c^2 \approx 0.6$  (rather than  $\Lambda_{QCD}^2/m_c^2$ ), it is not a priori clear whether formally higher order terms in the  $m_c$  expansion are numerically suppressed. More detailed investigations [42, 43, 44] have shown that higher order terms are indeed suppressed, because the corresponding expansion coefficients are small.

The analogous  $1/m_c^2$  effect has been found independently in the exclusive mode  $B \rightarrow K^* \gamma$  in ref. [45]. Numerically, the effect there is also at the few per cent level. Moreover, the analysis of the  $1/m_c^2$  effects was extended to the decay  $B \rightarrow X_s l^+ l^-$  in [44, 46].

As was recently emphasized by Misiak [47], an analogous systematic analysis of terms like  $\Gamma_{B \rightarrow X_s \gamma}^{(\mathcal{O}_2, \mathcal{O}_2)}$  at first order in  $\alpha_s$  is still missing. Rigorous techniques such as operator product expansions do not seem to be applicable in this case.

## 3.4 Theoretical status

### 3.4.1 $B \rightarrow X_s \gamma$

The theoretical prediction for the partonic  $b \rightarrow s \gamma$  decay rate is usually normalized by the semileptonic decay rate in order to get rid of uncertainties related with the CKM matrix elements and the fifth power of the  $b$  quark mass. Moreover, an explicit lower cut on the photon energy in the bremsstrahlung correction is often made:

$$R_{quark}(\delta) = \frac{\Gamma[b \rightarrow s \gamma] + \Gamma[b \rightarrow s \gamma gluon]_\delta}{\Gamma[b \rightarrow X_c e \bar{\nu}_e]} \quad (3.15)$$

where the subscript  $\delta$  means that only photons with energy  $E_\gamma > (1 - \delta)E_\gamma^{max} = (1 - \delta)\frac{m_b}{2}$  are counted. The ratio  $R_{quark}$  is divergent in the limit  $\delta \rightarrow 1$  due to the unphysical soft photon divergence in the subprocess  $b \rightarrow s \gamma gluon$ . In this limit only the sum of  $\Gamma[b \rightarrow s \gamma]$ ,  $\Gamma[b \rightarrow s gluon]$  and  $\Gamma[b \rightarrow s \gamma gluon]$  is a reasonable physical quantity, in which all divergences cancel out. In [26] it was shown that the theoretical result is rather sensitive to the unphysical soft-photon divergence; the choice  $\delta = 0.90$  was suggested as the optimized definition of the total decay rate. In the analysis presented in [31] the limit  $\delta \rightarrow 1$  is taken and the singularities are removed by adding the virtual photon corrections to  $b \rightarrow s gluon$ .

It is suggestive to give up the concept of a total decay rate of  $b \rightarrow s \gamma$  and compare theory and experiment using the same energy cut as CLEO ( $E_\gamma > 2.1$  GeV). Then also the theoretical uncertainty regarding the photon energy spectrum mentioned above would occur naturally in the theoretical prediction.

In the meanwhile detailed studies of the electroweak corrections were performed. In [48] part of the electroweak two-loop contributions, namely contributions from fermion loops in gauge boson propagators ( $\gamma$  and  $W$ ) and from short-distance photonic loop corrections, were calculated. Moreover, it was found that the on-shell value of the fine structure constant  $1/\alpha_{em} = 137$  is more appropriate for real photon emission than the value  $1/\alpha_{em} = (130.3 \pm 2.3)$  used in previous analyses. The QED loop calculations in [48] confirmed this expectation. This change in  $\alpha_{em}$  leads to a reduction of 5% in  $R_{quark}$ . In [26] the QED analysis made in [48] was improved by resumming the contributions of order  $\alpha \log(\mu_b/M)(\alpha_s \log(\mu_b/M))^n$  to all orders (while in [48] only the  $n = 0$  contribution was included). This resummation decreases the QED corrections. In [49] a complete analysis of the heavy top and the heavy Higgs corrections in the limit  $m_W \rightarrow 0$  was made. This analysis was recently refined in [50]. A 2% reduction of the branching ratio of  $B \rightarrow X_s \gamma$  due to purely electroweak corrections is found.

Using the measured semileptonic branching ratio  $\mathcal{B}_{exp.}^{sl}$ , the branching ratio  $\mathcal{B}(B \rightarrow X_s \gamma)$  is given by

$$\mathcal{B}(B \rightarrow X_s \gamma) = R_{quark} \times \mathcal{B}_{exp.}^{sl} (1 + \Delta_{nonpert}), \quad (3.16)$$

where the nonperturbative corrections scaling with  $1/m_b^2$  and  $1/m_c^2$ , summed in  $\Delta_{nonpert}$ , have a numerical effect of +1% [39, 40] and +3% [41], respectively, on the branching ratio only.

For a comparison with the ALEPH measurement (3.3) the measured semileptonic branching ratio  $\mathcal{B}(H_b \rightarrow X_{c,u} \ell \nu)$  should be used consistently. This leads to a larger theoretical prediction for the LEP experiments.

Including only the resummed QED corrections and the nonperturbative corrections discussed in section 3.3, using the on-shell value of  $\alpha_{em}$  and working with the convention  $\delta \rightarrow 1$  in  $R_{quark}$ , one ends up with the following theoretical prediction for the  $B \rightarrow X_s \gamma$  branching ratio [51]:

$$\mathcal{B}(B \rightarrow X_s \gamma) = (3.32 \pm 0.14 \pm 0.26) \times 10^{-4}, \quad (3.17)$$

where the first error represents the uncertainty regarding the scale dependences, while the second error is the uncertainty due to the input parameters. In the second error the uncertainty due to the parameter  $m_c/m_b$  is dominant.

Quite recently, quark mass effects within the decay  $B \rightarrow X_s \gamma$  were further analysed [55], in particular the definitions of the quark masses  $m_c$  and  $m_b$  in the matrix element  $\langle \mathcal{O}_2 \rangle \equiv \bar{X}_s \gamma |(\bar{s}c)_{V-A}(\bar{c}b)_{V-A}|b\rangle$ . Since the charm quark in the matrix element  $\langle \mathcal{O}_2 \rangle$  are dominantly off-shell (see fig. 7a) the authors argue that the running charm mass should be chosen instead of the pole mass. The latter choice was used in all previous analyses [31, 33, 35, 26, 51].

$$m_c^{\text{pole}}/m_b^{\text{pole}} \quad \Rightarrow \quad m_c^{\overline{\text{MS}}}(\mu)/m_b^{\text{pole}}, \quad \mu \in [m_c, m_b]. \quad (3.18)$$

Since the matrix element starts at NLL order and, thus, the renormalization scheme for  $m_c$  and  $m_b$  is an NNLL issue, one should regard this choice as an

educated guess of the NNLL corrections. However, this new choice is guided by the experience gained from many higher-order calculations in perturbation theory. Numerically, the shift from  $m_c^{\text{pole}}/m_b^{\text{pole}} = 0.29 \pm 0.02$  to  $m_c^{\overline{\text{MS}}}(\mu)/m_b^{\text{pole}} = 0.22 \pm 0.04$  is rather important and leads to a +11% shift of the central value of the  $B \rightarrow X_s \gamma$  branching ratio. The authors of [55] quote a weighted experimental world average using the preliminary data from CLEO and BELLE, (3.4) and (3.5), and the published ALEPH data (3.3):

$$\mathcal{B}(B \rightarrow X_s \gamma) = (2.96 \pm 0.35) \times 10^{-4}. \quad (3.19)$$

With their new choice of the charm mass and with  $\delta = 0.9$ , their theoretical prediction for the ‘total’ branching ratio is

$$\mathcal{B}(B \rightarrow X_s \gamma) = (3.73 \pm 0.30) \times 10^{-4}, \quad (3.20)$$

which means that the difference between the theoretical and the experimental value is consistent with zero at the level of  $1.6\sigma$  (if one assumes that a statistical interpretation of this difference is really possible). Because the choice of the renormalization scheme for  $m_c$  and  $m_b$  is a NNLL effect, one could argue for a larger theoretical uncertainty in  $m_c^{\overline{\text{MS}}}(\mu)/m_b^{\text{pole}}$  which includes also the value of  $m_c^{\text{pole}}$ . A more conservative choice would then be  $m_c^{\overline{\text{MS}}}(\mu)/m_b^{\text{pole}} = 0.22 \pm 0.07$  which would reduce the significance of the perceived discrepancy.

Instead of making a theoretical prediction for the branching ratio  $\mathcal{B}(B \rightarrow X_s \gamma)$ , one can use the experimental data and theory in order to directly determine the combination  $|V_{tb}V_{ts}^*|/|V_{cb}|$  of the CKM matrix elements; in turn, one can determine  $|V_{ts}|$  by making use of the relatively well known CKM matrix elements  $V_{cb}$  and  $V_{tb}$ . An update of the analysis in [56] was presented in [51]. Using the CLEO data (3.2), the ALEPH data (3.3), and the theoretical prediction (3.17), one finds [51]

$$\begin{aligned} \frac{|V_{ts}^*V_{tb}|}{|V_{cb}|} &= 0.95 \pm 0.08_{\text{exp.}} \pm 0.05_{\text{th.}} && \text{CLEO} \\ \frac{|V_{ts}^*V_{tb}|}{|V_{cb}|} &= 0.91 \pm 0.15_{\text{exp.}} \pm 0.04_{\text{th.}} && \text{ALEPH.} \end{aligned}$$

The average of the two measurements yields

$$\frac{|V_{ts}^*V_{tb}|}{|V_{cb}|} = 0.93 \pm 0.09 \pm 0.03 = 0.93 \pm 0.10 \quad (3.21)$$

where in the very last step the theoretical and experimental errors were added in quadrature. Using  $|V_{tb}| = 0.99 \pm 0.15$  from the CDF measurement and  $|V_{cb}| = 0.0393 \pm 0.0028$  extracted from semileptonic  $B$  decays, one obtains [51]

$$|V_{ts}| = 0.037 \pm 0.007, \quad (3.22)$$

where all the errors were added in quadrature. This is probably the most direct determination of this CKM matrix element. With an improved measurement of

$\mathcal{B}(B \rightarrow X_s \gamma)$  and  $V_{tb}$ , one expects to reduce the present error on  $|V_{ts}|$  by a factor of 2 or even more.

Finally, some remarks on the decay mode  $b \rightarrow s \text{ gluon}$  are in order. The effective Hamiltonian is the same as in the  $b \rightarrow s \gamma$  case. By replacing the photon by the gluon, the NLL QCD calculation of  $b \rightarrow s \gamma$  can also be used. However, in the calculation of the matrix element of the operator  $\mathcal{O}_2$ , further diagrams with the nonabelian three-gluon coupling have to be calculated [52]. Numerically, one obtains  $\mathcal{B}(b \rightarrow s \text{ gluon}) = (5.0 \pm 1.0) \times 10^{-3}$ , which is more than a factor of 2 larger than the former LL result  $\mathcal{B}(b \rightarrow s \text{ gluon}) = (2.2 \pm 0.8) \times 10^{-3}$  [29]. The mode  $b \rightarrow s \text{ gluon}$  represents one component to the inclusive charmless hadronic decays,  $B \rightarrow X_{\text{nocharm}}$ , where  $X_{\text{nocharm}}$  denotes any hadronic charmless final state. A measurement of the corresponding branching ratio would allow the extraction of the ratio  $|V_{ub}/V_{cb}|$ , which is poorly known at present [53]. At the quark level, there are decay modes with three-body final states,  $b \rightarrow q' \bar{q}' q$  ( $q' = u, d, s$ ;  $q = d, s$ ) and the modes  $b \rightarrow qg$ , with two-body final-state topology. The component  $b \rightarrow sg$  of the charmless hadronic decays is expected to manifest itself in kaons with high momenta (of order  $m_b/2$ ), owing to its two-body nature [54].

### 3.4.2 $B \rightarrow X_d \gamma$

With respect to new physics, also the  $B \rightarrow X_d \gamma$  decay is of specific interest, because its CKM suppression by the factor  $|V_{td}|^2/|V_{ts}|^2$  in the SM may not be true in extended models. Moreover, a future measurement of the  $B \rightarrow X_d \gamma$  decay rate will help to drastically reduce the currently allowed region of the CKM-Wolfenstein parameters  $\rho$  and  $\eta$ .

Most of the theoretical improvements carried out in the context of the decay  $B \rightarrow X_s \gamma$  (see sections 3.2 and 3.3) can straightforwardly be adapted for the decay  $B \rightarrow X_d \gamma$ . As for the former decay, the NLL-improved and power-corrected decay rate for  $B \rightarrow X_d \gamma$  has much reduced theoretical uncertainty, which would allow a more precise extraction of the CKM parameters from the measured branching ratio.

The perturbative QCD corrections in the decay  $B \rightarrow X_d \gamma$  can be treated in complete analogy to the ones in the decay  $B \rightarrow X_s \gamma$ . The effective Hamiltonian is the same in the processes  $b \rightarrow s \gamma$  and  $b \rightarrow d \gamma$  up to the obvious replacement of the  $s$ -quark field by the  $d$ -quark field. However, as  $\lambda_u$  for  $b \rightarrow d \gamma$  is not small with respect to  $\lambda_t$  and  $\lambda_c$ , one also has to encounter the operators proportional to  $\lambda_u$ . The matching conditions  $C_i(m_W)$  and the solutions of the RG equations, yielding  $C_i(\mu_b)$ , coincide with those needed for the process  $B \rightarrow X_s \gamma$ . The power corrections in  $1/m_b^2$  and  $1/m_c^2$  (besides the CKM factors) are also the same for the two modes.

The long-distance contributions from the intermediate  $u$ -quark in the penguin loops, however, are different. These are suppressed in the  $B \rightarrow X_s \gamma$  mode by the unfavourable CKM matrix elements. In  $B \rightarrow X_d \gamma$ , there is no CKM suppression and one has to include the long-distance intermediate  $u$ -quark contributions,

which can only be modelled at present. However, these contributions are estimated to be rather small [57]. Moreover, it must be stressed that there is no spurious enhancement of the form  $\log(m_u/\mu_b)$  in the perturbative contribution to the matrix elements  $\langle X_d\gamma|O_{iu}|B\rangle$  ( $i = 1, 2$ ) as shown by the explicit calculation in [31] and also discussed in [58]. In other words, the limit  $m_u \rightarrow 0$  can be taken.

The predictions for the  $B \rightarrow X_d\gamma$  decay given in [59] show that for  $\mu_b = 2.5$  GeV (and the central values of the input parameters) the difference between the LL and NLL results is  $\sim 10\%$ , increasing the branching ratio in the NLL case. For a fixed value of the CKM-Wolfenstein parameters  $\rho$  and  $\eta$ , the theoretical uncertainty of the branching ratio is:

$$\Delta\mathcal{B}(B \rightarrow X_d\gamma)/\mathcal{B}(B \rightarrow X_d\gamma) = \pm(6 - 10)\%. \quad (3.23)$$

Of particular theoretical interest is the ratio of the branching ratios, defined as

$$R(d\gamma/s\gamma) \equiv \frac{\mathcal{B}(B \rightarrow X_d\gamma)}{\mathcal{B}(B \rightarrow X_s\gamma)}, \quad (3.24)$$

in which a good part of the theoretical uncertainties cancels. This suggests that a future measurement of  $R(d\gamma/s\gamma)$  will have a large impact on the CKM phenomenology.

Varying the CKM-Wolfenstein parameters  $\rho$  and  $\eta$  in the range  $-0.1 \leq \rho \leq 0.4$  and  $0.2 \leq \eta \leq 0.46$  and taking into account other parametric dependences stated above, the results (without electroweak corrections) are

$$\begin{aligned} 6.0 \times 10^{-6} &\leq \mathcal{B}(B \rightarrow X_d\gamma) \leq 2.6 \times 10^{-5}, \\ 0.017 &\leq R(d\gamma/s\gamma) \leq 0.074. \end{aligned}$$

These quantities are expected to be measurable at the high-luminosity  $B$  facilities.

### 3.4.3 $B \rightarrow X_s l^+ l^-$

The inclusive  $B \rightarrow X_s l^+ l^-$  decay will also be accessible at the  $B$  factories. In comparison with the  $B \rightarrow X_s\gamma$  decay, it presents a complementary and also more complex test of the SM since different contributions add to the decay rate (fig. 9). Because of kinematic observables such as the invariant dilepton mass spectrum and the forward-backward asymmetry, it is particularly attractive. It is also dominated by perturbative contributions, if one eliminates  $c\bar{c}$  resonances with the help of kinematic cuts.

Using heavy quark expansion, nonperturbative corrections scaling with  $1/m_b^2$  and  $1/m_c^2$  can be calculated quite analogously to those in the decay  $B \rightarrow X_s\gamma$  [44]. However, there are also on-shell  $c\bar{c}$  resonances, which one has to take into account. While in the decay  $B \rightarrow X_s\gamma$  (on-shell photon) the intermediate  $\psi$  background for example, namely  $B \rightarrow \psi X_s$  followed by  $\psi \rightarrow X'\gamma$ , is suppressed and can be subtracted from the  $B \rightarrow X_s\gamma$  decay rate (see section 3.1), the  $c\bar{c}$  resonances show up as large peaks in the dilepton invariant mass spectrum in the decay

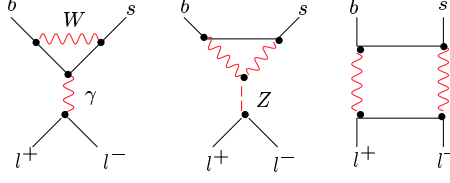


Figure 9: One-loop contributions to the decay  $B \rightarrow X_s l^+ l^-$ .

$B \rightarrow X_s l^+ l^-$  (off-shell photon). However, these resonances can be removed by appropriate kinematic cuts in the invariant mass spectrum: In the 'perturbative window', namely  $0.05 < \hat{s} = (m_{l^+ l^-} / m_b)^2 < 0.25$ , theoretical predictions for the invariant mass spectrum are dominated by the purely perturbative contributions, and theoretical precision comparable with the one reached in the decay  $B \rightarrow X_s \gamma$  is in principle possible.

The present status of the calculation of the perturbative contributions is the following: the effective Hamiltonian relevant to  $B \rightarrow X_s l^+ l^-$  in the SM reads

$$H_{eff}(B \rightarrow X_s l^+ l^-) = -\frac{4G_F}{\sqrt{2}} \lambda_t \sum_{i=1}^{10} C_i(\mu) \mathcal{O}_i(\mu) \quad , \quad (3.25)$$

Compared with the decay  $B \rightarrow X_s \gamma$  (see (3.6)), the effective Hamiltonian (3.25) contains in this case two additional operators:

$$\begin{aligned} \mathcal{O}_9 &= \frac{e^2}{16\pi^2} (\bar{s} \gamma_\mu P_L b) (\bar{l} \gamma^\mu l) \quad , \\ \mathcal{O}_{10} &= \frac{e^2}{16\pi^2} (\bar{s} \gamma_\mu P_L b) (\bar{l} \gamma^\mu \gamma_5 l) \quad . \end{aligned} \quad (3.26)$$

It turns out that the first large logarithm of the form  $\log(m_b/M)$  ( $M = m_W$ ) arises already without gluons, because the operator  $\mathcal{O}_2$  mixes into  $\mathcal{O}_9$  at one loop (the pair  $c\bar{c}$  in  $\mathcal{O}_2$  can be closed to form a loop, and an off-shell photon producing a  $l\bar{l}$  pair can be radiated from a quark line). This possibility has no correspondence in the  $B \rightarrow X_s \gamma$  case within the SM. Consequently, the decay amplitude is ordered according to

$$G_F \log(m_b/M) \quad (\alpha_s(m_b) \log(m_b/M))^n \quad (LL), \quad (3.27)$$

$$G_F \log(m_b/M) \alpha_s(m_b) \quad (\alpha_s(m_b) \log(m_b/M))^n \quad (NLL), \quad (3.28)$$

which should be compared with (2.2) and (2.3). To technically achieve the resummation of these terms, it is convenient to redefine magnetic, chromomagnetic and lepton-pair operators  $\mathcal{O}_7$ ,  $\mathcal{O}_8$ ,  $\mathcal{O}_9$ , and  $\mathcal{O}_{10}$  and the corresponding coefficients as follows [62, 63]:

$$\mathcal{O}_i^{new} = \frac{16\pi^2}{g_s^2} \mathcal{O}_i, \quad C_i^{new} = \frac{g_s^2}{16\pi^2} C_i \quad (i = 7, \dots, 10). \quad (3.29)$$

This redefinition enables one to proceed according to the three calculational steps presented in section 2, when calculating the decay amplitude [62, 63]. In particular, the one-loop mixing of the operator  $\mathcal{O}_2$  with the operator  $\mathcal{O}_9^{new}$  appears formally at order  $g_s^2$ , after the reshufflings in (3.29).

The QCD calculation up to NLL precision can be found in [62, 63]. However, the  $LL$  term in the series accidentally turns out to be small. In order to reach the same accuracy as in the case of the NLL prediction for  $B \rightarrow X_s \gamma$  one has to include the NNLL order contribution in the  $B \rightarrow X_s l^+ l^-$  calculation.

Large parts of the NLL calculation in the decay  $B \rightarrow X_s \gamma$ , reviewed in section 3.2, can be taken over and used in the NNLL calculation within the decay  $B \rightarrow X_s l^+ l^-$ . However, the *complete* NNLL enterprise - following the standard three steps in the formalism of effective theories (see section 2) - is a formidable task:

- Step 1: In [60] the complete Step 1 up to NNLL precision was presented. The authors did the two-loop matching for all the operators relevant to  $B \rightarrow X_s l^+ l^-$  (including a confirmation of the  $B \rightarrow X_s \gamma$  NLL matching results of [32, 34, 35, 36]). The inclusion of this NNLL contribution already removes the large matching scale ( $\mu_W$ ) uncertainty of around 16% present in the NLL prediction of  $B \rightarrow X_s l^+ l^-$ . As usual the partonic decay width is normalized by the semileptonic decay width in order to get rid of uncertainties due to the fifth power in  $m_b$ :

$$R_{quark}^{l^+ l^-}(\hat{s}) = \frac{1}{\Gamma(b \rightarrow X_c e \bar{\nu})} \frac{d\Gamma(b \rightarrow X_s l^+ l^-)}{d\hat{s}}. \quad (3.30)$$

One finds the following partial NNLL prediction [60]:

$$\begin{aligned} & \mathcal{B}(B \rightarrow X_s l^+ l^-)_{Cut: \hat{s} \in [0.05, 0.25]} = \\ &= \mathcal{B}(B \rightarrow X_c e \bar{\nu}) \int_{0.05}^{0.25} d\hat{s} [R_{quark}^{l^+ l^-}(\hat{s}) + \delta_{1/m_b^2} R(\hat{s}) + \delta_{1/m_c^2} R(\hat{s})] \\ &= 0.104 [(1.36 \pm 0.18_{scale}) + 0.06 - 0.02] 10^{-5} \\ &= (1.46 \pm 0.19_{scale}) 10^{-6} \end{aligned} \quad (3.31)$$

$\delta_{1/m_b^2} R(\hat{s})$  and  $\delta_{1/m_c^2} R(\hat{s})$  are the nonperturbative contributions discussed in section 3.3. The quoted error in (3.31) reflects only the  $\mu_b$  scale uncertainty. This purely perturbative uncertainty should get significantly reduced by contributions within Step 3 of the NNLL program, namely the two-loop QCD corrections to the matrix element of the four-quark operators  $\mathcal{O}_2$ . The error due to the uncertainties in the input parameters and to other contributions was not estimated in [60], at this intermediate stage of the NNLL calculation.

- Step 2: The most important NNLL contribution from the three-loop renormalization group evolution of the Wilson coefficients from the matching scale  $\mu_W$  to the low scale  $\mu_b$ , namely the three-loop anomalous dimensions

corresponding to the mixing of the four-quark operators  $\mathcal{O}_i$  ( $i = 1\dots 6$ ) into the dipole operators  $\mathcal{O}_7$  and  $\mathcal{O}_8$ , can be taken over from the NLL calculation in the decay  $B \rightarrow X_s \gamma$  [33]. However, the analogous three-loop anomalous dimensions corresponding to the mixing of the four-quark operators into the operator  $\mathcal{O}_9$  is missing. In [60] an estimate was made which suggests that the numerical influence of these missing NNLL contributions to the branching ratio of  $B \rightarrow X_s l^+ l^-$  is small.

- Step 3: Within the NLL  $B \rightarrow X_s \gamma$  calculation the two-loop matrix elements of the four-quark operator  $\mathcal{O}_2$  for an on-shell photon were calculated in [31] and quite recently confirmed in [37]. This calculation was extended to the case of an off-shell photon [61], which corresponds to a NNLL contribution relevant to the decay  $B \rightarrow X_s l^+ l^-$ . The calculation includes also that part of the corresponding gluon bremsstrahlung which is needed to cancel infrared and collinear singularities of the virtual corrections. If one includes also this NNLL piece in the partonic NNLL prediction for the decay  $B \rightarrow l^+ l^-$ , one gets [61]

$$\int_{0.05}^{0.25} d\hat{s} R_{quark}^{l^+ l^-}(\hat{s}) = (1.25 \pm 0.08_{scale}) \times 10^{-5} \quad (3.32)$$

Again the only error given corresponds to the uncertainty of the low scale  $\mu_b$ . As expected the inclusion of the two-loop virtual corections to the four-quark operator  $\mathcal{O}_2$  has reduced this scale ambiguity from  $\pm 13\%$  down to  $\pm 6.5\%$ . The authors of [61] also analyse the error due to the uncertainty in the input parameter  $m_c/m_b$  and find an uncertainty of  $\pm 7.6\%$  within the partonic quantity.

Within the Step 3 of the NNLL calculation, the renormalization group invariant two-loop matrix element of the operator  $\mathcal{O}_9$  is not calculated yet. Because this contribution includes no logarithms, the scale dependence of the NLL prediction is not sensitive to this NNLL contribution.

One could think that within this perturbative window at low  $\hat{s} \in [0.05, 0.25]$ , one is only sensitive to  $C_7$  which would be redundant information, since we already know it from the decay  $B \rightarrow X_s \gamma$ . However, as was explicitly shown in [62, 63], one is also sensitive to the new Wilson coefficients  $C_9$  and  $C_{10}$  and interference terms in the low  $\hat{s}$  regime with  $\hat{s} = m_{l^+ l^-}/m_b^2 \in [0.05, 0.25]$  (see fig. 10 where the various perturbative contributions to  $R_{quark}$  (with NLL precision) are plotted).

Together with the decay  $B \rightarrow X_s \gamma$ , the inclusive  $B \rightarrow X_s l^+ l^-$  decay will make precision flavour physics possible, if one can also measure the kinematic variables in the  $B \rightarrow X_s l^+ l^-$  decay precisely. As was first advocated in [64],

- the invariant dilepton mass spectrum

$$d\Gamma(B \rightarrow X_s l^+ l^-) / d\hat{s}, \quad (3.33)$$

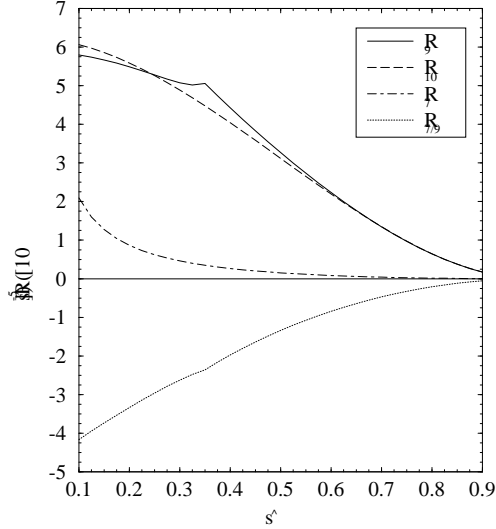


Figure 10: Comparison of the different short-distance contributions to  $R_{quark}(\hat{s})$  (NLL precision), from [63].

- the forward-backward charge asymmetry

$$A(s) = \int_{-1}^1 d\cos\theta \, d^2\Gamma(B \rightarrow X_s l^+ l^-) / d\hat{s} d\cos\theta \, \text{sgn}(\cos\theta) \quad (3.34)$$

- and the decay rate of  $B \rightarrow X_s \gamma$ ,

$$\Gamma(B \rightarrow X_s \gamma) \quad (3.35)$$

determine the magnitude and also the sign of the three Wilson coefficients  $C_7$ ,  $C_8$ , and  $C_{10}$ , and allow for a model-independent analysis of rare  $B$  decays. For the measurements of these kinematic distributions, however, high statistics will be necessary.

## 4 Indirect search for supersymmetry

Today supersymmetric models are given priority in our search for new physics beyond the SM. This is primarily suggested by theoretical arguments related to the well-known hierarchy problem. The decay  $B \rightarrow X_s \gamma$  is sensitive to the mechanism of supersymmetry breaking because in the limit of exact supersymmetry, the decay rate would be just zero:

$$\mathcal{B}(B \rightarrow X_s \gamma) = 0. \quad (4.1)$$

This follows from an argument first given by Ferrara and Remiddi in 1974 [65]. In that work the absence of the anomalous magnetic moment in a supersymmetric

abelian gauge theory was shown. The necessary mechanism of supersymmetry breaking, however, is unknown and leads to a proliferation of free parameters in the (unconstrained) minimal supersymmetric standard model (MSSM).

There are two types of new contributions to flavour changing neutral currents in the MSSM: CKM-induced contributions, which are induced by a charged Higgs or a chargino, and generic new contributions, which are induced by flavour mixing in the squark-mass matrix. The structure of the MSSM does not explain the suppression of flavour changing neutral currents which is observed in experiments. This is the essence of the well-known supersymmetric flavour problem.

In the framework of the MSSM there are at present three favoured concrete supersymmetric models. They solve the supersymmetric flavour problem by a specific mechanism through which the sector of supersymmetry breaking communicates with the sector accessible to experiments: in the minimal supergravity model (mSUGRA) [66], supergravity is the corresponding mediator; in the other two models this role is fulfilled by gauge interactions (GMSB) [67] and by anomalies (AMSB) [68]. Furthermore, there are other classes of models in which the flavour problem is solved by particular flavour symmetries [69].

Flavour violation thus originates from the interplay between the dynamics of flavour and the mechanism of supersymmetry breaking. The model-independent analysis of rare  $B$  and  $K$  decays therefore can contribute to the question of which mechanism ultimately breaks the supersymmetry and will thus yield important (indirect) information on the construction of supersymmetric extensions of the SM. In this context it is important to analyse the correlations between the different information from rare  $B$  and  $K$  decays.

As was already emphasized in the introduction, inclusive rare decays, as loop-induced processes, are particularly sensitive to new physics and theoretically clean. Neutral flavour transitions involving third-generation quarks, typically in the  $B$  system, do not pose yet serious threats to specific models. However, despite the relatively large experimental uncertainties, the rare decay  $B \rightarrow X_s \gamma$  has already carved out some regions in the space of free parameters of most of the models in the classes mentioned above (see [70],[71] and references therein). Once more precise data from the  $B$  factories are available, this decay will undoubtedly gain efficiency in selecting the viable regions of the parameter space in the various classes of models; this may help in discriminating between the models by then proposed. In view of this, it is important to calculate the rate of this decay with theoretical uncertainties reduced as much as possible, and general enough for generic supersymmetric models.

While in the SM, the rate for  $B \rightarrow X_s \gamma$  is known up to NLL in QCD, the calculation of this decay rate within supersymmetric models is still far from this level of sophistication. There are several contributions to the decay amplitude: besides the  $W t$ -quark and the  $H t$ -quark contributions, there are also the chargino, gluino and neutralino contributions. In most of the phenomenological analyses of the decay  $B \rightarrow X_s \gamma$  these nonstandard contributions were not investigated with NLL precision as the SM contribution. However, as has already been pointed

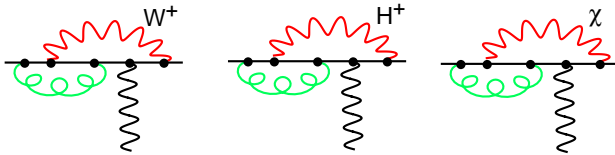


Figure 11: SM, charged Higgs and chargino contribution at the matching scale.

out, the step from the LL to the NLL precision is also necessary in order to check the validity of the perturbative approach in the model under consideration. It is possible that the restriction of the parameter space of nonstandard models, based on an LL analysis only, proves to be invalid after the NLL analysis is completed. Moreover, it was already shown in specific new physics scenarios that bounds on the parameter space of nonstandard models are rather sensitive to NLL contributions (see below).

Nevertheless, within supersymmetric models partial NLL results are available. The gluonic NLL two-loop matching contributions were recently presented [72]. A complete NLL calculation of the  $B \rightarrow X_s \gamma$  branching ratio in the simplest extension of the SM, namely the Two-Higgs-Doublet Model (2HDM), is already available [35, 73]. In the 2HDM of Type II (which already represents a good approximation for gauge-mediated supersymmetric models with large  $\tan \beta$  where the charged Higgs contribution dominates the chargino contribution), the  $B \rightarrow X_s \gamma$  is only sensitive to two parameters of this model, the mass of the charged Higgs boson and  $\tan \beta$ . Thus, the experimental data of the decay  $B \rightarrow X_s \gamma$  allows for stringent bounds on these two parameters which are much more restrictive than the lower bound on the charged Higgs mass found in the direct search at LEP. One also finds that these indirect bounds are very sensitive to NLL QCD corrections and even to the two-loop electroweak contributions (see [35, 73]).

In [74] a specific supersymmetric scenario is presented, where in particular the possibility of destructive interference of the chargino and the charged Higgs contribution is analysed. The analysis has been done under two assumptions. First it is assumed that the only source of flavour violation at the electroweak scale is that of the SM, encoded in the CKM matrix (minimal flavour violation). Therefore, the analysis applies to mSUGRA, GMSB and AMSB models (in which the same features are assumed at the messenger scale) only when the sources of flavour violation, generated radiatively between the supersymmetry breaking scale and the electroweak scale, can be neglected with respect to those induced by the CKM matrix. The second assumption is that there exists a specific mass hierarchy, in particular the heavy gluino limit. Indeed, the NLL calculation has been done in the limit

$$\mu_{\tilde{g}} \sim O(m_{\tilde{g}}, m_{\tilde{q}}, m_{\tilde{t}_1}) \gg \mu_W \sim O(m_W, m_{H^+}, m_t, m_\chi, m_{\tilde{t}_2}). \quad (4.2)$$

The mass scale of the charginos ( $\chi$ ), and of the lighter stop ( $\tilde{t}_2$ ) is the ordinary electroweak scale  $\mu_W$ , while the scale  $\mu_g$  is characteristic of all other strongly

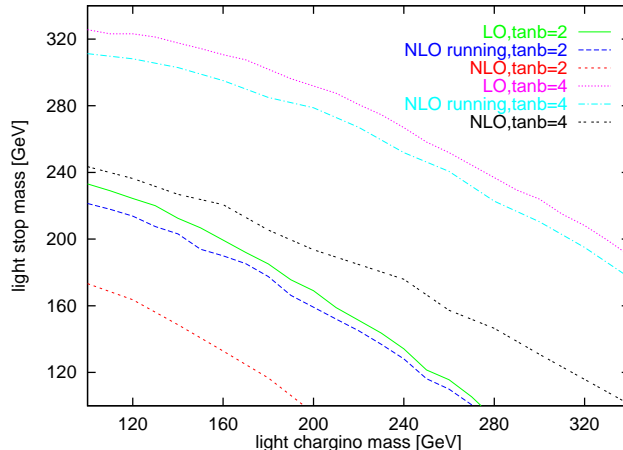


Figure 12: Upper bounds on the lighter chargino and stop masses from  $B \rightarrow X_s \gamma$  data in the scenario (4.2) if a light charged Higgs mass is assumed; for  $\tan \beta = 2$  (three lower curves) and 4 (three upper plots) the LL, NLL-running and NLL results (from the top to the bottom) are shown (see text), from [74].

interacting supersymmetric particles (squarks and gluinos) and is assumed to be of the order of 1 TeV. NLL QCD corrections have been calculated up to first order in  $\mu_W/\mu_{\tilde{g}}$  including the important nondecoupling effects [74].

At the electroweak scale  $\mu_W$ , the new contributions do not induce any new operators in this scenario. Thus, the only step in the new NLL calculation beyond the one within the SM is Step 1, the matching calculation at the scale  $\mu_W$  where we encounter the two new CKM-induced contributions of the charged Higgs and the chargino (see fig. 11):

$$C_{NLL}(\mu_W) = C_{NLL}^{SM}(\mu_W) + C_{NLL}^{H^+}(\mu_W) + C_{NLL}^X(\mu_W). \quad (4.3)$$

One finds [74] that, in this specific supersymmetric scenario, bounds on the parameter space are rather sensitive to NLL contributions and they lead to a significant reduction of the stop-chargino mass region where the supersymmetric contribution has a large destructive interference with the charged-Higgs boson contribution. In fig. 12 the upper bounds on the lighter chargino and stop masses from  $B \rightarrow X_s \gamma$  data in the scenario of (4.2) are illustrated if a light charged Higgs mass of  $m_{H^\pm} = 100$  GeV is assumed. The stop mixing is set to  $|\theta_{\tilde{t}}| < \pi/10$  which corresponds to the assumption of a mainly right-handed light stop. Moreover,  $|\mu| < 500$  GeV and all heavy masses are around 1 TeV. For  $\tan \beta = 2$  and 4 the results of the LL, ‘NLL running’ and NLL calculations are given. The result of neglecting the new NLL supersymmetric contributions to the Wilson coefficients is labelled as ‘NLL running’ and illustrates the importance of the NLL chargino contribution [74].

Quite recently, this minimal flavour violation scenario was refined and extended to the large  $\tan \beta$  regime by the resummations of terms of the form

$\alpha_s^n \tan^{n+1} \beta$  [75, 76]. The stability of the renormalization group improved perturbation theory was reassured for this specific scenario: the resummed NLL results in the large  $\tan \beta$  regime show constraints similar to the LL results (see also [77]).

For example, it is a well-known feature in the mSUGRA model, that depending on the sign of  $A_t \cdot \mu$  (where  $A_t$  denotes the stop mixing parameter) the chargino contribution can interfere constructively ( $A_t \cdot \mu > 0$ ) or destructively ( $A_t \cdot \mu < 0$ ) with the SM and the charged Higgs contribution. Therefore, the scenario  $A_t \cdot \mu > 0$  within this model requires very heavy superpartners in order to accommodate the  $B \rightarrow X_s \gamma$  data. But also the case  $A_t \cdot \mu < 0$  is constrained in the large  $\tan \beta$  regime where the chargino contribution is strongly enhanced (for details see [75, 76, 77]).

However, all these NLL analyses are valid only in the heavy gluino regime. Thus, these calculations cannot be used in particular directions of the parameter space of the above listed models in which quantum effects induce a gluino contribution as large as the chargino or the SM contributions. Nor can it be used as a model-discriminator tool, able to constrain the potentially large sources of flavour violation typical of generic supersymmetric models. A complete NLL calculation should also include contributions where the gluon is replaced by the gluino.

The flavour nondiagonal vertex gluino-quark-squark induced by the flavour violating scalar mass term and trilinear terms is particularly interesting. This is generically assumed to induce the dominant contribution to quark flavour transitions, as this vertex is weighted by the strong coupling constant  $g_s$ . Therefore, it is often taken as the only contribution to these transitions and in particular to the  $B \rightarrow X_s \gamma$  decay, when attempting to obtain order-of-magnitude upper bounds on flavour violating terms in the scalar potential [78, 79]. Once the constraints coming from the experimental measurements are imposed, however, the gluino contribution is reduced to values such that the SM and the other supersymmetric contributions can no longer be neglected. Any LL and NLL calculation of the  $B \rightarrow X_s \gamma$  rate in generic supersymmetric models, therefore, should then include all possible contributions.

The gluino contribution, however, presents some peculiar features related to the implementation of the QCD corrections. In ref. [80] this contribution to the decay  $B \rightarrow X_s \gamma$  has been investigated in great detail for supersymmetric models with generic soft terms. The gluino-induced contributions to the decay amplitude for  $B \rightarrow X_s \gamma$  are of the following form:

$$\alpha_s(m_b) (\alpha_s(m_b) \log(m_b/M))^n \quad (LL), \quad (4.4)$$

$$\alpha_s^2(m_b) (\alpha_s(m_b) \log(m_b/M))^n \quad (NLL). \quad (4.5)$$

In the matching calculation, all factors  $\alpha_s$ , regardless of their source, should be expressed in terms of the  $\alpha_s$  running with five flavours. In [80] it is shown that the relevant operator basis of the SM effective Hamiltonian gets enlarged to contain magnetic and chromomagnetic operators with an extra factor of  $\alpha_s$  and weighted by a quark mass  $m_b$  or  $m_c$ , and also magnetic and chromomagnetic operators of lower dimensionality where the (small) factor  $m_b$  is replaced by the gluino mass.

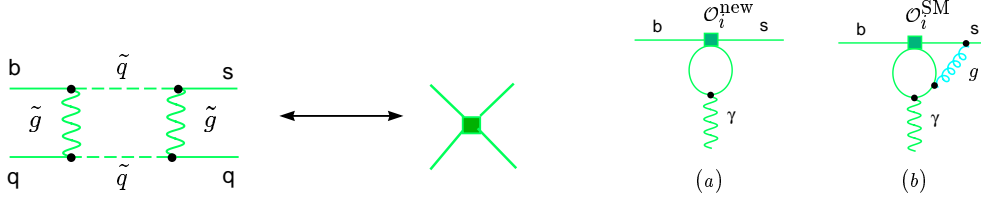


Figure 13: Matching of gluino-squark box on new scalar operators (left frame); mixing of new (scalar) operators at one-loop (a) in contrast to the vectorial operators of the SM (b) who mix at two-loop only (right frame).

Furthermore, one finds that gluino-squark boxes induce new scalar and tensorial four-quark operators, which are shown to mix into the magnetic operators without gluons. On the other hand, the vectorial four-quark operators mix only with an additional gluon into magnetic ones (fig. 13). Thus, they will contribute at the NLL order only. However, from the numerical point of view the contributions of the vectorial operators (although NLL) are not necessarily suppressed w.r.t. the new four-quark contributions; this is due to the expectation that the flavour-violation parameters present in the Wilson coefficients of the new operators are expected to be much smaller (or much more stringently constrained) than the corresponding ones in the coefficients of the vectorial operators. This feature shows that a complete order calculation is important.

In ref. [80] the effects of the LL QCD corrections on constraints on supersymmetric sources of flavour violation are analysed. To understand the sources of flavour violation that may be present in supersymmetric models in addition to those enclosed in the CKM matrix, one has to consider the contributions to the squark mass matrices

$$\mathcal{M}_f^2 = \begin{pmatrix} m_{f,LL}^2 & m_{f,LR}^2 \\ m_{f,RL}^2 & m_{f,RR}^2 \end{pmatrix} + \quad (4.6)$$

$$\begin{pmatrix} F_{f,LL} + D_{f,LL} & F_{f,LR} \\ F_{f,RL} & F_{f,RR} + D_{f,RR} \end{pmatrix}, \quad (4.7)$$

where  $f$  stands for up- or down-type squarks. In the super CKM basis where the quark mass matrices are diagonal and the squarks are rotated in parallel to their superpartners, the  $F$  terms from the superpotential and the  $D$  terms turn out to be diagonal  $3 \times 3$  submatrices of the  $6 \times 6$  mass matrices  $\mathcal{M}_f^2$ . This is in general not true for the additional terms (4.6), originating from the soft supersymmetric breaking potential. Because all neutral gaugino couplings are flavour diagonal in the super CKM basis, the gluino contributions to the decay  $b \rightarrow s\gamma$  are induced by the off-diagonal elements of the soft terms  $m_{f,LL}^2$ ,  $m_{f,RR}^2$ ,  $m_{f,RL}^2$ .

It is convenient to select one possible source of flavour violation in the squark sector at a time and assume that all the remaining ones are vanishing. It should be stressed that one already excludes any kind of interference effects between

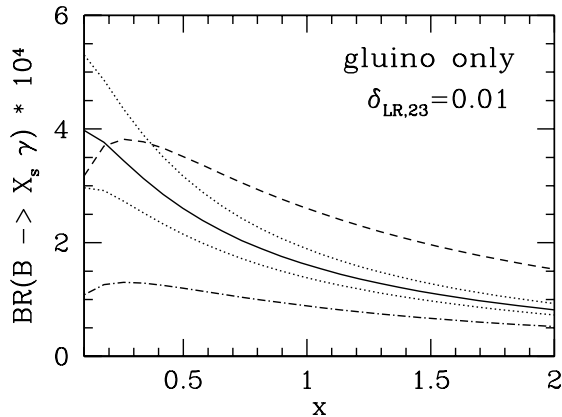


Figure 14: Gluino-induced branching ratio  $\mathcal{B}(B \rightarrow X_s \gamma)$  as a function of  $x = m_{\tilde{g}}^2/m_{\tilde{q}}^2$ , obtained when the only source of flavour violation is  $\delta_{LR,23}$  (see text).

different sources of flavour violation in this way. Following ref. [78], all diagonal entries in  $m_{d,LL}^2$ ,  $m_{d,RR}^2$ , and  $m_{u,RR}^2$  are set to be equal and their common value is denoted by  $m_{\tilde{q}}^2$ . The branching ratio can then be studied as a function of

$$\delta_{LL,ij} = \frac{(m_{d,LL}^2)_{ij}}{m_{\tilde{q}}^2}, \quad \delta_{RR,ij} = \frac{(m_{d,RR}^2)_{ij}}{m_{\tilde{q}}^2}, \quad (4.8)$$

$$\delta_{LR,ij} = \frac{(m_{d,LR}^2)_{ij}}{m_{\tilde{q}}^2} \quad (i \neq j). \quad (4.9)$$

The remaining crucial parameter needed to determine the branching ratio is  $x = m_{\tilde{g}}^2/m_{\tilde{q}}^2$ , where  $m_{\tilde{g}}$  is the gluino mass. Figures 14 and 15 show the LL QCD corrections to the gluino contribution.

In these figures the solid lines show the QCD corrected branching ratio, when only  $\delta_{LR,23}$  or  $\delta_{LL,23}$  are nonvanishing. The branching ratio is plotted as a function of  $x$ , using  $m_{\tilde{q}} = 500 \text{ GeV}$ . The dotted lines show the range of variation of the branching ratio, when the renormalization scale  $\mu$  varies in the interval 2.4–9.6 GeV. Numerically, the scale uncertainty in  $\mathcal{B}(B \rightarrow X_s \gamma)$  is about  $\pm 25\%$ . An extraction of bounds on the  $\delta$  quantities more precise than just an order of magnitude or less, would, therefore, require the inclusion of NLL QCD corrections. It should be noticed, however, that the inclusion of the LL QCD corrections has already removed the large ambiguity on the value to be assigned to the factor  $\alpha_s(\mu)$  in the gluino-induced operators. Before adding QCD corrections, the scale in this factor can assume all values from  $O(m_b)$  to  $O(m_W)$ : the difference between the value of  $\mathcal{B}(B \rightarrow X_s \gamma)$  obtained when taking  $\alpha_s(m_b)$  and that obtained when taking  $\alpha_s(m_W)$  is of the same order as the LL QCD corrections. The corresponding

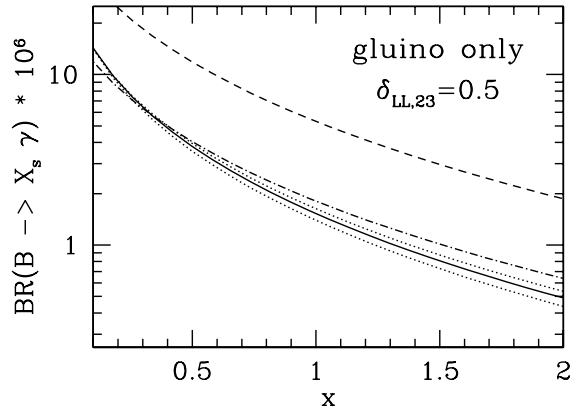


Figure 15: Gluino-induced branching ratio  $\mathcal{B}(B \rightarrow X_s \gamma)$  as a function of  $x = m_g^2/m_q^2$ , obtained when the only source of flavour violation is  $\delta_{LL,23}$  (see text).

values of  $\mathcal{B}(B \rightarrow X_s \gamma)$  for the two extreme choices of  $\mu$  are indicated in Figs. 14 and 15 by the dot-dashed lines ( $\mu = m_W$ ) and the dashed lines ( $\mu = m_b$ ). The choice  $\mu = m_W$  gives values for the non-QCD corrected  $\mathcal{B}(B \rightarrow X_s \gamma)$  relatively close to the band obtained when the LL QCD corrections are included, if only  $\delta_{LL,23}$  is nonvanishing. Finding a corresponding value of  $\mu$  that minimizes the QCD corrections in the case studied in Fig. 14, when only  $\delta_{LR,23}$  is different from zero, depends strongly on the value of  $x$ . In the context of the full LL result, it is important to stress that the explicit  $\alpha_s$  factor has to be evaluated - like the Wilson coefficients - at a scale  $\mu = O(m_b)$ .

In spite of the large uncertainties still affecting the branching ratio  $\mathcal{B}(B \rightarrow X_s \gamma)$  at LL in QCD, it is possible to extract indications of the size that the  $\delta$ -quantities may maximal acquire without inducing conflicts with the experimental measurements (see [80]).

Finally, it should be emphasized that a consistent analysis of the bounds on the sfermion mass matrix should also include interference effects between the various contributions. For this issue we refer to a quite recent paper [81], where the interplay between the various sources of flavour violation and the interference effects of SM, gluino, chargino, neutralino and charged Higgs boson contributions is systematically analysed. New bounds on simple combinations of elements of the soft part of the squark mass matrices are found to be, in general, one order of magnitude weaker than the bound on the single off-diagonal element  $\delta_{LR,23}$ , which was derived in previous work [78, 82] by neglecting any kind of interference effects.

## 5 Direct CP violation in $b/s$ transitions

Detailed measurements of CP asymmetries in rare  $B$  decays will be possible in the near future. Theoretical predictions for the *normalized* CP asymmetries of the inclusive channels (see [59, 83, 84]) within the SM lead to

$$\alpha_{CP}(B \rightarrow X_{s/d}\gamma) = \frac{\Gamma(\bar{B} \rightarrow X_{s/d}\gamma) - \Gamma(B \rightarrow X_{\bar{s}/\bar{d}}\gamma)}{\Gamma(\bar{B} \rightarrow X_{s/d}\gamma) + \Gamma(B \rightarrow X_{\bar{s}/\bar{d}}\gamma)} \quad (5.1)$$

$$\alpha_{CP}(B \rightarrow X_s\gamma) \approx 0.6\%, \quad \alpha_{CP}(B \rightarrow B_d\gamma) \approx -16\% \quad (5.2)$$

when the best-fit values for the CKM parameters [85] are used.

The leading partonic contribution to the CP asymmetries is given by

$$\begin{aligned} \alpha_{CP}(B \rightarrow X_{s/d}\gamma) &\simeq \frac{10^{-2}}{|C_7|^2} (1.17 \times \text{Im}[C_2 C_7^*] - 9.51 \times \text{Im}[C_8 C_7^*] \\ &+ 0.12 \times \text{Im}[C_2 C_8^*] - 9.40 \times \text{Im}[\epsilon_{s(d)} C_2 (C_7^* - 0.013 C_8^*)]); \\ \epsilon_s &= \frac{V_{us}^* V_{ub}}{V_{ts}^* V_{tb}} \simeq -\lambda^2(\rho - i\eta), \quad \epsilon_d = \frac{V_{ud}^* V_{ub}}{V_{td}^* V_{tb}} \simeq \frac{\rho - i\eta}{1 - \rho + i\eta}. \end{aligned} \quad (5.3)$$

The large coefficient of the second term in (5.3) has triggered an attractive scenario in which an enhanced chromomagnetic dipole contribution,  $C_8$ , induces a large direct CP violation in the decay  $B \rightarrow X_s\gamma$ . Such a possible enhancement of the chromomagnetic contribution would lead to a natural explanation of the phenomenology of semileptonic  $B$  decays and also of charm production in  $B$  decays [83].

An analysis for the leptonic counterparts is presented in [86]. The normalized CP asymmetries may also be calculated for exclusive decays; however, these results are model-dependent. An example of such a calculation may be found in [87].

CLEO has already presented a measurement of the CP asymmetry in inclusive  $b \rightarrow s\gamma$  decays, yielding [88]

$$\alpha_{CP}(B \rightarrow X_s\gamma) = (-0.079 \pm 0.108 \pm 0.022) \times (1.0 \pm 0.030), \quad (5.4)$$

which indicates that very large effects are already excluded.

Supersymmetric predictions for the CP asymmetries in  $B \rightarrow X_{s/d}\gamma$  depend strongly on what is assumed for the supersymmetry-breaking sector and are, thus, a rather model-dependent issue. The minimal supergravity model cannot account for large CP asymmetries beyond 2% because of the constraints coming from the electron and neutron electric dipole moments [89]. However, more general models allow for larger asymmetries, of the order of 10% or even larger [90, 83]. Recent studies of the  $B \rightarrow X_d\gamma$  rate asymmetry in specific models led to asymmetries between  $-40\%$  and  $+40\%$  [92] or  $-45\%$  and  $+21\%$  [91]. In general, CP asymmetries may lead to clean evidence for new physics by a significant deviation from the SM prediction. From (5.2), it is obvious that a large CP

asymmetry in the  $B \rightarrow X_s \gamma$  channel or a positive CP asymmetry in the inclusive  $B \rightarrow X_d \gamma$  channel would be a clear signal for new physics.

In [93] it was pointed out that the exclusive and inclusive decays of the form  $b \rightarrow s \gamma$  and  $b \rightarrow d \gamma$ , as well as their leptonic counterparts, provide a stringent test, if the CKM matrix is indeed the only source of CP violation. Using U-spin, which is the  $SU(2)$  subgroup of flavour  $SU(3)$  relating the  $s$  and the  $d$  quark and which is already a well-known tool in the context of nonleptonic decays [94, 95], one derives relations between the CP asymmetries of the exclusive channels  $B^- \rightarrow K^{*-} \gamma$  and  $B^- \rightarrow \rho^- \gamma$  and of the inclusive channels  $B \rightarrow X_s \gamma$  and  $B \rightarrow X_d \gamma$ . One should make use of the U-spin symmetry only with respect to the strong interactions. Moreover, within exclusive final states, the vector mesons like the U-spin doublet  $(K^{*-}, \rho^-)$  are favoured as final states because these have masses much larger than the (current-quark) masses of any of the light quarks. Thus one expects, for the ground-state vector mesons, the U-spin symmetry to be quite accurate in spite of the nondegeneracy of  $m_d$  and  $m_s$ . Defining the rate asymmetries (not the *normalized* CP asymmetries) by

$$\Delta\Gamma(B^- \rightarrow V^- \gamma) = \Gamma(B^- \rightarrow V^- \gamma) - \Gamma(B^+ \rightarrow V^+ \gamma) \quad (5.5)$$

one arrives at the following relation [93]:

$$\Delta\Gamma(B^- \rightarrow K^{*-} \gamma) + \Delta\Gamma(B^- \rightarrow \rho^- \gamma) = b_{exc} \Delta_{exc} \quad (5.6)$$

where the right-hand side is written as a product of a relative U-spin breaking  $b_{exc}$  and a typical size  $\Delta_{exc}$  of the CP violating rate difference. In order to give an estimate of the right-hand side, one can use the model result from [87] for  $\Delta_{exc}$ ,

$$\Delta_{exc} = 2.5 \times 10^{-7} \Gamma_B. \quad (5.7)$$

The relative breaking  $b_{exc}$  of U-spin can be estimated, e.g. from spectroscopy. This leads us to

$$|b_{exc}| = \frac{M_{K^*} - m_\rho}{\frac{1}{2}(M_{K^*} + m_\rho)} = 14\%. \quad (5.8)$$

Certainly, other estimates are also possible, such as a comparison of  $f_\rho$  and  $f_{K^*}$ . In this case one finds a very small U-spin breaking. Using the more conservative value for  $b_{exc}$ , which is also compatible with sum rule calculations of form factors (see [96]), one arrives at the standard-model prediction for the difference of branching ratios

$$|\Delta\mathcal{B}(B^- \rightarrow K^{*-} \gamma) + \Delta\mathcal{B}(B^- \rightarrow \rho^- \gamma)| \sim 4 \times 10^{-8} \quad (5.9)$$

Note that the right-hand side is model-dependent. Still (5.9) is of some use, since a value significantly above this estimate would be a strong hint that non-CKM sources of CP violation are active.

The issue is more attractive in the inclusive modes. Due to the  $1/m_b$  expansion for the inclusive process, the leading contribution is the free  $b$ -quark decay. In

particular, there is no sensitivity to the spectator quark and thus one arrives at the following relation for the CP rate asymmetries [93]:

$$\Delta\Gamma(B \rightarrow X_s\gamma) + \Delta\Gamma(B \rightarrow X_d\gamma) = b_{inc}\Delta_{inc}. \quad (5.10)$$

In this framework one relies on parton-hadron duality (besides in the long-distance contribution from up-quark loops, which is found to be rather small [57]). So one can actually compute the breaking of U-spin by keeping a nonvanishing strange quark mass. However, it is a formidable task to do this for the CP asymmetries and it has not yet been done. The typical size of  $b_{inc}$  can be roughly estimated to be of the order of  $|b_{inc}| \sim m_s^2/m_b^2 \sim 5 \times 10^{-4}$ ;  $|\Delta_{inc}|$  is again the average of the moduli of the two CP rate asymmetries. These have been calculated (for vanishing strange quark mass), e.g. in [59] and thus one arrives at

$$|\Delta\mathcal{B}(B \rightarrow X_s\gamma) + \Delta\mathcal{B}(B \rightarrow X_d\gamma)| \sim 1 \cdot 10^{-9}. \quad (5.11)$$

Again, any measured value in significant deviation of (5.11) would be an indication of new sources of CP violation. Although only an estimate is given here, it should again be stressed that in the inclusive mode the right-hand side in (5.11) can be computed in a model-independent way with the help of the heavy mass expansion.

## 6 $K_L \rightarrow \pi^0\nu\bar{\nu}$ and $K^+ \rightarrow \pi^+\nu\bar{\nu}$

The rare decays  $K_L \rightarrow \pi^0\nu\bar{\nu}$  and  $K^+ \rightarrow \pi^+\nu\bar{\nu}$  represent complementary opportunities for precision flavour physics. They are flavour changing current processes induced at the one-loop level (see fig. 16) and are exceptionally clean processes. In particular, the  $K_L \rightarrow \pi^0\nu\bar{\nu}$  amplitude can be calculated with a theoretical uncertainty below 3% [97].

This implies the important role of these decay modes for CKM phenomenology: they play a unique role among  $K$  decays, like the  $B_d \rightarrow \psi K_S$  mode among the  $B$  decays. They allow a measurement of one angle of the unitarity triangle without any hadronic uncertainties to a precision comparable to that obtained by the  $B_d \rightarrow \psi K_S$  mode before the LHC era [98]:

$$\sin 2\beta = \frac{2r_s}{1+r_s^2} \quad r_s = \sqrt{\sigma} \frac{\sqrt{\sigma(B_1 - B_2) - P_0(K^+)}}{\sqrt{B_2}} \quad (6.1)$$

where  $\sigma$  is just related to the Wolfenstein parameter  $\lambda = 0.22$  via  $(1 - \lambda^2/2)^{-2}$ ;  $P_0(K^+) = 0.40 \pm 0.06$  is the internal charm contribution to  $K^+ \rightarrow \pi^+\nu\bar{\nu}$ ; this quantity is known up to next-to-leading QCD precision, and the dependence on  $V_{tb}$  is only of second order in  $\lambda$ ;  $B_1$  and  $B_2$  represent here the reduced branching ratios  $B_1 = B(K^+ \rightarrow \pi^+\nu\bar{\nu})/(4.11 \times 10^{-11})$  and  $B_2 = B(K_L \rightarrow \pi^0\nu\bar{\nu})/(1.80 \times 10^{-10})$ .

The time-integrated CP violating asymmetry in  $B_d^0 \rightarrow \psi K_S$  is given by  $A_{CP}(\psi K_S) = -\sin 2\beta x_d/(1+x_d^2)$  where  $x_d = \Delta m/\Gamma$  gives the size of  $B_d^0 - \bar{B}_d^0$

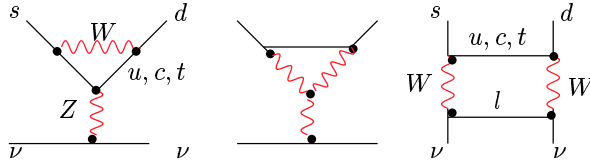


Figure 16: One-loop diagrams contributing to  $K \rightarrow \pi \nu \bar{\nu}$ .

mixing. With  $(\sin 2\beta)_{\pi \nu \bar{\nu}} = (\sin 2\beta)_{\psi K_S}$ , one obtains an interesting connection between rare  $K$  decays and  $B$  physics:

$$\frac{2r_s(B_1, B_2)}{1 + r_s^2(B_1, B_2)} = -A_{CP}(\psi K_S) \frac{1 + x_d^2}{x_d}, \quad (6.2)$$

which must be satisfied in the SM. As was stressed in [98], all quantities in this ‘golden relation’ (6.2) - except for  $P_0(K^+)$  - can be directly measured experimentally and the relation is almost independent of  $V_{cb}$ .

Besides their rich CKM phenomenology, the decays  $K_L \rightarrow \pi^0 \nu \bar{\nu}$  and  $K^+ \rightarrow \pi^+ \nu \bar{\nu}$  are very sensitive to new physics beyond the SM. In addition, the theoretical information is very clean and, thus, the measurement of these decays leads to very accurate constraints on any new physics model. Moreover, there is the possibility that these clean rare decay modes themselves lead to first evidence of new physics when the measured decay rates are not compatible with the SM.

New physics contributions in  $K_L \rightarrow \pi^0 \nu \bar{\nu}$  and  $K^+ \rightarrow \pi^+ \nu \bar{\nu}$  can be parametrized in a model-independent way by two parameters which quantify the violation of the golden relation (6.2) [99, 100]. New effects in supersymmetric models can get induced through new box diagram and penguin diagram contributions involving new particles such as charged Higgs or charginos and stops (fig. 17), replacing the  $W$  boson and the up-type quark of the SM (fig. 16).

In the constrained minimal supersymmetric standard model (MSSM), where all flavour changing effects are induced by contributions proportional to the CKM mixing angles the golden relation (6.2) is valid. Thus, the measurements of  $\mathcal{B}(K_L \rightarrow \pi^0 \nu \bar{\nu})$  and  $\mathcal{B}(K^+ \rightarrow \pi^+ \nu \bar{\nu})$  still directly determine the angle  $\beta$ , and a significant violation of (6.2) would rule out this model.

At the present experimental status of supersymmetry, however, a model-independent analysis including also flavour change through the squark mass matrices is more suitable. If the new sources of flavour change get parametrized by the mass-insertion approximation, an expansion of the squark mass matrices around their diagonal, it turns out that SUSY contributions in this more general setting of the unconstrained MSSM allow for a significant violation of the golden rule. An enhancement of the branching ratios by an order of magnitude (in the case of  $K^+ \rightarrow \pi^+ \nu \bar{\nu}$  by a factor 3) compared with the SM values is possible, mostly due to the chargino-induced Z-penguin contribution [101]. Recent analyses [101, 102, 103] within the uMSSM focused on the correlation of rare

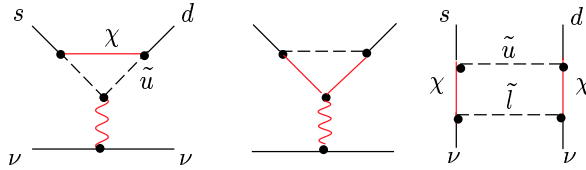


Figure 17: Supersymmetric contributions to  $K \rightarrow \pi \nu \bar{\nu}$ .

decays and  $\epsilon'/\epsilon$ , and led to reasonable upper bounds for the branching ratios:  $\mathcal{B}(K_L \rightarrow \pi^0 \nu \bar{\nu}) \leq 1.2 \times 10^{-10}$ , and  $\mathcal{B}(K^+ \rightarrow \pi^+ \nu \bar{\nu}) \leq 1.7 \times 10^{-10}$ . which should be compared with the latest numerical SM predictions [104]:  $\mathcal{B}(K^+ \rightarrow \pi^+ \nu \bar{\nu}) = (7.9 \pm 3.1) \times 10^{-11}$ ,  $\mathcal{B}(K_L \rightarrow \pi^0 \nu \bar{\nu}) = (2.8 \pm 1.1) \times 10^{-11}$ .

The rare decays  $K^+ \rightarrow \pi^+ \nu \bar{\nu}$  and  $K_L \rightarrow \pi^0 \nu \bar{\nu}$  are specifically interesting in view of the suggested experiments at the Brookhaven laboratory (USA) [108] and at FERMILAB (USA) [109] [110] and at KEK (Japan) [111]. The current Brookhaven experiment E787 has already observed a single, but clean candidate event for  $K^+ \rightarrow \pi^+ \nu \bar{\nu}$  in 1997 which corresponds to the following branching ratio [105]:

$$\mathcal{B}(K^+ \rightarrow \pi^+ \nu \bar{\nu}) = (1.5_{-1.2}^{+3.4}) \times 10^{-10}. \quad (6.3)$$

For the  $K_L \rightarrow \pi^0 \nu \bar{\nu}$  mode, there is only an upper bound available [106]:

$$\mathcal{B}(K_L \rightarrow \pi^0 \nu \bar{\nu}) < 5.9 \times 10^{-7}. \quad (6.4)$$

An indirect upper bound on  $\mathcal{B}(K_L \rightarrow \pi^0 \nu \bar{\nu})$ , using the current limit on  $\mathcal{B}(K^+ \rightarrow \pi^+ \nu \bar{\nu})$  and isospin symmetry, can be placed [107] at  $2 \times 10^{-9}$ .

## 7 Summary

In this paper we have reviewed the status of inclusive rare  $B$  decays, highlighting recent developments. These decays give special insight into the CKM matrix; moreover, as flavour changing neutral current processes, they are loop-induced and therefore particularly sensitive to new physics.

Decays modes such as  $B \rightarrow X_s \gamma$  and  $B \rightarrow X_s l^+ l^-$  (with specific kinematic cuts) represent laboratories for perturbative QCD. Nonperturbative contributions play a subdominant role and they are under control thanks to the heavy mass expansion. The inclusive rare  $B$  decays are or will be accessible at the present  $e^+ e^-$  machines with their low background and their kinematic constraints (CLEO, BaBar, BELLE) and will make precision flavour physics possible in the near future.

Significant progress has been made during the last couple of years. The calculation of NLL (or even NNLL) QCD corrections to these decay modes has been performed. The theoretical uncertainty has been reduced below the 10% level. As was emphasized, the step from LL to NLL precision within the framework of the

renormalization group improved perturbation theory is not only a quantitative, but also a qualitative one, which tests the validity of the perturbative approach in the given problem.

Inclusive rare  $B$  decays allow for an indirect search for new physics, a strategy complementary to the direct production of new (supersymmetric) particles, which is reserved for the planned hadronic machines such as the LHC at CERN. However, the indirect search at the  $B$  factories will imply significant restrictions for the parameter space of supersymmetric models and will thus lead to important theoretically clean information for the direct search of supersymmetric particles. Within supersymmetric models the QCD calculation of the inclusive rare  $B$  decays has not reached the sophistication of the corresponding SM calculation. However, NLL analyses in specific scenarios already show that bounds on the parameter space of nonstandard models are rather sensitive to NLL QCD contributions.

Detailed measurements of CP asymmetries in rare  $B$  decays will also be possible in the near future. They will allow for a stringent and clean test if the CKM matrix is indeed the only source of CP violation.

The rare kaon decays,  $K^+ \rightarrow \pi^+ \nu \bar{\nu}$  and  $K_L \rightarrow \pi^0 \nu \bar{\nu}$ , offer complementary opportunities for precision flavour physics. Besides the current Brookhaven experiment, several more are planned or suggested to explore these theoretically clean decay modes.

## Acknowledgements

I am grateful to Gerhard Buchalla and Christoph Greub for careful reading of the manuscript. I thank Thomas Besmer, Francesca Borzumati, Christoph Greub, Thomas Mannel, Mikolaj Misiak and Daniel Wyler for pleasant collaborations and countless discussions on many issues reviewed in this paper.

## References

- [1] M. Ciuchini *et al.*, “2000 CKM-triangle analysis: A critical review with updated experimental inputs and theoretical parameters,” hep-ph/0012308.
- [2] J. Lee, “Search for CP violation at CLEO,” Nucl. Phys. Proc. Suppl. **93**, 259 (2001);  
D. E. Jaffe, “Search for CP violation at CLEO,” Nucl. Phys. Proc. Suppl. **99**, 174 (2001) [hep-ex/0011021];  
see also <http://w4.lns.cornell.edu/public/CLEO> .
- [3] P. C. Bloom [BABAR Collaboration], “Results from BABAR / PEP-II: One year of operations,” Nucl. Phys. Proc. Suppl. **93**, 336 (2001);  
A. Ryd [BaBar Collaboration], “Studies of CP violation at BaBar,” Nucl.

- Instrum. Meth. A **462**, 57 (2001) [hep-ex/0103036];  
see also <http://www.slac.stanford.edu/BFROOT/> .
- [4] P. Chang [BELLE Collaboration], “Search for CP violation in Belle,” Nucl. Phys. A **684**, 704 (2001);  
B. A. Shwartz [Belle Collaboration], “Belle/KEKB status and performance,” Nucl. Phys. Proc. Suppl. **93**, 332 (2001);  
B. G. Cheon [BELLE Collaboration], “Recent analysis of B meson decays at BELLE,” Nucl. Phys. Proc. Suppl. **93**, 83 (2001);  
K. Kinoshita [BELLE Collaboration], “CP results from Belle,” Nucl. Instrum. Meth. A **462**, 77 (2001) [hep-ex/0101033];  
see also <http://bsunsrv1.kek.jp/> .
- [5] A. Cerri [CDF and D0 Collaborations], “Tevatron measurements related to CP violation,” Nucl. Phys. Proc. Suppl. **99**, 200 (2001);  
S. Bailey [CDF Collaboration], “CDF Run I B physics results,” Nucl. Instrum. Meth. A **462**, 156 (2001);  
R. Jesik [D0 Collaboration], “Prospects for D0 beauty physics measurements in Run II,” Nucl. Phys. Proc. Suppl. **93**, 313 (2001);  
A. Ruiz [CDF-II Collaboration], “CP violation and B mixing in CDF-II,” Nucl. Phys. Proc. Suppl. **93**, 356 (2001);  
see also <http://www-cdf.fnal.gov> and <http://www-d0.fnal.gov/> .
- [6] J. F. Libby [LHCb Collaboration], “Prospects for measuring CP-violating asymmetries with LHCb,” Nucl. Phys. Proc. Suppl. **93**, 352 (2001);  
F. Muheim [LHCb Collaboration], “Status of the LHCb experiment,” Nucl. Instrum. Meth. A **462**, 233 (2001) [hep-ex/0012059];  
see also <http://lhcb.cern.ch/> .
- [7] A. Kulyavtsev *et al.* [BTeV Collaboration], “BTeV: An experiment to measure mixing, CP violation, and rare decays of beauty and charm at the Fermilab collider,” hep-ex/0006037;  
Y. Kubota, “Status of BTeV,” Nucl. Phys. Proc. Suppl. **93**, 303 (2001);  
see also <http://www-btev.fnal.gov/btev.html> .
- [8] T. Hurth *et al.*, “Present and future CP measurements,” J. Phys. G **G27**, 1277 (2001) [hep-ph/0102159].
- [9] H. N. Brown *et al.* [Muon g-2 Collaboration], “Precise measurement of the positive muon anomalous magnetic moment,” Phys. Rev. Lett. **86**, 2227 (2001) [hep-ex/0102017].
- [10] K. Melnikov, “On the theoretical uncertainties in the muon anomalous magnetic moment,” hep-ph/0105267.
- [11] L. Lellouch and M. Luscher, “Weak transition matrix elements from finite-volume correlation functions,” Commun. Math. Phys. **219**, 31 (2001) [hep-lat/0003023];

- L. Lellouch, “Light hadron weak matrix elements,” Nucl. Phys. Proc. Suppl. **94**, 142 (2001) [hep-lat/0011088];
- C. Bernard, “Heavy quark physics on the lattice,” Nucl. Phys. Proc. Suppl. **94**, 159 (2001) [hep-lat/0011064];
- C. T. Sachrajda, “Lattice B physics,” Nucl. Instrum. Meth. A **462**, 23 (2001) [hep-lat/0101003].
- [12] P. Colangelo and A. Khodjamirian, “QCD sum rules: A modern perspective,” hep-ph/0010175;  
M. Shifman, “Snapshots of hadrons or the story of how the vacuum medium determines the properties of the classical mesons which are produced, live and die in the QCD vacuum,” Prog. Theor. Phys. Suppl. **131**, 1 (1998) [hep-ph/9802214];  
V. M. Braun, “Light-cone sum rules,” hep-ph/9801222;  
A. Khodjamirian and R. Ruckl, “QCD sum rules for exclusive decays of heavy mesons,” hep-ph/9801443;
- [13] J. D. Bjorken, “Topics In B Physics,” Nucl. Phys. Proc. Suppl. **11**, 325 (1989);  
M. J. Dugan and B. Grinstein, “QCD basis for factorization in decays of heavy mesons,” Phys. Lett. B **255**, 583 (1991);  
H. D. Politzer and M. B. Wise, “Perturbative corrections to factorization in anti-B decay,” Phys. Lett. B **257**, 399 (1991).
- [14] M. Beneke, G. Buchalla, M. Neubert and C. T. Sachrajda, “QCD factorization for exclusive, non-leptonic B meson decays: General arguments and the case of heavy-light final states,” Nucl. Phys. B **591**, 313 (2000) [hep-ph/0006124].
- [15] M. Beneke, G. Buchalla, M. Neubert and C. T. Sachrajda, “QCD factorization in  $B \rightarrow \pi K$ ,  $\pi \pi$  decays and extraction of Wolfenstein parameters,” hep-ph/0104110;  
M. Ciuchini, E. Franco, G. Martinelli, M. Pierini and L. Silvestrini, “Charming penguins strike back,” hep-ph/0104126.
- [16] J. Gasser, “Chiral perturbation theory,” hep-ph/9912548;  
G. Colangelo and G. Isidori, “An introduction to CHPT,” hep-ph/0101264.
- [17] M. Neubert, “Heavy quark symmetry,” Phys. Rept. **245** (1994) 259.
- [18] Courtesy of A. Lenz.
- [19] A. Ali and C. Greub, “Inclusive photon energy spectrum in rare B decays,” Z. Phys. C **49**, 431 (1991); “Photon energy spectrum in  $B \rightarrow X(s) + \gamma$  and comparison with data,” Phys. Lett. B **361**, 146 (1995) [hep-ph/9506374].

- [20] G. Altarelli, N. Cabibbo, G. Corbo, L. Maiani and G. Martinelli, “Leptonic Decay Of Heavy Flavors: A Theoretical Update,” Nucl. Phys. B **208**, 365 (1982);  
A. Ali and E. Pietarinen, “Semileptonic Decays Of Heavy Quarks In Quantum Chromodynamics,” Nucl. Phys. B **154**, 519 (1979).
- [21] M. S. Alam *et al.* [CLEO Collaboration], “First measurement of the rate for the inclusive radiative penguin decay  $b \rightarrow s \gamma$ ,” Phys. Rev. Lett. **74**, 2885 (1995).
- [22] S. Ahmed *et al.* [CLEO Collaboration], “ $b \rightarrow s \gamma$  branching fraction and CP asymmetry,” hep-ex/9908022.
- [23] K. Lingel, T. Skwarnicki and J. G. Smith, “Penguin decays of B mesons,” Ann. Rev. Nucl. Part. Sci. **48**, 253 (1998) [hep-ex/9804015].
- [24] R. Barate *et al.* [ALEPH Collaboration], “A Measurement of the inclusive  $b \rightarrow s \gamma$  branching ratio,” Phys. Lett. **B429**, 169 (1998).
- [25] Preliminary new results presented by T. Taylor for the BELLE Collaboration and by F. Blanc for the CLEO Collaboration can be found at the homepage of the XXXVI Rencontres de Moriond, 11-17 March 2001: <http://moriond.in2p3.fr/EW/2001/program.html>.
- [26] A.L. Kagan and M. Neubert, “QCD anatomy of  $B \rightarrow X(s \gamma)$  decays,” Eur. Phys. J. **C7**, 5 (1999) [hep-ph/9805303].
- [27] I. I. Bigi, M. Shifman, N. G. Uraltsev and A. Vainshtein, “QCD predictions for lepton spectra in inclusive heavy flavor decays,” Phys. Rev. Lett. **71**, 496 (1993) [hep-ph/9304225]; “On the motion of heavy quarks inside hadrons: Universal distributions and inclusive decays,” Int. J. Mod. Phys. A **9**, 2467 (1994) [hep-ph/9312359];  
A. V. Manohar and M. B. Wise, “Inclusive semileptonic B and polarized Lambda(b) decays from QCD,” Phys. Rev. D **49**, 1310 (1994) [hep-ph/9308246];  
M. Neubert, “QCD based interpretation of the lepton spectrum in inclusive anti-B  $\rightarrow X(u)$  lepton anti-neutrino decays,” Phys. Rev. D **49**, 3392 (1994) [hep-ph/9311325]; “Analysis of the photon spectrum in inclusive  $B \rightarrow X(s) \gamma$  decays,” Phys. Rev. D **49**, 4623 (1994) [hep-ph/9312311];  
T. Mannel and M. Neubert, “Resummation of nonperturbative corrections to the lepton spectrum in inclusive  $B \rightarrow X$  lepton anti-neutrino decays,” Phys. Rev. D **50**, 2037 (1994) [hep-ph/9402288];  
U. Aglietti and G. Ricciardi, “The structure function of semiinclusive heavy flavour decays in field theory,” Nucl. Phys. B **587**, 363 (2000) [hep-ph/0003146].
- [28] M. Misiak, “Status of theoretical anti-B  $\rightarrow X/s \gamma$  and  $B \rightarrow X/s$  lepton+ lepton- analyses,” hep-ph/0009033.

- [29] M. Ciuchini, E. Franco, G. Martinelli, L. Reina and L. Silvestrini, “Scheme independence of the effective Hamiltonian for  $b \rightarrow s$  gamma and  $b \rightarrow s g$  decays,” Phys. Lett. **B316**, 127 (1993) [hep-ph/9307364];  
M. Ciuchini, E. Franco, G. Martinelli and L. Reina, “The Delta  $S = 1$  effective Hamiltonian including next-to-leading order QCD and QED corrections,” Nucl. Phys. **B415**, 403 (1994) [hep-ph/9304257];  
G. Cella, G. Curci, G. Ricciardi and A. Vicere, “QCD corrections to electroweak processes in an unconventional scheme: Application to the  $b \rightarrow s$  gamma decay,” Nucl. Phys. **B431**, 417 (1994) [hep-ph/9406203];  
M. Misiak, “The  $b \rightarrow s e^+ e^-$  and  $b \rightarrow s$  gamma decays with next-to-leading logarithmic QCD corrections,” Nucl. Phys. B **393**, 23 (1993) [Erratum-ibid. B **439**, 461 (1993)].
- [30] N. Pott, “Bremsstrahlung corrections to the decay  $b \rightarrow s$  gamma,” Phys. Rev. **D54**, 938 (1996) [hep-ph/9512252].
- [31] C. Greub, T. Hurth and D. Wyler, “Virtual corrections to the decay  $b \rightarrow s \gamma$ ,” Phys. Lett. B **380**, 385 (1996) [hep-ph/9602281]; “Virtual  $O(\alpha_s)$  corrections to the inclusive decay  $b \rightarrow s \gamma$ ,” Phys. Rev. D **54**, 3350 (1996) [hep-ph/9603404].
- [32] K. Adel and Y. Yao, “Exact alpha-s calculation of  $b \rightarrow s + \text{gamma}$   $b \rightarrow s + g$ ,” Phys. Rev. D **49**, 4945 (1994) [hep-ph/9308349].
- [33] K. Chetyrkin, M. Misiak and M. Munz, “Weak radiative B meson decay beyond leading logarithms,” Phys. Lett. **B400**, 206 (1997) [hep-ph/9612313].
- [34] C. Greub and T. Hurth, “Two-loop matching of the dipole operators for  $b \rightarrow s$  gamma and  $b \rightarrow s g$ ,” Phys. Rev. D **56**, 2934 (1997) [hep-ph/9703349].
- [35] M. Ciuchini, G. Degrossi, P. Gambino and G.F. Giudice, “Next-to-leading QCD corrections to  $B \rightarrow X(s)$  gamma: Standard model and two Higgs doublet model,” Nucl. Phys. **B527**, 21 (1998) [hep-ph/9710335].
- [36] A.J. Buras, A. Kwiatkowski and N. Pott, “Next-to-leading order matching for the magnetic photon penguin operator in the  $B \rightarrow X(s)$  gamma decay,” Nucl. Phys. **B517**, 353 (1998) [hep-ph/9710336].
- [37] A. J. Buras, A. Czarnecki, M. Misiak and J. Urban, “Two-loop matrix element of the current-current operator in the decay  $b \rightarrow X/s$  gamma,” hep-ph/0105160.
- [38] C. Greub and T. Hurth, “Towards a next-to-leading logarithmic result in  $B \rightarrow X(s)$  gamma,” hep-ph/9608449.
- [39] A. F. Falk, M. Luke and M. J. Savage, “Nonperturbative contributions to the inclusive rare decays  $B \rightarrow X(s)$  gamma and  $B \rightarrow X(s)$  lepton+ lepton-,” Phys. Rev. D **49**, 3367 (1994) [hep-ph/9308288].

- [40] A. Ali, G. Hiller, L. T. Handoko and T. Morozumi, “Power corrections in the decay rate and distributions in  $B \rightarrow X/s l^+ l^-$  in the standard model,” *Phys. Rev. D* **55**, 4105 (1997) [hep-ph/9609449].
- [41] M.B. Voloshin, “Large  $O(m(c)^{-2})$  nonperturbative correction to the inclusive rate of the decay  $B \rightarrow X(s) \gamma$ ,” *Phys. Lett.* **B397**, 275 (1997) [hep-ph/9612483].
- [42] Z. Ligeti, L. Randall and M.B. Wise, “Comment on nonperturbative effects in anti- $B \rightarrow X(s) \gamma$ ,” *Phys. Lett.* **B402**, 178 (1997) [hep-ph/9702322].
- [43] A.K. Grant, A.G. Morgan, S. Nussinov and R.D. Peccei, “Comment on nonperturbative  $O(1/m(c)^2)$  corrections to  $\gamma$  (anti- $B \rightarrow X(s) \gamma$ ),” *Phys. Rev.* **D56**, 3151 (1997) [hep-ph/9702380].
- [44] G. Buchalla, G. Isidori and S. J. Rey, “Corrections of order  $\Lambda(\text{QCD})^2/m(c)^2$  to inclusive rare B decays,” *Nucl. Phys. B* **511**, 594 (1998) [hep-ph/9705253].
- [45] A. Khodjamirian, R. Ruckl, G. Stoll and D. Wyler, “QCD estimate of the long distance effect in  $B \rightarrow K^* \gamma$ ,” *Phys. Lett.* **B402**, 167 (1997) [hep-ph/9702318];
- [46] G. Buchalla and G. Isidori, “Nonperturbative effects in anti- $B \rightarrow X/s l^+ l^-$  for large dilepton invariant mass,” *Nucl. Phys. B* **525**, 333 (1998) [hep-ph/9801456].
- [47] M. Misiak, “Theory of radiative B decays,” hep-ph/0002007.
- [48] A. Czarnecki and W.J. Marciano, “Electroweak radiative corrections to  $b \rightarrow s \gamma$ ,” *Phys. Rev. Lett.* **81**, 277 (1998) [hep-ph/9804252].
- [49] A. Strumia, “Two loop heavy top corrections to the  $b \rightarrow s \gamma$  decay,” *Nucl. Phys.* **B532**, 28 (1998) [hep-ph/9804274].
- [50] P. Gambino and U. Haisch, “Electroweak effects in radiative B decays,” *JHEP* **0009**, 001 (2000) [hep-ph/0007259].
- [51] C. Greub and T. Hurth, “Radiative corrections in inclusive rare B decays,” *Nucl. Phys. Proc. Suppl.* **74**, 247 (1999) [hep-ph/9809468].
- [52] C. Greub and P. Liniger, “Calculation of next-to-leading QCD corrections to  $b \rightarrow s g$ ,” *Phys. Rev. D* **63**, 054025 (2001) [hep-ph/0009144].
- [53] A. Lenz, U. Nierste and G. Ostermaier, “Determination of the CKM angle  $\gamma$  and  $|V(ub)/V(cb)|$  from inclusive direct CP asymmetries and branching ratios in charmless B decays,” *Phys. Rev. D* **59**, 034008 (1999) [hep-ph/9802202].

- [54] A. L. Kagan and J. Rathsman, “Hints for enhanced  $b \rightarrow s g$  from charm and kaon counting,” hep-ph/9701300.
- [55] P. Gambino and M. Misiak, “Quark mass effects in anti- $B \rightarrow X/s \gamma$ ,” hep-ph/0104034.
- [56] A. Ali, “Theory of rare B decays,” hep-ph/9709507.
- [57] G. Ricciardi, “Short and long distance interplay in inclusive  $B \rightarrow X(d) \gamma$  decays,” Phys. Lett. B **355**, 313 (1995) [hep-ph/9502286];  
N. G. Deshpande, X. He and J. Trampetic, “Long distance contributions to penguin processes  $b \rightarrow s \gamma$  and  $b \rightarrow d \gamma$ ,” Phys. Lett. B **367**, 362 (1996).
- [58] M. Abud, G. Ricciardi and G. Sterman, “Light masses in short distance penguin loops,” Phys. Lett. **B437**, 169 (1998) [hep-ph/9712346].
- [59] A. Ali, H. Asatrian and C. Greub, “Inclusive decay rate for  $B \rightarrow X(d) + \gamma$  in next-to-leading logarithmic order and CP asymmetry in the standard model,” Phys. Lett. **B429**, 87 (1998) [hep-ph/9803314].
- [60] C. Bobeth, M. Misiak and J. Urban, “Photonic penguins at two loops and  $m(t)$ -dependence of  $BR(B \rightarrow X(s) l+ l-)$ ,” Nucl. Phys. B **574**, 291 (2000) [hep-ph/9910220].
- [61] H. H. Asatrian, H. M. Asatrian, C. Greub and M. Walker, “Two-loop virtual corrections to  $B \rightarrow X/s l+ l-$  in the standard model,” Phys. Lett. B **507**, 162 (2001) [hep-ph/0103087].
- [62] M. Misiak, “The  $b \rightarrow s e+ e-$  and  $b \rightarrow s \gamma$  decays with next-to-leading logarithmic QCD corrections,” Nucl. Phys. B **393**, 23 (1993) [Erratum-ibid. B **439**, 461 (1993)]
- [63] A. J. Buras and M. Munz, “Effective Hamiltonian for  $B \rightarrow X(s) e+ e-$  beyond leading logarithms in the NDR and HV schemes,” Phys. Rev. D **52**, 186 (1995) [hep-ph/9501281].
- [64] A. Ali, G. F. Giudice and T. Mannel, “Towards a model independent analysis of rare B decays,” Z. Phys. C **67**, 417 (1995) [hep-ph/9408213].
- [65] S. Ferrara and E. Remiddi, “Absence Of The Anomalous Magnetic Moment In A Supersymmetric Abelian Gauge Theory,” Phys. Lett. B **53**, 347 (1974).
- [66] A. H. Chamseddine, R. Arnowitt and P. Nath, “Locally Supersymmetric Grand Unification,” Phys. Rev. Lett. **49**, 970 (1982);  
R. Barbieri, S. Ferrara and C. A. Savoy, “Gauge Models With Spontaneously Broken Local Supersymmetry,” Phys. Lett. B **119**, 343 (1982);  
L. Hall, J. Lykken and S. Weinberg, “Supergravity As The Messenger Of Supersymmetry Breaking,” Phys. Rev. D **27** (1983) 2359.

- [67] M. Dine, W. Fischler and M. Srednicki, “Supersymmetric Technicolor,” Nucl. Phys. B **189**, 575 (1981);  
 S. Dimopoulos and S. Raby, “Supercolor,” Nucl. Phys. B **192**, 353 (1981);  
 M. Dine and A. E. Nelson, “Dynamical supersymmetry breaking at low-energies,” Phys. Rev. D **48**, 1277 (1993) [hep-ph/9303230];  
 M. Dine, A. E. Nelson and Y. Shirman, “Low-energy dynamical supersymmetry breaking simplified,” Phys. Rev. D **51**, 1362 (1995) [hep-ph/9408384];  
 M. Dine, A. E. Nelson, Y. Nir and Y. Shirman, “New tools for low-energy dynamical supersymmetry breaking,” Phys. Rev. D **53**, 2658 (1996) [hep-ph/9507378].
- [68] G. F. Giudice, M. A. Luty, H. Murayama and R. Rattazzi, “Gaugino mass without singlets,” JHEP **9812**, 027 (1998) [hep-ph/9810442];  
 L. Randall and R. Sundrum, “Out of this world supersymmetry breaking,” Nucl. Phys. B **557**, 79 (1999) [hep-th/9810155].
- [69] M. Dine, R. Leigh and A. Kagan, “Flavor symmetries and the problem of squark degeneracy,” Phys. Rev. D **48**, 4269 (1993) [hep-ph/9304299];  
 Y. Nir and N. Seiberg, “Should squarks be degenerate?,” Phys. Lett. B **309**, 337 (1993) [hep-ph/9304307].  
 M. Leurer, Y. Nir and N. Seiberg, “Mass matrix models: The Sequel,” Nucl. Phys. B **420**, 468 (1994) [hep-ph/9310320].  
 S. Dimopoulos and G. F. Giudice, “Naturalness constraints in supersymmetric theories with nonuniversal soft terms,” Phys. Lett. B **357**, 573 (1995) [hep-ph/9507282];  
 A. Pomarol and D. Tommasini, “Horizontal symmetries for the supersymmetric flavor problem,” Nucl. Phys. B **466**, 3 (1996) [hep-ph/9507462];  
 A. G. Cohen, D. B. Kaplan and A. E. Nelson, “The more minimal supersymmetric standard model,” Phys. Lett. B **388**, 588 (1996) [hep-ph/9607394];  
 R. Barbieri, G. Dvali and L. J. Hall, “Predictions From A U(2) Flavour Symmetry In Supersymmetric Theories,” Phys. Lett. B **377**, 76 (1996) [hep-ph/9512388].
- [70] H. Baer, M. Brhlik, D. Castano and X. Tata, “ $b \rightarrow s$  gamma constraints on the minimal supergravity model with large  $\tan(\beta)$ ,” Phys. Rev. D **58**, 015007 (1998) [hep-ph/9712305];  
 T. Goto, Y. Okada and Y. Shimizu, “Flavor changing neutral current processes in B and K decays in the supergravity model,” Phys. Rev. D **58**, 094006 (1998) [hep-ph/9804294].
- [71] F. M. Borzumati, M. Olechowski and S. Pokorski, “Constraints on the minimal SUSY SO(10) model from cosmology and the  $b \rightarrow s$  gamma decay,” Phys. Lett. B **349**, 311 (1995) [hep-ph/9412379];  
 F. M. Borzumati, “On the minimal messenger model,” hep-ph/9702307.

- [72] C. Bobeth, M. Misiak and J. Urban, “Matching conditions for  $b \rightarrow s$  gamma and  $b \rightarrow s$  gluon in extensions of the standard model,” Nucl. Phys. B **567**, 153 (2000) [hep-ph/9904413].
- [73] F.M. Borzumati and C. Greub, “2HDMs predictions for anti- $B \rightarrow X(s)$  gamma in NLO QCD,” Phys. Rev. **D58**, 074004 (1998) [hep-ph/9802391]; “Two Higgs doublet model predictions for anti- $B \rightarrow X(s)$  gamma in NLO QCD: Addendum,” Phys. Rev. **D59**, 057501 (1999) [hep-ph/9809438].
- [74] M. Ciuchini, G. Degrassi, P. Gambino and G.F. Giudice, “Next-to-leading QCD corrections to  $B \rightarrow X(s)$  gamma in supersymmetry,” Nucl. Phys. **B534**, 3 (1998) [hep-ph/9806308,v2].
- [75] M. Carena, D. Garcia, U. Nierste and C. E. Wagner, “ $b \rightarrow s$  gamma and supersymmetry with large  $\tan(\beta)$ ,” Phys. Lett. B **499**, 141 (2001) [hep-ph/0010003].
- [76] G. Degrassi, P. Gambino and G. F. Giudice, “ $B \rightarrow X/s$  gamma in supersymmetry: Large contributions beyond the leading order,” JHEP **0012**, 009 (2000) [hep-ph/0009337].
- [77] W. de Boer, M. Huber, A. V. Gladyshev and D. I. Kazakov, “The  $b \rightarrow X/s$  gamma rate and Higgs boson limits in the constrained minimal supersymmetric model,” hep-ph/0102163.
- [78] F. Gabbiani, E. Gabrielli, A. Masiero and L. Silvestrini, “A complete analysis of FCNC and CP constraints in general SUSY extensions of the standard model,” Nucl. Phys. B **477**, 321 (1996) [hep-ph/9604387].
- [79] J. S. Hagelin, S. Kelley and T. Tanaka, “Supersymmetric flavor changing neutral currents: Exact amplitudes and phenomenological analysis,” Nucl. Phys. B **415** (1994) 293.
- [80] F. Borzumati, C. Greub, T. Hurth and D. Wyler, “Gluino contribution to radiative B decays: Organization of QCD corrections and leading order results,” Phys. Rev. D **62**, 075005 (2000) [hep-ph/9911245]; T. Hurth, “Gluino-mediated rare B decays,” Nucl. Phys. Proc. Suppl. **86**, 503 (2000) [hep-ph/9911304]; C. Greub, T. Hurth and D. Wyler, “Indirect search for supersymmetry in rare B decays,” hep-ph/9912420.
- [81] T. Besmer, C. Greub and T. Hurth, “Bounds on flavour violating parameters in supersymmetry,” hep-ph/0105292.
- [82] A. Masiero and O. Vives, “New physics in CP violation experiments,” hep-ph/0104027.

- [83] A. L. Kagan and M. Neubert, “Direct CP violation in  $B \rightarrow X/s$  gamma decays as a signature of new physics,” *Phys. Rev. D* **58**, 094012 (1998) [hep-ph/9803368].
- [84] K. Kiers, A. Soni and G. Wu, “Direct CP violation in radiative b decays in and beyond the standard model,” *Phys. Rev. D* **62**, 116004 (2000) [hep-ph/0006280].
- [85] F. Caravaglios, F. Parodi, P. Roudeau and A. Stocchi, “Determination of the CKM unitarity triangle parameters by end 1999,” hep-ph/0002171.
- [86] A. Ali and G. Hiller, “A theoretical reappraisal of branching ratios and CP asymmetries in the decays  $B \rightarrow (X/d, X/s) l^+ l^-$  and determination of the CKM parameters,” *Eur. Phys. J. C* **8**, 619 (1999) [hep-ph/9812267].
- [87] C. Greub, H. Simma and D. Wyler, “Branching ratio and direct CP violating rate asymmetry of the rare decays  $B \rightarrow K^* \gamma$  and  $B \rightarrow \rho \gamma$ ,” *Nucl. Phys. B* **434**, 39 (1995) [Erratum-ibid. *B* **444**, 447 (1995)] [hep-ph/9406421].
- [88] T. E. Coan *et al.* [CLEO Collaboration], “CP asymmetry in  $b \rightarrow s$  gamma decays,” hep-ex/0010075.
- [89] T. Goto, Y. Y. Keum, T. Nihei, Y. Okada and Y. Shimizu, “Effect of supersymmetric CP phases on the  $B \rightarrow X/s$  gamma and  $B \rightarrow X/s l^+ l^-$  decays in the minimal supergravity model,” *Phys. Lett. B* **460**, 333 (1999) [hep-ph/9812369].
- [90] M. Aoki, G. Cho and N. Oshimo, “CP asymmetry for radiative B meson decay in the supersymmetric standard model,” *Nucl. Phys. B* **554**, 50 (1999) [hep-ph/9903385];  
 C. Chua, X. He and W. Hou, “CP violating  $b \rightarrow s$  gamma decay in supersymmetric models,” *Phys. Rev. D* **60**, 014003 (1999) [hep-ph/9808431];  
 Y. G. Kim, P. Ko and J. S. Lee, “Possible new physics signals in  $b \rightarrow s$  gamma and  $b \rightarrow s l^+ l^-$ ,” *Nucl. Phys. B* **544**, 64 (1999) [hep-ph/9810336];  
 S. Baek and P. Ko, “Probing SUSY-induced CP violations at B factories,” *Phys. Rev. Lett.* **83**, 488 (1999) [hep-ph/9812229];  
 L. Giusti, A. Romanino and A. Strumia, “Natural ranges of supersymmetric signals,” *Nucl. Phys. B* **550**, 3 (1999) [hep-ph/9811386];  
 E. J. Chun, K. Hwang and J. S. Lee, “CP asymmetries in radiative B decays with R-parity violation,” *Phys. Rev. D* **62**, 076006 (2000) [hep-ph/0005013];  
 D. Bailin and S. Khalil, “Flavor-dependent SUSY phases and CP asymmetry in  $B \rightarrow X/s$  gamma decays,” *Phys. Rev. Lett.* **86**, 4227 (2001) [hep-ph/0010058].
- [91] H. H. Asatrian and H. M. Asatrian, “CP asymmetry for inclusive decay  $B \rightarrow X/d + \gamma$  in the minimal supersymmetric standard model,” *Phys.*

- Lett. B **460**, 148 (1999) [hep-ph/9906221];  
H. H. Asatryan, H. M. Asatrian, G. K. Yeghiyan and G. K. Savvidy, “Direct CP-asymmetry in inclusive rare B decays in 2HDM,” hep-ph/0012085.
- [92] A. G. Akeroyd, Y. Y. Keum and S. Recksiegel, “Effect of supersymmetric phases on the direct CP asymmetry of  $B \rightarrow X/d$  gamma,” Phys. Lett. B **507**, 252 (2001) [hep-ph/0103008].
- [93] T. Hurth and T. Mannel, “CP asymmetries in  $b \rightarrow (s/d)$  transitions as a test of CKM CP violation,” hep-ph/0103331.
- [94] R. Fleischer, “New strategies to extract beta and gamma from  $B/d \rightarrow \pi^+ \pi^-$  and  $B/s \rightarrow K^+ K^-$ ,” Phys. Lett. B **459**, 306 (1999) [hep-ph/9903456].
- [95] M. Gronau and J. L. Rosner, “U-spin symmetry in doubly Cabibbo-suppressed charmed meson decays,” Phys. Lett. B **500**, 247 (2001) [hep-ph/0010237];  
M. Gronau, “U-spin symmetry in charmless B decays,” Phys. Lett. B **492**, 297 (2000) [hep-ph/0008292].
- [96] A. Ali, V. M. Braun and H. Simma, “Exclusive radiative B decays in the light cone QCD sum rule approach,” Z. Phys. C **63**, 437 (1994) [hep-ph/9401277];  
P. Ball and V. M. Braun, “Exclusive semileptonic and rare B meson decays in QCD,” Phys. Rev. D **58**, 094016 (1998) [hep-ph/9805422].
- [97] G. Buchalla and A. J. Buras, “QCD corrections to rare K and B decays for arbitrary top quark mass,” Nucl. Phys. B **400**, 225 (1993);  
M. Misiak and J. Urban, “QCD corrections to FCNC decays mediated by Z-penguins and W-boxes,” Phys. Lett. B **451**, 161 (1999) [hep-ph/9901278].
- [98] G. Buchalla and A. J. Buras, “Sin2beta from  $K \rightarrow \pi$  neutrino anti-neutrino,” Phys. Lett. B **333**, 221 (1994) [hep-ph/9405259].
- [99] Y. Nir and M. P. Worah, “Probing the flavor and CP structure of supersymmetric models with  $K \rightarrow \pi$  nu anti-nu decays,” Phys. Lett. B **423**, 319 (1998) [hep-ph/9711215].
- [100] A. J. Buras, A. Romanino and L. Silvestrini, “ $K \rightarrow \pi$  nu anti-nu: A model independent analysis and supersymmetry,” Nucl. Phys. B **520**, 3 (1998) [hep-ph/9712398].
- [101] G. Colangelo and G. Isidori, “Supersymmetric contributions to rare kaon decays: Beyond the single mass-insertion approximation,” JHEP **9809**, 009 (1998) [hep-ph/9808487].
- [102] A. J. Buras and L. Silvestrini, “Upper bounds on  $K \rightarrow \pi$  nu anti-nu and  $K(L) \rightarrow \pi^0 e^+ e^-$  from epsilon'/epsilon and  $K(L) \rightarrow \mu^+ \mu^-$ ,” Nucl. Phys. B **546**, 299 (1999) [hep-ph/9811471].

- [103] A. J. Buras, G. Colangelo, G. Isidori, A. Romanino and L. Silvestrini, “Connections between epsilon’/epsilon and rare kaon decays in supersymmetry,” Nucl. Phys. B **566**, 3 (2000) [hep-ph/9908371].
- [104] A. J. Buras, “CP violation and rare decays of K and B mesons,” hep-ph/9905437.
- [105] S. Adler *et al.* [E787 Collaboration], “Further search for the decay  $K^+ \rightarrow \pi^+ \nu \text{ anti-}\nu$ ,” Phys. Rev. Lett. **84**, 3768 (2000) [hep-ex/0002015]; see also <http://www.phy.bnl.gov/e787/e787.html> .
- [106] A. Alavi-Harati *et al.* [The E799-II/KTeV Collaboration], “Search for the decay  $K(L) \rightarrow \pi^0 \nu \text{ anti-}\nu$  using  $\pi^0 \rightarrow e^+ e^- \gamma$ ,” Phys. Rev. D **61**, 072006 (2000) [hep-ex/9907014]; see also <http://kpsa.fnal.gov:8080/public/ktev.html> .
- [107] Y. Grossman and Y. Nir, “ $K(L) \rightarrow \pi^0 \nu \text{ anti-}\nu$  beyond the standard model,” Phys. Lett. B **398**, 163 (1997) [hep-ph/9701313].
- [108] see <http://www.phy.bnl.gov/e949/> .
- [109] P. S. Cooper [CKM Collaboration], “CKM: Charged kaons at the main injector,” Nucl. Phys. Proc. Suppl. **99**, 121 (2001); see also <http://www.fnal.gov/projects/ckm/Welcome.html> .
- [110] see <http://kpsa.fnal.gov:8080/public/kami/kami.html> .
- [111] see <http://psux1.kek.jp/~satot/00e391a/index.html> .

# Higgs and Supersymmetry searches at the Large Hadron Collider

FRANÇOIS CHARLES

*Universit de Haute Alsace  
Mulhouse, France*

We present here the results for Higgs and Supersymmetry prospective searches at the Large Hadron Collider. We show that for one year at high luminosity, Standard Model and MSSM Higgs should be observed within the theoretically expected mass range. MSUGRA and restricted phenomenological MSSM searches lead to discovery of up to 2.5  $TeV$  squarks and gluinos.

Presented at the

5th International Symposium on Radiative Corrections  
(RADCOR-2000)

Carmel CA, USA, 11-15 September, 2000

# 1 Higgs searches

## 1.1 Standard Model Higgs

The search for the Higgs boson is one of the major task of the LHC. Several decay channels of Higgs have been explored at the LHC among them :  $ZZ, WW$  and  $\gamma\gamma$  provide the best discovery possibilities. We can see in figure 1 the expected branching ratio as function of the Higgs mass. We can notice that  $b\bar{b}$  and  $WW$  are the dominant mode.

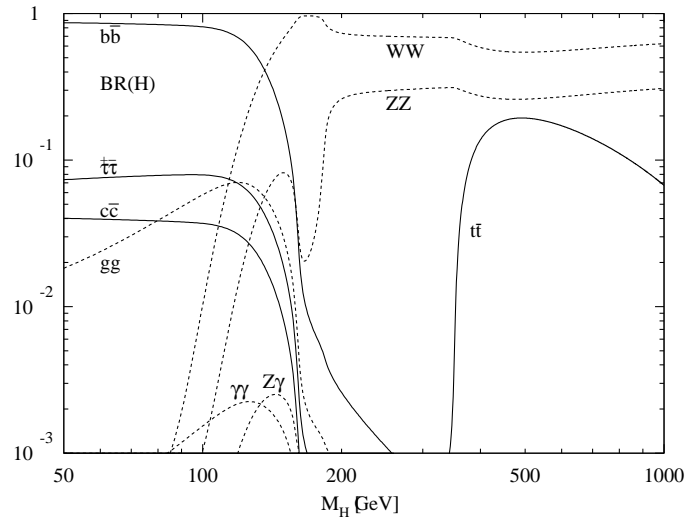


FIG. 1: Branching ratios for major Higgs decay channels as a function of its mass.

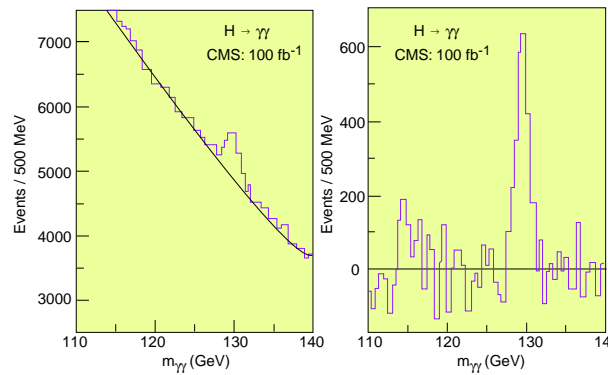


FIG. 2:  $H \rightarrow \gamma\gamma$  with CMS

One of the most important and challenging mode is  $H \rightarrow \gamma\gamma$  in the Higgs mass

range 100 GeV to 150 GeV. It requires excellent calorimetric precision both in energy and angular measurement. True  $\gamma\gamma$  production as well as reducible  $\gamma jet$  (with  $\pi^0$  faking photon) should constitute the main background. The figure 2 illustrate the diphoton invariant mass as expected with CMS detector for one year at high luminosity.

We can see in figure 3 the expected significance ( $S/\sqrt{B}$ ) for one year of high luminosity in ATLAS [1] experiment over the full Higgs mass range. Combining all possible channels should give more than  $5\sigma$ , even in the low luminosity regime.

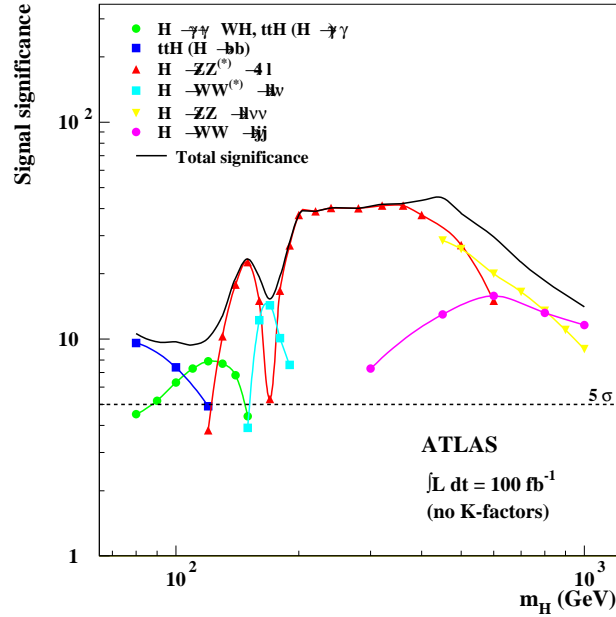


FIG. 3: Higgs boson discovery with ATLAS, high luminosity

## 1.2 Supersymmetry Higgses

In the Minimal Supersymmetric Standard Model, we expect 5 Higgses, two charged and 3 neutral Higgses. For the lightest Higgs,  $h \rightarrow bb$  remains the most important mode while for heavier Higgs :  $H/A \rightarrow \tau\tau, tt, \mu\mu$  are interesting modes. As can be seen from figure 4 in the case of minimal mixing, the full range  $m_A = 50 - 500 GeV$ ,  $\tan\beta = 1 - 50$  can be covered. The most difficult region correspond to intermediate  $m_A$  and  $\tan\beta$ . In the case of light SUSY particles we would also observe decay of Higgs into a pair of sparticles.

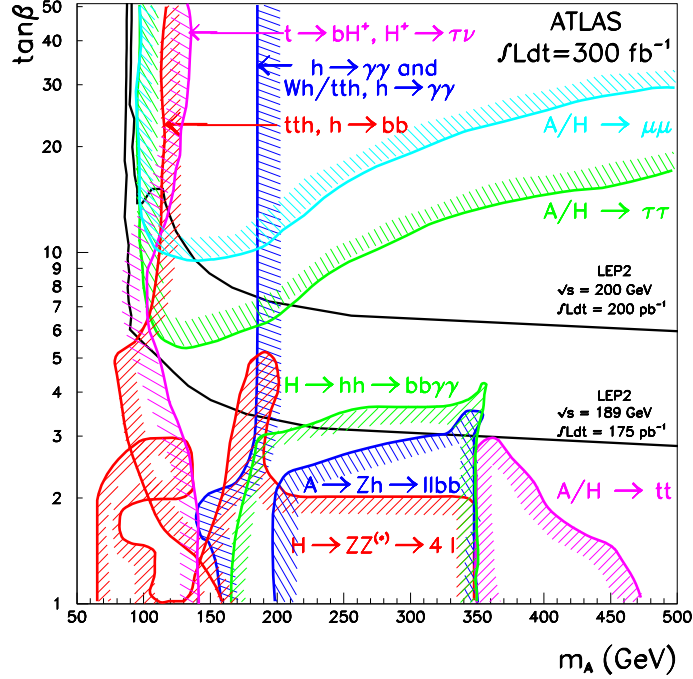


FIG. 4: MSSM Higgs boson discovery with ATLAS, high luminosity

## 2 Supersymmetry searches

### 2.1 Introduction

One of the aims of the LHC collider is to search for the physics beyond the Standard Model (SM). One of the direction of this search is a possible discovery of superpartners of ordinary particles as expected in Supersymmetric extensions of SM (SUSY). SUSY, if it exists, is expected to reveal itself at LHC via excess of (multilepton +) multijet +  $E_T^{miss}$  final states compared to Standard Model (SM) expectations .

The main goal of the LHC studies is to evaluate the potential of the CMS and ATLAS detectors [2,1], to find evidence for SUSY. It deals, first with a semi-inclusive search mainly squarks and gluino mass reach, as the production cross section of these strongly interacting sparticles (pair production or in association with charginos and neutralinos) dominates the total SUSY cross section over a wide region of the parameter space. These studies were done first in the framework of MSUGRA model and at a later stage in a constrained MSSM.

Finally we will consider more exotic models like R-parity violated and Gauge Mediated Supersymmetry Breaking models.

## 2.2 MSUGRA Studies

The large number of SUSY parameters even in the framework of Minimal extension of the SM (MSSM) makes it difficult to evaluate the general reach. So, for this study we restrict ourselves at present to the mSUGRA-MSSM model. This model evolves from MSSM, using Grand Unification Theory (GUT) assumptions (see more details in e.g. [3]). In fact, it is a representative model, especially in case of inclusive studies and reach limits are expressed in terms of squark and gluino mass values.

The mSUGRA model contains only five free parameters :

- a common gaugino mass ( $m_{1/2}$ ) ;
- a common scalar mass ( $m_0$ ) ;
- a common trilinear interaction amongst the scalars ( $A_0$ ) ;
- the ratio of the vacuum expectation values of the Higgs fields ;
- a Higgsino mixing parameter  $\mu$  which enters only through its sign ( $sign(\mu)$ ).

### 2.2.1 Simulation procedure

The PYTHIA 5.7 generator [4] is used to generate all SM background processes, whereas ISAJET 7.32 [5] is used for mSUGRA signal simulations. The CMSJET (version 4.51) fast MC package [7] is used to model the CMS detector response, since it still looks impossible to perform a full-GEANT [6] simulation for the present study, requiring to process multi-million samples of signal and SM background events.

The SM background processes considered are : QCD  $2 \rightarrow 2$  (including  $b\bar{b}$ ),  $t\bar{t}$ ,  $W + jets$ ,  $Z + jets$ . The  $\hat{p}_T$  range of all the background processes is subdivided into several intervals to facilitate accumulation of statistics in the high- $\hat{p}_T$  range : 100-200 GeV, 200-400 GeV, 400-800 GeV and  $> 800$  GeV (additional interval of 800-1200 GeV is reserved for QCD). The accumulated SM background statistics for all background channels amounts to about 200 millions events.

The grid of probed  $m_0$ ,  $m_{1/2}$  mSUGRA points has a cell size of  $\Delta m_0 = \Delta m_{1/2} = 100$  GeV for  $m_0 < 1000$  GeV and  $\Delta m_0 = 200$  GeV,  $\Delta m_{1/2} = 100$  GeV for  $m_0 > 1000$  GeV. This was also probed with the appropriate mixture of signal and pile-up events. The kinematics of signal events is usually harder than that of SM background for the interesting regions of maximal reach of squark-gluino masses . The cross section of the background is however higher by orders of magnitude and high- $p_T$  tails of different backgrounds can have a kinematics similar to that of the signal.

In figure 5 we compare some signal distributions for the point  $(m_0, m_{1/2}) = (1000, 800)$ , corresponding to  $m_{\tilde{g}} \approx m_{\tilde{q}_L} \approx 1900$  GeV,  $m_{\tilde{\chi}_1^0} = 351$  GeV,  $m_{\tilde{\chi}_2^0} = m_{\tilde{\chi}_1^\pm} = 668$  GeV, and distributions of the sum of all SM background processes for the  $E_T^{miss}$  signature.

Both signal and background histograms contain only events satisfying first level selection criteria ( $N_{jets} > 2$  and  $E_T^{miss} > 200\text{GeV}$ ). Only the hardest jet and lepton in the event are shown in distributions in figure 5.

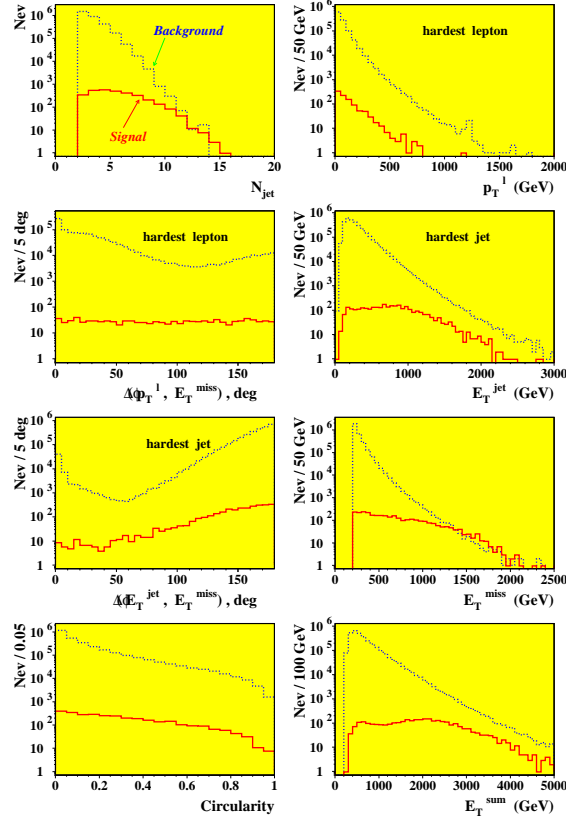


FIG. 5: Comparison of the mSUGRA signal and SM background, with  $100\text{fb}^{-1}$ , in one point of mSUGRA parameter space :  $m_0=1000\text{ GeV}$ ,  $m_{1/2}=800\text{ GeV}$  ( $m_{\tilde{g}}\approx m_{\tilde{q}_L}\approx 1900\text{ GeV}$ ) for the  $E_T^{miss}$  signature. Initial cuts are applied.

Since the topology of signal and background events is rather similar already after first level selection cuts, the difference in the angular distributions and circularity is not significant either, it is thus not very useful to apply cuts on these variables too. The difference in the lepton  $p_T$  distributions is also not very pronounced as signal leptons are produced in cascade decays, thus loosing “memory” about the hardness of the original process. But for extremely high masses of squarks or gluinos ( $\sim 2\text{ TeV}$ ), there is some difference in the angular and  $p_T^l$  distributions between signal and the total SM background. One can deduce from figures 5 that cuts on the jet multiplicity  $N_j$  and  $E_T^{miss}$  are the most profitable ones for background suppression . Of course,

there is inevitable correlation between variables both in signal and background, e.g. an obvious correlation between  $E_T^{miss}$  and the hardest jet  $E_T$  in QCD events, since there  $E_T^{miss}$  is mainly produced by neutrinos from b-jets and/or high- $E_T^{jet}$  mis-measurement. This can lead to a degradation of the efficiency of some cuts, if fixed cuts are used. It is thus more profitable to have adjustable cuts to meet various kinematical conditions in various domains of mSUGRA parameter space and take into account difference in topology between various signatures. For this reason, we search among 10000 cuts combination, the best selection at each generated MSUGRA point.

### 2.2.2 Results

Figures 6 and 7 show the main results of our study for mSUGRA assuming an integrated luminosity of  $100 \text{ fb}^{-1}$ . Figure 6 contains isomass contours for squarks ( $\tilde{q}$ ), gluino ( $\tilde{g}$ ) and lightest scalar Higgs ( $h$ ). Numbers in parenthesis denote mass values of corresponding isomass contour. The neutralino relic density contours from ref. [8], for mSUGRA domain  $m_0 < 1000 \text{ GeV}$ ,  $m_{1/2} < 1000 \text{ GeV}$ , are shown for  $\Omega h^2 = 0.15$ ,  $0.4$  and  $1.0$ . Value  $\Omega h^2 > 1$  would lead to a Universe age less than 10 billion years old, in contradiction with estimated age of the oldest stars. The region in between  $0.15$  and  $0.4$  is favoured by the Mixed Dark Matter (MDM) cosmological models. It is a rather general situation that for all investigated sets of mSUGRA parameters the best reach can be obtained with the  $E_T^{miss}$  signature. The more leptons required - the smaller reach, as can be seen from figures 7. The cosmologically preferred region  $\Omega h^2 < 0.4$  seems to be entirely within the reach of CMS. In figure 6 we also show our calculations for the  $E_T^{miss}$  signature reach for an integrated luminosity of  $300 \text{ fb}^{-1}$ , trying to estimate the ultimate CMS reach.

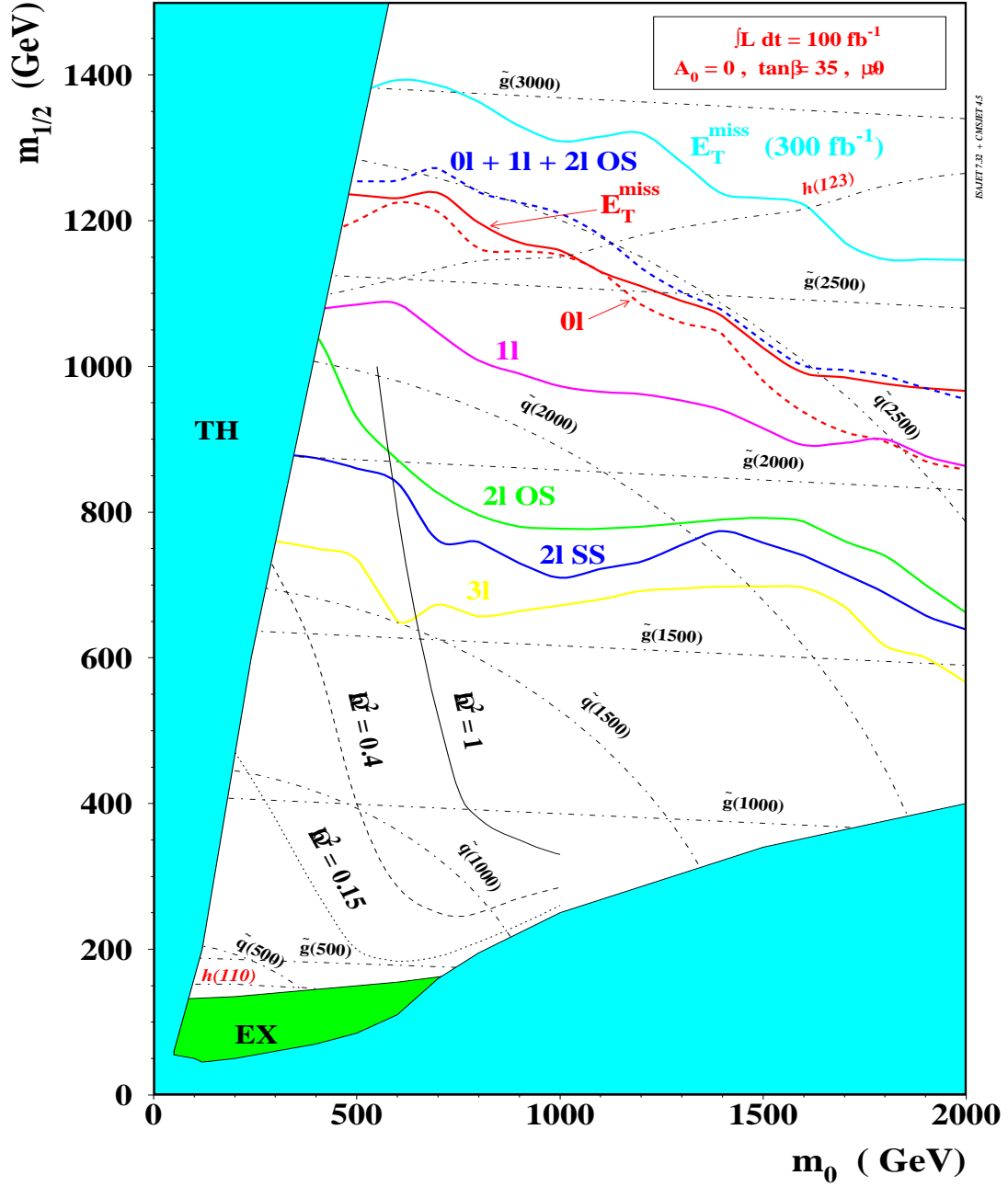


FIG. 6: 5 sigma reach contours for various final states with  $100 \text{ fb}^{-1}$  (see also comments in text).

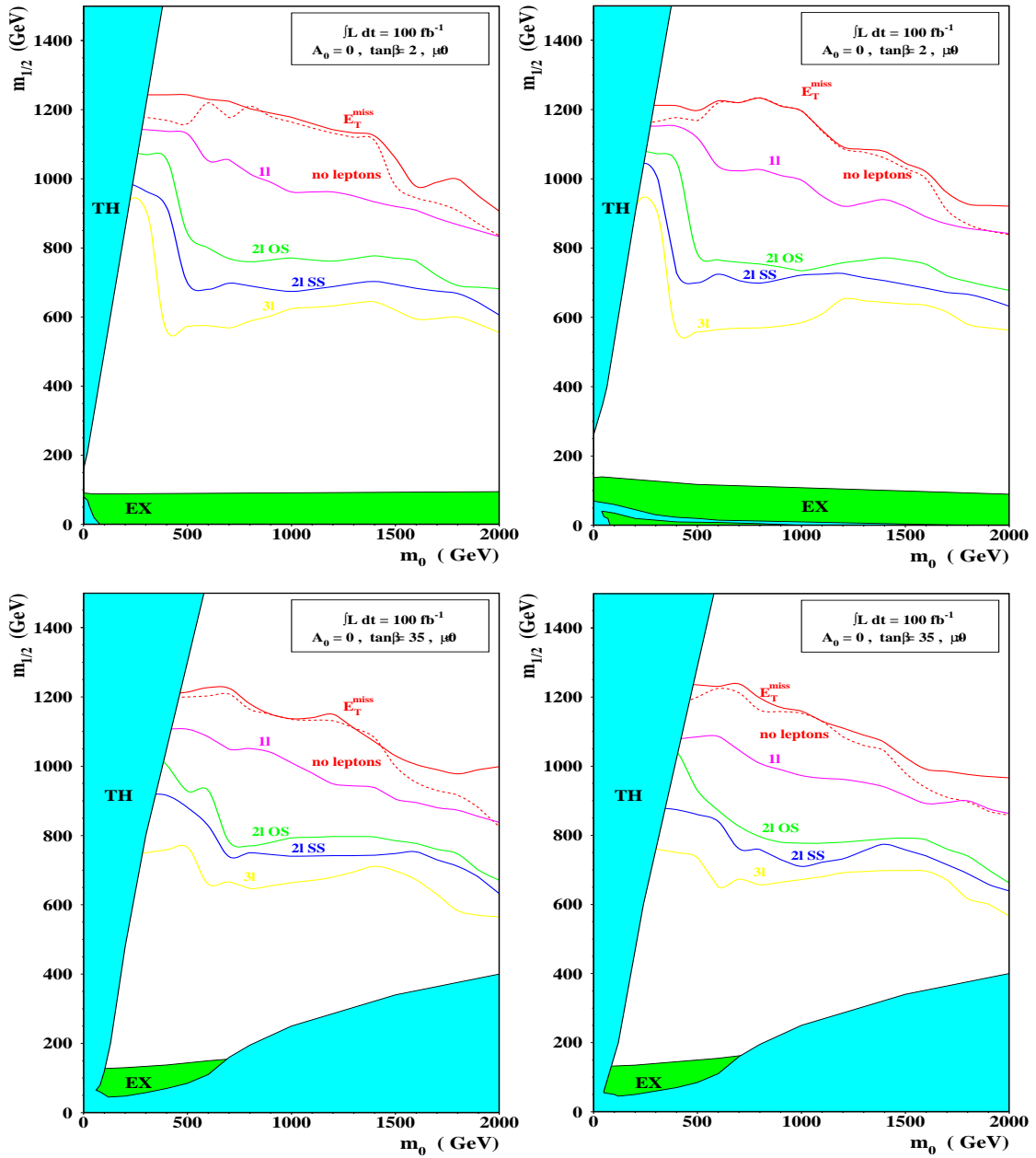


FIG. 7: Simplified figures gathered together.

## 2.3 MSSM

### 2.3.1 A restricted pMSSM

The model used in the next study is a phenomenological MSSM (19 parameters), but with a further reduction of the number of the parameters which allows us to perform simpler simulation, while keeping the diversity of the signatures of MSSM events. We take into account, respectively, the mass unification of squarks and sleptons (universality of the three particles generations) and the unification of trilinear coupling. This leads to 9 free parameters :  $\tan \beta$ ,  $M_A$ ,  $\mu$ ,  $M_1$ ,  $M_2$ ,  $M_{\tilde{g}}$ ,  $M_{\tilde{q}}$ ,  $M_{\tilde{l}}$ ,  $A_3$ .

### 2.3.2 Signal

The goal of this study is to evaluate the capacity of CMS detector to observe MSSM signals. Two reasons urge us to study this pMSSM after the MSUGRA study. First, MSUGRA is a rather constrained model with only five free parameters. Contrary to MSUGRA, the pMSSM has no fixed hierarchy of masses as shown later. Moreover, we try to estimate MSSM parameter values using kinematical quantities measured by CMS, using a fast simulation program. We use a model with 9 parameters, which constitute an hyperspace with 9 dimensions. In order to facilitate the analysis, we use a discretization of the parameters. The choice of the number of value of each parameters depends of the parameter sensitivity. We used a grid for squarks and gluinos masses with 9 values evenly spaced between 600 and 3000 GeV, because the events characteristics at LHC depend primarily on these two masses. On the other hand, the observables are not very dependant on the parameter  $\tan \beta$  and thus we only use two values in order to distinguish the larges ones and the small values from it parameters. Thus, the values which we selected for each parameter of this analysis are :

- $M_{\tilde{l}}$  : 200, 1000, 3000 GeV
- $M_1$  : 100, 500, 1000, 2000 GeV
- $M_2$  : 100, 500, 1000, 2000 GeV
- $M_A$  : 200, 1000, 3000 GeV
- $A_3$  : 0, 2000 GeV
- $\mu$  : 200, 500, 2000 GeV
- $\tan \beta$  : 2, 50
- $M_{\tilde{q}}$  : 600, 900, 1200, 1500, 1800, 2100, 2400, 2700, 3000 GeV
- $M_{\tilde{g}}$  : 600, 900, 1200, 1500, 1800, 2100, 2400, 2700, 3000 GeV

We end up with a total of 140000 different combination of parameters for each of which we generate 1000 events, a compromise between the limits imposed by handling the

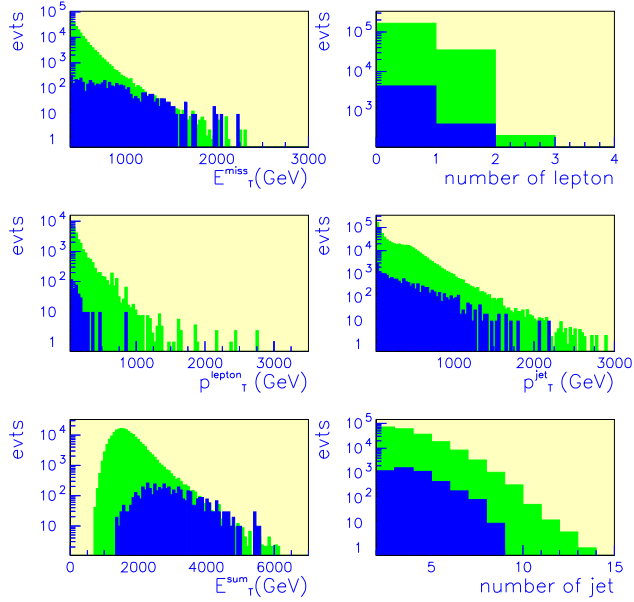


FIG. 8: Example 1 : distribution of signal and background for differents observables

data flow and sufficiently small statistical errors. The theoretical and experimental constraints make it possible to reduce the number of combination to a total of  $17 \cdot 10^3$ . The background production was estimated using Standard Model events leading to similar signatures as MSSM events, in order to study the possibility of extracting SUSY signals from the background. We illustrate in the following figure the background and signal distribution for various variables.

The values of MSSM parameter for the figure 8 are :

$$M_{\tilde{t}} = 1000 \text{ GeV}, M_1 = 100 \text{ GeV}, M_2 = 500 \text{ GeV}, M_{\tilde{q}} = 1800 \text{ GeV}, M_{\tilde{g}} = 1800 \text{ GeV}, M_A = 200 \text{ GeV}, \tan \beta = 50, \mu = 2000 \text{ GeV}, A_3 = 2000 \text{ GeV}.$$

Despite the corresponding low cross section  $\sigma = 77 \text{ fb}$ , the significance of this parameter set is, after application of optimisation cuts, equal to 21.

### 2.3.3 case of large and close hierarchy of masses.

For the first example (figure 9) the masses of neutralinos are much lower than the masses of squarks, gluinos and sleptons, the production will be dominated by neutralinos and charginos. The parameter values are the following :

$$M_{\tilde{t}} = 2000 \text{ GeV}, M_1 = 500 \text{ GeV}, M_2 = 500 \text{ GeV}, M_{\tilde{g}} = 2000 \text{ GeV}, M_{\tilde{q}} = 2000 \text{ GeV}, M_A = 1000 \text{ GeV}, \tan \beta = 50, \mu = 200 \text{ GeV}, A_3 = 0 \text{ GeV}.$$

The cross section of this set of parameters is  $\sigma = 1.22 \text{ pb}$  and despite the abundance

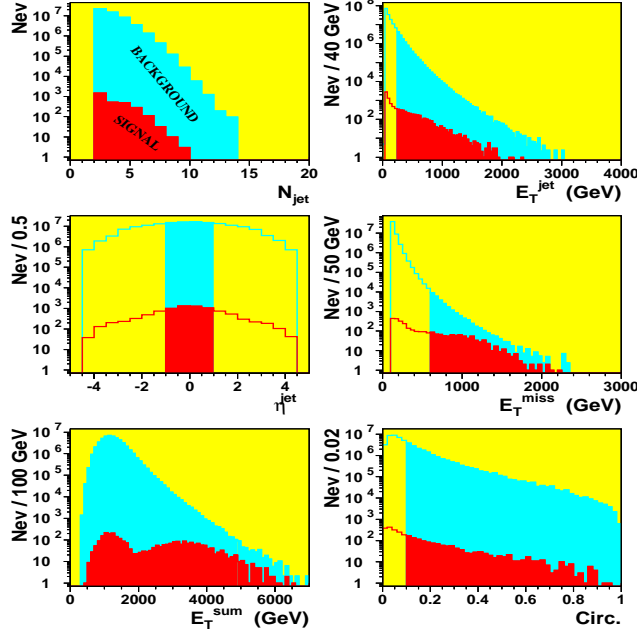


FIG. 9: Example 2 : distribution of signal and background

of neutralinos, the low production rate of gluinos and squarks allows nevertheless to obtain a significance equal to 10.2. The cuts for figures 9 and 10, are those giving the maximum significance (among the list of the optimization cuts).

For the second example (figure 10) the parameter values are the following :  $M_{\tilde{\gamma}} = 1500 \text{ GeV}$ ,  $M_1 = 940 \text{ GeV}$ ,  $M_2 = 2000 \text{ GeV}$ ,  $M_{\tilde{g}} = 1000 \text{ GeV}$ ,  $M_{\tilde{q}} = 1020 \text{ GeV}$ ,  $M_A = 1000 \text{ GeV}$ ,  $\tan \beta = 50$ ,  $\mu = 1050 \text{ GeV}$ ,  $A_3 = 0 \text{ GeV}$ . The masses of neutralinos, gluinos, squarks and sleptons are comparable. The main production proceeds via gluinos and squarks with a cross section  $\sigma = 2.0 \text{ pb}$  and a significance equal to 36.3.

For the third example (figure 11) the parameter values are the following :

$$M_{\tilde{\gamma}} = 1520 \text{ GeV}, M_1 = 1450 \text{ GeV}, M_2 = 2000 \text{ GeV}, M_{\tilde{g}} = 1500 \text{ GeV}, \\ M_{\tilde{q}} = 1520 \text{ GeV}, M_A = 1000 \text{ GeV}, \tan \beta = 50, \mu = 1500 \text{ GeV}, A_3 = 0 \text{ GeV}$$

The masses of neutralinos, gluinos, squarks and sleptons are comparable but with a higher value. The main production proceeds always via gluinos and squarks with, in this case, a cross section  $\sigma = 0.126 \text{ pb}$  and a significance equal to 3.2.

Even for the sets of parameters which would seem difficult (hierarchy of very close mass or on the contrary very separated), this method make it possible to obtain good results, but we observe a limitation in the case of close hierarchy of masses with a discovery limit of about 1.5 TeV instead of 2.5 TeV in the other case.

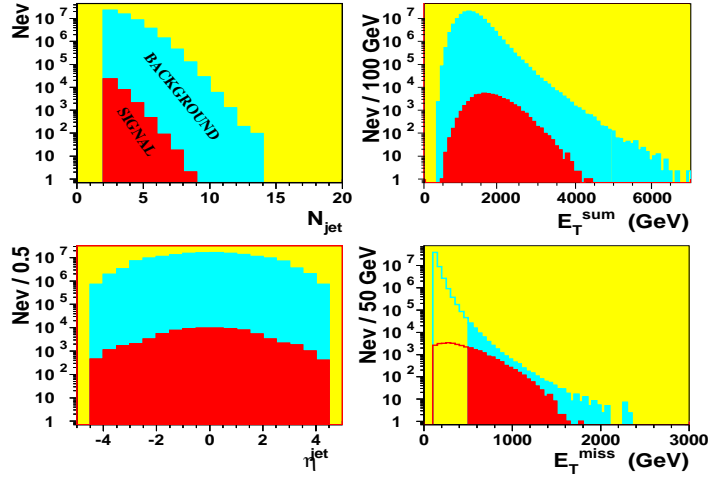


FIG. 10: Example 3 : distribution of signal and background

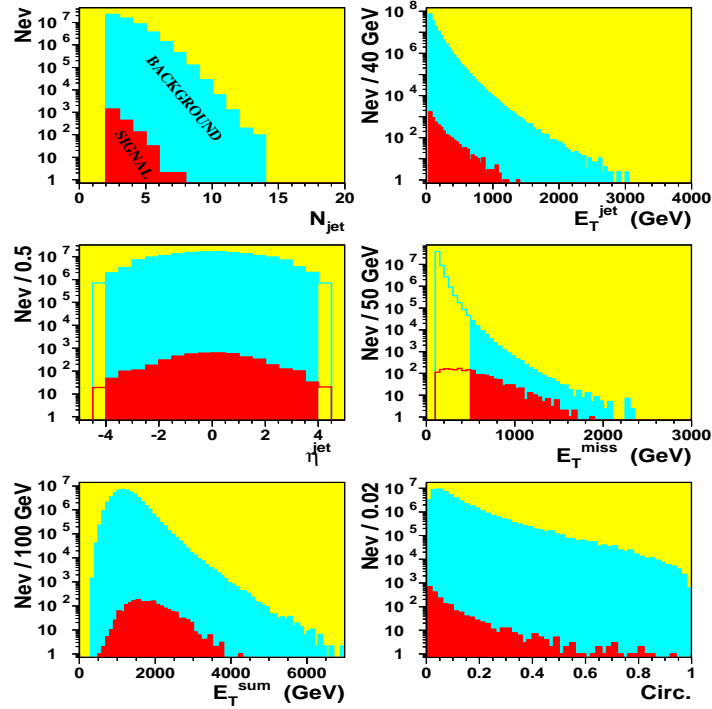


FIG. 11: Distribution of signal and background

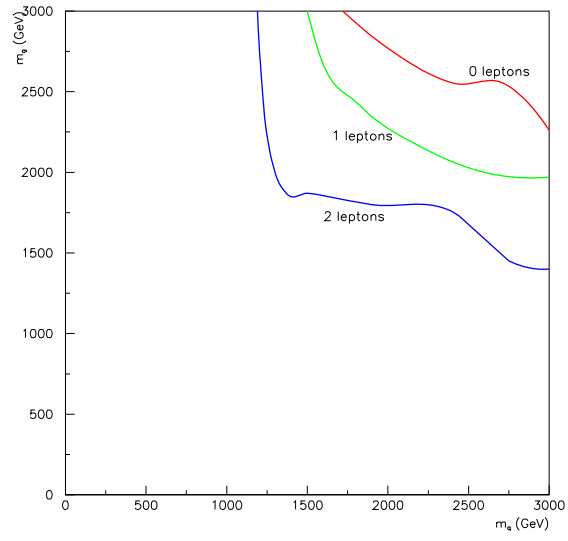


FIG. 12: Graph of exclusion in the plane  $m_{\tilde{q}} vs m_{\tilde{g}}$

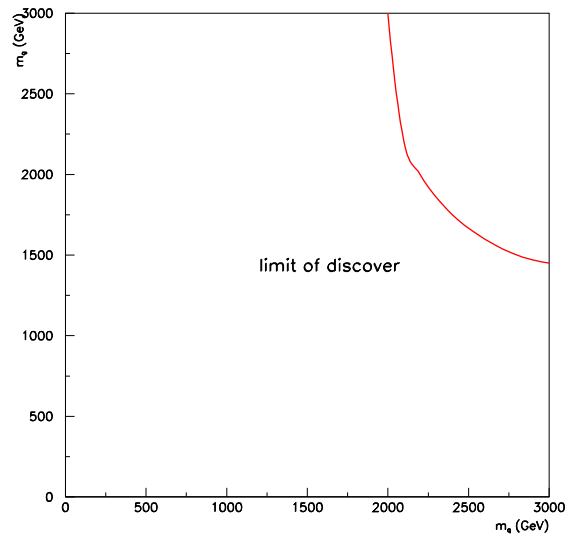


FIG. 13: limit of discovery of MSSM in plane  $m_{\tilde{q}} vs m_{\tilde{g}}$

### 2.3.4 Limit of discovery

We now will generalize this study in order to define limit of discovery for the MSSM. The significance was calculated for high luminosity  $\int L dt = 100 fb^{-1}$ . The isocurves of significance equal to 5 are given in Figure 12 in the plane  $m_{\tilde{q}}$  versus  $m_{\tilde{g}}$ , for the set of 7 different parameters :  $M_{\tilde{t}} = 3000 GeV$ ,  $M_1 = 100 GeV$ ,  $M_2 = 2000 GeV$ ,  $M_A = 200 GeV$ ,  $\tan\beta = 50$ ,  $\mu = 2000 GeV$ ,  $A_3 = 0 GeV$ . Each of these isocurves represent a specific cut on the number of leptons per event. The curves labelled  $0l$ ,  $1l$  and  $2l$  represent significance equal to 5 in case of each event taken into account in the calculation of signal and background possesses respectively 0, 1, 2 lepton(s). Figure 13 show the zone of discovery in plane  $m_{\tilde{q}}$  vs  $m_{\tilde{g}}$  for all the sets of parameter. There is a total of 3750 from the 17000 combinations of parameter which wouldn't be discovered. This lead to the limit of discovery of about 2 TeV.

## 2.4 Conclusion

We demonstrated the possibility to discover a phenomenological MSSM using an inclusive study in the MSSM parameters space. We can note, at the end of our study, that we observed little difference between MSUGRA and the pMSSM. The limit of discovery correspond to the limit of the cross section (2.7 TeV at CMS). The only difference appears for some points having a specific mass hierarchy. For example in the case of close masses, the limit we expect is about 1.5 TeV.

## 3 R parity violation

The conservation of this quantum quantity ( $R = (-1)^{3(B-L)+2S}$ ) allows to conserve baryonic and leptonic number. Nevertheless there is no theoretical reason to impose this conservation. We then expect several new terms to appear in the supersymmetric lagrangian depending on a  $\lambda$  coupling. Experimental constrains lead to very small value for the factor (usually less than  $\lambda < 10^{-1}$ ) multiplying the lagrangian terms violating the R parity. Phenomenologically for ( $\lambda < 10^{-6}$ ) we expect the LSP to decay outside our detectors thus behaving like R-parity conserved signature. We focused here on the intermediate situation ( $10^{-6} < \lambda < 10^{-2}$ ). The phenomenological behaviour correspond to R-parity conserved situation with the decay of the LSP in 3 jets or 3 leptons or 2 jets and one lepton. Figure 14 illustrates the 3 leptons case where the invariant dilepton mass is plotted. As is expected the edge of this distribution correspond to the LSP mass. This correspond to MSUGRA model with low  $m_0$  mass.

The expected reach for the 3 leptons case in the MSUGRA plane is illustrated in the following figure 15. We can note that the mass reach is roughly the same as in the R-parity conserved one. In the following figure 16, is plotted the invariant dijet and

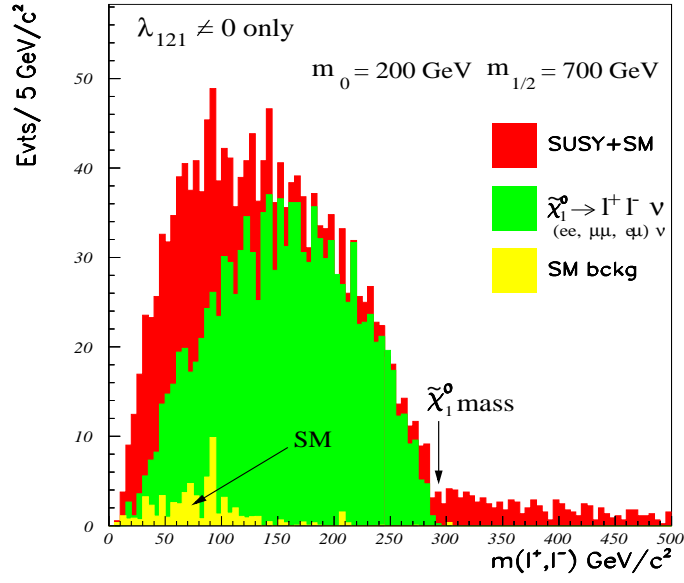


FIG. 14: Invariant dilepton mass for  $\lambda_{121} > 0$

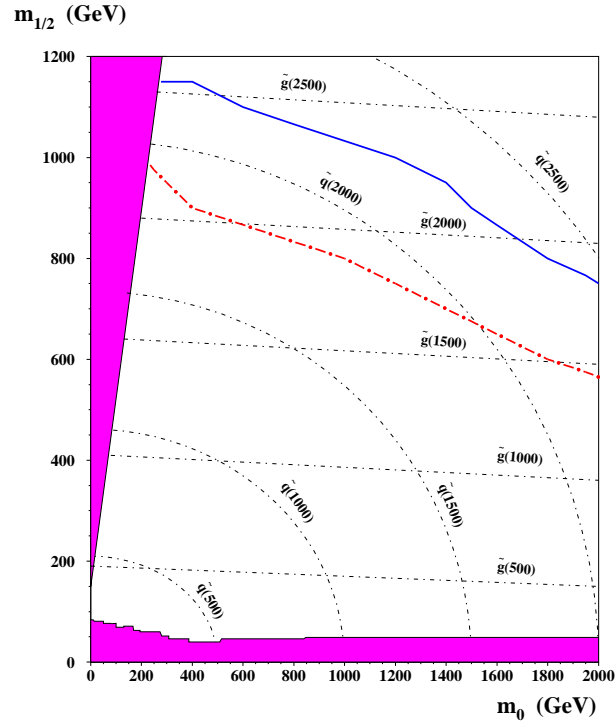


FIG. 15: MSUGRA mass reach for one year of low luminosity for  $\lambda_{121}$  or  $\lambda_{233}$  non zero

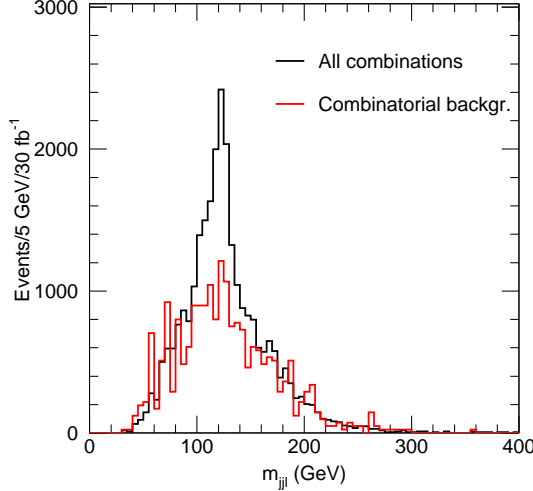


FIG. 16: invariant dilepton and jet mass for  $\lambda'$  non zero.

lepton invariant mass corresponding to  $\lambda'$  non zero. We can observe a reconstructed peak at 130 GeV matching the LSP mass.

## 4 Gauge Mediated Supersymmetry Breaking

In these model, SUSY breaking has its origin in a separate sector at a relatively low scale  $F_m = (10^{10} GeV)^2$  (compare to MSUGRA model). An important characteristic of this model is to lead to a very light gravitino mass much lower than the other spartners. In the minimal GMSB model 6 parameter are considered :  $M_m$  messenger scale,  $\Lambda = F_m/M_m$ ,  $N_5$  number of messenger family,  $\tan\beta$ ,  $sgn\mu$ ,  $C_{grav}$  ratio of the gravitino mass to its value if the only source of SUSY breaking is  $F_m$ . For LHC experiment it is extremely interesting to evaluate the response of the detector to the signature provided by these models as they present different phenomenology. We expect 2 possible scenarios :

$$- \tilde{\chi}_1^0 \rightarrow \tilde{G} + \gamma \quad (\tilde{\chi}_1^0 \text{ NLSP})$$

$$- \tilde{l}_R \rightarrow \tilde{G} + l \quad (\tilde{l}_R \text{ NLSP})$$

with the following signatures :

NSLP	$c\tau$ : short	$c\tau$ : average	$c\tau$ long
$\tilde{\chi}_1^0$	MSSM+2 $\gamma$	$c\tau$ measurement (ECAL, $\mu$ chamber)	MSSM
$\tilde{l}_R$	MSSM+2 $l$	$c\tau$ and mass measurement	mass measurement (TOF)

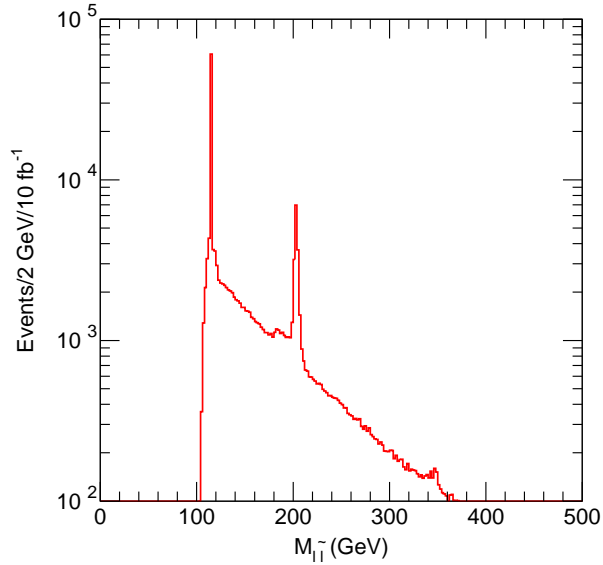


FIG. 17: Dilepton invariant mass reconstruction for slow ionizing slepton

In figure 17, we show the channel  $\tilde{\chi}_i^0 \rightarrow \tilde{l}_R l$  where we reconstruct a long living right slepton using TOF measurement as measured in the muon chamber. We observe 3 peaks corresponding to  $\tilde{\chi}_1^0, \tilde{\chi}_2^0$  and  $\tilde{\chi}_4^0$ . Figure 18 show the channel  $\tilde{l}_L \rightarrow \tilde{\chi}_i^0 l \rightarrow \tilde{l}_R ll$  : peak  $\tilde{l}_L$ , and  $\tilde{\chi}_1^\pm \rightarrow \tilde{\nu} l \rightarrow \tilde{l}_R \nu ll$ . Combine previous  $\tilde{\chi}_1^0$  invariant mass with any of 4 hardest jets provide the reconstruction of left squark (generated  $m_{\tilde{q}} = 648 \text{ GeV}$ , reconstructed 632 GeV) as can be seen in figure 19. From this study we can deduce that the full reconstruction chain can be performed.

#### 4.1 Conclusions

The main conclusions of our studies are the following : Standard Model Higgs as well MSSM Higgs should be visible over the complete theoretical expected range using various decay channels. The SUGRA model, investigated for SUSY search, would be detectable through an excess of events over SM expectations up to masses  $m_{\tilde{q}} \sim m_{\tilde{g}}$

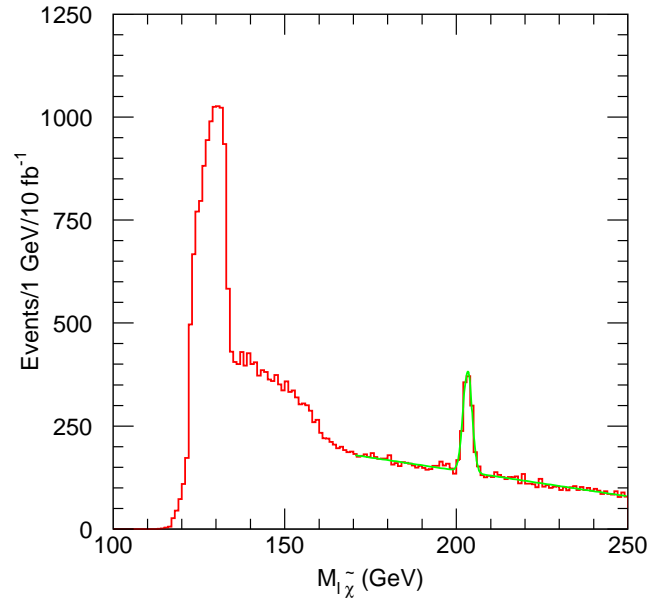


FIG. 18: Trilepton invariant mass

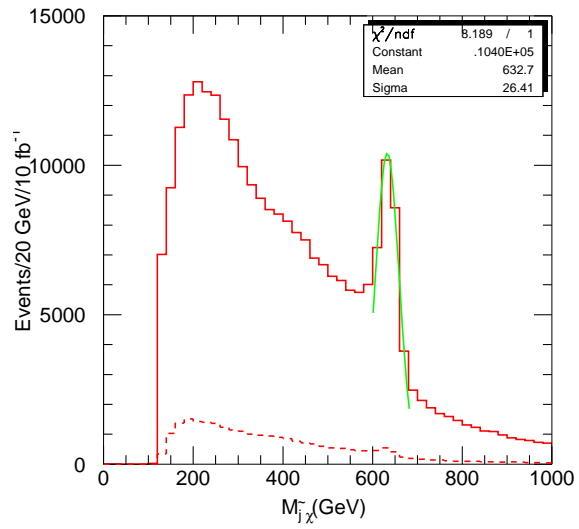


FIG. 19: Trilepton and jet invariant mass

$\sim 2.5$  TeV with  $100 \text{ fb}^{-1}$ . This means that the entire plausible domain of EW-SUSY parameter space for most probable values of  $\tan\beta$  can be probed. Furthermore, the S/B ratios are  $> 1$  everywhere in the reachable domain of parameter space (with the appropriate cuts) thus allowing a study of kinematics of  $\tilde{q}, \tilde{g}$  production and obtaining information on their masses. The cosmologically interesting region  $\Omega h^2 \leq 1$ , and even more the preferred region  $0.15 \leq \Omega h^2 \leq 0.4$ , can be entirely probed. The mass reach is up to  $\tilde{q}, \tilde{g} = 2.5 \text{ TeV}$  and the cosmologically interesting region is covered by CMS/ATLAS. Sleptons can be observed up to 400 GeV, LSP up to 400 GeV. LHC can perform exclusive studies : gluino, neutralino reconstruction and determine MSUGRA parameters. MSSM investigation show similarities with MSUGRA but some specific mass hierarchy might be difficult to explore. LHC can also strongly contribute in GMSB model and provide some insights for parameters determination. R parity violated ( $\lambda < 10^{-2}$ ) studied ( $\chi_1^0$  mass determination). These models lead to various experimental signature with which LHC detectors can cope.

## Références

- [1] Technical Proposal CERN/LHCC/94-43
- [2] CMS technical design report, CERN/LHCC/94-38 LHCCP1 (1994)
- [3] The Minimal Supersymmetric Standard Model : Group summary report A.Djouadi and al. PM/98-45 december 1998.
- [4] T.Sjostrand, Computer Phys. Comm. 82 (1994) 74.
- [5] ISAJET 7.48 a monte carlo event generator for  $pp, p\bar{p}$  and  $e^+e^-$  reaction - F.Paige, S.Protopopescu, H.Baer, X.Tata
- [6] GEANT 3 - R.brun and al CERN DD/EE/84-1 (1986)
- [7] CMSJET s.Abdullin, A.Khanov, N.Stepanov - CMS-TN/94-180
- [8] H. Baer and M.Brhlík, Phys.Rev. **D57**, 567 (1998).

ER/40685/964  
UB-HET-01-01  
UR-1629  
April 19, 2001  
hep-ph/0101254

# Theoretical Challenges for a Precision Measurement of the W Mass at Hadron Colliders\*

ULRICH BAUR

*Department of Physics  
State University of New York at Buffalo, Buffalo, NY 14260 USA*

DOREEN WACKEROTH

*Department of Physics and Astronomy  
University of Rochester, Rochester, NY 14627 USA*

We summarize the status of calculations of the electroweak radiative corrections to W and Z boson production via the Drell-Yan mechanism at hadron colliders. To fully exploit the precision physics potential of the high-luminosity environment of the Fermilab Tevatron  $p\bar{p}$  (Run II) and the CERN LHC  $pp$  colliders, it is crucial that the theoretical predictions are well under control. The envisioned precision physics program includes a precise measurement of the W boson mass and the (leptonic) weak mixing angle, as well as probing the Standard Model (SM) of electroweak interactions at the highest accessible center-of-mass energies. Some numerical results are presented.

Presented at the

5th International Symposium on Radiative Corrections  
(RADCOR-2000)  
Carmel CA, USA, 11–15 September, 2000

---

\*Work supported by NSF grants PHY-9970703 and PHY-9600155, and by the U.S. Department of Energy, under grant DE-FG02-91ER40685.

# 1 Introduction

The Standard Model of electroweak interactions (SM) so far withstood all experimental challenges and is tested as a quantum field theory at the 0.1% level [1]. However, the mechanism of mass generation in the SM predicts the existence of a Higgs boson which, so far, has eluded direct observation. Direct searches at LEP2 give a (preliminary) 95% confidence-level lower bound on the mass of the SM Higgs boson of  $M_H > 113.5$  GeV [2]. Indirect information on the mass of the Higgs boson can be extracted from the  $M_H$  dependence of radiative corrections to the W boson mass. With the present knowledge of the W boson and top quark masses, and the electromagnetic coupling constant,  $\alpha(M_Z^2)$ , the SM Higgs boson mass can be indirectly constrained to  $M_H = 77_{-39}^{+69}$  GeV [1] by a global fit to all electroweak precision data. Future more precise measurements of the W boson and top quark masses are expected to considerably improve the present indirect bound on  $M_H$ : with a precision of 30 MeV for the W boson mass,  $M_W$ , and 2 GeV for the top quark mass which are target values for Run II of the Tevatron [3],  $M_H$  can be predicted with an uncertainty of about 30%. In addition, the confrontation of a precisely measured W boson mass with the indirect SM prediction from a global fit to all electroweak precision data,  $M_W = 80.385 \pm 0.022$  GeV [1], will provide a stringent test of the SM. A detailed discussion of the prospects for the precision measurement of  $M_W$ , and of the (leptonic) effective weak mixing angle,  $\sin^2 \theta_{eff}^l$ , at Run II and the LHC is given in Refs. [3] and [4], respectively.

In order to measure  $M_W$  with high precision in a hadron collider environment it is necessary to fully control higher order QCD and electroweak radiative corrections to the W and Z production processes. The status of the QCD corrections to W and Z boson production at hadron colliders is reviewed in Refs. [5,6]. Here we discuss the electroweak  $\mathcal{O}(\alpha)$  corrections to  $p\bar{p}^{(-)} \rightarrow W^\pm \rightarrow l^\pm \nu_l$  and  $p\bar{p}^{(-)} \rightarrow \gamma^*, Z \rightarrow l^+ l^-$  ( $l = e, \mu$ ) as presented in detail in Refs. [7,8] and [9,10].

## 2 Electroweak $\mathcal{O}(\alpha)$ Corrections to $p\bar{p}^{(-)} \rightarrow W^\pm \rightarrow l^\pm \nu$

The full electroweak  $\mathcal{O}(\alpha)$  corrections to resonant W boson production in a general four-fermion process were calculated in Ref. [7] with special emphasis on obtaining a gauge invariant decomposition into a photonic and non-photonic part. It was shown that the cross section for resonant W boson production via the Drell-Yan mechanism at parton level,  $q_i \bar{q}_{i'} \rightarrow f \bar{f}'(\gamma)$ , can be written in the following form [8]:

$$\begin{aligned}
 d\hat{\sigma}^{(0+1)} &= d\hat{\sigma}^{(0)} [1 + 2\mathcal{R}e(\tilde{F}_{weak}^{initial}(\hat{s} = M_W^2) + \tilde{F}_{weak}^{final}(\hat{s} = M_W^2))] \\
 &+ \sum_{\substack{a=initial,final, \\ interf.}} [d\hat{\sigma}^{(0)} F_{QED}^a(\hat{s}, \hat{t}) + d\hat{\sigma}_{2 \rightarrow 3}^a], \quad (1)
 \end{aligned}$$

where the Born cross section,  $d\hat{\sigma}^{(0)}$ , is of Breit-Wigner form, and  $\hat{s}$  and  $\hat{t}$  are the usual Mandelstam variables in the parton center of mass frame. The (modified) weak corrections and the virtual and soft photon emission from the initial and final state fermions (as well as their interference) are described by the form factors  $\tilde{F}_{weak}^a$  and  $F_{QED}^a$ , respectively. The IR finite contribution  $d\hat{\sigma}_{2\rightarrow 3}^a$  describes real photon radiation away from soft singularities. Mass singularities of the form  $\ln(\hat{s}/m_f^2)$  arise when the photon is emitted collinear with a charged fermion and the resulting singularity is regularized by retaining a finite fermion mass ( $m_f$ ).  $F_{QED}^{initial}$  and  $d\hat{\sigma}_{2\rightarrow 3}^{initial}$  still include quark-mass singularities which need to be extracted and absorbed into the parton distribution functions (PDFs). The absorption of the quark-mass singularities into the PDFs can be done in complete analogy to gluon emission in QCD, thereby introducing a QED factorization scheme dependence. Explicit expressions for the  $W$  production cross section in the QED DIS and  $\overline{\text{MS}}$  scheme are provided in Ref. [8]. So far, in the extraction of the PDFs from data as well as in the PDF evolution, QED corrections are not taken into account. The latter result in a modified scale dependence of the PDFs, which is expected to have a negligible effect on the observable cross sections [4]. The numerical evaluation of the cross section is done with the parton level Monte Carlo program WGRAD [8]<sup>1</sup>, and results have been obtained for a variety of interesting  $W$  boson observables at the Tevatron [8] and the LHC [4].

In the past, fits to the distribution of the transverse mass of the final-state lepton neutrino system,  $M_T(l\nu)$ , have provided the most accurate measurements of  $M_W$  [11]. Photonic initial state and initial-final state interference corrections were found to have only a small effect on the  $M_T$  distribution, and weak corrections uniformly reduce the cross section by about 1%. However, final-state photon radiation significantly distorts the shape of the  $M_T$  distribution, and thus considerably affects the extracted value of  $M_W$ . In the electron case, when taking into account realistic lepton identification requirements to simulate the detector acceptance, the electroweak radiative corrections are strongly reduced because electron and photon momenta are combined for small opening angles between the two particles. This eliminates the mass singular terms associated with final state radiation. The ratio of the full  $\mathcal{O}(\alpha^3)$  and lowest order differential cross section as a function of  $M_T(l\nu)$  with and without lepton identification requirements taken into account is shown in Fig. 1.

A previous approximate calculation [12] took only the real photonic corrections properly into account while the effect of soft and virtual virtual photonic corrections were estimated from the inclusive  $W \rightarrow l\nu(\gamma)$  width. Weak corrections were ignored in Ref. [12]. Comparing the  $W$  mass shifts obtained using the calculations of Refs. [12] and [8], one finds that the proper treatment of virtual and soft corrections and the inclusion of weak corrections induces an additional shift of  $\mathcal{O}(10 \text{ MeV})$  in the extracted  $W$  boson mass.

---

<sup>1</sup>WGRAD is available from the authors.

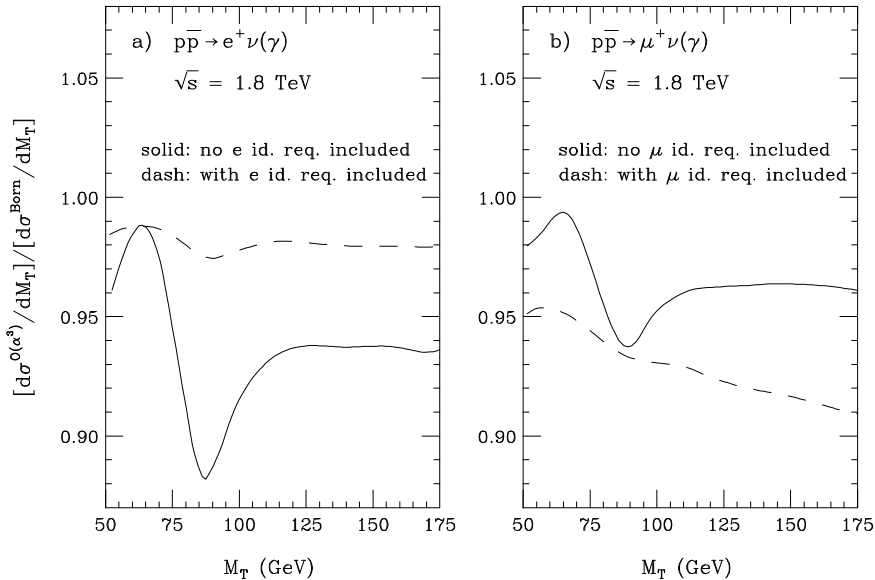


Figure 1: The relative corrections to the  $M_T(l\nu)$  distributions at the Tevatron when taking into account the full electroweak  $\mathcal{O}(\alpha)$  corrections (from Ref. [8]).

### 3 Electroweak $\mathcal{O}(\alpha)$ Corrections to $p\bar{p} \rightarrow \gamma^*, Z \rightarrow l^+l^-$

Neutral-current Drell-Yan production is interesting for several reasons:

1. Future precise measurements of the W boson mass at hadron colliders depend on a precise knowledge of the Z boson production process. When compared to the values measured at LEP, the measured Z boson mass and width help to determine the energy scale and resolution of the electromagnetic calorimeter.
2. Ratios of W and Z boson observables may yield a more precise measurement of  $M_W$  than the traditional technique of fitting the  $M_T$  distribution [3,13].
3. The forward-backward asymmetry in the vicinity of the Z resonance can be used to measure the (leptonic) effective weak mixing angle [4,9]. Studying the forward-backward asymmetry above the Z resonance probes the  $\gamma, Z$  interference at the highest available energies.
4. Finally, at large di-lepton invariant masses,  $m(l^+l^-)$ , deviations from the SM prediction could indicate the presence of new physics, such as new heavy gauge bosons  $Z'$  or extra spatial dimensions.

It is therefore important to determine the electroweak corrections for this process.

The electroweak  $\mathcal{O}(\alpha)$  corrections to neutral-current Drell-Yan processes naturally decompose into QED and weak contributions, i.e. they build gauge invariant subsets and thus can be discussed separately. The observable next-to-leading order (NLO) cross section is obtained by convoluting the parton cross section with the quark distribution functions  $q(x, Q^2)$  ( $\hat{s} = x_1 x_2 S$ ) [10]

$$d\sigma(S) = \int_0^1 dx_1 dx_2 q(x_1, Q^2) \bar{q}(x_2, Q^2) [d\hat{\sigma}^{(0+1)}(\hat{s}, \hat{t}) + d\hat{\sigma}_{\text{QED}}(\mu_{\text{QED}}^2, \hat{s}, \hat{t})], \quad (2)$$

where  $d\hat{\sigma}^{(0+1)}$  comprises the NLO cross section including weak corrections, and  $d\hat{\sigma}_{\text{QED}}$  describes the QED part, i.e. virtual corrections and real photon emission off the quarks and charged leptons. The PDFs depend on the QCD renormalization and factorization scales which we choose to be equal; the common scale is denoted by  $Q^2$ . The radiation of collinear photons off quarks requires the factorization of the arising mass singularities into the PDFs which introduces a dependence on the QED factorization scale,  $\mu_{\text{QED}}$ . The treatment of mass singularities is universal and thus the same as in the  $W$  case. The QED  $\mathcal{O}(\alpha)$  corrections to  $p\bar{p}^{(\pm)} \rightarrow \gamma^*, Z \rightarrow l^+l^-$  ( $l = e, \mu$ ) have been calculated and implemented in the parton level Monte Carlo program ZGRAD [9]<sup>2</sup> and their impact on the di-lepton invariant mass spectrum, the lepton transverse momentum distribution, and on the forward-backward asymmetry,  $A_{\text{FB}}$ , has been studied. In addition, the prospects for a precision measurement of  $\sin^2 \theta_{\text{eff}}^l$  extracted from  $A_{\text{FB}}$  at the Z resonance at the LHC were investigated.

In Fig. 2 we show the effect of the QED corrections on the invariant mass distribution of the final state lepton pair. Similar to the transverse mass distribution in the charged-current Drell-Yan process, final-state photon radiation strongly affects the shape of the  $m(l^+l^-)$  distribution. When lepton identification requirements are taken into account, the large contributions from mass singular logarithms largely cancel in the electron case. As in the charged-current Drell-Yan process, initial-final state interference is negligible, and the impact of initial-state radiation is small after factorizing the collinear singularities into the PDFs. The difference in the extracted Z boson mass when comparing the approximate calculation of Ref. [12] with the full calculation of the  $\mathcal{O}(\alpha)$  QED corrections is of  $\mathcal{O}(10 \text{ MeV})$ . Since the detector response is calibrated using Z boson observables, the shift in the Z boson mass is expected to slightly modify the W mass extracted from experiment.

For precision physics away from the Z resonance, the (non-universal) weak corrections must also be included. These corrections become important at large values of the di-lepton invariant mass due to the presence of large Sudakov-like electroweak logarithms of the form  $\ln(m(l^+l^-)/M_V)$ ,  $V = W, Z$ , which eventually may be resummed [15]. A calculation of the non-universal weak corrections in  $p\bar{p}^{(\pm)} \rightarrow \gamma^*, Z \rightarrow l^+l^-$  is currently in progress [10]. In the implementation of the weak corrections we

---

<sup>2</sup>ZGRAD is available from the authors.

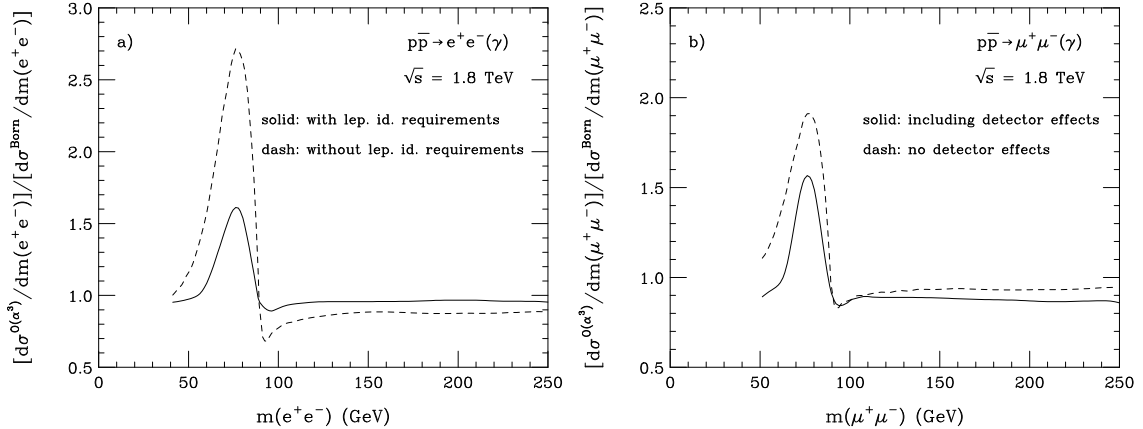


Figure 2: The relative corrections to the  $m(e^+e^-)$  and  $m(\mu^+\mu^-)$  distributions in Drell-Yan production at the Tevatron due to the  $\mathcal{O}(\alpha)$  QED corrections (from Ref. [9]).

closely follow Ref. [18], in particular for the treatment of higher-order corrections, which are important for a precise description of the Z resonance.

The NLO parton differential cross section, including weak  $\mathcal{O}(\alpha)$  and leading  $\mathcal{O}(\alpha^2)$  corrections, which enters eq. (2) is of the form [10]

$$d\hat{\sigma}^{(0+1)} = dP_{2f} \frac{1}{12} \sum |A_\gamma^{(0+1)} + A_Z^{(0+1)}|^2(\hat{s}, \hat{t}) + d\hat{\sigma}_{\text{box}}(\hat{s}, \hat{t}), \quad (3)$$

where the sum is taken over the spin and color degrees of freedom, and  $dP_{2f}$  denotes the two-particle phase space.  $d\hat{\sigma}_{\text{box}}$  describes the contribution of the box diagrams involving two massive gauge bosons. The matrix elements  $A_{\gamma,Z}^{(0+1)}$  comprise the Born matrix elements, the  $\gamma$ ,  $Z$ ,  $\gamma Z$  self energy insertions including a leading-log resummation of the terms involving the light fermions, and the one-loop vertex corrections. While  $A_{\gamma,Z}^{(0+1)}$  can be expressed in terms of effective vector and axial-vector couplings, the box contribution  $d\hat{\sigma}_{\text{box}}$  cannot be absorbed in effective couplings. However, in the Z resonance region the box diagrams can be neglected and the NLO cross section  $d\hat{\sigma}^{(0+1)}$  of eq. (3) has a Born-like structure. The leading universal electroweak corrections, i.e. the running of the electromagnetic charge and corrections connected to  $\Delta\rho$ , can be included in form of an effective Born approximation (EBA). Comparing results of the calculation which includes the full  $\mathcal{O}(\alpha)$  corrections with those obtained using the EBA together with the pure QED corrections reveals the effects of the genuine non-universal electroweak corrections such as box diagrams.

The weak corrections to neutral-current Drell-Yan processes as described above are currently being implemented in the parton level MC program ZGRAD2 [10]. A detailed numerical discussion of the effects of the electroweak  $\mathcal{O}(\alpha)$  corrections on distributions in  $p\bar{p} \rightarrow \gamma^*, Z \rightarrow l^+l^-(\gamma), l = e, \mu$  at the Tevatron and the LHC will be

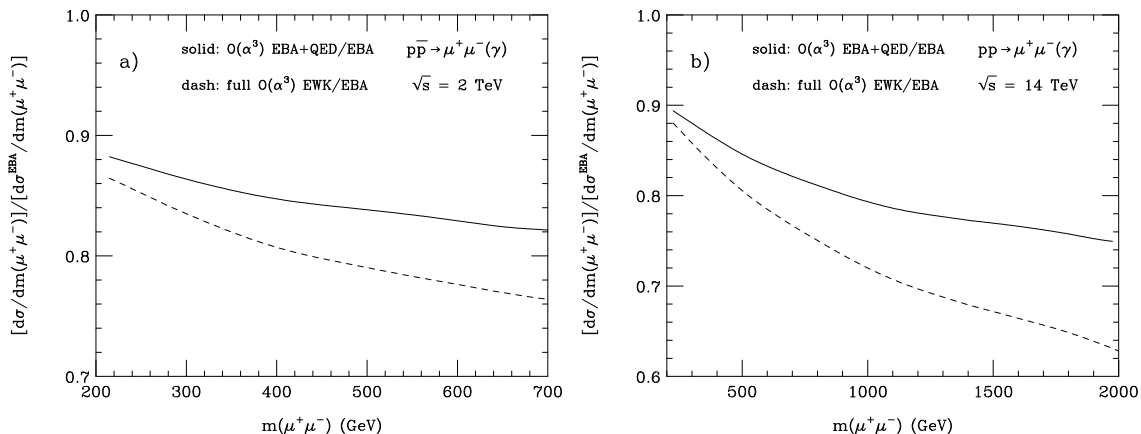


Figure 3: The relative corrections to the  $m(\mu^+\mu^-)$  distribution a) at the Tevatron and b) at the LHC when taking into account the universal corrections entering the EBA and QED corrections only (solid line), and when the full  $\mathcal{O}(\alpha)$  electroweak corrections are included in the calculation (dashed line).

given in Ref. [10]. Here we present some selected preliminary results for the di-lepton invariant mass distribution and the forward-backward asymmetry.

In Fig. 3 we show the  $\mu^+\mu^-$  invariant mass distribution including the full  $\mathcal{O}(\alpha)$  corrections normalized to the differential cross section in the EBA for large di-lepton invariant masses at the Tevatron and the LHC. Separation cuts and lepton identification requirements to simulate the detector acceptance as described in Ref. [9] (Tevatron) and Ref. [4] (LHC) are taken into account in Fig. 3. For comparison the relative corrections including the QED corrections only are also shown. As expected from the presence of large electroweak Sudakov-like logarithms, the weak corrections strongly increase in magnitude with increasing  $m(\mu^+\mu^-)$ , reaching about 10% at  $m(\mu^+\mu^-) = 1$  TeV. Both, the QED and the genuine weak corrections reduce the differential cross section. Qualitatively similar results are obtained in the  $e^+e^-$  case.

In Fig. 4, we show how the purely weak corrections affect the forward backward asymmetry at the LHC<sup>3</sup>. To illustrate the effect of the non-universal weak corrections, we plot the difference of the forward backward asymmetry including the full  $\mathcal{O}(\alpha)$  corrections, and the asymmetry which only takes into account QED corrections and the universal corrections which are included in the EBA. A genuine non-universal electroweak effect can be observed in the vicinity of  $m(l^+l^-) = M_W$  and  $2M_W$ , which is due to threshold effects in the box diagrams involving two W bosons. Results qualitatively similar to those shown in Fig. 4 are also obtained for the Tevatron.

<sup>3</sup>For a definition of  $A_{FB}$  at the LHC, see Ref. [9].

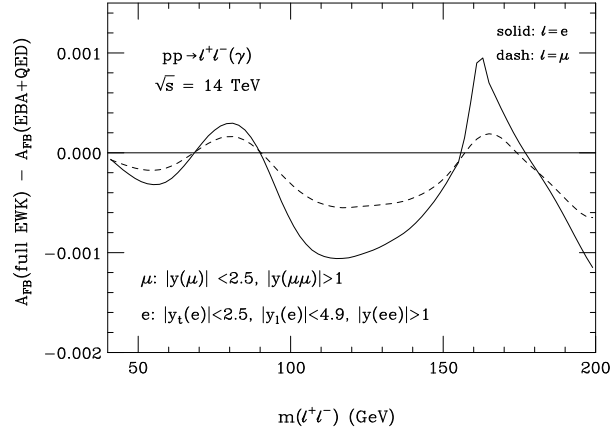


Figure 4: The forward-backward asymmetry including NLO electroweak corrections at the LHC, imposing the cuts and lepton identification requirements of Ref. [16]. The EBA and QED contribution have been subtracted (preliminary results).

The forward backward asymmetry at the LHC is very sensitive to the rapidity coverage of the leptons assumed. In Fig. 4, we have used the lepton rapidity coverages foreseen for the ATLAS detector [4,16]. For muon pairs, both muons are required to have rapidity  $|y(\mu)| < 2.5$ . For  $e^+e^-$  pairs, the leptons are required to have  $|y_l(e)| < 4.9$ , with one of them having to fulfill the more stringent requirement  $|y_t(e)| < 2.5$ . In addition, the lepton pair rapidity has to be  $|y(ll)| > 1$  for both electrons and muons in the final state. This cut substantially increases the magnitude of  $A_{\text{FB}}$  at the LHC [17].

It is interesting to check whether the threshold effect at  $m(l^+l^-) = 2M_W$  will be observable. In the electron case, the expected statistical uncertainty in  $A_{\text{FB}}$  for  $m(e^+e^-) = 2M_W \pm 5 \text{ GeV}$  and  $100 \text{ fb}^{-1}$  at the LHC is about  $(3 - 4) \times 10^{-3}$  per experiment. The size of the non-universal electroweak corrections in the region are of the order of  $10^{-3}$ . In a realistic calculation, contributions from  $W^+W^- \rightarrow l^+\nu_l l^-\bar{\nu}_l$ ,  $ZZ \rightarrow l^+l^-\bar{\nu}\nu$  and  $\bar{t}t$  production to the forward backward asymmetry need to be taken into account, which could well be of the same order as the genuine weak corrections. It will thus be difficult to observe a clear signal of the threshold effects originating from the box diagrams involving two W bosons in  $A_{\text{FB}}$  at the LHC. On the other hand, given the expected statistical precision, the genuine weak corrections cannot be neglected when comparing data with the SM prediction.

## 4 Conclusions

Our results show that, for the precision obtained in previous Tevatron runs, the existing calculations for W and Z boson production are sufficient. However, for future precision measurements the full electroweak  $\mathcal{O}(\alpha)$  corrections and probably also multiple photon radiation effects should be taken into account. The inclusion of the non-resonant contributions to W production in WGRAD is in progress [14] (see also Ref. [19]). As a first step towards a calculation of the  $\mathcal{O}(\alpha^2)$  QED corrections, the effects of two-photon radiation in W and Z boson production at hadron colliders have been computed in Ref. [20].

## Acknowledgments

We would like to thank the organizers of RADCOR-2000, especially H. Haber, for a delightful and inspiring conference experience, and for arranging the spectacular sunsets at Carmel beach. One of us (U.B.) is grateful to the Fermilab Theory Group, where part of this work was carried out, for its generous hospitality.

## References

- [1] D. Abbaneo *et al.*, CERN-EP-2000-016 (January 2000).
- [2] T. Junk, these proceedings and hep-ex/0101015; P. Igo-Kemenes, talk presented at the LEP Seminar at CERN, Nov. 3, 2000.
- [3] R. Brock *et al.*, “Report of the working group on precision measurements”, Proceedings of the Workshop on *QCD and Weak Boson Physics in Run II*, Fermilab-Pub-00/297, Fermilab, Batavia, Illinois, March – November 1999 (eds. U. Baur, R.K. Ellis and D. Zeppenfeld), p. 78, and hep-ex/0011009.
- [4] S. Haywood *et al.*, “Electroweak physics”, report of the Electroweak Physics Working Group of the *1999 CERN Workshop on SM physics (and more) at the LHC*, CERN-TH/2000-102 [hep-ph/0003275].
- [5] S. Catani *et al.*, “QCD”, report of the QCD Working Group of the *1999 CERN Workshop on SM physics (and more) at the LHC*, CERN-TH/2000-102 [hep-ph/0005025].
- [6] U. Baur *et al.*, “Report of the working group on photon and weak boson production”, Proceedings of the Workshop on *QCD and Weak Boson Physics in Run II*, Fermilab-Pub-00/297, Fermilab, Batavia, Illinois, March – November 1999 (eds. U. Baur, R.K. Ellis and D. Zeppenfeld), p. 115, hep-ph/0005226.

- [7] D. Wackeroth and W. Hollik, *Phys. Rev.* **D55**, (1997) 6788 [hep-ph/9606398].
- [8] U. Baur, S. Keller and D. Wackeroth, *Phys. Rev.* **D59**, (1999) 013002 [hep-ph/9807417].
- [9] U. Baur, S. Keller and W. K. Sakumoto, *Phys. Rev.* **D57**, (1998) 199 [hep-ph/9707301].
- [10] U. Baur, O. Brein, W. Hollik, C. Schappacher, and D. Wackeroth, in preparation.
- [11] B. Abbott *et al.* (DO Collaboration), *Phys. Rev.* **D58**, (1998) 012002; T. Affolder *et al.* (CDF Collaboration), hep-ex/0007044.
- [12] F. A. Berends and R. Kleiss, *Z. Phys.* **C27**, (1985) 365.
- [13] W. T. Giele and S. Keller, *Phys. Rev.* **D57**, (1998) 4433.
- [14] U. Baur and D. Wackeroth, in preparation.
- [15] A. Denner, these proceedings (hep-ph/0101213), and references therein.
- [16] A. Airapetian *et al.* (ATLAS Collaboration), CERN/LHCC/99-14 and CERN/LHCC/99-15 (1999).
- [17] M. Dittmar, *Phys. Rev.* **D55**, (1997) 161.
- [18] D. Bardin, W. Hollik and G. Passarino (eds), “Reports of the Working Group on Precision Calculations at the  $Z$  Resonance”, CERN 95-03 (1995).
- [19] S. Dittmaier and M. Krämer, in preparation.
- [20] U. Baur and T. Stelzer, *Phys. Rev.* **D61**, (2000) 073007 [hep-ph/9910206].

# WW Physics at Future $e^+e^-$ Linear Colliders

TIMOTHY L. BARKLOW\*

*Stanford Linear Accelerator Center  
Stanford, California 94309, USA*

Measurements of triple gauge boson couplings and strong electroweak symmetry breaking effects at future  $e^+e^-$  linear colliders are reviewed. The results expected from a future  $e^+e^-$  linear collider are compared with LHC expectations.

Presented at the

5th International Symposium on Radiative Corrections  
(RADCOR-2000)  
Carmel CA, USA, 11–15 September, 2000

---

\*Work supported by Department of Energy contract DE-AC03-76SF00515.

# 1 Introduction

The measurement of gauge boson self-couplings at a future  $e^+e^-$  collider will provide insight into new physics processes in the presence or absence of new particle production. In the absence of particle resonances, and in particular in the absence of a Higgs boson resonance, the measurement of gauge boson couplings will provide a window to the new physics responsible for electroweak symmetry breaking. If there are many new particles being produced – if, for example, supersymmetric particles abound – then the measurement of gauge boson couplings will prove valuable since the gauge boson couplings will reflect the properties of the new particles through radiative corrections.

Experiments at LEP2 have demonstrated the viability of measuring gauge boson self-couplings at an  $e^+e^-$  collider. Complex effects such as initial and final state radiation,  $\mathcal{O}(\alpha)$  electroweak radiative corrections, fragmentation, and detector bias are incorporated into analyses which utilize all decay modes of the  $W$  boson. The present LEP2 triple gauge boson precision of a few percent [1] exceeds the predictions for LEP2 sensitivity made a decade ago.

In this paper we review the prospect for studying triple gauge boson couplings and strong electroweak symmetry breaking effects at future  $e^+e^-$  linear colliders. We will deal primarily with the reaction  $e^+e^- \rightarrow W^+W^-$ . However, when discussing strong electroweak symmetry breaking we will also consider the processes  $e^+e^- \rightarrow \nu\bar{\nu}W^+W^-$ ,  $\nu\bar{\nu}ZZ$ , and  $\nu\bar{\nu}t\bar{t}$ . Triple gauge boson production is important for the study of quartic gauge boson couplings, but is beyond the scope of this paper.

## 2 Triple gauge boson couplings

Gauge boson self-couplings include the triple gauge couplings (TGCs) and quartic gauge couplings (QGCs) of the photon,  $W$  and  $Z$ . Of special importance at a linear collider are the  $WW\gamma$  and  $WWZ$  TGCs since a large sample of fully reconstructed  $e^+e^- \rightarrow W^+W^-$  events will be available to measure these couplings.

The effective Lagrangian for the general  $W^+W^-V$  vertex ( $V = \gamma, Z$ ) contains 7 complex TGCs, denoted by  $g_1^V$ ,  $\kappa_V$ ,  $\lambda_V$ ,  $g_4^V$ ,  $g_5^V$ ,  $\tilde{\kappa}_V$ , and  $\tilde{\lambda}_V$  [2]. The magnetic dipole and electric quadrupole moments of the  $W$  are linear combinations of  $\kappa_\gamma$  and  $\lambda_\gamma$  while the magnetic quadrupole and electric dipole moments are linear combinations of  $\tilde{\kappa}_\gamma$  and  $\tilde{\lambda}_\gamma$ . The TGCs  $g_1^V$ ,  $\kappa_V$ , and  $\lambda_V$  are C- and P-conserving,  $g_5^V$  is C- and P-violating but conserves CP, and  $g_4^V$ ,  $\tilde{\kappa}_V$ , and  $\tilde{\lambda}_V$  are CP-violating. In the SM at tree-level all the TGCs are zero except  $g_1^V = \kappa_V = 1$ .

If there is no Higgs boson resonance below about 800 GeV, the interactions of the  $W$  and  $Z$  gauge bosons become strong above 1 TeV in the  $WW$ ,  $WZ$  or  $ZZ$  center-of-mass system. In analogy with  $\pi\pi$  scattering below the  $\rho$  resonance, the

interactions of the  $W$  and  $Z$  bosons below the strong symmetry breaking resonances can be described by an effective chiral Lagrangian [3]. These interactions induce anomalous TGC's at tree-level:

$$\begin{aligned}\kappa_\gamma &= 1 + \frac{e^2}{32\pi^2 s_w^2} (L_{9L} + L_{9R}) \\ \kappa_Z &= 1 + \frac{e^2}{32\pi^2 s_w^2} \left( L_{9L} - \frac{s_w^2}{c_w^2} L_{9R} \right) \\ g_1^Z &= 1 + \frac{e^2}{32\pi^2 s_w^2} \frac{L_{9L}}{c_w^2},\end{aligned}$$

where  $s_w^2 = \sin^2 \theta_w$ ,  $c_w^2 = \cos^2 \theta_w$ , and  $L_{9L}$  and  $L_{9R}$  are chiral Lagrangian parameters. If we replace  $L_{9L}$  and  $L_{9R}$  by the values of these parameters in QCD,  $\kappa_\gamma$  is shifted by  $\Delta\kappa_\gamma \sim -3 \times 10^{-3}$ .

Standard Model radiative corrections [4] cause shifts in the TGCs of  $\mathcal{O}(10^{-4} - 10^{-3})$  for CP-conserving couplings and of  $\mathcal{O}(10^{-10} - 10^{-8})$  for CP-violating TGC's. Radiative corrections in the MSSM can cause shifts of  $\mathcal{O}(10^{-4} - 10^{-2})$  in both the CP-conserving [5] and CP-violating TGC's [6].

The methods used at LEP2 to measure TGCs provide a useful guide to the measurement of TGCs at a linear collider. When measuring TGCs the kinematics of an  $e^+e^- \rightarrow W^+W^-$  event can be conveniently expressed in terms of the  $W^+W^-$  center-of-mass energy following initial state radiation (ISR), the masses of the  $W^+$  and  $W^-$ , and five angles: the angle between the  $W^-$  and initial  $e^-$  in the  $W^+W^-$  rest frame, the polar and azimuthal angles of the fermion in the rest frame of its parent  $W^-$ , and the polar and azimuthal angles of the anti-fermion in the rest frame of its parent  $W^+$ .

In practice not all of these variables can be reconstructed unambiguously. For example, in events with hadronic decays it is often difficult to measure the flavor of the quark jet, and so there is usually a two-fold ambiguity for quark jet directions. Also, it can be difficult to measure ISR and consequently the measured  $W^+W^-$  center-of-mass energy is often just the nominal  $\sqrt{s}$ . Monte Carlo simulation is used to account for detector resolution, quark hadronization, initial- and final-state radiation, and other effects.

The TGC measurement error at a linear collider can be estimated to a good approximation by considering  $e\nu q\bar{q}$  and  $\mu\nu q\bar{q}$  channels only, and by ignoring all detector and radiation effects except for the requirement that the  $W^+W^-$  fiducial volume be restricted to  $|\cos\theta_W| < 0.9$ . Such an approach correctly predicts the TGC sensitivity of LEP2 experiments and of detailed linear collider simulations [7]. This rule-of-thumb approximation works because LEP2 experiments and detailed linear collider simulations also use the  $\tau\nu q\bar{q}$ ,  $\ell\nu\ell\nu$  and  $q\bar{q}q\bar{q}$  channels, and the increased sensitivity from these extra channels makes up for the lost sensitivity due to detector resolution, initial- and final-state radiation, and systematic errors.

TGC	error $\times 10^{-4}$			
	$\sqrt{s} = 500$ GeV		$\sqrt{s} = 1000$ GeV	
	Re	Im	Re	Im
$g_1^\gamma$	15.5	18.9	12.8	12.5
$\kappa_\gamma$	3.5	9.8	1.2	4.9
$\lambda_\gamma$	5.4	4.1	2.0	1.4
$g_1^Z$	14.1	15.6	11.0	10.7
$\kappa_Z$	3.8	8.1	1.4	4.2
$\lambda_Z$	4.5	3.5	1.7	1.2

Table 1: Expected errors for the real and imaginary parts of CP-conserving TGCs assuming  $\sqrt{s} = 500$  GeV,  $\mathcal{L} = 500$  fb $^{-1}$  and  $\sqrt{s} = 1000$  GeV,  $\mathcal{L} = 1000$  fb $^{-1}$ . The results are for one-parameter fits in which all other TGCs are kept fixed at their SM values.

TGC	error $\times 10^{-4}$			
	$\sqrt{s} = 500$ GeV		$\sqrt{s} = 1000$ GeV	
	Re	Im	Re	Im
$\tilde{\kappa}_\gamma$	22.5	16.4	14.9	12.0
$\tilde{\lambda}_\gamma$	5.8	4.0	2.0	1.4
$\tilde{\kappa}_Z$	17.3	13.8	11.8	10.3
$\tilde{\lambda}_Z$	4.6	3.4	1.7	1.2
$g_4^\gamma$	21.3	18.8	13.9	12.8
$g_5^\gamma$	19.3	21.6	13.3	13.4
$g_4^Z$	17.9	15.2	12.0	10.4
$g_5^Z$	16.0	16.7	11.4	10.7

Table 2: Expected errors for the real and imaginary parts of C- and P-violating TGCs assuming  $\sqrt{s} = 500$  GeV,  $\mathcal{L} = 500$  fb $^{-1}$  and  $\sqrt{s} = 1000$  GeV,  $\mathcal{L} = 1000$  fb $^{-1}$ . The results are for one-parameter fits in which all other TGCs are kept fixed at their SM values.

Table 1 contains the estimates of the TGC precision that can be obtained at  $\sqrt{s} = 500$  and 1000 GeV for the CP-conserving couplings  $g_1^V$ ,  $\kappa_V$ , and  $\lambda_V$ . These estimates are derived from one-parameter fits in which all other TGC parameters are kept fixed at their tree-level SM values. Table 2 contains the corresponding estimates for the C- and P-violating couplings  $\tilde{\kappa}_V$ ,  $\tilde{\lambda}_V$ ,  $g_4^V$ , and  $g_5^V$ . An alternative method of measuring the  $WW\gamma$  couplings is provided by the channel  $e^+e^- \rightarrow \nu\bar{\nu}\gamma$  [8].

The difference in TGC precision between the LHC and a linear collider depends on

the TGC, but typically the TGC precision at the linear collider will be substantially better, even at  $\sqrt{s} = 500$  GeV. Figure 1 shows the measurement precision expected for the LHC [9] and for linear colliders of three different energies for four different TGCs.

If the goal of a TGC measurement program is to search for the first sign of deviation from the SM, then one-parameter fits in which all other TGCs are kept fixed at their tree-level SM values are certainly appropriate. But what if the goal is to survey a large number TGCs, all of which seem to deviate from their SM value? Is a 28-parameter fit required? The answer is probably no, as illustrated in Fig. 2.

Figure 2 shows the histogram of the correlation coefficients for all 171 pairs of TGCs when 19 different TGCs are measured at LEP2 using one-parameter fits. The entries in Fig. 2 with large positive correlations are pairs of TGCs that are related to each other by the interchange of  $\gamma$  and  $Z$ . The correlation between the two TGCs of each pair can be removed using the dependence on electron beam polarization. The entries in Fig. 2 with large negative correlations are TGC pairs of the type  $Re(\tilde{\kappa}_\gamma)/Re(\tilde{\lambda}_\gamma)$ ,  $Re(\tilde{\kappa}_Z)/Re(\tilde{\lambda}_Z)$ , etc. Half of the TGC pairs with large negative correlations will become uncorrelated once polarized electron beams are used, leaving only a small number of TGC pairs with large negative or positive correlation coefficients.

### 3 Strong WW scattering

Strong  $W^+W^-$  scattering can be studied at a linear collider with the reactions  $e^+e^- \rightarrow \nu\bar{\nu}W^+W^-$ ,  $\nu\bar{\nu}ZZ$ ,  $\nu\bar{\nu}t\bar{t}$ , and  $W^+W^-$  [10]. The final states  $\nu\bar{\nu}W^+W^-$ ,  $\nu\bar{\nu}ZZ$  are used to study the I=J=0 channel in  $W^+W^-$  scattering, while the final state  $W^+W^-$  is best-suited for studying the I=J=1 channel. The  $\nu\bar{\nu}t\bar{t}$  final state can be used to investigate strong electroweak symmetry breaking in the fermion sector through the process  $W^+W^- \rightarrow t\bar{t}$ .

The first step in studying strong  $W^+W^-$  scattering is to separate the scattering of a pair of longitudinally polarized  $W$ 's, denoted by  $W_LW_L$ , from transversely polarized  $W$ 's, and from background such as  $e^+e^- \rightarrow e^+e^-W^+W^-$  and  $e^-\bar{\nu}W^+Z$ . Studies have shown that simple cuts can be used to achieve this separation in  $e^+e^- \rightarrow \nu\bar{\nu}W^+W^-$ ,  $\nu\bar{\nu}ZZ$  at  $\sqrt{s} = 1000$  GeV, and that the signals are comparable to those obtained at the LHC [11]. Furthermore, by analyzing the gauge boson production and decay angles it is possible to use these reactions to measure chiral Lagrangian parameters with an accuracy greater than that which can be achieved at the LHC [12].

The reaction  $e^+e^- \rightarrow \nu\bar{\nu}t\bar{t}$  provides unique access to  $W^+W^- \rightarrow t\bar{t}$  since this process is overwhelmed by the background  $gg \rightarrow t\bar{t}$  at the LHC. Techniques similar to those employed to isolate  $W_LW_L \rightarrow W^+W^-, ZZ$  can be used to measure the enhancement in  $W_LW_L \rightarrow t\bar{t}$  production [13]. Even in the absence of a resonance it

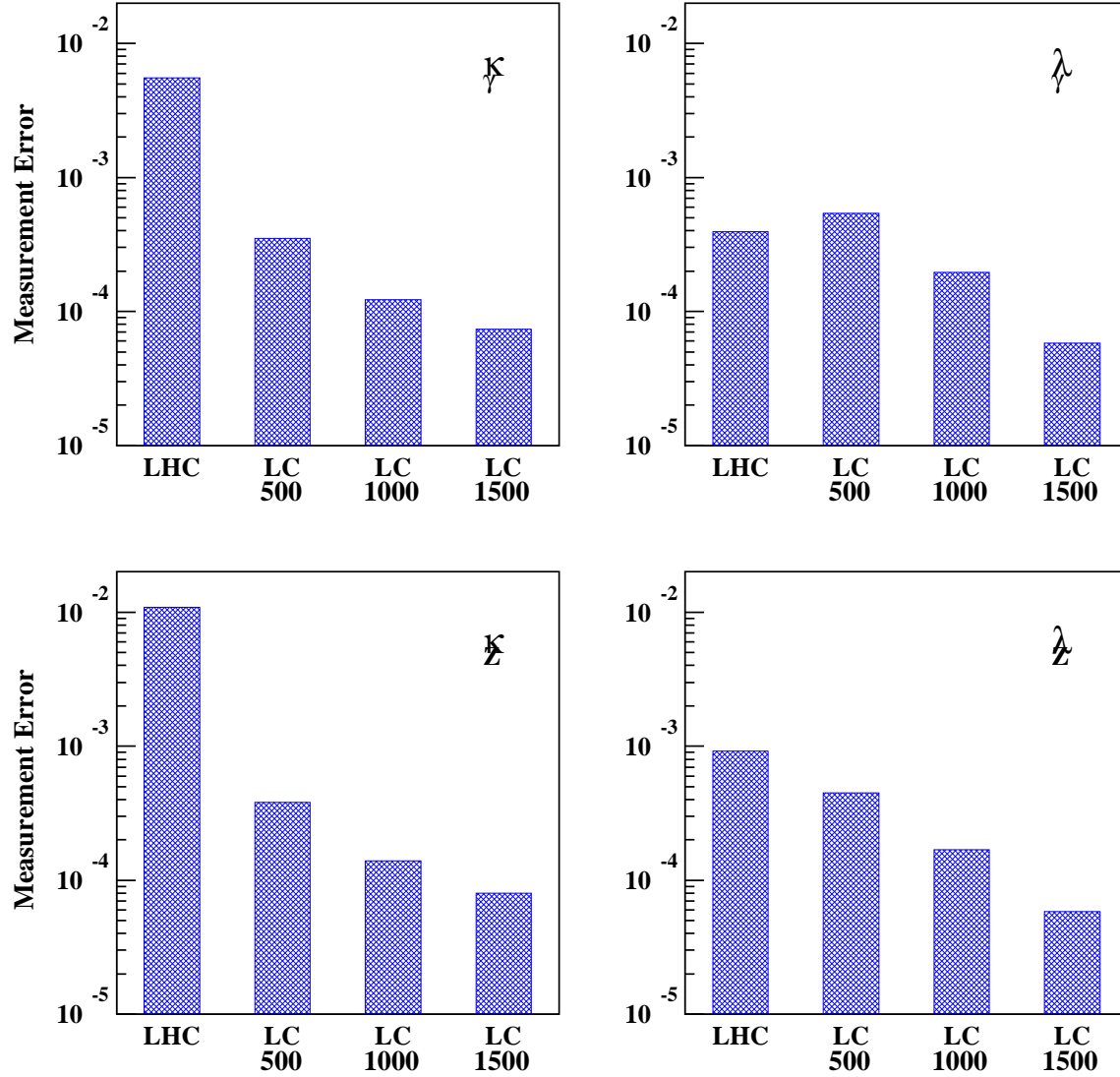


Figure 1: Expected measurement error for the real part of four different TGCs. The numbers below the “LC” labels refer to the center-of-mass energy of the linear collider in GeV. The luminosity of the LHC is assumed to be  $300 \text{ fb}^{-1}$ , while the luminosities of the linear colliders are assumed to be 500, 1000, and 1000  $\text{fb}^{-1}$  for  $\sqrt{s}=500, 1000,$  and  $1500 \text{ GeV}$  respectively.

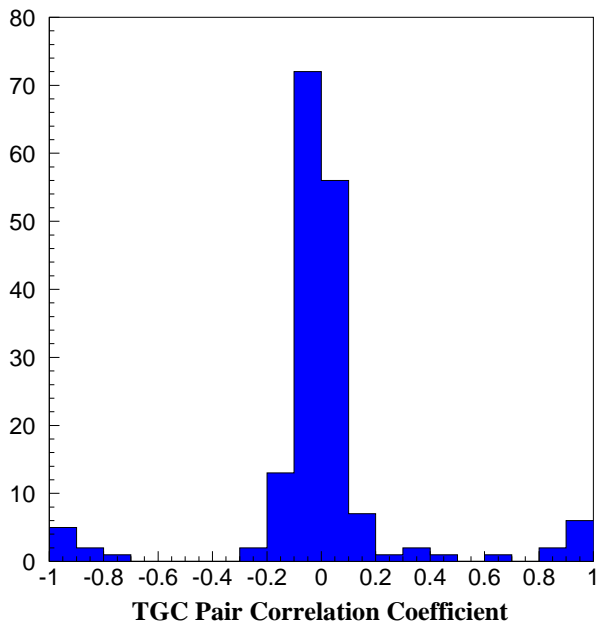


Figure 2: Histogram of correlation coefficients for all 171 pairs of TGCs when 19 different TGCs are measured using one-parameter fits at LEP2 (unpolarized beams). The 19 TGCs are made up of the real and imaginary parts of the 8 C- and P-violating couplings along with the real parts of the three CP-conserving couplings  $g_1^Z$ ,  $\kappa_\gamma$ ,  $\lambda_\gamma$ .

will be possible to clearly establish a signal. The ratio  $S/\sqrt{B}$  is expected to be 12 for a linear collider with  $\sqrt{s} = 1$  TeV and  $1000 \text{ fb}^{-1}$  and 80%/0% electron/positron beam polarization, increasing to 28 for the same data sample at  $\sqrt{s} = 1.5$  TeV.

There are two approaches to studying strong  $W^+W^-$  scattering with the process  $e^+e^- \rightarrow W^+W^-$ . The first approach was discussed in Section 2: a strongly coupled gauge boson sector induces anomalous TGCs which could be measured in  $e^+e^- \rightarrow W^+W^-$ . The precision of  $4 \times 10^{-4}$  for the TGCs  $\kappa_\gamma$  and  $\kappa_Z$  at  $\sqrt{s} = 500$  GeV can be interpreted as a precision of 0.26 for the chiral lagrangian parameters  $L_{9L}$  and  $L_{9R}$ . Assuming naive dimensional analysis [14], such a measurement would provide a  $8\sigma$  ( $5\sigma$ ) signal for  $L_{9L}$  and  $L_{9R}$  if the strong symmetry breaking energy scale were 3 TeV (4 TeV). The only drawback to this approach is that the detection of anomalous TGCs does not by itself provide unambiguous proof of strong electroweak symmetry breaking.

The second approach involves an effect unique to strong  $W^+W^-$  scattering. When  $W^+W^-$  scattering becomes strong the amplitude for  $e^+e^- \rightarrow W_L W_L$  develops a complex form factor  $F_T$  in analogy with the pion form factor in  $e^+e^- \rightarrow \pi^+\pi^-$  [15]. To

evaluate the size of this effect the following expression for  $F_T$  has been suggested:

$$F_T = \exp \left[ \frac{1}{\pi} \int_0^\infty ds' \delta(s', M_\rho, \Gamma_\rho) \left\{ \frac{1}{s' - s - i\epsilon} - \frac{1}{s'} \right\} \right]$$

where

$$\delta(s, M_\rho, \Gamma_\rho) = \frac{1}{96\pi} \frac{s}{v^2} + \frac{3\pi}{8} \left[ \tanh\left(\frac{s - M_\rho^2}{M_\rho \Gamma_\rho}\right) + 1 \right].$$

Here  $M_\rho, \Gamma_\rho$  are the mass and width respectively of a vector resonance in  $W_L W_L$  scattering. The term

$$\delta(s) = \frac{1}{96\pi} \frac{s}{v^2}$$

is the Low Energy Theorem (LET) amplitude for  $W_L W_L$  scattering at energies below a resonance. Below the resonance the real part of  $F_T$  is proportional to  $L_{9L} + L_{9R}$ , and can therefore be interpreted as a TGC. The imaginary part, however, is a distinctive new effect.

The real and imaginary parts of  $F_T$  are measured [16] in the same manner as the TGCs. The  $W^+ W^-$  production and decay angles are analyzed and an electron beam polarization of 80% is assumed. In contrast to TGCs, the analysis of  $F_T$  seems to benefit from even small amounts of jet flavor tagging. We therefore assume that charm jets can be tagged with a purity/efficiency of 100/33%. These purity/efficiency numbers are based on research [17] which indicates that it may be possible to tag charm jets with a purity/efficiency as high as 100/65% given that  $b$  jet contamination is not a significant factor in  $W^+ W^-$  pair-production and decay.

The expected 95% confidence level limits for  $F_T$  for  $\sqrt{s} = 500$  GeV and a luminosity of  $500 \text{ fb}^{-1}$  are shown in Fig. 3, along with the predicted values of  $F_T$  for various masses  $M_\rho$  of a vector resonance in  $W_L W_L$  scattering. The masses and widths of the vector resonances are chosen to coincide with those used in the ATLAS TDR [9]. The technipion form factor  $F_T$  affects only the amplitude for  $e^+ e^- \rightarrow W_L W_L$ , whereas TGCs affect all amplitudes. Through the use of electron beam polarization and the rich angular information in  $W^+ W^-$  production and decay, it will be possible to disentangle anomalous values of  $F_T$  from other anomalous TGC values and deduce the mass of a strong vector resonance well below threshold, as suggested by Fig. 3.

The signal significances obtained by combining the results for  $e^+ e^- \rightarrow \nu \bar{\nu} W^+ W^-$ ,  $\nu \bar{\nu} Z Z$  [11] with the  $F_T$  analysis of  $W^+ W^-$  [16] are displayed in Fig. 4 along with the results expected from the LHC [9]. The LHC signal is a mass bump in  $W^+ W^-$ ; the LC signal is less direct. Nevertheless, the signals at the LC are strong, particularly in  $e^+ e^- \rightarrow W^+ W^-$ , where the technirho effect gives a large enhancement of a very well-understood Standard Model process. Since the technipion form factor includes an integral over the technirho resonance region, the linear collider signal significance is relatively insensitive to the technirho width. (The real part of  $F_T$  remains fixed as the width is varied, while the imaginary part grows as the width grows.) The

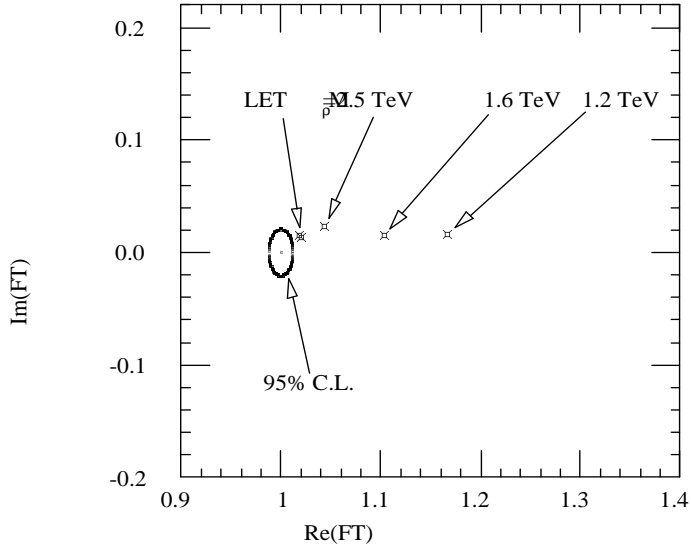


Figure 3: 95% C.L. contour for  $F_T$  for  $\sqrt{s} = 500$  GeV and  $500 \text{ fb}^{-1}$ . Values of  $F_T$  for various masses  $M_\rho$  of a vector resonance in  $W_L W_L$  scattering are also shown. The  $F_T$  point “LET” refers to the case where no vector resonance exists at any mass in strong  $W_L W_L$  scattering.

LHC signal significance will drop as the technirho width increases. The large linear collider signals can be utilized to study a vector resonance in detail; for example, the evolution of  $F_T$  with  $\hat{s}$  can be determined by measuring the initial state radiation in  $e^+e^- \rightarrow W^+W^-$ .

Only when the vector resonance disappears altogether (the LET case in the lower right-hand panel in Fig. 4) does the direct strong symmetry breaking signal from the  $\sqrt{s} = 500$  GeV linear collider drop below the LHC signal. At higher  $e^+e^-$  center-of-mass energies the linear collider signal exceeds the LHC signal.

## 4 Conclusion

A future  $e^+e^-$  linear collider operating in the center-of-mass energy range of 0.5 – 1.0 TeV will measure TGCs with an accuracy of order  $10^{-4}$ , which corresponds to an improvement of two orders of magnitude over present LEP2 measurements and one order of magnitude over what is expected from the LHC. Such a precision is sufficient to test electroweak radiative corrections to the TGCs.

Studies of strong electroweak symmetry breaking are enhanced by a future  $e^+e^-$  linear collider. Signal and background in  $WW$  scattering are limited to electroweak processes, so that a measurement of a structureless enhancement in the total  $WW$

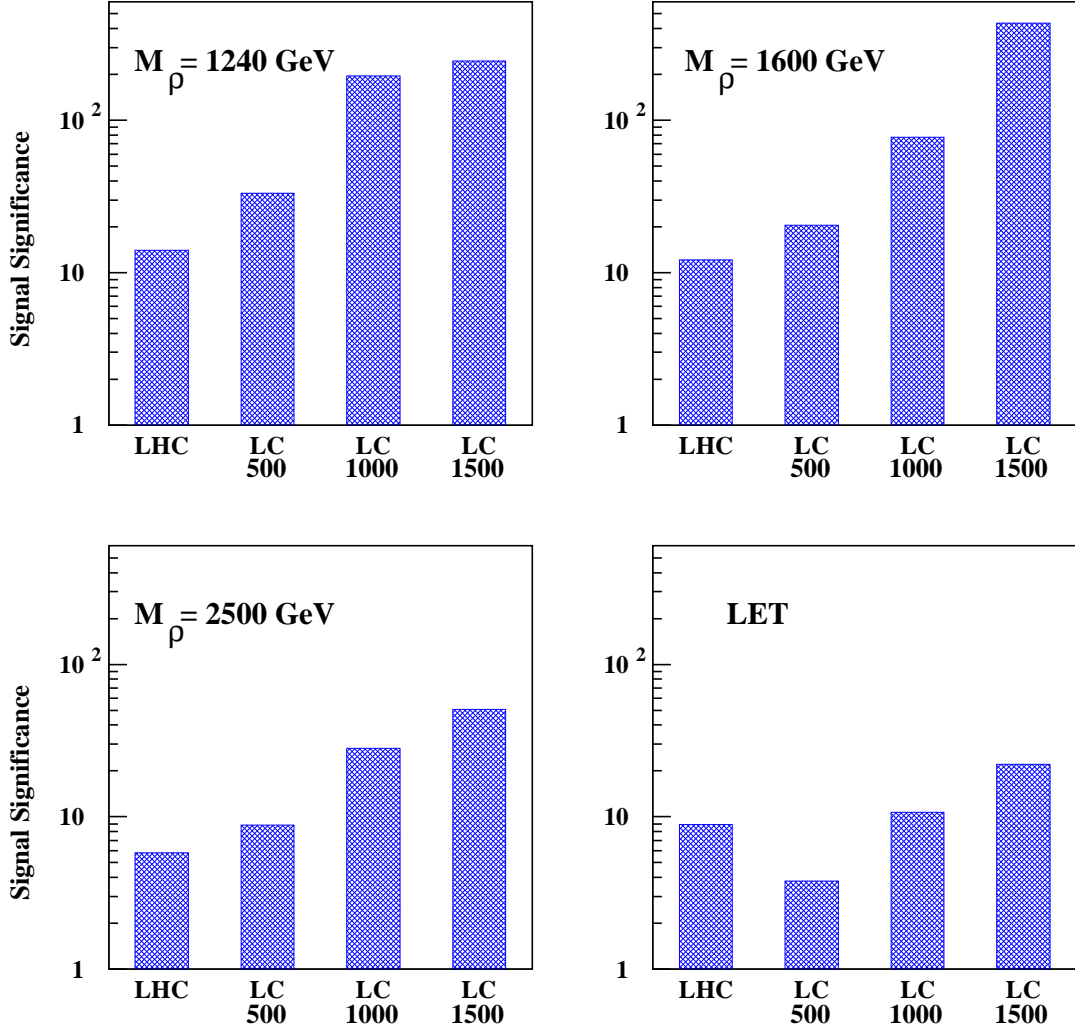


Figure 4: Direct strong symmetry breaking signal significance in  $\sigma$ 's for various masses  $M_\rho$  of a vector resonance in  $W_L W_L$  scattering. In the first three plots the signal at the LHC is a bump in the  $WW$  cross section; in the LET plot, the LHC signal is an enhancement over the SM cross section. The various LC signals are for enhancements of the amplitude for pair-production of longitudinally polarized  $W$  bosons. The numbers below the "LC" labels refer to the center-of-mass energy of the linear collider in GeV. The luminosity of the LHC is assumed to be  $300 \text{ fb}^{-1}$ , while the luminosities of the linear colliders are assumed to be 500, 1000, and 1000  $\text{fb}^{-1}$  for  $\sqrt{s}=500, 1000,$  and  $1500$  GeV respectively. The lower right hand plot "LET" refers to the case where no vector resonance exists at any mass in strong  $W_L W_L$  scattering.

scattering cross-section will have a smaller systematic error at an  $e^+e^-$  collider than at the LHC. In addition, an  $e^+e^-$  collider does an excellent job measuring the lowest order parameters of the chiral lagrangian for a strongly interacting gauge boson sector, as well as the technipion form factor for the pair-production of longitudinally polarized  $W$  bosons. Finally, an  $e^+e^-$  collider can provide unique access to the process  $W^+W^- \rightarrow t\bar{t}$ .

## Acknowledgments

I am grateful to Michael Peskin for many helpful discussions.

## References

- [1] S. Jezequel, “Charged boson triple gauge couplings at LEP:  $W W \gamma$ ,  $W W Z$  and  $W$  polarisation,” LAPP-EXP-2000-10.
- [2] K. Hagiwara, R. D. Peccei, D. Zeppenfeld and K. Hikasa, Nucl. Phys. **B282**, 253 (1987).
- [3] J. Bagger, S. Dawson, and G. Valencia, Nucl. Phys. **B399**, 264 (1993).
- [4] C. Ahn, M. E. Peskin, B. W. Lynn and S. B. Selipsky, Nucl. Phys. **B309**, 221 (1988); J. Fleischer, J. L. Kneur, K. Kolodziej, M. Kuroda and D. Schildknecht, Nucl. Phys. **B378**, 443 (1992) [Erratum-ibid. **B426**, 443 (1992)].
- [5] A. Arhrib, J. L. Kneur and G. Moultaka, Phys. Lett. **B376**, 127 (1996); E. N. Argyres, A. B. Lahanas, C. G. Papadopoulos and V. C. Spanos, Phys. Lett. **B383**, 63 (1996). G. Couture, J.N. Ng, J.L. Hewett, and T.G. Rizzo, Phys. Rev. **D38**, 860 (1988).
- [6] M. Kitahara, M. Marui, N. Oshimo, T. Saito and A. Sugamoto, Eur. Phys. J. **C4**, 661 (1998),
- [7] C. Burgard, in *Physics and Experiments with Future  $e^+e^-$  Linear Colliders*, E. Fernández and A. Pacheco, eds. (UAB Publications, Barcelona, 2000). W. Menges, “A Study of Charge Current Triple Gauge Couplings at TESLA.” LC-PHSM-2001-022. <http://www.desy.de/~lcnotes>.
- [8] D. Choudhury, J. Kalinowski, Nucl. Phys. **B491**, 129 (1997). D. Choudhury, J. Kalinowski, A. Kulesza, Phys. Lett. **B457**, 193 (1999).

- [9] ATLAS Detector and Physics Performance Technical Design Report, LHCC 99-14/15 (1999).
- [10] T. L. Barklow *et al.*, in *Proceedings of the 1996 DPF/DPB Summer Study On New Directions For High-Energy Physics* (Snowmass 96), D. G. Cassel, L. T. Gennari, and R. H. Siemann, eds. (SLAC,1997). [hep-ph/9704217].
- [11] V. Barger, K. Cheung, T. Han and R. J. Phillips, Phys. Rev. **D52**, 3815 (1995); E. Boos, H. J. He, W. Kilian, A. Pukhov, C. P. Yuan and P. M. Zerwas, Phys. Rev. **D57**, 1553 (1998); Phys. Rev. **D61**, 077901 (2000).
- [12] R. Chierici, S. Rosati, M. Kobel, “Strong electroweak symmetry breaking signals in WW scattering at TESLA.” LC-PHSM-2001-038 <http://www.desy.de/~lcnotes>.
- [13] T. L. Barklow, in *Proceedings of the 1996 DPF/DPB Summer Study On New Directions For High-Energy Physics* (Snowmass 96), D. G. Cassel, L. T. Gennari, and R. H. Siemann, eds. (SLAC,1997). E. Ruiz Morales and M. E. Peskin, hep-ph/9909383. T. Han, Y. J. Kim, A. Likhoded and G. Valencia, Nucl. Phys. **B593**, 415 (2001); F. Larios, T. M. Tait and C. P. Yuan, hep-ph/0101253.
- [14] A. Manohar and H. Georgi, Nucl. Phys. B **234**, 189 (1984).
- [15] M. Peskin, in *Physics in Collisions IV*, A. Seiden, ed. (Éditions Frontières, Gif-Sur-Yvette, France, 1984). F. Iddir, A. Le Yaouanc, L. Oliver, O. Pene and J. C. Raynal, Phys. Rev. **D41**, 22 (1990).
- [16] T. L. Barklow, “LET Signals in  $e^+e^- \rightarrow W^+W^-$  at  $\sqrt{s} = 800$  GeV” in Proceedings of 5th International Linear Collider Workshop (LCWS2000).
- [17] C. J. S. Damerell and D. J. Jackson, in *Proceedings of the 1996 DPF/DPB Summer Study On New Directions For High-Energy Physics* (Snowmass 96), D. G. Cassel, L. T. Gennari, and R. H. Siemann, eds. (SLAC,1997).

October 22, 2001  
hep-ph/0101135

# Precision Higgs Physics at a Future Linear Collider

DAVE RAINWATER

*Theoretical Physics Dept.*

*Fermi National Accelerator Laboratory, Batavia, IL 60510 USA*

Assuming that a Higgs sector is responsible for electroweak symmetry breaking, we attempt to address two important questions: How much better precision are various measurements of Higgs boson properties at a future linear collider than at the LHC? What can a future linear collider do for Higgs physics that the LHC cannot?

Presented at the

5th International Symposium on Radiative Corrections  
(RADCOR-2000)

Carmel CA, USA, 11-15 September, 2000

# 1 Introduction

The origin of electroweak symmetry breaking (EWSB) and fermion mass generation remains one of the most pertinent in the field of high energy physics today. Although there exist several explanations for EWSB, some dynamical and others spontaneous, preeminent among those is the existence of a Higgs sector, either one or two complex scalar doublets which acquire a vacuum expectation value (vev), or vevs, providing longitudinal degrees of freedom for the weak gauge bosons and additional physical observable Higgs boson states. For a single Higgs doublet, as in the Standard Model (SM), one neutral CP even Higgs ( $H$ ) would be observed. In a two-Higgs doublet model (2HDM), such as the MSSM, five physical Higgses would exist: light and heavy CP even neutral scalars ( $h, H$ ), a CP odd scalar ( $A$ ), and a charged Higgs and its conjugate  $H^\pm$ . Additionally, a set of Yukawa couplings of the Higgs to SM fermions ( $Y_f$ ), of unknown origin, generates the fermion masses.

No physical Higgs boson has yet been observed, although electroweak precision data has long suggested that the Higgs is light, of order 100 GeV. As such, it can possibly be accessed by present experiments, i.e. CERN's LEP II or the Fermilab Tevatron II. If neither of those experiments turns up evidence for a Higgs, the community will turn to the LHC, which will have the capability to detect a SM or at least one MSSM Higgs of any mass up to the unitarity limit.

Let us suppose that the LHC finds a Higgs candidate resonance, which could be either the solitary physical Higgs of a single Higgs doublet model, or a 2HDM neutral state. This could be confirmation of previous observation at LEP or Tevatron, or an LHC discovery. Either way, a narrow resonance  $\phi$  is found in one or more anticipated channels with rate commensurate with expectations. The task is then to determine the quantum numbers of  $\phi$ , first to confirm that it is a Higgs of some flavor, second to determine what model the Higgs belongs to. These quantum numbers are, with the expected value for a Higgs in brackets:

- charge [neutral]
- color [none]
- mass [ $\mathcal{O}(100)$  GeV]
- spin [0]
- couplings (gauge, Yukawa) [model dependent]
- total width
- self-coupling ( $\lambda$ ) [model dependent]
- CP [even, odd, mixture?]

The nature of the final state of the observed channel(s) gives us at least the first two quantum numbers, charge and color, immediately. For example, detecting a Jacobian peak in the dilepton-missing transverse momentum spectrum in  $\ell^+\ell^-jj\cancel{p}_T$  events, as expected in weak boson fusion and decay to a pair of  $W$  bosons, would indicate that the state is neutral and colorless. Likewise for finding a resonance in the two photon invariant mass spectrum, i.e. due to Higgs production,  $gg \rightarrow \phi \rightarrow \gamma\gamma$ . The latter process would further imply by Yang's Theorem that the state cannot be spin 1, also consistent with a Higgs boson. A fairly precise measurement of the state's mass would also be obtained.

These determinations are necessary, but not sufficient conditions for confirming the Higgs nature of an observed resonance. To go further we must measure the state's coupling to weak bosons, which must be a gauge coupling, perhaps modified by a mass mixing parameter  $\alpha$  and ratio of vevs in a 2HDM  $\tan\beta$ ; and its couplings to fermions, which must be Yukawa, i.e. proportional to the fermion mass. Were these couplings found to meet the requirements of a Higgs sector, it is likely that most members of the community would agree that a Higgs had been discovered. However, the issue of measuring a self-coupling clouds this. One could argue that this is merely an aspect of determining the exact model that is realized in nature. To this end we would also want to know the CP state of the resonance.

For a SM or MSSM Higgs, the LHC can, in fact, make quite good determinations of the mass and gauge coupling, a very good measurement of the total width (even for a Higgs width smaller than the width resolution of the detectors), and a good measurement of at least one Yukawa coupling,  $Y_\tau$  [1]. CP-dependent distributions in Higgs production are known [2], however observing them appears not to be possible in practice, due to detector effects [3]. A future International Linear Collider (ILC) can certainly do better than the LHC for the case of a light Higgs, approximately  $110 \leq M_H \leq 200$  GeV. How much better an ILC could measure these couplings, what additional couplings it would have access to, and its ability to go significantly beyond LHC physics by measuring a self-coupling  $\lambda$  or the CP nature of the Higgs sector are what I review here.

## 2 The Easy Quantum Numbers

Of greatest interest in Higgs physics is "Where is the Higgs?" That is, what is its mass? Precision fits to electroweak data suggest [4] it is very near the lower bound from experiment,  $M_H > 113$  GeV [5]. If a Higgs is found in the range  $M_H < 135$  GeV or so, then the MSSM is still a viable theory. Finding a much heavier Higgs would suggest a different form of new physics. At the LHC,  $M_H$  would be determined principally by observing the process  $gg \rightarrow H \rightarrow ZZ \rightarrow 4\ell$ , which is accessible at all masses. For example, at ATLAS for  $M_H < 400$  GeV, this would yield a 0.1%

or better mass measurement, depending ultimately on uncertainty in the calorimeter calibration [3].

For a light Higgs, an ILC would improve this roughly by a factor of two to three, around 0.03 – 0.05% uncertainty for a light Higgs, using a combination of data from the recoil mass spectrum in  $e^+e^- \rightarrow HZ \rightarrow \ell^+\ell^- + X$  and direct reconstruction of Higgs decay into dijets. A simulated recoil mass spectrum for  $M_H = 120$  GeV is shown in Fig. 1. Fig. 2 shows a comparison between CMS expectations and some different ILC energies and luminosities. However, this level of precision may be overkill. It would correspond to, for example, 4-loop radiative corrections in the MSSM! These are currently far from achievable. Additionally, the leading uncertainty in  $\Delta M_H$  in this case is due to the large uncertainty in the top quark mass,  $m_t$ , which will not improve enough in the LHC or conceivable ILC experiments to warrant calculation of MSSM 4-loop corrections to  $M_H$ , possibly even the 3-loop contributions.

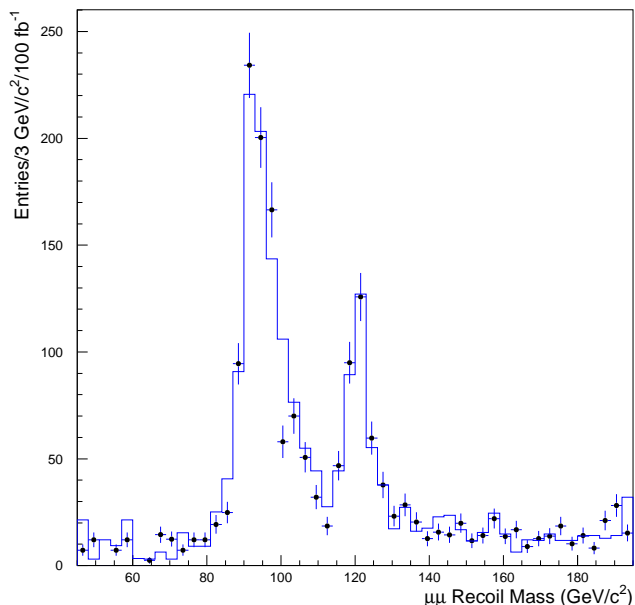


Figure 1:  $\mu\mu$  recoil mass for  $e^+e^- \rightarrow ZH \rightarrow \mu\mu + X$ , taken from Ref. [6].

Determining consistency of a resonance with spin-0 has been studied thoroughly for the LHC. There exist two methods: angular distributions in  $H \rightarrow \gamma\gamma$ , and also in the reconstructed  $Z$  bosons in  $H \rightarrow ZZ$ ! [3]. The LHC has no difficulty with this consistency check for  $M_H < 400$  GeV, so I do not discuss it further here.

Measurement of the resonance's couplings to the weak bosons, photon, gluons, and fermions is of much greater interest. Confirming that  $g_{HWW}, g_{HZZ}$  are gauge couplings and related by SU(2) is one of the key determinations to identifying the resonance as a Higgs boson. These couplings may be modified by mixing or other parameters of a 2HDM, which are well defined and appear only as overall factors.

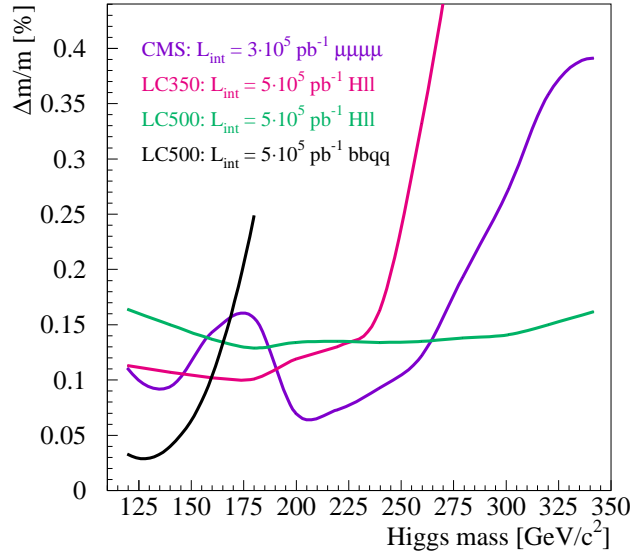


Figure 2: The expected Higgs mass resolution at CMS and at three linear collider options, taken from Ref. [7].

For example, the  $hWW$ ,  $HWW$  vertices are modified at tree level in the MSSM by  $\sin(\beta - \alpha)$ ,  $\cos(\beta - \alpha)$ , respectively. In this same vein, we would require that  $g_{H\gamma\gamma}$ ,  $g_{Hgg}$  are demonstrated to be loop-induced.

At the LHC,  $g_{HWW}$  may be determined to better than 5% for a light Higgs,  $M_H < 200$  GeV, for scenarios where the Higgs is relatively SM-like [1]; non-SM-like Higgs coupling extraction scenarios are just now beginning to be examined [8]. This is achieved by combining information from various decay channels in weak boson fusion Higgs production. This same method also allows the total width to be extracted indirectly, to about the 10 – 15% level. The best Yukawa coupling measurement can be made for taus, which is quite good at about 5 – 15% over the mass region  $115 < M_H < 150$  GeV, and work is progressing on  $H \rightarrow b\bar{b}$  but this measurement is not likely to be better than about 30% in the end [9]. Decays to  $c\bar{c}$  are completely inaccessible at the LHC, but the width to gluons could be determined to about 20% from the rate for  $gg \rightarrow H \rightarrow W^+W^-$  and the highly accurately known  $\text{BR}(WW)$ . These results would already be quite good and allow for considerable model determination, but an ILC could do far better.

The procedure for extracting couplings<sup>1</sup> is equally involved at the ILC. First, the recoil mass spectrum in  $ZH$  production would be used to determine  $\sigma_{ZH}$  to about

<sup>1</sup>We may alternatively discuss the measurement of partial widths, which are directly proportional to the coupling squared. If the total width cannot be determined, it is more appropriate to discuss measurement of branching ratios.

2% (TESLA) for a light Higgs, say  $110 < M_H < 150$  GeV. This measurement is the basis for extracting absolute branching ratios. Once the  $WW$  branching ratio is known ( $< 5\%$  for a light Higgs, possibly as good as 2%),  $g_{HWW}$  could be obtained to better than 2%. From there, Yukawa couplings could be extracted directly. The expected uncertainty in the branching ratio for decay to  $b\bar{b}$  is anticipated to be the lowest, about 2% for  $M_H = 120$  with reasonable luminosity; 8% for  $c\bar{c}$  and 6% for  $\tau^+\tau^-$ . Additionally,  $\text{BR}(gg)$  could be determined to about 8% for the same mass. Fig. 3 shows the probable branching ratio measurement precision at TESLA.

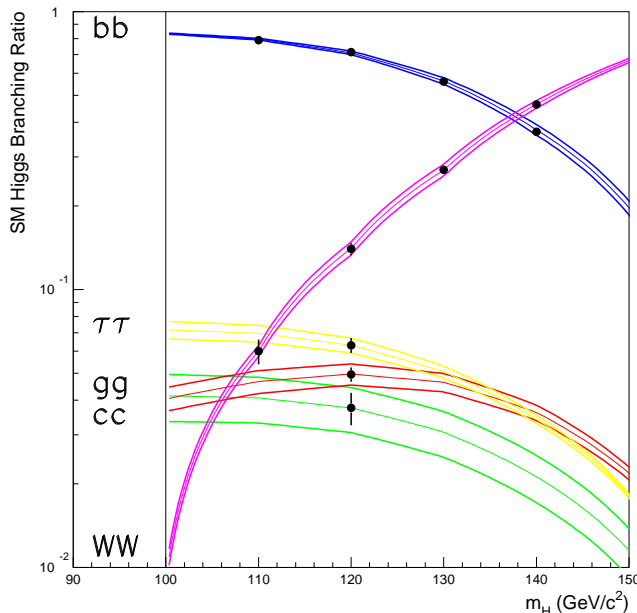


Figure 3: Estimated accuracy for SM Higgs branching fractions for  $500 \text{ fb}^{-1}$  of data at TESLA, taken from Ref. [6].

$t\bar{t}H$  production is possible for a high-energy ILC, being optimum at about  $\sqrt{s} = 800$  GeV for  $M_H = 120$  GeV. There is considerable discrepancy in the literature, however, as to the achievable precision in  $\delta g_{Htt}/g_{Htt}$ , ranging from 6% [10] on the optimistic end to as pessimistic as about 50% [11]. Clearly, more study is needed to resolve this disagreement. Finally, the total width could be had to better than 5% for  $M_H = 120$  GeV, or about 3% for  $M_H = 140$  GeV, using the  $H\nu\nu$  cross section as key input, which contains the already determined gauge coupling.

As far as distinguishing the SM from the MSSM, prospects appear good at the ILC but this subject begs for more study. Ratios of branching ratios are important, especially  $\text{BR}(b\bar{b})/\text{BR}(W^+W^-)$ , which could yield an indirect measurement of  $M_A$ . (It is possible that observing the CP odd state  $A$  itself could prove difficult.) Other important ratios are  $\text{BR}(c\bar{c})/\text{BR}(b\bar{b})$  and  $\text{BR}(gg)/\text{BR}(b\bar{b})$ . It is known that an MSSM Higgs sector can be established as non-SM-like at the 95% CL for  $M_A < 550$  or so at

TESLA, depending somewhat on  $\tan\beta$ . This is shown in Fig. 4 for 500 fb<sup>-1</sup> of data.

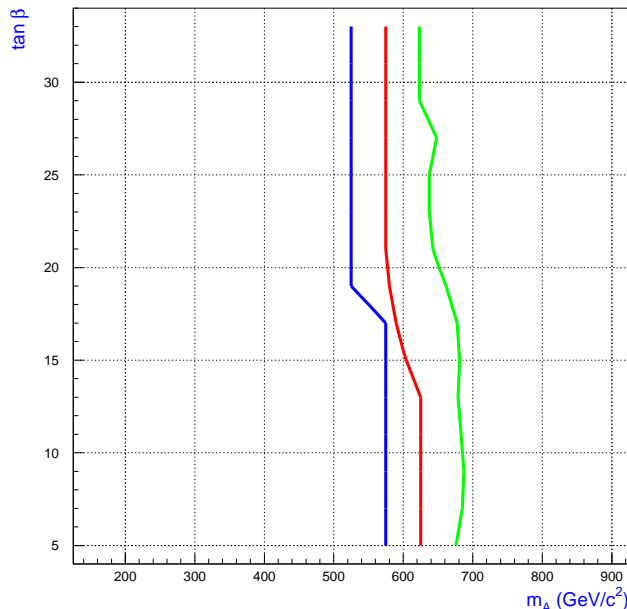


Figure 4: SM v. MSSM discriminating power as a function of  $M_A$  and  $\tan\beta$  for 500 fb<sup>-1</sup> of data at TESLA, taken from Ref. [6]. Parameter space to the right of the curves would appear SM-like. The blue curve is 95% CL, red is 90% CL, and green is 68% CL.

For a Higgs heavier than about 150 GeV, measurement of Yukawa couplings (other than to the top quark) are essentially inaccessible at any machine, except in certain restricted regions of a 2HDM. However, it is still highly desirable to know the gauge couplings and total width in this regions. Preliminary results indicate [12] that for the mass region  $150 < M_H < 300$  GeV an ILC could achieve 10% uncertainty for BR( $WW$ ) and 10 – 25% uncertainty for BR( $ZZ$ ), the latter depending strongly on  $M_H$ . For  $M_H > 300$  GeV, BR( $VV$ ) could be determined to a few percent, and BR( $t\bar{t}$ ) becomes accessible, probably at the 6% level. It is currently not known how to measure this at all at the LHC. For  $M_H > 230$  GeV or so, the Higgs width is expected to exceed detector resolution; the LHC and an ILC would have comparable ability here, at the few percent level for a heavy Higgs. A heavy Higgs is widely regarded as less interesting, and as such this scenario has not received as much attention in studies for an ILC.

It is easy to find already in the SM that radiative corrections are important. For example,  $\delta \text{BR}(b\bar{b}) > 30\%$  for  $M_H = 120$  GeV, simply due to the gluonic corrections. In extensions to the SM, such as the MSSM, large radiative corrections to the couplings (partial widths) lurk behind every corner. To take a couple examples, light squark corrections to  $h \rightarrow gg$  can be as large as factors of 2-3 in the partial width, but disappear as the squarks get heavy, greater than a few hundred GeV. Also, gluino

or chargino corrections to the  $b$ - $H$  vertices and  $H_1, H_2$  mixing can lead to order 1 corrections to the partial widths to  $b$  quarks or  $\tau$  leptons [13]. Considerable effort has been invested in calculating such corrections over the past decade, but the state of the art advances and interesting phenomenology continues to be revealed.

### 3 The Tough Quantum Numbers

While the “easy-to-determine” quantum numbers of a newly discovered resonance may be sufficient to establish it as part of a Higgs sector, in some sense the more difficult measurements are the interesting ones. These are the CP nature of the resonance, more specifically if there is any CP mixing in the neutral states in the case of a two Higgs doublet sector; and the self-coupling(s)  $\lambda_i$ . In the SM  $\lambda$  is related to the Higgs mass via  $M_H^2 = 2v^2\lambda$ , and as it is a free parameter,  $M_H$  is undetermined. In the MSSM, the various  $\lambda_i$  are gauge couplings, thus  $M_H$  is constrained. To be convinced that an observed Higgs sector (and perhaps other MSSM candidate states) belong to the MSSM, we would need to verify that these are, indeed, gauge couplings. Thus, multiple Higgs production would have to be observed.

Several studies have addressed the issue of multiple Higgs production at an ILC, highlighting scenarios where the cross section is large enough to obtain a substantial rate [14]. Only two groups have performed a signal  $v.$  background study at the phenomenological level (in the  $ZHH$  channel for the SM), and only one of those two groups, Castanier et al., included detector simulation. However, their results are quite promising. For a light SM Higgs, i.e.  $120 < M_H < 140$  GeV, their study suggests that the  $ZHH$  cross section could potentially be measured at the 12 – 18% level for large integrated luminosity,  $2000 \text{ fb}^{-1}$ . They further show that this would translate to about a 20% measurement of  $\lambda_{hhh}$ . It is clear that studies such as these at a future linear collider will depend critically on  $b$ -tagging performance. The studies go on to point out that in some MSSM parameter space regions, heavy Higgs decay to lighter Higgs states has significantly larger rates than the SM case, making the prospects for observation quite good. In contrast, it remains to be shown that the LHC has any capability to measure a Higgs sector self-coupling.

Research into methods to extract the CP nature of observed neutral Higgses is even less developed. Studies so far indicate that a CP = +1 state can be qualitatively distinguished from a CP = -1 state via angular distributions in  $ZH$  production [15], but if the state has mixed CP, the -1 component is very easily washed out. Additional work is sorely needed in this area, as the LHC again has no capability here, primarily due to the strong backgrounds and detector effects that hide the relevant distributions.

## 4 Conclusions

Prospects for observing a Higgs sector as the responsible mechanism for EWSB are quite good: precision fits to electroweak data suggest that the Higgs is light and thus accessible, perhaps by the Tevatron, and the LHC has the capability to observe a Higgs boson of any mass up to the unitarity limit. While the Tevatron could not make any serious measurements of couplings or other important properties of an observed resonance to completely convince one that it is part of a Higgs sector, the LHC can go a long way toward this goal. The LHC would determine the mass to a greater precision than can be matched theoretically, and would be able to determine the gauge coupling and total width of a Higgs boson, either directly or indirectly, to better than the 10% level. However, the LHC will have considerable difficulty to observe most fermionic decays, and will not have the capability to observe any self-couplings or identify CP mixing among the states of multiple physical Higgses.

An ILC extends our knowledge of a Higgs sector considerably. Its measurements of both gauge and Yukawa couplings would be superior over most of the mass range of a possible Higgs, and it would have access to additional fermionic decays as well as self-couplings and probably CP mixing, improving model discrimination. However, the state of the art on the last goal is still somewhat underdeveloped. Also lacking is a detailed overview of the capability of an ILC to distinguish different models based on coupling and mass measurements, although at least one study to address this is nearing completion [16]. So far, studies have presented levels of measurement precision based only on cross sections in the SM. If a Higgs sector turns out to be not very SM-like, then some of these levels of precision could be quite poor, while others are better than expected, and the restriction in model parameter space may or may not be satisfyingly small.

## Acknowledgments

I am grateful to the organizers of the conference and to the many physicists who have performed the LHC and LC Higgs studies which I have attempted to summarize here.

## References

- [1] D. Zeppenfeld, R. Kinnunen, A. Nikitenko and E. Richter-Was, Phys. Rev. D **62**, 013009 (2000) [hep-ph/0002036].
- [2] J. F. Gunion and X. He, Phys. Rev. Lett. **76**, 4468 (1996) [hep-ph/9602226];  
J. F. Gunion and J. Pliszka, Phys. Lett. **B444**, 136 (1998) [hep-ph/9809306].

- [3] ATLAS Collaboration, ATLAS TDR, report CERN/LHCC/99-15 (1999).
- [4] See, e.g.: W. J. Marciano, hep-ph/0003181;  
J. Erler, hep-ph/0010153.
- [5] P. Igo-Kemenes, LEP seminar, CERN, Nov.3, 2000;  
R. Barate *et al.* [ALEPH Collaboration], hep-ex/0011045;  
M. Acciarri *et al.* [L3 Collaboration], hep-ex/0011043.
- [6] M. Battaglia, talk presented at the Fermilab Linear Collider Study Group meeting, April 5, 2000.
- [7] A. Sopczak, talk presented at the 2nd ECFA/DESY Linear Collider Conference, Obernai, Oct. 16-19, 1999.
- [8] M. Carena, S. Heinemeyer, D. Rainwater, G. Weiglein and D. Zeppenfeld, in preparation.
- [9] D. Rainwater, hep-ph/0004119, to appear in Phys. Lett. **B**.
- [10] A. Juste and G. Merino, hep-ph/9910301.
- [11] H. Baer, S. Dawson and L. Reina, Phys. Rev. D **61**, 013002 (2000) [hep-ph/9906419]
- [12] A. Kronfeld et al., Fermilab Linear Collider Study Group Physics Report, FNAL-FN-701.
- [13] M. Carena, S. Mrenna and C. E. Wagner, Phys. Rev. D **60**, 075010 (1999) [hep-ph/9808312].
- [14] C. Castanier, P. Gay, P. Lutz and J. Orloff, talk presented at the 2nd ECFA/DESY Linear Collider Conference, Obernai, Oct. 16-19, 1999; hep-ex/0101028;  
D. J. Miller and S. Moretti, Eur. Phys. J. **C13**, 459 (2000) [hep-ph/9906395];  
A. Djouadi, W. Kilian, M. Muhlleitner and P. M. Zerwas, hep-ph/0001169;  
P. Osland and P. N. Pandita, Phys. Rev. D **59**, 055013 (1999) [hep-ph/9806351].
- [15] See e.g. talk presented by A. Skjold and P. Osland, hep-ph/9508223.
- [16] M. Carena, H. Haber, H. Logan and S. Mrenna, FNAL-00/334-T, in preparation.

# GigaZ: High Precision Tests of the SM and the MSSM

J. ERLER<sup>1</sup> AND S. HEINEMEYER<sup>2</sup>

<sup>1</sup>*Department of Physics and Astronomy, University of Pennsylvania,  
Philadelphia PA 19104-6396, USA*

<sup>2</sup>*BNL, Physics Department, Upton NY 11973, USA*

The high-energy  $e^+e^-$ -collider TESLA can be operated in the GigaZ mode on the  $Z$  resonance, producing  $\mathcal{O}(10^9)$   $Z$  bosons per year. This will allow the measurement of the effective electroweak mixing angle to an accuracy of  $\delta \sin^2 \theta_{\text{eff}} \approx \pm 1 \times 10^{-5}$ . Similarly the  $W$  boson mass is expected to be measurable with an error of  $\delta M_W \approx \pm 6$  MeV near the  $W^+W^-$  threshold. We discuss the impact of these observables on the accuracy with which the Higgs boson mass can be determined from loop corrections within the Standard Model. We also study indirect constraints on new mass scales within the Minimal Supersymmetric Standard Model.

Presented by JENS ERLER at the

5th International Symposium on Radiative Corrections  
(RADCOR-2000)

Carmel CA, USA, 11-15 September, 2000

# 1 Introduction

The high-energy  $e^+e^-$  linear collider TESLA is being designed to operate on top of the  $Z$  boson resonance by adding a bypass to the main beam line. Given the high luminosity,  $\mathcal{L} = 7 \times 10^{33} \text{cm}^{-2}\text{s}^{-1}$ , and the cross section,  $\sigma_Z \approx 30 \text{ nb}$ , about  $2 \times 10^9$   $Z$  events can be generated in an operational year of  $10^7$ s. We will therefore refer to this option as the GigaZ mode of the machine. Moreover, by increasing the collider energy to the  $W$ -pair threshold, about  $10^6$   $W$  bosons can be generated at the optimal energy point for measuring the  $W$  boson mass,  $M_W$ , near threshold and about  $3 \times 10^6$   $W$  bosons at the energy of maximal cross section. The large increase in the number of  $Z$  events by two orders of magnitude as compared to LEP1 and the increasing precision in the measurements of  $W$  boson properties, open new opportunities for high precision physics in the electroweak sector [1].

By adopting the Blondel scheme [2], the left-right asymmetry,  $A_{LR} \equiv 2(1 - 4\sin^2\theta_{\text{eff}})/(1 + (1 - 4\sin^2\theta_{\text{eff}})^2)$ , can be measured with very high precision,  $\delta A_{LR} \approx \pm 10^{-4}$  [3], when both, electrons and positrons, are polarized longitudinally. From  $A_{LR}$  the mixing angle in the effective leptonic vector coupling of the on-shell  $Z$  boson,  $\sin^2\theta_{\text{eff}}$ , can be determined to an accuracy [3],

$$\delta \sin^2\theta_{\text{eff}} \approx \pm 1 \times 10^{-5}, \quad (1)$$

while the  $W$  boson mass is expected to be measurable within [4]

$$\delta M_W \approx \pm 6 \text{ MeV}. \quad (2)$$

Besides the improvements in  $\sin^2\theta_{\text{eff}}$  and  $M_W$ , GigaZ has the potential to determine the total  $Z$  width within  $\delta\Gamma_Z = \pm 1 \text{ MeV}$ ; the ratio of hadronic to leptonic partial  $Z$  widths with a relative uncertainty of  $\delta R_l/R_l = \pm 0.05\%$ ; the ratio of the  $b\bar{b}$  to the hadronic partial widths with a precision of  $\delta R_b = \pm 1.4 \times 10^{-4}$ ; and to improve the  $b$  quark asymmetry parameter  $A_b$  to a precision of  $\pm 1 \times 10^{-3}$  [3]. These additional measurements offer complementary information on the Higgs boson mass,  $M_H$ , but also on the strong coupling constant,  $\alpha_s$ , which enters the radiative corrections in many places. This is desirable in its own right, and in the present context it is important to control  $\alpha_s$  effects from higher order loop contributions to avoid confusion with Higgs effects. Indirectly, a well known  $\alpha_s$  would also help to control  $m_t$  effects, since  $m_t$  from a threshold scan at a linear collider will be strongly correlated with  $\alpha_s$ . We find that via a precise measurement of  $R_l$ , GigaZ would provide a clean determination of  $\alpha_s$  with small error,

$$\delta\alpha_s \approx \pm 0.001, \quad (3)$$

and consequently a smaller uncertainty in  $\delta m_t$  compared to a linear collider, given identical threshold data ( $5 \times 10 \text{ fb}^{-1}$ ). The anticipated precisions for the most relevant

Table 1: Expected precision at various colliders for  $\sin^2\theta_{\text{eff}}$ ,  $M_W$ ,  $m_t$  and the (lightest) Higgs boson mass,  $M_H$ , at the reference value  $M_H = 110$  GeV. Run IIA refers to  $2 \text{ fb}^{-1}$  integrated luminosity per experiment collected at the Tevatron with the Main Injector, while Run IIB assumes the accumulation of  $30 \text{ fb}^{-1}$  by each experiment. LC corresponds to a linear collider without the GigaZ mode. (The entry in parentheses assumes a fixed target polarized Møller scattering experiment using the  $e^-$  beam.) Concerning the present value of  $M_W$  some improvement can be expected from the final analysis of the LEP 2 data.  $\delta m_t$  from the Tevatron and the LHC is the error for the top pole mass, while at the top threshold in  $e^+e^-$  collisions the  $\overline{\text{MS}}$  top-quark mass can be determined. The smaller value of  $\delta m_t$  at GigaZ compared to the LC is due to the prospective reduced uncertainty in  $\alpha_s$ , which affects the relation between the mass parameter directly extracted at the top threshold and the  $\overline{\text{MS}}$  top-quark mass.

	now	Run IIA	Run IIB	LHC	LC	GigaZ
$\delta \sin^2 \theta_{\text{eff}} (\times 10^5)$	17	50	13	21	(6)	1.3
$\delta M_W$ [MeV]	37	30	15	15	15	6
$\delta m_t$ [GeV]	5.1	4	2	2	0.2	0.13
$\delta M_H$ [MeV]	—	—	2000	100	50	50

electroweak observables at the Tevatron (Run IIA and IIB), the LHC, a future linear collider, LC, and GigaZ are summarized in Table 1.

In this talk, we discuss the potential impact of high precision measurements of  $\sin^2\theta_{\text{eff}}$ ,  $M_W$ , and other observables on the (indirect) determination of the Higgs boson mass in the SM and of non-SM mass scales in the MSSM. These unknown mass scales affect the predictions of the precision observables through loop corrections.

## 2 Higgs Sector of the SM

Within the SM, the precision observables measured at the  $Z$  peak are affected by two high mass scales: the top quark mass,  $m_t$ , and the Higgs boson mass,  $M_H$ . They enter into various relations between electroweak observables. For example, the radiative corrections entering the relation between  $M_W$  and  $M_Z$ , and between  $M_Z$  and  $\sin^2\theta_{\text{eff}}$ , have a strong quadratic dependence on  $m_t$  and a logarithmic dependence on  $M_H$ . We mainly focus on the two electroweak observables that are expected to be measurable with the highest accuracy at GigaZ,  $M_W$  and  $\sin^2\theta_{\text{eff}}$ . The current theoretical uncertainties [5] are dominated by the parametric uncertainties from the errors in the input parameters  $m_t$  (see Table 1) and  $\Delta\alpha$ . The latter denotes the QED-induced shift in the fine structure constant,  $\alpha \rightarrow \alpha(M_Z)$ , originating from charged-lepton and light-quark photon vacuum polarization diagrams. The hadronic

contribution to  $\Delta\alpha$  currently introduces an uncertainty of  $\delta\Delta\alpha = \pm 2 \times 10^{-4}$  [6]. Forthcoming low-energy  $e^+e^-$  annihilation experiments may reduce this uncertainty to about  $\pm 5 \times 10^{-5}$  [7]. Combining this value with future (indistinguishable) errors from unknown higher order corrections, we assign the total uncertainty of  $\delta\Delta\alpha = \pm 7 \times 10^{-5}$  to  $\Delta\alpha$ . For the future theoretical uncertainties from unknown higher-order corrections (including the uncertainties from  $\delta\Delta\alpha$ ) we assume,

$$\delta M_W(\text{theory}) = \pm 3 \text{ MeV}, \quad \delta \sin^2 \theta_{\text{eff}}(\text{theory}) = \pm 3 \times 10^{-5} \quad (\text{future}). \quad (4)$$

Given the high precision of GigaZ, also the experimental error in  $M_Z$ ,  $\delta M_Z = \pm 2.1 \text{ MeV}$ , results in non-negligible uncertainties of  $\delta M_W = \pm 2.5 \text{ MeV}$  and  $\delta \sin^2 \theta_{\text{eff}} = \pm 1.4 \times 10^{-5}$ . The experimental error in the top-quark mass,  $\delta m_t = \pm 130 \text{ MeV}$ , induces further uncertainties of  $\delta M_W = \pm 0.8 \text{ MeV}$  and  $\delta \sin^2 \theta_{\text{eff}} = \pm 0.4 \times 10^{-5}$ . Thus, while currently the experimental error in  $M_Z$  can safely be neglected, for the GigaZ precision it will actually induce an uncertainty in the prediction of  $\sin^2 \theta_{\text{eff}}$  that is larger than its experimental error.

- The relation between  $\sin^2 \theta_{\text{eff}}$  and  $M_Z$  can be written as,

$$\sin^2 \theta_{\text{eff}} \cos^2 \theta_{\text{eff}} = \frac{A^2}{M_Z^2(1 - \Delta r_Z)}, \quad (5)$$

where  $A = [(\pi\alpha)/(\sqrt{2}G_F)]^{1/2} = 37.2805(2) \text{ GeV}$  is a combination of two precisely known low-energy coupling constants, the Fermi constant,  $G_F$ , and the electromagnetic fine structure constant,  $\alpha$ . The quantity  $\Delta r_Z$  summarizes the loop corrections, which at the one-loop level can be decomposed as,

$$\Delta r_Z = \Delta\alpha - \Delta\rho^\dagger + \Delta r_Z^{\text{H}} + \dots \quad (6)$$

The leading top contribution to the  $\rho$  parameter [8], quadratic in  $m_t$ , reads,

$$\Delta\rho^\dagger = \frac{3G_F m_t^2}{8\pi^2 \sqrt{2}}. \quad (7)$$

The Higgs boson contribution is screened and logarithmic for large Higgs boson masses,

$$\Delta r_Z^{\text{H}} = \frac{G_F M_W^2}{8\pi^2 \sqrt{2}} \frac{1 + 9s_W^2}{3c_W^2} \log \frac{M_H^2}{M_W^2} + \dots \quad (8)$$

- An independent analysis can be based on the precise measurement of  $M_W$  near threshold. The  $M_W$ - $M_Z$  interdependence is given by,

$$\frac{M_W^2}{M_Z^2} \left( 1 - \frac{M_W^2}{M_Z^2} \right) = \frac{A^2}{M_Z^2(1 - \Delta r)}, \quad (9)$$

where the quantum correction  $\Delta r$  has the one-loop decomposition,

$$\Delta r = \Delta\alpha - \frac{c_W^2}{s_W^2} \Delta\rho^t + \Delta r^H + \dots, \quad (10)$$

$$\Delta r^H = \frac{G_F M_W^2}{8\pi^2 \sqrt{2}} \frac{11}{3} \log \frac{M_H^2}{M_W^2} + \dots, \quad (11)$$

with  $\Delta\alpha$  and  $\Delta\rho^t$  as introduced above.

Due to the different dependences of  $\sin^2 \theta_{\text{eff}}$  and  $M_W$  on  $m_t$  and  $M_H$ , the high precision measurements of these quantities at GigaZ (and other observables entering a global analysis) can determine  $m_t$  and  $M_H$ . The expected accuracy in the indirect determination of  $M_H$  from the radiative corrections within the SM is displayed in Fig. 1. To obtain these contours, the error projections in Table 1 are supplemented by central values equal to the current SM best fit values for the entire set of current high precision observables [9]. For the theoretical uncertainties, Eq. (4) is used, while the parametric uncertainties, such as from  $\alpha_s$  and  $M_Z$ , are automatically accounted for in the fits<sup>1</sup>. The allowed bands in the  $m_t$ - $M_H$  plane for the GigaZ accuracy are shown separately for  $\sin^2 \theta_{\text{eff}}$  and  $M_W$ . By adding the information on the top-quark mass, with  $\delta m_t \lesssim 130$  MeV obtained from measurements of the  $t\bar{t}$  production cross section near threshold, an accurate determination of the Higgs boson mass becomes feasible, from both,  $M_W$  and  $\sin^2 \theta_{\text{eff}}$ . If the two values are found to be consistent, they can be combined and compared to the Higgs boson mass measured in direct production through Higgs-strahlung [12] (see the last row in Table 1). In Fig. 1 this is shown by the shaded area, where the measurements of other  $Z$  boson properties as anticipated for GigaZ are also included. For comparison, the area corresponding to current experimental accuracies is also shown.

The results can be summarized by calculating the accuracy with which  $M_H$  can be determined indirectly. The expectations for  $\delta M_H/M_H$  in each step until GigaZ are collected in Table 2. It is apparent that GigaZ, reaching  $\delta M_H/M_H = \pm 7\%$ , triples the precision in  $M_H$  relative to the anticipated LHC status. On the other hand, a linear collider without the high luminosity option would provide only a modest improvement.

- A direct formal relation between  $M_W$  and  $\sin^2 \theta_{\text{eff}}$  can be established by combining the two relations (5) and (9) as,

$$M_W^2 = \frac{A^2}{\sin^2 \theta_{\text{eff}} (1 - \Delta r_W)}. \quad (12)$$

---

<sup>1</sup>All fit results in this Section were obtained using GAPP [11].

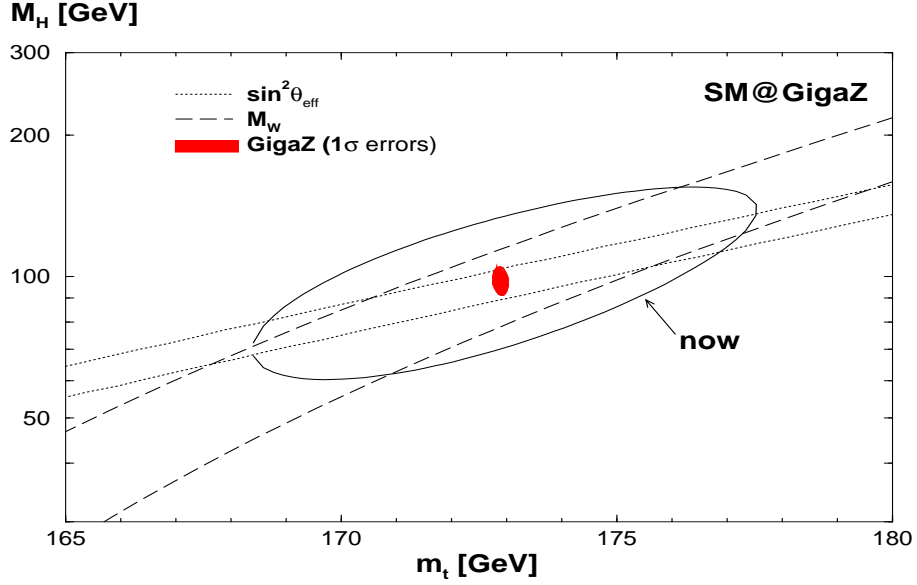


Figure 1:  $1\sigma$  allowed regions in the  $m_t$ - $M_H$  plane taking into account the current measurements and the anticipated GigaZ precisions for  $\sin^2 \theta_{\text{eff}}$ ,  $M_W$ ,  $\Gamma_Z$ ,  $R_l$ ,  $R_q$  and  $m_t$  (see text).

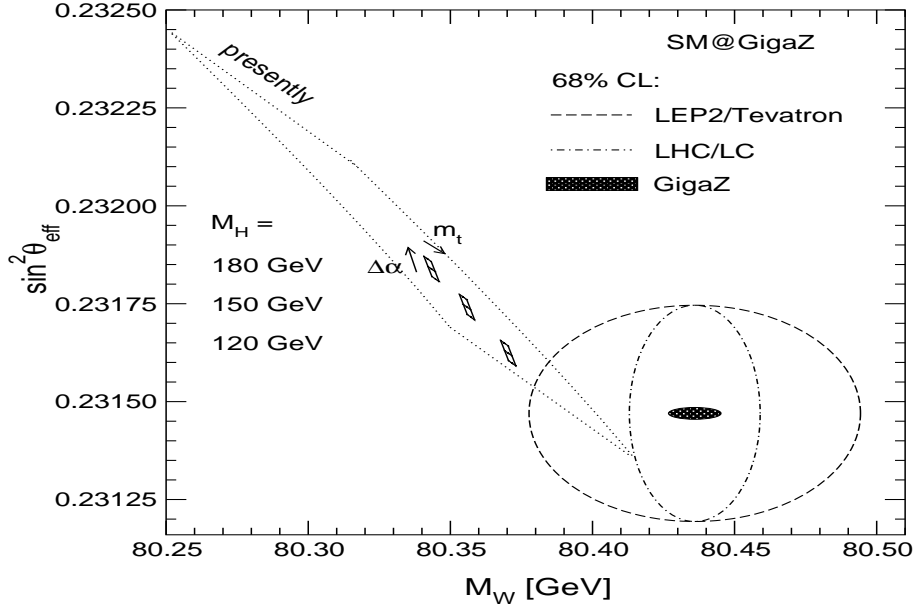


Figure 2: The theoretical prediction for the relation between  $\sin^2 \theta_{\text{eff}}$  and  $M_W$  in the SM for Higgs boson masses in the intermediate range is compared to the experimental accuracies at LEP 2/Tevatron (Run IIA), LHC/LC and GigaZ (see Table 1). For the theoretical prediction an uncertainty of  $\delta\Delta\alpha = \pm 7 \times 10^{-5}$  and  $\delta m_t = \pm 200$  MeV is taken into account.

Table 2: *Cumulative* expected precisions of indirect Higgs mass determinations, given the error projections in Table 1. Theoretical uncertainties and their correlated effects on  $M_W$  and  $\sin^2 \theta_{\text{eff}}$  are taken into account (see text). The last column shows the indirect Higgs mass determination from the full set of precision observables.

	$M_W$	$\sin^2 \theta_{\text{eff}}$	all
now	200 %	62 %	60 %
Tevatron Run IIA	77 %	46 %	41 %
Tevatron Run IIB	39 %	28 %	26 %
LHC	28 %	24 %	21 %
LC	18 %	20 %	15 %
GigaZ	12 %	7 %	7 %

The quantum correction  $\Delta r_W$  is independent of  $\Delta \rho^t$  in leading order and has the one-loop decomposition,

$$\Delta r_W = \Delta \alpha - \Delta r_W^{\text{H}} + \dots, \quad (13)$$

$$\Delta r_W^{\text{H}} = \frac{G_F M_Z^2}{24\pi^2 \sqrt{2}} \log \frac{M_H^2}{M_W^2} + \dots. \quad (14)$$

Relation (12) can be evaluated by inserting the measured value of the Higgs boson mass as predetermined at the LHC and the LC. This is visualized in Fig. 2, where the present and future theoretical predictions for  $\sin^2 \theta_{\text{eff}}$  and  $M_W$  (for different values of  $M_H$ ) are compared with the experimental accuracies at various colliders. Besides the independent predictions of  $\sin^2 \theta_{\text{eff}}$  and  $M_W$  within the SM, the  $M_W - \sin^2 \theta_{\text{eff}}$  contour plot in Fig. 2 can be interpreted as an additional indirect determination of  $M_W$  from the measurement of  $\sin^2 \theta_{\text{eff}}$ . Given the expected negligible error in  $M_H$ , this results in an uncertainty of

$$\delta M_W(\text{indirect}) \approx \pm 2 \text{ MeV} \pm 3 \text{ MeV}. \quad (15)$$

The first uncertainty reflects the experimental error in  $\sin^2 \theta_{\text{eff}}$ , while the second is the theoretical uncertainty discussed above (see Eq. (4)). The combined uncertainty of this indirect prediction is about the same as the one of the SM prediction according to Eq. (9) and is close to the experimental error expected from the  $W^+W^-$  threshold given in Eq. (2).

Consistency of all the theoretical relations with the experimental data would be the ultimate precision test of the SM based on quantum fluctuations. The comparison between theory and experiment can also be exploited to constrain possible physics

scales beyond the SM. These additional contributions can conveniently be described in terms of the S,T,U [13] or  $\epsilon$  parameters [14]. Adopting the notation of Ref. [9], the errors with which they can be measured at GigaZ are given as follows:

$$\begin{aligned} \Delta S &= \pm 0.05, & \Delta \hat{\epsilon}_3 &= \pm 0.0004, \\ \Delta T &= \pm 0.06, & \Delta \hat{\epsilon}_1 &= \pm 0.0005, \\ \Delta U &= \pm 0.04, & \Delta \hat{\epsilon}_2 &= \pm 0.0004. \end{aligned} \tag{16}$$

The oblique parameters in Eq. (16) are strongly correlated. On the other hand, many types of new physics predict  $U = \hat{\epsilon}_2 = 0$  or very small (see Ref.[9] and references therein). With the  $U$  ( $\hat{\epsilon}_2$ ) parameter known, the anticipated errors in  $S$  and  $T$  would decrease to about  $\pm 0.02$ , while the errors in  $\hat{\epsilon}_1$  and  $\hat{\epsilon}_3$  would be smaller than  $\pm 0.0002$ .

### 3 Supersymmetry

We now assume that supersymmetry would be discovered at LEP 2, the Tevatron, or the LHC, and further explored at an  $e^+e^-$  linear collider. The high luminosity expected at TESLA can be exploited to determine supersymmetric particle masses and mixing angles with errors from  $\mathcal{O}(1\%)$  down to one per mille, provided they reside in the kinematical reach of the collider, which we assume to be about 1 TeV.

In contrast to the Higgs boson mass in the SM, the lightest  $\mathcal{CP}$ -even MSSM Higgs boson mass,  $M_h$ , is not a free parameter but can be calculated from the other SUSY parameters. In the present analysis, the currently most precise result based on Feynman-diagrammatic methods [15] is used, relating  $M_h$  to the pseudoscalar Higgs boson mass,  $M_A$ . The numerical evaluation has been performed with the Fortran code *FeynHiggs* [16]. Later in our analysis we also assume a future uncertainty in the theoretical prediction of  $M_h$  of  $\pm 0.5$  GeV.

The relation between  $M_W$  and  $\sin^2 \theta_{\text{eff}}$  is affected by the parameters of the supersymmetric sector, especially the  $\tilde{t}$ -sector. At the LHC and in the first phase of LC operations, the mass of the light  $\tilde{t}$ ,  $m_{\tilde{t}_1}$ , and the  $\tilde{t}$ -mixing angle,  $\theta_{\tilde{t}}$ , may be measurable very well, particularly in the process  $e^+e^- \rightarrow \tilde{t}_1 \bar{\tilde{t}}_1$  (see the last paper of Ref. [1] and references therein). On the other hand, background problems at the LHC and lacking energy at the LC may preclude the analysis of the heavy  $\tilde{t}$ -particle,  $\tilde{t}_2$ .

In Fig. 3 we show in a first step of the analysis the effect of the precise determination of  $\sin^2 \theta_{\text{eff}}$  alone on the indirect determination of the heavier  $\tilde{t}$  mass,  $m_{\tilde{t}_2}$ . In this first step we neglect the variation of the SUSY parameters and the theoretical uncertainty of  $M_h$ . For the precision observables we have taken  $\sin^2 \theta_{\text{eff}} = 0.23140$  and  $M_h = 115$  GeV with the experimental errors given in the last column of Table 1. For  $\tan \beta$ , the ratio of the vacuum expectation values of the two Higgs doublets in the MSSM, we assume a relatively well determined  $\tan \beta = 3 \pm 0.5$ , as can be expected

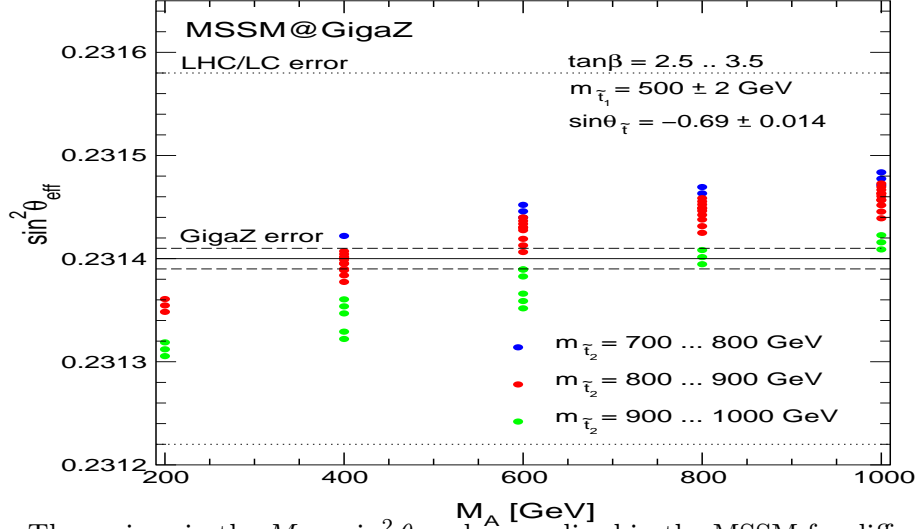


Figure 3: The regions in the  $M_A - \sin^2 \theta_{\text{eff}}$  plane realized in the MSSM for different values of  $m_{\tilde{t}_2}$ . The precision on  $\sin^2 \theta_{\text{eff}}$  obtainable at the LHC and the LC is compared to the prospective GigaZ precision around the value  $\sin^2 \theta_{\text{eff}} = 0.23140$ , for  $2.5 < \tan \beta < 3.5$  and the other experimental values as in Fig. 4. (See text for details.)

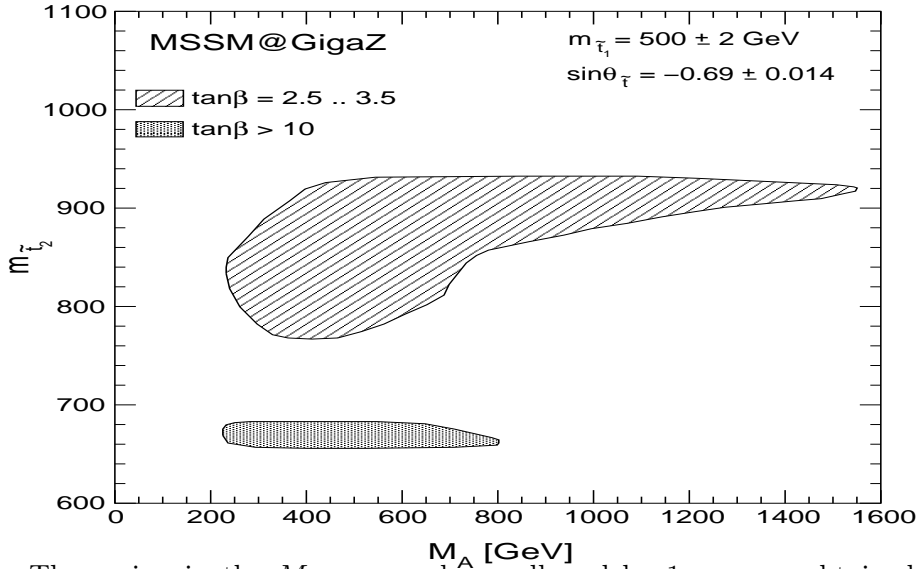


Figure 4: The region in the  $M_A - m_{\tilde{t}_2}$  plane, allowed by  $1\sigma$  errors obtained from the GigaZ measurements of  $M_W$  and  $\sin^2 \theta_{\text{eff}}$ :  $M_W = 80.40$  GeV,  $\sin^2 \theta_{\text{eff}} = 0.23140$ , and from the LC measurement of  $M_h$ :  $M_h = 115$  GeV. The experimental errors for the SM parameters are given in Table 1.  $\tan \beta$  is assumed to be experimentally constrained by  $2.5 < \tan \beta < 3.5$  or  $\tan \beta > 10$ . The other parameters including their uncertainties are given by  $m_{\tilde{t}_1} = 500 \pm 2$  GeV,  $\sin \theta_{\tilde{t}} = -0.69 \pm 2\%$ ,  $A_b = A_t \pm 10\%$ ,  $\mu = -200 \pm 1$  GeV,  $M_2 = 400 \pm 2$  GeV and  $m_{\tilde{g}} = 500 \pm 10$  GeV. For the uncertainties of the theoretical predictions we use Eq. (4).

from measurements in the gaugino sector (see e.g. Ref. [17]). As for the other parameters, the following values are assumed:  $m_{\tilde{t}_1} = 500 \pm 2$  GeV,  $\sin \theta_{\tilde{t}} = -0.69 \pm 2\%$ ,  $A_b = A_t$ ,  $\mu = -200$  GeV,  $M_2 = 400$  GeV and  $m_{\tilde{g}} = 500$  GeV. ( $A_{b,t}$  are trilinear soft SUSY-breaking parameters,  $\mu$  is the Higgs mixing parameter,  $M_2$  is one of the soft SUSY-breaking parameter in the gaugino sector, and  $m_{\tilde{g}}$  denotes the gluino mass.) In Fig. 3 the GigaZ precision for  $\sin^2 \theta_{\text{eff}}$  is compared to the precision obtainable at the LHC and a LC without the GigaZ option. While the LHC/LC precision gives no restrictions for  $m_{\tilde{t}_2}$  or  $M_A$ , the high GigaZ precision could give lower and *upper* bounds on both non-SM mass parameters.

However, a more realistic scenario includes the other precision observable that can be determined at GigaZ with extremely high precision,  $M_W$ . In addition, all uncertainties of the additional SUSY mass scales, as well as the theoretical uncertainty of the Higgs boson mass prediction have to be taken into account. Therefore, as a second step in our analysis we now consider  $\sin^2 \theta_{\text{eff}}$  and  $M_W$  and include all possible uncertainties. It is demonstrated in Fig. 4 how in this complete analysis limits on  $m_{\tilde{t}_2}$  and  $M_A$  can be derived from measurements of  $M_h$ ,  $M_W$ , and  $\sin^2 \theta_{\text{eff}}$ . As experimental values we assumed  $M_h = 115$  GeV,  $M_W = 80.40$  GeV, and  $\sin^2 \theta_{\text{eff}} = 0.23140$ , with the experimental errors given in the last column of Table 1, and the future theoretical uncertainty for the Higgs boson mass of  $\pm 0.5$  GeV. We now consider two cases for  $\tan \beta$ : the low  $\tan \beta$  region, where we assume a band,  $2.5 < \tan \beta < 3.5$  as for Fig. 3, and the high  $\tan \beta$  region where we assume a lower bound,  $\tan \beta \geq 10$  (see e.g. Ref. [17] and references therein). As for the other parameters, the following values are assumed, with uncertainties as expected from LHC and TESLA:  $m_{\tilde{t}_1} = 500 \pm 2$  GeV,  $\sin \theta_{\tilde{t}} = -0.69 \pm 2\%$ ,  $A_b = A_t \pm 10\%$ ,  $\mu = -200 \pm 1$  GeV,  $M_2 = 400 \pm 2$  GeV and  $m_{\tilde{g}} = 500 \pm 10$  GeV.

In this full analysis, taking into account all possible uncertainties, for low  $\tan \beta$  the heavier  $\tilde{t}$ -mass,  $m_{\tilde{t}_2}$ , can be restricted to  $760 \text{ GeV} \lesssim m_{\tilde{t}_2} \lesssim 930 \text{ GeV}$ . The mass  $M_A$  varies between 200 GeV and 1600 GeV. A reduction of this interval to  $M_A \geq 500$  GeV by its non-observation at the LHC and the LC does not improve the bounds on  $m_{\tilde{t}_2}$ . If  $\tan \beta \geq 10$ , the allowed region turns out to be much smaller ( $660 \text{ GeV} \lesssim m_{\tilde{t}_2} \lesssim 680 \text{ GeV}$ ), and  $M_A$  is restricted to  $M_A \lesssim 800$  GeV.

In deriving the bounds on  $m_{\tilde{t}_2}$ , both the constraints from  $M_h$  (see Ref. [18]) and  $\sin^2 \theta_{\text{eff}}$  play an important role. For the bounds on  $M_A$ , the main effect comes from  $\sin^2 \theta_{\text{eff}}$ . We have assumed a value for  $\sin^2 \theta_{\text{eff}}$  slightly different from the corresponding value obtained in the SM limit. For this value the (logarithmic) dependence on  $M_A$  (see also Fig. 3) is still large enough so that in combination with the high precision in  $\sin^2 \theta_{\text{eff}}$  at GigaZ an *upper limit* on  $M_A$  can be set. For an error as obtained at an LC without the GigaZ mode (see Table 1) no bound on  $M_A$  could be inferred. Thus, the high precision measurements of  $M_W$ ,  $\sin^2 \theta_{\text{eff}}$ , and  $M_h$  do not improve the direct lower bound on the mass of the pseudoscalar Higgs boson  $A$ , but instead they enable us to set an *upper bound*.

## 4 Conclusions

The opportunity to measure electroweak observables very precisely in the GigaZ mode of the projected  $e^+e^-$  linear collider TESLA, in particular the electroweak mixing angle  $\sin^2\theta_{\text{eff}}$  and the  $W$  boson mass, opens new areas for high precision tests of electroweak theories. We have analyzed in detail two examples: (i) The Higgs mass of the Standard Model can be extracted to a precision of a few percent from loop corrections. By comparison with the direct measurements of the Higgs mass, bounds on new physics scales can be inferred that may not be accessible directly. (ii) The masses of particles in supersymmetric theories, which for various reasons may not be accessible directly neither at the LHC nor at the LC, can be constrained. Typical examples are the heavy scalar top quark and the mass of the  $\mathcal{CP}$ -odd Higgs boson,  $M_A$ . (Further examples for the MSSM have also been studied in the original literature [1].) In the scenarios studied here, a sensitivity of up to order 2 TeV for the mass of the pseudoscalar Higgs boson and an upper bound of about 1 TeV for the heavy scalar top quark can be expected. Opening windows to unexplored energy scales renders these analyses of virtual effects an important tool for experiments in the GigaZ mode of a future  $e^+e^-$  linear collider.

## Acknowledgments

It is a pleasure for J.E. to thank the organizers for a very pleasant conference in a spectacular setting.

## References

- [1] See S. Heinemeyer, T. Mannel and G. Weiglein, e-print [hep-ph/9909538](#);  
J. Erler, S. Heinemeyer, W. Hollik, G. Weiglein, and P.M. Zerwas, *Phys. Lett.* **B486** (2000) 125;  
S. Heinemeyer and G. Weiglein, e-print [hep-ph/0012364](#); and references therein.
- [2] A. Blondel, *Phys. Lett.* **B202** (1988) 145.
- [3] R. Hawkings and K. Mönig, *EPJdirect* **C8** (1999) 1;  
K. Mönig, e-print [hep-ex/0101005](#).
- [4] G. Wilson, Proceedings, Linear Collider Workshop, Sitges 1999.
- [5] D. Bardin, M. Grünewald and G. Passarino, e-print [hep-ph/9802452](#).

- [6] M. Davier and A. Höcker, *Phys. Lett.* **B435** (1998) 427;  
 J. Kühn and M. Steinhauser, *Phys. Lett.* **B437** (1998) 425;  
 J. Erler, *Phys. Rev.* **D59** (1999) 054008;  
 F. Jegerlehner, e-print [hep-ph/9901386](#).
- [7] F. Jegerlehner, *The effective fine structure constant at TESLA energies*, LC-TH-2001-035.
- [8] M. Veltman, *Nucl. Phys.* **B123** (1977) 89.
- [9] J. Erler and P. Langacker, in Ref. [10].
- [10] D.E. Groom *et al.*, *Eur. Phys. J.* **C15** (2000) 1.
- [11] J. Erler, e-print [hep-ph/0005084](#).
- [12] J. Ellis, M. Gaillard and D. Nanopoulos, *Nucl. Phys.* **B106** (1976) 292;  
 B. Ioffe and V. Khoze, *Sov. J. Part. Nucl.* **9** (1978) 50;  
 B. Lee, C. Quigg and H. Thacker, *Phys. Rev.* **D16** (1977) 1519;  
 V. Barger, K. Cheung, A. Djouadi, B. Kniehl and P. Zerwas, *Phys. Rev.* **D49** (1994) 79.
- [13] M. Peskin and T. Takeuchi, *Phys. Rev.* **D46**, 381 (1992).
- [14] G. Altarelli and R. Barbieri, *Phys. Lett.* **B253**, 161 (1990).
- [15] S. Heinemeyer, W. Hollik and G. Weiglein, *Phys. Rev.* **D58** (1998) 091701; *Phys. Lett.* **B440** (1998) 296; *Eur. Phys. J.* **C9** (1999) 343.
- [16] S. Heinemeyer, W. Hollik and G. Weiglein, *Comp. Phys. Comm.* **124** (2000) 76; e-print [hep-ph/0002213](#).
- [17] S.Y. Choi, A. Djouadi, M. Guchait, J. Kalinowski, and P.M. Zerwas, *Eur. Phys. J.* **C14**, (2000) 535.
- [18] G. Weiglein, e-print [hep-ph/0001044](#).

FERMILAB-Conf-00/333-E  
July 26, 2001  
hep-ex/0012061

## QCD at the Tevatron: Status and Prospects

JOHN WOMERSLEY\*

*Fermi National Accelerator Laboratory  
Batavia, IL 60510 USA*

I shall review the present status of Tevatron QCD studies, focusing on the production of jets, vector bosons, photons and heavy quarks. In general there is good agreement between the results of current calculational tools and the experimental data. The major areas of discrepancy arise when the input parton distributions become uncertain (for example, jets at high  $E_T$ ) or when the momentum scales become relatively small (for example,  $b$  production at low  $p_T$ ). We can look forward to continued improvement in both calculations and measurements over the next decade. However, fully exploiting the power of the data will require considerable work, both from the experimentalists who must understand and publish all the systematic errors and their correlations, and from the phenomenologists who must understand the level of uncertainty in their calculations and in the parton distributions.

Presented at the

5th International Symposium on Radiative Corrections  
(RADCOR-2000)  
Carmel CA, USA, 11-15 September, 2000

---

\*womersley@fnal.gov

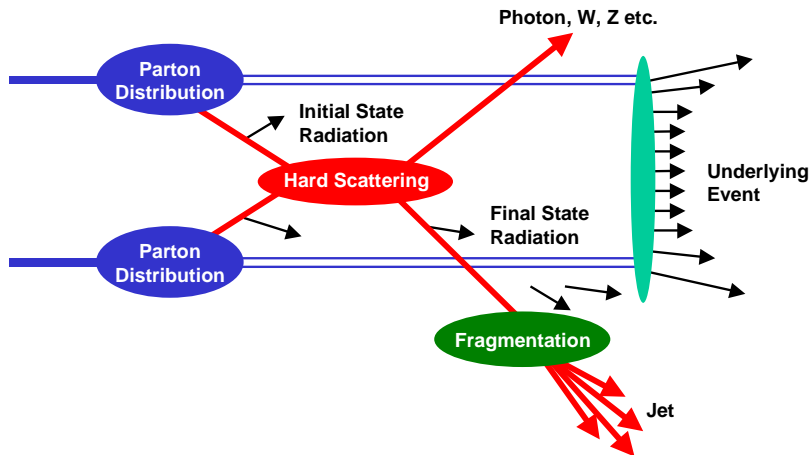


Figure 1: Schematic view of a hadron-hadron collision.

## 1 Introduction

It is over four years since data taking was completed in Run 1 at the Tevatron, so there are rather few new results to report. Instead, this presentation will be more of a review of the current state of knowledge, highlighting unresolved issues and prospects for Run 2. I shall briefly cover the production of jets, vector bosons, photons and heavy flavor. The opinions expressed are my own, and do not necessarily reflect the “party line” of the experiments.

The Tevatron collider recorded about  $100 \text{ pb}^{-1}$  of data during 1992–95 (Run 1), with two large detectors, CDF and DO. The results I shall show all come from this dataset, which was taken at  $\sqrt{s} = 1.8 \text{ TeV}$  (with a small amount of running at 630 GeV). The detectors are now nearing the completion of major upgrades, and data taking will resume in March 2001 (Run 2). The goal is to accumulate  $2 \text{ fb}^{-1}$  by 2003 and  $15 \text{ fb}^{-1}$  by 2007. In Run 2, the machine will operate at  $\sqrt{s} = 1.96 \text{ TeV}$ .

In hadron-hadron collisions, the simple picture of perturbative hard scattering between point-like particles, as described for  $e^+e^-$  collisions by earlier speakers at this meeting, becomes complicated by the additional effects shown in Fig. 1:

- parton distributions — a hadron collider is really a broad-band quark and gluon collider;
- fragmentation of final state quarks and gluons;
- both the initial and final states can be colored and can radiate gluons, which may interfere;
- the presence of an underlying event from proton remnants.

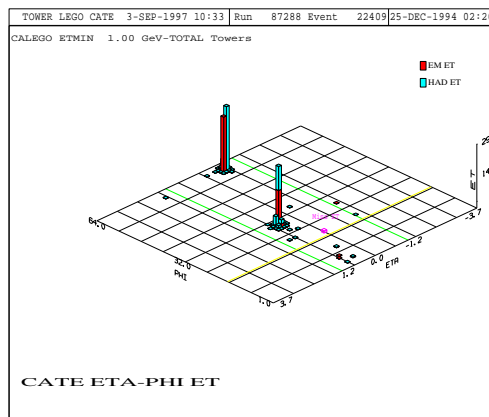


Figure 2: Lego plot of a high- $E_T$  dijet event in DO. Towers with  $E_T < 1$  GeV are suppressed.

Despite these potential complications, at sufficiently high energies the events appear quite simple: clear two-jet structure becomes obvious, as seen in Fig. 2, for example. Let us start by reviewing the status of jet production.

## 2 Jet Production

### 2.1 Inclusive Jet Cross sections at $\sqrt{s} = 1.8$ TeV

CDF[1] and DO[2] have both measured the cross section for  $R = 0.7$  cone jets in the central rapidity region. The cross section falls by seven orders of magnitude between  $E_T = 50$  and 450 GeV and both experiments' data are in pretty good agreement with NLO QCD over the whole range, as seen in Fig. 3. Looked at on a linear scale and normalized to the prediction, however, we have the situation shown in Fig. 4 (note that the CDF figure does not include systematic errors). The impression one gets is that there is a marked excess above QCD in the CDF data, which is not observed at DO. So much has been said about this discrepancy that it is difficult to know what can usefully be added<sup>1</sup> but I shall attempt to describe where we now stand.

In order to compare with CDF, DO carried out an analysis in exactly the same rapidity interval ( $0.1 < |\eta| < 0.7$ ). The results[4] are shown in Fig.5. Firstly we note that there is no actual discrepancy between the datasets. Secondly, for this plot the theoretical prediction was made using the CTEQ4HJ parton distribution, which has been adjusted to give an increased gluon density at large  $x$  while not violating any

<sup>1</sup>see Fig. 1 in [3].

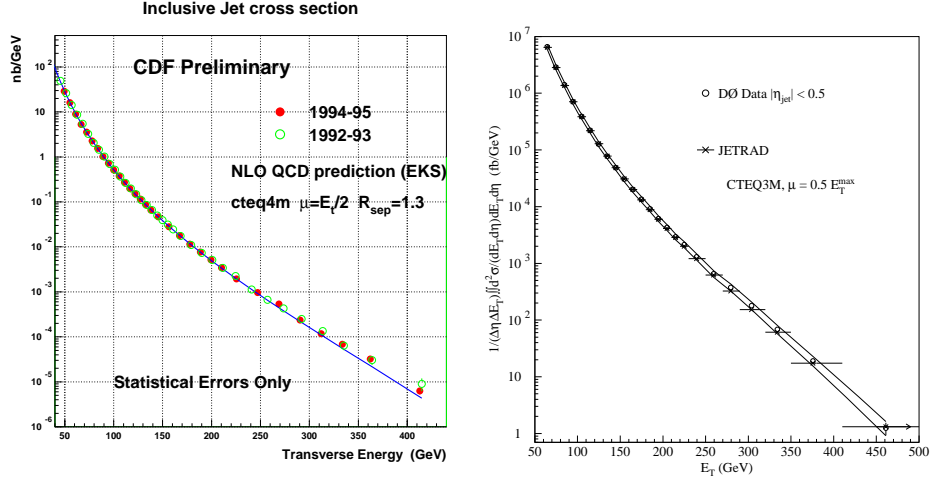


Figure 3: Inclusive jet cross sections measured at the Tevatron by CDF[1] (left, for  $0.1 < |\eta| < 0.7$ ) and DO[2] (right, for  $|\eta| < 0.5$ ), compared to the NLO QCD prediction.

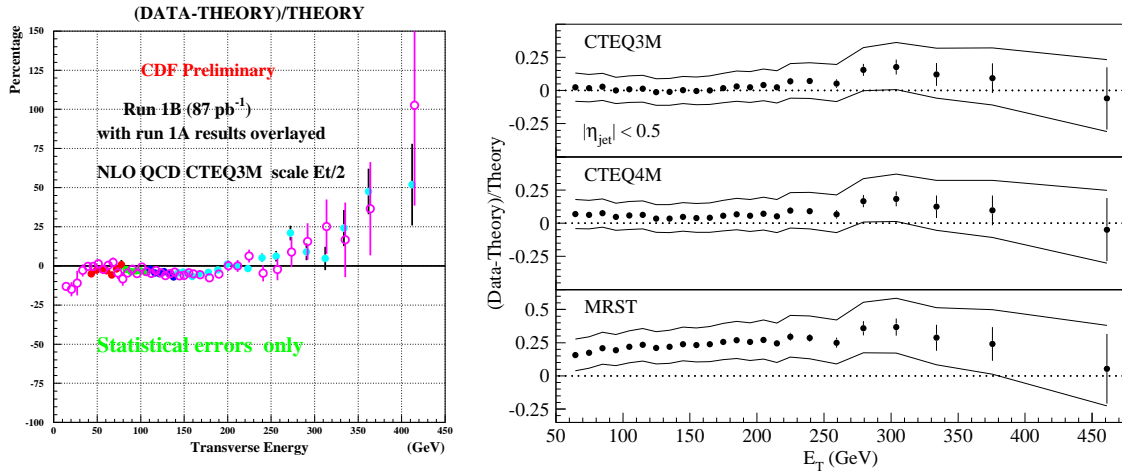


Figure 4: Inclusive jet cross sections measured at the Tevatron by CDF[1] (left, for  $0.1 < |\eta| < 0.7$ ) and DO[2] (right, for  $|\eta| < 0.5$ ), all normalized to the NLO QCD prediction.

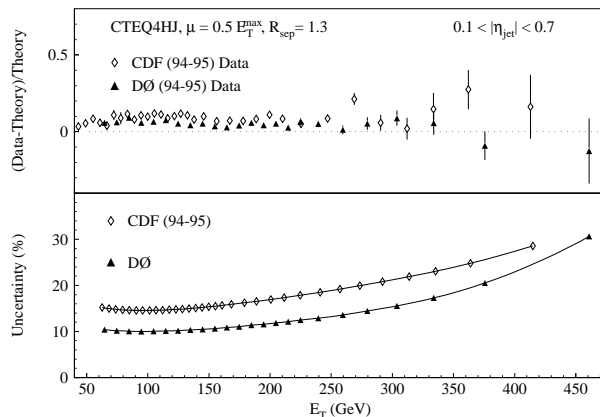


Figure 5: Inclusive jet cross sections for  $0.1 < |\eta| < 0.7$  from CDF and DO, compared with CTEQ4HJ distribution; and size of the systematic errors on the two measurements. Taken from [4].

experimental constraints (except perhaps fixed target photon production data, which in any case require big corrections before they can be compared to QCD, as we shall see later). The result of this increased gluon content is improved agreement especially with the CDF data points. The situation with the latest CTEQ5M and CTEQ5HJ parton distributions is shown in Fig. 6, and again, the enhanced gluon content in CTEQ5HJ brings the predicted cross section closer to the CDF data.

What then have we learned from this issue? In my opinion, whether the CDF data show a real excess above QCD, or just a “visual excess,” depends critically on understanding the systematic errors and their correlations as a function of  $E_T$ . Whether nature has actually exploited the freedom to enhance gluon distributions at large  $x$  will only be clear with the addition of more data — the factor of 20 increase in luminosity in the first part of Run 2 will extend the reach by 70–100 GeV in  $E_T$  and should therefore make the asymptotic high- $x$  behavior clearer. Whatever the Run 2 data show, this has been a useful lesson; it has reminded us all that parton distributions have uncertainties, whether made explicit or not, and that a full understanding of experimental systematics *and their correlations* is needed to understand whether experiments and theory agree or disagree.

DO[5] have extended their measurement of inclusive jet cross sections into the forward region. Figure 7 shows the measured cross sections up to  $|\eta| = 3$ . They are in good agreement with NLO QCD over the whole range of pseudorapidity and transverse energy; in fact both CTEQ4M and CTEQ4HJ parton distributions yield a good  $\chi^2$ .

Both Tevatron experiments have also studied dijet final states. CDF[6] has pre-

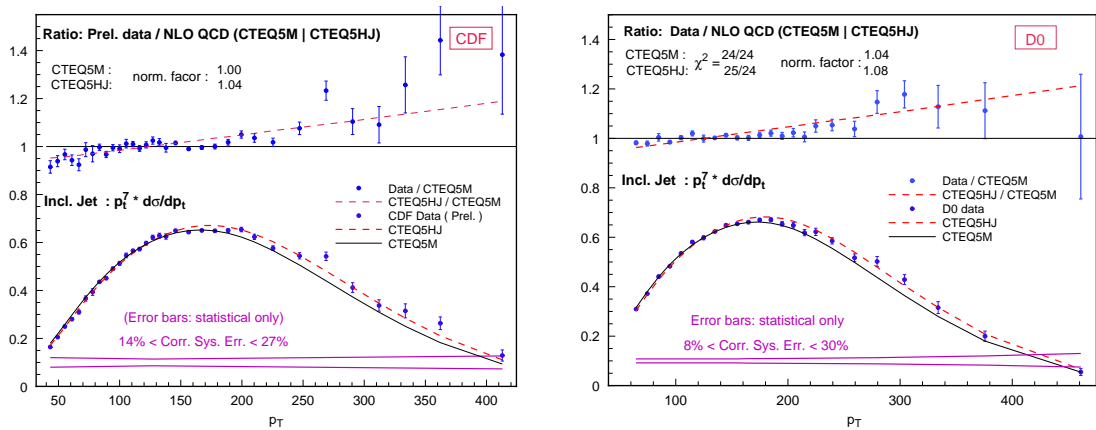


Figure 6: Inclusive jet cross sections measured by CDF (left) and DO (right), compared to the NLO QCD prediction using CTEQ5 parton distributions. The upper data points show  $(data-theory)/theory$ , while the lower points are the measured and predicted cross sections (approximately linearized through multiplication by  $E_T^7$ ).

sented cross sections for processes with one central jet ( $0.1 < |\eta_1| < 0.7$ ) and one jet allowed forward ( $|\eta_2|$  up to 3.0). In Fig. 8 these are compared with the NLO QCD prediction as a function of the central jet’s transverse energy ( $E_{T1}$ ). The data show an excess above the theory for large  $E_{T1}$ , just as seen in the inclusive cross section; but since these events are common to both samples, this is not surprising.

DO have measured[5] the cross sections for dijet production with both same-side ( $\eta_1 \approx \eta_2$ ) and opposite-side ( $\eta_1 \approx -\eta_2$ ) topologies, for four bins of  $|\eta|$  up to 2.0. The results are all in good agreement with the NLO QCD prediction.

All of these central, forward and dijet cross section measurements should really be used as input to the parton distribution fitting “industry”. Figure 9 shows where the Tevatron data lie on the plane of  $x$  and  $Q^2$ , indicating their complementarity to the fixed target and HERA deep-inelastic data. The apex of the Tevatron phase space is set by the highest  $Q^2$  event observed in Run 1, a spectacular dijet seen in DO with a jet-jet invariant mass of 1.2 TeV,  $Q^2 = 2.2 \times 10^5 \text{ GeV}^2$ , and  $x_1 = x_2 = 0.66$ .

## 2.2 Extraction of $\alpha_s$

CDF have carried out an interesting study with the aim of extracting  $\alpha_s$  from the inclusive jet cross section[7]; at NLO, the calculated cross section depends on  $\alpha_s$  with a coefficient which is predicted by JETRAD. The result,  $\alpha_s(m_Z) = 0.113_{-0.009}^{+0.008}$ , is consistent with the world average, and  $\alpha_s$  shows a nice evolution with scale (given by the jet transverse energy), as shown in Fig. 10. However the figure also shows that the measurement suffers from a large, and hard to quantify, sensitivity to the parton

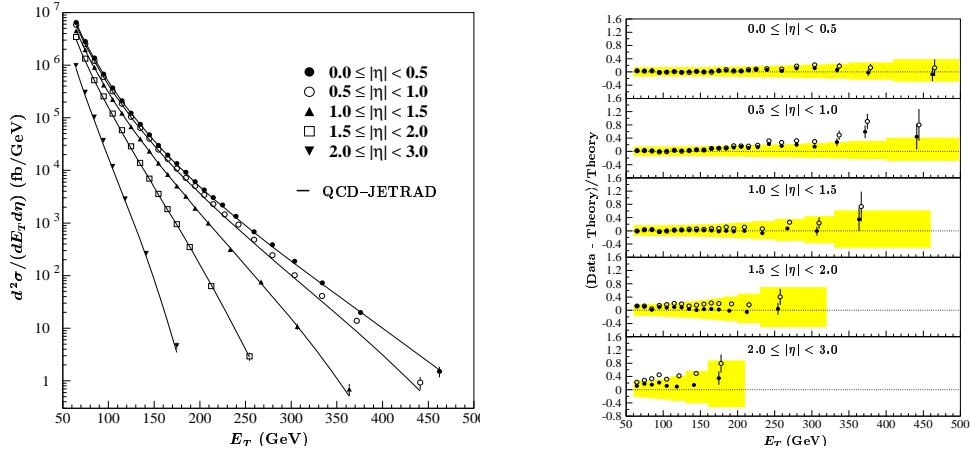


Figure 7: Inclusive jet cross sections measured up to  $|\eta| = 3$  by DO[5], compared to the NLO QCD prediction (using the JETRAD Monte Carlo). In the left hand plot the prediction uses CTEQ4M; in the right hand plot the solid points use CTEQ4HJ while the open points use CTEQ4M.

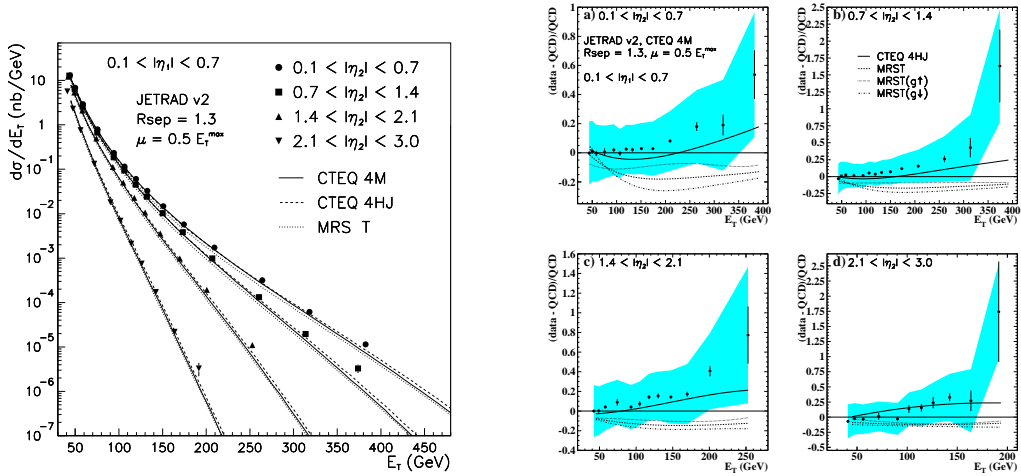


Figure 8: Dijet cross sections measured by CDF[6] for events with one central jet  $0.1 < |\eta_1| < 0.7$  and one jet allowed forward; left, as a function of the central jet  $E_T$  for various bins of  $|\eta_2|$ , and right, normalized to the NLO QCD prediction (from JETRAD).

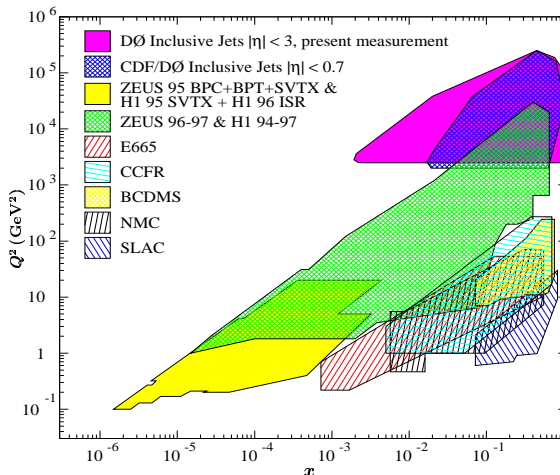


Figure 9: Phase space in  $x$  and  $Q^2$  probed by various experiments, showing the potential of central and forward jet production at the Tevatron to constrain parton distributions in regions complementary to deep inelastic scattering. Taken from [5].

distributions, especially to the value of  $\alpha_s$  assumed therein. At this time I think it must be characterized as a nice test of QCD and not really as a measurement of  $\alpha_s$ .

### 2.3 Cross section ratio 630 GeV/1800 GeV

Both CDF[8] and DO[9] have exploited a short period of data taking at reduced center of mass energy towards the end of Run 1, to measure the ratio of scale invariant jet cross sections,  $E_T^3 d^2\sigma/dE_T d\eta$  at  $\sqrt{s} = 1800$  and 630 GeV. This ratio, as a function of scaled jet transverse energy  $x_T = 2E_T/\sqrt{s}$ , is shown in Fig.11. The ratio is expected to be a rather straightforward quantity to measure and to calculate — it would be exactly 1 in the pure parton model. Unfortunately the two experiments are not obviously consistent with each other (especially at low  $x_T$ ) nor with NLO QCD (at any  $x_T$ ). At least two explanations have been suggested for the discrepancy. Firstly, different renormalization scales could be used for the theoretical calculations at the two energies. While allowed, this seems unappealing.<sup>2</sup> An alternative explanation is offered by Mangano[10], who notes that a shift of a few GeV in energy between parton and particle level jets would bring the data in line with the prediction. Such

<sup>2</sup>Glover has suggested that such a procedure is in fact natural when a scaling variable like  $x_T$  is used; because  $x_T$  differs by a factor of about three between the two center of mass energies for a given  $E_T$ , a factor of three difference in the renormalization scales is appropriate.

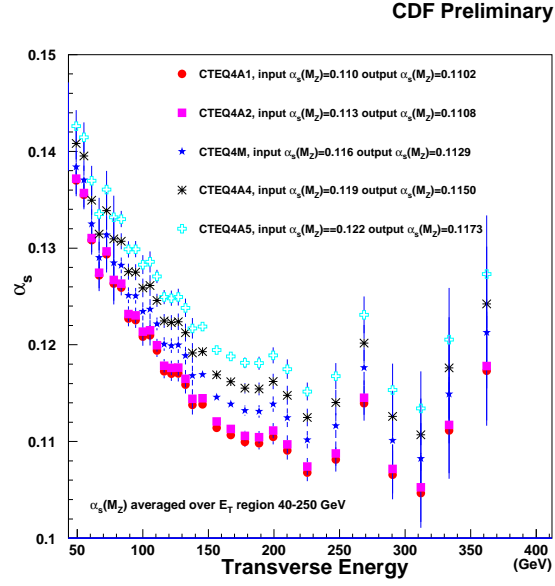


Figure 10: Value of  $\alpha_s$  as a function of scale (jet transverse energy) inferred by CDF from the inclusive jet cross section using the CTEQ4A series of parton distributions[7].

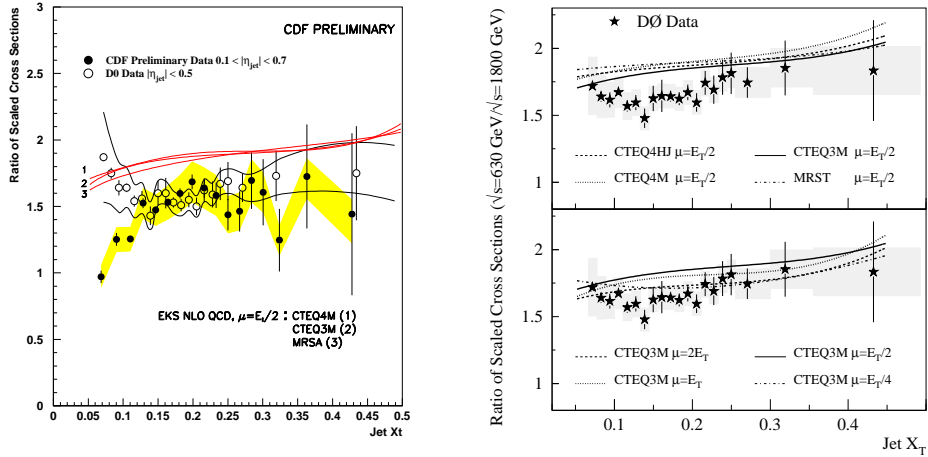


Figure 11: Scaled ratios of jet cross sections at  $\sqrt{s} = 630 \text{ GeV}$  to  $\sqrt{s} = 1800 \text{ GeV}$ , as a function of  $x_T = 2E_T/\sqrt{s}$ , as measured by CDF[8] and DO[9] and as predicted by NLO QCD.

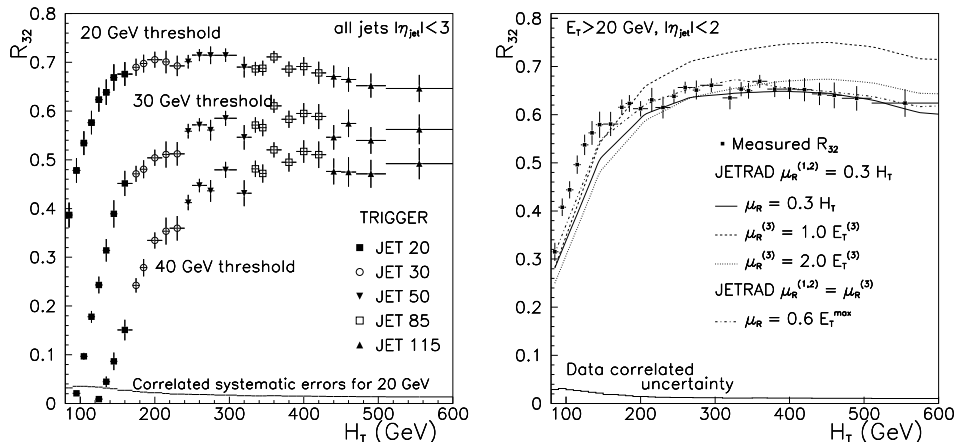


Figure 12: Ratio of events with three or more jets to those with two or more jets,  $R_{32}$ , measured as a function of  $H_T = \Sigma E_T^{\text{jets}}$ , for various jet thresholds (left) and compared with JETRAD (right).[11]

a shift might arise from non-perturbative effects such as losses outside the jet cone, underlying event energy, and intrinsic transverse momentum of the incoming partons; the shifts would likely be jet algorithm-dependent, and the two experiments might even obtain different results depending on how the jet energy scale corrections were done (based on data or Monte Carlo, for example). It seems that more work, both theoretical and experimental, is needed before this question can be resolved.

## 2.4 Ratio of 3-jet/2-jet Events

DO[11] have measured  $R_{32}$ , the ratio of events with  $\geq 3$  jets to those with  $\geq 2$  jets, as a function of  $H_T = \Sigma E_T^{\text{jets}}$ , for various third jet thresholds. This ratio (Fig. 12) is surprisingly large: two thirds of high- $E_T$  jet events have a third jet with  $E_T > 20$  GeV and about half have a third jet above 40 GeV. It is interesting to ask if this ratio can be predicted by QCD. The answer is yes, reasonably well, even by JETRAD (which of course is a leading order calculation of  $R_{32}$ ). DO have also attempted to extract information on the optimal renormalization scale for the emission of the third jet: should it be the same scale as the leading jets, or should the third jet emission be treated as part of a parton shower with an “evolving” scale related to the third jet’s  $E_T$ ? (A specially modified version of JETRAD was used for this study). They find that a scale tied to the first two jets is better than one related to the third jet  $E_T$ . Whether this tells us much about nature or merely about JETRAD I don’t know, but it’s interesting given the widespread use of the parton shower approximation to generate additional jets in HERWIG and PYTHIA.

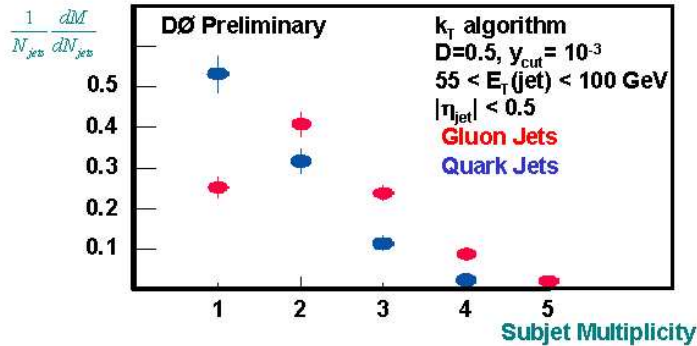


Figure 13: Subject multiplicities measured by DO using a  $k_T$  algorithm to find clusters within jets; distributions for quark and gluon jets are inferred using  $\sqrt{s} = 1800$  GeV and  $\sqrt{s} = 630$  GeV data[12].

## 2.5 Jet Structure and Quark/Gluon Separation

All the results presented so far have used a cone jet finder. By running a  $k_T$  jet finder inside previously identified jets, one can count the number of “subjets” or energy clusters. Doing this (rather than, for example, counting charged tracks) allows the *coarse* jet structure corresponding to the initial, perturbative part of fragmentation to be studied. DO[12] have made such a measurement and, by comparing jets of the same  $E_T$  and  $\eta$  recorded at  $\sqrt{s} = 1800$  and 630 GeV, have inferred the composition of pure quark and gluon jets. The extracted subjet multiplicity  $M$  for the two species is shown in Fig.13. The ratio of  $M - 1$  for the two cases, which might naively be expected to equal the ratio of gluon and quark colour charges, is found to be  $1.91 \pm 0.04$ , compared with  $1.86 \pm 0.04$  from HERWIG. This is very encouraging and might even suggest that we have glimpsed the holy grail of quark-gluon jet separation. The true test, however, remains the use of the subject multiplicity as a discriminant in an analysis like the search for  $t\bar{t} \rightarrow 6$  jets. Such a test will probably have to wait for Run 2.

## 3 Weak Boson production

Next-to-next-to leading order (order  $\alpha \cdot \alpha_s^2$ ) predictions exist for the  $W$  and  $Z$  production cross sections times decay branching ratios into leptons. The experimental values from CDF and DO (Fig. 14) are in excellent agreement with these predictions, both for electrons and muons. In fact, the careful reader will note that the CDF cross sections are a few percent higher than those from DO; this is consistent with the fact that CDF use a luminosity normalization which is 6.2% higher than DO’s (the two

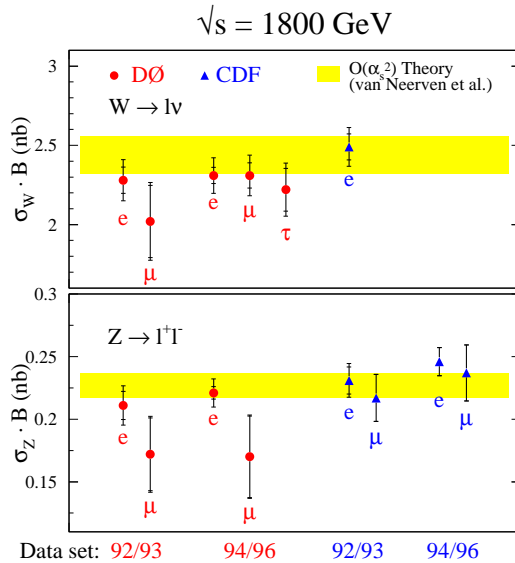


Figure 14: Vector boson production cross sections measured at the Tevatron by CDF and DO, compared to the NNLO QCD prediction.

experiments assume different total  $p\bar{p}$  inelastic cross sections). It is therefore tempting to conclude that the  $W/Z$  cross sections are the better known quantity, and indeed it has been seriously proposed to use  $\sigma_W$  as the absolute luminosity normalization basis in Run 2. Walter Giele’s contribution in these proceedings contains some more discussion of the systematics associated with such an approach.

### 3.1 $Z$ Transverse Momentum

As well as increasing the total cross section, the QCD predictions change the transverse momentum distribution of the produced boson. The most straightforward measurement is for the  $Z$  since it can be directly reconstructed from two decay leptons. Figure 15 show recent DO results on the transverse momentum distribution of the  $Z$  boson[13] compared with a variety of QCD predictions. Clearly the fixed-order NLO QCD is not a good match for the data, while the resummed formalism of Ladinsky and Yuan[14] fits rather well. This approach uses fixed-order QCD at high  $p_T^Z$  matched to a resummation of the large logarithms of  $m_Z^2/p_T^2$  at low  $p_T^Z$ . The resummed calculations always include some nonperturbative parameters that must be extracted from the data, and various authors have used different values for these. This probably accounts for the fact that the resummed calculations of Davies, Webber and Stirling[15], and of Ellis and Veseli[16] (also shown in the figure) do not offer quite as good a description of the data.

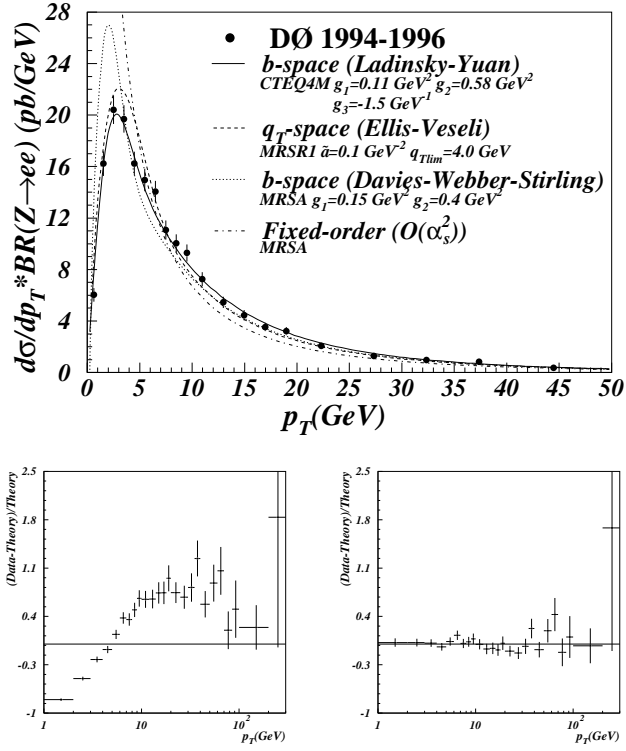


Figure 15: Transverse momentum distribution of the  $Z$ , as measured by DO[13]. The upper plot shows the data and various calculations. The lower left shows the data normalized to the fixed-order QCD prediction and the lower right shows the data normalized to the resummed calculation of Ladinsky and Yuan[14].

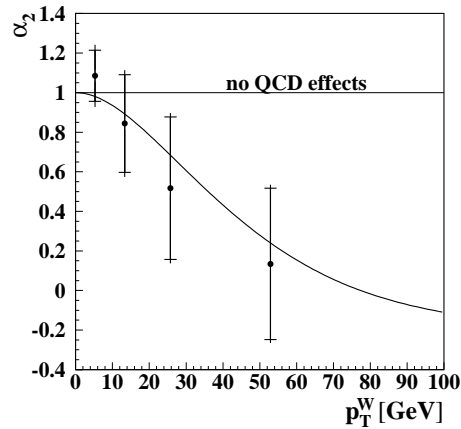


Figure 16: Extracted value [17] of  $\alpha_2$  (the coefficient of  $\cos^2 \theta^*$  in the angular distribution of electrons from  $W$  decay) as a function of  $p_T^W$ . The measurement is in good agreement with QCD.

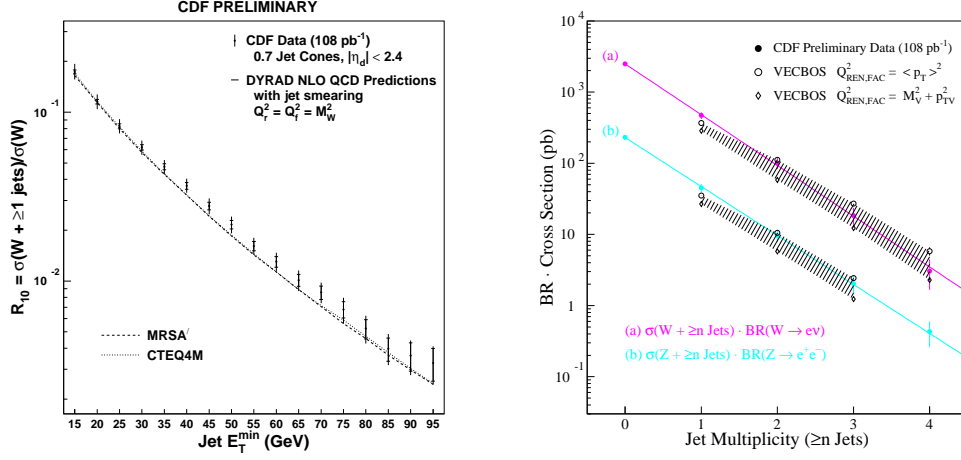


Figure 17: The left hand plot shows the ratio of the  $W +$  (one or more) jets cross section to the inclusive  $W$  cross section at the Tevatron, as measured by CDF[18]. The right hand plot shows the  $W + n$  jets and  $Z + n$  jets cross sections as a function of the number of jets  $n$ .

DO have also observed[17] the effect of QCD corrections in the angular distribution of electrons from  $W$  decay. Figure 16 shows the extracted value of  $\alpha_2$  (the coefficient of  $\cos^2 \theta^*$  in the angular distribution) as a function of  $p_T^W$ . The measurement is in good agreement with QCD.

### 3.2 $W + \text{jets}$

QCD also predicts the number and spectrum of jets produced together with the vector boson. DO used to show a cross section ratio  $(W + 1\text{jet})/(W + 0\text{jet})$  which was badly in disagreement with QCD. This is no longer shown: the data were basically correct, but there was a bug in the way DO extracted the ratio from the DYRAD theory calculation.

Recent CDF measurements of the  $W + \text{jets}$  cross sections[18] agree well with QCD, as shown in Fig. 17. The figure shows the fraction of  $W$ 's with 1 or more jets, compared with the NLO prediction; and the  $W + n$  jets rate, compared with the LO prediction (for a variety of renormalization scales). Alas, it seems that there is little prospect for being able to extract  $\alpha_s$  from these measurements, as had been hoped. This is because the  $W + \text{jet}$  cross section depends on  $\alpha_s$  both in the jet production vertex and in the parton distributions, and these two factors largely cancel in the kinematic range probed at the Tevatron.

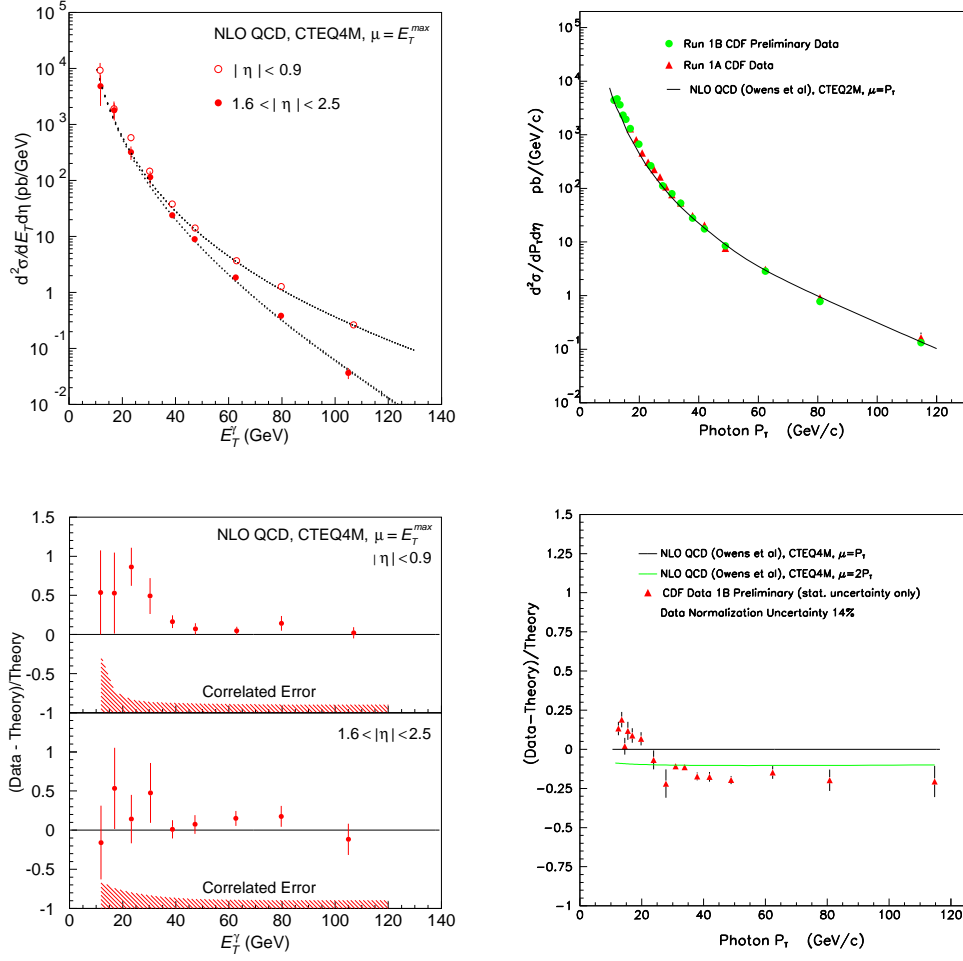


Figure 18: Inclusive isolated direct photon cross sections at the Tevatron; the left hand plots show DO[19] measurements and the right hand plots show the latest CDF results[20] (statistical errors only). All are compared with the NLO QCD prediction of Owens *et al.*[21].

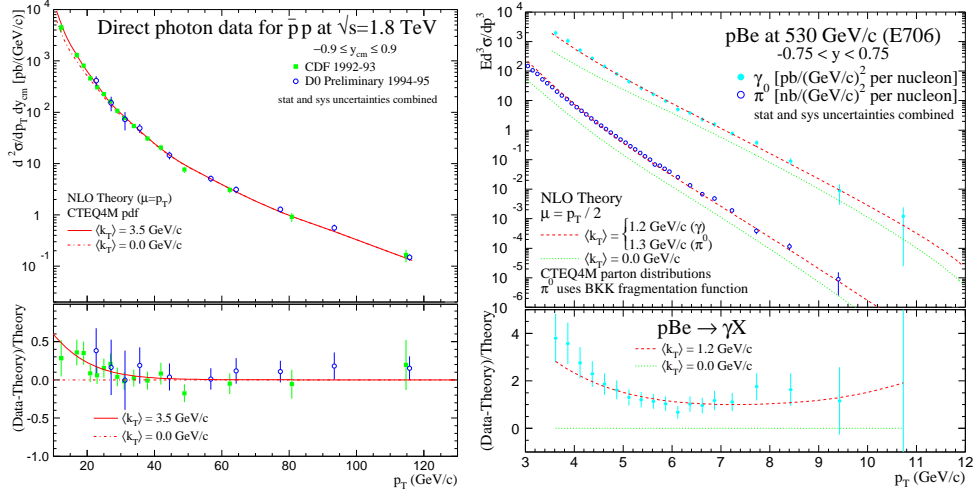


Figure 19: The isolated photon cross section at the Tevatron (left hand plots) showing the improved agreement with QCD if 3.5 GeV of transverse momentum smearing (“ $k_T$ ”) is added to account for soft gluon emission. The right hand plot shows the isolated photon and  $\pi^0$  cross sections measured by E706[23], compared with the NLO QCD prediction with and without 1.2 GeV of additional  $k_T$  smearing.

## 4 Isolated Photon Production

Historically, many authors hoped that measurements of direct (or prompt) photons would provide a clean test of QCD, free from the systematic errors associated with jets, and would help pin down parton distributions. In fact photons have not lived up to this promise — instead they revealed that there may be unaccounted-for effects in QCD cross sections at low  $E_T$ . (Because photons can typically be measured at lower energies than jets, they provide a way of exploring the low- $E_T$  regime). Results from the Tevatron experiments [19][20] are shown in Fig. 18. While the general agreement with the NLO calculation of Owens and collaborators[21] is good, there is a definite tendency for the data to rise above the theory at low transverse energies.

An often-invoked explanation for this effect is that there exists additional transverse momentum smearing of the partonic system due to soft gluon radiation. The magnitude of the smearing, or “ $k_T$ ”, is typically a few GeV (at the Tevatron), motivated in part by the experimentally measured  $p_T$  of the  $\gamma\gamma$  system in diphoton production which peaks around 3 GeV[22]. PYTHIA simulations of photon production also suggest that the most probable transverse momentum of radiated initial state gluons is 2–3 GeV[20]. Inclusion of such  $k_T$  through Gaussian smearing in the calculation gives much better agreement with the data, as shown in Fig. 19. Much larger deviations from QCD are observed in fixed-target experiments such as E706 at Fermilab[23]. Again, Gaussian smearing (with  $k_T \approx 1.2$  GeV in this case) can

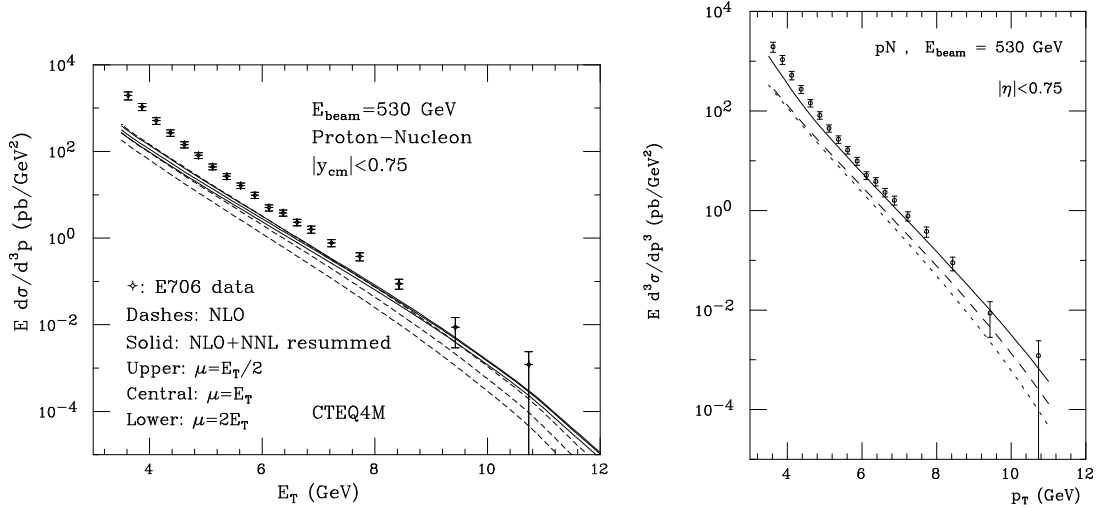


Figure 20: Resummed calculations of isolated photon production compared with the E706 data; left, by Catani *et al.*[25] and right, by Laenen, Sterman and Vogelsang[27].

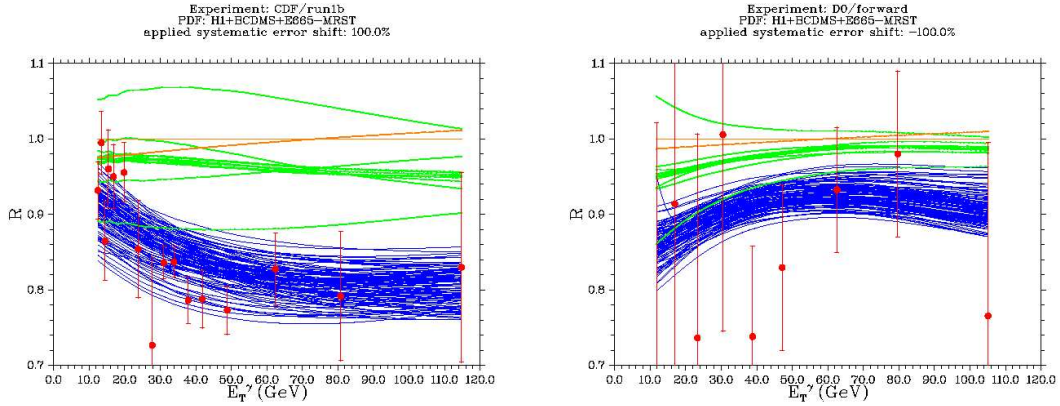


Figure 21: Isolated photon cross sections measured in the central region by CDF (left) and the forward region by DO (right), compared with NLO QCD predictions. The blue curves use an ensemble of PDF's proposed by Giele, Keller and Kosower, derived by fitting to H1, BCDMS and E665 data. The range of predictions gives a measure of the uncertainty on the PDF. The green curves use MRS99 distributions and the orange curves are CTEQ5M and 5L. No additional  $k_T$  smearing is included.

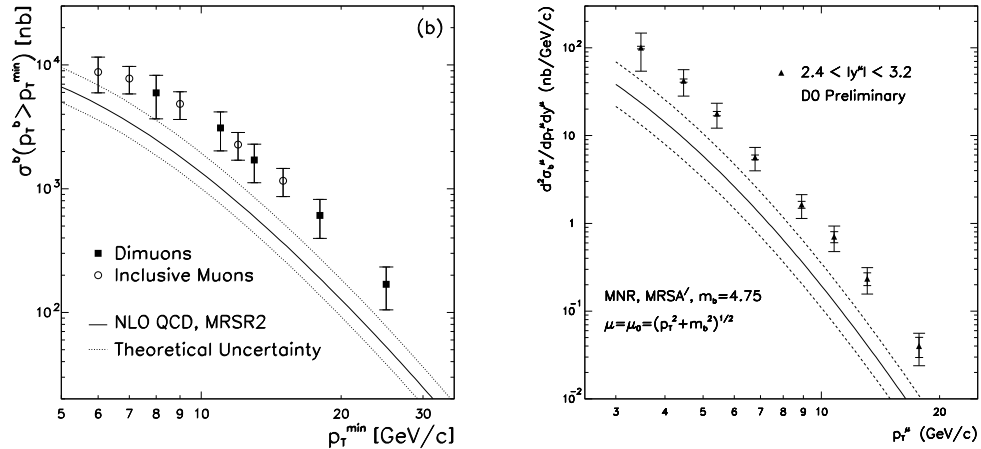


Figure 22: Cross sections for  $b$  production at the Tevatron compared with NLO QCD predictions, as measured by DO[29]; left, central rapidity region, and right, forward.

account for the data, as also shown in the figure.

Unfortunately the predictive power of Gaussian smearing is small: it cannot really tell us what happens to forward photons, or what happens at the LHC, for example. The “right way” to treat soft gluon emission should be through a resummation calculation which works nicely for  $\gamma\gamma$  and  $W/Z$  transverse momentum distributions. Initial attempts did not seem to model the E706 data[25][26], but more recent calculations include additional terms and look more promising[27] (Fig. 20).

A rather different view is expressed by Aurenche and collaborators[24], who find their calculations, *sans*  $k_T$ , to be consistent with all the ISR and fixed-target data with the sole exception of E706. They say, “it does not appear very instructive to hide this problem by introducing an arbitrary parameter fitted to the data at each energy,” by which they mean  $k_T$ .

The latest result in this saga is most interesting. Elsewhere in these proceedings, Walter Giele reports that he is able to obtain good agreement (Fig. 21) between the Tevatron data and QCD, without any  $k_T$ , with a newly derived set of PDF’s that are extracted from DIS data from H1, BCDMS and E665. If correct, this observation could render the whole discussion moot — there would be no discrepancy with QCD here at all, merely another indication that we need to understand parton distribution uncertainties!

In summary, direct photon production has proved extremely interesting and remains quite controversial. The appropriateness of a Gaussian  $k_T$  treatment is still hotly debated, the experiments may not all be consistent, and the latest results merely increase the mystery — is it all just the PDF’s?

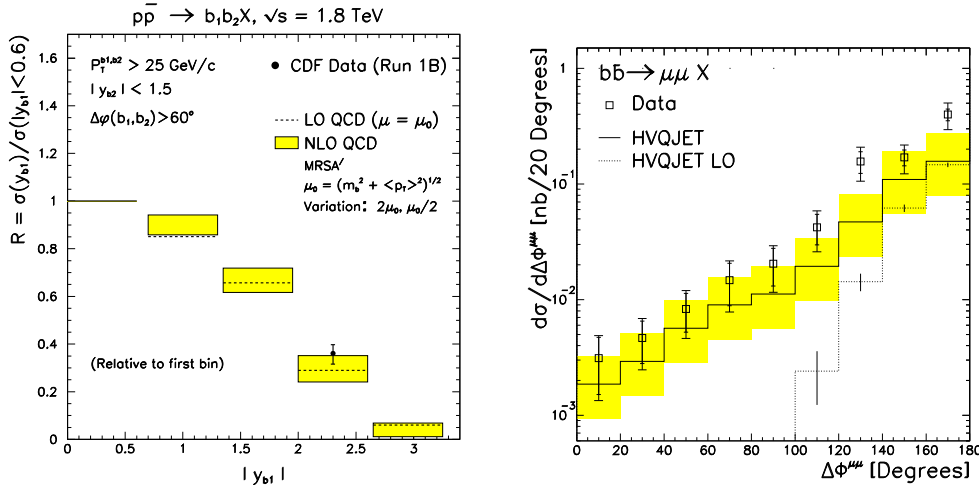


Figure 23: Correlations between  $b$ -jets at the Tevatron compared with NLO QCD predictions; (left) rapidity correlations as measured by CDF (normalized to the first bin), and (right) azimuthal angle correlations as measured by DO.

## 5 Heavy Flavour Production

At the Tevatron, the measured inclusive  $b$ -quark and  $B$ -meson production cross sections continue to lie a factor of about two above the NLO QCD expectation. This is seen by both CDF[28] and DO[29] in the central and forward regions (the difference is perhaps even larger for forward  $b$  production, as seen in Fig. 22). On the other hand, NLO QCD does a good job of predicting the shape of inclusive distributions, and of the correlations between  $b$  quark pairs (Fig. 23), so it seems unlikely that any exotic new production mechanism is responsible for the higher than expected cross section. In passing, it is interesting to note that a similar excess is also seen in  $b$ -production at HERA[32][33] and in  $\gamma\gamma$  collisions at LEP2[31].

Recently, DO have extended these measurements to higher transverse momenta (up to 100 GeV)[30]. The results (Fig.24) are interesting: the measured cross section comes closer to the prediction around  $p_T \sim 50$  GeV and above. It is therefore tempting to compare the shape of  $(Data - Theory) / Theory$  for  $b$ -jets and for photons, as I have done in Fig. 25. The plot compares DO photons, CDF photons (renormalized by 1.33) and DO  $b$ -jets (compared with the highest of the range of QCD predictions). The plot is perhaps quite suggestive that the same explanation may be relevant for photons and  $b$ -jets — whatever that may be!

If the heavy flavour is heavy enough, QCD seems to work rather better. The current state of measured and predicted top cross sections is summarised in Table 1. This includes the latest (revised) CDF measurement. There is an excellent agreement

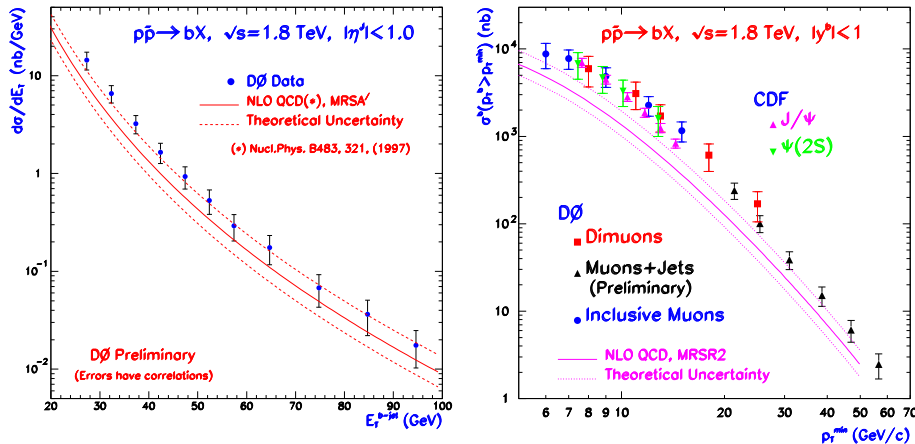


Figure 24: New measurements of high- $p_T$   $b$ -jet production at the Tevatron compared with NLO QCD predictions, as measured by DO[30]; (left) differential cross section as a function of  $E_T^{\text{jet}}$ ; (right) integral cross section as a function of  $p_T^b$ .

Authors	Cross Section (pb)
CDF[34]	$6.5_{-1.4}^{+1.7}$ (at $m_t = 175$ GeV)
DO[35]	$5.9 \pm 1.7$ (at $m_t = 172$ GeV)
Bonciani <i>et al.</i> [36]	$5.0 \pm 1.6$
Berger and Contopanagos[37]	$5.6_{-0.4}^{+0.1}$
Kidonakis[38]	6.3

Table 1: Top production cross sections at the Tevatron, measured and predicted.

between data and theory, though one may note that the most recent (resummation) calculation[38] lies outside the band of uncertainty claimed by earlier authors[37].

## 6 Prospects

What can we look forward to in Run 2 and beyond? Clearly there will be lots more data — the next decade belongs to the hadron colliders. We can also expect improved calculations (NNLO calculations, NLL resummations). There is a lot of work going on towards the goal of correctly treating uncertainties in PDF's, as manifested by Walter Giele's contribution to these proceedings. This is a great step forward, but it does impose significant work on the experiments, who must understand and publish all the errors and their correlations.

We can also look forward to improved jet algorithms. There is a CDF-DO accord

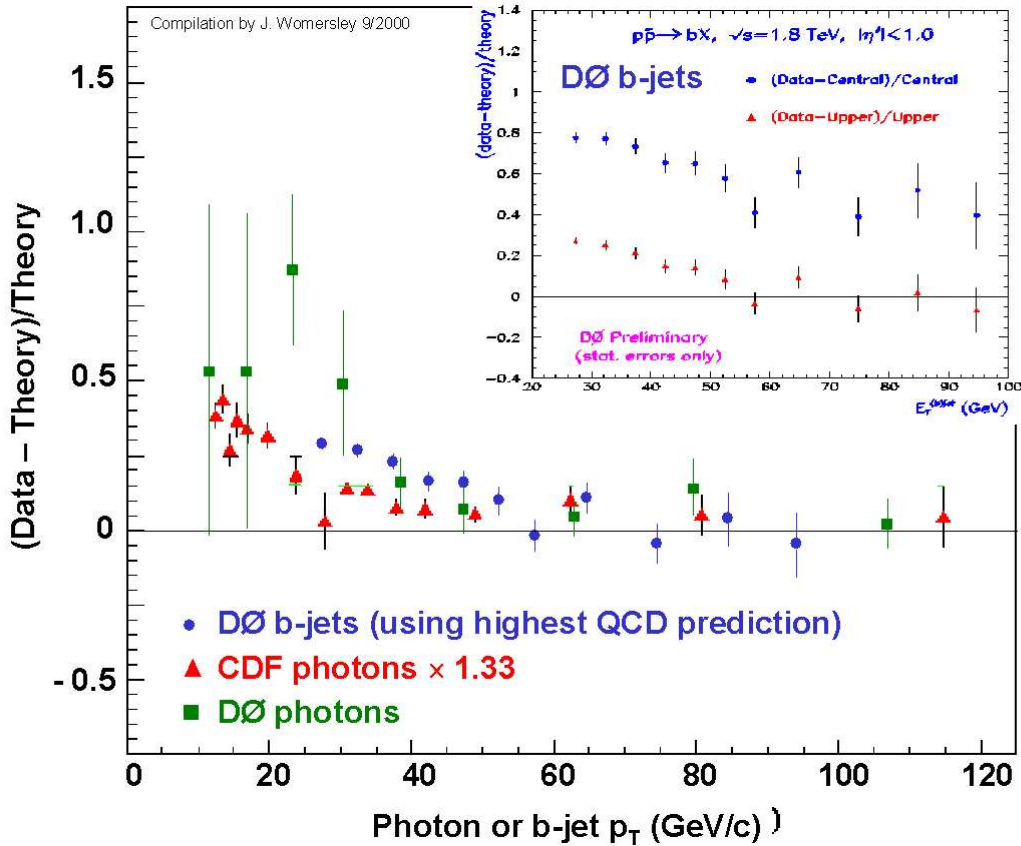


Figure 25: Compilation of  $b$ -jet and isolated photon cross sections compared with QCD.

from the Fermilab Run 2 QCD workshop. The  $k_T$  algorithm will be used from the start, and the experiments have agreed upon one common implementation. They will also try to make the cone algorithm theoretically more acceptable by modifying the choice of seeds (or even through a seedless version).

I would also like to see a theoretical and experimental effort to understand the underlying event, and include it in the predictions. The current approach is to subtract an “underlying event contribution” from the jet energies. This assumes factorization between the hard scattering and the underlying event, and while this is a reasonable approximation it is bound to break down at the GeV level because the hard event and the underlying event are color-connected. Indeed, HERWIG suggests that at the 1–2 GeV level jets pick up or lose energy to the rest of the event depending on the jet algorithm. This is another example of how greater precision demands greater care: approximations and assumptions that used to be “good enough” can no longer be taken for granted. In fact there are very nice new results from CDF on the under-

lying event[39]. Understanding the underlying event would also allow a consistent treatment of double parton scattering.

Finally, one may hope for a consistent approach to hard diffraction processes. High  $E_T$  jets and  $W$  production are hard processes which should be amenable to perturbative calculation, even if the final state is such that one of the nucleons does not break up. We need to break down the walls of the “pomeron ghetto” and stop trying to describe these processes in a language which, in my opinion, does not promote understanding.

## 7 Conclusions

Tevatron QCD measurements have become precision measurements. We are no longer testing QCD; we are testing our ability to make precise calculations within the framework of QCD. The state of the art is NNLO calculations, NLL resummations, and measurement errors at the 5% level. This level of precision demands considerable care both from the experimentalists and the phenomenologists, in understanding jet algorithms, jet calibrations, all the experimental errors and their correlations, and the level of uncertainty in the calculations and in the PDF's.

In general our calculational tools are working well. The open issues generally relate to attempts to push calculations closer to the few-GeV scale ( $b$  production at modest  $p_T$ , perhaps low- $E_T$  photons) and/or to regions where the parton distributions are uncertain (high- $E_T$  jets, and perhaps photons).

## Acknowledgments

I am grateful to Georgia Hamel and Jacqueline Pizzuti at SCIPP for their efficient administration of the conference, and to Howie Haber, Stan Brodsky and the other organizers of RADCOR-2000 for making the program both informative and enjoyable.

## References

- [1] F. Abe *et al.* [CDF Collaboration], Phys. Rev. Lett. **77**, 438 (1996).
- [2] B. Abbott *et al.* [D0 Collaboration], Phys. Rev. Lett. **82**, 2451 (1999).
- [3] J. Womersley, in *Proc. of the 19th Intl. Symp. on Photon and Lepton Interactions at High Energy LP99* ed. J.A. Jaros and M.E. Peskin, eConf **C990809**, 607 (2000) [hep-ex/9912009].

- [4] G. C. Blazey and B. L. Flaugher, *Ann. Rev. Nucl. Part. Sci.* **49**, 633 (1999) [[hep-ex/9903058](http://hep-ex/9903058)].
- [5] B. Abbott *et al.* [D0 Collaboration], [hep-ex/0011036](http://hep-ex/0011036).
- [6] T. Affolder *et al.* [CDF Collaboration], [hep-ex/0012013](http://hep-ex/0012013).
- [7] CDF note 4892, unpublished. These results are available at <http://www-cdf.fnal.gov>.
- [8] C. Mesropian, (for the CDF Collaboration) Fermilab-Conf-99/177-E, in the Proceedings of the 34th Rencontres de Moriond: QCD and Hadronic Interactions, Les Arcs, France, March 1999.
- [9] B. Abbott *et al.* [D0 Collaboration], [hep-ex/0008072](http://hep-ex/0008072).
- [10] M.L. Mangano, in the Proceedings of the International Europhysics Conference on High-Energy Physics (EPS-HEP 99), Tampere, Finland, July 1999.
- [11] B. Abbott *et al.* [D0 Collaboration], [hep-ex/0009012](http://hep-ex/0009012).
- [12] R. Snihur [DO Collaboration], [hep-ex/9907059](http://hep-ex/9907059).
- [13] B. Abbott *et al.* [D0 Collaboration], [hep-ex/9909020](http://hep-ex/9909020).
- [14] G.A. Ladinsky and C.P. Yuan, *Phys. Rev.* **D50**, 4239 (1994).
- [15] C.T. Davies, B.R. Webber and W.J. Stirling, *Nucl. Phys.* **B256**, 413 (1985).
- [16] R.K. Ellis and S. Veseli, *Nucl. Phys.* **B511**, 649 (1998).
- [17] B. Abbott *et al.* [D0 Collaboration], [hep-ex/0009034](http://hep-ex/0009034).
- [18] T. Affolder *et al.* [CDF Collaboration], FERMILAB-PUB-00-196-E; J.R. Dittmann, UMI-99-17363. These results are available at <http://www-cdf.fnal.gov>.
- [19] S. Abachi *et al.* [D0 Collaboration], *Phys. Rev. Lett.* **77**, 5011 (1996) [hep-ex/9603006](http://hep-ex/9603006).
- [20] U. Baur *et al.*, Report of the Working Group on Photon and Weak Boson Production (Workshop on QCD and Weak Boson Physics in Run II, Fermilab, 1999), [hep-ph/0005226](http://hep-ph/0005226).
- [21] H. Baer, J. Ohnemus and J.F. Owens, *Phys. Rev.* **D42**, 61 (1990).
- [22] P. Hanlet [D0 Collaboration], *Nucl. Phys. Proc. Suppl.* **64**, 78 (1998).

- [23] L. Apanasevich *et al.* [Fermilab E706 Collaboration], Phys. Rev. Lett. **81**, 2642 (1998).
- [24] P. Aurenche, M. Fontannaz, J.P. Guillet, B. Kniehl, E. Pilon and M. Werlen, Eur. Phys. J. **C9**, 107 (1999).
- [25] S. Catani, M.L. Mangano, P. Nason, C. Oleari and W. Vogelsang, JHEP **03**, 025 (1999).
- [26] N. Kidonakis and J. F. Owens, Phys. Rev. **D61**, 094004 (2000) [hep-ph/9912388].
- [27] E. Laenen, G. Sterman and W. Vogelsang, hep-ph/0010184.
- [28] F. Abe *et al.* [CDF Collaboration], Phys. Rev. Lett. **71**, 2396 (1993); Phys. Rev. **D53**, 1051 (1996).
- [29] S. Abachi *et al.* [D0 Collaboration], Phys. Rev. Lett. **74**, 3548 (1995); B. Abbott *et al.* [D0 Collaboration], hep-ex/9905024.
- [30] B. Abbott *et al.* [D0 Collaboration], hep-ex/0008021.
- [31] M. Acciarri *et al.* [L3 Collaboration], hep-ex/0011070.
- [32] C. Adloff *et al.* [H1 Collaboration], Phys. Lett.**B 467**, 156 (1999).
- [33] J. Breitweg *et al.* [ZEUS Collaboration], hep-ex/0011081.
- [34] F. Abe *et al.* [CDF collaboratipn], Phys. Rev. Lett. 82, 2808(E) (1999).
- [35] B. Abbott *et al.* [D0 Collaboration], Phys. Rev. **D60**, 012001 (1999).
- [36] R. Bonciani, S. Catani, M.L. Mangano and P. Nason, Nucl. Phys. **B529**, 424 (1998).
- [37] E.L. Berger and H. Contopanagos, Phys. Rev. **D57**, 253 (1998).
- [38] N. Kidonakis, hep-ph/0010002.
- [39] K. Ellis *et al.* Report of the QCD Tools Working Group (Workshop on QCD and Weak Boson Physics in Run II, Fermilab, 1999), hep-ph/0011122.

# Conformal Expansions: A Template for QCD Predictions

JOHAN RATHSMAN

*TH Division, CERN, CH-1211 Geneva 23, Switzerland*

The use of conformal expansions for predictions in quantum chromodynamics is discussed as a way to avoid renormalization scheme and scale ambiguities, as well as factorial growth of perturbative coefficients due to renormalons. Special emphasis is given to the properties of an assumed skeleton expansion and its relation to the Banks-Zaks expansion. The relation of BLM scale-setting to the skeleton expansion is also discussed and new criteria for the applicability of BLM scale-setting are presented.

Presented at the

5th International Symposium on Radiative Corrections  
(RADCOR-2000)

Carmel CA, USA, 11–15 September, 2000

# 1 Introduction

The apparent freedom in choosing the renormalisation scale and scheme for perturbative calculations of observables in quantum chromodynamics (QCD) introduces theoretical uncertainties which, if taken literally, prohibit absolute predictions beyond a qualitative level. The renormalisation scheme dependence can be solved by using a fixed reference scheme or, equivalently, by relating measurements of different observables to each other. The  $\overline{\text{MS}}$  scheme is the simplest choice from a calculational point of view but the question then arises if there exists a preferred scheme which is optimal from a physics point of view. A closely related question is how to choose the renormalisation scale which is important since most QCD observables are only known to next-to-leading order (NLO) where the renormalisation scale dependence is still sizable.

Another problem with perturbative QCD predictions is that the series is in fact asymptotic, *i.e.* after a given order the higher order contributions start to increase and make the series divergent. The most prominent source for this asymptotic behaviour is due to so-called renormalons which make the higher order coefficients grow factorially [1].

This talk presents an alternative approach which avoids, or at least minimizes, the problems outlined above by using conformal expansions and the closely related skeleton expansion. The presentation is mainly based on [2] which also contains a complete list of references. The relation between the skeleton expansion and the Banks-Zaks expansion [3], as well as the BLM scale-setting method by Brodsky, Lepage, and Mackenzie [4] and its generalizations [5,6,7,8], is also discussed.

## 2 Conformal relations

For definiteness and simplicity the discussion will be limited to single-scale space-like observables in massless QCD, but the approach can also be generalised to time-like and multi-scale observables. The perturbative expansion for such a single-scale observable can be written as,

$$R(Q^2) = R_{\text{QPM}}(Q^2) + R_0(Q^2) \frac{\alpha_s(\mu^2)}{\pi} + R_1(Q^2, \mu^2) \frac{\alpha_s^2(\mu^2)}{\pi^2} + R_2(Q^2, \mu^2, \beta_2) \frac{\alpha_s^3(\mu^2)}{\pi^3} + \dots,$$

where  $Q^2 = -q^2$  is the (space-like) physical scale,  $\mu^2$  is the renormalisation scale, and  $\beta_2$  is the next-to-next-to-leading order coefficient in the renormalisation group equation for the coupling,

$$\frac{da(\mu^2)}{d \log(\mu^2)} = -\beta_0 a^2(\mu^2) - \beta_1 a^3(\mu^2) - \beta_2 a^4(\mu^2) + \dots$$

where  $a = \alpha_s/\pi$ .

The truncation of the perturbative expansion at order  $N$  introduces a renormalisation scale and scheme uncertainty of order  $a^{N+1}$ . In addition the perturbative coefficients  $R_n$  will asymptotically grow factorially due to renormalons,  $R_n \sim n!\beta_0^n$ . This should be contrasted with the situation in the conformal (scale-invariant) limit where  $da/d\log(\mu^2) = 0$ . In this case there is no scale-ambiguity, and the coefficients  $R_n$  are free of factorial growth due to renormalons. The only remaining problem is the scheme uncertainty which can be circumvented by relating observables to each other instead of trying to make absolute predictions.

Before continuing it is useful to recall the concept of an effective charge [9] which collects all perturbative corrections to an observable. An observable  $R(Q^2)$  can then be written in terms of the effective charge  $a_R(Q^2)$  as,

$$R(Q^2) = R_{\text{QPM}}(Q^2) + R_0(Q^2)a_R(Q^2)$$

where

$$a_R(Q^2) = a(\mu^2) + r_1(Q^2, \mu^2)a^2(\mu^2) + r_2(Q^2, \mu^2, \beta_2)a^3(\mu^2) + \dots$$

and the perturbative coefficients  $r_i = R_i/R_0$ .

The most celebrated example of a conformal relation between observables is the Crewther relation [10,11,7] between the Adler D-function ( $a_D$ ) and the polarized Bjorken sum-rule for deep inelastic scattering ( $a_{g_1}$ ),

$$(1 + a_D)(1 - a_{g_1}) = 1.$$

Thus, the Crewther relation is simply a geometric series to all orders and there is no growth of higher order coefficients. The effective charges  $a_D$  and  $a_{g_1}$ , which appear in the relation, are defined by,

$$D(Q^2) = Q^2 \frac{d\Pi(Q^2)}{dQ^2} \equiv N_C \sum_f e_f^2 [1 + a_D(Q^2)]$$

$$\int_0^1 [g_1^p(x, Q^2) - g_1^n(x, Q^2)] dx \equiv \frac{g_A}{6g_V} [1 - a_{g_1}(Q^2)]$$

where  $\Pi(Q^2)$  is the hadronic correction to the vacuum polarisation of the photon, the spacelike continuation of  $R_{e^+e^-}(s)$ .

In general, conformal relations between two arbitrary observables  $A$  and  $B$  can be written as,

$$a_A = \sum_n c_n^{AB} a_B^n$$

where, as is evident, the conformal coefficients  $c_n^{AB}$  depend on which two observables that are related. Of course, in real life the QCD coupling is scale-dependent. Even so, the notion of conformal coefficients is still useful as will be shown below. The

main advantage is that by identifying the conformal part of the ordinary perturbative coefficients it is possible to treat all the running coupling effects separately and thus keeping the coefficients free from factorial growth due to renormalons which are instead resummed in the running of the coupling.

### 3 The skeleton expansion

The skeleton expansion [12] organizes the perturbative series in terms of contributions to fundamental skeleton graphs. A skeleton graph is defined by the requirement that the fundamental vertices and propagators contain no substructure. One example of an ordinary Feynman diagram and the corresponding skeleton graph is shown in Fig. 1.

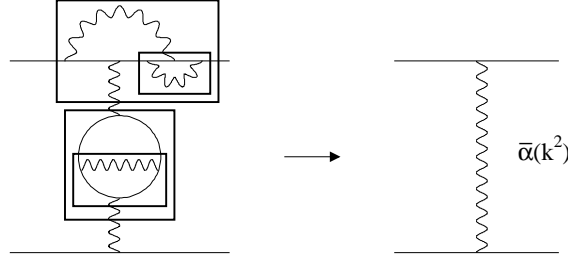


Figure 1: Example of an ordinary Feynman diagram (left) and the corresponding skeleton graph (right) in QED.

In QED, the skeleton expansion is straight-forward to construct thanks to the basic Ward identity,  $Z_1 = Z_2$ , from which it follows that charge renormalisation is given by photon propagator renormalisation ( $Z_3$ ). The coupling  $\bar{\alpha}$  that appears in the skeleton expansion is the Gell-Mann Low coupling which resums the Dyson series of the one-particle irreducible photon self-energy  $\Pi$ ,

$$\bar{\alpha}(Q^2) = \frac{\alpha_0}{1 - \Pi(Q^2)}.$$

The radiative corrections to the one-photon exchange skeleton graph, such as illustrated in Fig. 1, can then be written as an integral over the running coupling,

$$\int \bar{\alpha}(k^2) \phi_0 \left( \frac{k^2}{Q^2} \right) \frac{dk^2}{k^2}$$

where  $\phi_0$  is a momentum distribution function which has been normalised to 1 for convenience. (In the above example  $\phi_0 \left( \frac{k^2}{Q^2} \right) = \delta(k^2 - Q^2)$ .)

Adding the contributions from one-, two-, three-photon exchange etc., an effective charge can be written as

$$\begin{aligned}
a_R(Q^2) &= \int \bar{a}(k^2) \phi_0 \left( \frac{k^2}{Q^2} \right) \frac{dk^2}{k^2} + \bar{c}_1 \int \bar{a}(k_1^2) \bar{a}(k_2^2) \phi_1 \left( \frac{k_1^2}{Q^2}, \frac{k_2^2}{Q^2} \right) \frac{dk_1^2}{k_1^2} \frac{dk_2^2}{k_2^2} \\
&+ \bar{c}_2 \int \bar{a}(k_1^2) \bar{a}(k_2^2) \bar{a}(k_3^2) \phi_2 \left( \frac{k_1^2}{Q^2}, \frac{k_2^2}{Q^2}, \frac{k_3^2}{Q^2} \right) \frac{dk_1^2}{k_1^2} \frac{dk_2^2}{k_2^2} \frac{dk_3^2}{k_3^2} + \dots, \quad (1)
\end{aligned}$$

where  $\phi_i$  are the momentum distribution functions (normalised to 1) and the  $\bar{c}_i$  are the conformal coefficients in the skeleton scheme. For simplicity the above expression has been written including just one skeleton at each order but in general there can be several different skeletons which contribute at the same order. For comparison, the conformal theory gives  $a_R(Q^2) = \bar{a} + \bar{c}_1 \bar{a}^2 + \bar{c}_2 \bar{a}^3 + \dots$ .

Another important property of the skeleton expansion is that each term in the expansion is renormalisation scheme and scale-invariant by itself. In addition the skeleton coupling is gauge-invariant. The skeleton expansion thus provides an alternative way of writing the perturbative series for an observable in which each term is given by one or several integrals over the running coupling. One complication of the skeleton expansion is that in general one needs a diagrammatic construction to identify the different skeletons. However, at low orders this requirement can be bypassed.

In QCD, the existence of an all-order skeleton expansion has so far not been proved. The basic complication arises from the gluon self-interactions and the related difference between gluon-propagator and charge renormalisation. Nevertheless it is reasonable to assume that something similar to the skeleton expansion in QED can also be constructed for QCD. In fact, the so called pinch technique [13] provides a realisation of the skeleton expansion in QCD at the one-loop level. As an example Fig. 2 illustrates how the three-gluon vertex is divided into a pinch part which contributes to the renormalisation of the effective propagator and a non-pinch part which contributes to renormalisation of the “external” vertex.

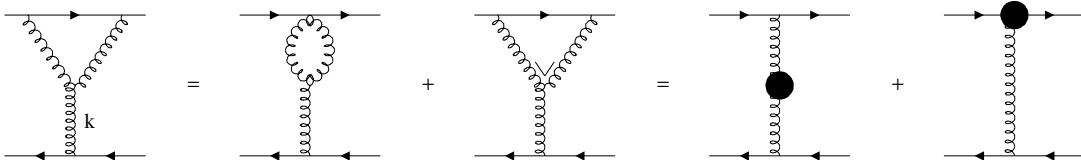


Figure 2: Illustration of the subdivision of the three-gluon vertex into a pinch part and a non-pinch part using the pinch technique

In this way the pinch technique arrives at the following QED-like Ward identities,

$$\begin{aligned} Z_1^{(PT)} &= Z_2^{(PT)} = 1 - \frac{1}{\varepsilon} \frac{C_F}{4} \bar{a} \\ Z_3^{(PT)} &= 1 + \frac{1}{\varepsilon} \left( \frac{11}{12} C_A - \frac{1}{3} T_F N_F \right) \bar{a} = 1 + \frac{1}{\varepsilon} \beta_0 \bar{a} \end{aligned}$$

such that all the one-loop running coupling effects are contained in the effective gluon propagator. The coupling defined by the pinch technique has a simple relation to the  $\overline{\text{MS}}$  scheme,

$$\bar{a}(Q^2) = a_{\overline{\text{MS}}}(\mu^2) + \left[ -\beta_0 \left( \log \frac{Q^2}{\mu^2} - \frac{5}{3} \right) + 1 \right] a_{\overline{\text{MS}}}^2(\mu^2) + \dots$$

Recently there has been progress in extending the pinch-technique to two loops [14] and this may eventually lead to an extension of the skeleton expansion in QCD to two loops as well. Another possibility may be to use light-front quantization of QCD in light-cone gauge [15].

## 4 Identifying conformal coefficients

Given the advantages of the skeleton expansion compared to the standard perturbative expansion, it is instructive to consider the following simplified ansatz for QCD as a starting point for further investigations: assume there is only one skeleton coupling, that there is only one skeleton graph at each order in  $\bar{a}$ , and that the dependence on the number of light flavours ( $N_F$ ) can be used to identify the non-conformal parts of the perturbative coefficients. Given these assumptions the first conformal coefficients in the skeleton expansion can be obtained from the perturbative ones in the following way [2].

The starting point is the skeleton expansion of an effective charge given by Eq. (1). Next the skeleton couplings  $\bar{a}(k^2)$  under the integration sign can be expanded in the coupling  $\bar{a}(Q^2)$  using the solution to the renormalisation group equation,

$$\bar{a}(k^2) = \bar{a}(Q^2) + \beta_0 \log \left( \frac{Q^2}{k^2} \right) \bar{a}^2(Q^2) + \left[ \beta_1 \log \left( \frac{Q^2}{k^2} \right) + \beta_0^2 \log^2 \left( \frac{Q^2}{k^2} \right) \right] \bar{a}^3(Q^2) + \dots$$

Inserting this into Eq. (1) then gives,

$$a_R(Q^2) = \bar{a}(Q^2) + (\bar{c}_1 + \beta_0 \phi_0^{(1)}) \bar{a}^2(Q^2) + (\bar{c}_2 + \bar{c}_1 \beta_0 \phi_1^{(1)} + \beta_1 \phi_0^{(1)} + \beta_0^2 \phi_0^{(2)}) \bar{a}^3(Q^2) + \dots$$

where  $\phi_i^{(n)}$  are log-moments of the momentum distribution functions,

$$\begin{aligned} \phi_0^{(n)} &= \int \log^n \left( \frac{Q^2}{k^2} \right) \phi_0 \left( \frac{k^2}{Q^2} \right) \frac{dk^2}{k^2} \\ \phi_1^{(1)} &= \int \left( \log \frac{Q^2}{k_1^2} + \log \frac{Q^2}{k_2^2} \right) \phi_1 \left( \frac{k_1^2}{Q^2}, \frac{k_2^2}{Q^2} \right) \frac{dk_1^2}{k_1^2} \frac{dk_2^2}{k_2^2}. \end{aligned}$$

This can now be directly compared with the standard perturbative expansion,

$$a_R(Q^2) = \bar{a}(Q^2) + \bar{r}_1 \bar{a}^2(Q^2) + \bar{r}_2 \bar{a}^3(Q^2) + \dots,$$

which gives the relations

$$\begin{aligned} \bar{r}_1 &= \bar{c}_1 + \beta_0 \phi_0^{(1)} \\ \bar{r}_2 &= \bar{c}_2 + \bar{c}_1 \beta_0 \phi_1^{(1)} + \beta_1 \phi_0^{(1)} + \beta_0^2 \phi_0^{(2)}. \end{aligned}$$

Based on the  $N_F$  dependence of the perturbative coefficients  $\bar{r}_i$  it is thus possible to identify in a unique way the conformal coefficients  $\bar{c}_1$  and  $\bar{c}_2$  as well as the log-moments  $\phi_0^{(1)}$ ,  $\phi_0^{(2)}$ , and  $\phi_1^{(1)}$ . (This follows since the coefficients  $\bar{r}_i$  are polynomials in  $N_F$  of order  $i$ .) In fact, given the assumptions made, it is possible to decompose the perturbative coefficients up to order  $\bar{a}^4$  without any additional information. At higher orders the  $N_F$  dependence alone does not provide enough information even with the simplifying assumptions that have been made.

In general there are several ways in which the assumed ansatz can break down. Most notably, at higher orders there are skeletons which are  $N_F$ -dependent by themselves. In contrast to QED where the  $N_F$ -dependent skeletons (such as the light-by-light scattering diagrams) can be easily identified based on the dependence on the external charge there is in general no such simple identification possible in QCD. Another complication is that there may be more than one skeleton at each order. To resolve these two problems one will need an explicit diagrammatic construction of the skeleton expansion. It may also be the case that the skeleton expansion in QCD can only be systematically extended to all orders by having several skeleton couplings. However, even if some of the assumptions that have been made are wrong, it may still be true that the general properties of the ansatz are valid. This includes the property that running-coupling effects can be associated with different skeleton graphs in a renormalisation-group-invariant way, and that the skeleton coefficients are conformal. In practice there is usually no problem in identifying the skeleton structure at next-to-leading order but special care has to be taken as will be discussed below when the application of BLM scale-setting to the thrust-distribution in  $e^+e^-$ -annihilation is re-examined.

## 5 Relation to the Banks-Zaks expansion

As already realised at the time of the discovery of asymptotic freedom, perturbative QCD has an perturbative infrared fixed-point [16] ( $k^2 \rightarrow 0$ ),

$$\frac{da_{\text{FP}}(k^2)}{d \ln k^2} = -\beta_0 a_{\text{FP}}^2(k^2) - \beta_1 a_{\text{FP}}^3(k^2) + \dots = 0$$

in the so called conformal window  $8 < N_F < 16$  since for this range of  $N_F$  the first two terms in the  $\beta$ -function have opposite signs,  $\beta_0 = \frac{11}{4} - \frac{1}{6}N_F > 0$  and  $\beta_1 = \frac{51}{8} - \frac{19}{24}N_F < 0$ .

If the coupling at the fixed point  $a_{\text{FP}}$  is small, such that perturbation theory is still applicable, then it can be written as a so called Banks-Zaks expansion [3] in the parameter  $a_0 = -\beta_0/\beta_1|_{\beta_0=0} = \frac{16}{107}\beta_0$ ,

$$a_{\text{FP}} = a_0 + v_1 a_0^2 + \dots ,$$

where the coefficients  $v_i$  can be calculated from the higher order terms ( $\beta_2$  etc.) in the  $\beta$ -function.

In the same way an arbitrary effective charge  $a_R$  can also be expanded in  $a_0$ . Starting from the ordinary perturbative expansion the coefficients  $r_i$  can be rewritten in terms of  $a_0$  using the polynomial  $N_F$ -dependence,

$$a_R(Q^2) = a(Q^2) + (r_{1,0} + r_{1,1}a_0)a^2(Q^2) + (r_{2,0} + r_{2,1}a_0 + r_{2,2}a_0^2)a^3(Q^2) + \dots .$$

From this it follows that it is also possible to get a relation between the fixed-point value of the effective charge  $a_R^{\text{FP}}$  and the coupling  $a_{\text{FP}}$ . Taking the limit  $Q^2 \rightarrow 0$  (assuming that this is well defined) and inserting  $a_0 = a_{\text{FP}} + u_1 a_{\text{FP}}^2 + \dots$  gives the fixed point relation,

$$a_R^{\text{FP}} = a_{\text{FP}} + r_{1,0}a_{\text{FP}}^2 + (r_{2,0} + r_{1,1})a_{\text{FP}}^3 + \dots .$$

Comparison with the conformal coefficients obtained from the skeleton decomposition of the perturbative coefficients shows that, if  $a_{\text{FP}}$  is identified with the skeleton coupling then, they are indeed the same, *i.e.*  $r_{1,0} = \bar{c}_1$  and  $r_{2,0} + r_{1,1} = \bar{c}_2$  etc. Thus, the conformal coefficients in QCD can also be obtained from the Banks-Zaks expansion by analytically continuing the number of light quark flavours into the conformal window and taking the infrared limit [2].

## 6 Connection to BLM scale-setting

Once the conformal coefficients have been identified one also has to evaluate the corresponding skeleton integrals. For the leading skeleton this can be done using the momentum distribution function calculated in the large  $\beta_0$ -approximation. At the same time the associated renormalon ambiguity indicates the form of the non-perturbative corrections in terms of power-corrections. The combination gives a framework for analysing the renormalon resummation and the non-perturbative corrections together [17,18]. An alternative is to approximate the skeleton integrals by using BLM scale-setting [4,5] as will be discussed below.

The starting point is the skeleton expansion of the effective charge in question where each integral is evaluated using the mean value theorem (MVT) in the following way,

$$\begin{aligned}
a_R(Q^2) &= \int \bar{a}(\ell^2) \phi_0 \left( \frac{\ell^2}{Q^2} \right) \frac{d\ell^2}{\ell^2} + \bar{c}_1 \int \bar{a}(\ell_1^2) \bar{a}(\ell_2^2) \phi_1 \left( \frac{\ell_1^2}{Q^2}, \frac{\ell_2^2}{Q^2} \right) \frac{d\ell_1^2}{\ell_1^2} \frac{d\ell_2^2}{\ell_2^2} \\
&+ \bar{c}_2 \int \bar{a}(\ell_1^2) \bar{a}(\ell_2^2) \bar{a}(\ell_3^2) \phi_2 \left( \frac{\ell_1^2}{Q^2}, \frac{\ell_2^2}{Q^2}, \frac{\ell_3^2}{Q^2} \right) \frac{d\ell_1^2}{\ell_1^2} \frac{d\ell_2^2}{\ell_2^2} \frac{d\ell_3^2}{\ell_3^2} + \dots \\
(\text{MVT}) &\equiv \bar{a}(k_0^2) + \bar{c}_1 \bar{a}^2(k_1^2) + \bar{c}_2 \bar{a}^3(k_2^2) + \dots
\end{aligned}$$

The ‘‘BLM’’ scales  $k_0, k_1, k_2$ , etc. are uniquely determined by requiring a one-to-one correspondence between the skeleton integrals and the terms in the ‘‘BLM’’ series [2]. In other words  $k_0$  depends only on  $\phi_0$ ,  $k_1$  on  $\phi_1$ , and so on. Thus there is no ambiguity in determining the scales as is the case for commensurate scale relations [6,7]. Expanding the couplings  $\bar{a}(k^2)$  in terms of  $\bar{a}(Q^2)$  under the integration sign the ‘‘BLM’’ scales are obtained as a perturbative series in the skeleton coupling with the coefficients given in terms of the moments of the distribution functions,

$$\begin{aligned}
\ln \frac{Q^2}{k_0^2} &= \phi_0^{(1)} + \left[ \phi_0^{(2)} - \left( \phi_0^{(1)} \right)^2 \right] \beta_0 \bar{a}(k_0^2) + \dots, \\
&\quad \text{mean} \qquad \qquad \text{variance} \\
\ln \frac{Q^2}{k_1^2} &= \frac{1}{2} \phi_1^{(1)} + \dots.
\end{aligned}$$

It is important to realize that this provides a systematic improvement of the original BLM-scale,  $k_{0,\text{BLM}}^2 = Q^2 \exp(-\phi_0^{(1)})$ . In the lowest order approximation the scale  $k_0$  is simply given by the mean of the momentum distribution as indicated above. By going to higher orders one then takes into account the variance of the distribution and so on. This corresponds to performing the skeleton integral with successively improved approximations to  $\phi_0$ .

Given the conformal expansions of two observables in the skeleton scheme it is also possible to eliminate the skeleton scheme and get a direct relation between the two observables – a so called commensurate scale relation (CSR). From renormalisation group transitivity it follows that the coefficients in the commensurate scale relation are also conformal and thus free of factorial growth due to renormalons. However, there is no clear interpretation of the scales that appear in the CSRs, and in addition there is no unique scale setting procedure as has been already mentioned.

## 7 Re-examining BLM scale-setting for thrust

The new insights gained from the relation between the skeleton expansion and BLM scale-setting makes it interesting to re-examine BLM scale-setting for event

shape observables in  $e^+e^-$  annihilation [19]. In the following the thrust distribution will be considered as a concrete example but general criteria for the applicability of BLM scale-setting will also be given.

Thrust is an event shape observable defined by,

$$T = \max_{\vec{n}_T} \frac{\sum_i \vec{n}_T \cdot \vec{p}_i}{\sum_i |\vec{p}_i|}$$

where the sum runs over all particles in the final state. The thrust-axis  $\vec{n}_T$  is varied until the maximal value for  $T$  is obtained. An event with two narrow back-to-back jets corresponds to  $T = 1$  whereas the minimal thrust value  $T = 0.5$  is obtained for an event with isotropic distribution of particles as illustrated in Fig. 3.

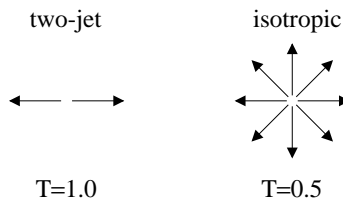


Figure 3: The values of thrust for an event with two narrow back-to-back jets (left) and an event with isotropic distribution of particles (right).

In the quark parton model the thrust distribution is a delta-function at  $T = 1$ . The leading order QCD-corrections have been calculated analytically [20] whereas the next-to-leading order QCD-corrections have only been calculated numerically [21,22]. From the definition of thrust one expects that at leading order there is only one skeleton which contributes and that all the  $N_F$ -dependence at next-to-leading order is from running coupling effects. Thus BLM scale-setting should be straight forward. There is however one possible complication, namely the non-inclusiveness of the definition. The easiest way to see this is that at leading order thrust can have values in the range  $2/3 < T < 1$  whereas at next-to-leading order the range is given by  $1/\sqrt{3} < T < 1$ . Thus, if the next-to-leading order  $N_F$ -dependence is non-zero for  $1/\sqrt{3} < T < 2/3$  then this cannot be attributed to the leading skeleton. However, as will be shown below the problems for the case of thrust are minimal.

At next-to-leading order the BLM series for the thrust-distribution can be written as,

$$\frac{1}{\sigma} \frac{d\sigma^{\text{BLM}}}{dT}(s, T) = \delta(1 - T) + R_0(T) \bar{a}(k_{0,\text{BLM}}^2(s, T)) + \bar{R}_1(T) \bar{a}^2(k_{0,\text{BLM}}^2(s, T)), \quad (2)$$

where the skeleton coupling has been identified with the pinch technique coupling,  $\bar{R}_1(T)$  is the conformal coefficient in the pinch scheme, and the BLM-scale  $k_{0,\text{BLM}}^2$  is

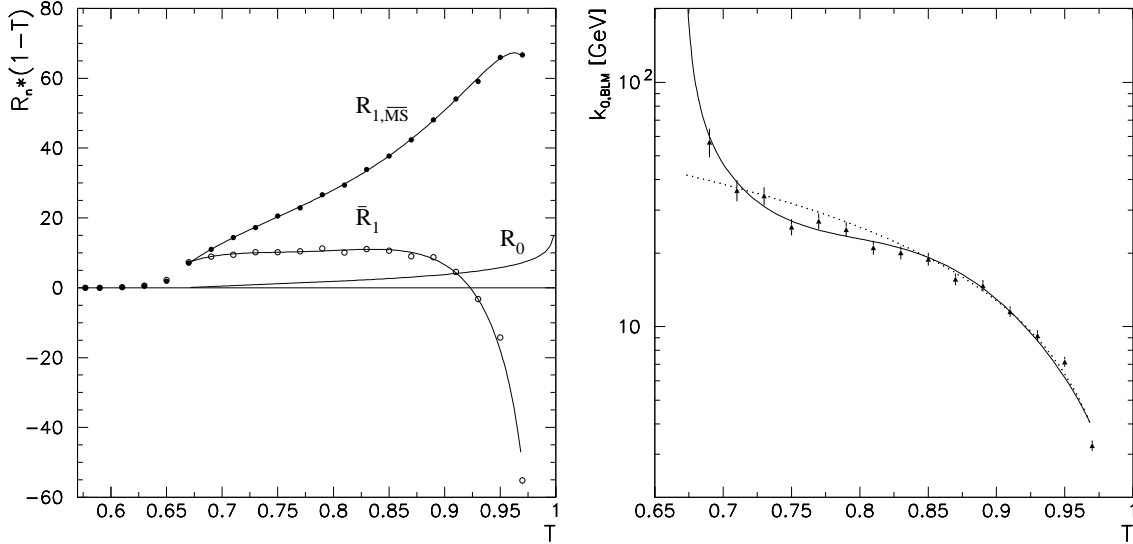


Figure 4: (a) The next-to-leading order conformal coefficient  $\bar{R}_1$  compared to the standard  $\overline{\text{MS}}$  coefficient  $R_{1,\overline{\text{MS}}}(\mu^2 = s, N_F = 5)$  and the leading order (scheme-invariant) coefficient  $R_0$ . (b) The BLM-scale for  $\sqrt{s} = M_Z$ . For both figures the points show the numerical values that have been calculated and the lines are fits to these points taking into account the known logarithmic terms. In (b) the dotted line show the approximation  $k_{0,\text{BLM}} \simeq 1.4(1-T)\sqrt{s}$ .

used to approximate the unknown scale  $k_1^2$  which should appear in the  $\bar{R}_1(T)$ -term. It is important to realize that the BLM-scale  $k_{0,\text{BLM}}^2(s, T)$  is a function of both kinematic variables,  $s$  and  $T$ . In addition the BLM scale is undefined for  $T < 2/3$  where  $R_0$  vanishes.

The expansion given above should be compared with the standard  $\overline{\text{MS}}$  expansion using  $\mu^2 = s$ ,

$$\frac{1}{\sigma} \frac{d\sigma^{\overline{\text{MS}}}}{dT}(s, T) = \delta(1-T) + R_0(T)a_{\overline{\text{MS}}}(s) + R_{1,\overline{\text{MS}}}(\mu^2 = s, N_F, T)a_{\overline{\text{MS}}}^2(s).$$

The leading order coefficient  $R_0$  is scheme-invariant and thus the same in both expansions. However, the next-to-leading order coefficient  $R_1$  is very different in the two cases as is illustrated in Fig. 4 which shows the conformal coefficient  $\bar{R}_1$  compared to the standard  $\overline{\text{MS}}$  coefficient  $R_{1,\overline{\text{MS}}}(\mu^2 = s, N_F = 5)$  and the leading order coefficient  $R_0$ . The coefficients have been calculated numerically using the Beowulf program [22] which is shown as points in the figures. The lines are fits to this points taking into account the know logarithmic parts of the coefficients [25].

From the figure it is clear that the next-to-leading order coefficient is large compared to the leading order one in both cases. However, the conformal coefficient is more stable over a large range of  $T$  (when multiplied with  $(1-T)$ ) except for  $T \rightarrow 1$

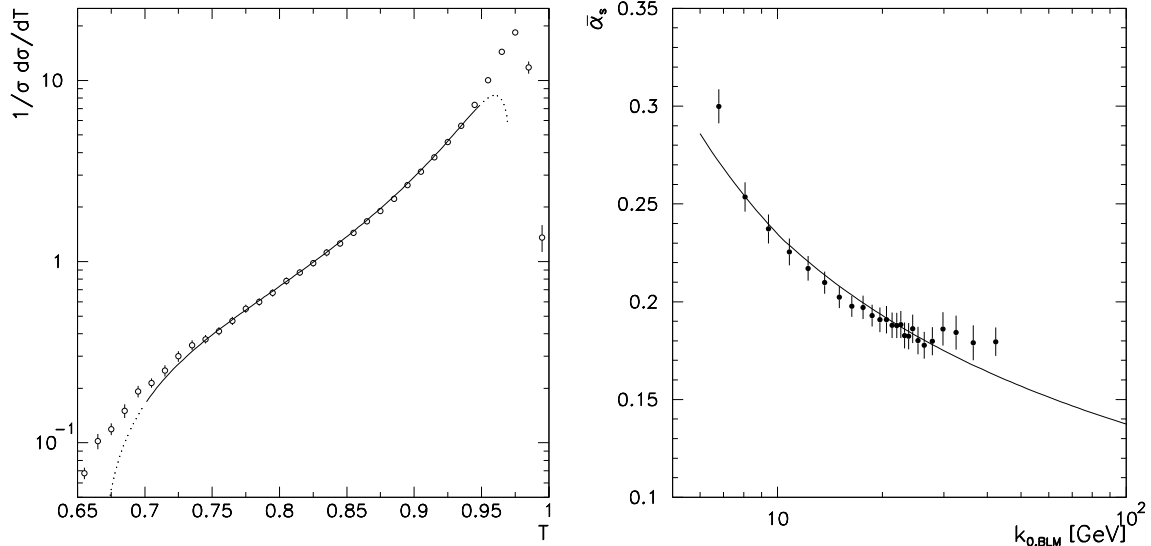


Figure 5: (a) Fit to OPAL data using the fixed order BLM series. The full line corresponds to the range fitted ( $0.7 < T < 0.95$ ). (b) Value of running coupling  $\bar{\alpha}_s$  extracted from OPAL data in the range  $0.7 < T < 0.95$  at the corresponding BLM-scale.

where it becomes negative. This is the Sudakov region which can only be properly treated by resumming all singular terms in the Sudakov form-factor. Another important feature which is clear from the figure is that the non-conformal part of  $R_1$  more or less vanishes for  $T < 2/3$ , which is a good indication that the  $N_F$  dependence can indeed be used to separate the conformal and non-conformal parts and that the problems with non-inclusiveness are only minor (see also [23,18,24]). This property is different for other event shape observables depending on how they are defined. For example, oblateness is defined as the difference between an observable that starts at order  $\alpha_s$  and one that starts at order  $\alpha_s^2$ . As a consequence there are  $N_F$  dependent contributions to the next-to-leading term which do not come from the leading skeleton. This could also explain why BLM scale-setting seems to fail for some event shape observables [19].

Fig. 4 also shows the resulting BLM-scale  $k_{0,\text{BLM}}(s, T)$  for the case  $\sqrt{s} = M_Z$ . From the figure it is clear that the scale vanishes as  $T \rightarrow 1$  which is reasonable since the available phase-space for gluon emission vanishes in this limit. For comparison the figure also shows the approximation  $k_{0,\text{BLM}} \simeq 1.4(1 - T)\sqrt{s}$  which gives an overall good description of the  $T$ -dependence. The scale can also be understood physically as the transverse momentum which approximately scales as  $(1 - T)\sqrt{s}$  for a three-jet configuration with one of the jets being much less energetic than the other two, *i.e.* in the soft limit. For  $T \rightarrow 2/3$  the BLM-scale grows rapidly since the  $R_0 \rightarrow 0$  but even at  $T = 0.69$  (the point with the smallest  $T$ -value shown in the figure) the BLM-scale

is still smaller than  $\sqrt{s}$  which should be true in a physical scheme following from the mean value theorem.

For illustration, the fixed order BLM expression for the thrust distribution given by Eq. (2) has been fitted to data from the OPAL collaboration [26] at  $\sqrt{s} = M_Z$  in the range  $0.70 < T < 0.95$  using a two-loop running coupling. The result of the fit, which is shown together with the data in Fig. 5, corresponds to the value  $\alpha_{\overline{\text{MS}}}(M_Z^2) = 0.117$ . (To translate the fit into a value for  $\alpha_{\overline{\text{MS}}}(M_Z^2)$  the commensurate scale relation,  $\bar{a}(e^{5/3}M_Z^2) = a_{\overline{\text{MS}}}(M_Z^2) + a_{\overline{\text{MS}}}^2(M_Z^2)$ , was used.) For comparison, using the fixed order  $\overline{\text{MS}}$  expression gives  $\alpha_{\overline{\text{MS}}}(M_Z^2) = 0.143$ . This illustrates the importance of taking running coupling effects into account. However, it should be kept in mind that a complete analysis should also include the Sudakov form-factor and non-perturbative effects.

It is also possible to see the running of the coupling  $\bar{\alpha}_s$  as a function of the BLM-scale  $k_{0,\text{BLM}}$  directly from the data. For each data point Eq. (2) is a simple second order equation which can be solved for  $\bar{a} = \bar{\alpha}_s/\pi$ . The resulting values of  $\bar{\alpha}_s$  obtained in this way are shown in Fig. 5 as a function of the corresponding BLM-scales. (The figure only shows the points that were used in the fit. For larger values of  $T$  the next-to-leading order coefficient  $\bar{R}_1$  is negative and for smaller values of  $T$  the next-to-leading order correction is larger than 100%.) Thus, even though the experiment is done at a fixed energy, it is still possible to observe the running of the coupling.

## 8 Conclusions

The standard perturbative expansion of observables in QCD is plagued by renormalisation scheme and scale ambiguities as well as higher order coefficients which grow factorially due to renormalons. In this talk I have presented an alternative approach which avoids, or at least minimizes, these problems by using conformal expansions, especially the skeleton expansion.

In contrast to the ordinary perturbative expansion the skeleton expansion is free of renormalisation scheme and scale ambiguities and the coefficients are free of factorial growth due to renormalons. Presently the pinch technique provides a realization of the skeleton expansion in QCD at next-to-leading order but it is not known whether an all-order expansion exists or not. Even so, the skeleton expansion has important phenomenological consequences.

The leading skeleton integral makes it possible to include non-perturbative effects in a consistent way which takes into account the arbitrariness of the definition of perturbation theory. The renormalon ambiguities which appear in the evaluation of the leading skeleton integral can be used to parametrize the non-perturbative contributions in the form of power-corrections.

By making a simple ansatz for the skeleton expansion in QCD the first steps in

making a more systematic study of its properties have been taken [2]. One result of this study is that the conformal coefficients coincide with the ones obtained in case QCD has a perturbative infrared fixed-point (the Banks-Zaks expansion).

The skeleton integrals which appear in the skeleton expansion can also be approximated by the BLM-scale setting method and its generalisations. Requiring a one-to-one correspondence between the BLM-scales and the skeleton integrals gives a unique prescription for setting the scales [2] in contrast to the situation for commensurate scale relations. The connection between the skeleton expansion and BLM scale-setting also gives new criteria for the applicability of the latter.

## Acknowledgments

I would like to thank Stan Brodsky and Einan Gardi for helpful comments on the manuscript. I would also like to thank the organizers for financial support and for organizing such an inspiring meeting.

## References

- [1] G. 't Hooft, in “The whys of subnuclear physics”, Erice 1977, Ed. Zichichi, Plenum (1977), p. 943; A.H. Mueller, Nucl. Phys. **B250** (1985) 327; Phys. Lett. **B308** (1993) 355; V.I. Zakharov, Nucl. Phys. **B385** (1992) 452; For a recent review see M. Beneke, Phys. Rept. **317** (1999) 1.
- [2] S.J. Brodsky, E. Gardi, G. Grunberg and J. Rathsmann, hep-ph/0002065.
- [3] T. Banks and A. Zaks, Nucl. Phys. **B196** (1982) 189.
- [4] S.J. Brodsky, G.P. Lepage and P.B. Mackenzie, Phys. Rev. D **28** (1983) 228.
- [5] G.P. Lepage and P.B. Mackenzie, Phys. Rev. **D48**, 2250 (1993).
- [6] S.J. Brodsky and H.J. Lu, Phys. Rev. D **51** (1995) 3652.
- [7] S.J. Brodsky, G.T. Gabadadze, A.L. Kataev and H. J. Lu, Phys. Lett. **B372** (1996) 133.
- [8] G. Grunberg and A.L. Kataev, Phys. Lett. **B279** (1992) 352; H.J. Lu and C.A. Sa de Melo, Phys. Lett. **B273** (1991) 260 (Erratum: *ibid.* **B285** (1992) 399); H.J. Lu, Phys. Rev. D **45** (1992) 1217; SLAC-0406 (Ph.D. Thesis) (1992); J. Rathsmann, Phys. Rev. D **54** (1996) 3420; M. Neubert, Phys. Rev. D **51** (1995) 5924; hep-ph/9502264; M. Beneke and V.M. Braun, Phys. Lett. **B348**

- (1995) 513; P. Ball, M. Beneke and V.M. Braun, Nucl. Phys. **B452** (1995) 563; C.N. Lovett-Turner and C.J. Maxwell, Nucl. Phys. **B452** (1995) 188; S.J. Brodsky, J. Ellis, E. Gardi, M. Karliner and M.A. Samuel, Phys. Rev. D **56** (1997) 6980; S.J. Brodsky, M.S. Gill, M. Melles and J. Rathsman, Phys. Rev. **D58** (1998) 116006; S.J. Brodsky, M. Melles and J. Rathsman, Phys. Rev. **D60** (1999) 096006; S.J. Brodsky and J. Rathsman, hep-ph/9906339.
- [9] G. Grunberg, Phys. Lett. **95B** (1980) 70, Erratum-ibid. **110B** (1982) 501; Phys. Rev. D **29** (1984) 2315.
- [10] R.J. Crewther, Phys. Rev. Lett. **28** (1972) 1421. Phys. Lett. **B397** (1997) 137.
- [11] D.J. Broadhurst and A.L. Kataev, Phys. Lett. **B315** (1993) 179.
- [12] J.D. Bjorken and S.D. Drell, *Relativistic Quantum Fields*, McGraw-Hill, New-York, 1965.
- [13] J. M. Cornwall, Phys. Rev. D **26** (1982) 1453; J. M. Cornwall and J. Papavasiliou, Phys. Rev. D **40** (1989) 3474; J. Papavassiliou, Phys. Rev. D **47** (1993) 4728; Phys. Rev. D **41** (1990) 3179; G. Degrossi and A. Sirlin, Phys. Rev. D **46** (1992) 3104; N. J. Watson, Nucl. Phys. **B494** (1997) 388.
- [14] N. J. Watson, Nucl. Phys. **B552** (1999) 461; J. Papavassiliou, Phys. Rev. Lett. **84** (2000) 2782; Phys. Rev. D **62** (2000) 045006.
- [15] P.P. Srivastava and S.J. Brodsky, hep-ph/0011372.
- [16] D.J. Gross and F. Wilczek, Phys. Rev. **D8** (1973) 3633; W.E. Caswell, Phys. Rev. Lett. **33** (1974) 244; S. A. Caveny and P. M. Stevenson, hep-ph/9705319; E. Gardi and M. Karliner, Nucl. Phys. **B529** (1998) 383; E. Gardi and G. Grunberg, JHEP**9903** (1999) 024.
- [17] G. Grunberg, JHEP**9811** (1998) 006.
- [18] E. Gardi and G. Grunberg, JHEP**9911** (1999) 016.
- [19] P.N. Burrows, H. Masuda, D. Muller and Y. Ohnishi, Phys. Lett. **B382** (1996) 157; P. Abreu *et al.* [DELPHI Collaboration], Eur. Phys. J. **C14** (2000) 557.
- [20] A. De Rujula, J. Ellis, E. G. Floratos and M. K. Gaillard, Nucl. Phys. **B138** (1978) 387.
- [21] R.K. Ellis, D.A. Ross and A.E. Terrano, Nucl. Phys. **B178** (1981) 421. Z. Kunszt, P. Nason, *QCD*, in *Z Physics at LEP 1*, vol. 1, p. 373, Eds. G. Altarelli, R. Kleiss, and C. Verzegnassi; S. Catani and M.H. Seymour, Phys. Lett. **B378** (1996) 287; Nucl. Phys. **B485** (1997) 291.

- [22] D.E. Soper, Phys. Rev. Lett. **81** (1998) 2638; Phys. Rev. D **62** (2000) 014009.
- [23] P. Nason and M.H. Seymour, Nucl. Phys. **B454** (1995) 291.
- [24] E. Gardi, JHEP**0004** (2000) 030.
- [25] S. Catani, L. Trentadue, G. Turnock and B.R. Webber, Nucl. Phys. **B407** (1993) 3.
- [26] P.D. Acton *et al.* [OPAL Collaboration], Z. Phys. **C59** (1993) 1.

# The Drell-Yan-Levy Relation: $ep$ vs $e^+e^-$ Scattering to $O(\alpha_s^2)^{*†}$

<sup>a</sup> J. BLÜMLEIN, <sup>b</sup> V. RAVINDRAN, AND <sup>c</sup> W.L. VAN NEERVEN

<sup>a</sup> *DESY Zeuthen, Platanenallee 6,  
D-15738 Zeuthen, Germany*

<sup>b</sup> *Harish-Chandra Research Institute, Chhatnag Road, Jhusi,  
Allahabad, 211019, India*

<sup>c</sup> *Instituut-Lorentz, Universiteit Leiden, P.O. Box 9506,  
2300 HA Leiden, The Netherlands.*

We study the validity of a relation by Drell, Levy and Yan (DLY) connecting the deep inelastic structure (DIS) functions and the single-particle fragmentation functions in  $e^+e^-$  annihilation which are defined in the spacelike ( $q^2 < 0$ ) and timelike ( $q^2 > 0$ ) regions, with respect to physical evolution kernels for the two processes to  $O(\alpha_s^2)$ . We also comment on a relation proposed by Gribov and Lipatov.

Presented at the

5th International Symposium on Radiative Corrections  
(RADCOR-2000)

Carmel CA, USA, 11–15 September, 2000

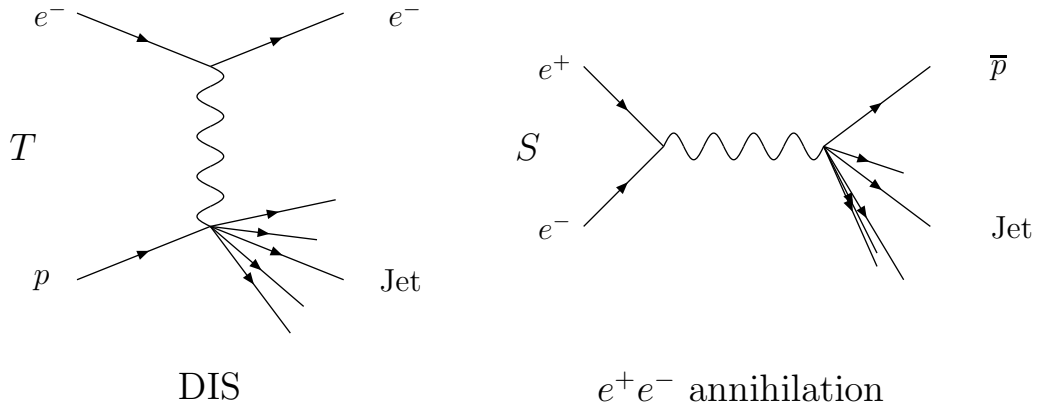
---

\*Presented by J. Blümlein

†Work supported in part by EU contract FMRX-CT98-0194 (DG 12-MIHT).

# 1 The DLY-Relation

Right after the discovery of the partonic structure of nucleons the question arose, whether at large virtualities of the exchanged photon the hard processes  $e^-p \rightarrow e^-X$  and  $e^+e^- \rightarrow \bar{p}X$  are related by crossing from the  $t$ - to the  $s$ -channel, [1,2].



For the two-fold differential scattering cross sections for both processes,

$$\frac{d^2\sigma}{dx dQ^2} \sim L_{\mu\nu} W^{\mu\nu} , \tag{1}$$

one may express channel crossing by the hadronic tensors  $W_{\mu\nu}$  as done by Drell, Levy, and Yan [1]

$$W_{\mu\nu}^{(S)}(q, p) = -W_{\mu\nu}^{(T)}(q, -p) . \tag{2}$$

At that time partons were assumed as fermionic particles, interacting via (pseudo) scalars, with  $\delta(1 - z)$ -sources, where  $z$  denotes the longitudinal momentum fraction. Considering only ladder graphs at lowest order, such a crossing could be envisaged for the whole hadronic tensor.

Viewing these reactions in QCD, the picture changes. The sources of the partons are extended non-perturbative distributions with  $z \in [0, 1]$ , about which perturbative QCD cannot make a statement, even resumming whole classes of graphs. However, at large scales of  $Q^2$  both processes factorize into the parton densities and perturbative evolution kernels, which rule the  $Q^2$  behaviour. The question of crossing from the  $t$ - to the  $s$ - channel can thus be modified in studying it for the *factorized* evolution kernels at the one side within *perturbative QCD* and leaving the related question for the non-perturbative sources to *Lattice Gauge Theory*.

The scaling variables describing deep inelastic scattering at the one side and hadron fragmentation on the other side are  $x_B$  and  $x_E$ ,

$$x_B = \frac{Q^2}{2p \cdot q}, \quad 0 \leq x_B \leq 1 \quad \text{DIS} \quad (3)$$

$$x_E = \frac{2p \cdot q}{Q^2}, \quad 0 \leq x_E \leq 1 \quad e^+e^- \text{ annihilation} . \quad (4)$$

The point  $x = 1$  connects both domains and is usually a singular point. One may now calculate QCD evolution kernels for both domains. The central question of the present paper is, what are the conditions to *continue* the kernel obtained in one domain into that of the other. In general one cannot expect to find an analytic continuation in an arbitrarily chosen factorization scheme in which the process independent splitting functions are evaluated. However, one may form *physical evolution kernels*, in both domains, which are scheme-invariant and study their crossing behaviour. Thus the above question is directed to the connection of the physical evolution behaviour of *observables* as the structure and fragmentation functions. In the present paper we study this relation up to  $O(\alpha_s^2)$ . Early related investigations (partly before the advent of QCD) were performed in Refs. [3]–[11], and more recently in Refs. [12]–[15].

## 2 Scheme-invariant Evolution Equations

To investigate the crossing behaviour for the evolution kernels of structure and fragmentation functions we first derive physical evolution equations. The twist-2 contributions to these functions can be expressed in the form

$$F_i(x, Q^2) = \sum_{l=q,g} \left( C_{i,l}(\alpha_s(\mu_r^2), \frac{Q^2}{\mu_f^2}, \frac{\mu_f^2}{\mu_r^2}) \otimes f_l(\alpha_s(\mu_r^2), \frac{\mu_f^2}{\mu^2}, \frac{\mu_f^2}{\mu_r^2}) \right) (x), \quad (5)$$

where  $C_{i,l}$  denote the Wilson coefficients,  $f_l$  the parton densities and  $\otimes$  is the Mellin convolution.  $\mu_f^2$  and  $\mu_r^2$  are the factorization and renormalization scales, respectively. Beyond leading order the parton densities and Wilson coefficients obey factorization scheme-dependent evolution equations and are thus no observables. Their dependence on  $\mu_f^2$  can, however, be eliminated in expressing the non-singlet and singlet parton densities via physical observables, the scale dependence of which is finally studied. For the singlet case one obtains

$$\frac{\partial}{\partial t} \begin{pmatrix} F_A^N \\ F_B^N \end{pmatrix} = -\frac{1}{4} \begin{pmatrix} K_{AA}^N & K_{AB}^N \\ K_{BA}^N & K_{BB}^N \end{pmatrix} \begin{pmatrix} F_A^N \\ F_B^N \end{pmatrix} . \quad (6)$$

Here the evolution kernels  $K_{IJ}^N$  written in Mellin-moment space are no longer process-independent quantities for the evolution of the pair of observables  $\{F_A^N, F_B^N\}$ , but

scheme-independent quantities. Eq. (6) refers to the evolution variable  $t = -(2/\beta_0) \times \ln(a_s(Q^2)/a_s(Q_0^2))$ .  $\beta_0$  is the lowest order  $\beta$ -function, and  $a_s(Q^2) = \alpha_s(Q^2)/(4\pi)$ . The physical evolution kernels read

$$K_{IJ}^N = \left[ -4 \frac{\partial C_{I,m}^N(t)}{\partial t} (C^N)_{m,J}^{-1}(t) - \frac{\beta_0 a_s(Q^2)}{\beta(a_s(Q^2))} C_{I,m}^N(t) \gamma_{mn}^N(t) (C^N)_{n,J}^{-1}(t) \right], \quad (7)$$

with  $\beta(a_s)$  the  $\beta$ -function and

$$K_{IJ}^N = \sum_{n=0}^{\infty} a_s^n(Q^2) (K^N)_{IJ}^{(n)}. \quad (8)$$

One easily sees that the kernels Eq. (7) are very difficult to obtain in  $x$ -space, due to the inverse coefficient functions to be evaluated. Instead they take a simple form for the Mellin-transforms. The transformed coefficient functions are needed in *analytic form* in  $N$ , which are usually polynomials out of multiple alternating and non-alternating harmonic sums [16,17]. These expressions have to be analytically continued to complex values of  $N$ . It turns out that all Wilson coefficients to  $O(\alpha_s^2)$  can be expressed by at most 26 basic functions of complex  $N$ , the analytic continuations of which can be found in Ref. [18].

Possible choices for the observables  $\{F_A^N, F_B^N\}$  are  $F_2, \partial F_2/\partial t, g_1, \partial g_1/\partial t$ , and  $F_2, F_L$ . Here we denote by  $F_i$  and  $g_i$  the respective unpolarized and polarized structure *and* fragmentation functions. The physical evolution kernels, as obtained from the anomalous dimensions and coefficient functions, read :

### System: $F_2, \partial F_2/\partial t$

Leading Order [19]:

$$\begin{aligned} K_{22}^{N(0)} &= 0 \\ K_{2d}^{N(0)} &= -4 \\ K_{d2}^{N(0)} &= \frac{1}{4} \left( \gamma_{qq}^{N(0)} \gamma_{gg}^{N(0)} - \gamma_{gg}^{N(0)} \gamma_{qq}^{N(0)} \right) \\ K_{dd}^{N(0)} &= \gamma_{qq}^{N(0)} + \gamma_{gg}^{N(0)} \end{aligned} \quad (9)$$

Next-to-Leading Order [19]:

$$\begin{aligned} K_{22}^{N(1)} &= K_{2d}^{N(1)} = 0 \\ K_{d2}^{N(1)} &= \frac{1}{4} \left[ \gamma_{gg}^{N(0)} \gamma_{qq}^{N(1)} + \gamma_{gg}^{N(1)} \gamma_{qq}^{N(0)} - \gamma_{qq}^{N(1)} \gamma_{gg}^{N(0)} - \gamma_{qq}^{N(0)} \gamma_{gg}^{N(1)} \right] \end{aligned}$$

$$\begin{aligned}
& -\frac{\beta_1}{2\beta_0} \left( \gamma_{qq}^{N(0)} \gamma_{gg}^{N(0)} - \gamma_{gq}^{N(0)} \gamma_{qg}^{N(0)} \right) \\
& + \frac{\beta_0}{2} C_{2,q}^{N(1)} \left( \gamma_{qq}^{N(0)} + \gamma_{gg}^{N(0)} - 2\beta_0 \right) \\
& - \frac{\beta_0}{2} \frac{C_{2,g}^{N(1)}}{\gamma_{qg}^{N(0)}} \left[ (\gamma_{qq}^{N(0)})^2 - \gamma_{qq}^{N(0)} \gamma_{gg}^{N(0)} + 2\gamma_{qg}^{N(0)} \gamma_{gq}^{N(0)} - 2\beta_0 \gamma_{qq}^{N(0)} \right] \\
& - \frac{\beta_0}{2} \left( \gamma_{qq}^{N(1)} - \frac{\gamma_{qq}^{N(0)} \gamma_{qg}^{N(1)}}{\gamma_{qg}^{N(0)}} \right)
\end{aligned} \tag{10}$$

The same structures apply to  $g_1, \partial g_1 / \partial t$ .

### System: $F_2, \hat{F}_L$

For convenience we define  $\hat{F}_L^N \equiv F_L^N / (a_s(Q^2) C_{L,g}^{N(1)})$ .

Leading Order [20]:

$$\begin{aligned}
K_{22}^{N(0)} &= \gamma_{qq}^{N(0)} - \frac{C_{L,q}^{N(1)}}{C_{L,g}^{N(1)}} \gamma_{qg}^{N(0)} \\
K_{2L}^{N(0)} &= \gamma_{qg}^{N(0)} \\
K_{L2}^{N(0)} &= \gamma_{gq}^{N(0)} - \left( \frac{C_{L,q}^{N(1)}}{C_{L,g}^{N(1)}} \right)^2 \gamma_{qg}^{N(0)} \\
K_{LL}^{N(0)} &= \gamma_{gg}^{N(0)} + \frac{C_{L,q}^{N(1)}}{C_{L,g}^{N(1)}} \gamma_{qg}^{N(0)} + \frac{C_{L,q}^{N(1)}}{C_{L,g}^{N(1)}} (\gamma_{qq}^{N(0)} - \gamma_{gg}^{N(0)})
\end{aligned} \tag{11}$$

Next-to-Leading Order [15]:

$$\begin{aligned}
K_{22}^{N(1)} &= \gamma_{qq}^{N(1)} - \frac{\beta_1}{\beta_0} \gamma_{qq}^{N(0)} - \frac{C_{L,q}^{N(1)}}{C_{L,g}^{N(1)}} \left( \gamma_{qg}^{N(1)} - \frac{\beta_1}{\beta_0} \gamma_{qg}^{N(0)} \right) \\
& + \frac{C_{L,q}^{N(1)}}{C_{L,g}^{N(1)}} C_{2,g}^{N(1)} \gamma_{qq}^{N(0)} - \frac{C_{L,q}^{N(1)}}{C_{L,g}^{N(1)}} C_{2,g}^{N(1)} \gamma_{gg}^{N(0)} \\
& - \left[ \frac{C_{L,q}^{N(2)}}{C_{L,g}^{N(1)}} + \left( \frac{C_{L,q}^{N(1)}}{C_{L,g}^{N(1)}} \right)^2 C_{2,g}^{N(1)} - \frac{C_{L,q}^{N(1)}}{C_{L,g}^{N(1)}} \frac{C_{L,g}^{N(2)}}{C_{L,g}^{N(1)}} \right] \gamma_{qg}^{N(0)}
\end{aligned}$$

$$\begin{aligned}
& + C_{2,g}^{N(1)} \gamma_{gq}^{N(0)} + 2\beta_0 \left( C_{2,q}^{N(1)} - \frac{C_{L,q}^{N(1)}}{C_{L,g}^{N(1)}} C_{2,g}^{N(1)} \right) \\
K_{2L}^{N(1)} &= \gamma_{qg}^{N(1)} - \frac{\beta_1}{\beta_0} \gamma_{qg}^{N(0)} - C_{2,g}^{N(1)} (\gamma_{qq}^{N(0)} - \gamma_{gg}^{N(0)}) + 2\beta_0 C_{2,g}^{N(1)} \\
& + \left( C_{2,q}^{N(1)} + \frac{C_{L,q}^{N(1)}}{C_{L,g}^{N(1)}} C_{2,g}^{N(1)} - \frac{C_{L,g}^{N(2)}}{C_{L,g}^{N(1)}} \right) \gamma_{qg}^{N(0)} \\
K_{L2}^{N(1)} &= \gamma_{gq}^{N(1)} - \frac{\beta_1}{\beta_0} \gamma_{gq}^{N(0)} + \frac{C_{L,q}^{N(1)}}{C_{L,g}^{N(1)}} \left( \gamma_{qq}^{N(1)} - \frac{\beta_1}{\beta_0} \gamma_{qq}^{N(0)} \right) \\
& - \left( \frac{C_{L,q}^{N(1)}}{C_{L,g}^{N(1)}} \right)^2 \left( \gamma_{qg}^{N(1)} - \frac{\beta_1}{\beta_0} \gamma_{qg}^{N(0)} \right) - \frac{C_{L,q}^{N(1)}}{C_{L,g}^{N(1)}} \left( \gamma_{gg}^{N(1)} - \frac{\beta_1}{\beta_0} \gamma_{gg}^{N(0)} \right) \\
& + \left[ \frac{C_{L,q}^{N(2)}}{C_{L,g}^{N(1)}} - \frac{C_{L,q}^{N(1)}}{C_{L,g}^{N(1)}} C_{2,q}^{N(1)} + \left( \frac{C_{L,q}^{N(1)}}{C_{L,g}^{N(1)}} \right)^2 C_{2,g}^{N(1)} \right] \gamma_{qg}^{N(0)} \\
& - \left[ \left( \frac{C_{L,q}^{N(1)}}{C_{L,g}^{N(1)}} \right)^3 C_{2,g}^{N(1)} + 2 \frac{C_{L,q}^{N(1)} C_{L,q}^{N(2)}}{C_{L,g}^{N(1)} C_{L,g}^{N(1)}} - \left( \frac{C_{L,q}^{N(1)}}{C_{L,g}^{N(1)}} \right)^2 \frac{C_{L,g}^{N(2)}}{C_{L,g}^{N(1)}} \right. \\
& \left. - \left( \frac{C_{L,q}^{N(1)}}{C_{L,g}^{N(1)}} \right)^2 C_{2,q}^{N(1)} \right] \gamma_{qg}^{N(0)} + 2\beta_0 \left( \frac{C_{L,q}^{N(2)}}{C_{L,g}^{N(1)}} - \frac{C_{L,q}^{N(1)} C_{L,g}^{N(2)}}{C_{L,g}^{N(1)} C_{L,g}^{N(1)}} \right) \\
& + \left( \frac{C_{L,q}^{N(1)}}{C_{L,g}^{N(1)}} C_{2,g}^{N(1)} - C_{2,q}^{N(1)} + \frac{C_{L,g}^{N(2)}}{C_{L,g}^{N(1)}} \right) \gamma_{gq}^{N(0)} \\
& - \left[ \frac{C_{L,q}^{N(2)}}{C_{L,g}^{N(1)}} + \left( \frac{C_{L,q}^{N(1)}}{C_{L,g}^{N(1)}} \right)^2 C_{2,g}^{N(1)} - \frac{C_{L,q}^{N(1)}}{C_{L,g}^{N(1)}} C_{2,q}^{N(1)} \right] \gamma_{gg}^{N(0)} \\
K_{LL}^{N(1)} &= \gamma_{gg}^{N(1)} - \frac{\beta_1}{\beta_0} \gamma_{gg}^{N(0)} + \frac{C_{L,q}^{N(1)}}{C_{L,g}^{N(1)}} \left( \gamma_{qg}^{N(1)} - \frac{\beta_1}{\beta_0} \gamma_{qg}^{N(0)} \right) \\
& - \frac{C_{L,q}^{N(1)}}{C_{L,g}^{N(1)}} C_{2,g}^{N(1)} \gamma_{qq}^{N(0)} + \left[ \frac{C_{L,q}^{N(2)}}{C_{L,g}^{N(1)}} - \frac{C_{L,q}^{N(1)} C_{L,g}^{N(2)}}{C_{L,g}^{N(1)} C_{L,g}^{N(1)}} \right. \\
& \left. + \left( \frac{C_{L,q}^{N(1)}}{C_{L,g}^{N(1)}} \right)^2 C_{2,g}^{N(1)} \right] \gamma_{qg}^{N(0)}
\end{aligned}$$

$$-C_{2,g}^{N(1)}\gamma_{gq}^{N(0)} + \frac{C_{L,q}^{N(1)}}{C_{L,g}^{N(1)}}C_{2,g}^{N(1)}\gamma_{gg}^{N(0)} + 2\beta_0\frac{C_{L,g}^{N(2)}}{C_{L,g}^{N(1)}} \quad (12)$$

### 3 DLY–Relations for Evolution Kernels

The original crossing relation [1]

$$W_{\mu\nu}^T(q, p) = -W_{\mu\nu}^S(q, -p) \quad (13)$$

is modified to [11]

$$F_i^{(S)}(x_B) = -(-1)^{2(s_1+s_2)}x_E F_i^{(T)}\left(\frac{1}{x_E}\right) \quad , \quad i = 1, 2, L \quad (14)$$

if particles of different spin  $s_i$  contribute, again considering ladder approaches to the problem with idealized sources.

In the following we give the analytic continuation relations, cf. Ref. [15], which yield the correct transformations for physical kernels up to  $O(\alpha_s^2)$ . They read :

$$P(z) \rightarrow zP(1/z) \quad (15)$$

$$P_{ii} \rightarrow -P_{ii} \quad (16)$$

$$P_{qg}, P_{gq} \rightarrow \text{cross color pre - factor} \quad (17)$$

$$\ln\left(Q^2/\mu_f^2\right)_{\text{space-like}} \rightarrow \ln\left(Q^2/\mu_f^2\right)_{\text{time-like}} - i\pi \quad (18)$$

$$\delta(1-z) \rightarrow -\delta(1-z) \quad (19)$$

$$\ln(1-z) \rightarrow \ln(1-z) - \ln(z) + i\pi \quad (20)$$

$$\ln(\varepsilon) \rightarrow \ln(\varepsilon) + i\pi \quad (21)$$

Due to Eq. (19), Eq. (14) does not hold for  $x_B = x_E = 1$ , even in leading order, where the physical evolution kernels are the splitting functions.

In next-to-leading order the differences between the analytically continued space-like splitting functions and the time-like splitting functions are :

$$\begin{aligned} \overline{P}_{qq}^{(1)S} - P_{qq}^{(1)T} &= -2\beta_0 Z_{qq}^{T(1)} + Z_{qq}^{T(1)} \otimes \overline{P}_{qq}^{(0)} - Z_{gq}^{T(1)} \otimes \overline{P}_{gq}^{(0)} \quad , \\ \overline{P}_{gq}^{(1)S} - P_{gq}^{(1)T} &= -2\beta_0 Z_{gq}^{T(1)} + Z_{gq}^{T(1)} \otimes (\overline{P}_{gg}^{(0)} - \overline{P}_{qq}^{(0)}) \\ &\quad + \overline{P}_{gq}^{(0)} \otimes (Z_{qq}^{T(1)} - Z_{gg}^{T(1)}) \quad , \\ \overline{P}_{gq}^{(1)S} - P_{gq}^{(1)T} &= -2\beta_0 Z_{gq}^{T(1)} + Z_{gq}^{T(1)} \otimes (\overline{P}_{qq}^{(0)} - \overline{P}_{gg}^{(0)}) \\ &\quad + \overline{P}_{gq}^{(0)} \otimes (Z_{gg}^{T(1)} - Z_{qq}^{T(1)}) \quad , \\ \overline{P}_{gg}^{(1)S} - P_{gg}^{(1)T} &= -2\beta_0 Z_{gg}^{T(1)} + Z_{gg}^{T(1)} \otimes \overline{P}_{gg}^{(0)} - Z_{qg}^{T(1)} \otimes \overline{P}_{qg}^{(0)} \quad , \end{aligned} \quad (22)$$

and do *not* vanish. Here we defined

$$Z_{ij}^{T(1)} = P_{ji}^{(0)} \cdot (\ln(z) + a_{ji}) ,$$

where for unpolarized scattering

$$a_{qq} = a_{gg} = 0 \quad , \quad a_{qg} = -\frac{1}{2} \quad , \quad a_{gq} = \frac{1}{2} , \quad (23)$$

and for polarized scattering

$$a_{ij} = 0 , \quad (24)$$

cf. also [13].

The transformation of the NLO coefficient functions  $C_{1,q(g)}$  and  $C_{L,q(g)}$  are :

$$\begin{aligned} C_{1,q}^{(T)(1)}(z) + \left\{ z C_{1,q}^{(S)(1)} \left( \frac{1}{z} \right) \right\} &= Z_{qq}^{(T)(1)} \\ \frac{1}{2} \left[ C_{1,g}^{(T)(1)}(z) - \frac{C_F}{2N_f T_f} \left\{ 2z C_{1,g}^{(S)(1)} \left( \frac{1}{z} \right) \right\} \right] &= Z_{gg}^{(T)(1)} , \end{aligned} \quad (25)$$

and

$$\begin{aligned} C_{L,q}^{(T)(1)}(z) - \frac{z}{2} C_{L,q}^{(S)(1)} \left( \frac{1}{z} \right) &= 0 , \\ \frac{1}{2} \left[ C_{L,g}^{(T)(1)}(z) + \frac{C_F}{2N_f T_f} \left\{ z C_{L,g}^{(S)(1)} \left( \frac{1}{z} \right) \right\} \right] &= 0 . \end{aligned} \quad (26)$$

Finally the NNLO unpolarized longitudinal coefficient functions [21] transform as [15] :

$$\begin{aligned} C_{L,q}^{(T)(2)}(z) + \left\{ -\frac{z}{2} C_{L,q}^{(S)(2)} \left( \frac{1}{z} \right) \right\} &= \\ Z_{qq}^{(T)(1)} \otimes \frac{z}{2} C_{Lq}^{(1)S} \left( \frac{1}{z} \right) + Z_{gg}^{(T)(1)} \otimes \frac{C_F}{2N_f T_f} \left\{ -\frac{z}{2} C_{L,g}^{(S)(1)} \left( \frac{1}{z} \right) \right\} , \\ \frac{1}{2} \left[ C_{L,g}^{(T)(2)}(z) + \frac{C_F}{2N_f T_f} \left\{ z C_{L,g}^{(S)(2)} \left( \frac{1}{z} \right) \right\} \right] &= \\ Z_{gg}^{(T)(1)} \otimes \frac{z}{2} C_{L,q}^{(S)(1)} \left( \frac{1}{z} \right) + Z_{gg}^{(T)(1)} \otimes \frac{C_F}{2N_f T_f} \left\{ -\frac{z}{2} C_{L,g}^{(1)S} \left( \frac{1}{z} \right) \right\} . \end{aligned}$$

The transformations for the other NNLO coefficient functions [21,22] are given in Ref. [15].

Let us define the difference between the time-like physical evolution kernel and the analytically continued space-like evolution kernel by

$$\delta K_{IJ} := K_{IJ}^T - \overline{K}_{IJ}^S. \quad (27)$$

Using identities for pair-convolutions of higher order Nielsen integrals, see Ref. [15], one finally obtains that

$$\begin{aligned}\delta K_{d2} &= 0 \\ \delta K_{dd} &= 0 ,\end{aligned}\tag{28}$$

and

$$\begin{aligned}\delta K_{22}^{N(1)} &= 0 \\ \delta K_{L2}^{N(1)} &= 0 \\ \delta K_{2L}^{N(1)} &= 0 \\ \delta K_{LL}^{N(1)} &= 0 ,\end{aligned}\tag{29}$$

showing explicitly the validity of the Drell–Levy–Yan relation for the physical evolution kernels in leading and next-to-leading order at the above choice of observables.

We finally would like to comment on a relation suggested by Gribov and Lipatov [23],

$$\overline{K}(x_E, Q^2) = K(x_B, Q^2)$$

This relation holds for the LO non-singlet contributions and some pieces in the NLO non-singlet contributions, but is generally violated beyond LO.

## 4 Conclusions

The scale evolution of structure and fragmentation functions can be represented in terms of physical evolution kernels and observable non-perturbative input distributions. The physical evolution kernels of either choice of observables are related for the evolution of structure and fragmentation functions by an analytic continuation (DLY relation) from  $0 \leq x < 1$  to  $1 < x < \infty$  up to  $O(\alpha_s^2)$ , for which transformation rules were derived. The Gribov–Lipatov relation is violated beyond LO. An extension of the present investigation to  $O(\alpha_s^3)$  requires the knowledge of the hitherto unknown 3-loop singlet anomalous dimensions. The DLY relation for the evolution kernels is not necessarily expected to hold to arbitrary high orders due to the emergence of new production thresholds for the s-channel process. An interesting test of QCD can be carried out in comparing the scaling violations of structure and fragmentation functions using factorization scheme-independent evolution equations.

## Acknowledgments

We would like to thank the organizers of the conference, H. Haber and S.J. Brodsky, for having organized a stimulating meeting.

## References

- [1] S.D. Drell, D.J. Levy, and T.M. Yan, Phys. Rev. **187** (1969) 2159; **D1** (1970) 1617.
- [2] J. Pestieau and P. Roy, Phys. Lett. **B30** (1969) 483.
- [3] S.D. Drell, D.J. Levy, and T.M. Yan, Phys. Rev. Lett. **22** (1969) 744;  
S.J. Chang and P.M. Fishbane, Phys. Rev. Lett. **24** (1970) 847; Phys. Rev. **D2** (1970) 1084, 1173;  
S.D. Drell and T.D. Lee, Phys. Rev. **D5** (1972) 1738;  
S.D. Drell, D.J. Levy and T.M. Yan Phys. Rev. **D1** (1970) 1035.
- [4] V.N. Gribov and L.N. Lipatov, Phys. Lett. **B37** (1971) 78.
- [5] P.M. Fishbane and J.D. Sullivan, Phys. Lett. **B37** (1971) 68.
- [6] A. Suri, Phys. Rev. **D4** (1971) 510;  
R. Gatto and G. Preparata, Nucl. Phys. **B47** (1972) 313;  
H.D. Dahmen and F. Steiner, Phys. Lett. **43B** (1973) 217.
- [7] R. Gatto and P. Menotti, Nuovo Cim. **2A** (1971) 881; **7A** (1972) 118;  
R. Gatto, P. Menotti, and I. Vendramin, Lett. Nuovo Cim. **4** (1972) 79; Ann. Phys. (New York) **79** (1973) 1;  
P.V. Landshoff, J.C. Polkinghorne, and R.D. Short, Nucl. Phys. **B28** (1971) 225;  
P.V. Landshoff and J.C. Polkinghorne, Phys. Rev. **D6** (1972) 3708; Nucl. Phys. **B53** (1973) 473;  
G. Altarelli and L. Maiani, Phys. Lett. **B41** (1972) 480; Nucl. Phys. **B51** (1973) 509.
- [8] P. Menotti, in: Proceedings of the Informal Meeting on Electromagnetic Interactions, Frascati, May 2–3, 1972, Pisa Preprint SNS 3/72.
- [9] P.V. Landshoff, Phys. Lett. **B32** (1970) 57.
- [10] L.N. Lipatov, Sov. J. Nucl. Phys. **20** (1975) 181.
- [11] A.P. Bukhvostov, L.N. Lipatov, and N.P. Popov, Sov. J. Nucl. Phys. **20** (1975) 287.
- [12] G. Curci, W. Furmanski and R. Petronzio, Nucl. Phys. **B175** (1980) 27;  
E.G. Floratos, R. Lacaze and C. Kounnas, Phys. Lett. **B98** (1981) 89, 285.
- [13] M. Stratmann and W. Vogelsang, Nucl. Phys. **B496** (1997) 41.

- [14] J. Blümlein, V. Ravindran and W.L. van Neerven, Acta Phys. Polon. **B29** (1998) 2581 and references therein; J. Phys. **G25** (1999) 1551; Nucl. Phys. **B** (Proc. Suppl.) **79** (1999) 169.
- [15] J. Blümlein, V. Ravindran and W.L. van Neerven, Nucl. Phys. **B586** (2000) 349.
- [16] J. Blümlein, S. Kurth, DESY-97-160, hep-ph/9708388; Phys. Rev. **D60** (1999) 014018.
- [17] J. Vermaseren and E. Remiddi, Int. J. Mod. Phys. **A15** (2000) 725;  
S. Moch and J. Vermaseren, Nucl. Phys. **B573** (2000) 853;  
W.L. van Neerven and A. Vogt, Nucl. Phys. **B586** (2000) 263, **B588** (2000) 345.
- [18] J. Blümlein, hep-ph/0003100, Computer Phys. Commun. **133** (2000) 76.
- [19] W. Furmanski and R. Petronzio, Z. Phys. **C11** (1982) 293.
- [20] S. Catani, Z. Phys. **C75** (1997) 665.
- [21] W.L. van Neerven and E.B. Zijlstra, Nucl. Phys. **B383** (1992) 525;  
P.J. Rijken and W.L. van Neerven, Nucl. Phys. **B487** (1997) 233; Phys. Lett. **B392** (1997) 207; **B386** (1996) 422. Nucl. Phys. **B523** (1998) 245;  
E. B. Zijlstra, Ph.D thesis, Leiden University (1993);  
P.J. Rijken, Ph.D thesis, Leiden University, (1997).
- [22] W.L. van Neerven and E.B. Zijlstra, Phys. Lett. **B272** (1991) 127, **B273** (1991) 476; **B297** (1992) 377; Nucl.Phys. **B417** (1994) 61, E: **B426** (1994) 245.
- [23] V.N. Gribov and L.N. Lipatov, Sov. J. Nucl. Phys. **15** (1972) 675.

ANL-HEP-CP-01-10  
October 19, 2001

## HERA Small- $x$ and/or Diffraction

RIK YOSHIDA

ON BEHALF OF THE ZEUS AND H1 COLLABORATIONS

*Argonne National Laboratory*

*9700 S. Cass Ave, Argonne, Illinois 60439, USA*

Recent HERA data on small- $x$  structure functions as well as DIS diffraction and diffractive vector meson production are presented. The relationship between these processes and possible indications of dynamics beyond the DGLAP formalism are discussed.

PRESENTED AT

5th International Symposium on Radiative Corrections  
(RADCOR-2000)

Carmel CA, USA, 11–15 September, 2000

# 1 Proton Structure Function $F_2$ at Small- $x$

## 1.1 Deep Inelastic Scattering and $F_2$

Deep Inelastic Scattering (DIS) of electrons (or positrons) with a proton is shown in Figure 1. The reaction proceeds through the exchange of a virtual boson; in the kinematic range covered in this talk, only photon exchange is important. The reaction can be described completely by two kinematic variables chosen to be the four-momentum transfer squared,  $Q^2 = -q^2$  (see Figure 1), and the Bjorken variable,  $x$ . In the Quark Parton Model,  $x$  is the fraction of the initial proton momentum carried by the struck parton.

The DIS cross-section factorizes into a short-distance part which is the partonic cross-section,  $\hat{\sigma}$ , which can be calculated perturbatively in QCD, and a long-distance non-perturbative part, the parton densities,  $f$ .

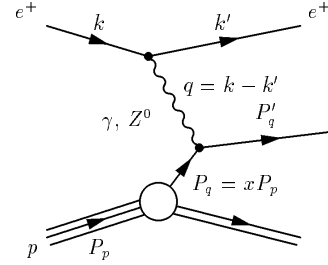


Figure 1: Collision of electron (positron),  $e^\pm$ , of four-momentum  $k$  with a proton,  $p$ , of four-momentum  $P_p$ .

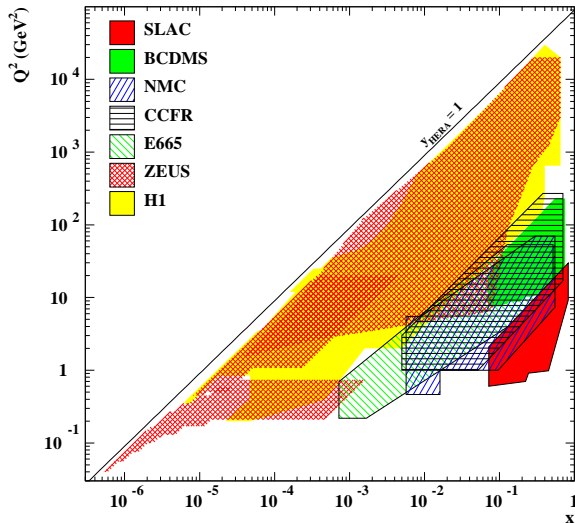


Figure 2: The kinematic region in which the proton  $F_2$  has been measured. H1 and ZEUS are the experiments at the HERA  $ep$  collider.

At sufficiently high  $Q^2$ , the parton densities,  $f$ , obey the DGLAP equation [1], which is written schematically as,

$$\frac{\partial f}{\partial \ln Q^2} \sim f \otimes P, \quad (1)$$

where  $P$  are the splitting functions that describe the branching of quarks and gluons, and  $\otimes$  symbolizes a convolution.

The DIS differential cross-section can be written in terms of the proton structure function  $F_2$  as

$$\frac{d\sigma^2}{dx dQ^2} = \frac{2\pi\alpha^2}{xQ^4} (1 + (1-y)^2) F_2(x, Q^2), \quad (2)$$

where  $y = Q^2/xs$  is the inelasticity parameter, and  $s$  is the CMS energy squared of the  $ep$  collision. The longitudinal structure function  $F_L$  and the effects of  $Z^0$  exchange have been neglected in Equation (2).

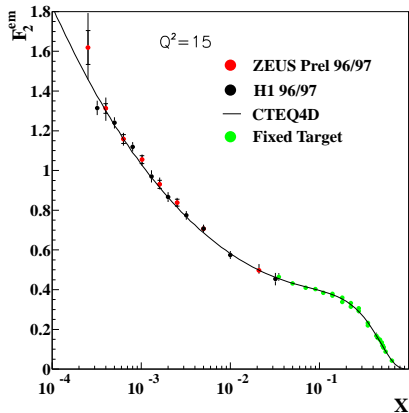


Figure 3: World's data on  $F_2$  at  $Q^2 = 15$   $\text{GeV}^2$  as a function of  $x$ . The solid line is a DGLAP fit by the CTEQ group [2].

$x^{-\lambda}$ , then  $\lambda$  falls as a function of  $Q^2$  from about 0.4 to 0.1 as  $Q^2$  falls from 200  $\text{GeV}^2$  to 1  $\text{GeV}^2$ . At  $Q^2$  of 10  $\text{GeV}^2$ ,  $\lambda$  is about 0.2 (Figure 4) [5, 6].

The naive physical interpretation of the small- $x$  rise of  $F_2$  is that it is caused by more and more gluons (and thus sea-quarks) being present at smaller and smaller fractional momenta values, i.e.  $x$ .

The scaling violations of  $F_2$  (i.e. the  $Q^2$  dependence of  $F_2$  at fixed  $x$ , as seen in Figure 5) at low  $x$  are related, in Leading Order (LO) DGLAP, simply to the gluon density of the proton [7],

$$\frac{\partial F_2(x/2, Q^2)}{\partial \ln Q^2} \propto \alpha_s x g(x, Q^2). \quad (4)$$

In Next-to-LO (NLO) DGLAP, the simple relationship of Equation (4) no longer holds. However, the gluon density may be extracted from the NLO DGLAP fits to  $F_2$ .

As an example of such fits, the one made by the H1 collaboration is briefly described [3].

The fit is made to the H1 data and the BCDMS  $\mu p$  data at  $Q^2 > 3.5$   $\text{GeV}^2$ . The flavor decomposition of  $F_2$  into the gluon  $xg$ , the valence component  $V$ , and the sea

At leading order,

$$F_2(x, Q^2) = x \sum_q e_q^2 (q(x, Q^2) + \bar{q}(x, Q^2)), \quad (3)$$

where  $q, \bar{q}$  are the quark and antiquark distributions, respectively.

Figure 2 shows the  $x$  and  $Q^2$  range of the currently available measurements of  $F_2$ . At the HERA  $ep$  collider, with  $\sqrt{s}$  of about 300  $\text{GeV}$ ,  $x$  and  $Q^2$  can be varied over six orders of magnitude. Of particular relevance to this talk is the region of smallest  $x$ , which is probed only at HERA.

The measurements of  $F_2$  at HERA show that the structure function rises steeply at small  $x$  (see Figure 3) [3, 4].

If  $F_2$  at  $x < 0.1$  is parameterized as  $\propto$

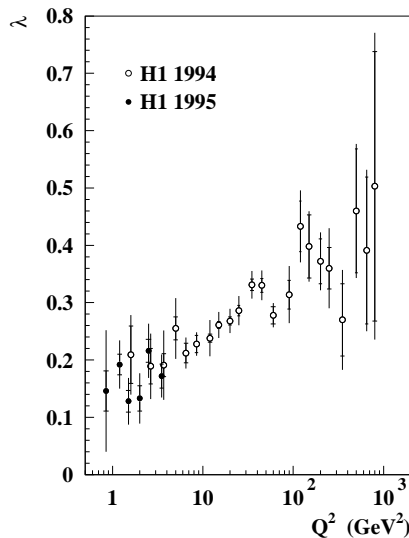


Figure 4: The parameter  $\lambda$  of the  $x$  dependence of  $F_2$ . See text and ref. [5].

component  $A$  is done in such a way as to allow the use of proton data only and avoid the deuteron data which introduces nuclear-correction uncertainties.

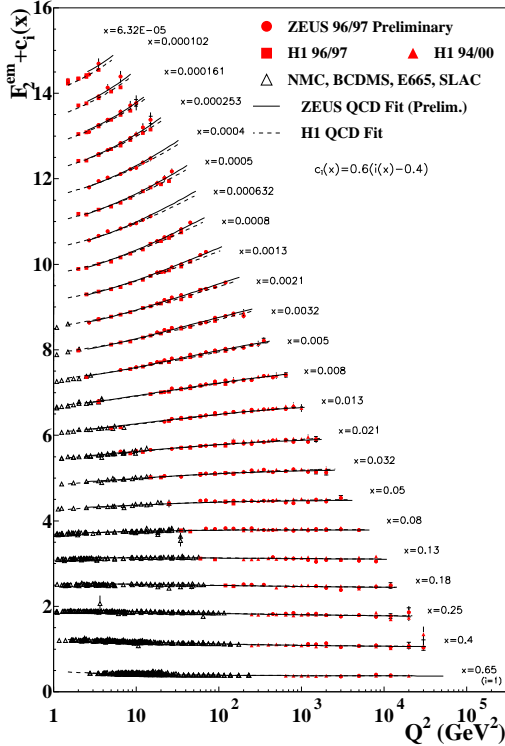


Figure 5: Proton  $F_2$  for fixed  $x$  as functions of  $Q^2$ . A constant,  $c_i$ , has been added to  $F_2$  in order to make all of the points visible.

$$W \approx \sqrt{Q^2/x}.$$

The total virtual-photon proton cross-section, at small- $x$ , can be written in terms of  $F_2$  as

$$\sigma_{tot}^{\gamma^*p}(W^2, Q^2) = \frac{4\pi^2\alpha}{Q^2} F_2(x, Q^2). \quad (5)$$

For fixed  $Q^2$ ,  $F_2 \propto x^{-\lambda}$  implies  $\sigma_{tot}^{\gamma^*p} \propto W^{2\lambda}$ . The structure function  $F_2$  must vanish as  $Q^2$ , for fixed  $W$ , as  $Q^2$  approaches 0, by conservation of EM current. At  $Q^2 = 0$  (photoproduction), the cross-section,  $\sigma_{tot}(W)$ , is described by Regge phenomenology, and is known to agree with the universal hadron-hadron cross-section behavior at high energies,  $\sigma_{tot}(W) \propto W^{2(\alpha_{\mathbb{P}}-1)}$  [8]. The Pomeron intercept  $\alpha_{\mathbb{P}}$  has the value 1.08 [9]. Thus at  $Q^2 = 0$ ,  $\sigma_{tot}(W) \propto W^{0.16}$ , in contrast to  $\sigma_{tot}^{\gamma^*p}(W^2, Q^2) \propto W^{0.4}$  at  $Q^2 \approx 10 \text{ GeV}^2$ .

The  $xg$ ,  $V$ , and  $A$  distributions are parameterized in the form  $ax^b(1-x)^c \times (1+d\sqrt{x}+ex)$ . The momentum sum rule is imposed leading to 16 parameters to be fitted including  $\alpha_s$ . The fits are made by employing Equations (1) and (3) (in their NLO versions).

Figure 6 shows the gluon density extracted from the fit. In keeping with the naive expectation of a gluon-driven  $F_2$ , the gluons also rise steeply at low  $x$ . As  $Q^2$  falls, the steepness of the gluon also becomes less, as in the case of  $F_2$  itself.

## 1.2 DIS and $\sigma_{tot}^{\gamma^*p}$

Figure 2 shows that due to the kinematic limit at HERA, the measurements of  $F_2$  at the smallest  $x$  values of  $10^{-6}$ – $10^{-5}$  correspond to rather small values of  $Q^2$ , well below  $1 \text{ GeV}^2$ . In this kinematic range, it is appropriate to describe DIS in the hadronic language of a collision between a virtual photon and a proton. The appropriate variable, in this case, becomes the virtual-photon proton CMS energy,

Figure 7 shows the measured  $F_2$  at fixed  $y = W^2/s$  down to the  $Q^2$  value of  $0.04 \text{ GeV}^2$ .  $F_2$  begins to fall as  $Q^2$  below  $Q^2 < 1 \text{ GeV}^2$ . The dashed line is a Regge inspired fit in the form  $F_2(x, Q^2) = (\frac{Q^2}{4\pi^2\alpha}) \cdot (\frac{M_0^2}{M_0^2 + Q^2}) \cdot (A_{\text{IR}} \cdot (W^2)^{\alpha_{\text{IR}} - 1} + A_{\text{IP}} \cdot (W^2)^{\alpha_{\text{IP}} - 1})$ . The  $\alpha_{\text{IP}}$  value of 1.1 gives a good fit. This is consistent with the value of Pomeron intercept discussed above [6].

Also shown in Figure 7 is a NLO DGLAP fit which gives a good description of the data from high  $Q^2$  down to about  $1 \text{ GeV}^2$ .

### 1.3 Beyond DGLAP?

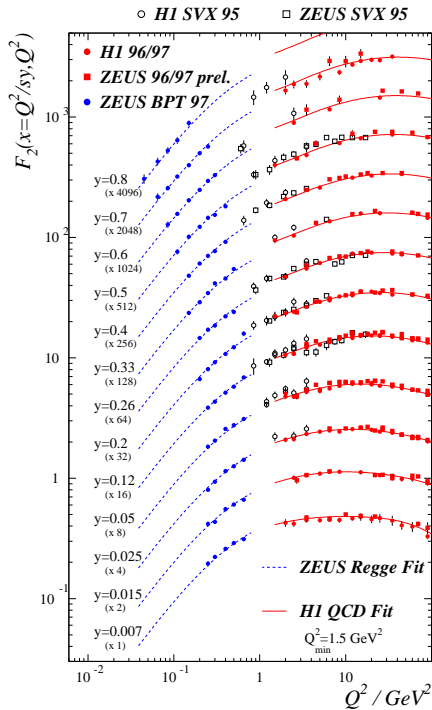


Figure 7:  $F_2$  as a function of  $Q^2$ . The lines are Regge and pQCD fits.

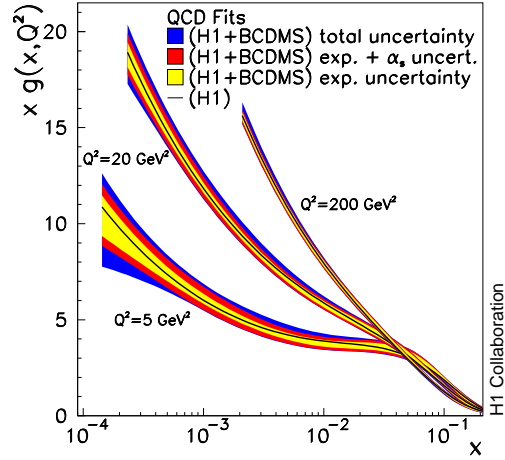


Figure 6: The gluon distribution extracted by the H1 Collab. See [3] for details.

The interest in small- $x$  physics is that the partons under study are the result of a large number of QCD branching processes. The evolution of the number of partons over a wide kinematic range in  $x$  and  $Q^2$  should be sensitive to the applicability of different perturbative approximations of QCD.

Figure 8 shows the qualitative expectation of applicability of various pQCD approaches. DGLAP is a resummation of terms proportional to  $(\ln Q^2)$  and is expected to hold in the region of large  $Q^2$ . BFKL [10] is a resummation of terms proportional to  $(\ln 1/x)$  and, while the stability of the perturbative expansion still under study [11, 12], it is expected to hold in the region of small  $x$ . The CCFM [13] equation incorporates both  $(\ln 1/x)$  and  $(\ln Q^2)$  terms.

At small enough  $x$ , the density of partons should become sufficiently large so that the interactions between them become important. This boundary is marked in Figure 8 by the line labeled “critical line”. The GLR equations [14, 15] attempt to take these saturation, or shadowing, effects into account.

It has been shown above that the DGLAP formalism is able to describe the currently available  $F_2$  data down to 1  $\text{GeV}^2$  and  $x$  of  $10^{-5}$  in apparent contradiction to Figure 8, at least with the  $1/x$  scale numbers as drawn.

On the other hand, there have also been successful fits to a wide range of  $F_2$  data using formalisms that incorporate the  $(\ln 1/x)$  terms as well as the  $(\ln Q^2)$  terms [16, 17].

In search of clarification, we turn next to the phenomenon of DIS diffraction, and vector meson production, before returning to consider if there are any indications in the  $F_2$  data for dynamics beyond DGLAP.

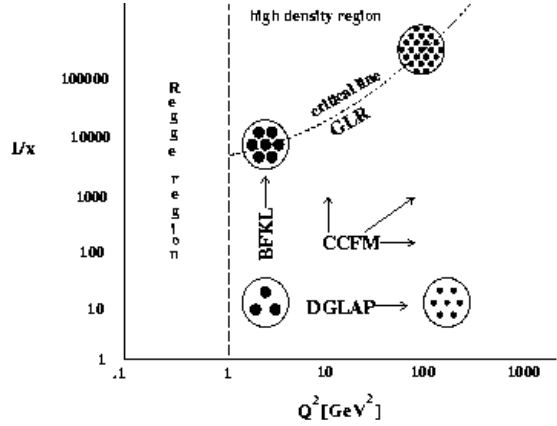


Figure 8: Schematic diagram of the applicability of different pQCD approximations.

## 2 Diffraction in DIS

One of the striking results from HERA is the presence of diffractive events in DIS [18, 19]. About 10% of all DIS events have a gap in particle emission between the final-state proton, or a low mass state, which travels down the beampipe, and the system  $X$ , which is measured in the detector (Figure 9). Such a reaction is usually described as an exchange of a colorless object, generically called the Pomeron ( $\mathbb{P}$ ).

In order to describe diffractive DIS, two kinematic variables in addition to  $x$  and  $Q^2$  are needed. These are  $t$ , which is the momentum transfer at the proton vertex and  $x_{\mathbb{P}}$ , which is the fractional momentum of the proton carried by the Pomeron. Another useful variable is  $\beta = x/x_{\mathbb{P}}$ , which has an interpretation as the fractional momentum of the Pomeron carried by the struck parton (i.e. the Pomeron analogue of  $x$  for the proton).

Any perturbative description of diffractive DIS must go beyond the simplest DGLAP picture; the lack of color connections between the system  $X$  and the proton must mean that at least two gluons are

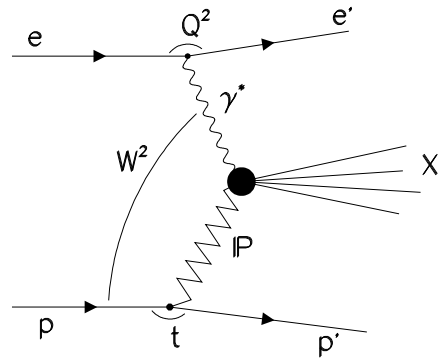


Figure 9: Diffractive DIS scattering.

exchanged. It is then interesting to investigate the connection between the high gluon densities implied by the  $F_2$  measurements and the phenomenon of DIS diffraction.

## 2.1 Diffractive Factorization and Pomeron Structure

The diffractive cross-section, in analogy with the total cross-section, is written in terms of the diffractive structure function  $F_2^D$  as

$$\frac{d^3\sigma^D}{d\beta dQ^2 dx_{\mathbb{P}}} = \frac{2\pi\alpha^2}{\beta Q^4} (1 + (1-y)^2) \times F_2^{D(3)}(\beta, Q^2, x_{\mathbb{P}}). \quad (6)$$

The cross-section has been integrated over  $t$ . It has been proven that  $F_2^D$  factorizes into a long and a short distance contributions, as does the inclusive  $F_2$ , i.e.  $F_2^D \sim f^D \otimes \hat{\sigma}$  where  $\hat{\sigma}$  are the usual pQCD hard cross-sections and  $f^D$  are the diffractive parton densities, which obey the usual DGLAP equations, and are universal [21]. By knowing  $f^D$ , we can calculate any diffractive DIS final state such as charm or jet production.

The diffractive parton densities are functions of four variables:  $x_{\mathbb{P}}$ ,  $t$ ,  $\beta$  and  $Q^2$ . However, the DGLAP evolution only concerns the variables  $x$  (or  $\beta$ ) and  $Q^2$ . If, for all relevant  $f^D$ 's, the  $x_{\mathbb{P}}$  and  $t$  dependences decouple from the  $\beta$  and  $Q^2$  dependence, *and* if the  $x_{\mathbb{P}}$  and  $t$  dependences are the *same* for all relevant partons, then we arrive at what is known as Regge factorization [22],

$$F_2^D(x_{\mathbb{P}}, t, Q^2, \beta) = f(x_{\mathbb{P}}, t) \cdot F_2^{\mathbb{P}}(\beta, Q^2). \quad (7)$$

In this case  $f(x_{\mathbb{P}}, t)$  can be interpreted as the flux factor of the Pomeron, and  $F_2^{\mathbb{P}}$  as the structure function of the Pomeron. In this case DGLAP analysis of  $F_2^{\mathbb{P}}$  becomes meaningful. It is a remarkable experimental fact that Regge factorization, which is not required by the diffractive factorization theorem, apparently holds over a large part of the measured phase-space, and that the flux factor,  $f(x_{\mathbb{P}}, t)$ , has approximately the form expected by Regge theory of  $1/x_{\mathbb{P}}^{2\bar{\alpha}_{\mathbb{P}}-1}$  [18, 19] (see also Figure 17a).

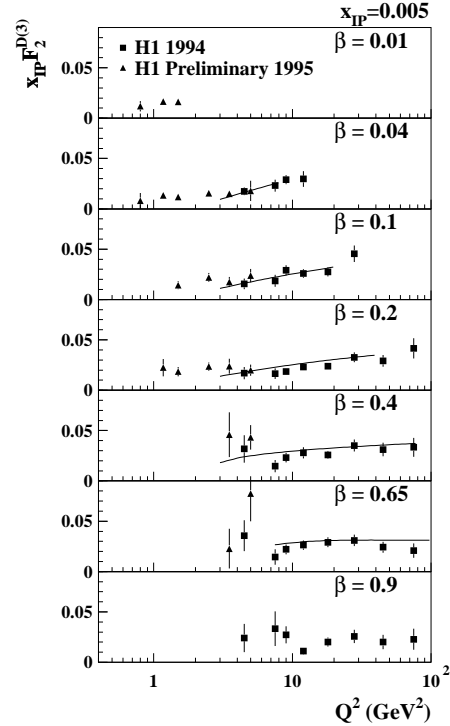


Figure 10: The diffractive structure function for a bin of  $x_{\mathbb{P}}$  measured by the H1 Collab. See text.

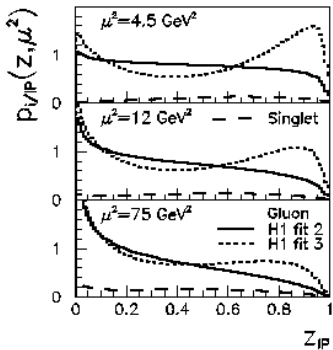


Figure 11: The parton distribution,  $P$ , of the Pomeron extracted by the H1 Collab. See text.

the DGLAP analysis can indeed be used to describe the dijet cross-section in diffractive events (Figure 12). The jet measurement favors the parton distributions labelled “fit 2” in Figure 11.

## 2.2 Diffraction and $F_2$ at Small- $x$

While the analyses based on diffractive factorization have been very successful and powerful, the question of the origin of the phenomenon of DIS diffraction remains unanswered. Furthermore, the relationship between the Pomeron structure and the proton structure is not clear.

Figure 13 shows the ratio, for fixed  $Q^2$ , of the DIS diffractive cross section to the total DIS cross-section as measured by the ZEUS collaboration. Although a cut has been made in the mass of the diffractive system,  $M_X$ , the conclusion is independent of  $M_X$ : the ratio is flat as a function of  $W$  or, equivalently for fixed  $Q^2$ , of  $x$  [18]. The flatness of the ratio implies that the energy dependence of DIS diffraction is the same as that of inclusive DIS, i.e.  $\propto W^{0.4}$  at  $Q^2 \approx 10 \text{ GeV}^2$ .

This result is surprising from several points of view. A naive expectation from the optical theorem would lead to diffractive cross sections

Figure 10 shows the measurements of  $F_2^{D(3)}$  by the H1 collaboration for  $x_{\text{IP}}$  of 0.005 [19, 20]. The lines are the results of the DGLAP analysis. The resulting parton distributions in the Pomeron is shown in Figure 11.

The analysis finds two stable solutions, one of which (dotted line) favors a rather large amount of gluons at  $z_{\text{IP}} = 1$ , and the second which does not (solid line). The fractional momentum carried by the parton in the Pomeron is denoted by  $z_{\text{IP}}$ , and the renormalization and factorization scale by  $\mu$ .

The recent measurement by H1 of dijet production in diffraction [23] shows that the Pomeron parton distributions extracted from

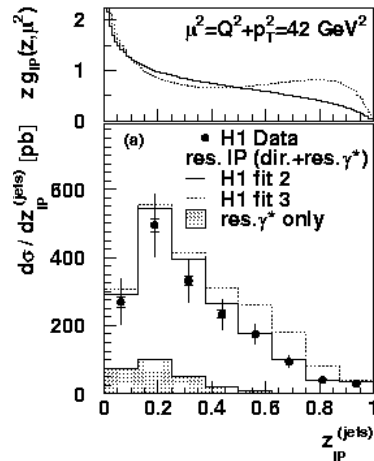


Figure 12: Dijet cross-section for diffractive events compared to predictions based on the gluon momentum distribution of the Pomeron,  $z g_{\text{IP}}$ . See text and ref [23].

that rise twice as fast as the inclusive one. In other words, if the rise of the inclusive cross-section is driven by a gluon density that rises as  $x^{-\lambda}$  (or  $W^{2\lambda}$ ), then for diffractive process that needs to couple to at least two gluons, the cross-section should rise as  $x^{-2\lambda}$ . At the same time, the energy dependence of the diffractive cross-section also contradicts Regge phenomenology, which expects an energy dependence of  $W^{0.25-0.3}$ .

The lines in Figure 13 that describe the data qualitatively are from the dipole model of Golec-Biernat and Wüsthoff [24, 25], briefly described below.

### 2.3 Impact Parameter Space (or Dipole) Models

The infinite momentum frame of DIS, which is appropriate for the DGLAP formalism, is obviously not the only possible frame of reference. In the impact parameter, or dipole, formalism, the appropriate frame of reference is that in which the virtual photon dissociates into a quark-anti quark pair (or a more complicated state), which forms a color dipole which collides with the proton (Figure 14).

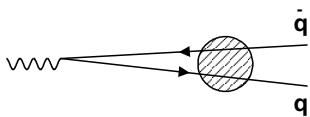


Figure 14: Color dipole picture of DIS

as  $r^2$  in keeping with the behavior of perturbative QCD. At large  $r$ ,  $\hat{\sigma}_{dipole}$  becomes constant to preserve unitarity. The saturation of the dipole cross-section can be qualitatively shown to correspond to the saturation of partons in the proton [27].

In the model, the point at which the  $r^2$  dependence of the cross-section changes to the constant behavior depends on the density of the partons in the proton. Specifically, a parameter,  $R_0 \sim 1/xg(x) \sim x^\lambda$ , which can be interpreted as the separation of

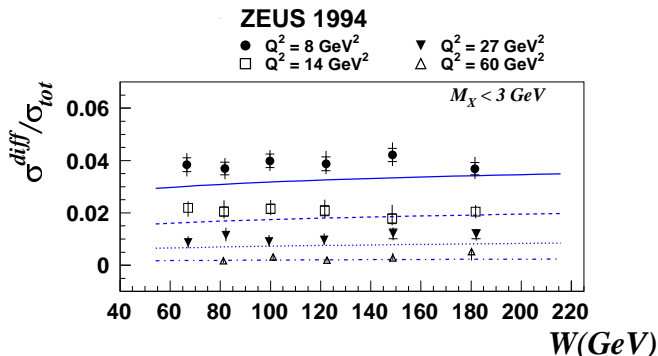


Figure 13: The ratio of diffractive to total DIS cross-section. The data have been binned in  $Q^2$  and a cut on the mass of the state  $X$ ,  $M_X < 3$  GeV has been made.

The description of the interaction of this color dipole with the proton distinguishes the various models of this type that have been proposed [26]. In this presentation, a particularly simple model due to Golec-Biernat and Wüsthoff (GB&W) will be described.

In the GB&W model, the cross-section of the dipole,  $\hat{\sigma}_{dipole}$ , with the proton is modeled simply as a function that smoothly interpolates between two limits (Figure 15); at small dipole radius,  $r$ ,  $\hat{\sigma}_{dipole}$  increases

partons in the proton, is introduced. When  $r \ll R_0$ ,  $\hat{\sigma}_{dipole}$  is in the “pQCD” region, while when  $r \gg R_0$ , it is in the saturation region (Figure 16a and 16b, respectively).

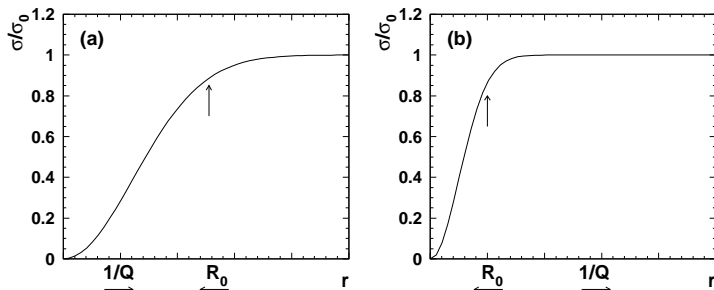


Figure 15: The dipole cross-section of the GB&W model for (a) the case of small dipole radius and (b) large dipole radius.

quarks in the dipole.

The diffractive cross-section is explicitly related to the total cross-section, which is,

$$\sigma_{tot} \propto \int d^2r \int dz |\Psi_\gamma(z, r)|^2 \hat{\sigma}_{dipole}(x, r). \quad (9)$$

The fact that  $\sigma^D/\sigma_{tot}$  is constant as a function of  $W$  (or  $x$ ), as shown in Figure 13, can be shown to occur only if the dipole cross-section is being probed in these processes beyond the small  $r$  region into the saturation region. The implication of this for the total cross-section will be discussed below.

In Figure 17a, the measurements of  $F_2^D$ , this time from the ZEUS collaboration, are shown along with the prediction of the GB&W model. There is qualitative agreement. Figure 17b shows the recent measurement of  $F_2^D$  at very low  $Q^2$  [28]. The GB&W model again describes the data qualitatively.

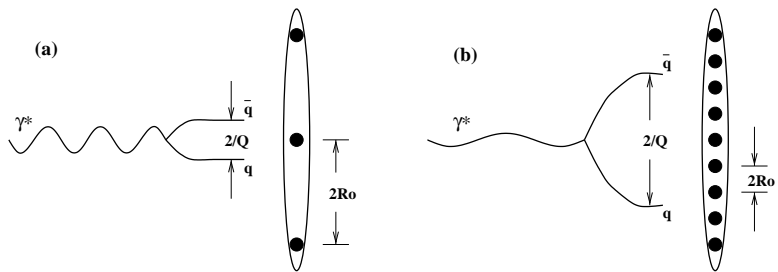


Figure 16: Schematic representation of the GB&W model. The characteristic radius of the dipole is proportional to the  $Q^2$  of the virtual photon,  $\gamma^*$ . The parameter  $R_0$  corresponds to the separation of the partons within the proton. The relative size of  $r$  and  $R_0$  determines the behavior of the dipole cross-section.

The dipole radius,  $r$ , enters through the wave function of the virtual photon,  $\Psi_\gamma$ , and the diffractive cross-section is written, up to a  $t$  dependence, as,

$$\sigma^D \propto \int d^2r \int dz \times |\Psi_\gamma(z, r)|^2 \hat{\sigma}_{dipole}^2(x, r), \quad (8)$$

where  $z$  is the fractional momentum of one of the

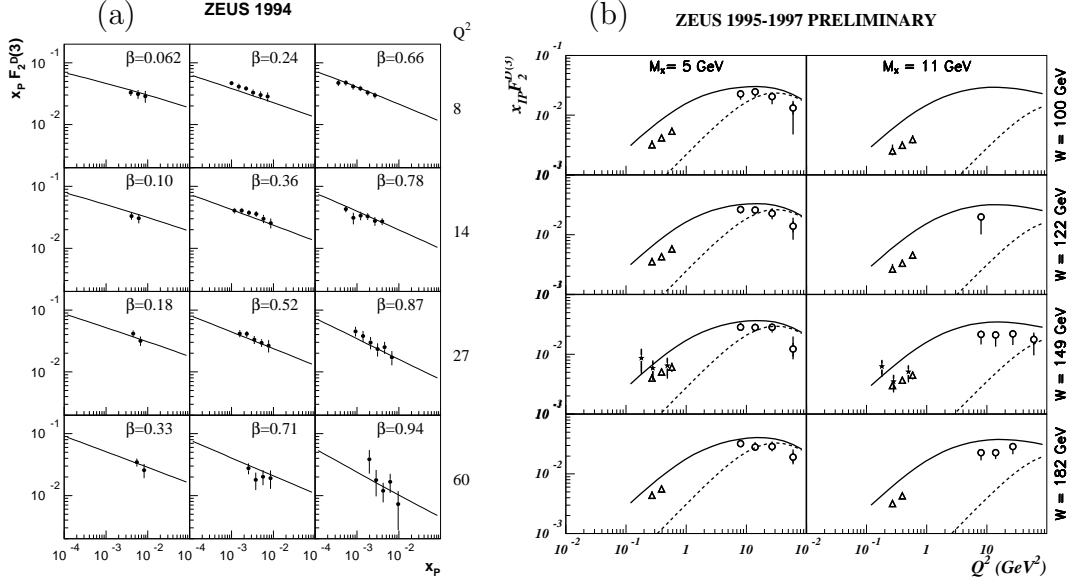


Figure 17: GB&W model (solid lines) compared to  $x_{\mathbb{P}}F_2^D(3)$  measurements. See text and refs [18, 25, 28].

### 3 Diffractive Vector Meson Production

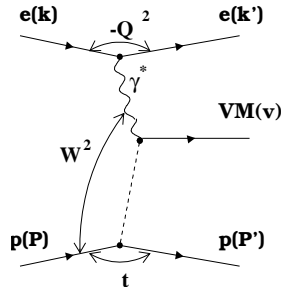


Figure 18: Diffractive VM production.

The exclusive production of vector mesons (VM) in DIS is a process which is closely related to DIS inclusive diffraction. As seen in Figure 18, the final state X in Figure 9 is replaced by a vector meson. Let us review the energy dependences of the processes we have discussed so far:

- The total real photoproduction cross-section,  $\sigma_{tot}^{\gamma p}$ , increases in accordance with the Regge expectation, i.e.  $W^{2(\alpha_{\mathbb{P}}-1)} \approx W^{0.16}$ .
- The total virtual-photon proton cross-section,  $\sigma_{tot}^{\gamma^* p}$ , at  $Q^2 \approx 10 \text{ GeV}^2$  increases approximately as  $W^{0.4}$ , corresponding to  $F_2$  rising as  $x^{-0.2}$ .
- The diffractive DIS cross-section,  $\sigma^D$ , has approximately the same energy dependence as  $\sigma_{tot}^{\gamma^* p}$ , i.e. increases as  $W^{0.4}$  at  $Q^2 \approx 10 \text{ GeV}^2$ .

The energy dependence of exclusive vector meson production at  $Q^2 = 0$  (photoproduction) is summarized in Figure 19. While the production of light vector mesons,  $\rho$ ,  $\phi$  and  $\omega$ , have a weak energy dependence consistent with Regge expectations, the  $J/\psi$  production cross-section rises rapidly with energy, as  $W^{0.8}$ , i.e. twice as fast as  $\sigma_{tot}^{\gamma^*p}$ , at  $Q^2 \approx 10 \text{ GeV}^2$ . It is the fastest energy dependence of the processes discussed so far [29, 30].

The  $Q^2$  dependence of the  $J/\psi$  production cross-section has been studied, but is still statistics limited. There is no evidence for a change of the energy dependence up to  $Q^2$  of 15  $\text{GeV}^2$  [31].

The  $Q^2$  dependence of  $\rho$  production cross-section is shown in Figure 20 [32], which shows  $\delta$ , as obtained from a fit to the form  $W^\delta$ , as a function of  $Q^2$ . The energy dependence clearly rises as a function of  $Q^2$ , although the precise form is not yet clear from the limited statistics.

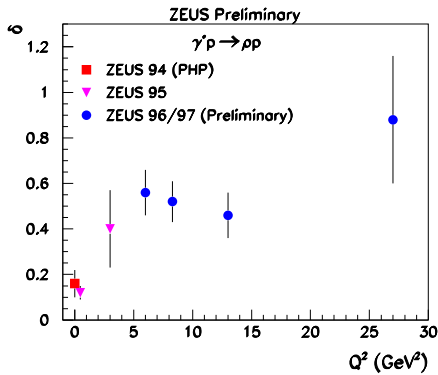


Figure 20: The energy dependence of  $\rho$  production as a function of  $Q^2$ .

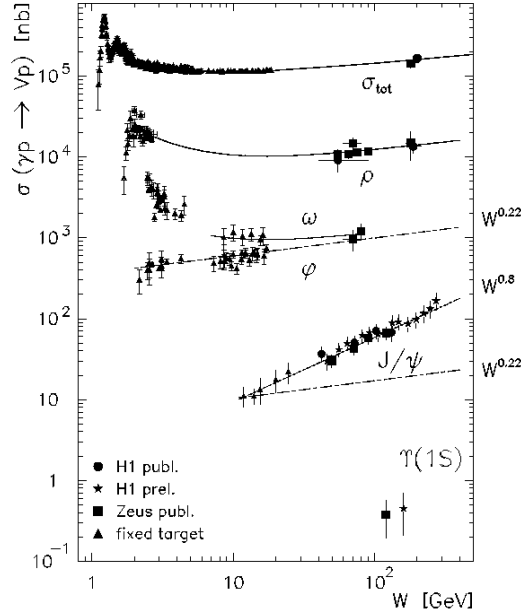


Figure 19: The  $W$  dependence of diffractive VM photoproduction.

In Figure 21,  $\delta$  for various species of vector mesons has been plotted as a function of  $Q^2 + M_{VM}^2$ , where  $M_{VM}$  is the mass of the vector meson. While the statistics are still limited, the data are consistent with a scaling of  $\delta$  with  $Q^2 + M_{VM}^2$ . If we recall that  $\delta = 2\lambda$  (see Section 1.2), we can compare the energy dependence of vector meson production with that of inclusive DIS.

Comparing Figure 21 with Figure 4 which shows  $\lambda$  extracted from fits to  $F_2$  to the form  $x^{-\lambda}$  for  $x < 0.1$ , it can be seen that  $\lambda_{(VM)}(Q^2 + M_{VM}^2) \approx 2\lambda_{(F_2)}(Q^2)$ . This means that the vector meson production has an energy dependence at  $Q^2 + M_{VM}^2$  which is twice as fast as that of the inclusive DIS cross-section at  $Q^2$ .

The ratio of cross-sections of different species of vector mesons to the  $\rho$  meson is shown in Figure 22 as a function of  $Q^2 + M_{VM}^2$ . The ratio is flat as a function of  $Q^2 + M_{VM}^2$  and is consistent with the ratios  $\rho : \omega : \phi : J/\psi$  being 9:1:2:8. Such ratios are expected from the coupling of a photon to a vector meson,  $f_{VM}^2$ , from simple charge counting of the quark content of the vector mesons.

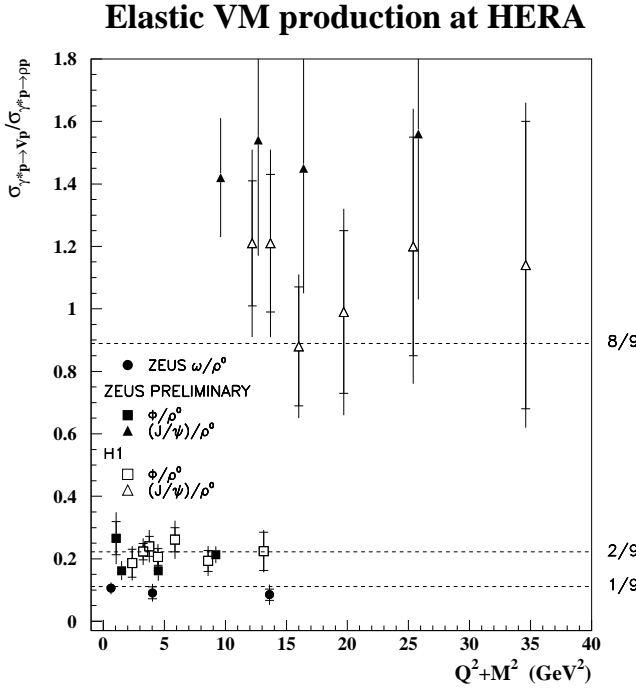


Figure 22: Ratios of diffractive VM production cross-sections to diffractive  $\rho$  production cross-section, as a function of  $Q^2 + M_{VM}^2$ .

Figure 23 shows the values of the  $t$  slope,  $b$ , where the vector meson cross-sections are parameterized as  $d\sigma_{VM}/d|t| \propto e^{-b|t|}$ . The parameter  $b$  is plotted as a function of  $Q^2 + M_{VM}^2$ . Within the statistical accuracy of the measurements,  $b$  scales with  $Q^2 + M_{VM}^2$  and decreases with increasing  $Q^2 + M_{VM}^2$ . This is an indication that  $Q^2 + M_{VM}^2$  is indeed giving the effective radius of the interaction, and thus the radius of the vector meson, or the color dipole.

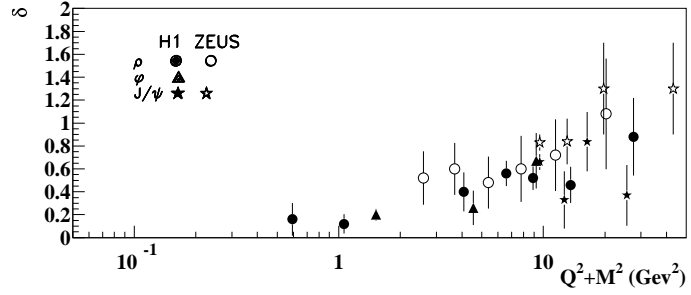


Figure 21: Energy dependence parameter  $\delta$  for different VM's plotted as a function of  $Q^2 + M_{VM}^2$ .

In the Vector Meson Dominance Model (VDM) of the production of vector mesons in photon (or virtual photon) proton collisions, the cross-section is given as  $\sigma_{VM} = f_{VM}^2 \cdot \sigma_{VMp}$ , where  $\sigma_{VMp}$  is the vector-meson proton cross-section. The fact that the ratio of the cross-sections is given by  $f_{VM}^2$  implies that  $\sigma_{VMp}$  for different species of vector mesons scales as  $Q^2 + M_{VM}^2$ . In the context of color dipole models, the implication is that  $Q^2 + M_{VM}^2$  gives a measure of the radius,  $r$ , of the color dipole, which is the primary variable on which the cross-section depends.

Figure 23 shows the values of the  $t$  slope,  $b$ , where the vector meson cross-sections are parameterized as  $d\sigma_{VM}/d|t| \propto e^{-b|t|}$ . The parameter  $b$  is plotted as a function of  $Q^2 + M_{VM}^2$ . Within the statistical accuracy of the measurements,  $b$  scales with  $Q^2 + M_{VM}^2$  and decreases with increasing  $Q^2 + M_{VM}^2$ .

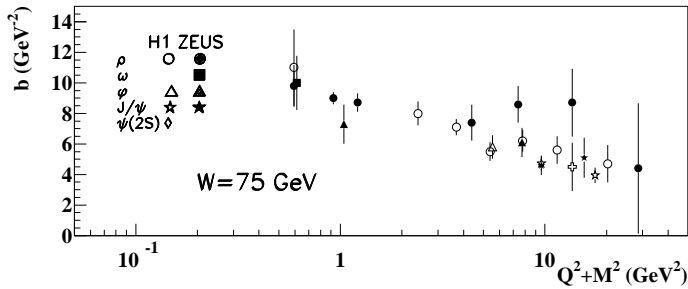


Figure 23: The slope dependence parameter  $b$  for different VM's plotted as a function of  $Q^2 + M_{VM}^2$ .

$\Psi_\gamma$ , is not a well known quantity. Recently, evaluation of vector meson production in the context of Equation (10) and the dipole cross-section,  $\hat{\sigma}_{dipole}$ , from the GB&W model has been made [33]. Simple wave-functions for the vector mesons were chosen. The results reproduce the elastic  $J/\psi$  cross-section and their energy dependence very well. For the lighter mesons,  $\phi$  and  $\rho$ , the calculations fail to give a good description of the magnitude of the cross-sections. However, the steepening of the energy dependence with increasing  $Q^2$  (Figure 20) is well reproduced.

## 4 $F_2$ at Small- $x$ Revisited

In the first part of this presentation, it was stated that the proton  $F_2$  measured so far at HERA and elsewhere is well described by fits using DGLAP equations above  $Q^2$  of  $1 \text{ GeV}^2$ , and a model combining Regge theory and Vector Meson Dominance has been shown to work well below  $1 \text{ GeV}^2$ .

The dipole model description of the total DIS cross-section (or  $F_2$ ) is given in Equation (9). Currently the formal connection between the DGLAP interpretation and the dipole models is far from clear [27, 34, 35]. However many dipole models, in particular the GB&W model, describe the dynamics of cross-section saturation which goes beyond the physics of the DGLAP picture. Thus, it is appropriate to revisit the inclusive DIS data and ask if there are any indications of behavior beyond DGLAP, even though the DGLAP fits are successful.

The DGLAP evolution equations, at low  $x$  and at LO, imply that the partial derivative of  $F_2$  with respect to  $(\ln Q^2)$  is proportional to  $xg(x, Q^2)$ , the gluon momentum density of the proton (Equation (4)). On the other hand, at sufficiently low  $Q^2$ ,  $F_2$  must vanish as  $Q^2$  from current conservation, a behavior built into the GB&W model but not in the DGLAP formulation of DIS:

$$\frac{\partial F_2}{\partial \log Q^2} \propto Q^2 \sigma_0. \quad (11)$$

The cross-section for diffractive vector meson production can be written in the color dipole model as,

$$\sigma_{VM} \sim \left| \int dz \int d^2 r \Psi_{VM} \times \hat{\sigma}_{dipole} \Psi_\gamma \right|^2, \quad (10)$$

where  $\Psi_{VM}$  is the wave function of the vector meson, which, in contrast to the virtual photon wave function,

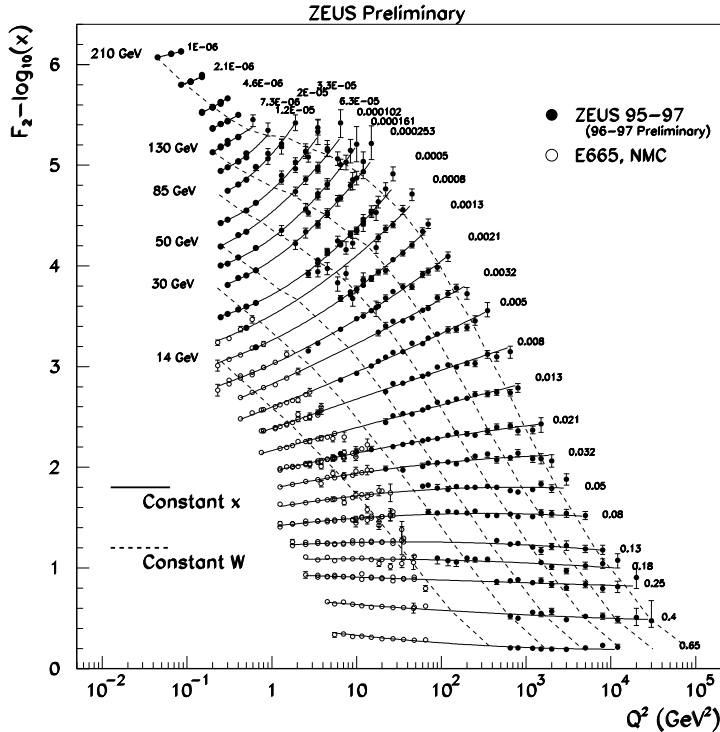


Figure 24:  $F_2$  measurements in bins of  $x$  as a function of  $Q^2$ . The solid lines are the results of the fits described in the text.

the nature of the transition [36].

Figure 24 shows recent measurements of  $F_2$  from the ZEUS collaboration along with the fixed target measurements [37] from the NMC and the E665 collaborations.  $F_2$  is shown as a function of  $Q^2$  for bins of fixed  $x$ . Where necessary, the measurements have been interpolated to the appropriate values of  $x$  using the ALLM parameterization [38]. The  $F_2$  in each bin of fixed  $x$  is offset by an additive factor of  $(-\log_{10} x)$  to ensure that the vertical separation between the bins is monotonic in  $x$ . Therefore, at low  $x$ , the line connecting  $F_2 - \log_{10} x$  at constant  $W$  would be a straight line, as a function of  $\log_{10} Q^2$ , if  $F_2$  were a constant and contained no dynamics.

The parameterization  $A(x) + B(x) \log_{10} Q^2 + C(x)(\log_{10} Q^2)^2$  has been used to fit the  $F_2$  measurements at each value of  $x$ . The quality of the fit is good, and the result is shown in Figure 24 as solid lines. The constant  $W$  points on the parameterizations have been found according to the formula  $W^2 = Q^2(1/x - 1)$ , and are indicated on the plot with dashed lines. It is interesting to note the distortion in the fixed- $W$  lines that occurs at  $x \approx 10^{-4}$  at relatively high  $Q^2 \approx 5 \text{ GeV}^2$  and at  $W$  above 85 GeV.

Since  $W$  at low  $x$  is related to  $x$  and  $Q^2$  by  $W^2 \approx Q^2/x$ , the plot of  $\partial F_2 / \partial \log Q^2$  at a constant  $W$ , over the  $Q^2$  range covered by the data, should show a transition from the behavior according to Equation (4) to that of Equation (11), provided  $xg(x, Q^2)$  has a weak  $Q^2$  dependence and  $\sigma_0$ , which corresponds to the photo-production cross-section, has a weak  $x$  (or equivalently energy) dependence. Since there is no quantitative prediction for the kinematic region in which the DGLAP formalism is applicable, the determination of the  $Q^2$  and  $x$  at which this transition occurs is of great interest and may help in clarifying

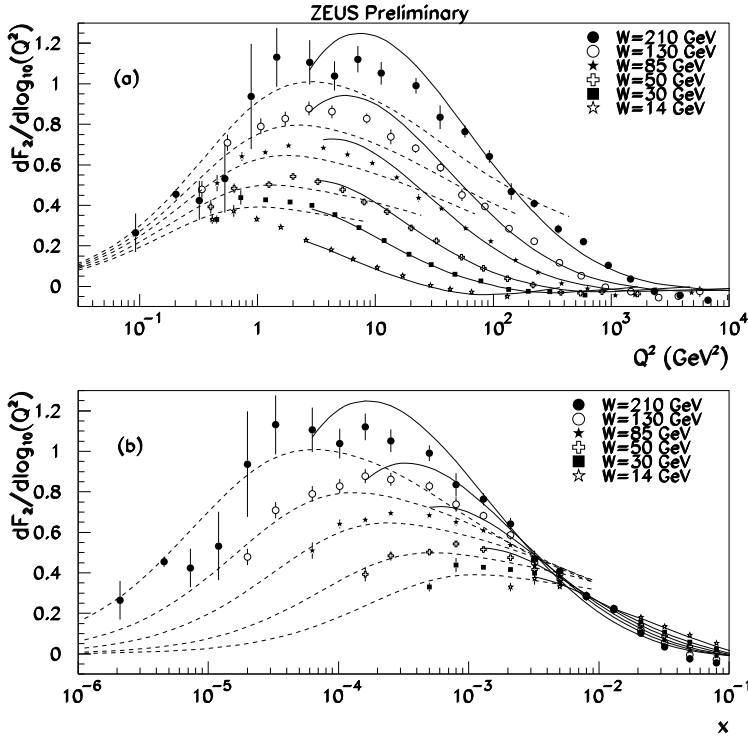


Figure 25: The logarithmic slope of  $F_2$  at a constant  $W$  as a function of  $Q^2$  and  $x$ . See text.

tion (11).

Figure 25b shows that at higher  $x$ , corresponding to higher  $Q^2$  in Figure 25a, the derivatives fall with increasing  $x$  and tend to become independent of  $W$  at  $x > 0.003$ , in line with the expectation of Equation (4), if  $xg(x, Q^2)$  has the form  $x^{-\lambda}$  and only a slow dependence on  $Q^2$ .

The value of  $Q^2$ , or  $x$ , where the slope of the derivatives changes sign can be read off from Figures 25a and 25b.

This transition, for values of  $W$  above 85 GeV, happens at a relatively high  $Q^2$  of 2-6 GeV<sup>2</sup> at the corresponding  $x$  of  $5 \cdot 10^{-4}$  to  $3 \cdot 10^{-3}$ .

The dashed lines in Figure 25 are the prediction of the GB&W model, which explicitly incorporates the transition between the behaviors described in Equations (11) and (4) as a

In Figure 25, the derivatives of  $F_2$ , evaluated from the fit  $B + 2C \log_{10} Q^2$ , are shown. The errors of the derivatives are evaluated using the errors on, and correlations between, the parameters  $B$  and  $C$  obtained from the polynomial fits. Figure 25a shows the derivatives at constant  $W$  as a function of  $Q^2$ , whereas Figure 25b shows the same as a function of  $x$ .

Figure 25a shows that at lower  $Q^2$ , corresponding to lower  $x$  in Figure 25b, the derivatives fall as  $Q^2$  decreases and tend to become independent of  $W$  at  $Q^2$  of about 0.4 GeV<sup>2</sup>. This is in line with the expectation of Equa-

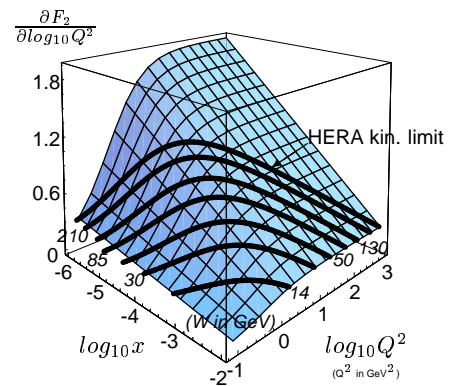


Figure 26: A schematic representation of Figure 25 in two dimensions. See text.

transition between the pQCD region and the saturation region of the dipole cross-section. The lines are drawn only at  $x < 0.01$  where the model is applicable. The solid line is the result of a DGLAP fit by the ZEUS collaboration. The line is drawn only above  $Q^2 > 2.7 \text{ GeV}^2$ , where data have been fit. In case of the DGLAP fit, the peaking behavior of Figure 25 is related to the rapid decrease of the gluon density at low  $x$  between  $Q^2$  of  $10 \text{ GeV}^2$  and  $1 \text{ GeV}^2$  [18, 39].

Figure 26 is a 2-dimensional visualization of the qualitative features of Figure 25. The lines of constant  $W$  (“trajectories”), plotted as thick solid lines, when projected to the  $Q^2$  and  $x$  axes, approximately give Figures 22a and 22b, respectively. The peak structure of the constant  $W$  lines represents the transition from the region where  $\partial F_2/\partial \log_{10} x$  is steeply rising with  $-\log_{10} x$  to the region where it is steeply rising with  $\log_{10} Q^2$ , behaviors corresponding to Equations (4) and (11), respectively. The position of the peak structure does not depend strongly on the “trajectory”,  $f(x, Q^2)$ , at which the derivatives are plotted, chosen to be  $W^2 \approx Q^2/x$  in Figure 25. Inspection of Figure 26 shows that almost any choice of a function  $f(x, Q^2)$ , which rises monotonically with decreasing  $x$  for a fixed  $Q^2$  will have a peak at the same  $(x, Q^2)$  position which correctly indicates the transition. In particular, an early ZEUS analysis, made with a more limited data set available at the time, shows (Figure 27) the same transitional behavior at the same  $(x, Q^2)$  position.

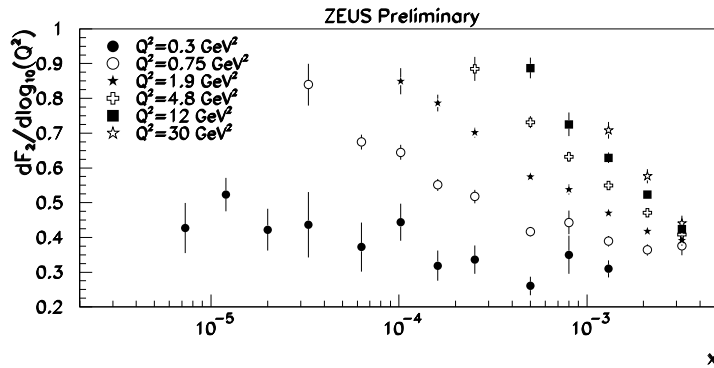


Figure 28: The logarithmic slope of  $F_2$  for fixed  $Q^2$  as a function of  $x$ .

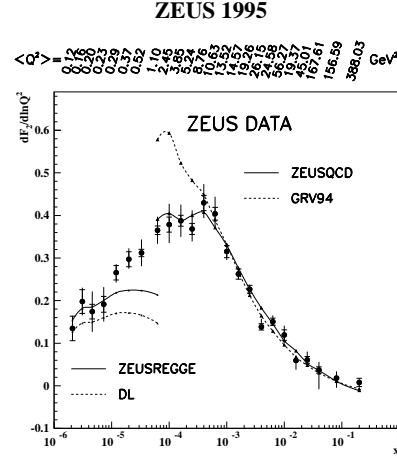


Figure 27: The logarithmic slope evaluated at  $Q^2$  (scale at the top) and  $x$  (scale at the bottom). See text.

Figure 28 shows the derivatives plotted for constant  $Q^2$ , as a function of  $x$ . At  $Q^2$  above  $1.9 \text{ GeV}^2$ , the derivatives rise rapidly as  $x$  decreases in line with the expectations of Equation (4) assuming  $xg(x, Q^2)$  has the form  $x^{-\lambda}$ . As  $Q^2$  falls, the rise of the derivative becomes less steep, as would be expected from Equation (11), if a mild energy

dependence, of the Regge type, is assumed for  $\sigma_0$ ; thus a turn-over in Figure 28 is not expected from the GB&W model, while naively one might expect it from Equation (4) with saturating gluons,  $xg$ . The statements sometimes found in the literature that the turn-over found in Figure 27 is “accidental” or “only kinematic in origin” [35, 40, 41, 42] arises from the combination of the expectation of a turn-over in Figure 28 as a manifestation of gluon saturation and the misunderstanding that Figure 27 is in some way an approximation of Figure 28; rather, it is an approximation of Figure 25.

## 5 Discussion and Outlook

The measurements of the proton structure at small  $x$  at HERA are now very precise. However, in spite of the expectation that these measurements should show some manifestation of dynamics beyond that incorporated in the  $(\ln Q^2)$  expansion of the DGLAP formalism, the DGLAP fits to the data give a good description above  $Q^2$  of about 1 GeV<sup>2</sup>.

The question of whether the success of DGLAP fits merely indicates the flexibility of the parton parameterizations and the still-limited  $(\ln Q^2)$  range of the measurement at small- $x$  is not likely to be answered by looking at  $F_2$  alone, at least in the currently available kinematic range. As discussed in Section 4, while the qualitative features of  $F_2$  at small- $x$  (and necessarily small  $Q^2$ ), show some characteristics expected by a saturation model, the DGLAP fits can reproduce those same features without any parton saturation, as a result of a rapidly evolving gluon density at low  $Q^2$ .

One of the most promising ways of investigating the small- $x$  proton structure is to look at the inclusive DIS measurements together (“and” rather than “or” of the title) with the diffractive DIS reactions. While the theoretical understanding of the relation of small- $x$  and diffraction is not yet very rigorous, the data sets from HERA provide many interesting indications of the underlying dynamics.

## ACKNOWLEDGEMENTS

It is a pleasure to thank the organizers for a most enjoyable Symposium. The experimental results presented here are due to a huge collaborative effort, over many years, of the large number of people in the H1 and ZEUS experiments. I had many interesting discussions on the subject matter of this talk with many of my colleagues in H1 and ZEUS; I would particularly like to thank Brian Foster. I would also like to thank John Collins, Krzysztof Golec-Biernat, Al Mueller and Mara Soares for illuminating discussions. Finally, Jim Whitmore, Peter Schleper and Brian Foster were kind enough to carefully check the manuscript.

## References

- [1] L. N. Lipatov, Sov. J. Nucl. Phys. **20**, 94 (1975);  
V. N. Gribov and L. N. Lipatov, Sov. J. Nucl. Phys. **15**, 438 (1972);  
G. Altarelli and G. Parisi, Nucl. Phys. **B126**, 298 (1977);  
Y. L. Dokshitzer, Sov. Phys. JETP**46**, 641 (1977).
- [2] H. L. Lai *et al.*, Phys. Rev. **D 55**, 1280 (1997) [hep-ph/9606399].
- [3] C. Adloff *et al.* [H1 Collaboration], hep-ex/0012053.
- [4] ZEUS Collaboration, paper 412, XXXth International Conference on High Energy Physics, July 27–August 2, 2000, Osaka, Japan.
- [5] C. Adloff *et al.* [H1 Collaboration], Nucl. Phys. B **497**, 3 (1997) [hep-ex/9703012].
- [6] J. Breitweg *et al.* [ZEUS Collaboration], Eur. Phys. J. **C7**, 609 (1999) [hep-ex/9809005].
- [7] K. Prytz, Phys. Lett. B **311**, 286 (1993).
- [8] M. Derrick *et al.* [ZEUS Collaboration], Z. Phys. **C63**, 391 (1994);  
S. Aid *et al.* [H1 Collaboration], Z. Phys. **C69**, 27 (1995) [hep-ex/9509001].
- [9] A. Donnachie and P. V. Landshoff, Nucl. Phys. **B231**, 189 (1984).
- [10] V. S. Fadin, E. A. Kuraev and L. N. Lipatov, Phys. Lett. **B60**, 50 (1975);  
E. A. Kuraev, L. N. Lipatov and V. S. Fadin, Sov. Phys. JETP**44** (1976) 443;  
E. A. Kuraev, L. N. Lipatov and V. S. Fadin, Sov. Phys. JETP**45** (1977) 199;  
I. I. Balitsky and L. N. Lipatov, Sov. J. Nucl. Phys. **28**, 822 (1978).
- [11] V. S. Fadin and L. N. Lipatov, Phys. Lett. **B429**, 127 (1998) [hep-ph/9802290];  
M. Ciafaloni and G. Camici, Phys. Lett. **B430**, 349 (1998) [hep-ph/9803389].
- [12] J. Blumlein and A. Vogt, Phys. Rev. D **57**, 1 (1998) [hep-ph/9707488].  
J. Blumlein, V. Ravindran, W. L. van Neerven and A. Vogt, hep-ph/9806368.
- [13] M. Ciafaloni, Nucl. Phys. **B296**, 49 (1988);  
S. Catani, F. Fiorani and G. Marchesini, Nucl. Phys. **B336**, 18 (1990);  
S. Catani, F. Fiorani and G. Marchesini, Phys. Lett. **B234**, 339 (1990).
- [14] L. V. Gribov, E. M. Levin and M. G. Ryskin, Phys. Rep. **100**, 1 (1983).
- [15] J. Bartels, G. A. Schuler and J. Blumlein, Z. Phys. C **50** (1991) 91.
- [16] R. S. Thorne, Nucl. Phys. **B512**, 323 (1998) [hep-ph/9710541].

- [17] H. Jung, Nucl. Phys. Proc. Suppl. **79**, 429 (1999) [hep-ph/9905554].
- [18] J. Breitweg *et al.* [ZEUS Collaboration], Eur. Phys. J. **C6**, 43 (1999) [hep-ex/9807010].
- [19] C. Adloff *et al.* [H1 Collaboration], Z. Phys. **C76**, 613 (1997) [hep-ex/9708016].
- [20] H1 Collaboration, paper 571, XXIXth International Conference on High Energy Physics, July 23–29, 1998, Tampere, Finland.
- [21] J. C. Collins, Phys. Rev. **D 57**, 3051 (1998) [hep-ph/9709499].
- [22] G. Ingelman and P. E. Schlein, Phys. Lett. **B152**, 256 (1985).
- [23] C. Adloff *et al.* [H1 Collaboration], hep-ex/0012051.
- [24] K. Golec-Biernat and M. Wusthoff, Phys. Rev. **D 59**, 014017 (1999) [hep-ph/9807513].
- [25] K. Golec-Biernat and M. Wusthoff, Phys. Rev. **D 60**, 114023 (1999) [hep-ph/9903358].
- [26] E. Gotsman, E. Levin and U. Maor, Nucl. Phys. **B493**, 354 (1997) [hep-ph/9606280];  
 E. Gotsman, E. Levin and U. Maor, Phys. Lett. **B425**, 369 (1998) [hep-ph/9712517];  
 E. Gotsman, E. Levin, U. Maor and E. Naftali, Nucl. Phys. **B539**, 535 (1999) [hep-ph/9808257];  
 N. N. Nikolaev and B. G. Zakharov, Z. Phys. **C49**, 607 (1991);  
 N. Nikolaev and B. G. Zakharov, Z. Phys. **C53**, 331 (1992);  
 V. Barone, M. Genovese, N. N. Nikolaev, E. Predazzi and B. G. Zakharov, Phys. Lett. **B326**, 161 (1994) [hep-ph/9307248];  
 J. R. Forshaw, G. Kerley and G. Shaw, Phys. Rev. **D 60**, 074012 (1999) [hep-ph/9903341];  
 W. Buchmuller, T. Gehrman and A. Hebecker, Nucl. Phys. **B537**, 477 (1999) [hep-ph/9808454];  
 A. H. Mueller and B. Patel, Nucl. Phys. **B425**, 471 (1994) [hep-ph/9403256];  
 A. H. Mueller, Nucl. Phys. **B415**, 373 (1994).  
 W. Buchmuller and A. Hebecker, Nucl. Phys. **B476**, 203 (1996) [hep-ph/9512329];  
 W. Buchmuller, M. F. McDermott and A. Hebecker, Nucl. Phys. **B487**, 283 (1997) [hep-ph/9607290].

- [27] A. H. Mueller, hep-ph/9911289.
- [28] ZEUS Collaboration, paper 435, XXXth International Conference on High Energy Physics, July 27–August 2, 2000, Osaka, Japan.
- [29] C. Adloff *et al.* [H1 Collaboration], Phys. Lett. **B483**, 23 (2000) [hep-ex/0003020].
- [30] ZEUS Collaboration, paper 437, XXXth International Conference on High Energy Physics, July 27–August 2, 2000, Osaka, Japan.
- [31] ZEUS Collaboration, paper 438, XXXth International Conference on High Energy Physics, July 27–August 2, 2000, Osaka, Japan.
- [32] ZEUS Collaboration, paper 439, XXXth International Conference on High Energy Physics, July 27–August 2, 2000, Osaka, Japan.
- [33] A. C. Caldwell and M. S. Soares, hep-ph/0101085.
- [34] J. Bartels, J. Phys. **G26**, 481 (2000).
- [35] M. F. McDermott, hep-ph/0008260.
- [36] ZEUS Collaboration, paper 416, XXXth International Conference on High Energy Physics, July 27–August 2, 2000, Osaka, Japan.
- [37] M. R. Adams *et al.* [E665 Collaboration], Phys. Rev. **D 54**, 3006 (1996);  
M. Arneodo *et al.* [New Muon Collaboration], Nucl. Phys. **B483**, 3 (1997) [hep-ph/9610231].
- [38] H. Abramowicz, E. M. Levin, A. Levy and U. Maor, Phys. Lett. **B269**, 465 (1991).  
H. Abramowicz and A. Levy, hep-ph/9712415.
- [39] A. D. Martin, R. G. Roberts, W. J. Stirling and R. S. Thorne, Eur. Phys. J. **C4**, 463 (1998) [hep-ph/9803445].
- [40] E. Gotsman, Nucl. Phys. Proc. Suppl. **79**, 192 (1999).
- [41] A. De Roeck, in the Proceedings of “Yalta 2000, new trends in high-energy physics”.
- [42] P. Schleper, hep-ex/0102051.

## Review of BFKL

CARL R. SCHMIDT\*

*Department of Physics and Astronomy  
Michigan State University, East Lansing, MI 48824 USA*

I describe the underlying physics behind the BFKL resummation and discuss some of the recent ideas and results in this field. On the theoretical side I consider the formalism in the next-to-leading logarithmic (NLL) approximation and the interpretation of the large corrections. On the phenomenological side I discuss several experiments that attempt to observe the BFKL effects in the high energy limit.

Presented at the

5th International Symposium on Radiative Corrections  
(RADCOR-2000)

Carmel CA, USA, 11–15 September, 2000

---

\*Work supported by the US National Science Foundation under grants PHY-9722144 and PHY-0070443.

# 1 Introduction to BFKL

Hadronic processes at high-energy colliders often involve more than one energy scale. As a consequence, calculations in perturbative Quantum Chromodynamics (QCD) can involve large logarithms of the ratio of these scales, which must be resummed to obtain a reliable prediction. Two processes where this might be necessary are Deep Inelastic Scattering (DIS) at small  $x$  and hadronic dijet production at large rapidity intervals  $\Delta y$ . In DIS the logarithm that appears is  $\ln(1/x)$ , with  $x \simeq Q^2/s$  the squared ratio of the momentum transfer to the photon-hadron center-of-mass energy. In large-rapidity dijet production the large logarithm is  $\Delta y \simeq \ln(\hat{s}/|\hat{t}|)$ , with  $\hat{s}$  the squared parton center-of-mass energy and  $|\hat{t}|$  of the order of the squared jet transverse energy. In both of these cases the large logarithms, which arise at each order in the coupling constant  $\alpha_s$ , can be resummed by means of the Balitsky-Fadin-Kuraev-Lipatov (BFKL) equation [1].

The most familiar prediction of the BFKL resummation in the leading logarithmic (LL) approximation is the power-law rise in the partonic cross section as a function of the energy:

$$\hat{\sigma} \approx e^{A\Delta y} \approx \hat{s}^A . \quad (1)$$

The quantity  $(1 + A)$  is often referred to as the BFKL Pomeron intercept, where at LL

$$A = \bar{\alpha}_s 4 \ln 2 \quad (2)$$

with  $\bar{\alpha}_s = N_c \alpha_s / \pi$  and  $N_c = 3$  the number of colors. Similarly, in DIS the structure functions are predicted to rise as  $x^{-A}$  at small  $x$ . One of the goals in BFKL physics has been to observe this power-law rise as a direct indication of the importance of the resummation. In this talk I will review the status of BFKL physics, both in its theoretical development at next-to-leading logarithm (NLL) and in its phenomenological application to experiment.

## 2 BFKL at LL

I begin by giving a simple physical picture of the BFKL resummation at leading logarithm (LL), where the large logarithm is taken to be the rapidity interval between two widely-separated partonic jets. Although this in no way can be considered a derivation of the BFKL equation, it is useful to show what assumptions go into the resummation and to show how the factors of  $\alpha_s \Delta y$  arise at each order and exponentiate.

The starting point is the factorization of the partonic cross section at large rapidity separation:

$$\frac{d\hat{\sigma}}{d^2 p_{a\perp} d^2 p_{b\perp}} = V_a(p_{a\perp}^2) f(\Delta y, p_{a\perp}, p_{b\perp}) V_b(p_{b\perp}^2) . \quad (3)$$

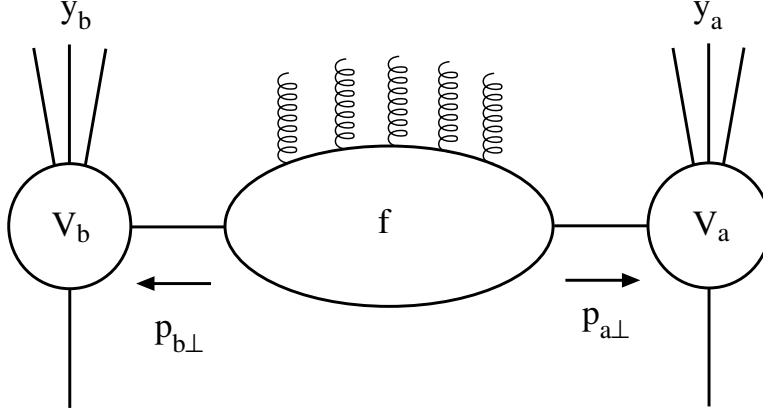


Figure 1: A schematic picture of the cross section for producing particles at large rapidity separation.

A physical interpretation of this factorization is represented in Fig. 1. The process consists of two distinct scatterings, which occur at widely-separated rapidities,  $y_a$  and  $y_b$ , and small transverse momenta  $|p_{a\perp}| \sim |p_{b\perp}|$ . The impact factors  $V(p_\perp^2)$  depend only on the transverse momentum exchanged and the specific partons involved in each scattering, but not on anything else that happens in the event. The function  $f(\Delta y, p_{a\perp}, p_{b\perp})$  connects the two scatterings by accounting for the emission of gluons in the rapidity interval. This function is universal and provides the exponentiation of the logarithms.

We can see this factorization directly in the Born cross section for gluon-gluon scattering at  $y_a \gg y_b$ , shown diagrammatically in Fig. 2(a):

$$\frac{d\hat{\sigma}_{gg}^{(0)}}{d^2p_{a\perp}d^2p_{b\perp}} = \left[ \frac{N_c\alpha_s}{p_{a\perp}^2} \right] \left[ \frac{1}{2}\delta^{(2)}(p_{a\perp} + p_{b\perp}) \right] \left[ \frac{N_c\alpha_s}{p_{b\perp}^2} \right], \quad (4)$$

where the central factor is the  $\mathcal{O}(\alpha_s^0)$  contribution to the function  $f$ , and we see that the leading-order gluon impact factor is

$$V_g(p_\perp^2) = \frac{N_c\alpha_s}{p_\perp^2}. \quad (5)$$

The real  $\mathcal{O}(\alpha_s^1)$  correction to  $f$  can be obtained by considering the emission of three gluons, strongly ordered in rapidity  $y_a \gg y_1 \gg y_b$ , shown diagrammatically in Fig. 2(b):

$$\frac{d\hat{\sigma}_{gg}^{(1r)}}{d^2p_{a\perp}d^2p_{b\perp}} = \left[ \frac{N_c\alpha_s}{p_{a\perp}^2} \right] \left[ \frac{\bar{\alpha}_s}{\pi} \int \frac{d^2k_{1\perp}dy_1}{k_{1\perp}^2} \frac{1}{2}\delta^{(2)}(p_{a\perp} + k_{1\perp} + p_{b\perp}) \right] \left[ \frac{N_c\alpha_s}{p_{b\perp}^2} \right]. \quad (6)$$

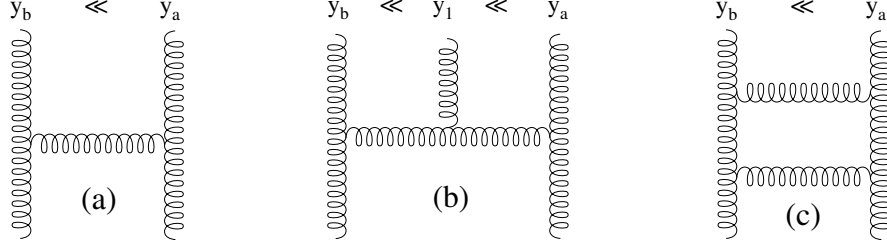


Figure 2: Contributions to LL BFKL ladder obtained from  $gg$  scattering: (a)  $(\alpha_s \Delta y)^0$  real. (b)  $(\alpha_s \Delta y)^1$  real. (c)  $(\alpha_s \Delta y)^1$  virtual.

From this formula, we easily see where the large logarithm comes from. It arises from the integral over the rapidity  $y_1$  of the intermediate gluon, resulting in a factor of  $\alpha_s \Delta y$ .

We can now generalize the form of these real corrections to an arbitrary number of emitted gluons:

- At each order, another gluon is inserted in the ladder with a weight given by

$$\frac{\bar{\alpha}_s d^2 k_{i\perp}}{\pi k_{i\perp}^2} .$$

- The emitted gluons conserve transverse momentum, as enforced by a delta-function factor

$$\frac{1}{2} \delta^{(2)}(p_{a\perp} + \sum_i k_{i\perp} + p_{b\perp}) .$$

- The intermediate gluons are integrated over the ordered rapidity-intervals,

$$y_b < y_1 < y_2 < \dots < y_n < y_a ,$$

producing an overall factor of

$$\frac{(\Delta y)^n}{n!} .$$

The real  $n$ -gluon contribution can be obtained directly from the tree-level  $(n+2)$ -gluon cross-section by assuming that all transverse momenta are comparable in size, while terms suppressed by  $\mathcal{O}(e^{-|y_i - y_j|})$  are neglected.

Of course, the real contributions by themselves are not infrared-safe, because they diverge when the  $k_\perp$  of any of the intermediate gluons vanishes. The cure for this is the inclusion of virtual corrections in the large  $\Delta y$  limit. The  $\mathcal{O}(\alpha_s^1)$  virtual correction

in  $gg$  scattering comes from the diagram in Fig. 2(c). Similar contributions must come in at each order to regularize the  $1/k_{\perp}^2$  infrared singularities. Including these corrections, we can understand the following form of the BFKL equation

$$\begin{aligned}
f(\Delta y, p_{a\perp}, p_{b\perp}) &= \frac{1}{2} \delta^{(2)}(p_{a\perp} + p_{b\perp}) \\
&+ (\Delta y) K \left[ \frac{1}{2} \delta^{(2)}(p_{a\perp} + p_{b\perp}) \right] \\
&+ \frac{1}{2!} (\Delta y)^2 K \left[ K \left[ \frac{1}{2} \delta^{(2)}(p_{a\perp} + p_{b\perp}) \right] \right] \\
&+ \frac{1}{3!} (\Delta y)^3 K \left[ K \left[ K \left[ \frac{1}{2} \delta^{(2)}(p_{a\perp} + p_{b\perp}) \right] \right] \right] \\
&+ \dots, \tag{7}
\end{aligned}$$

where the kernel  $K$  is an integral operator acting on a function  $\phi(p_{a\perp})$  by

$$K \left[ \phi(p_{a\perp}) \right] = \frac{\bar{\alpha}_s}{\pi} \int \frac{d^2 k_{\perp}}{k_{\perp}^2} \left[ \phi(k_{\perp} + p_{a\perp}) - \frac{p_{a\perp}^2}{k_{\perp}^2 + (k_{\perp} + p_{a\perp})^2} \phi(p_{a\perp}) \right]. \tag{8}$$

At LL, each operation of the kernel inserts one more real or virtual gluon in the ladder. The first term in (8) corresponds to a real gluon, while the second term is the virtual correction needed to regularize the soft singularity. The equation (7) is just the solution of the BFKL equation obtained by iteration.

A more compact form of the BFKL solution at LL is obtained by finding the eigenfunctions and eigenvalues of the kernel (8). This yields

$$f(\Delta y, p_{a\perp}, p_{b\perp}) = \frac{1}{i(2\pi)^2} \sum_{n=-\infty}^{\infty} e^{in\tilde{\phi}} \int_{1/2-i\infty}^{1/2+i\infty} d\gamma (p_{a\perp}^2)^{\gamma-1} (p_{b\perp}^2)^{-\gamma} e^{\bar{\alpha}_s \chi(n, \gamma) \Delta y}, \tag{9}$$

where  $\tilde{\phi} = \phi_a - \phi_b - \pi$ , the function

$$\bar{\alpha}_s \chi(n, \gamma) = \bar{\alpha}_s \left[ 2\psi(1) - \psi\left(\frac{n}{2} + \gamma\right) - \psi\left(\frac{n}{2} + 1 - \gamma\right) \right] \tag{10}$$

gives the eigenvalues of the LL BFKL kernel (8), and  $\psi$  is the logarithmic derivative of the gamma function. For very large  $\Delta y$ , the integral over  $\gamma$  in (9) can be performed in the saddle-point approximation. The  $n = 0$  term dominates, and one obtains the exponential rise in the cross section (1), displayed in the introduction with  $A = \bar{\alpha}_s \chi(0, \frac{1}{2}) = 4\bar{\alpha}_s \ln 2$ .

### 3 BFKL at NLL

At LL each application of the kernel gives a contribution of  $\mathcal{O}(\alpha_s \Delta y)$ . At NLL one also includes terms of  $\mathcal{O}(\alpha_s^2 \Delta y)$ . That is, we can reinterpret the kernel in (7) as a

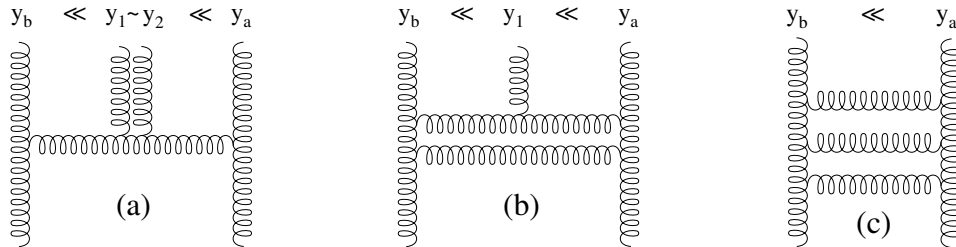


Figure 3: Contributions to NLL BFKL ladder at  $\mathcal{O}(\alpha_s^2 \Delta y)$  obtained from  $gg$  scattering.

power series  $K \equiv \bar{\alpha}_s K^{(1)} + \bar{\alpha}_s^2 K^{(2)} + \dots$ , where  $\bar{\alpha}_s K^{(1)}$  is the LL kernel, given in (8), and  $\bar{\alpha}_s^2 K^{(2)}$  includes the NLL corrections. There are three types of contributions at NLL, which are shown schematically, in the context of  $gg$  scattering, in Fig. 3. They consist of: (a) the emission of two gluons nearby in rapidity, (b) the virtual correction to the emission of one gluon, widely separated in rapidity, (c) the subleading purely-virtual corrections. These three types of contributions took many years and many papers to sort out the technical details<sup>1</sup>, with the final NLL kernel obtained in 1998 by Fadin and Lipatov [3]. Although the full kernel has not been checked in a completely independent manner, many of the pieces of the calculation have received independent confirmation. Two particularly significant checks are the calculation of the virtual correction to the gluon emission at large rapidity separation [4], and the compilation of the three NLL terms into a single kernel with the cancellation of all collinear and soft singularities [5].

The final result of this calculation is usually presented by applying the NLL kernel to the LL eigenfunctions, with azimuthal averaging, yielding

$$\begin{aligned}
 K_{\text{NLL}} \left[ (p_{a\perp}^2)^{\gamma-1} \right] &= \left\{ \bar{\alpha}_s(\mu) \chi(\gamma) \right\} (p_{a\perp}^2)^{\gamma-1} \\
 &= \left\{ \bar{\alpha}_s(\mu) \chi^{(1)}(\gamma) \left[ 1 - \bar{\alpha}_s(\mu) b_0 \ln(p_{a\perp}^2/\mu^2) \right] \right. \\
 &\quad \left. + \bar{\alpha}_s(\mu)^2 \chi^{(2)}(\gamma) \right\} (p_{a\perp}^2)^{\gamma-1}
 \end{aligned} \tag{11}$$

where  $\bar{\alpha}_s \chi^{(1)}(\gamma)$  is the LL eigenvalue for  $n = 0$  given in (10),  $b_0 = 11/12 - n_f/(6N_c)$ , and we have explicitly included the dependence on the  $\overline{\text{MS}}$  renormalization scale  $\mu$ . The NLL correction has been separated into two terms. The first term depends on the scale  $p_{a\perp}$  and is associated with the running of the coupling in the LL kernel:  $\alpha_s(\mu) \rightarrow \alpha_s(p_{a\perp})$ . The second term,  $\bar{\alpha}_s^2 \chi^{(2)}(\gamma)$ , is independent of scale and contains the remainder of the NLL corrections [3].

After completion of the NLL corrections to the BFKL kernel, several issues quickly became apparent. Roughly speaking, they can be separated into issues associated

<sup>1</sup>A list of references can be found in ref. [2], but with no guarantee of completeness.

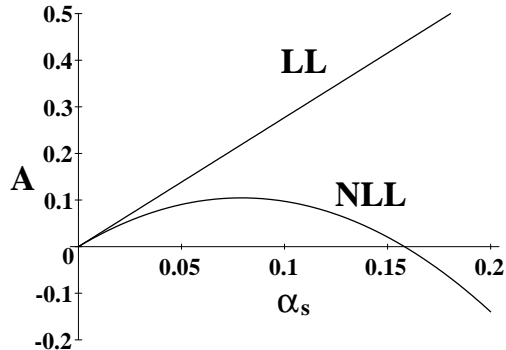


Figure 4: Leading BFKL eigenvalue  $A = \bar{\alpha}_s \chi(\frac{1}{2})$  at LL and NLL.

with the running coupling term and issues associated with the scale-invariant term. In this talk I will concentrate on the scale-invariant term. For analyses of the running coupling issues, see Refs. [6,7,8,9].

The first indication of problems with BFKL at NLL was seen immediately by Fadin and Lipatov. The corrections to the leading eigenvalue are large and negative! If we ignore the effects of running coupling, we obtain

$$\bar{\alpha}_s \chi(\frac{1}{2}) = 2.77\bar{\alpha}_s - 18.34\bar{\alpha}_s^2, \quad (12)$$

for three active flavors. This function is plotted in Fig. 4. At the not-unreasonable value of  $\alpha_s = 0.16$  the NLL corrections exactly cancel the LL term, while for larger values of  $\alpha_s$  the eigenvalue becomes negative. Naively, this would indicate that the BFKL Pomeron intercept also becomes negative, leading to a cross section that decreases, rather than increases, as a power of the energy.

Unfortunately, things get even worse. The standard BFKL power-law scaling of the partonic cross section (1) relies on the saddle-point evaluation of the NLL generalization of the BFKL solution (9). Upon closer analysis Ross [10] showed that the NLL eigenvalue function  $\chi(\gamma)$  no longer has a maximum at  $\gamma = \frac{1}{2}$ , but has a minimum with two maxima occurring symmetrically on either side of this point<sup>2</sup>. Performing a higher-order expansion of  $\chi(\gamma)$ , Ross found a smaller correction to the BFKL Pomeron intercept. However, the cross section he obtained was not positive definite. It contained oscillations as one varied  $p_{a\perp}$  and  $p_{b\perp}$ . This led Levin [8] to declare that NLL BFKL has a serious pathology.

<sup>2</sup>The standard procedure in these analyses is to modify the LL eigenfunctions used in eq. (11) in order to make the eigenvalues manifestly symmetric under  $\gamma \rightarrow 1 - \gamma$ , following ref. [3].

One might wonder whether the approximate evaluation of the integral performed by Ross is adequate at this stage. Perhaps an exact evaluation is necessary. However, negative cross sections have also arisen when the resummed small- $x$  anomalous dimensions, obtained from the NLL BFKL solution, were used to study DIS scattering at small- $x$  [11,12]. In any event the NLL corrections to the BFKL solution are large, leading one to question the stability and applicability of the BFKL resummation procedure in general.

## 4 Understanding the large NLL Corrections.

When any perturbation expansion has large corrections at higher orders, the natural thing to do is to try to reorganize the series so that it converges more rapidly. In this talk I will briefly discuss three different approaches to this reorganization.

The first proposal by Brodsky *et al.* [13] uses the freedom to choose the renormalization scheme. The NLL eigenvalue equation (12) is written in the  $\overline{\text{MS}}$  scheme. Brodsky *et al.* argued that a non-abelian physical scheme should be more natural for the BFKL resummation. Then they used the BLM procedure [14] to find the optimal scale for the QCD coupling. In this case the BLM procedure dictates a large scale, thereby reducing the effective  $\alpha_s$  (and the LL prediction) and also reducing the coefficient of the NLL  $\alpha_s^2$  term. This approach predicts a BFKL Pomeron intercept of  $A \sim 0.17$  for  $\alpha_s = 0.2$ . In addition it yields a very weak dependence on the gluon virtuality  $p_{a\perp}^2$  and leads to an approximate conformal invariance.

The motivation for the second proposal [2] (first suggested in [15] and [16]) can be seen from the discussion of the physics of BFKL at LL in section 2. The approximation used in deriving the LL contribution at each order in the BFKL ladder was to neglect terms of  $\mathcal{O}(e^{-|y_i - y_{i+1}|})$  in the QCD matrix elements, which is valid when the emitted gluons are all widely separated in rapidity. However, the gluon rapidity  $y_i$  is then integrated all the way up to  $y_{i+1}$ . Thus, the errors in the matrix elements are largest when  $y_i \sim y_{i+1}$ . This suggests that one enforce a condition  $y_{i+1} - y_i > \Delta$ , so that the gluons are required to be widely separated, and the kinematic approximations are good. The arbitrary parameter  $\Delta$  is assumed to be much smaller than the total rapidity interval. The excluded region is re-introduced at NLL, such that the change in the cross section due to shifting  $\Delta$  is always next-to-next-to-leading logarithm (NNLL). In this way, the dependence on  $\Delta$  can be regarded as an estimate of the uncertainty due to NNLL corrections (similar to the role of the renormalization scale  $\mu$  in the  $\overline{\text{MS}}$  scheme).

Fig. 5 shows the dependence on  $\Delta$  of the leading eigenvalue and its second derivative at LL and NLL for  $\alpha_s = 0.15$  in this modified BFKL theory. Note that the corrections to  $\bar{\alpha}_s \chi(\frac{1}{2})$  are not large for  $\Delta \gtrsim 2$  and have weak dependence on  $\Delta$  for large  $\Delta$ . Also, the point  $\gamma = \frac{1}{2}$  is a maximum for this coupling as long as  $\Delta \gtrsim 2.2$ .

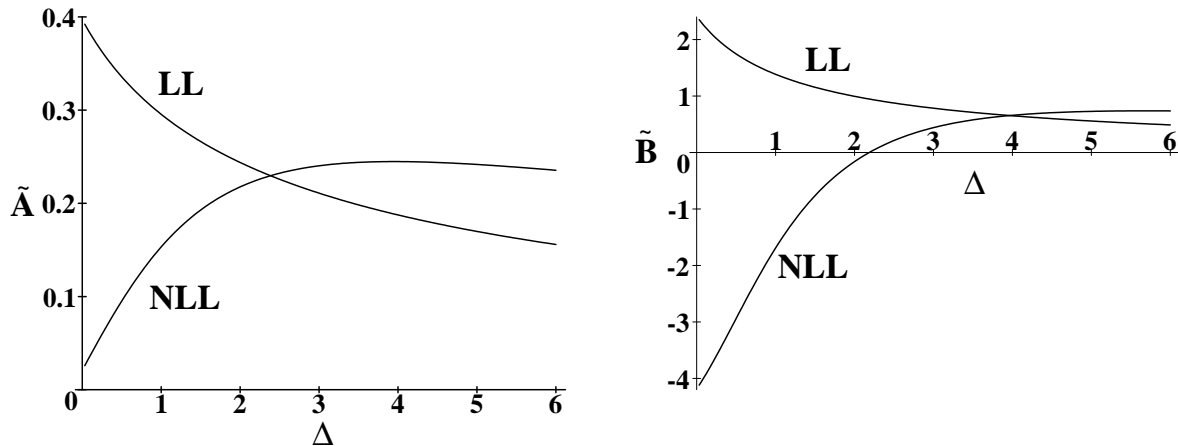


Figure 5: Dependence of  $\tilde{A} = \bar{\alpha}_s \chi(\frac{1}{2})$  and  $\tilde{B} = -\frac{1}{2} \bar{\alpha}_s \chi''(\frac{1}{2})$  on  $\Delta$  for  $\alpha_s = 0.15$ , from Ref. [2].

Thus, the BFKL resummation is stable for large enough  $\Delta$ . This modification of the BFKL resummation predicts a somewhat larger value of the BFKL pomeron intercept than the previous proposal. However, the implications of a large value of  $\Delta$  for the phenomenological use of BFKL is open to interpretation.

The third and perhaps most ambitious proposal [17,9] to control the large NLL corrections is to systematically include the largest collinearly-enhanced, but still sub-leading corrections into LL BFKL. The most important of these are energy-scale corrections [5]. To understand the origin of these corrections, note that in our discussion of BFKL at LL in section 2 we chose to work with the symmetric rapidity  $\Delta y = \ln \hat{s}/(p_{a\perp} p_{b\perp})$  as the large logarithm to resum. However, we could equally well have chosen  $y^+ = \ln x_a^+/x_b^+ = \ln \hat{s}/p_b^2$  or  $y^- = \ln x_b^-/x_a^- = \ln \hat{s}/p_a^2$ , where  $x_i^\pm$  is the momentum fraction along the positive or negative light-cone for the emitted gluon  $i$ . These choices are all equivalent at LL because the transverse momenta are treated as comparable in size; however, at NLL they are inequivalent. A change in the logarithm produces a change in the NLL kernel and can introduce double transverse logarithms of the form  $\bar{\alpha}_s \ln^2(p_{a\perp}^2/p_{b\perp}^2)$  into the resummation.

Motivated by DGLAP-type resummation [18] one finds that the appropriate choice is to resum  $y^+$  when  $p_{b\perp}^2 \gg p_{a\perp}^2$  and  $y^-$  when  $p_{a\perp}^2 \gg p_{b\perp}^2$ . The effect of these changes of the BFKL resummation variable was studied in refs. [5] and [3], and the corresponding terms in the NLL eigenvalue  $\chi^{(2)}(\gamma)$  were isolated and resummed in ref. [17]. Additional collinearly-enhanced terms due to the effects of the running

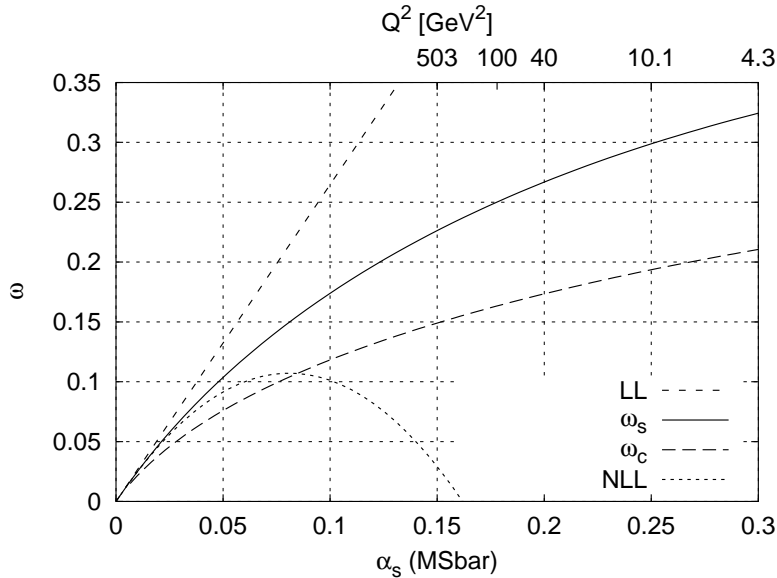


Figure 6: The BFKL Pomeron intercept (here labeled  $\omega$ ) at LL, NLL and with the collinearly-enhanced resummation included at NLL, from Ref. [9]. The curve  $\omega_s$  corresponds to the coefficient for the exponential rise in  $\Delta y$ , which is what we have focused on in this talk. The curve  $\omega_c$  corresponds to the power growth of the small- $x$  splitting functions. Although identical in LL BFKL, these two coefficients differ at NLL.

coupling and the non-singular part of the splitting functions have also been considered and resummed in Ref. [9]. A nice discussion of these ideas can be found in ref. [19].

A similar approach, advocated in Refs. [20], is to use the “duality” relations between the BFKL  $\ln(1/x)$  and the DGLAP  $\ln(Q^2)$  resummations to incorporate the dominant collinear effects into BFKL at small  $x$ . Adding contributions obtained from the known LO and NLO DGLAP anomalous dimensions, one gets a “double leading” expansion for the BFKL function  $\chi(\gamma)$ , which is better behaved and more stable in the collinear region near  $\gamma = 0$ .

Results of the collinearly-enhanced resummation from Ref.[9] are shown in Fig. 6, where the leading eigenvalue  $\omega_s = \bar{\alpha}_s \chi(\frac{1}{2})$  is plotted as a function of  $\bar{\alpha}_s$ . As in the other cases the eigenvalue is found to be positive after resummation, yielding a value of about  $\omega_s = 0.27$  for  $\alpha_s = 0.2$ . In addition the characteristic eigenvalue function of  $\gamma$  is stable for values of  $\alpha_s$  of interest.

The physical implications of the energy-scale dependence can be seen by further investigating the relation between resummation in  $y^\pm$  and  $\Delta y$ . When  $p_{b\perp}^2 \gg p_{a\perp}^2$ , the resummation in  $y^+$  requires the ordering  $x_a^+ > x_b^+$ . Translating back into the symmetric variable, this implies  $\Delta y > \ln(p_{b\perp}/p_{a\perp})$ . Similarly, when  $p_{a\perp}^2 \gg p_{b\perp}^2$ , the resummation in  $y^-$  requires the ordering  $x_b^- > x_a^-$ , implying  $\Delta y > \ln(p_{a\perp}/p_{b\perp})$ . These constraints hold for any two successively emitted gluons. Therefore, the incorporation

of these collinear effects corresponds to imposing a  $p_{\perp}$ -dependent cut,  $y_{i+1} - y_i > |\ln(p_{i\perp}/p_{i+1\perp})|$ , on the separation in rapidity between the neighboring gluons. Since this cut is very similar to the rapidity veto of proposal two, it is understandable that when both the collinear resummation and the rapidity veto are included, as studied in Ref. [21], the dependence on the parameter  $\Delta$  was significantly reduced, even for small  $\Delta$ .

## 5 Phenomenology of BFKL

Although the theoretical studies of BFKL have been focused on its behavior at NLL, the level of most phenomenological studies is still at LL. To treat a process consistently at NLL, one also must incorporate the  $\mathcal{O}(\alpha_s)$  corrections to the impact factors. Although these corrections are known for some processes, at least at the amplitude level, they have yet to be incorporated into a consistent calculation suitable for phenomenological studies.

In this section I will discuss several probes of BFKL physics in hadron-hadron, lepton-hadron, and  $\gamma^*\gamma^*$  collisions. I will only consider processes for which the relevant transverse scales  $p_{a\perp}, p_{b\perp}$  on both sides of the BFKL ladder can be considered perturbative. In particular, I will not consider the inclusive  $F_2(x, Q^2)$  in DIS, because it is necessarily dependent on non-perturbative inputs.

### 5.1 BFKL probes at the Tevatron

One of the most thoroughly studied searches for BFKL physics has been by the DØ collaboration in  $p\bar{p}$  collisions at the Fermilab Tevatron. As in all BFKL experimental studies, the basic idea is to analyze the events in a configuration which most closely approximates that used in the BFKL resummation. Jets, with transverse momentum above some  $E_{\perp\text{min}}$ , are tagged and ordered in rapidity. Then one defines observables as a function of  $\Delta y = y_a - y_b$ , where  $y_a$  and  $y_b$  are the rapidities of the most forward and backward jets, respectively.

The most natural BFKL signal would be the power-law growth in the partonic cross section with  $\Delta y$ , as in Eq. (1). However, at fixed center-of-mass energy this growth is swamped by the effects of steeply falling parton distribution functions (PDFs) which are relevant when far forward or backward jets are produced. Thus, the first observable to be considered was the decorrelation in azimuthal angle between the two tagged jets as a function of  $\Delta y$ . Physically, this effect is easy to understand. In the Born approximation, only two jets are produced, and by momentum conservation they must be back-to-back. However, as the rapidity interval increases, there is more room for additional jets, and the tagged jets become decorrelated. This can be seen directly in the BFKL solution (9). At small  $\Delta y$ , all terms in the Fourier series in  $\tilde{\phi} = \phi_a - \phi_b - \pi$  are approximately equal, producing a delta-function in  $\tilde{\phi}$

which forces the two jets to be back to back. As  $\Delta y$  increases, the higher order terms become smaller and smaller compared to the leading  $n = 0$  term, so the jets become completely decorrelated [22]. The simplest observable to display this effect is the moment  $\langle \cos \tilde{\phi} \rangle$ , which goes to 1 if the jet azimuthal angles are completely correlated and goes to 0 if they are completely decorrelated [23].

Even before the  $D\tilde{O}$  analysis was completed, however, it was realized that there was a serious problem in using LL BFKL for phenomenological analyses at hadron colliders: the BFKL resummation includes the contribution of energetically disfavored or disallowed configurations in its predictions. In principle these configurations are subleading, but in practice they are very important [24]. (In fact these effects could be considered to be a foreshadowing of the large corrections to BFKL at NLL.) We can understand this effect by considering the Feynman  $x$ -values used in the PDFs. The exact values are given by conservation of light-cone momentum along the beam axis and can be written

$$\begin{aligned} x_a &= \frac{1}{\sqrt{s}} \left( p_{a\perp} e^{y_a} + p_{b\perp} e^{y_b} + \sum_i k_{i\perp} e^{y_i} \right) \\ x_b &= \frac{1}{\sqrt{s}} \left( p_{a\perp} e^{-y_a} + p_{b\perp} e^{-y_b} + \sum_i k_{i\perp} e^{-y_i} \right), \end{aligned} \quad (13)$$

where the sum is over all partons produced in the event. In the “naive” LL BFKL one only keeps the leading contributions,

$$\begin{aligned} x_a^0 &= \frac{p_{a\perp} e^{y_a}}{\sqrt{s}} \\ x_b^0 &= \frac{p_{b\perp} e^{-y_b}}{\sqrt{s}}. \end{aligned} \quad (14)$$

That is, one convolutes the analytic LL BFKL solution (9) with the impact factors, using the PDFs evaluated at  $x_{a,b}^0$ . However, the true  $x_{a,b}$  are always larger than  $x_{a,b}^0$ , and the energy-momentum constraints  $x_{a,b} < 1$  are not enforced in the naive BFKL calculation. If the PDFs vary strongly with  $x$ , this can greatly overestimate the contributions from multi-jet events.

With the analytic LL BFKL solution (9) the phase space of the intermediate gluons has already been integrated over, so there is no choice but to use the leading  $x^0$ 's (14) in the PDFs. However, in a BFKL Monte Carlo solution [25,26] one generates the gluon ladder directly as in Eq. (7). Thus, one has information on all the produced partons, and one can enforce energy conservation on the solution by using the exact  $x$ 's (13) in the PDFs. This greatly improves the reliability of the BFKL prediction.

In Fig. 7 we show the  $D\tilde{O}$  azimuthal decorrelation data from Ref. [27] compared with the naive LL BFKL and a Monte Carlo BFKL calculation with energy conservation included. The data shows  $\langle \cos \tilde{\phi} \rangle$  as a function of  $\Delta y$  at  $\sqrt{s} = 1.8$  TeV,

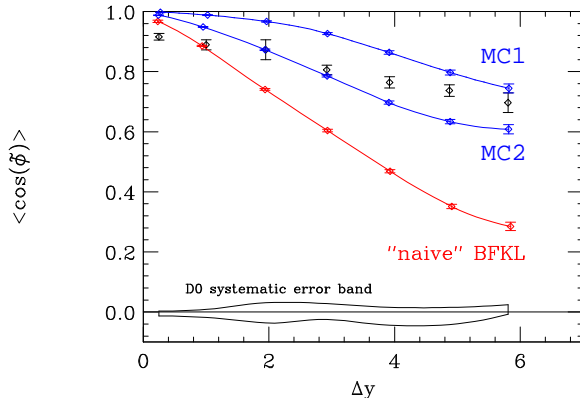


Figure 7: Azimuthal angle decorrelation as a function of rapidity interval. The DØ data is from [27], the lowest curve is “naive” BFKL, the two upper curves are BFKL Monte Carlo predictions. The correlated systematic error is due to jet energy scale uncertainty.

where the tagging jets are required to have  $E_{\perp} > 20$  GeV. The naive BFKL severely overestimates the rate of decorrelation with  $\Delta y$ , due to the overweighting of energetically disfavored or disallowed configurations. The two BFKL Monte Carlo curves are produced by the Monte Carlo in Ref. [25]. Both use the exact  $x$ 's in the PDFs, but use different approximations to relate the partonic to the hadronic cross sections in the high energy limit. The difference between the two approximations is subleading in the high energy limit. The BFKL Monte Carlo with energy conservation certainly works much better than the naive BFKL, but the subleading uncertainties are still sizeable, as displayed by the difference between the two Monte Carlo predictions.

An argument against the decorrelation measurement as a signal of BFKL is that it probes the region around  $\tilde{\phi} \approx 0$ , which is also most sensitive to Sudakov logarithms. It would be nicer to probe directly the rise in partonic cross section with the partonic energy as in Eq. (1). This became possible when the Tevatron collider was run at the lower energy of 630 GeV, allowing a comparison of dijet production at two different center-of-mass energies. By binning the events in the partonic  $x_a, x_b$  values rather than in  $\Delta y$ , the dependence on the PDFs should cancel in the ratio

$$R = \frac{\sigma(\sqrt{s_1} = 1800\text{GeV})}{\sigma(\sqrt{s_2} = 630\text{GeV})}. \quad (15)$$

This is the original proposal of Mueller and Navelet [28]. Using the asymptotic saddle point approximation, one obtains a prediction of

$$R_{\text{BFKL}} = \frac{e^{A(\Delta y_1 - \Delta y_2)}}{\sqrt{\Delta y_1 / \Delta y_2}}, \quad (16)$$

where  $\Delta y_i \approx \ln(\hat{s}_i / p_{a\perp} p_{b\perp}) \approx \ln(\hat{s}_i / E_{\perp\text{min}}^2)$ . This ratio was measured by the DØ collaboration, in several  $x$  bins, with the following cuts:  $E_{\perp\text{min}} > 20$  GeV,  $|y| < 3$ ,

$\Delta y > 2$ , and  $400 < Q^2 = E_{a\perp} E_{b\perp} < 1000 \text{ GeV}^2$ . Using the formula (16), a BFKL Pomeron intercept of  $A = 0.65 \pm 0.07$  was extracted [29].

This measurement is noteworthy in that it is probably the only current measurement which shows a rise in the cross section that is *larger* than the LL BFKL prediction. Using  $\alpha_s(20 \text{ GeV}) = 0.17$  in Eq. (2), one obtains a LL prediction of  $A = 0.45$ , which is almost 3 standard deviations below the extracted value. However, as discussed in Ref. [30], one must be careful in interpreting this measurement. First, the extraction of the BFKL Pomeron intercept from (16) assumes that the asymptotic BFKL expression is valid, and the experimental cuts and precise definition of the  $x$ 's do not significantly affect the asymptotics. In particular the cut on  $Q^2$  was seen to slow the approach to asymptotics, resulting in a smaller predicted value for the ratio  $R$ . The inclusion of energy conservation via a BFKL Monte Carlo further reduced the predicted ratio. Finally, it was shown that the use of equal  $E_\perp$  cuts on both of the tagging jets introduces the same large Sudakov logarithms that plague the decorrelation measurement. Thus, it seems unlikely that the large ratio found by the DØ collaboration can be attributed to perturbative BFKL.

## 5.2 BFKL probes at HERA

It is also possible to look for the BFKL rise in the cross section in deep inelastic scattering (DIS) by tagging a forward jet [31,32]. Referring to the high energy factorization picture of Fig. 1, the DIS setup consists of the scattering of an off-shell photon with virtuality  $Q^2$  and Bjorken  $x_{bj} = Q^2/s_{ep}$  on the left, the scattering of a forward jet of momentum fraction  $x_{\text{jet}} = E_{\text{jet}}/E_p$  and transverse momentum  $p_\perp$  on the right, connected by the BFKL ladder of gluon emissions in the middle. If  $Q^2 \sim p_\perp^2 \gg \Lambda_{QCD}^2$ , then the BFKL evolution is perturbative. The large logarithm that is resummed is  $\ln(x_{\text{jet}}/x_{bj})$ .

This DIS setup has several advantages over the  $p\bar{p}$  setup, due to its asymmetric nature. Note that in the high energy limit, the PDF of the proton is evaluated at  $x_{\text{jet}}$ . Thus, with  $x_{\text{jet}}$  fixed, one can vary the rapidity interval at a single collider energy by varying  $x_{bj}$ , without any change in the PDF. In addition, this suggests that the energy conservation effects mentioned above may be less important, or at least not so strongly dependent on  $x_{bj}$ . Finally, the resummation in  $\ln(x_{\text{jet}}/x_{bj})$ , rather than in the jet rapidity intervals, is more natural here, and perhaps more stable theoretically, since it corresponds to the standard DGLAP evolution variable when  $Q^2 > p_\perp^2$ . The only major disadvantage is that the virtual photon impact factor is more complicated theoretically than the gluon or quark impact factors. Indeed, it has not been calculated completely at NLO.

Both the H1 [33] and ZEUS [34] collaborations have measured this forward jet cross section. The main experimental cuts on the forward jet itself are  $x_{\text{jet}} > 0.035$ ,  $E_{\perp\text{jet}} > 3.5$  and  $5 \text{ GeV}$  for H1,  $x_{\text{jet}} > 0.036$ ,  $E_{\perp\text{jet}} > 5 \text{ GeV}$  for ZEUS, and  $0.5 < E_{\perp\text{jet}}^2/Q^2 < 2$  for both. The H1 data is displayed in Fig. 8. In Figs. 8(a) and (c) the

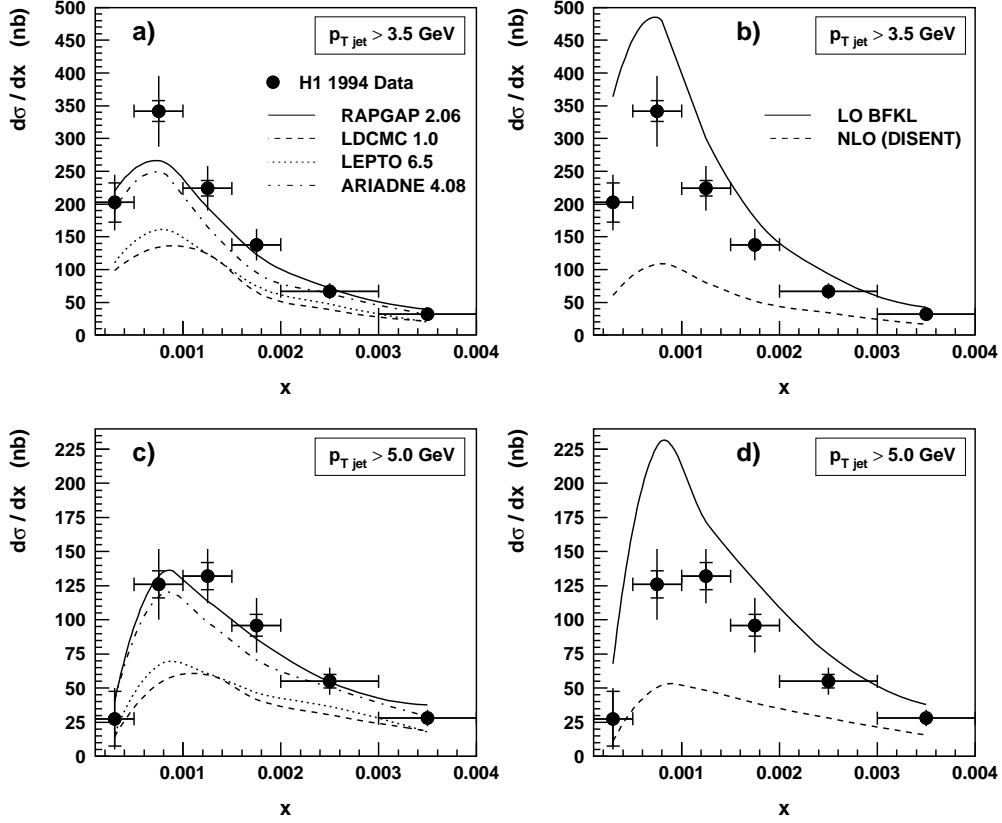


Figure 8: Forward jet cross-sections as a function of Bjorken- $x$  from H1 [33] for two  $p_{\perp}$  cuts of 3.5 and 5 GeV. The data in (a) and (c) are compared with Monte-Carlo model predictions, including hadronization. The data in (b) and (d) are compared with partonic NLO  $\mathcal{O}(\alpha_s^2)$  and LL BFKL calculations.

data is compared against several hadron-level Monte Carlo shower models attached to lowest order QCD matrix elements. The two that agree the best with the data are ARIADNE [35] and RAPGAP [36]. ARIADNE is based on the colour dipole model for gluon radiation which, like BFKL, lacks ordering in  $k_{\perp}$ . Gluon radiation in RAPGAP is based on DGLAP evolution, but this model also includes a resolved photon contribution to the basic QCD production mechanism. In Figs. 8(b) and (d) the H1 data is compared against a LL BFKL prediction [37] and a NLO QCD  $\mathcal{O}(\alpha_s^2)$  prediction [38], both at the parton levels. The NLO calculation significantly underestimates the data at small  $x_{bj}$ , whereas the BFKL calculation overestimates it. This is not unreasonable, given that NLL corrections to BFKL are expected to reduce the rise at small  $x_{bj}$ , and that the kinematic cuts could not be included exactly in the calculation. The ZEUS data [34], shown in Fig. 9, similarly is far above a NLO

## ZEUS 1995

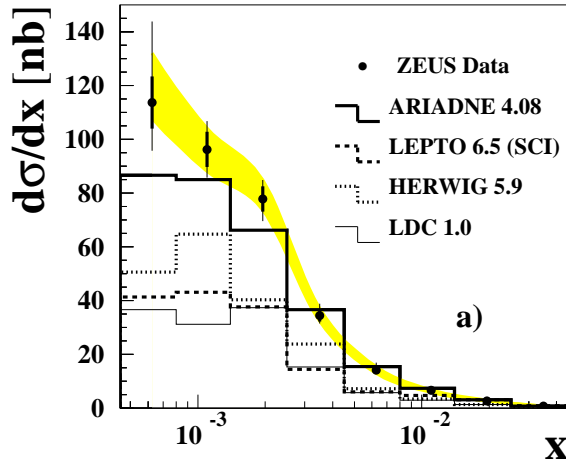


Figure 9: Forward jet cross-sections as a function of Bjorken- $x$  from ZEUS [34] for  $p_{\perp} > 5$  GeV. The data are compared with several Monte-Carlo model predictions at the hadron level.

QCD calculation [39], but below the LL BFKL expectations. A fit [40] to the data from both experiments using the LL BFKL cross section yielded an effective BFKL pomeron intercept corresponding to  $A = 0.43 \pm 0.025(\text{stat}) \pm 0.025(\text{sys})$ , compared to the LL prediction from Eq. (2) of  $A = 0.75$  for  $\alpha_s = 0.28$  at  $Q^2 = 10$  GeV<sup>2</sup>.

Recently, several forward jet calculations with different approaches have shown good agreement with the data. One calculation [41] is based on LL BFKL, but modified by a consistency condition containing effects similar to the dominant NLL energy-scale effects discussed in section 4. A second calculation [42] is with a hadron-level Monte Carlo generator, based on the CCFM evolution [43], which is designed to agree with both DGLAP and BFKL in their respective regimes of reliability. Since both of these calculations can be considered LL BFKL, with some dominant subleading corrections included, this looks promising for BFKL. A third approach [44] which also fits the data is a NLO calculation that includes a resolved photon contribution, similar in spirit to the RAPGAP Monte Carlo. Interestingly, it appears that the success of this approach relies not on the evolution in  $Q^2$  allowed by the inclusion of the photon PDF, but in the fact that it effectively approximates one term higher in  $\alpha_s$ , via the NLO resolved piece. This is not incompatible with BFKL, since the new  $\mathcal{O}(\alpha_s^3)$  contribution also includes the first gluon emission in the BFKL ladder. It is an interesting question to ask how the approximations in this picture of forward jet production mesh with those in the BFKL picture.

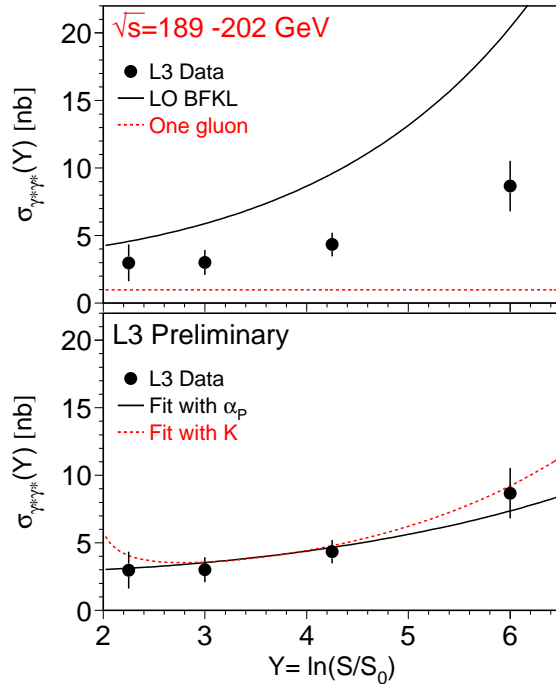


Figure 10: Two-photon cross-sections,  $\sigma_{\gamma^*\gamma^*}$ , after subtraction of the LO  $\gamma^*\gamma^* \rightarrow q\bar{q}$  contribution at  $\sqrt{s} \simeq 189-202$  GeV and  $4 < Q_{1,2}^2 < 40$  GeV<sup>2</sup>, from Ref. [47]. The top figure compares the data with LO BFKL in the saddle point approximation with  $A = \alpha_P - 1 = 0.53$  and with the one-gluon exchange diagram. The lower figure shows fits of the saddle-point BFKL expression to the data, allowing either  $\alpha_P$  or the normalization  $K$  to vary.

### 5.3 BFKL probes in $\gamma^*\gamma^*$

Another standard BFKL measurement [45] is to observe the total  $\gamma^*\gamma^*$  hadronic cross section as a function of  $\sqrt{s_{\gamma\gamma}}$ . This can be extracted from the process  $e^+e^- \rightarrow e^+e^- + \text{hadrons}$  by tagging on the forward and backward electrons. In this case the two independent scatterings of Fig. 1 are the off-shell photons of momenta  $Q_1^2$  and  $Q_2^2$  that break up into color dipoles ( $q\bar{q}$  pairs at leading order), which are then connected by the BFKL ladder. The large logarithm here is  $Y \approx \ln(s_{\gamma\gamma}/\sqrt{Q_1^2 Q_2^2})$ , in direct analogy to the hadron-hadron case.

This experiment has the advantage that, for large enough  $Q_{1,2}^2$ , there are no non-perturbative PDF inputs, so that in principle it is the cleanest probe, theoretically. However, from a purely calculational point of view, this process may be more complicated since it involves two off-shell photon impact factors. In particular, the cross-channel gluon on which the BFKL ladder is built does not even appear until NNLO in a standard perturbative QCD calculation..

The  $\gamma^*\gamma^*$  hadronic cross section has been measured by the L3 [46,47] and the

OPAL [48] collaborations at LEP. In Fig. 10 we display the most recent preliminary L3 data [47]. The data clearly shows a rise with  $Y$  as expected by BFKL, but much less steep than LO BFKL. However, the data is above both LO and NLO QCD predictions [49]. In addition the data is also above the prediction from the single-gluon exchange contribution (evaluated using the average value of  $\langle Q_{1,2}^2 \rangle = 15 \text{ GeV}^2$ ). In the lower figure the data is fitted to the asymptotic BFKL prediction

$$\sigma_{\gamma^*\gamma^*} = \frac{\sigma_0}{\sqrt{Q_1^2 Q_2^2 Y}} e^{AY} , \quad (17)$$

with either the overall normalization or the BFKL intercept  $A = \alpha_P - 1$  left as a free parameter. The preliminary result in the latter case gives  $A = 0.36 \pm 0.02$ , which is more in line with NLO expectations. The OPAL preliminary measurements [48] give qualitatively similar results, but with less statistical significance.

## 6 Summary and Conclusions.

In this talk I have presented some recent results in BFKL physics, both in the theory and in its phenomenological applications. On the theoretical side, the focus has been on the large NLL corrections. At this time, it seems fairly safe to say that the original catastrophe of falling, or even negative, cross sections has been averted. By understanding the origin of these effects in the collinear behavior of the gluons, one can reorganize the resummation in order to move the dominant corrections back into the LL theory. Then the NLL prediction for the BFKL intercept is stable and slightly smaller than the standard LL prediction.

On the phenomenological side, the results look suggestive, especially in the DIS and  $\gamma^*\gamma^*$  data. The cross sections are significantly above the state-of-the-art NLO QCD calculations, as they should be for a BFKL-enhanced observable. They are also in the range one might expect from a NLL BFKL calculation. However, the lesson learned from the analysis of the hadron-hadron experiments is that one must be very careful to consider how experimental cuts and kinematic effects, such as energy conservation, will affect these predictions. Although the asymmetric configuration of the DIS forward jet experiments and the lack of nonperturbative PDF-dependence in the  $\gamma^*\gamma^*$  (assuming  $Q^2$  is large enough) may make these observables less susceptible to large subleading effects, a thorough phenomenological analysis is certainly warranted.

With the completion and understanding of the NLL corrections to the BFKL kernel in hand, the next phase is to bring the phenomenological analyses up to the same NLL level. So far the major emphasis has been on the NLL BFKL intercept, but to make a full NLL prediction, with a reliable normalization, one also needs to combine this with NLO impact factors. In particular the NLO impact factor for the off-shell photon is crucial for the both the DIS and  $\gamma^*\gamma^*$  analyses. In addition

the analyses must be performed in such a way as to treat the kinematics and cuts as accurately as possible. Promising steps in this direction are Refs. [41,17], which incorporate the largest NLL corrections into BFKL via a consistency condition, or via a CCFM Monte Carlo, respectively. Another useful exercise would be to incorporate the largest NLL corrections to the BFKL ladder into the BFKL Monte Carlos [25,26] and to modify them for use in the other experimental environments. This would be helpful for gauging the sensitivity to subleading kinematic effects (which arise at least as much from the impact factors as from the actual BFKL ladder). However, the greatest progress would come with a full NLL calculation with full NLO impact factors included. There is much work left to be done.

## References

- [1] E. A. Kuraev, L. N. Lipatov and V. S. Fadin, Sov. Phys. JETP **44**, 443 (1976) [Zh. Eksp. Teor. Fiz. **71**, 840 (1976)];  
E. A. Kuraev, L. N. Lipatov and V. S. Fadin, Sov. Phys. JETP **45**, 199 (1977) [Zh. Eksp. Teor. Fiz. **72**, 377 (1977)];  
I. I. Balitsky and L. N. Lipatov, Sov. J. Nucl. Phys. **28**, 822 (1978) [Yad. Fiz. **28**, 1597 (1978)].
- [2] C. R. Schmidt, Phys. Rev. D **60**, 074003 (1999) [hep-ph/9901397].
- [3] V. S. Fadin and L. N. Lipatov, Phys. Lett. B **429**, 127 (1998) [hep-ph/9802290].
- [4] V. Del Duca and C. R. Schmidt, Phys. Rev. D **59**, 074004 (1999) [hep-ph/9810215].
- [5] G. Camici and M. Ciafaloni, Phys. Lett. B **412**, 396 (1997) [Erratum-ibid. B **417**, 390 (1997)] [hep-ph/9707390];  
Phys. Lett. B **430**, 349 (1998) [hep-ph/9803389].
- [6] Y. V. Kovchegov and A. H. Mueller, Phys. Lett. B **439**, 428 (1998) [hep-ph/9805208].
- [7] N. Armesto, J. Bartels and M. A. Braun, Phys. Lett. B **442**, 459 (1998) [hep-ph/9808340].
- [8] E. Levin, hep-ph/9806228.
- [9] M. Ciafaloni and D. Colferai, Phys. Lett. B **452**, 372 (1999) [hep-ph/9812366];  
M. Ciafaloni, D. Colferai and G. P. Salam, Phys. Rev. D **60**, 114036 (1999) [hep-ph/9905566].

- [10] D. A. Ross, Phys. Lett. B **431**, 161 (1998) [hep-ph/9804332].
- [11] R. D. Ball and S. Forte, hep-ph/9805315.
- [12] J. Blumlein and A. Vogt, Phys. Rev. D **58**, 014020 (1998) [hep-ph/9712546];  
J. Blumlein, V. Ravindran, W. L. van Neerven and A. Vogt, hep-ph/9806368.
- [13] S. J. Brodsky, V. S. Fadin, V. T. Kim, L. N. Lipatov and G. B. Pivovarov, JETP Lett. **70**, 155 (1999) [hep-ph/9901229].
- [14] S. J. Brodsky, G. P. Lepage and P. B. Mackenzie, Phys. Rev. D **28**, 228 (1983).
- [15] B. Andersson, G. Gustafson and J. Samuelsson, Nucl. Phys. B **467**, 443 (1996).
- [16] L.N. Lipatov, talk presented at the 4<sup>th</sup> Workshop on Small- $x$  and Diffractive Physics, Fermi National Accelerator Laboratory, Sept. 17-20, 1998.
- [17] G. P. Salam, JHEP **9807**, 019 (1998) [hep-ph/9806482].
- [18] Y. L. Dokshitzer, Sov. Phys. JETP **46**, 641 (1977) [Zh. Eksp. Teor. Fiz. **73**, 1216 (1977)];  
V. N. Gribov and L. N. Lipatov, Yad. Fiz. **15**, 781 (1972) [Sov. J. Nucl. Phys. **15**, 438 (1972)];  
G. Altarelli and G. Parisi, Nucl. Phys. B **126**, 298 (1977).
- [19] G. P. Salam, Acta Phys. Polon. B **30**, 3679 (1999) [hep-ph/9910492].
- [20] G. Altarelli, R. D. Ball and S. Forte, Nucl. Phys. B **575**, 313 (2000) [hep-ph/9911273];  
G. Altarelli, R. D. Ball and S. Forte, Nucl. Phys. B **599**, 383 (2001) [hep-ph/0011270].
- [21] J. R. Forshaw, D. A. Ross and A. Sabio Vera, Phys. Lett. B **455**, 273 (1999) [hep-ph/9903390].
- [22] V. Del Duca and C. R. Schmidt, Phys. Rev. D **49**, 4510 (1994) [hep-ph/9311290].
- [23] W. J. Stirling, Nucl. Phys. B **423**, 56 (1994) [hep-ph/9401266].
- [24] V. Del Duca and C. R. Schmidt, Phys. Rev. D **51**, 2150 (1995) [hep-ph/9407359].
- [25] C. R. Schmidt, Phys. Rev. Lett. **78**, 4531 (1997) [hep-ph/9612454].
- [26] L. H. Orr and W. J. Stirling, Phys. Rev. D **56**, 5875 (1997) [hep-ph/9706529].

- [27] B. Abbott *et al.* [D0 Collaboration], FERMILAB-CONF-97-371-E *Contributed to 18th International Symposium on Lepton - Photon Interactions (LP 97), Hamburg, Germany, 28 Jul - 1 Aug 1997, and Contributed to International Europhysics Conference on High-Energy Physics (HEP 97), Jerusalem, Israel, 19-26 Aug 1997*;  
S. Abachi *et al.* [D0 Collaboration], Phys. Rev. Lett. **77**, 595 (1996) [hep-ex/9603010].
- [28] A. H. Mueller and H. Navelet, Nucl. Phys. B **282**, 727 (1987).
- [29] B. Abbott *et al.* [D0 Collaboration], Phys. Rev. Lett. **84**, 5722 (2000) [hep-ex/9912032].
- [30] J. R. Andersen, V. Del Duca, S. Frixione, C. R. Schmidt and W. J. Stirling, JHEP **0102**, 007 (2001) [hep-ph/0101180].
- [31] A. Mueller, Nucl. Phys. B (Proc. Suppl.) **18C**, 125 (1991).
- [32] J. Kwiecinski, A. D. Martin and P. J. Sutton, Phys. Rev. D **46**, 921 (1992);  
J. Bartels, A. de Roeck and M. Loewe, Z. Phys. C **54**, 635 (1992);  
W. Tang, Phys. Lett. B **278**, 363 (1992).
- [33] C. Adloff *et al.* [H1 Collaboration], Nucl. Phys. B **538**, 3 (1999) [hep-ex/9809028].
- [34] J. Breitweg *et al.* [ZEUS Collaboration], Eur. Phys. J. C **6**, 239 (1999) [hep-ex/9805016].
- [35] L. Lonnblad, Comput. Phys. Commun. **71**, 15 (1992).
- [36] H. Jung, Comput. Phys. Commun. **86**, 147 (1995). H. Jung, L. Jonsson and H. Kuster, Eur. Phys. J. C **9**, 383 (1999) [hep-ph/9903306].
- [37] J. Bartels, V. Del Duca, A. De Roeck, D. Graudenz and M. Wusthoff, Phys. Lett. B **384**, 300 (1996) [hep-ph/9604272].
- [38] S. Catani and M. H. Seymour, Phys. Lett. B **378**, 287 (1996) [hep-ph/9602277].  
S. Catani and M. H. Seymour, Nucl. Phys. B **485**, 291 (1997) [Erratum-ibid. B **510**, 503 (1997)] [hep-ph/9605323].
- [39] E. Mirkes and D. Zeppenfeld, Phys. Rev. Lett. **78**, 428 (1997) [hep-ph/9609231].
- [40] J. G. Contreras, R. Peschanski and C. Royon, Phys. Rev. D **62**, 034006 (2000) [hep-ph/0002057];  
J. G. Contreras, Phys. Lett. B **446**, 158 (1999) [hep-ph/9812255].

- [41] J. Kwiecinski, A. D. Martin and J. J. Outhwaite, Eur. Phys. J. C **9**, 611 (1999) [hep-ph/9903439].
- [42] H. Jung and G. P. Salam, Eur. Phys. J. C **19**, 351 (2001) [hep-ph/0012143].
- [43] M. Ciafaloni, Nucl. Phys. B **296**, 49 (1988);  
S. Catani, F. Fiorani and G. Marchesini, Phys. Lett. B **234**, 339 (1990);  
S. Catani, F. Fiorani and G. Marchesini, Nucl. Phys. B **336**, 18 (1990).
- [44] G. Kramer and B. Potter, Phys. Lett. B **453**, 295 (1999) [hep-ph/9901314].
- [45] J. Bartels, A. De Roeck and H. Lotter, Phys. Lett. B **389**, 742 (1996) [hep-ph/9608401];  
S. J. Brodsky, F. Hautmann and D. E. Soper, Phys. Rev. D **56**, 6957 (1997) [hep-ph/9706427].
- [46] M. Acciarri *et al.* [L3 Collaboration], Phys. Lett. B **453**, 333 (1999).
- [47] L3 Collaboration, L3 Note 2568, presented at ICHEP 2000, Osaka, Japan.
- [48] OPAL Collaboration, OPAL Physics Notes PN456.
- [49] M. Cacciari, V. Del Duca, S. Frixione and Z. Trocsanyi, JHEP **0102**, 029 (2001) [hep-ph/0011368].

## $\varepsilon'/\varepsilon$ and Chiral Dynamics

ANTONIO PICH\*

*Departament de Física Teòrica, IFIC, Universitat de València – CSIC  
Edifici d'Instituts de Paterna, Apt. Correus 22085, E-46701 València, Spain*

The long-distance contributions to  $K \rightarrow 2\pi$  amplitudes can be pinned down, using well established Chiral Perturbation Theory techniques. The strong S-wave rescattering of the two final pions generates sizeable chiral loop corrections, which have an important impact on the direct CP violation ratio  $\varepsilon'/\varepsilon$  [1,2]. Including all large logarithmic corrections, both at short and long distances, the Standard Model Prediction for this observable is found to be [2]  $\text{Re}(\varepsilon'/\varepsilon) = (1.7 \pm 0.9) \cdot 10^{-3}$ , in good agreement with the most recent experimental measurements. A better estimate of the strange quark mass could reduce the theoretical uncertainty to 30%.

Presented at the

5th International Symposium on Radiative Corrections  
(RADCOR-2000)

Carmel CA, USA, 11–15 September, 2000

---

\*Work supported by the European Union TMR network *EURODAPHNE* (Contract No. ERBFMX-CT98-0169) and by DGESIC, Spain (Grant No. PB97-1261).

# 1 Introduction

The CP-violating ratio  $\varepsilon'/\varepsilon$  constitutes a fundamental test for our understanding of flavour-changing phenomena within the Standard Model framework. The experimental status has been clarified by the recent KTeV [3],  $\text{Re}(\varepsilon'/\varepsilon) = (28.0 \pm 4.1) \cdot 10^{-4}$ , and NA48 [4],  $\text{Re}(\varepsilon'/\varepsilon) = (15.3 \pm 2.6) \cdot 10^{-4}$ , measurements, which provide clear evidence for a non-zero value and, therefore, the existence of direct CP violation. The present world average is [3,4,5,6],

$$\text{Re}(\varepsilon'/\varepsilon) = (18.0 \pm 2.0) \cdot 10^{-4}, \quad (\chi^2/\text{ndf} = 10.8/3). \quad (1)$$

The theoretical prediction has been rather controversial since different groups, using different models or approximations, have obtained different results [7,8,9,10,11,12]. Although there was no universal agreement on the  $\varepsilon'/\varepsilon$  value predicted by the Standard Model, it has been often claimed that it is too small, failing to reproduce the experimental world average by at least a factor of two. This claim has generated a very intense theoretical activity, searching for new sources of CP violation beyond the Standard Model [13].

It has been pointed out recently [1] that the theoretical short-distance evaluations of  $\varepsilon'/\varepsilon$  had overlooked the important role of final-state interactions (FSI) in  $K \rightarrow \pi\pi$  decays. Although it has been known for more than a decade that the rescattering of the two final pions induces a large correction to the isospin-zero decay amplitude, this effect was not taken properly into account in the theoretical predictions. From the measured  $\pi$ - $\pi$  phase shifts one can easily infer [1] that FSI generate a strong enhancement of the  $\varepsilon'/\varepsilon$  prediction, by roughly the needed factor of two. This large correction is associated with infrared chiral logarithms involving the pion mass, which can be rigorously analyzed with standard Chiral Perturbation Theory ( $\chi$ PT) techniques [14,15,16]. A very detailed analysis, including all large logarithmic corrections both at short and long distances, has been presented in ref. [2]. The resulting Standard Model prediction [2],

$$\text{Re}(\varepsilon'/\varepsilon) = (17 \pm 9) \cdot 10^{-4}, \quad (2)$$

is in good agreement with the most recent measurements.

The following sections present a brief overview of the most important ingredients entering the theoretical prediction of  $\varepsilon'/\varepsilon$ :

1. A short-distance calculation at the electroweak scale and its renormalization-group evolution to the three-flavour theory ( $\mu \lesssim m_c$ ), which sums the leading and next-to-leading ultraviolet logarithms.
2. The matching to the  $\chi$ PT description, which so far has been done at leading order in the  $1/N_C$  expansion.
3. Chiral loop corrections, which induce large infrared logarithms related to FSI.

## 2 Theoretical framework

In terms of the  $K \rightarrow \pi\pi$  isospin amplitudes,  $\mathcal{A}_I = A_I e^{i\delta_I}$  ( $I = 0, 2$ ),

$$\frac{\varepsilon'}{\varepsilon} = e^{i\Phi} \frac{\omega}{\sqrt{2}|\varepsilon|} \left[ \frac{\text{Im}(A_2)}{\text{Re}(A_2)} - \frac{\text{Im}(A_0)}{\text{Re}(A_0)} \right]. \quad (3)$$

Owing to the well-known “ $\Delta I = 1/2$  rule”,  $\varepsilon'/\varepsilon$  is suppressed by the ratio  $\omega = \text{Re}(A_2)/\text{Re}(A_0) \approx 1/22$ . The strong S-wave rescattering of the two final pions generates a large phase-shift difference between the two isospin amplitudes, making the phases of  $\varepsilon'$  and  $\varepsilon$  nearly equal. Thus,

$$\Phi \approx \delta_2 - \delta_0 + \frac{\pi}{4} \approx 0. \quad (4)$$

The CP-conserving amplitudes  $\text{Re}(A_I)$ , their ratio  $\omega$  and  $\varepsilon$  are usually set to their experimentally determined values. A theoretical calculation is then only needed for the quantities  $\text{Im}(A_I)$ .

One starts above the electroweak scale where the flavour-changing process, in terms of quarks, leptons and gauge bosons, can be analyzed within the usual gauge-coupling perturbative expansion in a rather straightforward way. Since  $M_Z$  is much larger than the long-distance hadronic scale  $M_K$ , there are large short-distance logarithmic contributions which can be summed up using the Operator Product Expansion (OPE) [17] and the renormalization group. The proper way to proceed makes use of modern Effective Field Theory (EFT) techniques [18].

The renormalization group is used to evolve down in energy from the electroweak scale, where the top quark and the  $Z$  and  $W^\pm$  bosons are integrated out. That means that one changes to a different EFT where those heavy particles are no longer explicit degrees of freedom. The new Lagrangian contains a tower of operators constructed with the light fields only, which scale as powers of  $1/M_Z$ . The information on the heavy fields is hidden in their (Wilson) coefficients, which are fixed by “matching” the high- and low-energy theories at the point  $\mu = M_Z$ . One follows the evolution further to lower energies, using the EFT renormalization group equations, until a new particle threshold is encountered. Then, the whole procedure of integrating the new heavy scale and matching to another EFT starts again.

One proceeds down to scales  $\mu < m_c$  and gets finally an effective  $\Delta S = 1$  Lagrangian, defined in the three-flavour theory [19,20],

$$\mathcal{L}_{eff}^{\Delta S=1} = -\frac{G_F}{\sqrt{2}} V_{ud} V_{us}^* \sum_{i=1}^{10} C_i(\mu) Q_i(\mu), \quad (5)$$

which is a sum of local four-fermion operators  $Q_i$ , constructed with the light degrees of freedom, modulated by Wilson coefficients  $C_i(\mu)$  which are functions of the heavy

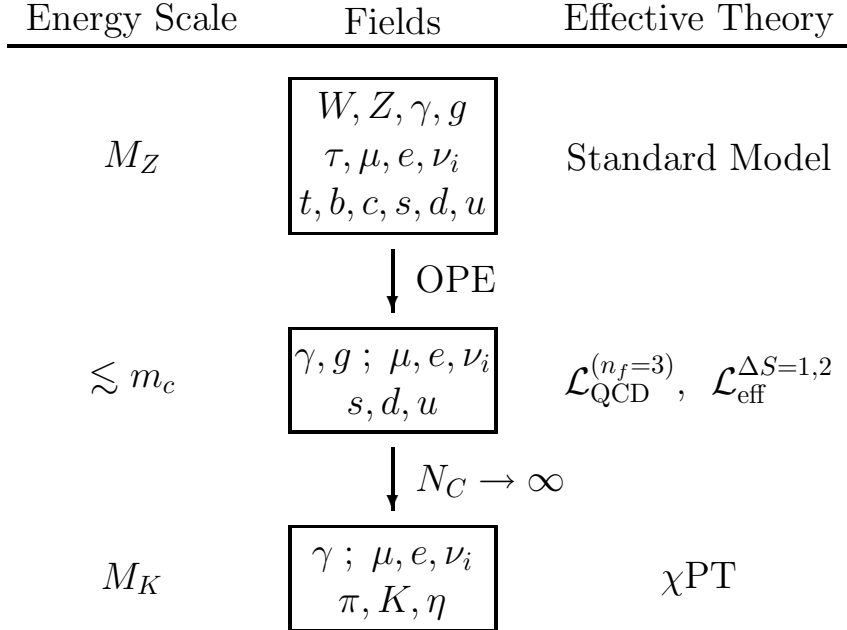


Figure 1: Evolution from  $M_Z$  to  $M_K$ .

masses. We have explicitly factored out the Fermi coupling  $G_F$  and the Cabibbo–Kobayashi–Maskawa (CKM) matrix elements  $V_{ij}$  containing the usual Cabibbo suppression of  $K$  decays. The unitarity of the CKM matrix allows to write

$$C_i(\mu) = z_i(\mu) + \tau y_i(\mu), \quad (6)$$

where  $\tau = -V_{td}V_{ts}^*/V_{ud}V_{us}^*$ . Only the  $y_i$  components are needed to determine the CP–violating decay amplitudes. The overall renormalization scale  $\mu$  separates the short– ( $M > \mu$ ) and long– ( $m < \mu$ ) distance contributions, which are contained in  $C_i(\mu)$  and  $Q_i$ , respectively. The physical amplitudes are of course independent of  $\mu$ .

Our knowledge of  $\Delta S = 1$  transitions has improved qualitatively in recent years, thanks to the completion of the next-to-leading logarithmic order calculation of the Wilson coefficients [21,22]. All gluonic corrections of  $O(\alpha_s^n t^n)$  and  $O(\alpha_s^{n+1} t^n)$  are known, where  $t \equiv \ln(M_1/M_2)$  refers to the logarithm of any ratio of heavy mass scales  $M_1, M_2 \geq \mu$ . Moreover, the full  $m_t/M_W$  dependence (at lowest order in  $\alpha_s$ ) is taken into account.

In order to predict physical amplitudes, however, one is still confronted with the calculation of hadronic matrix elements of the four–quark operators. This is a very difficult problem, which so far remains unsolved. Those matrix elements are usually parameterized in terms of the so-called bag parameters  $B_i$ , which measure them in units of their vacuum insertion approximation values.

To a very good approximation, the Standard Model prediction for  $\varepsilon'/\varepsilon$  can be written (up to global factors) as [7]

$$\frac{\varepsilon'}{\varepsilon} \sim \left[ B_6^{(1/2)}(1 - \Omega_{IB}) - 0.4 B_8^{(3/2)} \right]. \quad (7)$$

Thus, only two operators are numerically relevant: the QCD penguin operator  $Q_6$  ( $\Delta I = 1/2$ ) governs  $\text{Im}(A_0)$ , while  $\text{Im}(A_2)$  ( $\Delta I = 3/2$ ) is dominated by the electroweak penguin operator  $Q_8$ . The parameter

$$\Omega_{IB} = \frac{1}{\omega} \frac{\text{Im}(A_2)_{IB}}{\text{Im}(A_0)} \quad (8)$$

takes into account isospin-breaking corrections, which get enhanced by the large factor  $1/\omega$ .

The isospin-breaking correction coming from  $\pi^0$ - $\eta$  mixing was originally estimated to be  $\Omega_{IB}^{\pi^0\eta} = 0.25$  [23,24]. Together with the usual ansatz  $B_i \sim 1$ , this produces a large numerical cancellation in eq. (7) leading to low values of  $\varepsilon'/\varepsilon$  around  $7 \cdot 10^{-4}$ . A recent improved calculation of  $\pi^0$ - $\eta$  mixing at  $\mathcal{O}(p^4)$  in  $\chi$ PT has found the result [25]

$$\Omega_{IB}^{\pi^0\eta} = 0.16 \pm 0.03. \quad (9)$$

This smaller number, slightly increases the naive estimate of  $\varepsilon'/\varepsilon$ .

### 3 Chiral Perturbation Theory

Below the resonance region one can use global symmetry considerations to define another EFT in terms of the QCD Goldstone bosons ( $\pi$ ,  $K$ ,  $\eta$ ). The  $\chi$ PT formulation of the Standard Model [14,15,16] describes the pseudoscalar-octet dynamics, through a perturbative expansion in powers of momenta and quark masses over the chiral symmetry breaking scale ( $\Lambda_\chi \sim 1$  GeV).

Chiral symmetry fixes the allowed  $\chi$ PT operators. At lowest order in the chiral expansion, the most general effective bosonic Lagrangian with the same  $SU(3)_L \otimes SU(3)_R$  transformation properties as the short-distance Lagrangian (5) contains three terms, transforming as  $(8_L, 1_R)$ ,  $(27_L, 1_R)$  and  $(8_L, 8_R)$ , respectively. Their corresponding chiral couplings are denoted by  $g_8$ ,  $g_{27}$  and  $g_{ew}$ .

The tree-level  $K \rightarrow \pi\pi$  amplitudes generated by the lowest-order  $\chi$ PT Lagrangian do not contain any strong phases:

$$\begin{aligned} \mathcal{A}_0 &= -\frac{G_F}{\sqrt{2}} V_{ud} V_{us}^* \sqrt{2} f_\pi \left\{ \left( g_8 + \frac{1}{9} g_{27} \right) (M_K^2 - M_\pi^2) - \frac{2}{3} f_\pi^2 e^2 g_8 g_{ew} \right\}, \\ \mathcal{A}_2 &= -\frac{G_F}{\sqrt{2}} V_{ud} V_{us}^* \frac{2}{9} f_\pi \left\{ 5 g_{27} (M_K^2 - M_\pi^2) - 3 f_\pi^2 e^2 g_8 g_{ew} \right\}. \end{aligned} \quad (10)$$

Taking the measured phase shifts into account, the moduli of  $g_8$  and  $g_{27}$  can be extracted from the CP-conserving  $K \rightarrow 2\pi$  decay rates; one gets [26]  $|g_8| \approx 5.1$  and  $|g_{27}| \approx 0.29$ . The huge difference between these two couplings shows the well-known enhancement of octet  $|\Delta I| = 1/2$  transitions. The  $g_{ew}$  term is the low-energy realization of the electroweak penguin operator.

The isospin amplitudes  $\mathcal{A}_I$  have been computed up to next-to-leading order in the chiral expansion [2,27,28,29,30,31]. The only remaining problem is the calculation of the  $\chi$ PT couplings from the effective short-distance Lagrangian (5), which requires to perform the matching between the two EFTs. This can be easily done in the large- $N_C$  limit of QCD [32], because in this limit the four-quark operators factorize into currents which have well-known chiral realizations. The local  $\mathcal{O}(p^4)$  contributions to the amplitudes  $\mathcal{A}_I$  can be easily included in eqs. (10), through effective correction factors  $\Delta_C \mathcal{A}_I^{(R)}$  to the lowest-order  $g_R$  contributions. At leading order in  $1/N_C$ , one gets [2]:

$$\begin{aligned}
g_8^\infty \left[1 + \Delta_C \mathcal{A}_0^{(8)}\right]^\infty &= \left\{ -\frac{2}{5} C_1(\mu) + \frac{3}{5} C_2(\mu) + C_4(\mu) - 16 L_5 C_6(\mu) \left[ \frac{M_K^2}{(m_s + m_q)(\mu) f_\pi} \right]^2 \right\} f_0^{K\pi}(M_\pi^2), \\
g_{27}^\infty \left[1 + \Delta_C \mathcal{A}_0^{(27)}\right]^\infty &= g_{27}^\infty \left[1 + \Delta_C \mathcal{A}_2^{(27)}\right]^\infty = \frac{3}{5} [C_1(\mu) + C_2(\mu)] f_0^{K\pi}(M_\pi^2), \\
e^2 g_8^\infty \left[g_{ew} + \Delta_C \mathcal{A}_0^{(ew)}\right]^\infty &= -3 C_8(\mu) \left[ \frac{M_K^2}{(m_s + m_q)(\mu) f_\pi} \right]^2 \left[ 1 + \frac{4L_5}{f_\pi^2} M_K^2 \right] \\
&\quad - \frac{3}{4} [C_7 - C_9 + C_{10}](\mu) \frac{M_K^2 - M_\pi^2}{f_\pi^2} f_0^{K\pi}(M_\pi^2), \\
e^2 g_8^\infty \left[g_{ew} + \Delta_C \mathcal{A}_2^{(ew)}\right]^\infty &= -3 C_8(\mu) \left[ \frac{M_K^2}{(m_s + m_q)(\mu) f_\pi} \right]^2 \left[ 1 + \frac{4L_5}{f_\pi^2} M_\pi^2 \right] \\
&\quad + \frac{3}{2} [C_7 - C_9 - C_{10}](\mu) \frac{M_K^2 - M_\pi^2}{f_\pi^2} f_0^{K\pi}(M_\pi^2), \tag{11}
\end{aligned}$$

where  $f_0^{K\pi}(M_\pi^2) \approx 1 + 4L_5 M_\pi^2/f_\pi^2$  is the  $K\pi$  scalar form factor at the pion mass scale,  $L_5$  is a coupling of the  $\mathcal{O}(p^4)$  strong chiral Lagrangian and  $m_q \equiv m_u = m_d$ . In the limit  $N_C \rightarrow \infty$ ,  $L_5^\infty = \frac{1}{4} f_\pi^2 \left( \frac{f_K}{f_\pi} - 1 \right) / (M_K^2 - M_\pi^2) \approx 2.1 \cdot 10^{-3}$  and  $f_0^{K\pi}(M_\pi^2) \approx 1.02$ .

These results are equivalent to the usual large- $N_C$  evaluations of the  $B_i$  factors. In particular, for  $\varepsilon'/\varepsilon$  where only the imaginary part of the  $g_R$  couplings matter [i.e.  $\text{Im}(C_i)$ ] they amount to  $B_8^{(3/2)} \approx B_6^{(1/2)} = 1$ . Therefore, up to minor variations on some input parameters, the corresponding  $\varepsilon'/\varepsilon$  prediction reproduces the published results of the Munich [7] and Rome [8] groups.

The large- $N_C$  limit is only applied to the matching between the 3-flavour quark theory and  $\chi$ PT, as indicated in Figure 1. The evolution from the electroweak scale down to  $\mu < m_c$  has to be done without any unnecessary expansion in powers of  $1/N_C$ ; otherwise, one would miss large corrections of the form  $\frac{1}{N_C} \ln(M/m)$ , with  $M \gg m$  two widely separated scales [33]. Thus, the Wilson coefficients contain the full  $\mu$  dependence.

The large- $N_C$  factorization of the four-quark operators  $Q_i$  ( $i \neq 6, 8$ ) does not provide any scale dependence. Since the anomalous dimensions of these operators vanish when  $N_C \rightarrow \infty$  [33], a very important ingredient is lost in this limit [34]. To achieve a reliable expansion in powers of  $1/N_C$ , one needs to go to the next order where this physics is captured [34,35]. This is the reason why the study of the  $\Delta I = 1/2$  rule has proven to be so difficult. Fortunately, these operators are numerically suppressed in the  $\varepsilon'/\varepsilon$  prediction and their contributions can be easily corrected with the information provided by the measured CP-conserving rates [2,7].

The only anomalous dimensions which survive when  $N_C \rightarrow \infty$  are precisely the ones corresponding to  $Q_6$  and  $Q_8$  [24,33]. One can then expect that the matrix elements of these two operators are well approximated by this limit [34,35,36]. These operators factorize into colour-singlet scalar and pseudoscalar currents, which are  $\mu$  dependent. This generates the factors  $\langle \bar{q}q \rangle(\mu) \approx -f_\pi^2 M_K^2 / (m_s + m_q)(\mu)$ , which exactly cancel the  $\mu$  dependence of  $C_{6,8}(\mu)$  at large  $N_C$  [24,33,34,35,36,37]. It remains of course a dependence at next-to-leading order.

Therefore, while there are large  $1/N_C$  corrections to  $\text{Re}(g_I)$  [35], the large- $N_C$  limit is expected to give a good estimate of  $\text{Im}(g_I)$ .

## 4 Chiral loop corrections

The lowest-order calculation does not provide any strong phases  $\delta_I$ . Those phases originate in the final rescattering of the two pions and, therefore, are generated by chiral loops which are of higher order in both the momentum and  $1/N_C$  expansions. Analyticity and unitarity require the presence of a corresponding dispersive FSI effect in the moduli of the isospin amplitudes. Since the S-wave strong phases are quite large, specially in the isospin-zero case, one should expect large higher-order unitarity corrections.

The size of the FSI effect can be calculated at one loop in  $\chi$ PT. The dominant one-loop correction to the octet amplitude comes indeed from the elastic soft rescattering of the two pions in the final state. The existing one-loop analyses [2,27,28] show that pion loop diagrams provide an important enhancement of the  $\mathcal{A}_0$  amplitude, implying a corresponding reduction of the phenomenologically fitted value of  $|g_8|$ . This chiral loop correction destroys the accidental numerical cancellation in eq. (7), generating a sizeable enhancement of the  $\varepsilon'/\varepsilon$  prediction [1].

Let us decompose the isospin amplitudes in their different chiral components as  $\mathcal{A}_0 = \mathcal{A}_0^{(8)} + \mathcal{A}_0^{(27)} + \mathcal{A}_0^{(ew)}$  and  $\mathcal{A}_2 = \mathcal{A}_2^{(27)} + \mathcal{A}_2^{(ew)}$ . Moreover, we can write them in the form

$$\mathcal{A}_I^{(R)} = \mathcal{A}_I^{(R)\infty} \times \mathcal{C}_I^{(R)}, \quad (12)$$

where  $\mathcal{A}_I^{(R)\infty}$  are the large- $N_C$  results obtained in the previous section. The correction factors  $\mathcal{C}_I^{(R)} \equiv 1 + \Delta_L \mathcal{A}_I^{(R)}$  contain the chiral loop contributions  $\Delta_L \mathcal{A}_I^{(R)}$  that we are interested in. Their complete analytical expressions at one loop in  $\chi$ PT have been given in ref. [2], where the following numerical values have been obtained:

$$\begin{aligned} \mathcal{C}_0^{(8)} &= 1.27 \pm 0.05 + 0.46 i, \\ \mathcal{C}_0^{(27)} &= 2.0 \pm 0.7 + 0.46 i, \\ \mathcal{C}_0^{(ew)} &= 1.27 \pm 0.05 + 0.46 i, \\ \mathcal{C}_2^{(27)} &= 0.96 \pm 0.05 - 0.20 i, \\ \mathcal{C}_2^{(ew)} &= 0.50 \pm 0.24 - 0.20 i. \end{aligned} \quad (13)$$

The central values have been evaluated at the chiral renormalization scale  $\nu = M_\rho$ . To estimate the corresponding uncertainties we have allowed the scale  $\nu$  to change between 0.6 and 1 GeV. The scale dependence is only present in the dispersive contributions and should cancel with the corresponding  $\nu$  dependence of the local  $\chi$ PT counterterms. However, this dependence is next-to-leading in  $1/N_C$  and, therefore, is not included in the large- $N_C$  determination of the chiral couplings. The sensitivity of the results to the scale  $\nu$  gives a good estimate of those missing contributions. Notice that all amplitudes with a given isospin get the same absorptive contribution, as it should since they have identical strong phase shifts.

The numerical corrections to the 27-plet amplitudes do not have much phenomenological interest for CP-violating observables, because  $\text{Im}(g_{27}) = 0$ . Remember that the CP-conserving amplitudes  $\text{Re}(A_I)$  are set to their experimentally determined values. What is relevant for the  $\varepsilon'/\varepsilon$  prediction is the 35% enhancement of the isoscalar octet amplitude  $\text{Im}[A_0^{(8)}]$  and the 46% reduction of  $\text{Im}[A_2^{(ew)}]$ . Just looking to the simplified formula (7), one realizes immediately the obvious impact of these one-loop chiral corrections.

A complete  $\mathcal{O}(p^4)$  calculation [25,29] of the isospin-breaking parameter  $\Omega_{IB}$  is not yet available. The value 0.16 quoted in eq. (9) only accounts for the contribution from  $\pi^0$ - $\eta$  mixing [25] and should be corrected by the effect of chiral loops. Since  $|\mathcal{C}_2^{(27)}| \approx 0.98 \pm 0.05$ , one does not expect any large correction of  $\text{Im}(A_2)_{IB}$ , while we know that  $\text{Im}[A_0^{(8)}]$  gets enhanced by a factor 1.35. Taking this into account, one gets the corrected value

$$\Omega_{IB} \approx \Omega_{IB}^{\pi^0\eta} \left| \frac{\mathcal{C}_2^{(27)}}{\mathcal{C}_0^{(8)}} \right| = 0.12 \pm 0.05, \quad (14)$$

where the quoted error is an educated theoretical guess. This value agrees with the result  $\Omega_{IB} = 0.08 \pm 0.05 \pm 0.01$ , obtained in ref. [38] by using three different models [9,31,35,39,40,41] to estimate the relevant  $\mathcal{O}(p^4)$  chiral couplings.

The sensitivity to higher-order chiral loop corrections has been investigated in ref. [2] through an Omnès exponentiation of the dominant pion loops [1], using the experimental  $\pi\pi$  phase shifts. The standard one-loop  $\chi$ PT results and the Omnès calculation agree within errors, indicating a good convergence of the chiral expansion.

## 5 Numerical results and discussion

The infrared effect of chiral loops generates an important enhancement of the isoscalar  $K \rightarrow \pi\pi$  amplitude. This effect gets amplified in the prediction of  $\varepsilon'/\varepsilon$ , because at lowest order (in both  $1/N_C$  and the chiral expansion) there is an accidental numerical cancellation between the  $I = 0$  and  $I = 2$  contributions. Since the chiral loop corrections destroy this cancellation, the final result for  $\varepsilon'/\varepsilon$  is dominated by the isoscalar amplitude. Thus, the Standard Model prediction for  $\varepsilon'/\varepsilon$  is finally governed by the matrix element of the gluonic penguin operator  $Q_6$ .

A detailed numerical analysis has been provided in ref. [2]. The short-distance Wilson coefficients have been evaluated at the scale  $\mu = 1$  GeV. Their associated uncertainties have been estimated through the sensitivity to changes of  $\mu$  in the range  $M_\rho < \mu < m_c$  and to the choice of  $\gamma_5$  scheme. Since the most important  $\alpha_s$  corrections appear at the low-energy scale  $\mu$ , the strong coupling has been fixed at the  $\tau$  mass, where it is known [42] with about a few percent level of accuracy:  $\alpha_s(m_\tau) = 0.345 \pm 0.020$ . The values of  $\alpha_s$  at the other needed scales can be deduced through the standard renormalization group evolution.

Taking the experimental value of  $\varepsilon$ , the CP-violating ratio  $\varepsilon'/\varepsilon$  is proportional to the CKM factor  $\text{Im}(V_{ts}^* V_{td}) = (1.2 \pm 0.2) \cdot 10^{-4}$  [43]. This number is sensitive to the input values of several non-perturbative hadronic parameters adopted in the usual unitarity triangle analysis; thus, it is subject to large theoretical uncertainties which are difficult to quantify [44]. Using instead the theoretical prediction of  $\varepsilon$ , this CKM factor drops out from the ratio  $\varepsilon'/\varepsilon$ ; the sensitivity to hadronic inputs is then reduced to the explicit remaining dependence on the  $\Delta S = 2$  scale-invariant bag parameter  $\hat{B}_K$ . In the large- $N_C$  limit,  $\hat{B}_K = 3/4$ . We have performed the two types of numerical analysis, obtaining consistent results. This allows us to estimate better the theoretical uncertainties, since the two analyses have different sensitivity to hadronic inputs.

The final result quoted in ref. [2] is:

$$\text{Re}(\varepsilon'/\varepsilon) = (1.7 \pm 0.2^{+0.8}_{-0.5} \pm 0.5) \cdot 10^{-3} = (1.7 \pm 0.9) \cdot 10^{-3}. \quad (15)$$

The first error comes from the short-distance evaluation of Wilson coefficients and the choice of low-energy matching scale  $\mu$ . The uncertainty coming from varying the strange quark mass in the interval  $(m_s + m_q)(1 \text{ GeV}) = 156 \pm 25 \text{ MeV}$

[45,46,47,48,49,50,51] is indicated by the second error. The most critical step is the matching between the short- and long-distance descriptions. We have performed this matching at leading order in the  $1/N_C$  expansion, where the result is known to  $\mathcal{O}(p^4)$  and  $\mathcal{O}(e^2 p^2)$  in  $\chi$ PT. This can be expected to provide a good approximation to the matrix elements of the leading  $Q_6$  and  $Q_8$  operators. Since all ultraviolet and infrared logarithms have been resummed, our educated guess for the theoretical uncertainty associated with  $1/N_C$  corrections is  $\sim 30\%$  (third error).

Thus, a better determination of the strange quark mass would allow to reduce the uncertainty to the 30% level. In order to get a more accurate prediction, it would be necessary to have a good analysis of next-to-leading  $1/N_C$  corrections. This is a very difficult task, but progress in this direction can be expected in the next few years [9,11,35,52,53,54].

To summarize, using a well defined computational scheme, it has been possible to pin down the value of  $\varepsilon'/\varepsilon$  with an acceptable accuracy. Within the present uncertainties, the resulting Standard Model theoretical prediction (15) is in good agreement with the measured experimental value (1), without any need to invoke a new physics source of CP violation.

## Acknowledgments

I warmly thank Elisabetta Pallante and Ignazio Scimemi for a rewarding collaboration, and the RADCOR-2000 organizers for making possible a very stimulating workshop in such a nice environment.

## References

- [1] E. Pallante and A. Pich, *Phys. Rev. Lett.* **84** (2000) 2568; *Nucl. Phys.* **B592** (2000) 294; A. Pich, *Nucl. Phys. B (Proc. Suppl.)* **93** (2001) 253.
- [2] E. Pallante, A. Pich and I. Scimemi, hep-ph/0105011.
- [3] KTeV collaboration (A. Alavi-Harati *et al.*) *Phys. Rev. Lett.* **83** (1999) 22.
- [4] NA48 collaboration (V. Fanti *et al.*), *Phys. Lett.* **B465** (1999) 335; G. Unal, *A New Measurement of Direct CP Violation by NA48*, CERN Particle Physics Seminar (May 10, 2001), <http://www.cern.ch/NA48/Welcome.html>.
- [5] NA31 collaboration (H. Burkhardt *et al.*), *Phys. Lett.* **B206** (1988) 169; (G.D. Barr *et al.*), *Phys. Lett.* **B317** (1993) 233.

- [6] E731 collaboration (L.K. Gibbons *et al.*), *Phys. Rev. Lett.* **70** (1993) 1203.
- [7] A.J. Buras *et al.*, *Nucl. Phys.* **B592** (2001) 55; S. Bosch *et al.*, *Nucl. Phys.* **B565** (2000) 3; G. Buchalla *et al.*, *Rev. Mod. Phys.* **68** (1996) 1125; A.J. Buras *et al.*, *Nucl. Phys.* **B408** (1993) 209; *Phys. Lett.* **B389** (1996) 749.
- [8] M. Ciuchini *et al.*, *Nucl. Phys. B (Proc. Suppl.)* **99** (2001) 27; hep-ph/9910237; *Nucl. Phys.* **B523** (1998) 501, *Z. Phys.* **C68** (1995) 239; *Phys. Lett.* **B301** (1993) 263.
- [9] S. Bertolini *et al.*, *Rev. Mod. Phys.* **72** (2000) 65; *Phys. Rev.* **D63** (2001) 056009; *Nucl. Phys.* **B449** (1995) 197, **B476** (1996) 225, **B514** (1998) 63, 93; M. Fabbrichesi, *Phys. Rev.* **D62** (2000) 097902.
- [10] T. Hambye *et al.*, hep-ph/0001088; *Nucl. Phys.* **B564** (2000) 391; *Eur. Phys. J.* **C10** (1999) 271; *Phys. Rev.* **D58** (1998) 014017; Y.-L. Wu, *Phys. Rev.* **D64** (2000) 016001.
- [11] J. Bijnens and J. Prades, *JHEP* **06** (2000) 035; *Nucl. Phys. B (Proc. Suppl.)* **96** (2001) 354.
- [12] S. Narison, *Nucl. Phys.* **B593** (2001) 3; H.Y. Chen, *Chin. J. Phys.* **38** (2000) 1044; A.A. Belkov *et al.*, hep-ph/9907335.
- [13] There is a vast literature on this issue, which can be traced back from the recent review by A. Masiero and O. Vives, hep-ph/0104027.
- [14] S. Weinberg, *Physica* **96A** (1979) 327.
- [15] J. Gasser and H. Leutwyler, *Ann. Phys., NY* **158** (1984) 142; *Nucl. Phys.* **B250** (1985) 465; 517; 539.
- [16] G. Ecker, *Prog. Part. Nucl. Phys.* **35** (1995) 1; A. Pich, *Rep. Prog. Phys.* **58** (1995) 563; U.-G. Meissner, *Rep. Prog. Phys.* **56** (1993) 903.
- [17] K.G. Wilson, *Phys. Rev.* **179** (1969) 1499.
- [18] A. Pich, *Effective Field Theory*, in “Probing the Standard Model of Particle Interactions”, Proc. 1997 Les Houches Summer School, eds. R. Gupta *et al.* (Elsevier, Amsterdam, 1999), Vol. II, p. 949.
- [19] F.J. Gilman and M.B. Wise, *Phys. Rev.* **D20** (1979) 2392; **D21** (1980) 3150.
- [20] A.J. Buras, *Weak Hamiltonian, CP Violation and Rare Decays*, in “Probing the Standard Model of Particle Interactions”, Proc. 1997 Les Houches Summer School, eds. R. Gupta *et al.* (Elsevier, Amsterdam, 1999), Vol. I, p. 281.

- [21] A.J. Buras *et al.*, *Nucl. Phys.* **B400** (1993) 37, 75, **B370** (1992) 69.
- [22] M. Ciuchini *et al.*, *Nucl. Phys.* **B415** (1994) 403.
- [23] J.F. Donoghue *et al.*, *Phys. Lett.* **B179** (1986) 361 [Err: **B188** (1987) 511]; H.Y. Cheng, *Phys. Lett.* **B201** (1988) 155; M. Lusignoli, *Nucl. Phys.* **B325** (1989) 33.
- [24] A.J. Buras and J.-M. Gérard, *Phys. Lett.* **B192** (1987) 156.
- [25] G. Ecker, G. Müller, H. Neufeld and A. Pich, *Phys. Lett.* **B477** (2000) 88.
- [26] A. Pich, B. Guberina and E. de Rafael, *Nucl. Phys.* **B277** (1986) 197.
- [27] J. Kambor, J. Missimer and D. Wyler, *Nucl. Phys.* **B346** (1990) 17; *Phys. Lett.* **B261** (1991) 496; J. Kambor *et al.*, *Phys. Rev. Lett.* **68** (1992) 1818.
- [28] J. Bijnens, E. Pallante and J. Prades, *Nucl. Phys.* **B521** (1998) 305; E. Pallante, *JHEP* **01** (1999) 012.
- [29] G. Ecker, G. Müller, H. Neufeld and A. Pich, *Nucl. Phys.* **B591** (2000) 419.
- [30] V. Cirigliano, J.F. Donoghue and E. Golowich, *Phys. Lett.* **B450** (1999) 241; *Phys. Rev.* **D61** (2000) 093001 [Err: **D63** (2000) 059903], 093002; V. Cirigliano and E. Golowich, *Phys. Lett.* **B475** (2000) 351.
- [31] G. Ecker, J. Kambor and D. Wyler, *Nucl. Phys.* **B394** (1993) 101.
- [32] G. 't Hooft, *Nucl. Phys.* **B72** (1974) 461, **B75** (1974) 461; E. Witten, *Nucl. Phys.* **B149** (1979) 285, **B160** (1979) 57; *Ann. Phys.* **128** (1980) 363.
- [33] W.A. Bardeen, A.J. Buras and J.-M. Gérard, *Nucl. Phys.* **B293** (1987) 787; *Phys. Lett.* **B211** (1988) 343, **B192** (1987) 138, **B180** (1986) 133; A.J. Buras and J.-M. Gérard, *Nucl. Phys.* **B264** (1986) 371.
- [34] A. Pich, *Nucl. Phys. B (Proc. Suppl.)* **7A** (1989) 194.
- [35] A. Pich and E. de Rafael, *Nucl. Phys.* **B358** (1991) 311; *Phys. Lett.* **B374** (1996) 186.
- [36] M. Jamin and A. Pich, *Nucl. Phys.* **B425** (1994) 15.
- [37] E. de Rafael, *Nucl. Phys. B (Proc. Suppl.)* **7A** (1989) 1.
- [38] K. Maltman and C.E. Wolfe, *Phys. Lett.* **B482** (2000) 77; *Phys. Rev.* **D63** (2001) 014008.

- [39] G. Ecker, J. Gasser, A. Pich and E. de Rafael, *Nucl. Phys.* **B321** (1989) 311; G. Ecker, J. Gasser, H. Leutwyler, A. Pich and E. de Rafael, *Phys. Lett.* **B223** (1989) 425.
- [40] G. Ecker, A. Pich and E. de Rafael, *Phys. Lett.* **B237** (1990) 481.
- [41] S. Gardner and G. Valencia, *Phys. Lett.* **B466** (1999) 355.
- [42] A. Pich, *Nucl. Phys. B (Proc. Suppl.)* **98** (2001) 385.
- [43] M. Ciuchini *et al.*, hep-ph/0012308; A. Höcker *et al.*, hep-ph/0104062; D. Atwood and A. Soni, hep-ph/0103197.
- [44] A. Pich and J. Prades, *Phys. Lett.* **B346** (1995) 342.
- [45] S. Chen, M. Davier, E. Gámiz, A. Höcker, A. Pich and J. Prades, hep-ph/0105253; *Nucl. Phys. B (Proc. Suppl.)* **98** (2001) 319.
- [46] A. Pich and J. Prades, *JHEP* **10** (1999) 004, **06** (1998) 013.
- [47] ALEPH collaboration, *Eur. Phys. J.* **C11** (1999) 599; **C10** (1999) 1.
- [48] J. Kambor and K. Maltman, *Phys. Rev.* **D62** (2000) 093023; K.G. Chetyrkin *et al.*, *Nucl. Phys.* **B533** (1998) 473; J.G. Korner *et al.*, hep-ph/0003165.
- [49] M. Jamin, *Nucl. Phys. B (Proc. Suppl.)* **64** (1998) 250; K.G. Chetyrkin *et al.*, *Phys. Lett.* **B404** (1997) 337; P. Colangelo *et al.*, *Phys. Lett.* **B408** (1997) 340; C.A. Dominguez *et al.*, *Nucl. Phys. B (Proc. Suppl.)* **74** (1999) 313; K. Maltman, *Phys. Lett.* **B462** (1999) 195; S. Narison, *Phys. Lett.* **B466** (1999) 345.
- [50] V. Lubicz, *Nucl. Phys. B (Proc. Suppl.)* **94** (2001) 116; R. Gupta and K. Maltman, hep-ph/0101132.
- [51] J. Prades, *Nucl. Phys. B (Proc. Suppl.)* **64** (1998) 253; J. Bijnens, J. Prades and E. de Rafael, *Phys. Lett.* **B348** (1995) 226.
- [52] J.F. Donoghue and E. Golowich, *Phys. Lett.* **B478** (2000) 172.
- [53] M. Knecht, S. Peris and E. de Rafael, hep-ph/0102017; *Nucl. Phys. B (Proc. Suppl.)* **B86** (2000) 279; *Phys. Lett.* **B457** (1999) 227, **B443** (1998) 255; S. Peris and E. de Rafael, *Phys. Lett.* **B490** (2000) 213.
- [54] L. Lellouch and M. Lüscher, *Commun. Math. Phys.* **219** (2001) 31; M.F.L. Golterman and E. Pallante, *JHEP* **08** (2000) 023; C.-J.D. Lin *et al.*, hep-lat/0104006.

CERN-TH/2001-48  
MPI-PhT/2001-01  
February 2001  
hep-ph/0102292

# Light Quark Mass Effects in Bottom Quark Mass Determinations

ANDRÉ HOANG\*

*Theory Division, CERN,  
CH-1211 Geneva 23, Switzerland*

Recent results for charm quark mass effects in perturbative bottom quark mass determinations from  $\Upsilon$  mesons are reviewed. The connection between the behavior of light quark mass corrections and the infrared sensitivity of some bottom quark mass definitions is examined in some detail.

Presented at the

5th International Symposium on Radiative Corrections  
(RADCOR-2000)

Carmel CA, USA, 11–15 September, 2000

---

\*Permanent address: Max-Planck-Institut für Physik, Werner-Heisenberg-Institut, Föhringer Ring 6, D-80805 München, Germany.

# 1 Introduction

The mass of the bottom quark is an important parameter in the theoretical description of B meson decays. In particular, for the extraction of  $V_{ub}$  and  $V_{cb}$  from inclusive decays a precision in the bottom quark mass of the order 1% is desirable due to a strong mass dependence. Precise determinations of the bottom mass are available from Lattice QCD using the B mesons mass (see Refs. [1] for recent reviews) and from perturbative QCD. As the B meson binding energy is dominated by non-perturbative QCD, perturbative methods can only be applied to  $\Upsilon$  mesons, where the relevant dynamical scales, momentum  $\langle p \rangle \sim M_b v$  and energy  $\langle E \rangle \sim M_b v^2$ ,  $v$  being the bottom quark velocity, can be larger than the hadronization scale  $\Lambda_{\text{QCD}}$ .<sup>1</sup>

In recent time new perturbative bottom mass analyses have been carried out including newly available NNLO (i.e.  $\mathcal{O}(v^2, \alpha_s v, \alpha_s^2)$ ) corrections in the non-relativistic expansion for heavy quark–antiquark systems based on the concept of effective theories and employing properly defined short-distance quark mass definitions<sup>2</sup> that are adapted to the non-relativistic framework [3]. It has become practice to determine the bottom  $\overline{\text{MS}}$  mass  $\overline{m}_b(\overline{m}_b)$  as the reference mass to compare the various analyses among each other. The various results, which are based on experimental data on the  $\Upsilon$  mesons, show good agreement with a central value for  $\overline{m}_b(\overline{m}_b)$  of about 4.2 GeV and an uncertainty ranging from 50 to 80 MeV. It is important to note that the uncertainty is predominantly theoretical, and (as a necessary consequence) partly depends on the taste and believes of the respective authors. It is therefore impossible to interpret the value for the error in a statistical way. It will be the primary aim of future studies and analyses to achieve a better understanding of this theoretical uncertainty—not necessarily in order to reduce it further, but in order to put it on firmer ground.

One effect that has been neglected in previous bottom quark mass analyses is coming from the finite masses of the light quarks (u, d, s, c), where ”light” means ”lighter than the bottom quark mass”. In this talk I report on results and examinations on light quark mass corrections at NNLO in the non-relativistic expansion which have been presented in Refs. [4,5]. Light quark mass corrections are interesting because the non-relativistic  $b\bar{b}$  system is governed by a tower of scales:  $M_b$ ,  $\langle p \rangle \sim M_b v$  and  $\langle E \rangle \sim M_b v^2$ . For small velocities these scales form a hierarchy and their relations to  $\Lambda_{\text{QCD}}$  determines the theoretical approach that has to be used to describe the  $b\bar{b}$  dynamics. In the work discussed in this talk I assume that all three scales are much larger than  $\Lambda_{\text{QCD}}$  (i.e. that  $v$  is not smaller than about 0.3 for bottom quarks) as only for this case the relevant approach is well understood theoretically.

Whether the mass of a light quark can also be considered ”light” in the context of the non-relativistic  $b\bar{b}$  dynamics depends on its relation to the three scales mentioned

---

<sup>1</sup> At LEP the  $\overline{\text{MS}}$  bottom mass at the Z scale has been determined from the rate of 3 jet events containing a  $b\bar{b}$  pair [2]. This measurement established experimentally the ”running” of the bottom  $\overline{\text{MS}}$  mass. For this method, the uncertainties are, however, still too large that light quark mass effects would be irrelevant.

<sup>2</sup> I call a heavy quark mass definition without an  $\mathcal{O}(\Lambda_{\text{QCD}})$  ambiguity a short-distance mass.

above. The masses of the up, down and strange quarks are indeed much smaller than any of the three scales and one can expect that for them the massless approximation is a very good one, as an expansion in their masses is justified. The mass of the charm, however, can be about as large as  $\langle p \rangle$  and larger than  $\langle E \rangle$ , and it is clearly inappropriate to consider the massless approximation in the first place. I will show that the effects of the non-zero charm quark mass in bottom mass determinations can amount to up to several tens of MeV depending of the method and the bottom short-distance mass definition that is employed.

Apart from the resulting quantitative effects in the determination of bottom quark short-distance masses, light quark mass effects are also interesting conceptually because the massive quark loops provide an infrared cutoff of the momentum flow through gluon lines. The behavior of light quark mass corrections, in general, can therefore serve as a natural tool to monitor the degree of infrared (IR) sensitivity of various bottom quark mass definition and their resulting ambiguity. This is in close analogy to the well-known IR renormalon studies with a fictitious gluon mass, but with the difference that the light quark mass corrections are real.

## 2 Light Quark Mass Corrections in the Coulomb Potential

In order to account for the light quark mass effects in the non-relativistic quark-antiquark dynamics at NNLO we have to determine the light quark mass corrections to the Coulomb potential  $V_c(\mathbf{r}) = -\frac{C_F \alpha_s}{r} + \dots$  that occurs in the Schrödinger equation

$$\left( -\frac{\nabla^2}{M_b} - \frac{\nabla^4}{4M_b^3} + \left[ V_c(\mathbf{r}) + \dots \right] - E \right) G(\mathbf{r}, \mathbf{r}', E) = \delta^{(3)}(\mathbf{r} - \mathbf{r}'). \quad (1)$$

Here  $M_b$  is (just as a matter of convenience in writing down Eq. (1)) the bottom pole mass and  $E = E_{cm} - 2M_b$ ,  $E_{cm}$  being the center-of-mass energy. At NNLO, corrections to the Coulomb potential have to be taken into account up to order  $\alpha_s^3$ . For massless light quarks these two-loop corrections have been determined in Refs. [6]. At NNLO there is also a potential of order  $\alpha_s^2/(M_b r^2)$  and another of order  $\alpha_s/(M_b^2 r)$ . (The latter contains e.g. the Darwin and the spin-orbit interactions.) For these potentials light quark mass corrections do not have to be considered because they contribute only at NNLO, whereas for light quark mass corrections we gain at least one more power of  $\alpha_s$ . There are also no light quark mass corrections to the kinetic energy terms.

The light quark mass corrections to the Coulomb potential arise for the first time at order  $\alpha_s^2$  from the insertion of the light quark self energy into the gluon line (Fig. 1). These corrections contribute at NLO in the non-relativistic power counting. For one massive light quark flavor, and the other  $n_l - 1$  light quark flavors being massless, the correction reads ( $\tilde{m}_q = e^{\gamma_E} m_q$ ):

$$\delta V_{c,m}^{\text{NLO}}(\mathbf{r}) = -\frac{C_F \alpha_s^{(n_l)}}{r} \left( \frac{\alpha_s^{(n_l)}}{3\pi} \right) \left\{ \ln(\tilde{m}_q r) + \frac{5}{6} + \int_1^\infty dx f(x) e^{-2m_q r x} \right\},$$

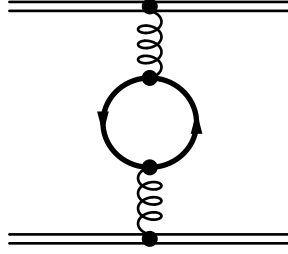


Figure 1: NLO contribution to the static potential coming from the insertion of a one-loop vacuum polarization of a light quark with finite mass.

$$f(x) \equiv \frac{1}{x^2} \sqrt{x^2 - 1} \left( 1 + \frac{1}{2x^2} \right). \quad (2)$$

The light quark mass corrections vanish for  $m_q r \rightarrow 0$ . This is related to the definition of  $\alpha_s$  that is (here and for the rest of this presentation) chosen to include the evolution originating from the massive light quark. In other words, the massive light quark is not integrated out. I emphasize that the statements about the size and behavior of the light quark mass corrections I will make later, are only true for this definition of  $\alpha_s$ . It is straightforward to generalize Eq. (2) to arbitrary numbers of massive light quark species and different definitions of  $\alpha_s$ . However, I emphasize that all previous analyses, where the light quark masses were neglected have naturally adopted the same scheme, so the results discussed here can be directly interpreted as additive corrections.

In Eq. (2) the NLO light quark mass corrections to the Coulomb potential are given in terms of a subtracted dispersion relation, where  $f$  is the absorptive part of the vacuum polarization. This representation is advantageous for determining the effects of the light quark masses to heavy-quark–antiquark bound state properties in Rayleigh-Schrödinger perturbation theory due to the simplicity of the dependence on  $\mathbf{r}$ . The remaining dispersion integration can then be carried out numerically (or if possible analytically) at the very end. In particular, for the determination of multiple potential insertions at higher orders in time-independent perturbation theory this method is probably the only feasible one. On the other hand, the dispersion representation makes the choice of definition for  $\alpha_s$  manifest.

At NNLO the light quark mass corrections to the Coulomb potential arise from dressing the one-loop diagram in Fig. (1) with additional gluon, ghost and light quark lines. The resulting diagrams were calculated numerically by Melles [7]. Using again the dispersion relation representation it is possible to rewrite Melles' results in a form that is simple to use for determining the light quark mass corrections. With the same conventions as for the NLO result, and adopting the pole mass definition for  $m_q$ , the result reads [5]:

$$\delta V_{c,m}^{\text{NNLO}}(\mathbf{r}) = -\frac{C_F \alpha_s^{(n_l)}}{r} \left( \frac{\alpha_s^{(n_l)}}{3\pi} \right)^2 \left\{ \left[ 3 \left( \ln(\tilde{m}_q r) + \frac{5}{6} \right) \left( \beta_0 \ln(\tilde{\mu} r) + \frac{a_1}{2} \right) + \beta_0 \frac{\pi^2}{4} \right. \right.$$

$$\begin{aligned}
& -\frac{3}{2} \int_1^\infty dx f(x) e^{-2m_q r x} \left( \beta_0 \left( \ln \frac{m_q^2}{\mu^2} + g_1(x, m_q, r) \right) - a_1 \right) \Big] \\
& - \left[ - \left( \ln(\tilde{m} r) + \frac{5}{6} \right)^2 - \frac{\pi^2}{12} + \int_1^\infty dx f(x) e^{-2m_q r x} \left( g_2(x) + g_1(x, m_q, r) - \frac{5}{3} \right) \right] \\
& + \left[ \frac{57}{4} \left( \ln(\tilde{m}_q r) + \frac{161}{228} + \frac{13}{19} \zeta_3 + c_1 \int_{c_2}^\infty \frac{dx}{x} e^{-2m_q r x} + d_1 \int_{d_2}^\infty \frac{dx}{x} e^{-2m_q r x} \right) \right] \Big\}, \quad (3)
\end{aligned}$$

where

$$\begin{aligned}
g_1(x, m_q, r) &= \ln(4x^2) - \text{Ei}(2m_q x r) - \text{Ei}(-2m_q x r), \\
g_2(x) &= \frac{5}{3} + \frac{1}{x^2} \left( 1 + \frac{1}{2x} \sqrt{x^2 - 1} (1 + 2x^2) \ln \left( \frac{x - \sqrt{x^2 - 1}}{x + \sqrt{x^2 - 1}} \right) \right). \quad (4)
\end{aligned}$$

The first three lines in Eq. (3) are exact and involve corrections coming from one and two insertions of the one-loop massive light quark vacuum polarization. The fourth line involves all other corrections and is parametrized by four numerical constants. Of these constants only two are independent, because the corrections have to vanish for  $m_q \rightarrow 0$ . A useful parameterization of the constants reads [5]

$$c_1 = \frac{\ln \frac{A}{d_2}}{\ln \frac{c_2}{d_2}}, \quad d_1 = \frac{\ln \frac{c_2}{A}}{\ln \frac{c_2}{d_2}}, \quad A = \exp \left( \frac{161}{228} + \frac{13}{19} \zeta_3 - \ln 2 \right), \quad (5)$$

where for the constants  $c_2$  and  $d_2$  one can obtain the following numerical results from the results of Refs. [7],

$$c_2 = 0.470 \pm 0.005 \quad d_2 = 1.120 \pm 0.010. \quad (6)$$

### 3 1S Mass, $n = 1$ ${}^3S_1$ Binding Energy and Upsilon Expansion

Naively one might think, that – at least up to some non-perturbative effects – the mass spectrum for  $b\bar{b}$  mesons could be obtained from solving the Schrödinger equation (1). However, the theoretical formalism from which it has been derived is becoming unreliable for higher radial excitations ( $n \gtrsim 2$ ), because the average momentum  $\langle p \rangle \sim \frac{M_b \alpha_s}{n}$  and the average energy  $\langle E \rangle \sim \frac{M_b \alpha_s^2}{n^2}$  become comparable or even smaller than  $\Lambda_{\text{QCD}}$ .

For the ground state ( $n = 1$ ), however, the formalism for the perturbative contributions is likely to work, and one can determine e.g. the  $\overline{\text{MS}}$  value of the bottom quark mass from comparing the  $\Upsilon(1S)$  mass with the result for the  $n = 1$ ,  ${}^3S_1$   $b\bar{b}$  bound state energy once an estimate for the non-perturbative corrections is made [8,9].

On the other hand, one can use the perturbation series for a  $n = 1$ ,  ${}^3S_1$  bound state mass obtained from Eq. (1) as a formal short-distance mass definition, because

it is free of the strong linear infrared sensitivity that leads to an ambiguity of order  $\Lambda_{\text{QCD}}$  in the pole mass definition [10,11]. In Ref. [12] the so called 1S mass has been defined as one half of the perturbative  $n = 1$ ,  ${}^3S_1$  bound state mass obtained from Eq. (1). It has been demonstrated that the 1S bottom quark mass leads to a very well convergent perturbative series for totally inclusive B decay rates [13]. Physically this behavior can be understood from the fact that the 1S mass is adapted to the situation where heavy quarks are very close to their mass shell, a situation that is realized for heavy-heavy as well as for heavy-light bound state systems. Heavy quark mass definitions that have this property are called "threshold masses" [14]. There are other heavy quark threshold mass definitions in the literature, such as the PS mass [11] and the kinetic mass [15], which will, however, not be further discussed in this talk.

The light quark mass corrections to the Coulomb potential presented in the previous section can be used to determine the light quark mass corrections in the  $b\bar{b}$  bound state energies. Here we will, as indicated earlier, only consider the binding energy of the  $n = 1$ ,  ${}^3S_1$  triplet ground state, but the calculation can be generalized without difficulty to arbitrary quantum numbers. In Dirac notation the NNLO result for the light quark mass corrections reads

$$\begin{aligned}
2 \left[ M_b^{\text{1S}} - M_b \right]_m &= \left[ M_{b\bar{b},1}{}^3S_1 - 2M_b \right]_m = \langle 1S | \delta V_{c,m}^{\text{NLO}} | 1S \rangle \\
&+ \langle 1S | \delta V_{c,m}^{\text{NNLO}} | 1S \rangle + \sum_{i \neq 1S} \langle 1S | \delta V_{c,m}^{\text{NLO}} \frac{|i\rangle\langle i|}{E_{1S} - E_i} \delta V_{c,m}^{\text{NLO}} | 1S \rangle \\
&+ 2 \sum_{i \neq 1S} \langle 1S | \delta V_{c,m}^{\text{NLO}} \frac{|i\rangle\langle i|}{E_{1S} - E_i} V_{c,\text{massless}}^{\text{NLO}} | 1S \rangle. \tag{7}
\end{aligned}$$

The first term on the RHS of Eq. (7) is the NLO correction of order  $M_b \alpha_s^3$  (in the non-relativistic power counting) and the terms in the second and third line are the NNLO corrections of order  $M_b \alpha_s^4$ . The explicit result based on the dispersion relation representation is given in Ref [5]. The NLO contribution has already been calculated earlier in Ref. [16] and agrees with the result here. The corrections coming from gluons and massless quarks (not displayed in Eq. (7), and called "massless corrections" from now on) have first been calculated in Ref. [8].

It is not possible to use Eq. (7) directly for any phenomenological analysis that intends a precision better than order  $\Lambda_{\text{QCD}}$ , because it is written in terms of the bottom pole mass. Nevertheless, it is instructive to have a closer look at the behavior of the light quark mass corrections in the bottom 1S-pole mass relation displayed in Eq. (7). For  $M_b = 4.9$  GeV,  $\overline{m}_c(\overline{m}_c) = 1.5$  GeV for the  $\overline{\text{MS}}$  charm quark mass and  $\alpha_s^{(4)}(\mu = 4.7 \text{ GeV}) = 0.216$  we obtain

$$\begin{aligned}
M_b^{\text{1S}} &= \left\{ 4.9 - \left[ 0.051 \right]_{\text{LO}} - \left[ 0.074 + 0.0045_m \right]_{\text{NLO}} \right. \\
&\quad \left. - \left[ 0.099 + 0.0121_m \right]_{\text{NNLO}} \right\} \text{GeV}, \tag{8}
\end{aligned}$$

where the charm mass corrections are indicated by the subscript  $m$  and the numbers without subscript are from the massless corrections. We stress that because  $M_b\alpha_s \approx 1.5$  GeV the charm mass correction shown in Eq. (8) cannot be obtained by an expansion in the light quark mass. To obtain the numbers shown in Eq. (8) it is essential that the complete expressions for the corrections given in Eqs. (2) and (3) are taken into account. We see that neither the massless corrections nor the charm mass corrections are converging. This is a consequence of the fact that I have used the bottom pole mass as an input parameter and the practical reason why Eq. (7) has only limited use for a phenomenological analysis. Another interesting point I would like to mention is that the NNLO charm mass corrections arising from double insertions of NLO potentials (the last two terms on the RHS of Eq. (7)) make for less than 10% of the full NNLO charm mass corrections for  $\mu$  between 1.5 and 5 GeV. This property will be important for the analysis of the charm mass effects in the  $\Upsilon$  sum rules (Sec. 7).

It is interesting that the linear sensitivity to small momenta contained in the pole mass definition is directly reflected in the analytic behavior of the light quark mass corrections in Eq. (7) for  $m_q \rightarrow 0$  ( $a_s \equiv \alpha^{(n)}(\mu)$ ):

$$\begin{aligned}
[M_b^{1S} - M_b]_m &\longrightarrow -C_F \left(\frac{a_s}{\pi}\right)^2 \left\{ \frac{\pi^2}{8} m_q + \dots \right\}_{\text{NLO}} \\
&\quad - C_F \left(\frac{a_s}{\pi}\right)^3 \left\{ \frac{\pi^2}{16} m_q \left[ \beta_0 \left( \ln \frac{\mu^2}{m_q^2} - 4 \ln 2 + \frac{14}{3} \right) \right. \right. \\
&\quad \left. \left. - \frac{4}{3} \left( \frac{59}{15} + 2 \ln 2 \right) + \frac{76}{3\pi} \left( c_1 c_2 + d_1 d_2 \right) \right] + \dots \right\}_{\text{NNLO}}. \quad (9)
\end{aligned}$$

Using the fact that the dispersion integrations in Eqs. (2) and (3) can be interpreted as an integration over a gluon mass, one can show (see Ref. [17]) that the linear light quark mass terms in Eq. (9) are directly related to the linear gluon mass terms frequently used in renormalon analyses. A different way to look at this feature is that the mass of the light quark provides an infrared cutoff for gluon lines due to decoupling at very small momentum transfers. On the other hand, if we express the 1S mass in terms of another short-distance mass, such as the  $\overline{\text{MS}}$  mass, these linear light quark mass terms do not arise. I will come back to this point later in this talk.

I also would like to point out that the structure of the linear light quark mass corrections in Eq. (9) themselves reveals their infrared origin. First of all, the linear dependence on the light quark mass is non-analytic since it comes from the square root of  $m_q^2$ . On the other hand, the full vacuum polarization of the quark loop does only depend on the square of the quark mass, so the linear mass terms cannot be obtained from expanding in the light quark mass before doing the integration over the gluon momentum. Consequently the linear mass terms arise from gluon momenta of the order of the light quark mass. This feature is also reflected in the BLM scale in the NNLO term in Eq. (9) which is of order  $m_q$  rather than  $M_b\alpha_s$ . Another observation is that the non-analyticity of the linear mass terms is associated with an enhancement

factor  $\pi^2$ . This is a common feature of contributions that originate from infrared momenta. We will see later that this enhancement will help us a lot to determine the three-loop light quark corrections to the  $\overline{\text{MS}}$ -pole mass relation.

Another feature of expression (9) is that the linear light quark mass corrections at NLO (NNLO) are multiplied by  $\alpha_s^2$  ( $\alpha_s^3$ ), which appears to contradict the non-relativistic power counting mentioned before. However, one has to take into account that the light quark mass corrections are  $M_b$  times a function of the ratio  $m_q/(M_b\alpha_s)$ . Thus there is no contradiction with the non-relativistic power counting.<sup>3</sup> On the other hand, one can also show that the linear light quark mass terms are in fact completely independent of the quantum number of the bound state. This can be seen from the fact that the terms displayed in Eq. (9) are equal to the linear light quark mass terms contained in  $\frac{1}{2}[\delta V_{c,m}^{\text{NLO}}(\mathbf{r}) + \delta V_{c,m}^{\text{NNLO}}(\mathbf{r})]$ . Because the linear terms are  $r$ -independent they are just multiplied by the norm of the bound state wave function, i.e. by 1. [The suppression of the NNLO charm mass corrections from double insertions of NLO potentials mentioned above, can be understood from the dominance of the linear and  $r$ -independent light quark mass terms in the potential: constant corrections to potentials give zero in higher order time-independent perturbation theory.] This means that the term  $\propto \alpha_s^2$  ( $\alpha_s^3$ ) in Eq. (9), can equally well be considered as two (three) loop contributions. This interesting feature is giving us a direct hint how one has to combine a usual loop expansion in powers of  $\alpha_s$  (such as the perturbative series for the  $\overline{\text{MS}}$ -pole mass relation) with a non-relativistic expansion that is in  $\alpha_s$  and the velocity  $v$  (such as the 1S-pole mass relation). The guiding principle to combine the two types of expansions is the cancellation of corrections that are linearly sensitive to small momenta. The resulting prescription is called *upsilon expansion* [13] and has been devised first for the massless corrections based on more general arguments. The *upsilon expansion* states that we have to consider corrections of  $N^{n-1}\text{LO}$  in the non-relativistic expansion (which contains itself a resummation of certain corrections to all orders in  $\alpha_s$ ) as of order  $\alpha_s^n$  in the usual expansion in the number of loops.

## 4 Heavy Quark $\overline{\text{MS}}$ -Pole Mass Relation

The pole mass parameter is quite convenient in intermediate steps of calculating the dynamics of a non-relativistic  $Q\bar{Q}$  pair, because the Schrödinger equation takes its standard QED-like form only in the pole mass scheme (see Eq. (1)). However, for practical applications (were a precision better than  $\Lambda_{\text{QCD}}$  is relevant) the pole mass needs to be replaced by a short-distance mass parameter. The standard choice is the  $\overline{\text{MS}}$  mass definition.

The *upsilon expansion* tells us that, if we want to describe the non-relativistic  $Q\bar{Q}$  dynamics at NNLO, the heavy quark  $\overline{\text{MS}}$ -pole mass relation has to be known at order  $\alpha_s^3$ . The massless two-loop corrections have been determined a long time ago in Ref. [18] and the massless three-loop corrections can be found in Refs. [19]. In Ref. [18]

---

<sup>3</sup>At NNLO the energy scale  $M_b\alpha_s^2$  does not yet arise as a relevant dynamical scale.

also the two-loop light quark mass corrections were determined fully analytically for any value of the mass. For  $m_q \ll M_b$  the light quark mass corrections at two loops read

$$\left[\overline{M}_b(\overline{M}_b) - M_b\right]_m \longrightarrow -C_F \left(\frac{a_s}{\pi}\right)^2 \left\{ \frac{\pi^2}{8} m_q - \frac{3}{4} \frac{m_q^2}{M_b} + \dots \right\}. \quad (10)$$

It is remarkable that the linear two-loop term is equal to the NLO term displayed in Eq. (9). This is, of course, not an accident, but related to the universality of the linear light quark mass correction, already mentioned before. However, the reason for this is more general: it has been shown in Refs. [10,11] that the total static energy of a  $Q\overline{Q}$  pair,  $E_{\text{stat}} = 2M_Q + V(\mathbf{r})$  is free of any linear dependence on small momenta to all orders of perturbation theory. Therefore, also the three-loop linear light quark mass corrections in  $[\overline{M}_b(\overline{M}_b) - M_b]$  are given by the NNLO linear terms displayed in Eq. (9). From this fact alone we would not gain much because we cannot get any information on the size of the three-loop correction with higher powers of the light quark mass from this argument. However, we have seen before that the non-analytic linear light quark mass terms are enhanced by a factor  $\pi^2$  with respect to the analytic terms with higher powers of the light quark mass. This feature is also clearly visible in Eq. (10). Comparing the size of the full two-loop light quark mass corrections to the size of the linear term we find that the difference is at most 15% for  $m/M_b < 0.3$ . We therefore conclude (or conjecture) that the three-loop linear light quark mass corrections dominate the yet uncalculated full three-loop light quark mass corrections in a similar way and that the linear light quark mass terms provide a very good approximation at the level of 10% to the full light quark mass corrections. Some more numerical examinations based on BLM type three loop corrections have been carried out in Ref. [5] and are compatible with the conjecture. It even seems likely that the two- and three-loop differences between linear mass approximation and full results have a different sign, so that the difference in the sum might be much below 10%.

To conclude the discussion of the light quark mass corrections to the  $\overline{\text{MS}}$ -pole mass relation let me also show some numerical values. For  $\overline{M}_b(\overline{M}_b) = 4.2$  GeV,  $\overline{m}_c(\overline{m}_c) = 1.5$  GeV for the  $\overline{\text{MS}}$  charm quark mass and  $\alpha_s^{(4)}(\mu = 4.7 \text{ GeV}) = 0.216$  we obtain

$$M_b = \left\{ 4.2 + \left[0.385\right]^{\mathcal{O}(\alpha_s)} + \left[0.197 + 0.0117_m\right]^{\mathcal{O}(\alpha_s^2)} + \left[0.142 + 0.0176_m\right]^{\mathcal{O}(\alpha_s^3)} \right\} \text{ GeV}. \quad (11)$$

The massless corrections are somewhat better behaved than for the 1S-pole mass relation (but not what one would honestly call "convergent"), but the charm mass corrections (which are in the linear approximation) are again quite badly behaved. If we evaluate the charm mass corrections for  $\mu = \overline{m}_c(\overline{m}_c) = 1.5$  GeV, which is the natural scale for the linear mass terms, we obtain 36 MeV for the order  $\alpha_s^2$  corrections and 32 MeV for the order  $\alpha_s^3$  terms.

## 5 Heavy Quark $\overline{\text{MS}}$ -1S Mass Relation

The perturbative relation between the bottom 1S and the  $\overline{\text{MS}}$  mass can be used for two purposes. First, one can extract the bottom  $\overline{\text{MS}}$  mass from the experimental number for the mass of the  $\Upsilon(1S)$  (with a model-dependence from the estimate of non-perturbative corrections). Second, one can determine the bottom  $\overline{\text{MS}}$  mass from determinations of the 1S mass from methods that are less sensitive to non-perturbative effects, such as the  $\Upsilon$  sum rules.

Using the results of the two previous sections and combining them using the epsilon expansion to eliminate the pole mass parameter (which is absolutely crucial!) it is straightforward to derive this relation to order  $\alpha_s^3$  (or NNLO in the non-relativistic expansion). The full analytic expression for the resulting perturbative series can be found in Ref. [5].

To illustrate the behavior of the series let me show here again some numerical results. For  $M_b^{1S} = 4.7$  GeV,  $\overline{m}_c(\overline{m}_c) = 1.5$  GeV and  $\alpha_s^{(4)}(\mu = 4.7 \text{ GeV}) = 0.216$  we obtain

$$\begin{aligned} \overline{M}_b(\overline{M}_b) = & \left\{ 4.7 - \left[ 0.382 \right]^{\mathcal{O}(\alpha_s), \text{LO}} - \left[ 0.098 + 0.0072_m \right]^{\mathcal{O}(\alpha_s^2), \text{NLO}} \right. \\ & \left. - \left[ 0.030 + 0.0049_m \right]^{\mathcal{O}(\alpha_s^3), \text{NNLO}} \right\} \text{ GeV}. \end{aligned} \quad (12)$$

Comparing this result to Eqs. (8) and (11) we see that now the massless corrections show a quite good convergence and the charm mass corrections a fairly good one. This behavior reflects the fact that the  $\overline{\text{MS}}$  and the 1S mass definition both are short-distance masses, i.e. they do not have an ambiguity of order  $\Lambda_{\text{QCD}}$  such as the pole mass. It is therefore possible to reliably extract e.g. the bottom  $\overline{\text{MS}}$  mass from a given value for the 1S mass with a precision better than  $\Lambda_{\text{QCD}}$ .

The reason why the convergence of the charm mass corrections in our numerical example is not much better is the fact that the natural choice of the renormalization scale for the charm mass corrections is of the order of the charm mass and not the bottom mass, as used in Eq. (12). For  $\mu = 1.5$  GeV we find that the order  $\alpha_s^2$  ( $\alpha_s^3$ ) charm mass corrections amount to  $-16$  MeV ( $-1$  MeV). However, for  $\mu = 1.5$  GeV we also find  $(-570, 33, 55)$  MeV for the order  $(\alpha_s, \alpha_s^2, \alpha_s^3)$  massless corrections, because for them the characteristic scale is larger than the charm mass. Because the massless corrections are the dominant ones it is, of course, more suitable to choose the larger scale as we did in Eq. (12). Thus we find that the charm mass corrections lead to a shift of about  $-15$  MeV in the value of  $\overline{M}_b(\overline{M}_b)$  for a given value for  $M_b^{1S}$ . We note that the size of the charm mass corrections is larger than one would estimate from an effect of order  $(\frac{\alpha_s}{\pi})^2 \frac{m^2}{M_b}$ . The size arises from the incomplete cancellation of the linear light quark mass term in the bottom  $\overline{\text{MS}}$ -pole mass relation, since we are not allowed to expand in the charm mass in the bottom 1S-pole mass relation. On the other hand, for the up, down and strange quarks we are allowed to use the light quark mass expansion (because their masses are smaller than  $\langle p \rangle \sim M_b \alpha_s$  and  $\langle E \rangle \sim M_b \alpha_s^2$ ) and the linear mass terms are canceled, leaving a tiny correction that is quadratic in

the light quark masses. For  $\overline{m}_q(\overline{m}_q) = 0.1$  GeV the light quark mass corrections are well below the 1 MeV level. Thus the mass effects from the quarks lighter than the charm can be neglected.

The expression for the order  $\alpha_s^3$  (NNLO) relation between the bottom 1S and  $\overline{\text{MS}}$  is quite complicated, but it turns out that for  $\overline{m}_q(\overline{m}_q) > 0.4$  GeV and  $\mu \gtrsim 2.5$  GeV the dependence of the bottom  $\overline{\text{MS}}$ -1S mass relation at order  $\alpha_s^3$  on all parameters is approximately linear. This allows for the derivation of a handy approximation formula [5], which is applicable to all cases of interest and allows for a quick determination of the charm quark mass effects:

$$\begin{aligned} \overline{M}_b(\overline{M}_b) = & \left[ 4.169 \text{ GeV} - 0.01 \left( \overline{m}_c(\overline{m}_c) - 1.4 \text{ GeV} \right) + 0.925 \left( M_b^{1\text{S}} - 4.69 \text{ GeV} \right) \right. \\ & \left. - 9.1 \left( \alpha_s^{(5)}(M_Z) - 0.118 \right) \text{ GeV} + 0.0057 \left( \mu - 4.69 \right) \text{ GeV} \right]. \end{aligned} \quad (13)$$

## 6 Bottom $\overline{\text{MS}}$ Mass from $M(\Upsilon(1S))$

We can apply Eq. (13) to extract the bottom  $\overline{\text{MS}}$  mass from the mass of the  $\Upsilon(1S)$  meson, if we assume that  $\langle p \rangle$  and  $\langle E \rangle$  both are larger than  $\Lambda_{\text{QCD}}$  for the 1S state. Because for higher radial excitations  $\Upsilon(2S), \dots$  this assumption is more difficult to justify, we do not attempt a similar analyses for them. Recalling that the 1S mass just incorporates the perturbative effects, we need an estimate of the size of non-perturbative effects in the  $\Upsilon(1S)$  bound state. Using the gluon condensate contribution obtained by Voloshin and Leutwyler [20] we get

$$\left[ M(\Upsilon(1S)) \right]^{\text{non-pert}} \approx \frac{1872}{1275} \frac{M_b \pi}{(M_b C_F \alpha_s)^4} \langle \alpha_s \mathbf{G}^2 \rangle. \quad (14)$$

Using the standard literature range  $\langle \alpha_s \mathbf{G}^2 \rangle = 0.05 \pm 0.03 \text{ GeV}^4$  the non-perturbative correction can range from anywhere between 10 and 200 MeV due to the strong dependence on the renormalization scale in  $\alpha_s$ . Taking this estimate and  $M(\Upsilon(1S)) = 9460$  MeV we arrive at

$$M_b^{1\text{S}} = \frac{1}{2} \left\{ M(\Upsilon(1S)) - \left[ M(\Upsilon(1S)) \right]^{\text{non-pert}} \right\} = 4.68 \pm 0.05 \text{ GeV}. \quad (15)$$

From Eq. (13) we then obtain

$$\overline{M}_b(\overline{M}_b) = 4.16 \pm 0.06 \text{ GeV} \quad (16)$$

for the bottom  $\overline{\text{MS}}$  mass for  $\overline{m}_c(\overline{m}_c)$  around 1.3 GeV and adding the uncertainty in  $\alpha_s(M_Z)$  quadratically. The charm mass corrections amount to about  $-15$  MeV and are smaller than the uncertainty.

## 7 $\Upsilon$ Sum Rules

A method that is in principle much less sensitive to non-perturbative effects is to extract the bottom quark mass from moments of the  $b\bar{b}$  total cross section in  $e^+e^-$  annihilation:

$$P_n = \int_{s_{\min}}^{\infty} \frac{ds}{s^{n+1}} R(s). \quad (17)$$

Here  $R$  is the inclusive  $b\bar{b}$  cross section normalized to the muon pair cross section and  $s$  the square of the c.m. energy. The idea of the  $\Upsilon$  sum rules is to determine the bottom quark mass from comparing theoretical calculations of the moments  $P_n$  with moments obtained from experimental data [21]. Non-perturbative effects can, in contrast to calculations of the  $b\bar{b}$  spectrum, be suppressed by hand by choosing the parameter  $n$  small enough such that the size of the effective integration range in the c.m. energy in (17) is much larger than  $\Lambda_{\text{QCD}}$  [22]. For  $n \lesssim 15 - 20$  the gluon condensate corrections to the theoretical moments turn out to be smaller than a percent and can be neglected [21]. On the other hand, one would like to suppress the influence of the quite badly known  $b\bar{b}$  continuum in the experimental moments. This can be achieved by choosing  $n$  large, so that non-relativistic dynamics dominates the (theoretical and experimental) moments. In this case the only experimental input needed for the determination of the experimental moments are the masses and the electronic partial widths of the  $\Upsilon$  mesons. The continuum can be approximated by a crude model. Due to the large size of the bottom quark mass one can easily find a window,  $4 \lesssim n \lesssim 15$ , for which both requirements can be met. One can show that the average relative velocity of  $b\bar{b}$  pairs that dominate the moments is of order  $v_{\text{eff}} = 1/\sqrt{n}$ . So, by restricting  $n$  to the values just mentioned we find that  $\langle p \rangle \sim M_b v_{\text{eff}}$  and  $\langle E \rangle \sim M_b v_{\text{eff}}^2$  form a hierarchy and are larger than  $\Lambda_{\text{QCD}}$ . Thus the Schrödinger equation (1) can be safely used to describe the dynamics encoded in the moments.

For the case of massless light quarks a number of NLO [21,23] and NNLO [3,24] analyses have been carried out. For the restricted range of  $n$  the theoretical moments are directly related to the Green function  $G(0, 0, E)$  of the Schrödinger equation (1). It is also necessary to include, for the NNLO moments, a two-loop renormalization of an external current that describes the annihilation of a  $b\bar{b}$  pair into a photon. One can either calculate the bound state resonances and the continuum explicitly and carry out the energy integration in Eq. (17) on the real energy axis, or one uses the analyticity properties of the Green function and integrates instead in the negative complex energy plane. The calculations involved in these computations are quite extensive and shall not be describe here in more detail.

The light quark mass corrections to the moments have been determined in Ref. [5]. The NLO and NNLO corrections to the Green function  $G(0, 0, E)$  are determined with time-independent perturbation theory in analogy to Eq. (7). In Ref. [5] only the light quark mass corrections at NLO were fully determined, whereas at NNLO only the single insertion contribution (corresponding to the second term on the RHS of

Eq. (7)) was calculated. The NNLO double insertion contributions (last two terms on the RHS of Eq. (7)) were neglected based on the assumption that the suppression of the double insertion corrections (last two terms on the RHS of Eq. (7)) is as effective as for the calculation of the 1S mass.

The light quark mass corrections to the two-loop renormalization of the current were neglected because they are expected to be of order  $(\alpha_s/\pi)^2(m/M_b)^2$ , which is at the permille level even for charm quarks. There are no linear light quark mass corrections to the current renormalization because it only contains effects from momenta of order  $M_b$ . This means that non-analytic, and in particular  $\pi^2$ -enhanced linear light quark mass corrections do not exist.

In Ref. [5] a detailed analysis of the light quark mass correction in the 1S mass scheme has been carried out. The mass effects from up, down and strange quarks are negligible. For typical choices for the renormalization scales,  $\alpha_s(M_Z)$  and the 1S mass we find that the NNLO charm mass corrections are around -1% for  $n = 4$  and around -5% for  $n = 10$ , for  $\bar{m}_c(\bar{m}_c) \approx 1.5$  GeV. Thus the charm mass corrections in the bottom 1S mass are negative. From dimensional analysis we see that the moments  $P_n$  are proportional to  $(M_b^{1S})^{-2n}$ , so we can estimate that the charm mass corrections amount to about -15 MeV. (In the pole mass scheme the corrections are considerably larger due to the large non-analytic charm mass corrections that we have already discussed in the bottom 1S-pole mass relation. By using the bottom 1S mass in the moments these large corrections are canceled. The same is true for the massless corrections, see e.g. Ref. [25] for a comparison of results in different mass schemes.)

In Ref. [5] I have carried out a more thorough NLO and NNLO analysis based on a  $\chi^2$ -procedure, where several (theoretical and experimental) moments have been fitted simultaneously. This fitting procedure puts more statistical weight on the relative than on the absolute size of the moments. Interestingly, the relative size of the theoretical moments turns out to have smaller perturbative corrections than their absolute size. This is an issue that is well known from the total cross section for  $t\bar{t}$  production close to threshold in  $e^+e^-$  annihilation, where the line-shape for the NNLO prediction has much smaller perturbative corrections than the height (see Ref. [14] for a review). Recently, using renormalization group improved perturbation theory in the framework of "vNRQCD" [26] the height of the line-shape has been considerably stabilized by summation of logarithms of the top velocity at NNLL [27]. I will be quite interesting to see whether a summation of these logarithms can improve the behavior of the absolute size of the moments as well.

The result for the allowed values for the bottom 1S mass from the  $\chi^2$ -procedure based on the NNLO theoretical moments is displayed in Fig. 2 for  $\bar{m}_c(\bar{m}_c) = 0.0$  and 1.3 GeV. The dots represent points of minimal  $\chi^2$  for a large number of random choices of renormalization scales and sets of  $n$ 's for given values of  $\alpha_s^{(5)}(M_Z)$ . Experimental errors at 95% CL are displayed as vertical lines. (See Ref. [5] for more details.) The dependence of the 1S mass on the input value for  $\alpha_s^{(5)}(M_Z)$  turns out to be quite weak, particularly if the charm mass corrections are taken into account. For

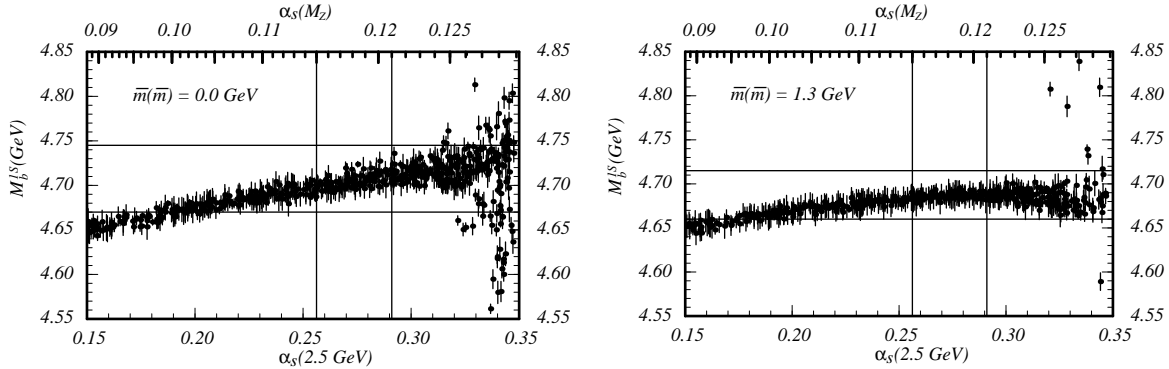


Figure 2: Results for the allowed range of  $M_b^{1S}$  for given values of  $\alpha_s^{(5)}(M_Z)$  at NNLO for  $\overline{m}_c(\overline{m}_c) = 0.0$  and  $1.3$  GeV. It is illustrated by the vertical and horizontal lines how the allowed range for  $M_b^{1S}$  is obtained, if  $0.115 \leq \alpha_s^{(5)}(M_Z) \leq 0.121$  is taken as an input.

$\overline{m}_c(\overline{m}_c) = 1.4 \pm 0.3$  GeV we obtain

$$M_b^{1S} = 4.69 \pm 0.03 \text{ GeV} \quad (18)$$

for the bottom 1S mass. The charm mass corrections shift the 1S mass by about -20 MeV, which is compatible with the crude estimate mentioned above. It is quite interesting that this result is compatible with the determination of the 1S mass from  $M(\Upsilon(1S))$  (see Eq. (15)). The difference to Eq. (15) is that the central value and the error from the sum rule determination are completely independent of the estimate for the size of the non-perturbative gluon condensate contribution. In this respect the result in Eq. (18) should be considered as more solid than the one in Eq. (15).

Taking the approximation formula (13) we then arrive at

$$\overline{M}_b(\overline{M}_b) = 4.17 \pm 0.05 \text{ GeV}, \quad (19)$$

for the bottom  $\overline{MS}$  mass, where we have added quadratically the uncertainties from  $M_b^{1S}$  (30 MeV),  $\alpha_s^{(5)}(M_Z) = 0.118 \pm 0.003$  (30 MeV),  $\mu = 4.7 \pm 3$  GeV (15 MeV) and  $\overline{m}_c(\overline{m}_c) = 1.4 \pm 0.3$  GeV (5 MeV). We note that the charm mass corrections in the  $\Upsilon$  sum rules and those in the  $\overline{MS}$ -1S mass relation are additive and lead to an overall shift of about -30 MeV in  $\overline{M}_b(\overline{M}_b)$  compared to an analysis where the charm mass is neglected altogether. Thus the charm mass effects are relevant for the sum rule method, in particular if it should turn out that the perturbative uncertainties in the moments can be decreased in the future.

## 8 Conclusions

In this talk I have reviewed recent results for light quark mass effects in perturbative bottom quark mass determinations from  $\Upsilon$  mesons [4,5]. We find that the effects of the charm mass are non-negligible in view of the present theoretical uncertainties.

Light quark mass corrections were determined for the 1S-pole mass relation at NNLO, for the  $\overline{\text{MS}}$ -pole mass relation at order  $\alpha_s^3$  and for the  $\Upsilon$  sum rules at NNLO. In the determination of the bottom  $\overline{\text{MS}}$  mass,  $\overline{M}_b(\overline{M}_b)$ , from the mass of the  $\Upsilon(1S)$  meson the charm mass corrections shift the value of  $\overline{M}_b(\overline{M}_b)$  by about -15 MeV. In the determination of the bottom 1S mass,  $M_b^{1S}$ , from the  $\Upsilon$  sum rules the charm mass corrections shift the value of  $M_b^{1S}$  by about -20 MeV. The overall shift of  $\overline{M}_b(\overline{M}_b)$  obtained from the  $\Upsilon$  sum rule analysis is about -30 MeV. The sign and size of the charm mass corrections shows agreement with a recent unquenched lattice determination of  $\overline{M}_b(\overline{M}_b)$  [28].

On the conceptual side light quark mass corrections are interesting because they provide a natural tool to investigate the sensitivity the heavy quark mass definitions to infrared momenta.

## Acknowledgments

This work was supported in part by the EU Fourth Framework Program “Training and Mobility of Researchers”, Network “Quantum Chromodynamics and Deep Structure of Elementary Particles”, contract FMRX-CT98-0194 (DG12-MIHT).

## References

- [1] C. T. Sachrajda, hep-lat/0101003; V. Lubicz, hep-lat/0012003.
- [2] G. Dissertori, hep-ex/0010005. A. Brandenburg, P. N. Burrows, D. Muller, N. Oishi and P. Uwer, Phys. Lett. B **468**, 168 (1999).
- [3] K. Melnikov and A. Yelkhovsky, Phys. Rev. D **59**, 114009 (1999); A. H. Hoang, Phys. Rev. D **61**, 034005 (2000); M. Beneke and A. Signer, Phys. Lett. B **471**, 233 (1999).
- [4] A. H. Hoang and A. V. Manohar, Phys. Lett. B **483**, 94 (2000).
- [5] A. H. Hoang, hep-ph/0008102.
- [6] Y. Schroder, Phys. Lett. B **447**, 321 (1999); M. Peter, Phys. Rev. Lett. **78**, 602 (1997).
- [7] M. Melles, Phys. Rev. D **62**, 074019 (2000); Phys. Rev. D **58**, 114004 (1998).
- [8] A. Pineda and F. J. Yndurain, Phys. Rev. D **58**, 094022 (1998); S. Titard and F. J. Yndurain, Phys. Rev. D **49**, 6007 (1994).
- [9] F. J. Yndurain, Nucl. Phys. Proc. Suppl. **93**, 196 (2001).

- [10] A. H. Hoang, M. C. Smith, T. Stelzer and S. Willenbrock, Phys. Rev. D **59**, 114014 (1999).
- [11] M. Beneke, Phys. Lett. B **434**, 115 (1998).
- [12] A. H. Hoang and T. Teubner, Phys. Rev. D **60**, 114027 (1999).
- [13] A. H. Hoang, Z. Ligeti and A. V. Manohar, Phys. Rev. D **59**, 074017 (1999); Phys. Rev. Lett. **82**, 277 (1999).
- [14] A. H. Hoang *et al.*, Eur. Phys. J. directC **3**, 1 (2000).
- [15] I. Bigi, M. Shifman, N. Uraltsev and A. Vainshtein, Phys. Rev. D **56**, 4017 (1997).
- [16] D. Eiras and J. Soto, Phys. Lett. B **491**, 101 (2000).
- [17] A. Hoang, PhD thesis, University of Karlsruhe, RX-1578 (AACHEN).
- [18] N. Gray, D. J. Broadhurst, W. Grafe and K. Schilcher, Z. Phys. C **48**, 673 (1990).
- [19] K. Melnikov and T. v. Ritbergen, Phys. Lett. **B482**, 99 (2000). K. G. Chetyrkin and M. Steinhauser, Nucl. Phys. **B573**, 617 (2000).
- [20] M. B. Voloshin, Yad. Fiz. **36**, 247 (1982) [Sov. J. Nucl. Phys. **36**,1 (1982)]; H. Leutwyler, Phys. Lett. **B98**, 447 (1981).
- [21] M. B. Voloshin, Int. J. Mod. Phys. **A10**, 2865 (1995).
- [22] E. C. Poggio, H. R. Quinn and S. Weinberg, Phys. Rev. D **13**, 1958 (1976).
- [23] J. H. Kuhn, A. A. Penin and A. A. Pivovarov, Nucl. Phys. B **534**, 356 (1998).
- [24] A. H. Hoang, Phys. Rev. D **59**, 014039 (1999); A. A. Penin and A. A. Pivovarov, Phys. Lett. B **443**, 264 (1998); Nucl. Phys. B **549**, 217 (1999);
- [25] A. H. Hoang, Nucl. Phys. Proc. Suppl. **86**, 512 (2000).
- [26] M. E. Luke, A. V. Manohar and I. Z. Rothstein, Phys. Rev. D **61**, 074025 (2000); A. V. Manohar and I. W. Stewart, Phys. Rev. D **62**, 014033 (2000); Phys. Rev. D **62**, 074015 (2000); Phys. Rev. D **63**, 054004 (2001). A. H. Hoang, A. V. Manohar and I. W. Stewart, hep-ph/0102257.
- [27] A. H. Hoang, A. V. Manohar, I. W. Stewart and T. Teubner, hep-ph/0011254.
- [28] V. Gimenez, L. Giusti, G. Martinelli and F. Rapuano, JHEP**0003**, 018 (2000).

## Exclusive QCD

MARKUS DIEHL

*Deutsches Elektronen-Synchrotron DESY, 22603 Hamburg, Germany*

I give a brief introduction to the physics of generalized parton distributions and distribution amplitudes. I then report on the status of the calculation of radiative corrections for the exclusive processes where these quantities occur.

Presented at the

5th International Symposium on Radiative Corrections  
(RADCOR-2000)

Carmel CA, USA, 11–15 September, 2000

# 1 Introduction

In recent years a formalism has been developed which highlights the close connection between exclusive and inclusive strong interaction processes. The cornerstones of this formalism are the concepts of generalized parton distributions and generalized distribution amplitudes. These quantities contain valuable information on the non-perturbative transition between partons and hadrons, whose understanding remains one of the great outstanding tasks in QCD. They can be accessed in several exclusive reactions that are within the reach of current and planned experimental facilities. In this contribution I will first give a brief overview of the formalism and the physics behind it, and then report on the status of the calculation of radiative corrections in this context.

A key process in the development of the QCD improved parton model has been inclusive deep inelastic scattering,  $ep \rightarrow eX$ , which via the optical theorem is conveniently expressed in terms of the imaginary part of the forward Compton amplitude,  $\gamma^*(q) + p(p) \rightarrow \gamma^*(q) + p(p)$ . In the Bjorken region of large photon virtuality  $Q^2 = -q^2$  and c.m. energy  $(p + q)^2$ , this amplitude factorizes into a perturbatively calculable scattering process at the level of quarks and gluons and process independent matrix elements

$$\langle p(p) | \mathcal{O}(\lambda) | p(p) \rangle. \quad (1)$$

Here  $\mathcal{O}(\lambda)$  stands for quark or gluon operators  $\bar{\psi}(0) n_\mu \gamma^\mu \psi(\lambda n)$ ,  $\bar{\psi}(0) n_\mu \gamma^\mu \gamma_5 \psi(\lambda n)$ ,  $n_\mu n_\nu F^{\mu\alpha}(0) F^\nu{}_\alpha(\lambda n)$ ,  $n_\mu n_\nu F^{\mu\alpha}(0) \tilde{F}^\nu{}_\alpha(\lambda n)$ , whose fields are separated by a light-like distance  $\lambda n$  (*i.e.*,  $n^2 = 0$ ). These matrix elements, represented by a blob in fig. 1a, are parameterized by parton distributions; they describe the transition between hadronic and partonic degrees of freedom.

This factorization into short- and long-distance dynamics is actually more general.

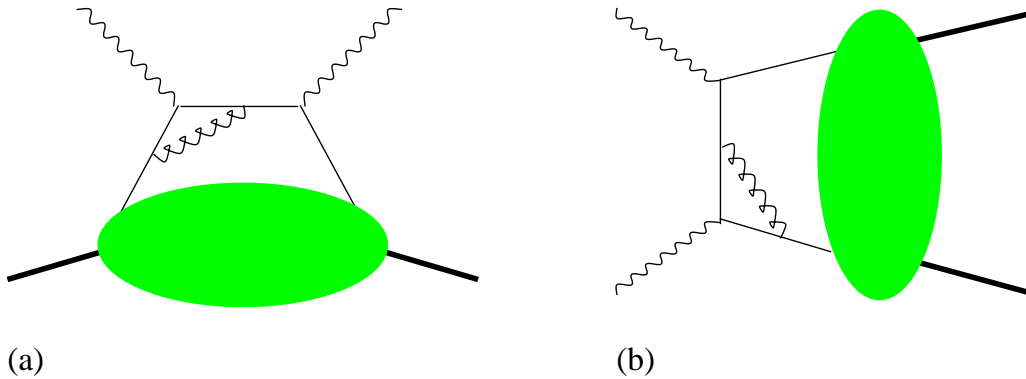


Figure 1: (a) A diagram for the Compton amplitude  $\gamma^*p \rightarrow \gamma^*p$  in Bjorken kinematics. (b) A diagram for the corresponding amplitude  $\gamma^*\gamma^* \rightarrow p\bar{p}$  in the crossed channel.

It also holds for the nonforward Compton amplitude,  $\gamma^*(q) + p(p) \rightarrow \gamma^*(q') + p(p')$ , in a generalization of Bjorken kinematics, namely if the c.m. energy  $(p + q)^2$  and at least one of the photon virtualities  $|q^2|$ ,  $|q'^2|$  are large while the invariant momentum transfer  $(p - p')^2$  is small [1,2,3]. In the particular case where the outgoing photon is on shell, one speaks of deeply virtual Compton scattering, which can be accessed in the physical process  $ep \rightarrow ep\gamma$ , *i.e.*, in exclusive electroproduction of a photon. The non-perturbative physics is now described by matrix elements with the *same* operators as before, but between *different* hadron states,

$$\langle p(p') | \mathcal{O}(\lambda) | p(p) \rangle. \quad (2)$$

The nonzero momentum transfer to the proton implies that the momenta of the two parton lines attached to the blob in fig. 1a must differ as well. A simple calculation shows that in particular their momentum fractions with respect to the hadrons cannot be equal. For this reason, the generalized parton distributions which parameterize the matrix elements (2) are often called “skewed”.

A completely analogous type of factorization occurs in the crossed channel, *i.e.*, in  $\gamma^*(q) + \gamma^*(q') \rightarrow p(p) + \bar{p}(p')$ , if at least one of the photon virtualities is large, in particular compared with the invariant mass  $(p + p')^2$  of the produced hadron pair [1,4]. A corresponding diagram is shown in fig. 1b. Matrix elements

$$\langle p(p) \bar{p}(p') | \mathcal{O}(\lambda) | 0 \rangle \quad (3)$$

with again the same operators as before now parameterize the non-perturbative transition from a quark-antiquark or gluon pair to the final state hadrons. In addition to the  $p\bar{p}$  system one can consider a wide range of hadrons, say  $\pi\pi$  or  $KK$ , which are not easily available as beam particles in Compton scattering. The production mechanism represented in fig. 1b is the same as in the process  $\gamma^*\gamma \rightarrow \pi$ , where the nonperturbative input is represented by the quark-antiquark distribution amplitude of the pion. Data on this process have in fact provided one of the best available constraints so far on this important quantity [5]. The matrix elements (3) are a direct generalization of usual distribution amplitudes, where  $\langle p\bar{p} |$  is replaced by a single-meson state.

## 2 Some physics aspects

As a consequence of the finite momentum transfer to the proton, generalized parton distributions admit two different kinematical regimes. In the first, they describe the emission of a parton with momentum fraction  $x + \xi$  from the parent hadron and its reabsorption with momentum fraction  $x - \xi$ , see fig. 2a. In the limit where  $p = p'$  one has  $\xi = 0$  and recovers the usual parton distributions. In a second regime, which does not exist for  $p = p'$ , one has the coherent emission of a quark-antiquark or gluon

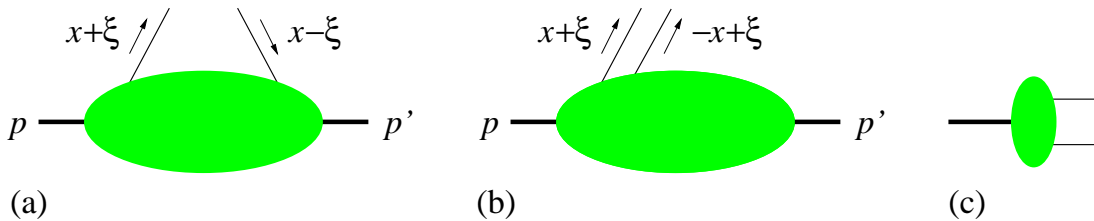


Figure 2: (a) The kinematical regime where a generalized parton distribution describes the emission and reabsorption of a parton. (b) The regime where it describes the emission of a quark-antiquark or gluon pair. This is reminiscent of a meson distribution amplitude, shown in (c).

pair from the parent hadron of momentum  $p$ , leaving the hadron with momentum  $p'$ , see fig. 2b. One is thus sensitive to aspects of the proton structure that cannot be accessed by the ordinary parton densities. The second regime is reminiscent of a distribution amplitude, shown in fig. 2c, where there is no hadron left behind after emission of the partons. We will encounter an important manifestation of this similarity in section 4.1.

It has long been known that the usual parton distributions can be represented in terms of light-cone wave functions, which completely specify the structure of a hadron in terms of quark and gluon configurations [6]. In this representation, depicted in fig. 3a, the wave functions appear *squared*, which reflects the crucial parton model feature that parton densities can be understood as classical probabilities for the emission of a parton from a hadron. The wave function representation of generalized parton distributions [7] provides a key to their physical interpretation: they are not probabilities but *interference* terms of wave functions for different parton configurations in a hadron. In this sense they contain characteristic information on the quantum fluctuations of QCD bound states, going beyond the classical probability picture of the parton model.

Generalized parton distributions have a rich structure in spin, since the helicities of the partons and the hadrons can be varied independently. Of particular interest are those combinations where the helicity difference on the hadron side is not compensated on the parton side: in that case angular momentum conservation must be ensured by a transfer of orbital angular momentum, which is possible if there is a finite transfer of transverse momentum. Thus, generalized distributions carry information on the orbital angular momentum of partons—information that is hard to access otherwise. If one takes moments of the generalized distributions in the momentum fraction  $x$ , the operators in the matrix elements (2) are transformed into local operators, *i.e.*, one obtains form factors of various local currents. A sum rule due to Ji [2] states that the second moment of a particular combination of generalized distributions gives a form factor whose value at zero momentum transfer is the *total* angular momentum

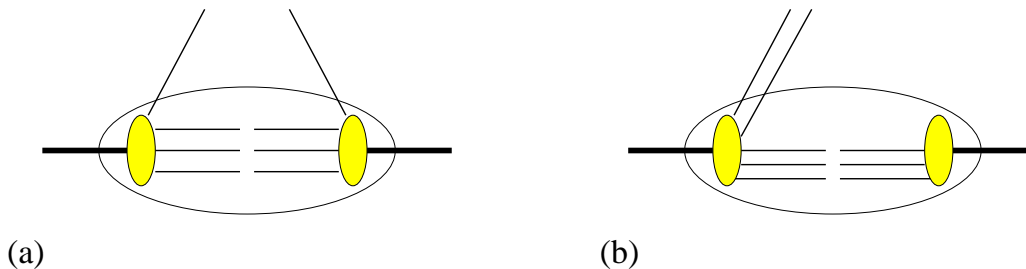


Figure 3: Representation of a parton distribution in terms of light-cone wave functions, denoted by small blobs, in the two regimes of fig. 2a and b. Notice that the second regime involves wave functions with different parton content.

of quarks in the proton, consisting both of a spin and an orbital part.

The generalized distribution amplitudes of fig. 1b are intimately connected with generalized parton distributions by crossing symmetry. Their moments are in fact related by an analytic continuation in the Mandelstam invariant, *i.e.*,  $t = (p - p')^2$  for distributions and  $s = (p + p')^2$  for distribution amplitudes. On the other hand, generalized distribution amplitudes contain physics quite distinct from that of parton distributions: they involve not only the partonic structure of a single hadron, but also the interactions between hadrons. They parameterize what one might call the “exclusive limit” of fragmentation, *i.e.*, of the transition between parton and hadron degrees of freedom. It is interesting to note that one can make a connection with phenomenologically successful pictures of hadronization such as the Lund string model [8].

### 3 Processes

As we saw in the introduction, generalized parton distributions can be accessed in deeply virtual Compton scattering, measurable by electroproduction  $ep \rightarrow ep\gamma$ . Another class of processes where they occur is exclusive electroproduction of a meson instead of a photon,  $ep \rightarrow ep\rho^0$ ,  $ep \rightarrow en\pi^+$ , etc. Example diagrams are shown in fig. 4. Notice that for vector mesons both quark and gluon distributions contribute at leading order in  $\alpha_s$ . This is in contrast to Compton scattering, where gluons only appear at the level of one-loop corrections, as they do in inclusive deep inelastic scattering.

To date, we have no experimental determinations of generalized parton distributions. However, first measurements of the above processes in the relevant kinematical domain have been performed, in particular by HERMES, H1, and ZEUS at DESY. Further and more precise investigations are planned Jefferson Lab and at CERN (COMPASS), and several future accelerator projects would be well suited for in-depth

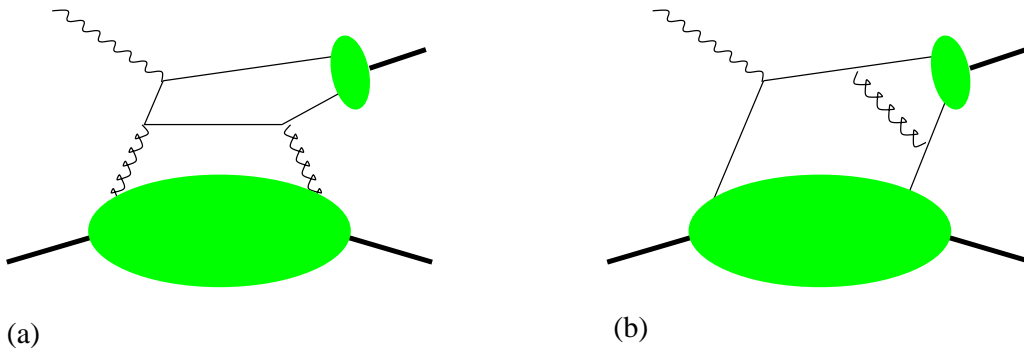


Figure 4: Born level diagrams for the exclusive production of a meson from a deeply virtual photon. The large blobs denote generalized gluon or quark distributions, and the small blobs the meson distribution amplitude. Diagram (a) only contributes for mesons with negative charge conjugation parity.

studies of these processes.

Generalized distribution amplitudes can be accessed in  $\gamma^*\gamma^*$  or  $\gamma^*\gamma$  processes at  $e^+e^-$  colliders, and cross section estimates [9] indicate that the production of pion pairs  $\gamma^*\gamma \rightarrow \pi\pi$  should be well in the reach of BABAR, BELLE, and CLEO.

## 4 Radiative Corrections

As in all applications of QCD factorization, radiative corrections in our context manifest themselves in two ways. The process independent hadronic matrix elements depend on a factorization scale via evolution equations, whose kernels can be calculated in perturbation theory. On the other hand, there are radiative corrections to the hard scattering subprocesses for each individual reaction.

### 4.1 Evolution

The evolution of generalized distribution amplitudes is exactly the same as the one of the usual distribution amplitudes for mesons, described by the ERBL equations [15]. This is not surprising, since evolution arises from the renormalization of the bilocal operators  $\mathcal{O}(\lambda)$  and is insensitive to whether the matrix elements (3) involve a single meson or a two-particle state with the same quantum numbers.

The evolution of general parton distributions on the other hand, is more complex and of considerable theoretical interest. It is in fact this aspect on which the earliest studies of these quantities have focused on [1,14]. In the regime of fig. 2a, the evolution is similar to the standard DGLAP evolution of parton densities, with a kernel that depends on the parameter  $\xi$  describing the longitudinal momentum transfer to the

partons (see fig. 2). In the regime of fig. 2b, evolution acts in a similar way as ERBL evolution, which highlights the close analogy between figs. 2b and c. The evolution equations for ordinary parton distributions and for distribution amplitudes, although acting in quite different ways, are thus intimately related, which stems from the fact that these quantities are defined through the same bilocal operators  $\mathcal{O}(\lambda)$ . The evolution kernels for generalized parton distributions, called “extended ERBL kernels”, contain the usual DGLAP and ERBL kernels as limiting cases; in this sense the evolution of generalized parton distributions *interpolates* between the two extremes of DGLAP and ERBL evolution.

The extended ERBL kernels have been calculated to LO by many groups. They can be found to NLO accuracy in [16], where conformal and supersymmetric constraints were employed in order to reconstruct them from the known NLO DGLAP kernels. A numerical study (limited to parton helicity independent distributions) showed that the effect of NLO evolution was moderate compared with LO evolution [17]. For the model distributions used there, the difference between NLO and LO evolution was a few percent for non-singlet distributions and not more than 10 to 30% in the singlet sector.

## 4.2 The two-photon processes

The one-loop corrections to deeply virtual Compton scattering have been independently calculated by three groups [10,11]. In addition to diagrams like the one in fig. 1a they involve diagrams with the generalized gluon distributions in the proton. In [10] one finds the NLO results for the general nonforward amplitude  $\gamma^*(q) + p(p) \rightarrow \gamma^*(q') + p(p')$ ; in the limit  $q = q'$  their imaginary parts reduce to the well-known expressions for unpolarized and polarized deep inelastic scattering. In [11] a numerical study for  $\gamma^*p \rightarrow \gamma p$  was performed, making an ansatz for the yet unknown generalized quark and gluon distributions. It was found that the NLO corrections can be large, up to about 50%, and depend sensitively on the value of the Bjorken variable  $x_B = Q^2/(2p \cdot q)$ .

By an analytic continuation of the hard scattering kernel, the one-loop corrections for  $\gamma^*\gamma \rightarrow \pi\pi$  have been obtained from those for the general nonforward Compton amplitude [12]. Numerical studies show that the size of the corrections is very sensitive to the relative size of the two-gluon and the quark-antiquark distribution amplitudes [12,13]. In other words, this process may offer an interesting way to investigate how strongly the two-pion system couples to  $gg$  in comparison with  $q\bar{q}$ .

## 4.3 Power corrections

The factorized description discussed so far is valid in the limit of infinitely large photon virtuality  $Q^2$ , and at finite  $Q^2$  there are as usual corrections suppressed by powers of  $1/Q$ , up to logarithmic terms.

An estimation of  $1/Q^2$  corrections to deeply virtual Compton scattering and to pion electroproduction has been made in [18] with the help of the renormalon technique, resumming vacuum polarization insertions in the gluon lines of figs. 1a and 4b. The corrections, evaluated at  $Q^2 = 4 \text{ GeV}^2$ , were found to grow with  $x_B$  and to be important (of order 10 to 50%) for the Compton process. For pion production they came out substantially larger (100% and more), with a strong dependence on the ansatz made for the generalized quark distributions.

The structure of the  $1/Q$  corrections to the Compton process [19] and its crossed counterpart in  $\gamma^*\gamma$  collisions [20] has been completely classified in the framework of the operator product expansion. These corrections factorize into a hard scattering subprocess and generalized parton distributions of twist 3, in contrast to the twist-2 distributions discussed so far. The evolution equations of the twist-3 distributions are known [21], in part to LO and in part to NLO, whereas the NLO corrections to the hard scattering have not been calculated as yet. It is worth mentioning that the  $1/Q$  suppressed terms contribute only to amplitudes where the helicities of the two photons differ by 1, whereas the leading contributions only feed amplitudes where the photon helicities are equal or differ by 2. The corresponding helicity amplitudes can be separated using appropriate angular distributions [9,22]; the two-photon processes might therefore provide a window on twist-3 effects that are not masked by large twist-2 pieces.

#### 4.4 Meson production

For meson electroproduction, the one-loop corrections to the hard scattering kernels have not yet been evaluated. In the case of pion production, they are closely connected with the one-loop corrections to the pion form factor in the hard-scattering formalism of Brodsky and Lepage. In fact, the Feynman diagrams for the latter can be obtained from those for pion electroproduction (see fig. 4b) by replacing the quark distribution in the proton with the pion distribution amplitude. The NLO corrections to the pion form factor can but need not be important, depending crucially on the choice of renormalization scale in  $\alpha_s$  [23].

For the production of vector mesons, the additional calculation of the one-loop corrections to the gluon exchange diagrams (see fig. 4a) is necessary for a complete NLO evaluation. It would be very interesting to know the size of these corrections. Frankfurt *et al.* [24] have studied the tree level diagrams, including in the hard scattering process the transverse momentum  $k_T$  of the quark-antiquark pair in the vector meson, *i.e.*, replacing the meson distribution amplitude in fig. 4a with the  $k_T$  dependent light-cone wave function. This inclusion of this finite  $k_T$  effects led to a very strong suppression of the amplitude when a meson wave function was taken that decreases as slowly as  $1/k_T^2$  at large transverse momentum. This large- $k_T$  falloff is, however, mediated by hard gluon exchange between the quark and antiquark forming

the meson, and as such should be included not in the meson wave function but in the hard scattering process, where it is a *part* of the NLO corrections.

## 5 Summary

Generalized parton distributions and distribution amplitudes provide novel tools to study the interplay between partons and hadrons in QCD. They connect several well-studied concepts such as parton densities, distribution amplitudes, form factors, and light-cone wave functions, and contain information beyond what can be learned from each of these.

These novel quantities can be studied in certain exclusive processes at large momentum transfer, whose investigation is in reach of present-day and future experiments. The description of these processes relies on factorization theorems and thus has a solid basis in QCD.

A quantitatively reliable extraction of generalized parton distributions and distribution amplitudes will require a sufficient understanding of and control over radiative corrections. The logarithmic evolution of these quantities is well studied and the kernels are known to NLO. As to the corrections to the hard scattering subprocess, they are known to NLO in the case of Compton scattering and of  $\gamma^*\gamma$  collisions, but a deeper understanding of when and why they are large is still to be achieved. Not much is known about the NLO corrections to meson production, but some pieces of evidence exist that they may be important in certain kinematical situations.

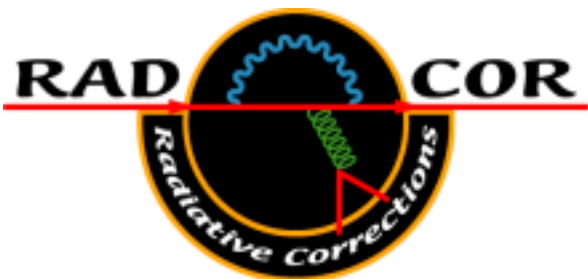
## Acknowledgments

I gratefully acknowledge the financial support of RADCOR–2000 and of the SLAC theory group.

## References

- [1] D. Müller *et al.*, Fortsch. Phys. **42**, 101 (1994) [hep-ph/9812448].
- [2] X. Ji, Phys. Rev. Lett. **78** (1997) 610 [hep-ph/9603249].
- [3] A. V. Radyushkin, Phys. Rev. **D56**, 5524 (1997) [hep-ph/9704207];  
J. C. Collins and A. Freund, Phys. Rev. **D59** (1999) 074009 [hep-ph/9801262].
- [4] M. Diehl *et al.*, Phys. Rev. Lett. **81**, 1782 (1998) [hep-ph/9805380].

- [5] J. Gronberg *et al.* (CLEO Collaboration), Phys. Rev. **D57**, 33 (1998) [hep-ex/9707031].
- [6] S. J. Brodsky and G. P. Lepage, in: *Perturbative Quantum Chromodynamics*, edited by A. H. Mueller (World Scientific, Singapore 1989).
- [7] S. J. Brodsky, M. Diehl and D. S. Hwang, hep-ph/0009254; M. Diehl, T. Feldmann, R. Jakob and P. Kroll, hep-ph/0009255.
- [8] M. Maul, Phys. Rev. **D63**, 036003 (2001) [hep-ph/0003254].
- [9] M. Diehl *et al.*, Phys. Rev. **D62**, 073014 (2000) [hep-ph/0003233].
- [10] X. Ji and J. Osborne, Phys. Rev. **D58**, 094018 (1998) [hep-ph/9801260]; L. Mankiewicz *et al.*, Phys. Lett. **B425**, 186 (1998) [hep-ph/9712251].
- [11] A. V. Belitsky *et al.*, Phys. Lett. **B474**, 163 (2000) [hep-ph/9908337].
- [12] N. Kivel *et al.*, Phys. Lett. **B467**, 263 (1999) [hep-ph/9908334].
- [13] N. Kivel and L. Mankiewicz, Eur. Phys. J. **C18**, 107 (2000) [hep-ph/0008168].
- [14] J. Blümlein *et al.*, Phys. Lett. **B406**, 161 (1997) [hep-ph/9705264].
- [15] G. P. Lepage and S. J. Brodsky, Phys. Lett. **B87**, 359 (1979); A. V. Efremov and A. V. Radyushkin, Phys. Lett. **B94**, 245 (1980).
- [16] A. V. Belitsky *et al.*, Nucl. Phys. **B574**, 347 (2000) [hep-ph/9912379].
- [17] A. V. Belitsky *et al.*, Nucl. Phys. **B546**, 279 (1999) [hep-ph/9810275]; A. V. Belitsky *et al.*, Phys. Lett. **B437**, 160 (1998) [hep-ph/9806232].
- [18] M. Vanttinen, L. Mankiewicz and E. Stein, hep-ph/9810527.
- [19] A. V. Radyushkin and C. Weiss, hep-ph/0010296, and references therein.
- [20] N. Kivel and L. Mankiewicz, hep-ph/0010161.
- [21] A. V. Belitsky and D. Müller, Nucl. Phys. **B589**, 611 (2000) [hep-ph/0007031].
- [22] M. Diehl *et al.*, Phys. Lett. **B411**, 193 (1997) [hep-ph/9706344].
- [23] B. Melić *et al.*, Phys. Rev. **D60**, 074004 (1999) [hep-ph/9802204].
- [24] L. Frankfurt *et al.*, Phys. Rev. **D54**, 3194 (1996) [hep-ph/9509311].



# Organizing Committees

[HOME](#) [COMMITTEES](#) [PARTICIPANTS](#) [PROCEEDINGS](#) [PROGRAM](#)

[BULLETIN](#) [HOTEL](#) [REGISTRATION](#) [TRAVEL INFO](#)

## International Organizing Committee

- G. Altarelli (CERN)
- S. Bethke (MPI, Munich)
- R. Clare (MIT)
- N. Dombey (Sussex)
- J. Ellis (CERN)
- E. Fernandez (UAB, Barcelona)
- K. Hagiwara (KEK)
- W. Hollik (Karlsruhe)
- S. Jadach (Cracow)
- P. Janot (CERN)
- R.D. Peccei (UCLA)
- G.G. Ross (Oxford)
- J. Sola (UAB, Barcelona)
- B.F.L. Ward (Tennessee)
- S. Weinberg (Texas, Austin)
- P.M. Zerwas (DESY)

## Local Organizing Committee

- H.E. Haber, Chair (UCSC)
- S.J. Brodsky, Vice-Chair (SLAC)
- Z. Bern (UCLA)
- L. Dixon (SLAC)
- M.L. Graesser (UCSC)
- J.F. Gunion (UCD)
- J.L. Hewett (SLAC)
- G. Hiller (SLAC)
- K. Melnikov (SLAC)
- M.E. Peskin (SLAC)
- T.G. Rizzo (SLAC)
- P.C. Rowson (SLAC)
- B.A. Schumm (UCSC)



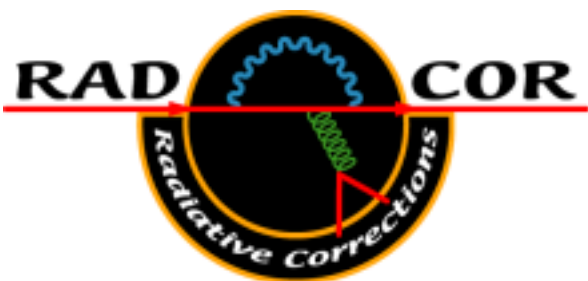
■ [Home](#) ■ [Committees](#) ■ [Participants](#) ■ [Proceedings](#) ■ [Program](#)

■ [Bulletin](#) ■ [Hotel](#) ■ [Registration](#) ■ [Travel Info](#)

5th International Symposium on Radiative Corrections  
Carmel Mission Inn, Carmel, CA  
September 11 - 15, 2000

[Jones](#)

Last Update: Monday, 20 November 2000



# Participants

**HOME COMMITTEES PARTICIPANTS PROCEEDINGS PROGRAM**  
**BULLETIN HOTEL REGISTRATION TRAVEL INFO**

Name	Organization	Email Address
Afanasev, Andrei	NCCU/Jlab	<a href="mailto:afanas@jlab.org">afanas@jlab.org</a>
Akushevich, Igor	NCCU/Jlab	<a href="mailto:aku@jlab.org">aku@jlab.org</a>
Barker, Tony	University of Colorado, Boulder	<a href="mailto:tonyb@cuhep.colorado.edu">tonyb@cuhep.colorado.edu</a>
Barklow, Timothy	SLAC	<a href="mailto:timb@slac.stanford.edu">timb@slac.stanford.edu</a>
Baur, Ulrich	State University of New York at Buffalo	<a href="mailto:baur@ubhep.physics.buffalo.edu">baur@ubhep.physics.buffalo.edu</a>
Beneke, Martin	RWTH Aachen	<a href="mailto:mbeneke@physik.rwth-aachen.de">mbeneke@physik.rwth-aachen.de</a>
Berger, Edmond	Argonne National Laboratory	<a href="mailto:berger@anl.gov">berger@anl.gov</a>
Bern, Zvi	UCLA	<a href="mailto:bern@physics.ucla.edu">bern@physics.ucla.edu</a>
Bertolini, Stefano	INFN and SISSA	<a href="mailto:bertolin@he.sissa.it">bertolin@he.sissa.it</a>
Binger, Michael	SLAC	<a href="mailto:mwbinger@stanford.edu">mwbinger@stanford.edu</a>
Blumlein, Johannes	DESY	<a href="mailto:blumlein@ifh.de">blumlein@ifh.de</a>
Brodsky, Stanley	SLAC	<a href="mailto:sjbth@slac.stanford.edu">sjbth@slac.stanford.edu</a>
Carena, Marcela	Fermilab	<a href="mailto:carena@fnal.gov">carena@fnal.gov</a>
Chang, Darwin	SLAC and N. Tsing-Hua University	<a href="mailto:chang@fnal.gov">chang@fnal.gov</a>
Charles, François	GRPHE/UHA	<a href="mailto:charles@sbgpcs10.in2p3.fr">charles@sbgpcs10.in2p3.fr</a>
Chetyrkin, Konstantin	Albert-Ludwigs Univ. Freiburg	<a href="mailto:chet@particle.physik.uni-karlsruhe.de">chet@particle.physik.uni-karlsruhe.de</a>
Czarnecki, Andrzej	University of Alberta	<a href="mailto:czar@phys.ualberta.ca">czar@phys.ualberta.ca</a>

<b>Dalley, Simon</b>	<b>Centre for Mathematical Sciences</b>	<a href="mailto:sd214@damtp.cam.ac.uk"><u>sd214@damtp.cam.ac.uk</u></a>
<b>Denner, Ansgar</b>	<b>Paul Scherrer Institut</b>	<a href="mailto:Ansgar.Denner@psi.ch"><u>Ansgar.Denner@psi.ch</u></a>
<b>Diehl, Markus</b>	<b>SLAC</b>	<a href="mailto:mdiehl@slac.stanford.edu"><u>mdiehl@slac.stanford.edu</u></a>
<b>Dittmaier, Stefan</b>	<b>University of Bielefeld</b>	<a href="mailto:Stefan.Dittmaier@cern.ch"><u>Stefan.Dittmaier@cern.ch</u></a>
<b>Dixon, Lance</b>	<b>SLAC</b>	<a href="mailto:lance@slac.stanford.edu"><u>lance@slac.stanford.edu</u></a>
<b>El-Khadra, Aida</b>	<b>University of Illinois, Dept. of Physics</b>	<a href="mailto:axk@uiuc.edu"><u>axk@uiuc.edu</u></a>
<b>Ellis, Keith</b>	<b>Fermilab</b>	<a href="mailto:ellis@fnal.gov"><u>ellis@fnal.gov</u></a>
<b>Erlar, Jens</b>	<b>University of Pennsylvania</b>	<a href="mailto:erler@langacker.hep.upenn.edu"><u>erler@langacker.hep.upenn.edu</u></a>
<b>Garcia-Murchat, David</b>	<b>CERN, TH</b>	<a href="mailto:dgarcia@mail.cern.ch"><u>dgarcia@mail.cern.ch</u></a>
<b>Gehrmann, Thomas</b>	<b>Univ. Karlsruhe</b>	<a href="mailto:gehrt@particle.uni-karlsruhe.de"><u>gehrt@particle.uni-karlsruhe.de</u></a>
<b>Ghinculov, Adrian</b>	<b>UCLA</b>	<a href="mailto:adriangh@physics.ucla.edu"><u>adriangh@physics.ucla.edu</u></a>
<b>Giele, Walter</b>	<b>Fermilab</b>	<a href="mailto:giele@fnal.gov"><u>giele@fnal.gov</u></a>
<b>Graesser, Michael</b>	<b>University of California, Santa Cruz</b>	<a href="mailto:graesser@scipp.ucsc.edu"><u>graesser@scipp.ucsc.edu</u></a>
<b>Grassi, Pietro Antonio</b>	<b>New York University</b>	<a href="mailto:pag5@nyu.edu"><u>pag5@nyu.edu</u></a>
<b>Guasch, Jaume</b>	<b>Institut fuer Theoretische Physik Universitaet Karlsruhe</b>	<a href="mailto:guasch@particle.physik.uni-karlsruhe.de"><u>guasch@particle.physik.uni-karlsruhe.de</u></a>
<b>Gunion, John</b>	<b>U.C. Davis</b>	<a href="mailto:jfgucd@higgs.ucdavis.edu"><u>jfgucd@higgs.ucdavis.edu</u></a>
<b>Haber, Howard</b>	<b>University of California, Santa Cruz</b>	<a href="mailto:haber@scipp.ucsc.edu"><u>haber@scipp.ucsc.edu</u></a>
<b>Hagiwara, Kaoru</b>	<b>KEK Theory Division</b>	<a href="mailto:kaoru.hagiwara@kek.jp"><u>kaoru.hagiwara@kek.jp</u></a>
<b>Harlander, Robert</b>	<b>Brookhaven National Laboratory</b>	<a href="mailto:rharlan@bnl.gov"><u>rharlan@bnl.gov</u></a>
<b>Heinemeyer, Sven</b>	<b>DESY</b>	<a href="mailto:Sven.Heinemeyer@desy.de"><u>Sven.Heinemeyer@desy.de</u></a>
<b>Herrero, Maria</b>	<b>Universidad Autonoma de Madrid</b>	<a href="mailto:herrero@delta.ft.uam.es"><u>herrero@delta.ft.uam.es</u></a>
<b>Hiller, Gudrun</b>	<b>SLAC</b>	<a href="mailto:ghiller@slac.stanford.edu"><u>ghiller@slac.stanford.edu</u></a>
<b>Hoang, Andre</b>	<b>CERN</b>	<a href="mailto:Andre.Hoang@cern.ch"><u>Andre.Hoang@cern.ch</u></a>

<b>Hollik, Wolfgang</b>	<b>Universität Karlsruhe</b>	<a href="mailto:Wolfgang.Hollik@physik.uni-karlsruhe.de"><u>Wolfgang.Hollik@physik.uni-karlsruhe.de</u></a>
<b>Hurth, Tobias</b>	<b>CERN</b>	<a href="mailto:tobias.hurth@cern.ch"><u>tobias.hurth@cern.ch</u></a>
<b>Isidori, Gino</b>	<b>INFN - Laboratori Nazionali di Frascati</b>	<a href="mailto:Gino.Isidori@lnf.infn.it"><u>Gino.Isidori@lnf.infn.it</u></a>
<b>Jones, Tim</b>	<b>Liverpool University</b>	<a href="mailto:drtj@liverpool.ac.uk"><u>drtj@liverpool.ac.uk</u></a>
<b>Junk, Tom</b>	<b>CERN</b>	<a href="mailto:Tom.Junk@cern.ch"><u>Tom.Junk@cern.ch</u></a>
<b>Kreimer, Dirk</b>	<b>Mainz University</b>	<a href="mailto:dirk.kreimer@uni-mainz.de"><u>dirk.kreimer@uni-mainz.de</u></a>
<b>Kuehn, Johann</b>	<b>Inst. f. Theor. Teilchenphysik, Univ. Karlsruhe</b>	<a href="mailto:Johann.Kuehn@Physik.Uni-Karlsruhe.de"><u>Johann.Kuehn@Physik.Uni-Karlsruhe.de</u></a>
<b>Lebed, Richard</b>	<b>Jefferson Lab</b>	<a href="mailto:lebed@jlab.org"><u>lebed@jlab.org</u></a>
<b>Leibovich, Adam</b>	<b>Carnegie Mellon University</b>	<a href="mailto:adaml@cmuhep2.phys.cmu.edu"><u>adaml@cmuhep2.phys.cmu.edu</u></a>
<b>Lepage, Peter</b>	<b>Cornell University</b>	<a href="mailto:gpl@mail.lns.cornell.edu"><u>gpl@mail.lns.cornell.edu</u></a>
<b>Luke, Michael</b>	<b>University of Toronto</b>	<a href="mailto:luke@physics.utoronto.ca"><u>luke@physics.utoronto.ca</u></a>
<b>Lykken, Joseph</b>	<b>Fermilab</b>	<a href="mailto:lykken@fnal.gov"><u>lykken@fnal.gov</u></a>
<b>Marciano, William</b>	<b>Brookhaven National Lab</b>	<a href="mailto:marciano@bnl.gov"><u>marciano@bnl.gov</u></a>
<b>Martin, Stephen</b>	<b>Northern Illinois U. and Fermilab</b>	<a href="mailto:spmartin@niu.edu"><u>spmartin@niu.edu</u></a>
<b>McFarland, Kevin</b>	<b>University of Rochester</b>	<a href="mailto:ksmcf@pas.rochester.edu"><u>ksmcf@pas.rochester.edu</u></a>
<b>Mele, Salvatore</b>	<b>CERN</b>	<a href="mailto:Salvatore.Mele@cern.ch"><u>Salvatore.Mele@cern.ch</u></a>
<b>Melnikov, Kirill</b>	<b>SLAC</b>	<a href="mailto:melnikov@slac.stanford.edu"><u>melnikov@slac.stanford.edu</u></a>
<b>Narayanan, Rajamani</b>	<b>American Physical Society</b>	<a href="mailto:rajamani@bnl.gov"><u>rajamani@bnl.gov</u></a>
<b>Nierste, Ulrich</b>	<b>Fermilab</b>	<a href="mailto:nierste@fnal.gov"><u>nierste@fnal.gov</u></a>
<b>Orr, Lynne</b>	<b>University of Rochester</b>	<a href="mailto:orr@pas.rochester.edu"><u>orr@pas.rochester.edu</u></a>
<b>Passarino, Giampiero</b>	<b>Universita` Torino</b>	<a href="mailto:giampiero@to.infn.it"><u>giampiero@to.infn.it</u></a>
<b>Peskin, Michael</b>	<b>SLAC</b>	<a href="mailto:mpeskin@slac.stanford.edu"><u>mpeskin@slac.stanford.edu</u></a>
<b>Pich, Antonio</b>	<b>IFIC, Universidad de Valencia</b>	<a href="mailto:Antonio.Pich@uv.es"><u>Antonio.Pich@uv.es</u></a>
<b>Prigl, Ralf</b>	<b>BNL</b>	<a href="mailto:prigl@bnl.gov"><u>prigl@bnl.gov</u></a>

<b>Quimbay, Carlos</b>	<b>Universidad Nacional de Colombia</b>	<a href="mailto:carloqui@ciencias.ciencias.unal.edu.co"><u>carloqui@ciencias.ciencias.unal.edu.co</u></a>
<b>Rainwater, David</b>	<b>Fermilab</b>	<a href="mailto:dlrain@fnal.gov"><u>dlrain@fnal.gov</u></a>
<b>Rathsman, Johan</b>	<b>CERN</b>	<a href="mailto:Johan.Rathsman@cern.ch"><u>Johan.Rathsman@cern.ch</u></a>
<b>Riemann, Tord</b>	<b>DESY</b>	<a href="mailto:Tord.Riemann@ifh.de"><u>Tord.Riemann@ifh.de</u></a>
<b>Rivas, Siannah Penaranda</b>	<b>Universidad Autonoma de Madrid</b>	<a href="mailto:siannah@delta.ft.uam.es"><u>siannah@delta.ft.uam.es</u></a>
<b>Rizzo, Thomas</b>	<b>SLAC</b>	<a href="mailto:rizzo@slac.stanford.edu"><u>rizzo@slac.stanford.edu</u></a>
<b>Rowson, P.C.</b>	<b>SLAC</b>	<a href="mailto:rowson@slac.stanford.edu"><u>rowson@slac.stanford.edu</u></a>
<b>Satpathy, Asish</b>	<b>Dept. of Physics, University of Cincinnati</b>	<a href="mailto:satpathy@bsunsv1.kek.jp"><u>satpathy@bsunsv1.kek.jp</u></a>
<b>Schmidt, Carl</b>	<b>Michigan State University</b>	<a href="mailto:schmidt@pa.msu.edu"><u>schmidt@pa.msu.edu</u></a>
<b>Schumm, Bruce</b>	<b>UC Santa Cruz</b>	<a href="mailto:schumm@scipp.ucsc.edu"><u>schumm@scipp.ucsc.edu</u></a>
<b>Smirnov, Vladimir</b>	<b>Nuclear Physics Institute of Moscow State University</b>	<a href="mailto:smirnov@theory.npi.msu.su"><u>smirnov@theory.npi.msu.su</u></a>
<b>Solà, Joan</b>	<b>Univ. Autònoma de Barcelona</b>	<a href="mailto:sola@ifae.es"><u>sola@ifae.es</u></a>
<b>Soper, Davison</b>	<b>University of Oregon</b>	<a href="mailto:soper@bovine.uoregon.edu"><u>soper@bovine.uoregon.edu</u></a>
<b>Spira, Michael</b>	<b>II. Inst. Theor. Physik, Hamburg University</b>	<a href="mailto:spira@desy.de"><u>spira@desy.de</u></a>
<b>Strom, David</b>	<b>University of Oregon</b>	<a href="mailto:strom@bovine.uoregon.edu"><u>strom@bovine.uoregon.edu</u></a>
<b>Touramanis, Christos</b>	<b>University of Liverpool</b>	<a href="mailto:christos@slac.stanford.edu"><u>christos@slac.stanford.edu</u></a>
<b>Trentadue, Luca</b>	<b>Universita' di Parma-Dipartimento di Fisica</b>	<a href="mailto:luca.trentadue@fis.unipr.it"><u>luca.trentadue@fis.unipr.it</u></a>
<b>Verbeni, Michela</b>	<b>Universita' di Parma-Dipartimento di Fisica</b>	<a href="mailto:verbeni@fis.unipr.it"><u>verbeni@fis.unipr.it</u></a>
<b>Wackerroth, Doreen</b>	<b>University of Rochester</b>	<a href="mailto:dow@pas.rochester.edu"><u>dow@pas.rochester.edu</u></a>
<b>Wagner, Carlos E.M.</b>	<b>Argonne National Lab and University of Chicago</b>	<a href="mailto:cwagner@pcl10.hep.anl.gov"><u>cwagner@pcl10.hep.anl.gov</u></a>
<b>Ward, Bennie</b>	<b>University of Tennessee</b>	<a href="mailto:bflw@slac.stanford.edu"><u>bflw@slac.stanford.edu</u></a>
<b>Was, Zbigniew</b>	<b>Institute of Nuclear Physics</b>	<a href="mailto:z.was@cern.ch"><u>z.was@cern.ch</u></a>

Willenbrock, Scott	U. of Illinois at Urbana-Champaign	<a href="mailto:willen@uiuc.edu">willen@uiuc.edu</a>
Womersley, John	Fermilab	<a href="mailto:womersley@fnal.gov">womersley@fnal.gov</a>
Wyler, Daniel	University of Zurich	<a href="mailto:wyler@physik.unizh.ch">wyler@physik.unizh.ch</a>
Wynhoff, Stephan	CERN	<a href="mailto:stephan.wynhoff@cern.ch">stephan.wynhoff@cern.ch</a>
Yakovlev, Oleg	University of Michigan	<a href="mailto:yakovlev@umich.edu">yakovlev@umich.edu</a>
Yoshida, Rik	Argonne National Laboratory	<a href="mailto:rik.yoshida@desy.de">rik.yoshida@desy.de</a>
Zhao, Xin	University of Kansas	<a href="mailto:xinz@mail.lns.cornell.edu">xinz@mail.lns.cornell.edu</a>

90 participants



- [Home](#) ■ [Committees](#) ■ [Participants](#) ■ [Proceedings](#) ■ [Program](#)
- [Bulletin](#) ■ [Hotel](#) ■ [Registration](#) ■ [Travel Info](#)

5th International Symposium on Radiative Corrections  
Carmel Mission Inn, Carmel, CA  
September 11 - 15, 2000

[Jones](#)

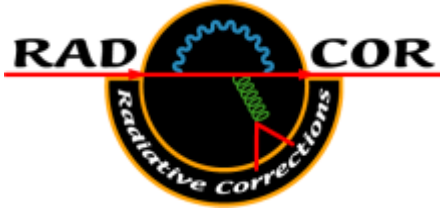
Last Update: Thursday, 13 December 2001



# 5th International Symposium on Radiative Corrections

## Carmel Mission Inn, Carmel, CA

### September 11 - 15, 2000



# Program

## Overview

Day	Date	Start	End	Event
Sunday	Sept 10	6:00 pm	9:00 pm	Registration and Reception
Monday	Sept 11	9:00 am	12:30 pm	<a href="#">Electroweak Physics I</a>
		12:30 pm	2:30 pm	Lunch
		2:30 pm	6:00 pm	<a href="#">Heavy Quark Physics I</a>
Tuesday	Sept 12	9:00 am	12:30 pm	<a href="#">e+e- Physics at Present and Future Facilities</a>
		12:30 pm	2:30 pm	Lunch
		2:30 pm	6:00 pm	<a href="#">QCD Physics I</a>
<b>Note:</b> The Wednesday sessions will be held at UC Santa Cruz in Room B-206 of the Earth and Marine Sciences (EMS) Building. All other conference sessions will be held at the Carmel Mission Inn.				
Wednesday	Sept 13	9:45 am	1:00 pm	<a href="#">Beyond the Standard Model I</a>
		1:00 pm	2:30 pm	Lunch
		2:30 pm	6:00 pm	<a href="#">Heavy Quark Physics II</a>
		7:00 pm	10:00 pm	Banquet (Chaminade at Santa Cruz)
Thursday	Sept 14	9:00 am	12:30 pm	<a href="#">QCD Physics II</a>
		12:30 pm	2:30 pm	Lunch
		2:30 pm	6:00 pm	<a href="#">Computational Methods in Quantum Field Theory</a>
Friday	Sept 15	9:00 am	12:30 pm	<a href="#">Electroweak Physics II and Beyond the Standard Model II</a>
		12:30 pm	2:30 pm	Lunch
		2:30 pm	6:00 pm	<a href="#">Precision Physics at Future Colliders and Conference Summary</a>
<b>End of Conference</b>				

# Schedule of Talks

## Monday, September 11, 2000, 9 am -- 12:30 pm: Electroweak Physics I

Chair: Stanley Brodsky (SLAC)

TIME	SPEAKER	TITLE
9:00 - 9:10	Howard Haber (UC Santa Cruz)	Introduction to RADCOR-2000
9:10 - 9:40	David Strom (Oregon)	Precision Electroweak Observables at LEP and SLD
9:40 - 10:10	Kaoru Hagiwara (KEK)	Precision Electroweak Measurements--a theorist's perspective
10:10 - 10:30	Tord Riemann (DESY, Zeuthen)	S-matrix approach to the Z resonance
10:30 - 11:00	COFFEE BREAK	
11:00 - 11:40	Kevin McFarland (Rochester)	Electroweak Physics at the Tevatron
11:40 - 12:10	Scott Willenbrock (Illinois)	Precision Top Physics
12:10 - 12:30	Andrzej Czarnecki (Alberta)	Radiative corrections to bound state properties in QED

## Monday, September 11, 2000, 2:30 -- 6 pm: Heavy Quark Physics I

Chair: Bruce Schumm (UC Santa Cruz)

TIME	SPEAKER	TITLE
2:30 - 2:50	Christos Touramanis (Liverpool)	First Results from Babar
2:50 - 3:10	Asish Satpathy (Cincinnati)	First Results from Belle
3:10 - 3:30	Xin Zhao (Kansas)	The Measurement of $V_{cb}$ and Charmless Hadronic B Decays at CLEO
3:30 - 4:00	Aida El-Khadra (Illinois U., Urbana)	Results from the Lattice
4:00 - 4:30	COFFEE BREAK	
4:30 - 5:10	Salvatore Mele (CERN, INFN Napoli)	Overview, and rho-eta fit
5:10 - 5:40	Martin Beneke (Aachen)	Factorization in Hadronic B-Decays
5:40 - 6:00	Ulrich Nierste (Fermilab)	The width difference of $B_s$ mesons

## Tuesday, September 12, 2000, 9 am -- 12:30 pm: e+e- Physics at Present and Future Facilities

Chair: Peter Rowson (SLAC)

TIME	SPEAKER	TITLE
9:00 - 9:30	Tom Junk (Carlton)	Searches at LEP2: Higgs and physics beyond the Standard Model
9:30 - 10:00	Stephan Wynhoff (CERN)	Standard Model Physics Results from LEP2
10:00 - 10:30	Stefan Dittmaier (Bielefeld)	Four-fermion production in e+e- annihilation
10:30 - 11:00	COFFEE BREAK	
11:00 - 11:20	Ansgar Denner (PSI)	Leading electroweak logarithms at one loop
11:20 - 11:40	Giampiero Passarino (Torino)	Single-W production, Fermion-Loop and ISR
11:40 - 12:10	Bennie Ward (Tennessee)	Precision Predictions for WW/4f Production in e+e- Annihilation: YFSWW3/KoralW1.42/YFSZZ
12:10 - 12:30	Zbigniew Was (INP, Cracow)	Coherent Exclusive Exponentiation of 2f Processes in e+e- Annihilation

## Tuesday, September 12, 2000, 2:30 -- 6 pm: QCD Physics I

Chair: Lance Dixon (SLAC)

TIME	SPEAKER	TITLE
2:30 - 3:10	John Womersley (Fermilab)	QCD at the Tevatron: current results and future prospects
3:10 - 3:40	R. Keith Ellis (Fermilab)	NLO QCD corrections to femtobarn processes
3:40 - 4:00	Walter Giele (Fermilab)	Phenomenological implications of parton density function uncertainties
4:00 - 4:30	COFFEE BREAK	
4:30 - 5:10	Konstantin Chetyrkin (Karlsruhe)	Review of multi-loop QCD computations such as: beta functions, anomalous dimensions, quark mass relations; applications and future prospects
5:10 - 5:40	Johan Rathsmann (CERN)	Conformal expansions: a template for QCD predictions
5:40 - 6:00	Johannes Bluemlein (DESY, Zeuthen)	On the Drell-Yan-Levy Relation to $O(\alpha_s^2)$

## Wednesday, September 13, 2000, 9:45 am -- 1 pm: Beyond the Standard Model I

Chair: Michael Graesser (UC Santa Cruz)

TIME	SPEAKER	TITLE
9:45 - 10:05	Edmond Berger (ANL)	Predictions for Associated Production of a Gaugino and a Gluino at Hadron Colliders in SUSY-QCD at NLO
10:05 - 10:25	Michael Spira (Paul Scherrer Institut)	Higgs Radiation off Quarks in Supersymmetric Theories at e+e- Colliders
10:25 - 10:45	Sven Heinemeyer (DESY)	New results for Feynman-diagrammatic higher order corrections in the MSSM
10:45 - 11:05	Marcela Carena (Fermilab)	MSSM Higgs sector phenomenology with explicit CP violation
11:05 - 11:35	COFFEE BREAK	
11:35 - 11:55	David Garcia (CERN)	Quantum corrections for the MSSM Higgs couplings to Standard Model fermions
11:55 - 12:15	Maria Herrero (Madrid)	Decoupling properties of MSSM particles in Higgs and top decays
12:15 - 12:35	Joan Sola (Barcelona)	FCNC top quark decays beyond the Standard Model
12:35 - 12:55	D.R. Tim Jones (Liverpool)	Exact results for soft supersymmetry-breaking beta-functions and their applications

## Wednesday, September 13, 2000, 2:30 -- 6 pm: Heavy Quark Physics II

Chair: Gudrun Hiller (SLAC)

TIME	SPEAKER	TITLE
2:30 - 2:50	Tony Barker (Colorado)	KTeV Present and Future
2:50 - 3:10	Stefano Bertolini (INFN, SISSA)	Theory of $\epsilon_s'/\epsilon_s$
3:10 - 3:40	Gino Isidori (INFN, Frascati)	Supersymmetric effects in rare semileptonic decays of B & K mesons
3:40 - 4:00	Richard Lebed (Arizona State)	Weak Annihilation Radiative Decays
4:00 - 4:30	COFFEE BREAK	
4:30 - 4:50	Adam Leibovich (Carnegie Mellon)	$V_{ub}$ from semileptonic decay and $b \rightarrow s$ gamma
4:50 - 5:10	Michael Luke (Toronto)	A new method for obtaining $V_{ub}$
5:10 - 5:40	Daniel Wyler (Zurich)	Extraction of CKM angles in the presence of new physics
5:40 - 6:00	Tobias Hurth (CERN)	Rare B Decays at the NLL level

## Thursday, September 14, 2000, 9 am -- 12:30 pm: QCD Physics II

Chair: Zvi Bern (UCLA)

TIME	SPEAKER	TITLE
9:00 - 9:40	Rik Yoshida (ANL)	HERA small-x and/or diffraction
9:40 - 10:20	Carl Schmidt (Michigan State)	Review of BFKL
10:20 - 10:50	COFFEE BREAK	
10:50 - 11:20	Antonio Pich (Valencia)	Chiral perturbation theory
11:20 - 11:50	Simon Dalley (Cambridge)	Light-cone QCD on the lattice
11:50 - 12:10	Andre Hoang (CERN)	Charm Effects in Perturbative Bottom Mass Determination
12:10 - 12:30	Markus Diehl (SLAC)	Exclusive QCD

## Thursday, September 14, 2000, 2:30 -- 6 pm: Computational Methods

Chair: Kirill Melnikov (SLAC)

TIME	SPEAKER	TITLE
2:30 - 2:50	Rajamani Narayanan (APS and BNL)	Nonperturbative simulation of chiral fermions
2:50 - 3:10	Robert Harlander (BNL)	Application of Pade's to fixed-order QCD computations
3:10 - 3:30	Thomas Gehrmann (Karlsruhe)	Multi-loop non-propagator integrals
3:30 - 4:00	Vladimir A. Smirnov (Moscow)	"Strategy of regions" --- expansions of Feynman diagrams in both Euclidean and pseudo-Euclidean regimes
4:00 - 4:30	COFFEE BREAK	
4:30 - 4:50	Davison Soper (Oregon)	Purely numerical calculations of event-shape variables
4:50 - 5:10	Pietro Anonio Grassi (NYU)	Practical Algebraic Renormalization
5:10 - 5:30	Adrian Ghinculov (UCLA)	Electroweak two-loop corrections: Reduction and evaluation of massive graphs
5:30 - 6:00	Dirk Kreimer (Mainz)	Polylogarithms, Knots and Feynman Diagrams

## Friday, September 15, 2000, 9 am -- 12:30 pm: Electroweak Physics II and Beyond the Standard Model II

Chair: Thomas Rizzo (SLAC)

TIME	SPEAKER	TITLE
9:00 - 9:20	Ralf Prigl (BNL)	Recent Experimental Results for g-2
9:20 - 9:50	Bill Marciano (BNL)	Theoretical Implications of g-2
9:50 - 10:10	Zvi Bern (UCLA)	Perturbative Quantization of Gravity Theories
10:10 - 10:30	Wolfgang Hollik (Karlsruhe)	2-loop electroweak contributions to $\Delta_r$
10:30 - 11:00	COFFEE BREAK	
11:00 - 11:20	John Gunion (UC Davis)	Do precision electroweak constraints guarantee e+e- collider discovery of at least one Higgs boson of a two-Higgs-doublet model?
11:20 - 11:40	Stephen Martin (Northern Illinois)	Constraints on ultraviolet stability of gauge couplings in realistic supersymmetric models
11:40 - 12:00	Carlos Wagner (ANL)	Electroweak Baryogenesis in the MSSM
12:00 - 12:30	Joe Lykken (Fermilab)	A practical guide to higher dimensional quantum gravity

## Friday, September 15, 2000, 2:30 -- 6 pm: Precision Physics at Future Colliders and Conference Summary

Chair: Michael Peskin (SLAC)

TIME	SPEAKER	TITLE
2:30 - 3:00	Francois Charles (Strasbourg)	Precision Physics at the LHC
3:00 - 3:20	Doreen Wackerroth (Rochester)	Theoretical challenges for a precision measurement of the W mass at hadron colliders
3:20 - 3:50	Tim Barklow (SLAC)	WW Physics at Present and Future e+e- Colliders
3:50 - 4:20	COFFEE BREAK	
4:20 - 4:50	David Rainwater (Fermilab)	Precision Higgs Physics at the NLC
4:50 - 5:10	Jens Erler (U. Penn.)	Physics Impact of a Giga Z
5:10 - 5:50	Johann Kuehn (Karlsruhe)	Conference Summary